Inositol Polyphosphates and Analogues: Synthesis & Chemical Biology

Megan Shipton

A thesis submitted to the University of Oxford for the degree of Doctor of Philosophy

University of Oxford

Department of Pharmacology

July 2021

Abstract

In this work, *myo*-inositol phosphates and pyrophosphates were investigated to facilitate further understanding of their chemical biology and biological functions. The synthesis of novel carbohydrate-based polyphosphate analogues of lower inositol phosphates, including the second messenger D-*myo*-inositol 1,4,5-trisphosphate [Ins(1,4,5)P_3], was undertaken, and novel routes for some naturally-occurring inositol pyrophosphates were designed.

Synthetic routes for the *meso myo*-inositol pyrophosphates 5-PP-InsP_5 (5-IP_7) and 5-PP-InsP_4, as well as both the racemic and chiral versions of D-1,5-$(PP)_2$-InsP_4 (D-1,5-IP_8), were successfully executed. These approaches incorporated the hitherto little-used methylsulfonylethyl (MSE)-protecting group, allowing its versatility to be explored. Final products were then used with collaborators to investigate: substrate binding to the yeast diphosphoinositol polyphosphate phosphohydrolase through a structural biology approach; the potential scope of a novel pyrophosphate-monitoring, europium-based luminescence assay; and structure-activity (SAR) aspects of the inositol 1,4,5,6-tetrakisphosphate binding site in the histone deacetylase 3 - SMRT corepressor (HDAC3-SMRT) complex.

The SAR investigation for HDAC3-SMRT featured seven glucose-based polyphosphate compounds (two known, five novel) that were designed, synthesised and biologically evaluated. The L-glucose-based ligands were found to be the first carbohydrate-based ligands able to activate the complex, while their D-glucose-based enantiomers were inactive. A binding site region suspected to be able to accommodate steric bulk was explored, and it also was concluded that inositol pyrophosphates are unlikely to be physiologically relevant endogenous activators for the HDAC3-SMRT complex.

A further six novel glucose-based polyphosphates were synthesised to investigate calcium release via the Ins(1,4,5)P_3 receptor (InsP_3R). Two ligands, α-D-glucopyranosyl 1,3,4-trisphosphate and β-D-glucopyranosyl 1,3,4-trisphosphate, were full agonists, the latter equipotent to Ins(1,4,5)P_3 itself. These two ligands were also substrates for *Arabidopsis* inositol tetrakisphosphate kinase-1 (ITPK1). Although unconfirmed, it is proposed that ITPK1 phosphorylates the 6-position primary hydroxyl. Both ligands were uniquely co-crystallised with Ins(1,4,5)P_3 3-kinase. The crystallographically-solved ternary complexes also revealed the primary hydroxyl group to be well-situated for potential phosphorylation.

Two of the InsP_3R-study ligands, methyl α-L-glucopyranoside 2,3,6-trisphosphate and methyl α-L-glucopyranoside 2,4,6-trisphosphate, were low-affinity, low-efficacy partial agonists. From the presumed binding mode of the latter, structurally-inspired *myo*-inositol pyrophosphate-containing compounds were designed, targeting a potential higher-affinity partial agonist or antagonist. Using techniques earlier developed, three novel inositol pyrophosphates were synthesized, 4-PP-Ins(5)P, 5-PP-Ins(4)P and 4-PP-Ins$(1,5)_2$, which are the first examples of an Ins(1,4,5)P_3 pyrophosphate analogue modified at the 4,5-vicinal bisphosphate pharmacophore. Biological evaluation of these compounds is currently underway.

Acknowledgements

Firstly, I would like to thank my main supervisor Professor Barry Potter for giving me the opportunity to join the lab group and carry out this DPhil. It was a somewhat unconventional start to a DPhil, and Barry went out of his way to help me join his group and undertake this project, for which I am so thankful. Throughout my time here he has been a brilliant supervisor who, despite his busy schedule, always made time to answer any of my questions and provide me with very useful feedback and suggestions. I would also like to thank my other main supervisor Dr Andrew Riley, who helped support me throughout this degree with endless kindness and patience. He taught me so much about practical synthetic chemistry and was always there to provide good advice about my research. My thanks also to the other members of the lab, Dr Wolfgang Dohle, Dr Stephen Mills and Dr Xiangdong Su, who provided invaluable assistance and a really friendly atmosphere in the lab. You guys are wonderful and I am going to miss everyone in the Potter lab so much–it has already been hard having everyone leave one by one as the lab winds down. You all made me feel that I belonged in the group – thank you so much! These have been some of the happiest and most interesting years of my life and I am so grateful.

I would like to thank my third supervisor Prof Stuart Conway, who although I did not see much of him in person, supported me so much, providing a crucial safety net to enable me to carry out this degree in the Potter group. He also coordinated my access to the NMR facilities in the CRL when I lost admittance to the department due to the pandemic, and helped reinstate my access as soon as possible. On that note, I would also like to thank all of the Conway group postdocs who collected and ran my many NMR samples when I could not access the walk-up machines myself: Dr Pascal Heitel, Dr Maria Odyniec, Dr Jessica Reynolds, Dr Antoine Wallabregue and Dr Glen Brodie. I would not have been able to carry out even half of the synthetic work I managed to in the last year without all of your help in analysing my many samples – without a doubt, you rescued my project. Thank you!

I am grateful to Mrs Maria Marshall, Prof Tim Claridge, Dr Nader Amin and Miss Tina Jackson from the NMR faculty who ran some of my more challenging NMR samples and still provided me with lovely spectra. Additional thanks to Dr Victor Mikhailov and Dr James Wickens for running my high-resolution mass spectrometry samples and sticking with the trickier products (deprotected phosphates) until they succeeded in obtaining results.

Many thanks to all of our collaborators: Dr Stephen Butler, Ms F. A. Jamion, Prof Beatriz González and her lab group, Prof Charles Brearley, Dr Hayley Whitfield, Prof John Schwabe, Dr Yun Song, Dr Jennifer Gurnett, Mr Ed Brown, Prof Antony Galione, Dr Lianne Davis, Prof Colin Taylor and Dr Ana Rossi. It was a pleasure to work with you!

Additionally, I would like to thank my GTC college advisor, Prof Garrett Morris, for his support and friendly advice. I am so grateful to him for checking in periodically to make sure I was doing well and inviting me to lunches so we could catch up. You really helped me settle in to college life, and it was so reassuring to know you had my back – thank you!

Lastly, I would like to thank my family for their unerring support (with a special shout out to Dad for proof-reading this thesis). Mom, Dad, Poodle and Saffy, thank you so much – I could not have gotten here without you!

Table of Contents

Abstract II

Acknowledgements III

Compounds Synthesised VIII

Associated publications XII

Abbreviations XIII

(1) Introduction 1

1.1 Inositol phosphates 1

1.1.1 Inositol phosphates introduction and overview 1

1.1.2 Inositol phosphate biosynthesis 3

1.1.3 Interconversion, abundance and biological roles of inositol phosphates 6

1.2 Inositol pyrophosphates 8

1.2.1 Interconversion and abundance of inositol pyrophosphates 8

1.2.2 Biological function of inositol pyrophosphates 11

1.3 Carbohydrate chemistry 14

1.3.1 Anomeric effect 15

1.4 Inositol chemistry 16

1.5 Phosphate chemistry 17

1.6 Pyrophosphate chemistry 20

1.6.1 Chemical synthesis methods 20

1.6.2 MSE-phosphitylating agent 22

1.6.3 Pyrophosphate Mimics 24

1.6.4 Biological methods 26

1.7 Strategies to overcome cell impermeability 26

1.8 Aims 27

(2) Inositol pyrophosphates: 5-PP-InsP$_5$ and 5-PP-InsP$_4$ 29

2.1 Biological relevance of 5-PP-InsP$_5$ and 5-PP-InsP$_4$ 29

2.2 Previous syntheses of 5-PP-IP$_5$ 31

2.3 Previous syntheses of 5-PP-InsP$_4$ *34*

*2.4 Synthesis of 5-PP-InsP$_5$ (**2**) and 5-PP-InsP$_4$ (**3**)* *36*

2.4.1 Shared synthetic route of 5-PP-InsP$_5$ (**2**) and 5-PP-InsP$_4$ (**3**) 38

2.4.2 Final steps in route to synthesise 5-PP-InsP$_5$ (**2**) 40

2.4.3 Continuation of the synthesis of 5-PP-InsP$_4$ (**3**) from the point of divergence 53

2.5 ScDDP1 crystal structures *55*

2.6 Europium complex assay *62*

(3) Inositol pyrophosphate: 1,5-(PP)$_2$-InsP$_4$ **72**

3.1 Specific biological roles of 1,5-(PP)$_2$-InsP$_4$ *72*

3.2 Previous syntheses of 1,5-(PP)$_2$-InsP$_4$ *73*

3.3 1,5-(PP)$_2$-InsP$_4$ synthesis *75*

3.4 Dictyostelium InsP$_8$ *88*

3.4.1 *Dictyostelium* inositol pyrophosphates overview 88

3.4.2 Attempted synthesis of *Dictyostelium* InsP$_8$ model compound 90

3.5 Biological evaluations of D-1,5-(PP)$_2$-InsP$_4$ *97*

(4) HDAC3-SMRT and inositol 1,4,5,6-tetrakisphosphate **98**

4.1 Histone deacetylases (HDACs) – biological background *98*

4.2 HDAC3-SMRT and Ins(1,4,5,6)P$_4$ *100*

4.3 Proposed HDAC3-SMRT regulators *103*

4.3.1 Binding mode predictions for the proposed carbohydrate-based HDAC3-SMRT ligands 104

4.3.2 GOLD docking predictions for the proposed carbohydrate-based HDAC3-SMRT ligands 107

4.4 Synthesis of the carbohydrate-based potential HDAC3-SMRT ligands *109*

4.5 HDAC3-SMRT biological results *117*

4.5.1 HDAC3-SMRT deacetylation assay: carbohydrate-based ligands 117

4.5.2 HDAC3-SMRT deacetylation assay: inositol pyrophosphates and analogues 125

(5) Inositol 1,4,5-trisphosphate and calcium signalling **137**

5.1 Ins(1,4,5)P_3 and calcium signalling – background overview *137*
5.1.1 Ins(1,4,5)P_3 binding to InsP_3R 138
5.1.2 Adenophostin A, a potent InsP_3R agonist 144
5.1.3 Development and summary of antagonists and partial agonists of InsP_3R 146
5.2 Proposed InsP_3R ligands *149*
5.2.1 Methyl α-L-glucopyranoside 2,3,6-trisphosphate (**58**) InsP_3R binding predictions 151
5.2.2 Methyl α-L-glucopyranoside 2,4,6-trisphosphate (**59**) InsP_3R binding predictions 153
5.2.3 Methyl α-D-glucopyranoside 2,3,6-trisphosphate (**60**) and methyl α-D-glucopyranoside 2,4,6-trisphosphate (**61**) InsP_3R binding predictions 155
5.2.4 α-D-glucopyranosyl 1,3,4-trisphosphate (**62**) and β-D-glucopyranosyl 1,3,4-trisphosphate (**63**) InsP_3R binding predictions 155
5.3 Synthesis of the carbohydrate-based potential InsP_3R ligands *158*
*5.4 Stability analysis of α-D-glucopyranosyl 1,3,4-trisphosphate (**62**) and β-D-glucopyranosyl 1,3,4-trisphosphate (**63**)* *168*
5.5 InsP_3R biological results *171*
5.5.1 Calcium release and competition binding assays 171
5.5.2 Sea urchin egg homogenate assay 175
5.6 Discussion of the biological activities of the InsP_3R ligands *177*
5.6.1 Anomeric phosphate agonists: α-D-glucopyranosyl 1,3,4-trisphosphate (**62**) and β-D-glucopyranosyl 1,3,4-trisphosphate (**63**) 177
5.6.2 Partial agonist: methyl α-L-glucopyranoside 2,3,6-trisphosphate (**58**) and its inactive enantiomer, methyl α-D-glucopyranoside 2,3,6-trisphosphate (**60**) 180
5.6.3 Partial agonist: methyl α-L-glucopyranoside 2,4,6-trisphosphate (**59**) and its inactive enantiomer, methyl α-D-glucopyranoside 2,4,6-trisphosphate (**61**) 182
5.7 Arabidopsis ITPK1 and the carbohydrate-based Ins(1,4,5)P_3 mimics *184*
5.7.1 Ins(1,4,5)P_3 analogues with ITPK1 186
5.7.2 NMR analysis of ITPK1 product 188
5.8 IP_3-3K and the carbohydrate-based Ins(1,4,5)P_3 mimics *198*

(6) Pyrophosphate-containing Ins(1,4,5)P_3 derivatives **200**

6.1 Introduction and design of lower inositol pyrophosphates 200

6.2 Docking simulations for the lower inositol pyrophosphates 204

6.3 Synthesis of PP-InsP and PP-InsP_2 products *206*

6.3.1 Early and shared steps in the synthetic route 207

6.3.2 PP-InsP "model" compounds (**77** and **78**) divergence 208

6.3.3 Continuation of route to PP-InsP_2 compounds (**79** and **80**) 215

6.4 Biological evaluation of PP-InsP and PP-InsP_2 compounds *226*

(7) Conclusions and future work **228**

(8) Experimental **233**

Biological methods *233*

*Sc*DDP1 co-crystallization 233

Europium complex luminescence emission assay protocol 233

HPLC protocol 235

HDAC3-SMRT activity assay protocol 236

Ins(1,4,5)P_3R assay protocol 236

ITPK1 assay 238

IP3-3K co-crystallisation 239

Chemical Methods *240*

GOLD Molecular Modelling 240

General Synthetic Chemistry 250

References **327**

Spectra **363**

Compounds Synthesised

Synthesis of 5-PP-InsP$_5$ and 5-PP-InsP$_4$ 252

2-*O*-Benzyl-1,6:3,4-bis-*O*-(2,3-dimethoxybutane-2,3-diyl)-*myo*-inositol (**5**)..... 253

N,N-Diisopropylamino-bis-[2-(methylsulfonyl)ethyloxy]phosphine (**1**) 253

2-*O*-Benzyl-1,6:3,4-bis-*O*-(2,3-dimethoxybutane-2,3-diyl)-*myo*-inositol-5-bis[2-(methanesulfonyl)ethyl]phosphate (**6**)..... 254

2-*O*-Benzyl-*myo*-inositol-5-bis[2-(methanesulfonyl)ethyl]phosphate (**7**)..... 255

myo-Inositol-5-bis[2-(methanesulfonyl)ethyl]phosphate (**8**)..... 256

myo-Inositol-1,2,3,4,6-pentakis(dibenzyl)phosphate-5-bis[2-(methanesulfonyl)ethyl]-phosphate (**9**).....256

5-Diphospho-*myo*-inositol-1,2,3,4,6-pentakisphosphate triethylammonium salt (**2**) 257

2-*O*-Benzyl-*myo*-inositol-1,3,4,6-tetrakis(dibenzyl)phosphate-5-bis[2-(methanesulfonyl)ethyl]-phosphate (**11**) 258

5-Diphospho-*myo*-inositol-1,3,4,6-tetrakisphosphate triethylammonium salt (**3**)...259

Synthesis of 1,5-bis(diphospho)-*myo*-inositol tetrakisphosphate [1,5-(PP)$_2$-InsP$_4$]..... 261

myo-Inositol orthobenzoate (**17**)..... 262

2,4,6-Tri-*O*-benzyl-*myo*-inositol orthobenzoate (**18**) 262

2,3,4,6-Tetra-*O*-benzyl-*myo*-inositol (**19**) 263

2,3,4,6-Tetra-*O*-benzyl-*myo*-inositol-1,5-bis{bis[2-(methanesulfonyl)ethyl]phosphate} (**20**).....264

myo-Inositol-1,5-bis{bis[2-(methanesulfonyl)ethyl]phosphate} (**21**)..... 265

myo-Inositol-1,5-bis{bis[2-(methanesulfonyl)ethyl]phosphate}-2,3,4,6-tetrakis(dibenzylphosphate) (**22**) 266

1,5-Bis(diphospho)-*myo*-inositol-2,3,4,6-tetrakisphosphate triethylammonium salt (**16**) 267

Synthesis of HDAC3-SMRT carbohydrate polyphosphates 269

Methyl α-D-glucopyranoside (**42**).....269

Methyl 4,6-*O*-benzylidene-α-D-glucopyranoside (**44**) 270

Methyl 6-*O*-benzyl α-D-glucopyranoside (**45**) 271

Methyl 2,3-di-*O*-benzoyl-4,6-*O*-benzylidene-α-D-glucopyranoside (**46**)……272

Methyl 2,3-di-*O*-benzoyl-6-*O*-benzyl-α-D-glucopyranoside (**47**) ……272

Methyl 6-*O*-benzyl-α-D-glucopyranoside 2,3,4-tris(dibenzylphosphate) (**48**)……..273

Methyl 6-*O*-benzyl-α-D-glucopyranoside 2,3,4-trisphosphate triethylammonium salt (**37**)…… 274

Methyl α-D-glucopyranoside 2,3,4-trisphosphate triethylammonium salt (**38**) …….275

Methyl α-D-glucopyranoside 2,3,4,6-tetrakis(dibenzylphosphate) (**43**) ……..276

Methyl α-D-glucopyranoside 2,3,4,6-tetrakisphosphate triethylammonium salt (**36**) ……..277

Methyl β-D-glucopyranoside 2,3,4,6-tetrakis(dibenzylphosphate) (**57**) ……..278

Methyl β-D-glucopyranoside 2,3,4,6-tetrakisphosphate triethylammonium salt (**56**) ……..278

Methyl α-L-glucopyranoside (**49**) ……280

Methyl 4,6-*O*-benzylidene-α-L-glucopyranoside (**51**) ……280

Methyl 2,3-di-*O*-benzoyl-4,6-*O*-benzylidene-α-L-glucopyranoside (**52**) ……..281

Methyl 2,3-di-*O*-benzoyl-6-*O*-benzyl-α-L-glucopyranoside (**53**) ……281

Methyl 6-*O*-benzyl-α-L-glucopyranoside (**54**) ……..282

Methyl 6-*O*-benzyl-α-L-glucopyranoside 2,3,4-tris(dibenzylphosphate) (**55**) ……..282

Methyl 6-*O*-benzyl-α-L-glucopyranoside 2,3,4-trisphosphate triethylammonium salt (**41**) ……283

Methyl α-L-glucopyranoside 2,3,4-trisphosphate triethylammonium salt (**40**) …….284

Methyl α-L-glucopyranoside 2,3,4,6-tetrakis(dibenzylphosphate) (**50**) ……..284

Methyl α-L-glucopyranoside 2,3,4,6-tetrakis phosphate triethylammonium salt (**39**) ……..285

Synthesis of $InsP_3R$ carbohydrate polyphosphates…… 286

Methyl 4,6-*O*-benzylidene-3-*O*-benzyl-α-D-glucopyranoside (**66**) ……287

Methyl 3-*O*-benzyl-α-D-glucopyranoside (**67**) ……288

Methyl 3-*O*-benzyl-α-D-glucopyranoside 2,4,6-tris(dibenzylphosphate) (**68**) ……289

Methyl α-D-glucopyranoside 2,4,6-trisphosphate triethylammonium salt (**61**) …….290

Methyl 3-*O*-benzyl-4,6-*O*-benzylidene-α-L-glucopyranoside (**71**) ……291

Methyl 3-*O*-benzyl-α-L-glucopyranoside (**72**) ……291

Methyl 3-*O*-benzyl-α-L-glucopyranoside 2,4,6-tris(dibenzylphosphate) (**73**) ……292

Methyl α-L-glucopyranoside 2,4,6-trisphosphate triethylammonium salt (**59**) …….293

Methyl 4-*O*-benzyl-α-D-glucopyranoside (**64**) ……293

Methyl 4-*O*-benzyl-α-D-glucopyranoside 2,3,6-tris(dibenzylphosphate) (**65**) ……295

Methyl α-D-glucopyranoside 2,3,6-trisphosphate triethylammonium salt (**60**) …….296

Methyl 4-*O*-benzyl-α-L-glucopyranoside (**69**) ……297

Methyl 4-*O*-benzyl-α-L-glucopyranoside 2,3,6-tris(dibenzylphosphate) (**70**) ……297

Methyl α-L-glucopyranoside 2,3,6-trisphosphate triethylammonium salt (**58**) …….298

2,6-di-*O*-benzyl-D-glucopyranose (**74**) ……299

2,6-di-*O*-benzyl-D-glucopyranosyl 1,3,4-tris(dibenzylphosphate) (**75** and **76**) ……299

β-D-glucopyranosyl 1,3,4-trisphosphate triethylammonium salt (**63**) ……301

α-D-glucopyranosyl 1,3,4-trisphosphate triethylammonium salt (**62**) ……302

Synthesis of diphospho-*myo*-inositol bisphosphate and diphospho-*myo*-inositol phosphate [PP-InsP$_2$/PP-InsP] target compounds…….. 303

DL-1,2-isopropylidene-*myo*-inositol (**81**) ……303

DL-3,6-Di-*O*-benzyl-1,2-isopropylidene-*myo*-inositol (**82**) ……304

DL-3,6-Di-*O*-benzyl-*myo*-inositol (**83**) ……304

DL-3,6-Di-*O*-benzyl-4,5-*O*-(2,3-dimethoxybutane-2,3-diyl)-*myo*-inositol (**84**) ……305

Synthesis of diphospho-*myo*-inositol phosphate [PP-InsP] targets ……306

DL-1,2,3,6-Tetra-*O*-benzyl-4,5-*O*-(2,3-dimethoxybutane-2,3-diyl)-*myo*-inositol (**85**) ……307

DL-1,2,3,6-Tetra-*O*-benzyl-*myo*-inositol (**28**)…… 307

DL-1,2,3,6-Tetra-*O*-benzyl-*myo*-inositol-5-bis[2-(methanesulfonyl)ethyl]phosphate (**86**), DL-1,2,3,6-tetra-*O*-benzyl-*myo*-inositol-4-bis[2-(methanesulfonyl)ethyl]phosphate (**87**) and DL-1,2,3,6-tetra-*O*-benzyl-*myo*-inositol-4,5-bisbis[2-(methanesulfonyl)ethyl]phosphate (**29**) ……308

DL-1,2,3,6-Tetra-*O*-benzyl-*myo*-inositol-4-dibenzylphosphate-5-bis[2-(methanesulfonyl)ethyl]phosphate (**88**) ……311

DL-5-Diphospho-*myo*-inositol-4-phosphate triethylammonium salt (**77**) ……312

DL-1,2,3,6-Tetra-*O*-benzyl-*myo*-inositol-5-dibenzylphosphate-4-bis[2-(methanesulfonyl)ethyl]phosphate (**89**) ……313

DL-4-Diphospho-*myo*-inositol-5-phosphate triethylammonium salt (**78**) ……314

Synthesis of diphospho-*myo*-inositol bisphosphate [PP-InsP$_2$] targets……. 316

DL-3,6-Di-*O*-benzyl-4,5-*O*-(2,3-dimethoxybutane-2,3-diyl)-1-*O*-*para*-methoxybenzyl-*myo*-inositol (**96**) ……316

DL-2,3,6-Tri-*O*-benzyl-4,5-*O*-(2,3-dimethoxybutane-2,3-diyl)-1-*O*-*para*-methoxybenzyl-*myo*-inositol (**97**) ……317

DL-2,3,6-Tri-*O*-benzyl-4,5-*O*-(2,3-dimethoxybutane-2,3-diyl)-*myo*-inositol (**98**) ……318

DL-2,3,6-Tri-*O*-benzyl-*myo*-inositol (**99**) ……319

Fe(dpm)$_3$ (dpm = 2,2,6,6-tetramethyl-3,5-heptanedionate) (**108**) ……319

DL-2,3,6-Tri-*O*-benzyl-4-*O*-para-methoxybenzyl-*myo*-inositol (**100**) and DL-2,3,6-tri-*O*-benzyl-5-*O*-para-methoxybenzyl-*myo*-inositol (**101**) ……320

DL-2,3,6-Tri-*O*-benzyl-4-O-*para*-methoxybenzyl-*myo*-inositol 1,5-bis(dibenzylphosphate) (**102**) ……322

DL-2,3,6-Tri-*O*-benzyl-*myo*-inositol 1,5-bis(dibenzylphosphate) (**103**)…… 323

DL-2,3,6-Tri-*O*-benzyl-*myo*-inositol-1,5-bis(dibenzylphosphate)-4-bis[2-(methanesulfonyl)-ethyl]phosphate (**104**) ……324

DL-4-Diphospho-*myo*-inositol 1,5-bisphosphate triethylammonium salt (**80**) …….325

Associated publications

Shipton, M. L.; Riley, A. M.; Rossi, A. M.; Brearley, C. A.; Taylor, C. W.; Potter, B. V. L. Both D- and L-Glucose Polyphosphates Mimic D-*Myo*-Inositol 1,4,5-Trisphosphate: New Synthetic Agonists and Partial Agonists at the Ins(1,4,5)P_3 Receptor. *J. Med. Chem.* **2020**, *63* (10), 5442–5457

Márquez-Moñino, M. Á.; Ortega-García, R.; Shipton, M. L.; Franco-Echevarría, E.; Riley, A. M.; Sanz-aparicio, J.; Potter, B. V. L.; González, B. Multiple Substrate Recognition by Yeast Diadenosine and Diphosphoinositol Polyphosphate Phosphohydrolase through Phosphate Clamping. *Sci. Adv.* **2021**, *7*, 1–16.

Abbreviations

AdA	Adenophostin A
ADP	Adenosine diphosphate
ADPR	Adenosine diphosphate ribose
AMP	Adenosine monophosphate
AMP-PNP	Adenylyl-imidodiphosphate
ATP	Adenosine trisphosphate
cADPR	Cyclic adenosine diphosphate ribose
BDA	Butane diacetal
bm	Binding mode
BSTFA	*N,O*-Bis(trimethylsilyl)trifluoroacetamide
CCDC	Cambridge Crystallographic Data Centre
CLM	Cytosol-like medium
COSY	^{1}H COrrelated SpectroscopY
DBU	1,8-Diazabicyclo[5.4.0]undec-7-ene
DCM	Dichloromethane
DDQ	2,3-Dichloro-5,6-dicyano-1,4-benzoquinone
DIPP	Diphosphoinositol polyphosphate phosphohydrolase
DMF	dimethylformamide
DMSO	dimethyl sulfoxide
dpm	dipivaloylmethane
EDTA	Ethylenediaminetetraacetic acid
EGTA	Ethylene glycol-bis(β-aminoethyl ether)-*N,N,N',N'*-tetraacetic acid
ER	Endoplasmic reticulum
FITC	Fluorescein isothiocyanate
G6P	Glucose 6-phosphate
GOLD	Genetic Optimisation for Ligand Docking

HAT	Histone acetyltransferase
HDAC	Histone deacetylase
HEK	Human Embryonic Kidney cells
HEPES	4-(2-hydroxyethyl)-1-piperazineethanesulfonic acid
HMBC	Heteronuclear Multiple Bond Correlation
HPLC	High-Performance Liquid Chromatography
IBC	Inositol 1,4,5-trisphosphate binding core
Ins	Inositol
$InsP_3R$	Inositol 1,4,5-trisphosphate receptor
IP_3-3K	Inositol 1,4,5-trisphosphate 3-Kinase
IP6K	$InsP_6$ kinase
ITPK	Inositol tetrakisphosphate 1-kinase
*m*CPBA	*meta*-Chloroperoxybenzoic acid
mRNA	Messenger ribonucleic acid
MSE	Methylsulfonylethyl
N-CoR	Nuclear receptor CoRepressor
NAADP	Nicotinic acid adenine dinucleotide phosphate
NAADP-R	Nicotinic acid adenine dinucleotide phosphate receptor
NMR	Nuclear Magnetic Resonance
NPP	Nucleoside polyphosphate
P	Phosphate
PA	Phosphonoacetate
PCP	Methylene bisphosphonate
PDB	Protein Database
PH	Pleckstrin homology
PIP_2	Phosphatidylinositol 4,5-bisphosphate
PMB	*para*-Methoxybenzyl

PolyP	Inorganic polyphosphate
PP	Pyrophosphate
PPi	Inorganic pyrophosphate
ppm	Parts per million
PPIP5K	PP-InsP_5 kinase
py	pyridine
RMSD	Root Mean Square Deviation
RT	Room temperature
SAHA	Suberoylanilide hydroxamic acid
SANT	Switching-defective protein 3 (Swi3), adaptor 2 (Ada2), nuclear receptor co-repressor (N-CoR), transcription factor (TF)IIIB
SAR	Structure-activity relationship
SD	Suppressor Domain
SMRT	Silencing Mediator of Retinoid and Thyroid receptors
SPX	SYG1/Pho81/XPR1
SUEH	Sea Urchin Egg Homogenate
TBAB	Tetrabutylammonium bromide
TBAI	Tetrabutylammonium iodide
TEA	Triethylamine
TEAB	Triethylammonium bicarbonate
TFA	Trifluoroacetic acid
THF	Tetrahydrofuran
TLC	Thin Layer Chromatography
TMDS	1,1,3,3-Tetramethyldisiloxane
TSA	Trichostatin A

(1) Introduction

1.1 Inositol phosphates

1.1.1 Inositol phosphates introduction and overview

Inositol phosphates are an important group of molecules that participate in cellular signalling in organisms across multiple taxa, mediating a number of different biological functions including calcium signalling, transcription, stress response, export and translation of mRNA and insulin signalling.[1–3]

Inositol (1,2,3,4,5,6-cyclohexanehexol, generally abbreviated to "Ins") is a six-membered carbon ring structure with hydroxyl groups attached to every position around the ring. There are nine possible stereoisomers of inositol determined by the orientation of the hydroxyl groups, eight of which occur naturally (Figure 1, *allo*-, D-*chiro*-, L-*chiro*-, *epi*-, *muco*-, *myo*-, *neo*-, *scyllo*-, and the unnatural *cis*- isomer).[1]

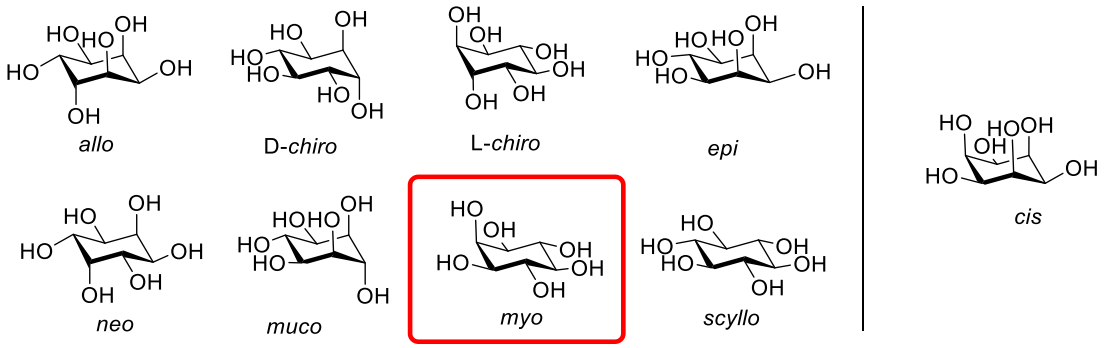

Figure 1: Structures of the stereoisomers of inositol. The eight stereoisomers on the left have been found to occur naturally, and the stereoisomer on the right has not been found in nature. The predominant stereoisomer found in most organisms, *myo*-inositol, has been highlighted in red.

Although there are multiple naturally occurring isomers of inositol, one stereoisomer in particular, *myo*-inositol, appears to predominate in most organisms, and its phosphorylated derivatives serve vital roles as cellular messengers.[1,4] The inositol stereoisomer used in this body of work was *myo*-inositol (if the stereoisomer of inositol is not explicitly stated, it should be assumed to be *myo*-inositol), which has one axial hydroxyl attached to the 2-position of the ring, while the remaining hydroxyls are in the equatorial orientation. A structural mnemonic called Agranoff's Turtle has previously been employed to describe the orientation of the hydroxyl groups in *myo*-inositol (Figure 2), likening the appearance of the molecule to a turtle with one hydroxyl sticking up to represent the head (axial 2-position) and the other five hydroxyls representing the four legs and tail (equatorial 1-, 3-, 4-, 5- and 6-positions).[5] *Myo*-inositol is also able to ring-flip to its less energetically favoured conformation,

which possesses one equatorial hydroxyl (2-position) and five axial hydroxyls, although this conformation has been calculated to be 6.683 kcal/mol higher in energy and so this stereoisomer of inositol usually exists as the conformer described by Agranoff's Turtle.[6]

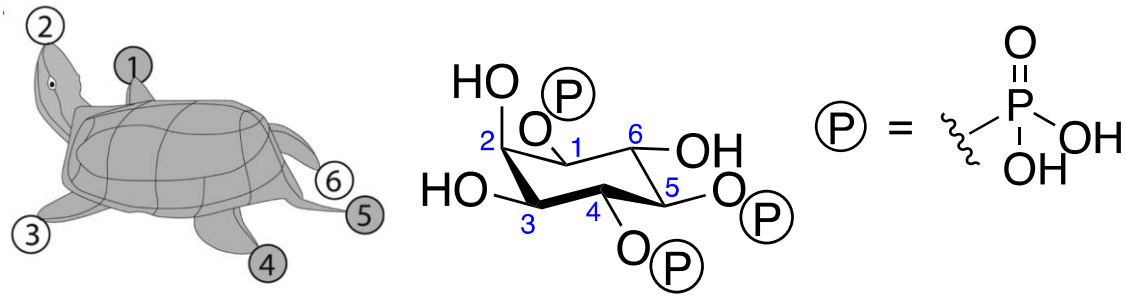

Figure 2: A depiction of Agranoff's Turtle reproduced from its original publication,[5] in which the head of the turtle is shown sticking up to correlate to the axial 2-position hydroxyl of *myo*-inositol 1,4,5-trisphosphate (left) alongside the structure of *myo*-inositol 1,4,5-trisphosphate. An inositol phosphate derivative was used to describe the basic structure of inositol as the numbering conventions of the structure are different for myo-inositol and its symmetrical derivatives.

Investigation into the potential biological roles of inositol phosphates began following the discovery that inositol 1,4,5-trisphosphate [Ins(1,4,5)P_3, depicted in Figure 2] is able to trigger calcium release from intracellular stores.[7] A wide variety of inositol phosphates, with different numbers of phosphate groups arranged in different positions around the central inositol ring, have been found to occur with different biological roles since identified for some of the regioisomers (Section 1.1.3). There are sixty-three different possible isomers for *myo*-inositol phosphates, and approximately half of these hypothetical compounds have been identified in nature.[5]

Inositol pyrophosphates, such as 5-PP-InsP_5 (also known as 5-InsP_7), are inositol derivatives that have at least one pyrophosphate group attached to one of the hydroxyl groups around the ring, with the other positions usually having monophosphates attached (Figure 3).

Pyrophosphates, also referred to as diphosphates in official IUPAC nomenclature, are functional groups that comprise two individual phosphate moieties chained together via a shared oxygen in a phosphoanhydride linkage. The prefix "pyro-" in pyrophosphate is derived from the Ancient Greek word for *fire* and was readily adopted to indicate the high energy of the phosphoanhydro bond.[8]

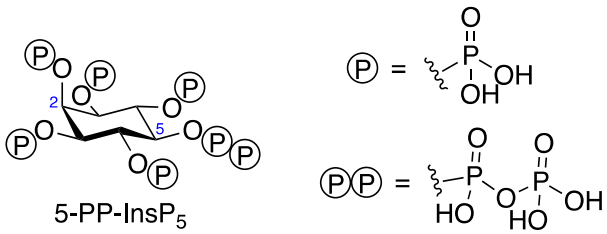

Figure 3: Example structure of the inositol pyrophosphate 5-PP-InsP$_5$. The notation for referring to the different phosphates in the pyrophosphate group is indicated.

The phosphoanhydride linkage of pyrophosphates is vulnerable to hydrolysis. Upon hydrolysis, pyrophosphates release a large amount of energy due to overall stabilisation through solvation, phosphate resonance and new electrostatic interactions.[9] The bond energies calculated for the hydrolysis of InsP$_7$ and ADP provide evidence of this with the respective bond energies of 6.6 kcal/mol and 6.4 kcal/mol (as a comparison, cleavage of one of the monophosphates attached to the inositol ring is calculated to be 3.4-4.0 kcal/mol).[10] The pyrophosphate group attached to an inositol pyrophosphate is even more susceptible to hydrolysis than in other pyrophosphate-containing compounds due to the steric interference from the surrounding negatively charged monophosphates around the inositol ring; hydrolysis can provide relief from both the electrostatic and steric congestion.[11] Under physiological conditions, both monophosphates and pyrophosphate moieties in inositol polyphosphates would be expected to be negatively charged (with the pyrophosphate likely accommodating two or more negative charges).[12–14]

1.1.2 Inositol phosphate biosynthesis

There are two natural pathways by which inositol phosphates can be synthesised: the lipid-dependent pathway and the lipid-independent pathway. The lipid-dependent pathway was the initial focus for investigating the biosynthesis of inositol phosphates, due in part to this pathway being the only biosynthetic route utilised to generate inositol phosphates in yeast, as well as the ubiquitous presence of this route in multiple organisms. A second biosynthetic pathway that is lipid-independent appears to be present in some organisms and seems to be independently regulated from the lipid-dependent pathway.[15]

Lipid-dependent biosynthesis

The lipid-dependent biosynthetic pathway generates $Ins(1,4,5)P_3$ from the phospholipase C-catalysed hydrolysis of membrane lipid phosphatidylinositol 4,5-bisphosphate (PIP_2), and in doing so liberates diacylglycerol, another second messenger in its own right (Figure 4).[7,16,17]

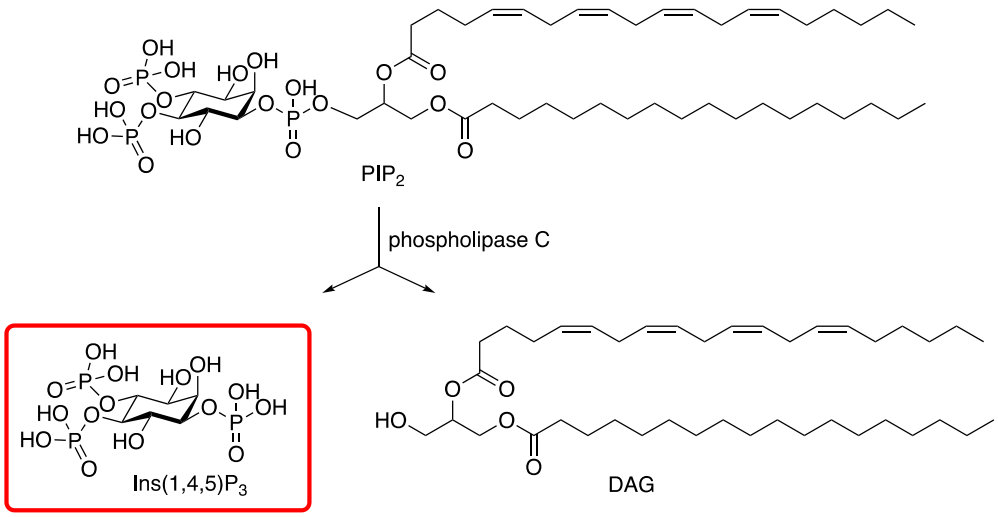

Figure 4: Biosynthesis of $Ins(1,4,5)P_3$ (highlighted in red) and diacylglycerol (DAG) from PIP_2 in the lipid-dependent inositol phosphate synthesis pathway.

From $Ins(1,4,5)P_3$, through the action of different kinases (sourcing phosphate from ATP) and phosphatases, a variety of different inositol phosphates are generated, each of which can, at least hypothetically, carry out different biological functions (Section 1.1.3).[18]

Lipid-independent biosynthesis

Some organisms have been found to be able to generate inositol phosphates with strictly no inclusion of lipids (Figure 5). This lipid-independent pathway was initially thought to be restricted to social amoeba (such as *Dictyostelium discoidem*) and plants,[15,19] although there has recently been some evidence that mammals may also be able be able to employ this biosynthetic route.[15]

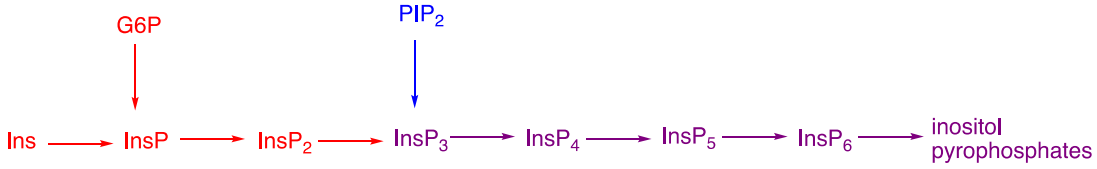

Figure 5: A very simplified depiction of the lipid-dependent synthesis route (shown in blue); the lipid-independent route from inositol (Ins) and/or glucose 6-phosphate (G6P), which is only observed in select organisms (shown in red); and the shared phosphorylation steps to generate higher inositol phosphates (shown in purple).[15]

Only some organisms have been identified to have suitable kinases to phosphorylate inositol directly including plants, amoebae and archaea but not animals.[15] Animals have been found to utilise another potential in-road to inositol phosphate synthesis, however, through the *de novo* synthesis of inositol 3-phosphate from glucose 6-phosphate (G6P). This conversion occurs through the action of inositol 3-phosphate synthase enzymes (referred to as ISYNA1 in mammals and Ino1 in yeast) that sequentially oxidise, cyclise and reduce the substrate to generate an inositol phosphate product (Figure 6).[15,20,21] Organisms that have been found directly to phosphorylate inositol after importing it into cells appear to use the isomerisation of G6P as well to generate sufficient quantities of inositol phosphates.[22]

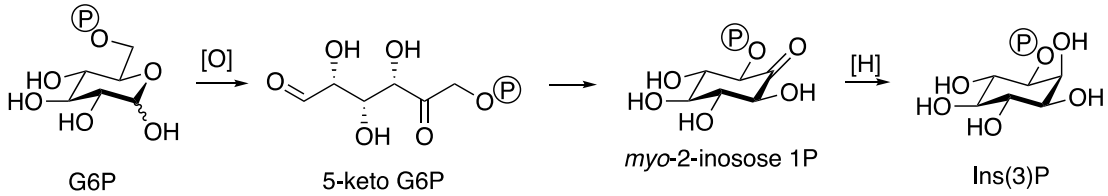

Figure 6: Synthesis of *myo*-inositol 3-phosphate [Ins(3)P] from glucose 6-phosphate (G6P) catalysed by an inositol 3-phosphate synthase demonstrating the two intermediates of the isomerisation: 5-keto-glucose 6-phosphate following oxidation and *myo*-2-inosose 1-phosphate, which is formed upon cyclisation. The myo-2-inosose 1P intermediate is then reduced to form the inositol 3-phosphate product.[20,23]

A recent investigation into the inositol tetrakisphosphate 1-kinase 1 (ITPK1) in mammals indicated that this enzyme is able to phosphorylate both Ins(1)P and Ins(3)P regioisomers to an inositol pentakisphosphate, $InsP_5$ (the regioisomer of which was not identified in the study).[15] The capabilities of ITPK1s and their homologues in a variety of organisms are currently a topic of interest being probed further and, in fact, this thesis features an investigation into the plant *Arabidopsis thaliana* (thale cress) ITPK1 in Chapter 5.

1.1.3 Interconversion, abundance and biological roles of inositol phosphates

Over thirty different inositol phosphates have been isolated from eukaryotic organisms, although only a fraction of these has been identified in animals.[18,24] These inositol phosphates interconvert rapidly through the action of a number of kinases and phosphatases (Figure 7).[18]

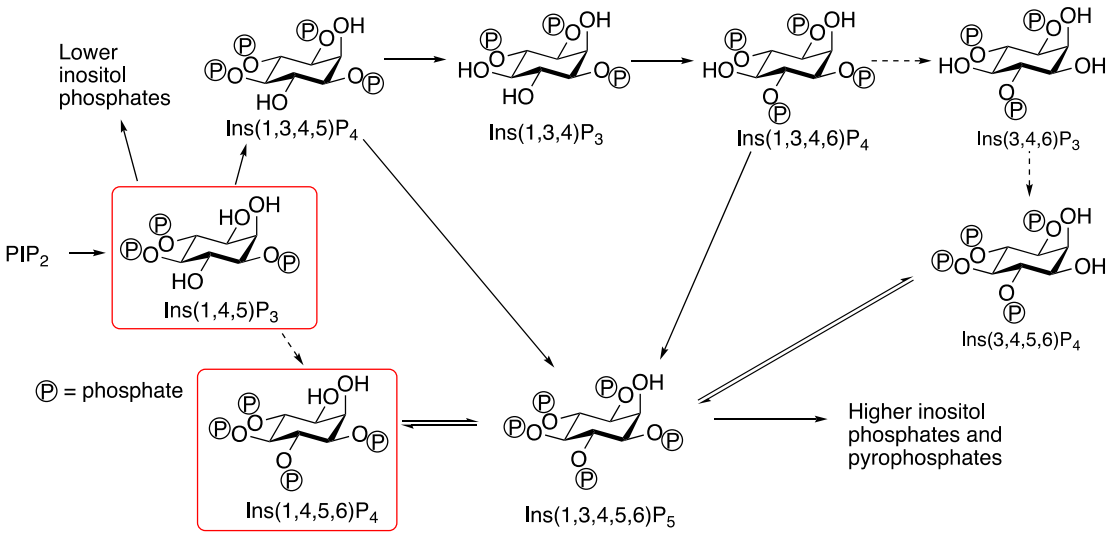

Figure 7: Some of the interconversions between lower inositol phosphates in animals (with major pathways indicated with solid arrows and some of the minor pathways indicated with dashed arrows).[18,25] Inositol 1,4,5-trisphosphate [Ins(1,4,5)P_3], which is important in calcium signalling, has been highlighted in red and is the focus of Chapters 5 and 6. Inositol 1,4,5,6-tetrakisphosphate [Ins(1,4,5,6)P_4], which is involved in gene expression, has also been highlighted in red and is discussed further in Chapter 4. "Lower inositol phosphates" in this figures indicates inositol phosphates that have one or two phosphate groups attached, while "higher inositol phosphates and pyrophosphates" have six or more phosphate groups attached as either monophosphates or pyrophosphates.

The concentrations of inositol phosphates in cells vary depending on a number of different factors, including organism type and metabolic state, but the approximate quantities present in mammalian cells have been reported in a few different studies (Table 1). Due to difficulties in quantification of these compounds such as their lack of a chromophore, presence of multiple regioisomers, low abundance, high charge density, and the fact that many of the methods used to determine their intracellular concentrations would not be able to account for the inositol phosphates derived from glucose-6-phosphate as they employ isotopically labelled inositol, the levels of inositol phosphates in cells may be higher than initially reported.[21]

Inositol phosphate	Approximate abundance
Ins(1,4,5)P_3	0.5 μM (lit. [26])
Ins(1,3,4)P_3	1-5 μM (lit. [26])
Ins(3,4,6)P_3	Levels not detected/reported in literature.
Ins(1,3,4,5)P_4	trace-1 μM (lit. [26,27])
Ins(3,4,5,6)P_4	trace-1 μM (lit. [27–29])
Ins(1,4,5,6)P_4	0.5-1 μM (lit. [27,29])
Ins(1,3,4,6)P_4	trace- 0.2 μM (lit. [29])
Ins(1,3,4,5,6)P_5	2-120 μM (lit. [21,27,30])
$InsP_6$	10-100 μM (lit. [21,31–33])

Table 1: The approximate abundance of inositol phosphates in mammalian (and yeast) cells. The inositol phosphates that are relevant to later chapters are in bold: Ins(1,4,5,)P_3 (Chapters 5 and 6) and Ins(1,4,5,6)P_4 (Chapter 4).

Inositol phosphates are ubiquitous in a number of different kingdoms of organisms and participate in a large variety of cellular functions, including calcium signalling, gene expression, insulin signalling and stress response.[1–3,18] While some functions have been determined for individual inositol phosphate regioisomers, not every regioisomer has been assigned a biological role and further investigation into of these compounds is required.

Of the $InsP_3$ regioisomers, Ins(1,4,5)P_3 is the most thoroughly studied due to its role as a second messenger in calcium signalling (discussed further in Chapter 5).[7,18] The Ins(1,3,4)P_3 regioisomer has also been found to regulate the synthesis of other inositol phosphates through inhibiting Ins(3,4,5,6)P_4 1-kinase enzymes.[18]

A number of different biological roles have been identified for different regioisomers of $InsP_4$. The Ins(1,4,5,6)P_4 regioisomer has been recently discovered to activate the HDAC3-SMRT histone deacetylase complex (discussed further in Chapter 4), as well as possibly inhibiting phosphatidylinositol 3-kinase (PI3K) signalling *via* an unknown mechanism.[18] The Ins(3,4,5,6)P_4 regioisomer has been found to have a role in regulating the voltage-gated ClC-3 chloride channel found in the plasma membrane.[34] The Ins(1,3,4,5)P_4 regioisomer has been implicated in regulating phosphatidylinositol-3,4,5-trisphosphate signalling in neutrophils, as well as protecting Ins(1,4,5)P_3 from hydrolysis and regulating calcium signalling.[18,35,36]

The most abundant regioisomer of $InsP_5$, Ins(1,3,4,5,6)P_5, has not had a clear function identified beyond being a pool for inositol phosphate and pyrophosphate turnover.[18]

In addition to acting as a crucial precursor to the formation of inositol pyrophosphates, $InsP_6$ is thought to have an impact on several biological functions by interacting with a variety of proteins (including the activation of protein kinase C and inhibition of protein phosphatases) and may also play a role in mRNA transport.[18] $InsP_6$ has also been found to facilitate the virulence of *C. difficile* through allosteric activation of protease domains involved in intracellular auto-proteolysis, resulting in a growing interest in the development of $InsP_6$ analogues that could potentially interfere with this process.[37] There is also interest in developing crops that possess lower levels of $InsP_6$ (referred to in plants as phytate), as this inositol phosphate acts as an anti-nutrient that prevents the absorption of minerals as a result of chelation in non-ruminant animals that consume crops with high levels of phytate. It should be noted, however, that too great a reduction leads to the impaired biosynthesis of inositol pyrophosphates naturally derived from $InsP_6$.[19]

1.2 Inositol pyrophosphates

1.2.1 Interconversion and abundance of inositol pyrophosphates

Inositol pyrophosphates were first discovered in 1992 and 1993 independently through research carried out on the *Dictyostelium discoideum* slime mould (although the inositol pyrophosphates initially isolated were later established to be unusual regioisomers, discussed further in Chapter 3)[10,38] and mammalian cells[39]. Although it has been almost thirty years since their discovery, many of the exact functions of inositol pyrophosphates are not well understood and are currently still under investigation.

Not long after their initial discovery, it was found that the generation and turnover of inositol pyrophosphates in cells occurs quite quickly. In mammalian cells, the stores of inositol phosphate precursors, $InsP_6$ and $InsP_5$, were found to be converted to inositol pyrophosphates by approximately 50% and 20% respectively every hour (Figure 8).[39] The inositol pyrophosphates themselves were found to have even higher turnover rates, with the pool of $InsP_7$ being found to turn over ten times in only 40 minutes in mammalian hepatocytes.[40]

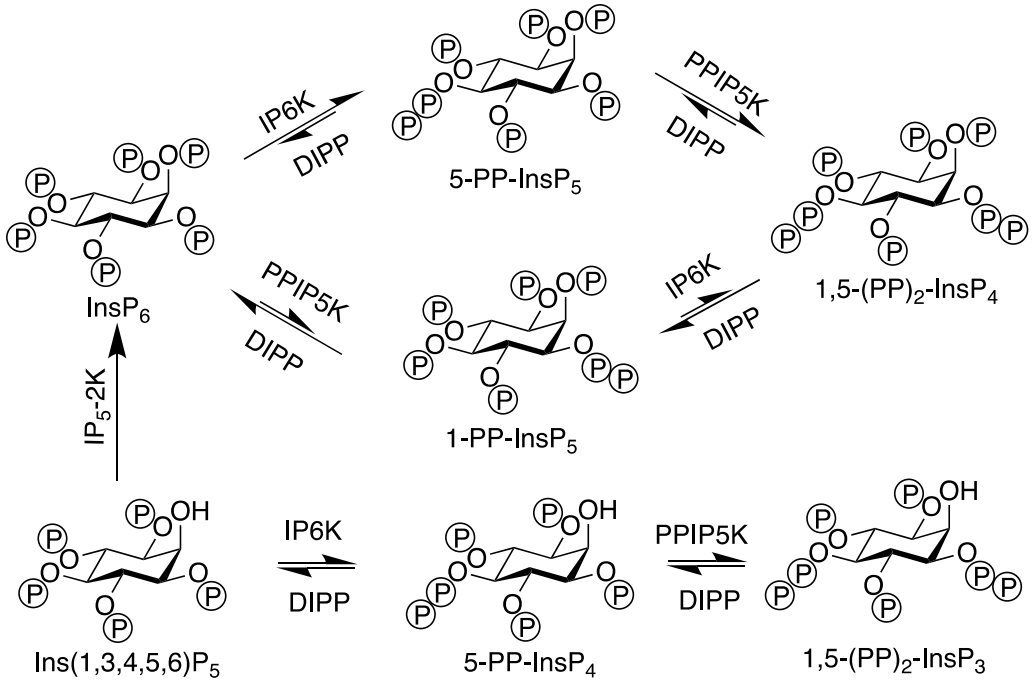

Figure 8: Some of the possible interconversions of inositol pyrophosphates in humans.[9,33,41]

$InsP_6$ kinases (IP6Ks, kcs1 in *Saccharomyces cerevisiae*) attach the γ-phosphate from a molecule of ATP to the 5-position phosphate of $InsP_6$ and 1-PP-$InsP_5$ to generate 5-PP-$InsP_5$ and 1,5-$(PP)_2$-$InsP_4$ respectively. There have been three subtypes of IP6K found in humans.[42,43]

A structurally unrelated group of kinases, PP-$InsP_5$ kinases (PPIP5Ks, Vip1 in *Saccharomyces cerevisiae*), was found to be responsible for creating the pyrophosphate in the 1-position of inositol phosphate of both $InsP_6$ and 5-PP-$InsP_5$ to generate 1-PP-$InsP_5$ and 1,5-$(PP)_2$-$InsP_4$ respectively.[44–47] Two mammalian PPIP5Ks have been identified.[48]

Although there are two possible routes for the biosynthesis of 1,5-$(PP)_2$-$InsP_4$, the main route proceeds from $InsP_6$ through 5-PP-$InsP_5$. IP6Ks phosphorylate both $InsP_6$ and 1-PP-$InsP_5$ but exhibit a preference for $InsP_6$ as a substrate. PPIP5Ks have also been found to preferentially phosphorylate 5-PP-$InsP_5$ over $InsP_6$.[44–47,49] While 1,5-$(PP)_2$-$InsP_4$ is predominantly generated via 5-PP-$InsP_5$, the fact that it is also synthesised via 1-PP-$InsP_5$ in a secondary, unfavoured route renders the concentration of 1,5-$(PP)_2$-$InsP_4$ not dependent solely on the concentration of 5-PP-$InsP_5$.[49]

The formation of pyrophosphate groups has been found to be reversible through the action of diphosphoinositol polyphosphate phosphohydrolases (DIPPs), a group of promiscuous phosphatases.[50–52] There are five isoforms of DIPP that have been identified in humans.[48]

In addition to the substrate preferences of the kinases supporting 5-PP-$InsP_5$ as the main intermediate in the generation of 1,5-$(PP)_2$-$InsP_4$, the DIPP hydrolases that are responsible for removing the β-phosphate from a pyrophosphate moiety favour removal of the 5-position pyrophosphate group of 1,5-$(PP)_2$-$InsP_4$ to generate 1-PP-$InsP_5$.[53] DIPPs have also been found to cleave preferentially the pyrophosphates of 1-PP-$InsP_5$ over its regioisomer, 5-PP-$InsP_5$.[53,54] Further evidence of this substrate regioisomer preference was provided by Wu *et al*. when the hydrolysis-resistant analogue of the 1-PP-$InsP_5$ was shown to bind to the hDIPP1 phosphatase with higher potency than the 5-position regioisomer.[55] A further study on the action of the yeast analogue phosphatase, *Sc*DDP1, is described in Chapter 2.

Although not normally detected within cells, the inositol pyrophosphates 5-PP-$InsP_4$ and 1,5-$(PP)_2$-$InsP_3$ are generated in quantifiable amounts when the formation of $InsP_6$ is prevented through deletion of a kinase.[56] Both IP6Ks and PPIP5Ks are able to treat Ins(1,3,4,5,6)P_5 as a substrate and form a pyrophosphate group in the 5- and 1-position respectively.[30,57]

The absolute cellular levels of inositol pyrophosphates are difficult to determine as there are technical limitations to the current methods available for isolation and quantification,[41] although there has been progress in the development of several methods. Quantitative HPLC methods that do not rely on radiolabelling, but instead monitor light absorbance of the sample in the presence of ferric nitrate, have been developed,[58–60] as well as a method utilizing capillary electrophoresis coupled to electrospray ionization mass spectrometry.[21]

It must also be noted that the concentrations of inositol phosphates and pyrophosphates vary quite significantly depending on tissue type and organism.[33] The levels of inositol pyrophosphates within a single cell can also fluctuate significantly during stress responses, at different stages in the cell cycle and depending on organism age.[41] Despite these difficulties in measuring their quantities, approximate concentration ranges of inositol phosphates have been reported in various studies (Table 2).

Inositol phosphates/pyrophosphates	Approximate abundance
$InsP_6$	10-100 μM (lit. [21,31–33])
$Ins(1,3,4,5,6)P_5$	2-120 μM (lit. [21,27,30])
5-PP-$InsP_4$	Very low levels (not successfully isolated from wild type cells)[30,61]
$1,5\text{-}(PP)_2\text{-}InsP_3$	Very low levels (not successfully isolated from wild type cells)[30]
1-PP-$InsP_5$	0.1-0.2 μM (lit. [31,32,53])*
5-PP-$InsP_5$	0.5-5 μM (lit.[9,21,31–33,61])
$1,5\text{-}(PP)_2\text{-}InsP_4$	<0.05-1 μM (lit.[31,33])

Table 2: The approximate abundance of inositol pyrophosphates and their immediate inositol phosphate precursors in most eukaryotes (with the exception of some organisms such as slime moulds). The inositol pyrophosphates that are relevant to later chapters are in bold: 5-PP-$InsP_4$ and 5-PP-$InsP_5$ (Chapter 2) and $1,5\text{-}(PP)_2\text{-}InsP_4$ (Chapter 3).*A recent study reported that 1-PP-$InsP_5$ can be the major regioisomer in plant seedlings.[21]

As in the case of quantifying inositol phosphates, the actual intracellular levels of inositol pyrophosphates may be higher than initially reported due to the difficulties associated in measuring these compounds, including the fact that many of the methods could not account for inositol pyrophosphates originally derived from glucose-6-phosphate.[21] Even if the intracellular concentrations of inositol pyrophosphates are low, local concentrations may also be higher due to possible compartmentalisation of these compounds in organelles.[31]

1.2.2 Biological function of inositol pyrophosphates

Due to the high turnover rates of inositol pyrophosphates, before any definite biological roles were established, it was believed that these compounds could behave as molecular switches.[56] Many experiments have since been carried out to investigate the action of inositol pyrophosphates, usually by preventing their formation through the genetic attenuation of pyrophosphate-forming kinases, and from these experiments inositol pyrophosphates have been implicated in many biological roles including cell growth, insulin signalling, phosphate homeostasis, glycolysis regulation, intracellular trafficking, telomere maintenance, immune response, environmental stress response, tumour cell motility and ribosome biogenesis.[9,30,56,62–66] These and other biological roles have been reviewed by Thota and Bhandari, Wilson *et al.*,

Chakraborty, Shah *et al*. and Wundenberg and Mayr.[8,32,33,41,48] However, due to the broad nature of knockout and knockdown genetic experiments, it has been challenging to assign roles to specific inositol pyrophosphates and determine their mechanism of action.

There are several mechanisms by which inositol pyrophosphates are thought to participate in cellular functions (lit. [32,48]):

Protein binding

There is a growing list of biological roles in which inositol pyrophosphates seem to act as ligands for the binding sites of enzymes or receptors. Many of the proteins identified to bind inositol pyrophosphates possess a pleckstrin homology (PH) domain that the inositol pyrophosphates compete with phosphatidylinositol 3,4,5-phosphate [PtdIns(3,4,5)P_3] to occupy. A wide array of PH-domain-containing proteins has been confirmed to interact with inositol pyrophosphates including: mammalian Akt,[55,67–70] GRP1 (general receptor for phosphoinositides 1),[67] PIKE (nuclear phosphatidylinositol 3-kinase enhancer),[70] Tiam (T-lymphoma invasion and metastasis protein)[70] and SIN1 (stress-activated protein kinase-interaction protein 1)[67] as well as *Dictyostelium* Crac (cytosolic regulator of adenylyl cyclase)[70]. There have also been a number of non-PH-domain-containing proteins found to bind to inositol pyrophosphates including the yeast cyclin-CDK-CDK-inhibitor complex,[71] CK2 protein[72] and a number of proteins with SPX domains (named for some of the proteins that feature this binding domain: SYG1/Pho81/XPR1).[73]

In some biological assays, different regioisomers of inositol pyrophosphates have also been found to bind preferentially to their protein targets, making clear the stereospecificity requirements.[67,71] Due to the difficulties in procuring specific inositol pyrophosphates until relatively recently, it has also been suggested that some proteins that have been assumed to bind to $InsP_6$ may in fact physiologically bind preferentially to an inositol pyrophosphate, although this claim remains to be investigated.[70]

Protein pyrophosphorylation

Inositol pyrophosphates have demonstrated the unique ability *in vitro* to transfer their β-phosphate onto pre-phosphorylated serine residues to form pyrophosphate groups on proteins.[41,74,75] This process requires the presence of divalent cations but is not dependent on enzymes.[75] Further calculations have also indicated that β-phosphate transfer is more thermodynamically favourable for inositol pyrophosphates than for inorganic pyrophosphate or even ATP and ADP.[11]

The biological purpose of pyrophosphorylation is not yet fully understood, although it is presumed to play a similar role to mono-phosphorylation of proteins, which is known to cause changes to protein conformation, catalytic activity, localisation and protein-protein interactions.[74] Due to the pyrophosphorylated protein product being resistant to many phosphatases, pyrophosphorylation is thought to be a more stable modification than simple phosphorylation, despite pyrophosphates being inherently less stable structures than monophosphates.[8,74] Although comparatively robust, pyrophosphorylation is still thought possibly to be a reversible process involved in signalling pathways, as prolonged incubation with alkaline phosphatases have been found to cleave the β-phosphate groups.[76] Due to the ubiquitous expression of $InsP_7$, but the lack of conservation of binding targets across kingdoms, it has been suggested that pyrophosphorylation could be the primary mechanism by which inositol pyrophosphates impact cellular biology.[8]

To date, several proteins have been identified as probable targets for inositol pyrophosphate-mediated pyrophosphorylation including the yeast Nsr1 and Srp40 proteins,[74,75] the RNA Pol I enzyme,[77] the IRF3 transcription factor[63] and the AP3β1 protein complex subunit[78].

Pyrophosphorylation can be theoretically achieved with any inositol pyrophosphate regioisomer, but the possibility of regioselectivity for a specific phosphoserine acceptor protein cannot be eliminated until this process is better understood.[32,74] There has only been one reported instance of pyrophosphorylation being carried out preferentially by an individual inositol pyrophosphate, and that is the transcription factor IRF3, which seems to be pyrophosphorylated by 1-PP-$InsP_5$ (not 5-PP-$InsP_5$ or a non-hydrolysable analogue of 1-PP-$InsP_5$).[41,63]

In addition to protein binding and pyrophosphorylation, inositol pyrophosphates are also thought to impact protein-protein interactions as well as regulate the amounts of inorganic polyphosphate (polyP) within cells.[48]

The interest in inositol pyrophosphates and their roles in signalling has been growing and their binding sites may prove to be useful drug targets.[1] As a result of the increase in interest, new methods, both chemical and biological, by which pyrophosphates can be generated are being developed.

1.3 Carbohydrate chemistry

Carbohydrates are a widespread group of naturally occurring compounds with the general formula of $C_x(H_2O)_y$. The relevant subgroup of carbohydrates relevant to this work are hexoses (with a general formula of $C_6H_{12}O_6$), which can exist as single monosaccharide units or be chained into disaccharides, oligosaccharides or polysaccharides. Monosaccharides exist as pairs of enantiomers that are denoted D- and L- (named after Latin *dexter* and *laevus*, right and left) in accordance with their relative configurations to the enantiomers of glyceraldehyde that rotate polarized light right or left.

Carbohydrates, specifically both D- and L-isomers of glucose, are substrates of interest for mimicking *myo*-inositol-based compounds due to their structural similarities (Figure 9). As described in later chapters, D- and L-glucose were used as the starting material for the generation of Ins(1,4,5,6)P_4 and Ins(1,4,5)P_3 analogues (discussed further in Chapters 4 and 5 respectively).

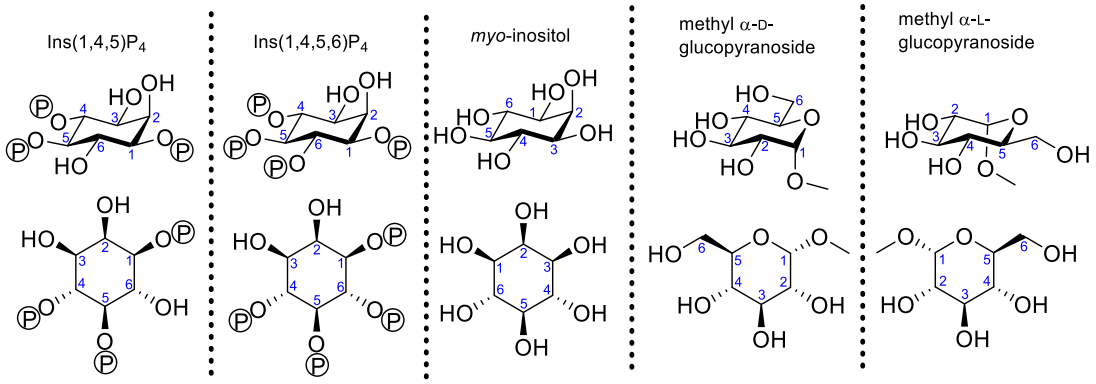

Figure 9: Structures from left to right of Ins(1,4,5)P_3, Ins(1,4,5,6)P_4, *myo*-inositol, methyl α-D-glucopyranoside and methyl α-L-glucopyranoside with numbering. Note that the numbering of *myo*-inositol, symmetrical derivatives and L-enantiomers of asymmetrical derivatives is clockwise, but D-enantiomers of asymmetrical derivatives is anticlockwise as viewed from above the axial 2-OH position.

There are several advantages to using carbohydrate-based mimics of lower inositol phosphates. In addition to the similarities in the stereochemistry of some of the hydroxyl groups between glucose and *myo*-inositol, there are some slight structural differences which could be beneficial in generating analogues of inositol phosphates that can aid in probing structural requirements for their binding sites. The fact that both enantiomers of glucose are readily available commercially (and cheap in the case of D-glucose) allows for both to be used as convenient chiral starting materials, thereby eliminating the need for the often laborious optical resolution typically required in inositol chemistry.

There are several limitations on using carbohydrate structures to mimic inositol phosphates as well, however. Firstly, the 6-position hydroxymethyl group of glucose

extends one of the hydroxyl groups of the structure further from the central ring, which is a structural difference to inositol that may prevent glucose-based mimics from being sufficiently close structural analogues to inositol phosphates.

Another limitation on the use of carbohydrates is the need to attach a group (such as a methyl group) to the anomeric hydroxyl to fix the product as a single stereoisomer and prevent anomerisation. If a group is attached to this position, however, the 1-position of the carbohydrate can no longer mimic the hydroxyl of an inositol derivative and instead serves as a source of steric bulk that may otherwise interfere with the potential ligand binding of a carbohydrate-based inositol polyphosphate analogue. While it is possible to affix a phosphate group to the hydroxyl connected to the anomeric centre (see Chapter 5 for more details), the stability of these phosphate groups, especially when protected, can restrict the possible subsequent reactions following phosphorylation.

As an additional consequence of the carbohydrate structure containing a pyranosyl ring oxygen, the central ring structure is distorted from the perfect cyclohexane chair observed in inositol (particularly when the 1-position substituent is axial: refer to the anomeric effect, section 1.3.1).

Finally, due to the inclusion of the pyranosyl ring oxygen, a phosphate group cannot be hosted at every position around the 6-membered glucose ring, thereby rendering it less suitable to mimic higher inositol phosphates.

Although there are complications associated with attaching robust functional groups to the anomeric 1-position of monosaccharides, this position can be regioselectively modified more easily as a result of its chemically distinct environment due to the proximity of the pyranosyl ring oxygen. The neighbouring pyranosyl ring oxygen may influence the orientation in which substituents are attached to the 1-position of the carbohydrate because of the anomeric effect.

1.3.1 Anomeric effect

The anomeric effect can be observed through polar substituents attached to the 1-position in sugars adopting an axial orientation preferentially, as opposed to equatorial.[79] This contradicts the usual pattern of substituents around a cyclohexane ring favouring equatorial orientations to minimise steric clashes.[80]

The anomeric effect is thought to arise from a combination of hyperconjugation, electrostatic/steric interactions or exchange effects, with contributions depending on the structure of the compound in question, particularly the substituent attached to the anomeric hydroxyl, and the surrounding medium. Although there are some

studies that support electrostatic interactions (dipole repulsion) or exchange effects, hyperconjugation is usually considered to dominate.[81]

The hyperconjugation explanation for the anomeric effect involves the selective stabilisation of the axially oriented anomer of a compound as a result of orbital mixing: the antibonding C-X 1-position orbital (LUMO, with X being the substituent attached to the 1-position hydroxyl) mixing with the parallel lone pair orbital on the pyranosyl ring oxygen (HOMO). This orbital mixing, which is only possible when the substituent attached to the 1-position carbon is in the axial orientation to maximise orbital overlap, results in electron delocalisation that stabilises the compound (Figure 10).

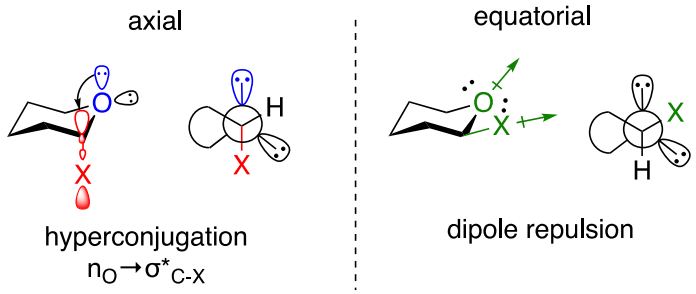

Figure 10: On the left is the hyperconjugation explanation for the anomeric effect. The $n_O \rightarrow \sigma^*_{C\text{-}X}$ orbital mixing stabilises the axially oriented α-anomer. These orbitals are only allowed to mix when they are antiperiplanar to each other, as depicted in the Newman projection when the 1-position substituent is axial. On the right is the dipole repulsion explanation for the anomeric effect that suggests the equatorial β-anomer is disfavoured due to electrostatic interactions. A Newman projection of the β-anomer is also shown to demonstrate that the orbitals cannot substantially mix in this orientation to result in the hyperconjugation observed in the α-anomer.[81]

As a result of the anomeric effect, the carbohydrate ring structure, particularly that of the α-anomer, is further distorted from the regular structure of cyclohexane. The bond between the pyranosyl ring oxygen and the 1-position carbon is shortened, while the bond between the 1-position carbon and the axial substituent attached to this position is lengthened. The difference in bond lengths can be rationalised by orbital mixing and thus this observed trend serves as evidence for hyperconjugation.[81] In part as a consequence of this distortion, however, the carbohydrate ring is not equally proportioned and renders glucose a slightly less close structural analogue of inositol.

1.4 Inositol chemistry

By using *myo*-inositol as a starting material, endogenous inositol phosphates and pyrophosphates can be synthesised as well as potentially more closely related structural mimics. This is especially pertinent for higher inositol phosphates and

inositol pyrophosphates that require each position around the ring to have a phosphate group attached.

Although there are some similarities between using carbohydrates and inositol in syntheses, such as the highly polar, hydrophilic nature of the hydroxyl group-rich starting materials, using inositol is more challenging due to the lack of distinct chemical environments around the ring. Although carbohydrate compounds are rich in hydroxyls, inositol contains a slightly greater number making it a more hydrophilic structure (rendering purification via silica column chromatography slightly more challenging, especially when hydrophilic moieties such as MSE-protected phosphates are attached). This also results in slightly more difficult initial steps in the earlier stages of synthetic routes, as it can be more challenging to find appropriate solvents. Due to the similar chemical environments of the hydroxyls around *myo*-inositol (only one axial hydroxyl), longer synthetic routes are required to position necessary protecting groups correctly prior to phosphorylation in the syntheses of inositol phosphates.

In addition to the increased difficulty of protecting group manipulation, inositol phosphate products which are not symmetrical would be synthesised as a racemic product requiring chiral resolution for any biological applications. Chiral resolution can be introduced as a step in a synthetic route to separate the chemically indistinguishable enantiomers by means of generating separable diastereomers. This can be achieved through reacting exposed hydroxyls with chiral auxiliary agents such as (1*S*)-(-)-camphanic chloride or (*S*)-O-Acetylmandeloyl chloride to generate diastereomer esters or, depending on the intended final product, desymmetrisation can occur through phosphorylation with a C_2-symmetric phosphoramidite.[82] However, chiral resolutions are often time-consuming, reduce yields and may not always be successful.

1.5 Phosphate chemistry

Phosphate groups can be attached to hydroxyls through either direct addition of a protected phosphate moiety using a P(V) reagent or in a two-step procedure that comprises first attaching a protected P(III) phosphite moiety that is subsequently oxidised to form a protected phosphate.

Traditionally, the one-step P(V) phosphorylation method that attaches a protected phosphate to the target compound was favoured. Direct P(V) phosphorylation can be achieved with reagents including chlorophosphates and phosphoroimidazolates.[83,84] One of the main advantages of using P(V) methods is the higher relative stability of the necessary reagents, although the yields are often lower than in the later developed P(III) reagent methods.[85]

There are a variety of P(III) phosphitylation agents including phosphites, chlorophosphites and phosphoramidites.[86,87] As well as offering higher yields, P(III) methods allow for the synthesis of more sterically-congested polyphosphate products due to the lower steric demands of phosphites over phosphates. Indeed, one of the main disadvantages of P(V) methodologies is the difficulty in attaching phosphates to vicinal hydroxyl groups due to steric clash following the first phosphorylation and also competing cyclisation side reactions that occur through attack by the neighbouring, exposed hydroxyl group.[2,88]

Phosphoramidites are the main type of P(III) phosphitylating agents currently used, and this is due to their stable nature and the diversity of commercially-available reagents which are able to introduce protecting groups that can be used orthogonally to each other (Figure 11).[87]

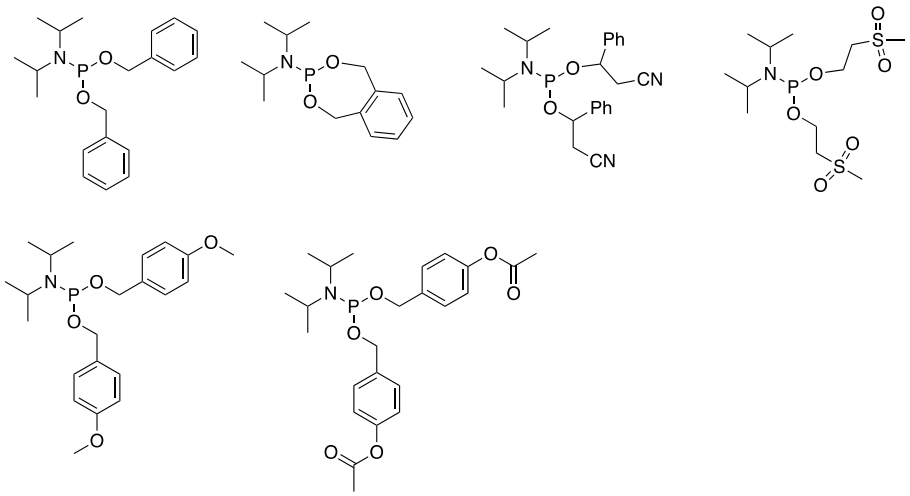

Figure 11: Examples of phosphoramidite phosphitylating agents including: (top row left to right) benzyl phosphitylaing agent, XEPA phosphitylating agent,[37] cyano-containing phosphitylating agent,[89,90] methylsulfonylethyl phosphitylating agent,[91] (bottom row left to right) PMB phosphitylating agent[92] and acyloxybenzyl phosphitylating agent.[93]

Before phosphoramidites can attach the protected phosphite moiety to a given starting material, they must first be activated by an acid. The activators most commonly used are weak nitrogenous acids such as tetrazole or 5-phenyl-1*H*-tetrazole, which react with phosphoramidites to displace the stable diisopropylidene group to yield a tetrazolide species as the active phosphitylating agent (Figure 12).[87,94]

Although the tetrazole reagent acts as a catalyst in phosphitylations, it is required in stoichiometric quantities due to the diisopropylamine side product generated, which increases the pH of the reaction, possibly deprotonating the remaining tetrazole and rendering a smaller quantity of the catalyst active.[87] The tetrazole catalyst can be salvaged through the addition of isocyanate scavengers, although these are usually omitted in favour of adding excess tetrazole.[87]

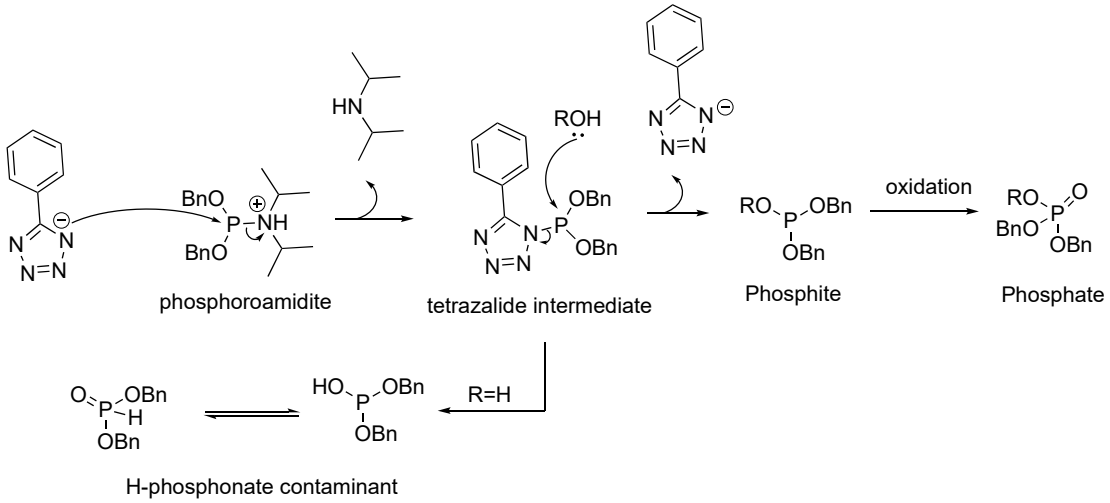

Figure 12: Mechanism for phosphitylation. Formation of the H-phosphonate contaminant that arises from water in the reaction has also been depicted.

Following successful phosphitylation, the P(III) phosphite signals can be observed in the ^{31}PNMR spectra in approximately the 130-150 ppm region. In the second step, the phosphite groups are oxidized to protected phosphates by an oxidizing agent, most commonly *m*CPBA. The P(V) phosphate signals of the oxidized product can be observed in the ^{31}PNMR spectra in the region of 0 ppm.

The most commonly observed protecting group for phosphates is benzyl, which can be cleaved in a final hydrogenation reaction usually catalyzed by a palladium catalyst. Palladium hydroxide on carbon, Pearlman's catalyst, is one of the two most common palladium catalysts used in hydrogenations, the other being palladium on carbon.[95] Palladium hydroxide on carbon was thought to be a better choice of catalyst to use in hydrogenations throughout this study, as it is not as pyrophoric.[96]

Following deprotection, phosphates exist as free acids unless the hydrogenation step was carried out in the presence of source of counterions (a base such as sodium bicarbonate or triethylammonium bicarbonate) or the product was later exposed to them.

1.6 Pyrophosphate chemistry

Inositol pyrophosphates have some of the highest electron densities of all organic compounds, with multiple, densely packed, negatively charged phosphate groups. This can be observed in electron density maps of the 1,5-$(PP)_2$-$InsP_4$ structure in the literature.[11,97] Due to the sterically bulky, highly polar nature of inositol phosphates, their synthesis proves to be quite challenging. Their protected precursors are especially difficult to handle as they are inherently unstable and prone to hydrolysis and cyclisation mid-synthesis.

1.6.1 Chemical synthesis methods

Pyrophosphate chemistry was initially developed in order to synthesise nucleotides and their derivatives. The first chemical methods developed to synthesise pyrophosphates employed P(V) phosphate donors such as phosphoromorpholidate, phosphoimidazolidate or phosphoimidazolide derivatives to react with acceptor monophosphate moieties.[84,92,98–100] Most of these P(V)-P(V) reactions suffered from side reactions, product instability, long reaction times and low-to-moderate yields, although these methods have been found to be very useful to generate pyrophosphate groups that are not a terminal substituent on the target compound.[84,98]

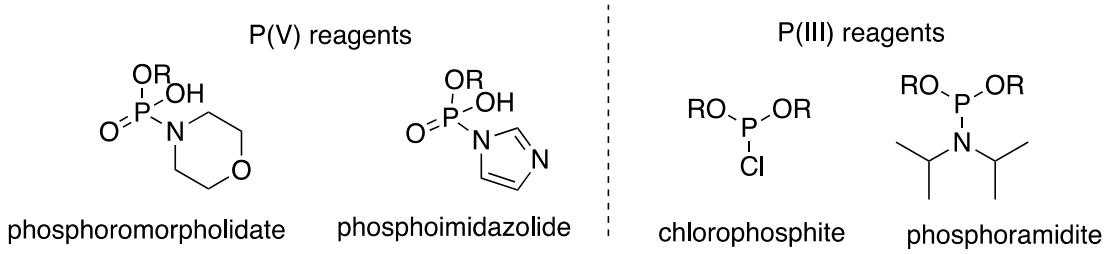

Figure 13: P(V) Phosphorylating agents that have been used to phosphorylate phosphate groups to generate protected pyrophosphates (left).[84,92,98–100] P(III) donor reagents that have been used to generate P(III)-P(V) intermediates through the phosphitylation of phosphates before the mixed anhydride species are oxidised to protected pyrophosphate group (right).[89,93,101]

Alternative methods were developed to form pyrophosphate groups through the generation of P(III)-P(V) mixed anhydrides or P(III)-P(III) precursors that subsequently undergo oxidation to form the terminally protected pyrophosphate groups.[100,102] The most commonly used method of synthesising pyrophosphate groups in inositol pyrophosphates is through the generation of a mixed P(III)-P(V) anhydride species.[89,93,101]

Methods that generate P(III)-P(V) intermediates initially used a number of different P(III) donor reagents such as chlorophosphites, until phosphoramidates became the predominant reagent (Figure 13).[86,102] Highly reactive phosphoramidites were found to provide the highest yields but require the application of protecting group chemistry to ensure no off-target phosphitylation occurs.[102] P(III)-P(V) methods have also recently been employed in nucleotide synthesis, and although the starting materials for the coupling are more challenging to generate, the pyrophosphate product yield was reported to be higher than in some of the traditional P(V)-P(V) routes.[99,103]

In order to synthesise pyrophosphate groups selectively at specific positions on substrates that contain multiple other phosphate groups, the α-phosphate precursor(s) must be protected by orthogonal protecting groups to those attached to the remaining phosphates. This allows for the selective deprotection of specific phosphate groups, rendering only certain exposed positions viable for further phosphorylation.

Benzyl groups are one of the most commonly used protecting groups for phosphates and, as a result, in most cases the protecting groups attached to the α-phosphate precursor(s) must be completely cleaved under conditions in which benzyl groups are stable. The most common orthogonal protecting strategy appears to be the use of protecting groups such as cyanoethyl that can be removed through base-driven β-elimination (Figure 14).

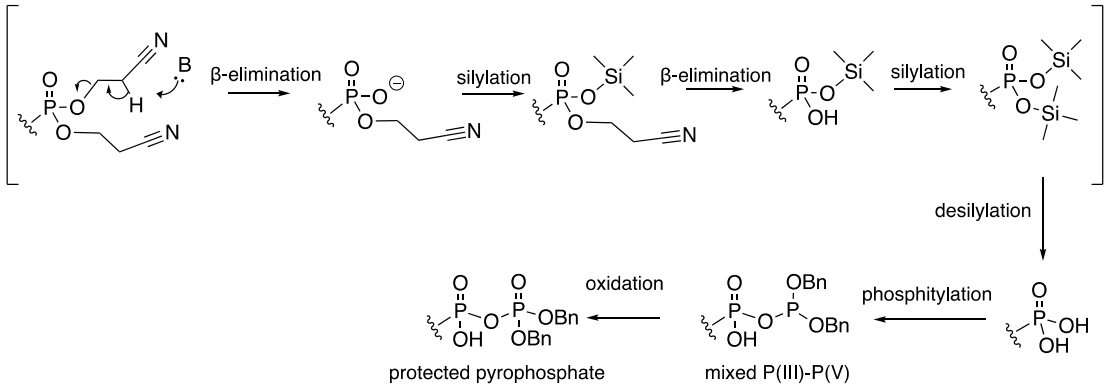

Figure 14: Example synthesis of a pyrophosphate through a P(III) stepwise route. The starting material features a phosphate protected with cyanoethyl groups (an example of a protecting group removed through β-elimination) as employed in the route reported in Wang *et al*.[47] The silylation and β-elimination steps would occur in a single reaction to result ultimately in the persilylated phosphate precursor. Following desilylation, phosphorylation with a benzyl-protected P(III) agent such as a phosphoramidite would then result in the formation of a benzyl-protected P(III)-P(V) mixed anhydride, which could subsequently be oxidised to the protected pyrophosphate.

To ensure that both protecting groups are removed from the α-phosphate precursor(s), the basic protecting group cleavage is carried out with a simultaneous

silylation that temporarily masks the negative charge exposed through deprotection of the first protecting group, thereby allowing the base-driven β-elimination of the remaining second protecting group.[86,89]

Following deprotection of silyl groups, the exposed phosphate(s) can be phosphitylated (usually by means of an activated phosphoramidite) to generate the P(III)-P(V) mixed anhydride(s). Oxidation of the β-phosphite(s) results in the formation of the protected pyrophosphate(s). At this stage, the pyrophosphate moiety is less stable than in its final salt form, as the protected β-phosphate is a better leaving group for cyclisation or hydrolysis reactions than the negatively charged terminal phosphate in the debenzylated product. Pyrophosphates become more stable when deprotected as the negative charges of the exposed phosphates repel nucleophilic attack at either phosphate centre.[93]

The final deprotection step in the syntheses of inositol pyrophosphates is hydrogenation due to the prevalence of benzyl groups being used to protect phosphates. This step is usually carried out in the presence of a base (such as sodium bicarbonate or triethylammonium bicarbonate) to provide counterions for the phosphate groups, thereby preventing them from remaining as free acids in solution and improving the stability of the final product.[74,104–107]

Pyrophosphates become less susceptible to hydrolysis with the inclusion of counterions, as seen by a subsequent decrease in hydrolysis free energy upon formation of a salt form.[108] Different counterions for the phosphate groups in a deprotected pyrophosphate product are believed to have an impact on the overall energy of the compound, although further analysis is required to determine the degree to which they affect pyrophosphate stability.[11] Trialkylammonium counterions such as triethylammonium have been previously noted as being preferred counterions for conferring stability to triphosphate-containing nucleosides as opposed to metal ions, which are better Lewis acids. The denser positive charge of metal counterions may render the central phosphate more electrophilic than in pyrophosphates with triethylammonium counterions.[84] The Potter group has always stored inositol pyrophosphates as triethylammonium salts, rather than the often used sodium salts, and has observed higher stability than expected (unpublished results).

1.6.2 MSE-phosphitylating agent

N,N-Diisopropylamino-bis-[2-(methylsulfonyl)ethyloxy] phosphine (**1**), the MSE-phosphitylating agent, is a relatively little-used phosphitylating agent that has been employed by the Potter lab previously to synthesise pyrophosphate groups in inositol pyrophosphates.[91] It is also the phosphitylating agent that was used in this study to

synthesise inositol pyrophosphates, and one aim of this work was to investigate its wider utility through its inclusion in novel synthetic routes to generate highly sought-after, known inositol pyrophosphates (5-PP-InsP_5 and 5-PP-InsP_4: Chapter 2; 1,5-$(PP)_2$-InsP_4: Chapter 3) and novel inositol pyrophosphates (Chapter 6).

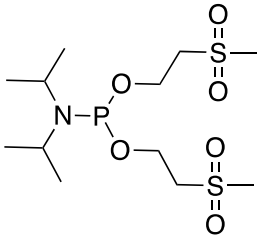

Figure 15: MSE-phosphitylating agent (*N,N*-diisopropylamino-bis-[2-(methylsulfonyl)ethyloxy] phosphine) (**1**) structure.

The MSE-phosphitylating agent (**1**) is used to form phosphate groups that can be selectively deprotected in the presence of benzyl-protected phosphates (allowing for the synthesis of pyrophosphates). As in the case of the previously employed β-cyanoethyl-protecting group,[89,101,107] the MSE-protecting group can be cleaved through β-elimination upon exposure to base (Figure 16). The proximity of the sulphone group to the neighbouring protons increases their acidity and facilitates their removal to initiate basic deprotection.

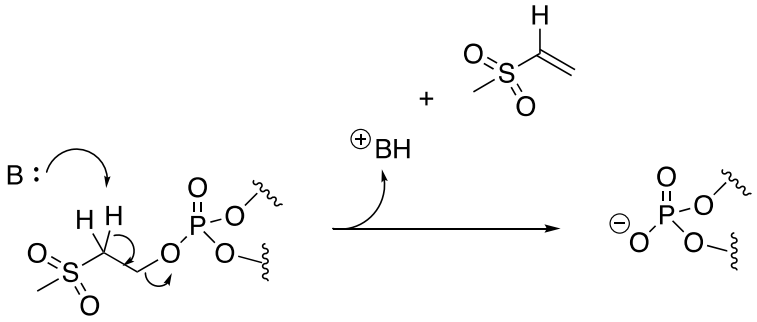

Figure 16: Basic cleavage of the MSE-protecting group from a phosphate. Elimination probably proceeds via a concerted mechanism.[109]

There are several advantages to using the MSE reagent (**1**) as the orthogonal protecting group to benzyl over other phosphorylating agents removed through β-elimination, including its resistance to hydrogenation and ability to withstand acidic conditions. The MSE P(III) agent (**1**) is also attractively a crystalline solid and therefore easier to purify, dry and store. Another advantage is that more of the phosphorylation by-products are water soluble and removed during the aqueous work-up.

There are some disadvantages to using the MSE phosphorylating agent (**1**), however, such as its highly hygroscopic nature. The phosphitylation reactions are also more difficult to monitor with ^{31}PNMR spectroscopy, as the signal for the activated

tetrazolide cannot be observed (which is suspected to be the result of its highly reactive nature). The introduction of the highly polar MSE group after phosphorylation can also lead to slightly more challenging purification of the phosphorylated products, which become more hygroscopic and tend to stick longer to silica chromatography columns. The phosphitylating agent is also not commercially available, although its synthesis is straightforward (refer to the Experimental).

1.6.3 Pyrophosphate Mimics

Pyrophosphates are negatively charged at physiological pH and are thus difficult to replace with neutral functional group mimics that could render analogues slightly less hydrophilic while maintaining biological activity.[110] A small number of functional groups have been identified and used as a substitute for the less chemically and biologically stable pyrophosphate moiety to further probe the biological functions of pyrophosphate-containing endogenous compounds (Figure 17).

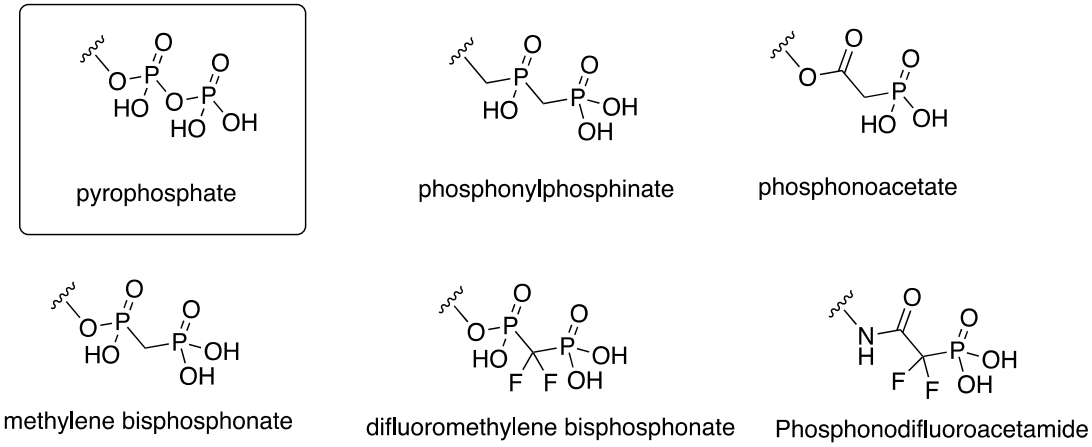

Figure 17: Structures of a pyrophosphate group and structural mimics used to generate more stable analogues including: phosphonylphosphinate,[111] phosphonoacetate,[112,113] methylene bisphosphonate,[55,106] difluoromethylene bisphosphonate and phosphonodifluoroacetamide groups.[114]

By replacing pyrophosphate groups with similar moieties which have the β-phosphate equivalent bound to a carbon atom rather than an oxygen, analogue mimics are rendered stable to hydrolysis and isomerization and also become resistant to DIPP-mediated decomposition. These non-hydrolysable pyrophosphate analogues are very useful tools in determining the mechanism by which inositol pyrophosphates interact with specific proteins. However, these pyrophosphate mimics possess differences in

electron distribution, bond angles, bond length and pK_as that could result in lower potency at inositol pyrophosphate binding sites.[114,115]

Non-hydrolysable analogues may be tolerated in inositol pyrophosphate binding sites, but pyrophosphorylation would not be possible as the terminal β-phosphate equivalent would not be able to detach and transfer to a protein subtrate.[55,113] However, the use of stable pyrophosphate mimics allows for other biological analyses to take place, through structural modifications that can introduce fluorophores and resin-immobilised groups to the analogues.[113]

The phosphonoacetate (PA) moiety was the first group to be used as a non-hydrolysable replacement for inositol pyrophosphates and has the advantage of being relatively easy to synthesise.[112,113] However, the lack of an α-phosphate equivalent reduces the capacity of the phosphonoacetate to accommodate negative charge, and the planar carbonyl group extending the terminal phosphate further from the ring would be more rigid than a phosphate or simple hydrocarbon linkage. The inclusion of the carbonyl group also results in the PA-analogues being susceptible to chemical and enzyme-catalysed hydrolysis, unlike some of the other pyrophosphate analogues. Additionally, the greater differences in bond angle, bond length and pK_a can result in phosphonoacetates not performing as well as other mimics of pyrophosphates.[114,116]

The later-developed methylene bisphosphonate (PCP) analogues are now more commonly used as hydrolysis-resistant mimics of inositol pyrophosphates, as the PCP moiety preserves an α-phosphate equivalent group.[55,106] The methylene linkage of methylene bisphosphonate moieties is less inductively electron withdrawing than the bridging oxygen in pyrophosphates, which results in the pK_a of the pyrophosphate groups being larger.[114] Structurally similar phosphonylphosphinates have also been employed to mimic pyrophosphates, although these analogues are not as close a mimic of pyrophosphates.[111]

Another variant of methylene bisphosphonates is difluoromethylene bisphosphonates, although this moiety has not been used to generate mimics of inositol pyrophosphates yet due to the difficulty in synthesising the analogues.[42,106,114,115,117] The inclusion of the electronegative fluorine atoms in the methylene linkage of this moiety renders the phosphate groups incorporated in the structure more acidic. As well as resulting in closer pK_as to pyrophosphates, the fluorine atoms also make the methylene linkage of the phosphates a closer match sterically to the bridging oxygen of a pyrophosphate group.[114]

The electron-withdrawing effects of fluorine have also been incorporated into another group designed to mimic pyrophosphates, phosphonodifluoroacetamide. This derivative of the PA group has a more acidic terminal phosphate due to the proximity

of the fluorine atoms, although the structure had to be further modified by also replacing the ester linkage with an amide group to prevent excessive hydrolysis.[114]

1.6.4 Biological methods

In addition to the chemical methods outlined above, there are also biological methods by which inositol pyrophosphates can be synthesised. Traditionally these methods have been plagued by low yields and contamination with related biological products.[55] Recently progress have been made by the Fiedler group in employing kinases to generate natural inositol pyrophosphates on a relatively large scale.[118] Although biological synthesis has become extraordinarily efficient in synthesising naturally occurring regioisomers of inositol pyrophosphates, it is constrained by the substrates that the enzymes will tolerate and the subsequent products that they can form. Chemical syntheses have not lost their relevance as they enable the generation of both natural and unnatural inositol pyrophosphates, as well as structurally similar analogues that cannot made with kinases.

1.7 Strategies to overcome cell impermeability

Due to their highly charged nature, inositol phosphates and inositol pyrophosphates, as well as their similar structural mimics, are cell-impermeable. Although this puts some potential constraints on the usage of these compounds, there are a number of chemical and biological strategies that can either render compounds temporarily cell-permeable or circumvent the need to cross the hydrophobic cell membrane.[119]

To render these compounds temporarily cell-permeable through chemical means, the negative charges of the phosphate groups can be masked with protecting groups that can be cleaved by esterases within the cell cytoplasm or photolabile groups that can be cleaved following deliberate light exposure.

When acyl moieties which can be cleaved by enzymes (such as propionyloxymethyl, butyryloxymethyl and acetoxybenzyl)[90,120–124] are used to protect the phosphate groups, there is a delayed onset and gradual response of any ligands delivered to cells due to the necessity of protecting group cleavage.[90,119]

Protection of pyrophosphates with acyl groups has been found to be less straightforward than the protection of monophosphates, however, as the phosphoanhydride bond is prone to hydrolysis without the exposed negative charges of the phosphate moieties. Protection of only the β-phosphate with an enzyme-cleavable protecting group can render pyrophosphate-containing compounds

temporarily cell-permeable, but the α-phosphate must remain unmasked to deter nucleophilic cleavage of the phosphoanhydride bond.[93]

There are a number of photolabile groups that can be used to protect phosphates (with the protection referred to as 'caging' for photolabile groups), including: 2-nitrobenzyl derived groups (such as 1-(2-nitrophenyl)ethyl [NPE] and 4,5-dimethoxy-2-nitrobenzyl [DMNB])[120]; 3-dinitrophenyl and 3,5-dinitrophenyl (DNP);[120] α-benzoyl-3,5-dimethoxybenzyl[120] and [7-(diethylamino)coumarin-4-yl]methyl (DEACM).[123,124] As well as caging phosphates, some of these protecting groups have been used to cage hydroxyl groups.[122] However, as in the case of enzyme-cleavable acyl protecting groups, compounds with photolabile protecting groups also suffer delayed release of the active, deprotected form.[119]

There are also a number of experimental techniques to bypass the lipid bilayer and place charged or highly hydrophilic compounds into the cytoplasm of cells without any chemical modification of the compounds. These techniques include microinjection, patch-clamp, electroporation and rendering cells permeable with detergents such as saponin.[90,120] There are disadvantages to using these methods as well, including the possible loss of molecules and proteins that regulate cellular functions, damaging cell structure and decreasing longer term viability of cells.[90,120]

Another possible biological technique to avoid temporary chemical protection of the phosphate groups is to deliver the compounds with liposomes, as recently described by Li *et al*.[125]

1.8 Aims

This study has been carried out to address multiple aims, which can be grouped into two main categories: first, furthering the knowledge associated with the chemical synthesis of *myo*-inositol polyphosphates and related pyrophosphates; and secondly, to probe some of the emerging biological roles already identified for such inositol phosphates through the generation of specially tailored structural analogues.

The first aim of furthering the field of inositol pyrophosphate synthesis is addressed through the synthesis of the naturally occurring inositol pyrophosphates, 5-PP-InsP_5 and its analogue 5-PP-InsP_4 (Chapter 2), as well as 1,5-$(PP)_2$-InsP_4 (Chapter 3). The synthetic route to generate 5-PP-InsP_5 was designed such that the route could easily be diverged from midway to enable the synthesis of the structurally related 5-PP-InsP_4 product. The route to synthesise 1,5-$(PP)_2$-InsP_4 was developed to employ milder reaction conditions and more readily attainable reagents than the only other previously reported chemical route.[97] The purification of the 1,5-$(PP)_2$-InsP_4 product

was also investigated to determine if the desired product could be successfully isolated from contaminating $InsP_7$ side-product.[97] Both synthetic routes to generate these three, known inositol pyrophosphate products employed the little-used methylsulfonylethyl (MSE) group to protect orthogonally the phosphate groups that were precursors to the α-phosphates of the pyrophosphates from the benzyl groups used to protect the monophosphate precursors. Upon successful synthesis of the inositol pyrophosphate products, some aspects of their biological function were probed through a number of collaborations detailed in their respective chapters.

In addition to investigating some of the biological roles of the inositol pyrophosphates, a number of carbohydrate-based ligands were designed and synthesised to probe the biological functions of some of the lower inositol phosphates, namely inositol 1,4,5,6-tetrakisphosphate [$Ins(1,4,5,6)P_4$] and its involvement in gene expression through activation of the HDAC3-SMRT complex (Chapter 4), and inositol 1,4,5-trisphosphate [$Ins(1,4,5)P_3$] and its role in calcium signalling (Chapter 5).

Seven polyphosphate ligands derived from D- and L-glucose were designed and synthesised to expand the knowledge obtained from the initial investigation into the SAR of $Ins(1,4,5,6)P_4$ in the HDAC3-SMRT binding site (Chapter 4).[112] Glucose was used as a convenient chiral scaffold to generate chiral analogues of $Ins(1,4,5,6)P_4$ that probed the tolerance of the binding site to different changes to the structure of the endogenous ligand.

A further six D- and L-glucose-derived polyphosphates were generated with the intention of developing novel $InsP_3R$ agonists and ideally partial agonists or even antagonists (Chapter 5). Glucose was again used as a scaffold to mimic *myo*-inositol, as the usage of its D-enantiomer enabled the synthesis of two heavily truncated analogues of the InsP3R agonist, adenophostin A, while its L-enantiomer could be used to generate analogues of $Ins(1,4,5)P_3$ that were predicted to be potential partial agonists of the receptor. Two of the D-glucose derived trisphosphates designed for the InsP3R study were also found to bind to inositol phosphate kinases, thereby furthering the investigations into the binding requirements of these enzymes.

Finally, following the initial results of the carbohydrate-based analogues at the $Ins(1,4,5)P_3$ receptor that included the successful design of a low efficacy $InsP_3R$ partial agonist, a series of inositol pyrophosphate $Ins(1,4,5)P_3$ analogues were created to further the investigation into the development of potential partial agonists for this receptor: 4-PP-$Ins(1,5)P_2$ and two regioisomers of PP-InsP, 5-PP-Ins(4)P and 4-PP-Ins(5)P (Chapter 6). These inositol pyrophosphates were generated using the techniques developed and practised to make the natural inositol pyrophosphates described earlier in the study (Chapters 2 and 3), thereby combining the development of inositol pyrophosphate chemistry with the investigation into the biological roles of lower inositol phosphates.

(2) Inositol pyrophosphates: 5-PP-InsP$_5$ and 5-PP-InsP$_4$

2.1 Biological relevance of 5-PP-InsP$_5$ and 5-PP-InsP$_4$

The most abundant inositol pyrophosphate naturally occurring in yeast and mammals, usually by a reasonable margin, is 5-diphosphoinositol pentakisphosphate, 5-PP-InsP$_5$ (Figure 18), which reaches concentrations of around 0.5-5 µM.[9,31–33] Due to the high relative abundance of this InsP$_7$ regioisomer, it is often the inositol pyrophosphate initially suspected of being involved in biological functions. Additionally, a large variety of studies have confirmed biological roles specifically for the 5-PP-InsP$_5$ regioisomer.[9,126–131] 5-PP-InsP$_5$ is believed to participate in a great number of biological processes including apoptosis, cytokine signalling, nuclear dynamics, chemotaxis, kinase regulation, protein pyrophosphorylation and vacuole biogenesis, in addition to many other processes.[9,41,48,61,70,72,77,132]

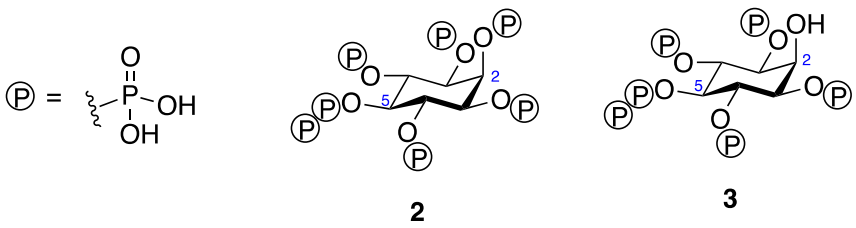

Figure 18: Structures of 5-PP-InsP$_5$ (**2**, left) and 5-PP-Ins(1,3,4,6)P$_4$ (from here on referred to as 5-PP-InsP$_4$ or **3**, right) with the 2-positions and 5-positions indicated.

From genetic knockout and knockdown experiments, it is thought that the 5-PP-InsP$_5$ regioisomer of InsP$_7$ could be involved in a number of different cellular processes, ultimately influencing metabolic homeostasis [although it should be noted that these studies are not able to isolate responses for the absence of 5-PP-InsP$_5$ compared with that of 1,5-(PP)$_2$-InsP$_4$].[127–130]

It has also been found that 5-PP-InsP$_5$ specifically inhibits the release of neurotransmitters from synaptic vesicles, while 1-PP-InsP$_5$ was not an effective inhibitor in comparison.[9,131]

This regioisomer has also been found to destabilise the Na^+/K^+-ATPase-α1 enzyme, thereby negatively regulating its activity. It was found that neither InsP$_6$ nor 1-PP-InsP$_5$ were able to fulfil this function and, although InsP$_8$ was not included in the study and may be able to destabilise the enzyme, the substantially lower physiological concentrations of this inositol pyrophosphate make its hypothetical contribution unlikely to be too significant.[126]

5-PP-InsP$_5$ has been found to compete for PH (pleckstrin homology) domains which have previously been known to bind to PtdIns(3,4,5)P$_3$.[70] PH domains feature in a large variety of proteins, including Crac (cytosolic regulator of adenylyl cyclase), Akt/PKB, PhdA, SIN1 and GRP1, resulting in the 5-PP-InsP$_5$ competition for ligand binding having an effect on a variety of biological functions (including insulin release, neutrophil superoxide production and phagocytosis).[9,34,69,133] These PH domain-containing proteins display some degree of specificity for 5-PP-InsP$_5$ over the other regioisomers of InsP$_7$.[67]

In addition to PH domains, it was recently discovered that 5-PP-InsP$_5$ is able to compete for SPX [named for three of the proteins in which this domain is present: Suppressor of Yeast gpa1 (SYG1); yeast Phosphatase 81 (Pho81); and human Xenotropic and Polytropic Retrovirus receptor 1 (XPR11)] domains that feature in some proteins associated with phosphate metabolism.[73,127,134–137] This includes playing a regulatory role in the synthesis of inorganic polyphosphate (polyP) and the inorganic phosphate efflux through binding to the VTC and TbPho91 proteins respectively.[73,134,136] It is also thought that 5-PP-InsP$_5$ plays an important role in regulating the interaction between the SPX-containing OsSPX4 and OsPHR2 transcription factors.[127,136] 5-PP-InsP$_5$ specifically has also been discovered to drive virulence of fungal disease through the stabilisation of the CDK inhibitor Pho81, which does not have a mammalian analogue and could prove to be a viable target for the future development of antifungals.[137]

As well as these discoveries of 5-PP-InsP$_5$ binding to different proteins, there are on-going efforts to investigate the intricacies of how this inositol pyrophosphate binds to, and is subsequently dephosphorylated by, Diphosphoinositol Polyphosphate Phosphohydrolase (DIPP) enzymes.[138,139] As mentioned in Chapter 1, DIPPs are responsible for regulating inositol pyrophosphate levels by cleaving the phosphoanhydride bond, thereby impacting cellular metabolism.[140] To further the understanding of inositol pyrophosphate binding to DIPPs, the 5-PP-InsP$_5$ synthesised in this study was used in a structural biology collaboration with the Beatriz González lab in Madrid. The results are discussed later in the chapter (Section 2.5).

The structurally related 5-PP-InsP$_4$ (Figure 18), is presumed to be present in extremely low levels intracellularly, although it has not yet been isolated from wild type cells.[30] It has been found to be possible to alter cells to produce measurable levels of 5-PP-InsP$_4$ through the deletion of IPK1, the kinase responsible for converting Ins(1,3,4,5,6)P$_5$ to InsP$_6$. The morphology of the mutant yeast cells with this deletion was found to appear identical to their wild-type counterparts, leading to the assumption that the 5-PP-InsP$_4$ and 1,5-(PP)$_2$-Ins(3,4,6)P$_3$ detected in the mutant cells were able to satisfy any signalling roles of 5-PP-InsP$_5$ and 1,5-(PP)$_2$-InsP$_4$ respectively.[56] Further studies have found that, while 5-PP-InsP$_4$ is able to alleviate some of the defects observed in *kcs1*Δ-specific phenotype, it is not able to completely fulfil the role

of 5-PP-InsP$_5$ in phosphate signalling.[141] Although no specific functions for 5-PP-InsP$_4$ have been conclusively identified, there remains the possibility that this inositol pyrophosphate also has a role in regulating telomere length and inositol phosphate metabolism.[9,41,127,142,143]

As there have been several biological functions already attributed to 5-PP-InsP$_5$ and more are still being discovered, there is a demand for synthetic 5-PP-InsP$_5$ for the purpose of further study. Fortunately, 5-PP-InsP$_5$ is also one of the more straightforward inositol pyrophosphates to synthesise owing to its symmetrical structure (the final product and all of the precursors are *meso* compounds with a C-2—C-5 plane symmetry), which precludes the need for the often difficult separation of chiral enantiomers.

2.2 Previous syntheses of 5-PP-IP$_5$

The first regioisomers of InsP$_7$ chemically synthesised were 1-PP-InsP$_5$ and 3-PP-InsP$_5$ by Falck *et al*. in 1995.[104] A few years later, the same group was the first to synthesise 5-PP-InsP$_5$ (Figure 19).[105]

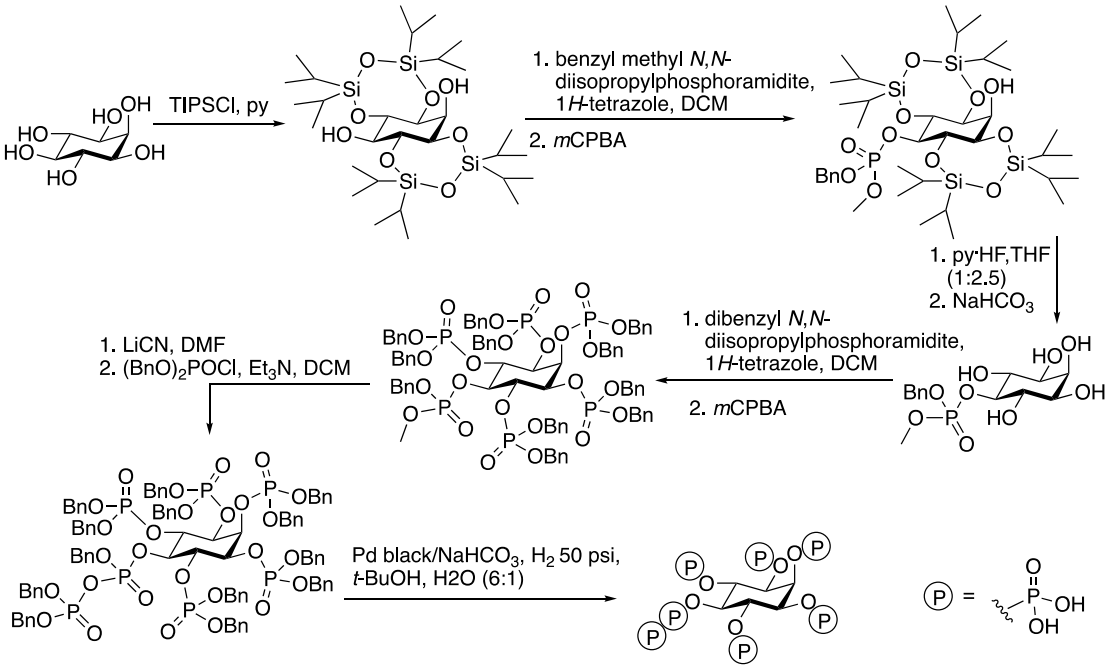

Figure 19: Reddy *et al.* synthesis route for 5-PP-InsP$_5$ which was also later used by Bhandari *et al.*[74,105]

The Reddy *et al.* synthesis started with the regioselective hydroxyl protection with a silicon-based diol protecting group, using a method described by Watanabe *et al.*[144] The diol was then phosphorylated using standard stepwise P(III) phosphoramidite

methodology (Chapter 1), using a phosphoramidite that attached a phosphate with both a benzyl and a methyl-protecting group.[105]

This phosphorylation generated a mixture of products and the desired 5-position monophosphate was purified from the resultant mixture. Subsequent acidic deprotection of silicon-based groups formed the 5-phosphate pentaol. This pentaol then underwent phosphorylation, again with a phosphoramidite and activator followed by oxidation, to yield the protected hexakisphosphate.[105]

The pyrophosphate was then constructed following the selective cleavage of the methyl group from the 5-position phosphate, which was achieved with lithium cyanide. The β-phosphate was then attached to the partially exposed 5-position phosphate with dibenzyl chlorophosphonate in a direct P(V) coupling.[105]

Finally, hydrogenation in the presence of sodium bicarbonate deprotected the precursor to yield 5-PP-InsP_5 as a sodium salt in 13% overall yield (39% yield for the pyrophosphate sequence, referring to the initial deprotection of the monophosphate on position 5 to the final product).[105]

This initial synthesis route was then repeated and adapted by Bhandari *et al.* in 2007 with only minor differences in reaction times, solvents, reagent equivalent and oxidising agent, with 6% overall yield (25% yield for the pyrophosphate sequence).[74]

As pyrophosphate synthesis methodology evolved, the synthesis of 5-PP-InsP_5 was carried out again by Zhang *et al.* as well as by Wu *et al.*, who employed alternative protecting group strategies to construct the pyrophosphate in a more scalable route (Figures 20).[101,106]

In the Zhang *et al.* method, an orthoformate-protecting group was temporarily used to attach a benzoyl group selectively to the axial 2-position hydroxyl. As in the Reddy *et al.* synthesis, the 1- and 6- as well as the 3- and 4-position hydroxyls were protected with diol protecting groups,[105] leaving only the 5-position hydroxyl exposed. This remaining hydroxyl was then protected with the more robust PMB-protecting group in the next step. Following deprotection of the acetonide groups, the resultant pentaol was phosphorylated with standard phosphoramidite methodology (Chapter 1) to generate XEPA-protected phosphates. The PMB attached to the 5-position was then selectively cleaved and a phosphoramidite was again employed to attach a phosphate with a benzyl and cyanoethyl-protecting group to this newly exposed hydroxyl.

The construction of the pyrophosphate then began with the selective deprotection of the cyanoethyl group by way of base-driven β-elimination. The partially deprotected 5-position phosphate was phosphorylated again with the direct addition of a protected β-phosphate with dibenzyl phosphoryl chloride. It should be noted that the tri-protected P(V)-P(V) moiety constructed in the penultimate step of these syntheses is highly unstable.[145]

Wu *et al.* found that HPLC purification was required after this step, prior to the final hydrogenation deprotection, to ensure sufficient product purity.[106] In the original Zhang *et al.* route, the final deprotection used platinum oxide to catalyse the hydrogenation, yielding the final product as a free acid before purification with Dowex-Na^+ exchange resin (6% overall yield), while Wu *et al.* employed palladium black in the presence of sodium bicarbonate.[101,106]

The yields for the majority of the Wu *et al*. route were not reported but the yield of the pyrophosphate-forming sequence was lower than that described in the Zhang *et al.* route (38% compared to 75%).[101,106] This decrease in yields following the Wu *et al.* modifications of the Zhang *et al*. route might be explained in part by the difference in scale, with the Wu *et al*. route using smaller quantities of reagents.

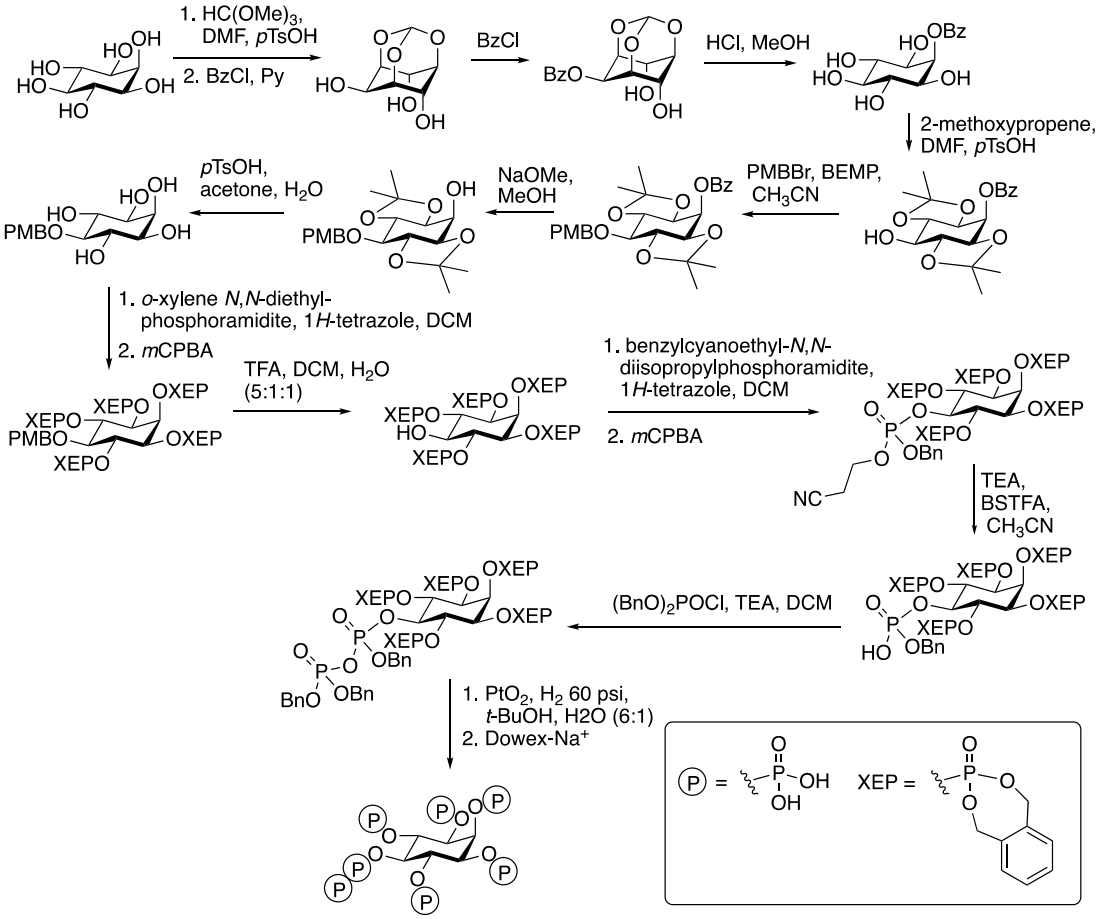

Figure 20: Zhang *et al.* synthesis route for 5-PP-InsP_5.[101] Wu *et al.* also used an adapted version of this route.[106]

The Zhang *et al.* route reports that the diisopropylidene and benzoyl-protected precursor four steps into the route can be generated on a multigram scale from inexpensive starting materials (although with an overall yield of 18%). From this point

though, the remaining steps to synthesise 5-PP-InsP$_5$ were completed in 33% yield (including the pyrophosphate sequence, which was completed with 75% yield).[101]

Apart from greater suitability to being scaled up, another advantage the Zhang *et al.*/Wu *et al.* route has over the original Reddy *et al*./Bhandari *et al.* route is the improved stability of the XEPA-protecting groups over benzyl groups on the phosphates in the last few steps involving the construction of the pyrophosphate moiety.[74,101,105,106] The point is also made that the Zhang *et al.* route had a higher yield in the final three pyrophosphate construction steps than the Bhandari *et al.* route (75% in comparison with 25%), and it was speculated that the benzyl-protected precursor was significantly less stable than the XEPA-protected precursor and was responsible for the lower yield.[101] While there are some obvious advantages to using XEPA-protecting groups, the required XEPA phosphoramidite is significantly more expensive than the benzyl phosphoramidite (approximately five times as expensive from Sigma Aldrich in 2020).

In addition to these methods of chemical synthesis of 5-PP-InsP$_5$, it should be noted that a scalable chemoenzymatic synthesis has also been recently reported by Puschmann *et al.,* as mentioned in Chapter 1.[118]

In addition to 5-PP-InsP$_5$, there is some interest in analysing possible functions of 5-PP-Ins(1,3,4,6)P$_4$ (hence referred to as 5-PP-InsP$_4$), resulting in a need for the scalable synthesis of this inositol pyrophosphate as well. A synthesis route that could therefore diverge at a late stage to form either 5-PP-InsP$_5$ or 5-PP-InsP$_4$ would be the ideal way to generate these structurally similar inositol pyrophosphates.

The Reddy *et al.* and Bhandari *et al.* route (Figure 19) could be modified through the introduction of a benzyl group to the 2-position hydroxyl following the initial phosphorylation of the 5-position hydroxyl in the second step. The Zhang *et al.* and Wu *et al.* routes could similarly be adapted with the introduction of a benzyl group to the 2-position hydroxyl by benzylating the 2-position hydroxyl following the debenzoylation in the sixth step. Although theoretically possible, these divergent routes to 5-PP-InsP$_4$ were not pursued.

2.3 Previous syntheses of 5-PP-InsP$_4$

As 5-PP-InsP$_4$ has not been isolated from wild type cells due to its presumed extremely low cellular concentrations, the drive to analyse this compound and determine if it might have physiological relevance in biological settings has been less urgent, and the chemical synthesis was not completed until the involvement of the Potter group, as reported in Wang *et al.* in 2014 (Figure 21).[107]

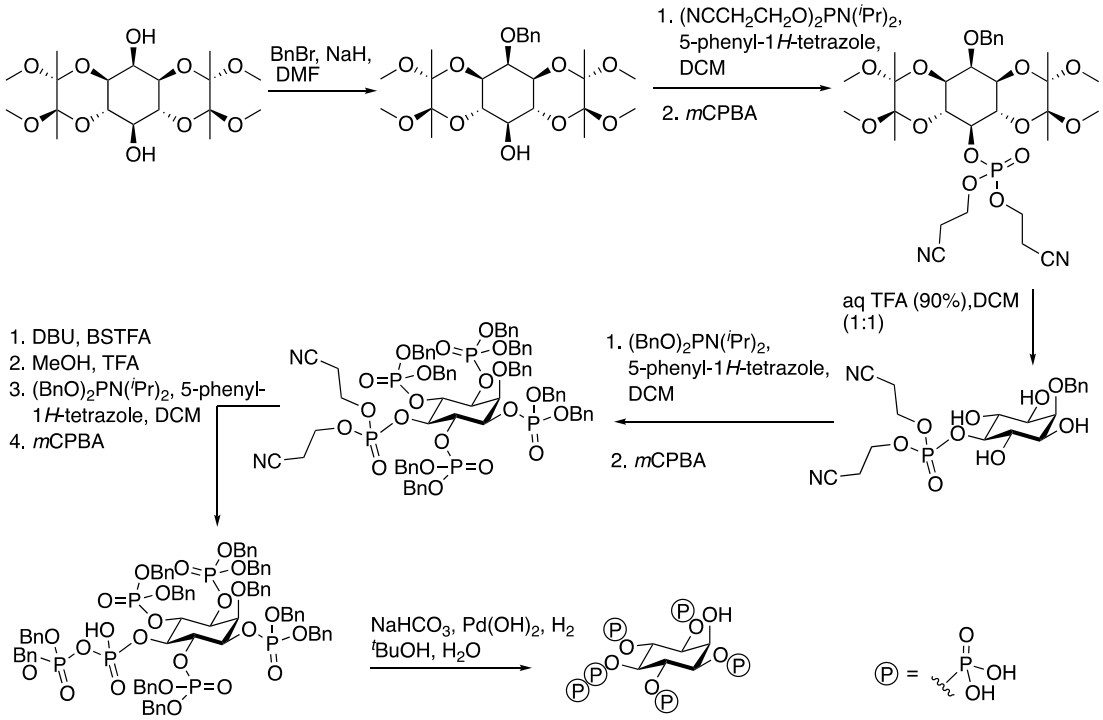

Figure 21: Synthesis route carried out by Wang *et al.* to produce 5-PP-InsP$_4$.[107]

As in the previously reported routes for synthesising 5-PP-InsP$_5$,[74,101,105,106] the synthesis began with the attachment of diol protecting groups to the 1 and 6 as well as 3 and 4-positions, although the protecting group used in this case was butane diacetal (BDA), a more stable acetal-protecting group than the isopropylidene used by Zhang *et al.* and Wu *et al.*[101,106,107]

The next step involved the protection of the 2-position hydroxyl with a benzyl moiety, leaving only the 5-position hydroxyl exposed for phosphorylation in the next step. The phosphate was added to this position through the now common P(III) methodology using a phosphoramidite with cyanoethyl-protecting groups. These cyanoethyl-protecting groups on the 5-position phosphate are able to withstand acidic conditions, which were required to remove the BDA-protecting groups in the next step. The phosphorylation of the tetraol was then carried out, attaching benzyl-protected phosphates by way of another phosphorylation using a benzyl-protected phosphoramidite.[107]

The final reaction sequence was the generation of the pyrophosphate moiety and deprotection of the compound. The pyrophosphate sequence began with the selective deprotection of the cyanoethyl groups and subsequent silylation of the phosphate attached to the 5-position, through base-driven β-elimination using DBU and BSTFA. The silyl groups were then cleaved with the sequential addition of methanol followed by TFA. The β-phosphate of the pyrophosphate was attached with a phosphoramidite as a benzyl-protected phosphite prior to subsequent oxidation. This is one of the first

instances of a pyrophosphate moiety being constructed using P(III) methodology resulting in a mixed P(III)-P(V) pyrophosphate precursor, with the first time reported by Capolicchio *et al.* in their synthesis of asymmetric regioisomers of $InsP_7$ in 2013.[89] The mixed P(III)-P(V) anhydride moiety is oxidised in the final phosphorylation to a di-protected P(V)-P(V) species lacking a protecting group on the α-phosphate, which, although still unstable, is more robust than the tri-protected analogue.

The final hydrogenation in the presence of sodium bicarbonate removed all of the benzyl-protecting groups and yielded 5-PP-$InsP_4$ as a sodium salt (36% overall yield from the BDA-protected diol).[107]

It is important to note that this synthetic scheme could not be directly diverged from to form 5-PP-$InsP_5$. The benzyl group attached to the 2-position would need to be removed after the first phosphorylation and prior to the second phosphorylation. This benzyl deprotection would necessitate a hydrogenation that would reduce the cyanoethyl-protecting groups from the 5-position phosphate in an undesired side reaction.

There are currently no other reported chemical synthesis routes for 5-PP-$InsP_4$, but Wilson *et al*. have also achieved its synthesis using enzymes.[127]

2.4 Synthesis of 5-PP-$InsP_5$ (**2**) and 5-PP-$InsP_4$ (**3**)

The first inositol pyrophosphate successfully synthesised for this thesis project was the symmetrical regioisomer of $InsP_7$, namely 5-PP-$InsP_5$. This inositol pyrophosphate was chosen to be the first synthetic target because its symmetrical structure allowed for a comparatively easy synthetic route that did not need to include chiral resolution steps. As the most abundant naturally occurring regioisomer of $InsP_7$, this product is also a compound of potential interest in a number of biological studies (some of which will be discussed later in this chapter, see sections 2.5 and 2.6).

Following the successful synthesis of 5-PP-$InsP_5$, the route was adapted to diverge partway through to generate also the structurally related 5-PP-$InsP_4$ inositol pyrophosphate.

The route used to achieve the synthesis of 5-PP-$InsP_5$ and 5-PP-$InsP_4$ (Scheme 1) was largely derived from the similar route to synthesise 5-PP-$InsP_4$ by Wang *et al*. (Figure 21) and the Riley *et al.* route to synthesise 1-PP-Ins(4,5)P_2.[91,107] The main difference that allowed the route in this study to diverge and generate two final inositol pyrophosphate products rather than one was the use of the hydrogenation-resistant methylsulfonylethyl (MSE)-protecting group on the phosphate attached to the 5-position, thereby further exploring the synthetic applications of this protecting group.

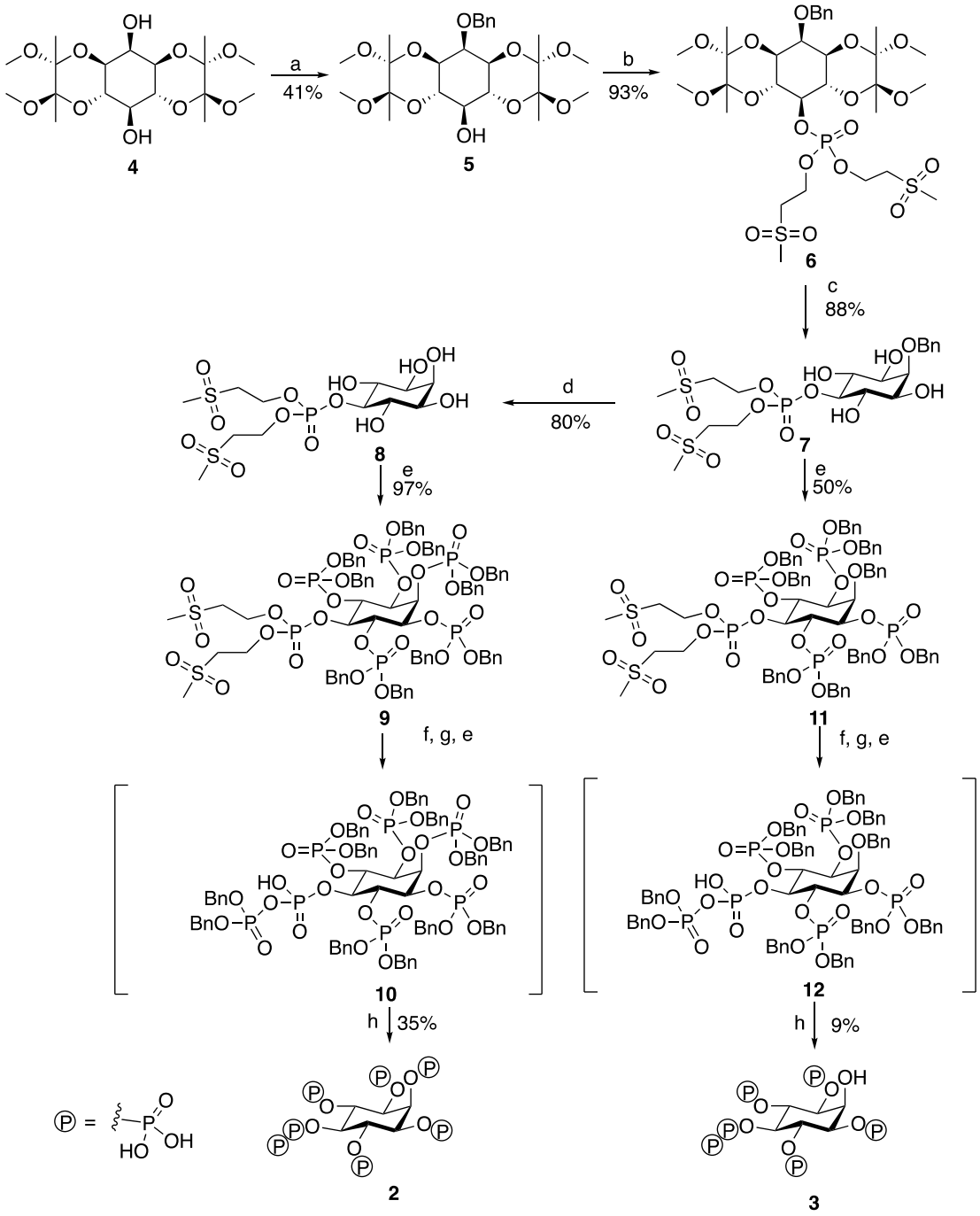

Scheme 1: Divergent Syntheses of 5-PP-InsP_5 and 5-PP-InsP_4 carried out in this study.

Reagents and conditions: (a) DMF, NaH, BnBr; (b) 1. DCM, 5-phenyl-1*H*-tetrazole, $(OMSE)_2PN(^iPr)_2$ (**1**), 20h 2. *m*CPBA, -78°C-RT; (c) TFA, H_2O; (d) THF, CH_3COOH, H_2O, H_2, $Pd(OH)_2/C$; (e) 1. DCM, 5-phenyl-1*H*-tetrazole, $(OBn)_2PN(^iPr)_2$, 20h 2. *m*CPBA, -78°C-RT; (f) DBU, BSTFA; (g) MeOH, TFA; (h) MeOH, THF, 1 M TEAB/$NaHCO_3$, H_2, $Pd(OH)_2/C$, 24h.

As in the case of the previously described routes for 5-PP-InsP_5, the point for facile divergence to 5-PP-InsP_4 in this route (Scheme 1) was situated in the middle of the route, after step 4 out of 8 (with the hypothetical divergence point to synthesise 5-PP-InsP_4 in the Zhang *et al.*/Wu *et al*. route being after step 7 out of 14, and for the Reddy

et al./Bhandari *et al.* route after step 3 out of 6, although these divergent routes were not pursued in the original studies).[74,101,105,106]

The route in this study, however, crucially differs from the previous synthesis routes for 5-PP-InsP_5 through the use of different protecting groups and the pyrophosphate construction method.

2.4.1 Shared synthetic route of 5-PP-InsP_5 (**2**) and 5-PP-InsP_4 (**3**)

The route begins with 1,6:3,4-bis-[*O*-(2,3-dimethoxybutane-2,3-diyl)]-*myo*-inositol (**4**), which can be synthesised from inositol as described by Riley *et al.*,[146] being regioselectively benzylated at the axial 2-position hydroxyl. This was accomplished with the slow addition of sodium hydride to a suspension of the starting material, followed by benzyl bromide, as described by Wang *et al.*[107] The reaction was allowed to stir overnight before being worked up to yield the 2-position mono-benzylated product (**5**) at 41% yield (with no appearance of the other 5-position mono-benzylated regioisomer). This regioselectivity of this reaction has been observed before, although the reason for its occurrence is not evident.[113]

The next step in the route was the introduction of a protected phosphate to the available 5-position hydroxyl, which would later serve as the α-phosphate of the pyrophosphate moiety of both final products.

This 5-position phosphate was attached to the protected inositol precursor using standard P(III) phosphoramidite methodology. Importantly, the phosphoramidite employed in this reaction was protected with MSE-protecting groups. As mentioned in Chapter 1, the MSE-protecting group is useful, as it remains stable under acidic conditions and is not reduced in hydrogenation.

The MSE-protected phosphoramidite required for the necessary phosphorylation, bis[(methylsulfonyl)ethyl]diisopropylphosphoramidite (**1**), had to first be synthesised. This was achieved in the one-pot reaction described by Engelsma *et al.*[147] Although the reaction was carried out as reported, the recommended purification technique described in said method, as well as another purification technique reported in an alternative method of synthesising the MSE phosphoramidite, as described by Bradshaw *et al.*,[148] were found to be unsuitable: the recommended recrystallisation from acetone/hexane did not remove all of the contaminants from the product;[147] the recommended silica column chromatography with a column deactivated with triethylamine did allow for the isolation of the mostly pure product as a waxy, off-white solid, but the product was found to degrade rapidly even when stored in the freezer.[148] We instead found that recrystallisation of the product in the minimum

amount of DCM (approx. 2 mL) followed by diethyl ether (150 mL), resulted in the product precipitating overnight as pure, white needle-like crystals that did not show any signs of degradation following filtering, drying and storage in the freezer. The reaction was repeated a number of times to generate sufficient amounts of MSE phosphoramidite, and the yield of the reaction varied during the reaction repeats (approximately 10-40% yield), with the variation thought to be the result of differences in water content in some of the reagents [the 2-(methylsulfonyl)ethanol was found to be particularly hygroscopic] as well as decomposition of product during purification. Although the yields were generally low (the highest obtained being 49%), the starting materials were easily obtained and the reaction did not necessitate the consumption of our supply of *N,N*-diisopropylphosphoramide dichloride, a reagent that is very valuable for the synthesis of more complicated phosphoramidites.

Following phosphitylation, oxidation and work-up, the product was purified with silica column chromatography, during which the product eluted later than expected despite having no exposed hydroxyls and the reasonably hydrophobic BDA- and benzyl-protecting groups. This late elution is thought to be due to the extremely polar nature of the MSE-protecting groups attached to the newly added phosphate. This phosphorylated product (**6**) was collected as a white foam (93% yield).

In the next step, the BDA-protecting groups were removed in a straightforward acidic hydrolysis reaction. Acidic conditions would also be suitable for removing other acetal-protecting groups such as isopropylidene, which was used in the other 5-PP-InsP_5 synthesis routes.[55,101] Unlike isopropylidene, the BDA structure contains *O*-methoxy groups that stabilise the protecting group through the anomeric effect, resulting in more forcing acidic conditions being required for the removal of the protecting group. As mentioned before, the MSE groups protecting the phosphate attached to the 5-postion are resistant to acidic conditions and were not removed when exposed to TFA. In fact, leaving trace amounts of TFA at this stage was expected to ensure the MSE groups were not cleaved in the next step of the route and, as a result, the product (**7**) was not dried excessively. This deprotection reaction was achieved at 88% yield.

Removal of the benzyl group attached to the 2-position via hydrogenation marks the point of divergence for synthesising 5-PP-InsP_5 (**2**) instead of 5-PP-InsP_4 (**3**). The discussion from this point will continue along the route to synthesis 5-PP-InsP_5 and will later return to the synthesis of 5-PP-InsP_4.

2.4.2 Final steps in route to synthesise 5-PP-InsP$_5$ (**2**)

As described previously, one of the benefits of the MSE-protecting groups of the phosphate attached to the 5-position is that they are resistant to hydrogenation and therefore will not be affected during the removal of the benzyl attached to the 2-position. The protecting groups used for the 5-position phosphate in the Zhang *et al*./Wu *et al*. synthetic routes, cyanoethyl, would be unable to withstand hydrogenation and would be reduced.[101,106] Following this first hydrogenation, the compound was not purified or even allowed to stay in solution for very long, as previous attempts had shown it to be prone to rapid degradation in d6-DMSO solution at this point (as well as degradation being observed at the analogous step in the synthesis of InsP$_8$, Chapter 3). Unfortunately, it is not immediately apparent why the benzyl-deprotected pentaol product should be unstable compared to the preceding compound in the route. The product was lyophilised to a white solid (80% yield), and while a small portion was removed for NMR analysis, the rest was carried through to the next step.

To continue the route to generate 5-PP-InsP$_5$, the pentaol hydrogenation product (**8**) was phosphorylated with the benzyl-protected phosphoramidite and 5-phenyl-1*H*-tetrazole. This second phosphorylation in the route had to attach phosphates to the product that were protected by an orthogonally-stable protecting group to the MSE groups attached to the phosphate at position-5. Benzyl-protecting groups were deemed to be the best choice as the benzyl moiety would not be removed by the basic conditions later used to deprotect the MSE groups. Benzyl-protecting groups were also used instead of the XEPA groups used in the previous syntheses of 5-PP-InsP$_5$, due to the comparative ease with which the required dibenzyl phosphoramidite can be commercially obtained over the XEPA analogue.[101,106]

Despite its apparent similarities to other polyol phosphorylations carried out in this work (as seen in Chapters 4 and 5), this particular reaction proved to be more problematic. The phosphorylation of the pentaol (**8**) in this route failed multiple times before it was successfully completed. This reaction is now believed to have failed due to trace amounts of water, despite the other analogous phosphorylations not showing similar levels of moisture sensitivity. The combination of the five exposed hydroxyl groups with the highly polar MSE-protected phosphate group resulted in the starting material being very hygroscopic and thus challenging to dry. Insufficient drying resulted in the activated tetrazolide in the phosphorylation being consumed by any water present in the reaction.

A number of slightly different reaction conditions and drying methods were attempted before the reaction was successfully completed (Table 3).

Reaction code	Reaction conditions changed	Outcome and theories
107	5-phenyl-1*H*-tetrazole activator (7.5 equiv) and benzyl phosphitylating agent (6.8 equiv) were added at the beginning of the reaction. Commercially dried DCM used. Note: small scale (27 mg pentaol **8** starting material used).	Reaction failed. Insolubility of the starting material was suspected to be slowing the reaction (noting that the phosphite intermediates tend to break down if left for too long in solution).
109/111/120/ 121	Used a sonicator to dissolve the starting material in the DCM. 5-phenyl-1*H*-tetrazole activator (7.5 equiv) and benzyl phosphitylating agent (6.8 equiv) were added at the beginning of the reaction. The DCM was also thoroughly dried with phosphorus pentoxide and molecular sieves and more was used in the reactions. The tetrazolide was also allowed to preform before being added to the pentaol. Note: small scale (16/24/40/38 mg pentaol **8** starting material used respectively).	Reactions failed. Following these failures, trace water consuming the phosphorylating agent became the new theory for an explanation.
149	Used a sonicator to dissolve the starting material in the DCM. 5-phenyl-1*H*-tetrazole activator (7.5 equiv) and benzyl phosphitylating agent (6.8 equiv) were added at the beginning of the reaction with additional portions (respectively 7.5 equiv and 6.8 equiv) being added after a few hours after ^{31}PNMR indicated the reaction had not progressed. The DCM was also dried with phosphorus pentoxide and molecular sieves. Note: small scale (14 mg pentaol **8** starting material used).	Reaction failed. Water is believed to have been the reason. More equivalents of the phosphorylating reagents added from the beginning may overcome water present.
150	Extra equivalents of 5-phenyl-1*H*-tetrazole activator (20 equiv) and benzyl phosphitylating agent (15 equiv) used from the beginning of the reaction. The pentaol starting material was dissolved in dry solvents and concentrated (dry acetonitrile three times, then dry DCM) followed by drying thoroughly on a vacuum line. The DCM was also dried with phosphorus pentoxide and molecular sieves. Note: small scale (15 mg pentaol **8** starting material used).	Reaction successful with 80% yield of **9**.
164	Extra equivalents of 5-phenyl-1*H*-tetrazole activator (15 equiv) and benzyl phosphitylating agent (10 equiv) used from the beginning of the reaction. The pentaol starting material was dissolved in dry solvents and concentrated (dry acetonitrile three times, then dry DCM) followed by drying thoroughly on a vacuum line. The DCM was also dried with phosphorus pentoxide and molecular sieves. Note: larger scale (110 mg pentaol **8** starting material used).	Reaction successful with 97% yield of **9**. Larger reaction scale believed to be contributing factor in increased yield.

Table 3: Different phosphorylation attempts for the pentaol (**8**) in the 5-PP-InsP_5 (**2**) synthesis route to generate the protected hexakisphosphate (**9**).

To add to the initial confusion as to the reason for the failure of this phosphorylation, the ^{31}PNMR signals observed after phosphorylation but prior to oxidation seemed to indicate that activated tetrazolide appeared to be present in the solution with a peak at 128 ppm, but not reacting with the hydroxyls of the pentaol (**8**). The signal that was initially believed to be the activated tetrazolide in the reactions that failed is now suspected of being a phosphitylated side-product of the hydrolysed phosphitylating agent (Figure 22). To investigate this possibility, a phosphorylation in the absence of target substrate was carried out and this 'blank' sample demonstrated the formation of two peaks around 128 ppm, the activated tetrazolide and the presumed phosphorylated hydrolysed phosphitylating agent (this sample was oxidised and hydrogenated to yield inorganic phosphate and trace amounts of inorganic pyrophosphate).

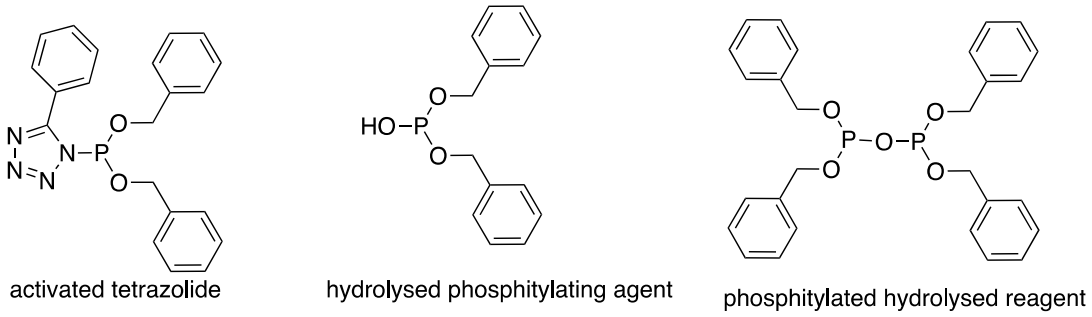

Figure 22: Structures of the activated tetrazolide, hydrolysed tetrazolide and the phosphorylated hydrolysed phosphitylating agent, which may be the source of the observed 128 ppm species present in the failed phosphitylation reactions.

It also became apparent in the third-attempted phosphorylation that the addition of more phosphoramidite and 5-phenyl-1*H*-tetrazole activator mid-reaction does not always promote further progress of the reaction. In this case, the reason for this is thought to be the propensity for the phosphitylating agent apparently to react with other reaction side products preferentially over the starting material, in addition to the diisopropylamine by-product consuming the additional 5-phenyl-1*H*-tetrazole activator.[87]

It should be noted that there are side reactions that could have potentially occurred during this phosphorylation, such as the migration of the 5-position phosphate to neighbouring hydroxyls prior to phosphorylation or the cleavage of the MSE groups. The proximity of the newly deprotected hydroxyl groups in the 4- or 6-position could enable them hypothetically to form a cyclic phosphate through nucleophilic attack on the MSE-protected phosphate attached to the 5-position, thereby displacing one of the MSE-protecting groups. Once a cyclic phosphate forms, hydrolysis could take place to open the cyclic phosphate in either direction, possibly resulting in phosphate migration.[149] While the possibility of phosphate migration was present, it was

believed to be unlikely due to the excess of the acidic tetrazole activator present in the reaction and the propensity for migration to occur under basic conditions. These more acidic conditions resulting from the larger quantities of 5-phenyl tetrazole were also expected to suppress the cleavage of the MSE groups, which occurs readily under basic conditions. Indeed, neither unwanted side reaction was observed in any of the reaction attempts.

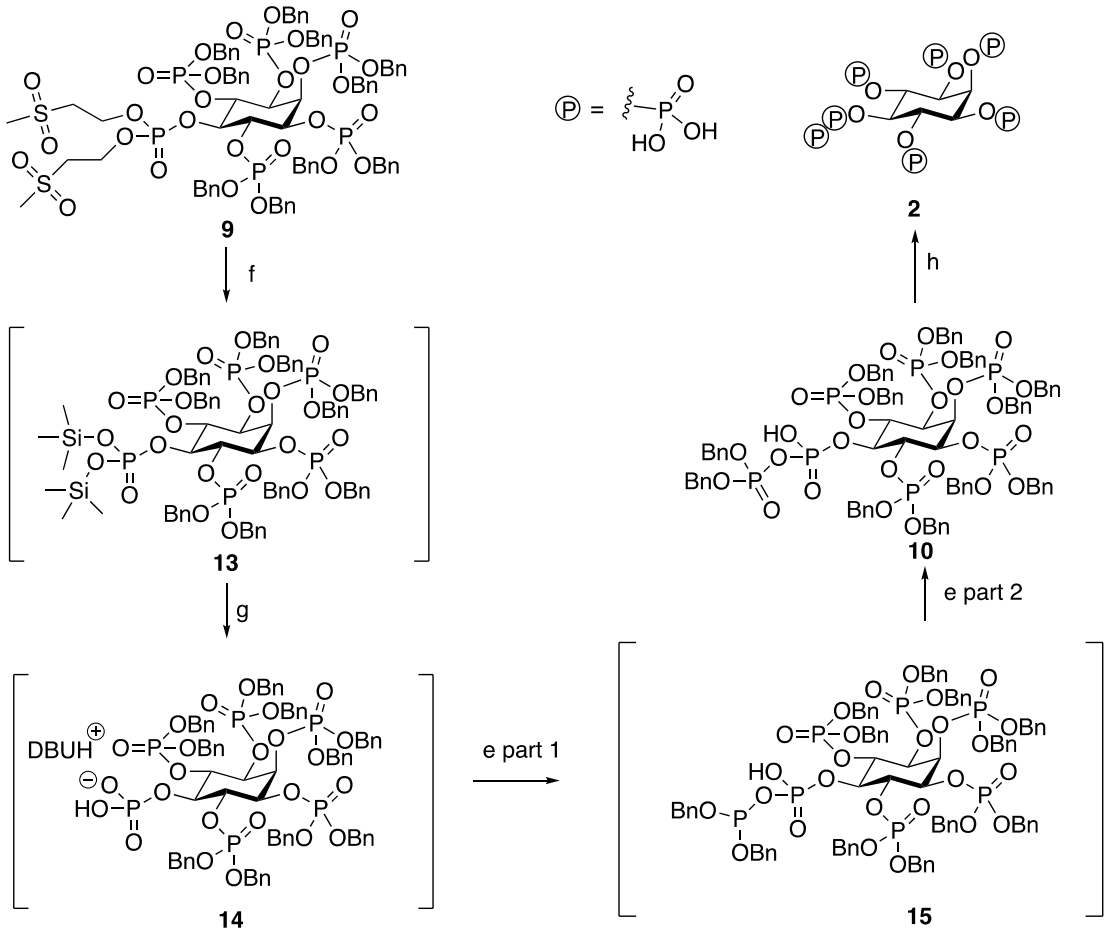

Scheme 2: Expanded final steps in the 5-PP-InsP_5 synthetic route shown previously in Scheme 1 to show the pyrophosphorylation sequence intermediates.

Reagents and conditions: (e) 1. DCM, 5-phenyl-1*H*-tetrazole, $(OBn)_2PN(^iPr)_2$, 20h 2. *m*CPBA, -78°C-RT; (f) DBU, BSTFA; (g) MeOH, TFA; (h) MeOH, THF, 1 M TEAB/$NaHCO_3$, H_2, $Pd(OH)_2/C$, 24h.

The next step in the reaction route is a multi-step sequence (Scheme 2) to construct the pyrophosphate moiety at the 5-position. These steps had to be performed in quick succession as some of the intermediates proved to be unstable. The first step in this sequence to generate the pyrophosphate moiety was the cleavage of the MSE groups protecting the phosphate attached to the 5-position. The base-labile MSE groups were first cleaved with DBU [1,8-diazabicyclo(5.4.0)undec-7-ene], a non-nucleophilic base. DBU alone is unable to cleave both MSE groups from the phosphate, however, as the

newly exposed negative charge following the first MSE deprotection would repel DBU and prevent it from approaching to remove the second MSE group. To circumnavigate this problem, the partially deprotected phosphate was protected again with a trimethylsilyl (TMS) group that temporarily masked the negative charge and allowed DBU access to the remaining MSE group.[89] An excess of *N,O*-bis(trimethylsilyl) trifluoroacetamide (BSTFA) was used to silylate the phosphate groups (with additional equivalents required to account for the reagent being consumed by water present in the DBU supply). ^{31}PNMR spectroscopy was used to monitor the silylation reaction and ensure completion (Figure 23).[89]

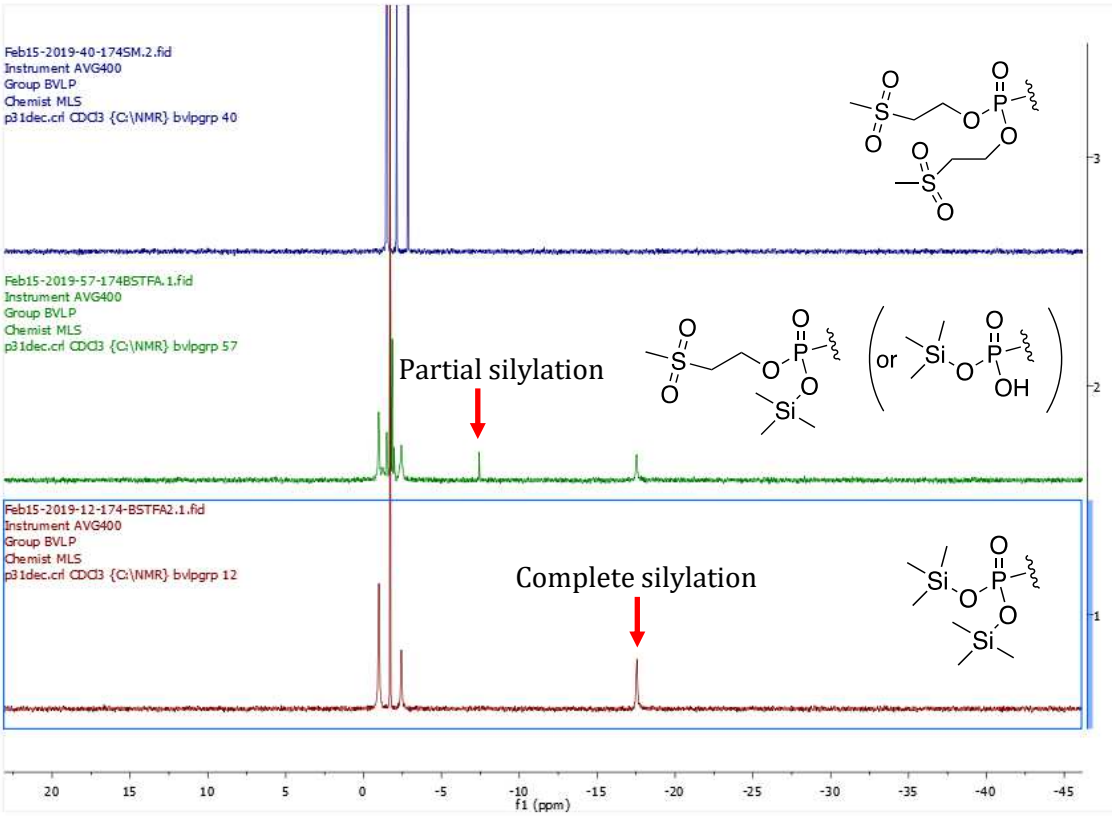

Figure 23: ^{31}PNMR spectra showing the cleavage of the MSE and subsequent silylation in progress during the synthesis of 5-PP-InsP$_5$, with structures corresponding to the 5-position phosphate on the right for each spectrum. The blue trace shows the starting material (with the 5-position phosphate protected by MSE groups); the green trace shows partial silylation (with some of the material protected by only one silyl group at the 5-position phosphate); and the red trace, which was obtained following the addition of more BSTFA, shows complete silylation of the 5-position phosphate (now protected completely with two silyl groups, **13**).

It should be noted that the ^{31}PNMR signals for phosphates with only one silyl group through either monosilylation or hydrolysis of the doubly-silylated phosphate will appear in a similar region (around -10 ppm). Despite anecdotal evidence from other members of the lab of silyl groups being hydrolysed at this stage in pyrophosphate

formation, degradation of the silyl-protected phosphates was not observed in these reactions prior to deliberate removal.

The next step of the sequence, the cleavage of the silyl groups through methanolysis, required precise timing of reagent addition [although no difficulties were encountered in the 5-PP-$InsP_5$ synthesis route at this stage, the analogous step in the 1,5-$(PP)_2$-$InsP_4$ route (Chapter 3) had been attempted once before and proved to be more difficult].

Once methanol was added to the reaction mixture, the silyl groups were cleaved and the unmasked, nucleophilic phosphate attached to the 5-position became able potentially to attack neighbouring phosphate benzyl esters. To suppress these hypothetical cyclisation reactions, trifluoroacetic acid (TFA) had to be added to render the deprotected phosphates less nucleophilic.[89] As well as preventing cyclisation side reactions, the TFA plays an important role in the next reaction by protonating the DBU (thereby preventing it from slowing down the subsequent phosphorylation).

However, it was found that if the TFA was added too soon, it severely slowed methanolysis (resulting in silyl-protecting groups remaining attached after days, after which time degradation of the product was observed). It should be noted though, that some synthetic routes included the simultaneous addition of MeOH and TFA and did not report sluggish silyl cleavage.[89] The time between addition of methanol and TFA was monitored to ensure cleavage of the silyl groups, while also preventing incomplete reaction (Table 4).

Reaction code	Time between adding MeOH and TFA	Result
166	7 minutes	complete desilylation
169/172	30 seconds	complete desilylation
176	10 seconds	incomplete desilylation
178	3 minutes	complete desilylation

Table 4: Desilylation step attempts in the route to synthesise 5-PP-$InsP_5$ to generate **14** from **13**. The time allowed between the addition of MeOH and TFA and the resulting reaction outcome are reported.

No cyclisation was observed during the desilylation phase of the synthesis of 5-PP-$InsP_5$, although it was found to occur during the analogous step in attempts to synthesise 1,5-$(PP)_2$-$InsP_4$ (Chapter 3). However, an unwanted cyclisation side reaction was observed in the next step of the route to generate 5-PP-$InsP_5$.

In this next step of the route, the deprotected 5-position phosphate (**14**) was phosphorylated with the benzyl phosphoroamidite reagent to make a mixed P(III)-P(V)

anhydride moiety (**15**). Upon oxidation with *m*CPBA, the phosphite intermediate was converted to a phosphate and the protected pyrophosphate was formed (**10**). Although P(III) methodology had not previously been employed in the synthesis of 5-PP-InsP$_5$ (instead, the β-phosphate was attached in a P(V) state),[55,74,101,105] it has been used in the reported synthesis of 5-PP-InsP$_4$,[107] as well as in routes to generate other regioisomers of InsP$_7$ and InsP$_8$.[89,97]

This phosphorylation step to form the sterically congested 5-PP-InsP$_5$ precursor (**10**, Figure 24) proved to be more sensitive and prone to failure than previous phosphorylations due to cyclisation side reactions and product instability.

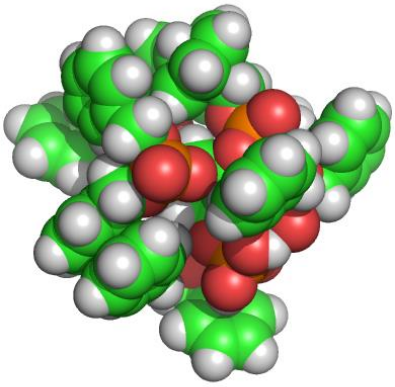

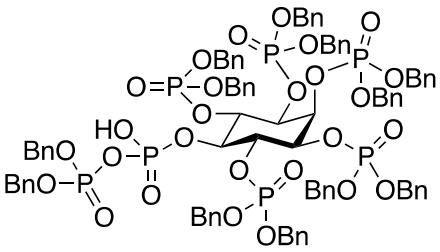

10

Figure 24: Space-filling CPK model to indicate the sterically-congested nature of the protected 5-PP-InsP$_5$ precursor, *myo*-inositol-1,2,3,4,6-pentakis(dibenzyl)phosphate-5-dibenzyl diphosphate (**10**). Carbon atoms are depicted in green, oxygen in red, hydrogen in white and phosphorus in orange.

The first problem encountered was the formation of cyclisation products. These cyclic products were observed in the ^{31}PNMR spectrum (Figure 25) as pyrophosphate signals that formed before the addition of an oxidising agent (ie. before any possible conversion of phosphites to phosphates, ruling out the intended pyrophosphate product).

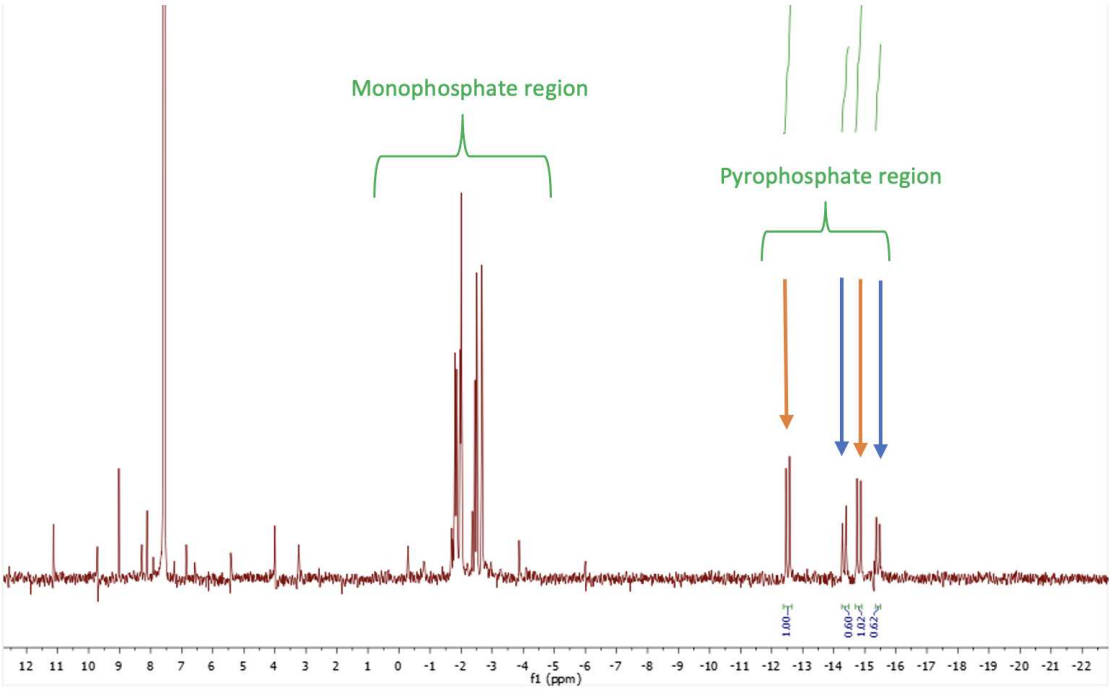

Figure 25: ^{31}PNMR spectrum showing two cyclised products that formed during the final phosphorylation reaction in the route to synthesise 5-PP-InsP_5. The two colours of arrows correspond to different diastereoisomers of cyclic pyrophosphates in an approx. 10:6 ratio.

There are four potential cyclisation products that could form following deprotection of the 5-position phosphate depending on the direction of cyclisation to either the 4- or 6-position phosphates, as well as the orientation of the protecting groups on the attacked phosphate (Figure 26). As these products are two sets of enantiomers, only two products would be expected to be detected by NMR spectroscopy.

Indeed, there were two pyrophosphate-containing compounds visible in the ^{31}PNMR (Figure 25) in an approximate 6:10 ratio (as integration of ^{31}PNMR cannot be used to accurately represent quantities). The presumed nucleophilic attack of the phosphate attached to position-5 on either neighbouring phosphate (position 4/6) appears to take place more easily when the substituents of the phosphate are in a certain orientation resulting in the preferential formation of one of the two racemic diastereoisomers.

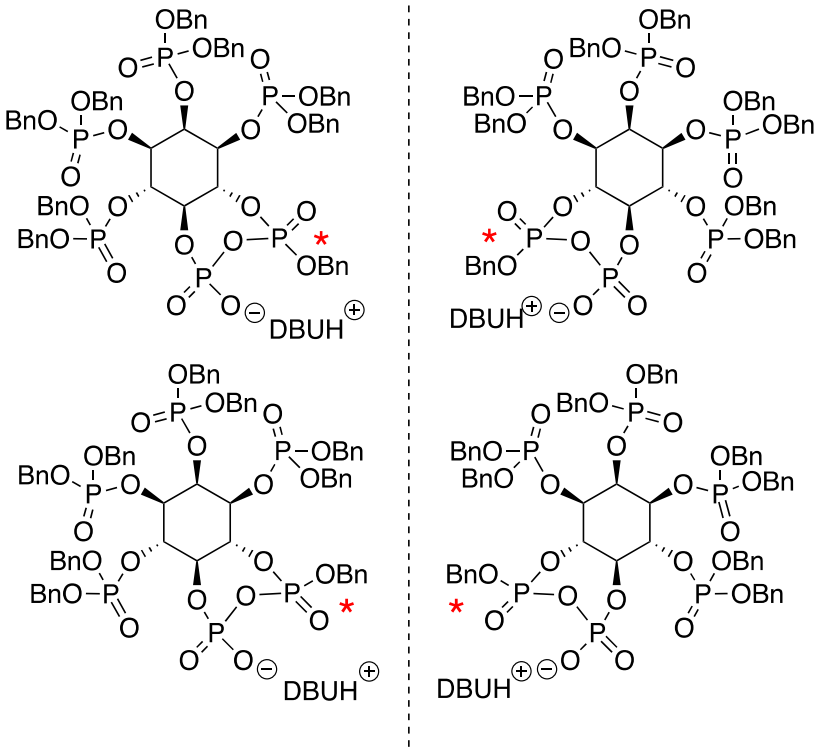

Figure 26: Structures of possible products of cyclisation. The stereogenic centre of the phosphate in the cyclic pyrophosphate group is indicated with a red asterisk in all four compounds. There are two pairs of enantiomers (mirror plane down the middle) resulting in only two cyclic products being observed in the ^{31}PNMR spectrum as diastereoisomers.

A number of reaction conditions were trialled to reduce or prevent the cyclisation side reactions and promote the desired phosphorylation. These conditions and their results are summarised below in Table 5.

Reaction	Reaction conditions	Result
167	The reaction was initially started with 1.7 equivalents of the phosphorylating agent and 2.2 equivalents of the 5-phenyl-1*H*-tetrazole. As the reaction did not seem to be progressing after an hour, another 1.7 equivalents of the phosphorylating agent were added.	Two cyclised products emerged in the ^{31}PNMR (with the amounts increasing when more P(III) reagent was added).
170	As before, the reaction was initially started with 1.7 equivalents of the phosphorylating agent and 2.2 equivalents of the 5-phenyl-1*H*-tetrazole. This time only an additional 0.8 equiv of the phosphitylating agent was added and the reaction was left for a couple of hours longer.	Two cyclised products emerged in the ^{31}PNMR (with the amounts increasing when more P(III) reagent was added).
175	As before, the reaction was initially started with 1.7 equivalents of the phosphorylating agent and 2.2 equivalents of the 5-phenyl-1*H*-tetrazole. This time the activated tetrazolide species was allowed to preform before the starting material was added to the reaction.	Two cyclised products emerged in the ^{31}PNMR (with the amounts increasing when more P(III) reagent was added).
177	As before, the reaction was initially started with 1.7 equivalents of the phosphorylating agent and 2.2 equivalents of the 5-phenyl-1*H*-tetrazole. After an hour, a ^{31}PNMR spectrum was obtained and another 1.7 equiv of phosphorylating agent and an additional 4.4 equiv of 5-phenyl-1*H*-tetrazole were added to the reaction. It was noted that the pH of the reaction was slightly acidic (approx. 6). The progress of the reaction was checked by NMR after another hour and then left to stir overnight.	Initially, only phosphonate was observed with trace amounts of cyclisation. After more reagents were added, the desired phosphite intermediate (**15**) started to form. The reaction was left overnight and this intermediate was found to have degraded during this time.
179	This time an excess of the phosphorylating agent and the 5-phenyl-1*H*-tetrazole were added from the start of the reaction (2.7 equiv and 6.6 equiv respectively). After a short period of time an additional 2.7 equiv of phosphorylating agent was added. The reaction was only allowed to progress for three hours and was not left overnight.	No cyclisation was observed and the desired P(III)-P(V) intermediate (**15**) was successfully generated before being oxidised to form the protected pyrophosphate.

Table 5: Summarising the reaction conditions and results for the different attempts to phosphorylate the hexakisphosphate precursor (**14**) to generate benzyl-protected 5-PP-InsP_5 (**10**).

In the first three reaction attempts, significant levels of cyclisation were observed. After the first reaction, it was initially hoped that this side reaction could be controlled by fine-tuning the equivalents of the phosphorylating agent and reaction time, although the changes made for the second attempt proved to be insufficient.

In the third attempt, while the equivalents of the phosphorylating agent and the activator were unchanged, the order in which the reagents were combined was altered so that the activated tetrazolide species was allowed to preform for 15 minutes before the inositol hexakisphosphate starting material (**14**) was added. This approach was trialled, as it was theorised that if the phosphorylation could take place as quickly as possible, the desired formation of the phosphite intermediate (**15**) might outcompete at least some of the basic cyclisation mechanism which could take place when the starting material alone is left in solution (Figure 27). The introduction of a phosphite group to the 5-position phosphate provides another possible mechanism by which the compound can cyclise (Figure 27), although this mechanism was thought to be less likely. Unfortunately, preforming the tetrazolide did not appear to have any effect on the formation of the cyclic products and a new strategy was devised.

In the fourth iteration of the phosphorylation attempt, it was speculated that forcing more acidic conditions might suppress cyclisation assuming the basic mechanism was taking place. Although both excessively acidic or basic conditions could hypothetically be responsible for the cyclisation observed (Figure 27), the basic mechanism was predicted to be the more likely option and more acidic conditions should prevent this side reaction. To render the reaction more acidic, the equivalents of 5-phenyl-1*H*-tetrazole (a weak acid) were increased significantly.

The results of this reaction supported the conclusion that the basic mechanism was probably the favoured route by which cyclisation had been occurring, as the cyclisation side reaction was mostly suppressed under more acidic conditions and the formation of the desired phosphite intermediate (**15**) could be observed in the ^{31}PNMR spectrum after a few hours. It was hoped that a longer reaction time would allow more phosphite (**15**) to form and the reaction was left overnight.

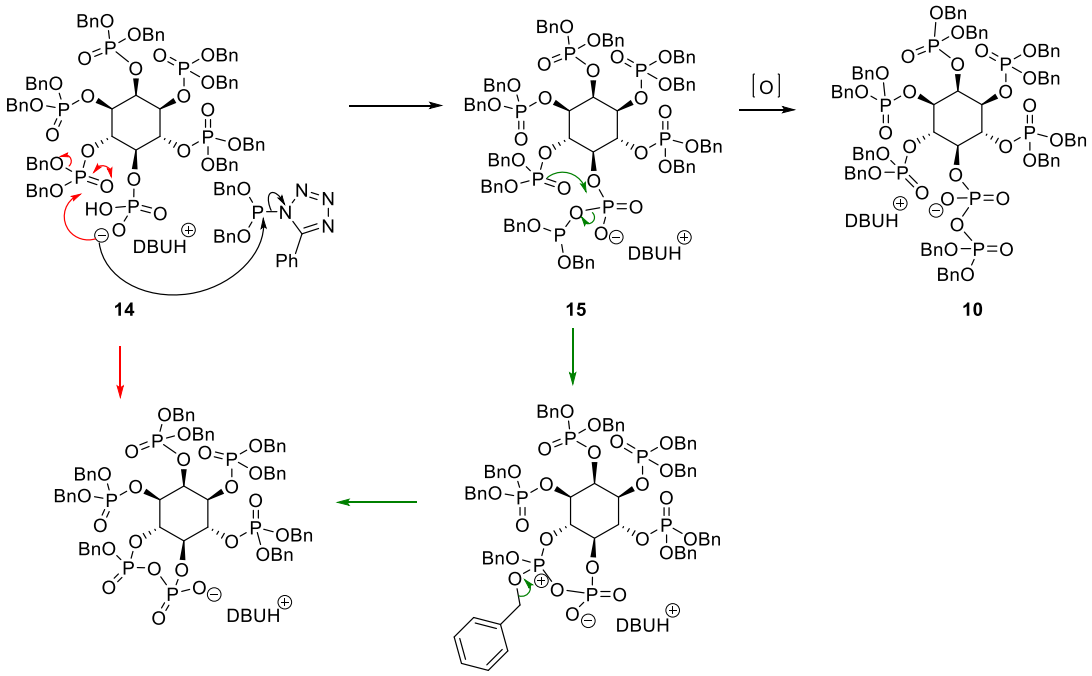

Figure 27: Possible mechanisms for cyclisation observed as a side reaction during the phosphorylation step in the pyrophosphate-forming sequence in the 5-PP-InsP$_5$ route. For simplicity, only one possible cyclisation product is shown when the 5-position phosphate could attack the 4-position phosphate in a slightly different orientation resulting in a different diastereoisomer as shown in Figure 26. The acidic mechanism can be seen by following the green arrows and the basic mechanism can be seen by following the red arrows. The desired reaction to the protected pyrophosphate intermediate (**10**) can be seen by following the black arrows.

Unfortunately, it was found that the P(III)-P(V) intermediate (**15**) degraded overnight, unlike the phosphite intermediates in other phosphorylations described throughout this study. The reason for this could have been the inherent instability of the highly phosphorylated intermediate or as a consequence of the increased acidity of the solution promoting acidic hydrolysis. From NMR spectroscopic evidence, it seemed that the reaction could be sufficiently completed within a few hours, so the phosphite (**15**) could be generated and oxidised successfully while avoiding both cyclisation and degradation.

In the final iteration of the reaction, more equivalents of both the 5-phenyl-1*H*-tetrazole and phosphorylating agent (with more of the former to ensure suppression of cyclisation) were used in the phosphorylation. In this final attempt, no unwanted cyclisation was observed and only the phosphite intermediate (**15**) could be seen forming in the ^{31}PNMR spectrum. The reaction was only allowed to stir for three hours before being oxidised with *m*CPBA to yield the protected pyrophosphate (**10**).

Upon completion of the reaction, the protected pyrophosphate (**10**) generated was not expected to be very stable and, as a result, the usual aqueous work-up for phosphorylations was bypassed. Although still prone to degradation through

hydrolysis or cyclisation, the protected inositol pyrophosphate precursor (**10**) was able to withstand purification with quick silica column chromatography, using a column deactivated with TEA prior to use. Following the column, the product was immediately hydrogenated, as the protected inositol pyrophosphate (**10**) appeared to become unstable. This decrease in stability is thought to possibly be the result of removing the stabilising protonated DBU ions.

The final step to generate the inositol pyrophosphate product was hydrogenation to remove the benzyl-protecting groups from the phosphates attached to the 1, 2, 3, 4 and 6-positions, as well as the β-phosphate of the pyrophosphate. Once the β-phosphate was deprotected in particular, the compound was expected to become less prone to cyclisation and other unwanted side reactions.

Due to the inherent instability of pyrophosphates, sodium bicarbonate is usually included in final hydrogenations to provide counter ions for the negatively charged phosphate groups as they were exposed (including in the previously described syntheses for 5-PP-Ins$P_{5/4,}$ apart from in the Zhang *et al*. route which generated the free acid and converted the product to a sodium salt after hydrogenation).[74,101,105–107] In the first chemical synthesis of an inositol pyrophosphate by Falck *et al.*, it was noted that the omission of a base in this final hydrogenation step led to the generation of more contaminants.[104] However, the inclusion of a base in the final hydrogenation reaction would be expected to slow the rate of debenzylation. Fortunately, the only benzyl groups which require cleavage in the synthesis of 5-PP-InsP_5 are attached to phosphates, and this occurs more readily than the cleavage of benzyl ether groups.

In the route detailed in this work, the final hydrogenation for 5-PP-InsP_5 was carried out in the presence of TEAB buffer rather than sodium bicarbonate. Using TEAB buffer also has the advantage of bypassing the need to measure precisely sodium hydrogen carbonate because, unlike sodium hydrogen carbonate, excess triethylammonium carbonate can be destroyed with successive co-evaporations with methanol. The use of TEAB buffer also eliminates the need to convert the salt form of the final product in purification. As the hydrogenation was found to take several days to be completed in the presence of TEAB buffer and the crude product contained several contaminants, sodium bicarbonate was used for future pyrophosphorylation sequence hydrogenations (requiring less time for full deprotection).

In the synthesis of 5-PP-InsP_5 (**2**), although the hydrogenation product generated was slightly contaminated, the reaction was found to be successful with sufficiently high yield.

The ^{31}PNMR signals of inositol pyrophosphates are often sharper prior to final purification with RP-18 chromatography, which can have a peculiar broadening effect on the phosphate peaks. Pyrophosphate signals in ^{31}PNMR spectra are sensitive to both counterions present and the pH of the solution in which they are analysed.[84]

Specifically, the signal of the β-phosphate significantly broadens and shifts upon exposure to extremes of pH, likely due to differences in internal hydrogen bonding and pK_a effects.[150] The addition of TEA base was found to aid in sharpening the signals of the slightly acidic product solution generated by the final hydrogenation. As a reverse-phase column would immediate follow and ideally remove all contaminants, the chelating agent EDTA (ethylenediaminetetraacetic acid) was also added to optimise the ^{31}PNMR spectra through the sequestering of trace metal cations that broaden the phosphate peaks through exchange processes.[84]

The final 5-PP-InsP_5 product (**2**) was then purified with a reverse-phase ion pair chromatography column (0-10% MeCN in 0.05 M TEAB), with the fractions containing phosphate-containing product identified with a qualitative Briggs Assay (refer to Experimental for details). Excess buffer present with the purified product was broken down through successive additions of methanol and vacuum-drying. The product was then analysed by NMR spectroscopy and was found to be sufficiently pure (no other phosphorus-containing species was found to co-elute with the product) to not require further purification with an ion exchange column and second reverse-phase column (30% yield for the pyrophosphorylation sequence).

The purified 5-PP-InsP_5 product (**2**) was then lyophilised to a colourless glass and stored as the triethylammonium salt in the -20°C freezer. The number of triethylammonium counterions was determined through integration of the ^{1}HNMR spectrum. As a precaution, this compound was treated as if it were unstable, but the final product appeared to be more stable than initially expected. Indeed, the triethylammonium salt of 5-PP-InsP_5 showed no signs of degradation when left in a solution of deuterated methanol at room temperature for over a month. It might be speculated that the salt form of the final product may contribute to the stability of the pyrophosphate product, although more analysis would be required to determine conclusively the impact of the counterion.

2.4.3 Continuation of the synthesis of 5-PP-InsP_4 (**3**) from the point of divergence

As shown previously, it was possible to diverge halfway through the synthesis route for 5-PP-InsP_5 (**2**) to generate 5-PP-InsP_4 (**3**) also (Scheme 1). The point of divergence was at the fourth step in the route to 5-PP-InsP_5 (**2**), immediately after the removal of the BDA-protecting groups (**7**). Rather than carrying out a hydrogenation to remove the benzyl-protecting group attached to the 2-position, the benzyl was allowed to remain in place to prevent the 2-position hydroxyl from being phosphorylated in the following step.

In an analogous fashion to the synthesis of 5-PP-InsP_5, the next step was the phosphorylation of the tetraol starting material (**7**) with dibenzyl phosphoramidite

followed by oxidation. As in the case of the pentaol (**8**) in the 5-PP-InsP_5 route, this phosphitylation proved to be more moisture-sensitive than other polyol phosphorylations (refer to Chapters 4 and 5), although to a lesser extent than in the 5-PP-InsP_5 route (**11**, 47% yield).

The pyrophosphate construction sequence (MSE deprotection and silylation, desilylation, phosphitylation, oxidation) to generate the protected 5-PP-InsP_4 precursor was completed in a similar manner as the equivalent pyrophosphate-forming steps of the 5-PP-InsP_5 synthesis route. Following the results in the differences in time between adding the TFA following the methanol previously in the desilylation step (Table 4), the time was allowed to be three minutes and the desilylation was confirmed through ^{31}PNMR to be complete.

With the knowledge accrued in the trial attempts to phosphorylate the 5-position phosphate in the 5-PP-InsP_5 route (Table 5), the final phosphorylation for 5-PP-InsP_4 was carried out with an excess of the weakly acidic activator and a shorter reaction time to prevent cyclisation and degradation respectively. As in the 5-PP-InsP_5 route, the protected pyrophosphate (**12**) was quickly purified using silica column chromatography prior to the final deprotection.

The hydrogenation to generate 5-PP-InsP_4 (**3**) was carried out in the presence of sodium bicarbonate rather than TEAB buffer to protect the pyrophosphate as it formed. It was hoped that the use of sodium bicarbonate and a slightly longer reaction time would allow for a cleaner reaction, while still removing the stubborn 2-position benzyl ether-protecting group, which was anticipated to be more difficult to remove than those attached as phosphate esters. Unfortunately, the hydrogenation still generated a number of contaminants so the product was purified with a reverse-phase ion-pair column, which also served to change the counterion from sodium to triethylammonium. After identifying the product-containing fractions through a qualitative Briggs assay, the product was found still to be slightly contaminated and was then purified on an anion exchange column. Due to the significantly higher concentration of TEAB buffer required for the ion exchange column resulting in the introduction of some hydrophobic contaminants, a final RP-18 column was required.

Before this final RP-18 column was carried out though, a sharp ^{31}PNMR spectrum of the product was obtained using addition of EDTA, which was subsequently removed in the final column. Finally, the purified product (**3**) was isolated, lyophilised to a colourless glass and stored as the triethylammonium salt in the -20°C freezer (9% yield). This product was then utilised by our collaborators in a crystallographic study of the *Sc*DDP1 enzyme (Section 2.5) as well as in the development of a europium-based inositol pyrophosphate luminescence probe (Section 2.6).

2.5 *Sc*DDP1 crystal structures

DIPPs (Diphosphoinositol Polyphosphate Phosphohydrolases) are the phosphatases responsible for dephosphorylating inositol pyrophosphates in humans.[42,50–52] They are part of a wider grouping of enzymes called nudix (nucleoside diphosphate linked moiety X) hydrolase enzymes, categorised because of their shared nudix motif (also known as the MutT domain), which acts as a dephosphorylating catalytic domain.[51,151] DIPPs, and their orthologues in other organisms, are able to cleave pyrophosphate bonds in many different substrates including inositol pyrophosphates (Figure 28), nucleoside diphosphates, nucleoside triphosphates, dinucleotides, RNA caps and inorganic polyphosphates (polyP).[54,151–153] The complete significance of DIPP function is not yet fully understood, though studies to determine the nuances of their activity are currently ongoing.[48,154]

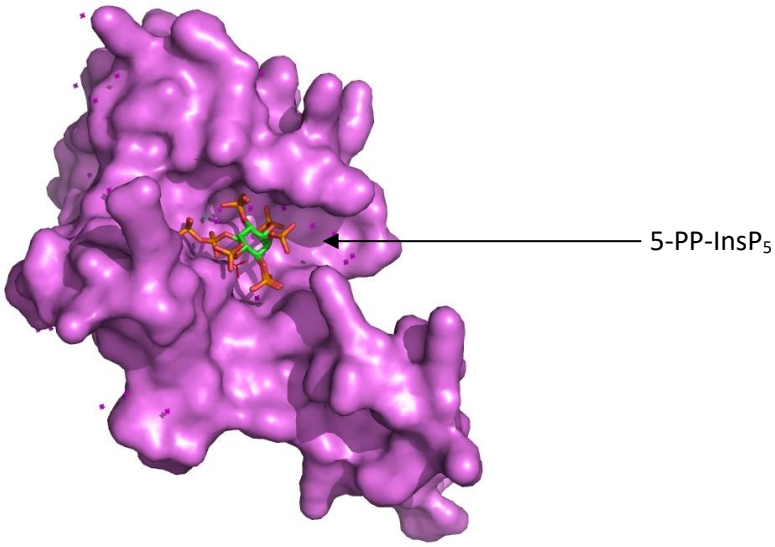

Figure 28: Structure of *Sc*DDP1 (yeast orthologue of DIPP) in complex with 5-PP-InsP_5, bound in its productive mode, in the presence of magnesium ions (PDB: 7AUL).

In mammals, five isoforms of DIPP exist and the genes which encode them have been identified: the *NUDT3* gene encodes for DIPP1; *NUDT4* for DIPP2 (existing as spliced isoforms DIPP2α and DIPP2β); *NUDT10* for DIPP3α; and *NUDT11* for DIPP2β.[48,52,140,155] DIPP1 appears to be the most active isoform, as it is approximately ten-fold to sixty-fold more active than either DIPP2 isoforms or DIPP3 isoforms, depending on substrate.[53] Although there are variations in substrate preference for the DIPP isoforms, the order in which inositol pyrophosphates are preferentially cleaved tends to the following: 1-PP-InsP_5 > 5-PP-InsP_5 = 1,5-PP-InsP_4.[154]

In addition to furthering the understanding of the intricacies of DIPP-catalysed dephosphorylations in mammals, there is additional interest in investigating the fungal orthologues of the enzymes due to the established connection between phosphorus metabolism and fungal virulence (e.g. 5-PP-InsP$_5$ is necessary for *Cryptococcus neoformans* pathogenicity).[137,141] Improved understanding of the enzymes crucial to maintaining levels of inositol pyrophosphates in fungi could hopefully lead to the development of selective drugs.[156]

Our collaborators in Madrid, the Beatriz González group, have been investigating how inositol pyrophosphates bind to the yeast orthologue of human DIPPs, *Sc*DPP1.[156] As in the case of the DIPP enzymes, *Sc*DPP1 does not exclusively dephosphorylate inositol pyrophosphates and also acts on a variety of pyrophosphate-containing substrates, such as diadenosine polyphosphates and inorganic polyphosphates (Figure 29).[54,156] In another similarity to its human orthologues, *Sc*DPP1 also displays a preference for dephosphorylating 1-PP-InsP$_5$ faster than both 5-PP-InsP$_5$ and 1,5-(PP)$_2$-InsP$_4$.[53] The work carried out in this investigation is, to our knowledge, the first to report crystal structures of the yeast *Sc*DPP1 enzyme, and also provides co-crystal structures to probe the structural basis for the observed promiscuity of a pyrophosphate phosphatase with its three main substrate types.[156]

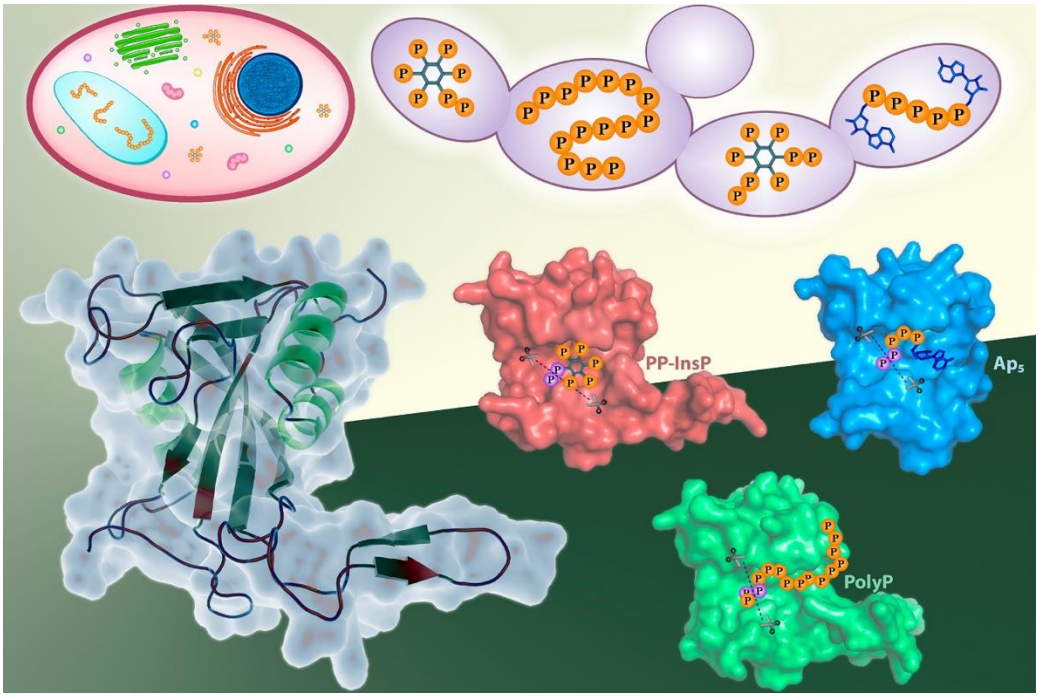

Figure 29: Schematic structure of *Sc*DDP1 in complex with its three main classes of substrates: inositol pyrophosphates (*Sc*DDP1 structure depicted in red), nucleotide polyphosphates (*Sc*DDP1 structure depicted in blue), and inorganic polyphosphates (*Sc*DDP1 structure depicted in green). Figure generated by the Beatriz González group for our collaborative Márquez-Moñino *et al.* study.[156]

The 5-PP-$InsP_5$ synthesised in this body of work (**2**, Section 2.4) was included in our recent collaborative crystallographic study into *Sc*DDP1 binding, along with $InsP_6$, 1-PP-$InsP_5$, and some non-hydrolysable analogues of inositol pyrophosphates prepared in the group: 1-PCP-$InsP_5$, 5-PCF-$InsP_5$, 1,5-$(PCP)_2$-$InsP_4$ and 1,5-$(PA)_2$-$InsP_4$ (Figure 30). In addition to the inositol pyrophosphates and their analogues, our collaborators co-crystallised *Sc*DDP1 with adenylyl-imidodiphosphate (AMP-PNP), adenosine 5'-triphosphate (ATP), HMP (hexametaphosphate), and Ap_5A, although these crystal structures will not be discussed in this thesis.[156]

When the inositol pyrophosphates and their analogues were co-crystallised with *Sc*DDP1 by the González group, it was found that some of the ligands were capable of occupying the enzyme active site in multiple orientations. Due to the differences in placement of the pyrophosphate group, some of the binding modes for the inositol pyrophosphates were predicted to be productive, while others appear to be unproductive.[156]

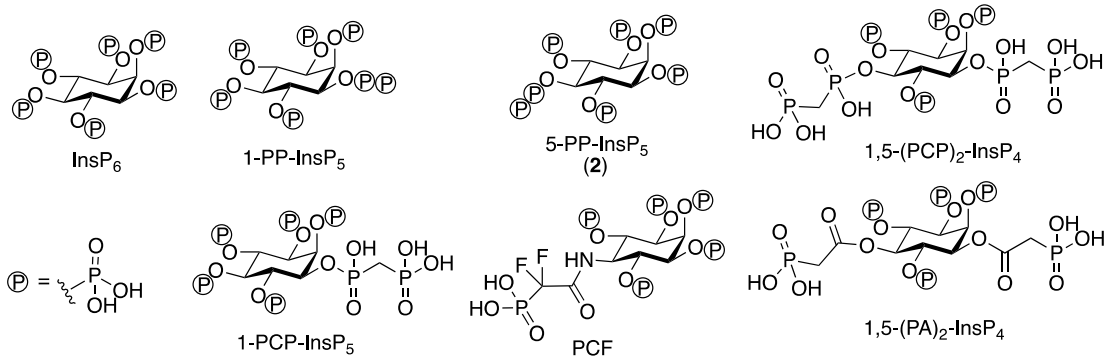

Figure 30: Inositol-based ligands that were co-crystallised with *Sc*DDP1. 5-PP-$InsP_5$ was synthesised in this study and the other ligands were synthesised previously by the Potter group.

When 5-PP-$InsP_5$ was crystallised with *Sc*DDP1, it appeared to bind in two different modes dubbed: bm1, which is thought to be non-productive (Figure 31) and bm3, which is thought to be productive (Figure 32).[156]

The non-catalytic binding mode of 5-PP-$InsP_5$-*Sc*DDP1, bm1, which is also the mode in which $InsP_6$ binds to *Sc*DDP1, positions the pyrophosphate group of 5-PP-$InsP_5$ away from the catalytic site of the enzyme (Figure 31). It appears as though this non-productive binding mode may even be the more energetically favoured of the possible binding orientations of 5-PP-$InsP_5$. All of the 5-PP-$InsP_5$ crystals that were generated in this study contained at least some amount of the bm1 binding mode.[156]

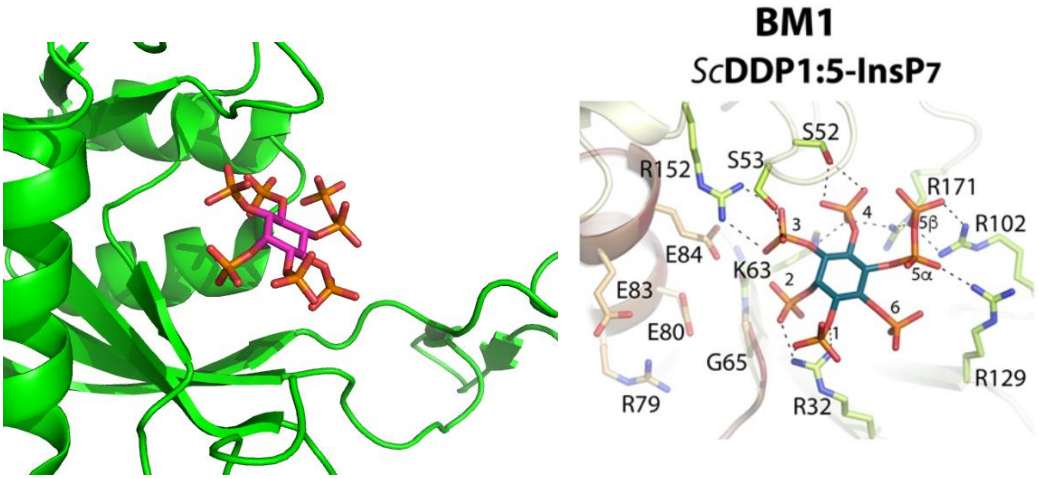

Figure 31: The panel on the left shows the crystal structure of the non-productive binding mode for 5-PP-InsP$_5$ in *Sc*DDP1 in the absence of magnesium (7AUK, 5-PP-InsP$_5$ in pink, *Sc*DDP1 in green).[156] The panel on the right is reproduced from Márquez-Moñino *et al.* and depicts the same non-productive binding mode (dubbed bm1) with some of the key residues involved in binding labelled and interactions shown (7AUK, 5-PP-InsP$_5$ in teal, *Sc*DDP1 in light green or cream).[156]

There is a possibility that the non-productive binding mode was only generated due to the non-physiological conditions, which do not accurately reflect cellular conditions. The notably low pH necessary to prevent pyrophosphate cleavage and, in some cases, the complete absence of magnesium ions used to generate some of the crystal structures could lead to the formation of binding modes that would not form under physiological conditions.

On the other hand, the presence of this non-productive binding mode could explain the observed ligand preference of *Sc*DDP1 in that 5-PP-InsP$_5$ is dephosphorylated much more slowly than its regioisomer, 1-PP-InsP$_5$. Indeed, in an enzyme kinetics study, it has been found that *Sc*DDP1 dephosphorylates 5-PP-InsP$_5$ at a rate approximately five times slower than it dephosphorylates 1-PP-InsP$_5$, although both regioisomers displayed similar K_m values (indicating similar affinity for the substrates binding to the enzyme).[53] These previous findings are in line with the theory that the preferred binding orientation of 5-PP-InsP$_5$ in *Sc*DDP1 is non-productive, while the preferred binding orientation of 1-PP-InsP$_5$ is productive.[53]

The other binding mode, bm3 (Figure 32), was expected to be productive due to the required placement of the pyrophosphate moiety in the catalytic domain. This binding mode was only observed when the enzyme was crystallised in the presence of magnesium ions, unlike bm1 which could form in their absence.[156] A magnesium ion was found to be incorporated into this binding mode, coordinating to both the α- and β-phosphates of the pyrophosphate group.

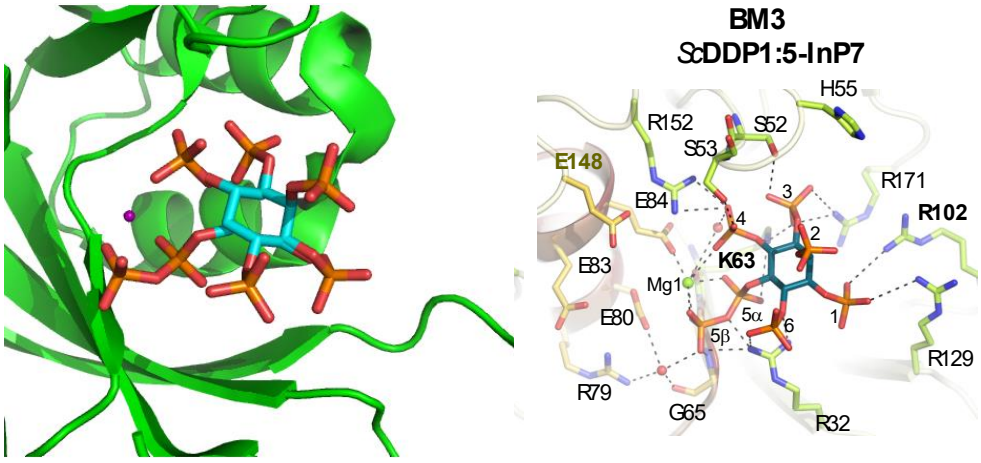

Figure 32: The panel on the left shows the productive binding mode of 5-PP-InsP$_5$-*Sc*DDP1 (bm3, 7AUL, 5-PP-InsP$_5$ in aqua, *Sc*DDP1 in green, magnesium ion in magenta).[139,156] The panel on the right is reproduced from Márquez-Moñino *et al.* and depicts the same *Sc*DDP1 productive binding mode (dubbed bm3) with the some of the key residues involved in binding labelled (bolded residues specific to *Sc*DDP1) and interactions shown (7AUL, 5-PP-InsP$_5$ in teal, *Sc*DDP1 in light green or cream).[156]

The analogue of 5-PP-InsP$_5$, 5-PCF-InsP$_5$ was found to bind in an orientation somewhat similar to bm1, although the placement of the pyrophosphate-mimicking PCF group differs slightly. Thus 5-PCF-InsP$_5$ was established to occupy *Sc*DDP1 in a new binding mode dubbed bm4.[156]

Crystal structures of the other naturally occurring regioisomer of InsP$_7$ in most organisms, 1-PP-InsP$_5$, as well as its non-hydrolysable analogue, 1-PCP-InsP$_5$, bound to *Sc*DDP1 were also obtained in this study. Both ligands were found to occupy the binding site in the same mode dubbed bm2, which positioned the axial phosphate attached to the 2-position out into solvent and the pyrophosphate group (or bisphosphonate analogue) into the catalytic site.[156]

Although InsP$_8$ itself was not included in the study, two non-hydrolysable analogues, 1,5-(PCP)$_2$-InsP$_4$ and 1,5-(PA)$_2$-InsP$_4$, were used to obtain *Sc*DDP1 crystal structures. The 1,5-(PA)$_2$-InsP$_4$ analogue was found to bind in the non-productive bm1 mode, whereas the 1,5-(PCP)$_2$-InsP$_4$ analogue, which is a closer structural mimic to 1,5-(PP)$_2$-InsP$_4$, was found to bind in a new mode dubbed bm5 that significantly twisted the substrate to position the 1-position bisphosphonate group in the catalytic site. Docking simulations carried out by the González group indicated that 1,5-(PP)$_2$-InsP$_4$ probably adopts the bm3 binding mode in *Sc*DDP1, as this would allow for the cleavage of the 5-position pyrophosphate while the 1-position pyrophosphate could face out of the binding site and not interfere with the substrate being accommodated by the enzyme.[156]

Although there are no other crystal structures of DDP1, there have been a few crystallographic studies which have investigated substrate binding to DIPPs, the

human orthologue of *Sc*DDP1.[138,139,154] The initial study detailed in Thorsell *et al.* produced two crystal structures that demonstrated that $InsP_6$, the product of $InsP_7$ dephosphorylation, is able to bind to DIPP1 in two different conformations (one of which is now thought to be a longer-lived binding mode that keeps the enzymes in an inhibited state).[138,154]

The study initially predicted the wrong isomer of $InsP_8$ [3,5-$(PP)_2$-$InsP_4$] as being the endogenous ligand of DIPP1 due to the ligand interactions calculated in molecular docking, although this was later corrected to naturally occurring regioisomer [1,5-$(PP)_2$-$InsP_4$].[47,138] A later study by Dollins *et al.* reported high resolution (1.2 Å) crystal structures of DIPP1 in complex with 1-PP-$InsP_5$ (PMB: 6PCK) and 5-PP-$InsP_5$ (PMB: 6PCL).[139] The crystal structures of DIPP1 in complex with its substrates were obtained at low pH, which prevented the phosphatase activity of the enzyme, preserving the phosphoanhydride bond of the inositol pyrophosphate in the enzyme active site.[139] A recent study has also been reported by Zong *et al.* that further investigated the binding of inositol phosphates, inositol pyrophosphates and their non-hydrolysable (PCP) analogues to *Hs*DIPP1.[154]

From comparison of the binding modes of the orthologues, it is apparent that the productive binding mode of 5-PP-$InsP_5$-*Sc*DDP1, bm3, matches the orientation of the analogous 5-PP-$InsP_5$-*Hs*DIPP1 crystal structure (6PCL, human diphosphoinositol polyphosphate phosphohydrolase) structure (Figure 33).[139,156] The magnesium ion present in bm3 also appears to be located in approximately the same region as one of the three magnesium ions present in the 5-PP-$InsP_5$-*Hs*DIPP1 structure (Mg1).[139,156]

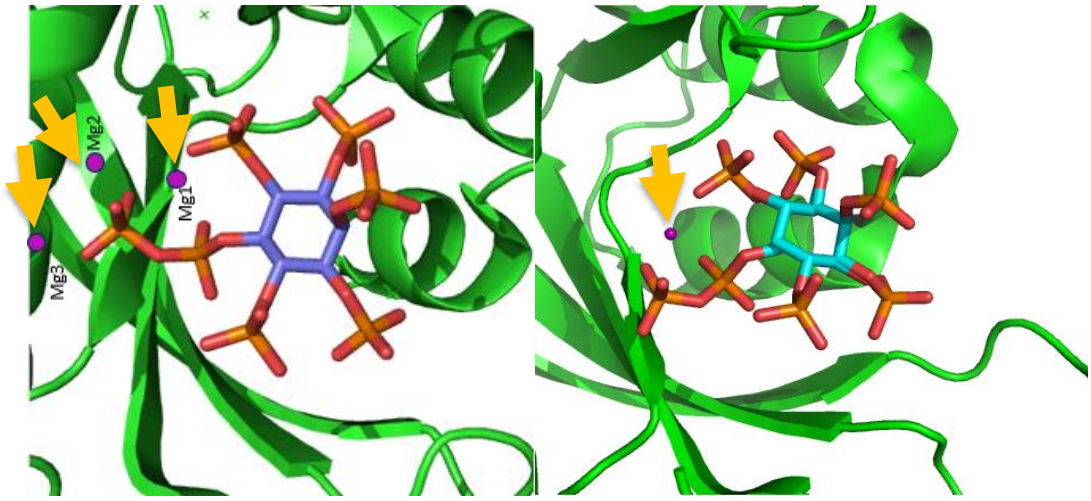

Figure 33: Comparison of the crystal structures of 5-PP-$InsP_5$-*Hs*DIPP1 (6PCL, left panel, 5-PP-$InsP_5$ in purple, *Hs*DIPP1 in green, magnesium ions in magenta with large yellow arrows indicating their positions) and the productive binding mode of 5-PP-$InsP_5$-*Sc*DDP1 (bm3, 7AUL, right panel, 5-PP-$InsP_5$ in aqua, *Sc*DDP1 in green, magnesium ion in magenta, indicated with a yellow arrow).[139,156]

The three different magnesium ions in the 5-PP-InsP$_5$-*Hs*DIPP1 are expected to play different roles in the human DIPP1 enzyme complex including: the correct positioning of the substrate (Mg1 and Mg3); influencing catalytic activity of the enzyme (Mg2 and Mg3); and possibly even promoting the nucleophilic attack of a water molecule on the pyrophosphate phosphodiester linkage (Mg3).[138,139,154,156]

There is a possibility that the artificially acidic crystallisation conditions may have interfered with the magnesium ion placement in the 5-PP-InsP$_5$-*Sc*DDP1 complex, and three magnesium ions may be present when the complex forms under biological conditions (although the human orthologue complex was also crystallised under physiological and acidic conditions).[139,156] However, the yeast orthologue of DDP1 may only require one magnesium ion positioned in the active site to successfully catalyse pyrophosphate cleavage.[156]

There are a number of conserved glutamic acid, arginine and glycine residues that interact with the same phosphates of 5-PP-InsP$_5$ in both *Hs*DIPP1 and *Sc*DDP1 binding sites.[138,154,156] There are two key residues involved in substrate binding in *Sc*DDP1, Lys63 and Arg102, which do not have equivalents in the orthologues of the enzyme. It is hoped that these unique residues may allow for the future development of selective inhibitors.

Ultimately, this latest study into the binding of inositol pyrophosphates and analogues to *Sc*DDP1 has furthered the general understanding of inositol pyrophosphate metabolism and how these pyrophosphates are cleaved. In addition to obtaining crystal structures of multiple binding modes of multiple substrates and pseudo-substrates for this yeast enzyme, this study was able to suggest an explanation for the substrate specificity of InsP$_7$ regioisomers (due to the possibility that the non-productive binding mode for 5-PP-InsP$_5$ seems to be favoured). It is hoped that the new information concerning details of substrate-binding to *Sc*DDP1 might aid in the development of fungal-specific DIPP inhibitors.[156]

2.6 Europium complex assay

Lanthanide complexes have been found to be useful in a number of different biological contexts including as MRI contrast agents, therapeutic agents and luminescent sensors that allow for cellular imaging.[157,158]

Our collaborators, the Stephen Butler lab in Loughborough University, have designed a selection of europium complexes to monitor levels of nucleoside polyphosphate (NPP) anions at physiological pH in real-time with a microplate assay. This allows for easy tracking of the activity of kinases and glycotransferases in a non-invasive, high-throughput method suitable for compound screening.[159] Only a small amount of europium complex was found to be required (5 μM) to generate a sufficient luminescence signal and, due to the fast and reversible binding of NPP anions to the complexes, the presence of the europium complex was not expected to have a significant effect on the concentrations of ATP within cells and should not interfere with the monitoring of, for example, ATPase activity.[159] It has been found to be a viable method for tracking the ratio of ATP to ADP through analysis of luminescence emission.[160]

In addition to phosphate-containing compounds, europium luminescence probes have previously been used to track levels of citrate and lactate in biological settings.[161]

As 5-PP-InsP_5 and other inositol pyrophosphates are present in cells, it was of interest to explore if a novel assay method for their detection and breakdown against the background of other cellular phosphate and pyrophosphate-containing ligands might be possible, and this was the stimulus for the collaboration. The 5-PP-InsP_5 synthesised in this project (**2**) has therefore been used to determine if the scope of these europium-based luminescence assays could, in principle, be expanded to track intracellular levels of inositol pyrophosphates.

Europium complex assays have several advantages over some of the other techniques by which enzymes can be monitored including elimination of the need for expensive antibodies and chemically labelled substrates. Additionally, the luminescence complex allows for real-time quantitative monitoring that does not require isolation or purification steps of the product.[160]

During the luminescence assays, the europium complex is initially irradiated with UV light, after which the excited europium centre decays to emit visible light, with specific emission spectra affected by the ligands bound to the europium centre. Upon irradiation with UV light, europium ion electrons could theoretically undergo f-f orbital transitions in a direct excitation, although these transitions are symmetry forbidden (Laporte forbidden). Despite being forbidden on symmetry grounds, the f-f transitions are allowed to hypothetically take place when the symmetry of the complex is

distorted, such as by asymmetric vibrations resulting in weak absorption. Sensitisation of the lanthanide ion from chelating organic chromophores in the 'antenna effect' is a much more effective excitation method that allows the Laporte selection rule to be overcome and the $^5D_0$ Eu excited state to be populated.[162,163] The antenna effect is the phenomenon by which energy is transferred from a strongly absorbing chromophore ligand to the lanthanide ion centre. Chelating ligand cages can be constructed that contain strongly UV-absorbing moieties such as the aromatic quinoline rings, which are able to efficiently collect and transfer energy to the europium ion centre.[160,162] The excited europium centre decays through the emission of visible light in the red-orange region of the visible light spectrum: 580-720 nm (Figure 34).[162]

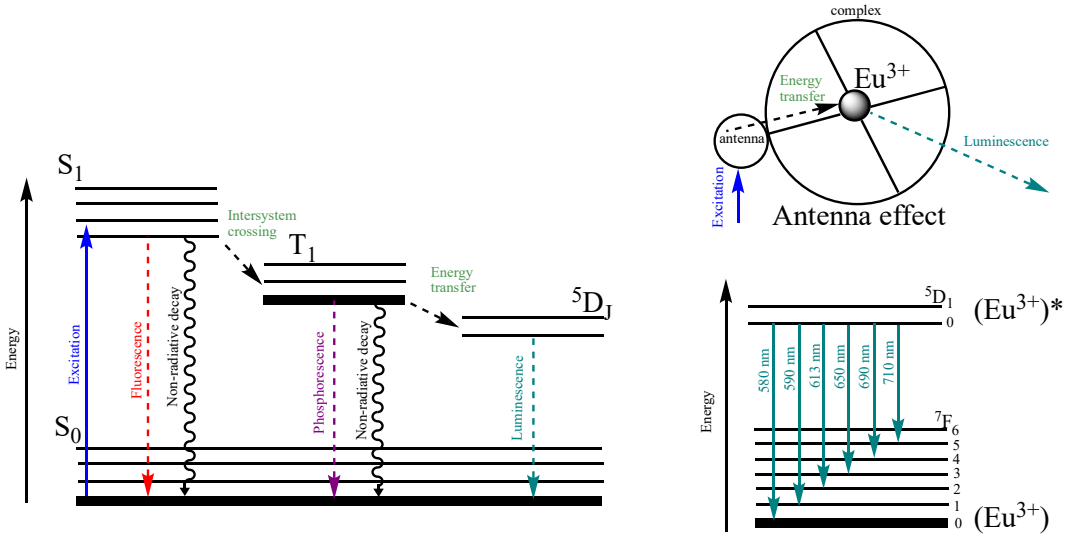

Figure 34: On the left is a simplified Jablonski diagram indicating the main energy pathways involved in europium sensitisation. The top right displays a diagram illustrating the antenna effect and the bottom right displays a simplified Jablonski diagram that shows the 4f-4f transitions of europium ions with the corresponding luminescence wavelengths shown.[164,165]

The luminescence decay emissions for these lanthanide complexes follow an f-f orbital transition from the excited ion in a Laporte forbidden transition, which, as a consequence, occurs on a longer timescale.[166,167] Rather than fluorescence, the term *luminescence* was coined in the 1800s to describe both short- and long-lived emissions that are independent of temperature (whereas fluorescence is usually reserved for only short-lived emissions on a nanosecond scale).[162] It is this long-lived nature (milliseconds for europium complexes) of the light emission that allows for the easy separation of the lanthanide complex luminescence from any endogenous fluorescence that would occur from biological samples, rendering lanthanide complexes exceptionally useful for cellular imaging.[158,162]

In addition to collecting UV energy and transferring it to the central europium ion, the ligands function to shield the metal centre from the aqueous environment and

prevent the coordination of water, thereby minimising non-radiative decay of the excited europium ion.[162,167] The ligands typically used are nonadentate or octadentate to ensure that water molecules are completely, or near-completely, excluded from the europium centre.[162] The octadentate complexes have one position available for coordination of a single water molecule that subsequently quenches europium luminescence. Displacement of this single water molecule can then occur with the reversible binding of ligands, rendering these complexes potentially useful as probes (Figure 35).

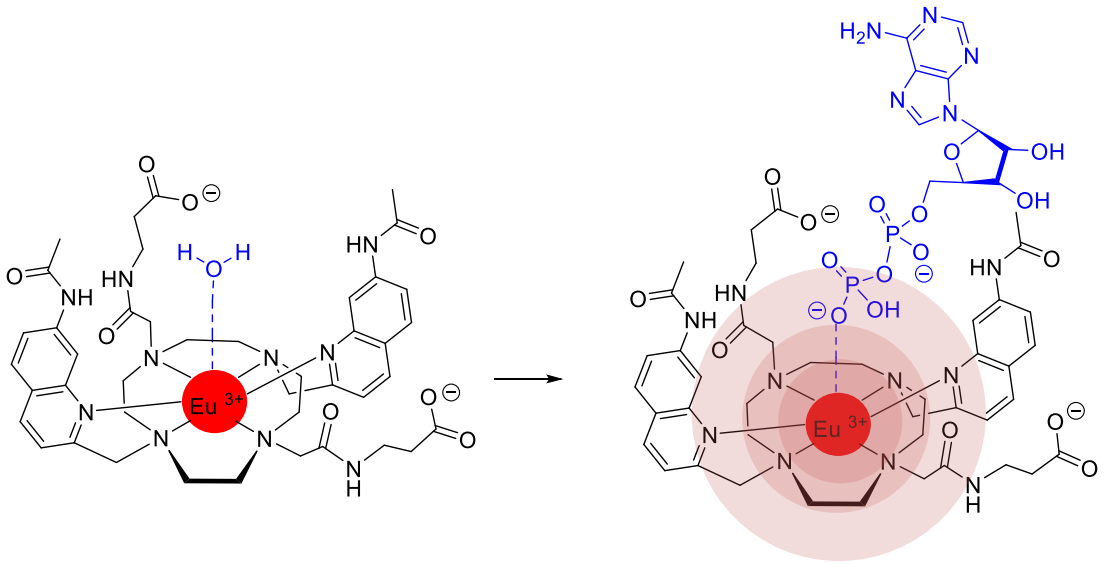

Figure 35: Structure of the Eu.L5 europium complex coordinated first with a molecule of water that quenches luminescence emission and then with ADP, which displaces the water molecule and promotes luminescence.[166]

The structure of the octodentate ligand that chelates the central europium ion can be adjusted to improve the ability of the complex to differentiate between different NPP substrates and affinity for certain ligands. Distinct detection of NPPs should then be possible, as the emission spectra obtained from the europium complexes when bound to different NPP ligands varies.[159]

In this study, a series of europium complexes first described in the Mailhot *et al*. study (Figure 36) were investigated to determine which would provide the best emission spectrum with 5-PP-InsP_5, assuming this pyrophosphate-containing compound would be able to bind sufficiently in the assays.[159] One complex, referred to as Eu.L5, was found to generate the most luminescence when bound to 5-PP-InsP_5, while also producing a weaker response to InsP_6 binding, indicating some sensitivity and selectivity for inositol pyrophosphates for the assay (Figure 37).

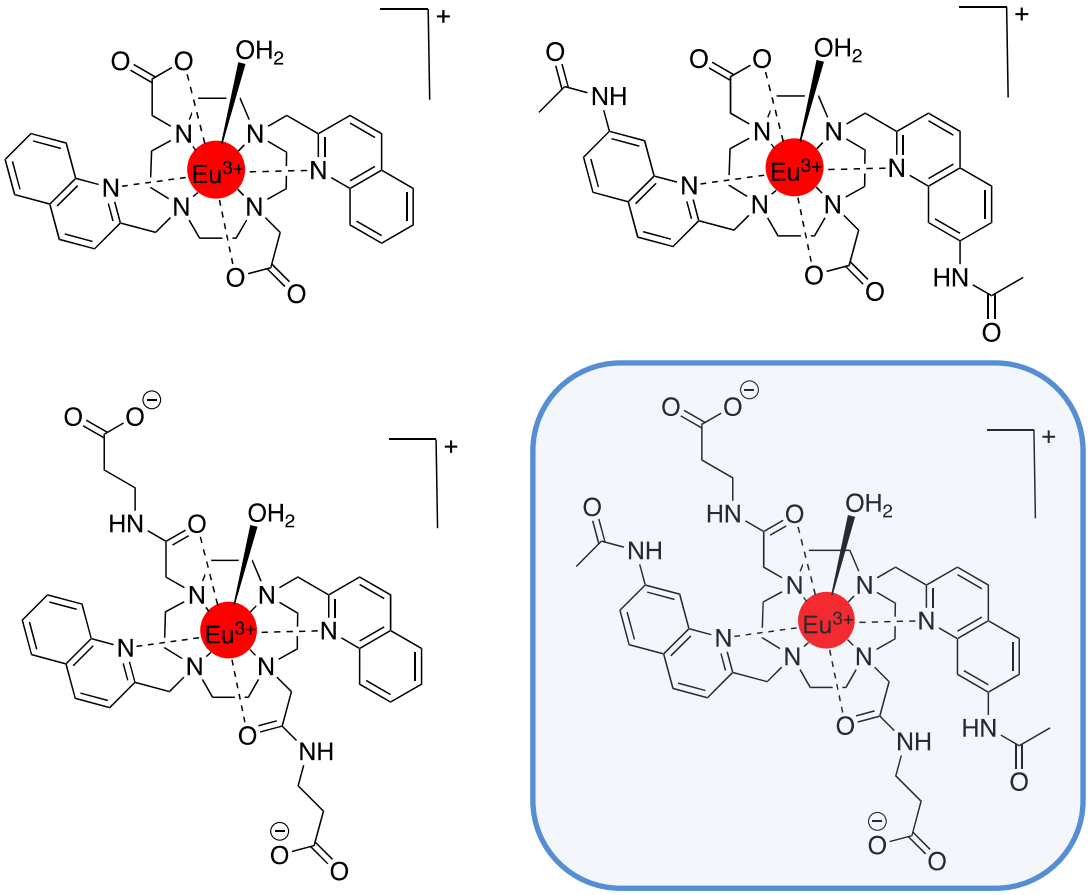

Figure 36: Structures of octadentate europium complexes (originally described in Mailhot *et al.*) used in this body of work to determine if 5-PP-InsP$_5$ can be differentiated from InsP$_6$.[159] The complex highlighted in blue, dubbed [Eu.3]$^+$ in the original study but later referred at as Eu.L5, was found to be the most effective in detecting and differentiating inositol pyrophosphates and inositol phosphates.

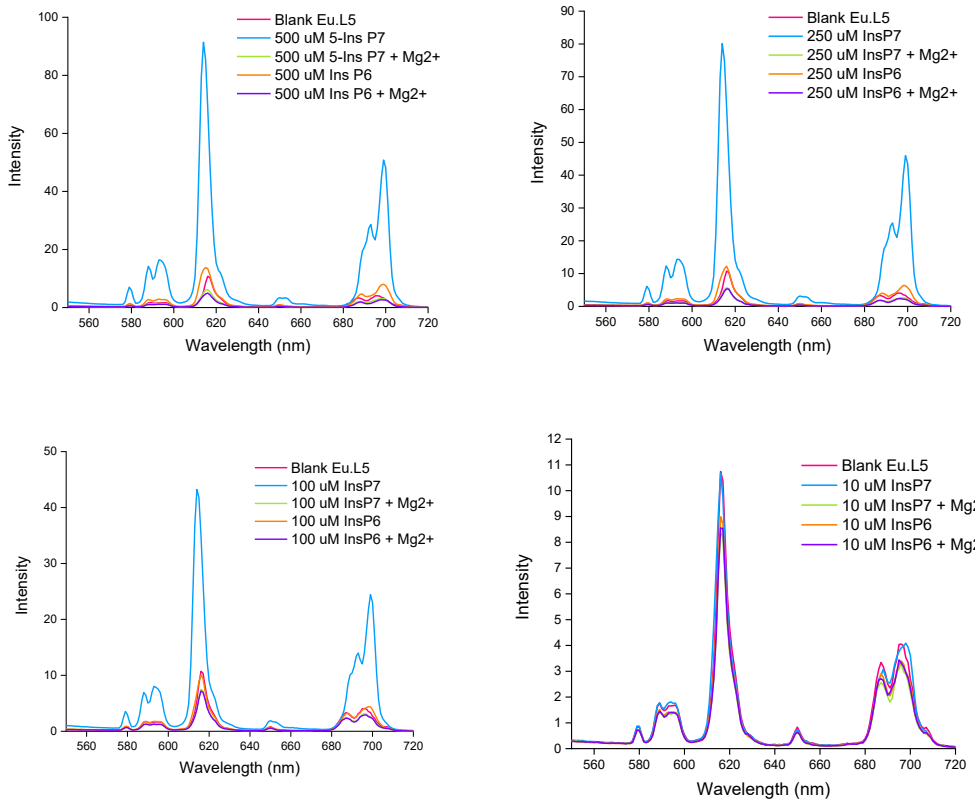

Figure 37: Overlaid luminescence emission spectra of the most effective europium complex, Eu.L5 (Figure 36) coordinated to 5-PP-InsP$_5$ (labelled 5-InsP$_7$ or InsP$_7$) and InsP$_6$ at different concentrations in the presence or absence of magnesium ions. Luminescence assay performed by F. A. Jamion from the Stephen Butler lab.

The Eu.L5 complex was one of two octodentate complexes tested that contained neutral carbonyl amide hydrogen bond donor groups to improve the selectivity of the complex for binding to more negative ligands. Indeed, these complexes were proved to be better at differentiating the more negative pyrophosphate-containing 5-PP-InsP$_5$ over the InsP$_6$ anions, which possesses only monophosphate groups and a weaker overall negative charge.[159]

In addition to the amide groups, there were a few other features that improved the ability of Eu.L5 to bind to 5-PP-InsP$_5$. This complex also features amide-derivatised quinoline groups which are able to hydrogen bond to the europium centre, thereby increasing the electropositivity of the central ion and facilitating coordination to ligand pyrophosphate moieties. The terminal carboxylate groups in the Eu.L5 complex improve solubility of the complex in an aqueous solution.[160]

The Eu.L5 europium complex has previously been found to be suitably sensitive to monitor endogenous levels of ATP (around 1 mM) in the presence of biologically relevant levels of magnesium ions. From initial experiments to investigate the

sensitivity of the Eu.L5 complex, it was thought that the complex may not be useful in biological contexts as it did not appear to be able to detect 5-PP-InsP$_5$ at 10 µM (Figure 37). Subsequent investigation, however, found that the complex was able to successfully detect 5-PP-InsP$_5$ at 25 µM, which could be suitably sensitive for tracking this inositol pyrophosphate in at least some biological contexts.

The distinct shapes of the spectral emissions from the complex when bound to different ligands indicate changes in the coordination environment around the europium centre (as a result of different binding geometries). The Eu.L5 complex has previously been shown to produce different luminescence emission spectra following binding to ATP, ADP and AMP in a HEPES-buffered solution that mimics intracellular conditions. The spectra generated by ATP and ADP were sufficiently different to allow the ratio of these two compounds within cells to be tracked.[166] In this study, the luminescence emission spectra generated by the Eu.L5 complex in the presence of ATP, ADP, PPi and 5-PP-InsP$_5$ were collected and compared to determine if the patterns of emission bands varied enough to distinguish the inositol pyrophosphate signals (Figure 38).

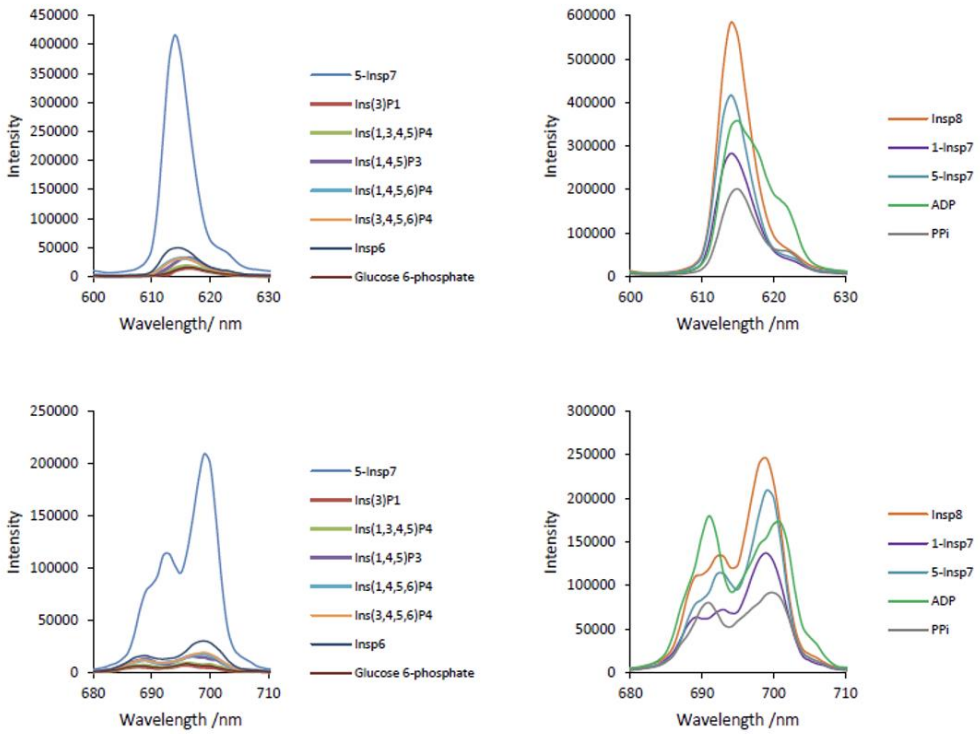

Figure 38: Luminescence emission spectra for the Eu.L5 complex when in the presence of different ligands between 600-630 nm for the ΔJ= 2 band (top row) and 680-710 nm for the ΔJ= 4 band (bottom row). Luminescence assay performed by F. A. Jamion from the Stephen Butler lab.

While the emission spectrum for 5-PP-InsP$_5$ binding to Eu.L5 was found broadly to be similar to those generated following the coordination of other pyrophosphate-

containing ligands, there were a few pronounced differences between some of the emission bands in some of the ligands (Figure 38).

Specifically, between 600-630 nm (corresponding to a ΔJ= 2 emission as shown in the simplified Jablonski diagram for the europium luminescence emission in Figure 34) the emission spectrum for 5-PP-InsP_5 displayed a single intense peak in this region (around 615 nm), while the spectra for ADP and PPi contained an additional secondary peak (around 620 nm) absent in the inositol pyrophopshate spectra (Figure 38).[165]

Another difference in the emission spectra can be observed between 680-710 nm (corresponding to a ΔJ= 4 emission as shown in Figure 34) in which 5-PP-InsP_5 and the other inositol pyrophosphates possess a more intense peak around 700 nm, while the emission peaks for ADP and PPi are slightly shifted and their other peaks in the region (around 690 nm) are more prominent (Figure 38).[165]

Although further experiments will be required to determine how the emission spectra can be used to track levels of inositol pyrophosphates in the presence of other pyrophosphate-containing ligands, the minor differences in the emission spectra presented here are a promising start. Unfortunately, the emission spectra generated by the different inositol pyrophosphates, 1-PP-InsP_5, 5-PP-InsP_5 and 1,5-$(PP)_2$-InsP_4, appear to be too similar to differentiate, although further investigation into the possibility of distinguishing assay responses generated by these inositol pyrophosphates is underway. Due to the very low endogenous quantities of 1-PP-InsP_5 and 1,5-$(PP)_2$-InsP_4 compared to 5-PP-InsP_5, the ability of the assay to differentiate inositol pyrophosphates also may not be critical, depending on the proposed usage of the assay.

The Butler group generated proposed binding modes for the 5-PP-InsP_5 using computational methods, first building and optimising the structures in Avogadro before employing Q-chem to further optimise the structures and determine likely binding orientations and calculating associated binding energies. It was determined through this computational model that 5-PP-InsP_5 is able to bind in two possible modes, one of which is monodentate and the other bidentate (Figure 39).

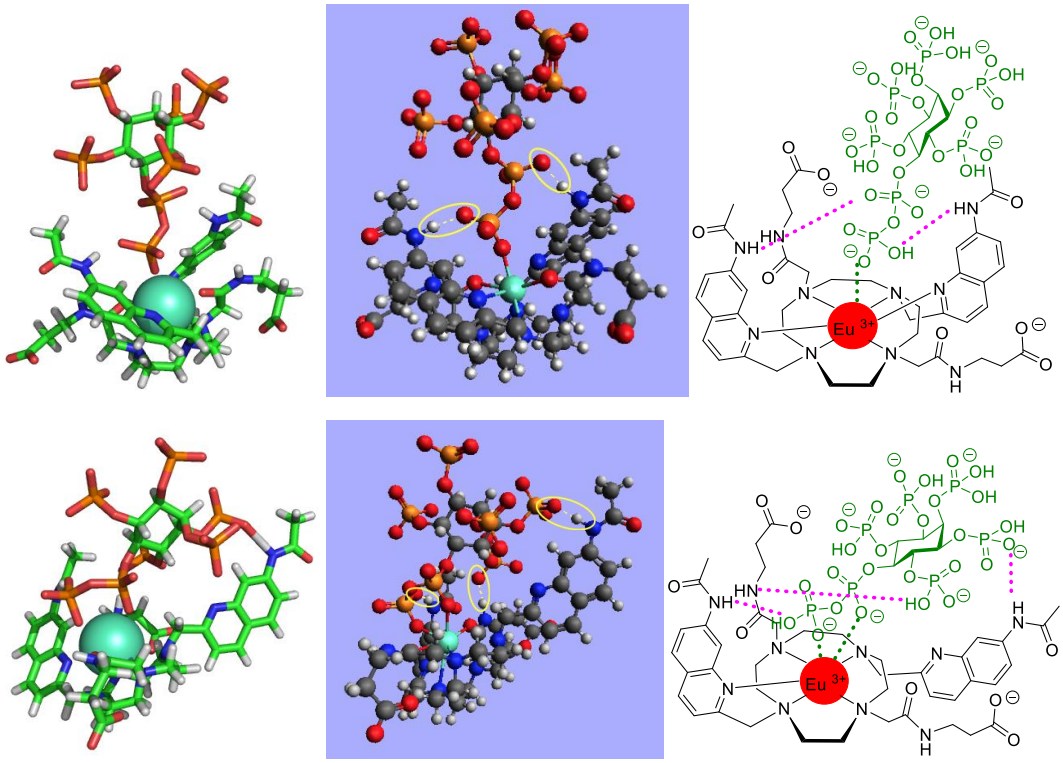

Figure 39: The proposed monodentate binding mode for 5-PP-InsP$_5$ in the Eu.L5 complex (top row) and the proposed bidentate binding mode for 5-PP-InsP$_5$ in the Eu.L5 complex (bottom row). The binding modes were generated in a computational study carried out by the Butler group using Avogadro and Q-chem software. The figures on the left display 5-PP-InsP$_5$ in the Eu.L5 complex with the europium ion in teal, carbon atoms in green, oxygen atoms in red, phosphorus atoms in orange, nitrogen atoms in blue and hydrogen atoms in white. The figures in the centre depict the binding modes with the hydrogen bonds circled in yellow (and the same colours for the atoms as the figures on the left apart from carbon depicted in grey). The figures on the right depict both binding modes with the hydrogen bonds between the 5-PP-InsP$_5$ ligands and the Eu.L5 complex shown in dotted pink lines. Modelling performed by F. A. Jamion of the Stephen Butler group.

The monodentate binding mode, which appeared to be superficially similar to the calculated binding mode for InsP$_6$, was determined to include two hydrogen bonds between the quinolone side arms of the complex and phosphate groups of the inositol pyrophosphate. The bidentate mode for 5-PP-InsP$_5$ binding is thought to be the more likely binding mode, however, due to the fact that the calculations indicated it is more stable than the monodentate mode by 27 kJ/mol. The accommodation for the pyrophosphate group to form two bonds to the europium centre is possible due to the apparent displacement of one of the quinolone side arms of the complex. Additionally, the bidentate mode appears to include the formation of three hydrogen bonds to the phosphate groups from the complex side arms.

As it has been established that the europium complex is able to generate luminescence, further experiments were carried out to investigate the viability of the assay for potentially monitoring phosphatase or kinase activity through tracking

$InsP_6$/5-PP-$InsP_5$ levels. It was first determined that Eu.L5 complexed with 5-PP-$InsP_5$ is very stable and the luminescence only decreased by 6% after one hour, rendering the assay potentially useful for high-throughput screening.

It was also found in a preliminary binding titration study that the europium complex binds to 5-PP-$InsP_5$ with a binding affinity of $LogK_a$ = 4.71±0.09, which is approximately 100-fold greater than the binding affinity of $InsP_6$, which has a binding affinity of $LogK_a$ = 2.85±0.06 (although the binding affinity of $InsP_6$ must be treated with caution until it can be repeated, as the initial experiment could not reach the maximum concentration of the ligand due to stock shortages).

A further investigation into the ability of this assay to distinguish 5-PP-$InsP_5$ from $InsP_6$ at low concentrations, an enzyme simulation study, was carried out through measuring the luminescence emission generated as the Eu.L5 complex was exposed to a systematically increasing ratio of 5-PP-$InsP_5$/$InsP_6$, with the total concentration of inositol phosphates remaining fixed (Figure 40). The increase in emission observed was found approximately to correlate linearly with the ratio of 5-PP-$InsP_5$ in solution (with 25 µM being the lowest viable concentration for signal detection), which is a promising result for the prospect of being able to use this assay to indicate the progress of enzymes that consume or create this inositol pyrophosphate.

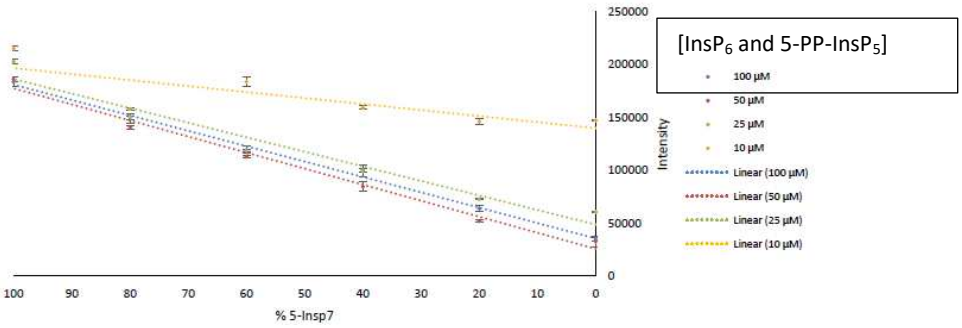

Figure 40: Enzyme simulation study indicating the decrease in the intensity of the luminescence emission of Eu.L5 when exposed to different total concentrations of 5-PP-$InsP_5$/$InsP_6$ as the ratio of 5-PP-$InsP_5$ decreases in the fixed total inositol polyphosphate concentration. This enzyme simulation assay was performed by F. A. Jamion of the Stephen Butler group.

Following the success of the enzyme simulation study, the Eu.L5 complex assay was used to track the progress of a DIPP1 phosphatase cleaving the pyrophosphate of 5-PP-$InsP_5$ (Figure 41). The correlation between enzyme activity and luminescence emission in the first forty-five minutes was the most reliable, as the effect of photobleaching and background hydrolysis was minimal until approximately that point. The emission intensity appeared to decrease with enzyme activity until it reached a plateau, having decreased by approximately 20% of the initial luminescence. While it is possible to monitor the activity of the enzyme with this

change in luminescence, the decrease is significantly less dramatic than expected from the previously established low emission intensity generated by $InsP_6$ (Figure 40). The unexpectedly low decrease in luminescence emission intensity requires further investigation.

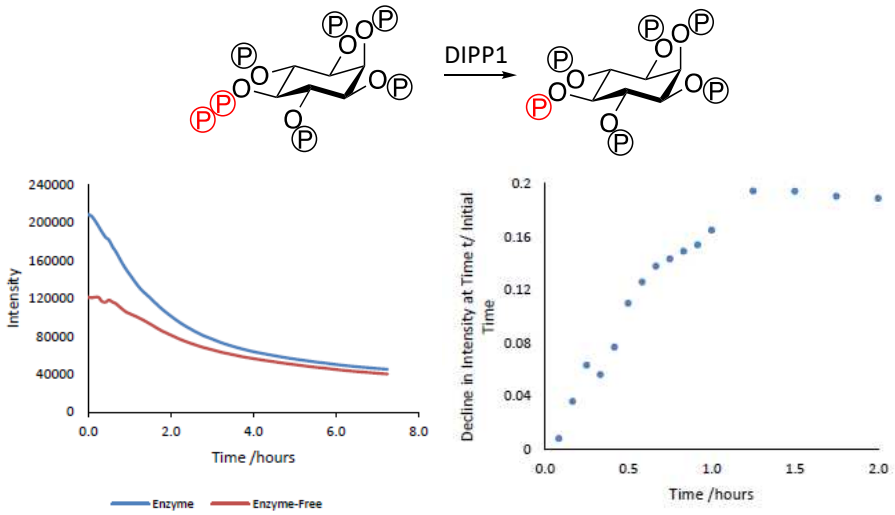

Figure 41: On the left is the decay curves of enzyme reaction (converting 5-PP-insP_5 to $InsP_6$, shown above) and the enzyme-free control. Measurements were taken every 5 minutes for the first hour, then every 15 minutes between 2-7 hours, with the average of triplicate reactions depicted. On the right, the decrease in the emission intensity of the Eu.L5 assay over time indicating the activity of DIPP1 is depicted. Surprisingly the final net decrease in luminescence emission intensity appeared to plateau at approximately 20%. These enzyme assay were performed by F. A. Jamion of the Stephen Butler group.

Although the unexpectedly low decrease in observed luminescence emission in preliminary DIPP1 study must be investigated, this experiment demonstrated that the Eu.L5 complex seems to be able to indicate the progress of a DIPP enzyme reaction through tracking levels of 5-PP-$InsP_5$ in the presence of $InsP_6$. The use of the europium luminescence assay to monitor phosphatase activity is currently being further optimised.

Further investigations are also required before the full scope of using europium complex assays to monitor inositol pyrophosphates is explored in other settings including: investigating what effect the presence of a wider range of anions abundant in cells (such as citrate and bicarbonate) has on the emission spectra; further investigating the binding affinities of the inositol pyrophosphates and $InsP_6$ through titration experiments; and determining the possible reason for the lower observed emissions from 1-PP-$InsP_5$ compared to its regioisomer 5-PP-$InsP_5$ through further computational modelling.

The results included in this body of work are a promising start for the possible development of a high-throughput screening method to identify potential inhibitors for DIPPs, which could prove to be useful in the development of therapeutic agents targeting these enzymes.

(3) Inositol pyrophosphate: 1,5-$(PP)_2$-$InsP_4$

3.1 Specific biological roles of 1,5-$(PP)_2$-$InsP_4$

In many organisms including animals and yeast, the most common regioisomer of $InsP_8$, D-1,5-$(PP)_2$-$InsP_4$, has the pyrophosphate groups attached to the *myo*-inositol ring at the 1- and 5-positions (Figure 42).[46,47] Although it is not usually present in very high concentrations in cells (<0.05-1 µM, lit.[31,33]), it is believed to be involved in a number of biological roles including cell growth, phosphate homeostasis, cell proliferation, protein pyrophosphorylation and cellular metabolism.[48,61] While the exact contribution of 1,5-$(PP)_2$-$InsP_4$ towards these biological functions is not yet well understood, a few studies have begun investigating the specific involvement of this inositol pyrophosphate.

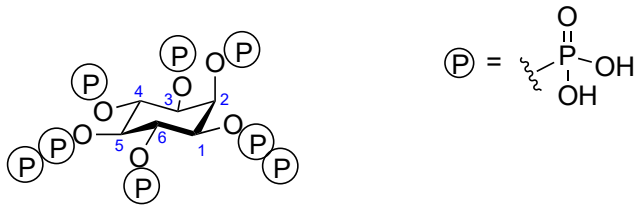

Figure 42: Structure of D-1,5-$(PP)_2$-$InsP_4$ (**16**).

Unlike 5-PP-$InsP_5$, cellular levels of 1,5-$(PP)_2$-$InsP_4$ appear to be linked to energy homeostasis.[64] It has also been found that the cellular levels of 1,5-$(PP)_2$-$InsP_4$ increased significantly when cells were put under hyperosmotic or thermal stress (through stress-elevated PPIP5K activity), but decrease when under bioenergetic stress.[64,168,169] It was also found that levels of 1,5-$(PP)_2$-$InsP_4$ fluctuate much more dramatically than those of $InsP_7$ or ATP when cells are starved of inorganic phosphate (P_i), indicating that 1,5-$(PP)_2$-$InsP_4$ likely has its own distinct role in signalling in phosphate homeostasis.[170] Further evidence for the involvement of 1,5-$(PP)_2$-$InsP_4$ in phosphate homeostasis has been recently found in the ability of this specific inositol pyrophosphate to regulate the SPX-domain containing XPR1 P_i exporter protein.[125]

The role of 1,5-$(PP)_2$-$InsP_4$ in plants is also under investigation, with some evidence that this inositol pyrophosphate acts specifically as the main mediator of the Phosphate Starvation Response Regulator 1 transcription factor (PHR1), forming a complex with SPX domain-containing proteins.[19]

There may also be a connection between irregular cellular levels of 1,5-$(PP)_2$-$InsP_4$ and keratoconus, a condition that results in vision impairment, due to the genetic factor linked to pathogenesis. A variant of the PPIP5K2 gene, which promotes the

synthesis of 1,5-$(PP)_2$-$InsP_4$ through both an increase in its kinase activity and decrease in its phosphatase activity, has been found to be potentially associated with the disease.[171]

Another study identified a variant of PPIP5K2 with hyperkinase activity and decreased phosphatase activity [resulting in 1,5-$(PP)_2$-$InsP_4$ levels that are approx. 60% higher than in WT cells] that seems to be associated with sensorineural hearing loss. These conditions associated with PPIP5K2 variants could be due to changes in 1-PP-$InsP_5$ levels [although the Yousaf *et al.* study on hearing loss suggested that this is unlikely, due to the significantly lower levels of 1-PP-$InsP_5$ than 1,5-$(PP)_2$-$InsP_4$].[172]

Due to the involvement of 1,5-$(PP)_2$-$InsP_4$ in a variety of biological roles, many of which are still being discovered or further investigated, there is a demand for synthetic 1,5-$(PP)_2$-$InsP_4$ that can aid in these studies.

3.2 Previous syntheses of 1,5-$(PP)_2$-$InsP_4$

Prior to the synthesis of the most common naturally occurring regioisomer of $InsP_8$ in yeast and mammals, 1,5-$(PP)_2$-$InsP_4$, the first regioisomer of $InsP_8$ to be synthesised was the unnatural *meso*-isomer *myo*-2,5-$(PP)_2$-$InsP_4$.[46] The synthesis of 1,5-$(PP)_2$-$InsP_4$ was then reported by Capolicchio *et al*. (Figure 43) in their divergent route to synthesise both 1,5-$(PP)_2$-$InsP_4$ and 3,5-$(PP)_2$-$InsP_4$.[97] This is currently the only chemical synthetic route in the literature to generate 1,5-$(PP)_2$-$InsP_4$. It should be noted that the route calls for the use of some unusual reagents which are hard to obtain, as well as some forcing reaction conditions, and also lacks a final purification step (generating a final product reported to contain 10% $InsP_7$),[97] leading to our interest in the development of an alternative route.

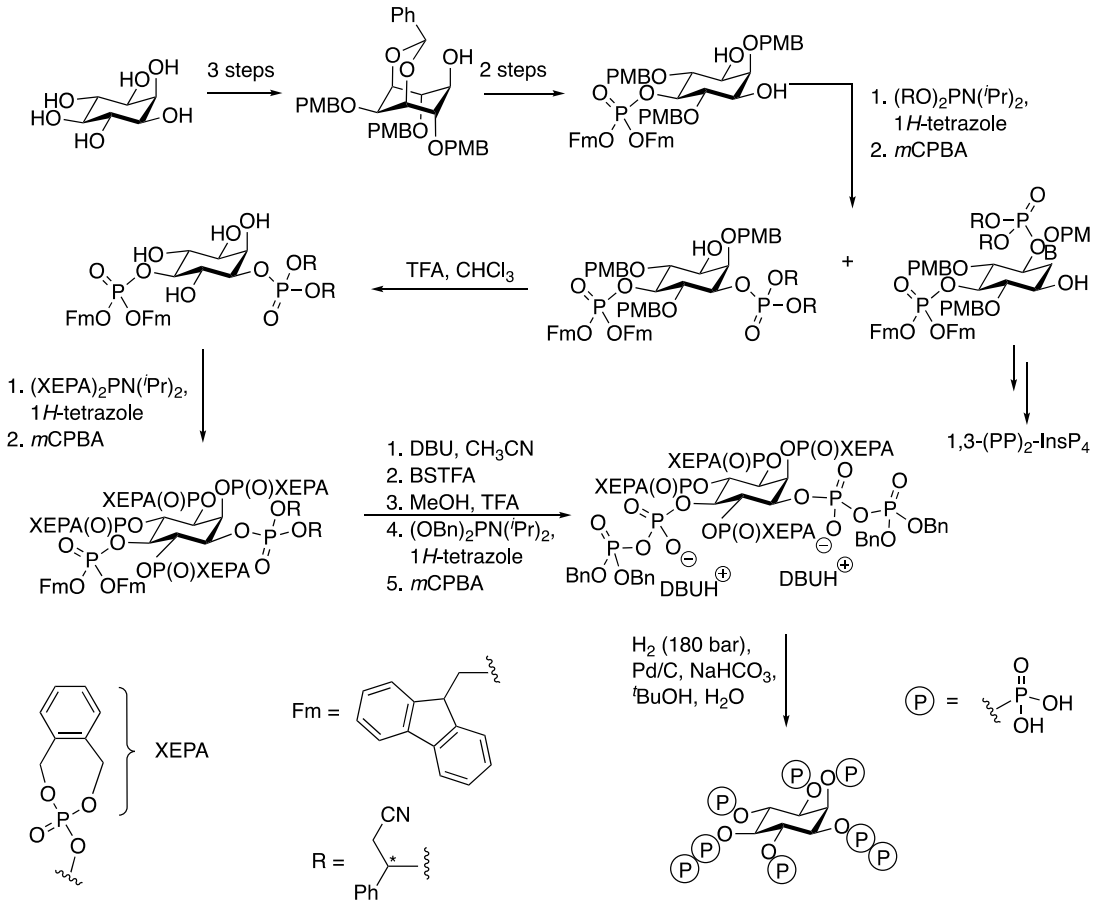

Figure 43: The synthesis of 1,5-$(PP)_2$-$InsP_4$ reported by Capolicchio *et al.*[97]

In the Capolicchio *et al.* route,[97] following the initial protecting group manipulations to expose only the hydroxyl group attached to the 5-position, P(III) phosphoramidite methodology was used to add a bis-fluorenyl-protected phosphate to this position.

After removal of the benzylidene-protecting group to expose the hydroxyls in the 1- and 3-positions, the next step was another phosphorylation with a C_2-symmetric nitrile-containing phosphoramidite that results in desymmetrisation of the *meso* starting material and the generation of separable diastereomers that were used to generate both 1,5-$(PP)_2$-$InsP_4$ and 3,5-$(PP)_2$-$InsP_4$. An analogous phosphorylation had previously been reported by the same lab group in the synthesis of 1-PP-$InsP_5$ and 3-PP-$InsP_5$.[89,97]

The PMB-protecting groups were removed under acidic conditions rather than hydrogenation, which had to be avoided to prevent the reduction of the cyano-ethyl group used to protect one of the phosphates and the possible cleavage of the fluorenyl group.[173] Following deprotection, the resulting tetraol bisphosphates were phosphorylated again with a XEPA-protected phosphoramidite to generate the protected hexakisphosphate.[97]

The pyrophosphorylation sequence was then initiated with the simultaneous deprotection of the fluorenyl and cyanoethyl-containing protecting groups attached to the phosphates at the 5 and 1(/3)-positions through silyl-facilitated basic cleavage using BSTFA and DBU. Following desilylation, the exposed phosphates were then phosphorylated again with benzyl-protected phosphoramidite to generate a mixed P(III)-P(V) intermediate that was subsequently oxidised with *m*CPBA to yield the protected inositol pyrophosphate.[97]

This protected pyrophosphate precursor was purified through crystallisation, which is thought to be possible as a result of the use of the XEPA-protecting groups, thereby removing many of the potential contaminants of the final product. The final deprotection of 1,5-$(PP)_2$-$InsP_4$ was carried out with a palladium-catalysed hydrogenation in a steel autoclave at 180 bar, although it is not clear why such extreme conditions were required for hydrogenolytic deprotection and they appeared to result in degradation of some of the $InsP_8$ product to $InsP_7$. Following hydrogenation, the palladium catalyst was removed through centrifugation and the product was collected without further purification in 13.5% overall yield from inositol orthoformate (with approximately 10% $InsP_7$).[89,97]

Although there are no other synthetic routes reported in the literature for 1,5-$(PP)_2$-$InsP_4$, there are a few routes available detailing the synthesis of non-hydrolysable analogues of the inositol pyrophosphate, namely 1,5-$(PA)_2$-$InsP_4$ and 1,5-$(PCP)_2$-$InsP_4$ (as mentioned in the DPP1 study in Chapter 2).[174] Several of the protecting group manipulation steps early in these routes were utilised in the synthetic route developed for 1,5-$(PP)_2$-$InsP_4$ described in this study.[175,176]

In addition to this reported chemical synthetic route for 1,5-$(PP)_2$-$InsP_4$, as in the case of 5-PP-$InsP_5$ and 5-PP-$InsP_5$, a scalable chemoenzymatic route has also been reported by Puschmann *et al*.[118]

3.3 1,5-$(PP)_2$-$InsP_4$ synthesis

While there are some similarities to the previous synthesis of $InsP_8$, the route in this study bears a closer resemblance to the synthetic routes to 5-PP-$InsP_5$ (**2**) and 5-PP-$InsP_4$ (**3**) described in Chapter 2 (Scheme 1) and was also designed to explore the applicability of the MSE phosphate protection strategy.

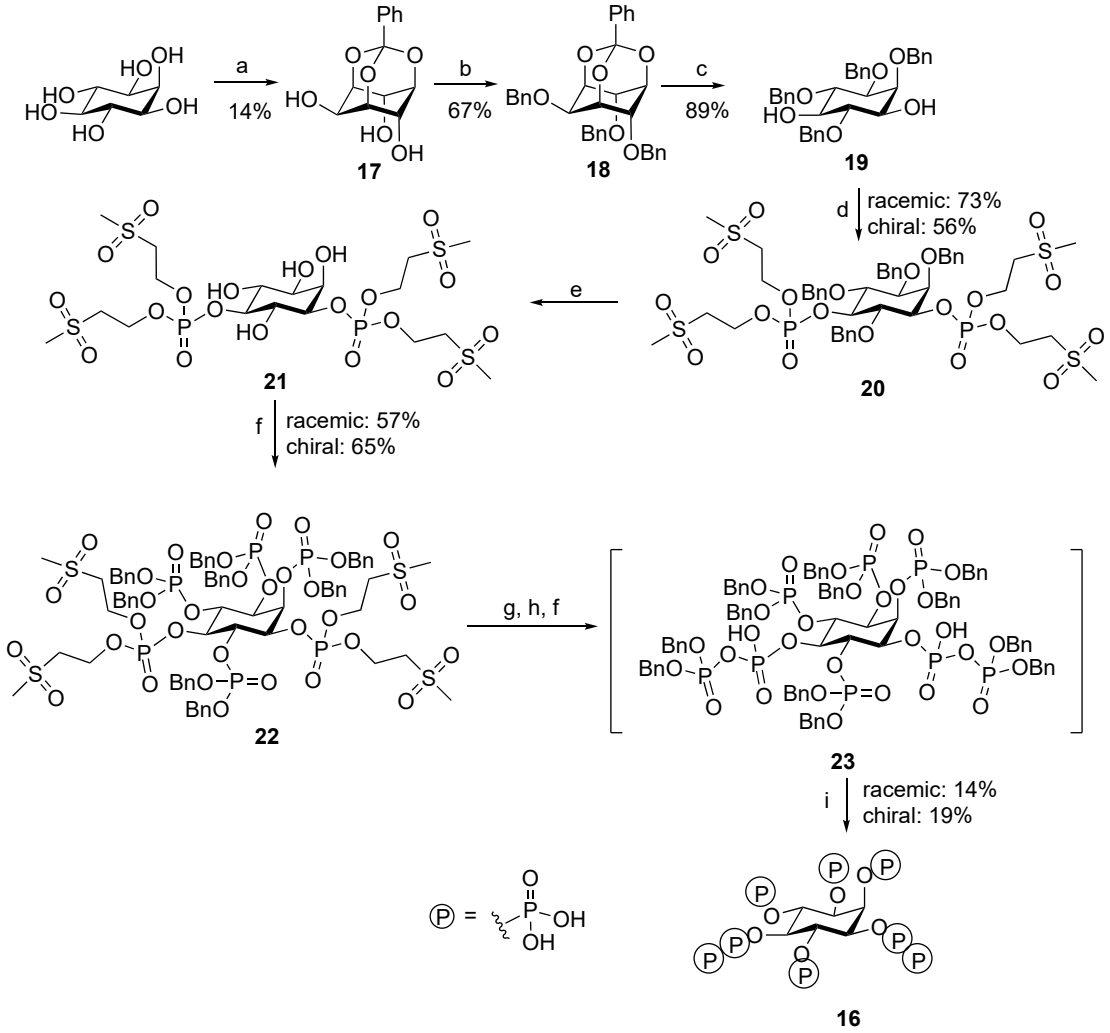

Scheme 3: Synthetic route to 1,5-$(PP)_2$-$InsP_4$ (**16**). This route was initially carried out with racemic material before being repeated from (**19**) with chiral material.

Reagents and conditions: (a) Trimethyl orthobenzoate, H_2SO_4-silica, DMSO, 80°C, 10h ; (b) BnBr, NaH, DMF, 0°C-RT, overnight; (c) DIBAL-H in toluene (1M), DCM, -78°C -RT, overnight; (d) 1. DCM, 5-phenyl-1*H*-tetrazole, $(OMSE)_2PN(^iPr)_2$ (**1**), 20h 2. *m*CPBA, -78°C-RT; (e) THF, CH_3COOH, H_2O, H_2, $Pd(OH)_2/C$; (f) 1. DCM, 5-phenyl-1*H*-tetrazole, $(OBn)_2PN(^iPr)_2$, 20h 2. *m*CPBA, -78°C -rt; (g) DBU, BSTFA; (h) MeOH, TFA; (i) MeOH, THF, 1 M TEAB, $NaHCO_3$, H_2, $Pd(OH)_2/C$.

The first step involved the protection of *myo*-inositol with an orthobenzoate group originally described by Riley *et al*.,[176] using a version of the protocol that employed H_2SO_4-silica as a catalyst that generated the *myo*-inositol 1,3,5-orthobenzoate product (**17**) in 14% yield.[177] This reaction required relatively high temperatures to allow the myo-inositol starting material to ring-flip to its less favoured conformer (five axial hydroxyls, one equatorial),[6] before being fixed in this conformation by the orthobenzoate group. The remaining three exposed hydroxyls were then benzylated with benzyl bromide and sodium hydride to yield 2,4,6-tri-*O*-benzyl inositol 1,3,5-orthobenzoate (**18**) in 67% yield.

The orthobenzoate group of **18** was then regioselectively opened with DIBAL-H to yield the 1,-5-diol (**19**) as a white solid in 89% yield, as reported by Swarbrick *et al*.[175] This reductive orthobenzoate opening is thought to take place via a bridging 1,3-*O*-benzylidene acetal intermediate that subsequently undergoes further reduction to yield the racemic 1/3-*O*-benzyl ether-protected product (**19**).[175]

This is the point in the reaction scheme at which the racemic material can be separated into its chiral enantiomers through resolution of its (-)-(1*S*)-monocamphanate ester derivative diastereoisomers (Figure 44).[174,178] Our group had a supply of previously synthesised chiral D-2,3,4,6-tetra-*O*-benzyl inositol,[174] and thus this resolution was unnecessary to repeat. The synthetic scheme was initially carried out using racemic material, but was later repeated with chiral material.

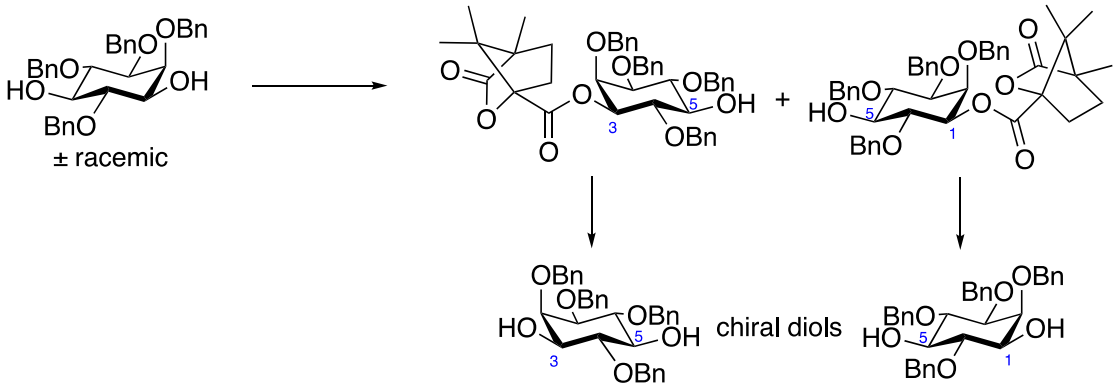

Figure 44: Chiral resolution of the racemic 2,3,4,6-tetra-*O*-benzyl-*myo*-inositol (**19**) through the generation of separable diastereomers with (–)-(1*S*)-camphanic chloride.[174] None of the unwanted diastereoisomer was observed in the ^{1}HNMR precursor to chiral D-2,3,4,6-tetra-*O*-benzyl inositol following separation of the camphanate diastereoisomers via flash chromatography and recrystallisation (estimated enantiopurity >98%).[174]

The remaining two exposed hydroxyls of 2,3,4,6-tetra-*O*-benzyl *myo*-inositol (**19**) were then phosphorylated via a phosphitylation-oxidation P(III) methodology using the MSE-protected phosphoramidite and 5-phenyl-1*H*-tetrazole followed by *m*CPBA. This phosphorylation generated the protected bisphosphate product (**20**) in 73% yield.

Following this initial phosphorylation, the benzyl-protecting groups of 2,3,4,6-tetra-*O*-benzyl-*myo*-inositol-1,5-bis{bis[2-(methanesulfonyl)ethyl]phosphate} (**20**) were removed through hydrogenation to expose the 2-, 3-, 4- and 6-position hydroxyls for a second phosphorylation. It should be noted that this deprotection method was only viable due to the MSE-protecting groups on the phosphates attached to the 1- and 5-positions being resistant to reduction. The protecting group for these phosphates used in the initial synthesis, fluorenyl,[97] might not be suitable in a direct substitution as

there is some evidence that this group might be slowly cleaved during hydrogenation.[173]

Following hydrogenation to remove the benzyl-protecting groups, the *myo*-inositol-1,5-bis{bis[2-(methanesulfonyl)ethyl]phosphate} tetraol (**21**) was not characterised, but instead immediately phosphorylated to prevent degradation. Although the exact mechanism of the degradation observed in the NMR samples allowed to remain in deuterated DMSO solution is not known, it is suspected to involve hydrolytic cleavage of the phosphate groups. The ^{1}HNMR spectrum of the degraded product in DMSO solution indicated that hydroxyl groups had become exposed over the course of a few days, which had been previously phosphorylated. This phenomenon has also been observed in analogous reactions in the syntheses of other inositol pyrophosphates (Chapter 2).

As in the case of the analogous step in the 5-PP-InsP_5 synthesis route (Chapter 2), the phosphorylation of *myo*-inositol-1,5-bis{bis[2-(methanesulfonyl)ethyl]phosphate} (**21**) proved to be a surprisingly challenging reaction, due to the hygroscopic nature of the MSE-protected bisphosphate, which was also prone to degradation, resulting in limited drying options. With excess reagents and careful drying (lyophilisation for the protected bisphosphate, **21**), the phosphorylation was successfully carried out with phosphitylation with dibenzyl phosphoramidite and 5-phenyl-1*H*-tetrazole followed by oxidation with *m*CPBA. The phosphorylation to generate the protected hexakisphosphate (**22**) was eventually achieved in 57% yield.

The next steps in the route were the pyrophosphate-forming sequence: silylation, desilylation, phosphitylation, oxidation and hydrogenation, as previously described in Chapters 1 and 2 (Scheme 4).

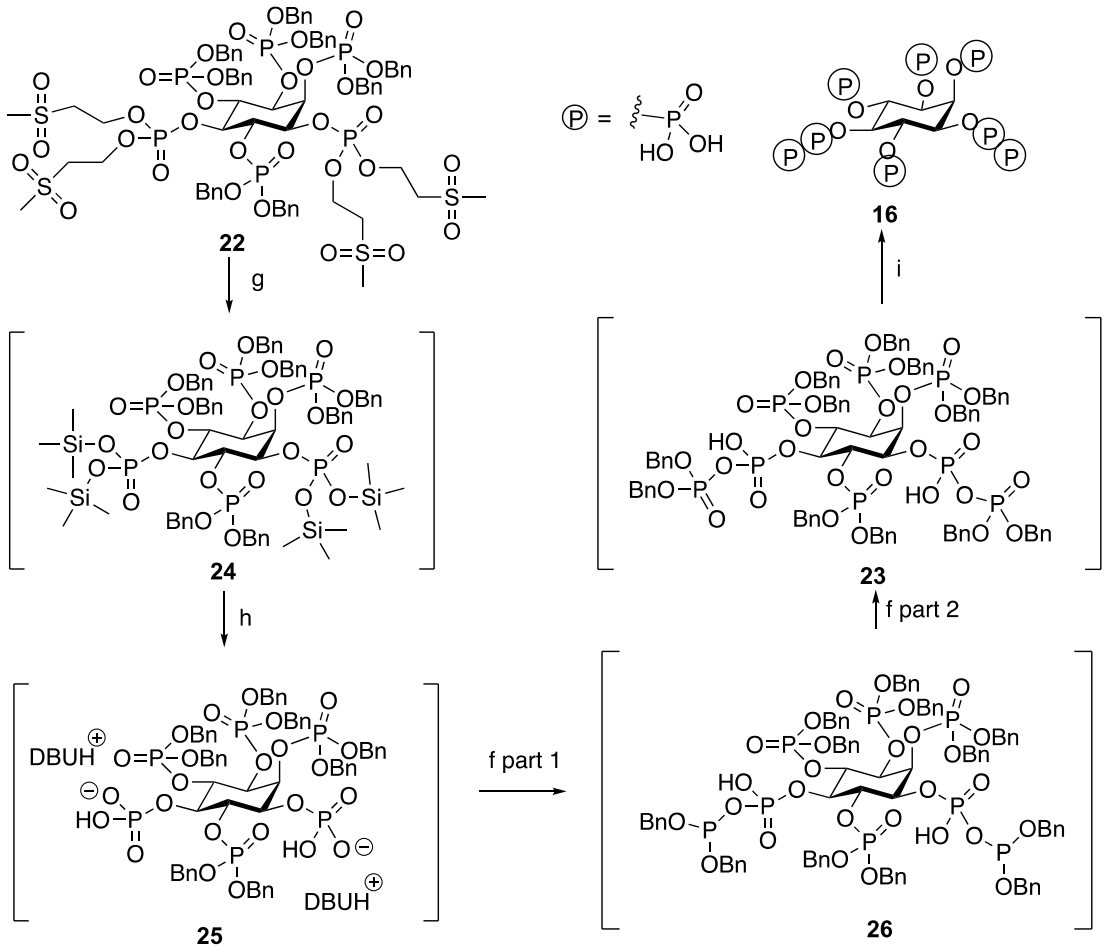

Scheme 4: Expanded final steps in the synthesis route for 1,5-$(PP)_2$-InsP_4 (Scheme 3) to show the intermediates formed during the construction of the pyrophosphate groups in the final reaction sequence.

Reagents and conditions: (f) 1. DCM, 5-phenyl-1*H*-tetrazole, $(OBn)_2PN(^iPr)_2$, 20h 2. *m*CPBA, -78°C-RT; (g) DBU, BSTFA; (h) MeOH, TFA; (i) MeOH, THF, 1 M TEAB, $NaHCO_3$, H_2, $Pd(OH)_2/C$.

Although the combined MSE-deprotection and silylation step took place without any problems (generating **24**), as in the synthesis of 5-PP-InsP_5 and 5-PP-InsP_4 (Chapter 2), the desilylation step proved to be challenging. The first time this step was attempted, the precursor cyclised to form a pyrophosphate moiety after the addition of methanol but before the addition of TFA. The cyclised product was quickly deprotected via hydrogenation to attempt to preserve this side product before decomposition could occur, as deprotected pyrophosphate moieties are more stable than their protected precursors. The cyclised product was then analysed through a proton-phosphorus-correlated HMBC spectrum (Figure 45) and, although the exact direction of cyclisation could not be determined, it was found that the axial 2-position phosphate was not involved in the newly-formed cyclic pyrophosphate group.

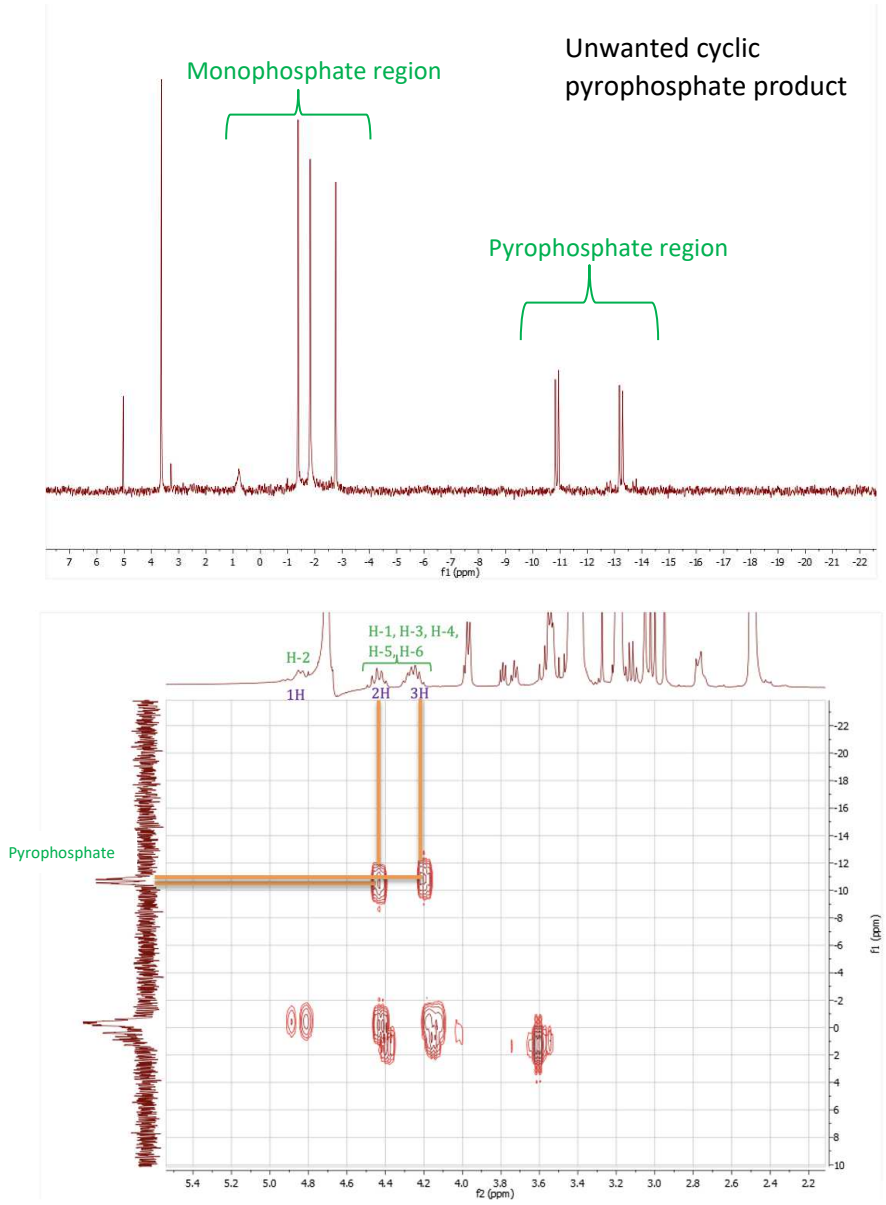

Figure 45: Cyclised side product generated in the $InsP_8$ route that formed during the desilylation (top row ^{31}PNMR spectrum, bottom row HMBC spectrum). The top row indicates the presence of a pyrophosphate moiety through the presence of signals around -11 and -13 ppm. This pyrophosphate formed prior to the phosphorylation step that was meant to introduce such a group, thereby indicating cyclisation. The bottom row depicts an HMBC spectrum that has the integrations for the proton spectrum in purple text underneath the inositol signals and the signal assignments in green text above. The HMBC spectrum shows that the cyclic pyrophosphate did not form in a way that involved the axial 2-position phosphate, although there are still three possible locations for the cyclic pyrophosphate group: 1-position – 6-position, 4-position – 5-position, 5-position – 6-position (Figure 46).

While it cannot be conclusively determined from this data where the suspected cyclic pyrophosphate is situated in the compound, there are three possible regioisomers that could be formed from reactions with the deprotected phosphates and their benzyl-protected neighbours, having eliminated one regioisomer that would require involvement of the axial 2-position phosphate (Figure 46).

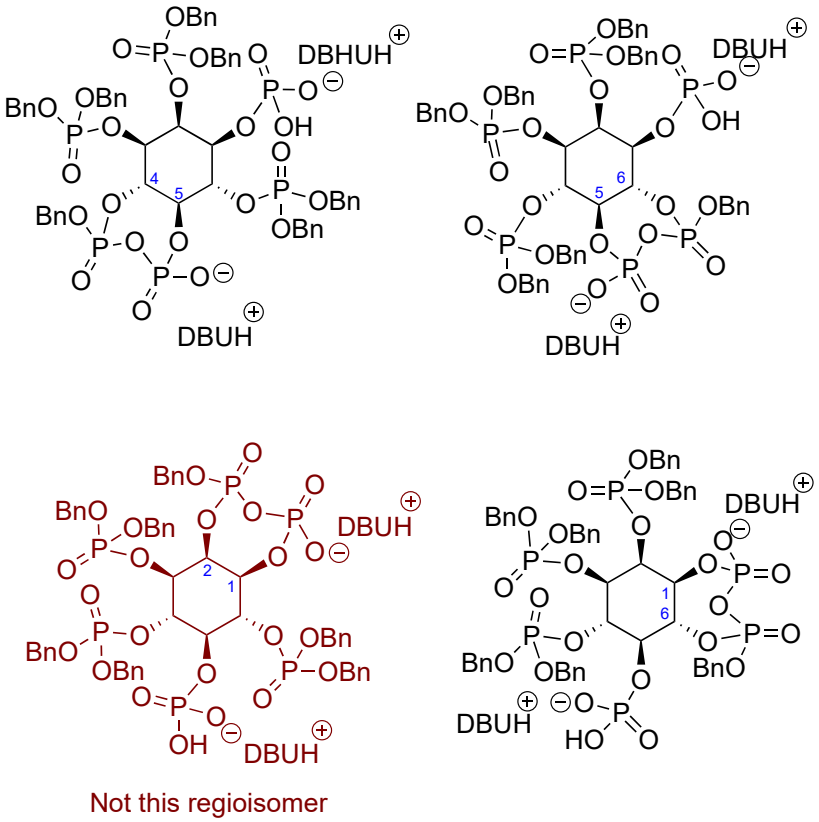

Figure 46: Possible cyclised products generated during the desilylation stage of a failed synthesis of 1,5-$(PP)_2$-$InsP_4$. Following analysis of the product, one of the four possible regioisomers was ruled out leaving three remaining possible structures: 4,5-cyclic pyrophosphate, 5,6-cyclic pyrophosphate (which are enantiomers that would be indistinguishable by NMR) or 1,6-cyclic pyrophosphate. It should be noted that all of these compounds are racemic but only the products of the chiral 1,5-$(PP)_2$-$InsP_4$ are shown.

It can also be speculated that the attack by the 5-position phosphate to either neighbouring 4-position or 6-position phosphates might be more likely than the 1-position phosphate attacking the 6-position phosphate (Figure 47). This is because, in unpublished data from the Potter lab, no cyclisation was observed during the synthesis of 1-PP-$InsP_5$, whereas in the synthesis of 5-PP-$InsP_5$ in this work, cyclisation was observed in the final phosphorylation step (Chapter 2). However, the evidence for the apparent proclivity for cyclisation of the phosphates attached to different positions of inositol from the precursors for the different regioisomers of $InsP_7$ may not necessarily reflect how the precursor to $InsP_8$ cyclises, as the increased electron density from inclusion of two deprotected phosphate groups (and later pyrophosphates) may impact on the direction of cyclisation.

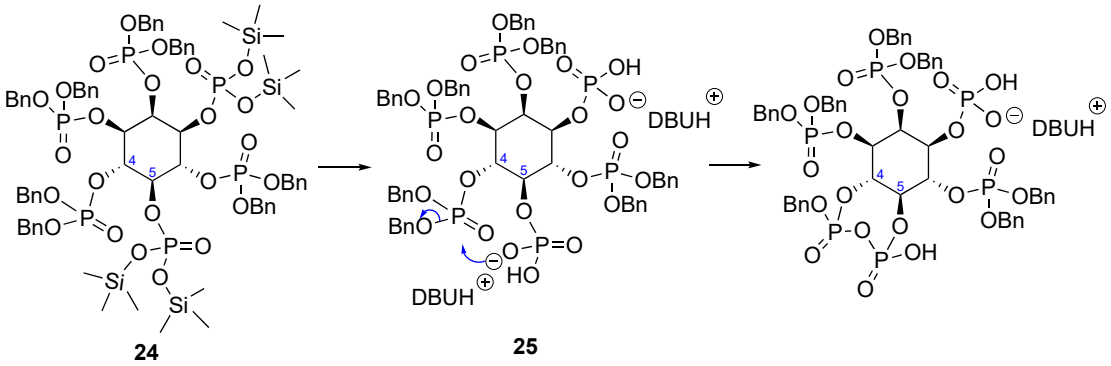

Figure 47: Possible cyclisation mechanism observed following the desilylation of the phosphate groups attached to the 1 and 5-positions in the pyrophosphate construction sequence to form one of the three possible cyclic products, the 4,5-cyclic pyrophopshate.

It was found that, to ensure that the desilylation step did not result in the formation of unwanted side products, the timings used between the addition of methanol and TFA had to be carefully monitored (Table 6).

Reaction code	Time between adding MeOH and TFA	Result
89 (racemic)	15 minutes	More than 50% of the material cyclised
392 (racemic)	2 minutes 30 seconds	Fully desilylated and no cyclisation observed
411 (chiral)	2 minutes 30 seconds	Fully desilylated and no cyclisation observed

Table 6: Desilylation step attempts in the route to synthesise 1,5-$(PP)_2$-$InsP_4$. The time allowed between the addition of MeOH and TFA and the resulting reaction outcome are reported.

The cyclisation occurred quite quickly following the addition of methanol, and from the success of cleaving the silyl groups in the analogous step in the formation of 5-PP-$InsP_5$ (Chapter 2), it was hoped that a short reaction time would be sufficient to cleave the silyl groups fully prior to the addition of TFA. As the cyclisation side reaction was thought to be the result of charged, deprotected phosphate attacking their protected neighbouring phosphates, decreasing the time before TFA was added was expected to suppress this unwanted side reaction. It was indeed found that, by limiting the time between addition of methanol and TFA to two minutes thirty seconds, cyclisation could be effectively prevented during desilylsation.

Following successful desilylation (**25**), the deprotected phosphates in the 1 and 5 positions were phosphorylated in a stepwise P(III) method with dibenzyl phosphoramidite and 5-phenyl tetrazole via a P(III)-P(V) intermediate. Following the cyclisation side-reaction observed in the analogous step during the synthesis of 5-PP-$InsP_5$ (Chapter 2), the phosphorylation in this route was adapted to minimise the possibility of similar cyclisation side reactions occurring. To suppress the basic mechanism of cyclisation, the reaction was kept more acidic through the inclusion of a larger excess of 5-phenyl-1*H*-tetrazole than would otherwise be used in a phosphorylation. To ensure the phosphite intermediate (**26**) did not decompose in the more acidic conditions, the reaction was only allowed to take place over the course of a few hours to minimise intermediate degradation prior to oxidation. Thankfully, unlike in the synthesis of 5-PP-$InsP_5$, no cyclisation was observed in the final phosphorylation step in the 1,5-$(PP)_2$-$InsP_4$ route, most likely due to the pre-emptive adjustments made to the usual phosphorylation protocol.

Following oxidation, as in the reaction routes for 5-PP-$InsP_5$ and 5-PP-$InsP_4$, the usual aqueous work-up was not carried out to prevent degradation of the presumed unstable protected pyrophosphate groups.

Indeed, early trials proved that protected pyrophosphate precursor of 1,5-$(PP)_2$-$InsP_4$ (**23**) is even less stable than the equivalent precursors of 5-PP-$InsP_5$ and 5-PP-$InsP_4$, and is unable to withstand a quick purification via silica flash column chromatography. While bypassing the silica column and proceeding directly to hydrogenation following oxidation would lead to more contaminants being generated in the final product, even partial deprotection of the pyrophosphate product would improve the stability of the product and allow for feasible purification.

The product of the initial hydrogenation was first purified with ion-pair reverse-phase column chromatography, for which the phosphate-containing fractions were tracked using a qualitative Briggs assay. Interestingly, the main phosphate-containing compound seemed to elute only after the end of the programmed automated column run (560 ml, 0-10% MeCN in 0.05 M TEAB), eluting when the column was washed with 70% acetonitrile in 0.05 M TEAB. This late elution seemed to indicate a much less polar product than expected for $InsP_8$. Upon analysis by ^{1}HNMR spectroscopy, it became apparent that the inositol pyrophosphate species still contained aromatic groups and the hydrogenation was incomplete.

The identity of the inositol pyrophosphate species collected after the first RP-18 column could not be confirmed, as the product initially coeluted with contaminants, although the presence of broad peak at -10 ppm in the ^{31}PNMR indicated the presence of a pyrophosphate group.

Although integration of signals in ^{31}PNMR spectra cannot reliably be used to quantify accurately phosphorus atoms in a chemical environment, it can give an approximate

estimation. In the case of this unknown product, integration of the ^{31}PNMR signal around -10 ppm only seemed to indicate the presence of two phosphorus atoms, potentially implying the presence of only one pyrophosphate group and thus the formation of an isomer of $InsP_7$ as a side product. It should be noted that phosphorus signals for the β-phosphate of the pyrophosphate are often broadened and shifted by a number of different factors (predominantly pH) and can sometimes be indistinguishable from background noise in the ^{31}PNMR spectrum, so even though only half of the required pyrophosphate signals appeared to be present in the sample, the possibility that this product was 1,5-$(PP)_2$-$InsP_4$ was not discarded.

As it was not possible to isolate a signal from the ^{1}HNMR spectrum of a proton on the inositol ring to which integrations could be normalized, the number of benzyl groups attached to the inositol pyrophosphate could not be quantified at this stage of the purification. It was predicted that the partial deprotection of the compound had at least cleaved the benzyl groups protecting the β-phosphates of the pyrophosphate, as this would account for the apparent stability of the compound (having not degraded during the RP-18 purification). Exposure of the negative charges on the β-phosphate groups would be expected to prevent hydrolysis and cyclisation by rendering them poorer leaving groups.[179]

The reason for the limited success of the initial hydrogenation is thought to be a consequence of the organic contaminants from the previous steps in the pyrophosphate sequence that were expected to severely slow hydrogenation. The main contaminant suspected of interfering with the hydrogenation was DBU, which was removed during the syntheses of 5-PP-$InsP_5$ and 5-PP-$InsP_4$ through silica column chromatography purification of the protected pyrophosphates immediately prior to the final deprotection of these compounds.

The pyrophosphate-containing compound isolated following the first hydrogenation in the 1,5-$(PP)_2$-$InsP_4$ route was subjected to a repeated hydrogenation. Following the second hydrogenation, the NMR spectra of the product indicated that all of the aromatic groups appeared to have been successfully cleaved, which was most likely possible due to the removal of most of the contaminants from the initial hydrogenation including the DBU. The product was again purified through reverse-phase column chromatography (0-10% MeCN in 0.05 M TEAB), but the collected product appeared to co-elute with a small amount of inositol phosphate contaminants, which were presumably $InsP_7$(s) and $InsP_6$ (Figure 48). Ion exchange column chromatography was hoped to be the suitable method for separating these negatively charged side-product contaminants that co-eluted with the 1,5-$(PP)_2$-$InsP_4$ product with RP-18.

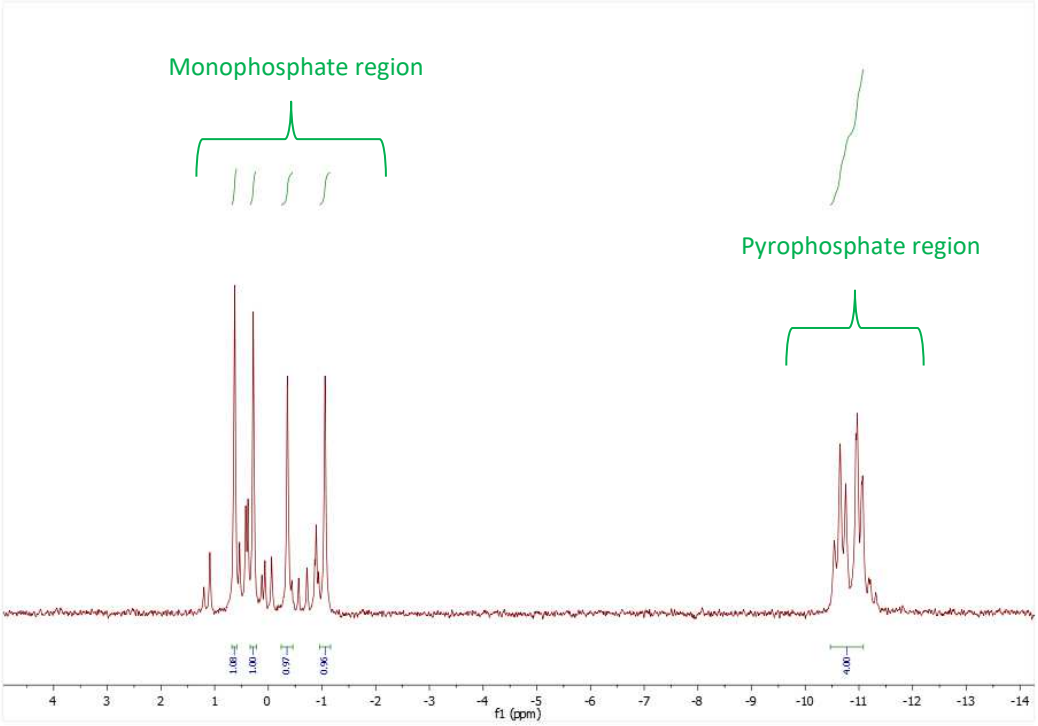

Figure 48: ^{31}PNMR spectrum of the inositol pyrophosphate product fractions of the RP-18 column that followed the second hydrogenation in the final deprotection step of the 1,5-$(PP)_2$-$InsP_4$ route.

Unfortunately, the first batch of DL-1,5-$(PP)_2$-$InsP_4$ synthesised was lost on the ion exchange column. This was later determined to be due to insufficiently concentrated buffer (2M was used first when later it was found that 1,5-$(PP)_2$-$InsP_4$ appeared to only elute when 2.5M TEAB was used). It should be noted that this was the first time 1,5-$(PP)_2$-$InsP_4$ had been purified by ion exchange chromatography, as the previously-reported synthesis concluded with purification of the product through only centrifugation to remove the palladium hydrogenation catalyst, without any column chromatography yielding material still slightly contaminated with partially dephosphorylated side-products.[97]

The synthesis of racemic 1,5-$(PP)_2$-$InsP_4$ was repeated exactly as initially carried out to return to the part in the purification where ion exchange was deemed necessary to remove the contaminating phosphate side products. As mentioned above, 1,5-$(PP)_2$-$InsP_4$ was found only to elute from the ion exchange column at a very high buffer concentration (2.5M TEAB). Fortunately, the ion exchange column with a steeper TEAB concentration gradient was successful in both removing the contaminating inositol phosphates and pyrophosphates and eluting the desired product from the column (Figure 49).

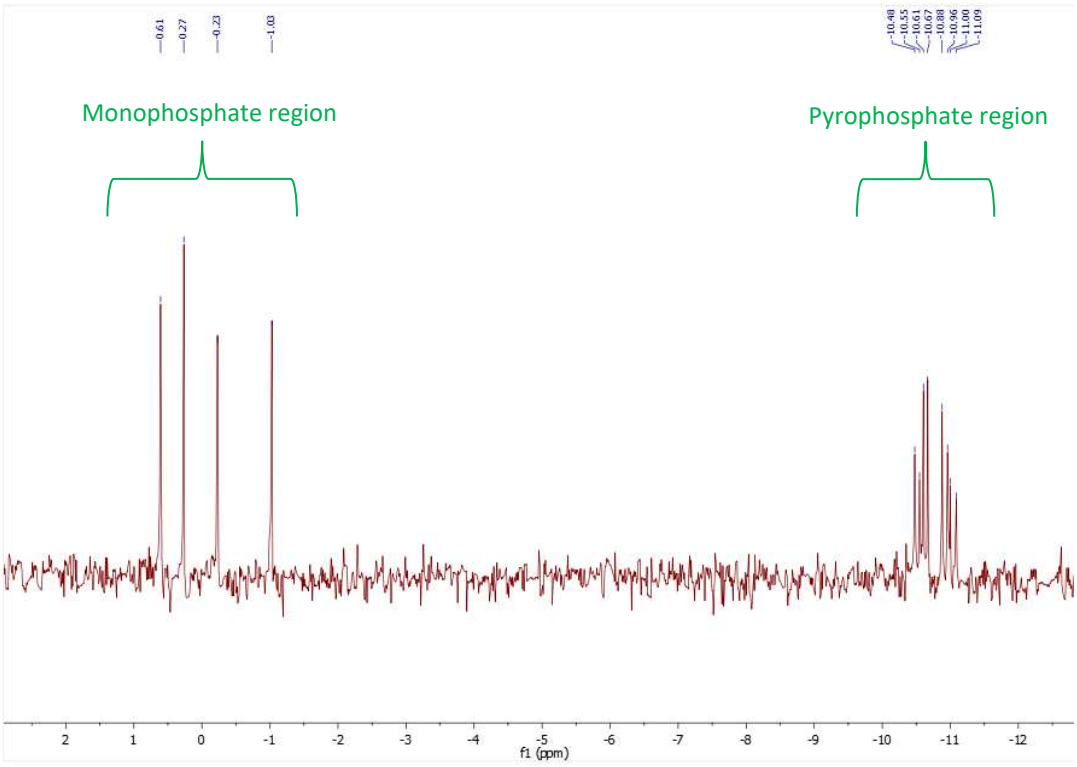

Figure 49: ^{31}PNMR spectrum of the repeated inositol pyrophosphate product fractions of the ion exchange column that followed the two RP-18 columns and two hydrogenations in the final deprotection step of the 1,5-$(PP)_2$-$InsP_4$ route.

A final reverse-phase column was carried out to remove some of the organic contaminants introduced via the highly concentrated buffer necessitated in the ion exchange column.

Following the final RP-18 column and lyophilisation, the final product, the racemic triethylammonium salt of 1,5-$(PP)_2$-$InsP_4$ (**16**), was collected as an off-white glass (14% yield for the pyrophosphate-forming sequence). The route was then repeated exactly as described for the racemic diol with chiral D-2,3,4,6-tetra-*O*-benzyl-*myo*-inositol previously synthesised by the Potter group,[174] to also generate the chiral D-1,5-$(PP)_2$-$InsP_4$ (19% yield for the pyrophosphate-forming sequence).

Preliminary HPLC analysis of both the racemic and chiral 1,5-$(PP)_2$-$InsP_4$ products has been carried out by our collaborator Charles Brearley (University of East Anglia) and indicates that both samples only seem to contain the desired product (Figure 50). Higher resolution HPLC will be conducted at a later date to accurately quantify the purity of both products (although a second, still preliminary, HPLC has already been carried out for the racemic 1,5-$(PP)_2$-$InsP_4$ sample using a steeper methanesulfonic acid gradient that indicates the product is >96% pure).

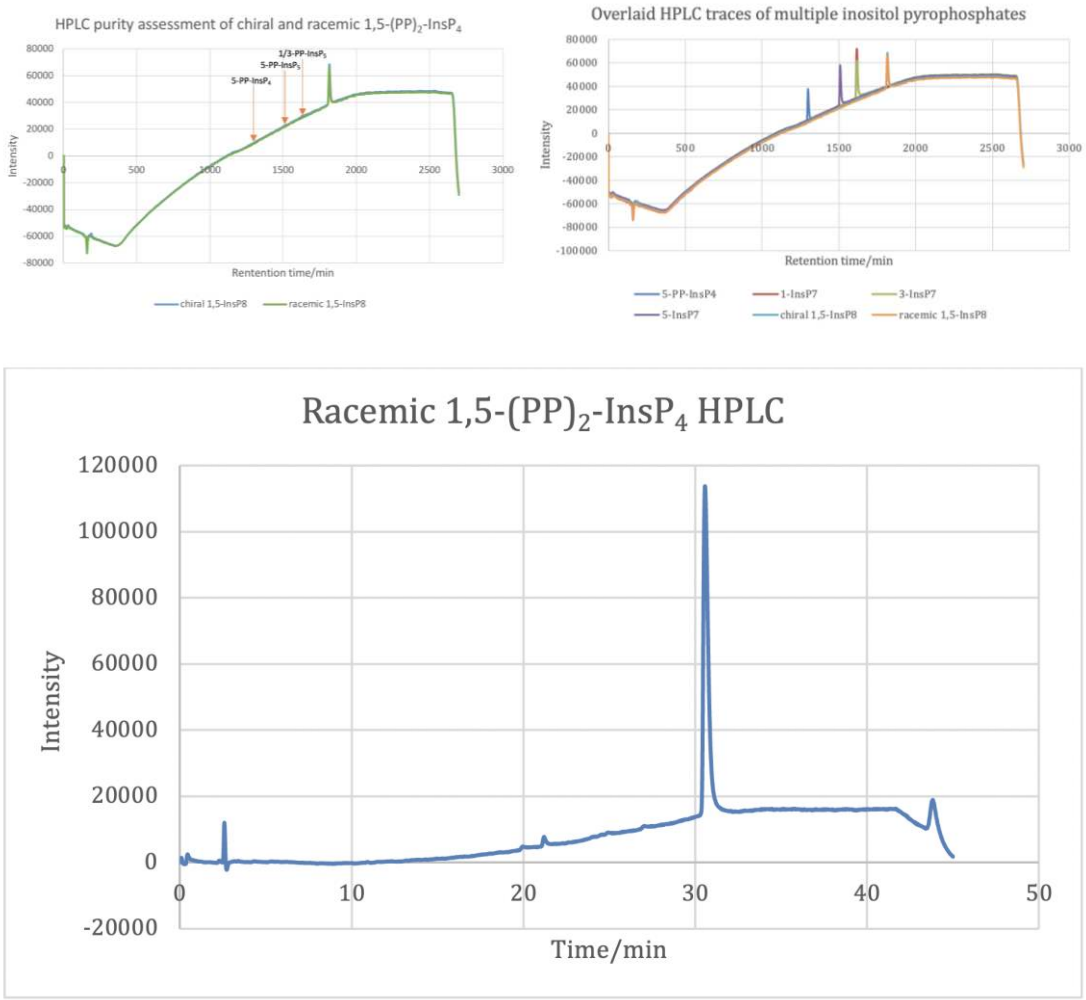

Figure 50: The top row on the left shows the overlaid HPLC traces of both the chiral and racemic 1,5-$(PP)_2$-$InsP_4$ products. The single peak present at around 1800 min was generated by the $InsP_8$ and arrows indicate the HPLC retention times for other inositol pyrophosphates which were found not to be present in either product. The top row on the right shows the overlaid HPLC traces of a number of other inositol pyrophosphates which could have hypothetically been side products of the $InsP_8$ synthesis as well as the traces for the $InsP_8$ products. The bottom row shows the racemic 1,5-$(PP)_2$-$InsP_4$ HPLC trace obtained using a steeper methanesulfonic acid gradient, which indicates that the product is >96% pure.

While the route to synthesise 1,5-$(PP)_2$-$InsP_4$ (**16**) detailed in this study requires further optimisation to improve reaction yields, it does successfully generate the pure target inositol pyrophosphate using comparatively milder conditions and more easily obtained reagents than the previously reported chemical synthesis of this compound.[97] The synthetic route in this study is also more easily generalised and can be adapted to synthesise different inositol pyrophosphate target compounds. One such inositol pyrophosphate target considered was the regioisomer of $InsP_8$ found in the slime mould *Dictyostelium discoideum* (Section 3.4).

3.4 *Dictyostelium* $InsP_8$

3.4.1 *Dictyostelium* inositol pyrophosphates overview

Although many organisms generate 1,5-$(PP)_2$-$InsP_4$ as the main regioisomer of $InsP_8$, there are a number of organisms that favour the formation of other regioisomers. The slime mould *Dictyostelium discoideum* proved to be one such organism, from which a variety of unusual *myo*-inositol based metabolites have been isolated.[150,180,181] Two main inositol pyrophosphates, one regioisomer of $InsP_7$ and one regioisomer of $InsP_8$, were initially isolated as the main *Dictyostelium* metabolites, with larger quantities of $InsP_8$ than $InsP_7$ detected.[41]

From the initial NMR studies of the isolated inositol pyrophosphates, it was not possible to determine if the mono-pyrophosphate was 6-PP-$InsP_5$ or 4-PP-$InsP_5$ and if the di-pyrophosphate was 5,6-$(PP)_2$-$InsP_4$ or its enantiomer, 4,5-$(PP)_2$-$InsP_4$.[150] A further enzymatic study was carried out utilising a purified 5-kinase from *Dictyostelium,* revealing that the correct isomers are 5,6-$(PP)_2$-$InsP_4$ and 6-PP-$InsP_5$ (Figure 51).[180]

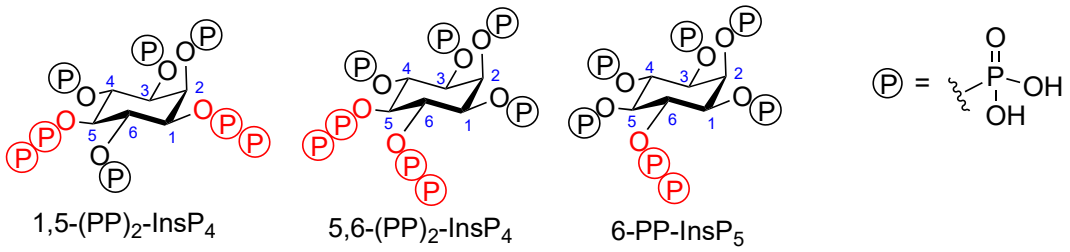

Figure 51: Structure of 1,5-$(PP)_2$-$InsP_4$ (left), the regioisomer of $InsP_8$ generated by most organisms, and the structures of the main inositol pyrophosphates generated in *Dictyostelium*, 5,6-$(PP)_2$-$InsP_4$ (centre) and 6-PP-$InsP_5$ (right).[180] The pyrophosphate groups for all of the compounds have been highlighted in red.

The structure for *Dictyostelium* $InsP_8$, which positions the two pyrophosphate groups adjacent to one another, was very unexpected, as it was initially thought that the high density of negative charges and steric congestion associated with this vicinal positioning would render the formation of this regioisomer improbable.[10,150] Inositol pyrophosphates represent some of the most charge dense and crowded molecules known,[182] and vicinal positioning of the pyrophosphate groups would only intensify these qualities.

As the vicinal pyrophosphate species has been proven to exist, speculation as to its biological properties abounded. As a result of the likely unstable bispyrophosphate group, it has been suggested that the metabolite may be involved in phosphotransferase reactions.[10,150,180] Due to the densely packed negative charge and steric congestion of the vicinal pyrophosphate pair, hydrolysis and phosphate transfer reactions from the 5,6-$(PP)_2$-$InsP_4$ regioisomer would be expected to be more energetically efficient.[11,46]

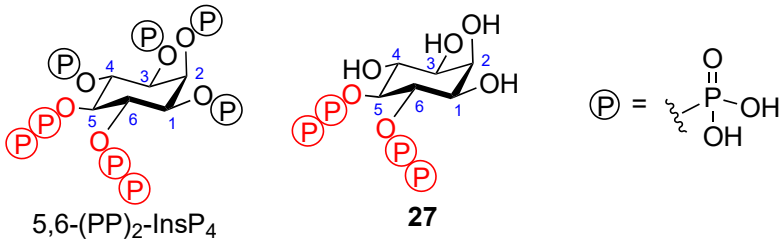

Figure 52: Structures of 5,6-$(PP)_2$-$InsP_4$ (left) and proposed model compound 5,6-$(PP)_2$-Ins (right). The pyrophosphate groups for all of the compounds have been highlighted in red.

Vicinal pyrophosphates have not been previously synthesised and, due to the steric clashes and electrostatic repulsion of the highly negatively charged vicinal pyrophosphate group, they were expected to be very challenging targets. A model compound (**27**) was first chosen as a synthetic target to ensure the vicinal pyrophosphate pair could be synthesised before any route to synthesise a natural *Dictyostelium* $InsP_8$ was designed (Figures 52 and 53).

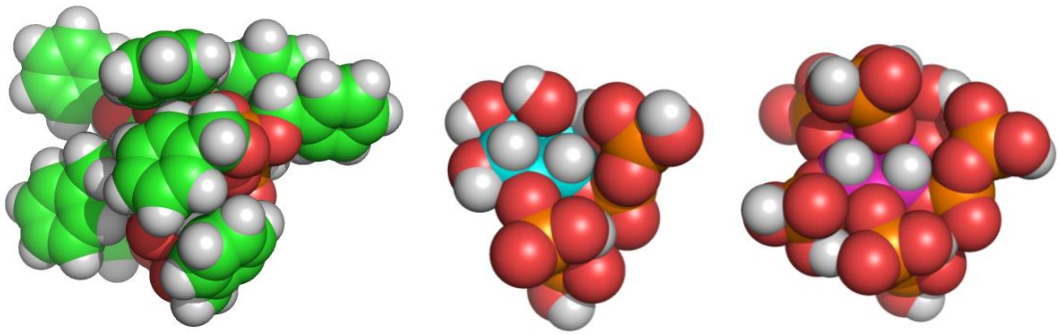

Figure 53: Space filling models of the model benzyl-protected inositol 5,6-bis-pyrophosphate (**33**, left), the model deprotected inositol 5,6-bis-pyrophosphate (**27**, centre) and the *Dictyostelium* regioisomer of $InsP_8$, 5,6-$(PP)_2$-$InsP_4$ (right). The oxygen atoms are shown in red, hydrogen in white, phosphorus in orange and carbon in green/aqua/pink respectively. Note that these models depict the D-enantiomers of all of the compounds.

3.4.2 Attempted synthesis of *Dictyostelium* $InsP_8$ model compound

It was deemed necessary to investigate if a vicinal pyrophosphate could be generated using the standard pyrophosphorylation protocol used throughout this study by synthesising a model of the 5,6-$(PP)_2$-Ins product (**27**, Scheme 5) before the synthesis of 5,6-$(PP)_2$-$InsP_4$ could be attempted.

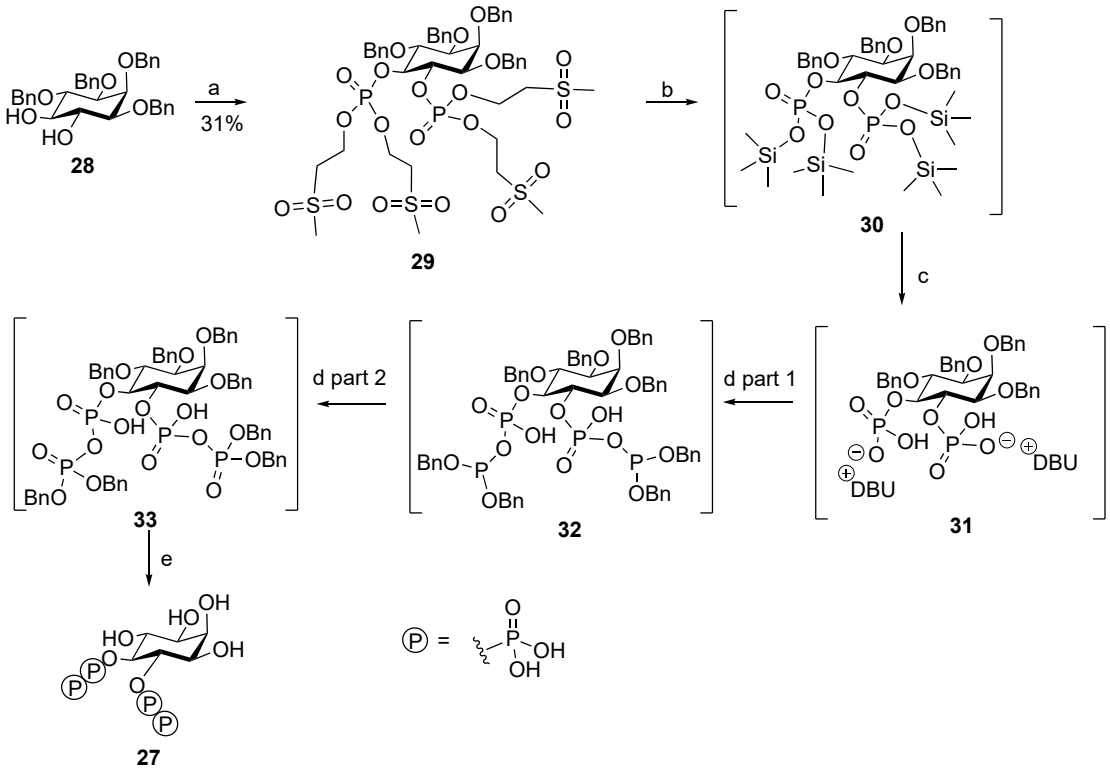

Scheme 5: Route to model compound for *Dictyostelium* $InsP_8$ (**27**).

Reagents and conditions: (a) 1. DCM, 5-phenyl-1*H*-tetrazole, $(OMSE)_2PN(^iPr)_2$ (**1**), 20h 2. *m*CPBA, -78°C -RT; (b) DBU, BSTFA; (c) MeOH, TFA; (d) 1. DCM, 5-phenyl-1*H*-tetrazole, $(OBn)_2PN(^iPr)_2$, 2h 2. *m*CPBA, -78°C-RT; (e) MeOH, mQ, $NaHCO_3$, H_2, $Pd(OH)_2/C$.

The first step of the synthetic route to the model compound was to phosphorylate 1,2,3,4-tetra-*O*-benzyl inositol (**28**, a starting material generated as part of the synthetic route outlined in Chapter 6) with the MSE-phosphitylating agent (**1**). The bisphosphorylated product, 1,2,3,4-tetra-*O*-benzyl inositol-1,5-bis{bis[2-(methanesulfonyl)ethyl]phosphate} (**29**), was also generated in the synthetic route outlined in Chapter 6 as a side product of a monophosphorylation reaction (with one iteration of the phosphorylation producing 33% monophosphates and 31% bisphosphate yields).

Following the phosphorylation, the next step in the reaction route was the beginning of the reaction sequence to generate the pyrophosphate groups. The first step of this sequence was the basic deprotection of the MSE groups and silylation of the exposed phosphate groups (**30**) by means of exposure to DBU and BSTFA. ^{31}PNMR spectroscopy was used to confirm that both this step and the following methanolysis of the silyl groups was successful (this was completed with eleven minutes between methanol and TFA addition and did not show any signs of potential cyclisation). The deprotected bisphosphate precursor (**31**) was then thoroughly dried on a vacuum line, prior to a second phosphorylation step to generate the two neighbouring pyrophosphate groups via phosphitylation to create two P(III)-P(V) groups (**32**) which could be subsequently oxidised to the protected pyrophosphate precursor (**33**).

As a precaution, and due to the assumed product instability, the phosphorylated product (initially presumed to be **33**) was not subjected to an aqueous work-up; nor was it purified through silica column chromatography. The crude mixture containing the presumed protected pyrophosphate product (**33**) was immediately hydrogenated, as it was hoped that if at least the β-phosphates had their benzyl-protecting groups removed, the product would be more stable and less prone to cyclisation or other methods of elimination of the β-phosphate.

The crude hydrogenation product was purified through reverse-phase chromatography to remove any organic contaminants that were believed to hinder debenzylation (primarily DBU) before the compound was subjected to a second hydrogenation. Unfortunately, following the second hydrogenation, the ^{31}PNMR signals around -10 ppm simplified to indicate that there was probably only a single pyrophosphate group present in solution (Figure 54).

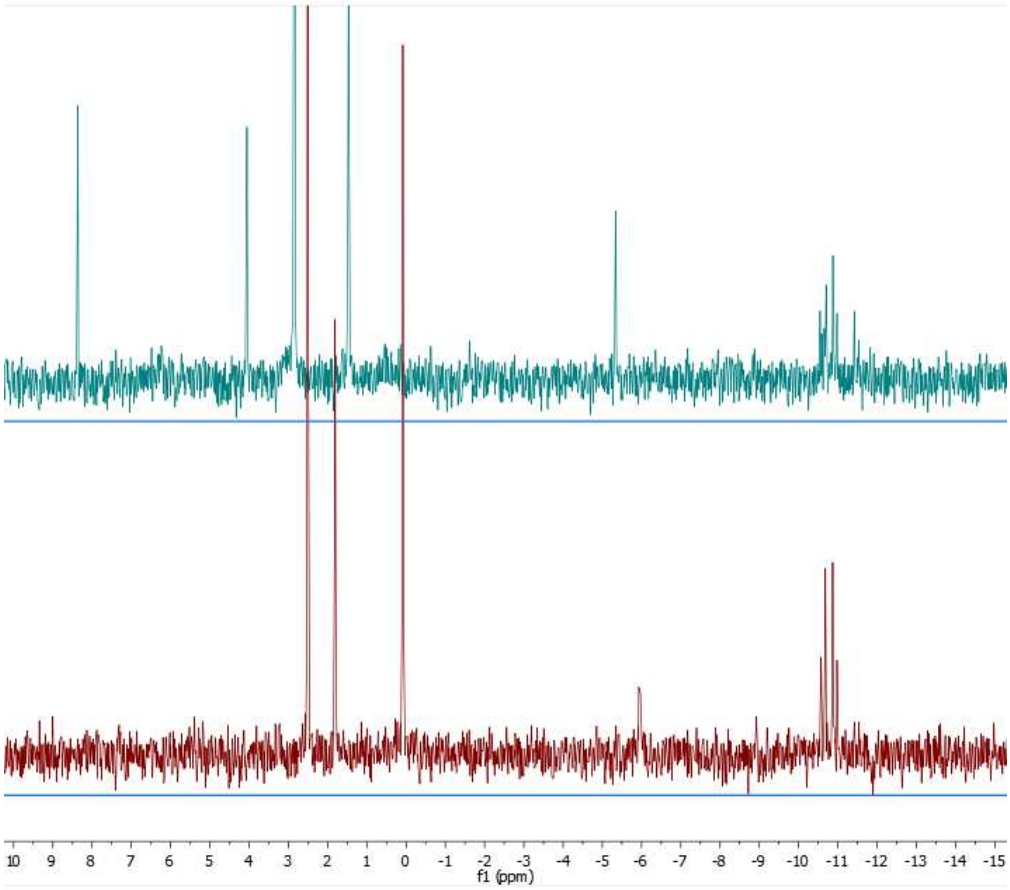

Figure 54: ^{31}PNMR Spectra of the *Dictyostelium* model product after RP-18 but before the second hydrogenation (top), and after the second hydrogenation and a second RP-18 column (bottom). The peak present at around -6 ppm is thought to be the reagent dimer after partial hydrolysis and phosphorylation (as shown in the blank pyrophosphorylation in Chapter 2).

This simplification of the signals was initially thought to indicate that either the desired bis-pyrophosphate product (**27**) was created but proceeded to decompose during the second hydrogenation, or that the pyrophosphate product initially observed was a mixture of partially benzylated pyrophosphate species that coalesced to a single apparent pyrophosphate-containing product (containing a single pair of doublets in the pyrophosphate region of the ^{31}PNMR spectrum) when all of the benzyl groups were successfully cleaved. Regardless of which method resulted in its formation, the isolated pyrophosphate-containing compound was expected to be either 5-PP-Ins(6)P or 6-PP-Ins(5)P. However, this hypothesis was disproven after a proton-phosphorus correlation HMBC spectrum was obtained (Figure 55), which indicated that the product generated was likely a cyclic pyrophosphate (**34**, Figure 56).

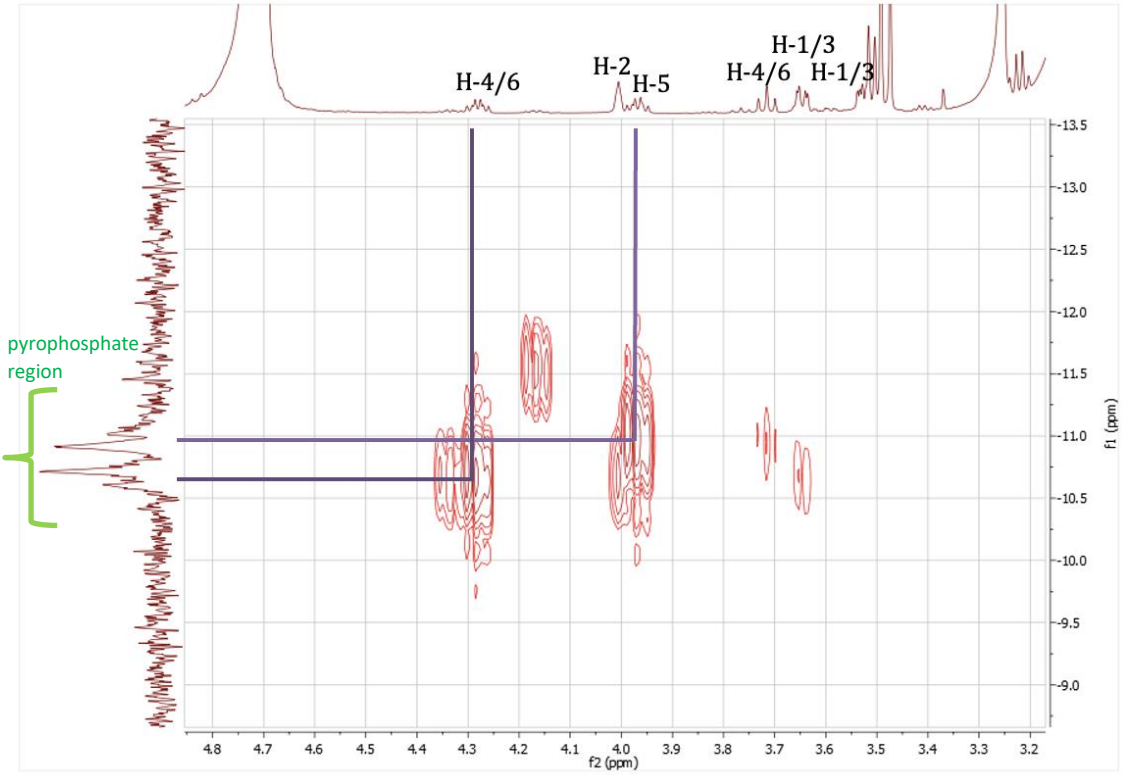

Figure 55: Proton-phosphorus correlation HMBC of the *Dictyostelium* model compound pyrophosphate-containing product fractions.

The HMBC spectrum indicated that both of the observed peaks in the pyrophosphate region of the ^{31}PNMR spectrum are coupled to different inositol ring protons in the ^{1}HNMR spectrum. It should be noted that this pyrophosphate-containing product co-eluted with a few other phosphate-containing compounds in both the ion exchange column and reverse-phase column (hence the inclusion of signals from contaminants in the HMBC).

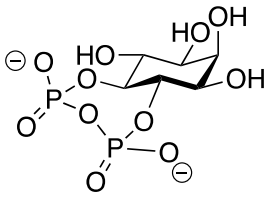

Figure 56: Structure of the proposed cyclised product (**34**) from the attempted synthesis of the *Dictyostelium* model compound.

It is difficult to determine if the cyclisation occurred during the phosphitylation step of the phosphorylation to generate the protected pyrophosphates or after oxidation (as the ^{31}PNMR spectrum acquired prior to oxidation was inconclusive). The formation of the pyrophosphate likely took place during the phosphitylation step, as in the synthesis of 5-PP-InsP_5 (Chapter 2), in an similar mechanism to that described in the

Pavlovic *et al*. paper, with one of the negatively charged deprotected phosphates attacking its neighbour when a protected P(III)-P(V) species is formed, resulting in the cleavage of the protected β-phosphite (Figure 57).[179]

This outcome was perhaps to be expected due to the steric congestion that would be created upon formation of a pair of vicinal pyrophosphate groups. When the P(III)-P(V) mixed anhydride formed on either exposed phosphate during the phosphitylation, the second phosphitylation to generate the neighbouring pyrophosphate group was likely hindered by steric interference, thereby allowing cyclisation to outcompete the formation of the second P(III)-P(V) moiety. It should be noted that, as in the synthesis of 5-PP-InsP_5, 5-PP-InsP_4 (Chapter 2) and 1,5-$(PP)_2$-InsP_4 (Chapter 3), a large excess of 5-phenyl-1*H*-tetrazole had been included in the final phosphorylation reaction in the attempt to suppress the nucleophilic attack of deprotected phosphate groups on adjacent P(III)-P(V) mixed anhydrides, although evidently this precaution was insufficient to prevent cyclisation in the model *Dictyostelium* reaction.

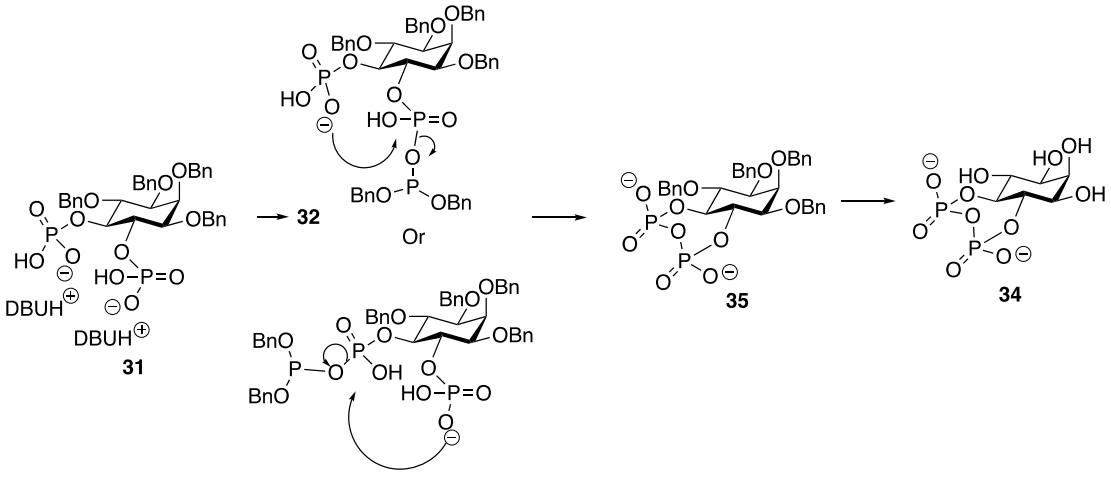

Figure 57: A possible mechanism by which the cyclisation could have taken place during the phosphitylation step of the pyrophosphate-forming reaction sequence. The initial phosphitylation could occur at either the 5-position or 6-position phosphate, as subsequent cyclisation results in the same product. Note that, as in the phosphorylation reactions used to generate the β-phosphates of pyrophosphate groups of the other inositol pyrophosphate products, the reaction contained an excess of 5-phenyl-1*H*-tetrazole to attempt to suppress cyclisation. All of the compounds depicted are racemic.

Although the *myo*-inositol-4,5-cyclic-pyrophosphate (**34**, or its 5,6-cyclic-pyrophosphate enantiomer) has not been synthesised previously, analogues have been intentionally synthesised that feature this functional group including cyclohexane-1,2-cyclic-pyrophosphate and *myo*-inositol 1-phosphate-4,5-cyclic pyrophosphate through desulfurisation of the vicinal phosphorothioates.[183,184] The signals for the cyclic pyrophosphate group in the reported ^{31}PNMR spectra for these compounds bear some resemblance to the observed pyrophosphate product signals

(Figure 58), -8.76 ppm (d, *J*= 18.5 Hz) and -10.13 ppm (d, *J*= 19.9 Hz) with the cyclohexane-1,2-cyclic-pyrophosphate containing a peak around -11.4 ppm and *myo*-inositol 1-phosphate-4,5-cyclic pyrophosphate containing peaks at -11.61 ppm (AB, *J*= 16.8 Hz) and -12.02 ppm (AB, *J*= 16.8 Hz). [183,184] It should be noted that the differences in chemical shift for the pyrophosphate peaks between the observed pyrophosphate product and the literature values for the similar pyrophosphate-containing products can be accounted for by differences in pH of the NMR samples, in addition to the subtly different chemical environments of the pyrophosphates in these related but distinct compounds.

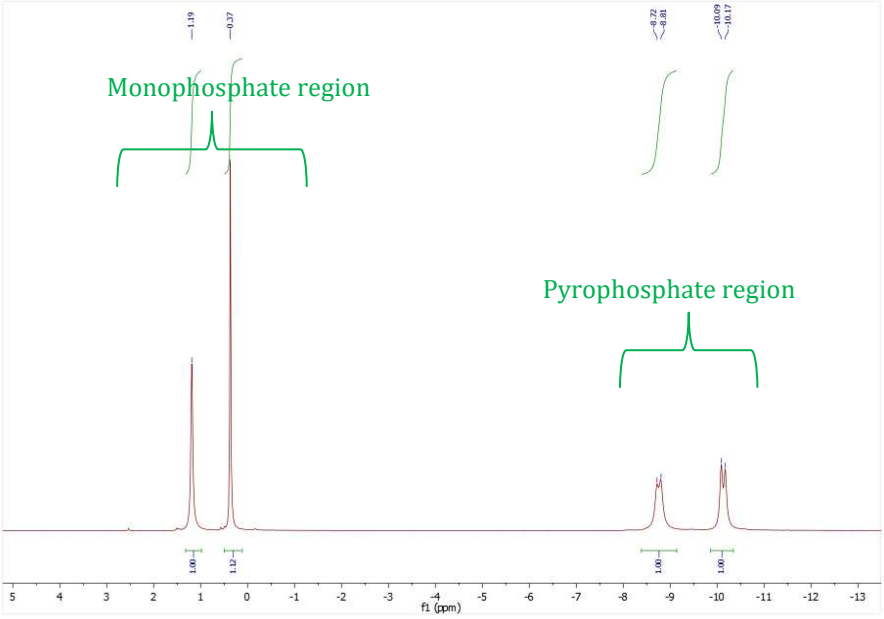

Figure 58: ^{31}PNMR Spectrum of the pyrophosphate-containing product mixture obtained from the *Dictyostelium* model compound synthesis following its final purification via ion-pair reverse-phase column chromatography. The signals from the cyclic-pyrophosphate product can be observed around -10 ppm, while the signals indicating the presence of a co-eluting species containing monophosphate groups can be seen around 1 ppm.

Further evidence that the pyrophosphate-containing product was *myo*-inositol-4,5-cyclic-pyrophosphate (**34**) was provided in the successful identification of the $[M-H]^-$ ion peak in the accurate mass electrospray ionization mass spectroscopy spectrum (Figure 59).

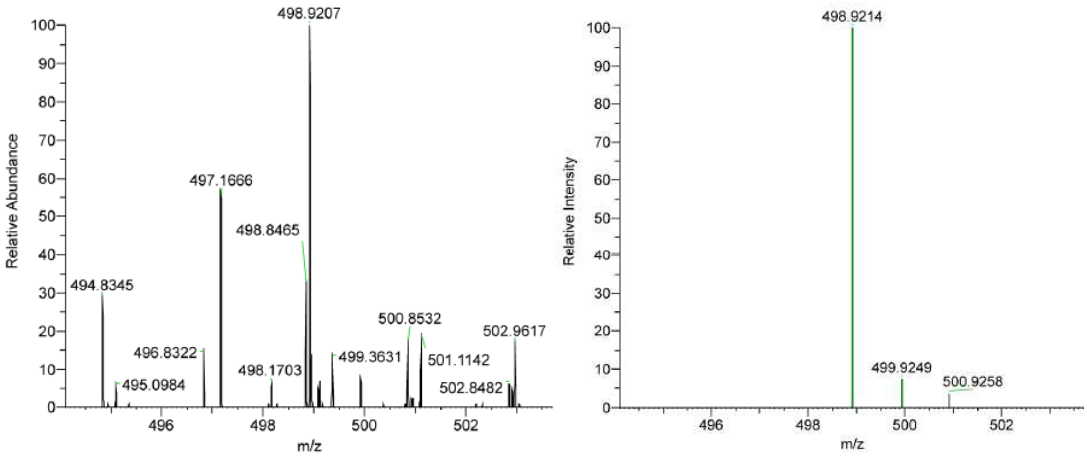

Figure 59: Found (left) and theoretical (right) mass spectroscopy spectra of racemic *myo*-inositol-4,5-cyclic-pyrophosphate (**34**) showing the $[M-H]^-$ ion peak at 498.92 m/z.

Unfortunately, there was insufficient time to optimise reaction conditions potentially to prevent the formation of this unwanted cyclised side product (**34**) and generate the actual vicinal pyrophosphate moiety (**27**). As there was no success with generating this key functional group in the model compound, the synthesis of 5,6-$(PP)_2$-$InsP_4$ was abandoned. It would be interesting to see if a compound such as these target products containing vicinal pyrophosphate groups could be generated via chemical synthesis at a later date, but this work seems to confirm that the intrinsic steric and charge congestion may be hard to overcome synthetically.

As the benzyl-protecting groups used in this model synthesis were a source of significant steric hinderance, perhaps the use of more space-restrained protecting groups on the 1-, 2-, 3- and 4-positions might create sufficient space in the molecule for the second phosphitylation to become competitive with the cyclisation side reaction. There are a few potential alternative model compounds that might suit this purpose including 1,2,3,6-tetramethyl-*myo*-inositol or even trans-cyclohexane 1,2-diol. Reducing sterically demanding neighbouring groups alone may not be sufficient to prevent cyclisation from occurring in the final phosphorylation step though.

This difficulty in synthesising a vicinal pyrophosphate moiety bears some resemblance to the historical problem encountered in synthesising vicinal monophosphates using P(V) methodology that had also been reported to lead to the unwanted formation of cyclic phosphates. This undesired cyclisation was overcome for vicinal bisphosphates in part by the development of less sterically demanding P(III) methods.[88] Perhaps a new phosphorylation strategy might be developed that would enable the formation of vicinal pyrophosphate moieties.

3.5 Biological evaluations of D-1,5-$(PP)_2$-$InsP_4$

The chiral D-1,5-$(PP)_2$-$InsP_4$ synthesised in this study was used as part of the investigation into the structural requirements for ligand binding at the HDAC3-SMRT enzyme complex $InsP_4$ site (described later in Chapter 4). In addition to further probing binding requirements for this site, D-1,5-$(PP)_2$-$InsP_4$ was included in the study to determine if this inositol pyrophosphate could be a potential endogenous activator of the complex.

The chiral 1,5-$(PP)_2$-$InsP_4$ synthesised in this study is also currently being tested with the europium complex luminescence assay (described previously in Chapter 2) to further investigate the scope of this assay in its ability to monitor inositol pyrophosphates. These results will be reported later following completion of the study.

Further collaborations are also currently underway with both the racemic and chiral 1,5-$(PP)_2$-$InsP_4$, although no results are available at the time of the submission of this thesis.

(4) HDAC3-SMRT and inositol 1,4,5,6-tetrakisphosphate

4.1 Histone deacetylases (HDACs) – biological background

Acetylation of histones is one of several factors that determine chromatin structure and accessibility of genes for transcription.[185] HDACs (Histone deacetylases) are enzymes that influence gene expression through the removal of post-translational acetyl groups from lysine residues in histones.[186,187] Although there are a number of processes that can influence gene expression, the activity of HDACs often leads to the repression or silencing of genes, while the activity of histone acetyltransferases (HATs) generally promotes gene activation.[188]

There are eighteen different HDAC enzymes that have been identified in humans, and these are divided into four classes based on their structural similarities to analogous yeast proteins. Class 1 HDACs (HDAC1, HDAC2, HDAC3 and HDAC8), grouped for similarities to the RPD3 yeast deacetylase, are relatively small enzymes with molecular masses in the range of 22-55 kDa and are found almost exclusively in the nucleus of cells.[187,189]

The catalytic site for deacetylation is highly conserved across all of the HDAC enzymes within each class.[190,191] The tubular binding pocket for Class 1 HDACs contains a zinc ion, two crucial histidine residues and a tyrosine residue that assist in the hydrolysis of acetamide-containing substrates (Figure 60).[187] The tyrosine residue and zinc ion are thought to polarise the carbonyl bond of the acetyl moiety, rendering the ligand more susceptible to nucleophilic attack by water, facilitated by the histidine residues.[187]

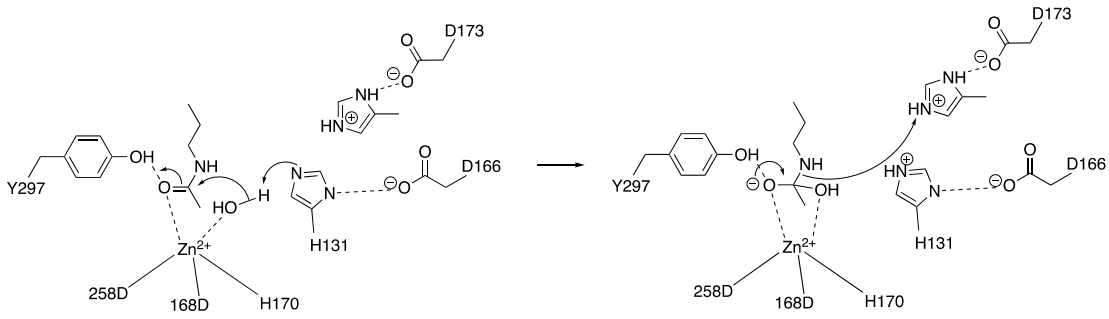

Figure 60: Proposed mechanism for deacetylation by HDAC1, HDAC2 and HDAC3 enzymes (adapted from Seto and Yoshida).[187]

Abnormal HDAC activity has been associated with a number of diseases and cancers.[187,190,191] There are several HDAC inhibitors that have been clinically approved, but these available drugs are not very specific as they target multiple HDAC enzymes and cause severe side effects.[190]

Due to the conserved nature of the HDAC ligand binding sites, targeting an individual HDAC enzyme at the deacetylation site has proven to be unfeasible, with only limited differentiation seen between the active sites in the HDAC classes.[192–194] Targeting HDAC protein *complexes* rather than the conserved HDAC active sites may instead be an effective method to generate new, selective HDAC inhibitors.[112,192,194]

HDAC3 is not active when it is not in a complex with either the corepressor SMRT (silencing mediator of retinoic acid) protein or with the N-CoR (nuclear receptor co-repressor) protein. These complexes form after HDAC3 is primed by cellular chaperones including the TCP-1 ring complex (TRiC), which actively ensures the correct folding of HDAC3 before being displaced by the corepressor (SMRT or N-Cor) to yield an active enzymatic complex. While HDAC3 is found in both the cytoplasm and the nuclei of healthy cells, the localisation and activity of HDAC3 is controlled and limited to the nucleus, in part through the necessity of complexation with co-repressor proteins.[195]

The co-repressor SMRT possesses a deacetylase activating domain (DAD) which crucially features a SANT [switching-defective protein 3 (Swi3), adaptor 2 (Ada2), nuclear receptor co-repressor (N-CoR), transcription factor (TF)IIIB] domain. The SMRT DAD is able to activate and bind to HDAC3, forming an active and stable catalytic protein complex HDAC3-SMRT.[195]

It was recently discovered that a molecule of D-*myo*-inositol 1,4,5,6-tetrakisphosphate, Ins(1,4,5,6)P_4, binds between HDAC3 and the SMRT co-repressor protein in the HDAC3-SMRT enzyme complex (Figure 61).[112,196]

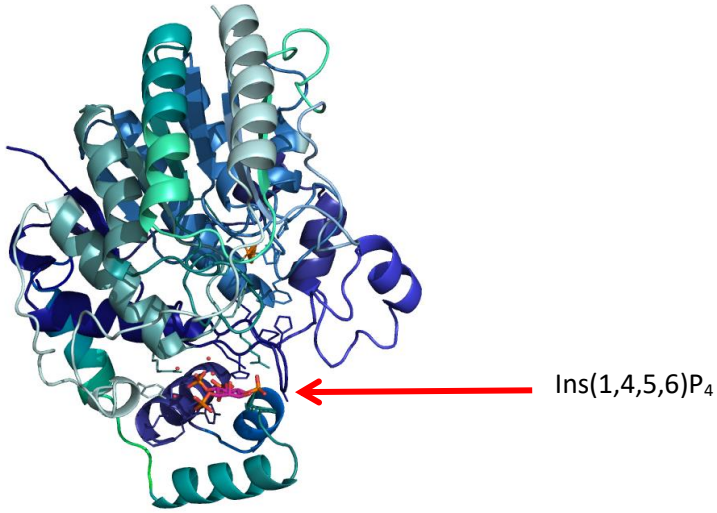

Figure 61: Crystal structure of Ins(1,4,5,6)P_4 binding in the HDAC3-SMRT complex, PDB: 4A69.[196]

There are multiple HDAC complexes for which interaction with inositol phosphates has been found to be important to enzyme activity. Specifically, HDAC1:MTA1 and HDAC1:MIDEAS complexes have been found also to be activated by Ins(1,4,5,6)P_4,

and it is suspected that other HDAC complexes with SANT or equivalent domains might be activated by inositol phosphates.[112,197,198] It was also discovered that the presence of inositol phosphates as activators of histone deacetylases is even more widespread, as the SAP30-HDAC1 complex, which lacks a SANT domain, is also activated by Ins(1,4,5,6)P_4.[199]

4.2 HDAC3-SMRT and Ins(1,4,5,6)P_4

The molecule of D-*myo*-inositol 1,4,5,6-tetrakisphosphate, Ins(1,4,5,6)P_4, was found to bind between the HDAC3 protein and SMRT co-repressor in the HDAC3-SMRT enzyme complex, and this was first reported in an X-ray crystallographic study carried out by Watson *et al.*[196]

While initially believed to be a form of 'molecular glue' that holds the SMRT and HDAC3 proteins together,[196] the role of the inositol phosphate molecule has instead now been established to be that of an activator for the HDAC3-SMRT complex.[112,198] It has been established that the enzyme complex could not be activated in the absence of Ins(1,4,5,6)P_4, and binding at the inositol phosphate site is thought to produce a dynamic allosteric effect on the active site of the complex.[112,187,194,196]

The initial study that investigated the binding requirements for compounds at the Ins(1,4,5,6)P_4 binding site of HDAC3-SMRT designated four regions of the binding pocket as A, B, C and D to correspond respectively to the locations in which the 4-, 5-, 6- and 1-position phosphates of D-*myo*-inositol 1,4,5,6-tetrakisphosphate bind (Figure 62).[112]

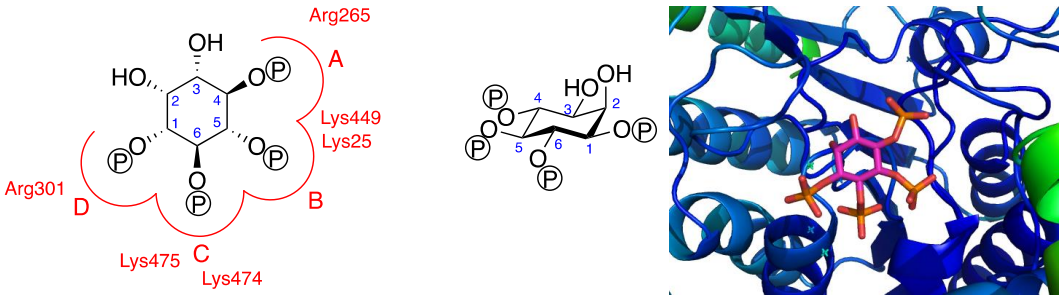

Figure 62: Binding site for Ins(1,4,5,6)P_4 in the HDAC3-SMRT complex with some of the amino acid residues with flexible side-chains involved in binding explicitly labelled (left) and the numbered structure of Ins(1,4,5,6)P_4 (centre) and the crystal structure of Ins(1,4,5,6)P_4 (depicted in pink) bound in the HDAC3-SMRT (PBD: 4A69).[196]

The initial Watson *et al.*[112] study outlined a few potential binding requirements for ligands at the HDAC3-SMRT binding site that can be summarised as follows:

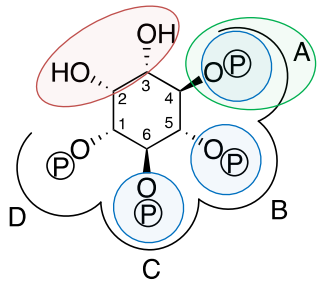

- Three consecutive phosphate groups are necessary for activation.
- A phosphate should be positioned in the A region of the binding site to form a salt bridge with the Arg265 residue (crucial to HDAC3-SMRT activation).
- The A region of the binding site is thought to be unable to tolerate even conservative additions of steric bulk or a change in orientation of any substituent in this position (even axial hydroxyl groups are not expected to be tolerated).
- The hydroxyl groups attached to the 2- and 3-positions of Ins(1,4,5,6)P_4 face out into solvent and are able to host bulky substituents with minimal decrease in affinity.
- The chair conformation of Ins(1,4,5,6)P_4 is thought to be important for positioning the phosphates in the required regions of the binding site [planar benzene 1,2,3,4-tetrakisphosphate was significantly less active than Ins(1,4,5,6)P_4].

The necessity of three consecutive phosphate groups was determined by the inability of Ins(1,4,5)P_3 to activate the HDAC3 complex.[112] It is thought that phosphate groups must be positioned by the ligand in the A, B and C regions for compounds to bind (as opposed to the B, C and D regions), due to the fact that, upon binding, the ligand is thought to be required to form a salt bridge in the A region with Arg265 to activate the enzyme complex. Furthering this theory, when the phosphates were systematically removed in Autodock models, the binding energy was reduced significantly more when the phosphate was removed from the A region (5.4 $kcalmol^{-1}$) than from the D region (1.2 $kcalmol^{-1}$).[112]

It should also be noted that none of the docking solutions generated in the modelling carried out in the initial study positioned phosphates in the B, C and D regions rather than the A, B, C regions.[112] The fourth phosphate which interacts with the D region of

the site (position 1 in Ins(1,4,5,6)P_4), is therefore thought to improve ligand affinity, but not be necessary for ligand binding or complex activation.[112]

The formation of the salt bridge between the phosphate occupying the A region of the binding site and the R265 residue is thought to improve ligand affinity and, crucially, immobilize the very flexible R265 residue side chain, resulting in a subtle change in the structure of the protein that leads to activation of the enzyme complex.[112] It has also been found that the HDAC3-SMRT enzyme activity is abolished following the mutation of this particular arginine residue (R265).[196,198] Although R265 mutation has been proven to prevent deacetylation, ligands have been found to be able still to bind to the mutated HDAC3-SMRT complex through analysis of the binding of the fluorescently tagged 2-FAM-Ins(1,3,4,5,6)P_5 (which was previously designed by the Potter group) in both the unaltered and mutated HDAC3-SMRT binding site.[112] The R265 arginine residue has been found to be of particular importance to HDAC3 specifically, as the mutation of its equivalent residue in HDAC1, Arg270, results in only a minor effect on deacetylase activity.[112,194]

While it has not been conclusively established that a phosphate must be positioned in the A region rather than the D region (as the compounds analysed are able theoretically to bind in multiple conformations that would allow for either A or D to be occupied), the role of R265 in forming an important salt bridge and the differences in calculated energy and molecular modelling results indicate that the occupation of the A region by a phosphate is likely a binding requirement for the enzyme complex.

Computational studies in the initial investigation of the inositol phosphate HDAC3-SMRT binding site seemed to indicate that the A region would tolerate steric bulk very poorly, even suggesting that an axial hydroxyl group in this position would result in too many steric clashes.[112] As a result, binding modes that position bulky or axial groups in the A pocket of the binding site are considered unlikely to be adopted by ligands.

The interactions between the phosphate groups and the deeply buried residues in the B and C pockets of the binding site are thought to be the key thermodynamic driving force in ligand binding.[112] Structural disturbances to the phosphate groups of Ins(1,4,5,6)P_4 analogues that are predicted to bind to these regions have previously been shown to result in a significant decrease in the activity observed for the HDAC3-SMRT complex. When a pyrophosphate group was positioned in the B region [5-PP-Ins(1,3,4,6)P_4], the activity of the complex was seen to drop drastically [60% of the activity of Ins(1,4,5,6)P_4] and the corresponding phosphonoacetate mimic [2-OH-5-PA-Ins(1,3,5,6)P_4] was found to be entirely unable to activate the HDAC3-SMRT complex. The difference in activity of these analogues is thought to be due to the carbonyl group of 2-OH-5-PA-Ins(1,3,5,6)P_4 being unable to mimic a phosphate to

satisfy the apparent requirement of having three consecutive phosphate groups present to activate the enzyme complex.[112]

When Ins(1,4,5,6)P_4 binds to the HDAC3-SMRT binding site, the 2- and 3-position hydroxyls face out into solvent and do not appear to have any significant effect on compound binding. Analogues of Ins(1,4,5,6)P_4 with benzyl groups attached to these positions have also been shown to suffer only a small decrease in complex activity, and *scyllo*-Ins(1,3,4,5,6)P_5, which changes the orientation of the 2-position hydroxyl and includes an additional phosphate attached to the 3-position, was found to activate HDAC3-SMRT to a similar extent to Ins(1,4,5,6)P_4.[112]

The three-dimensional chair structure of the 6-membered inositol ring was found to be important in aligning the phosphate groups such that they can they interact with relevant residues in the binding pocket. This was determined when the flat benzene analogue of Ins(1,4,5,6)P_4, benzene(1,4,5,6)P_4, was found to be unable to activate the HDAC3-SMRT complex to any substantial degree.[112]

To confirm and determine other requirements for this binding site in a continuing structure-activity study, more compounds were synthesised and analysed in an HDAC3-SMRT activity assay, in collaboration with colleagues in the Schwabe group at Leicester University.

4.3 Proposed HDAC3-SMRT regulators

To expand on the previously proposed binding requirements and, for the first time, to explore the potential of sugar-based mimics of Ins(1,4,5,6)P_4 at the HDAC3-SMRT binding site, six glucose-based compounds (Figure 63, four novel, two known) were synthesised. These carbohydrate phosphates were originally designed following preliminary molecular modelling initially performed by Dr Andrew Riley in our group.

By using D- and L-glucose as the basis for the synthesising these potential HDAC3-SMRT ligands, it was hoped that the minor structural differences between the carbohydrates and *myo*-inositol would enable the binding requirements of the Ins(1,4,5,6)P_4 to be further probed. These starting materials also provide the advantage of being chiral, thereby eliminating the need for a lengthy stereoisomer separation via an optical resolution step which would be required to generate enantiopure chiral inositol phosphates.

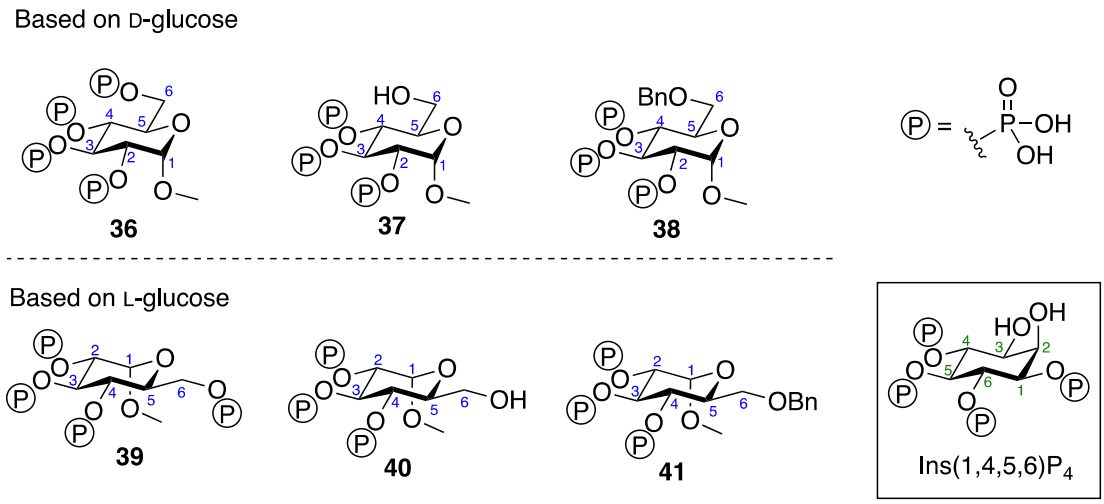

Figure 63: The carbohydrate compounds synthesised and tested at the Ins(1,4,5,6)P_4 HDAC3-SMRT binding site: methyl α-D-glucopyranoside 2,3,4,6-tetrakisphosphate (**36**), methyl α-D-glucopyranoside 2,3,4-trisphosphate (**37**), methyl 6-*O*-benzyl α-D-glucopyranoside 2,3,4-trisphosphate (**38**), methyl α-L-glucopyranoside 2,3,4,6-tetrakisphosphate (**39**), methyl α-L-glucopyranoside 2,3,4-trisphosphate (**40**) and methyl 6-*O*-benzyl α-L-glucopyranoside 2,3,4-trisphosphate (**41**).

In addition to these carbohydrate compounds, a number of compounds previously synthesised by the Potter group, including inositol pyrophosphates and their non-hydrolysable analogues, were evaluated biologically in concert to start building a wider structure-activity relationship of the Ins(1,4,5,6)P_4 binding site in the HDAC3-SMRT complex (Figure 74).

4.3.1 Binding mode predictions for the proposed carbohydrate-based HDAC3-SMRT ligands

As mentioned in the Introduction, the structures of *myo*-inositol and D- and L-glucose are quite similar for half of the ring structures, and it was hoped that it might be possible to generate carbohydrate-based activators for the HDAC3-SMRT complex. Taking into consideration the binding requirements established in the initial study into the HDAC3-SMRT Ins(1,4,5,6)P_4 binding site,[112] it was determined that some of the potential binding modes for the six carbohydrate compounds generated in this study may be more likely than others (Figure 64).

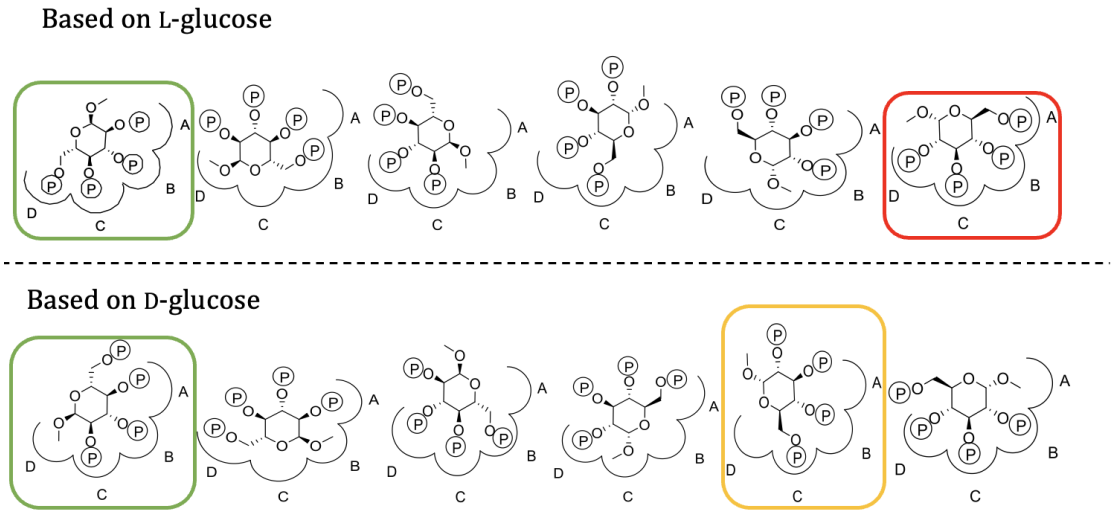

Figure 64: Predicted binding modes for methyl α-L-glucopyranoside 2,3,4,6-tetrakisphosphate (**39**, top row) and methyl α-D-glucopyranoside 2,3,4,6-tetrakisphosphate (**36**, bottom row). Binding modes expected to be favourable have been circled in green, a mode expected to unfavourable despite having three consecutive phosphate groups in red, and a mode that could be tolerated but would require unusual rotation of the ligand in the binding site is circled in yellow.

From the predicted binding modes, methyl α-L-glucopyranoside 2,3,4,6-tetrakisphosphate (**39**) was anticipated to be best suited to bind to the Ins(1,4,5,6)P_4 site as it could conceivably adopt two orientations that would place phosphates into all four of the same regions of the binding site as Ins(1,4,5,6)P_4. However, as steric bulk is not anticipated to be tolerated in the A region of the binding site,[112] one of these binding modes was predicted to be significantly less favourable as it would place the extended 6-position carbohydrate hydroxyl into this region (Figure 64, shown circled in red).

Due to the fact that methyl α-L-glucopyranoside 2,3,4,6-tetrakisphosphate (**39**) was expected to occupy the site in a probable binding mode that positions four phosphates and methyl α-D-glucopyranoside 2,3,4,6-tetrakisphosphate (**36**) was only expected to be able to bind with a maximum of three phosphates, the L-glucose-derived compound was expected to be the favoured enantiomer. There was a possibility that the D-enantiomer could bind reasonably well, however, as in one of the possible binding modes (Figure 64, circled in green on the bottom row), in addition to satisfying the requirement of having three consecutive phosphates in the A, B and C regions of the binding site, the fourth phosphate attached to the extended 6-position might be able to form a new interaction with the residues at the edge of the A region (such as Arg265).

A second possible binding mode could also potentially satisfy the ligand binding requirements for methyl α-D-glucopyranoside 2,3,4,6-tetrakisphosphate (**36**, Figure

64, circled in yellow), although this would necessitate the C region of the binding site accommodating the extended carbohydrate phosphate, which might not be tolerated. From the initial study into this binding site, it was determined that the B and/or C region is capable of accommodating a pyrophosphate group, albeit with an accompanying decrease in complex activation, but not a phosphonoacetate group,[112] which might be a closer structural analogue to the extended phosphate of methyl α-D-glucopyranoside 2,3,4,6-tetrakisphosphate (**36**) as both functional groups lack an equivalent to the α-phosphate of a pyrophosphate.

From considering the potential binding modes of methyl α-L-glucopyranoside 2,3,4-trisphosphate (**40**) and methyl α-D-glucopyranoside 2,3,4-trisphosphate (**37**), it was less clear which enantiomer might be better tolerated by the enzyme complex, as both were expected to be able to bind to the site in an orientation that positions the three phosphates in the likely required A, B, and C regions. Any disparity in activity observed between these enantiomers will probably be due to the substituent situated in the D region of the binding site (an axial *O*-methyl in the D-enantiomer and an extended equatorial hydroxyl in the L-enantiomer) being tolerated to different extents.

The remaining two carbohydrate-based compounds synthesised in the originally tested batch, methyl 6-*O*-benzyl-α-L-glucopyranoside 2,3,4-trisphosphate (**41**) and methyl 6-*O*-benzyl-α-D-glucopyranoside 2,3,4-trisphosphate (**38**), incorporated pendant benzyl groups into the ligand structure. Presuming that the benzyl groups would not be allowed into the depths of the binding pocket, the potential orientations of any binding modes should be restricted and the SARs more straightforward to determine. In the original study by Watson *et al*.,[112] it was determined that analogues of Ins(1,4,5,6)P_4 with benzyl groups attached to the 2- and or 3-position (2-*O*-Bn-Ins(1,4,5,6)P_4 and 2,3-di-*O*-Bn-Ins(1,4,5,6)P_4) are able to activate the enzyme complex, so the pendant benzyl groups of the carbohydrate compounds might also be tolerated.

It was even hoped these benzyl substituents might be able to form hydrophobic binding interactions which could compensate for the loss of the fourth phosphate group (particularly for methyl 6-*O*-benzyl-α-L-glucopyranoside 2,3,4-trisphosphate, **41**, which would be expected to position the benzyl group potentially near the Lys475 residue and the distant Arg301 in the D region). If such a hydrophobic interaction could be formed to improve ligand affinity, it could allow for less polar, more hydrophobic drug-like complex activators to be developed in the future.

4.3.2 GOLD docking predictions for the proposed carbohydrate-based HDAC3-SMRT ligands

Molecular modelling programs (such as GOLD: Genetic Optimisation for Ligand Docking) enable predictions to be made concerning the nature of small molecules interacting with protein binding sites. These programs carry out a search algorithm recursively to determine low-energy solutions detailing orientations in which ligands can occupy protein structure (acquired through X-ray crystallography). These solutions are assigned a 'fitness' score that can be used to rank the orientations calculated for a ligand within the binding site and determine which solution is more likely to result in favourable ligand binding.

The glucose-based ligands were docked in the crystal structure of the HDAC3-SMRT Ins(1,4,5,6)P_4 binding site (PDB: 4A69)[196] using an optimised GOLD procedure (refer to the Experimental for details regarding the docking software optimisation and some of the highest and lowest ranked exact docking scores). Interestingly, it was found that the L-glucose-based compounds consistently scored higher than their D-glucose-based enantiomers in the optimised docking protocols.

Methyl α-L-glucopyranoside 2,3,4,6-tetrakisphosphate (**39**) tended to score highest out of all of the glucose-based ligands assessed. Although several different binding modes were generated in the top scoring solutions, two orientations seemed to predominate: one in which the carbohydrate ligand was slightly shifted from the location of bound Ins(1,4,5,6)P_4 to accommodate the extended phosphate in the D region (Figure 64, circled in green on the top row) as initially predicted; and another, in which the ring structure of the docked ligand was dramatically shifted to position the extended phosphate in the A region (Figure 64, circled in red).

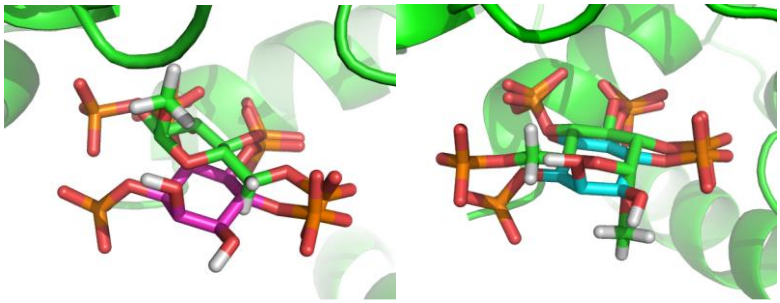

Figure 65: On the left, Ins(1,4,5,6)P_4 (coloured pink) and methyl α-L-glucopyranoside 2,3,4,6-tetrakisphosphate (**39**, coloured green) are shown in one possible binding orientation that positions the extended phosphate of the carbohydrate compound in the A region (docking solution 4, GOLDscore fitness: 146.4667, corresponding to the binding mode in Figure 64 circled in red). On the right, Ins(1,4,5,6)P_4 (coloured aqua) and methyl α-L-glucopyranoside 2,3,4,6-tetrakisphosphate (**39**, coloured green) are shown with the glucose phosphate in a different possible binding orientation that positions the extended phosphate in the D region (docking solution 35, GOLDscore fitness: 169.0041, corresponding to the binding mode in Figure 64 circled in green on the top row). Docking solutions were obtained with GOLD in the 4A69 crystal structure.[196]

The docking solutions for methyl α-L-glucopyranoside 2,3,4,6-tetrakisphosphate (**39**) that positioned the extended 6-position phosphate into the D region (Figure 65, right) mirrored the binding mode predicted to be most likely to be achieved by this ligand. As the extended phosphate group appears to be tolerated deeper within the D region in some of the docking solutions, the possibility that this phosphate may be able to form stronger interaction with residues such as Arg301 remains.

The docking solutions that positioned the extended 6-position phosphate into the A region of the binding site (Figure 65, left) appeared to force the ligand to shift significantly from its expected plane of binding to be accommodated. By shifting in this way, the extended 6-position phosphate does not appear to be placed deeper into the protein binding site and instead occupies the usual location of the 4-position phosphate of Ins(1,4,5,6)P_4, thereby aligning with the assumption that the A region cannot tolerate steric bulk.

The methyl α-D-glucopyranoside 2,3,4,6-tetrakisphosphate (**36**) was also predicted to bind to the HDAC3-SMRT site in a number of different orientations in the top-scoring docking solutions. The binding modes varied such that the extended 6-position phosphate could be positioned out into solvent, into the C region of the binding site or, in the most commonly observed orientation, into the A region of the binding site which resulted in the ligand being displaced from its expected plane of binding to be accommodated by the binding site (Figure 66).

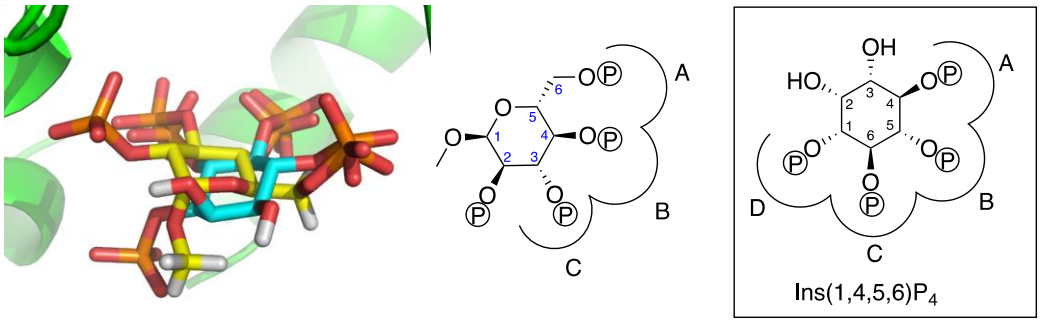

Figure 66: On the left, Ins(1,4,5,6)P_4 (shown in aqua) and methyl α-D-glucopyranoside 2,3,4,6-tetrakisphosphate (**36**, shown in yellow) are shown in an orientation in which the extended 6-position phosphate occupies the A region of the HDAC3-SMRT binding site (docking solution 13, GOLDscore fitness: 141.8075) generated using the PDB: 4A69.[196] In the centre is a ChemDraw depiction approximately corresponding to the binding mode on the left, which shows the axial methoxy group and the 2-position phosphate group bending out of the D site to allow the other phosphates of methyl α-D-glucopyranoside 2,3,4,6-tetrakisphosphate (**36**) to be accommodated. On the right is the binding orientation of Ins(1,4,5,6)P_4.

Both methyl α-L-glucopyranoside 2,3,4-trisphosphate (**40**) and methyl α-D-glucopyranoside 2,3,4-trisphosphate (**37**) were expected to bind less efficiently to the HDAC3-SMRT site compared to their corresponding tetrakisphosphates, and this was

reflected in poorer-scoring docking solutions. The highest-scoring solutions for both enantiomers also demonstrated a small range of docking orientations in the binding site, but these tended to significantly shift the central carbohydrate ring out of the plane in which Ins(1,4,5,6)P_4 binds.

Although in the docking experiments there appeared to be a few binding modes of both methyl 6-*O*-benzyl-α-L-glucopyranoside 2,3,4-trisphosphate (**41**) and methyl 6-*O*-benzyl-α-D-glucopyranoside 2,3,4-trisphosphate (**38**) that were calculated to be favourable, the majority of the one hundred docking solutions generated for each enantiomer did not predict that either of the compounds would bind well. The higher-scoring docking solutions of both compounds usually depicted the glucose ring structure forced further into the binding site, while the benzyl group occupied either the edge of the D region or faced out into solvent. The distant possibility that a cation-π interaction might form between the pendant benzyl groups at the outer edge of the binding pocket and some of the nearby residues remained, however, as the binding simulation may not be able to account for this interaction, should it occur.

4.4 Synthesis of the carbohydrate-based potential HDAC3-SMRT ligands

The D-glucose-based ligands were synthesised first (Scheme 6), and the reactions in the synthetic route were optimised before they were repeated with the considerably more expensive enantiomer, L-glucose, as a starting material (Scheme 7).

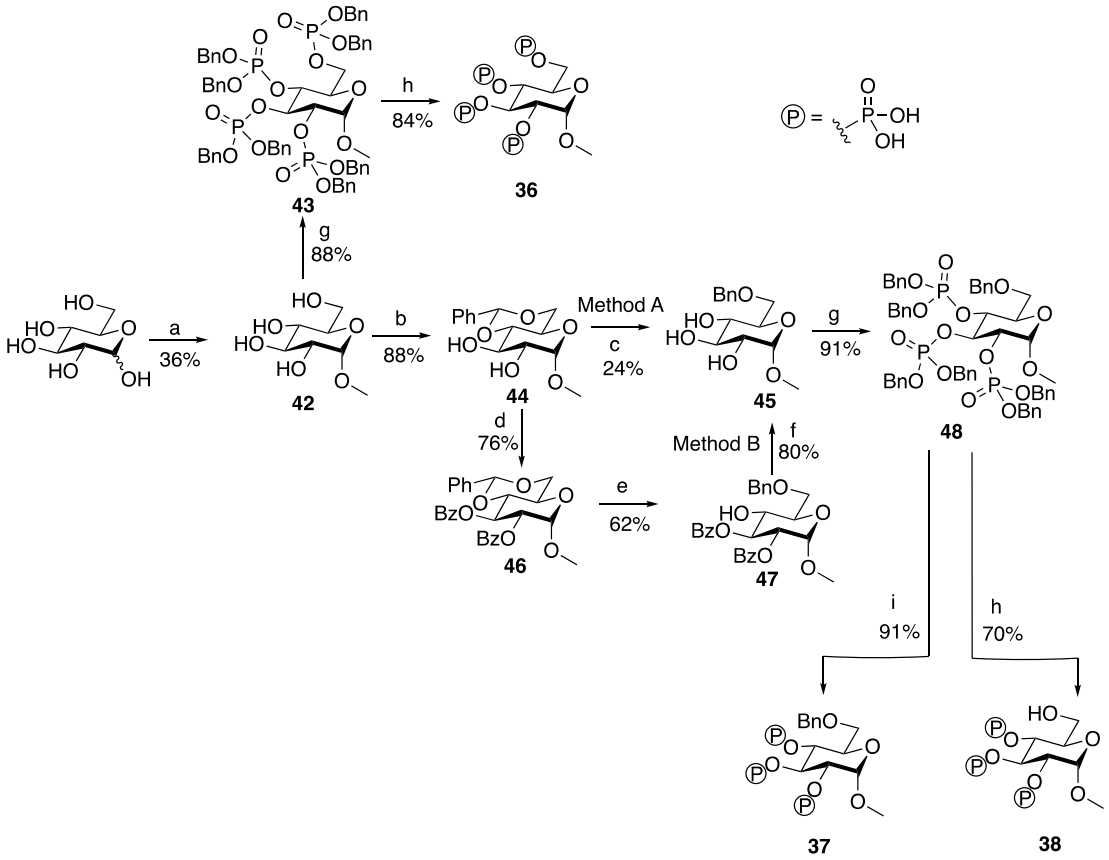

Scheme 6: Synthetic route for the D-glucose based HDAC ligands: methyl α-D-glucopyranoside 2,3,4,6-tetrakisphosphate (**36**), methyl α-D-glucopyranoside 2,3,4-trisphosphate (**37**) and methyl 6-*O*-benzyl α-D-glucopyranoside 2,3,4-trisphosphate (**38**).

Reagents and conditions: (a) CH_3COCl, MeOH; (b) $PhCH(OMe)_2$, cat. CSA, MeCN; (c) TMDS, $AlCl_3$, DCM; (d) BzCl, py; (e) $Me_3N.BH_3$, $AlCl_3$, THF, H_2O; (f) NaOH, MeOH; (g) 1. dibenzyl phosphoramidite, 5-Phenyl-*1H*-tetrazole, DCM, 2. *m*CPBA; (h) 1. $Pd(OH)_2/C$, H_2, MeOH, H_2O, 2. TEA; (i) 1. TMSBr, DCM, 2. TEAB.

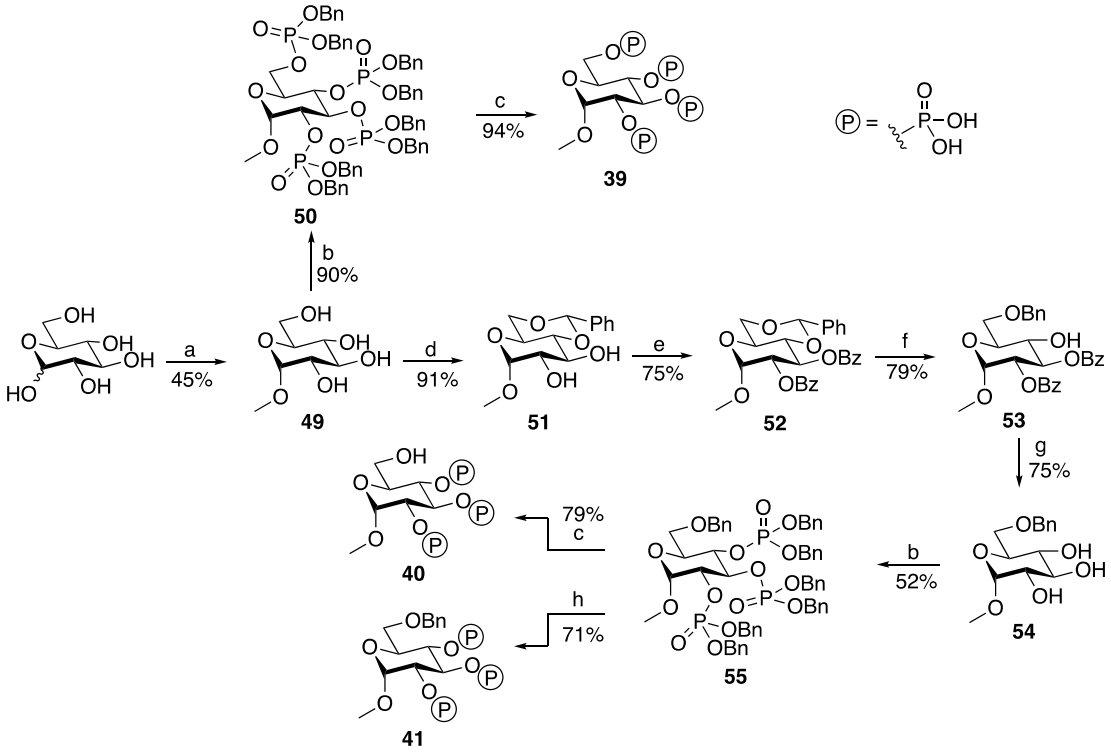

Scheme 7: Synthetic route for the L-glucose based HDAC ligands: methyl α-L-glucopyranoside 2,3,4,6-tetrakisphosphate (**39**), methyl α-L-glucopyranoside 2,3,4-trisphosphate (**40**) and methyl 6-*O*-benzyl α-L-glucopyranoside 2,3,4-trisphosphate (**41**).

Reagents and conditions: (a) CH_3COCl, MeOH; (b) 1. Benzyl P(III) agent, 5-Phenyl-*1H*-tetrazole, DCM, 2. *m*CPBA; (c) 1. $Pd(OH)_2/C$, H_2, MeOH, H_2O, 2. TEA; (d) $PhCH(OMe)_2$, cat. CSA, MeCN; (e) BzCl, py; (f) $Me_3N.BH_3$, $AlCl_3$, THF; (g) NaOH, MeOH; (h) 1. TMSBr, DCM, 2. TEAB.

For all of the carbohydrate-based ligands designed for HDAC3-SMRT, the first step in the synthesis was the methylation of glucose, which was carried out using the method described in Li *et al.*[200] The five-day reflux provided a sufficiently long period of time for the ratio of the stereoisomeric products to equilibrate and favour the formation of the more thermodynamically stable α-anomer. In every iteration of the reaction, the first recrystallization from ethanol of the crude product resulted in obtaining primarily the α-anomer, with only approximately 3% of the β-anomer. Upon a second recrystallization, the product could be isolated as pure methyl-α-glucospyranoside without any trace of the β-anomer. It was possible to increase the reaction yield by recycling the mother liquor of the recrystallisations into a second glycosylation reflux to re-equilibrate the product and obtain more of the desired α-anomer upon further repeated recrystallisations (**42**, D: 36% yield; **49**, L: 45% yield).

Following methylation, the synthetic route diverged to generate either the tetrakisphosphate product or the trisphosphate products. To continue the route to methyl α-glucopyranoside 2,3,4,6-tetrakisphosphate, the next reaction was the

stepwise phosphorylation of methyl-α-glucopyranoside. The phosphitylation was carried out with dibenzyl phosphoramidite, which was activated with 5-phenyl-1*H*-tetrazole and the resultant phosphite intermediate was subsequently oxidized with *m*CPBA to yield the protected tetrakisphosphate product (**43**, D: 88% yield; **50**, L: 90% yield).

The last step in the route to synthesise both enantiomers of the methyl glucopyranoside 2,3,4,6-tetrakisphosphate product was to cleave the benzyl groups from the protected precursors via hydrogenation. The hydrogenation was catalysed by palladium hydroxide on carbon and allowed to take place over twenty-four hours. The hydrogenation was found to be sufficiently clean that purification was not deemed necessary and the methyl glucopyranoside 2,3,4,6-tetrakisphosphate product, initially collected as a free acid, was converted to triethylammonium salt prior to storage and subsequent biological evaluation (**36**, D: 84% yield; **39**, L: 94% yield).

To generate the remaining trisphosphate target compounds, the methyl α-glucopyranoside from the initial divergence point was regioselectively protected with a benzylidene group at the 4- and 6-position hydroxyls. This benzylidene protection was accomplished by refluxing the methyl α-glucopyranoside with benzaldehyde dimethyl acetal and catalytic camphorsulphonic acid in chloroform, as described by Tseberlidis *et al.*[201] The inclusion of the acidic catalyst in this benzylidene protection has been previously studied and found markedly to increase the reaction yield.[202] Although this reaction is technically reversible, the yields in this study did not indicate that the consumption of the protected product, methyl 4,6-benzylidene α-glucopyranoside, was an issue on the scale used (D: 88% yield, L: 91% yield). The benzylidene acetal moiety is a popular protecting group in carbohydrate chemistry, as it is very stable under basic conditions but labile under acidic conditions. It is also possible reductively to open the benzylidene acetal regioselectively to yield either the 4-*O*-benzyl-protected product or the 6-*O*-benzyl-protected product, which proved to be useful in the following step.[203–205]

The next step in the synthetic route for both remaining trisphosphate targets was the regioselective opening of the benzylidene group to generate methyl 6-*O*-benzyl α-glucopyranoside. For the reaction route to the target ligands in this HDAC3-SRMT study, the 6-*O*-benzyl α-glucopyranoside product regioisomer was desired, whereas in the investigation into the synthesis of glucose-based $InsP_3R$ ligands (Chapter 5), this benzylidene opening was revisited with different reaction conditions to favour the other product regioisomer, 4-*O*-benzyl α-D-glucopyranoside. It was found to be important to control the direction in which the benzylidene group was opened carefully, as the mono-benzyl-protected product regioisomers (methyl 6-*O*-benzyl α-glucopyranoside and methyl 4-*O*-benzyl α-glucopyranoside) proved very difficult to

separate. Fortunately, the direction in which the benzylidene ring opens can be controlled through careful tuning of the reaction conditions.

The regioselectivity of the benzylidene opening can be influenced by a number of factors including the Lewis acid, the solvent and the choice of reducing agent used.[206–208] However, depending on the reducing agent used, the choice of Lewis acid is not always thought to have a very significant impact on the regioselectivity of the reaction and often instead appears mostly to affect the rate of benzylidene opening.[72] It is also possible for the steric bulk of substituents attached to the neighbouring 3-position hydroxyl to have an effect on the regioselectivity, but this is not thought to be a major influence compared to other variables.[206,208]

The regioselectivity is largely determined by which species in the reaction is the most electrophilic and will preferentially attack the most nucleophilic oxygen on the benzylidene acetal (the 6-position oxygen). The most electrophilic species is usually the Lewis acid, be it solvated or unsolvated, unless the reducing agent employed in the reaction is a borane reagent that can be activated by the Lewis acid to become the most electrophilic species. If a borane electrophile cannot be activated by the Lewis acid, the Lewis acid is instead expected to be the first species to coordinate to the most nucleophilic oxygen of the benzylidene acetal (usually the 6-position). This allows the borane electrophile to coordinate to the exposed 4-position of the acetal and open the benzylidene ring to yield the 4-*O*-benzyl product regioisomer (employed in a synthetic route described in Chapter 5).[206]

The choice of solvent aids in controlling the order in which the reagents coordinate to the benzylidene group through differing degrees of solvation of the reagents or cationic intermediates formed during the reaction, thereby influencing the major product regioisomer formed.[206,208] It should be noted, however, that the use of unsolvated electrophiles has been known to lead to lower yields and regioselectivities of benzylidene openings.[209,210]

The first set of conditions attempted to generate the desired methyl 6-*O*-benzyl α-D-glucopyranoside product used aluminium chloride and 1,1,3,3-tetramethyldisiloxane (TMDS) in DCM, as described by Zhang *et al.* (Figure 67),[211] which was initially carried out on a relatively large scale (1.0 g). The regioselectivity of benzylidene openings using TMDS as a reducing agent has been demonstrated to be controlled through the choice of Lewis acid, with $Cu(OTf)_2$ resulting in the preferential formation of the 4-*O*-benzyl product and $AlCl_3$ resulting in the 6-*O*-benzyl product.[211] Although the 6-position oxygen is likely the most nucleophilic in the acetal starting material and therefore favoured for Lewis Acid coordination, the aluminium chloride would also be expected to coordinate to the 4-position oxygen, thereby forming two possible oxocarbenium intermediate regioisomers. The reduction of the oxocarbenium intermediate, which is thought to be the rate-determining step of the TMDS-driven

benzylidene opening reaction,[211] appeared to favour selectively the reduction of the intermediate resulting in the 6-*O*-benzyl product.

Although successful in generating the desired methyl 6-*O*-benzyl α-D-glucopyranoside (**45**, D: 24% yield), the yield of the reaction was deemed to be unsuitable for repetition in the L-glucose synthetic route due to the limited supply of the starting material, and so different benzylidene opening conditions were investigated.

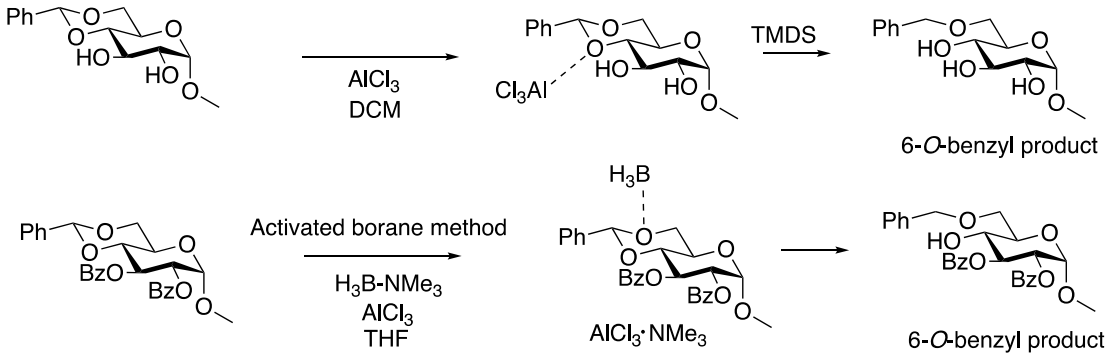

Figure 67: The two different reaction conditions attempted to regioselectively open the benzylidene ring to the 6-*O*-benzyl-protected product, using $AlCl_3$ and TMDS, as described by Zhang *et al.*,[211] and using $AlCl_3$ and borane-trimethylamine in the modified Garegg activated borane method.[206,210]

While it has already been reported that protecting the 2- and 3-position hydroxyls of a benzylidene-protected carbohydrate material is not necessary for opening the benzylidene group attached to the 4- and 6-positions, it has been found that allowing these hydroxyls to remain exposed can, although will not necessarily, reduce the regioselectivity and yield of the reaction.[206,211,212] To try to improve the yield of the benzylidene opening, the 2- and 3-position hydroxyls of the methyl 4,6-*O*-benzylidene α-glucopyranoside were protected with benzoyl groups prior to the next regioselective opening attempt with benzoyl chloride, as described by Ansell and Honeyman (**46**, D: 76% yield; **52** L: 75% yield).[213]

The next set of reaction conditions trialled for the regioselective reductive benzylidene opening of the methyl 2,3-*O*-di-benzoyl-4,6-*O*-benzylidene α-glucopyranoside was a modified version of the Garegg *et al.* method that employed aluminium chloride and borane trimethylamine in THF and water (Figure 67).[206,210]

In this reaction, rather than directly coordinating to the benzylidene starting material, the aluminium chloride instead coordinates first to the borane trimethylamine complex, thereby rendering the borane species the Lewis acid in the benzylidene ring opening that can coordinate to the most nucleophilic oxygen in the benzylidene acetal.[208] The regioselectivity of this borane trimethylamine complex reaction can be tuned to open the benzylidene group in either direction depending on the solvent used. Should the reaction employ a polar solvent (such as THF), the activation of the

borane species would be allowed to take place, leading to the preferential formation of the 6-*O*-benzyl product regioisomer, but in a non-polar solvent (such as toluene), the aluminium chloride would not activate the borane but instead coordinate directly to the benzylidene acetal, resulting in the preferential formation of the 4-*O*-benzyl product regioisomer.[209,210,214]

Although a small amount of water was added to the reaction, the competing hydrolysis reaction to cleave the benzylidene group did not appear to occur to a large extent. These conditions for the benzylidene opening proved to be sufficiently regioselective and high-yielding to allow both methyl 2,3-di-*O*-benzoyl-6-*O*-benzyl α-glucopyranoside product enantiomers to be isolated in reasonable yield (**47**, D: 62% yield; **53**, L: 79% yield).

The benzoyl-protecting groups were then selectively cleaved from the methyl 2,3-di-*O*-benzoyl-6-*O*-benzyl α-glucopyranoside in a simple alkaline solvolysis, as described by Marchant *et al.,*[215] to generate methyl 6-*O*-benzyl glucopyranoside (**45**, D: 80% yield; **54**, L: 75% yield).

Following the deprotection of the benzoyl groups, the next step carried out in the synthetic route was the phosphorylation of the newly exposed hydroxyl groups, which proceeded via a P(III) method, as described in the Introduction. The 6-*O*-benzyl α-glucopyranoside was phosphorylated with dibenzyl phosphoramidite and 5-phenyl-1*H*-tetrazole followed by *m*CPBA to form the protected 6-*O*-benzyl α-glucopyranoside 2,3,4-tris(dibenzylphosphate) products (**48**, D: 91% yield; **55**, L: 52% yield).

Another point of divergence occurs at the final step in the synthesis route, the deprotection of the benzyl-protecting groups. To synthesise the methyl 6-*O*-benzyl α-glucopyranoside 2,3,4-trisphosphate product, milder debenzylation conditions were required to prevent the benzyl ether group protecting the 6-position from being cleaved, while the methyl α-glucopyranoside 2,3,4-trisphosphate product required more forcing deprotection conditions to ensure complete debenzylation.

To generate the fully deprotected methyl α-glucopyranoside 2,3,4-trisphosphate, the benzyl-protecting groups were cleaved through palladium hydroxide on carbon catalysed hydrogenation. As both methyl α-glucopyranoside 2,3,4-trisphosphate enantiomer products were found to be suitably clean following filtration of the catalyst, purification was not deemed necessary and the products were converted from free acids to triethylammonium salts through exposure to triethylamine prior to storage and biological evaluation (**37**, D: 70% yield; **40**, L: 79% yield).

As a standard hydrogenation procedure would be unsuitable for the milder, partial deprotection required to generate methyl 6-*O*-benzyl α-glucopyranoside 2,3,4-trisphosphate, an alternative debenzylation method was employed. The selective debenzylation of the benzyl ester groups was achieved using trimethylsilyl bromide

(TMSBr), which has previously been demonstrated in literature to cleave alkyl-protecting groups from phosphates.[216,217] Deprotection of benzyl ester groups using TMSBr first proceeds via silylation of the phosphate groups (displacing the alkyl-protecting groups), followed by solvolysis (Figure 68).[217]

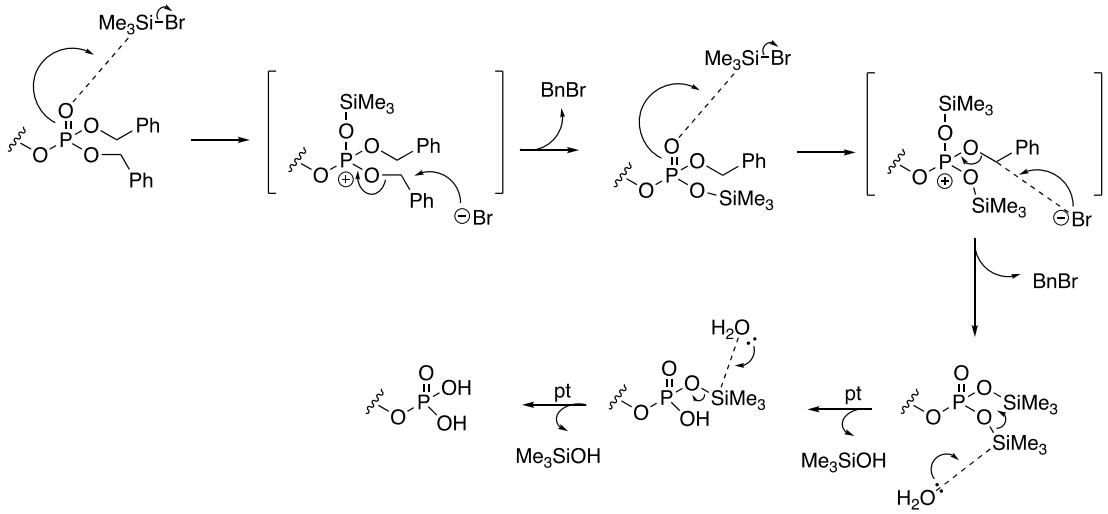

Figure 68: Mckenna *et al.* mechanism for the TMSBr-mediated deprotection of phosphates demonstrated with a dibenzyl-protected phosphate.[218]

In the first step of the TMSBr deprotection, the protected trisphosphate was allowed to stir with TMSBr in dry DCM for three hours to allow silylation to occur. The silylated material was not isolated or characterised, but instead purified with a diethyl ether wash before being hydrolysed by TEAB buffer to yield the deprotected phosphate groups as triethylammonium salts. Unlike the hydrogenation deprotection, the TMSBr-mediated debenzylation was not a clean reaction and the final trisphosphate product generated required purification. Although the benzyl ester groups were preferentially cleaved from the phosphates, the minor side product generated by the TMSBr reactions appeared to be the fully deprotected methyl α-glucopyranoside 2,3,4-trisphosphate following cleavage of the 6-position benzyl ether group.

Although benzyl ester groups attached to phosphates would be expected to be more labile than the benzyl ether groups protecting hydroxyl groups, the benzyl attached to the primary 6-position of a carbohydrate ring has been found to be more readily cleaved than benzyl ethers bound to any of the other secondary hydroxyl positions.[219] This unwanted cleavage of the 6-position benzyl group was expected to a certain extent, as TMSBr has been previously reported to cleave other ether-protecting groups, although not as readily as the related TMSI reagent.[220] It would have been possible to synthesise the methyl α-glucopyranoside 2,3,4-trisphosphate product by repeating the TMSBr reaction with longer reaction times to allow the deliberate cleavage of the 6-position benzyl group to take place, although this option was not pursued due to the clean and efficient nature of the alternative hydrogenation

debenzylation. As reported in other studies, the methyl group attached to the anomeric position hydroxyl resisted deprotection entirely under these deprotection conditions.[217,220]

The methyl 6-*O*-benzyl α-glucopyranoside 2,3,4-trisphosphate product enantiomers were both purified using reverse-phase column chromatography, and a qualitative Briggs phosphate assay (details in the Experimental) was carried out after each column to confirm the presence of product in the collected fractions. The triethylammonium salts of the methyl 6-*O*-benzyl α-glucopyranoside 2,3,4-trisphosphate enantiomer products were lyophilised and collected as colourless glasses (**38**, D: 91% yield; **41**, L: 71% yield).

4.5 HDAC3-SMRT biological results

4.5.1 HDAC3-SMRT deacetylation assay: carbohydrate-based ligands

The ability of each compound to activate the HDAC3-SMRT complex was investigated by our collaborators Dr Jennifer Gurnett, Mr Ed Brown and Dr Yun Song from the Schwabe lab (University of Leicester). The activity of the HDAC3-SMRT complex in the presence of each ligand was measured in a homogenous fluorogenic assay using a BOC-Lys-AMC substrate, as first described by Wegener *et al*.[221] The Schwabe group used this assay in the initial study on HDAC3-SMRT activation, reported in Watson *et al.*[112]

The first step of the assay involved the incubation of the inositol phosphate ligand or analogue under investigation (each in a different well on the plate) with recombinant HDAC3-SMRT from which the endogenous co-purified Ins(1,4,5,6)P_4 ligand had been stripped.

This activated HDAC3-SMRT complex was then incubated with the BOC-Lys-AMC substrate, during which time the activated enzyme complex cleaved the acetyl group from the lysine moiety of the substrate (Figure 69). The progress of deacetylation was then halted through the addition of the developer solution that contained Trichostatin A (TSA) to inhibit further HDAC3-SMRT activity as well as trypsin, which cleaved only the deacetylated BOC-Lys-AMC substrate, thereby releasing the fluorescent 4-amino 7-methylcoumarin and indicating successful activation of the enzyme complex.

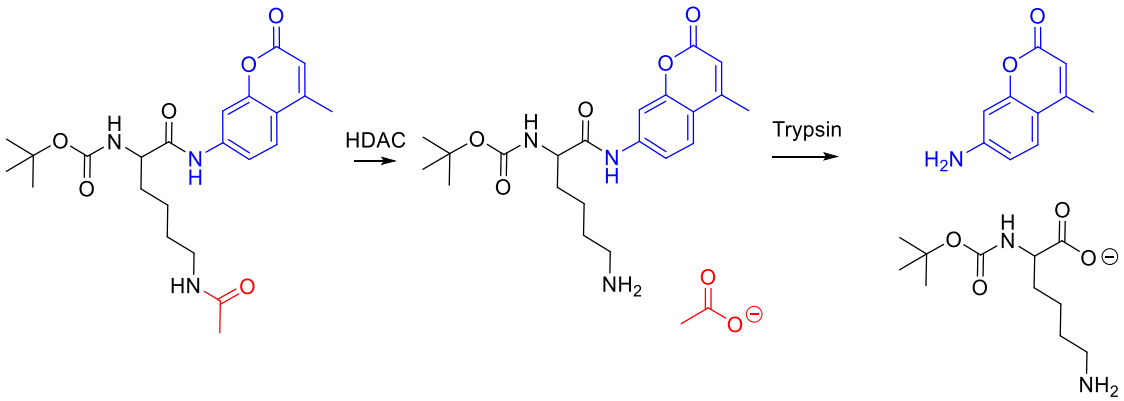

Figure 69: The BOC-Lys-AMC substrate in the HDAC binding assay. The first step, exposure to the activated HDAC3-SMRT enzyme, results in the cleavage of the acetyl group (depicted in red). The second step, exposure to the trypsin-containing developer solution, results in the trypsin-driven cleavage of the fluorescent 4-amino 7-methylcoumarin group (depicted in blue), which can only take place if the acetyl group has been cleaved.

The amount of fluorescence generated by each ligand as a result of the release of 4-amino 7-methylcoumarin (measured in a plate reader at 335/460 nm) was indicative of the extent to which each ligand (100 µM) was able to activate the HDAC3-SMRT complex and facilitate deacetylation. For more detailed protocol for this assay, refer to the Experimental section.

The carbohydrate-based ligands were analysed first in the HDAC3-SMRT assay (Figure 70 and Table 7).

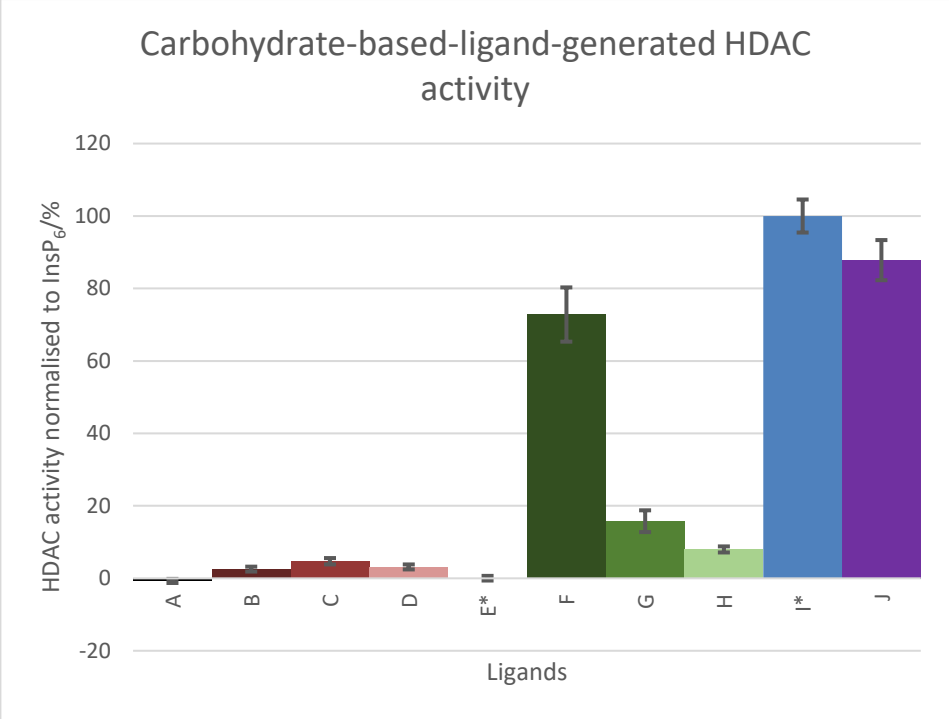

Ligand	HDAC activity normalised to $InsP_6$
A. Protein only	-0.7
B. α-D-Glu(2,3,4,6)P_4OMe, **36**	2.5
C. D-6OHGlu(2,3,4)P_3OMe, **37**	4.7
D. D-6OBnGlu(2,3,4)P_3OMe, **38**	3.1
E.* β-D-Glu(2,3,4,6)P_4OMe, **56**	0.0
F. L-Glu(2,3,4,6)P_4OMe, **39**	72.8
G. L-6OHGlu(2,3,4)P_3OMe, **40**	15.8
H. L-6OBnGlu(2,3,4)P_3OMe, **41**	8.0
I. $InsP_6$	100.0
J. Ins(1,4,5,6)P_4	87.8

Figure 70 and Table 7: The normalised activity of the carbohydrate-based ligands in the HDAC assay carried out by Jennifer Gurnett and Dr Yun Song from the Schwabe lab (University of Leicester). The assay was repeated in technical triplicate and the mean values for each ligand were normalised to the activity generated by $InsP_6$ and are reported in the table on the right. The entry with an asterisk indicates that the assay for this compound was carried out at a later date to the other results under the same conditions by Ed Brown from the Schwabe lab. Error bars indicate ± s.e.m (n=3).

The compound that was predicted to be the most active of the carbohydrate-based compounds from comparison of the hypothetical binding modes and supported by the results of the docking studies, methyl-α-L-glucopyranoside 2,3,4,6-tetrakisphosphate (**39**, Figure 70 and Table 7), was indeed the most active of this set. In fact, it proved to

be the only glucose-based ligand tested to induce reasonably high HDAC activity [approx. 83% of the activity observed with Ins(1,4,5,6)P_4 and 73% of the observed activity of InsP_6].

Although not pursued in this study, as methyl α-L-glucopyranoside 2,3,4,6-tetrakisphosphate (**39**) was found to be reasonably active at the HDAC3-SMRT site, it might be interesting to see if analogues of this structure could potentially also be generated. As the methyl group bound to the anomeric centre is presumed to face out into solvent and have a minimal impact on binding, it may be possible to substitute this moiety for a group that might be more easily derivatised to allow for the synthesis of potential probes or affinity columns.

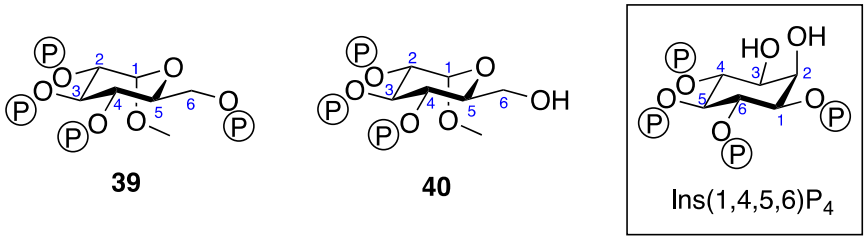

Figure 71: Structures of methyl-α-L-glucopyranoside 2,3,4,6-tetrakisphosphate (**39**, left) and methyl α-L-glucopyranoside 2,3,4-trisphosphate (**40**, centre), the carbohydrate-based ligands found to generate the highest HDAC3-SMRT activity, as well as the endogenous ligand Ins(1,4,5,6)P_4 (right).

The activity of the methyl α-L-glucopyranoside 2,3,4-trisphosphate (**40**, Figure 70 and Table 7) was significantly less than that of methyl α-L-glucopyranoside 2,3,4,6-tetrakisphosphate [approx. 18% of the activity observed with Ins(1,4,5,6)P_4 and 16% of the observed activity of InsP_6], which seems to indicate that the phosphate attached to the extended 6-position of the latter (presumably occupying the D position of the binding site) contributes positively to ligand binding. Although a decrease in activity was expected due to the absence of a fourth phosphate, the observed reduction in activity was far more dramatic than anticipated. In the initial Watson *et al.* study, it was found that inositol phosphates with three consecutive phosphates, presumed to occupy the A, B and C site pockets, were able to activate the HDAC3-SMRT complex to a reasonable extent [Ins(1,5,6)P_3 and Ins(4,5,6)P_3 achieved approx. 60% and 85% respectively of the activity of Ins(1,4,5,6)P_4].[112] As the α-L-glucopyranoside trisphosphate (**40**) produced significantly less activity in comparison, this could indicate that the extended 6-position hydroxyl is not tolerated in the D region of the binding site as well as hydroxyls bound directly to the ligand central ring structure.

Methyl 6-*O*-benzyl-α-L-glucopyranoside 2,3,4-trisphosphate (**41**) was not very well tolerated by the enzyme complex, with only weak deacetylase activity observed [approx. 9.1% that of Ins(1,4,5,6)P_4 and 8.0% that of InsP_6]. Assuming this compound would orient itself in the binding site such that the A, B and C regions are occupied by

phosphates, the equatorial benzyl group of this compound would be forced to be accommodated in the D region of the binding site. The minimal, but present, activity generated by this ligand may be the result of the pendant benzyl group being sufficiently flexible to be positioned as far from the D site as possible and out into solvent, as this and other results found in the study seem to indicate that the D region is unable to tolerate steric bulk.

Although a slight decrease in activity for the D-glucose series of compounds had been somewhat expected after comparison of the predicted binding modes and trends observed in the docking experiments of the enantiomer pairs, it had not been anticipated that these compounds would be virtually inactive. Further work needs to be carried out to determine exactly why the D-glucose-based compounds were completely unable to activate the HDAC complex.

Methyl α-D-glucopyranoside 2,3,4,6-tetrakisphosphate (**36**) was found to be the least active compound of all of those tested in the initial carbohydrate series with an activity of only 3.6% that of Ins(1,4,5,6)P_4 and 2.5% that of InsP_6. The contrast between the activities of the enantiomeric pair of methyl α-L-glucopyranoside 2,3,4,6-tetrakisphosphate (**39**) and methyl α-D-glucopyranoside 2,3,4,6-tetrakisphosphate (**36**) is much more marked than for any other pair of enantiomers previously tested at the HDAC3-SMRT allosteric binding site [Ins(1,4,5,6)P_4 and Ins(3,4,5,6)P_4 have previously been shown to be able to activate the complex with respective Kd_{app} values of 10 μM and 41 μM].[112] Due to the expectation that this ligand would bind to the HDAC3-SMRT site with three phosphate groups as opposed to four (like its enantiomer), only a slight decrease in activity had been anticipated (Figure 64). Evidently, the D-glucose-based enantiomer is not able to activate the deacetylase complex at all, presumably due to an inability to bind.

Methyl α-D-glucopyranoside 2,3,4-trisphosphate (**37**) was also found to be inactive at the HDAC3-SMRT site with a residual activity of 5.4% that of Ins(1,4,5,6)P_4 and 4.7% that of InsP_6. This is perhaps unsurprising given the inactivity of the tetrakisphosphate enantiomer, as the phosphate attached to the 6-position of methyl α-D-glucopyranoside 2,3,4,6-tetrakisphosphate (**36**), which the trisphosphate analogue lacks, had been expected to have a reasonably small effect on hypothetical ligand binding, as the binding mode deemed most likely positioned this group out of the binding site (Figure 64).

The last of the initial batch of carbohydrate-based compounds, methyl 6-*O*-benzyl-α-D-glucopyranoside 2,3,4-trisphosphate (**38**), was also found to be virtually inactive, registering only 3.6% of the activity of Ins(1,4,5,6)P_4 and 3.1% that of InsP_6. Due to the fact that all of the D-glucose-based compounds proved to be inactive, the possibility that the placement of the benzyl group near the A region of the binding site cannot be ruled out as a potential means of forming new hydrophobic interactions for ligands

of the HDAC3-SMRT inositol phosphate site, as there is evidently some other structural feature preventing the D-glucose-based series from binding.

The current theory for the failure of the α-D-glucose-based to activate the HDAC3-SMRT complex is that the axial methoxy group attached at the anomeric centre creates too much steric bulk in the D region of the binding site (in what is assumed to be the most promising hypothetical binding orientation for the ligands). It appears as though steric bulk cannot be tolerated in either the A region (as previously determined in the initial study)[112] or the D region, although the extent of the possible tolerance for larger steric groups in this region is not entirely clear yet, as some ligands (L-glucose-derived series) predicted to position bulkier groups in this region have been shown to retain some activity.

Further evidence of the D region being unable to tolerate much steric bulk, particularly in an axial orientation, can be gleaned from the currently unpublished results of the other Potter group compounds, which indicated that inositol pyrophosphate analogues that positioned axially oriented phosphate groups in the D region of the binding site are less active than regioisomers that do not (*vide infra* Section 4.4.3).

There is a possibility that the D region of the binding site is unable to tolerate steric bulk specifically in the *axial* orientation due to possible steric clashes with residues such as Arg301, and that substituents that are equatorially orientated may be better tolerated. Due to the fact that there is a slightly higher activity observed in methyl 6-*O*-benzyl- α-L-glucopyranoside 2,3,4-trisphosphate than for either the protein-only control or any of the D-glucose-based compounds, the binding site might be able at least partially to tolerate the benzyl-protecting group attached in an equatorial orientation to the extended 6-position in the D region. However, the hydrocarbon 6-position extension, which is predicted to be positioned in the D region in the most probable L-glucose derivative binding modes, might enable the moieties attached to the 6-position of these ligands to bend slightly out of the binding pocket to minimize steric clash in this region (Figure 72).

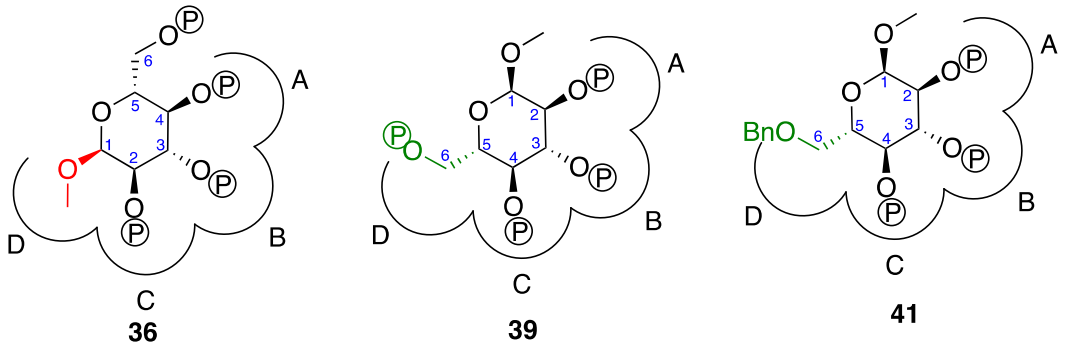

Figure 72: The hypothetical binding modes predicted to be the most favourable for methyl α-D-glucopyranoside 2,3,4,6-tetrakisphosphate (**36**, left), methyl α-L-glucopyranoside 2,3,4,6-tetrakisphosphate (**39**, centre) and methyl 6-*O*-benzyl-α-L-glucopyranoside 2,3,4-trisphosphate (**41**, right) in the HDAC3-SMRT site. The axial methyl group in methyl α-D-glucopyranoside 2,3,4,6-tetrakisphosphate (**36**) is believed to be responsible for the inability of this ligand to bind and has been highlighted in red. The equatorial extended phosphate and benzyl group which are predicted to be positioned in the same region of the binding site and have been highlighted in green are thought to be at least partially tolerated as both of these L-glucose-derived ligands were found to be able to activate the HDAC3-SMRT complex. The flexible nature of these extended equatorial groups might enable them partially to bend out of the binding site to minimize steric clashes in the D region.

As a follow-up to investigate the unexpected inactivity of the α-D-glucose series, methyl β-D-glucopyranoside 2,3,4,6-tetrakisphosphate (**56**, Figure 73) was synthesised and analysed at the HDAC3-SMRT site in the second set of potential ligands investigated. The synthesis to generate this ligand was identical to the route for methyl α-D-glucopyranoside 2,3,4,6-tetrakisphosphate, starting from a commercial supply of methyl β-D-glucopyranoside [via methyl β-D-glucopyranoside 2,3,4,6-tetrakis(dibenzylphosphate), **57**].

The inclusion of this compound in the second HDAC3-SMRT activation assay was to determine if, by merely changing the orientation of the methyl group from axial to equatorial, it might be possible to accommodate the steric bulk of the methyl group in the D region of the binding site (if indeed the compound is able to bind in this presumed orientation).

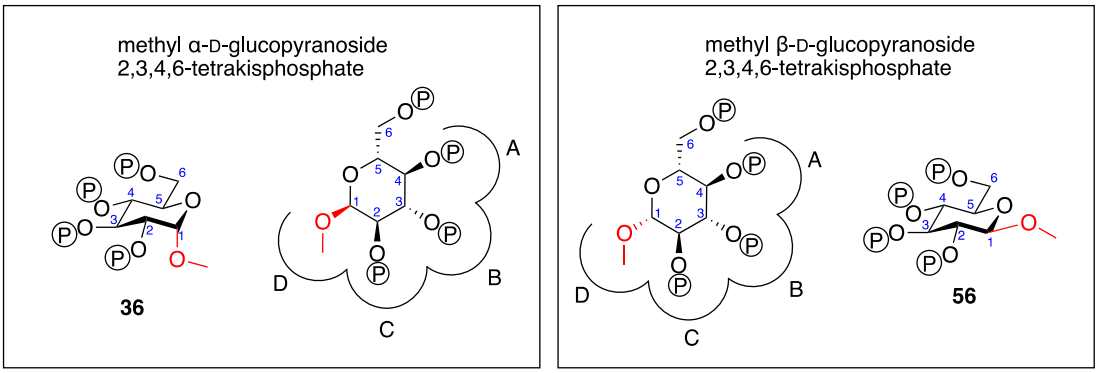

Figure 73: Predicted hypothetical binding modes deemed to be the most likely for methyl α-D-glucopyranoside 2,3,4,6-tetrakisphosphate (**36**, left) and methyl β-D-glucopyranoside 2,3,4,6-tetrakisphosphate (**56**, right) to adopt in the HDAC3-SMRT site. The 1-position methyl group, which is believed to be responsible for the inactivity of the D-glucose-based series is highlighted in red and this is the moiety that differs in orientation in these two tetrakisphosphate products.

It was found, however, that methyl β-D-glucopyranoside 2,3,4,6-tetrakisphosphate (**56**) was also unable to activate the active HDAC3-SMRT enzyme, as virtually no deacetylase activity was detected. This could indicate that the D region of the HDAC3-SMRT binding site is unable to tolerate steric bulk in either the equatorial or axial orientation, although this hypothesis remains to be proven conclusively.

Even if some steric bulk could be tolerated equatorially in the D region, the nature of the methyl group itself may be a factor preventing binding due to its lack of charge and relatively inflexible nature. Should the predicted binding modes for the L-glucose series be correct, the D region would be expected to tolerate a phosphate group attached to the extended 6-position (in methyl α-L-glucopyranoside 2,3,4,6-tetrakisphosphate, **39**) as well as, at least to a limited extent, a benzyl group also attached to the extended 6-position (in methyl 6-*O*-benzyl-α-L-glucopyranoside 2,3,4-trisphosphate, **41**). As mentioned previously, however, the flexible extension to these moieties, particularly the benzyl group, might allow them to bend out of the D region to avoid steric clashes (Figure 72).

To further probe the tolerance of the D region of the binding site, it may be interesting to investigate if D-glucopyranosyl 2,3,4,6-tetrakisphosphophosphate, which is entirely lacking in the anomeric methyl group, would be able to bind to the HDAC3-SMRT site (although this compound would be generated as a mixture of interconverting sugar stereoisomers rather than a single product). Another potential D-glucose-based compound that could prove to be active are the α- and β-glucopyranoside pentakisphosphates which would be predicted to position respectively an axial or equatorial phosphate in the D region. The presence of a charged phosphate in the D region may be sufficient to allow these D-glucose-based ligands to bind and activate the HDAC3-SMRT complex.

4.5.2 HDAC3-SMRT deacetylation assay: inositol pyrophosphates and analogues

In a genetic experiment carried out by Worley *et al.* on the class 1 HDAC yeast homologue Rpd3L, it was discovered that the function of this deacetylase was impaired following the deletion of the kcs1 and vip1 genes, which code for inositol pyrophosphate synthases in yeast. This indicates that Rpd3L, the class 1 HDAC homologue, might require the presence of an inositol pyrophosphate to be activated.[62] An allosteric inositol phosphate binding site has also been identified for Rpd3L, and it has been found that point mutations of residues in this binding site result in enzyme inactivity (although it is not known if the yeast enzyme forms a complex with a co-repressor protein analogous to SMRT).[62]

Due to the similar structure of Rpd3L and Class 1 HDACs, it has been suggested that the HDAC3-SMRT enzyme complex, featuring the Class 1 HDAC3, might bind to 1-PP-InsP_5, 5-PP-InsP_5, 5-PP-InsP_4 or 1,5-$(PP)_2$-InsP_4 as additional endogenous regulators of the enzyme.[62,112] Worley *et al.* proposed that the 1-PP-InsP_5 regioisomer, in particular, was a promising possible physiological activator of Rpd3L and therefore possibly also of HDAC3-SMRT. This choice of regioisomer was due to the expectation that the pyrophosphate would be accommodated by the D region of the binding site in one of the more likely binding modes (a mode that would position the axial 2-position substituent out of the binding site).[62] The results of this study cast some doubt on the ability of the D region to accommodate steric bulk however, although the use of charged moieties in this position seem to mitigate some of the steric clashes and allow for ligand binding (methyl α-L-glucopyranoside 2,3,4,6-tetrakisphosphate, **39**, is expected to position an extended phosphate in this region and this seems to be fairly well tolerated as the ligand is able to activate HDAC3-SMRT).

In addition to the evidence of inositol pyrophosphates seeming to activate Rpd3L, inspection of the HDAC3-SMRT allosteric binding site shows that a large portion of the bound Ins(1,4,5,6)P_4 is exposed to solvent, lending credence to the original suggestion that bulkier inositol pyrophosphates can be accommodated in the site.[62,112] Several ligands have also already been identified that have bulky groups attached to the 2- and 3-positions of Ins(1,4,5,6)P_4 such as benzyl groups, which are well tolerated, as well as phosphate groups, which have been found to generate more potent ligands.[112] The reason that both Ins(1,3,4,5,6)P_5 and InsP_6 were able to bind to the HDAC3-SMRT site with higher apparent affinity than Ins(1,4,5,6)P_4 is suspected to be an effect of the increased overall negative charge of these compounds as they interact with the positively charged binding site in HDAC3-SMRT, which is an effect that the inositol pyrophosphates and their highly charged analogues were also expected to benefit from.[112]

It should be reiterated that despite the apparent high affinity for the HDAC3-SMRT site displayed by Ins(1,3,4,5,6)P_5 and InsP_6 in the initial study,[112] and the interest in inositol pyrophosphates as potential endogenous activators, Ins(1,4,5,6)P_4 is still thought to be a major physiological activator of the enzyme complex as this is the inositol phosphate that was bound when the deacetylase was co-purified.[112]

It has already been found that 5-PP-InsP_4 and the 1-PP-InsP_5 mimic 1-PA-InsP_5 are able to activate the HDAC3-SMRT complex significantly [to 60% and 80% of the activity of Ins(1,4,5,6)P_4 respectively], while the 2-OH-5-PA-InsP_4 analogue is practically inactive.[112] This result for 5-PP-InsP_4 was significant because it demonstrated that the pyrophosphate group of 5-PP-InsP_4, which was likely accommodated deep within the binding site, is tolerated by the HDAC3-SMRT enzyme complex. The inactivity of the 2-OH-5-PA-InsP_4 analogue likely indicates that the carbonyl moiety that is located in the equivalent position to the α-phosphate of a pyrophosphate is an insufficient phosphate mimic and cannot form the necessary interactions in the binding site to allow the ligand to bind.[112]

The initial study of the HDAC3-SMRT binding site did not assess 1-PP-InsP_5, 5-PP-InsP_5 and 1,5-$(PP)_2$-InsP_4 as potential ligands for the enzyme complex,[112] leaving the possibility of inositol pyrophosphates being physiological regulators of the enzyme complex not being fully explored prior to this work. As part of this current investigation, a number of regioisomers of InsP_7 (naturally occurring 5-PP-InsP_5 and 1-PP-InsP_5 and the unnatural regioisomer 3-PP-InsP_5) and their bisphosphonate (PCP) analogues previously synthesised in the Potter group were included in the ligand sets analysed at the HDAC3-SMRT binding site. Following the completion of its synthesis, 1,5-$(PP)_2$-InsP_4 (**16**, Chapter 3) was also analysed, along with its hydrolysis-resistant PCP analogue, thereby ensuring the three relatively abundant inositol pyrophosphates generated in most organisms [5-PP-InsP_5, 1-PP-InsP_5 and 1,5-$(PP)_2$-InsP_4] were assessed. In addition to these inositol pyrophosphates and their non-hydrolysable analogues, a pair of ligands was included in the investigation, featuring both a benzyl group and a bisphosphonate moiety to probe further what can be tolerated in the HDAC3-SMRT binding site (Figure 74).

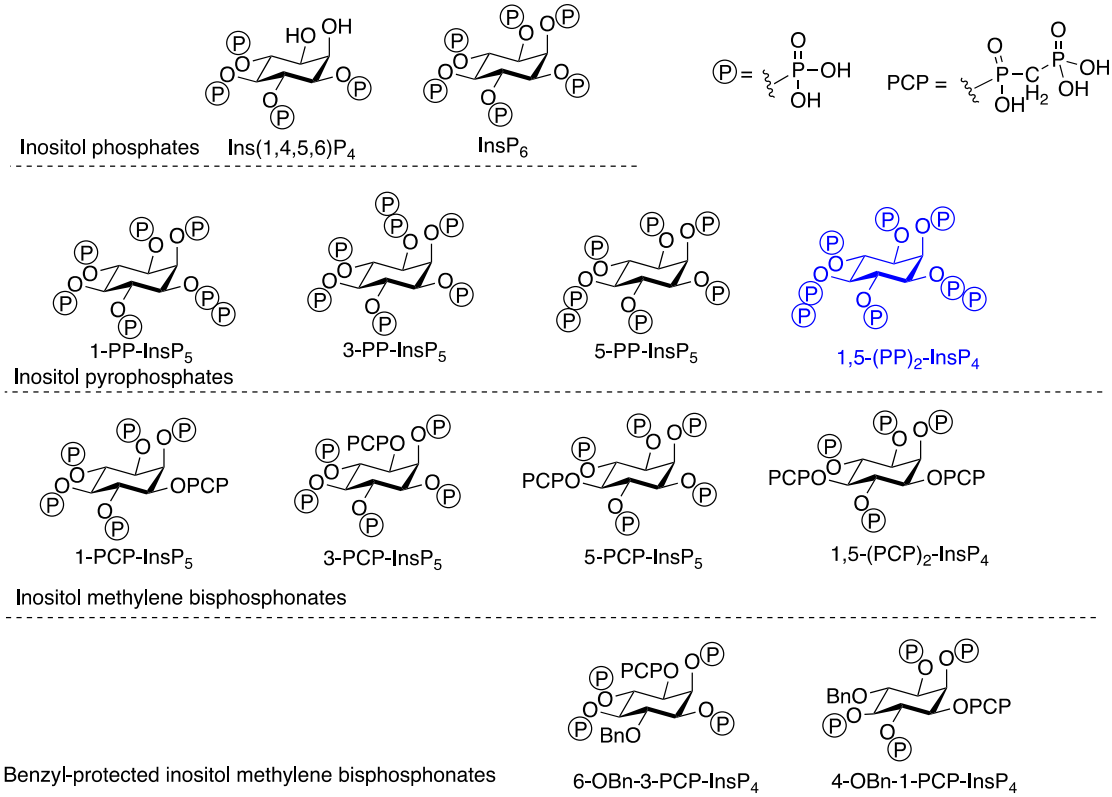

Figure 74: The inositol phosphates, inositol pyrophosphates and non-hydrolysable inositol pyrophosphate analogues and derivatives that were evaluated at the Ins(1,4,5,6)P_4 HDAC3-SMRT binding site. All of these compounds (except 1,5-$(PP)_2$-InsP_4, **16**, highlighted in blue) had been previously synthesised in the Potter lab. The 1,5-$(PP)_2$-InsP_4 which was synthesised as part of this study (Chapter 3) was analysed in the HDAC3-SMRT binding site in a later assay to the other compounds. Note that the chiral enantiomer of each of these compounds was analysed where applicable (some of the ligands are *meso*).

All of the pyrophosphates and bisphosphonate-containing compounds (Figure 74) were expected to be able to activate the complex *prima facie* as they were all predicted to be able to bind in modes in which regions A, B and C of the binding site are occupied by phosphates. The extent to which these inositol-based compounds might be able to activate the HDAC3-SMRT complex was not known, however, and the degree to which these compounds activate the enzyme complex might elucidate whether any of the inositol pyrophosphates tested could be potential physiological activators.

The hydrolysis-resistant bisphosphonate (PCP) analogues for each of the inositol pyrophosphates were analysed at the enzyme complex to provide evidence that any observed activity of the inositol pyrophosphates was probably not the result of ligand hydrolysis generating InsP_6. It was also hoped that, in addition to providing evidence towards the stability of the inositol pyrophosphates, the bisphosphonate analogues would perform well in activating the complex, despite the slightly different pKas of the groups rendering the potential activators slightly less charged.

All of the inositol pyrophosphate ligands and their bisphosphonate (PCP) analogues were indeed found to be able to activate the HDAC3-SMRT complex, although all to an equal or lesser extent than $InsP_6$ (Figure 75 and Table 8).

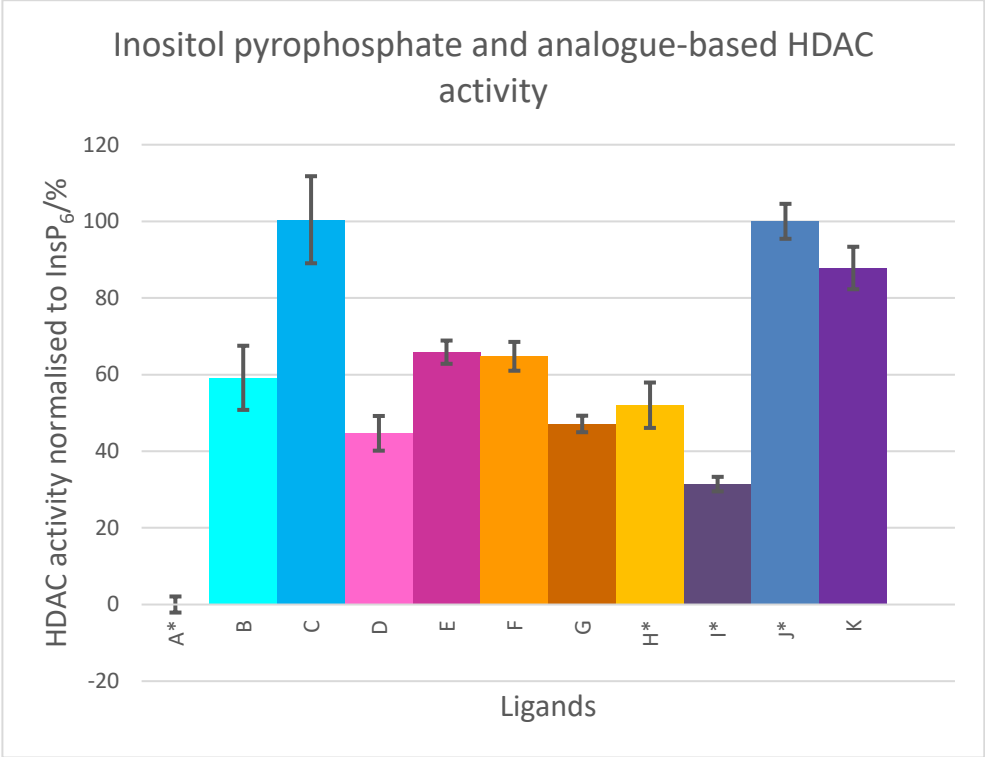

Ligand	HDAC activity normalised to $InsP_6$
A.* Protein only	0.0
B. 1-PP-Ins(2,3,4,5,6)P_5	59.2
C. 1-PCP-Ins(2,3,4,5,6)P_5	100.4
D. 3-PP-Ins(1,2,4,5,6)P_5	44.7
E. 3-PCP-Ins(1,2,4,5,6)P_5	65.9
F. 5-PP-Ins(1,2,3,4,6)P_5	64.8
G. 5-PCP-Ins(1,2,3,4,6)P_5	47.1
H.* 1,5-$(PP)_2$-Ins(2,3,4,6)P_4	52.0
I.* 1,5-$(PCP)_2$-Ins(2,3,4,6)P_4	31.4
J.* $InsP_6$	100.0
K. Ins(1,4,5,6)P_4	87.8

Figure 75 and Table 8: The normalised activity of the inositol pyrophosphate ligands and their non-hydrolysable analogues in the HDAC assay carried out by Dr Jennifer Gurnett and Dr Yun Song from the Schwabe lab (University of Leicester). The assay was repeated in technical triplicate and the mean values for each ligand were normalised to the activity generated by $InsP_6$ and reported in the table below. The entries with asterisks were carried out at a later date to the other results under the same conditions by Ed Brown from the Schwabe lab (University of Leicester). Error bars indicate ± s.e.m (n=3).

Interestingly, the activities generated by the inositol pyrophosphates differed to a certain extent from the activities generated by their bisphosphonate (PCP) analogues, with the bisphosphonate analogues of 1-PP-InsP_5 and 3-PP-InsP_5 proving to activate the enzyme complex more effectively than the corresponding pyrophosphate ligand. This result was surprising as bisphosphonate (PCP) analogues are slightly less charged than their pyrophosphate counterparts and thus it was expected that, as the inositol pyrophosphates and their bisphosphonate analogues would likely bond in equivalent binding modes, the higher charge of the pyrophosphate ligands were expected to give these compounds a slight advantage in binding to the HDAC3-SMRT site. There are multiple possible explanations for the hydrolysis-resistant analogues acting as more efficient activators than the natural pyrophosphate including differences in pKas, rigidity, capacity to form hydrophobic interactions and differences in displacement of the water molecules from the binding site. The increased activity of the mimics could also be due to the differences in the exact placement of the terminal (β) phosphonate, as a result of differences in the P-C-P and bond angles or lengths compared to those in the P-O-P pyrophosphate group. Different placement of the terminal (β) phosphonate could potentially allow the ligand to form stronger interactions with key residues, such as Arg301 or Lys475, or cause less steric clashing in the A or D region.

The results of the HDAC3-SMRT activity assay did not support the theory that 1-PP-InsP_5 (67% the activity of Ins(1,4,5,6)P_4 and 59% that of InsP_6) is the favoured regioisomer of InsP_7 because, although it triggered more activity than 3-PP-InsP_5 (51% the activity of Ins(1,4,5,6)P_4 and 45% that of InsP_6), it did not activate the HDAC3-SMRT complex as much as 5-PP-InsP_5 (74% the activity of Ins(1,4,5,6)P_4 and 65% that of InsP_6).

If it is assumed that binding modes that do not position the axial 2-position phosphate in the binding site are more likely, there are two possible likely orientiations for 1-PP-InsP_5 that position the pyrophosphate group in either the A or D region (Figure 76). It had initially been thought that the D region might be a suitable location for the placement of a pyrophosphate, although it has since become apparent that steric clashes may make this placement unsuitable. The remaining orientations that place the axially oriented phosphate in the binding pocket may in fact be better tolerated than positioning the pyrophosphate in either of these regions.

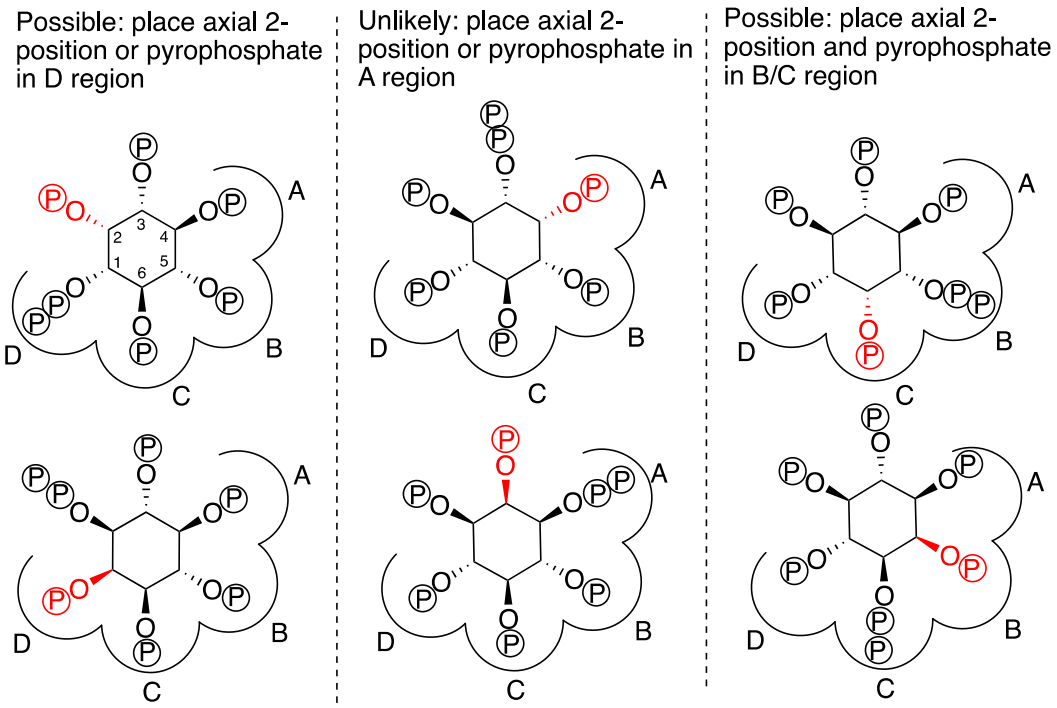

Figure 76: The predicted binding modes for 1-PP-InsP$_5$ in the HDAC3-SMRT binding site assuming the ligand binds in the same plane as Ins(1,4,5,6)P$_4$ and that the inositol ring pucker will match that of the endogenous ligand. The axial 2-position phosphate has been highlighted in red.

Molecular modelling of both 1-PP-InsP$_5$ and 1-PCP-InsP$_5$ could not support any particular predictions on what might be a possible preferred binding modes for either ligand, as docking solutions for both depicted the ligands bound in many different orientations in the HDAC3-SMRT site. There was a slight tendency for the docking solutions to place the pyrophosphate (or bisphosphonate) group near the Arg265 residue in the A region of the binding site (rather than near the Arg301 in the D region, as initially predicted). As mentioned previously in the chapter, the A region of the binding site is not thought to be able to tolerate steric bulk, but the binding modes that predicted that the pyrophosphate group (or mimic) be placed in this region avoided steric clashes in this region by displacing the inositol ring of the ligand away from the Arg265 residue, ensuring that these longer substituents do not extend any further into the A region than the phosphate of Ins(1,4,5,6)P$_4$.

This study found that 5-PP-InsP$_5$ is the most active regioisomer of InsP$_7$ (74% the activity of Ins(1,4,5,6)P$_4$ and 65% that of InsP$_6$) and that its non-hydrolysable analogue 5-PCP-InsP$_5$ is fairly active as well (54% the activity of Ins(1,4,5,6)P$_4$ and 47% that of InsP$_6$). If the binding modes that position the axial phosphate outside of the binding pocket are considered to be more likely, there are two probable binding modes that position the pyrophosphate (or bisphosphonate in the PCP analogue) deep into the binding pocket in either region B or C (Figure 77). As in the case of 5-PP-InsP$_4$, which was analysed in the previous Watson *et al.* study, 5-PP-InsP$_5$ was expected to position

its pyrophosphate group deep in the binding site and allow the α-phosphate (or α-phosphonate for 5-PCP-InsP$_5$) to mimic a monophosphate, thereby maintaining the "three phosphates in a row" motif thought to be required for binding.[112]

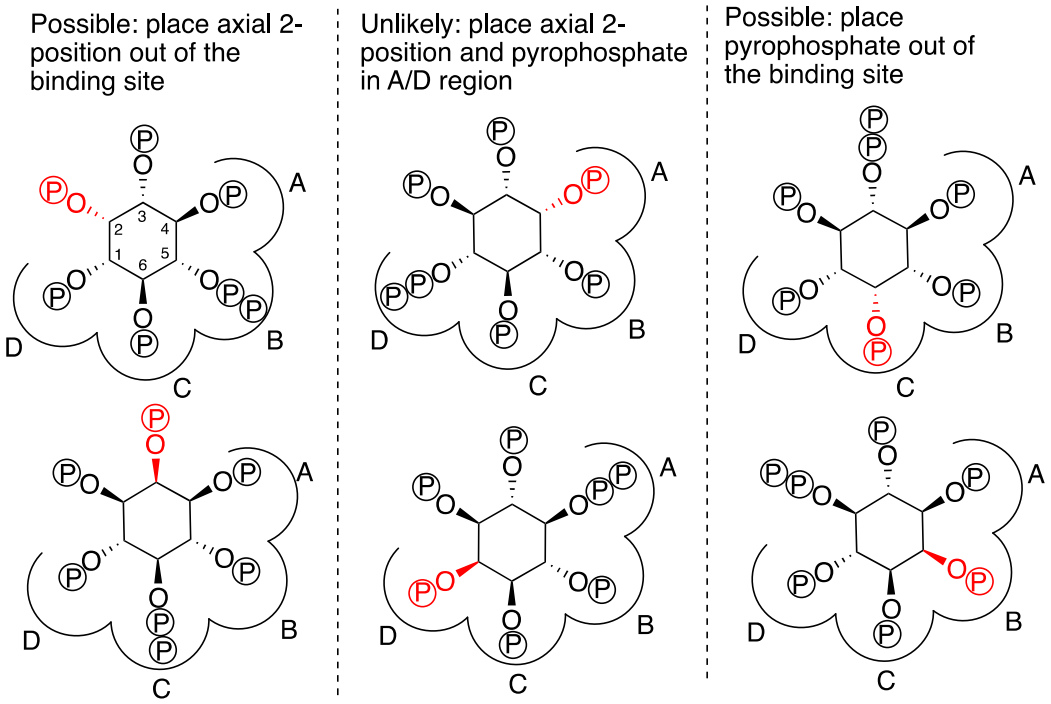

Figure 77: The predicted binding modes for 5-PP-InsP$_5$ in the HDAC3-SMRT binding site assuming that the ligand binds in the same plane as Ins(1,4,5,6)P$_4$ and the inositol ring pucker will match that of the endogenous ligand. The axial 2-position phosphate has been highlighted in red.

The docking solutions for both 5-PP-InsP$_5$ and 5-PCP-InsP$_5$ tended to shift the ligands deeper into the binding pocket and significantly change the angle at which the inositol ring is situated compared to Ins(1,4,5,6)P$_4$. With the pyrophosphate group (or bisphosphonate group) predicted to occupy the B or C pocket of the binding site, the ligands may even be able to form stronger interactions with some of the important lysine residues (Lys475, Lys475, Lys449, Lys25) involved in ligand binding in these regions.

Although 3-PP-InsP$_5$ is not a naturally occurring regioisomer of InsP$_7$ (unlike 1-PP-InsP$_5$ and 5-PP-InsP$_5$), both 3-PP-InsP$_5$ [51% activity of Ins(1,4,5,6)P$_4$ and 45% that of InsP$_6$] and its hydrolysis-resistant mimic, 3-PCP-InsP$_5$ [75% activity of Ins(1,4,5,6)P$_4$ and 66% that of InsP$_6$], proved to be able to activate the HDAC3-SMRT complex. From consideration of possible binding modes of this compound, it was predicted that this ligand would favour orientations that would position both of the axial phosphate and the pyrophosphate group out of the binding site into solvent (Figure 78). This prediction was supported by the molecular modelling results in which, although there

were a number of different orientations observed in docking solutions, the pyrophosphate group of 3-PP-InsP$_5$ tended to be positioned out into solvent, while the bisphosphonate group of 3-PCP-InsP$_5$ tended to be situated near the edge of the D region.

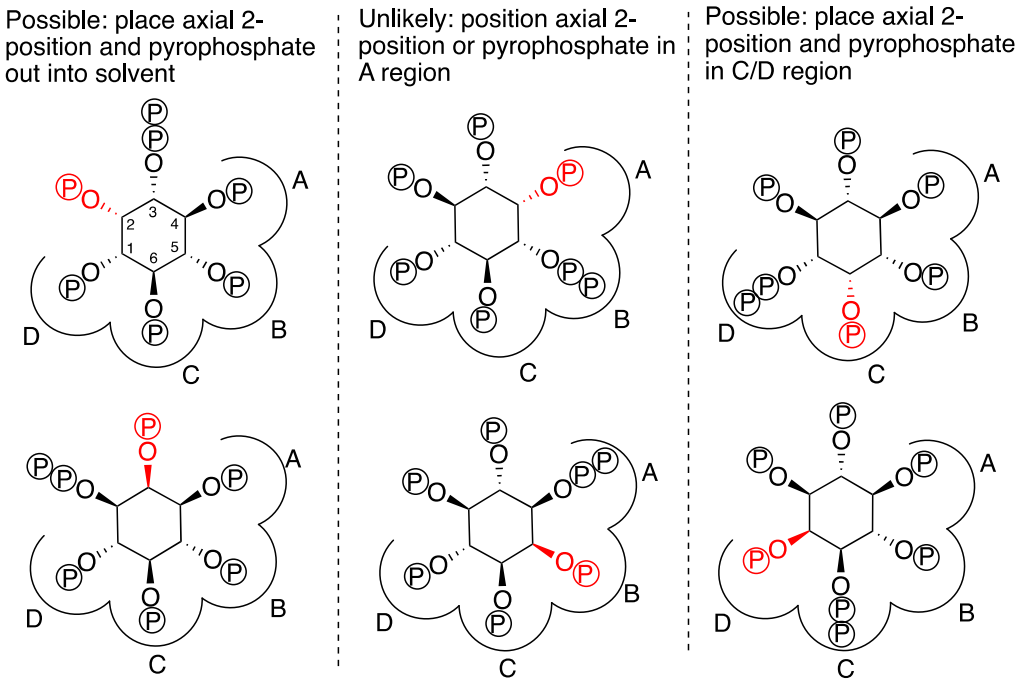

Figure 78: The predicted binding modes for 3-PP-InsP$_5$ in the HDAC3-SMRT binding site assuming that the ligand binds in the same plane as Ins(1,4,5,6)P$_4$ and the inositol ring pucker will match that of the endogenous ligand. The axial 2-position phosphate has been highlighted in red.

Despite the prediction, based on examination of the possible binding modes and docking simulation, that the pyrophosphate group and axial phosphate of 3-PP-InsP$_5$ would extend out of the binding site and not contribute to steric clashes, the activity of the ligand at the HDAC3-SMRT binding site was surprisingly low. This regioisomer of InsP$_7$ had been expected to be similar in activity to InsP$_6$, as every region of the binding site could be occupied by an equatorial monophosphate and the remaining axial phosphate and pyrophosphate group (or bisphosphonate group in the PCP analogue) could extend out of the binding site. The larger overall negative charge aquired from the pyrophosphate group was also predicted to assist in increasing interactions with the binding site. The result of the lower activity generated by these ligands seems to suggest that the the pyrophosphate or axial phosphate are preferentially participating in binding over the four consecutive equatorial phosphates and are less effective in interacting with the binding site and activating the complex.

In addition to the $InsP_7$ regioisomers and their hydrolysis-resistant PCP analogues, two inositol phosphates with bisphosphoate groups (PCP) positioned opposite to benzyl groups (4-*O*-benzyl-1-PCP-$InsP_4$ and 6-*O*-benzyl-3-PCP-$InsP_4$, Figure 74) that had been previously synthesised by the Potter group were assessed as HDAC3-SMRT activators (Figure 79 and Table 9).

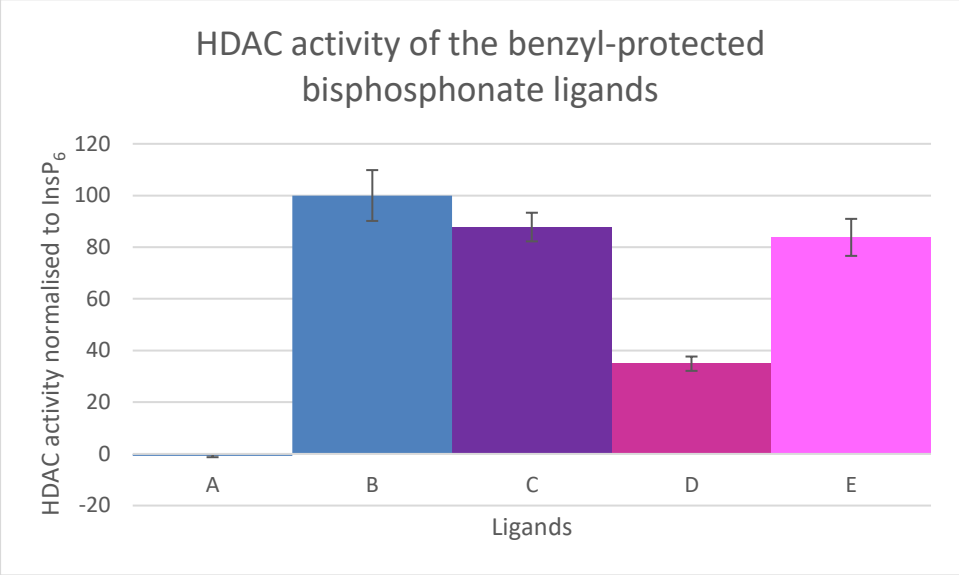

Ligand	HDAC activity normalised to $InsP_6$
A. protein alone	-0.7
B. $InsP_6$	100
C. Ins(1,4,5,6)P_4	87.8
D. 6-OBn-3-PCP-Ins(1,2,4,5)P_4	34.9
E. 4-OBn-1-PCP-Ins(2,3,5,6)P_4	83.8

Figure 79 and Table 9: The results of the HDAC3-SMRT assay carried out by Dr Yun Song and Jennifer Gurnett (University of Leicester) for 4-*O*-benzyl-1-PCP-$InsP_4$ and 6-*O*-benzyl-3-PCP-$InsP_4$ with the results for $InsP_6$ and Ins(1,4,5,6)P_4 included for comparison. The assay was repeated in technical triplicate and the mean values for each ligand were normalised to the activity generated by $InsP_6$ and reported in the table below. Error bars indicate ± s.e.m (n=3).

Neither 4-*O*-benzyl-1-PCP-$InsP_4$ or 6-*O*-benzyl-3-PCP-$InsP_4$ had been expected to be especially effective activators of the HDAC3-SMRT complex, because in any possible binding orientation, the binding pocket would have to accommodate either a bulky bisphosphonate group (PCP) or a bulky benzyl group in the centre of the binding pocket, assuming the modes that would position these groups in the A/D regions could be discarded. If it is assumed that both compound regioisomers bind such that the

benzyl groups are outside the binding site and the bisphosphonate group (PCP) within the binding pocket (with the α-phosphonate of the PCP mimicking a single phosphate in either the B or C region), both molecules have two likely binding modes (Figure 80). These compounds had both still been exptected to be activators of HDAC3-SMRT, however, due to the fact that the initial Watson *et al.* study provided evidence that a pyrophosphate group can be accomodated in the complex binding site, likely in the B or C region (because of the activity generated by 5-PP-InsP$_4$).[112]

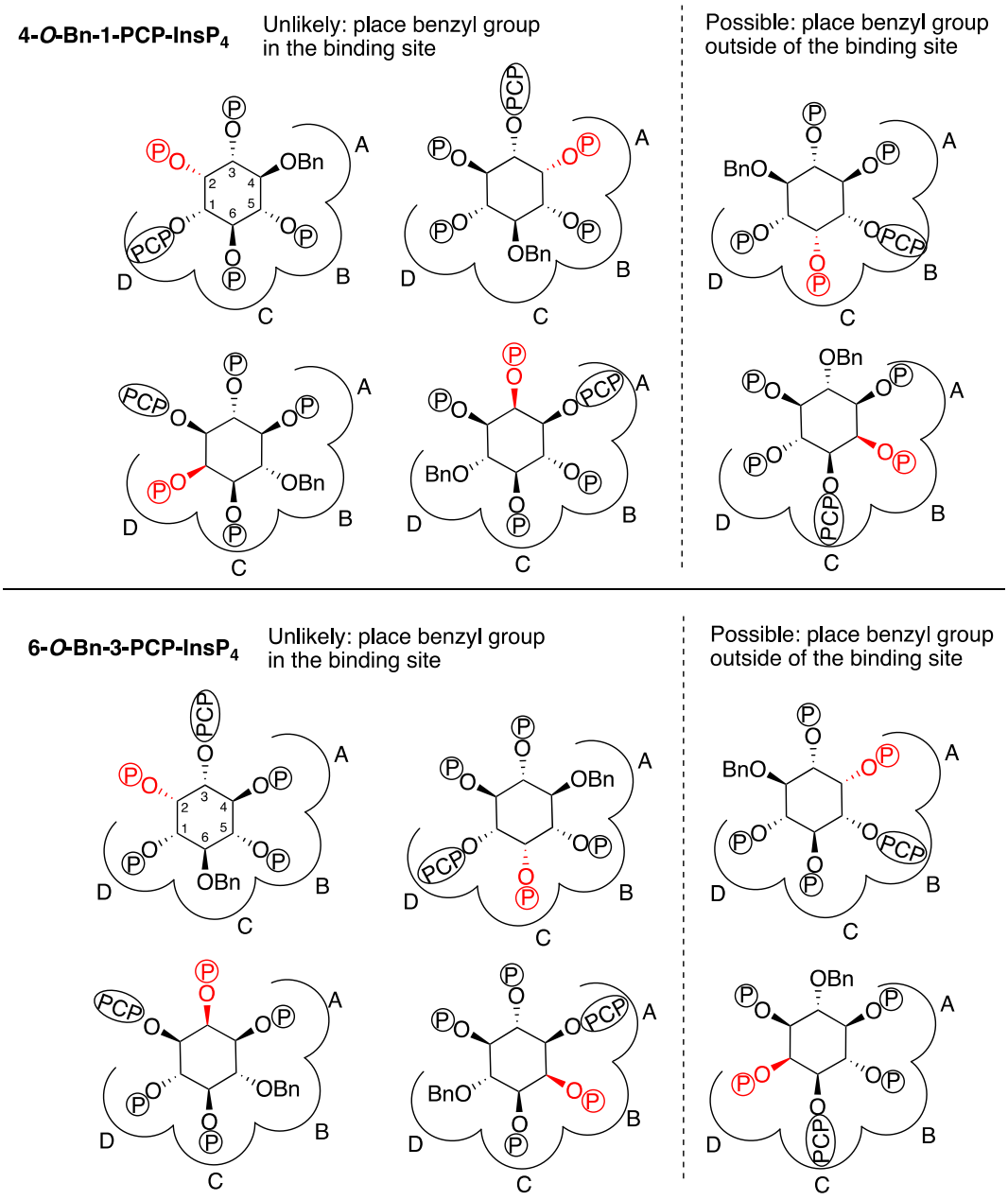

Figure 80: Possible binding modes for 4-*O*-benzyl-1-PCP-InsP$_4$ and 6-*O*-benzyl-3-PCP-InsP$_4$. The more likely binding modes (that position the benzyl group out of the binding pocket) have been highlighted.

It had not been anticipated that one regioisomer of the compounds would prove to be a significantly better activator of HDAC3-SMRT than the other, but 4-*O*-benzyl-1-PCP-InsP$_4$ (95% the activity of Ins(1,4,5,6)P$_4$ and 84% the activity of InsP$_6$) proved to be considerably more active than 6-*O*-benzyl-3-PCP-InsP$_4$ (40% the activity of Ins(1,4,5,6)P$_4$ and 35% the activity of InsP$_6$).

Although the two likely binding modes for 4-*O*-benzyl-1-PCP-InsP$_4$ or 6-*O*-benzyl-3-PCP-InsP$_4$ appear to be quite similar, there is a difference in the placement of the axial 2-position phosphate that may explain the difference in extent to which these regioisomers activate the HDAC3-SMRT complex. When 4-*O*-benzyl-1-PCP-InsP$_4$ binds, the axial 2-position phosphate is expected to occupy either the B or C region of the binding site, whereas when 6-*O*-benzyl-3-PCP-InsP$_4$ binds, the axial 2-position phosphate is expected to occupy either the A or D region. It was known that the A region would likely not be able to tolerate stereochemical inversion well from the initial Watson *et al.* study concerning activators of HDAC3-SMRT, but the D region had been expected to tolerate steric bulk.[112] This result is another piece of evidence that can be combined with the differences in activity of the carbohydrate-based enatiomers to support the theory that the D region of the HDAC3-SMRT site is unable to tolerate introduction of steric bulk or inversion.

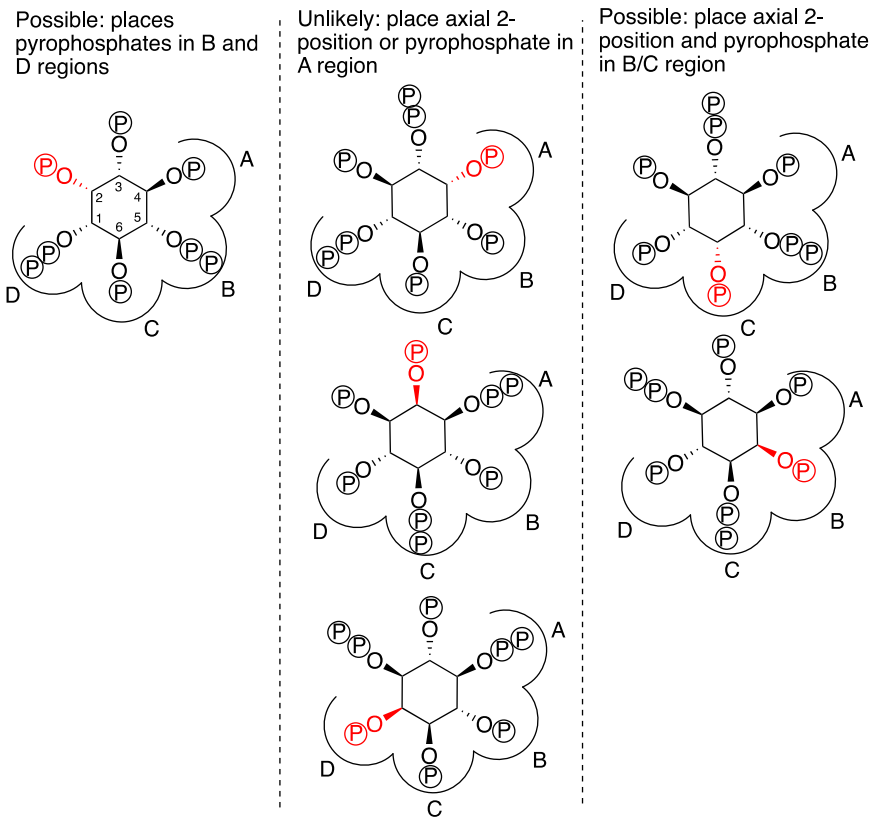

Figure 81: The predicted binding modes for 1,5-(PP)$_2$-InsP$_4$ in the HDAC3-SMRT binding site, assuming that the ligand binds in the same plane as Ins(1,4,5,6)P$_4$ and the inositol ring pucker will match that of the endogenous ligand. The axial 2-position phosphate has been highlighted in red.

Initially, only the non-hydrolysable analogue of 1,5-$(PP)_2$-$InsP_4$ was assessed as a possible HDAC3-SMRT activator but, following the completion of its synthesis (Chapter 3, **16**), 1,5-$(PP)_2$-$InsP_4$ was also analysed with the deacetylase complex. Both the inositol pyrophosphate and its bisphosphonate analogue were found to have only moderate activity at the HDAC3-SMRT complex (52% of the activity of $InsP_6$ for the pyrophosphate and 31% of the activity of $InsP_6$ for the bisphosphonate), which is slightly lower than the activities generated by the two structurally related regioisomers of $InsP_7$ (1-PP-$InsP_5$ and 5-PP-$InsP_5$) and their corresponding hydrolysis-resistant analogues (1-PCP-$InsP_5$ and 5-PCP-$InsP_5$).

The lower observed activity of 1,5-$(PP)_2$-$InsP_4$ compared to the $InsP_7$ regioisomers can perhaps be rationalised through analysis of the predicted binding modes (Figure 81). Although 1,5-$(PP)_2$-$InsP_4$ possesses a higher negative charge that would be expected to facilitate ligand binding, the positioning of the pyrophosphate groups around the inositol ring is such that all of the possible binding modes for this ligand require the binding site to accommodate at least one pyrophosphate in the binding pocket, with no option of having both be directed out into solvent. Although the increased negative charge from the additional phosphate groups would mitigate this hinderance to ligand binding, the inclusion of two pyrophosphate groups introduces steric bulk to the ligand, which could then be responsible for the observed lower HDAC3-SMRT activity generated by 1,5-$(PP)_2$-$InsP_4$. The successful activation of the HDAC3-SMRT site with 1,5-$(PP)_2$-$InsP_4$, despite the slightly lower enzyme activity observed, further confirms that pyrophosphate groups can be accommodated in the binding site with only some decrease in activator efficiency.

Although all of the natural inositol pyrophosphates are able to activate the HDAC3-SMRT complex, they were found to be less potent activators than Ins(1,4,5,6)P_4 and $InsP_6$, which renders 1-PP-$InsP_5$, 5-PP-$InsP_5$ and 1,5-$(PP)_2$-$InsP_4$ unlikely, but not impossible, to be important endogenous activators of this protein complex.

Now that a ligand set comprising of inositol pyrophosphates and their non-hydrolysable analogue has been assembled, it might be interesting to investigate other inositol phosphate binding sites identified in different HDAC complexes (such as HDAC1:MTA1, HDAC1:MIDEAS and SAP30-HDAC1)[112,197–199] to determine if they share SAR with HDAC3-SMRT.

(5) Inositol 1,4,5-trisphosphate and calcium signalling

5.1 Ins(1,4,5)P_3 and calcium signalling – background overview

It was first discovered in 1983 that D-*myo* inositol 1,4,5-trisphosphate [Ins(1,4,5)P_3] is able to act as a second messenger and release calcium from intracellular stores. Upon binding to Ins(1,4,5)P_3 receptors ($InsP_3R$), the release of calcium ions (Ca^{2+}) from the endoplasmic reticulum (ER) to the cytoplasm of cells is triggered.[7,222]

Calcium signalling has a large impact on many biological processes including apoptosis, cell proliferation and differentiation, gene transcription, secretion, metabolism and muscle contraction.[1,223,224] There are a number of different receptors that regulate intracellular calcium stores that recognise usually one of four second messengers: cyclic adenosine 5'-diphosphate ribose (cADPR) at ryanodine receptors; adenosine 5'-diphosphate ribose (ADPR) at transient receptor potential melastatin 2 (TRPM2); nicotinic acid adenine dinucleotide phosphate (NAADP) at the NAADP receptor (NAADP-R); and Ins(1,4,5)P_3 at $InsP_3R$.[119,223] Among these second messengers, Ins(1,4,5)P_3 is one of the longer known and better understood.

$InsP_3R$ is a tetrameric calcium ion channel formed from the oligomerisation of four monomer subunits that are each required to bind to a molecule of Ins(1,4,5)P_3 in order to prime the receptor for opening and allowing the efflux of calcium ions through the central receptor pore.[225,226]

There are three subtypes of $InsP_3R$ receptor subunits expressed in animal cells that share 60-70% of their amino acid sequence, $InsP_3R1$, $InsP_3R2$ and $InsP_3R3$.[227–230] These monomer isoforms can combine to form homotetrameric or heterotetrameric $InsP_3Rs$.[228,231] Although the subtypes of the receptor broadly perform the same role in calcium signalling, there is some variation in their expression, ligand affinities and exact biological function.[230–232] $InsP_3R2$ subtype has been found to have the highest affinity for Ins(1,4,5)P_3, followed by $InsP_3R1$ and then $InsP_3R3$.[229,233] The $InsP_3R1$ subtype is the best characterised and studied because it is expressed mostly as homotetramers in many tissue types (particularly neuronal), allowing for easier analysis.[230,231]

Ins(1,4,5)P_3 is metabolised by two distinct pathways: dephosphorylation with a 5-phosphatase to yield Ins(1,4)P_2, or by phosphorylation of the 3-position hydroxyl via Ins(1,4,5)P_3-3-kinase to yield Ins(1,3,4,5)P_4.[234] The role of Ins(1,3,4,5)P_4 in calcium signalling is still not entirely clear, with some studies indicating that it had no impact at all on Ca^{2+} mobilisation[235–237] or that it acts only on a distinct receptor[237–240], although it is now generally thought to be a weak full agonist of $InsP_3R$ that

participates in various regulatory calcium release feedback loops (still resulting in the overall dampening of calcium release compared to the effect of Ins(1,4,5)P_3).[35,241–246]

5.1.1 Ins(1,4,5)P_3 binding to InsP_3R

Ins(1,4,5)P_3 binds to a region of the InsP_3R receptor called the Ins(1,4,5)P_3-binding core (IBC). This region is a clamshell-like structure made up of an α-helical domain and a β-trefoil domain with a deep cleft between the domains that is rich in basic residues (Figures 82 and 83).[247,248]

When Ins(1,4,5)P_3 enters the IBC cleft, the phosphate groups attached to the 4- and 5-positions interact with the β-domain and α-domain respectively and, by doing so, pull the clam-like binding site domains closer together.[225,247,249,250] The closure of the IBC induced by Ins(1,4,5)P_3 binding results in the formation of a calcium ion binding site. Following Ca^{2+} binding, the IBC undergoes a conformational change that is translated to the rest of the receptor, ultimately resulting in the opening of the receptor pore, allowing the efflux of calcium ions into the cell cytoplasm.[225,249,251] Although calcium ions are required to bind to the activated InsP_3R to open the receptor ion channel pore, it has been found that very high concentrations of calcium ions can inhibit InsP_3R opening through a number of regulatory feedback interactions (including stimulating the synthesis of Ins(1,3,4,5)P_4 to deplete Ins(1,4,5)P_3 levels).[223,252–255]

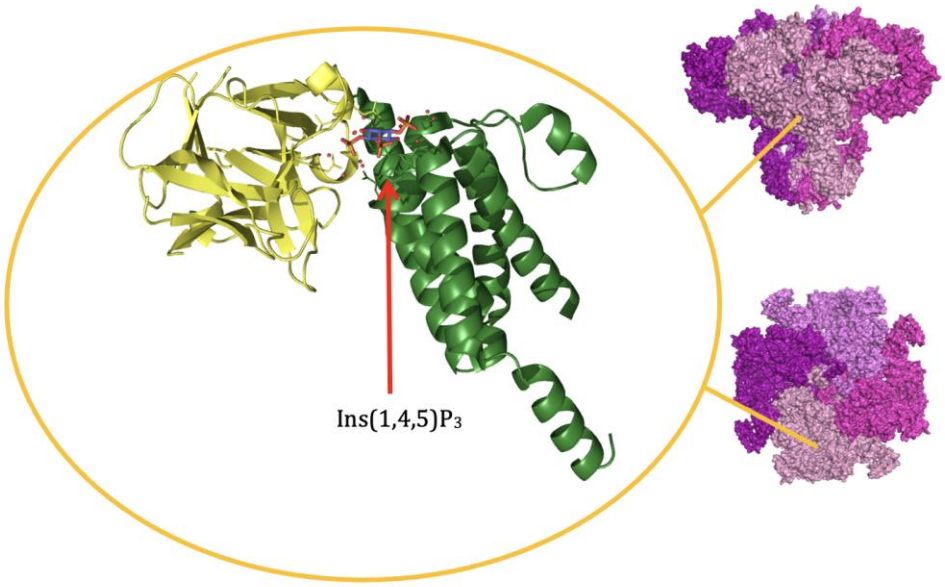

Figure 82: On the left, the crystal structure of Ins(1,4,5)P_3 bound to the IBC of InsP_3R (1N4K, the α-domain is depicted in green, and the β-domain in yellow).[247] The full InsP_3R receptor (7LHF) can be seen in two different orientations of a cryo-EM structure (resolution: 2.96 Å) with the different monomer subunits depicted in different shades of purple and the yellow lines indicating the approximate location of one of the four IBCs of the receptor.[256]

The IBC is located at the N-terminus of the protein and is connected to a suppressor domain (SD), which translates the conformational changes that occur in the IBC upon ligand binding to the rest of the receptor pore structure.[250] The IBC is highly conserved amongst the different isoforms of $InsP_3R$ and the minor differences in ligand affinity may in part stem from structural differences in the suppressor domains.[257]

The chiral nature of the receptor is reflected in the stark difference in the activities of potent D-*myo*-Ins(1,4,5)P_3 and its enantiomer, L-*myo*-Ins(1,4,5)P_3, which has been reported as being approximately 1000 times less potent if not fully inactive.[242,243,258]

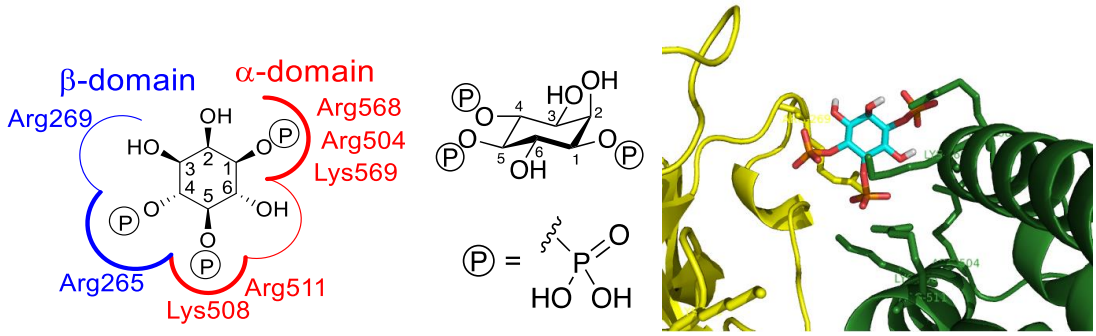

Figure 83: Ins(1,4,5)P_3 bound to the IBC of $InsP_3R1$ (residues 224-604) with some of the amino acid residues that are more involved in ligand binding labelled (left); structure of Ins(1,4,5)P_3 indicating the inositol ring-pucker (centre); and the Ins(1,4,5)P_3 bound crystal structure of the IBC of $InsP_3R1$ (1N4K)[247] with the α-domain of the IBC shown in green and the β-domain in yellow (right).

In addition to Ins(1,4,5)P_3, other potent agonists have been identified that are able to bind to the receptor such as the fungal nucleotide adenophostin A (Section 5.1.2).[259–261] Although there has been some success in finding agonists, there is a dearth of selective, potent antagonists for the receptor (Section 5.1.3). There has been an ongoing collective endeavour for decades to investigate the binding requirements for the IBC of $InsP_3R$ and also, through better understanding of ligand binding, to attempt to develop suitable receptor antagonists (Section 5.1.3).[251,262–265]

The structure-activity-relationships for Ins(1,4,5)P_3 at the $InsP_3R$ IBC can be summarised as follows:

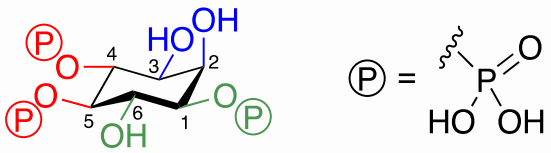

- The phosphates attached to the 4- and 5-positions are necessary for ligand binding.[266,267]
- The phosphate attached to the 1-position significantly improves ligand binding but is not strictly essential and modifications can be tolerated.[264]
- The 6-position hydroxyl is important to ligand binding.[263,268]
- The 3-position hydroxyl is of limited importance, but the region of the binding site that it occupies does not tolerate steric bulk well.[269]
- The 2-position hydroxyl in the axial orientation faces out into solvent and does not appear to participate in binding. Some steric bulk can be accommodated at this position.[250,270]
- The chair conformation of the inositol ring seems to be important in the correct placement of the hydroxyl and phosphate groups for many of the receptor ligands.[258]

4- and 5-position phosphates

The phosphate groups attached to the 4- and 5-positions of Ins(1,4,5)P_3 are generally considered essential for ligand binding to InsP_3R.[267] As mentioned earlier, each phosphate interacts with one of the IBC domains (the 5-position phosphate with the α-domain and the 4-position phosphate with the β-domain), and in doing so pulls the clamshell structure of the InsP_3R binding site closed upon ligand binding.[225,247,249,250]
It has been determined that the phosphate attached to the 5-position is the more dominant of the pair through a study involving the successive substitution of each phosphate group in Ins(1,4,5)P_3 with phosphorothioates.[266,271,272] This was later confirmed through the synthesis and testing of more analogues of Ins(1,4,5)P_3, with different groups attached to the 4- or 5-position.[251,262,273]

The importance of the exact placement in the InsP_3R binding site of the 4- and 5-position phosphates was demonstrated by studies that analysed analogues with axially oriented phosphates, deleted phosphates or 4,5-cyclic pyrophosphates which possessed decreased or abolished calcium release activities [or even partial agonist activity in the case of Ins(1,2,3,5)P_4].[241,267,274,275]
As discussed later (Section 5.1.3), a number of compounds with slight modifications to the 4- or 5-position phosphates have been identified as partial agonists or weak full agonists.[241,266,276–280]

It has previously been predicted by Bello *et al*. that modifying the phosphate bound to the 4-position may interfere with the ability of a ligand to close the clamshell binding site through prevention of interactions with the β-domain of the IBC and thereby allow the development of partial agonists or antagonists.[251] It was expected that this would be better tolerated than introducing structural differences to the dominant 5-position phosphate. It was also hoped that the 4-position would be a better target to inhibit clamshell closing, as only the 4-position phosphate interacts with the β-domain while both the 5-position and 1-position phosphates bind to the α-domain. Ligands that are unable to close the clamshell structure should be unable to trigger the conformational changes to the receptor that result in the opening of the calcium channel.[251] Unfortunately, the analogues developed in this study, although featuring only seemingly minor modifications to the 4-position phosphate, were found to be completely inactive at the $InsP_3R$.[251] However, this result could merely indicate that the structural changes attempted were too extreme to be tolerated by the IBC, and other 4-position modified Ins(1,4,5)P_3 analogues might be able to act as partial agonists as initially predicted.

Surprisingly, there has also been some evidence that minor modification only to the 5-position phosphate is able to generate ligands that appear to be weak antagonists or partial agonists of $InsP_3R$ (although further biological evaluation of these compounds would be beneficial).[262,273]

1-position phosphate

Unlike the phosphates attached to the 4- and 5-positions, the phosphate attached to the 1-position is not strictly necessary for $InsP_3R$ ligand binding. The presence of the 1-position phosphate does enhance ligand affinity significantly, however, as its deletion results in a sixty-fold decrease in potency.[267]

This auxiliary phosphate can be positioned in slightly different regions of the IBC compared to where the 1-position phosphate of Ins(1,4,5)P_3 binds and still meaningfully contribute to ligand binding [Ins(2,4,5)P_3 is significantly more potent than Ins(4,5)P_2].[267] Through the exploration of the agonist adenophostin A and its analogues (section 5.1.2), it has also been determined that modifications that position the auxiliary phosphate equivalent to the 1-position phosphate of Ins(1,4,5)P_3 further from the main ligand ring can be tolerated by $InsP_3R$.[264,270,289–292,281–288]

6-position hydroxyl

Although the interactions that the Ins(1,4,5)P_3 hydroxyl groups are able to form with the IBC are less strong than those formed with the charged phosphate groups, these moieties can be very important to ligand binding in multiple capacities. The hydroxyl

groups of the ligand are able to act as hydrogen bond donors or acceptors to the residues of the receptor binding site, as well as form intramolecular hydrogen bonds with the phosphates around the central inositol ring to fix their orientation and aid in their optimal positioning within the binding site.[293]

The hydroxyl attached to the 6-position of Ins(1,4,5)P_3 seems to be the most important hydroxyl in binding to the IBC, as its deletion results in a substantially larger loss of affinity compared to deletion of either hydroxyls attached to the 2- or 3-positions.[263,268]

Modifications at the 6-position such as deletion, substitution or inversion of the hydroxyl from an equatorial orientation to an axial orientation, while still partially tolerated, tend to lead to a dramatic loss of ligand potency. [232,242,293–295] From the low affinity of the 6-F-Ins(1,4,5)P_3 analogue, it has been suggested that this hydroxyl acts as a hydrogen bond donor rather than acceptor when binding to InsP_3R.[294,295]

3-position hydroxyl

The hydroxyl attached to the 3-position of Ins (1,4,5)P_3 is thought to have limited involvement in binding to InsP_3R. Removal of this hydroxyl has been found to result in a slightly less potent agonist of InsP_3R, although this decrease in potency was greater than that observed upon analogous removal of the 2-position hydroxyl.[263,293]

Minor modifications to this hydroxyl (including deletion, substitution with limited steric bulk introduced and inversion) have been found to result in InsP_3R ligands with slightly decreased potency.[232,265,275,278,279,296–299] The near equipotency of 3-F-Ins(1,4,5)P_3 to Ins(1,4,5)P_3 itself indicated that the 3-position hydroxyl likely acts as a hydrogen bond acceptor in ligand binding rather than a hydrogen bond donor (although it should be noted that while fluorine is unable to act as a hydrogen bond donor, the ability of the group to act as an effective hydrogen bond acceptor has come into question).[232,241,265,297,298,300]

Following numerous studies it has been determined that the 3-position hydroxyl can tolerate minor modifications and the addition of smaller functional groups, but is unable to tolerate large amounts of steric bulk.[232,269,276,301–304] When the equatorial 3-position hydroxyl group is replaced by increasingly bulky functional groups, the affinity of the ligands for the receptor decreases.[269,276,302–305]

Disruption to the structure of Ins(1,4,5)P_3 in the equivalent of the 3-position hydroxyl, usually in conjunction with modification to the equivalents of the phosphates attached to the 4- and 5-positions,[241,266,278,279] can result in the generation of partial agonists of InsP_3R (Section 5.1.3).[306]

2-position hydroxyl

The axial hydroxyl attached to the 2-position of Ins(1,4,5)P_3 appears to face out of the receptor binding pocket into solvent and is not thought to be involved in binding.[247,301] Inversion, removal or substitution of this hydroxyl usually only results in only a small reduction in ligand potency.[232,263,270,280,298,307,308]

The minimal decrease in potency for 2-F-Ins(1,4,5)P_3 compared to Ins(1,4,5)P_3 indicates that the 2-position hydroxyl likely acts, in its limited capacity to assist binding, as a hydrogen bond acceptor as opposed to a hydrogen bond donor.[280,309]

It should be noted, however, that if the substituent attached to the 2-position hydroxyl is sufficiently sterically bulky, the ligand can act as a partial agonist. This is thought to be due to the bulky 2-position substituent disrupting the communication between the IBC and the suppressor domain, which is necessary to convey the conformational change of the clamshell closure to open the calcium release pore (section 5.1.3).[250,310]

Chair-structure of *myo*-inositol

The correct positioning of the phosphates and hydroxyl groups of Ins(1,4,5)P_3 is achieved with the three-dimensional puckered chair-structure of the central *myo*-inositol ring.[258] In addition to inositol, glucose has been shown to be a viable 6-membered central ring structure that can position the substituents around the central ring with suitable stereochemistry, as demonstrated by the high activity observed in the glucose-containing adenophostin A agonist and its analogues (Section 5.1.3).

The preservation of a ring pucker appears to be quite important for ensuring the optimal placements of ligand functional groups within the InsP_3R binding site, as can be seen by the low activity of the flat, benzene trisphosphate Ins(1,4,5)P3 analogue.[311] Several benzene-trisphosphate dimer ligands have been identified as InsP_3R antagonists, although it has not been determined exactly how these bind to InsP_3R (section 5.1.3).[312]

It has also been determined that a 5-membered contracted central ring structure can position the phosphate and hydroxyl substituents of a ligand in the required regions of the IBC, albeit with a slight decrease in agonist potency compared to Ins(1,4,5)P_3.[313] This indicates that a 6-membered core ring structure in a chair confirmation is not strictly necessary for binding but beneficial.

5.1.2 Adenophostin A, a potent $InsP_3R$ agonist

For many years, there has been interest in identifying compounds that activate or inhibit the action of $InsP_3R$. As described previously in the known binding requirements for $InsP_3R$ (Section 5.1.1), the receptor does not tolerate many structural modifications, making the identification of more potent agonists challenging until the fortuitous discovery of the adenophostins.[260]

In 1993, it was discovered that a pair of adenosine-derived glyconucleotides isolated from P*enicillium brevicompactum* SANK 11991 and SANK 12177 were potent agonists of $InsP_3R$.[260,314] These nucleotides were named adenophostin A and B (Figure 84). Both adenophostin A and B proved to be 10-100 times more potent than $Ins(1,4,5)P_3$ in releasing calcium ions from all subtypes of $InsP_3Rs$.[259,315] Due to the fact that adenophostin A (AdA) was found to be marginally more potent than adenophostin B in releasing calcium and also is made up of a slightly simpler chemical structure lacking the acetyl group bound to the glucose ring, it became the more-studied metabolite.[259]

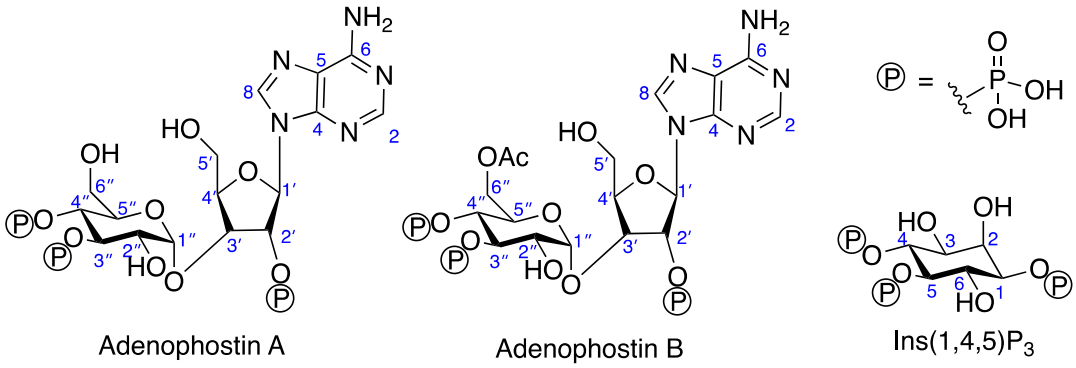

Figure 84: Structure of $InsP_3R$ agonist adenophostin A (AdA), adenophostin B and $Ins(1,4,5)P_3$.

Following the discovery of AdA, many synthetic analogues have been made to investigate the rationale behind its very high potency at $InsP_3R$.[259,261,289–291,315–321,264,322,282–288]

Through the systematic elimination or replacement of fragments of the AdA structure, it has been determined that the vicinal phosphate pair is important to activity and that the exact positioning of the third auxiliary phosphate can significantly improve the potency of an analogue.[261,282] The adenine moiety, or the inclusion of a similar aromatic group, has also been found to be a vital factor in increasing the potency above that of $Ins(1,4,5)P_3$.[283,323]

It was initially suggested that the adenine improved the potency of ligands by acting to help position the auxiliary phosphate in a supra-optimal position.[323–325] A later, and now commonly accepted, idea is that the adenine group forms additional interactions

with the binding site.[325,326] From molecular docking studies and later targeted mutagenesis, it was determined that the adenine ring of AdA forms a cation-π interaction with the guanidinium side chain of Arg504 in the IBC of $InsP_3R1$.[283,288,310,322,327,328]

The auxiliary 2'-position phosphate significantly improves the potency of a ligand, and the exact nature of how this moiety interacts with the binding site has been probed with a series of AdA anologues. In part to probe the possibility of supra-optimal positioning for the auxiliary phosphate, a large number of adenophostin A analogues with different degrees of truncation and substitution were generated to investigate the ideal spacer linkage for the 1-position phosphate equivalent group.[215,264,316–318,320,323,328–330,282–284,286–290] It was found that the longer the hydrocarbon chain used to space the auxiliary phosphate from the central ring structure, the greater the decrease in ligand affinity. The orientation of the spacer linkage from the central ring structure also proved to impact ligand affinity, with the axially-oriented spacers proving more potent than their equatorial analogues. Finally, it was also found that the ligands that incorporated ring structures to render the spacer section less flexible also tended to have higher receptor affinity than their more flexible analogues.[264,282,331]

The auxiliary 2'-position phosphate in AdA is thought to occupy a slightly different position in the IBC than that occupied by the 1-position phosphate in $Ins(1,4,5)P_3$ due to the increased distance between the 2-position phosphate on the ribose and the bisphosphate pair on the glucose moiety.[324,325] From docking studies, the 2'-postion phosphate is predicted to interact with the Lys569 and Arg504 in addition to, or instead of, Arg568.[283]

In a recent cryo-EM study, it was suggested that the structural resemblance between $Ins(1,4,5)P_3$ and AdA was coincidental and the binding modes of these agonists in the IBC were significantly different.[332] There is also some evidence that supports that AdA occupy slightly different positions within the IBC from entropic and enthalpic binding calculations, as well as the high activity of adenophostin B despite the presence of its acyl group.[301,310] However, this conclusion is not supported by the results of mutagenic studies and the observed activities of many truncated Ada analogues.[250,259,264,321,322,327,332]

It seems reasonable for now to proceed with the theory that the 3” and 4” phosphates of AdA mimic the 4 and 5 phosphates of $Ins(1,4,5)P_3$, and the 2’ phosphate at least partially mimics the 1-position phosphate.

5.1.3 Development and summary of antagonists and partial agonists of $InsP_3R$

Although very potent agonists have been identified for the receptor (eg. adenophostin A and B),[259,260] no selective potent antagonists have been identified, despite the binding site being investigated for the last thirty-five years.[1,333]

There are a number of antagonists identified for $InsP_3R$ (Figure 85), but none is universally suitable and they often suffer from various drawbacks including cell impermeability, numerous off-target effects, low potency and inconsistent antagonist activity.[301,306,333,334]

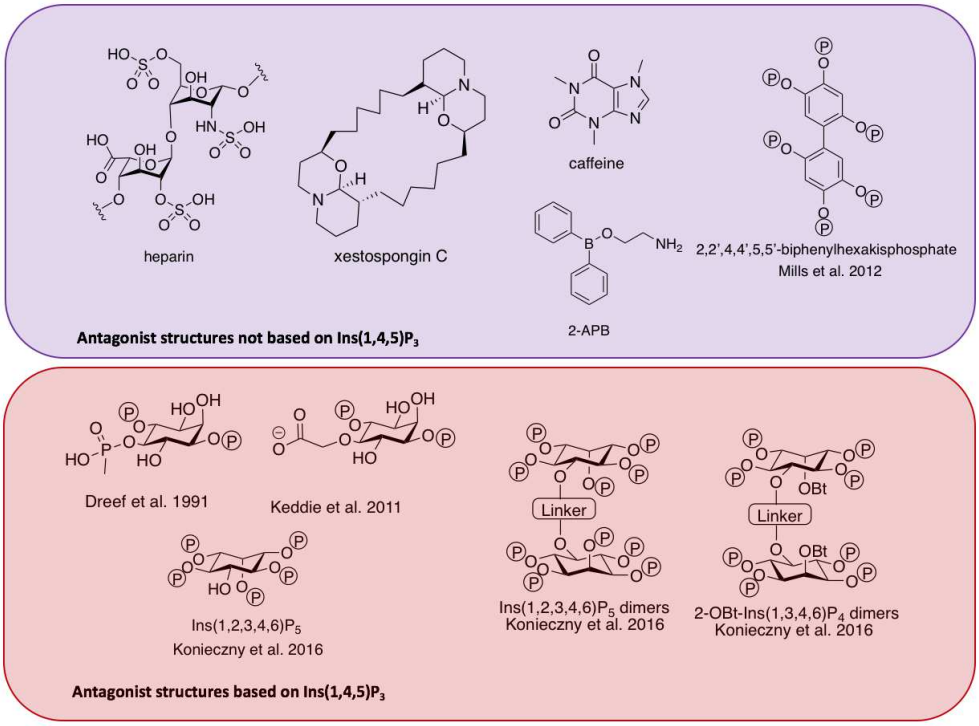

Figure 85: A diagram displaying some of the antagonists of $InsP_3R$ grouped according to whether they mimic $Ins(1,4,5)P_3$ structure or not. The studies in which certain antagonists were created are also included in the some of the structure labels and correspond to the following references.[262,273,306,312]

Investigations of structures derived from $Ins(1,4,5)P_3$ with the goal of designing $InsP_3R$ antagonists have been underway for a long time, although only a small number have been identified (Figure 85). There are multiple advantages as to why these potential antagonists and partial agonists should be derived from $Ins(1,4,5)P_3$, including the increased probability of the compounds being able to bind successfully to the unforgiving $InsP_3R$ IBC and the decreased likelihood of them being unselective and causing off-target effects. Another advantage of using $Ins(1,4,5)P_3$ mimics to pursue hypothetical partial agonists and antagonists is that analogues of this structure can be chemically protected and rendered cell permeable (refer to the Introduction), unlike the $InsP_3R$ antagonist heparin.

The first-identified Ins(1,4,5)P_3-derived antagonist was the 5-position-modified analogue initially synthesised by Dreef *et al.*, although no biological data were published until further studies were carried out by Keddie *et al.* twenty years later.[262,273] The Konieczny *et al.* study has also reported a few low-potency (Kd 7-8 µM) inositol phosphate InsP_3R antagonists.[306]

While there has been very limited success in developing selective InsP_3R antagonists, the development of partial agonists of the receptor has delivered more results (Figure 86). It is hoped that through the better understanding of which ligand structural features result in partial agonist activity, improved, lower-efficacy partial agonists and even potentially antagonists could be rationally designed.

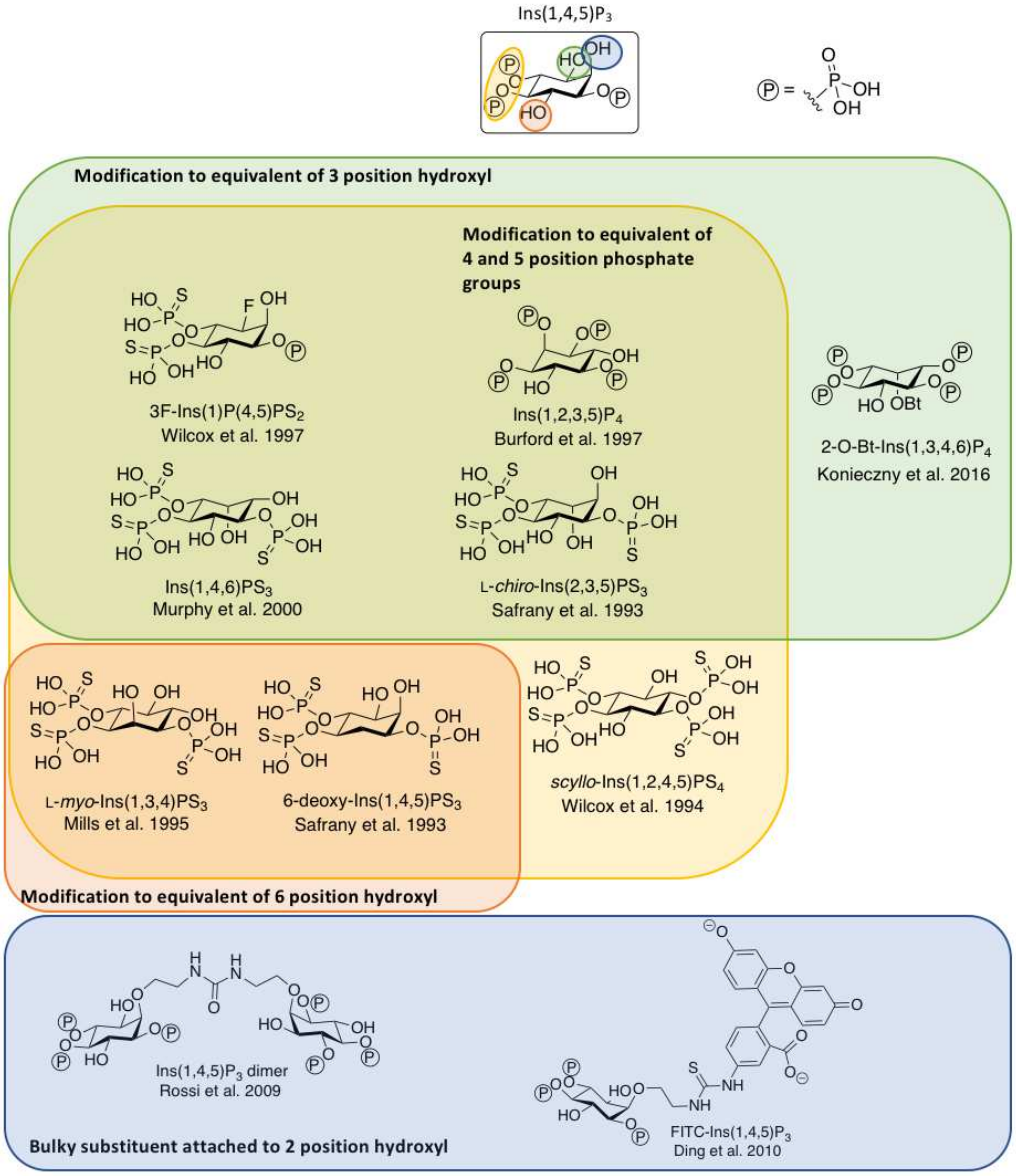

Figure 86: Some of the partial agonist Ins(1,4,5)P_3 mimics grouped according to which region of the Ins(1,4,5)P_3 structure have been modified. The studies in which the partial agonists were created are also included in the labels for the partial agonist structures and correspond to the following references.[241,250,266,277–280,306,310]

Two methods of modifying chemical structure to achieve partial agonism have been identified: interfering with the interactions of the ligand within the IBC to prevent full clamshell closure, and disrupting interactions between the IBC and SD through steric interference.[250]

The majority of the Ins(1,4,5)P_3-derived partial agonists identified are thought to exploit the first method of interfering with ligand binding and closure of the IBC clamshell. These partial agonist ligands tend to feature structural disruptions to the equivalents of the Ins(1,4,5)P_3 vicinal phosphates in combination with another modification in a different position around the central ring.[241,266,278,279]

Unfortunately, the minor modifications to the Ins(1,4,5)P_3 structure required to generate partial agonist activity have a detrimental effect on the affinity of the ligands for the receptor to different extents. Some of the structural changes, such as those to the position-3 hydroxyl region, have improved potency compared to analogues with perturbations at groups more crucial to binding like the 6-position hydroxyl.[279]

The second method found to generate partial agonists was to prevent conformational changes outside of the IBC by way of steric interference from a bulky group attached to the axial 2-position hydroxyl such as fluorescein 5-isothiocyanate (FITC) or a second inositol trisphosphate as part of a dimer connected at the 2-position.[250,310] In addition to the Ins(1,4,5)P_3 dimer depicted (Figure 86), the Rossi *et al*. study described an additional six other InsP_3R partial agonists that also feature bulky substituents attached to the axial 2-position hydroxyl.[250]

Although a number of partial agonists for InsP_3R have been identified, most of them suffer from low receptor affinity relative to that of Ins(1,4,5)P_3, resulting in their potential practical uses being limited and necessitating the development of improved partial agonists and antagonists for the receptor.

The exceptions which appear to have higher affinity than Ins(1,4,5)P_3 are the partial agonists with bulky groups attached to the 2-position. The bulky groups attached to the 2-position of these partial agonists are thought to interfere with the interaction between the IBC and SD and prevent transmission of conformational change in the receptor upon ligand binding, thereby reducing the binding energy used by the rest of the receptor.[250,310]

5.2 Proposed $InsP_3R$ ligands

In this body of work, six novel ligands based on L-glucose or D-glucose were designed, synthesised and evaluated for biological activity at $InsP_3R$ (Figure 87).[335] As mentioned in the Introduction, glucose was expected to be a suitable scaffold from which mimics of lower *myo*-inositol phosphates could be generated. Novel aspects of this idea were further pursued by generating glucose-based mimics of $Ins(1,4,5)P_3$ that could be used to investigate binding to $InsP_3R$, in addition to the glucose-based $Ins(1,4,5,6)P_4$ analogues generated to investigate the inositol phosphate binding site of the HDAC3-SMRT complex (Chapter 4). Unfortunately, none of the glucose phosphate compounds previously synthesised for the HDAC3-SMRT investigation would be viable candidates for $InsP_3R$ ligands due to their inclusion of three consecutive phosphates [and so lack of an equivalent to the crucial 6-position hydroxyl of $Ins(1,4,5)P_3$] and so they were not pursued in this regard.

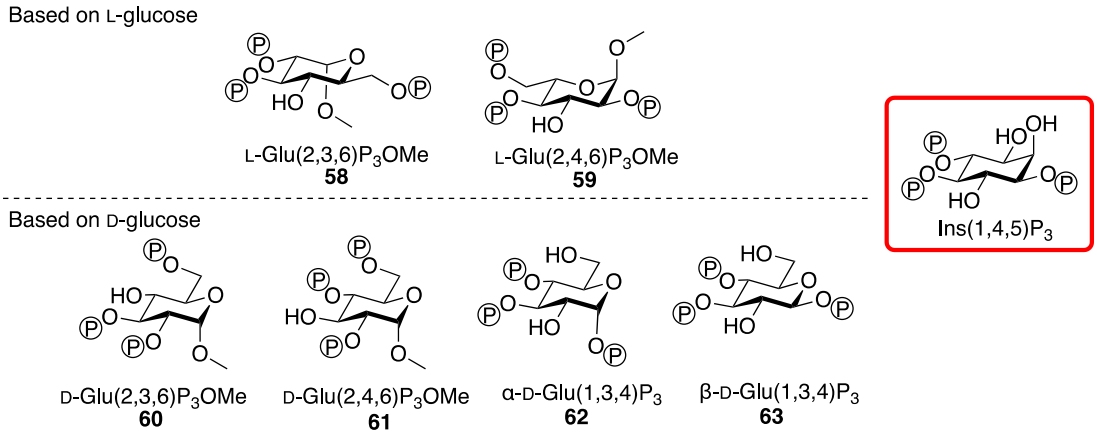

Figure 87: Ligands tested at $InsP_3R$ grouped according to which sugar enantiomer they are derived from and a structure of $Ins(1,4,5)P_3$ for comparison: methyl α-L-glucopyranoside 2,3,6-trisphosphate (**58**), methyl α-L-glucopyranoside 2,4,6-trisphosphate (**59**), methyl α-D-glucopyranoside 2,3,6-trisphosphate (**60**), methyl α-D-glucopyranoside 2,4,6-trisphosphate (**61**), α-D-glucosyl 1,3,4-trisphosphate (**62**) and β-D-glucosyl 1,3,4-trisphosphate (**63**).

Of the six ligands constructed for $InsP_3R$, only four were expected *prima facie* to show activity at the receptor: methyl α-L-glucopyranoside 2,3,6-trisphosphate (**58**), methyl α-L-glucopyranoside 2,4,6-trisphosphate (**59**), α-D-glucosyl 1,3,4-trisphosphate (**62**) and β-D-glucosyl 1,3,4-trisphosphate (**63**). Both of the L-glucose-based ligands, as well as the 1-position phosphate-containing D-glucose-based ligands, should be able to adopt binding modes that might satisfy the ligand binding requirements for the IBC of $InsP_3R$, although some feature minor structural perturbations that might not be tolerated by the receptor (Figure 88). Crucially, all four of these ligands should be able to bind in a mode that positions three phosphate groups in the regions of the IBC

occupied by the Ins(1,4,5)P_3 phosphates, as well as including an equivalent hydroxyl to the 6-position hydroxyl of Ins(1,4,5)P_3 and maintaining the expected pucker of the central 6-membered ring structure.

The remaining two compounds, methyl α-D-glucopyranoside 2,3,6-trisphosphate (**60**) and methyl α-D-glucopyranoside 2,4,6-trisphosphate (**61**), would be able to act as important controls for their L-glucose enantiomers. Both of these D-glucose-based ligands were not anticipated to bind to InsP_3R due to their inability to bind in an orientation that would satisfy the known binding requirements of the receptor.

The predictions for which ligands would be tolerated by InsP_3R were based on comparison of potential binding modes (Figure 88) in combination with GOLD docking simulations (refer to Experimental for optimised docking protocol and some of the highest and lowest ranked exact docking scores). Despite having reasonable hypothetical binding modes and docking solutions, it was still not certain if the structural differences from Ins(1,4,5)P_3 of the ligands, particularly those of methyl α-L-glucopyranoside 2,3,6-trisphosphate (**58**) and methyl α-L-glucopyranoside 2,4,6-trisphosphate (**59**), would be tolerated by the sensitive InsP_3R binding site.

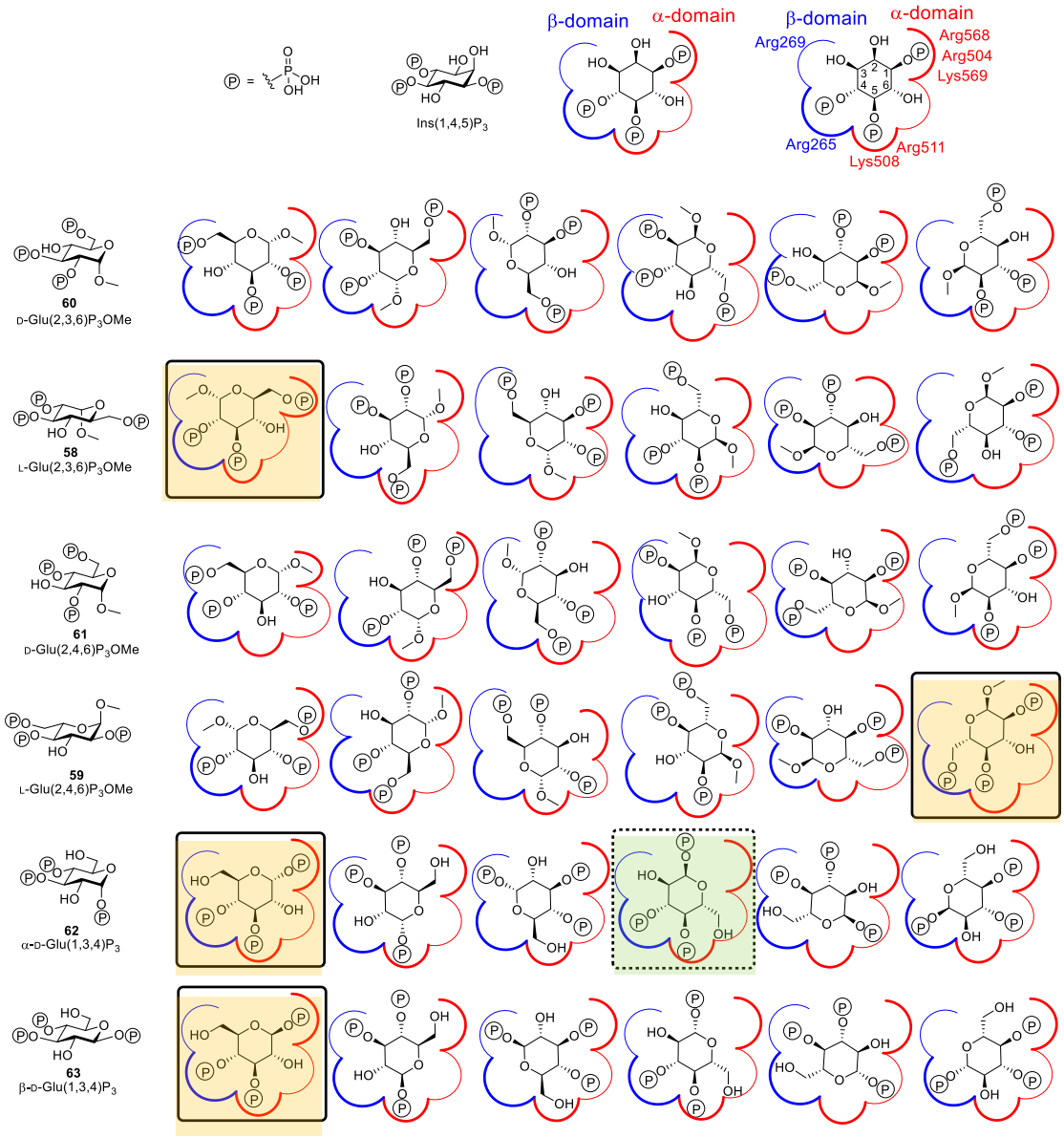

Figure 88: Possible binding modes for the novel synthetic $InsP_3R$ ligands. The α- and β- domains of the IBC have been colour-coded (red and blue respectively) and the regions in which phosphates are required to bind have been made bold. The likely binding modes that could plausibly mimic $Ins(1,4,5)P_3$ binding have been highlighted in yellow, and a second possible binding mode for **62** has been highlighted in green.

5.2.1 Methyl α-L-glucopyranoside 2,3,6-trisphosphate (**58**) $InsP_3R$ binding predictions

The main points of deviation of methyl α-L-glucopyranoside 2,3,6-trisphosphate (**58**) from the $Ins(1,4,5)P_3$ structure are the axial methyl group positioned in the equivalent of the 3-position hydroxyl, the extended phosphate in the equivalent of the 1-position phosphate and the pyranosyl ring oxygen in the equivalent of the axial 2-position hydroxyl.

The extended phosphate (attached to the 6-position of **58**) was expected to mimic the auxiliary phosphate that, while not crucial to binding, increases the binding affinity of ligands.[264] Although this phosphate was positioned further from the central ring structure than the 1-position Ins(1,4,5)P_3 phosphate, it was still expected to be tolerated by the IBC. This is due to the fact that a number of studies have demonstrated that truncated AdA analogues with the auxiliary phosphate extended from the central ring by different linkages can be accommodated by the receptor; additionally, a recent study by the Potter group proved that a pyrophosphate could be tolerated in the place of the 1-position phosphate.[91,261]

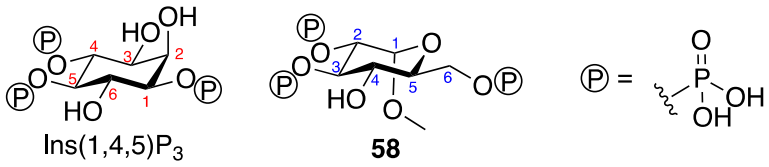

Figure 91: Comparison of numbered structures of Ins(1,4,5)P_3 (left) and methyl α-L-glucopyranoside 2,3,6-trisphosphate (**58**, right).

In agreement with the most likely binding mode (Figure 88), methyl α-L-glucopyranoside 2,3,6-trisphosphate (**58**) was also predicted to position the extended phosphate into the region occupied by the position-1 phosphate in the highest scoring docking predictions (Figure 92).

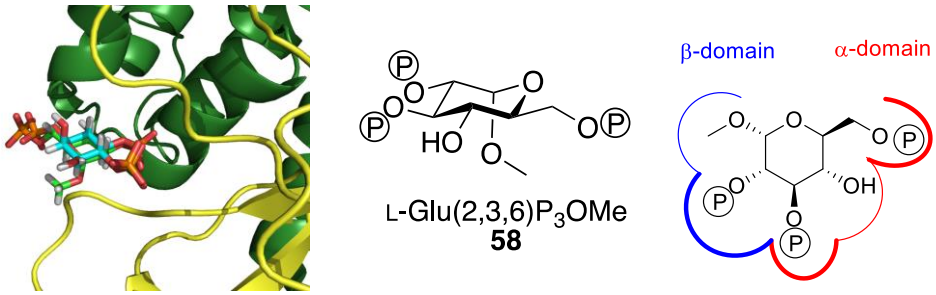

Figure 92. The most favourable docking conformation of methyl α-L-glucopyranosyl 2,3,6-trisphosphate (**58,** green, docking solution 8, GOLDscore fitness: 140.3659) with bound Ins(1,4,5)P_3 (**1**, aqua) in the IBC with the α-domain shown in dark green and β-domain shown in yellow (1N4K).[247] Figure adapted from Shipton *et al*. study.[335]

The highest-scoring docking predictions reflected that the positioning of the vicinal phosphates in methyl α-L-glucopyranoside 2,3,6-trisphosphate (**58**) would overlap near-perfectly with the vicinal phosphates of endogenously bound Ins(1,4,5)P_3, ensuring these crucial interactions with the binding site are preserved. By adopting this orientation, the auxiliary phosphate was predicted to extend further into the

binding site yet still retain its interaction with Arg568, although this residue was repositioned slightly upon ligand binding to accommodate the extended 6-position phosphate.

The pyranosyl ring oxygen was expected to be in the position usually occupied by the 2-position hydroxyl in Ins(1,4,5)P_3, which is thought to have a minimal contribution to binding; thus, this structural difference is not expected to effect ligand binding.[247,301]

Finally, it was not certain if the axial methyl group, which was predicted to occupy the region of the binding site that interacts with the 3-position hydroxyl of Ins(1,4,5)P_3, would be tolerated as this region of the IBC is thought to tolerate limited equatorial steric bulk only reasonably.[269,281]

5.2.2 Methyl α-L-glucopyranoside 2,4,6-trisphosphate (**59**) InsP_3R binding predictions

As can be seen in a comparison of the structures of Ins(1,4,5)P_3 and methyl α-L-glucopyranoside 2,4,6-trisphosphate (**59**), the compounds share some functional groups and their stereochemical aspects are conserved, but there are also a number of structural differences (Figure 89).

The structural deviation predicted to result in the largest impact on hypothetical binding to the IBC is the extended phosphate group attached to the 6-position of **59,** which could mimic the 4-phosphate group of Ins(1,4,5)P_3. It was not known, however, if the receptor would tolerate this hydrocarbon extension in the equivalent of the crucial 4-position phosphate, as some minor modifications to the vicinal phosphate pair have previously been shown to result in ligand inactivity (Section 5.1.1).[251]

There have also been reported cases in which conservative structural changes to the equivalent of the 4-position phosphate of Ins(1,4,5)P_3 can be tolerated by the IBC and are even thought to contribute, in conjunction with other structural modifications, to partial agonist behaviour in some ligands (Section 5.1.3).[266,276–278]

It was hoped that, as postulated by Bello *et al*., by modifying the equivalent of the 4-position phosphate specifically, the ligand may not be able to interact with the β-domain as effectively, thereby preventing IBC clamshell closure upon ligand binding and generating partial agonist activity.[251] However, the possibility remained that, as in the case of the 4-position-modified Ins(1,4,5)P_3 analogues synthesised in the Bello *et al*. study,[251] the structural difference to Ins(1,4,5)P_3 would be too drastic and the 6-position extended phosphate might prevent methyl α-L-glucopyranoside 2,4,6-trisphosphate (**59**) from binding to the IBC.

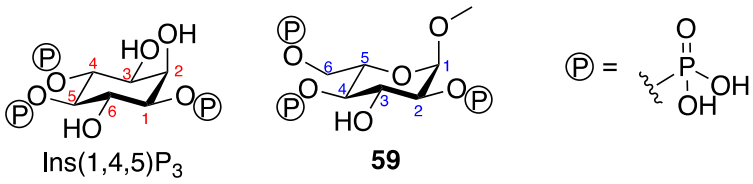

Figure 89: Comparison of numbered structures of Ins(1,4,5)P_3 (left) and methyl α-L-glucopyranoside 2,4,6-trisphosphate (**59**, right).

As predicted from the binding modes (Figure 88), higher-scoring docking solutions also often positioned the methyl α-L-glucopyranoside 2,4,6-trisphosphate (**59**) such that the extended phosphate was accommodated in the region of the binding site normally occupied by the 4-phosphate of Ins(1,4,5)P_3 (Figure 90).

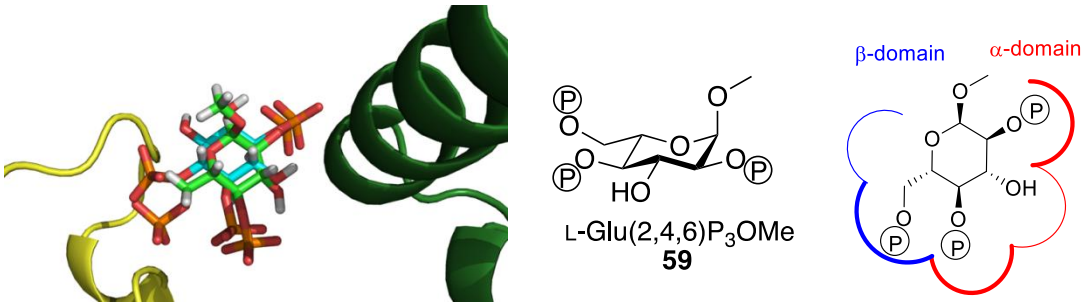

Figure 90: docking solution for methyl α-L-glucopyranoside 2,4,6-trisphosphate (**59**, green, docking solution 42, GOLDscore fitness: 135.9563) overlapping with the endogenous Ins(1,4,5)P_3 (aqua) in the IBC of InsP_3R (1N4K).[247] Figure reproduced from Shipton *et al*. study.[335]

This extended phosphate was therefore expected to interact with the Arg265 residue side chain and, as a result, the central ring of the ligand appeared to be slightly shifted from the position of Ins(1,4,5)P_3 to accommodate this interaction. As a consequence of the central ring shifting, the axial *O*-methyl of **59** was predicted to be able to point out of the binding site and into solvent.

The last main difference between Ins(1,4,5)P_3 and methyl α-L-glucopyranoside 2,4,6-trisphosphate (**59**) that could be reasonably expected to interfere with ligand binding was the absence of an equivalent to the 3-position hydroxyl of Ins(1,4,5)P_3 due to the location of the pyranosyl ring oxygen. While the lack of an equivalent hydroxyl in this position will likely result in a decrease in ligand affinity, this structural difference should not prevent ligand binding, as deletion of the 3-position hydroxyl of Ins(1,4,5)P_3 has already been demonstrated to be tolerated by InsP_3R.[263,293]

5.2.3 Methyl α-D-glucopyranoside 2,3,6-trisphosphate (**60**) and methyl α-D-glucopyranoside 2,4,6-trisphosphate (**61**) $InsP_3R$ binding predictions

As mentioned previously, both methyl α-D-glucopyranoside 2,3,6-trisphosphate (**60**) and methyl α-D-glucopyranoside 2,4,6-trisphosphate (**61**) were not expected to be able to bind to $InsP_3R$, as neither are able to be positioned such that the $InsP_3R$ binding requirements are met (Figure 88).

The docking solutions for both methyl α-D-glucopyranoside 2,3,6-trisphosphate (**60**) and methyl α-D-glucopyranoside 2,4,6-trisphosphate (**61**) tended to score poorly compared to the other ligands from this study included in the simulation. The highest-scoring docking solutions for both D-glucose-based enantiomers were also inconsistent in the orientation of the ligands in the $InsP_3R$ binding site.

5.2.4 α-D-glucopyranosyl 1,3,4-trisphosphate (**62**) and β-D-glucopyranosyl 1,3,4-trisphosphate (**63**) $InsP_3R$ binding predictions

Due to their structural similarities with $Ins(1,4,5)P_3$, both α-D-glucopyranosyl 1,3,4-trisphosphate (**62**) and β-D-glucopyranosyl 1,3,4-trisphosphate (**63**) were expected to be effective $Ins(1,4,5)P_3$ mimics and agonists of $InsP_3R$ (Figure 93).

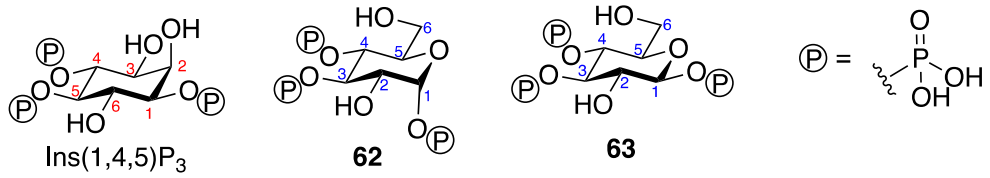

Figure 93: Comparison of numbered structures of $Ins(1,4,5)P_3$ (left), α-D-glucopyranosyl 1,3,4-trisphosphate (**62**, centre) and β-D-glucopyranosyl 1,3,4-trisphosphate (**63**, right).

D-Glucose-based ligands with modifications to the 1-position (the auxiliary phosphate) have been developed previously to investigate the unusually high potency of adenophostin A binding at $InsP_3R$ (Section 5.1.2). All of these glucose-based AdA analogues, including the heavily truncated analogues that did not feature either the adenine or ribose rings of AdA but instead positioned the auxiliary phosphate further from the glucose ring with a simple, hydrocarbon linkage, were found to be agonists of $InsP_3R$.[264,316,317,336] As a result, both α-D-glucopyranosyl 1,3,4-trisphosphate (**62**) and β-D-glucopyranosyl 1,3,4-trisphosphate (**63**), which to our knowledge have not been synthesised previously and could be considered heavily truncated analogues of AdA, were expected also to display agonist behaviour.

The relatively high potencies of the heavily truncated AdA analogues, thought to be fixed in a binding orientation analogous to Ins(1,4,5)P_3 by their 3,4-position vicinal phosphate pair (unlike less truncated analogues that might bind in slightly different orientations as result of the additional hydrophobic interactions between the IBC and ligand), demonstrate that the intrinsic differences between inositol and glucose structures will probably be tolerated by the IBC in this orientation.[264,282,284,305,331] This means that the extended hydroxyl in the equivalent of the 3-position hydroxyl, as well as the pyranosyl ring oxygen in the equivalent of the 2-position hydroxyl of both α-D-glucopyranosyl 1,3,4-trisphosphate (**62**) and β-D-glucopyranosyl 1,3,4-trisphosphate (**63**), should be tolerated.

The previous analogues of AdA have not included the auxiliary phosphate bound directly to the central ring and instead have always had it extended further into the binding site, as there had been concerns about the stability of the ligands, particularly the β–epimer.[264] The phosphates bound to the anomeric position were expected to bind well to the IBC in either orientation as, although an axial 1-position phosphate has not been previously analysed as part of a carbohydrate ligand, inositol-based ligands with axially oriented 1-position phosphates have been proven to be agonists.[281] However, the extent to which the axial orientation of the phosphate group in **62** impacts the affinity of a glucose-based ligand would be interesting to determine.

The structural differences between β-D-glucopyranosyl 1,3,4-trisphosphate (**63**) and Ins(1,4,5)P_3 are the same as for α-D-glucopyranosyl 1,3,4-trisphosphate (**62**), with the exception of the orientation of the 1-position phosphate. As a result, assuming sufficient stability, β-D-glucopyranosyl 1,3,4-trisphosphate (**63**) was expected to be more potent than its epimer, as the equatorial 1-position phosphate allows for the compound to mimic the structure of Ins(1,4,5)P_3 more closely.

In agreement with the predicted binding modes, the top-scoring docking solution from the GOLD molecular modelling positioned both **62** and **63** such that they overlapped quite closely with the position in which Ins(1,4,5)P_3 binds within the crystal structure (Figure 94).

The top-scoring docking solutions predicted that the axial phosphate in α-D-glucopyranosyl 1,3,4-trisphosphate (**62**) would displace the central ring slightly from the location of bound Ins(1,4,5)P_3 to ensure the 1-postion phosphate could be accommodated. In some of the highest-docking solutions for α-D-glucopyranosyl 1,3,4-trisphosphate (**62**), the axial phosphate appears to be positioned closer to the Arg504 residue, perhaps allowing it to form a stronger interaction with this residue. However, this change in position of the 1-position phosphate also results in it being further from the Arg568 residue, which is known to interact with the 1-position phosphate of Ins(1,4,5)P_3.

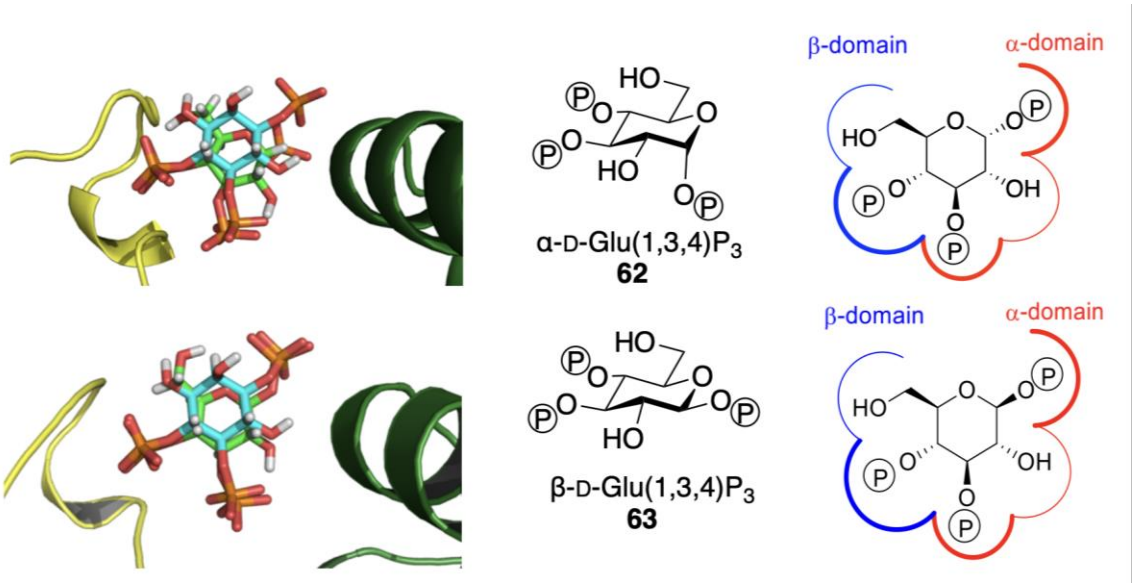

Figure 94. The highest-scoring docking conformations of **62** (green, top row, docking solution 56, GOLDscore fitness: 134.7244) and **63** (green, bottom row, docking solution 14, GOLDscore fitness: 143.1274) and bound Ins(1,4,5)P_3 (aqua) in the IBC of InsP_3R (1N4K), which has the α-domain shown in dark green and the β-domain in yellow.[247] Figure adapted from Shipton *et al.* study.[335]

The highest-scoring docking solutions for β-D-glucopyranosyl 1,3,4-trisphosphate (**63**) showed near-perfect overlap with the Ins(1,4,5)P_3 bound in the crystal structure, thereby presumably sustaining many of the same interactions between the three phosphate groups and the key binding residues in the IBC.

It was not initially clear if α-D-glucopyranosyl 1,3,4-trisphosphate (**62**) or especially β-D-glucopyranosyl 1,3,4-trisphosphate (**63**) would be sufficiently stable for accurate assessment via biological assay, due to the potentially labile nature of the phosphate attached to the anomeric hydroxyl.[264] Both α-D-glucopyranosyl 1,3,4-trisphosphate (**62**) and β-D-glucopyranosyl 1,3,4-trisphosphate (**63**) were successfully synthesised, however, and their stabilities analysed, as discussed later in the chapter (Section 5.4).

5.3 Synthesis of the carbohydrate-based potential $InsP_3R$ ligands

As in the case of the glucose-based inositol phosphate analogues synthesised for the HDAC3-SMRT study (Chapter 4), the syntheses of the compounds for this project were first carried out using the much cheaper D-glucose (Scheme 8) before being repeated with L-glucose (Scheme 9).

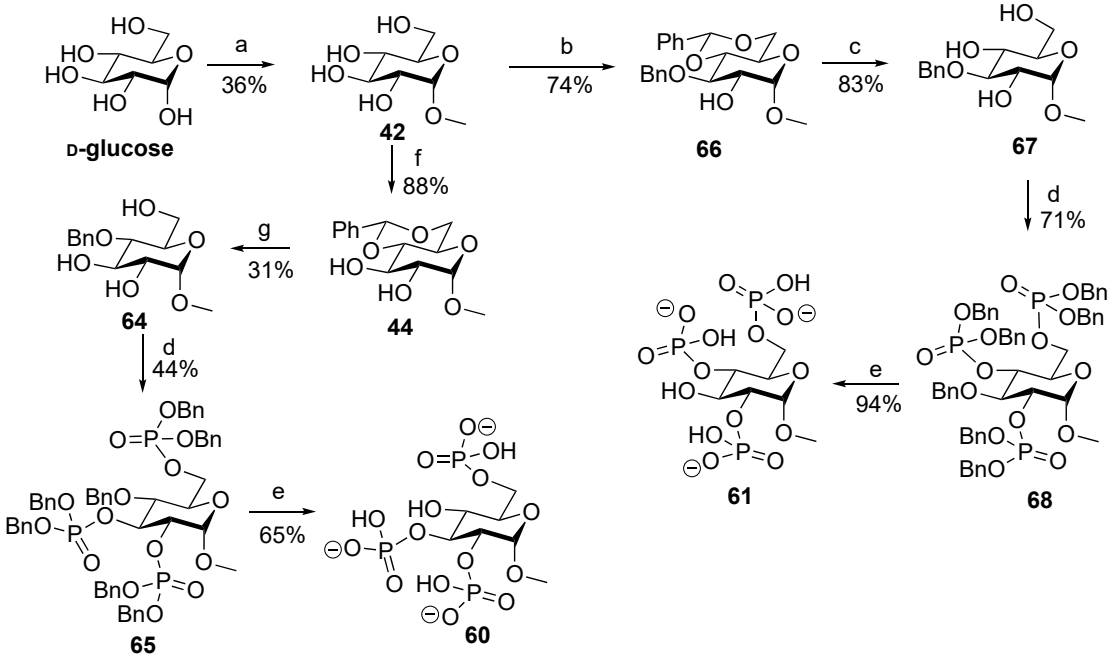

Scheme 8: Synthetic routes for the $InsP_3R$ ligands derived from D-glucose: methyl α-D-glucopyranoside 2,3,6-trisphosphate (**60**) and methyl α-D-glucopyranoside 2,4,6-trisphosphate (**61**).

Reagents and conditions: (a) MeOH, AcCl, reflux, 5d; (b) 1. TMSCl, py, 22h 2. DCM, benzaldehyde, $Fe(II)Cl_2 \bullet 6H_2O$, MeCN, triethylsilane, 0°C-rt, 1.5h; (c) MeOH, H_2O, 1M $HCl_{(aq)}$, Reflux, 3h; (d) 1. DCM, 5-phenyl-1*H*-tetrazole, $(OBn)_2PN(^iPr)_2$, 20h 2. *m*CPBA, -78°C-RT; (e) MeOH:H_2O (10:1 v/v), cat. $Pd(OH)_2/C$, H_2, 24h; (f) MeCN, benzaldehyde dimethyl acetal, cat. CSA, 24h; (g) BH_3-THF, $La(Tf)_3$, 7d.

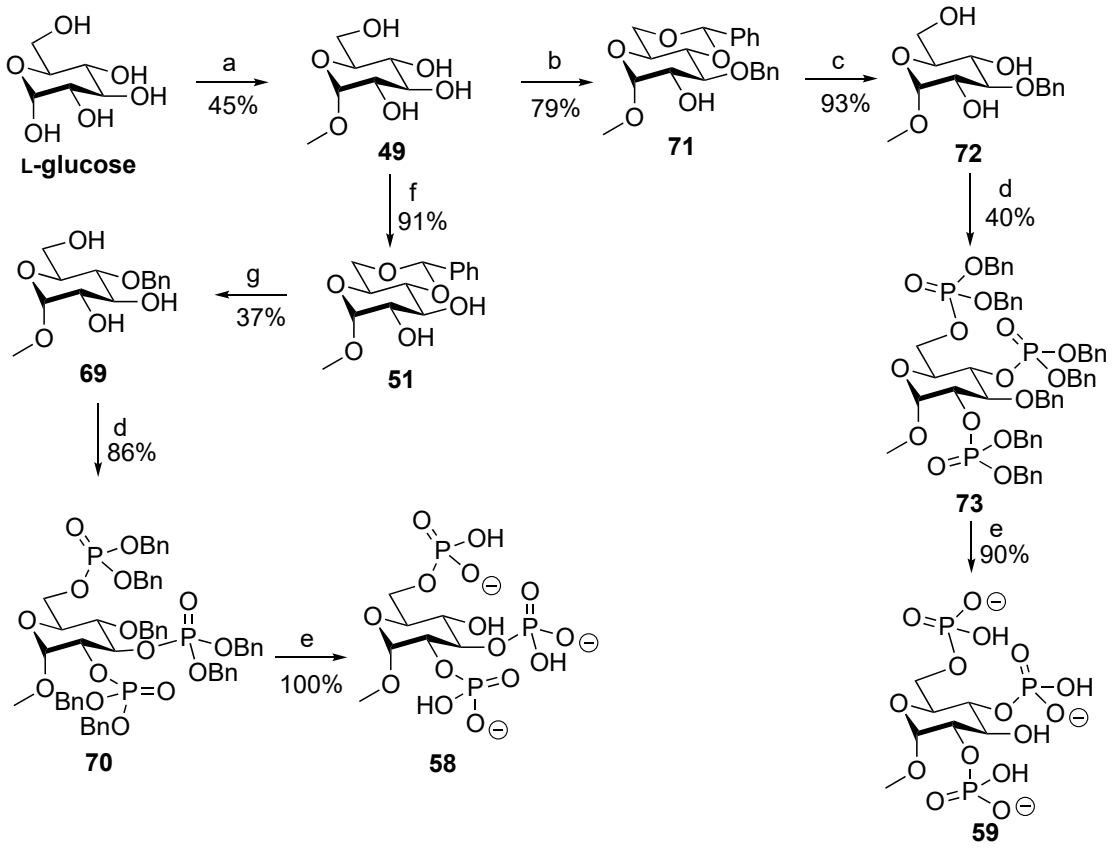

Scheme 9: Synthetic routes for the $InsP_3R$ ligands derived from L-glucose: methyl α-L-glucopyranoside 2,3,6-trisphosphate (**58**) and methyl α-L-glucopyranoside 2,4,6-trisphosphate (**59**)

Reagents and conditions: (a) MeOH, AcCl, reflux, 5d; (b) 1. TMSCl, py, 22h 2. DCM, benzaldehyde, $Fe(II)Cl_2{\cdot}6H_2O$, MeCN, triethylsilane, 0°C-rt, 1.5h; (c) MeOH, H_2O, 1M $HCl_{(aq)}$, Reflux, 3h; (d) 1. DCM, 5-phenyl-1*H*-tetrazole, $(OBn)_2PN(^iPr)_2$, 20h 2. *m*CPBA, -78°C-RT; (e) MeOH:H_2O (10:1 v/v), cat. $Pd(OH)_2/C$, H_2, 24h; (f) MeCN, benzaldehyde dimethyl acetal, cat. CSA, 24h; (g) BH_3-THF, $La(Tf)_3$, 7d.

The first step to synthesise four of the six target compounds, methylation of glucose, was the same first step in the syntheses of the HDAC3-SMRT glucose-based ligands (Chapter 4). After allowing the reaction to reflux for several days, the pure methyl α-glucopyranoside product was isolated from the α/β-epimer product mixture by means of repeated recrystallisations from ethanol (mostly α-epimer with approximately 3-5% β-epimer after the first recrystallisation, 100% α-epimer after the second). To maximize the yield for the methylation of L-glucose, the mother liquors of the recrystallisations were equilibrated in another reflux with methanol and acetyl chloride before more of the desired α-epimer was isolated from successive recrystallisations (45% overall yield for methyl α-L-glucopyranoside, **49**; 36% overall yield for the D-enantiomer, **42**). After this point, the synthetic routes diverged with different protecting group manipulations to generate the methyl α-glucopyranoside

2,3,6-trisphosphate and methyl α-glucopyranoside 2,4,6-trisphosphate enantiomer pairs.

To synthesise methyl α-L-glucopyranoside 2,3,6-trisphosphate (**58,** and analogously for methyl α-D-glucopyranoside 2,3,6-trisphosphate, **60**) the next step in the route was the benzylidene protection of the 4- and 6-position hydroxyls of methyl α-L-glucopyranoside, using benzaldehyde dimethyl acetal and catalytic camphor sulfonic acid (**44**, D:88 % yield; **51**, L:91% yield).

The benzylidene group of methyl 4,6-benzylidene α-glucopyranoside was then regioselectively opened to yield the methyl 4-*O*-benzyl α-glucopyranoside product. This is the opposite direction to the regioselective opening of methyl 4,6-benzylidene α-glucopyranoside described in the synthesis of some of the HDAC3-SMRT ligands (Chapter 4). As previously described, there are a number of factors that influence the regioselectivity of reductive benzylidene cleavage. The formation of the initial complex between the starting material and the Lewis acid is thought to be particularly important though, as this is the rate determining step of the reaction and can have a large impact on the regioselectivity of the product formed.[206]

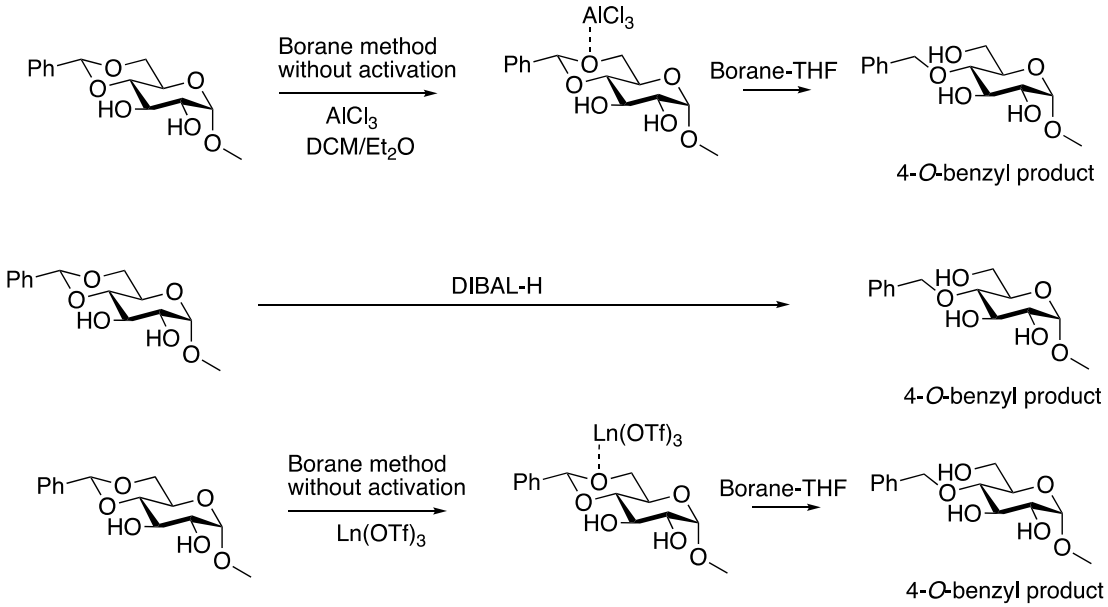

Figure 95: Different conditions used to open regioselectively methyl 4,6-benzylidene α-glucopyranoside in order to generate methyl 4-*O*-benzyl α-glucopyranoside.[208,209,337,338]

The benzylidene opening in this route was first attempted with borane-THF and aluminium chloride in dry DCM and diethyl ether (Figure 95). The 2- and 3-position hydroxyls of the starting methyl 4,6-benzylidene α-glucopyranoside were left unprotected as the reaction should still be feasible with exposed hydroxyls with possibly only a minor reduction in yield.[212,339,340] It is thought that aluminium chloride favours complexation to the relatively unhindered, more nucleophilic 6-position

oxygen of the benzylidene acetal and, in binding at this position, the benzylidene acetal is cleaved to yield the methyl 4-*O*-benzyl α-glucopyranoside product.[208] The potential side reaction of benzylidene acetal hydrolysis from trace amounts of water was largely prevented as an excess of borane was used in the reaction, which reacted readily with any water present.[212]

Although hydrolysis and over-reduction of the starting material were not observed, the benzylidene opening reaction suffered from poorer regioselectivity than hoped and a not-insignificant amount of methyl 6-*O*-benzyl α-glucopyranoside product was generated. Although multiple attempts to purify the product through silica column chromatography proved fruitless, it was found that following phosphorylation of slightly contaminated methyl 4-*O*-benzyl α-glucopyranoside, the contaminants [including the trace amount of methyl 6-*O*-benzyl α-glucopyranoside 2,3,4-tris(dibenzylphosphate) generated] could be separated from the desired methyl 4-*O*-benzyl α-glucopyranoside 2,3,6-tris(dibenzylphosphate) product with relative ease. However, a cleaner method of benzylidene was required to characterise the pure products of this benzylidene opening.

To this end, the next set of reaction conditions attempted employed DIBAL-H as both the reducing agent and Lewis acid to reductively open the benzylidene group regioselectively to the 4-position benzylated product (Figure 95).[209,337] While these conditions generated methyl 4-*O*-benzyl α-glucopyranoside as the main product, the reaction was insufficiently regioselective and too much methyl 6-*O*-benzyl α-glucopyranoside also formed, leading to other reaction conditions being investigated.

The next set of reaction conditions trialled for the regioselective opening of the benzylidene group was borane-THF with lanthanum triflate stirring at room temperature for a week in an adapted version of the Shie *et al.* protocol.[338] A number of lanthanide triflates have been previously reported to be used as Lewis acids in conjunction with borane-THF to open methyl 4,6-benzylidene α-glucopyranoside regioselectively to form methyl 4-*O*-benzyl α-glucopyranoside.[338,341] Lanthanide triflates are moisture-sensitive and expensive, but our lab had a viable supply of lanthanum triflate to attempt a benzylidene opening. Lanthanum triflate is a very sterically bulky Lewis acid that would be expected to coordinate preferentially to the relatively unhindered 6-position oxygen of the benzylidene acetal in an analogous fashion to aluminium chloride.

The lanthanum triflate reaction conditions were found to be more regioselective than the aluminium chloride conditions, and the desired methyl 4-*O*-benzyl glucopyranoside product could be successfully separated from the traces of methyl 6-*O*-benzyl glucopyranoside side-product generated. Although the lanthanum triflate method resulted in pure product, the low yield (**64**, D: 31% yield; **69**, L: 37%) and long reaction time resulted in the aluminium chloride method being used to generate the

majority of the methyl 4-*O*-benzyl α-glucopyranoside brought through for the remaining steps of the reaction route (with the contaminants of the benzylidene opening step, including the unwanted 6-*O*-benzyl regioisomer, being completely removed during purification of the protected trisphosphate product in the following phosphorylation reaction).

The phosphorylation of methyl 4-*O*-benzyl α-L-glucopyranoside (**69**, and methyl 4-*O*-benzyl α-D-glucopyranoside, **64**) proceeded in a stepwise phosphitylation-oxidation using dibenzyl phosphoramidite and 5-phenyl-1*H*-tetrazole followed by *m*CPBA to generate the pure methyl 4-*O*-benzyl α-glucopyranoside 2,3,6-tris(dibenzylphosphate) product as a colourless oil following purification by silica column chromatography (**65**, D: 44% yield; **70**, L: 86% yield).

In the final deprotection step, the benzyl-protected trisphosphate was hydrogenated with Pearlman's catalyst to yield the methyl α-glucopyranoside 2,3,6-trisphosphate, which was initially collected as a free acid. Both enantiomers of the product were found to be sufficiently clean not to require purification following filtration of the catalyst. The product was converted to triethylammonium salt through the addition of triethylamine, concentrated *in vacuo* and lyophilized to be collected as a colourless glass (**60**, D: 65% yield; **58**, L: 100% yield).

To synthesise the methyl α-L-glucopyranoside 2,4,6-trisphosphate (**59**) and methyl α-D-glucopyranoside 2,4,6-trisphosphate (**61**) final products, the first step of the synthetic route following the methylation of glucose was the simultaneous regioselective monobenzylation and benzylidene protection, as described by Bourdreux *et al*., in an iron (III) chloride hexahydrate catalysed acetal formation and reductive etherification.[342,343] One of the reasons this one-pot reaction was so attractive is that it bypassed the need to use an organotin-mediated regioselective protecting strategy to differentiate between the vicinal, equatorial 2- and 3-position hydroxyls.[344] The first step in this one-pot protection sequence was the persilylation of methyl α-glucopyranoside with TMSCl. Although this persilylated product was not purified, its formation was confirmed with ^{1}HNMR before the continuation to the second step of the reaction.

Persilylation had previously been determined to be necessary prior to introduction of the protecting groups in the second step, as the protection of carbohydrate starting materials with exposed hydroxyls tended to fail, in part due to their lower degree of solubility in the organic solvents necessary for the subsequent step.[345]

The persilylated methyl α-glucopyranoside, after being thoroughly dried through repeated co-evaporation with toluene, was then dissolved in DCM and to this solution benzaldehyde was added with catalytic iron (III) chloride hexahydrate. Several Lewis acids have been found to be effective for catalysing this reaction other than iron (III) chloride hexahydrate including copper (II) triflate, trimethylsilyl triflate, bismuth

triflate, halfnium triflate and vanadium triflate, but iron (III) chloride hexahydrate was used as it was reported to produce some of the highest yields and was readily available.[342,345]

In the second step of this reaction, the benzaldehyde formed two benzylidene acetal groups, a stable 4,6-benzylidene acetal and an unstable 2,3-acetal that was reductively opened *in situ* by an organosilane regioselectively to yield a 3-position benzyl group.[345] The 2,3-acetal appeared to open only to form the 3-position benzyl product as opposed to the 2-position benzyl regioisomer, which was not observed in the reactions in this body of work or in the analogous reactions carried out in the Français *et al*. study.[345] The regioselectivity of this benzylidene opening is thought to be due to the increased reactivity of the acetal bond at the 2-position, as well as the steric and inductive effects that decrease the nucleophilicity of the oxygen attached at the 3-position.[343,345,346]

Regioselective monobenzylation of the 3-position was also carried out on methyl 4,6-benzylidene α-glucopyranoside as described by Wang *et al*. to determine if a stepwise addition of the protecting groups would generate a higher yield.[343] It was found not to be necessary to attach the benzylidene group prior to the persilylation-benzylation reaction, however, as the yield for the reaction sequence to generate methyl 3-benzyl-4,6-benzylidene α-glucopyranoside proved to be higher from methyl α-glucopyranoside than from methyl 4,6-benzylidene α-glucopyranoside (74% yield and 46% yield respectively).

Following the one-pot simultaneous benzyl and benzylidene protection (**66**, D: 74% yield; **71**, L: 79% yield), the benzylidene group was selectively removed via acidic hydrolysis. This was achieved by refluxing the methyl 3-*O*-benzyl-4,6-benzylidene α-glucopyranoside starting material in methanol with hydrochloric acid to yield methyl 3-*O*-benzyl α-glucopyranoside (**67**, D: 83% yield; **72**, L: 93% yield).

The methyl 3-*O*-benzyl α-glucopyranoside was then phosphorylated in a two-step phosphitylation-oxidation using dibenzyl phosphoramidite and 5-phenyl-1*H*-tetrazole followed by *m*CPBA to generate the benzyl-protected trisphosphate product as a colourless oil after purification by silica column chromatography (**68**, D: 71% yield; **73**, L: 40% yield).

The benzyl groups of the protected precursors were subsequently removed in a palladium hydroxide-catalysed hydrogenation to yield methyl α-glucopyranoside 2,4,6-trisphosphate as a free acid. As in the case of the methyl α-glucopyranoside 2,3,6-trisphosphate route, this final hydrogenation step was found to be sufficiently clean and purification of the methyl α-glucopyranoside 2,4,6-trisphosphate product was not required following filtration of the palladium catalyst. The product was converted into a triethylammonium salt by exposure to triethylamine before being lyophilised to a colourless glass (**61**, D: 94% yield; **59**, L: 90% yield).

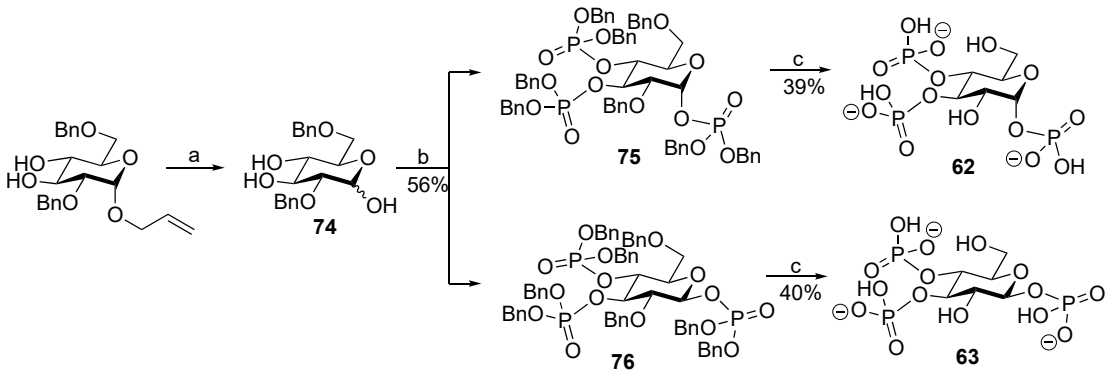

Scheme 10: Synthesis of the D-glucose based $InsP_3R$ ligands that have phosphates bound to the 1-position anomeric hydroxyl: α-D-glucosyl 1,3,4-trisphosphate (**62**) and β-D-glucosyl 1,3,4-trisphosphate (**63**).

Reagents and conditions: (a) MeOH, cat. $PdCl_2$, 6h; (b) 1. DCM, 5-phenyl-1*H*-tetrazole, $(OBn)_2PN(^iPr)_2$, 20h 2. *m*CPBA, -78°C -RT; (c) MeOH:H_2O (10:1 v/v), cat. $Pd(OH)_2/C$, H_2, $NaHCO_3$, 24h.

The synthesis of α-D-glucopyranosyl 1,3,4-trisphosphate (**62**) and β-D-glucopyranosyl 1,3,4-trisphosphate (**63**) began with allyl 2,6-dibenzyl-α-D-glucopyranoside (Scheme 10), which can be synthesised from D-glucose in a five-step route as described by Rosenberg *et al*.[282] There is precedence for the allyl functional group being used as an orthogonal protection group to benzyl groups to allow for selective protecting group manipulations at the anomeric position of a sugar.[347–352]

The first step in this synthetic route was the selective deprotection of the allyl group to expose the 1-position hydroxyl for subsequent phosphorylation. Deallylation of allyl 2,6-dibenzyl-α-D-glucopyranoside was carried out as described by Ogawa and Yamamoto in a palladium chloride catalyzed methanolysis.[353] The palladium catalyst isomerized the allyl group to the far more labile cis-prop-1-enyl, allowing for cleavage to take place under mild conditions.[348,349,354]

The allyl protecting group was ideal to use for this purpose as, when similar selective deprotection of the anomeric position is attempted with methyl glycosides, stronger acidic conditions and prolonged reaction times are required to hydrolyse the group attached to the 1-position, and such harsh conditions have been reported to result in low yields due to decomposition and cleavage of benzyl ether-protecting groups.[351,352] The milder reactions conditions needed to cleave allyl groups from the anomeric position are sufficiently gentle to avoid the unwanted cleavage of the benzyl-protecting groups.[347,355] This is particularly important for retaining the benzyl ether group attached to the primary 6-position hydroxyl, as groups in this position have been found to be particularly sensitive and can be cleaved under acidic conditions faster than benzyl ether attached to other positions around a carbohydrate ring.[347,348,356]

While the removal of the allyl group was successful, the subsequent mixture of anomers could not be fully purified from various reaction contaminants (in the literature, the compound has relatively little characterisation available).[357] Fortunately, following phosphorylation in the next step of the synthetic route, the resultant protected trisphosphate product epimers could be successfully purified and partially separated.

The slightly impure 2,6-dibenzyl glucose (**74**) was phosphorylated using the two-step phosphitylation-oxidation method with dibenzyl phosphoramidite and 5-phenyl-1*H*-tetrazole followed by *m*CPBA to generate both product anomeric epimers (**75** and **76**). The β-epimer was favoured slightly in the phosphorylation with the first product ratio of α:β-epimers being 1:2.5, and the second product ratio upon a repeat of the reaction being 1:1.2.

It was unclear if the benzyl-protected anomeric phosphate epimers would be sufficiently stable to allow the products to be purified by silica column chromatography, as there are some reports of protected β-epimers decomposing during aqueous work-ups or purification,[358,359] but others where they remain stable (Section 5.4).[358–363] There have also been accounts in the literature that describe the β-glycosyl phosphates anomerising to the more stable α-epimers,[362] but this phenomenon was not observed in this study. While no anomerisation took place, some degradation could be observed in the protected β-glycosyl phosphate product after three weeks at 4°C (approx. 30%. by ^{31}PNMR), while the protected α-glycosyl phosphate product remained intact.

Prior to hydrogenation, the benzyl-protected phosphate attached to the anomeric position is more vulnerable to hydrolysis due to the absence of an exposed charge on the phosphate which would render it a poorer leaving group and repel approaching nucleophiles. It has been suggested in the literature that to prevent hydrolysis of the protected anomeric phosphate species, the usual aqueous work-up that follows phosphorylation should be avoided altogether or kept basic to supress acidic hydrolysis[359,361,363] In the synthesis of 2,6-di-*O*-benzyl D-glucopyranosyl 1,3,4-trisphosphate, the alkaline aqueous work-up was included, although the total yield of this phosphorylation was slightly lower (56% yield) than some of the other phosphorylations of glucose in this study, which may be indicative of product decomposition during the work-up. The potentially lower yield as a result of the aqueous work-up was deemed acceptable, however, as this work-up eliminated impurities that would otherwise need to be removed with the potentially product-degrading silica column chromatography purification that also had to complete the difficult separation of the product epimers.

While it was found that the glycosyl phosphates could withstand purification via silica column chromatography, the α- and β-epimers of the desired product proved to be

very challenging to separate, and only partial separation was achieved after multiple columns (56% yield total: 14% yield α-epimer, **75**; 19% yield, β-epimer, **76**; 23% mixed epimers).[360] Despite the suggestion of one source to deactivate the acidic silica column with triethylamine prior to use in order to minimise product degradation,[363] the 2,6-di-*O*-benzyl D-glucopyranosyl 1,3,4-trisphosphate epimers were purified without deactivation to improve separation of the products (with only limited product loss observed after each column).

The final step in the route to generate α-D-glucopyranosyl 1,3,4-trisphosphate (**62**) and β-D-glucopyranosyl 1,3,4-trisphosphate (**63**) was the deprotection of the benzyl groups through a palladium-catalysed hydrogenation reaction. Hydrogenation reactions of organic phosphates become more acidic as the reaction progresses, a feature that is normally viewed as beneficial in accelerating debenzylation.

In an attempt to supress an acidic hydrolysis side reaction of the protected 1-position phosphate groups, the hydrogenation reactions to deprotect both **75** and **76** were carried out as a precaution with sodium bicarbonate. Several analogous reactions using sodium bicarbonate had previously been carried out by Fylaktakidou *et al*., and the authors reported that these hydrogenations produced high yields with no phosphate migration observed.[361] However, the inclusion of a base in the final deprotection of the glycosyl phosphate products may have been unnecessary, as there have been reported syntheses of similar hydrogenations carried out, without the presence of a base, that generated glycosyl phosphate products in reasonable yields.[364]

Both α-D-glucopyranosyl 1,3,4-trisphosphate (**62**) and β-D-glucopyranosyl 1,3,4-trisphosphate (**63**) products were purified through reverse-phase column chromatography, during which the salt form of the product was converted from sodium to triethylammonium. Both products were collected from their respective columns and lyophilised to yield the triethylammonium salts as colourless glasses (**62**, α: 39% yield; **63**, β: 40% yield).

The purity of all of the Ins(1,4,5)P_3 analogues was assessed through HPLC analysis by our collaborator Professor Charles Brearley at the University of East Anglia (Figure 96 and Table 10). The HPLC analysis was carried out using a highly specialised system to enable these products to be detected, as they lack a chromophore group which would be required for standard HPLC methods (details in Experimental).

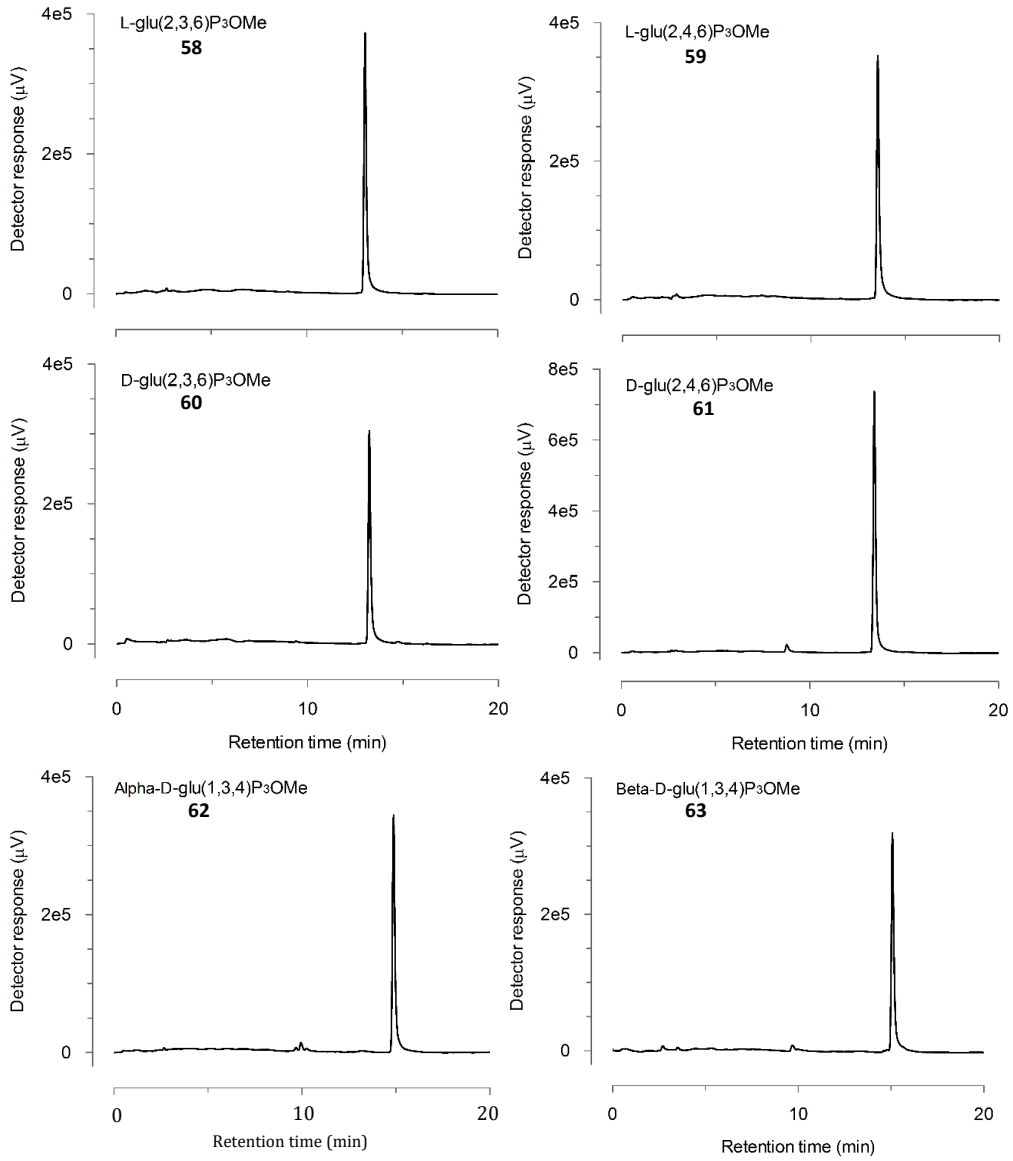

Compound	Mean integration %	Standard deviation %
methyl α-L-glucopyranosyl 2,3,6-trisphosphate (**58**)	99.15	0.06
methyl α-L-glucopyranosyl 2,4,6-trisphosphate (**59**)	99.83	0.08
methyl α-D-glucopyranoside 2,3,6-trisphosphate (**60**)	97.21	0.71
methyl α-D-glucopyranoside 2,4,6-trisphosphate (**61**)	96.87	0.23
α-D-glucopyranosyl 1,3,4-trisphosphate (**62**)	94.53	0.10
β-D-glucopyranosyl 1,3,4-trisphosphate (**63**)	95.43	0.58

Figure 96 and Table 10: Data reproduced from Shipton *et al*.[335] for the HPLC traces, confirming the purity for compounds **58**, **59**, **60**, **61**, **62** and **63**. The table gives values of the integrated peak area as a % of total peaks in each chromatogram.

5.4 Stability analysis of α-D-glucopyranosyl 1,3,4-trisphosphate (**62**) and β-D-glucopyranosyl 1,3,4-trisphosphate (**63**)

There is no clear consensus on the stability of phosphates bonded to the anomeric hydroxyl of carbohydrates (particularly β-epimers), as some compounds with these groups have been reported to be very fragile and prone to anomerisation or hydrolysis (often when the phosphates are still protected),[264,358,359,362,365] while others have been reported to be reasonably robust under neutral conditions.[359–363] An ancillary study into the stability of α-D-glucopyranosyl 1,3,4-trisphosphate (**62**) and β-D-glucopyranosyl 1,3,4-trisphosphate (**63**) was carried out to ensure that any biological results obtained for these compounds would not be compromised by compound degradation.

Phosphates bound to the anomeric centre can be removed through either acidic or basic hydrolysis (Figure 97). Through a study with isotopically labelled oxygen, it was previously discovered that under acidic conditions the phosphate is cleaved at the bond between the carbon and oxygen, whereas under basic conditions the phosphate was cleaved at the bond between the oxygen and the phosphorus.[366] Although both hydrolysis mechanisms are possible, the acidic pathway seemed to occur more readily. Of the two trisphosphate product anomers, hydrolysis of the β-epimer would be expected to be more facile as this stereoisomer is not stabilised by the anomeric effect (refer to Chapter 1).

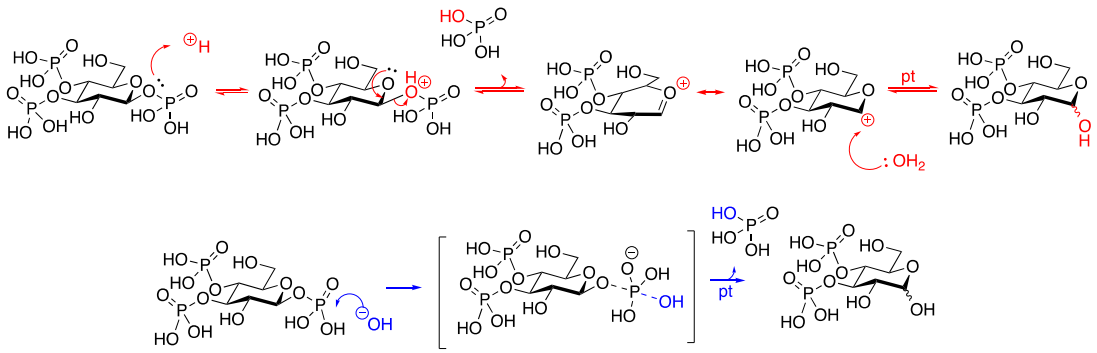

Figure 97: Mechanisms for acidic (top row) and basic (bottom row) hydrolysis of β-D-glucopyranosyl 1,3,4-trisphosphate (**63**). In the acidic mechanism, a lone pair of electrons on the pyranosyl oxygen can assist in the ejection of the phosphate from the anomeric position (resulting in the β-anomer being especially vulnerable to acidic decomposition, as it is not stabilised by the anomeric effect).[366,367]

It has been reported that carbohydrates with a deprotected phosphate bound to the anomeric position can be stored as a solid at 4°C for months without significant degradation.[363] This appears pleasingly to be the case for the glucopyranosyl 1,3,4-trisphosphate epimers in this study as well, as they have shown no signs of degradation after months at 4°C and approximately a year in the freezer at -20°C.

In addition to monitoring the stability of the glucopyranosyl 1,3,4-trisphosphate anomers as solids, the conditions of the epimers were tracked with ^{1}HNMR when in aqueous solution over time and when exposed to different pHs (Figure 98 and Table 11).

It was found that at neutral pH, neither α-D-glucopyranosyl 1,3,4-trisphosphate (**62**) nor β-D-glucopyranosyl 1,3,4-trisphosphate (**63**) showed any signs of degradation after over a month in aqueous solution. It took surprisingly forcing conditions to degrade the epimers, as demonstrated in Figure 98. ^{1}HNMR spectroscopy was used to track the degradation of both epimers in a mixture through integration of characteristic proton signals, thereby allowing relative decomposition of the regioisomers to be monitored under different conditions.

Under mild acidic conditions, only limited hydrolysis of the β-epimer was observed relative to the α-epimer, but when the acidity was increased, both regioisomers decomposed completely. On the other hand, under mildly basic conditions there was no apparent hydrolysis of either epimer, and only limited hydrolysis of the β-epimer relative to the α-epimer was observed under more basic conditions. It should be noted that only one product of hydrolysis can be observed in the ^{1}HNMR signals (with the other hidden underneath the HDO peak), but the integration of this peak was not used to indicate extent of hydrolysis due to the ease of interconversion between the two hydrolysed products.

Both α-D-glucopyranosyl 1,3,4-trisphosphate (**62**) and β-D-glucopyranosyl 1,3,4-trisphosphate (**63**) proved to be much more stable than initially expected. It should be safe to assume that both compounds are stable under the near neutral conditions employed in the biological studies described later in this Chapter (Section 5.5).

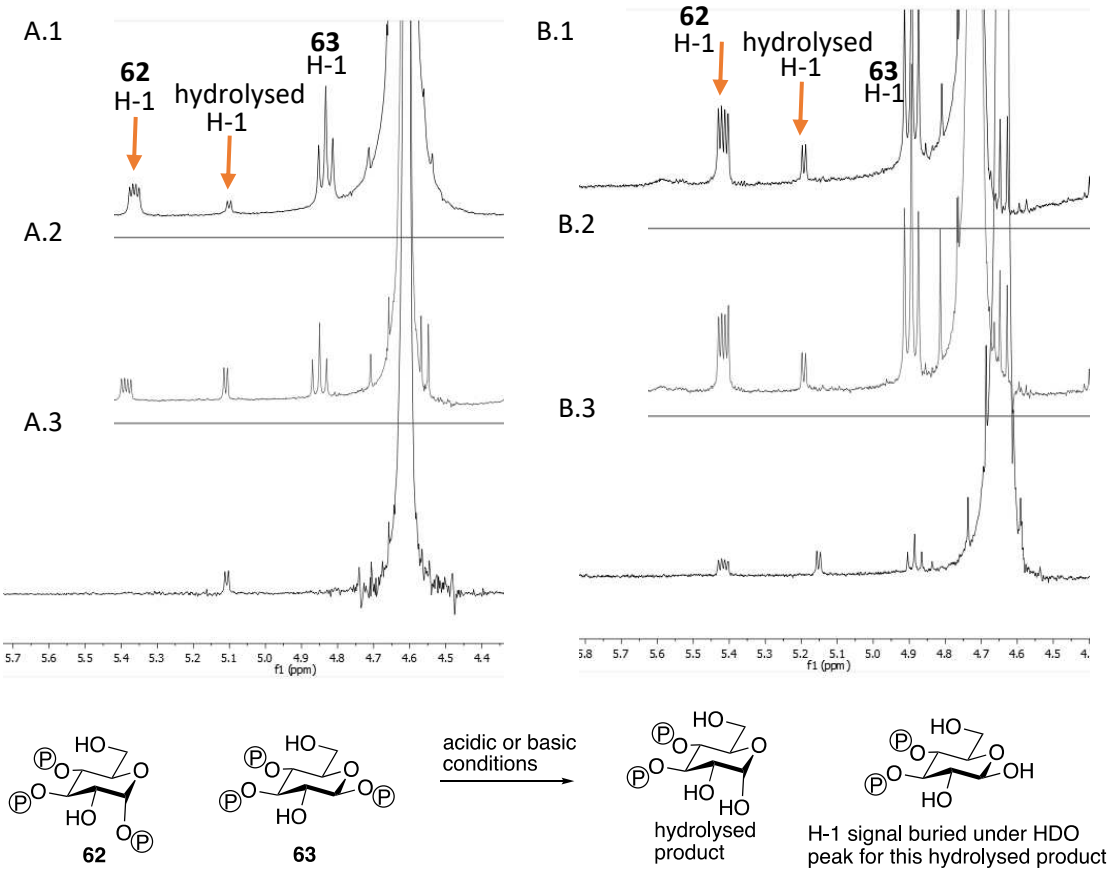

[1]HNMR trace	Conditions	Relative integration of 63 compared to normalised 62 peak
A.1	Neutral pH at RT	2.3
A.2	pH 3 for a week at RT	1.6
A.3	pH 1 for 1 day at RT	complete hydrolysis
B.1	Neutral pH at RT	2.3
B.2	pH 10 for a week at RT	2.3
B.3	pH 14 for 1 day at RT	1.7

Figure 98 and Table 11: Stability test for α-D-glucopyranosyl 1,3,4-trisphosphate (**62**) and β-D-glucopyranosyl 1,3,4-trisphosphate (**63**). The **A.** column on the left shows the compounds under increasingly acidic conditions and the **B.** column on the right shows the compounds under increasingly basic conditions. A small degree of hydrolysis occurred in the protected phosphate precursors prior to hydrogenation, resulting in the presence of a small amount of hydrolysed product present initially in panels A1 and B1. Diagram and table reproduced from Shipton *et al*.[335]

5.5 $InsP_3R$ biological results

Our collaborator Dr Ana Rossi from Professor Colin Taylor's lab in the University of Cambridge carried out both calcium release assays and $InsP_3R$ binding assays to determine the ability of the $Ins(1,4,5)P_3$ mimics in this study to affect $InsP_3R$. These results have been published in the *Journal of Medicinal Chemistry*.[335]

5.5.1 Calcium release and competition binding assays

The ability of the $Ins(1,4,5)P_3$ analogues to release calcium from intracellular stores of permeabilised HEK-$InsP_3R1$ cells was first determined in a fluorescence-based calcium release assay (details in the Experimental).

In addition to the six carbohydrate-based analogues of $Ins(1,4,5)P_3$, $Ins(1,4,5)P_3$ itself and the agonist AdA were included in the calcium release assay as controls. The permeabilized HEK-IP_3R1 cells were exposed to increasing concentrations of each potential receptor agonist, and the amounts of calcium subsequently released were tracked (Figure 99). A large range of concentrations was used for each of the ligands to ensure any ability the compounds had to trigger calcium release would be detected.

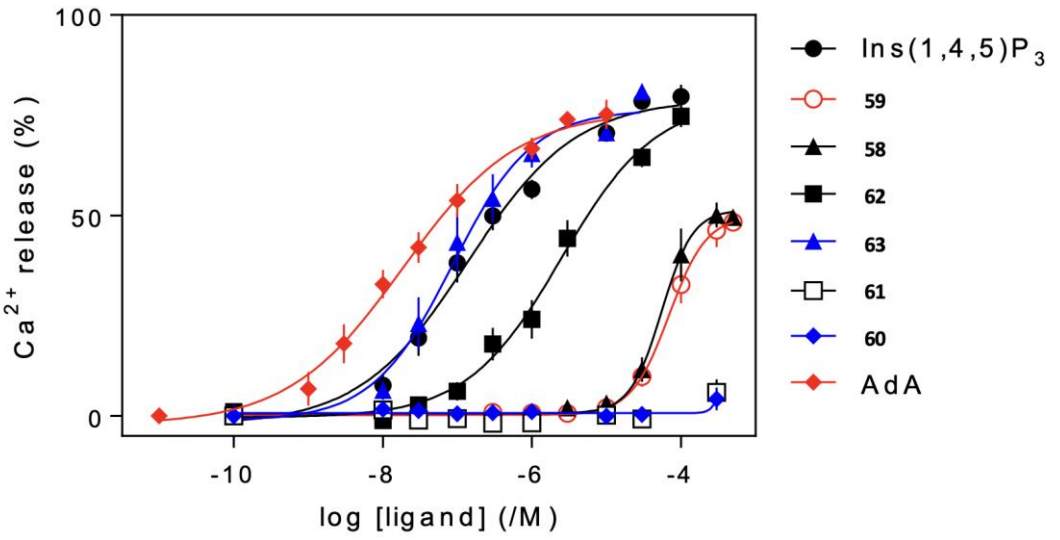

Figure 99: Dose-response curves reproduced from Shipton *et al*.[335] for the concentration-dependent effects of IP_3 and related ligands on the Ca^{2+} release from intracellular stores of permeabilized HEK-IP_3R1 cells. Results are mean ± SEM from 5-11 independent experiments each run in duplicate. Biological data were provided by Dr Ana Rossi from Professor Colin Taylor's lab (University of Cambridge).

Both α-D-glucopyranosyl 1,3,4-trisphosphate (**62**) and β-D-glucopyranosyl 1,3,4-trisphosphate (**63**) were shown to be full agonists of $InsP_3R$ through their ability to release the same quantity of intracellular Ca^{2+} as $Ins(1,4,5)P_3$ (approximately 80%).

The calcium release assay indicated that even at very high concentrations, both methyl α-L-glucopyranoside 2,3,6-trisphosphate (**58**) and methyl α-L-glucopyranoside 2,4,6-trisphosphate (**59**) were unable to release fully the calcium stores, with the total amount released for both ligands plateauing at approximately 50% (when approximately 80% would be expected for a full agonist). The inability of the compounds to release the calcium stores fully demonstrated that both ligands function as partial agonists, although their potency is low, as relatively high concentrations of the ligands were required before this behaviour could be observed.

The enantiomers of these newly-identified partial agonists, methyl α-D-glucopyranoside 2,3,6-trisphosphate (**60**) and methyl α-D-glucopyranoside 2,4,6-trisphosphate (**61**), proved to be unable to evoke any calcium release.

Following the calcium release assay, a competition binding assay using [^{3}H]-$Ins(1,4,5)P_3$ was carried out (Figure 100). The results from this binding assay were important in assessing the efficacy of methyl α-L-glucopyranoside 2,3,6-trisphosphate (**58**) and methyl α-L-glucopyranoside 2,4,6-trisphosphate (**59**) as partial agonists.

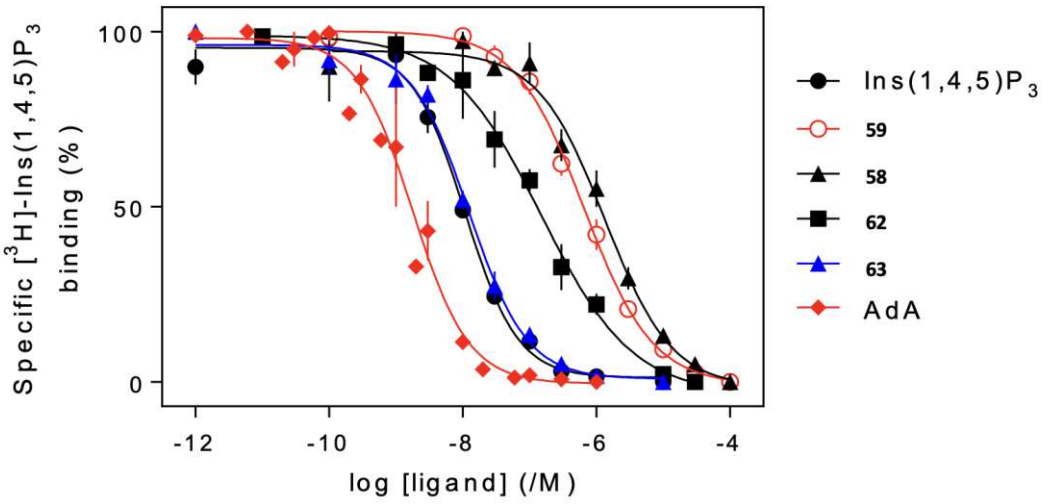

Figure 100: Dose-response curves reproduced from Shipton *et al.*[335] for the equilibrium-competition binding to cerebellar membranes using [^{3}H]-$Ins(1,4,5)P_3$ (1.5nM) and the indicated concentrations of $Ins(1,4,5)P_3$ or related ligands. Results are means ± SEM from 3 independent experiments. The results for $Ins(1,4,5)P_3$ and AdA have been published (Mills *et al.*)[368]. Biological data were provided by Dr Ana Rossi (University of Cambridge). Although not shown, both methyl α-D-glucopyranoside 2,3,6-trisphosphate (**60**) and methyl α-D-glucopyranoside 2,4,6-trisphosphate (**61**) were tested as well and confirmed to be inactive at $InsP_3R$.

The competition binding assay indicated that, of the glucose-based ligands, β-D-glucopyranosyl 1,3,4-trisphosphate (**63**) appeared to bind with the highest affinity, seemingly equal to Ins(1,4,5)P_3, followed by α-D-glucopyranosyl 1,3,4-trisphosphate (**62**) and then the partial agonists, methyl α-L-glucopyranoside 2,3,6-trisphosphate (**58**) and methyl α-L-glucopyranoside 2,4,6-trisphosphate (**59**). Although the data have not been included in the competition binding assay graph (Figure 100), both D-glucose based enantiomers (**60** and **61**) of the partial agonists were confirmed to be inactive at $InsP_3R$.

The data for the calcium release assay and binding competition assay were then combined to determine EC_{50}/K_d ratios for the ligands (Table 12). The EC_{50} is the concentration at which 50% of the maximum calcium release is induced, the K_d is the dissociation constant, and the ratio of these values can be used to gauge the efficacy of ligands as partial agonists.

	Ca^{2+} release			*Binding*			
	pEC_{50} **EC_{50}**	Release (%)	H	pK_d **K_d (nM)**	h	EC_{50}/K_d	$^{\wedge}EC_{39}/K_d$
$Ins(1,4,5)P_3$	6.90 ± 0.12 **126nM**	78.8 ± 1.3	0.7 ± 0.1	8.06 ± 0.03 **8.7**	1.1 ± 0.2	14 (5 - 46)	17 (5 - 63)
58	4.06 ± 0.09* **87.7µM**	56.2 ± 2.6*	1.4 ± 0.2	5.91 ± 0.03* **1230**	0.9 ± 0.1	71 (34 – 148)	132 (49 – 355)
59	3.98 ± 0.04* **104µM**	53.1 ± 5.0*	1.3 ± 0.2	6.26 ± 0.07* **549**	0.9 ± 0.1	191* (123 – 295)	462* (128 – 1667)
60	ND	4.3 ± 2.1#	ND	48 ± 12$	ND	ND	
61	ND	5.9 ± 2.1#	ND	53 ± 3$	ND	ND	
62	5.53 ± 0.20* **2.96µM**	78.8 ± 3.0	0.9 ± 0.2	6.89 ± 0.09* **129**	0.7 ± 0.1	23 (5 - 105)	
63	7.09 ± 0.18 **80nM**	75.2 ± 1.4	1.0 ± 0.1	7.95 ± 0.05 **11.2**	1.1 ± 0.2	7 (2 - 29)	
AdA	7.62 ± 0.12* **24nM**	77.8 ± 4.5	0.8 ± 0.1	8.86 ± 0.14* **1.4**	1.2 ± 0.2	17 (5 – 51)	

Table 12: Data reproduced from Shipton *et al.*[335] for the binding and calcium release assay data for AdA, $Ins(1,4,5)P_3$ and its analogues at $InsP_3R$.

[a]Effects of ligands on Ca^{2+} release from the intracellular stores of permeabilized HEK-$InsP_3R1$ cells and on [^{3}H]-$Ins(1,4,5)P_3$ binding to cerebellar membranes are summarized. Results from functional assays are means ± SEM (pEC_{50} (-log of the half-maximally effective concentration), Ca^{2+} release (%) and Hill coefficient, *h*) and means (EC_{50}) from 5-11 independent experiments, each performed in duplicate. Results from binding experiments are means ± SEM (pK_d (-log of the equilibrium dissociation constant) and *h*) and means (K_d) from three independent experiments. The pK_d values for $Ins(1,4,5)P_3$ and AdA have been published (Mills *et al.*)[368] and are reproduced with permission. Final columns show EC_{50}/K_d or (for partial agonists and $Ins(1,4,5)P_3$) EC_{39}/K_d (mean and 95% CI). ND, not determined. $^*P < 0.05$ relative to $Ins(1,4,5)P_3$.

#Ca^{2+} release evoked by 300 µM of the ligand

$Specific binding of [^{3}H]-$Ins(1,4,5)P_3$ in presence of 30µM of competing ligand

$^{\wedge}EC_{39}$ reports the concentration of ligand required to evoke the same Ca^{2+} release (39% of the intracellular stores) as evoked by a half- maximally effective concentration of $Ins(1,4,5)P_3$.

From the combined data of the two assays, the β-D-glucopyranosyl 1,3,4-trisphosphate epimer (**63**) can be seen to be near-equipotent with Ins(1,4,5)P_3 (approximately 1.5 times more potent).

The α-D-glucopyranosyl 1,3,4-trisphosphate epimer was still very active at the receptor as well, but was determined to be approximately twenty-fold less potent than Ins(1,4,5)P_3. It is perhaps unsurprising that **63** proved to be more active than **62**, as the 1-position phosphate of the β-epimer has the same stereochemistry as the equivalent phosphate in Ins(1,4,5)P_3. As further confirmation that both **62** and **63** are full agonists of InsP_3R, it can be noted that their EC_{50}/K_d values (23 and 7, respectively) are comparable with Ins(1,4,5)P_3 (14), as well as that of the confirmed agonist AdA (17).

As both L-glucose based ligands (**58** and **59**) were unable to evoke full calcium release, their receptor binding was further analysed through calculating their EC_{39} values as opposed to only their EC_{50} values [EC_{39} was chosen as this is the Ins(1,4,5)P_3 concentration that evokes half of the maximum Ca^{2+} release of the ligand]. The data confirmed that both (**58** and **59**), with their higher EC_{39}/K_d values (462 and 132, respectively) than Ins(1,4,5)P_3 (17), are partial agonists with low potency and efficacy.

5.5.2 Sea urchin egg homogenate assay

In addition to the more extensive investigation into the ability of these Ins(1,4,5)P_3 analogues to trigger the release of calcium in mammalian cells, their ability to cause the release of calcium in a sea urchin (*Lytechinus pictus*) egg homogenate assay (SUEH) was also assessed. For this study, the SUEH assay was prepared with Dr Lianne Davis from Professor Antony Galione's lab (University of Oxford, Pharmacology Dept), as detailed by Morgan and Galione, including the use of Fluo-3 to enable the monitoring of calcium concentration in the homogenate.[369]

The SUEH assay is a potentially high-throughput screening method that allows calcium release triggered by cell-impermeable compounds to be monitored with fluorimetry. The assay can be used to confirm which receptor a ligand acts on (InsP_3R, NAADPR and ryanodine receptors).

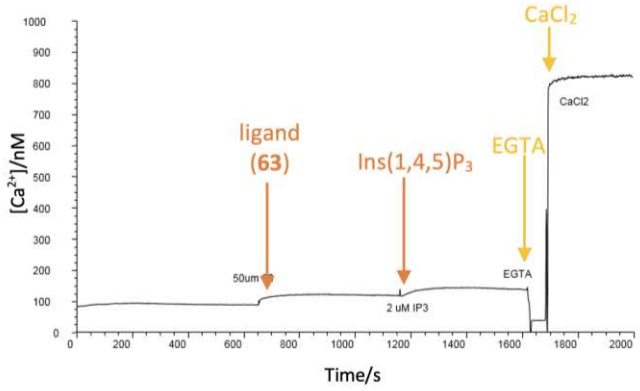

Ligand / (concentration of the 6 μL added to assay)	$[Ca^{2+}]$ released/ nM
$Ins(1,4,5)P_3$ (2 μM)	44.0
63 (50 μM)	20.5
62 (50 μM)	7.0
49 (50 μM)	7.3
69 (50 μM)	6.5
64 (50 μM)	11.6

Figure 101 and Table 13: On the left, an example of the graphs recorded during the SUEH assay for each of the compounds with calcium concentration (in nM) over time (s) as different compounds were added to the assay, with labels on the graph indicating time of addition. Following measurement of the change in calcium concentration from the addition of the ligand followed by $Ins(1,4,5)P_3$, EGTA then calcium chloride were added to calibrate the results. On the right, is a table indicating the increase in calcium concentration observed for each $Ins(1,4,5)P_3$ mimic, with $Ins(1,4,5)P_3$ itself included as a control. The calcium released for $Ins(1,4,5)P_3$ in the table above is the average of nine separate runs. The result for **63**, highlighted in the table, corresponds to the graph on the left.

Surprisingly, the SUEH assay seemed to indicate that only β-D-glucopyranosyl 1,3,4-trisphosphate (**63**) was an agonist of $InsP_3R$, and not its epimer α-D-glucopyranosyl 1,3,4-trisphosphate (**62**), which appeared to show the same inactivity as the other ligands tested (Figure 101 and Table 13).

The potency of the glucose-based ligands in the SUEH assay was also much lower than that of $Ins(1,4,5)P_3$, which could generate a calcium release response when 6 μL of 2 μM solution was added. The only carbohydrate-based ligand to trigger a substantial calcium release in the SUEH assay, β-D-glucopyranosyl 1,3,4-trisphosphate (**63**), required the use of 50 μM solution, after 2 μM solution was found to generate no response. The calcium released by this larger concentration was also significantly less than the response observed from $Ins(1,4,5)P_3$. The stark difference in potency between $Ins(1,4,5)P_3$ and the **62** and **63** agonists was unexpected, especially for **63,** which had been shown to be equipotent to $Ins(1,4,5)P_3$ in the other $InsP_3R$ assays (Section 5.5.1).

This discrepancy in observed potency could be due to possible differences between mammalian and sea urchin $InsP_3Rs$ (there is likely only one subtype present in *Lytechinus pictus* and although it has not been sequenced yet, it appears to have a significantly higher molecular mass than mammalian or amphibian *Xenopus laevis* $InsP_3Rs$).[370] It should also be noted that there have been reported incidents in which the results of SUEH assays have been found not to correlate with the results of mammalian calcium release assays for cADPR analogues at ryanodine receptors (and the isoform of ryanodine receptors in sea urchins has also been found to be

significantly different to its mammalian, avian, piscine and amphibian counterparts).[370,371] The abilities of the glucose-based Ins(1,4,5,)P_3 analogues to release calcium from the InsP_3R receptor, and any possible discrepancies between the results of the SUEH assay and the mammalian calcium release and competition binding assays, require further investigation but were not pursued in this study due to limited availability of the materials for the SUEH assay.

Despite the apparent differences in potency, it could clearly be detected that the prior addition of **63** appeared to desensitize the InsP_3R to subsequent additions of Ins(1,4,5)P_3 (calcium concentration increased by only 16.7 nM, compared to the 44.0 nM change observed previously), indicating that both ligands are acting on the same receptors and calcium stores.

5.6 Discussion of the biological activities of the InsP_3R ligands

5.6.1 Anomeric phosphate agonists: α-D-glucopyranosyl 1,3,4-trisphosphate (**62**) and β-D-glucopyranosyl 1,3,4-trisphosphate (**63**)

The high level of calcium release and corresponding ligand binding indicated that both α-D-glucopyranosyl 1,3,4-trisphosphate (**62**) and β-D-glucopyranosyl 1,3,4-trisphosphate (**63**) are full agonists of InsP_3R. Due to the similarities in structure of both of these ligands to Ins(1,4,5)P_3 (Figure 102), as well as their efficient docking in modelling simulations, the agonist activities of these ligands at InsP_3R were perhaps to be expected, but the degree of the ligand affinities for InsP_3R needed to be determined.

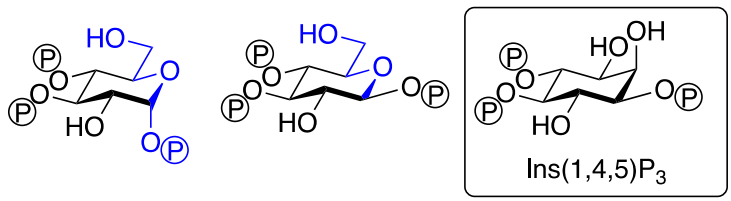

Figure 102: Structures of α-D-glucopyranosyl 1,3,4-trisphosphate (**62**, left) and β-D-glucopyranosyl 1,3,4-trisphosphate (**63**, middle) and Ins(1,4,5)P_3 (right). The main structural differences between the glucose-based ligands and Ins(1,4,5)P_3 are indicated in blue.

The closest structural mimic of Ins(1,4,5)P_3, β-D-glucopyranosyl 1,3,4-trisphosphate (**63**), was found to be equipotent to Ins(1,4,5)P_3 itself in both its capacity to trigger Ca^{2+} release and ability to bind to InsP_3R. The prediction that this ligand in particular might be an effective agonist for InsP_3R was supported by the molecular modelling results, which predicted near-perfect overlap of the top docking solutions for the ligand with the endogenous Ins(1,4,5)P_3 bound in the crystal structure.

The α-D-glucopyranosyl 1,3,4-trisphosphate (**62**), with its slightly lower potency [37-fold lower than β-D-glucopyranosyl 1,3,4-trisphosphate (**63**) and 23-fold lower than Ins(1,4,5)P_3] provided more evidence for the receptor tolerating ligands that position the auxiliary phosphate in a slightly different region of the binding site. Although the potency is lower than that of the β-epimer (**63**), it is still relatively high compared to some other reported agonists of InsP_3R [and considerably higher than the previously established activity of α-D-glucopyranosyl 3,4-bisphosphate, which is approximately 1000-fold less potent than Ins(1,4,5)P_3, confirming the participation of the axial phosphate in binding and giving further evidence for the stability of both epimers].[261,322]

Apart from the 1-position phosphates, both α-D-glucopyranosyl 1,3,4-trisphosphate (**62**) and β-D-glucopyranosyl 1,3,4-trisphosphate (**63**) can be considered as a fragment of the InsP_3R agonist adenophostin A (Figure 103). As mentioned previously (section 5.1.2), a large number of truncated analogues of AdA have been generated, although none with the auxiliary phosphate bound directly to the glucose ring.

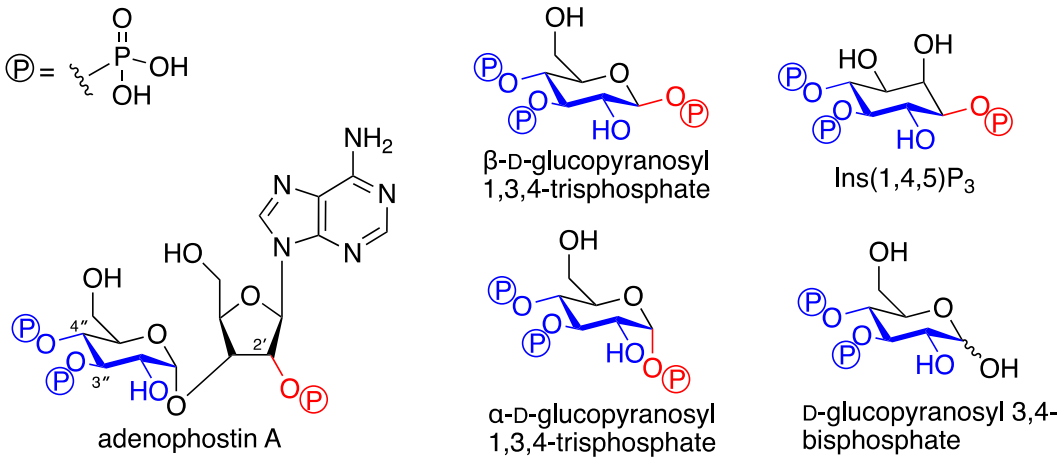

Figure 103: Structural comparison of Ins(1,4,5)P_3, AdA and some of its truncated analogues including α-D-glucopyranosyl 1,3,4-trisphosphate (62) and β-D-glucopyranosyl 1,3,4-trisphosphate (**63**). The conserved functional groups of the structures involved in binding are coloured in blue, while the auxiliary phosphate is shown in red.

As mentioned in Section 5.1.2, there have been numerous studies to investigate how AdA binds to InsP_3R, and there is not complete consensus on the positioning of the agonist within the IBC. There has been a long-held view that the 3", 4" and 2' phosphates of AdA at least partially mimic the 4, 5 and 1 phosphates of Ins(1,4,5)P_3 respectively.[250,259] From the structure of AdA, it is apparent that the positions of all three phosphates cannot closely be mimicked simultaneously due to the ribose moiety forcing the auxiliary phosphate further from the bisphosphate-supporting glucose ring structure. There is a general consensus that the auxiliary 2'-position phosphate in AdA can be tolerated in a slightly different region of the InsP_3R binding site to the 1-position

phosphate of Ins(1,4,5)P_3, while still making a positive contribution to ligand binding.[261,282]

Many truncated analogues of AdA have been synthesised to investigate the binding of agonists to the InsP_3R IBC. It was found that the exact three-dimensional positioning of this auxiliary phosphate in IBC receptor, determined by length, rigidity and orientation of the tethering group to the glucose ring, has a large impact on ligand affinity. The general trend observed in previous truncated AdA analogues has been that ligands are more potent when the linkage is shorter and more rigid. Ligands with auxiliary phosphate containing moieties that were oriented axially on the glucose ring also tended to have higher potencies than their equatorially oriented counterparts (although the analogues described in these studies were found to be weaker InsP_3R agonists than both β-D-glucopyranosyl 1,3,4-trisphosphate (**63**) and Ins(1,4,5)P_3).[264,286]

There have been recent relevant studies that have also probed the impact that the glucopyranosyl ring has on the binding of AdA and its analogues through the substitution of this group with D-*chiro*-inositol in AdA and ribophostin, resulting in a moderate and significant increase in potency respectively.[321,368]

The 3- and 4-position phosphates of both α-D-glucopyranosyl 1,3,4-trisphosphate (**62**) and β-D-glucopyranosyl 1,3,4-trisphosphate (**63**) are thought to mimic the vicinal 4,5-bisphosphate of Ins(1,4,5)P_3 closely and be the main functional groups responsible for pulling the α- and β-domains of the IBC closed.

The potency of α-D-glucopyranosyl 1,3,4-trisphosphate (**62**) and particularly β-D-glucopyranosyl 1,3,4-trisphosphate (**63**) demonstrate that the extended 6-position hydroxyl group and pyranosyl ring oxygen can be accommodated, presumably equivalent to the 3-position and 2-position hydroxyls of Ins(1,4,5)P_3 respectively, with no real decrease in ligand activity. Given the apparent tolerance of the binding site to the extended 6-position hydroxyl and pyranosyl ring oxygen in both of these ligands, it logically follows that the potency of α-D-glucopyranosyl 1,3,4-trisphosphate (**62**) should reflect that of one of its closest inositol phosphate analogues, D-*chiro*-Ins(1,3,4)P_3 [reported to be 25-fold less potent than Ins(1,4,5)P_3],[281,372] which indeed the results of this study supports.

The high activities of α-D-glucopyranosyl 1,3,4-trisphosphate (**62**) and β-D-glucopyranosyl 1,3,4-trisphosphate (**63**) have provided additional evidence as to the possible binding modes of InsP_3R agonists, including contributing to the knowledge of AdA binding, and thus add to the panoply of SAR studies carried out on both Ins(1,4,5)P_3 and Ada.[368]

The high potency of both of the truncated AdA ligands in this study provides some evidence that AdA itself may be able to bind in the IBC of InsP3R in the same region as

Ins(1,4,5)P_3, in that the inclusion of the extended hydroxyl group and pyranosyl ring oxygen in the glucose ring appear to have no detrimental effect on ligand affinity. However, this is by no means proof that AdA binds in an mode that mimics α-D-glucopyranosyl 1,3,4-trisphosphate (**62**) and β-D-glucopyranosyl 1,3,4-trisphosphate (**63**), as the different placement of the auxiliary phosphate and inclusion of the ribose and adenine groups in the AdA structure could substantially affect the way this agonist binds to the receptor.[264,282,283,316–318]

5.6.2 Partial agonist: methyl α-L-glucopyranoside 2,3,6-trisphosphate (**58**) and its inactive enantiomer, methyl α-D-glucopyranoside 2,3,6-trisphosphate (**60**)

The binding and calcium release triggered by methyl α-L-glucopyranoside 2,3,6-trisphosphate (**58**) indicated that the compound was a low-potency partial agonist.

The control enantiomer, methyl α-D-glucopyranoside 2,3,6-trisphosphate (**60**), was found to be entirely inactive. Due to the fact that this ligand cannot achieve a hypothetical binding mode in which all of the binding requirements of InsP_3R can be met (suitable placement of hydroxyl and phosphate groups in the IBC with simultaneous optimal stereochemistry of the ring substituents), it had been thought to be likely that this enantiomer would be unable to bind to the receptor and trigger calcium release.

The partial agonist activity of methyl α-L-glucopyranoside 2,3,6-trisphosphate (**58**) is thought to be primarily due to the axial methyl group occupying the region of the binding site occupied by the 3-position hydroxyl of Ins(1,4,5)P_3 (Figure 104). Steric interference from this axial *O*-methyl group could possibly hinder the full closure of the clamshell-like IBC domains upon ligand binding or interfere with the ability of the ligand to interact with the β-domain.

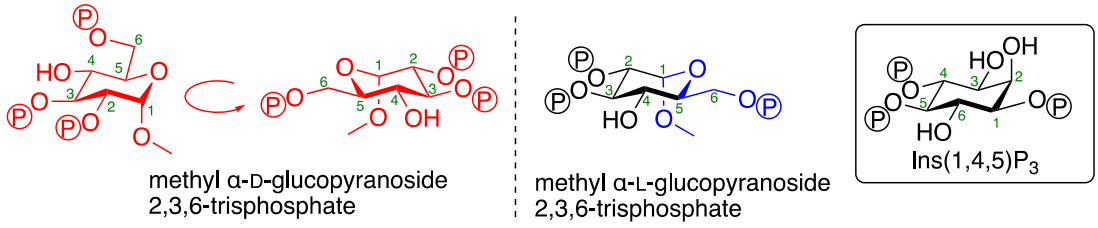

Figure 104: from left to right, structures of methyl α-D-glucopyranoside 2,3,6-trisphosphate (**60**, shown in red in two different orientations), methyl α-L-glucopyranoside 2,3,6-trisphosphate (**58**, with the important structural differences to Ins(1,4,5)P_3 highlighted in blue) and Ins(1,4,5)P_3. Methyl α-D-glucopyranoside 2,3,6-trisphosphate (**60**), depicted in red, is not expected to be able to adopt an orientation in which it can successfully mimic Ins(1,4,5)P_3, unlike its enantiomer, methyl α-L-glucopyranoside 2,3,6-trisphosphate (**58**).

As mentioned previously (Section 5.13), disruption to the structure of the ligand at the equivalent of the 3-position hydroxyl, albeit usually in combination with a further modification to the vicinal phosphates, can result in partial agonist activity.[241,266,278,279,306] It appears that in the case of methyl α-L-glucopyranoside 2,3,6-trisphosphate (**58**), disruption of binding at the 3-position without further significant modifications to the key vicinal phosphates is sufficient to generate partial agonist activity (as has been seen before in 2-*O*-butyryl-Ins(1,3,4,6)P_4).[306]

The extended phosphate equivalent to the auxiliary 1-position phosphate in Ins(1,4,5)P_3 is not thought to significantly impact the binding of the ligand, as it has already been established that the InsP_3R binding site is able to accommodate more sterically demanding functional groups in this region.[264,270,289–291,281–288] Another such example is the recently reported 1-PP-Ins(4,5)P_2 ligand from the Potter group, which contains a pyrophosphate group attached to the 1-position but produces approximately the same activity as Ins(1,4,5)P_3.[91] This 1-PP-Ins(4,5)P_2 agonist provided the first evidence that this region of the InsP_3R binding site could also tolerate an additional negative charge.[91]

Unfortunately, the affinity of methyl α-L-glucopyranoside 2,3,6-trisphosphate (**58**) was very low, and this is thought to be a consequence of the axial *O*-methyl group in the equivalent position to the 3-position hydroxyl of Ins(1,4,5)P_3, which is also the suspected structural difference responsible for the observed partial agonist activity. As described in Section 5.1.1, there have been several studies that have shown that while small substitutions are reasonably well tolerated, the larger the substituents attached to the 3-position hydroxyl, the weaker the binding of the ligand.[269,276,301–304] Additionally, it has been reported that inverting the 3-position hydroxyl causes a slight decrease in potency,[265,296] although there has been some precedence of ligands with smaller axial functional groups proving to be surprisingly potent agonists [3CF_3-Ins(1,4,5)P_3 as reported by Wilcox *et al.*].[276]

While the low affinity of methyl α-L-glucopyranoside 2,3,6-trisphosphate (**58**) may result in this compound not being investigated further as a basis for generating more partial agonists of InsP_3R, it is an interesting compound that could aid in the further understanding of generating future partial agonists and antagonists of InsP_3R.

5.6.3 Partial agonist: methyl α-L-glucopyranoside 2,4,6-trisphosphate (**59**) and its inactive enantiomer, methyl α-D-glucopyranoside 2,4,6-trisphosphate (**61**)

Excitingly, the calcium release and binding assays indicated that methyl α-L-glucopyranoside 2,4,6-trisphosphate (**59**) is also a partial agonist of $InsP_3R$. This ligand proved to be a more potent, lower-efficacy partial agonist compared to the other partial agonist identified, methyl α-L-glucopyranoside 2,3,6-trisphosphate (**58**), with a lower K_d value (549 nM compared to 1230 nM) and substantially higher EC_{39}/K_d ratio (462 compared to 132).

As in the case of the other partial agonist in this study, the D-glucose-based enantiomer of this newly identified partial agonist, methyl α-D-glucopyranoside 2,4,6-trisphosphate (**61**), was found to be completely inactive at the receptor. This inactivity was expected as, from comparison of binding modes, methyl α-D-glucopyranoside 2,4,6-trisphosphate (**61**) appeared to be unable to adopt an orientation in the IBC that would satisfy both the preferred placement of the phosphate groups as well as the maintaining the ideal stereochemistry of the substituents around the central ring.

The ability of methyl α-L-glucopyranoside 2,4,6-trisphosphate (**59**) to act as a partial agonist is thought to be due to the disruption to binding caused by the extended phosphate into the region of the binding site that is occupied by the 4-position phosphate in $Ins(1,4,5)P_3$ (Figure 105). In this predicted orientation, the pyranosyl ring oxygen occupies the same region of the IBC that the 3-position hydroxyl of $Ins(1,4,5)P_3$ does, while the axial *O*-methyl faces out into solvent and is not expected either to participate in or hinder ligand binding.

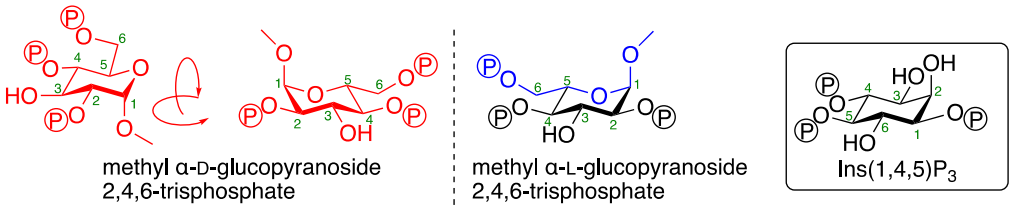

Figure 105: from left to right, structures of methyl α-D-glucopyranoside 2,4,6-trisphosphate (**61**, shown in red in two different orientations), methyl α-L-glucopyranoside 2,4,6-trisphosphate [**59**, with the important structural differences to $Ins(1,4,5)P_3$ highlighted in blue] and $Ins(1,4,5)P_3$. Methyl α-D-glucopyranoside 2,4,6-trisphosphate (**61**) is not expected to be able to adopt an orientation in which it can successfully mimic $Ins(1,4,5)P_3$, unlike its enantiomer, methyl α-L-glucopyranoside 2,4,6-trisphosphate (**59**).

As mentioned earlier in the chapter (section 5.1.1), it has previously been predicted that by modifying the equivalent of the 4-position phosphate in an $Ins(1,4,5)P_3$ analogue, the ligand binding may not result in the closure of the IBC. This could be due to the ligand being unable to form sufficiently strong interactions with the β-domain to pull the two sides of the clamshell structure together, or be the result of steric interference near the hinge of the IBC clamshell structure preventing the binding site

from fully closing around the ligand. The impediment to full IBC closure by either hypothetical method could then prevent the usual conformational changes to the rest of the receptor that take place upon agonist binding, thereby stopping the receptor pore from fully opening.[251]

The combination of modifications to the vicinal bisphosphates, in particular with modifications to the 3-position hydroxyl of Ins(1,4,5)P_3, has been shown previously to result in the development of partial agonists of InsP_3R.[241,266,278,279] The absence of an equivalent to the 3-position hydroxyl of Ins(1,4,5)P_3, due to the placement of the pyranosyl ring oxygen in methyl α-L-glucopyranoside 2,4,6-trisphosphate (**59**), may be a contributing factor in the partial agonist behaviour observed for this compound.

A few partial agonists have also been identified that have structural disturbances at the vicinal phosphates without changes to the 3-position hydroxyl,[276–278] meaning the effective absence of an equivalent for this hydroxyl in methyl α-L-glucopyranoside 2,4,6-trisphosphate (**59**) may not be necessary for partial agonism. The omission of an equivalent to the 3-position Ins(1,4,5)P_3 in methyl α-L-glucopyranoside 2,4,6-trisphosphate (**59**) may only result in lower affinity of the ligand as Ins(1,4,5)P_3 analogues lacking this group have previously been shown to be less potent InsP_3R agonists.[263,293]

The low efficacy of methyl α-L-glucopyranoside 2,4,6-trisphosphate (**59**) as a partial agonist makes this ligand a very promising result in furthering the development of partial agonists and antagonists of InsP_3R, but its low affinity is a significant drawback that limits its potential uses. Unfortunately, the hydrocarbon linkage intrinsic to carbohydrate structure that extends the 6-position phosphate further from the central glucose ring is thought to be the cause of both the low affinity of the ligand and also its partial agonist behaviour.

However, this compound does provide more evidence that the disruption of the 4-position phosphate is a method by which partial agonists can be generated.[251] Further modifications would be necessary to further lower the efficacy and, most crucially, increase the affinity of this ligand.

Based upon our speculated reasonings as to the structural determinant of the partial agonist activity of methyl α-L-glucopyranoside 2,4,6-trisphosphate (**59**), a new potential InsP_3R ligand was designed and synthesised, as described in Chapter 6 (Figure 106).

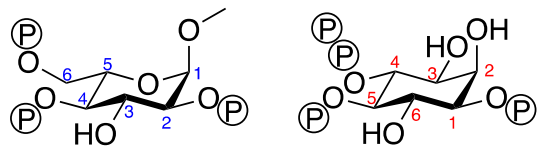

Figure 106: Structures of the $InsP_3R$ partial agonist methyl α-L-glucopyranoside 2,4,6-trisphosphate (**59**, left) and the newly designed analogue, 4-PP-Ins(1,5)P_2 (**80**, right), described further in Chapter 6.

This new potential analogue of methyl α-L-glucopyranoside 2,4,6-trisphosphate (**59**), 4-PP-Ins(1,5)P_2 (**80**), utilises an inositol template for the central ring structure but was designed to incorporate a pyrophosphate group attached to the 4-position to disrupt also ligand binding in the same region of the IBC, and in doing so hopefully also result in partial agonist/antagonist activity for the ligand.

5.7 Arabidopsis ITPK1 and the carbohydrate-based Ins(1,4,5)P_3 mimics

Ins(1,3,4)P_3 5/6-kinases (ITPKs) are members of the ATP-grasp family of proteins conserved between animals and plants.[373,374] ITPKs have been found to be remarkably versatile kinases that have been found to phosphorylate a number of lower inositol phosphates (including Ins(1)P, Ins(3)P, Ins(1,3,4)P_3, Ins(1,4,6)P_3, Ins(3,4,6)P_3, Ins(1,4,5)P_3, Ins(3,4,5,6)P_4 and Ins(1,4,5,6)P_4, Figure 107) and non-inositol-based substrates (including c-Jun, ATF-2, IκBα and p53) in certain organisms.[15,373,375–378] Additionally, ITPK enzymes have been found to be able to dephosphorylate certain positions of inositol phosphates and pyrophosphates.[378,379]

Recently, it has been discovered that *Arabidopsis thaliana* (thale cress) ITPK1 and ITPK2 catalyse the formation of a pyrophosphate moiety on the 5-position of $InsP_6$ (Figure 107).[380] Prior to this discovery, it had not been known that ITPK enzymes could generate pyrophosphates. A further study by our collaborators, Whitfield *et al.*, then demonstrated that *Arabidopsis* ITPK1 is able to phosphorylate Ins(1,2,3,4,5)P_5 to a product which is not $InsP_6$ but instead a regioisomer of PP-$InsP_4$ (suspected to be 5-PP-Ins(1,2,3,4)P_4).[378] An independent study, subsequently reported by Riemer *et al.,* also described isolating an unidentified regioisomer of PP-$InsP_4$ from *Arabidopsis* (and speculated that it might be derived from the $InsP_5$ regioisomer ITPK1 substrate identified in the Whitfield *et al.* study).[379]

As indicated by the name of the kinase, all homologues of the protein in different organisms appear to be able to phosphorylate either the 5- or 6-position hydroxyls of Ins(1,3,4)P_3 as one of the main substrates of this enzyme, although the ratio of products varies in different organisms.[374] It has been found that ITPKs in animals tend

to favour phosphorylation of the 6-position of Ins(1,3,4)P_3 to generate Ins(1,3,4,6)P_3,[373] whereas the opposite preference is observed in plants, with Ins(1,3,4,5)P_3 being the favoured product.[375,381] The region of the binding site associated with phosphorylating the 5-position or 6-position hydroxyl of Ins(1,3,4)P_3 was dubbed the A and B regions in the *Entamoeba histolytica* ITPK1 structure by Miller *et al.*, and the inability of the binding site to tolerate steric bulk in this region is thought to be the reason phosphorylation is not observed in both positions.[374] Although the substrate binding site is largely conserved for enzymes across different organisms, minor differences are present (usually further from highly conserved phosphorylation region in the binding site) and are thought to be responsible for the different distributions of phosphorylated products.[15]

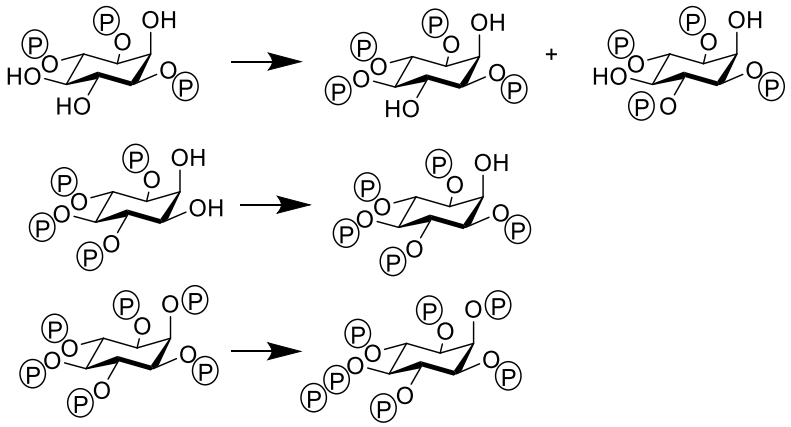

Figure 107: Some of the known endogenous inositol phosphate substrates for ITPKs and their resultant products: Ins(1,3,4)P_3 converted to both Ins(1,3,4,5)P_4 and Ins(1,3,4,6)P_4 (top row), Ins(3,4,5,6)P_4 converted to Ins(1,3,4,5,6)P_5 (middle row) and InsP_6 converted to 5-PP-InsP_5 (bottom row).

It has been found that the ITPK1 in the amoeba *E. histolytica* can, in addition to the seemingly ubiquitous action of phosphorylating Ins(1,3,4)P_3, phosphorylate Ins(1,4,5)P_3 to Ins(1,3,4,5)P_4. Currently Ins(1,4,5)P_3 appears to only be a substrate for the amoeba ITPK, as it is not phosphorylated by either *Arabidopsis* or human ITPKs under regular physiological conditions.[374,377] It should also be noted that the inositol phosphates found in *E. histolytica* appear to be derived from *neo*-inositol as opposed to *myo*-inositol, although the enzyme is able to phosphorylate both inositol stereoisomers.[374,382] Interestingly, although human ITPK1 cannot normally phosphorylate Ins(1,4,5)P_3, the enzyme becomes capable of phosphorylating the 3-position of Ins(1,4,5)P_3 upon the mutation of a single glycine residue (Gly-301).[374]

By screening different substrates with ITPKs, it may shed light on some of the other possible biological roles these enzymes could be capable of, based on which substrates they are able to phosphorylate or even pyrophosphorylate (potentially making a case for the existence of lower-inositol pyrophosphates, which are yet to be confirmed in nature).

5.7.1 Ins(1,4,5)P_3 analogues with ITPK1

In this study, the ITPK1 of *Arabidopsis thaliana* was used in an attempt to generate phosphorylated products from the six carbohydrate-based mimics of Ins(1,4,5)P_3 designed as InsP_3R ligands, in addition to glucose 4,5-bisphosphate and inositol hexakisphosphate (Figure 108). The aim would then be to characterise structurally any product formed.

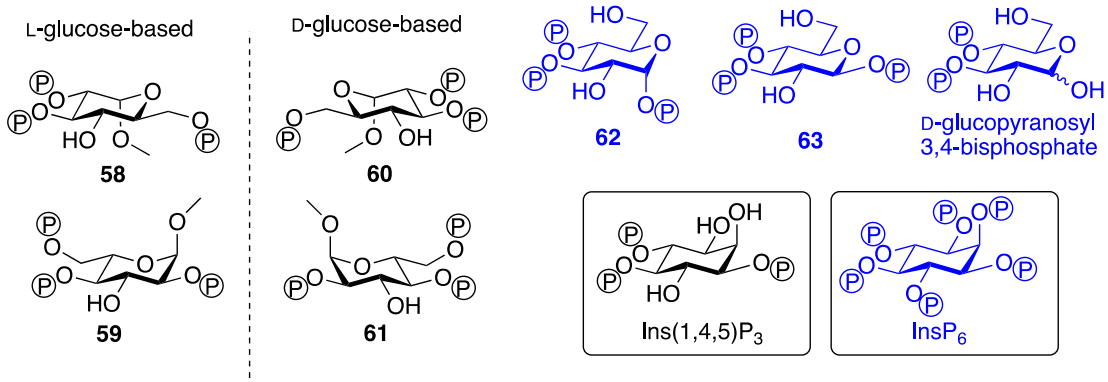

Figure 108: Structures of the compounds that were assessed as potential substrates of Arabidopsis ITPK1. The structures on the left in black [both L- and D-enantiomers of methyl α-glucopyranoside 2,3,6-trisphosphate (**58** and **60**) and methyl α-glucopyranoside 2,4,6-trisphosphate (**59** and **61**), as well as Ins(1,4,5)P_3] were not phosphorylated by the enzyme, but the structures on the right in blue [α-D-glucopyranosyl-1,3,4-trisphosphate (**62**), β-D-glucopyranosyl-1,3,4-trisphosphate (**63**), glucose 4,5-bisphosphate and InsP_6] were phosphorylated.

Following exposure of the compounds to *Arabidopsis* ITPK1 in a buffer with ATP and creatine phosphate (required for the creatine kinase ATP regenerating system), the product or recovered starting materials was analysed by HPLC. The HPLC product traces were compared with the traces of the respective potential enzyme substrate as a control. The longer retention times for a peak in the HPLC spectra of α-D-glucopyranosyl 1,3,4-trisphosphate (**62**), β-D-glucopyranosyl 1,3,4-trisphosphate (**63**), InsP_6 and glucose 3,4-bisphosphate indicated that these substrates were successfully phosphorylated by ITPK1 (Figure 109).

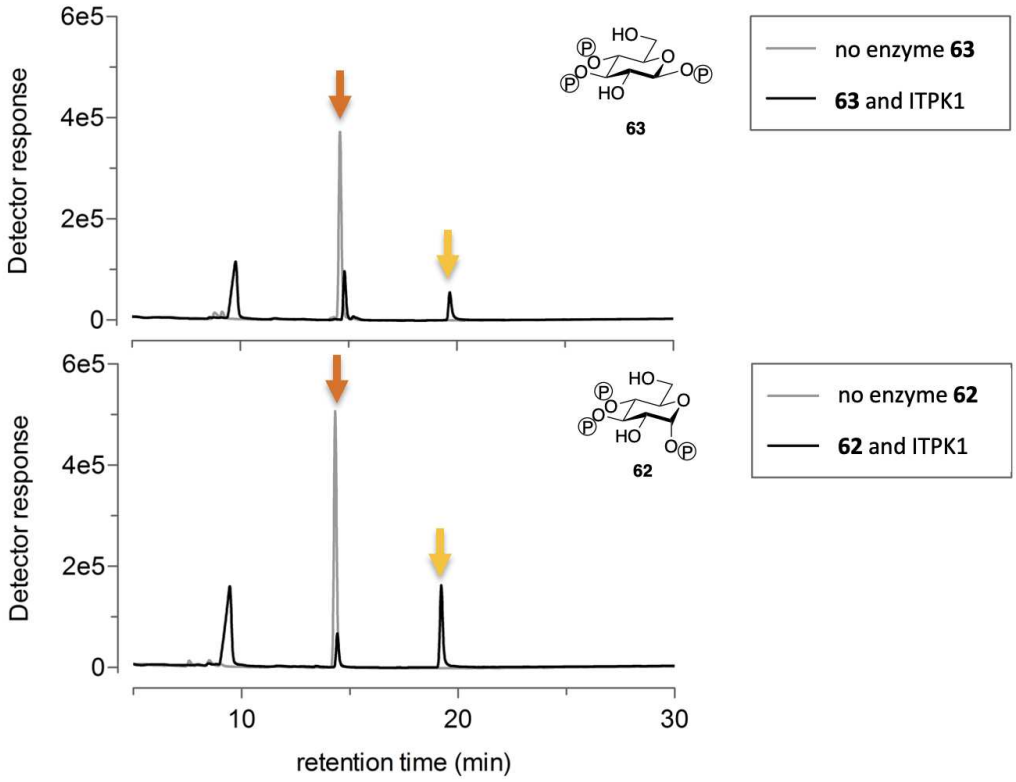

Figure 109: HPLC spectral traces for α-D-glucopyranosyl-1,3,4-trisphosphate (**62**) and β-D-glucopyranosyl-1,3,4-trisphosphate (**63**) overlaid with the corresponding HPLC traces for the ITPK1 products. The peaks for the trisphosphate starting materials (**62**/**63**) are indicated with orange arrows, and the peaks for the ITPK1 phosphorylated products are indicated with yellow arrows.

Due to the versatile nature of the ITPK1 kinase, it is clear that there are a number of possible products that could be generated from the phosphorylation of these four substrates. For the remainder of this section, only the products of α-D-glucopyranosyl-1,3,4-trisphosphate (**62**) and β-D-glucopyranosyl-1,3,4-trisphosphate (**63**) will be considered.

The ITPK1 enzyme could potentially add a phosphate group to either of the exposed hydroxyls attached to the 2-position or the extended 6-position, as well as there being a chance that the phosphate could be attached to one of the existing phosphates on the substrate, generating a pyrophosphate (Figure 110).

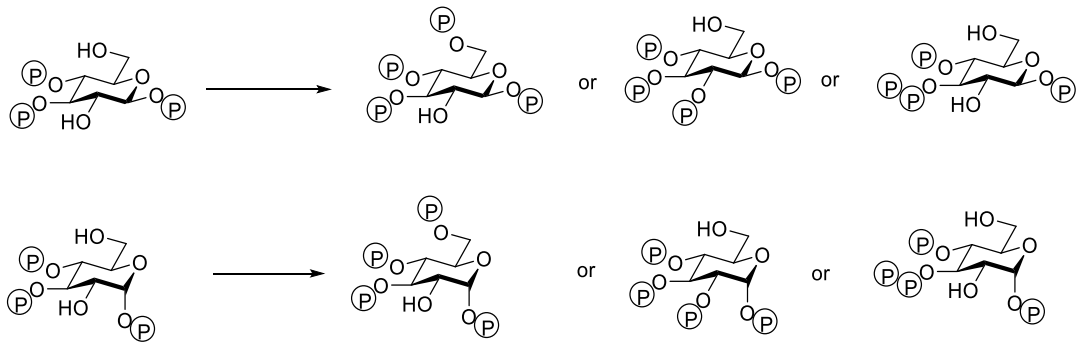

Figure 110: Some of the potential *Arabidopsis* ITPK1 phosphorylated products of α-D-glucopyranosyl-1,3,4-trisphosphate (**62**) and β-D-glucopyranosyl-1,3,4-trisphosphate (**63**).

The next step was to determine the structure for the phosphorylated products through NMR analysis.

The *Arabidopsis* ITPK1 product of α-D-glucose 1,3,4-trisphosphate (**62**) was generated in an optimised assay by Dr Hayley Whitfield in Professor Charles Brearley's lab (University of East Anglia), such that the product turnover was as efficient as possible while the reagents and by-products were minimised. This was achieved through an optimised, ATP-regenerating system (see the Experimental for more detail).

Analysis proceeded on a larger scale using α-D-glucose 1,3,4-trisphosphate (**62**) as a precaution to avoid any stability issues that may have arisen with the β-anomeric phosphate (although the stability of this phosphate had been investigated previously and found to be remarkable stable, see Section 5.4). The final turnover rate achieved for α-D-glucose 1,3,4-trisphosphate (**62**) was 93% and 3 µmole was converted into the enzyme product.

5.7.2 NMR analysis of ITPK1 product

Although the enzyme turnover had been successfully optimised, the crude product still contained a number of phosphorus-containing contaminants including ATP, ADP, unphosphorylated starting material and creatine phosphate, which prevented useful data being obtained from ^{31}PNMR analysis of the crude product. Purification through ion exchange chromatography (0-2M TEAB) prior to further NMR analysis was necessary.

From the proton-decoupled ^{31}PNMR spectrum initially obtained after the ion exchange column (Figure 111), it appeared that the product possessed five phosphorus signals, implying that the substrate had been phosphorylated at both the 6-position and the 2-position hydroxyls. Crucially, the absence of any peaks found in the ^{31}PNMR spectrum in the -10 ppm region indicated that no pyrophosphate groups

had formed, thereby eliminating the possibility of the product being a PP-InsP$_2$ regioisomer.

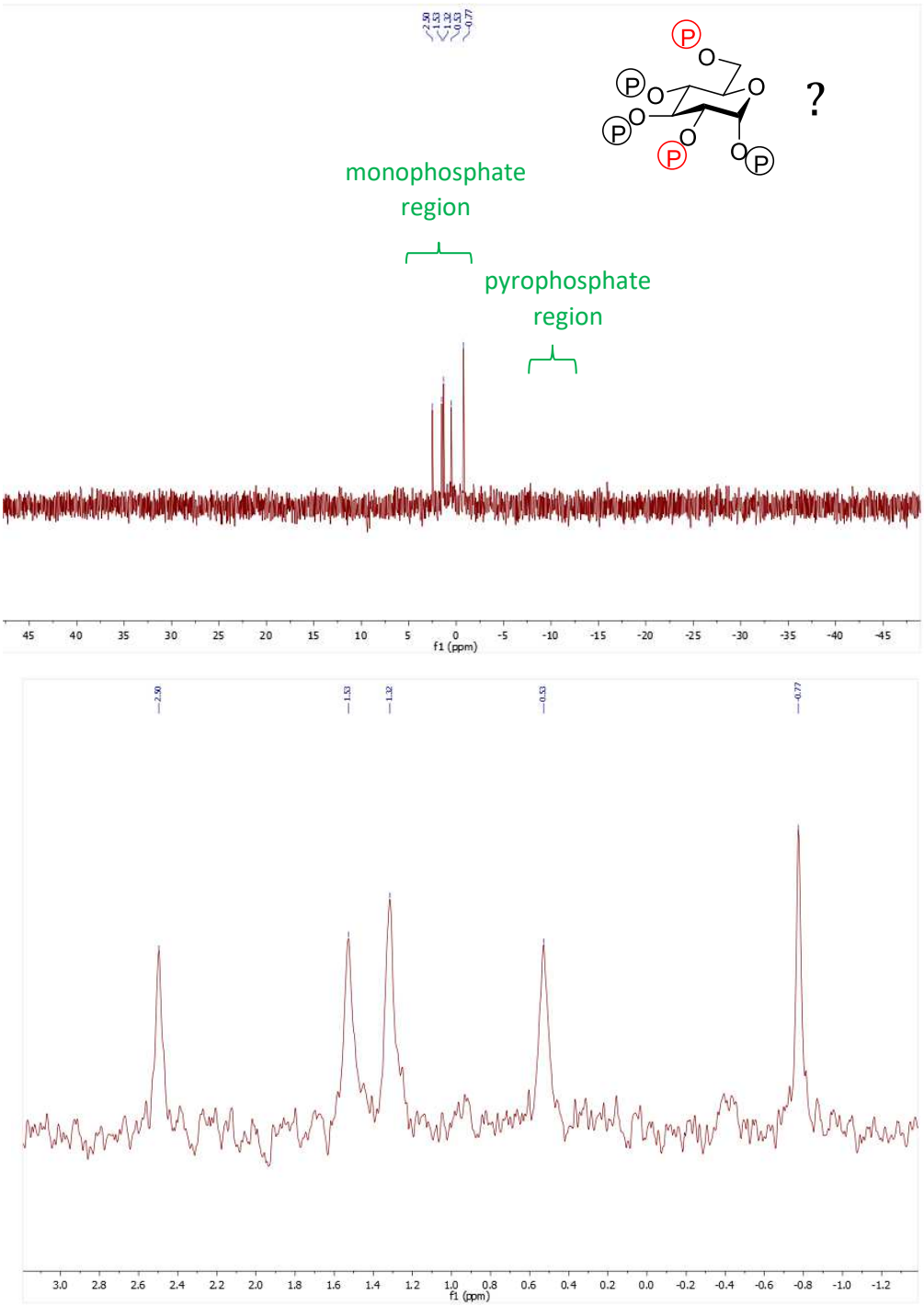

Figure 111: Proton-decoupled ^{31}PNMR spectrum of purified enzyme product, with subsequently added EDTA, depicting five phosphate signals with chemical shifts in the region for monophosphates (around 0 ppm) with a wider chemical shift range (top) and zoomed in to show the monophosphate signals (bottom). The structure of the initially proposed product is shown, with the phosphates attached by the *Arabidopsis* ITPK1 indicated in red.

For different reasons, both hydroxyl positions available for phosphorylation in the α-D-glucopyranosyl 1,3,4-trisphosphate (**62**) appear to be unlikely targets, as phosphorylation at the 2-position would be very sterically demanding in a region of the binding site not thought to tolerate steric bulk, while phosphorylation at the 6-position would entail phosphorylation of a primary hydroxyl group, which this enzyme is not known to be able to achieve in an inositol phosphate analogue.

A proton-coupled ^{31}PNMR spectrum was then obtained, with the hope that the presence of a phosphate attached to the primary 6-position might be possible to be confirmed through the splitting of one of the phosphate signal peaks into a doublet of doublets, whereas those phosphates attached to a secondary hydroxyl group should split into only a doublet. Unfortunately, the very small amount of compound isolated rendered obtaining a coupled spectrum extremely difficult. The proton-coupled ^{31}PNMR spectrum of the enzyme product was somewhat inconclusive regarding analysis of splitting patterns of most of the phosphate peaks; however, one of the peaks did not appear to broaden, indicating that this phosphate did not couple to any neighbouring protons. This raised the possibility that the glucose phosphate product fractions collected from the ion exchange column contained approximately the same amount of another phosphate-containing species that co-eluted with the product. Due to the lack of any pyrophosphate signals, this contaminant was predicted to most likely be creatine phosphate (Figure 112).

Upon discovery of this probable co-eluting contaminant, the theorised phosphorylated product of α-D-glucopyranosyl 1,3,4-trisphosphate (**62**) was revised to a tetrakisphosphate. There are still two possible product regioisomers that could have formed, however: α-D-glucopyranosyl 1,2,3,4-tetrakisphosphate or α-D-glucopyranosyl 1,3,4,6-tetrakisphosphate.

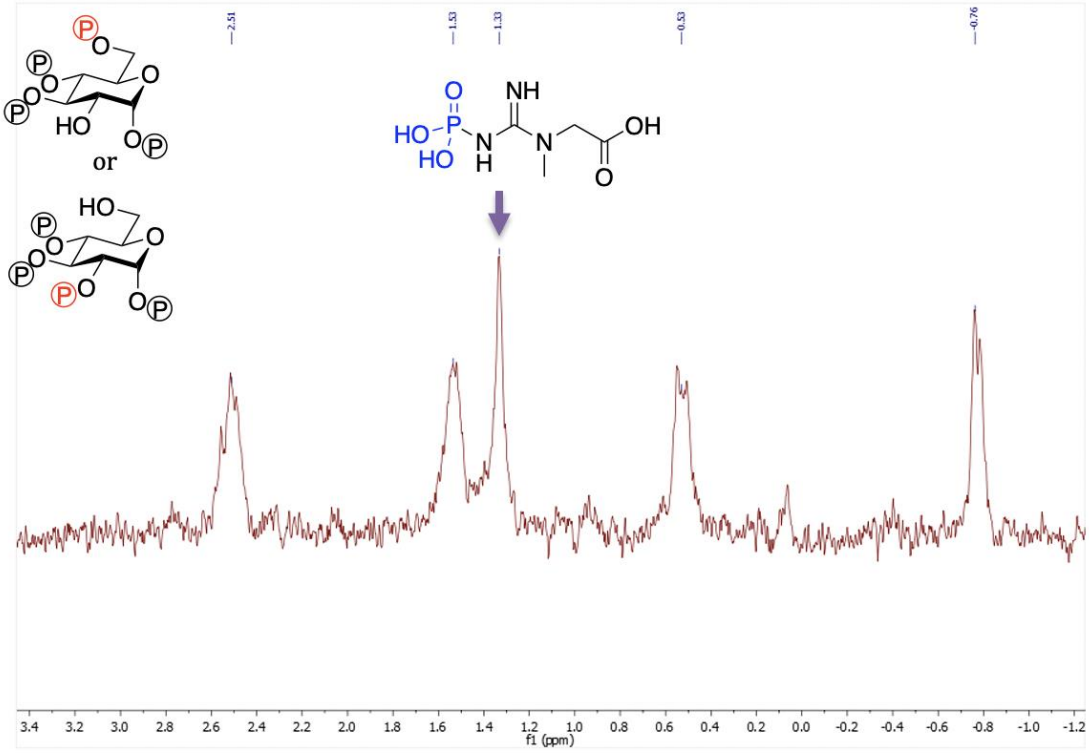

Figure 112: Proton-coupled ^{31}PNMR spectrum of purified enzyme product, with added subsequent EDTA, depicting four of the five phosphate signals broadening to indicate proton coupling with one peak remaining sharp, indicating that it does not have neighbouring protons to couple with. The structures of the possible proposed products, α-D-glucopyranosyl 1,3,4,6-tetrakisphosphate (top) or α-D-glucopyranosyl 1,2,3,4-tetrakisphosphate (bottom), are shown with the phosphates attached by *Arabidopsis* ITPK1 in red, as well as the structure of creatine phosphate with the phosphate group that might be responsible for the signal which did not broaden, indicated with a purple arrow, in blue.

The purified enzyme product was returned to Prof Charles Brearley, who confirmed through HPLC analysis that the product indeed still contained creatine phosphate, which must have co-eluted with the unknown glucose tetrakisphosphate product (data not shown). In an attempt to analyse the enzyme product further, possibly to determine which regioisomer of glucose tetrakisphosphate product had formed, a phosphorus-decoupled ^{1}HNMR, phosphorus-coupled ^{1}HNMR, COSY and proton-phosphorus HMBC spectra were obtained.

Unfortunately, due to the very small amount, the signals from the enzyme product were difficult to see in the ^{1}HNMR spectra. This difficulty in analysing the weak product proton signals was compounded by the remaining contaminants that remained from the enzyme turnover or were introduced in the TEAB buffer during purification. In fact, the signals from the co-eluting contaminants completely overwhelmed the product peaks in the COSY spectrum.

The phosphorus-proton correlated HMBC spectrum allowed the weak proton peaks of the glucose tetrakisphosphate product to be identified (Figure 113). The HMBC spectrum also appeared to indicate that one of the phosphate peaks (labelled P-6) correlates to two different regions of the proton spectrum, thereby providing some evidence that the product formed might be α-D-glucopyranosyl 1,3,4,6-tetrakisphosphate. However, this result is not definitive as this could be an artefact (as a few artefacts can be seen further upfield around 3.5 ppm), and the proton peaks are completely obscured by contaminants or too weak to provide corroborating evidence. The weak proton peaks identified for the product that were not obscured by contaminants could be seen to broaden in the phosphorus-coupled proton spectrum, compared to the corresponding peaks in the phosphorus-decoupled spectrum.

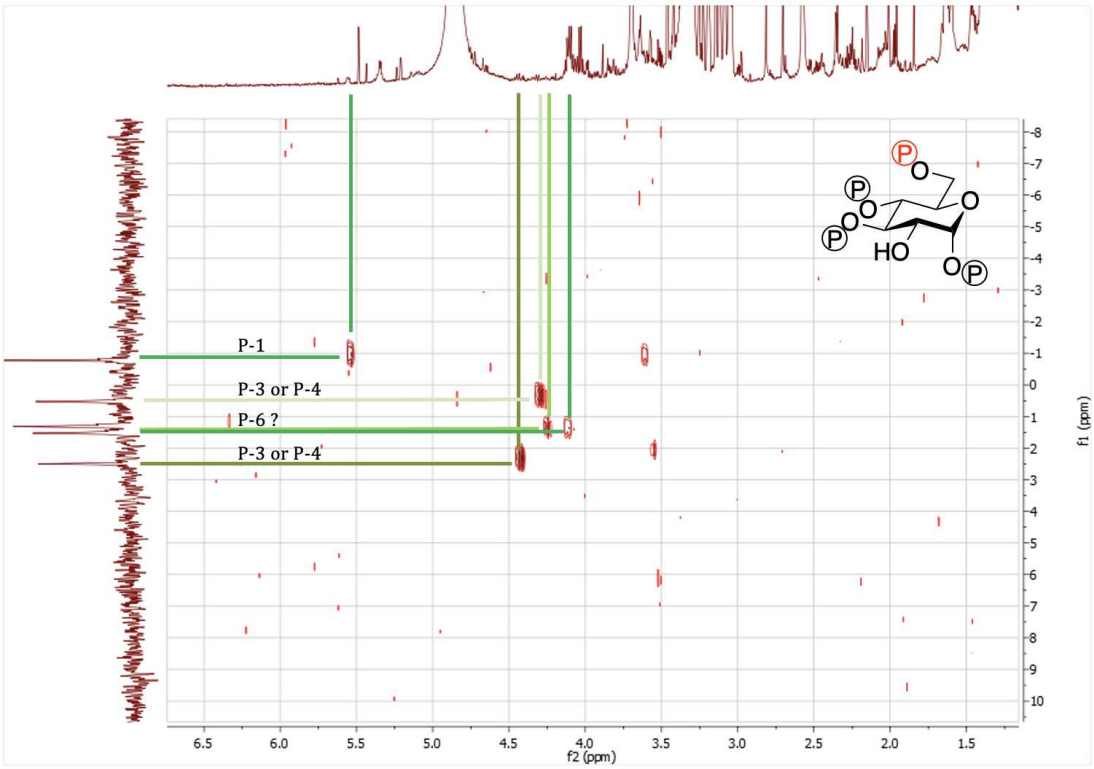

Figure 113: Proton-phosphorus correlated HMBC of the enzyme product. Despite product purification with ion exchange, there are still many unaccounted peaks present in the ^{1}HNMR spectrum, but there is an insufficient amount of product to purify it again safely. These contaminants are very minor, but are exacerbated by the very small quantity of product isolated, and they are usually derived from buffer and column contaminants. Moreover, indicatively they do not correlate with the phosphorus resonances. Green lines have been used to indicate the barely-detectable proton signals that correspond to the phosphorus signals for the enzyme product (with P-1, P-3, P-4 and P-6 labelled). The phosphate peak next to the phosphate designated P-6 is expected to be generated by creatine phosphate, and thus would not be expected to correlate to a proton signal.

Although the current NMR analysis of the enzyme product was not entirely conclusive, it did indicate that α-D-glucopyranosyl 1,3,4,6-tetrakisphosphate was the more likely

product to be formed. The substrates and products previously determined for *Arabidopsis* ITPK1 can allow for further speculation on product formation as well.

Arabidopsis ITPK1 is known to phosphorylate Ins(1,3,4)P_3 to generate both Ins(1,3,4,5)P_4 (major product) and Ins(1,3,4,6)P_4 (minor product), as well as Ins(1,4,5,6)P_4 and Ins(3,4,5,6)P_4 to form Ins(1,3,4,5,6)P_5 (Figure 114). Although this enzyme is able to phosphorylate both of the Ins(1,4,5,6)P_4 and Ins(3,4,5,6)P_4 inositol tetrakisphosphates, Ins(3,4,5,6)P_4 is the clearly favoured substrate of the enantiomers.[378]

From molecular modelling of the binding site, there are two regions that appear to form the most important interactions with phosphate moieties of a substrate dubbed the C and F regions (notation established by the Miller *et al.* study of *E. histolytica* ITPK1).[374,378]

Phosphorylation is thought to occur at the A site where an exposed hydroxyl in this region would be positioned suitably close to the γ-phosphate of the ATP bound in the active site. It has been proposed that the B region might also be sufficiently close to the γ-phosphate in the binding site of some organisms (*E. histolytica*) to also permit phosphorylation in this region, although alternatively the two phosphorylated regioisomer products of Ins(1,3,4)P_3 could be explained by the substrate adopting a second binding mode.[374,383,384]

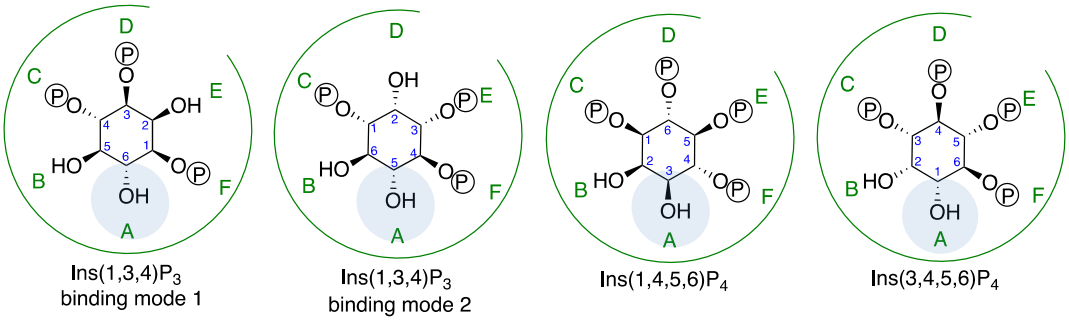

Figure 114: Predicted binding modes of Ins(1,3,4)P_3, Ins(1,4,5,6)P_4 and its enantiomer Ins(3,4,5,6)P_4 in *Arabidopsis* ITPK1. Ins(1,3,4)P_3 has been proposed to have two possible binding modes in human ITPK1 to generate both of the product regioisomers, and these may also be applicable to the *Arabidopsis* enzyme.[383,384] The A-F notations for the regions of the binding sites were originally coined by Miller *et al.* for *E. histolytica* ITPK1 and were later applied to *Arabidopsis* ITPK1 in Whitfield *et al*.[374,378] The area of the binding site where phosphorylation is expected to occur is the A region, which has been highlighted in blue.

The lower-inositol phosphates appear to bind in the same plane, but the higher-inositol phosphates, Ins(1,2,3,4,5)P_5 and InsP_6, have been predicted to bind perpendicularly, with the central inositol ring sitting higher in the binding site, even encroaching into the D region to allow the 5-position phosphate to be accommodated by the phosphorylating A region.[378]

From comparison of the predicted binding modes of α-D-glucopyranosyl 1,3,4-trisphosphate (**62**) remaining in the plane predicted for lower inositol phosphate binding modes, there are several possible binding orientations that the substrate could adopt to be phosphorylated by ITPK1 to a tetrakisphosphate product (Figure 115). These proposed binding modes meet the requirements of positioning a hydroxyl group in the A region to be phosphorylated (or B region for one of the modes that contained an extended moiety) and have phosphates occupying the C and F regions of the binding site, which are believed to be the regions of the binding site that form the most crucial interactions with the substrate.[378]

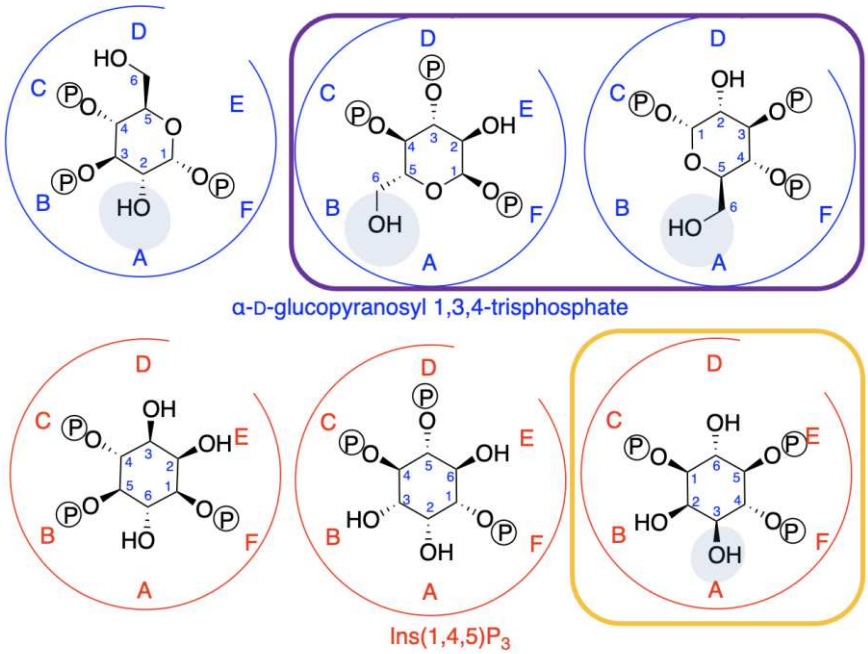

Figure 115: Possible binding modes of α-D-glucopyranosyl 1,3,4-trisphosphate (**62**, top row) with the corresponding hypothetical binding mode of Ins(1,4,5)P_3 (bottom row), although Ins(1,4,5)P_3 is not a substrate for *Arabidopsis* ITPK1 unlike α-D-glucopyranosyl 1,3,4-trisphosphate (**62**). The predicted binding modes leading to the potentially more likely α-D-glucopyranosyl 1,3,4,6-tetrakisphosphate product have been circled in purple and the suspected binding mode that Ins(1,4,5)P_3 adopts in *E. histolytica* ITPK1 has been circled in orange.[374] The area of the binding sites where phosphorylation can, at least hypothetically, occur is highlighted in blue.

There are two binding modes that would result in the formation of the 6-position phosphate product, through placing the extended 6-position hydroxyl of the substrate in the A or B region (Figure 115). One argument for the primary hydroxyl attached to the 6-position being the most likely location for phosphorylation is that one of the binding modes to generate this regioisomer would be equivalent to the suspected mode adopted by Ins(1,4,5)P_3 in *Entamoeba histolytica* ITPK1 that results in phosphorylation of the 3-position hydroxyl to generate Ins(1,3,4,5)P_4.[374] It should be reiterated that *Arabidopsis* ITPK1 is known to be unable to phosphorylate Ins(1,4,5)P_3;

however, the structural differences between Ins(1,4,5)P_3 and D-glucopyranosyl-1,3,4-trisphosphate (**62** and **63**) may be sufficient to allow these glucose-based substrates into the binding site, which is inaccessible to Ins(1,4,5)P_3. Should the glucopyranosyl trisphosphate substrates adopt either binding mode that would result in the phosphorylation of the 6-position hydroxyl, the main structural change that would be expected to improve binding comparted to inactive Ins(1,4,5)P_3 would be the extended 6-position itself; the hydrocarbon spacer for the 6-position hydroxyl may position the hydroxyl in a suitable location within the A/B region to be phosphorylated by the γ-phosphate of ATP that the 3-position hydroxyl of Ins(1,4,5)P_3 is unable to reach in *Arabidopsis* ITPK1.

In addition to the extended nature of the 6-position hydroxyl potentially facilitating phosphorylation, the absence of a neighbouring group protruding from the glucose ring structure, due to the placement of the pyranosyl ring oxygen, might also aid in binding through reducing the steric demands of the ligand in the A/B regions of the binding site, which are not thought to tolerate steric bulk well.[374]

As the A and B regions are thought to only be able to tolerate limited steric bulk, the extended nature of the hydroxyl attached to the 6-position might only interfere with binding and prevent the substrate from adopting orientations that would position this hydroxyl deep in the binding site, potentially resulting in the preferential binding via the mode that generates the 2-position phosphorylated product. The secondary nature of the 2-position hydroxyl may be preferred by the *Arabidopsis* kinase, as there have not been any reported primary hydroxyls phosphorylated by ITPK1 on inositol phosphate analogues (although it is thought that the ITPK1 enzyme can phosphorylate the serine/threonine residues of protein substrates).[373,375] However, the 2-position hydroxyl has phosphate groups attached to both neighbouring positions and, to our knowledge, there are no lower-inositol substrates that are phosphorylated at such sterically congested hydroxyls, as minimal steric bulk is thought to be tolerated in the enzyme binding site around the phosphorylation region.[374]

There is a possibility that the substrate would not bind in the same plane as lower-inositol phosphates, however, as Ins(1,2,3,4,5)P_5 and InsP_6 are expected to be accommodated in a perpendicular orientation higher in the D region of the binding site.[378] Should the α-D-glucopyranosyl 1,3,4-trisphosphate (**62**) bind with some aspects of the higher inositol binding, the extended 6-position hydroxyl might be able to fit further in the D site, in addition to the glucose ring being shifted further up into the D region as well. If the entire substrate could shift further into the D region, this could be a possible solution to mitigate the steric clash in the A and B regions encountered by having phosphates bound to both neighbouring 1- and 3-positions in the substrate. However, there is no apparent reason why α-D-glucopyranosyl 1,3,4-trisphosphate (**62**) might be accommodated in a slightly different region of the *Arabidopsis* binding site to be tolerated as a substrate when Ins(1,4,5)P_3 is not. In the

case of the binding mode required to generate the 2-position phosphate product, in addition to there being no obvious reason that the substrate might potentially be accommodated in a slightly different binding plane, it is not immediately evident how an extended 6-position hydroxyl in the D region, combined with the absence of a hydroxyl in the E region due to the presence of the pyranosyl ring oxygen, might facilitate substrate binding.

If the steric clash generated by the existence of neighbouring phosphates to target hydroxyl groups is sufficient to prevent glucose phosphates from being substrates of *Arabidopsis* ITPK1, this can also be used to rationalise why the remaining four carbohydrate phosphate compounds were inactive, in addition to helping to identify the binding mode and subsequent product regioisomer of α-D-glucopyranosyl 1,3,4-trisphosphate (Figure 116).

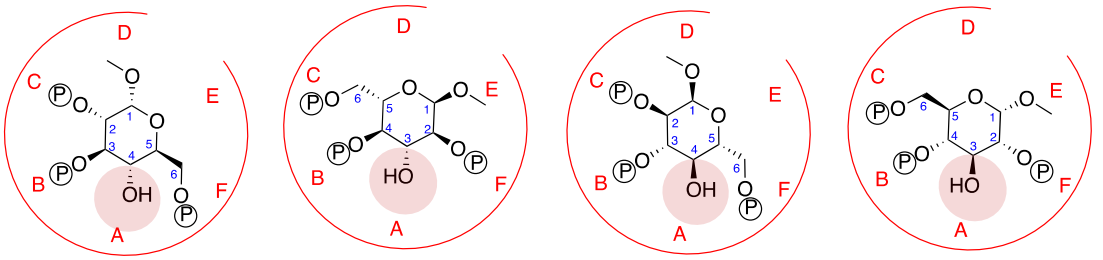

methyl α-L-glucopyranoside 2,3,6-trisphosphate **58**

methyl α-L-glucopyranoside 2,4,6-trisphosphate **59**

methyl α-D-glucopyranoside 2,3,6-trisphosphate **60**

methyl α-D-glucopyranoside 2,4,6-trisphosphate **61**

Figure 116: Hypothetical binding modes for methyl α-L-glucopyranoside 2,3,6-trisphosphate (**58**), methyl α-L-glucopyranoside 2,4,6-trisphosphate (**59**), methyl α-D-glucopyranoside 2,3,6-trisphosphate (**60**) and methyl α-D-glucopyranoside 2,4,6-trisphosphate (**61**), which were found not to be substrates for *Arabidopsis* ITPK1. The potential locations where phosphorylation could have taken place (although it did not for any of the substrates) are highlighted in red.

Although all of the compounds (**58**, **59**, **60** and **61**) can theoretically adopt binding modes that position phosphate groups in the C and F regions, as well as the exposed hydroxyl in the phosphorylating A region, none of the glucopyranoside trisphosphates were treated as substrates by *Arabidopsis* ITPK1. All of the potential binding modes positioned a phosphate group in the B region, which is thought to be sufficiently sterically demanding to prevent neighbouring exposed hydroxyl from occupying the A region. This phenomenon has already been proposed as the reason this kinase phosphorylates either the 5- or 6-position of Ins(1,3,4)P_3, but not both.[374]

Other factors might be preventing these compounds from being substrates of the *Arabidopsis* ITPK1 enzyme, however, as they feature the extra steric bulk associated with the incorporation of an axial methyl group attached to the 1-position, in addition to other structural differences such as the extended phosphate attached to the 6-position.

Two compounds previously synthesised by the Potter group, a D-glucose-based truncated AdA analogue dubbed furanophostin and its xylopyranoside-based derivative,[385,386] were also evaluated as potential substrates of *Arabidopsis* ITPK1 (Figure 117). It was hoped that the enzyme might be able to phosphorylate the furanophostin but not its xylopyranoside-derivative, as this would be further evidence that the phosphorylation of α-D-glucopyranosyl 1,3,4-trisphosphate (**62**) likely occurs at the primary 6-position hydroxyl, a moiety that the *xylo*-derivative entirely lacks. Unfortunately, the enzyme was not able to phosphorylate either substrate, probably due to the additional steric bulk from the furan ring structures preventing these compounds from binding. It would be interesting to see if a pair of structurally simpler glucose/xylose-based analogues could be assessed as possible ITPK1 substrates, but there was insufficient time to generate compounds that would allow the pursuit of this experiment.

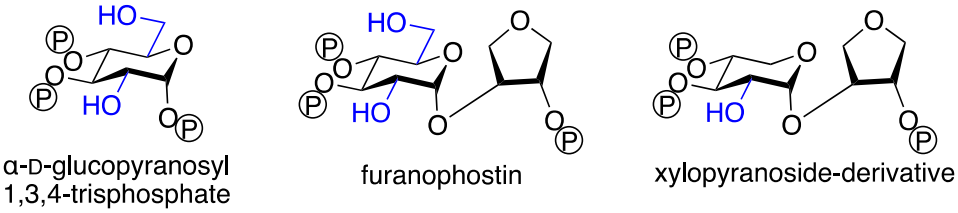

Figure 117: Structures of α-D-glucopyranosyl 1,3,4-trisphosphate (**62**), furanophostin and the xylopyranoside-derivative of furanophostin with the hydroxyl groups that could hypothetically be phosphorylated by ITPK1 highlighted in blue.

There was also insufficient time to characterise the ITPK1 product generated from the other glucose-based trisphosphate stereoisomer, β-D-glucopyranosyl 1,3,4-trisphosphate (**63**), but this substrate would be expected to bind in an equivalent mode to its α-anomer (**62**) and also likely result in the formation of the 6-position phosphorylated product (β-D-glucopyranosyl 1,3,4,6-tetrakisphosphate), although this would require further investigation to confirm.

While further study needs to be carried out to determine the exact products formed in the *Arabidopsis* ITPK1-mediated phosphorylation of not only α-D-glucopyranosyl 1,3,4-trisphosphate (**62**), but also β-D-glucopyranosyl 1,3,4-trisphosphate (**63**) and D-glucose 3,4-bisphosphate, this study has determined for the first time that *Arabidopsis* ITPK1 is able to phosphorylate carbohydrate-based substrates. It has been established that α-D-glucopyranosyl 1,3,4-trisphosphate (**62**) is phosphorylated to one of either two regioisomers, α-D-glucopyranosyl 1,2,3,4-tetrakisphosphate or α-D-glucopyranosyl 1,3,4,6-tetrakisphosphate, and does not form a pyrophosphate as initially speculated; and although the identity of the product remains to be fully confirmed, it is suggested that α-D-glucopyranosyl 1,3,4,6-tetrakisphosphate is the more likely product, which would be to our knowledge, the first time a primary hydroxyl has been phosphorylated on a non-protein substrate by ITPK1.

5.8 IP_3-3K and the carbohydrate-based Ins(1,4,5)P_3 mimics

Very recently, with our collaborators in Madrid, the Beatriz González group (Institute of Physical-Chemistry Rocasolano), it was possible to show for the first time in atomic detail that both α-D-glucopyranosyl 1,3,4-trisphosphate (**62**) and β-D-glucopyranosyl 1,3,4-trisphosphate (**63**) are able to bind to the Ins(1,4,5)P_3 3-kinase (IP_3-3K) enzyme. However, it still remains to be confirmed that these glucose trisphosphates are substrates of the enzyme.

The IP_3-3K enzyme, as the name suggests, normally phosphorylates the 3-position hydroxyl of Ins(1,4,5)P_3 to generate Ins(1,3,4,5)P_4.[387] There three different isoforms of the kinase have been identified in mammals (A, B and C), which all share a conserved kinase domain active site as well as a calmodulin-binding domain.[255]

The González group has obtained preliminary crystal structures of both ligands bound in the IP_3-3K A active site; these structures indicate their binding orientations in the enzyme (Figure 118 and Figure 119). The crystal structures will be further refined in the future.

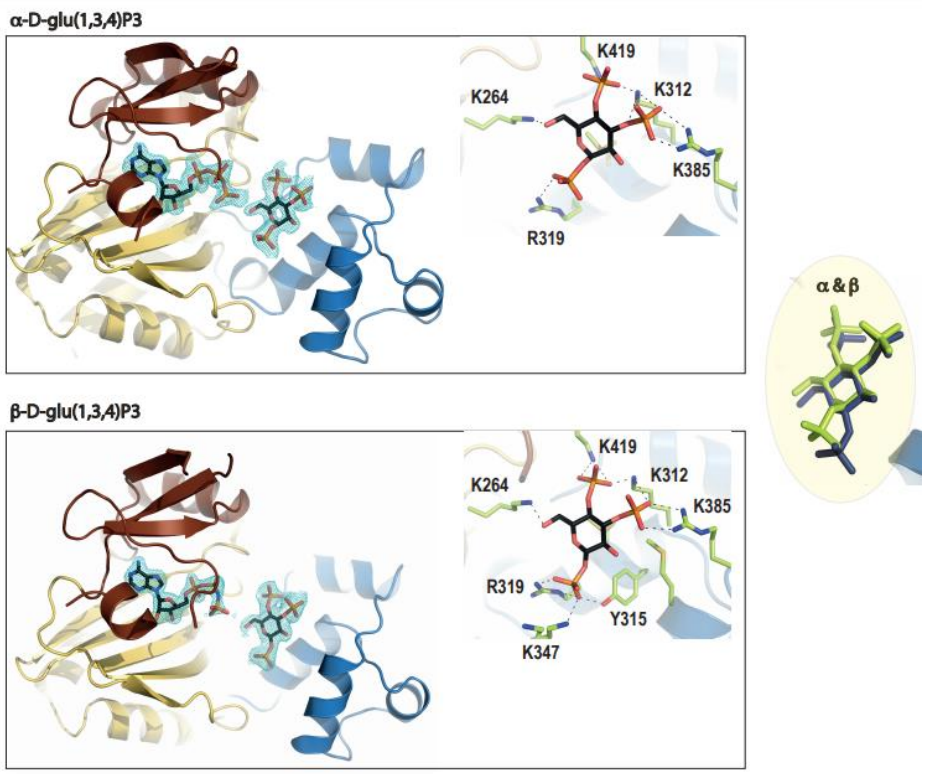

Figure 118: Crystals structures of the IP_3-3K (unpublished), displaying electron densities for ternary complexes of α-D-glucopyranosyl 1,3,4-trisphosphate (**62**, top panel) with ATP and for β-D-glucopyranosyl 1,3,4-trisphosphate (**63**, bottom panel) with the non-hydrolysable ATP analogue, AMP-PNP, binding to the enzyme active site. Both panels feature close-ups of their respective ligand binding orientations with some of the key residues involved in binding labelled. On the far right is the binding orientations of α-D-glucopyranosyl 1,3,4-trisphosphate (**62**) and β-D-glucopyranosyl 1,3,4-

trisphosphate (**63**) overlaid, indicating the similarities in the binding orientations of both ligands, which appear to be situated such that the extended 6-positions occupy the active phosphorylating region of the IP_3-3K binding site. Figure was provided by Prof Beatriz González (Institute of Physical-Chemistry Rocasolano).

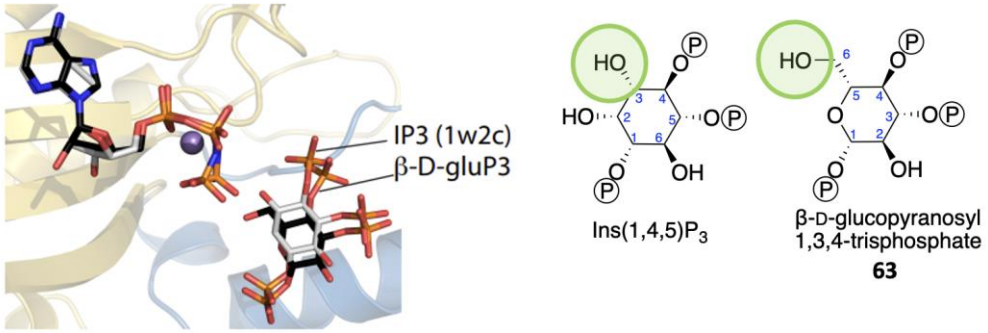

Figure 119: On the left, the binding modes of $Ins(1,4,5)P_3$ (shown in white) in the previously published binding site (PDB: 1W2C)[255] is shown overlaid with the binding mode for β-D-glucopyranosyl 1,3,4-trisphosphate (**63**, shown in black) in the IP_3-3K active site. The 3-position hydroxyl of $Ins(1,4,5)P_3$ and the primary, extended 6-position hydroxyl of β-D-glucopyranosyl 1,3,4-trisphosphate are both positioned in the active phosphorylation region of the binding site. Both ATP and AMP-PNP are also shown overlaid. Figure was provided by Prof Beatriz González (Institute of Physical-Chemistry Rocasolano). On the right are the corresponding binding orientations of $Ins(1,4,5)P_3$ and β-D-glucopyranosyl 1,3,4-trisphosphate (**63**) with the phosphorylation region highlighted in green.

The electron densities of both of the ligands appear to suggest that they are oriented in the binding site such that the primary 6-position hydroxyl would be phosphorylated. It can be seen in the comparison of β-D-glucopyranosyl 1,3,4-trisphosphate (**63**) and $Ins(1,4,5)P_3$ binding that the central carbohydrate ring structure is slightly shifted from the position that the endogenous inositol phosphate binds in so that the extended hydroxyl can more closely mimic the 3-position hydroxyl of $Ins(1,4,5)P_3$. In both cases, interestingly, the 6-position hydroxyl group maintains an important interaction with the lysine K264 residue, which has been shown to be essential for normal catalysis. The occupancy and density is much better for the β-anomer (**63**) than the α-anomer, which is not unexpected, as the former has already been shown to be a superior mimic to $Ins(1,4,5)P_3$ (Section 5.5.1).

To the best of our knowledge, it has not been previously established if $InsP_3$-3K would be able to phosphorylate a primary hydroxyl on a substrate. This discovery is exciting in and of itself, and it also could support the theory that α-D-glucopyranosyl 1,3,4,6-tetrakisphosphate might indeed be the phosphorylation product of ITPK1, as it demonstrates a possible precedent for an inositol phosphate kinase being able to phosphorylate an extended primary hydroxyl of a lower inositol phosphate analogue. However, the ability of the $InsP_3$-3K kinase to phosphorylate these glucose polyphosphates needs to be further substantiated in real enzyme assays in the future.

(6) Pyrophosphate-containing Ins(1,4,5)P_3 derivatives

6.1 Introduction and design of lower inositol pyrophosphates

Following the discovery that one of the carbohydrate-based ligands analysed at InsP_3R, methyl α-L-glucopyranoside 2,4,6-trisphosphate (**59**), is a promising partial agonist (Chapter 5), a new series of compounds was designed, based upon the SAR considerations established for the receptor, to investigate if an improved ligand with higher affinity and lower efficacy could be discovered.

The proposed binding modes for methyl α-L-glucopyranoside 2,4,6-trisphosphate (**59**) were discussed in detail earlier (Chapter 5), but one main structural feature thought to be potentially responsible for the partial agonist behaviour of the ligand is the extended phosphate group attached to the 6-position. This extended phosphate is predicted to be positioned in the region of the binding site occupied by the 4-position phosphate of Ins(1,4,5)P_3 and therefore may be able to generate partial agonist activity by preventing the full closure of the clam-shell like IBC, through either inadequate interaction with the β-domain or through steric interference (Figure 120).[251]

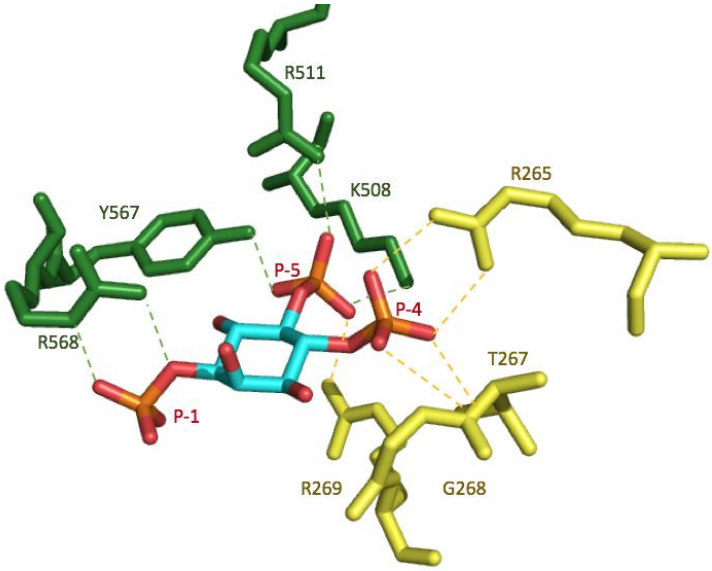

Figure 120: Some of the key IBC residues and their interactions with bound Ins(1,4,5)P_3 are shown [PDB: 1N4K, adapted from Riley *et al.*[91], InsP_3R residues in the α-domain are depicted in green and residues in the β-domain are depicted in yellow, Ins(1,4,5)P_3 phosphorus atoms are shown in orange, oxygen in red and carbon in aqua and the phosphate moieties are numbered]. Some of the main interactions between the IBC and Ins(1,4,5)P3 are shown with dashed lines, with the interactions with the α-domain in green and β-domain in yellow. The 4-position phosphate interacts exclusively with the β-domain, whereas the 5-position phosphate interacts mostly with the α-domain (but forms one important interaction to a β-domain residue side chain).

While the extension in the equivalent of the 4-position phosphate was hypothesized to be responsible for the observed partial agonism, the hydrocarbon nature of the linkage extending this phosphate further from the central glucose ring could potentially be one of the factors reducing the potency of the ligand.

The region of the IBC that the extended 6-position phosphate of the partial agonist [and the 4-position phosphate of Ins(1,4,5)P_3] is expected to bind to is rich with hydrophilic amino acid residues that bind well to polar groups.[247] Ligands that position more hydrophilic moieties in this region may be able to form more effective interactions with the binding site. It was thus hoped that, if an analogue was synthesised in which the hydrocarbon linkage was replaced by a more polar, charged group such as a pyrophosphate, the ligand might retain the ability to prevent the IBC clamshell from closing entirely (resulting in partial agonism) but also bind to the receptor with higher affinity.

A selection of novel PP-InsP_2 and model PP-InsP compounds were, therefore, planned as target compounds (Figure 121). The Potter group also recently published the synthesis of a PP-InsP_2 regioisomer, 1-PP-Ins(4,5)P_2, which was found to be a well-tolerated InsP_3R agonist.[91] The placement of the pyrophosphate moiety in 1-PP-Ins(4,5)P_2 is far from the crucial 4,5-vicinal phosphate system, however, and therefore the newly proposed PP-InsP_2 regioisomers in this study were not expected necessarily to demonstrate InsP_3R binding similar to this ligand.

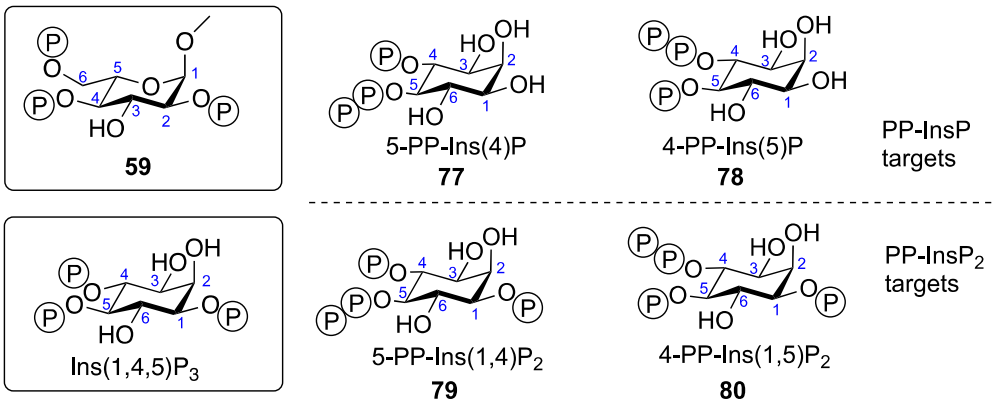

Figure 121: Structures of the target inositol pyrophosphate compounds with the structure of methyl α-L-glucopyranoside 2,4,6-trisphosphate (**59**) and Ins(1,4,5)P_3 for comparison in the box on the left. The top row displays the two regioisomers of PP-InsP synthesised, 5-PP-Ins(4)P (**77**) on the left and 4-PP-Ins(5)P (**78**) on the right. The bottom row displays the two target regioisomers of PP-InsP_2, 5-PP-Ins(1,4)P_2 (**79**) on the left and 4-PP-Ins(1,5)P_2 (**80**) on the right.

Of these four planned compounds, 4-PP-Ins(1,5)P_2 (**80**) was predicted to be able to adopt a binding mode closest to that assumed to be used by methyl α-L-glucopyranoside 2,4,6-trisphosphate (**59**, Figure 123). It was hoped that by recreating a structural disturbance in the equivalent of the 4-position phosphate of Ins(1,4,5)P_3

(and presumably the extended 6-position phosphate of methyl α-L-glucopyranoside 2,4,6-trisphosphate, **59**), 4-PP-Ins(1,5)P_2 (**80**) might act as a partial agonist of InsP_3R.

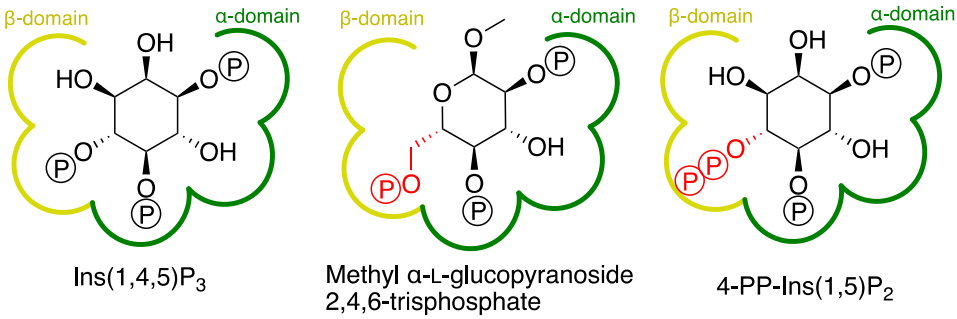

Figure 123: Comparison of the predicted binding modes for Ins(1,4,5)P_3, methyl α-L-glucopyranoside 2,4,6-trisphosphate (**59**) and 4-PP-Ins(1,5)P_2 (**80**) in the IBC of InsP_3R. The α-domains is depicted in green and the β-domain in yellow. The extended phosphate of methyl α-L-glucopyranoside 2,4,6-trisphosphate (**59**) believed to be responsible for the partial agonist activity of the ligand has been highlighted in red, as well as the 4-position pyrophosphate group of 4-PP-Ins(1,5)P_2 (**80**), which is also hoped to act as a partial agonist.

It should be noted that none of these proposed target compounds (Figure 121) is a particularly close structural analogue of methyl α-L-glucopyranoside 2,4,6-trisphosphate (**59**), as there are several structural differences associated with substituting the L-glucose central ring for *myo*-inositol.

By employing *myo*-inositol, the pyrophosphate moiety of 4-PP-Ins(1,5)$_2$ (**80**) could be attached directly to the central ring structure and would not be expected to bind much deeper within the IBC binding site than the hydrocarbon-extended 6-position phosphate of methyl α-L-glucopyranoside 2,4,6-trisphosphate (**59**). Changing the ligand structure from L-glucose enabled the incorporation of this more polar group in the equivalent position of the ligand in a more synthetically straightforward way (as opposed to attempting somehow to replace the 6-position extended hydrocarbon group with a pyrophosphate). As this change would also lead to the ligands being closer in structure to the endogenous agonist, Ins(1,4,5)P_3, it was hoped that these inositol pyrophosphates might be better tolerated by the InsP_3R binding site.

However, switching the scaffold from L-glucose to *myo*-inositol could diminish the potential ability of 4-PP-Ins(1,5)P_2 (**80**) to act as a partial agonist at InsP_3R, as this change in structure reintroduces the 3-position hydroxyl, which is absent in methyl α-L-glucopyranoside 2,4,6-trisphosphate (**59**) due to the placement of the pyranosyl ring oxygen. It was not known if the absence of an equivalent to the 3-position hydroxyl of Ins(1,4,5)P_3 might be required in combination with the extended phosphate for methyl α-L-glucopyranoside 2,4,6-trisphosphate (**59**) to behave as a partial agonist.

As described in the background information concerning development of antagonists and partial agonists of InsP_3R (Chapter 5), several of the partial agonists identified

previously include structural changes to the crucial vicinal phosphates, as well as in a different part of the ligand such as the equivalent to the 3-position or 6-position hydroxyls of Ins(1,4,5)P_3.[241,266,278,279] There have also been reported ligands that possess structural differences to Ins(1,4,5)P_3 only at the equivalent positions of the vicinal phosphates that demonstrate only weak full agonist activity.[184,271,388] Also, a ligand has been reported that features structural perturbation at the equivalent of the 3-position of Ins(1,4,5)P_3, but not the vicinal phosphate pair, which acts as a partial agonist.[306]

However, there have also been partial agonists identified with structural disruption at the vicinal phosphates, but not the equivalent of the 3-position hydroxyl,[276–278] as well as some evidence that structural disruption to solely the equivalent of the 5-position phosphate group can lead to InsP_3R antagonist behaviour.[262,273] The lack of an equivalent to the 3-position hydroxyl in methyl α-L-glucopyranoside 2,4,6-trisphosphate, due to the placement of the pyranosyl ring oxygen, could be contributing to the rendering the ligand a partial agonist, but it could also only be reducing the affinity of the ligand. Regardless of whether the absence of the 3-position hydroxyl equivalent contributes to the partial agonist activity, this structural difference is likely causing a significant decrease in ligand affinity, as can be seen in the weaker 3-deoxy-analogues of Ins(1,4,5)P_3.[263,299] Furthermore, the disruptions to the equivalent of the 3-position hydroxyl previously reported featured structural changes that introduced steric bulk to regions of the IBC through substitution or inversion,[241,266,278,279,306] whereas the pyranosyl ring oxygen in methyl α-L-glucopyranoside 2,4,6-trisphosphate (**59**) would be expected to contribute minimal steric bulk.

The only remaining major structural difference resulting in changing the structures of the loose methyl α-L-glucopyranoside 2,4,6-trisphosphate (**59**) mimics from L-glucose to *myo*-inositol is the replacement of the axial *O*-methyl group attached to the anomeric position with the axial 2-position hydroxyl of *myo*-inositol. As the axial *O*-methyl group of methyl α-L-glucopyranoside 2,4,6-trisphosphate (**59**) is expected to point out of the binding site into solvent and is not excessively sterically demanding, it is not expected to impact ligand binding either positively or negatively; thus its replacement with a hydroxyl group should have little effect on activity.[247,301]

An additional positive outcome of switching to using *myo*-inositol instead of L-glucose is that the synthesis of 4-PP-Ins(1,5)P_2 (**80**) and 5-PP-Ins(1,4)P_2 (**79**) would complete the series of Ins(1,4,5)P_3 analogues containing a single pyrophosphate group, which was begun earlier by the Potter lab with the synthesis of 1-PP-Ins(4,5)P_2.[91]

It was not known how the other PP-InsP_2 regioisomer, 5-PP-Ins(1,4)P_2 (**79**), might bind, although there is a chance this compound could behave as another partial agonist or antagonist. There has been some evidence that Ins(1,4,5)P_3 analogues with structural

disruptions solely to the equivalent of the 5-position phosphate have displayed this activity, although these antagonists might benefit from further biological analysis as they were initially assessed using only a SUEH assay.[262,273]

The two regioisomers of PP-InsP (**77** and **78**, Figure 121) were designed and synthesised mostly to explore the chemistry required to generate the PP-InsP_2 target regioisomers. The loss of the auxiliary 1-position phosphate group in both of these ligands was expected to result in a significant decrease in ligand affinity at InsP_3R [analogous to Ins(4,5)P_2, which was found to be approximately sixty-fold less potent than Ins(1,4,5)P_3].[267]

It should be noted that there have been a few references in literature that mention 5-PP-Ins(1,4)P_2 (**79**) as a naturally occurring product from Ins(1,4,5)P_3 in yeast.[3,389,390] However, none of these sources contain evidence of the discovery or characterisation of such an inositol pyrophosphate. It seems entirely possible in principle that pyrophosphate analogues of lower inositol phosphates such as Ins(1,4,5)P_3 (referred to as lower inositol pyrophosphates), could exist in nature, although this remains to be conclusively established. Through chemically synthesising these lower inositol pyrophosphates and fully characterising them, this study may aid in future attempts to identify these compounds more conclusively, should they ever be isolated from a biological source.

6.2 Docking simulations for the lower inositol pyrophosphates

Binding to the IBC of InsP_3R was modelled for all four of the lower-inositol pyrophosphate compounds, using the same GOLD docking conditions initially optimised for docking the carbohydrate-based Ins(1,4,5)P_3 analogues described in Chapter 5 (refer to the Experimental for the optimised docking procedure and some of the highest and lowest ranked exact docking scores).

In the docking predictions, all four of the ligands appeared to perform reasonably well, with the PP-InsP_2 regioisomers (**79** and **80**) tending to score more highly than both the PP-InsP regioisomers (**77** and **78**) and Ins(1,4,5)P_3 (Figure 124).

Both regioisomers of PP-InsP (**77** and **78**) appeared to be positioned in the binding site in numerous binding modes that were not always analogous to bound Ins(1,4,5)P_3. Although some of the binding modes predicted overlapped with bound Ins(1,4,5)P_3 structure, others shifted the central inositol ring to a slightly different plane. In all of the docking solutions, the exact placement of the pyrophosphate group within the IBC was found to vary, although usually it could be observed in the region occupied by the 4- or 5-position phosphates of Ins(1,4,5)P_3.

While some of the higher scoring docking solutions for the PP-InsP_2 compounds (**79** and **80**) also positioned the ligands such that they were oriented in the binding site effectively overlapping with the bound Ins(1,4,5)P_3, some of the docking solutions generated for both regioisomers did not correlate as closely. In some of the top-scoring docking results for the 4-PP-Ins(1,5)P_2 (**80**), the pyrophosphate group was positioned such that it often occupied the region of the binding site closer to the position occupied by the 5-position phosphate of Ins(1,4,5)P_3. The high-scoring docking solutions for 5-PP-Ins(1,4)P_2 (**79**) positioned the ligand more often to overlap with the bound Ins(1,4,5)P_3 structure, but there were still some solutions that positioned the pyrophosphate in different regions of the binding site, including the area where the 4-position phosphate of Ins(1,4,5)P_3 binds.

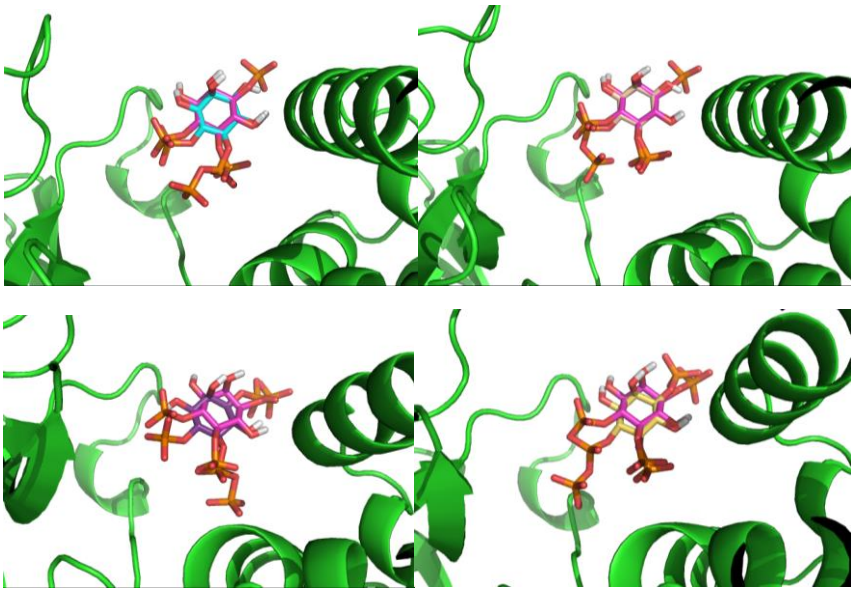

Figure 124: Docking studies for the prospective pyrophosphate containing Ins(1,4,5)P_3 analogues. In all of the diagrams, InsP_3R is shown in green and the Ins(1,4,5)P_3 bound in the crystal structure (1N4K) is shown in pink.[247] The compounds are docked: 5-PP-Ins(4)P (**77**, top left, depicted in aqua, docking solution 8, GOLDscore fitness: 93.5178), 4-PP-Ins(5)P (**78**, top right, depicted in light pink, docking solution 5, GOLDscore fitness: 98.6225), 5-PP-Ins(1,4)P_2 (**79**, bottom left, depicted in purple, docking solution 3, GOLDscore fitness: 111.0768), 4-PP-Ins(1,5)P_2 (**80**, bottom right, depicted in cream, docking solution 1, GOLDscore fitness: 106.9509).

Due to the nature of the calculations involved in GOLD molecular docking, it was expected that the docking solutions for the ligands with higher negative charge [such as the PP-InsP_2 regioisomers (**79** and **80**) compared to Ins(1,4,5)P_3] would score highly, indicating that these ligands would bind favourably at InsP_3R. These predictions must be treated with caution, however, as the majority of the docking conformations generated for all four pyrophosphate-containing ligands necessitate positioning the sterically demanding pyrophosphate deep into the binding cavity of the IBC, in a region of the binding site known to be intolerant to changes to the regular vicinal phosphates of the endogenous ligand.[251,262,266,271–273]

6.3 Synthesis of PP-InsP and PP-InsP$_2$ products

An ambitious branching synthetic route was devised that could generate all four target PP-InsP$_2$/PP-InsP compounds (Scheme 11).

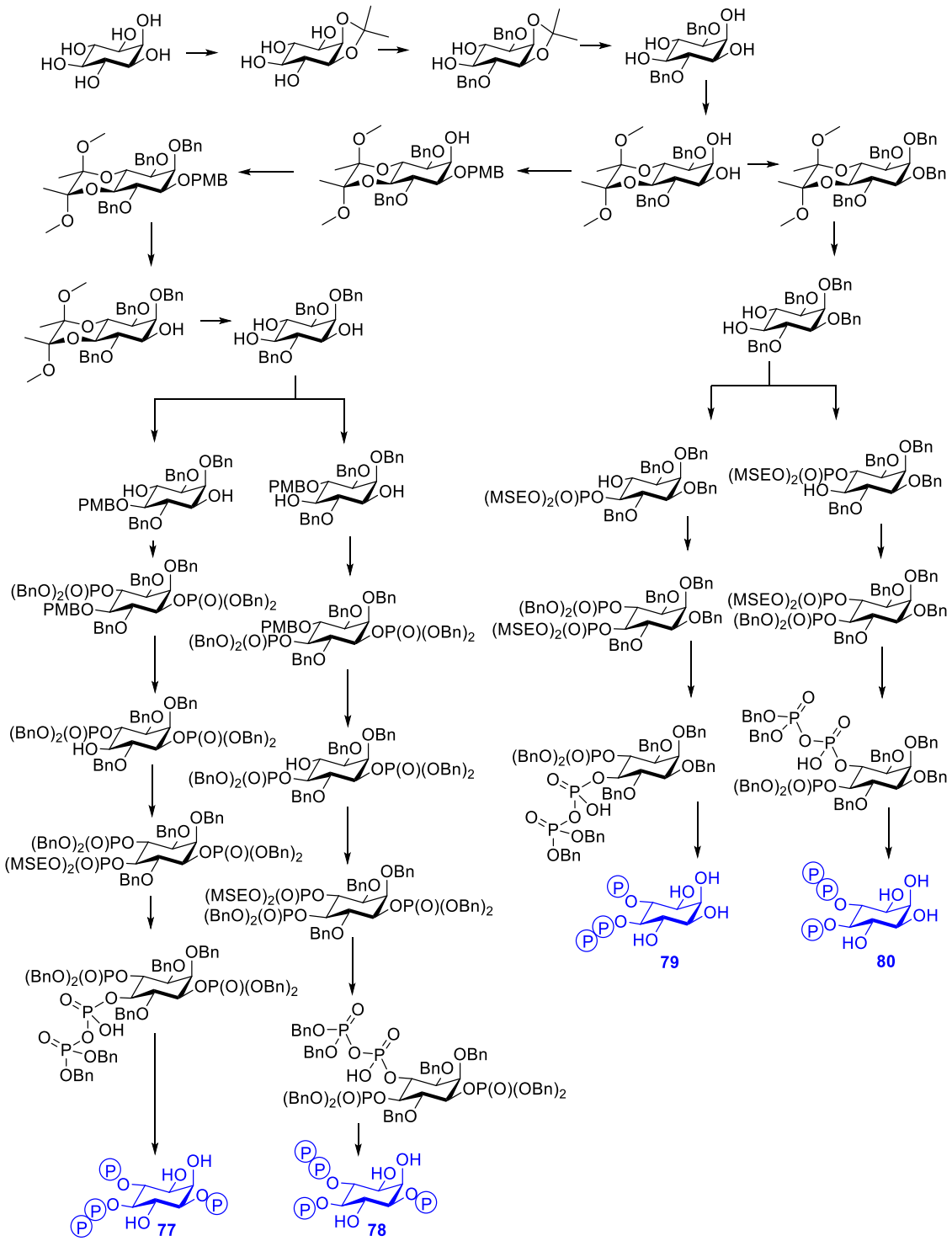

Scheme 11: Proposed divergent synthesis route from *myo*-inositol to the target PP-InsP and PP-InsP$_2$ compounds (**77**, **78**, **79** and **80**, highlighted in blue).

6.3.1 Early and shared steps in the synthetic route

The first steps in the branching synthetic routes for both the PP-InsP$_2$ and PP-InsP target compounds starting from *myo*-inositol are conserved (Scheme 12).

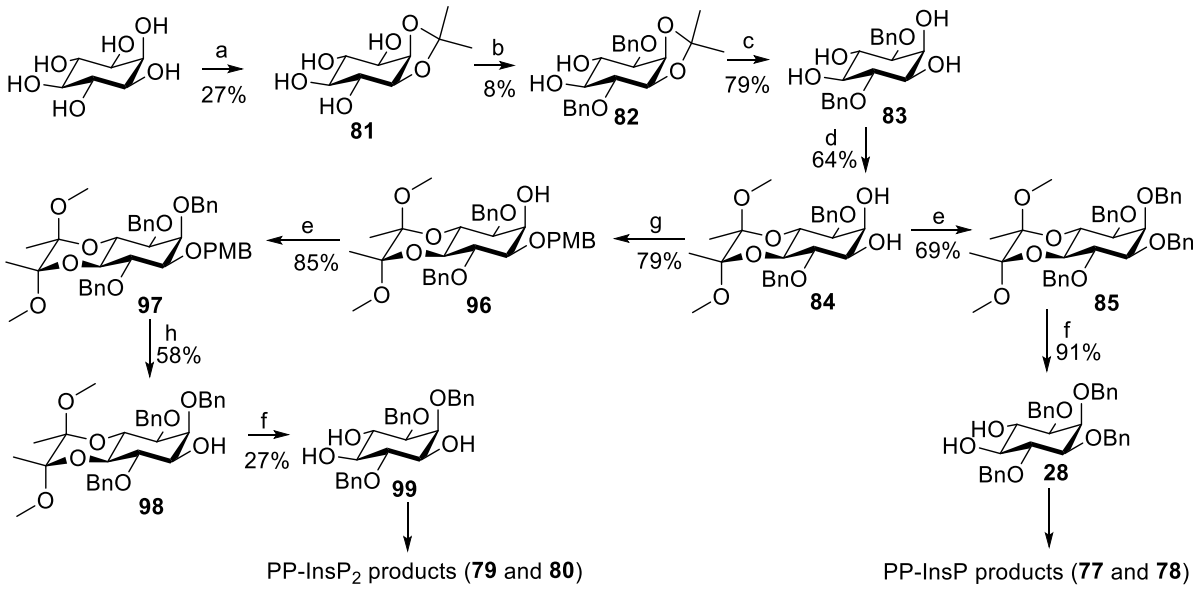

Scheme 12: Early synthetic steps in the routes to generate PP-InsP and PP-InsP$_2$ products: 5-PP-Ins(4)P (**77**), 4-PP-Ins(5)P (**78**), 5-PP-Ins(1,4)P$_2$ (**79**) and 4-PP-Ins(1,5)P$_2$ (**80**).

Reagents and conditions: (a) 2,2-isopropylidene, *p*TSA, DMSO, 110°C, 3h; (b) Bu_2SnO, BnBr, TBAB, MeCN, reflux, 24h; (c) 80% AcOH, 100°C, 4h; (d) trimethyl orthoformate, butanedione, CSA, MeOH, reflux, 24h; (e) BnBr, NaH, DMF, 0°C-RT, 3h; (f) TFA, H_2O, RT, 10 min; (g) 1. Bu_2SnO, MeOH, reflux, 24h, 2. PMBCl, CsF, DMF; (h) DDQ, DCM, H2O, RT, 90 min.

The synthetic route began with the generation of racemic 1,2-isopropylidene inositol from *myo*-inositol, using the method originally reported by Gigg *et al.*[391] During this reaction, the isopropylidene cyclic acetal preferentially formed at the *cis*-hydroxyl groups, leading to some selectivity for the desired 1,2-isopropylidene inositol product,[392] although other accounts of this reaction have reported that side products can also form with additional isopropylidene groups attached in different orientations to the *myo*-inositol ring.[393] The product (**81**) was purified through recrystallisation from boiling ethanol to be collected as a white, crystalline solid in 27% yield.

Following protection of the 1- and 2-position hydroxyls with the isopropylidene group, the compound was further protected with benzyl groups via a tin-mediated reaction that regioselectively protected the 3- and 6-position hydroxyls, as described by Desai *et al.*[393,394] In this one pot-reaction, dibutyltin oxide binds to the exposed hydroxyls in the first step to generate stannnylene acetals, which appear to exist in solution in dimers or higher oligomers.[395,396] By first carrying out a stannylation, the hydroxyl groups are effectively activated for alkylation and will react more readily with the

electrophiles present in solution, namely the benzyl bromide introduced in the second step.[396] Although the 3,6-di-*O*-benzyl regioisomer has previously been reported to be the favoured product,[394] this reaction was found to generate many different side products. The racemic 3,6-di-*O*-benzyl 1,2-isopropylidene inositol product (**82**) was eventually isolated following multiple silica chromatography columns (1. Et_2O 2. Pet. ether- Et_2O, 0-100%), after which it was collected as a white solid (8% yield).

The isopropylidene group was then cleaved with acidic hydrolysis to yield racemic 3,6-di-*O*-benzyl inositol (**83**), following recrystallisation from ethanol, as a white solid (79% yield).

The next step in the route was the regioselective protection of the 4- and 5-position hydroxyls with a butane diacetal (BDA) protecting group, as described by Riley *et al.*[397] Butanedione, trimethyl orthoformate and 3,6-di-*O*-benzyl inositol were refluxed in methanol with camphorsulfonic acid to yield the product (**84**) as a white solid (64% yield). This reaction selectively protected the *trans*-vicinal equatorial hydroxyl groups attached to the 4- and 5-positions rather than the *cis*-vicinal hydroxyl groups attached to the 1- and 2-positions.[398]

Following the addition of the BDA protecting group, the synthetic route diverged so that either the target PP-InsP products (**77** and **78**, Section 6.2.2) or PP-InsP_2 products (**79** and **80**, Section 6.2.3) could be generated.

6.3.2 PP-InsP "model" compounds (**77** and **78**) divergence

The first step diverging to the synthesis of the PP-InsP compounds (**77** and **78**) was the benzylation of the remaining exposed hydroxyls attached to the 1- and 2-positions. This was achieved with sodium hydride and benzyl bromide, generating the 1,2,3,6-tetra-*O*-benzyl 4,5-*O*-(2,3-dimethoxybutane-2,3-diyl) inositol (**85**) in 69% yield.

Following this benzylation, the BDA group was selectively cleaved with acidic hydrolysis using TFA and water to yield 1,2,3,6-tetra-*O*-benzyl inositol (**28**) in 91% yield. In addition to being able to proceed in this route to generate the PP-InsP targets (**77** and **78**), this diol product was also used in the attempted synthesis of the model *Dictyostelium* pyrophosphate (Chapter 3).

In continuing the synthetic route to both PP-InsP compounds (Scheme 13), the next step was a monophosphorylation reaction to attach a phosphate group to either the 5-position or 4-position hydroxyl and, in doing so, establish the protected phosphate that would later become the α-phosphate of the pyrophosphate group of 5-PP-Ins(4)P (**77**) and 4-PP-Ins(5)P (**78**) respectively. The phosphorylation was carried out in a two-

step phosphitylation-oxidation reaction, with the diol starting material (**28**) first being phosphitylated with 1.2 equivalents of the MSE-protected phosphoramidite (**1**) and 5-phenyl-1*H*-tetrazole before it was oxidised to generate a mixture of phosphate-containing products. This reaction was not regioselective and generated a mixture of both monophosphorylated regioisomers (**86** and **87**), as well as some bisphosphorylated product (**29**, which was used in the model *Dictyostelium* $InsP_8$ route in Chapter 3).

It had not been known if the MSE-protected phosphoramidite (**1**) could be used to generate separable mono-phosphorylated products (**86** and **87**) from the diol 1,2,3,6-tetra-*O*-benzyl inositol starting material (**28**). A similar monophosphorylation using the P(V) phosphorylating agent bis(2,2,2-trichloroethyl)phosphorochloridate was carried out in the Cooke *et al.* route, detailing the synthesis of an $Ins(1,4,5)P_3$ analogue.[272] In the Cooke *et al.* phosphorylation, no bisphosphoryalted product was observed, although this was believed to be a result of the sterically demanding P(V) phosphorylating agent used [the P(III) phosphoramidite method is better able to incorporate sterically bulky groups to substrates]. While multiple columns were required to separate the MSE-protected monophosphate products (**86** and **87**) generated in the synthetic route in this study, both regioisomers were at least partially successfully isolated (Figure 125, combined monophosphate regioisomers collected in 52% yield).

It should be noted that Cooke *et al.* reported that purification of their monophosphorylated products proved to be challenging due to cyclisation of the 4- or 5-position protected phosphate group with its neighbouring exposed hydroxyl.[272] Fortunately, no cyclisation or phosphate migration was observed in the purification of 1,2,3,6-tetra-*O*-benzyl inositol 5-bis[2-(methanesulfonyl)ethyl]phosphate (**86**) and 1,2,3,6-tetra-*O*-benzyl inositol 4-bis[2-(methanesulfonyl)ethyl]phosphate (**87**). The lack of phosphate cyclisation in this study could be due to the lack of pyridine used in the original phosphorylation as well, as it was reported in Cooke *et al.* that the amount of pyridine used in the P(V) phosphorylation reaction had to be reduced as it was found to promote phosphate cyclisation.[272]

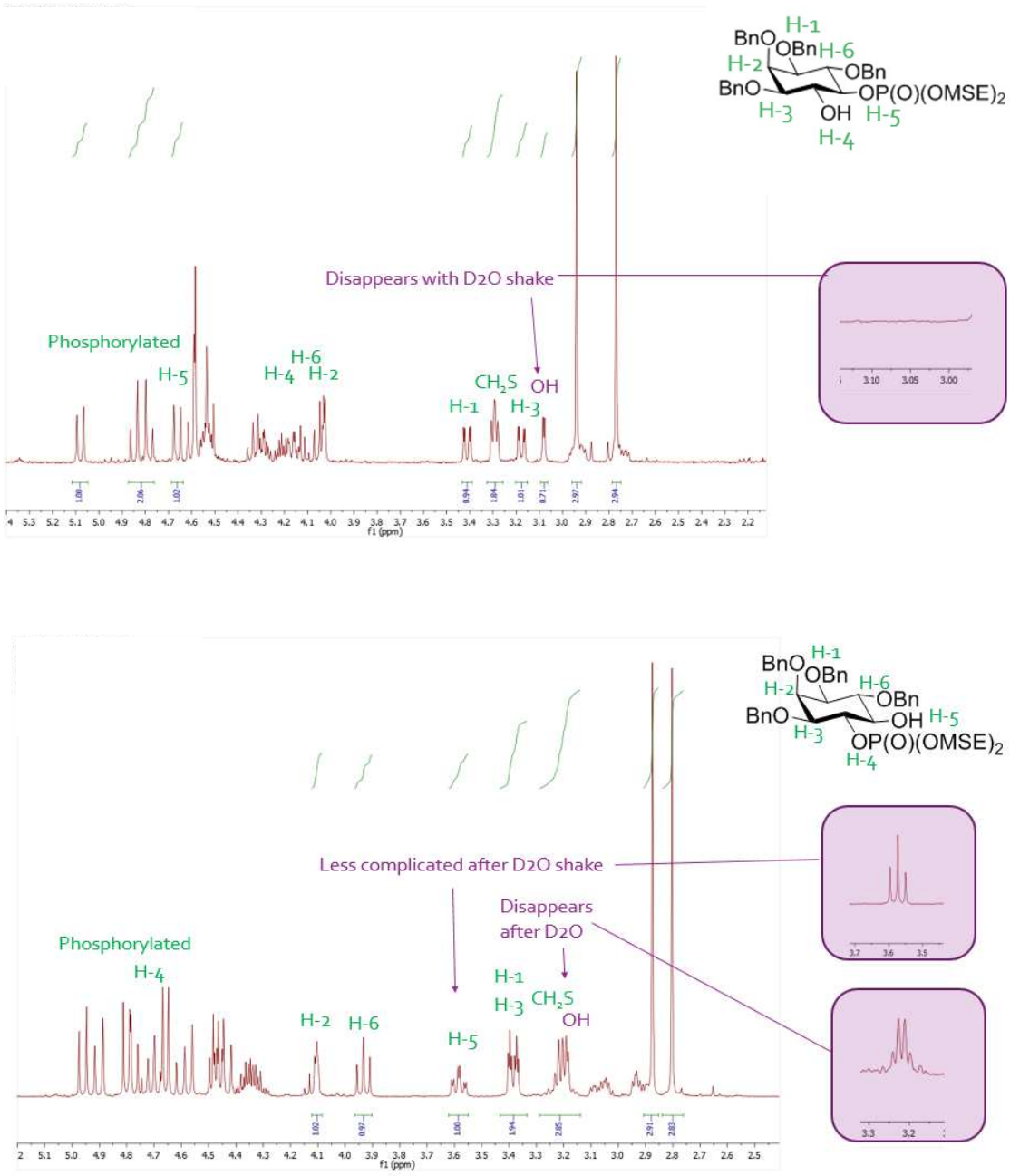

Figure 125: Assigned ^{1}HNMR spectra for the monophosphorylated product regioisomers, 1,2,3,6-tetra-*O*-benzyl inositol 5-bis[2-(methanesulfonyl)ethyl]phosphate (**86**, top spectrum) and 1,2,3,6-tetra-*O*-benzyl inositol 4-bis[2-(methanesulfonyl)ethyl]phosphate (**87**, bottom spectrum), with panels indicating which signals disappear or simplify following addition of D_2O.

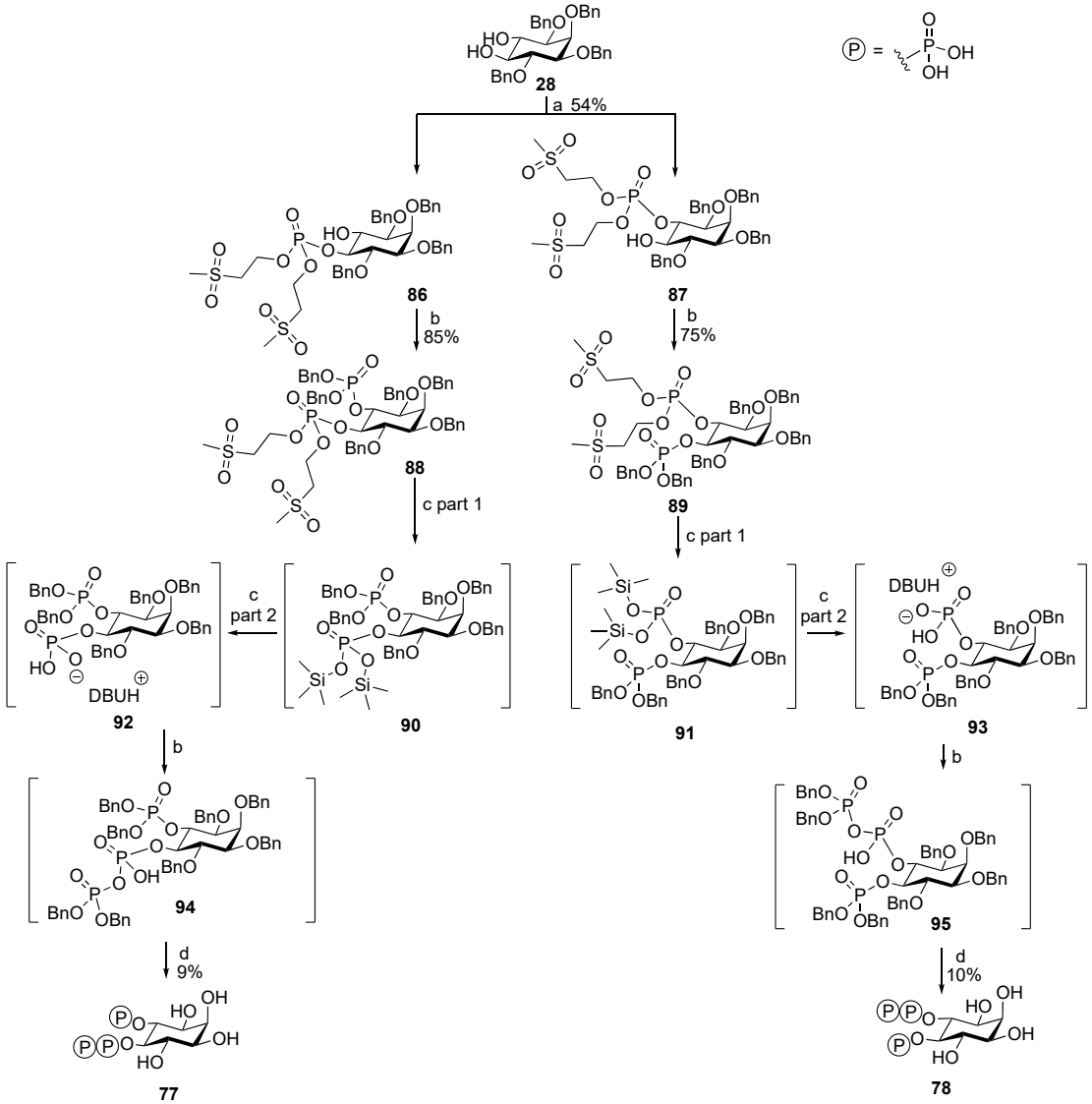

Scheme 13: Later steps in the synthetic route to form both target racemic regioisomers of PP-InsP:5-PP-Ins(4)P (**77**) and 4-PP-Ins(5)P (**78**).

Reagents and conditions: (a) 1. *N,N*-diisopropylamino-bis-[2-(methylsulfonyl)ethyloxy]phosphine (**1**), 5-phenyl-1*H*-tetrazole, DCM, RT, 3h, 2. *m*CPBA, -78°C -0°C, 10 min; (b) 1. dibenzyl diisopropylphosphoramidite, 5-phenyl-1*H*-tetrazole, DCM, RT, 3h, 2. *m*CPBA, -78°C -0°C, 10 min; (c) 1. BSTFA, $CDCl_3$ 2. MeOH, TFA; (d) H_2, $Pd(OH)_2/C$, $NaHCO_3$, H_2O, isopropanol. Non-isolated intermediates are shown in brackets.

Following the monophosphorylation, both isolated regioisomers (**86** and **87**) were thoroughly dried before being subjected to a second phosphorylation reaction that attached a benzyl-protected phosphate to the remaining exposed hydroxyl group. Both phosphorylations took place as step-wise phosphitylation-oxidation reactions that used dibenzylphosphoramidite and phenyl-1*H*-tetrazole, followed by *m*CPBA, to generate 1,2,3,6-tetra-*O*-benzyl inositol 4-dibenzylphosphate-5-bis[2-

(methanesulfonyl)ethyl]phosphate (**88**, 85% yield) and 1,2,3,6-tetra-*O*-benzyl inositol 5-dibenzylphosphate-4-bis[2-(methanesulfonyl)ethyl]phosphate (**89**, 75% yield).

The final steps for both target compounds in the PP-InsP route was the formation of the pyrophosphate moiety, which was achieved with an analogous sequence of reactions as those described for 5-PP-InsP_5, 5-PP-InsP_4 and 1,5-$(PP)_2$-InsP_4 (Chapters 2 and 3). The reaction sequence used to generate the pyrophosphate moieties for the PP-InsP product regioisomers was the same, unless otherwise explicitly stated.

The first step in the pyrophosphorylation sequence was the selective deprotection of the MSE groups from one of the protected phosphates and subsequent replacement of this protecting group with silyl moieties, which was carried out using DBU and BSTFA. Once ^{31}PNMR spectroscopy had been used to confirm complete silylation (**90**/**91**), the silyl groups were cleaved with methanol, with TFA added after seven minutes to prevent possible cyclisation side reactions and protonate the DBU. Fortunately, as in the synthesis of 5-PP-InsP_5 and 5-PP-InsP_4 (Chapter 2) but not the synthesis of 1,5-$(PP)_2$-InsP_4 (Chapter 3), there was no apparent cyclisation observed during the cleavage of the silyl groups of the PP-InsP precursors.

The partially deprotected bisphosphate (**92**/**93**) was allowed to dry overnight, before the pyrophosphate moiety was constructed through phosphitylation and subsequent oxidation via a mixed P(III)-P(V) intermediate.

Following construction of the benzyl-protected pyrophosphate moiety, both benzyl-protected PP-InsP precursor regioisomers (**94**/**95**) were quickly hydrogenated without purification. The previous syntheses of inositol pyrophosphates demonstrated that purifying the protected pyrophosphate phosphorylation product before the final hydrogenation by means of silica column chromatography can result in the product becoming more unstable after purification (5-PP-InsP_5, Chapter 2) or in complete loss of the product [1,5-$(PP)_2$-InsP_4, Chapter 3].

The synthesis of 1,5-$(PP)_2$-InsP_4 (Chapter 3) demonstrated that the final hydrogenation step to deprotect inositol pyrophosphates could be carried out on crude material with partial success. The partial debenzylation of the crude inositol pyrophosphate precursor was assumed to include the successful cleavage of the more labile benzyl ester groups attached to the β-phosphate of the pyrophosphate moiety, thereby rendering the compound more stable for subsequent purifications and hydrogenations.

Although it may be possible to purify the benzyl-protected PP-InsP precursors (**94**/**95**), it was not investigated during this study, and the initial deprotection reactions were carried out on the crude protected pyrophosphates, as this was thought to be the safer method to avoid product degradation. This decision was made due to the expectation that the protected pyrophosphate would likely become more unstable

following purification, and time-sensitive investigation of the product fractions collected following a silica column would not be possible because of pandemic-related restrictions on accessing spectroscopy facilities.

The construction of the pyrophosphate group of 4-PP-Ins(5)P was carried out first, and so this was the first regioisomer to undergo the final deprotection step via hydrogenation of the crude material. The protected pyrophosphate precursor (**95**) was dissolved in a mixture of mQ water and isopropanol, and to this solution sodium bicarbonate and palladium hydroxide on carbon were added followed by a hydrogen balloon and the hydrogenation was allowed to take place overnight.

As no purification had been carried out prior to the hydrogenation of the protected pyrophosphate, the starting material (**95**) for this reaction would be contaminated with a large number of reagents and side products from previous reactions including DBU, *m*CPBA and 5-phenyl-*1H*-tetrazole, the presence of which made the degree of debenzylation difficult to determine from the ^{1}HNMR spectrum of the crude hydrogenation product. The initial purification was carried out with reverse-phase column chromatography (0-10% MeCN in 0.05 M TEAB), although the product was only collected after the column was washed with 70% MeCN in 0.05 M TEAB. It was determined that the first hydrogenation had only been partially successful, as the ^{1}HNMR spectrum indicated the presence of several benzyl groups remaining (although crucially, the benzyl groups attached to the β-phosphate of the pyrophosphate groups were presumed to have been among those cleaved, resulting in a more stable compound).

A second hydrogenation was then attempted on the partially deprotected inositol pyrophosphate, using the same method described previously, except the sodium bicarbonate was omitted from the reaction, as triethylammonium counterions would be present in solution. However, this hydrogenation was also proven to be unable to cleave all of the remaining benzyl groups attached to the 4-PP-Ins(5)P precursor.

From integration of ^{1}HNMR signals, approximately two benzyl groups remained attached to the inositol pyrophosphate compound and, although the structures of these intermediates were not analysed, these benzyl groups were hypothesized to be those attached to the 1- and 2-positions. This is because these are benzyl ether groups, which are less labile than the benzyl ester groups that were used to protect the phosphate moieties, and neither position has a neighbouring phosphate group, the proximity of which seems to aid debenzylation (a trend previously observed in the Potter lab). Previous reported inositol phosphate syntheses have also noted that benzyl-protecting groups attached to the axial 2-position are notoriously resistant to hydrolytic cleavage, even when adjacent to phosphorous groups.[112]

Another factor believed to contribute to the prevention of complete debenzylation was the presence of some of the organic hydrophobic contaminants (including some

DBU), which appeared to co-elute with the partially deprotected product. A second reverse-phase column was therefore carried out with a steeper solvent gradient (0-70% MeCN in 0.05 M TEAB) to isolate the partially debenzylated pyrophosphate product from the remaining contaminants.

Following this second column, the collected inositol pyrophosphate product was subjected to another repeat of the hydrogenation protocol (again omitting the sodium bicarbonate). The third hydrogenation was found to be successful in fully deprotecting the product, and after further purification with an anion exchange column and a final reverse-phase column, 4-PP-Ins(5)P (**78**, Figure 126) was lyophilised and collected as an off-white glass (10% yield for the pyrophosphorylation sequence).

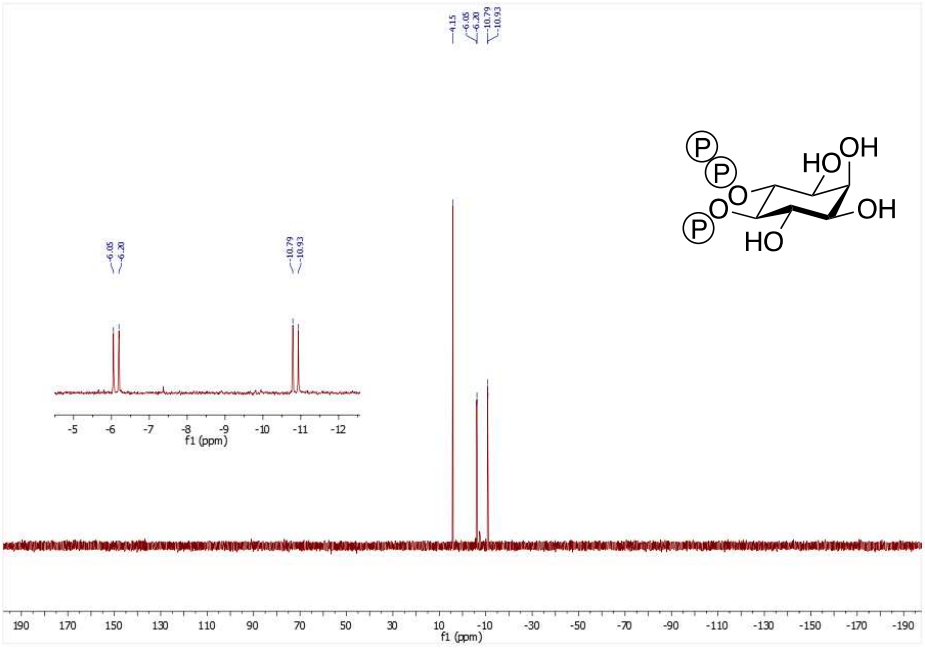

Figure 126: ^{31}PNMR spectrum of 4-PP-Ins(5)P (**78**) following the anion exchange column with EDTA added to the sample to sharpen the signal peaks by chelating trace metal ions that could broaden the 31PNMR signal peaks. The EDTA was removed in the following final reverse-phase column. The insert depicts the expanded pyrophosphate region of the spectrum (around -10 ppm) to more clearly show the two doublets generated by the pyrophosphate group.

Following successful deprotection and purification of 4-PP-Ins(5)P (**78**), the pyrophosphorylation sequence was repeated for its regioisomer to generate the benzyl-protected precursor to 5-PP-Ins(4)P (**77**). The final hydrogenation reaction of the inositol pyrophosphate synthesis was also carried out on the crude phosphorylation product (**94**) to yield the partially debenzylated precursor of the final product.

The initial reverse-phase column used to purify the partially deprotected 5-PP-Ins(4)P precursor was run with a steeper solvent gradient (0-70% MeCN in 0.05 M TEAB) than

that used in the initial purification of its regioisomer to improve separation of the inositol pyrophosphate and the organic contaminants from the preceding steps.

The product fractions from the first column were collected and then hydrogenated a second time (omitting the sodium bicarbonate due to the presence of triethylammonium counterions) to yield the fully debenzylated product. The product was purified with an anion exchange column, followed by a final reverse-phase column, before 5-PP-Ins(4)P (**77**, Figure 127) was lyophilised and collected as an off-white glass (9% yield for the pyrophosphorylation sequence).

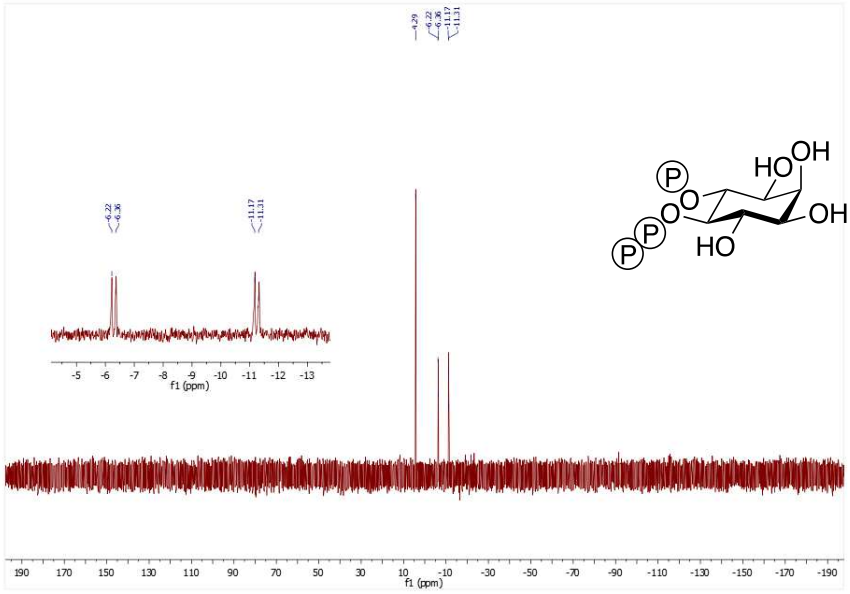

Figure 127: ^{31}PNMR spectrum of 5-PP-Ins(4)P (**77**) following the anion exchange column with EDTA added to the sample to sharpen the signal peaks by chelating trace metal ions that could broaden the 31PNMR signal peaks. The EDTA was removed in the following final reverse-phase column. The insert depicts the expanded pyrophosphate region of the spectrum (around -10 ppm) to more clearly show the two doublets generated by the pyrophosphate group.

Both racemic PP-InsP regioisomers (**77** and **78**) were then sent to Dr Ana Rossi (University of Cambridge) for biological evaluation of the inositol pyrophosphates in calcium release and $InsP_3R$ competition binding assays (Section 6.4)

6.3.3 Continuation of route to PP-$InsP_2$ compounds (**79** and **80**)

The first step in the synthetic route for the divergence to the PP-$InsP_2$ target compounds from their PP-InsP analogues was the regioselective protection of the 2-position hydroxyl of 3,6-di-*O*-benzyl-4,5-*O*-(2,3-dimethoxybutane-2,3-diyl) inositol

(**84**) with a *para*-methoxy-benzyl (PMB)-protecting group in a tin-mediated reaction, as described by Riley *et al.*[399]

In the first step of the reaction, the dibutyltin oxide formed a stannylene acetal at the exposed 1- and 2-positions of the inositol, which was subsequently alkylated regioselectively at the equatorial 1-position, as opposed to the axial 2-position. The 1-*O*-PMB product regioisomer was generated as the predominant product in this reaction with none of the 2-*O*-PMB regioisomer detected, allowing 3,6-di-*O*-benzyl-4,5-*O*-(2,3-dimethoxybutane-2,3-diyl) 1-*O*-PMB-inositol (**96**) to be purified and collected in 79% yield.

Following the regioselective PMB-protection, the remaining exposed axial hydroxyl attached to the 2-position was then protected with a benzyl group to yield 2,3,6-tri-*O*-benzyl-4,5-*O*-(2,3-dimethoxybutane-2,3-diyl) 1-*O*-PMB-inositol (**97**, 85% yield).

While it would have been ideal to cleave selectively the BDA-protected group at this stage to then follow a synthetic route that would more closely resemble that of the PP-InsP model compounds [**77** and **78**, with the next hypothetical reaction being monophosphorylation with the MSE-protected phosphitylation agent (**1**), followed by PMB deprotection and a second phosphorylation], it was predicted that the conditions required to remove the BDA would also result in the simultaneous deprotection of the PMB group.

The PMB group was instead selectively cleaved with DDQ to produce 2,3,6-tri-*O*-benzyl-4,5-*O*-(2,3-dimethoxybutane-2,3-diyl) inositol (**98**, 58% yield). It should be noted that although the cleavage of this PMB group could be achieved during the next step, the removal of the BDA group by means of TFA, the stepwise approach was deemed to be the more advantageous option. This was due to the expectation that, should the route eventually be repeated with optically-resolved enantiomers to generate chiral final products, this intermediate would be expected to be ideal for potential chiral resolutions *via* esterification of the 1/3-position hydroxyls, to form, for example, the camphanate or acetylmandelate diastereomers.[287,393,400,401] Unfortunately, there was insufficient time to repeat the synthetic route from this step to generate the chiral PP-InsP_2 products during this study.

The next step was the acidic cleavage of the BDA-protecting group with TFA and water to generate 2,3,6-tri-*O*-benzyl inositol (**99**, 27% yield). This deprotected triol was hoped to be the point at which the syntheses of the 4-PP-Ins(1,5)P_2 (**80**) and 5-PP-Ins(1,4)P_2 (**79**) regioisomers could diverge (Scheme 14).

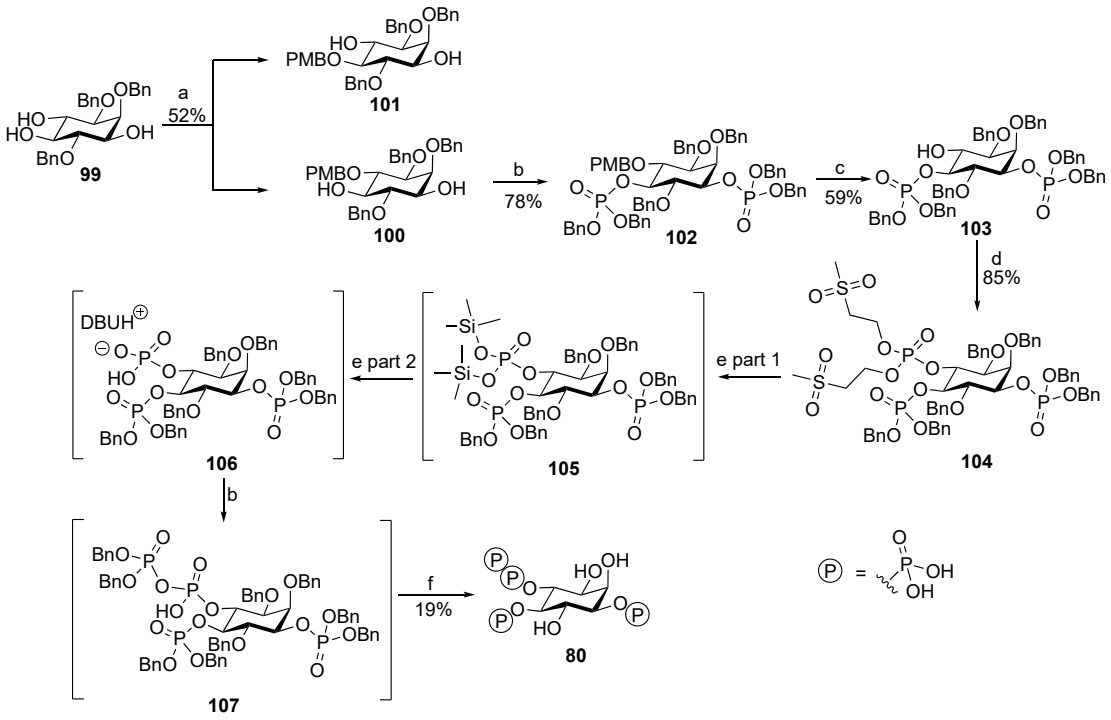

Scheme 14: Later steps in synthesis route to generate the racemic PP-InsP_2 product: 4-PP-Ins(1,5)P_2 (**80**).

Reagents and conditions: (a) 1. Bu_2SnO, MeCN, reflux, 24h, 2. PMBCl, TBAI, reflux, 24h; (b) 1. dibenzyl diisopropylphosphoramidite, 5-phenyl-1*H*-tetrazole, DCM, RT, 3h, 2. *m*CPBA, -78°C -0°C, 10 min; (c) DDQ, DCM, H2O, rt, 90 min; (d) 1. *N,N*-diisopropylamino-bis-[2-(methylsulfonyl)ethyloxy]phosphine (**1**), 5-phenyl-1*H*-tetrazole, DCM, RT, 3h, 2. *m*CPBA, -78°C -0°C, 10 min; (e) 1. BSTFA, $CDCl_3$ 2. MeOH, TFA; (f) H_2, $Pd(OH)_2/C$, $NaHCO_3$, H_2O, isopropanol.

The next step in the route was the regioselective protection of either the 4-position or 5-position hydroxyls of 2,3,6-tri-*O*-benzyl inositol (**99**) with a PMB group. A reaction was needed that was regioselective for these two positions (not the exposed 1-position hydroxyl) and would generate a mixture of both 5-*O*-PMB (**101**) and 4-*O*-PMB (1**00**) product regioisomers. It then also remained to be determined if the product regioisomers synthesised would be separable via silica column chromatography.

To attempt to control the regioselectivity of the protection of the 4- or 5-position hydroxyls, reaction conditions were investigated that featured a metal complex (such as dibutyltin oxide) that could coordinate to the diol on the starting material and selectively activate these positions for alkylation. While neither the formation of the 1-*O*-PMB product regioisomer or 4,5-*O*-bis-alkylated product was observed in any of the reaction attempts, generating both desired product regioisomers cleanly and in reasonable yield proved to be more difficult than anticipated, resulting in a number of reaction conditions being trialled (Table 14).

Reaction code	Method: key reagents	Approx. product regioisomer ratio	Unseparated products/ mg	Yield of unseparated products/%
414	method A: dibutyltin oxide, TBAI	1 (5-PMB) : 2 (4-PMB)	111.4	45
296	method A: dibutyltin oxide, TBAI	1 (5-PMB) : 1.4 (4-PMB)	130*	52
294	method B: $Fe(dpm)_3$, Ag_2O, TBAB	1 (5-PMB) : 2.6 (4-PMB)	30.7	12
299	method B: $Fe(dpm)_3$, Ag_2O, TBAB	1 (5-PMB) : 2.7 (4-PMB)	73.2	30
368	method C: dibutyltin oxide, CsF	1 (5-PMB) : 6 (4-PMB)	70.1	11

Table 14: Different reaction conditions and outcomes of attempts to protect regioselectively the 4-position and 5-position hydroxyls in of 2,3,6-tri-*O*-benzyl inositol (**99**). *Product was successfully partially separated: 35.9 mg (4-*O*-PMB product, **100**), 24.1 mg (5-*O*-PMB product, **101**), 70 mg still unseparated regioisomers.

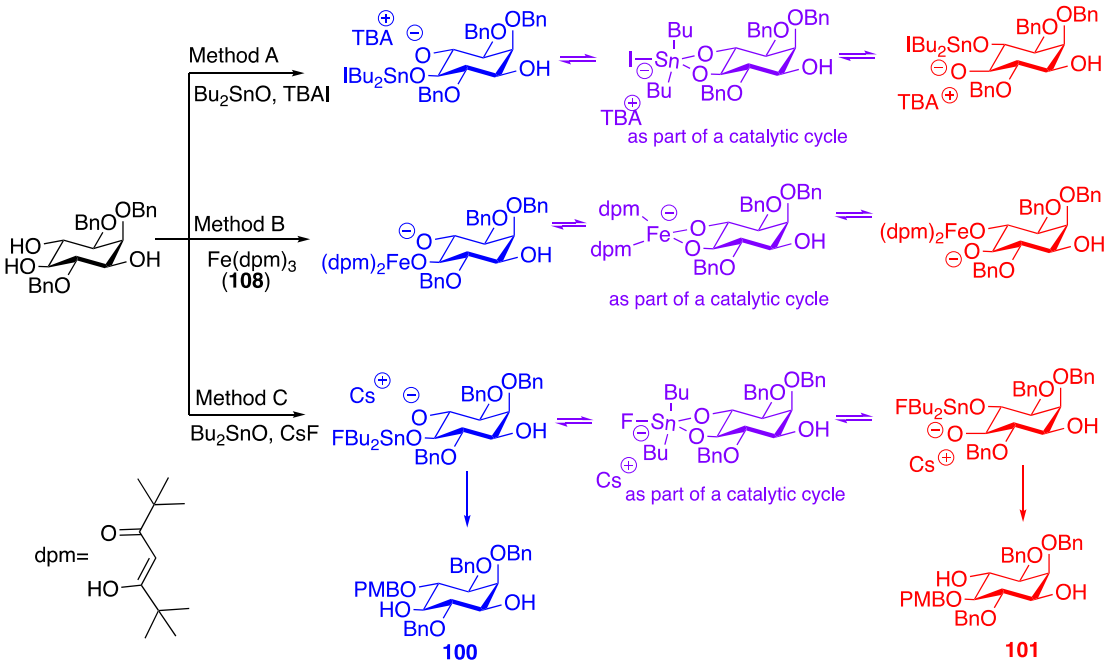

Figure 128: Proposed mechanisms for the three different methods of PMB-protection corresponding to the results listed in Table 14.[402–406]

All of the reaction attempts appeared to generate a mixture of products that contained three separate species containing a single PMB group (determined through ^{1}HNMR spectra analysis around the 3.8 ppm region, which corresponds to signals

generated by the methoxy protons of a PMB group). Two of the PMB-containing products were determined to be the 4-*O*-PMB (**100**) and 5-*O*-PMB (**101**) regioisomers, while the third was found not to contain an inositol ring and was suspected to be the *para*-methoxybenzyl alcohol (PMBOH).

It was possible to identify both alkylated product regioisomers (**100** and **101**) through analysis of their ^{1}HNMR COSY spectra, which indicated correlation between inositol ring protons and the remaining exposed hydroxyl protons allowing for structural assignments (Figure 129). Following identification of signals corresponding to the methoxy group of each product regioisomer, it was possible to determine that the 4-*O*-PMB regioisomer (**100**) was the favoured product in all of the crude products of the PMB-protections attempted.

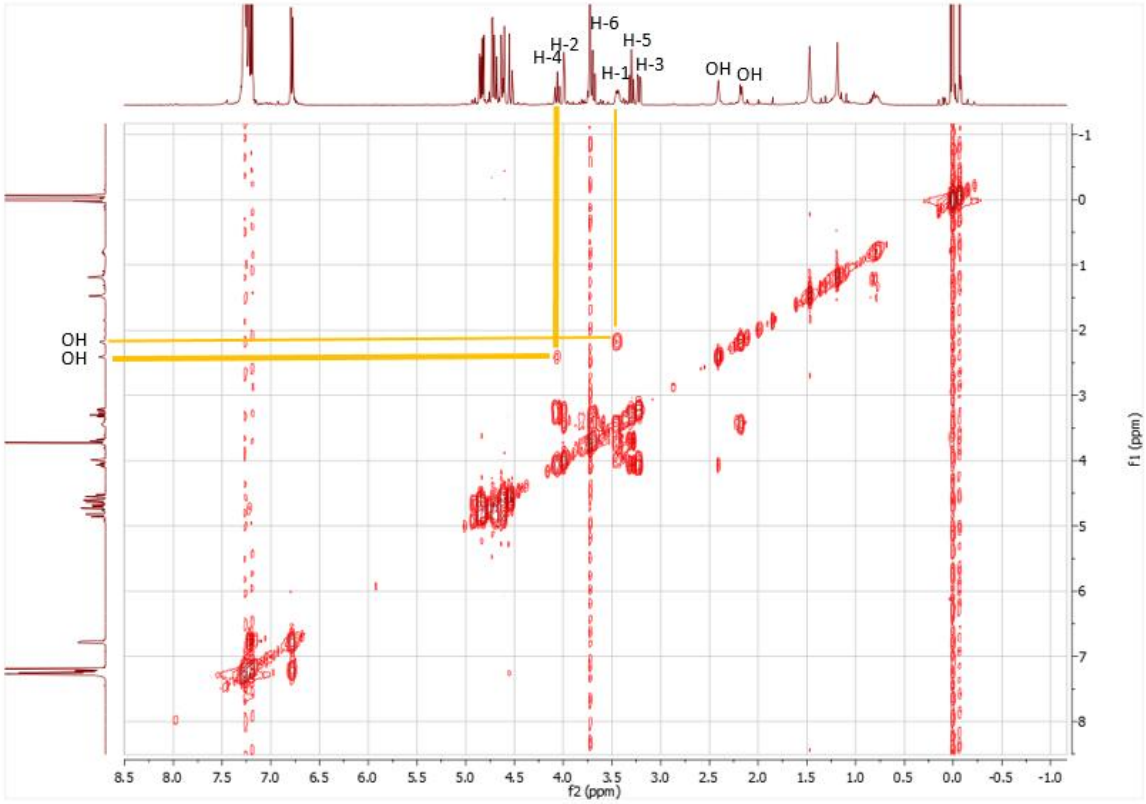

Figure 129: The assigned COSY spectrum of 2,3,6-tri-*O*-benzyl 4-*O*-PMB-inositol (**100**). The signals generated by the inositol ring protons and hydroxyl groups have been labelled on the horizontal ^{1}HNMR spectrum and the hydroxyl group signals have been labelled on the vertical ^{1}HNMR spectrum. Correlation can be observed between the H-4 proton and one of the hydroxyls (indicated with bold yellow lines) as well as the H-1 proton and the other hydroxyl signal.

The first set of reaction conditions attempted for the regioselective PMB-protection was a two-step alkylation that used dibutyltin oxide and tetra-*N*-butylammonium iodide (TBAI).[407] A stannylene acetal intermediate formed in the first step of the reaction, in which the starting of 2,3,6-tri-*O*-benzyl inositol (**99**) was allowed to reflux

with dibutyltin oxide for a day. Alkylation then took place upon the addition of *para*-methoxybenzyl chloride (PMBCl) and TBAI.

It was originally thought that the regioselectivity of the alkylation of a *trans*-diol was determined by the orientation of the dimer structures formed in solution,[395,396] although there is now some evidence that the regioselectivity is actually controlled by stereoelectronic effects within the polyol starting material; the product distribution is thought to be influenced by the orientation and nature of the substituents neighbouring the diol, which can affect the nucleophilicity of oxygen atoms in the diol as well as impact the preferential cleavage of the SnO bonds in the pentacoordinated tin intermediates.[344]

The reaction is proposed to proceed through a penta-coordinated tin structure (Figure 128) that forms when the TBAI reacts with the stannylene acetal intermediate as a Lewis base.[344,402] The unstable penta-coordinated tin complex dissociates into different alkoxide intermediates that subsequently react with the alkylating agent.

The reaction led to the preferential formation of the 4-*O*-PMB product, although the relatively low regioselectivity of the reaction appeared to demonstrate that the penta-coordinate tin complex could open to form either alkoxide regioisomer (but slightly favoured opening to expose the 4-position for alkylation).

Although these reaction conditions generated both 5-*O*-PMB (**101**) and 4-*O*-PMB (**100**) product regioisomers, it was found that the contaminants, particularly the large amount of PMB alcohol that co-eluted mostly with the 5-*O*-PMB regioisomer (**101**), were very difficult to separate from the desired products. As it was also hoped that both PMB product regioisomers could be isolated for continuation of the branching synthetic route, conditions that could generate the 5-*O*-PMB (**101**) and 4-*O*-PMB (**100**) products in a 1:1 ratio would be preferable to those that favour the formation of one regioisomer.

While the regioselectivity and yield for the initial attempt using these reaction conditions (method A) were tolerable, it was hoped that different protocols might yield superior results, and so alternative conditions were investigated.

The next set of conditions attempted for the regioselective PMB-protection (method B) was through catalysis using the $Fe(dpm)_3$ (dpm: dipivaloylmethane) complex (**108**, Figure 128), as described by Ren *et al.*[404] This iron catalyst was initially developed as a more environmentally friendly catalyst for the monoalkylations of diols that was also more cost effective to synthesise than other iron catalysts previously developed for this purpose. This set of conditions would also have the advantage of being better for the environment through avoiding the usage of highly toxic organotin reagents.[404] It was hoped that purification of the product regioisomers (**100** and **101**) generated in this reaction might also be easier due to the absence of tin-based contaminants.

Before this reaction could be attempted, the iron complex (**108**) first had to be synthesised. This was accomplished in a version of the method originally described by Hammond *et al.*[408] with 2,2,6,6-tetramethylheptan-3,5-dione and iron (III) chloride that formed the product as a bright-orange solid (84% yield).

The regioselective PMB-protection itself then proceeded in a single step with the $Fe(dpm)_3$ complex (**108**), silver (II) oxide, tetra-*N*-butylammonium bromide and potassium carbonate being allowed to stir for 12 hours at room temperature with the triol starting material, 2,3,6-tri-*O*-benzyl inositol, and PMBCl. The yield of the reaction improved upon using fresh silver (II) oxide (Table 14, reaction 299 used a fresh supply of Ag_2O).

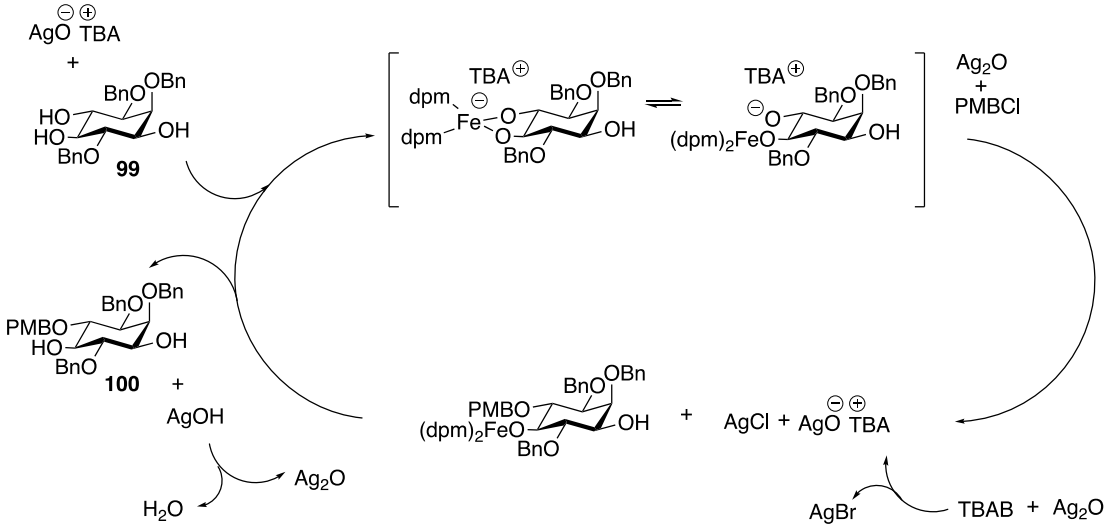

Figure 130: Proposed catalytic mechanism for the $Fe(dpm)_3$ (**108**) catalysed PMB-protection (method B) adapted from Ren *et al.*[405] The mechanism only depicts the formation of the 4-*O*-PMB product regioisomer (**100**), although the iron complex intermediate would be expected to be able to open in either direction, leading to the formation of both regioisomers (Figure 128). It should be noted that this is a simplified catalytic mechanism for the $Fe(dpm)_3$ alkylation, and the same group that proposed this mechanism have also reported a more complicated catalytic cycle for the reaction that incorporates the formation of substrate dimers.[404]

The silver oxide and TBAB acted as co-catalysts to deprotonate the hydroxyls of the starting material (**99**) and allow the iron complex (**108**) to bind to the diol group (Figure 130). As in the case of the dibutyltin oxide mechanism, the iron catalyst (**108**) was expected to form a complex with the vicinal hydroxyls attached to the 4- and 5-positions in a dioxolane intermediate, which could open in either direction to yield an alkoxide that could subsequently react with the alkylating agent.[404] The regioselectivity of the reaction would, therefore, be predicted to reflect which position of the 2,3,6-tri-*O*-benzyl inositol (**99**) diol group is more suited to host the negative charge prior to alkylation.

As in the case of the original dibutyltin oxide reaction (method A), the product distributions for the $Fe(dpm)_3$ (**108**) reactions (method B) were slightly skewed in favour of the of 4-PMB regioisomer (**100**), again indicating that the 4-position seems to be more suitable to host the alkoxide charge prior reaction with PMBCl. Although the regioselectivity observed in the initially attempted dibutyltin oxide method (method A) had demonstrated that the 4-*O*-PMB product (**100**) would likely be the major regioisomer (due to the similarities in the proposed mechanisms for the reactions), the regioselectivity for the 4-*O*-PMB product (**100**) was slightly more pronounced under this second set of conditions (method B).

Unfortunately, despite the benefits of avoiding dibutyltin oxide, the insufficient yields and unwanted regioselectivity of this method led to the investigation of other alkylation conditions.

The final set of reaction conditions that were attempted to regioselectively protect the 4- and 5-position hydroxyls of **99** employed dibutyltin oxide with caesium fluoride instead of TBAI (Table 14, method C). The use of caesium fluoride to promote tin-mediated alkylation reactions was initially suggested by Nagashima and Ohno in 1991.[403] The inclusion of caesium fluoride in these dibutyltin oxide reactions was reported to allow these alkylation reactions to occur under milder conditions and generate higher yields.[403]

The reaction proceeded in two steps, the first of which involved the formation of the dibutyltin oxide complex intermediate in methanol, before this stannylene acetal was concentrated to a residue and redissolved in DMF. In the second step, caesium fluoride was used to activate the stannylene complex for monoalkylation with PMBCl through forming a penta-coordinated tin complex with the fluoride ion.[403] As in the case of both the dibutyltin oxide/TBAI reaction conditions (method A) and the $Fe(dpm)_3$ (**108**) reaction conditions (method B), the penta-coordinated complex would be expected to open reversibly in both directions to form highly nucleophilic alkoxide anions which can subsequently react with PMBCl. The regioselectivity is thought to be determined by which of the reversibly formed alkoxide intermediate regioisomers is more reactive, rather than other factors such as steric bulk of the alkylation substrate or type of metal halide used.[403] Although this would indicate that the favoured product would likely still be the 4-*O*-PMB regioisomer (**100**), it was hoped that the yield of the reaction would be higher and the ratio of products generated would be balanced enough to produce a sufficient quantity of both regioisomers.

Unfortunately, the ratio of products formed was further from the ideal mixture than the previously attempted reaction conditions, with approximately six-fold more 4-*O*-PMB product (**100**) generated than the 5-*O*-PMB regioisomer (**101**).

It should also be noted that off-target alkylation has been previously observed in these reactions in stannylene acetal complexes that possess exposed hydroxyl groups, due

to the caesium fluoride activating the exposed hydroxyls sufficiently for alkylation.[403] However, this did not appear to occur in this study as no 1-*O*-PMB regioisomer was detected.

Due to the poor yield and unwanted regioselectivity observed with these conditions, the initial reaction conditions (method A) using dibutyltin oxide and tetrabutylammonium iodide were revisited, and the PMB-protection was repeated to generate product for the next step in the synthetic route.

As mentioned, there were multiple issues with the purification of these products, with the 5-*O*-PMB regioisomer (**101**) proving to be particularly difficult to separate from contaminating PMBOH and trace amounts of 4-PMB regioisomer (**100**), regardless of the reaction conditions used. The difficulty in purifying the product regioisomers in combination with the unwanted regioselectivity of the PMB-protection led to only a small quantity of 2,3,6-tri-*O*-benzyl 5-*O*-PMB inositol (**101**) being completely isolated, which was insufficient to be carried through to the remaining steps of the initially planned route (Scheme 14).

It was possible, however, to continue the synthetic route with the separated 4-*O*-PMB regioisomer (**100**), which was then phosphorylated in the next step with the benzyl-protected phosphitylating agent, dibenzyl phosphoramidite, and 5-phenyl-1*H*-tetrazole followed by *m*CPBA to generate 2,3,6-tri-*O*-benzyl 4-*O*-PMB inositol 1,5-bis(dibenzylphosphate) (**102**, 78% yield).

Following this first phosphorylation, the PMB-protecting group was removed with DDQ to yield 2,3,6-tri-*O*-benzyl inositol 1,5-bis(dibenzylphosphate) (**103**). The yield of this PMB-deprotection was relatively low (59% yield), but the reaction was clean, the product easy to purify and the reaction conditions were suitably mild not to result in the cleavage of the benzyl-protecting groups.

Following PMB-deprotection, the benzyl-protected bisphosphate compound (**103**) had a single hydroxyl exposed attached to the 4-position. After thorough drying, the 2,3,6-tri-*O*-benzyl inositol 1,5-bis(dibenzylphosphate) (**103**) was phosphorylated again using the MSE phosphitylating agent (**1**) and 5-phenyl-1*H*-tetrazole, followed by *m*CPBA, to generate the protected trisphosphate, 2,3,6-tri-*O*-benzyl inositol 1,5-bis(dibenzylphosphate)-4-bis[2-(methylsulfonyl)ethyl]phosphate (**104**, 85% yield).

The last stage in the reaction route was the construction of the pyrophosphate moiety through a pyrophosphorylation reaction sequence. There were a few minor differences in the pyrophosphorylation sequence used in the synthesis of 4-PP-Ins(1,5)P_2 (**80**) compared to that of the model compounds [4-PP-Ins(5)P (**78**) and 5-PP-Ins(4) (**77**)], as will be described.

The first step in the pyrophosphate sequence, the combined deprotection of the MSE groups and silylation of the α-phosphate precursor, took place without any difficulties, and full silylation (**105**) was confirmed through ^{31}PNMR spectroscopy.

The cleavage of these silyl groups was found to be incomplete after the first attempt in which the TFA was added seven minutes after the methanol. The majority of the compound in solution appeared to be the monosilylated intermediate (Figure 131), but subjecting the partially deprotected intermediate to a repeat of this deprotection step was sufficient to successfully remove the remaining silyl groups.

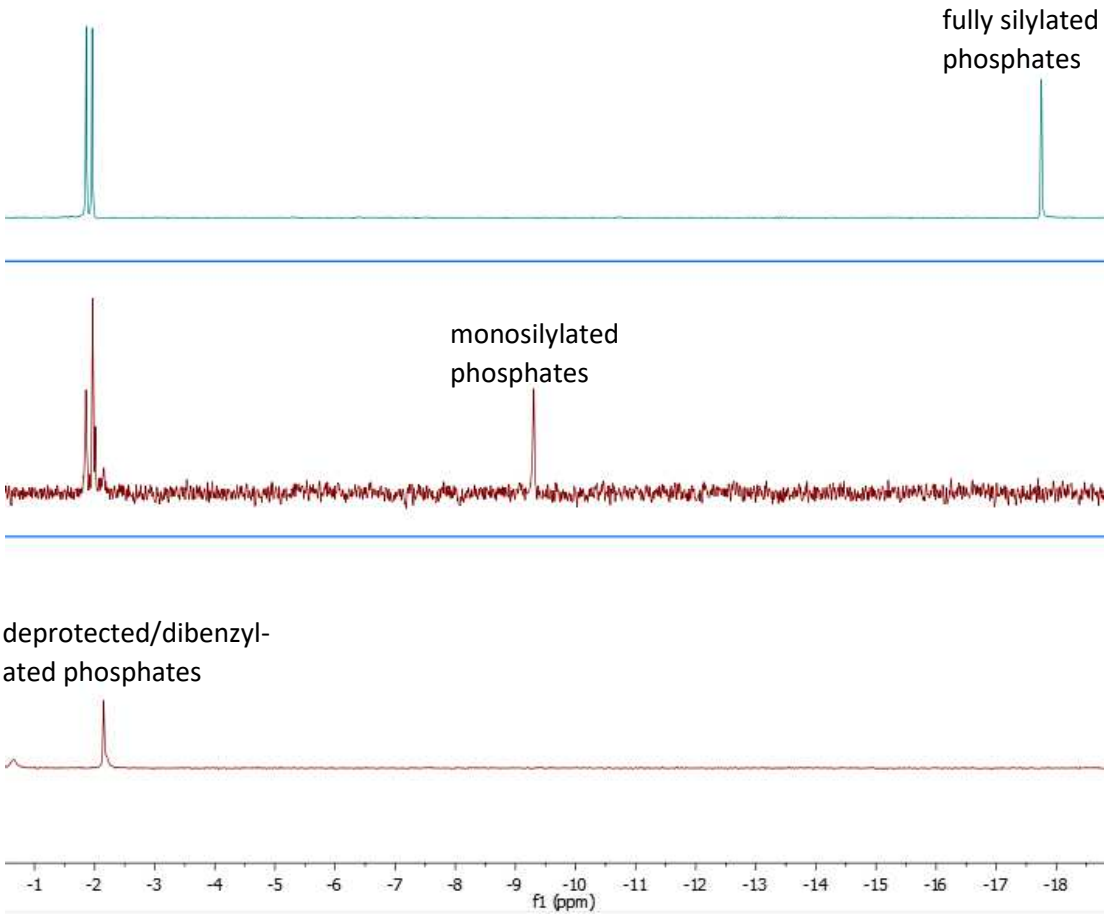

Figure 131: ^{31}PNMR spectra of different stages of the construction of the pyrophosphate group of 4-PP-Ins(1,5)P_2 (**80**) indicating signals for the fully silylated product (**105**, top row), the partially deprotected (monosilylated) intermediate (middle row), and the fully deprotected product without any remaining silyl groups (**106**, bottom row).

Following complete cleavage of the silyl groups, the product (**106**) was thoroughly dried prior to phosphorylation. In the subsequent phosphorylation, the benzyl-protected pyrophosphate was constructed at the 4-position phosphate via a P(III)-P(V) intermediate. Unlike in the analogous phosphorylation steps for the model PP-InsP compounds (**77** and **78**), this phosphorylation was followed by a short aqueous work-

up after the oxidation, as well as a very rapid purification via silica column chromatography.

Although normally omitted after the synthesis of the protected pyrophosphate product, the aqueous work-up was included in this synthetic route as it was hoped that the lower number of protected phosphates and pyrophosphates attached to the central ring would enable effective partitioning of the benzyl-protected product into the organic phase and slower hydrolysis of the pyrophosphate product. While the majority of syntheses for inositol pyrophosphates omit the aqueous work-up, there has been at least one route that incorporated a successful aqueous wash following phosphorylation.[107] As this protected pyrophosphate product appeared to be able to withstand this exposure to water without being hydrolysed, the inclusion of this aqueous work-up appeared to provide an efficient method of removing a significant amount of the organic contaminants from the crude product.

Following the aqueous work-up, the product was also purified via silica chromatography. The protected pyrophosphate precursor to 4-PP-Ins(1,5)P_2 (**107**) was expected to remain sufficiently stable during this process, as both PP-InsP_5 and PP-InsP_4 (Chapter 2) were found to withstand the column (although they became unstable immediately afterwards) and it has been previously reported that the protected precursor to 1-PP-Ins(4,5)P_2 could be purified by silica column as well.[91]

Although there was insufficient time to repeat the route to confirm, the model PP-InsP products discussed earlier (Section 6.3.2) would also likely be able to withstand an aqueous work-up following the final phosphorylation, as well as purification of the protected pyrophosphate product via silica column chromatography prior to the final debenzylation.

Care was taken to begin the hydrogenation step as quickly as possible following the column, as other inositol pyrophosphates such as 5-PP-InsP_5 (Chapter 2) were found to be unstable following purification (thought to be due to the removal of DBU). Following determination of the protected pyrophosphate product, the compound was hydrogenated for 24 hours in the presence of $NaHCO_3$. It was found that this single hydrogenation was sufficient for all of the aromatic groups to be fully cleaved from the compound and a second hydrogenation would not be necessary, unlike in the syntheses of the model PP-InsP compounds.

The reason for the complete success of this first hydrogenation is thought to be due to both the purification of the protected pyrophosphate prior to the final deprotection, as well as the positioning of the phosphate groups around the inositol ring. The silica column used to purify the benzyl-protected 4-PP-Ins(1,5)P_2 precursor (**107**) succeeded in removing many of the organic contaminants (including DBU) that were expected to slow debenzylation. The cleavage of the benzyl groups was also anticipated to be easier due to the inclusion of a 1-position phosphate group in this

compound, resulting in all of the benzyl ether groups attached to the inositol ring having a neighbouring phosphate group, which are suspected to render nearby benzyl groups more labile. The inositol pyrophosphate was then purified through RP-18 (0-10% MeCN in 0.05 M TEAB), ion exchange (0-2 M TEAB) and a final RP-18 column (0-10% MeCN in 0.05 M TEAB), before 4-PP-Ins(1,5)P_2 (**80**, Figure 132) was lyophilised and collected as an off-white glass (19% yield).

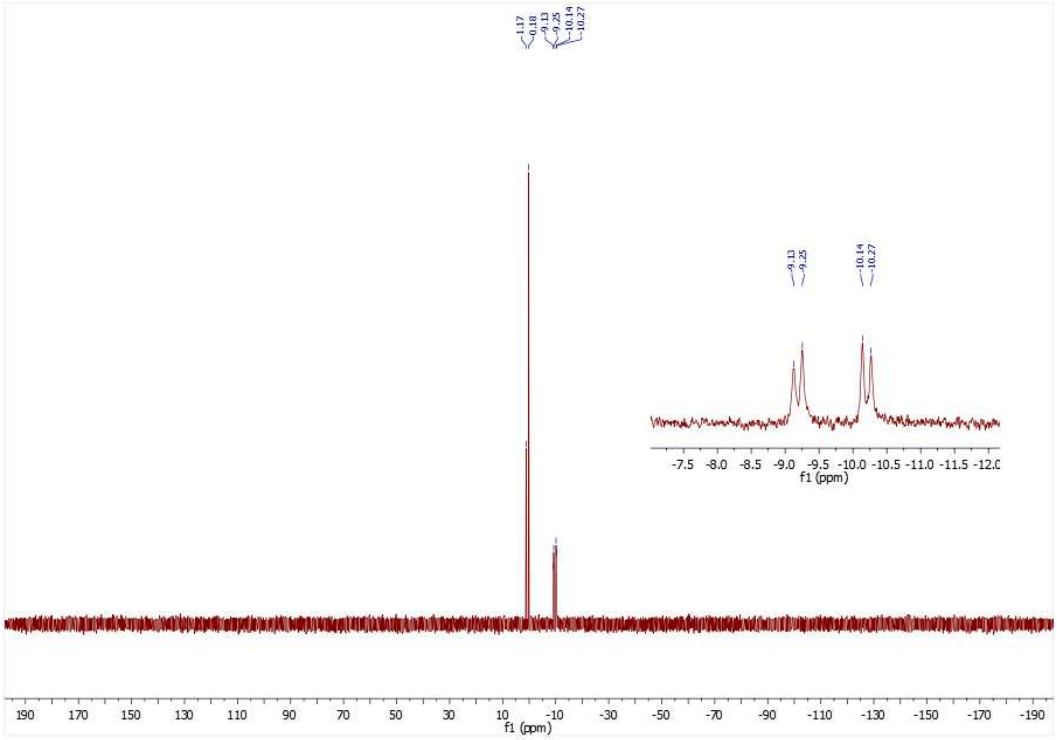

Figure 132: ^{31}PNMR spectrum of 4-PP-Ins(1,5)P_2 (**80**) following the anion exchange column, with EDTA added to the sample to sharpen the signal peaks. The EDTA was removed in the following final reverse-phase column.

There was insufficient time to find an alternate route to 5-PP-Ins(1,4)P_2 (**79**)and repeat the synthesis of both PP-InsP_2 regioisomers with chiral material during this study. The synthesis of chiral 4-PP-Ins(1,5)P_2 (**80**) and 5-PP-Ins(1,4)P_2 (**79**) will be pursued through different routes to enable both compounds to be biologically evaluated at InsP_3R at a later date, after the submission of this thesis.

6.4 Biological evaluation of PP-InsP and PP-InsP_2 compounds

Currently only the model PP-InsP compounds (**77** and **78**) have been analysed in a calcium-flux assay, as used to assess the carbohydrate-based Ins(1,4,5)P_3 analogues (Chapter 5), by our collaborator Dr Ana Rossi (University of Cambridge). The preliminary results for both 4-PP-Ins(5)P (**78**) and 5-PP-Ins(4)P (**77**) indicated that both

compounds are inactive in the $InsP_3R$ calcium release assay (Figure 133), although more detailed experiments have been planned including repeat calcium flux assays and competition binding assays.

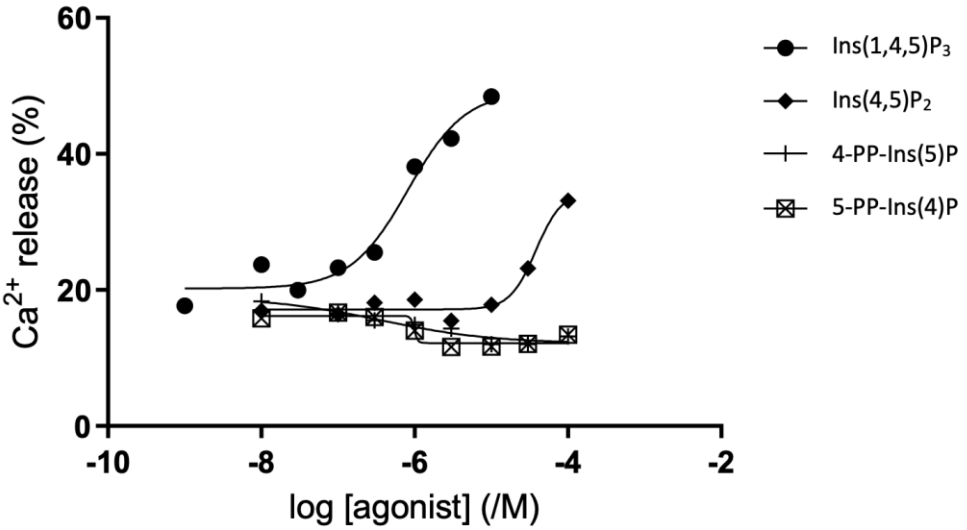

Figure 133: Preliminary calcium release study with the PP-InsP ligands [4-PP-Ins(5)P (**78**) and 5-PP-Ins(4)P (**77**)]. Data provided by Dr Ana Rossi (University of Cambridge).

The inactivity of the PP-InsP regioisomers is perhaps unsurprising, given that their close structural analogue $Ins(4,5)P_2$, has significantly lower receptor affinity due to the absence of 1-position phosphate,[258,267] and, moreover, the long-established dogma is that a vicinal 4,5-bisphosphate motif is needed for Ca^{2+}-releasing activity in flux assays. Further calcium release assays and binding competition assays will later be used to assess fully the binding affinity of these inositol pyrophosphates (**77** and **78**) at $InsP_3R$ and determine if they might potentially bind to $InsP_3R$, but not behave as agonists and instead display partial agonist or antagonist activity.

When the racemic 4-PP-$Ins(1,5)P_2$ (**80**) generated in this study is assessed at the $InsP_3R$, it will be interesting to compare its activity to that of methyl α-L-glucopyranoside 2,4,6-trisphosphate (**59**). Should it prove to be a weak full agonist rather than a partial agonist, this would not necessarily indicate that a pyrophosphate group attached at the 4-position is less suitable than the carbohydrate extended phosphate, and it may instead indicate that structural disruption at the 3-position hydroxyl is required for partial agonism.

The syntheses of chiral 4-PP-$Ins(1,5)P_2$ (**80**) and 5-PP-$Ins(1,4)P_2$ (**79**) are currently being pursued via a different method that avoids the difficult regioselective alkylation of the 4- and 5-position hydroxyls with PMB. Upon completion of these routes, both products will also be evaluated as potential $InsP_3R$ ligands.

(7) Conclusions and future work

Inositol pyrophosphates are a class of naturally-occurring compounds of which the physiological importance is steadily becoming more recognized. In this work, novel synthetic routes for the *meso myo*-inositol pyrophosphates 5-PP-InsP_5 and 5-PP-InsP_4 (Chapter 2), as well as both the racemic and chiral versions of D-1,5-$(PP)_2$-InsP_4 (Chapter 3), were successfully devised and executed.

These syntheses were carried out utilising the relatively little-used methylsulfonylethyl (MSE)-protecting group, and one particular key aim was to explore the versatility of this protecting group for this class of compound, as well as synthesize compounds for biological evaluation and exploitation. Although there are a few disadvantages to using the MSE-protecting groups [including the fact that the necessary phosphitylating agent (**1**) is not commercially available, and that products containing MSE-protected phosphates are rendered more hygroscopic], the MSE-protecting group proved to be highly useful in the syntheses of inositol pyrophosphates. Due to the ability of the MSE-protecting group to tolerate both acidic conditions and hydrogenation, a branching synthetic scheme could be developed to synthesise multiple inositol pyrophosphate products that would not be possible using some of the other previously used protecting groups orthogonal to benzyl such as β-cyanoethyl and its derivatives.[89,101,107] Also, although not commercially available, the synthesis of the MSE-phosphitylating agent (**1**) can be achieved in one simple reaction,[147] and the hygroscopic nature of the products can be overcome with careful drying conditions prior to protection of all of the inositol ring hydroxyl groups.

Following the synthesis of the first inositol pyrophosphate in this study, 5-PP-InsP_5 (**2**, Chapter 2), a sample was used in a collaboration with colleagues in the Institute of Physical-Chemistry Rocasolano in Madrid investigating the unique binding site of the diphosphoinositol polyphosphate phosphohydrolase (DDP1) yeast enzyme.[156] In this collaboration, the binding modes of the diverse substrate classes of the enzyme (dinucleotides, inorganic polyphosphates and inositol pyrophosphates) were investigated.[156] Upon co-crystallisation of the enzyme with a number of inositol pyrophosphate ligands, including 5-PP-InsP_5 (**2**), and their non-hydrolysable analogues, a variety of binding mode orientations was identified for ligands in the *Sc*DIPP1 active site, allowing for a hypothesis to be developed to explain the substrate selectivity of the enzyme for different regioisomers of inositol pyrophosphates, and more widely to explain the substrate promiscuity of the enzyme.

The 5-PP-InsP_5 (**2**) generated in this study was also used to help determine the potential scope of a europium-based pyrophosphate monitoring assay by our collaborators in Loughborough University. It was found that 5-PP-InsP_5 generates a usable luminescence emission spectrum at a reasonably low concentration, and the

pattern of peaks observed in this spectrum was subtly different to some other pyrophosphate-containing anions (ADP and PPi). After it was determined that the luminescence assay could be used to track a phosphatase simulation with systematically varying concentrations of 5-PP-InsP_5 and InsP_6, it was established that the assay could also be used to monitor real enzyme activity through tracking the dephosphorylation of 5-PP-InsP_5 by DIPP1 (although the decrease in observed intensity was less than anticipated). Further experiments are being carried out to: determine the sensitivity of the assay to 5-PP-InsP_5 in the presence of different anions; investigate the possibility of differentiating the spectra generated by different inositol pyrophosphates; investigate the limited change in luminescence emission detected in the enzyme study; as well as to determine why the intensity of the luminescence emission observed upon 1-PP-InsP_5 binding appears to be less than that generated by its regioisomer, 5-PP-InsP_5.

Multiple biological investigations involving the D-1,5-$(PP)_2$-InsP_4 (**16**) generated in this study (Chapter 3) are also currently underway, in addition to its inclusion in the investigation into the allosteric inositol polyphosphate ligand binding site of the HDAC3-SMRT deacetylase complex (see below and Chapter 4) and the investigation into the potential wider scope of the europium-based assay (Chapter 2).

The binding requirements for the previously identified *myo*-inositol 1,4,5,6-tetrakisphosphate [Ins(1,4,5,6)P_4] binding site in the histone deacetylase 3- SMRT corepressor (HDAC3-SMRT) complex were further investigated as part of this study (Chapter 4), initially through the design and synthesis of six glucose-based ligands (**36**, **37**, **39**, **39**, **40** and **41**), followed by a seventh glucose-based compound (**56**) and 1,5-$(PP)_2$-InsP_4.[112,196] A key subject of this investigation was to explore, for the first time, the potential tolerance of this binding site to carbohydrate-based polyphosphate ligands rather than natural inositol polyphosphates. This also allowed for the use of chiral sugar-based precursors that avoid potentially tedious resolution strategies for inositol phosphate precursors.

The initial investigation into the HDAC3-SMRT binding site identified four regions in the binding pocket that the phosphates of Ins(1,4,5,6)P_4 interact with (dubbed A, B, C and D), and it had been speculated that the binding site appeared to be relatively open in the crystal structure around the D region and might be able to accommodate larger groups.[62,112] The L-glucose-based compounds (**39**, **40** and **41**) were found to be able to activate the deacetylase complex to differing extents [with the tetrakisphosphate ligand (**39**) being a reasonably potent activator, while the other two ligands (**40** and **41**) proved to be less effective]. This marked the first successful activation of the HDAC3-SMRT complex with a carbohydrate. Surprisingly, however, the enantiomers of these ligands, the D-glucose-based compounds (**36**, **37** and **39**), proved to be entirely inactive. Following comparison of hypothetical binding modes for the D-glucose based series (**36**, **37** and **39**), it was theorised that the reason for their inability

to activate the enzyme complex is likely a result of the D region of the binding site [occupied by the phosphate attached to the 6-position in Ins(1,4,5,6)P_4] being less tolerant to steric bulk than initially thought and preventing their binding.

After it was found that the yeast histone deacetylase homologue, Rpd3L, appears to be activated by inositol pyrophosphates, it was speculated that inositol pyrophosphates might also be endogenous activators of the HDAC3-SMRT site.[62] Evaluation of inositol pyrophosphates [including the 1,5-$(PP)_2$-InsP_4 (**16**) synthesised in this work] showed that they were considerably weaker activators of deacetylation than Ins(1,4,5,6)P_4 or InsP_6, indicating that the natural 5-PP-InsP_5, 1-PP-InsP_5 and 1,5-$(PP)_2$-InsP_4 may not be physiologically relevant activators of HDAC3-SMRT.

Another six glucose-based ligands (**58**, **59**, **60**, **61**, **62** and **63**) were also synthesised to mimic *myo*-inositol 1,4,5-trisphosphate [Ins(1,4,5)P_3] and further probe the Ins(1,4,5)P_3 receptor [InsP_3R] (Chapter 5), with the intention to identify novel receptor agonists and partial agonists (or ideally antagonists). Two of these ligands, α-D-glucopyranosyl 1,3,4-trisphosphate (**62**) and β-D-glucopyranosyl 1,3,4-trisphosphate (**63**), were proven to be potent receptor agonists, with the latter anomer demonstrating equipotent activity to Ins(1,4,5)P_3 itself. The high affinities of both compounds for InsP_3R contribute to the base of knowledge concerning the binding of the most potent InsP_3R agonist, adenophostin A.

In addition to being agonists of InsP_3R, it was found that both of these ligands (**62** and **63**) are substrates for the *Arabidopsis* inositol tetrakisphosphate kinase-1 (ITPK1) enzyme, making them the first ever carbohydrate polyphosphate substrates identified for the enzyme. *Arabidopsis* ITPK1 is known to be a promiscuous enzyme that can phosphorylate a number of inositol phosphates to generate a number of products, even including inositol pyrophosphates.[378,380] The ability of the enzyme to phosphorylate either glucopyranosyl trisphosphate compound was somewhat surprising, however, as after the possibility of the enzyme forming a pyrophosphate had been eliminated, the two possible hydroxyl groups that could have been phosphorylated were both considered unlikely in two different ways: the phosphorylation of the 6-position would be the first instance of this kinase phosphorylating a primary hydroxyl on lower inositol phosphate analogue; while phosphorylation of the 2-position would necessitate the substrate positioning the neighbouring phosphate groups in a region of the binding site not thought to tolerate steric bulk well (the more sterically demanding inositol pyrophosphates are thought to be accommodated in a different binding plane to lower inositol phosphates).[378] Although the structures of these phosphorylated products remain to be determined conclusively, an NMR spectroscopy study of the enzyme product generated from the α-anomer (**62**) and comparison of its potential binding modes led us to posit the product is α-D-glucopyranosyl 1,3,4,6-tetrakisphosphate.

Following the ITPK1 investigation, it was found that both glucopyranosyl trisphosphates (**62** and **63**) are able to bind to the Ins(1,4,5)P_3 3-Kinase (IP_3-3K), as preliminary crystal structures of these ligands occupying the kinase active site in complex with ATP or its non-hydrolysable analogue have been obtained by the Beatriz González group. The electron densities of the glucose-based ligands in the enzyme active site seem to indicate that both ligands are slightly shifted from the position that Ins(1,4,5)P_3 binds in, so that the extended 6-position hydroxyl of the ligands can be accommodated into the phosphorylating region of the site, mimicking the 3-position hydroxyl of Ins(1,4,5)P_3. While it remains to be confirmed that these ligands are actually IP_3-3K substrates, these crystal structures lend some credence to the possibility of ITPK1 phosphorylating the primary 6-position.

Another outcome of the initial InsP_3R binding/flux activity investigations was the discovery of two new partial agonists: methyl α-L-glucopyranoside 2,3,6-trisphosphate (**58**) and methyl α-L-glucopyranoside 2,4,6-trisphosphate (**59**). Both of these ligands were found to be low-affinity, low-efficacy partial agonists that contain deviations to the accepted Ins(1,4,5)P_3 structure that are thought to result in partial agonist activity, by either interfering with the ability of the ligand to bind to the β-domain of the inositol trisphosphate binding core (IBC) or preventing the full closure of the IBC upon ligand binding due to steric interference.

The partial agonist activity of methyl α-L-glucopyranoside 2,3,6-trisphosphate (**58**) is thought to be primarily the result of the axial *O*-methyl group, which is predicted occupy the same region of the IBC as the 3-position hydroxyl of Ins(1,4,5)P_3 and therefore interfere with some of the interactions of the ligand to the β-domain, as well as act as a source of steric bulk.

The superior partial agonist found in the study (higher-affinity and lower-efficacy), methyl α-L-glucopyranoside 2,4,6-trisphosphate (**59**), is predicted to act as a partial agonist predominantly as a result of the extended methylene phosphate system behaving as the equivalent of the 4-position phosphate in Ins(1,4,5)P_3, and thereby disrupting β-domain binding and IBC closure. The partial agonist activity of this ligand could also possibly be influenced by the replacement of the 3-position hydroxyl by the pyranosyl ring oxygen (in another position that usually interacts with the β-domain), although in known SAR this modification is relatively benign.[263,299]

While the discovery of these novel L-glucose-based partial agonists (**58** and **59**) was exciting, their low affinities render them unlikely to be very useful themselves, but it is hoped that they could prove to be starting points from which structurally related, improved partial agonists or even antagonists, with lower efficacy and higher receptor affinity, could be generated. The elusive goal of designing an effective and simple small molecule antagonist has still not been met.

An attempt to generate such a structurally-inspired, improved partial agonist (or ideally an antagonist) was indeed carried out later in this study (Chapter 6). Particular interest was paid to the better of the two partial agonists, methyl α-L-glucopyranoside 2,4,6-trisphosphate (**59**), and the idea that introducing a different functional group to an equivalent to the 4-position phosphate of Ins(1,4,5)P_3 could generate partial agonists. The work in this study then came full circle through the design and synthesis of lower *myo*-inositol pyrophosphates that are hoped might function as partial agonists of InsP_3R. A series of Ins(1,4,5)P_3 analogues with disruptions to the 4-position phosphate (or 5-position phosphate) by means of incorporating a pyrophosphate were designed: 5-PP-Ins(4)P (**77**) and 4-PP-Ins(5)P (**78**) as analogues of Ins(4,5)P_2 and 5-PP-Ins(1,4)P_2 (**79**) and 4-PP-Ins(1,5)P_2 (**80**) as an analogue of Ins(1,4,5)P_3. Due to the unexpected regioselectivity in one of the steps in the reaction route, only three of the four planned compounds could be synthesised (**77**, **78** and **80**) within the available time (not 5-PP-Ins(1,4)P_2, **79**). The synthetic techniques used in the synthesis of 5-PP-InsP_5 (**2**), 5-PP-InsP_4 (**3**) and 1,5-$(PP)_2$-InsP_4 (**16**) were employed to synthesise racemic 5-PP-Ins(4)P (**77**), 4-PP-Ins(5)P (**78**) and 4-PP-Ins(1,5)P_2 (**80**). Only preliminary investigations into the activities of these compounds at InsP_3R have been carried out, but it appears as though both 5-PP-Ins(4)P (**77**) and 4-PP-Ins(5)P (**78**) are inactive in the calcium flux assay. Full biological evaluation for all three of these compounds (**77**, **78** and **80**) is currently underway.

As interest develops in the biological functions of individual inositol phosphates and pyrophosphates, further work will be required to generate these compounds, as well as chemically relevant and tailored structural analogues that can act as chemical biology tools and facilitate pharmacological investigations. Work on efficiently synthesizing inositol pyrophosphates and understanding their biology, in particular, is still in its infancy. It is hoped that the work detailed in this thesis will provide a useful contribution to the collective knowledge of both the biological roles of inositol phosphates and inositol pyrophosphates, as well as to the chemistry required to synthesise these naturally-occurring compounds and their artificial analogues.

(8) Experimental

Biological methods

*Sc*DDP1 co-crystallization

Method reported in Márquez-Moñino *et al.* study,[156] carried out by the Beatriz González lab (Institute of Physical-Chemistry Rocasolano) and reproduced below. Refer to the original study for details on protein expression and purification.

DDP1 cocrystallization with ligands. wt-DDP1 was cocrystallized by the sitting drop vapor diffusion method at 291 K, with three groups of ligands: based on inositol, polyphosphates, or adenosine. The initial crystallization conditions [20% (v/v) polyethylene glycol, molecular weight 6000, 0.1 M sodium acetate (pH 5.0), and lithium chloride] were found after setting up four commercial crystallization screenings: PACT (Jena Bioscience), Crystal Screen (Hampton Research), Index (Hampton Research), and JCSG (Jena Bioscience) using a Nanodrop robot (Innovadyne Technologies Inc.), 250:250 nL protein:precipitant drop ratio in 96-well sitting drop plates. PCT Pre-Crystallization Test (Hampton Research) was performed to optimize protein concentration at 6 mg/mL. All wt-DDP1 crystals were obtained only in the presence of any of the three groups of ligands. The best cocrystallization conditions for each ligand were discovered by optimization in 48-well plates (Hampton Research). Drop sizes and protein:precipitant ratio were adjusted for each case. Final crystallization conditions for each crystal complex are listed in table S2 in the Márquez-Moñino *et al.* study[156]. Sequentially microseeding and a protein:precipitant 3:1 ratio were necessary to improve the quality of the ScDDP1Δ*nose* crystals. Several cryoprotectants were tested, being usually the original crystallization conditions with slightly increased precipitant concentration and plus 25 to 30% (v/v) of cryo-protectant. After gradually changing the crystal drop solution by cryoprotectant solution, crystals were flash cooled in liquid nitrogen (77 K). We performed similar crystallization experiments to obtain structures for mutants and, in the case of DDP1-K63A mutant, obtained crystals in the absence of any ligand

Europium complex luminescence emission assay protocol

The protocol for the europium complex luminescence emission assay was originally written by F. A. Jamion (Loughborough University), who also carried out the

experiments. An edited version of the protocol is given below. Additional details for a number of these experiments can be found in related studies from the Butler lab group, such as Mailhot *et al*.[159]

General Procedure for the luminescence emission assay. Anion stock solutions of 5-PP-$InsP_5$ and $InsP_6$ (5 mM) were made up to 100 µL of 10 mM, pH 7.0 HEPES buffer from 0.5 µmole. Other samples received were used for anion screening, including regioisomers of $InsP_3$ and $InsP_4$ as well as 1,5-$(PP)_2$-$InsP_4$ (0.25 µmole), which were diluted to 50 µL of 10 mM, pH 7.0 HEPES buffer. PPi and glucose 6-phosphate (25 mM) were diluted by a factor of 5 to give samples in 5 mM. Solid Ins(3)P_1 was purchased from ThermoFisher (0.1 mg), and was made to a 5 mM solution in 10 mM HEPES buffer.

The luminescence generated by each sample was recorded using a Camlin Photonics luminescence spectrometer with FluoroSENS version 3.4.7.2024 software. Experimental parameters were λex = 330 nm, 1 nm increments, and 100 ms integration time. Before the anions were screened, a control was carried out in the absence of phosphate ligands with 40 µL of 5 µM europium complex. The anions (250 µM) were then added to the europium complex solution to make a total volume of 42 µL in a quartz cuvette. The emission spectra were collected for each compound from 550-720 nm. This wavelength was chosen as it was the peak of the ΔJ=2 band and gave similar results to taking the sum of the ΔJ=2 band. A graph of emission intensity versus wavelength with each anion set and probe in the absence of anions were plotted for comparison.

Anion Titrations. Known volumes of the relevant anion stock were added to 5 µM of europium complex in 10 mM, pH 7.0 HEPES in a quartz cuvette. The anion concentration increased steadily, keeping the europium complex concentration constant. The emission spectra were recorded after each addition. The emission intensities at 615 nm were plotted against anion concentration and analysed by fitting the data to a non-linear polynomial fitting procedure based on a 1:1 binding model using Origin Lab. The K_a values were calculated using the K_d (mM) values generated from the 1:1 binding curve plotted on the OriginLab 2020 (64-bit) ver. 9.7.5,184 software, multiplying it by 1000 to give K_a (M^{-1}) before conversion to a logarithmic scale ($\log K_a$) to aid in comparing the results of the anions.

Enzyme simulation assay. Solutions were made of a mixture of: 1) 5 µM europium complex, $InsP_6$, and 10 mM, pH 7.0 HEPES and 2) 5 µM europium complex, 5-PP-$InsP_5$, and 10 mM, pH 7.0 HEPES with the concentrations of the anions being 10, 25, 50, and 100 µM. These solutions were added to a plate reader, where each well equated to 40 µL. The emission values were recorded to deduce the selectivity of the assay, after which the emission values were obtained in triplicate data at 25 and 100 µM for the first 15 minutes. These measurements were recorded using a Clariostar BMGLabTech

multimode microplate reader with Clariostar MARS data analysis software ver 3.31. The additives were prepared by calculating the masses of the solid $CaCl_2$ and BSA required using their molecular masses, ensuring the solutions made up to the required volumes using 10 mM HEPES buffer. The following mixtures were made up: 1) 5 µM Europium complex, 25 µM $InsP_6$, 25 µM $CaCl_2$/ 0.2mg/mL BSA / 10% v/v DMSO, and 10 mM, pH 7.0 HEPES, and 2) 5 µM Europium complex, 25 µM 5-PP-$InsP_5$, 25 µM $CaCl_2$/ 0.2mg/mL BSA / 10% v/v DMSO, and 10 mM, pH 7.0 HEPES. These solutions were added to a plate reader where each well equated to 40 µL and the emission values were recorded for the first 15 minutes using a Clariostar BMGLabTech multimode microplate reader with Clariostar MARS data analysis software ver 3.31.

Phosphatase enzyme reaction. To 36.8 µL of solution containing 5-PP-$InsP_5$ (100 µM), europium complex (5 µM) Na_2EDTA (1 mM), KCl (50 mM) and BSA (0.05 mg/mL) in 50 mM HEPES at pH 7.047 in a 384-well plate, 3.2 µL of phosphatase solution (1.6 µg) or HEPES solution was added. The plate was read immediately, with luminescence measurements taken with excitation at 292 – 366 nm, and emission using time-resolved measurements at 615 – 625 nm using an integration time of 60 – 400 µs at 5-minute time intervals for the first hour, then every 15-minutes in the following 1-7 hours. Assays were run in triplicate, and the averaged ratio values were taken and plotted against time. Where appropriate, photobleaching (no enzyme) experiments were taken away from experiments containing phosphatase.

HPLC protocol

The HPLC protocol was reported in the Shipton *et al*.[335] study, carried out by Prof Charles Brearley (University of East Anglia) and reproduced below. This method describes the analysis of the glucose-derived inositol phosphate analogues (Chapter 5), but was also adapted to analyse the samples of racemic and chiral 1,5-$(PP)_2$-$InsP_4$ (Chapter 3).

For analysis and stability experiments, the sugar phosphates were resolved by anion-exchange HPLC on a 3 × 250 mm CarboPac PA200 column (Dionex) fitted with 3 × 50 mm guard cartridge of the same material. Compounds were eluted with a gradient derived from buffer reservoirs containing water (A) and 0.6 M methanesulfonic acid (B) delivered at a flow rate of 0.4 mL min−1 according to the following schedule: time (min), % B; 0, 0; 20, 80; 21, 0; and 31, 0. Compounds were detected with the phosphate detection reagent of Phillippy and Bland.[58] For this purpose, the column eluate was mixed in a mixing Tee with a solution of 0.1% (w/v) ferric nitrate nonahydrate in 2% (w/v) perchloric acid delivered at a flow rate of 0.2 mL min^{-1} and passed through a 0.192 mL internal volume knitted reaction coil before being transferred to a UV

detector set at 290 nm. Typically, samples of 40 µL of 500 µM solutions in water were injected. Data were exported from the ChromNav2 software as x,y data files and redrawn in GraFit.v7.73

HDAC3-SMRT activity assay protocol

The protocol for the HDAC assay which was carried out by Dr Jennifer Gurnett, Dr Yun Song and Mr Ed Brown (University of Leicester), was adapted from the original Watson *et al*.[112] Refer to the original study for details on protein preparation.

HDAC Activity Assays. The purified HDAC3-SMRT complex (0-400 nM) was incubated with BOC-Lys-AMC substrate (100 µM, BaChem) in a final volume of 50 µl buffer A (50 mM Tris/Cl pH 7.5, 50 mM NaCl, 5% glycerol) for 30 min at 37 °C in a 96-well plate (Corning). To test the ability of the inositol phosphates and other analogues to activate the HDAC3-SMRT complex, the HDAC3-SMRT complex (50-100 nm) was incubated with 100 µM of the potential ligands for 30 min at 37 °C before addition of the BOC-Lys-AMC substrate. Following incubation with the BOC-Lys-AMC substrate, the assay was then developed with the addition of 50 µl of developer buffer (50 mM Tris/Cl PH 7.5, 100 mM NaCl, 10 µg/µl trypsin), which had 2 µM of Trichostatin A (TSA), an HDAC inhibitor, added immediately prior to the developer buffer being added to the wells. HDAC activities were measured by detecting fluorescence using a Victor X5 plate reader (Perkin Elmer) with an excitation wavelength of 335 nm and an emission wavelength of 460 nm. All measurements were performed in triplicate and the data analysed using GraphPad Prism (version 7.0, GraphPad Software, Inc).

Ins(1,4,5)P_3R assay protocol

Calcium release assay

Method reported in Shipton *et al*.[335] study, carried out by Dr Ana Rossi (University of Cambridge) and reproduced below. Refer to the original study for details on cell culture and data analysis.

Ca^{2+} Release Assays. The free [Ca^{2+}] within the lumen of the endoplasmic reticulum (ER) was measured using the low-affinity Ca^{2+} indicator Mag-fluo-4.[409,410] The ER of

HEK-Ins(1,4,5)P_3R1 cells was loaded with the Ca^{2+} indicator by incubating cells (2.4 x 10^7 cells/mL, 1 h, 22°C) in HEPES-buffered saline (HBS; 135 mM NaCl, 5.9 mM KCl, 11.6 mM HEPES, 1.5 mM $CaCl_2$, 11.5 mM glucose, 1.2 mM $MgCl_2$, pH 7.3) supplemented with BSA (1 mg/mL), Pluronic F127 (0.4 mg/mL) and Mag-fluo-4 AM (20 μM). Cells were then suspended in Ca^{2+}-free cytosol-like medium (CLM: 20 mM NaCl, 140 mM KCl, 1 mM EGTA, 20 mM Pipes, 2 mM $MgCl_2$, pH 7.0) and permeabilized with saponin (10 μg/mL, 3 min, 37°C). Permeabilized cells were centrifuged (650 xg, 3 min), and incubated in CLM (7 min, 37°C) to allow the Ca^{2+} stores to empty. Cells were then centrifuged (650 xg, 3 min) and re-suspended in CLM without Mg^{2+}, but supplemented with 375 μM $CaCl_2$ to give a final free [Ca^{2+}] of 220 nM after addition of 1.5 mM MgATP. Cells (~4 x 10^5/well) were added to poly-L-lysine-coated half-area 96-well black-walled plates. Fluorescence was recorded at 20 °C at intervals of 1.44 s using a FlexStation III plate-reader (Molecular Devices, Sunnyvale, CA, USA) with excitation and emission wavelengths of 485 nm and 520 nm, respectively. MgATP (1.5 mM) was added to initiate Ca^{2+} uptake, and when the ER had loaded to steady-state (~2.5 min), *cyclopiazonic acid* (*CPA, 10* μM) was added to inhibit the ER Ca^{2+} pump. Ins(1,4,5)P_3 or other ligands were added after a further 60 s. The amount of Ca^{2+} released was calculated as a percentage of the fluorescence signal from fully loaded stores (F_{full}) minus the signal from non-loaded stores ($F_{full} - F_{empty}$).

Competition binding assay

Method reported in Shipton *et al*.[335] study, carried out by Dr Ana Rossi (University of Cambridge) and reproduced below. Refer to the original study for details on cell culture and data analysis.

[^{3}H]-Ins(1,4,5)P_3 binding to cerebellar membranes. Cerebellar membranes, which are rich in Ins(1,4,5)P_3R1, were prepared from the cerebella of adult Wistar rats. Frozen cerebella were homogenized at 4°C in homogenization medium (HM: 1 mM EDTA, 50 mM Tris, protease inhibitors, pH 8.3) supplemented with 100 mM NaCl. After centrifugation (130,000 x*g*, 1 hr, 4°C), the membranes were resuspended in HM (~6 mg protein/mL) and stored at -80°C. Equilibrium-competition binding assays were performed at 4°C in a final volume of 500 μL of Tris-EDTA medium (TEM: 50 mM Tris, 1 mM EDTA, pH 8.3) with [^{3}H]-Ins(1,4,5)P_3 (19.3 Ci/mmol, 1.5 nM), competing ligands and 25 μL of membranes.[250] After 5 min, during which equilibrium was attained, bound and free ligand were separated by centrifugation (20,000 xg, 5 min, 4°C), the pellet was then rinsed and resuspended in TEM (200 μL) before liquid scintillation counting (1 mL, Ecoscint-A). Non-specific binding, determined by addition of 10 μM Ins(1,4,5)P_3 was always <10% of total binding, and <10% of the added [^{3}H]-Ins(1,4,5)P_3 was bound.

Sea urchin egg homogenate (SUEH) assay

The SUEH assay was prepared with Dr Lianne Davis (University of Oxford), using the method described by Morgan and Galione.[369] Refer to the original study for details on egg collection, preparation and homogenization.

The sea urchin (*Lytechinus pictus*) egg homogenate (50% v/v), initially stored at -80°C, was warmed to RT gradually over approx. 3 h and diluted 20-fold (allowing for the Ca^{2+} stores to load optimally) with Glucamine Intracellular Medium (GluIM) and ATP-regenerating system [NMDG, potassium gluconate, $MgCl_2$, HEPES pH 7.2, ATP, CPK, PCr]. To this solution, the fluorescent Ca^{2+} indicator, Fluo-3-Ca^{2+}, was added as well. The homogenate was then carefully pipetted into a semi-micro cuvette with a micro-flea stirring in the bottom. A LS-50B Perkin Elmer fluorescence spectrometer was then used to measure the fluorescence detected in the cuvettes: before the addition of anything (control), after the addition of ligand (response), after the addition of EDTA (calibration minimum, F_{min}) and after the addition of $CaCl_2$ (calibration maximum, F_{max}). The amount of calcium released upon the addition of each ligand could then be calculated by from the detected fluorescence emissions of each sample with the following equation:

$$[\mathrm{Ca}^{2+}] = K_d \times \frac{(F - F_{min})}{(F_{max-F})}$$

Where the $[Ca^{2+}]$ is given in the same units as the K_d value (0.4 µM or 400 nM for fluo-3).

ITPK1 assay

The protocol for the ITPK1 assay was originally written by Dr Hayley Whitfield (University of East Anglia), who also carried out the experiments. The method is an adaption of the ITPK1 assay described in Whitfield *et al.*[378] Refer to the original study for details on protein preparation.

Determining whether sugar phosphates are ITPK1 substrates. AtITPK1 (33.6 µM) was incubated in 10 mM HEPES pH 7.5, 1 mM $MgCl_2$ under regenerating conditions with 1 mM sugar phosphate substrate, 5 mM phosphocreatine, 3 U creatine kinase and 1 mM ATP at 25 °C for various time points between 20 mins and overnight. Assays were stopped by the addition of an equal volume of 60 mM $(NH_4)_2HPO_4$ pH 3.5. Samples were clarified by centrifugation at 14 000×***g*** for 5 min and 50 µL injected for HPLC analysis.

Optimised ITPK1 turnover for experiments requiring complete conversion of the sugar phosphate. The ITPK1 assay was repeated as described but used only 1.5 mM phosphocreatine and 0.25 mM ATP and was allowed to take place overnight.

IP3-3K co-crystallisation

The protocol for the IP_3-3K co-crystallisation was originally written by Professor Beatriz González (Institute of Physical-Chemistry Rocasolano), who also carried out the experiments with her group. The IP_3-3K catalytic domain (residues 183-461) was purified following the reported protocol in Franco-Echevarría *et al*.[255]

IP_3-3K (18 mg/ml) was crystallized in 0.81-0.84M sodium citrate + 0.1M Tris pH 8.5, using vapor diffusion technique in a sitting drop set-up. Crystals appeared from 3-7 days and streak seeding was required to reproduce them effectively. The mother liquor was exchanged very slowly with the soaking solution (1.5M LiSO4 + 3mM ATP or AMP-PNP + 3 mM $MgCl_2$ or $MnCl_2$ + 5mM $InsP_3$ analogue)*. The crystals were left 2 hours in soaking solution after which they were frozen and data collection was performed at ID23-1 ESRF (α-D-glucopyranosyl 1,3,4-trisphosphate) and ALBA (β-D-glucopyranosyl 1,3,4-trisphosphate) synchrotrons. The data was processed with XDS, solved by Fourier difference synthesis using the structure of IP_3-3K catalytic domain (PDB: 1W2C),[255] and refined with Refmac (ccp4 suite). The model building in electron density maps was performed using coot.

* The α-D-glucopyranosyl 1,3,4-trisphosphate was soaked with ATP and $MnCl_2$; The β-D-glucopyranosyl 1,3,4-trisphosphate was soaked with AMP-PNP and $MgCl_2$.

Chemical Methods

GOLD Molecular Modelling

GOLD (Genetic Optimisation for Ligand Docking) is a program designed by the Cambridge Crystallographic Data Centre that employs a non-deterministic genetic algorithm to find favourable binding modes for ligands inserted into a specified binding site in a protein crystal structure.[411] GOLD is a very popular program used in protein-ligand docking for structure-based virtual screening.[412,413] The genetic algorithm that is the basis for GOLD was originally designed to focus on the hydrogen bonds that form between the binding site and the ligand, but also takes into account: the total acyclic ligand flexibility; limited cyclic ligand flexibility; and limited flexibility of the residues within the binding site; with even more interactions being recognised in later versions. Crucially, the program also accounts for the required displacement of weakly bound water molecules from the binding site upon successful docking of a ligand through inclusion of an energy penalty in the calculations.[411,414]

Small molecule ligands, drawn and minimized (in this work using Chemdraw 3D and Mercury programs), can be docked into binding sites by GOLD. In an attempt to avoid bias in the docking results, prior to insertion of the ligand into the binding site, the ligand undergoes a random translation and the rotatable bonds are randomised with regard to rotational and torsional degrees of freedom.[411] The docking solutions for each ligand are returned, having received a 'fitness' score that indicates how well the ligand is able to slot into the binding site of the protein. There are numerous parameters that can be altered to improve the accuracy of ligands binding to a crystal structure. Docking protocols are typically considered to be successful if the native ligand can be reinserted into the binding site with a RMSD of less than 2 Å.[412,413]

The GOLD program offers a number of different scoring and rescoring functions that can be used to determine the ability of the ligand to fit into the binding site. Each of these scoring functions uses different criteria to determine the fitness of a docking solution. For different binding site-ligand combinations, different criteria will be most appropriate and deliver the most reliable results. The scoring function for each docking result is used by the algorithm to mimic evolution and aid in the generation of high-scoring solutions (but the rescoring function value is not included in calculations for further results). In the docking protocols used in this study, it was found that the best results were generated when Goldscore was used as the scoring function and ChemPLP was used to rescore. Goldscore is a force field-based, molecular-mechanics-like scoring function originally designed for the GOLD program; it usually performs best when the interaction between the ligand and the binding site

is dominated by the formation of hydrogen bonds (ionic hydrogens in particular, in favour of neutral hydrogen bonds).[412,413] ChemPLP is an empirical scoring function which relies on steric factors to determine interactions between residues in the binding pocket and the ligand.[413] One of the limitations of an empirical scoring function is that larger ligands tend to have higher scores as a result of being able to form a greater number of non-specific interactions with the binding site.[412]

The GOLD program has been found to be less accurate when docking large, flexible, hydrophobic ligands.[411] Insufficiently high resolution of the crystal structure used in docking will also result in lower quality results and may be indicative of high mobility of the protein. Increased mobility of the protein residues could suggest that there may not be a well-defined binding mode for the ligands, resulting in difficulties in predicting docking solutions through computational means in some cases.[411,412]

Fortunately, the ligands docked into either the $InsP_3R$ binding site or HDAC3-SMRT binding site in this study are highly polar, and the resolution of both crystal structures used are reasonably high (1N4K: 2.2 Å and 4A69: 2.06 Å respectively for the PDB structures), so it was predicted that GOLD would be a suitable modelling program.[196,247] Both docking simulations were carried out in version 5.5 of GOLD with optimised protocols.

Docking for the HDAC3-SMRT Investigation

The HDAC3-SMRT PDB file (4A69)[196] was prepared prior to use in the GOLD ligand docking simulation through deletion of one half of the dimer, removal of the majority of the water molecules outside of the binding site and correction of the tautomeric states of the histidine residue side chains.

The docking settings were initially optimised through identifying settings that best favoured reinsertion of Ins(1,4,5,6)P_4 into the HDAC3-SMRT binding site crystal structure. Following the HDAC3-SMRT assay results of the first six D- and L-glucose-based compounds, the settings were further improved such that the docking simulation somewhat reflected activities of the synthesised ligands. If not explicitly mentioned, any other conditions used in the GOLD docking were on the default settings.

From the position of the extracted reference ligand, Ins(1,4,5,6)P_4, the binding site was determined to extend by a radius of approximately 10 Å. Within this established binding site, there are six residues with long, flexible side chains: Lys25, Lys449, Lys474, Lys475, Arg265 and Arg301. The best results were found when the lysine

residue side chains were allowed to rotate according to the rotatory library settings and the arginine residue side chains were allowed constrained rotation, thereby mimicking the flexible nature of the binding site. Taking into account the flexibility of the Arg265 residue side chain in particular is especially important for the HDAC3-SMRT Ins(1,4,5,6)P_4 binding site, as this residue side chain participates in the formation of a salt bridge upon activator binding, and this induces a conformational change leading to the activation of the complex.[112]

Four water molecules within the HDAC3-SMRT Ins(1,4,5,6)P_4 binding site were identified as being potentially involved in ligand binding: 2009, 2010, 2120 and 2121. The best results were achieved when the 2009 and 2010 waters were removed, and the 2120 and 2121 waters were allowed to toggle and spin in place. The 2120 and 2121 waters happened to have lower b-factors, indicating that the positioning and presence of these water molecules is more certain in the binding site (Figure 134).

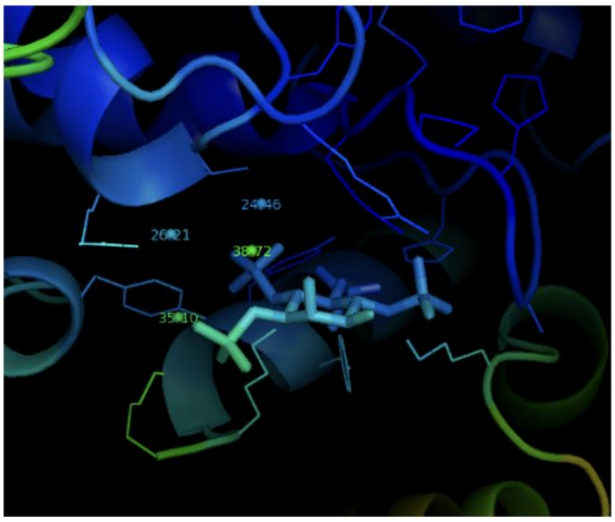

water	b-factor
2009	35.10
2010	38.72
2120	24.46
2121	26.21

Figure 134: Ins(1,4,5,6)P_4 bound to the HDAC3-SMRT inositol phosphate binding site coloured to indicate the b-factors of the ligand, protein crystal structure and four important water molecules that are involved in binding. A table is provided to give the numerical values for the b-factors of the four water molecules with the two waters that have lower b-factors highlighted in yellow. The highlighted water molecules, 2120 and 2121, were allowed to toggle and spin in the docking protocol, while the other two water molecules were removed from the simulation.

Because the algorithm used in GOLD is non-deterministic, each ligand was docked 100 times to yield a range of results enabling the most suitable docking modes to be identified.[411] Early termination of the genetic algorithm upon production of the same binding solution was not allowed. The RMSD for binding was calculated for each ligand docking result compared to the docking of the native Ins(1,4,5,6)P_4 ligand originally extracted from the crystal structure.

Goldscore was used as the scoring function, and the ChemPLP function was used to rescore the results. With the Goldscore scoring option, the ligands with more phosphate groups (such as all of the regioisomers of $InsP_7$ molecules and their PCP mimics) consistently outperformed all of the carbohydrate-based ligands, as expected for a scoring function that favours the formation of hydrogen bonds. When the ChemPLP scoring function was used to rescore the results, the highest-scored ligand was consistently methyl 6-*O*-Bn α-L-glucopyranoside as expected for a scoring function that places more emphasis on hydrophobic interactions.

Docking Solution Identifier	PLP.Fitness	Goldscore.Fitness	Reference.RMSD
129|3-PP-InsP5|mol2|1|dock3|1	5.3011	180.2509	4.0441
134|3-PP-InsP5|mol2|1|dock8|1	-16.3606	178.7532	3.4583
515|3-PP-InsP5|mol2|1|dock92|1	-7.0018	178.4118	3.2334
268|1-PP-InsP5|mol2|1|dock34|1	9.3433	175.9407	3.1374
955|6-O-Bn-3-PCP-InsP5|mol2|1|dock57|1	43.0454	175.2286	5.3936
487|3-PP-InsP5|mol2|1|dock64|1	-12.712	174.256	3.1416
660|1-PCP-InsP5|mol2|1|dock56|1	1.3397	171.7969	3.0488
245|1-PP-InsP5|mol2|1|dock11|1	-12.0668	171.5941	2.9312
756|3-PCP-InsP5|mol2|1|dock60|1	15.8947	171.4371	1.6025
267|1-PP-InsP5|mol2|1|dock33|1	40.8393	170.9385	3.2144
573|5-PP-InsP5|mol2|1|dock60|1	36.0928	170.3174	1.5223
479|3-PP-InsP5|mol2|1|dock56|1	-15.1016	169.9098	3.2645
517|3-PP-InsP5|mol2|1|dock94|1	0.8507	169.7497	3.0104
913|6-O-Bn-3-PCP-InsP5|mol2|1|dock15|1	-31.6617	169.7301	5.4521
1332|Me_a_L_glucp4|mol2|1|dock35|1	39.5511	169.0041	4.8526
291|1-PP-InsP5|mol2|1|dock57|1	-10.3014	169.0019	2.9828
117|1-PP-InsP5|mol2|1|dock9|1	8.8236	168.8252	4.7159
1341|Me_a_L_glucp4|mol2|1|dock44|1	41.0672	167.4383	4.8565
83|InsP6|InsP6|mol2|1|dock84|1	16.559	167.3175	2.9906
279|1-PP-InsP5|mol2|1|dock45|1	37.2045	167.2221	2.9916
475|3-PP-InsP5|mol2|1|dock52|1	-9.9392	166.6303	3.1359
239|1-PCP-InsP5|mol2|1|dock5|1	11.8266	166.5328	2.5535
800|4-O-Bn-1-PCP-InsP5|mol2|1|dock1|1	47.3869	165.5774	5.0825
569|5-PP-InsP5|mol2|1|dock56|1	-21.6822	165.2986	3.0265
751|3-PCP-InsP5|mol2|1|dock55|1	5.3012	165.2937	4.3958
1399|Me_a_L_glucp4|mol2|1|dock100|1	32.1777	165.2517	5.0011
1355|Me_a_L_glucp4|mol2|1|dock58|1	47.0919	164.9642	4.9006
443|3-PP-InsP5|mol2|1|dock20|1	15.4121	164.2793	2.9778
130|3-PP-InsP5|mol2|1|dock4|1	-10.9448	164.0228	3.1139
488|3-PP-InsP5|mol2|1|dock65|1	25.5159	164.0082	4.3708

Table 15: The 30 highest-scoring docking solutions of the initial HDAC3-SMRT ligands (Chapter 4) in the HDAC3 model ranked according to Goldscore Fitness.

Docking Solution Identifier	PLP.Fitness	Goldscore.Fitness	Reference.RMSD
1467|6_Bn_Me_a_D_glucp3|mol2|1|dock59|1	27.1245	80.7543	5.9563
878|4-O-Bn-1-PCP-InsP5|mol2|1|dock70|1	-33.5017	80.5874	6.0251
1506|6_Bn_Me_a_D_glucp3|mol2|1|dock98|1	29.567	80.5606	5.4484
926|6-O-Bn-3-PCP-InsP5|mol2|1|dock28|1	-4.6308	80.5465	4.9296
1443|6_Bn_Me_a_D_glucp3|1|dock35|1	32.9783	80.0643	5.7111
1013|Me_a_L_glucp3|mol2|1|dock5|1	-0.4888	80.0625	4.9547
1463|6_Bn_Me_a_D_glucp3|1|dock55|1	15.8225	79.9775	6.075
1499|6_Bn_Me_a_D_glucp3|mol2|1|dock91|1	19.5074	79.8722	5.1188
1146|Me_a_L_glucp3| mol2|1|dock30|1	3.0373	79.5519	4.9202
1517|6_Bn_Me_a_L_glucp3|mol2|1|dock19|1	2.2445	79.4685	4.9125
1029|Me_a_D_glucp3| mol2|1|dock12|1	14.8036	79.2081	5.5296
1116|Me_a_D_glucp3| mol2|1|dock99|1	16.3114	79.1191	5.2189
1591|6_Bn_Me_a_L_glucp3|mol2|1|dock93|1	12.6246	78.9322	4.9664
1186|Me_a_L_glucp3|mol2|1|dock70|1	2.3859	78.9289	4.9997
1505|6_Bn_Me_a_D_glucp3|mol2|1|dock97|1	34.3135	78.8618	5.4306
1594|6_Bn_Me_a_L_glucp3|mol2|1|dock96|1	24.1063	78.4397	5.0099
925|6-O-Bn-3-PCP-InsP5|mol2|1|dock27|1	-14.6399	78.2763	4.9343
1490|6_Bn_Me_a_D_glucp3|mol2|1|dock82|1	38.438	78.1835	4.9845
1586|6_Bn_Me_a_L_glucp3|mol2|1|dock88|1	5.118	77.4502	5.2483
1211|Me_a_L_glucp3|mol2|1|dock95|1	18.9508	76.9449	4.82
1503|6_Bn_Me_a_D_glucp3|mol2|1|dock95|1	28.1491	76.8549	5.1654
1209|Me_a_L_glucp3| mol2|1|dock93|1	11.0424	76.1978	5.0075
1543|6_Bn_Me_a_L_glucp3|mol2|1|dock45|1	29.3602	76.0841	6.0239
960|6-O-Bn-3-PCP-InsP5|mol2|1|dock62|1	1.5867	74.8895	5.1032
1414|6_Bn_Me_a_L_glucp3|mol2|1|dock6|1	1.9405	74.3463	5.0093
1587|6_Bn_Me_a_L_glucp3|mol2|1|dock89|1	15.3097	72.3868	4.892
1457|6_Bn_Me_a_D_glucp3|mol2|1|dock49|1	-8.8606	70.9685	5.3101
1540|6_Bn_Me_a_L_glucp3|mol2|1|dock42|1	13.1143	68.9288	5.1436
1092|Me_a_D_glucp3| mol2|1|dock75|1	6.2716	68.6459	5.2811
905|4-O-Bn-1-PCP-InsP5|mol2|1|dock97|1	9.6392	61.9439	5.5029

Table 16: The 30 lowest-scoring docking solutions of the initial HDAC3-SMRT ligands (Chapter 4) in the HDAC3 model ranked according to Goldscore Fitness.

Docking for the $InsP_3R$ investigation

The GOLD settings for docking ligands into $InsP_3R$ were first optimised through docking $Ins(1,4,5)P_3$ and adenophostin A, and then further improved with the results generated by the six glucose-based ligands synthesised in this study. As before, if not explicitly mentioned, the docking conditions used were set to the default settings.

It was found that the most accurate results were achieved when all of the lysine residue side chains in the binding site were allowed constrained rotation, while all of the remaining residues were kept rigid (including even the flexible arginine residues). Inclusion of internal H bonds in the ligands also proved to improve the accuracy of the results.

Of the seven water molecules originally allowed in the binding site, only two (1139 and 1198) were allowed to toggle and spin and the rest were removed in the final docking conditions. One of the water molecules, 1139, had the lowest b-factor, indicating that its position was most certain (rendering its inclusion in the docking procedure logical). Surprisingly, it was found that the most accurate modelling conditions were then achieved when the water molecule with the highest b-factor, 1198, was included as well (Figure 135).

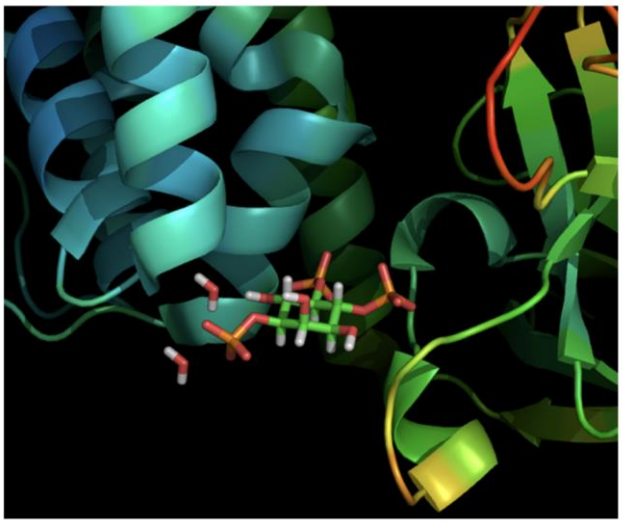

water	b-factor
1126	26.62
1128	34.30
1139	19.02
1146	26.97
1148	28.92
1157	33.11
1198	43.16

Figure 135: Ins(1,4,5)P_3 (green) bound in the InsP_3R binding site coloured to indicate the b-factors of the residues in the binding site with the two waters involved in the docking protocol explicitly shown (1139 and 1198). The orange loop in the bottom right corner contains the residue arginine 269 and the large red loop in the top right corner contains the lysine 412 residue.

Again, as in the case of the docking conditions for the HDAC3-SMRT Ins(1,4,5,6)P_4 analogues, the Goldscore function was used to score the results of the InsP_3R docking, and ChemPLP was used to rescore.

Docking solution Identifier	PLP.Fitness	Goldscore.Fitness	Reference.RMSD
2|1,4,5-IP3|mol2|1|dock3|1	76.2071	144.0946	0.6666
0|1,4,5-IP3|mol2|1|dock1|1	75.2336	143.7598	0.828
113|Beta anomeric|mol2|1|dock14|1	76.0397	143.1274	5.0282
1|1,4,5-IP3|mol2|1|dock2|1	75.6088	142.8951	0.7795
109|Beta anomeric|mol2|1|dock10|1	73.9057	142.8053	5.043
170|Beta anomeric|mol2|1|dock71|1	76.5656	142.4204	5.0426
6|1,4,5-IP3|mol2|1|dock7|1	77.614	142.4095	0.878
4|1,4,5-IP3|mol2|1|dock5|1	76.9376	142.0455	0.8073
187|Beta anomeric|mol2|1|dock88|1	76.8526	141.5897	5.0229
75|1,4,5-IP3|mol2|1|dock76|1	80.864	141.4267	0.4238
29|1,4,5-IP3|mol2|1|dock30|1	77.6565	141.4021	0.7018
24|1,4,5-IP3|mol2|1|dock25|1	81.1515	141.3651	0.4603
27|1,4,5-IP3|mol2|1|dock28|1	77.8962	141.333	0.8302
63|1,4,5-IP3|mol2|1|dock64|1	79.8225	141.0763	0.5075
20|1,4,5-IP3|1|dock21|1	76.1674	140.9011	0.4305
156|Beta anomeric|mol2|1|dock57|1	76.7562	140.8102	5.0297
67|1,4,5-IP3|mol2|1|dock68|1	78.6379	140.7387	0.5635
28|1,4,5-IP3|mol2|1|dock29|1	77.5123	140.7238	0.6936
57|1,4,5-IP3|mol2|1|dock58|1	77.047	140.5989	0.754
120|Beta anomeric|mol2|1|dock21|1	76.9456	140.3755	5.02
225|Me-L-Glu-2,3,6-P3|1|dock8|1	76.0172	140.3659	5.5509
77|1,4,5-IP3|mol2|1|dock78|1	79.9486	140.237	0.573
100|Beta anomeric|mol2|1|dock1|1	74.1735	140.2146	5.0789
59|1,4,5-IP3|mol2|1|dock60|1	78.3478	140.1901	0.72
475|Me-L-Glu-2,3,6-P3|mol2|1|dock69|1	80.2752	140.1814	5.5486
18|1,4,5-IP3|mol2|1|dock19|1	80.135	140.1665	0.7384
13|1,4,5-IP3|mol2|1|dock14|1	77.165	140.0412	0.6965
11|1,4,5-IP3|mol2|1|dock12|1	77.5192	139.805	1.1024
62|1,4,5-IP3|mol2|1|dock63|1	77.0284	139.5856	0.7147
65|1,4,5-IP3|mol2|1|dock66|1	78.2137	139.5434	0.7104

Table 17: The 30 highest-scoring docking solutions of the carbohydrate-based ligands (Chapter 5) and Ins(1,4,5)P_3 in the InsP_3R model ranked according to Goldscore Fitness.

Docking solution Identifier	PLP.Fitness	Goldscore.Fitness	Reference.RMSD
628|alpha-D-Glu-1,3,4-P3|mol2|1|dock29|1	68.289	102.0187	4.6008
209|Me-D-Glu-2,4,6-P3|mol2|1|dock1|1	22.2542	101.9949	5.6775
525|Me-L-Glu-2,4,6-P3|mol2|1|dock29|1	52.0898	101.4402	5.0842
367|Me-D-Glu-2,4,6-P3|mol2|1|dock51|1	36.2068	101.4392	4.9944
638|alpha-D-Glu-1,3,4-P3|mol2|1|dock39|1	42.328	101.3805	5.7381
351|Me-D-Glu-2,4,6-P3|mol2|1|dock35|1	48.9369	101.2505	5.042
691|alpha-D-Glu-1,3,4-P3|mol2|1|dock92|1	45.1903	101.2418	5.7676
688|alpha-D-Glu-1,3,4-P3|mol2|1|dock89|1	46.1228	101.1296	5.7238
597|Me-D-Glu-2,4,6-P3|mol2|1|dock100|1	29.6391	101.0877	4.6268
269|Me-D-Glu-2,3,6-P3|mol2|1|dock43|1	46.1821	101.0754	4.865
660|alpha-D-Glu-1,3,4-P3|mol2|1|dock61|1	46.5867	101.0535	5.7181
302|Me-D-Glu-2,3,6-P3|mol2|1|dock76|1	47.3934	100.4782	4.8599
462|Me-L-Glu-2,3,6-P3|mol2|1|dock56|1	39.6875	100.0309	4.5337
241|Me-D-Glu-2,3,6-P3|mol2|1|dock15|1	54.8642	99.9607	5.7325
237|Me-D-Glu-2,3,6-P3|mol2|1|dock11|1	58.6783	99.8919	5.4579
496|Me-L-Glu-2,3,6-P3|mol2|1|dock90|1	49.6639	99.5243	6.2108
363|Me-D-Glu-2,4,6-P3|mol2|1|dock47|1	52.4031	99.2003	4.9814
640|alpha-D-Glu-1,3,4-P3|mol2|1|dock41|1	43.6799	98.7296	5.7093
428|Me-L-Glu-2,3,6-P3|mol2|1|dock22|1	41.4496	98.4082	5.2196
360|Me-D-Glu-2,4,6-P3|mol2|1|dock44|1	33.4203	98.1898	4.8694
204|Me-D-Glu-2,3,6-P3|mol2|1|dock5|1	43.2129	97.9608	4.7017
266|Me-D-Glu-2,3,6-P3|mol2|1|dock40|1	57.1419	97.6416	5.3888
371|Me-D-Glu-2,4,6-P3|mol2|1|dock55|1	57.4887	96.8702	5.124
206|Me-D-Glu-2,3,6-P3|mol2|1|dock7|1	50.2542	96.7218	4.881
409|Me-D-Glu-2,4,6-P3|mol2|1|dock93|1	30.0333	96.6838	4.6824
387|Me-D-Glu-2,4,6-P3|mol2|1|dock71|1	49.8281	94.0534	5.3531
168|Beta anomeric|mol2|1|dock69|1	73.556	93.7447	5.0603
448|Me-L-Glu-2,3,6-P3|mol2|1|dock42|1	54.0592	90.2085	5.4758
521|Me-L-Glu-2,4,6-P3|mol2|1|dock25|1	58.2864	88.6299	6.1226
379|Me-D-Glu-2,4,6-P3|mol2|1|dock63|1	-23.6815	26.0936	5.5319

Table 18: The 30 lowest-scoring docking solutions of the carbohydrate-based ligands (Chapter 5) and Ins(1,4,5)P_3 in the InsP_3R model ranked according to Goldscore Fitness.

Docking Solutions	PLP.Fitness	Goldscore.Fitness
210|1|gold_5PP1_4_IP2_m1|mol2|1|dock2|1	70.8636	117.4744
401|1_4_5-IP3|mol2|1|dock2|1	80.677	116.3225
10|1|gold_5PP4_IP_m1|mol2|1|dock2|1	76.0257	114.8919
223|1|gold_4PP1_5_IP2_m1|mol2|1|dock15|1	74.7729	113.5494
211|1|gold_5PP1_4_IP2_m1|mol2|1|dock3|1	71.0099	111.0768
21|1|gold_4PP5_IP_m1|mol2|1|dock13|1	69.1009	110.0799
201|1|gold_4PP1_5_IP2_m1|mol2|1|dock2|1	49.6468	109.4394
234|1|gold_4PP1_5_IP2_m1|mol2|1|dock26|1	66.5411	109.0443
200|1|gold_4PP1_5_IP2_m1|mol2|1|dock1|1	56.2869	106.9509
403|1_4_5-IP3|mol2|1|dock4|1	65.8805	106.6163
213|1|gold_5PP1_4_IP2_m1|mol2|1|dock5|1	66.0217	106.0598
219|1|gold_4PP1_5_IP2_m1|mol2|1|dock11|1	58.0921	105.999
322|1|gold_5PP1_4_IP2_m1|mol2|1|dock24|1	69.9555	104.9525
311|1|gold_5PP1_4_IP2_m1|mol2|1|dock13|1	48.1468	104.8004
212|1|gold_5PP1_4_IP2_m1|mol2|1|dock4|1	61.0783	104.4798
315|1|gold_5PP1_4_IP2_m1|mol2|1|dock17|1	59.4386	104.3491
205|1|gold_4PP1_5_IP2_m1|mol2|1|dock6|1	70.6524	103.8112
324|1|gold_5PP1_4_IP2_m1|mol2|1|dock26|1	52.1798	103.6475
360|1|gold_5PP1_4_IP2_m1|mol2|1|dock62|1	55.4361	103.5739
209|1|gold_5PP1_4_IP2_m1|mol2|1|dock1|1	52.5836	103.467
1|1|gold_4PP5_IP_m1|mol2|1|dock2|1	59.7796	102.501
320|1|gold_5PP1_4_IP2_m1|mol2|1|dock22|1	57.4916	102.1632
231|1|gold_4PP1_5_IP2_m1|mol2|1|dock23|1	72.6249	101.9295
217|1|gold_5PP1_4_IP2_m1|mol2|1|dock9|1	42.2209	101.4826
23|1|gold_4PP5_IP_m1|mol2|1|dock15|1	59.3177	100.9781
248|1|gold_4PP1_5_IP2_m1|mol2|1|dock40|1	71.8232	100.9398
208|1|gold_4PP1_5_IP2_m1|mol2|1|dock9|1	54.0567	100.6208
204|1|gold_4PP1_5_IP2_m1|mol2|1|dock5|1	46.2905	100.4751
245|1|gold_4PP1_5_IP2_m1|mol2|1|dock37|1	61.7909	98.9379
413|1_4_5-IP3|mol2|1|dock14|1	59.1972	98.7773

Table 19: The 30 highest-scoring docking solutions of the inositol pyrophosphate ligands (Chapter 6) and Ins(1,4,5)P_3 in the InsP_3R model ranked according to Goldscore Fitness.

Docking Solutions	PLP.Fitness	Goldscore.Fitness
142|1|gold_5PP4_IP_m1|mol2|1|dock44|1	45.4613	63.5198
198|1|gold_4PP5_IP_m1|mol2|1|dock100|1	17.9098	63.5186
493|1_4_5-IP3| mol2|1|dock94|1	45.3532	63.2926
192|1|gold_5PP4_IP_m1|mol2|1|dock94|1	53.8491	63.0314
495|1_4_5-IP3|mol2|1|dock96|1	26.31	62.9195
147|1|gold_5PP4_IP_m1|mol2|1|dock49|1	34.0216	62.7089
98|1|gold_4PP5_IP_m1|mol2|1|dock90|1	42.7155	62.5517
159|1|gold_5PP4_IP_m1|mol2|1|dock61|1	57.3205	62.3615
174|1|gold_5PP4_IP_m1|mol2|1|dock76|1	41.1183	62.3039
84|1|gold_4PP5_IP_m1|mol2|1|dock76|1	43.1622	62.244
82|1|gold_4PP5_IP_m1|mol2|1|dock74|1	33.1057	62.1825
93|1|gold_4PP5_IP_m1|mol2|1|dock85|1	33.7441	61.0608
88|1|gold_4PP5_IP_m1|mol2|1|dock80|1	33.8428	61.0599
101|1|gold_4PP5_IP_m1|mol2|1|dock93|1	34.1762	61.0474
73|1|gold_4PP5_IP_m1|mol2|1|dock65|1	28.911	61.0281
154|1|gold_5PP4_IP_m1|mol2|1|dock56|1	38.7602	60.9125
479|1_4_5-IP3|mol2|1|dock80|1	24.9024	60.8667
171|1|gold_5PP4_IP_m1|mol2|1|dock73|1	21.7002	60.6852
83|1|gold_4PP5_IP_m1|mol2|1|dock75|1	34.9174	60.6779
102|1|gold_4PP5_IP_m1|mol2|1|dock94|1	36.5027	60.4079
450|1_4_5-IP3|mol2|1|dock51|1	36.123	60.3941
85|1|gold_4PP5_IP_m1|mol2|1|dock77|1	53.6466	60.3325
138|1|gold_5PP4_IP_m1|mol2|1|dock40|1	40.7605	59.9877
68|1|gold_4PP5_IP_m1|mol2|1|dock60|1	36.3824	59.868
197|1|gold_5PP4_IP_m1|mol2|1|dock99|1	44.6279	59.7321
80|1|gold_4PP5_IP_m1|mol2|1|dock72|1	42.2027	59.4819
194|1|gold_5PP4_IP_m1|mol2|1|dock96|1	36.5758	58.5856
477|1_4_5-IP3|mol2|1|dock78|1	40.1029	58.5821
148|1|gold_5PP4_IP_m1|mol2|1|dock50|1	35.7776	57.8555
165|1|gold_5PP4_IP_m1|mol2|1|dock67|1	37.4213	56.7834

Table 20: The 30 lowest-scoring docking solutions of the inositol pyrophosphate ligands (Chapter 6) and Ins(1,4,5)P_3 in the InsP_3R model ranked according to Goldscore Fitness.

General Synthetic Chemistry

Chemicals were purchased from Sigma-Aldrich, Acros, or Alfa Aesar. Anhydrous solvents were purchased from Sigma-Aldrich. TLC was performed on precoated plates (Merck Aluminum sheets silica 60 F254, art No. 5554). Chromatograms were visualised under UV light and by dipping plates into phosphomolybdic acid in EtOH, followed by heating; or $KMnO_4$ in water with K_2CO_3 and NaOH, followed by heating. Flash column chromatography was performed using RediSep Rf disposable silica flash columns on an ISCO CombiFlash Rf automated flash chromatography machine. Ion-pair reverse-phase chromatography was performed on LiChroprep RP-18 (25-40 µm, Merck) using a BioLogic LP system (BioRad), eluting at 5 mL/min with a gradient of 0−10/70% MeCN in 0.05 M triethylammonium bicarbonate (TEAB) buffer, collecting 7 mL fractions. Gradient elution anion exchange chromatography was performed on Q Sepharose Fast Flow resin, eluting at 5 mL/min with a gradient of 0-100% TEAB buffer (1-2.5 M) in mQ. Fractions containing the target polyphosphate were identified using a qualitative Briggs phosphate assay. Proton ^{1}HNMR and COSY spectra were recorded on a Bruker Avance III (400 MHz) spectrometer. Proton chemical shifts are reported in ppm (δ) relative to internal tetramethylsilane (TMS, δ 0.0 ppm) or with the solvent reference relative to TMS employed as the internal standard ($CDCl_3$, δ 7.26 ppm; CD_3OD, δ 3.31 ppm). The following abbreviations are used to describe the multiplicity of the chemical shifts: s, singlet; d, doublet; t, triplet; dd, double doublet; q, quartet; m, multiplet; br, broad; apt, apparent. ^{13}CNMR and HSQC spectra were recorded on a Bruker Avance III (100 MHz) spectrometer with complete proton decoupling. Carbon chemical shifts are reported in ppm (δ) relative to TMS with the respective solvent resonance as the internal standard ($CDCl_3$, δ 77.0 ppm, d4-MeOH, δ 49.0 ppm). ^{31}PNMR spectra were recorded on a Bruker Avance III (162 MHz) spectrometer with complete proton decoupling (unless explicitly labelled as proton-coupled). Phosphorus chemical shifts are reported in ppm (δ) relative to an 85% H_3PO_4 external standard (H_3PO_4, δ 0.0 ppm). All NMR data were collected at 25°C. Optical rotations were measured at ambient temperature using a Unipol Schmidt Haensch polarimeter in a cell volume of either 1 cm^3 or 5 cm^3, and specific rotation is given in $10^{-1}degcm^3g^{-1}$. Melting points were determined using a Stanford Research Systems Optimelt MPA100 automated melting point system and are uncorrected. Mass spectra were recorded on a GC-MS (Agilent 7200). All reactions were carried out under an argon atmosphere employing oven-dried glassware unless stated otherwise.

Qualitative modified Briggs Assay (as described by Lampe *et al*.[415])

With a Gilson pipette, 200 µL of each fraction to be analysed was added to a Pyrex test tube in a metal rack. This rack was then placed in an oven, and the samples were

allowed to heat to dryness (180 °C for approximately 30 min). After this time, 4 drops of conc. H_2SO_4 was added to each test tube and the rack was returned to the oven for at least an hour. During this time, the three indicator solutions should be prepared: Solution 1 was made up of ammonium molybdate (2.5 g) in mQ water (20 mL) and conc. H_2SO_4 (8 mL); solution 2 was made up of hydroquinone (0.1 g) in mQ water (20 mL) with one drop of conc. H_2SO_4; and solution 3 was made up of sodium sulphite (4 g) in mQ water (20 mL). The test tubes were then allowed to cool to RT, and 250 µL mQ water was added to each tube. To each fraction sample, solution 1 (500 µL), solution 2 (250 µL) and solution 3 (250 µL) were sequentially added, and the test tube was heated to boiling with a heat gun. Fractions that contained phosphate turned blue permanently (fractions without phosphate turned blue while boiling, but immediately returned to yellow when allowed to cool).

Synthesis of 5-PP-InsP$_5$ (2) and 5-PP-InsP$_4$ (3)

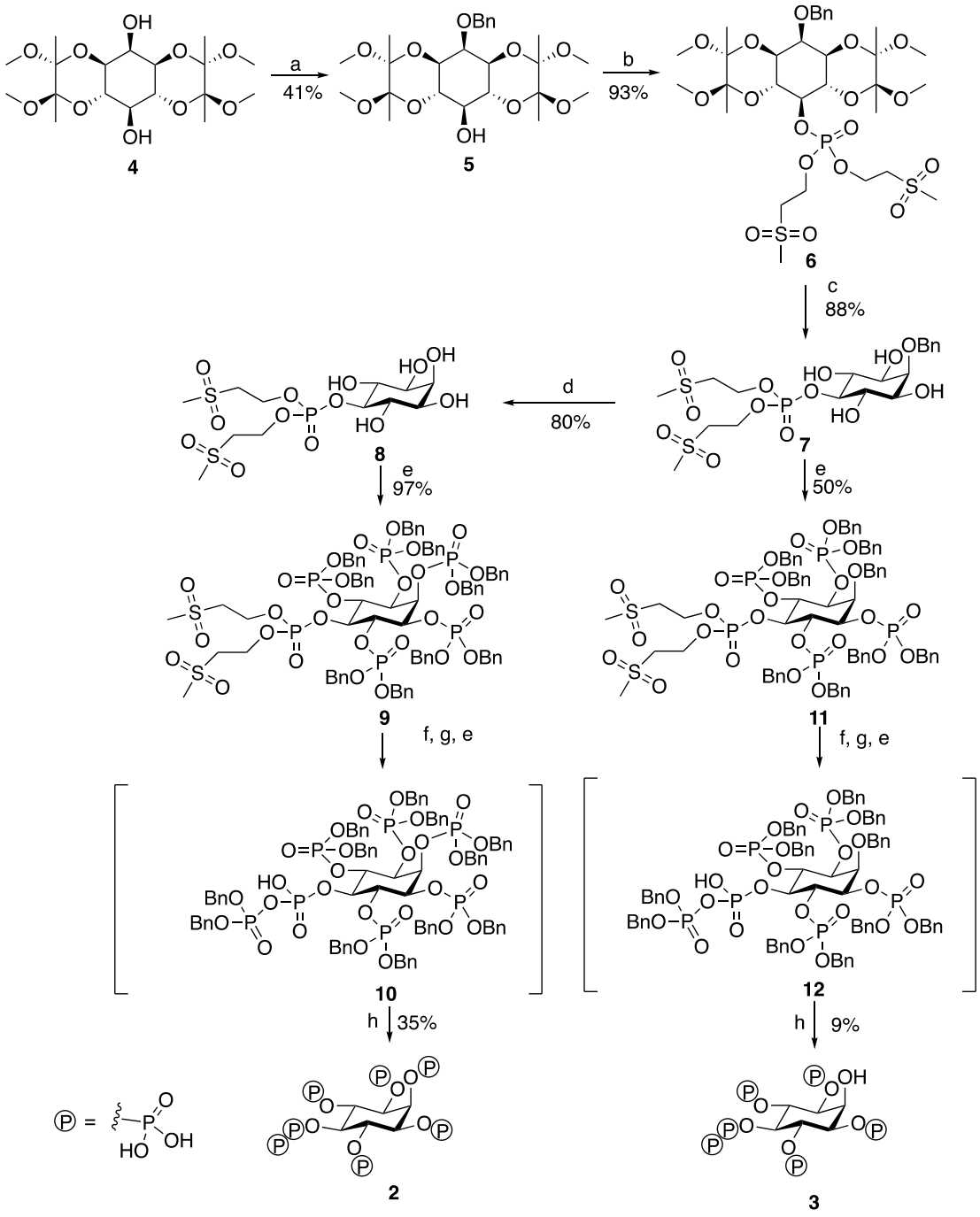

Scheme 1: Divergent Syntheses of 5-PP-InsP$_5$ and 5-PP-InsP$_4$ carried out in this study.

Reagents and conditions: (a) DMF, NaH, BnBr; (b) 1. DCM, 5-phenyl-1*H*-tetrazole, (OMSE)$_2$PN(^{i}Pr)$_2$ (**1**), 20h 2. *m*CPBA, -78°C-RT; (c) TFA, H_2O; (d) THF, CH_3COOH, H_2O, H_2, Pd(OH)$_2$/C; (e) 1. DCM, 5-phenyl-1*H*-tetrazole, (OBn)$_2$PN(^{i}Pr)$_2$, 20h 2. *m*CPBA, -78°C-RT; (f) DBU, BSTFA; (g) MeOH, TFA; (h) MeOH, THF, 1 M TEAB/$NaHCO_3$, H_2, Pd(OH)$_2$/C, 24h.

2-*O*-Benzyl-1,6:3,4-bis-*O*-(2,3-dimethoxybutane-2,3-diyl)-*myo*-inositol (**5**)

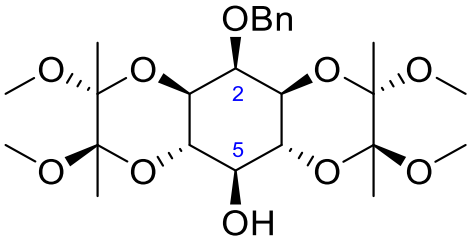

As described by Wang *et al.,*[107] sodium hydride (149 mg, 5.88 mmol, 1.2 equiv) was added over 10 minutes to a suspension of 1,6:3,4-bis-*O*-(2,3-dimethoxybutane-2,3-diyl)-*myo*-inositol (synthesised as described by Riley *et al.*,[146] 2.00 g, 4.90 mmol) in dry DMF (120 mL) under argon. After an hour of stirring at RT, benzyl bromide (0.64 mL, 5.39 mmol, 1.1 equiv) was added slowly over 30 minutes. The reaction was then allowed to stir at RT for 20 h. Completion of the reaction was confirmed with TLC, before the excess sodium hydride was destroyed through the dropwise addition of MeOH (10 mL). The solution was concentrated *in vacuo* and the residue dissolved in DCM (200 mL). The organic layer was washed with water (200 mL) and brine (200 mL), before being dried over $MgSO_4$ and concentrated. The crude product was purified by flash chromatography (P.E.-EtOAc, 0-100%) to give the pure product as a white solid (1009.9 mg, 2.03 mmol, 41% yield). **m.p.** 207.9- 212.0 °C (lit[113] 214– 216 °C); **^{1}HNMR** ($CDCl_3$, 400 Hz): 7.53-7.51 (m, 2H, Ar), 7.34-7.23 (m, 3H, Ar), 4.87 (s, 2H, C*H*$_2$Ar), 4.08 (t, *J*= 9.9 Hz, 2H, H-4 and H-6), 3.82 (t, *J*= 2.5 Hz, 1H, H-2), 3.67 (t, *J*= 9.5 Hz, 1H, H-5), 3.54 (dd, *J*= 2.5, 10.2 Hz, 2H, H-1 and H-3), 3.28 (s, 6H, OC*H*$_3$), 3.23 (s, 6H, OC*H*$_3$), 2.46 (s, 1H, OH), 1.32 (s, 12H, CC*H*$_3$); **^{13}CNMR** ($CDCl_3$, 100 Hz): 139.8 (Ar), 128.0 (Ar), 127.8 (Ar), 127.1 (Ar), 99.8 (*C*CH$_3$), 99.3 (*C*CH$_3$*)*, 76.4 (C-2), 74.0 (*C*H$_2$Ar), 70.8 (C-5), 69.5 (C-4 and C-6), 69.3 (C-1 and C-3), 48.1 (O*C*H$_3$), 48.0 (O*C*H$_3$), 17.9 (C*C*H$_3$), 17.8 (C*C*H$_3$); **HRMS (ESI)**: *m/z* calcd $[M+Na]^+$ for $C_{25}H_{38}O_{10}$: 521.2357, found: 521.2359.

N,N-Diisopropylamino-bis-[2-(methylsulfonyl)ethyloxy]phosphine (**1**)

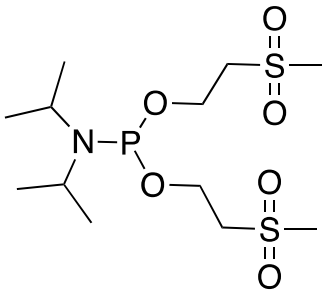

In a version of the method described by Engelsma *et al.,*[147] trichlorophosphane (0.50 mL, 5.73 mmol) was added to a solution of DIPEA (2.00 mL, 11.46 mmol, 2 equiv) in dry DCM (20 mL) under argon. This solution was then cooled to 0°C before diisopropylamine (1.63 mL, 11.46 mmol, 2 equiv) was added. The reaction was allowed

to stir for 10 min at 0°C. Methylsulfonylethanol (1.42 g, 11.46 mmol, 2 equiv) dissolved in dry DCM (30 mL) was then added dropwise to the reaction. The reaction was then allowed to warm to RT and left to stir for 3 h. The completion of the reaction was determined with ^{31}PNMR (diagnostic product signal at 149 ppm). The reaction was then diluted with EtOAc (200 mL), washed with sat. sodium bicarbonate (100 mL) and brine (100 mL). The organic layer was dried over $MgSO_4$ and concentrated *in vacuo* to yield the crude product as a yellow oil. The crude product was purified by flash chromatography (column deactivated with 1% TEA in PE prior to use, petroleum ether and EtOAc, 30 to 100%) and then recrystallized (minimum amount of DCM, approx. 2 mL, and then 150 mL diethyl ether) to give the pure product as a white, crystalline solid (1060 mg, 2.81 mmol, 49% yield). **m.p.** 73.3- 74.1 °C (lit value[91] 75.5-77.0 °C); ^{1}**HNMR** ($CDCl_3$, 400 Hz): 4.13-4.03 (m, 4H, C*H*$_2$C*H*$_2$), 3.61-3.55 [m, 2H, C*H*$(CH_3)_2$], 3.29-3.25 (m, 4H, C*H*$_2$C*H*$_2$), 3.00 (s, 6H, SC*H*$_3$), 1.20 [s, 6H, CH(C*H*$_3$)$_2$], 1.18 [s, 6H, CH(C*H*$_3$)$_2$]; ^{31}**PNMR** ($CDCl_3$, 162 Hz): 149.06; ^{13}**CNMR** ($CDCl_3$, 100 Hz): 57.8 (*C*H$_2$*C*H$_2$), 57.6 (*C*H$_2$*C*H$_2$), 56.4 (*C*H$_2$*C*H$_2$), 56.3 (*C*H$_2$*C*H$_2$), 43.5 [*C*H$(CH_3)_2$], 43.4 [*C*H$(CH_3)_2$], 43.0 (S*C*H$_3$), 24.8 [s, 6H, CH(*C*H$_3$)$_2$], 24.7 [s, 6H, CH(*C*H$_3$)$_2$]; **HRMS (ESI)**: *m/z* calcd $[M+Na]^+$ for $C_{12}H_{28}NO_6PS_2$: 400.1007, found: 400.0996.

2-*O*-Benzyl-1,6:3,4-bis-*O*-(2,3-dimethoxybutane-2,3-diyl)-*myo*-inositol-5-bis[2-(methanesulfonyl)ethyl]phosphate (**6**)

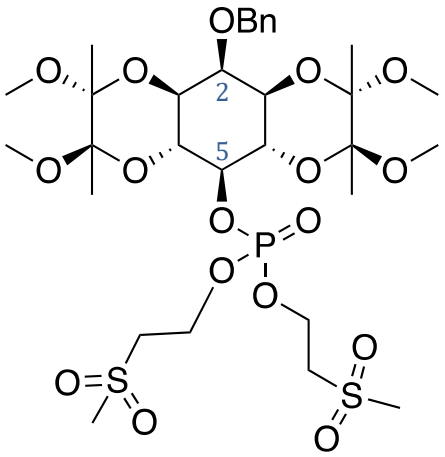

2-*O*-Benzyl-1,6:3,4-bis-*O*-(2,3-dimethoxybutane-2,3-diyl)-*myo*-inositol (**5,** 909 mg, 1.82 mmol) was dissolved in dry DCM (18 mL) and put under argon. To this solution, 5-phenyl-1*H*-tetrazole (400 mg, 2.73 mmol, 1.5 equiv) followed by *N,N*-diisopropylamino-bis-[2-(methylsulfonyl)ethyloxy]phosphine (**1**, 826 mg, 2.19 mmol, 1.2 equiv) were added. The reaction was allowed to stir at RT for 16 h. Prior to oxidation, the reaction was analysed by ^{31}PNMR spectroscopy to confirm phosphitylation had been successful. The reaction was then cooled to -78 °C, before *m*CPBA (900 mg, 70% pure, 3.65 mmol, 2.0 equiv) was added. The solution was allowed to warm to RT and was then diluted with EtOAc (150 mL). This organic phase

was washed with 10% sodium sulphite solution (3x20 mL), dried over $MgSO_4$ and concentrated *in vacuo* to yield the crude product. The product was purified by flash chromatography (EtOAc-MeOH, 0-20%) and the pure product collected as a white foam (1339 mg, 1.69 mmol, 93% yield). **^{1}HNMR** ($CDCl_3$, 400 Hz): 7.44-7.42 (m, 2H, Ar), 7.27-2.17 (m, 3H, Ar), 4.77 (s, 2H, C*H*$_2$Ar), 4.60-4.57 (m, 2H, MSE CH_2), 4.53-4.48 (m, 2H, MSE CH_2), 4.33 (q, *J*= 9.0 Hz, 1H, H-5), 4.11 (t, *J*= 9.8 Hz, 2H, H-4 and H-6), 3.75 (s, 1H, H-2), 3.50 (d, *J*= 10.0 Hz, 2H, H-1 and H-3), 3.45-3.39 (m, 2H, MSE CH_2), 3.30-3.26 (m, 2H, MSE CH_2), 3.19 (s, 6H, OC*H*$_3$), 3.15 (s, 6H, OC*H*$_3$), 2.94 (s, 6H, SC*H*$_3$), 1.24 (s, 6H, CC*H*$_3$), 1.20 (s, 6H, CC*H*$_3$); **^{31}PNMR** ($CDCl_3$, 162 Hz): -2.44; **^{13}CNMR** ($CDCl_3$, 100 Hz): 139.4 (Ar), 128.1 (Ar), 127.8 (Ar), 127.3 (Ar), 99.8 (*C*CH_3), 99.5 (*C*CH_3), 78.3 (C-5), 76.0 (C-2), 74.2 (*C*H_2Ar), 68.9 (C-1 and C-3), 68.1 (C-4 or C-6), 68.0 (C-4 or C-6), 61.6 (MSE CH_2), 61.5 (MSE CH_2), 55.2 (MSE CH_2), 55.1 (MSE CH_2), 48.2 (OCH_3x2), 42.8 (SCH_3), 17.79 (CCH_3), 17.75 (CCH_3); **HRMS (ESI)**: *m/z* calcd $[M+Na]^+$ for $C_{31}H_{51}O_{17}PS_2$: 813.2197, found: 813.2188.

2-*O*-Benzyl-*myo*-inositol-5-bis[2-(methanesulfonyl)ethyl]phosphate (**7**)

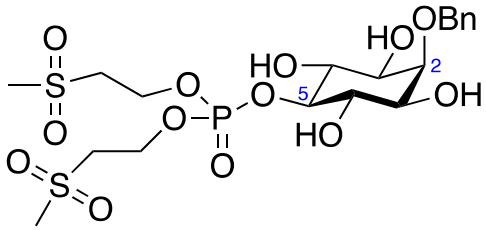

2-*O*-Benzyl-1,6:3,4-bis-*O*-(2,3-dimethoxybutane-2,3-diyl)-*myo*-inositol-5-bis[2-(methanesulfonyl)ethyl]phosphate (**6**, 396 mg, 0.50 mmol) was dissolved in a mixture of TFA (4.5 mL) and water (0.5 mL). The reaction was allowed to stir for 10 min under argon, during which time the solution turned dark yellow. The solution was then concentrated *in vacuo* without heating. The resultant residue was dissolved in methanol and concentrated *in vacuo* to yield the crude product as a white solid. The product was purified by recrystallization from boiling ethanol to yield the pure product as colourless crystals (249 mg, 0.44 mmol, 88% yield). **^{1}HNMR** (d4-MeOH, 400 Hz): 7.43- 7.41 (m, 2H, Ar), 7.33- 7.23 (m, 3H, Ar), 4.61-4.56 (m, 6H, C*H*$_2$Ar and MSE CH_2), 4.10 (q, *J*= 9.0 Hz, 1H, H-5), 3.92 (t, *J*= 2.6 Hz, 1H, H-2), 3.82 (t, *J*= 9.6 Hz, 2H, H-4 and H-6), 3.53 (t, *J*= 5.5 Hz, 4H, MSE CH_2), 3.48 (dd, *J*= 9.9, 2.5 Hz, 2H, H-1 and H-3), 3.04 (s, 6H, SC*H*$_3$); **^{31}PNMR**: (d6-dmso, 162 Hz) -2.26; **^{13}CNMR** (d6-dmso, 100 Hz): 139.8 (Ar), 128.0 (Ar), 127.1 (Ar), 83.5 (C-5), 81.8 (C-2), 74.4 (*C*H_2Ar), 71.5 (C-1 and C-3), 71.4 (C-4 and C-6), 61.11 (MSE CH_2), 61.06 (MSE CH_2), 54.2 (MSE CH_2), 54.1 (MSE CH_2), 42.0 (SCH_3); **HRMS (ESI)**: *m/z* calcd $[M+H]^+$ for $C_{19}H_{31}O_{13}PS_2$: 563.1016, found: 563.1014.

myo-Inositol-5-bis[2-(methanesulfonyl)ethyl]phosphate (**8**)

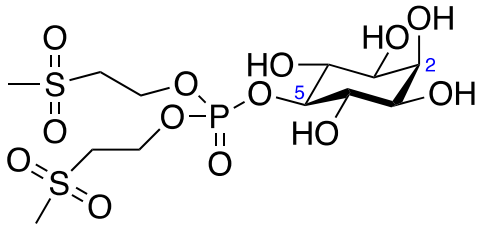

2-*O*-Benzyl-*myo*-inositol-5-bis[2-(methanesulfonyl)ethyl]phosphate (**7**, 100 mg, 0.178 mmol) was dissolved in THF (2.5 mL) and ultrapure water (0.5 mL). To this solution, three drops of acetic acid and palladium hydroxide on carbon (20 mg, 20%) were added. The reaction was allowed to stir under hydrogen for 24 hours at RT. The catalyst was then filtered off, and the solution was concentrated *in vacuo*. The residue was dissolved in ultrapure water and lyophilised to yield the product as a white solid (66.9 mg, 0.142 mmol, 80% yield). Due to compound instability when in solution, the compound was only partially characterised before being used in the next step. **^{1}HNMR** (d6-dmso, 400 Hz): 4.98 (d, *J*= 5.7 Hz, 2H), 4.70 (d, *J*= 3.7 Hz, 1H), 4.69 (d, *J*= 5.9 Hz, 2H), 4.44-4.34 (m, 4H), 3.93 (q, *J*= 9.1 Hz, 1H), 3.71 (q, *J*= 3.0 Hz, 1H), 3.60-3.54 (m, 2H), 3.51 (t, *J*=5.7 Hz, 4H), 3.23-3.18 (m, 2H), 3.01 (s, 6H); **^{31}PNMR** (d6-dmso, 162 Hz): -2.21.

myo-Inositol-1,2,3,4,6-pentakis(dibenzyl)phosphate-5-bis[2-(methanesulfonyl)ethyl]-phosphate (**9**)

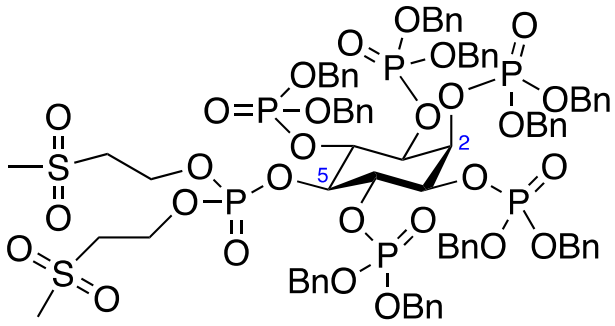

myo-Inositol-5-bis[2-(methanesulfonyl)ethyl]phosphate (**8**, 110 mg, 0.233 mmol) was dissolved in dry MeCN and concentrated *in vacuo* three times, then suspended in dry DCM and concentrated again to thoroughly dry the starting material. The starting pentaol (**8**) was then suspended in dry DCM (15 mL) and put under argon. To this suspension, 5-phenyl-1*H*-tetrazole (510 mg, 3.49 mmol, 15.0 equiv) and dibenzyl phosphoramidite (0.8 mL, 2.33 mmol, 10.0 equiv) were added, and the reaction was allowed to stir at RT for 16 h. The solution was then cooled to -78 °C before *m*CPBA (858 mg, 70%, 3.49 mmol, 15.0 equiv) was added. The reaction was allowed to warm to RT, and was then diluted with EtOAc (150 mL). The reaction solution was washed

with 10% aq. Na_2SO_3 (2 x 30 mL) and 1.0 M HCl (30 mL), and then dried over $MgSO_4$ and concentrated *in vacuo*. The residue was purified by flash column chromatography (P.E.-EtOAc, 0-100%) to give the pure product as a colourless oil (329.1 mg, 0.225 mmol, 97% yield).**^{1}HNMR** ($CDCl_3$, 400Hz): 7.32-7.23 (m, 46H, Ar), 7.17-7.15 (m, 4H, Ar), 5.67 (br d, *J*= 9.0 Hz, 1H, H-2), 5.23-5.19 (m, 2H, C*H*$_2$Ar), 5.14-4.90 (m, 18 H, H-4 and H-6 and C*H*$_2$Ar), 4.82-4.77 (m, 2H, C*H*$_2$Ar), 4.54 (q, *J*= 9.5 Hz, 1H, H-5), 4.49-4.43 (m, 2H, MSE CH_2), 4.39-4.28 (m, 4H, H-1 and H-3 and MSE CH_2), 3.19-3.06 (m, 4H, MSE CH_2), 2.76 (s, 6H, SC*H*$_3$); **^{31}PNMR** ($CDCl_3$, 100 Hz): -1.47 (2P), -1.49 (2P), -2.13, -2.84; **^{13}CNMR** ($CDCl_3$, 100 Hz): 135.8-135.5 (m, Ar), 128.9-128.8 (m, Ar), 128.0 (Ar), 77.4 (C-5), 75.6 (C-2), 74.7 (C-4 and C-6), 73.3 (C-1 and C-3), 70.4-70.0 (m, *C*H_2Ar), 62.21 (MSE CH_2), 62.17 (MSE CH_2), 54.5 (MSE CH_2), 54.4 (MSE CH_2), 42.5 (S*C*H_3); **HRMS (ESI)**: *m/z* calcd $[M+H]^+$ for $C_{82}H_{90}O_{28}P_6S_2$: 1773.3558, found: 1773.3518.

5-Diphospho-*myo*-inositol-1,2,3,4,6-pentakisphosphate triethylammonium salt (**2**)

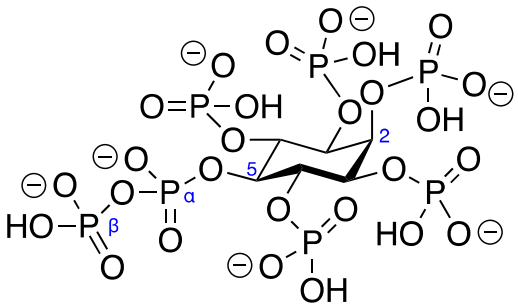

myo-Inositol-1,2,3,4,6-pentakis(dibenzyl)phosphate-5-bis[2-(methanesulfonyl)ethyl]-phosphate (**9**, 65.2 mg, 0.045 mmol) was dissolved in $CDCl_3$ (2 mL) in an NMR tube, and to this solution DBU (25 µL, 177 µmol, 4.0 equiv) followed by BSTFA (114 µL, 461 µmol, 10.3 equiv) were added. ^{31}PNMR was used to ensure the silylation was complete with singlets at -0.97 (2P), -1.70 (2P), -2.42 (1P) and a diagnostic singlet at -17.51 (1P). Methanol (26 µL, 2.05 mmol) was then added to the reaction and, after 3 min, TFA (27 µL, 0.347 mmol) was added. ^{31}PNMR confirmed that desilylation was completed with signals at 2.64 (1P), -1.62 (2P) and -1.94 (3P). The reaction was concentrated and the residue was thoroughly dried on a vacuum line.

This crude residue was then dissolved in $CDCl_3$ and to this solution, 5-phenyl-1*H*-tetrazole (42.9 mg, 0.29 mmol, 6.6 equiv) and dibenzyl phosphoramidite (41 µL, 0.12 mmol, 2.7 equiv) were added. After an hour, an additional portion of phosphitylating agent (41 µL, 0.12 mmol, 2.7 equiv) was added, and the reaction was allowed to stir for another 2h. ^{31}PNMR spectroscopy confirmed successful phosphitylation with a signal at 139.6 (β-P). The reaction was then cooled to -78 °C, before *m*CPBA (13 mg, 70%, 0.052 mmol, 2 equiv) was added. The solution was allowed to warm to RT, before

being concentrated *in vacuo* without heat. This residue (**10**) was purified by column chromatography (EtOAc and MeOH, 0-20%), before being immediately deprotected via hydrogenation (the compound was not studied at this stage as the product proved to be unstable following purification.

The protected pyrophosphate (**10**, 40.8 mg, assumed 0.0224 mmol) was dissolved in a mixture of THF (4.6 mL), MeOH (3 mL) and 1M TEAB (2.1 mL). To this solution, $Pd(OH)_2/C$ (20%, ≥50% wet, 27.2 mg) was added. The flask was evacuated and flushed with hydrogen three times before being left to stir in an atmosphere of hydrogen. The solution was allowed to stir at RT under hydrogen for 3 days. The crude product was purified on an RP-18 column, and the product was identified in the column fractions using a Briggs qualitative phosphate assay. The product fractions were concentrated *in vacuo* without heat, lyophilised and collected as an off-white glass (21.7 mg, calculated 6.5 TEA counterions per molecule of product, 0.0155 mmol, 35% yield). **^{1}HNMR** (d4-MeOH, 400 Hz): 4.97 (dt, *J*= 2.9, 10.4Hz, 1H, H-2), 4.60 (q, *J*= 9.7 Hz, 2H, H-4 and H-6), 4.35-4.25 (m, 3H, H-1, H-3 and H-5), 3.15 (s, approx. 39H, TEA CH_2), 1.30 (s, approx. 59H, TEA CH_3); **^{31}PNMR** (d4-MeOH, 162 Hz): 0.87 (2P), 0.68 (2P), -0.29, -10.70 (d, *J*= 22.8 Hz, pyrophosphate β-P), -11.81 (d, *J*= 22.8 Hz, pyrophosphate α-P); **^{13}CNMR** (d4-MeOH, 100 Hz): 79.4 (C-5), 77.5 (C-4 and C-6), 76.8 (C-2), 75.5 (C-1 and C-3), 47.2 (TEA CH_2), 9.3 (TEA CH_3); **HRMS (ESI)**: *m/z* calcd $[M-H]^-$ for $C_6H_{19}O_{27}P_7$: 738.8204, found: 738.8206.

2-*O*-Benzyl-*myo*-inositol-1,3,4,6-tetrakis(dibenzyl)phosphate-5-bis[2-(methanesulfonyl)ethyl]-phosphate (**11**)

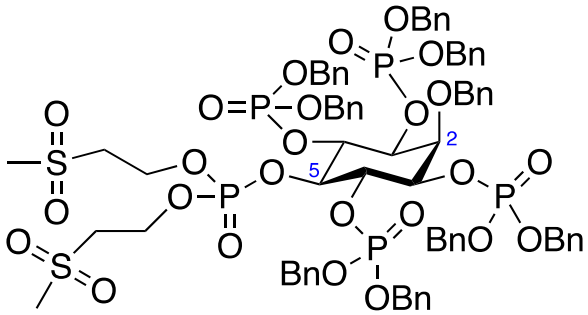

2-*O*-Benzyl-*myo*-inositol-5-bis[2-(methanesulfonyl)ethyl]phosphate (**7**, 50 mg, 0.0890 mmol) was first dissolved in dry toluene and concentrated in vacuo to remove as much water as possible. The dried tetraol (**7**) was then dissolved in dry DCM (5 mL). To this solution, 5-phenyl-1*H*-tetrazole (156 mg, 1.07 mmol, 12 equiv) and dibenzyl phosphoramidite (0.25 mL, 0.712 mmol, 8 equiv) were added. The solution was allowed to stir at RT for 2 hours, before the reaction progress was checked with ^{31}PNMR. The success of the phosphitylation was confirmed with signals at 144.42, 144.38, 141.13 and 141.10 ppm in the pre-oxidation ^{31}PNMR spectrum. The reaction

was then cooled to -78 °C and *m*CPBA (70%, 262 mg, 1.07 mmol, 12 equiv) was added. The solution was diluted with EtOAc (150 mL), washed with 10% aq. Na_2SO_3 (2 x 30 mL) and 1.0 M HCl (30 mL), and then dried over $MgSO_4$ and concentrated *in vacuo*. The product was purified using silica column chromatography (1 P.E.-EtOAc, 0-100%, 2. P.E.-EtOAc 70-100%). The pure product was collected as a colourless oil (66.4 mg, 0.0414 mmol, 47% yield). **^{1}HNMR** ($CDCl_3$, 400 Hz): 7.28-7.18 (m, 45H, Ar), 5.05-4.86 (m, 18H, C*H*$_2$Ar, H-4 and H-6), 4.76 (apt s, 3H, C*H*$_2$Ar, H-2), 4.47-4.40 (m, 3H, MSE CH_2 and H-5), 4.34-4.23 (m, 4H, MSE CH_2 and H-1 and H-3), 3.18-3.08 (m, 4H, MSE CH_2), 2.75 (s, 6H, SC*H*$_3$); **^{31}PNMR** ($CDCl_3$, 162 Hz): -1.71 (2P), -1.77 (2P), -2.82 (1P); **^{13}CNMR** ($CDCl_3$, 100 Hz): 128.9-127.6 (m, Ar), 77.4 (C-2), 76.8 (C-5), 76.3 (*C*H_2Ar), 75.5 (C-4 and C-6), 75.1 (C-1 and C-3), 70.2-69.9 (m, *C*H_2Ph), 62.21 (MSE CH_2), 62.16 (MSE CH_2), 54.6 (MSE CH_2), 54.5 (MSE CH_2), 42.5 (S*C*H_3); **HRMS (ESI)**: *m/z* calcd $[M+H]^+$ for $C_{73}H_{85}O_{25}P_5S_2$: 1603.34016, found: 1603.33533.

5-Diphospho-*myo*-inositol-1,3,4,6-tetrakisphosphate triethylammonium salt (**3**)

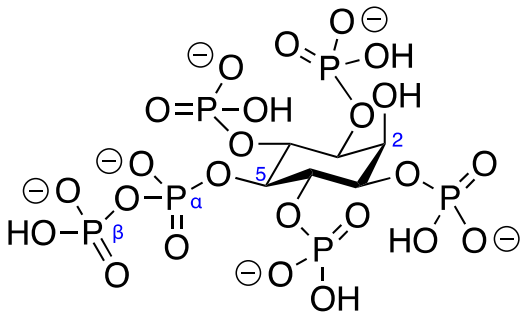

myo-Inositol-1,3,4,6-tetrakis(dibenzyl)phosphate-5-bis[2-(methanesulfonyl)ethyl]phosphate (**11**, 71.2 mg, 44.4 µmol) was dissolved in $CDCl_3$ (1.5 mL) in an NMR tube. To this solution DBU (27 µL, 178 µmol, 4.0 equiv), followed by BSTFA (220 µL, 888 µmol, 20 equiv) were added. ^{31}PNMR was used to ensure the silylation was complete with singlets at -1.56 (2P), -2.09 (2P), and a diagnostic singlet at -17.44 (1P). Methanol (90 µL, 2.23 mmol, 50 equiv) was then added to the reaction and, after 7 min, TFA (29 µL, 379 µmol, 8.5 equiv) was added. ^{31}PNMR spectroscopy confirmed that desilylation was completed with signals at -0.02 (1P), -1.98 (2P) and -3.49 (2P). The reaction was concentrated and the residue was thoroughly dried on a vacuum line.

This crude residue was then dissolved in dry DCM (8 mL), and to this solution, 5-phenyl-1*H*-tetrazole (64.8 mg, 0.444 mmol, 10 equiv) and dibenzyl phosphoramidite (0.08 mL, 0.355 mmol, 8 equiv) were added. ^{31}PNMR spectroscopy was used to track the progress of the reaction after 1 h, and more benzyl phosphitylating agent (0.1 mL) was added as the phosphitylation was not yet complete. After another 2 h, ^{31}PNMR confirmed successful phosphitylation with a P(III) signal at 139.6 ppm. The reaction

was then cooled to -78 °C, before *m*CPBA (61.3 mg, 70%, 0.355 mmol, 8 equiv) was added. The solution was allowed to warm to RT, before being concentrated *in vacuo* without heat. This residue (**12**) was purified by column chromatography (EtOAc-MeOH, 0-20%), before being immediately deprotected via hydrogenation (the compound was not studied or even thoroughly dried at this stage as the product proved to be unstable following purification).

The protected pyrophosphate compound (**12**, assumed 44.4 µmol) was dissolved in a mixture of isopropanol (8 mL) and mQ (2 mL). To this solution, sodium bicarbonate (40.6 mg, 0.483 mmol, 10.9 equiv) and $Pd(OH)_2/C$ (20%, ≥50% wet, 30 mg) were added. The flask was evacuated and flushed with hydrogen three times before being left to stir in an atmosphere of hydrogen. After 20 min, an additional 6 mL of mQ was added to the reaction, and the flask was evacuated and flushed with hydrogen three times again. The solution was allowed to stir at RT under hydrogen overnight. The crude product was purified on an RP-18 column, followed by an ion exchange column, then a final RP-18 column. The presence of product in the collected fractions was confirmed using a Briggs qualitative phosphate assay. The product-containing fractions of the columns were concentrated *in vacuo* without heat. The final product was lyophilised and collected as an off-white glass (6.5 mg, calculated 6.2 TEA counterions per molecule of product, 0.0039 mmol, 9% yield). **^{1}HNMR** (D_2O, 400 Hz): 4.44 (apt. q, *J*= 9.5 Hz, 2H, H-4 and H-6), 4.24 (t, *J*= 2.4 Hz, 1H, H-2), 4.17-4.22 (m, 1H, H-5), 4.10 (apt. dt, *J*= 2.4, 9.8 Hz, 2H, H-1 and H-3), 3.09 (q, *J*= 7.4 Hz, approx. 37H, TEA CH_2), 1.17 (t, *J*= 7.4 Hz, approx. 57H, TEA CH_3); **^{31}PNMR** (D_2O, 162 Hz): 0.58 (2P), 0.13 (2P), -11.01 (d, *J*= 24.3 Hz, 1P, pyrophosphate β-P), -11.34 (d, *J*= 20.8 Hz, 1P, pyrophosphate α-P); **^{13}CNMR** (D_2O, 100 Hz): 78.6 (C-5), 75.9 (C-4 and C-6), 74.1 (C-1 and C-3), 70.6 (C-2), 46.7 (TEA CH_2), 8.2 (TEA CH_3); **HRMS (ESI)**: *m/z* calcd $[M-H]^-$ for $C_6H_{18}O_{24}P_6$: 658.85300, found: 658.85303.

Synthesis of 1,5-bis(diphospho)-myo-inositol tetrakisphosphate [1,5-(PP)$_2$-InsP$_4$]

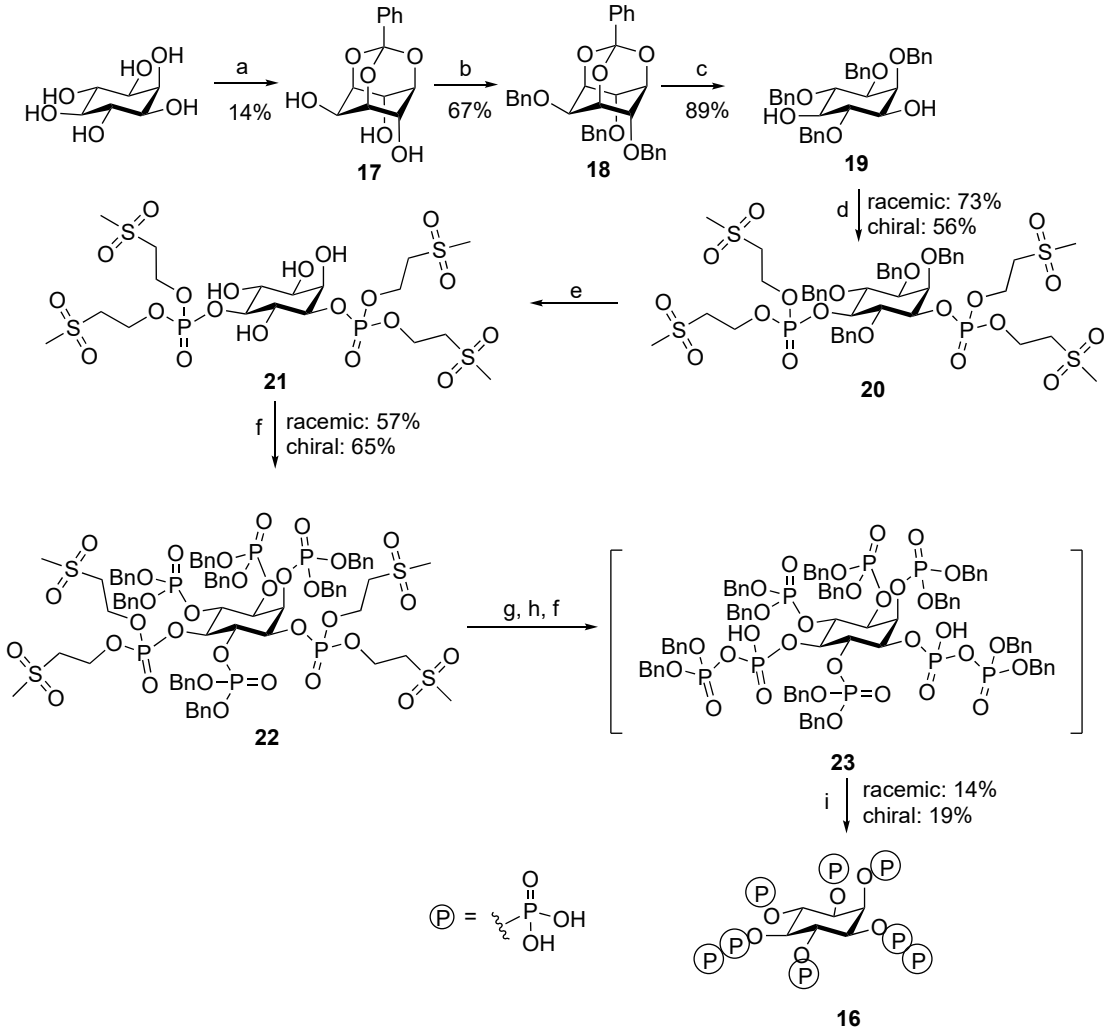

Scheme 3: Synthetic route to 1,5-(PP)$_2$-InsP$_4$ (**16**).

Reagents and conditions: (a) Trimethyl orthobenzoate, H_2SO_4-silica, DMSO, 80°C, 10h ; (b) BnBr, NaH, DMF, 0°C-RT, overnight; (c) DIBAL-H in toluene (1M), DCM, -78°C -RT, overnight; (d) 1. DCM, 5-phenyl-1*H*-tetrazole, (OMSE)$_2$PN(^{i}Pr)$_2$ (**1**), 20h 2. *m*CPBA, -78°C-RT; (e) THF, CH_3COOH, H_2O, H_2, Pd(OH)$_2$/C; (f) 1. DCM, 5-phenyl-1*H*-tetrazole, (OBn)$_2$PN(^{i}Pr)$_2$, 20h 2. *m*CPBA, -78°C-RT; (g) DBU, BSTFA; (h) MeOH, TFA; (i) MeOH, THF, 1 M TEAB, $NaHCO_3$, H_2, Pd(OH)$_2$/C.

myo-Inositol orthobenzoate (**17**)

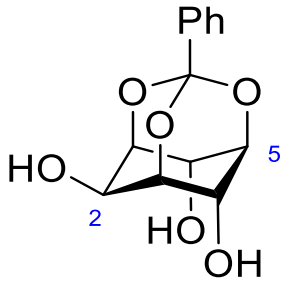

As described by Hussain *et al*.,[177]in an adaptation of the original Riley *et al.* method,[176] *myo*-inositol (2.25 g, 1 mmol) was dissolved in dry DMSO (20 mL), and to this solution H_2SO_4-silica (100 mg) was added to act as a catalyst, followed by trimethyl orthobenzoate (2.5 mL, 1.2 mmol, 1.2 equiv). The reaction was heated to 80°C and allowed to stir for 10 h. The progress of the reaction was confirmed with TLC, before the reaction was cooled to RT. Saturated sodium bicarbonate solution (100 mL) was added to the reaction, followed by ethyl acetate (200 mL). The organic layer was separated, dried over $MgSO_4$ and concentrated *in vacuo* to yield the crude product. The product was purified with silica column chromatography (DCM-MeOH, 0-10%) and was collected as an off-white solid (373 mg, 14% yield). **m.p.** 207.0-209.4°C (lit value.[177] 210-214°C); **^{1}HNMR** (d6-dmso, 400 Hz): 7.56-7.54 (m, 2H, Ar), 7.37-7.31 (m, 3H, Ar), 5.51 (d, *J*= 6.4 Hz, 2H, OH), 5.34 (d, *J*= 6.4 Hz, 1H, OH), 4.42-4.38 (m, 2H, H-4 and H-6), 4.22- 4.19 (m, 1H, H-5), 4.16-4.14 (m, 2H, H-1 and H-3), 4.08 (dt, *J*= 1.8, 6.4 Hz, 1H, H-2); **^{13}CNMR** (d6-dmso, 100 Hz): 137.9 (quaternary Ar), 129.0 (Ar), 127.6 (Ar), 125.5 (Ar), 106.5 (quaternary C in orthobenzoate group), 75.8 (C-1 and C-3), 70.2 (C-5), 67.2 (C-4 and C-6), 57.8 (C-2).

2,4,6-Tri-*O*-benzyl-*myo*-inositol orthobenzoate (**18**)

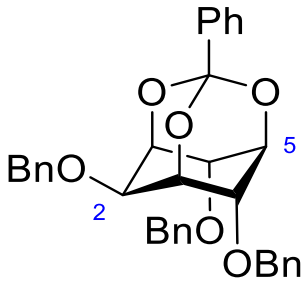

myo-Inositol orthobenzoate (**17**, 500 mg, 1.88 mmol) was dissolved in dry DMF (10 mL) and the solution was cooled to 0°C. To this solution, sodium hydride (270 mg, 11.25 mmol, 6 equiv) was added, and the solution was allowed to stir for 10 minutes. After this time, benzyl bromide (1.34 mL, 11.27 mmol, 6 equiv) was added, and the reaction was allowed to warm to RT and stir overnight. Following confirmation that the reaction was complete with TLC, a few drops of methanol were added to quench

the reaction. The reaction solution was then concentrated *in vacuo* to yield a residue, which was taken up in dichloromethane (200 mL) and washed with water (100 mL) and brine (100 mL). The organic layer was dried over $MgSO_4$ and concentrated to yield the crude product, which was purified by silica column chromatography (1. DCM-EtOAc, 0-100%, 2. P.E.-EtOAc, 0-100%) to yield the pure product as a white solid (675.4 mg, 1.26 mmol, 67% yield). **m.p.** 83.4-84.9°C (lit. value.[416] 84-85°C); **^{1}HNMR** ($CDCl_3$, 400 Hz): 7.59-7.56 (m, 2H, Ar), 7.32-7.30 (m, 2H, Ar), 7.25-7.18 (m, 12H, Ar), 7.13-7.11 (m, 4H, Ar), 4.58-4.52 (m, 4H, C*H*$_2$Ar), 4.48-4.45 (m, 1H, H-5), 4.42-4.38 (m, 6H, C*H*$_2$Ar and H-1, H-3, H-4 and H-6), 4.02 (t, *J*= 1.6 Hz, 1H, H-2); **^{13}CNMR** ($CDCl_3$, 100 Hz): 138.2 (Ar), 137.8 (Ar), 137.3 (Ar), 129.5 (Ar), 128.5 (Ar), 128.1 (Ar), 128.0 (Ar), 127.9 (Ar), 127.8 (Ar), 127.7 (Ar), 125.5 (Ar), 108.0 (quaternary C in orthobenzoate group), 74.2 (C-4 and C-6), 72.0 (C-1 and C-3), 71.7 (*C*H$_2$Ar), 71.3 (*C*H$_2$Ar), 69.2 (C-5), 66.3 (C-2).

2,3,4,6-Tetra-*O*-benzyl-*myo*-inositol (**19**)

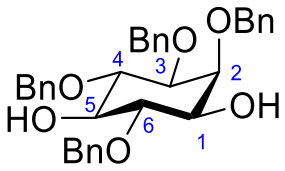

As described by Swarbrick *et al*.,[175] 2,4,6-tri-*O*-benzyl-*myo*-inositol orthobenzoate (**18**, 1000 mg, 1.86 mmol) was dissolved in dry DCM (30 mL), and this solution was then cooled to -78°C before DIBAL-H in toluene (7.44 mL, 1.0 M, 7.44 mmol, 4 equiv) was added dropwise. The reaction was allowed to gradually warm to RT and then allowed to stir overnight. The progress of the reaction was confirmed with TLC, after which the reaction was carefully quenched through the dropwise addition of water (20 mL). Hydrochloric acid (1.0 M, 20 mL) was then also added to the flask followed by more DCM (100 mL). The organic layer was isolated and more DCM (100 mL) was used to extract from the aqueous layer again. The organic layers were combined, dried over $MgSO_4$ and concentrated *in vacuo* to yield the crude product. The product was purified with silica column chromatography (P.E.-EtOAc, 0-100%) to yield the pure product as a white solid (898 mg, 1.66 mmol, 89% yield). **m.p.** 99.5-101.6 °C (lit. value.[174] 83.5-85.5°C); **^{1}HNMR** ($CDCl_3$, 400 Hz): 7.39-7.26 (m, 20H, Ar), 5.00 (AB, *J*= 11.6 Hz, 1H, C*H*$_2$Ar), 4.99 (AB, *J*= 11.2 Hz, 1H, C*H*$_2$Ar), 4.91 (AB, *J*= 11.4 Hz, 1H, C*H*$_2$Ar), 4.80 (AB, *J*= 12.0 Hz, 1H, C*H*$_2$Ar), 4.77 (AB, *J*= 11.4 Hz, 1H, C*H*$_2$Ar), 4.74 (AB, *J*= 11.5 Hz, 1H, C*H*$_2$Ar), 4.69 (brs, 2H, C*H*$_2$Ar), 4.07 (t, *J*= 2.5 Hz, 1H, H-2), 3.91 (t, *J*= 9.4 Hz, 1H, H-6), 3.70 (t, *J*= 9.3 Hz, 1H, H-4), 3.55 (dd, J= 1.9, 9.2 Hz, 1H, H-3), 3.52-3.48 (m, 1H, H-5), 3.46 (dd, J= 2.3, 9.7 Hz, 1H, H-1), 2.49 (d, *J*= 1.9 Hz, 1H, OH), 2.30 (d, *J*= 6.3 Hz, 1H, OH); **^{13}CNMR** ($CDCl_3$, 100 Hz): 138.8 (Ar), 138.2 (Ar), 128.54 (Ar), 128.53 (Ar), 128.50 (Ar), 128.4 (Ar), 128.1 (Ar), 128.0 (Ar), 127.82 (Ar), 127.78 (Ar), 127.67 (Ar), 127.65 (Ar), 81.7 (C-4),

81.4 (C-6), 80.9 (C-1), 77.2 (C-2), 75.5 (CH_2Ar), 75.1 (C-5), 74.9 (CH_2Ar), 74.8 (CH_2Ar), 72.7 (CH_2Ar), 72.2 (C-3).

DL-2,3,4,6-Tetra-*O*-benzyl-*myo*-inositol-1,5-bis{bis[2-(methanesulfonyl)ethyl]phosphate} (**20**)

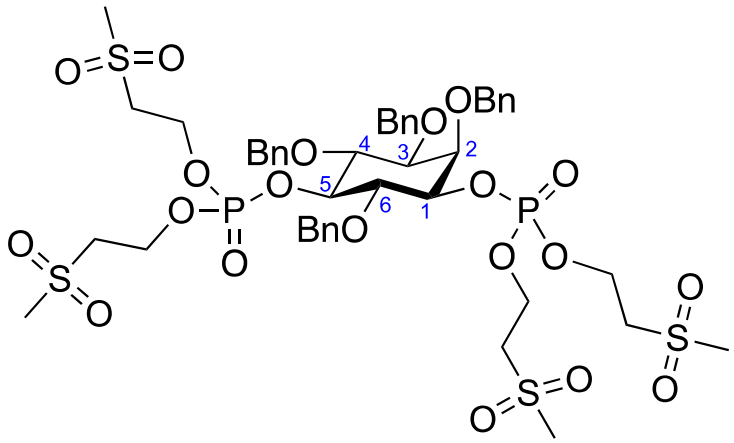

DL-2,3,4,6-Tetra-*O*-benzyl-*myo*-inositol (**19**, 147 mg, 0.272 mmol) was dissolved in dry toluene and concentrated *in vacuo* twice to thoroughly dry the starting material prior to use. The starting material diol (**19**) was then dissolved in dry DCM (10 mL). To this solution, 5-phenyl-1*H*-tetrazole (159 mg, 1.09 mmol, 4 equiv) and methylsulfonylethyl phosphitylating agent (**1**, 267 mg, 0.707 mmol, 2.6 equiv) were added. The reaction was allowed to stir at RT for 16 hours. After confirming the progression of the reaction with ^{31}PNMR, the reaction flask was cooled to -78°C, and *m*CPBA (268 mg, 1.09 mmol, 70% pure, 4 equiv) was added. The reaction was then allowed to warm to RT before it was diluted with EtOAc, washed with 10% sodium sulphite (2x30 mL) and 1M HCl (30 mL), dried over $MgSO_4$ and concentrated *in vacuo* to yield the crude product. The product was purified with silica column chromatography (DCM-MeOH, 0-10%) to yield the pure product as a colourless oil (223 mg, 0.198 mmol, 73% yield). The reaction was repeated with the chiral diol precursor (123 mg, 0.228 mmol) to generate chiral D-bisphosphate as a colourless oil (142.5 mg, 0.127 mmol, 56% yield). The D-chiral product was found to have a very small optical rotation: **[α]$^{21}_D$** 2.3 (*c*= 1.03, $CHCl_3$).

^{1}HNMR ($CDCl_3$, 400 Hz): 7.46-7.28 (m, 20H, Ar), 5.09 (AB, *J*= 11.4 Hz, 1H, C*H*$_2$Ph), 4.99 (AB, *J*= 11.9 Hz, 1H, C*H*$_2$Ph), 4.89-4.62 (m , 6H, C*H*$_2$Ph), 4.48 (q, *J*= 9.3 Hz, 1H, H-5), 4.41-4.04 (m, 12H, H-2, H-1 or H-3, H-4, H-6, 8xPOC*H*$_2$CH$_2$S), 3.60 (dd, *J*= 9.8, 2.0 Hz, 1H, H-1 or H-3), 3.23-3.06 (m, 3H, 3xPOCH$_2$C*H*$_2$S), 3.01-2.69 (m, 5H, 5xPOCH$_2$C*H*$_2$S), 2.88 (s, 3H, SMe), 2.81 (s, 3H, SMe), 2.75 (s, 3H, SMe), 2.73 (s, 3H, SMe); **^{31}PNMR** ($CDCl_3$, 162 Hz): -2.61, -3.24; **^{13}CNMR** ($CDCl_3$, 100 Hz): 138.50, 138.46, 138.1, 137.6 (4 x *ipso-C* of POCH$_2$Ph), 128.7-127.2 (m, Ar), 80.5 (m, C-5), 79.9 (C-1 or C-3), 78.8 and 78.4-78.2 (m, C-1 or C-3, C-4, C-6), 75.8 (C-2), 75.3, 74.6, 74.5, 72.8 (4x*C*H$_2$Ph), 61.6-61.3

(overlapping 4xPO*C*H_2CH_2S), 54.5-54.2 (overlapping 4xPOCH$_2$*C*H_2S), 42.54, 42.52, 42.46 and 42.44 (4xS*C*H_3); **HRMS** (*m*/*z*) $[M+H]^+$ calcd. for $C_{46}H_{62}O_{20}P_2S_4$; 1125.2241; found 1125.2256

DL-*myo*-Inositol-1,5-bis{bis[2-(methanesulfonyl)ethyl]phosphate} (**21**)

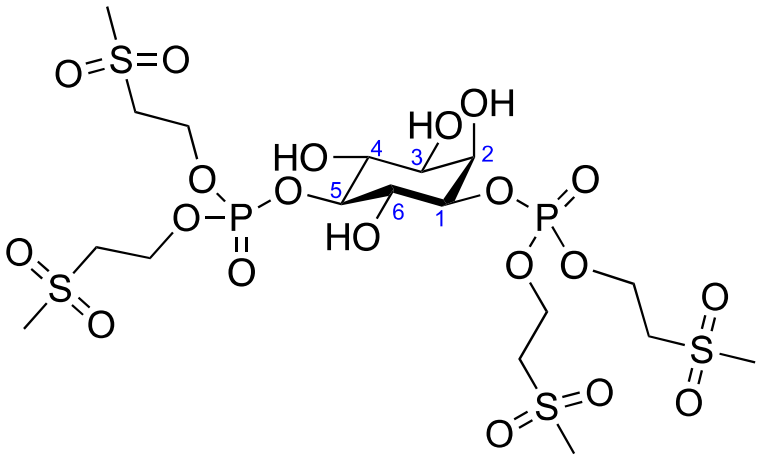

DL-2,3,4,6-Tetra-*O*-benzyl-*myo*-inositol-1,5-bis{bis[2-(methanesulfonyl)ethyl]phosphate} (**20**, 287 mg, 0.255 mmol) was dissolved in THF (10 mL) and distilled water (2 mL). To this solution, 5 drops of glacial acetic acid and $Pd(OH)_2$/C (20% Fluka, 50% water, 66 mg) were added. The reaction was then allowed to stir for 24 h under hydrogen, after which an additional amount of distilled water (10 mL) was added, and the reaction was allowed to stir under hydrogen for a further 24 h. The reaction was then filtered and concentrated *in vacuo*, before being lyophilised to yield the product as a white solid (151.2 mg, 0.198 mmol, 78% yield). A full characterisation was not carried out due to the instability of the compound (degradation can be observed in the ^{31}PNMR spectrum). ^{1}HNMR spectroscopy was used to confirm that the hydrolysis of the benzyl groups was complete (with an absence of signals around 7 ppm). The next step in the synthetic route (Scheme 3) was started as soon as possible. This reaction was initially carried out with the racemic protected bisphosphate (**20**) before being repeated with the D-chiral starting material.

^{1}HNMR (d6-dmso, 400 Hz): 5.60 (d, *J*= 6.8 Hz, 1H), 5.26 (d, *J*= 4.4 Hz, 1H), 5.16 (d, *J*= 5.7 Hz, 1H), 5.01 (d, *J*= 5.7 Hz, 1H), 4.42-4.36 (m, 9H), 4.29-4.19 (m, 1H),4.14-4.09 (m, 1H), 4.05-3.96 (m, 2H), 3.81-3.75 (m, 2H), 3.59-3.51 (m, integration distorted by neighbouring HDO peak but expected to be 7H), 3.03 (s, 3H, SCH_3), 3.02 (s, 3H, SCH_3), 3.01 (s, 6H, SCH_3); **^{31}PNMR** (d6-dmso, 162 Hz): -2.29, -2.81; **HRMS** (*m*/*z*) $[M+Na]^+$ calcd. for $C_{18}H_{38}O_{20}P_2S_4$; 787.0207; found 787.0201.

DL-*myo*-Inositol-1,5-bis{bis[2-(methanesulfonyl)ethyl]phosphate}-2,3,4,6-tetrakis(dibenzylphosphate) (**22**)

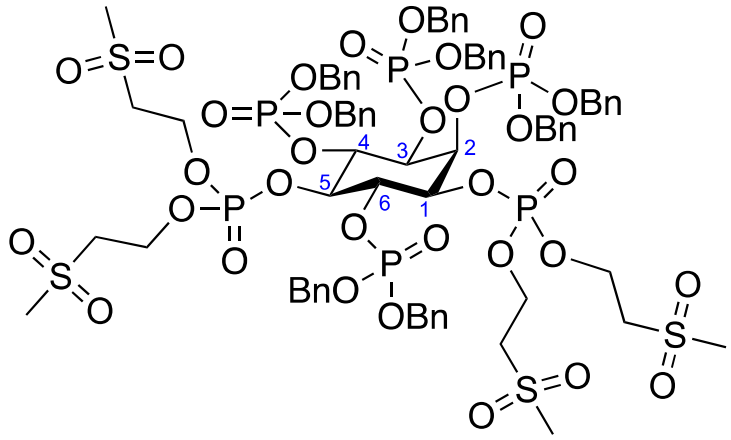

Prior to beginning the reaction, the solid starting materials, reaction flask and stirrer bar were dried overnight in a vacuum desiccator with fresh silica desiccant and P_2O_5. DL-*myo*-inositol-1,5-bis{bis[2-(methanesulfonyl)ethyl]phosphate} (**21**, 418 mg, 0.547 mmol) was dissolved in dry DCM (20 mL). To this solution, 5-phenyl-1*H*-tetrazole (600 mg, 4.10 mmol, 7.5 equiv) and dibenzyl phosphoramidite (1.2 mL, 3.56 mmol, 6.5 equiv) were added, and the reaction was put under argon and allowed to stir at RT overnight. After confirmation of successful phosphitylation through ^{31}PNMR spectroscopy, the reaction was cooled to -78 °C and *m*CPBA (70%, 1079 mg, 4.38 mmol, 8 equiv) was added to the flask. The reaction was allowed to warm to RT and stir for 5 min, before being diluted with ethyl acetate (200 mL), washed with 10% aqueous sodium sulphite (100 mL) and aqueous hydrochloric acid (100 mL, 1 M). The organic phase was dried over $MgSO_4$ and concentrated to yield the crude product. The product was purified with silica column chromatography (MeOH-EtOAc, 0-10%) to yield the product as a colourless oil (217.9 mg, 0.310 mmol, 57% yield). The reaction was repeated with the chiral bisphosphate precursor (D-**21**, 53.8 mg, 0.070 mmol) to generate chiral D-hexakisphosphate as a colourless oil (82.0 mg, 0.045 mmol, 65% yield). The D-chiral product was found to have a very small optical rotation: **[α]$^{21}_{D}$** 2.1 (*c*= 0.68, $CHCl_3$).

^{1}HNMR: 7.38-7.12 (m, 40H, Ar), 5.65 (dt, *J*= 2.1, 9.0 Hz, 1H, Ins-H), 5.20-4.86 (m, 17H, ArC*H*$_2$, 2xIns-H), 4.82-4.73 (m, 2H, ArC*H*$_2$ and Ins-H), 4.67-4.31 (m, 10H, MSE C*H*$_2$, 2xIns-H), 3.31-3.25 (m, 1H, MSE C*H*$_2$), 3.23-3.20 (m, 2H, MSE C*H*$_2$), 3.18-3.06 (m, 5H, MSE C*H*$_2$), 2.90 (s, 3H, MSE SC*H*$_3$), 2.84 (s, 3H, MSE SC*H*$_3$), 2.79 (s, 3H, MSE SC*H*$_3$), 2.76 (MSE SC*H*$_3$); **^{31}PNMR** ($CDCl_3$, 162 Hz): -0.91, -1.33, -1.67, -2.47, -2.74, -3.79; **^{13}CNMR**: 135.8-135.4 (m, Ar), 129.0 (Ar), 128.9 (Ar), 128.83 (Ar), 128.80 (Ar), 128.78 (Ar), 128.7 (Ar), 128.6 (Ar), 128.5 (Ar), 128.4 (Ar), 128.2 (Ar), 128.12 (Ar), 128.05 (Ar), 76.5 (Ins-C), 76.2 (Ins-C), 75.2 (Ins-C), 74.6 (Ins-C), 73.1 (Ins-C), 71.5 (Ins-C), 70.4-70.0 (*C*H$_2$Ar), 62.3-62.1 (MSE *C*H$_2$), 61.6 (MSE *C*H$_2$), 54.5-54.4 (MSE *C*H$_2$), 42.5 (MSE *C*H$_3$), 42.39 (MSE

CH_3), 42.36 (MSE *C*H_3), 42.1 (MSE *C*H_3); **HRMS** (*m/z*) $[M + 2H]^{2+}$ calcd. for $C_{74}H_{90}O_{32}P_6S_4$; 903.1423; found 903.1398.

1,5-Bis(diphospho)-*myo*-inositol-2,3,4,6-tetrakisphosphate triethylammonium salt (**16**)

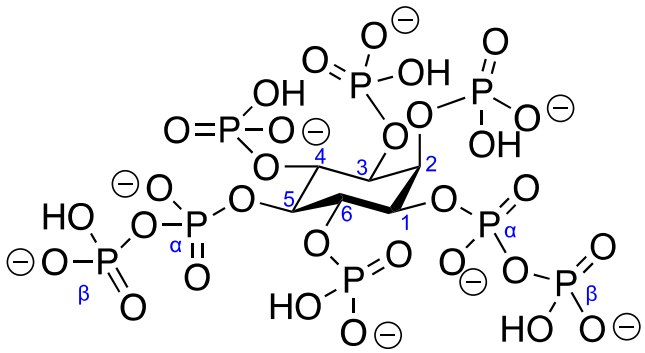

myo-Inositol-2,3,4,6-tetrakis(dibenzyl)phosphate-5-bis[2-(methanesulfonyl)ethyl]phosphate (**22**, 54.5 mg, 30.2 µmol) was dissolved in $CDCl_3$ (1.5 mL) in an NMR tube, and to this solution DBU (36 µL, 241 µmol, 8 equiv), followed by BSTFA (243 µL, 906 µmol, 30 equiv) were added. ^{31}PNMR spectroscopy was used to ensure the silylation was complete with singlets at -0.93, -0.96, -0.99 and -2.82, and diagnostic singlets at -17.36 and -19.14. Methanol (70 µL, 1.71 mmol, 56.7 equiv) was then added to the reaction and, after 3 min, TFA (22.2 µL, 290 µmol, 9.6 equiv) was added. ^{31}PNMR spectroscopy confirmed that desilylation was complete with all of the signals being positioned around 0 ppm (rather than around -10 ppm indicating partial silylation or -20 ppm indicated complete silylation). The reaction was concentrated and the residue was thoroughly dried on a vacuum line.

This crude residue was dissolved in dry DCM (10 mL), and to this solution, 5-phenyl-1*H*-tetrazole (211 mg, 1.44 mmol, 16 equiv) and a portion of the dibenzyl phosphoramidite (0.19 mL; total amount: 0.27 mL, 0.770 mmol, 8.5 equiv) were added and the reaction was allowed to stir at RT for an hour. The remaining dibenzyl phosphoramidite (0.08 mL) was then added and the phosphitylation was allowed to stir for another hour. The reaction was then cooled to -78 °C, before *m*CPBA (356 mg, 70%, 1.44 mmol, 16 equiv) was added. The solution was allowed to warm to RT before being concentrated *in vacuo* without heat. Unlike 5-PP-InsP_4 or 5-PP-InsP_5, the residue generated at this point in the reaction (**23**) could not be purified by column chromatography and was instead immediately deprotected crude via hydrogenation (the compound was not studied or even thoroughly dried at this stage as the protected pyrophosphate precursor tended to degradation).

The protected pyrophosphate compound (**23**, assumed 30 µmol) was dissolved in a mixture of isopropanol (8 mL) and mQ (2 mL). To this solution, sodium bicarbonate

(27.6 mg, 0.328 mmol, 10.9 equiv) and $Pd(OH)_2/C$ (20%, ≥50% wet, 120 mg) were added. The flask was evacuated and flushed with hydrogen three times before being left to stir in an atmosphere of hydrogen. After 2 h, an additional 6 mL of mQ was added to the reaction and the flask was evacuated and flushed with hydrogen three times again. The solution was allowed to stir at RT under hydrogen overnight before the catalyst was filtered out. The crude product was purified on an RP-18 column (1. 0-10% MeCN in 0.05 TEAB, 2. 0-10% MeCN in 0.05 TEAB). Following these columns, ^{1}HNMR spectroscopy indicated that not all of the benzyl protecting groups had been successfully cleaved from the phosphate groups, and the hydrogenation was repeated with the same quantities of reagents (omitting the $NaHCO_3$) and left for a further 24h, after which total cleavage of the benzyl groups was confirmed. ^{31}PNMR spectroscopy results indicated the presence of another contaminated inositol pyrophosphate (possibly $InsP_7$), thus the product was purified by an ion exchange column (30-100% 2.5M TEAB), followed by a final RP-18 column (0-10% MeCN in 0.05 TEAB). The presence of product in the collected fractions of each column was confirmed with a Briggs qualitative phosphate assay, and the product-containing fractions were concentrated *in vacuo* without heat. The excess TEAB buffer was decomposed through successive additions of methanol and *in vacuo* concentration. The racemic final product was lyophilised and collected as an off-white glass (7.2 mg, calculated 8.7 TEA counterions per molecule of product, 4.25 µmol, 14% yield). The reaction was repeated with the chiral hexakisphosphate precursor (D-**22**, 74.5 mg, 0.041 mmol) to generate chiral D-1,5-$(PP)_2$-$InsP_4$ as an off-white glass (13.9 mg, calculated 9.5 TEA counterions per molecule of product, 7.94 µmol, 19% yield).

^{1}HNMR (D_2O, 500 Hz): 4.84 (brd d, *J*= 9.8 Hz, 1H, H-2), 4.43 (t, *J*= 9.6 Hz, 1H, H-6), 4.40 (t, *J*= 9.4 Hz, 1H, H-4), 4.22-4.15 (m, 2H, H-5 and H-1), 4.07 (brt, *J*= 9.7 Hz, 1H, H-3), 3.10 (q, *J*= 7.3 Hz, approx. 51H, TEA CH_2), 1.18 (t, *J*= 7.3 Hz, approx. 79H, TEA CH_3); **^{31}PNMR** (D_2O, 202 Hz): 0.60 (P-4), 0.25 (P-3), -0.24 (P-6), -1.04 (P-2), -10.56 (d, *J*= 20.0 Hz, pyrophosphate β-P), -10.62 (d, *J*= 19.5 Hz, pyrophosphate β-P), -10.95 (d, *J*= 18.2 Hz, pyrophosphate α-P), -11.04 (d, *J*= 19.5 Hz, pyrophosphate α-P); **^{13}CNMR** (D_2O, 125 Hz): 77.6 (C-1 or C-5), 75.9 (C-4), 75.6 (C-2), 74.8 (C-6), 73.7 (C-1 or C-5), 73.6 (C-3), 46.6 (TEA CH_2), 8.2 (TEA CH_3); **HRMS (ESI)**: *m/z* calcd $[M-H]^-$ for $C_6H_{20}O_{30}P_8$: 818.7857, found: 818. 7868.

Synthesis of HDAC3-SMRT carbohydrate polyphosphates

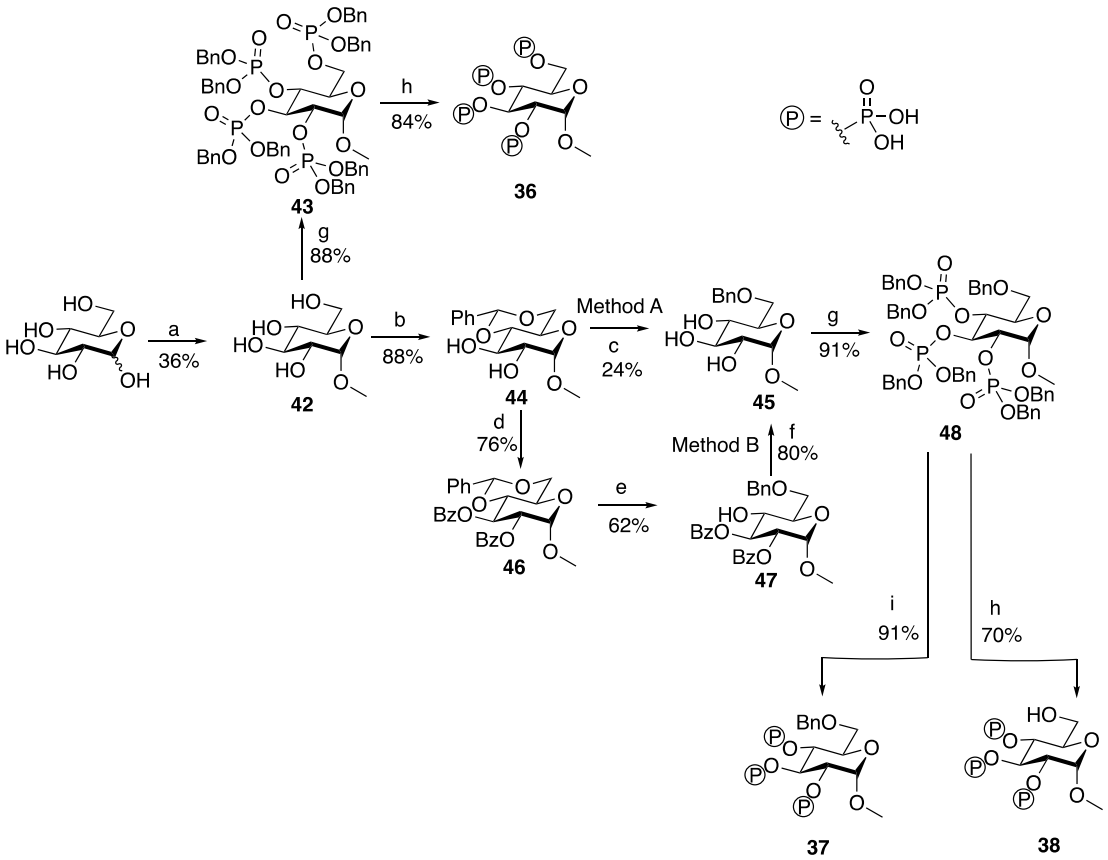

Scheme 6: Synthetic route for the D-glucose based HDAC ligands: methyl α-D-glucopyranoside 2,3,4,6-tetrakisphosphate (**36**), methyl α-D-glucopyranoside 2,3,4-trisphosphate (**37**) and methyl 6-*O*-benzyl α-D-glucopyranoside 2,3,4-trisphosphate (**38**).

Reagents and conditions: (a) CH_3COCl, MeOH; (b) $PhCH(OMe)_2$, cat. CSA, MeCN; (c) TMDS, $AlCl_3$, DCM; (d) BzCl, py; (e) $Me_3N.BH_3$, $AlCl_3$, THF, H_2O; (f) NaOH, MeOH; (g) 1. dibenzyl phosphoramidite, 5-Phenyl-*1H*-tetrazole, DCM, 2. *m*CPBA; (h) 1. $Pd(OH)_2/C$, H_2, MeOH, H_2O, 2. TEA; (i) 1. TMSBr, DCM, 2. TEAB.

Methyl α-D-glucopyranoside (**42**)

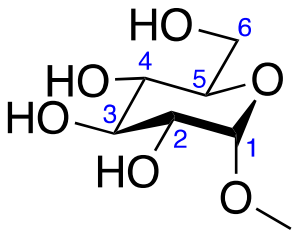

As described by Li *et al.*,[200] D-glucose (850 mg, 4.7 mmol) was dissolved in anhydrous MeOH (6.5 mL). A solution of hydrogen chloride was prepared by adding acetyl chloride (0.25 mL) to anhydrous MeOH (1.5 mL) at 0°C, and this solution was added

dropwise to the glucose solution. The reaction was refluxed for 5 days under nitrogen before the MeOH was evaporated to yield the crude product. The product was recrystallized from EtOH as a white crystalline solid, which contained approximately 5% of the β-anomer. The product was recrystallized from EtOH again to yield the pure α-anomer of the product as white crystals. The mother liquor of the recrystallisations was combined and thoroughly dried before the reflux was repeated using this residue to maximise the total yield of the reaction. More of the pure α-anomer product was obtained following successive recrystallisations of the product of the second reflux and combined with the α-anomer crystals isolated after the initial reflux (overall: 330.5 mg, 1.70 mmol, 36% yield). **m.p.** (from EtOH) 163.6-165.6 °C [Lit.[200] (from EtOH) 163-165°C]; **[α]$^{21}_{D}$** 161.9 (*c*= 1.00, MeOH) [Lit.[417] [α]$_D$ 158.0 (H_2O)]; **^{1}HNMR** (d4-MeOH, 400 MHz): δ 4.66 (d, *J*= 3.8 Hz, 1H, H-1), 3.81 (dd, *J*= 11.8, 2.4 Hz, 1H, H-6), 3.66 (dd, *J*= 11.8, 5.7 Hz, 1H, H-6), 3.61 (t, *J*= 9.3 Hz, 1H, H-3), 3.54-3.50 (m, 1H, H-5), 3.40 (s, 3H, OMe), 3.38 (dd, *J*= 9.7, 3.8 Hz, 1H, H-2), 3.27 (dd, *J*=9.9, 8.9 Hz, 1H, H-4); **^{13}CNMR** (d4-MeOH, 100 MHz): δ 101.2 (C-1), 75.1 (C-3), 73.54 (C-5), 73.53 (C-2), 71.8 (C-4), 62.7 (C-6), 55.5 (OMe).

Methyl 4,6-*O*-benzylidene-α-D-glucopyranoside (**44**)

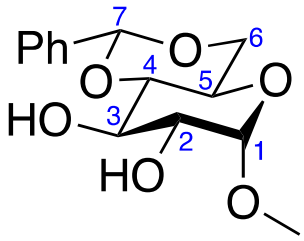

As described by Tseberlidis *et al.*,[201] methyl-α-D-glucopyranoside (**42**, 500 mg, 2.57 mmol, 1.0 equiv) was suspended in dry MeCN (8.5 mL) and put under a nitrogen atmosphere. To this suspension, benzaldehyde dimethyl acetal (1.2 mL, 7.73 mmol, 3 equiv) and catalytic camphor-10-sulphonic acid (8 mg, 0.034 mmol) were added, and the reaction was allowed to stir at RT overnight. After 24 h, the reaction was neutralised with a few drops of triethylamine, and evaporated *in vacuo* to yield the crude product as a white crystalline solid. The crude product was purified with flash chromatography (P.E.-EtOAc, 0-100%) and the pure product was collected as a white, crystalline solid (0.6391 g, 2.26 mmol, 88% yield). **m.p**: 161.5-164.1 °C (Lit.[418] (from $CHCl_3$) 159-161 °C); **[α]$^{21}_{D}$** 112.8 (*c*= 1.00, $CHCl_3$) [Lit.[418] [α]$^{22}_{D}$ 116.7 (c= 1.0, $CHCl_3$); **^{1}HNMR** ($CDCl_3$, 400 MHz): δ 7.50-7.48 (m, 2H, Ar), 7.40-7.35 (m, 3H, Ar), 5.52 (s, 1H, H-7), 4.78 (d, *J*= 3.9 Hz, 1H, H-1), 4.29 (dd, *J*= 9.6, 4.3 Hz, 1H, H-6), 3.92 (ap t, *J*= 9.3 Hz, 1H, H-3), 3.83-3.77 (m, 1H, H-5), 3.75 (ap q, *J*= 9.7 Hz, 1H, H-6), 3.62 (dd, *J*= 9.2, 3.9 Hz, 1H, H-2), 3.48 (ap t, *J*= 9.3 Hz, 1H, H-4), 3.45 (s, 3H, OMe), 2.61 (brs, 2H, 2 x OH);

^{13}CNMR ($CDCl_3$, 100 MHz): δ 137.2 (Ar), 129.4 (Ar), 128.5 (Ar), 126.4 (Ar), 102.1 (C-7), 99.9 (C-1), 81.0 (C-4), 73.0 (C-2), 71.9 (C-3), 69.1 (C-6), 62.5 (C-5), 55.7 (OMe).

Methyl 6-*O*-benzyl α-D-glucopyranoside (**45**)

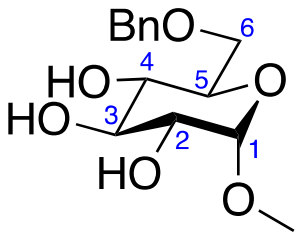

Method A: As described by Zhang *et al.*,[211] methyl 4,6-*O*-benzylidene-α-D-glucopyranoside (**44**, 1.0 g, 3.5 mmol, 1 equiv), was dissolved in dry DCM (25 mL) and cooled to -78 °C. $AlCl_3$ (708 mg, 5.3 mmol, 1.5 equiv), followed by 1,1,3,3-tetramethyldisiloxane (0.94 mL, 5.3 mmol, 1.5 equiv), were added to the solution. The reaction was allowed to warm to RT and stirred for 3 h. The reaction was then quenched with 1 M HCl (30 mL), and the product was extracted with DCM (4 x 20 mL) then EtOAc (2 x 20 mL). The combined organic layers were dried over $MgSO_4$ and concentrated to yield the crude product as a white solid. The product was purified with flash chromatography (DCM-MeOH, 0-10%). The collected mixed fractions were further purified by recrystallization from acetone and diisopropyl ether. The pure product was collected as a white crystalline solid (245 mg, 0.862 mmol, 24% yield).

Method B: As described by Marchant *et al.,*[215] methyl 2,3-di-*O*-benzoyl-6-*O*-benzyl-α-D-glucopyranoside (**47**, 100 mg, 0.20 mmol) was dissolved in MeOH (11.6 mL). NaOH (46 mg, 1.16 mmol, 5.7 equiv) was added to the solution and the reaction was refluxed for 30 min. The solution was then allowed to cool to RT, before being neutralised through the addition of solid CO_2. The solution was concentrated under reduced pressure to yield a solid residue. The residue was taken up in EtOAc, washed with water, dried over $MgSO_4$ and concentrated to yield the crude product. The product was purified with flash chromatography (DCM-MeOH, 0-10%) to yield the pure product (46.2 mg, 0.163 mmol, 80% Yield).

m.p. 60.2-63.6 °C (lit.[419] 58-60 °C); **$[\alpha]^{23}_D$** 78.5 (*c*= 0.518, $CHCl_3$) [lit.[419] $[\alpha]_D$ 82.0 (*c*= 0.62, $CHCl_3$)]; **^{1}HNMR** (d6-DMSO, 400 MHz): δ 7.37-7.25 (m, 5H, Ar), 4.99 (d, *J*= 5.9 Hz, 1H, OH), 4.80 (d, *J*= 5.0 Hz, 1H, OH), 4.74 (d, *J*= 6.4 Hz, 1H, OH), 4.53 (d, *J*= 6.4 Hz, 1H, H-1), 4.50 (s, 2H, C*H*$_2$Ar), 3.70-3.64 (m, 1H, H-5), 3.54-3.48 (m, 2H, H-6 x2), 3.40-3.37 (m, 1H, H-3), 3.26 (s, 3H, OMe), 3.21-3.16 (m, 1H, H-2), 3.09-3.03 (m, 1H, H-4); **^{13}CNMR** (d^6-DMSO, 100 MHz): δ 138.7 (Ar), 128.2 (Ar), 127.4 (Ar), 127.3 (Ar), 99.7 (C-1), 73.4 (C-3), 72.3 (CH_2Ar), 71.9 (C-2), 71.1 (C-6), 70.4 (C-4), 69.9 (C-5), 54.4 (OMe).

Methyl 2,3-di-*O*-benzoyl-4,6-*O*-benzylidene-α-D-glucopyranoside (**46**)

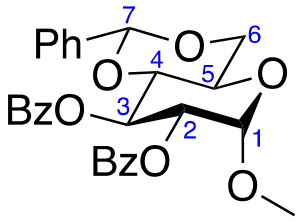

As described by Ansell and Honeyman,[213] methyl 4,6-*O*-benzylidene-α-D-glucopyranoside (**44**, 500 mg, 1.77 mmol) was dissolved in dry pyridine (3.5 mL). To this solution, benzoyl chloride (0.7 mL, 6.03 mmol, 3.4 equiv) was added dropwise. The reaction was allowed to stir at RT for 3 h, before being diluted with DCM (50 mL). The solution was washed with 1 M HCl (30 mL), sat. $NaHCO_{3\,(aq)}$ (30 mL) and brine (30 mL). The organic layer was dried over $MgSO_4$, and concentrated under reduced pressure to yield the crude product as a white solid. The product was purified by recrystallization from EtOAc and petroleum ether, and collected as white crystals (0.6592 g, 1.34 mmol, 76% yield). **m.p.** (from EtOAc and petroleum ether) 153.4-154.1 °C (Lit.[418] (from $CHCl_3$) m.p. 150-152 °C); **[α]$^{21}_D$** 93.6 (*c*= 1.00, $CHCl_3$) [Lit.[418] [α]$^{22}_D$ 95.0 (*c*= 1.0, $CHCl_3$)]. **^{1}HNMR** ($CDCl_3$, 400 MHz): δ 8.00-7.31 (m, 15H, Ar), 6.06 (t, *J*= 9.8 Hz, 1H, H-3), 5.57 (s, 1H, H-7), 5.24 (dd, *J*= 9.9, 3.7 Hz, 1H, H-2), 5.18 (d, *J*= 3.7 Hz, 1H, H-1), 4.38 (dd, *J*= 10.3, 4.8 Hz, 1H, H-6), 4.08 (m, 1H, H-5), 3.90 (t, *J*= 9.6 Hz, 1H, H-4), 3.87 (t, *J*= 10.3 Hz, 1H, H-6), 3.44 (s, 3H, OMe); **^{13}CNMR** ($CDCl_3$, 100 MHz): δ 166.2 (*C*(O)Ph), 165.7 (*C*(O)Ph), 137.0 (Ar), 133.5 (Ar), 133.1 (Ar), 130.1 (Ar), 129.9 (Ar), 129.2 (Ar), 128.6 (Ar), 128.4 (Ar), 128.3 (Ar), 126.3 (Ar), 101.8 (C-7), 98.0 (C-1), 79.6 (C-4), 72.7 (C-2), 69.7 (C-3), 69.1 (C-6), 62.7 (C-5), 55.7 (OMe).

Methyl 2,3-di-*O*-benzoyl-6-*O*-benzyl-α-D-glucopyranoside (**47**)

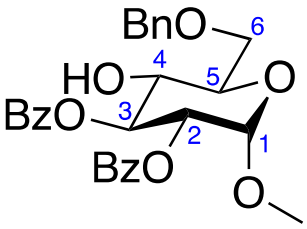

In a modified version of the of the Garegg *et al.* method,[206,210] methyl 2,3-di-*O*-benzoyl-4,6-*O*-benzylidene α-D-glucopyranoside (**46**, 200 mg, 0.408 mmol) was dissolved in dry THF (7.5 mL). To this solution, $Me_3N.BH_3$ (119 mg, 1.63 mmol, 4 equiv) was added followed by $AlCl_3$ (326 mg, 2.45 mmol, 6 equiv), which was added to the stirring solution very gradually. Ultrapure water (15 µL, 0.815 mmol, 2 equiv) mixed with dry THF (0.5 mL) was then added to the reaction. The reaction was allowed to stir

at RT for 5 h before being terminated with the addition of water (10 mL), followed by 1 M $HCl_{(aq)}$ (10 mL). The product was extracted with EtOAc (3 x 30 mL), and the combined organic fractions were washed with brine (30 mL), dried over $MgSO_4$ and concentrated under reduced pressure. The crude product was purified with flash chromatography (P.E.-EtOAc, 0-100%) to yield the pure product as a colourless oil (125 mg, 0.254 mmol, 62% yield). **$[\alpha]^{23}_D$** 127.4 (*c*= 1.00, DCM) [Lit.[420] $[\alpha]_D$ 123 (*c*=0.63, $CHCl_3$)]; **^{1}HNMR** ($CDCl_3$, 400 MHz): δ 8.00-7.97 (m, 4H, Ar), 7.53-7.48 (m, 2H, Ar), 7.39-7.29 (m, 9H, Ar), 5.74 (dd, *J*= 10.0, 8.6 Hz, 1H, H-3), 5.26 (dd, *J*= 10.1, 3.7 Hz, 1H, H-2), 5.13 (d, *J*= 3.6 Hz, 1H, H-1), 4.64 (q, *J*= 12.1 Hz, 2H, C*H*$_2$Ph x2), 4.02-3.93 (m, 2H, H-4, H-5), 3.88-3.79 (m, 2H, H-6 x2), 3.43 (s, 3H, OMe), 3.00 (d, *J*= 3.6 Hz, 1H, OH); **^{13}CNMR** ($CDCl_3$, 100 MHz): δ 167.4 (*C*(O)Ph), 166.1 (*C*(O)Ph), 137.9 (Ar), 133.48 (Ar), 133.45 (Ar), 130.0 (Ar), 129.4 (Ar), 129.3 (Ar), 128.6 (Ar), 128.53 (Ar), 128.52 (Ar), 127.94 (Ar), 127.85 (Ar), 97.2 (C-1), 74.3 (C-3), 73.9 (*C*H_2Ph), 71.6 (C-2), 70.8 (C-4 or 5), 70.3 (C-4 or 5), 69.6 (C-6), 55.6 (OMe).

Methyl 6-*O*-benzyl-α-D-glucopyranoside 2,3,4-tris(dibenzylphosphate) (**48**)

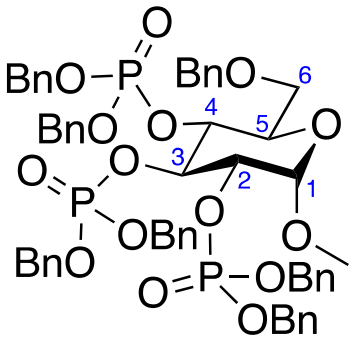

Methyl 6-*O*-benzyl-α-D-glucopyranoside (**45**, 100 mg, 0.35 mmol, 1 equiv) and 5-phenyl-1*H*-tetrazole (308 mg, 2.11 mmol, 6 equiv) were dissolved in dry DCM (4 mL) and put under a nitrogen atmosphere. To this white suspension, the phosphitylating agent dibenzyl phosphoramidite (547 mg, 1.58 mmol, 4.5 equiv) was added, and the reaction was allowed to stir at RT for 1 h. ^{31}PNMR was used to ensure that the phosphitylation was complete. The solution was then cooled to -78 °C and *m*CPBA (522 mg, 2.11 mmol, 6 equiv) was added. The solution was allowed to warm to RT, diluted with EtOAc (30 mL), washed twice with 10% sodium sulphite solution (2 x 30 mL), dried over $MgSO_4$ and evaporated *in vacuo* to form the crude product. The product was purified with flash chromatography (1. P.E.-EtOAc, 0-100%, 2. DCM-EtOAc, 0-100%) to yield the pure product as a colourless oil (341 mg, 0.320 mmol, 91% yield). **$[\alpha]^{20}_D$** 38.0 (*c*= 0.90, $CHCl_3$); **^{1}HNMR** ($CDCl_3$, 400 MHz): δ 7.24-7.06 (m, 35H, Ar), 5.06 (d, *J*= 3.6 Hz, 1H, H-1), 5.00-4.85 (m, 13H, H-3, C*H*$_2$Ph x12), 4.50 (q, *J*= 9.5 Hz, 1H, H-4), 4.45 (AB, *J*= 11.9 Hz, 1H, C-6*H*$_2$Ph), 4.33 (AB, *J*= 11.9 Hz, 1H, C*H*$_2$Ph), 4.23 (ddd, *J*= 9.6, 6.1, 3.5 Hz, 1H, H-2), 3.84-3.80 (m, 1H, H-5), 3.74 (dd, *J*= 11.0, 4.2 Hz, 1H, H-6),

3.69 (dd, *J*= 10.9, 2.1, 1H H-6), 3.25 (s, 3H, OMe); **^{31}PNMR** ($CDCl_3$, 162 MHz): δ -1.23, -2.18, -2.21; **^{13}CNMR** ($CDCl_3$, 100 MHz): δ 138.3 (Ar), 136.3-135.7 (m, Ar), 128.7-127.6 (m, Ar), 97.4 (C-1), 75.1 (C-2), 74.3 (C-4), 73.3 (*C*-6H_2Ph), 70.0-69.5 (m, C-3, C-5, *C*H_2Ph x6), 68.1 (C-6), 55.6 (OMe); **HRMS (ESI)**: *m/z* calcd $[M+H]^+$ for $C_{56}H_{59}O_{15}P_3$: 1065.31396, found: 1065.31327.

Methyl 6-*O*-benzyl-α-D-glucopyranoside 2,3,4-trisphosphate triethylammonium salt (**37**)

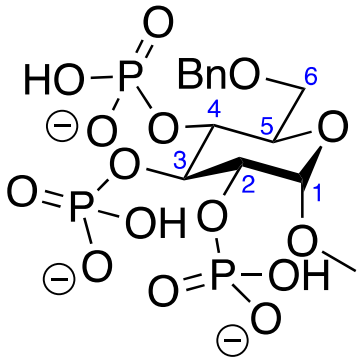

Methyl 6-*O*-benzyl-α-D-glucopyranoside 2,3,4-tris(dibenzylphosphate) (**48**, 50 mg, 0.047 mmol) was dissolved in dry DCM (1.5 mL), and the solution was cooled to -78 °C. TMSBr (0.1 mL, 0.75 mmol, 16 equiv) was added to the solution, and the reaction was allowed to warm to RT as it stirred under nitrogen for 3 h. The solution was then concentrated *in vacuo* to yield a white gum. This white residue was washed with diethyl ether (3 x 5 mL), before being dissolved in fresh TEAB buffer (1 M, 6 mL, pH 7.6). The TEAB solution was washed with diethyl ether (3 x 5 mL) and concentrated under reduced pressure to yield a white solid. This solid was dissolved in MeOH and evaporated three times, after which the residue was collected as the crude product. The product was purified by ion-pair reverse-phase column chromatography (0-30%, MeCN in 0.05 M TEAB). Phosphate-containing fractions were detected using the Briggs Phosphate Assay, combined and concentrated *in vacuo*. The product was dissolved in ultrapure water and lyophilised to yield the pure product as a colourless glass (36.7 mg, calculated 3.4 TEA counterions per molecule of product, 0.043 mmol, 91% yield). **[α]$^{23}_D$** 21.4 (*c*=0.72, MeOH); **^{1}HNMR** (d4-MeOH, 400 MHz): δ 7.38-7.23 (m, 5 H, Ar), 4.90 (d, *J*= 3.6 Hz, 1H, H-1), 4.61 (s, 2H, C*H*$_2$Ph x2), 4.56 (q, *J*= 9.3 Hz, 1H, H-3), 4.14-4.01 (m, 3H, H-2, H-4, H-6), 3.86 (dt, *J*= 1.6, 8.7 Hz, 1H, H-5), 3.68 (dd, *J*= 7.4, 11.1 Hz, 1H, H-6), 3.40 (s, 3H, OMe), 3.18 (q, *J*= 7.0 Hz, approx. 20H, TEA C*H*$_2$CH$_3$), 1.60 (t, *J*= 7.0 Hz, approx. 31H, TEA CH$_2$C*H*$_3$); **^{31}PNMR** (d4-MeOH, 162 MHz): δ 1.38, 1.13, -0.15; **^{13}CNMR** (d4-MeOH, 100 MHz): δ 140.1 (Ar), 129.3 (Ar), 128.7 (Ar), 128.4 (Ar), 100.2 (C-1), 78.1 (m, C-3), 75.8 (m, C-2), 75.5 (m, C-4), 74.4 (*C*-6H_2Ph), 72.0 (m, C-5), 71.5 (C-6), 55.4 (OMe), 47.1 (TEA *C*H_2CH$_3$), 9.1 (TEA CH$_2$*C*H$_3$); **HRMS (ESI)**: *m/z* $[M-H]^-$ calcd for $C_{14}H_{23}O_{15}P_3$: 523.01770, found: 523.01777.

Methyl α-D-glucopyranoside 2,3,4-trisphosphate triethylammonium salt (**38**)

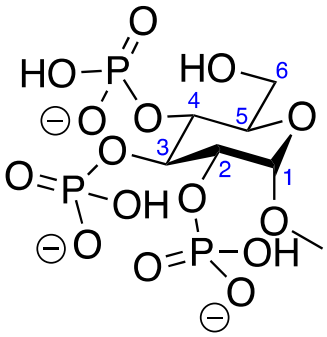

Methyl 6-*O*-benzyl-α-D-glucopyranoside tris(dibenzylphosphate) (**48**, 100 mg, 0.094 mmol, 1 equiv) was dissolved in MeOH (5 mL). Ultrapure water (0.5 mL) was added dropwise to the solution, ensuring that the precipitate that formed dissolved back into solution. 20% $Pd(OH)_2/C$ (≥50% wet, 50 mg,) was then added, and the reaction flask was flushed with hydrogen before being left to stir RT for 24 h. The catalyst was then filtered off using a PTFE syringe filter, and the collected filtrate was evaporated to yield the product as a free acid. Upon NMR analysis, no further purification steps were deemed necessary. To sharpen ^{31}PNMR signals and improve stability, the product was converted into the triethylammonium salt through the addition of excess triethylamine and subsequent concentration. The triethylammonium salt was lyophilised and collected as a colourless glass (53.8 mg, calculated 3.7 TEA counterions per molecule of product, 0.066 mmol, 70% yield). **$[\alpha]^{23}_D$** 49.4 (*c*= 1.08, MeOH) [lit.[361] $[\alpha]^{20}_D$ 56.4 (*c*= 0.5, H_2O) for the sodium salt]; **^{1}HNMR** (d4-MeOH, 400 MHz): δ 4.90 (d, *J*= 3.7 Hz, 1H, H-1), 4.56 (q, *J*= 9.4 Hz, 1H, H-3), 4.16-4.08 (m, 2 H, H-2, H-4), 3.95 (dd, *J*= 12.8, 4.0 Hz, 1H, H-6), 3.72 (dd, 1H, *J*= 12.8, 1.5 Hz, 1H, H-6), 3.60 (brdd, *J*= 9.9, 1.9 Hz, 1H, H-5), 3.37 (s, 3H, OMe), 3.19 (q, *J*= 6.6 Hz, approx. 22H, TEA CH_2CH_3), 1.31 (t, *J*= 6.6 Hz, approx. 33H, TEA CH_2CH_3); **^{31}PNMR** (d4-MeOH, 162 MHz): δ 1.56, 0.84, 0.53; **^{13}CNMR** (D_2O, 100 MHz): δ 98.2 (C-1), 76.2 (C-3), 74.0 (C-2), 72.4 (C-4), 70.8 (C-5), 60.3 (C-6), 54.9 (OMe), 46.5 (TEA CH_2CH_3), 8.2 (TEA CH_2CH_3); **HRMS (ESI)**: *m/z* calcd $[M-H]^-$ for $C_{14}H_{23}O_{15}P_3$: 432.97075, found 432.97061.

Methyl α-D-glucopyranoside 2,3,4,6-tetrakis(dibenzylphosphate) (**43**)

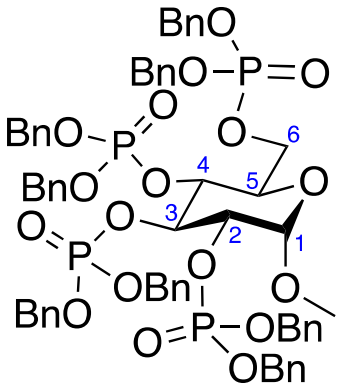

5-Phenyl-1*H*-tetrazole (292 mg, 2 mmol, 8 equiv) was dissolved in dry DCM (3 mL) and put under a nitrogen atmosphere. To this white suspension, the phosphitylating agent, dibenzyl diisopropylphosphoramidite (0.52 mL, 1.5 mmol, 6 equiv), was added and the solution was allowed to stir for 5 min (in which time, the white solid reacted and dissolved). Over the course of an hour, the methyl 6-*O*-benzyl-α-D-glucopyranoside (**42**, 48.5 mg, 0.25 mmol, 1 equiv) was added, and then the reaction was allowed to stir at RT overnight. After 18 h, the solution was cooled to -78 °C, and *m*CPBA (70% pure, 494 mg, 2 mmol, 8 equiv) was added. After 10 min, the solution was diluted with EtOAc (30 mL), washed twice with 10% sodium sulphite solution (2 x 30 mL), dried over $MgSO_4$ and evaporated *in vacuo* to yield the crude product. The product was purified with flash chromatography (DCM-EtOAc, 0-100%) to be collected as a thick, colourless oil (270.5 mg, 0.219 mmol, 88% yield). **$[\alpha]^{21}_D$** 28.0 (*c*=1.00, DCM) [lit.[361] $[\alpha]^{20}_D$ 45.5 (*c*= 1.00, DCM)]; **^{1}HNMR** ($CDCl_3$, 400 MHz): δ 7.32-7.15 (m, 40H, Ar), 5.07-4.94 (m, 18 H, 16 x C*H*$_2$Ph, H-1, H-3), 4.47-4.30 (m, 3H, H-4, 2 x H-6), 4.22 (ddd, *J*= 3.7, 6.0, 9.6 Hz, 1H, H-2), 3.89 (dd, *J*= 4.9, 9.8 Hz, 1H, H-5), 3.36 (s, 3H, OMe); **^{31}PNMR** ($CDCl_3$, 162 MHz): δ -0.99, -1.27, -1.90, -2.22; **^{13}CNMR** ($CDCl_3$, 100 MHz): δ 136.2-135.7 (m, Ar), 128.7-128.0 (m, Ar), 97.3 (C-1), 76.6-76.4 (m, C-3), 74.9 (d, *J*= 4.3 Hz, C-2), 73.7 (C-4), 70.1 (d, *J*= 5.8 Hz, *C*H$_2$Ph), 70.0 (d, *J*= 5.4 Hz, *C*H$_2$Ph), 69.8 (d, *J*= 5.7 Hz, *C*H$_2$Ph), 69.7-69.6 (m, 3 x *C*H$_2$Ph), 69.4 (m, 2 x *C*H$_2$Ph), 68.8 (m, C-5), 66.0 (d, *J*= 5.4 Hz, C-6), 55.8 (OMe); **HRMS (ESI)**: *m/z* calcd $[M+Na]^+$ for $C_{63}H_{66}O_{18}P_4$: 1257.30918, found 1257.30461.

Methyl α-D-glucopyranoside 2,3,4,6-tetrakisphosphate triethylammonium salt (**36**)

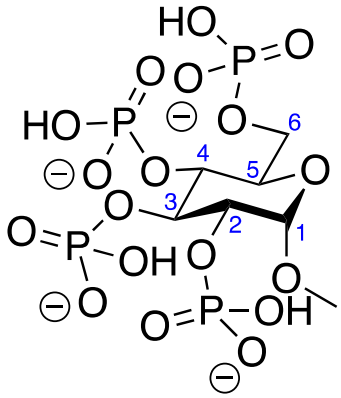

Methyl α-D-glucopyranoside 2,3,4,6-tetrakis(dibenzylphosphate) (**43**, 100 mg, 0.081 mmol) was dissolved in MeOH (5 mL). Ultrapure water (0.5 mL) was then added dropwise, ensuring that precipitate that formed re-dissolved. 20% $Pd(OH)_2/C$ (≥50% wet, 50 mg) was added to the solution and the reaction flask was flushed with hydrogen. The reaction was left to stir at RT for 24 h. The catalyst was then filtered, and the collected filtrate was evaporated to yield the free acid of the product. Upon NMR analysis, no purification steps were deemed to be necessary, but triethylamine was added to sharpen the ^{31}PNMR signals and convert the free acid into the triethylammonium salt of the product. The product was lyophilised and collected as a colourless glass (63.8 mass, calculated 4.2 TEA counterions per molecule of product, 0.068 mmol, 84% yield). **$[\alpha]^{22}_D$** 33.5 (*c*= 1.53, MeOH) [lit.[361] $[\alpha]^{20}_D$ 52.6 (*c*= 0.5, H_2O) for the sodium salt]; **^{1}HNMR** (d4-MeOH): δ 4.88 (d, *J*= 3.7 Hz, 1H, H-1), 4.60 (q, *J*= 9.4 Hz, 1H, H-3), 4.29 (q, *J*= 9.5 Hz, 1H, H-4), 4.23 (ddd, *J*= 10.8, 6.8, 3.6, 1H, H-6), 4.12-4.06 (m, 2H, H-2. H-6), 3.73 (brd, *J*= 9.4 Hz, 1H, H-5), 3.38 (s, 3H, OMe), 3.17 (q, *J*= 7.2 Hz, approx. 25H, TEA C*H*$_2$CH$_3$), 1.30 (t, *J*= 7.2 Hz, approx. 38H, TEA CH$_2$C*H*$_3$); **^{31}PNMR** (d4-MeOH): δ 1.97, 1.58, 1.16, -0.37; **^{13}CNMR** (d4-MeOH): δ 100.6 (C-1), 77.9 (m, C-3), 75.9 (d, *J*= 5.2 Hz, C-2), 74.6 (m, C-4), 71.9-71.8 (m, C-5), 64.7 (C-6), 55.4 (OMe), 46.9 (TEA *C*H$_2$CH$_3$), 9.2 (TEA CH$_2$*C*H$_3$); **HRMS (ESI)**: m/z calcd $[M-H]^-$ for $C_7H_{18}O_{18}P_4$: 512.93708, found: 512.93734;

Methyl β-D-glucopyranoside 2,3,4,6-tetrakis(dibenzylphosphate) **(57)**

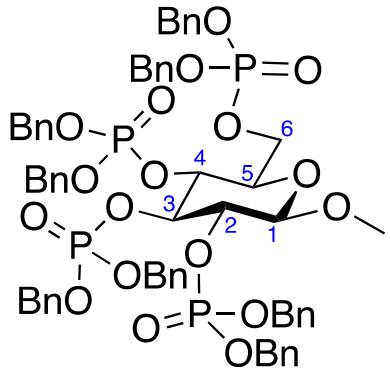

Methyl β-D-glucopyranoside 2,3,4,6-tetrakis(dibenzylphosphate) (**57**) was synthesised using the same method as that used to make methyl α-D-glucopyranoside 2,3,4,6-tetrakis(dibenzylphosphate) (**43**) using methyl β-D-glucopyranoside (100 mg, 0.515 mmol) as the carbohydrate starting material. The product was purified with column chromatography (DCM-EtOAc, 0-100%), and collected as a colourless oil (531.6 mg, 0.430 mmol, 84% yield); **$[\alpha]^{21}_{D}$** 3.93 (c= 1.0, $CHCl_3$); **^{1}HNMR** (d4-MeOH): δ 7.33-7.14 (m, 40H, Ar), 5.09-4.91 (m, 16H, C*H*$_2$Ar), 4.73 (q, *J*= 8.9 Hz, 1H, H-1,2 or 3), 4.52 (ddd, *J*= 2.1, 7.1, 11.4 Hz, 1H, H-6), 4.44-4.32 (m, 3H, H-4 and 1, 2 or 3), 4.25 (ddd, *J*= 1.5 Hz, 6.0, 13.2 Hz, 1H, H-6), 3.66-3.62 (m, 1H, H-5), 3.34 (s, 3H, OMe); **^{31}PNMR** (d4-MeOH): δ -1.26, -1.65, -1.91, -2.60; **^{13}CNMR** (d4-MeOH): δ 136.2-135.6 (m, Ar), 128.7-127.9 (m, Ar), 101.6 (C-1,2,3 or 4), 78.8 (C-1,2 or 3), 77.4 (C-1,2,3 or 4), 73.6 (C-1,2,3 or 4), 73.0 (C-5), 70.1-69.4 (*C*H_2Ar), 66.1 (C-6), 57.2 (CH_3); **HRMS (ESI)**: *m/z* calcd $[M+H]^+$ for $C_{63}H_{66}O_{18}P_4$: 1257.30918, found 1257.30461.

Methyl β-D-glucopyranoside 2,3,4,6-tetrakisphosphate triethylammonium salt (**56**)

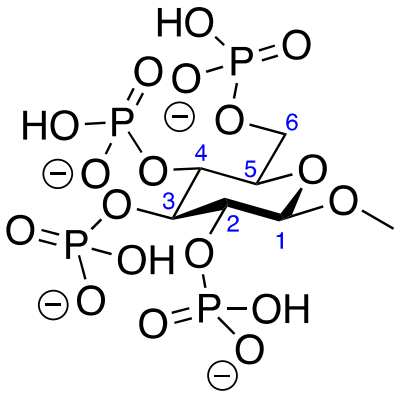

Methyl β-D-glucopyranoside 2,3,4,6-tetrakisphosphate (**56**) was synthesised from methyl β-D-glucopyranoside 2,3,4,6-tetrakis(dibenzylphosphate) (**57**, 233 mg, 0.189 mmol) with the same method used to make methyl α-D-glucopyranoside 2,3,4,6-

tetrakisphosphate (**36**). The product was collected as a white glass (174 mg, calculated 4.1 TEA counterions per molecule of product, 0.189 mmol, 100% yield); **[α]$^{20}_{D}$** -5.3 (*c*=1.0, methanol); **^{1}H NMR** (d4-MeOH): δ 4.40-4.33 (m, 2H), 4.28 (t, *J*= 9.6 Hz, 1H), 4.25-4.19 (m, 1H), 4.14 (dt, *J*= 2.6, 11.2 Hz, 1H), 4.07-4.00 (m, 1H), 3.51 (brd, 1H), 3.48 (s, 3H, OMe), 3.17 (q, *J*= 7.3 Hz, approx. 25H, TEA C*H*$_2$), 1.31 (t, *J*= 7.3 Hz, approx. 37H, TEA C*H*$_3$); **^{31}P NMR** (d4-MeOH): δ 1.54, -0.16, -0.34; **^{13}C NMR** (d4-MeOH): δ 104.4, 81.0, 78.2, 75.6, 74.3, 64.8, 57.0, 47.1 (TEA *C*H$_2$), 9.1 (TEA *C*H$_3$); **HRMS (ESI)**: *m/z* calcd [M-H]$^-$ for $C_7H_{18}O_{18}P_4$: 512.9371, found 512.9369.

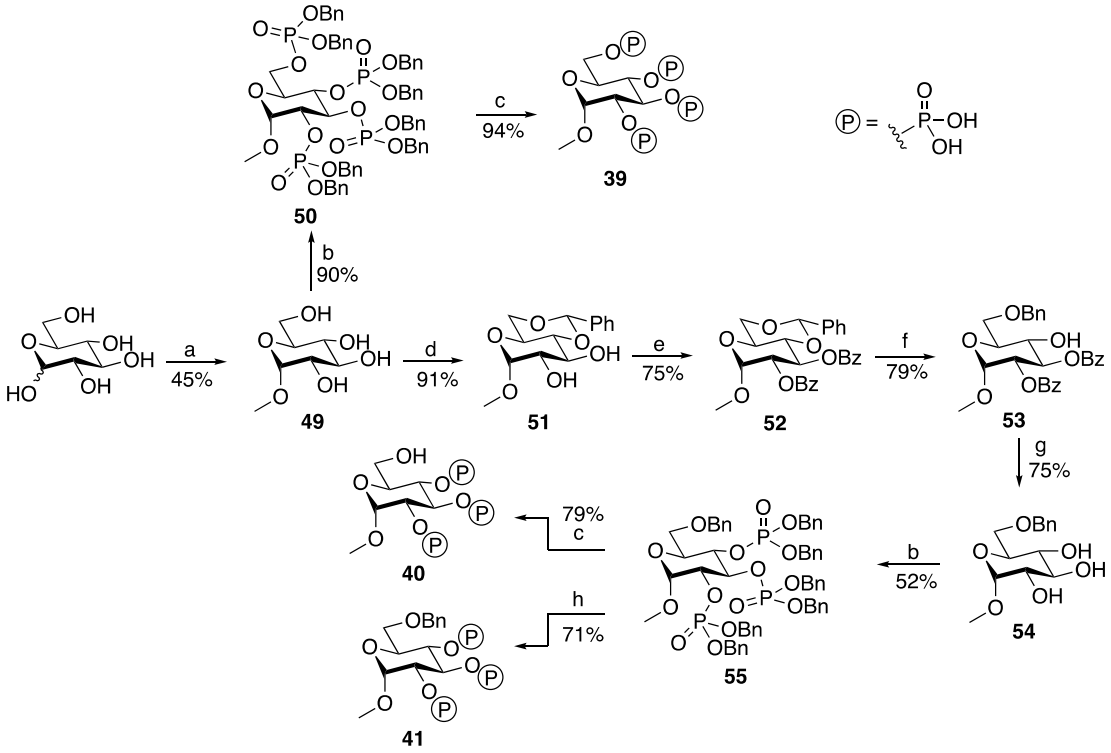

Scheme 7: Synthetic route for the L-glucose based HDAC ligands: methyl α-L-glucopyranoside 2,3,4,6-tetrakisphosphate (**39**), methyl α-L-glucopyranoside 2,3,4-trisphosphate (**40**) and methyl 6-*O*-benzyl α-L-glucopyranoside 2,3,4-trisphosphate (**41**).

Reagents and conditions: (a) CH_3COCl, MeOH; (b) 1. Benzyl P(III) agent, 5-Phenyl-*1H*-tetrazole, DCM, 2. *m*CPBA; (c) 1. $Pd(OH)_2/C$, H_2, MeOH, H_2O, 2. TEA; (d) $PhCH(OMe)_2$, cat. CSA, MeCN; (e) BzCl, py; (f) $Me_3N.BH_3$, $AlCl_3$, THF; (g) NaOH, MeOH; (h) 1. TMSBr, DCM, 2. TEAB.

Methyl α-L-glucopyranoside (**49**)

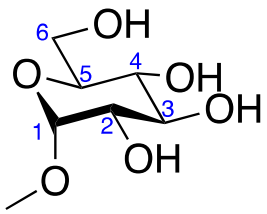

Methyl α-L-glucopyranoside (**49**) was prepared from L-glucose (850 mg, 4.7 mmol) with the same method used to make methyl α-D-glucopyranoside (**42**). The crude product was recrystallized twice from EtOH to isolate the pure α-anomer product as white crystals (414 mg, 2.13 mmol, 45% yield). **m.p.** (from EtOH) 167.2-168.1°C (Lit.[421] m.p. (from EtOH) 161-163 °C); **[α]$^{23}_{D}$** -168.4 (*c*= 1.00, MeOH) [Lit.[421] [α]$_D$ -161 (c= 1.0, MeOH)]; **^{1}HNMR** (d4-MeOH, 400 MHz): δ 4.67 (d, *J*= 3.8 Hz, 1H, H-1), 3.81 (dd, *J*= 11.8, 2.4 Hz, 1H, H-6), 3.67 (dd, *J*= 11.8, 5.8 Hz, 1H, H-6), 3.61 (t, *J*= 9.2 Hz, 1H, H-3), 3.55-3.50 (m, 1H, H-5), 3.41 (s, 3H, OMe), 3.38 (dd, *J*= 9.7, 3.8 Hz, 1H, H-2), 3.27 (dd, *J*= 10.0, 9.0 Hz, 1H, H-4); **^{13}CNMR** (d4-MeOH, 100 MHz): δ 101.2 (C-1), 75.1 (C-3), 73.54 (C-5), 73.53 (C-2), 71.8 (C-4), 62.7 (C-6), 55.5 (OMe).

Methyl 4,6-*O*-benzylidene-α-L-glucopyranoside (**51**)

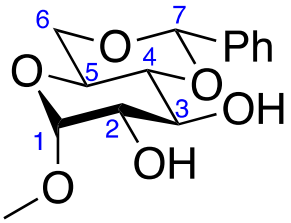

Methyl 4,6-*O*-benzylidene-α-L-glucopyranoside (**51**) was prepared from methyl α-L-glucopyranoside (**49**, 100 mg, 0.514 mmol) using the same method as for the synthesis of methyl 4,6-*O*-benzylidene-α-D-glucopyranoside (**44**). The crude product was purified through flash chromatography (P.E.-EtOAc, 0-100%) and the pure product was collected as a white solid (132.6 mg, 0.470 mmol, 91% yield). **m.p.** 163.1-164.4 °C (Lit.[421] 161-162 °C); **[α]$^{21}_{D}$** -110.5 (*c*= 0.69, $CDCl_3$) [Lit.[421] [α]$_D$ -95 (*c*= 1.0, MeOH)]; **^{1}HNMR** ($CDCl_3$, 400 MHz): δ 7.51-7.48 (m, 2H, Ar), 7.40-7.34 (m, 3H, Ar), 5.53 (s, 1H, H-7), 4.79 (d, *J*= 4.0 Hz, 1H, H-1), 4.29 (dd, *J*= 9.6, 4.3 Hz, 1H, H-6), 3.93 (apt td, *J*= 9.3, 2.2 Hz, 1H, H-3), 3.84-3.78 (m, 1H, H-5), 3.75 (apt q, *J*= 10.3 Hz, 1H, H-6), 3.63 (apt td, *J*= 9.3, 3.9 Hz, 1H, H-2), 3.49 (apt t, *J*= 9.3 Hz, 1H, H-4), 3.46 (s, 3H, OMe), 2.76 (d, *J*= 2.2 Hz, 1H, OH), 2.30 (d, *J*= 9.5 Hz, 1H, OH); **^{13}CNMR** ($CDCl_3$, 100 MHz): δ 137.2 (Ar),

129.4 (Ar), 128.5 (Ar), 126.4 (Ar), 102.1 (C-7), 99.9 (C-1), 81.1 (C-4), 73.0 (C-2), 72.0 (C-3), 69.1 (C-6), 62.5 (C-5), 55.7 (OMe).

Methyl 2,3-di-*O*-benzoyl-4,6-*O*-benzylidene-α-L-glucopyranoside (**52**)

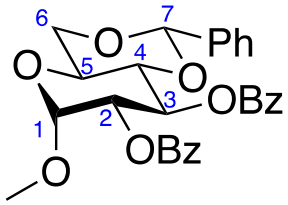

Methyl 2,3-di-*O*-benzoyl-4,6-*O*-benzylidene-α-L-glucopyranoside (**52**) was prepared with methyl 4,6-*O*-benzylidene-α-L-glucopyranoside (**51**, 126 mg, 0.446 mmol) using the same method as that for methyl 4,6-benzylidene-2,3-di-*O*-benzoyl-α-D-glucopyranoside (**46**). The crude product was purified with flash chromatography (1.P.E.-EtOAc, 0-100%, 2. P.E.-EtOAc, 0-100%) to yield the pure product as a white solid (164 mg, 0.334 mmol, 75% yield). **m.p.** 153.0-154.0 °C; **[α]$^{22}_{D}$** -96.8 (*c*=1.02, $CHCl_3$); **^{1}HNMR** ($CDCl_3$, 400 MHz): δ 8.00-7.97 (m, 4H, Ar), 7.53-7.30 (m, 11H, Ar), 6.06 (t, 1H, *J*= 9.7 Hz, H-3), 5.57 (s, 1H, H-7), 5.25 (dd, 1H, *J*= 9.9, 3.7 Hz, H-2), 5.18 (d, 1H, *J*= 3.7 Hz, H-1), 4.38 (dd, 1H, *J*= 10.3, 4.7 Hz, H-6), 4.08 (dt, 1H, 9.9, 4.9 Hz, H-5), 3.90 (t, 1H, *J*= 9.6 Hz, H-4), 3.87 (t, 1H, *J*= 10.3 Hz, H-6), 3.44 (s, 3H, OMe); **^{13}CNMR** ($CDCl_3$, 100 MHz): δ 166.2 (*C*(O)Ph), 165.7 (*C*(O)Ph), 137.1 (Ar), 133.5 (Ar), 133.1 (Ar), 130.1 (Ar), 129.9 (Ar), 129.18 (Ar), 129.15 (Ar), 128.6 (Ar), 128.4 (Ar), 128.3 (Ar), 126.3 (Ar), 101.8 (C-7), 98.0 (C-1), 79.6 (C-4), 72.7 (C-2), 69.7 (C-3), 69.1 (C-6), 62.7 (C-5), 55.7 (OMe).

Methyl 2,3-di-*O*-benzoyl-6-*O*-benzyl-α-L-glucopyranoside (**53**)

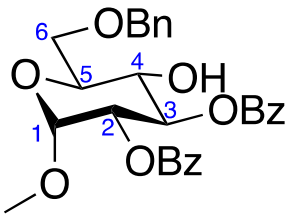

Methyl 2,3-di-*O*-benzoyl-6-*O*-benzyl-α-L-glucopyranoside (**53**) was prepared from methyl 2,3-di-*O*-benzoyl-4,6-*O*-benzylidene-α-L-glucopyranoside (**52**, 98.3 mg, 0.200 mmol) using the same method as for the synthesis of methyl 2,3-di-*O*-benzoyl-6-*O*-benzyl-α-D-glucopyranoside (**47**). The crude product was purified with flash chromatography (P.E.-EtOAc, 0-100%) to yield the product as a colourless oil (77.6 mg, 0.158 mmol, 79% yield). **[α]$^{22}_{D}$** -137.8 (*c*= 1.06, DCM); **^{1}HNMR** ($CDCl_3$, 400 MHz): δ 8.00-7.97 (m, 4H, Ar), 7.53-7.29 (m, 11H, Ar), 5.75 (t, *J*= 9.1 Hz, 1H, H-3), 5.26 (dd, *J*= 10.1, 3.6 Hz, 1H, H-2), 5.13 (d, *J*= 3.5 Hz, 1H, H-1), 4.64 (q, *J*= 12.0 Hz, 2H, CH_2Ph x2), 4.02-

3.93 (m, 2H, H-4, H-5), 3.88-3.79 (m, 2H, H-6 x2), 3.43 (s, 3H, OMe), 3.04 (brs, 1H, OH); **^{13}CNMR** ($CDCl_3$, 100 MHz): δ 167.5 (*C*(O)Ph), 166.1 (*C*(O)Ph), 137.9 (Ar), 133.49 (Ar), 133.46 (Ar), 130.0 (Ar), 129.4 (Ar), 129.3 (Ar), 128.6 (Ar), 128.54 (Ar), 128.52 (Ar), 128.0 (Ar), 127.9 (Ar), 97.2 (C-1), 74.3 (C-3), 73.9 (*C*H_2Ph), 71.6 (C-2), 70.8 (C-4 or 5), 70.3 (C-4 or 5), 69.6 (C-6), 55.6 (OMe).

Methyl 6-*O*-benzyl-α-L-glucopyranoside (**54**)

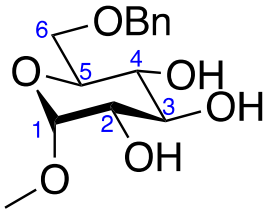

Methyl 6-*O*-benzyl-α-L-glucopyranoside (**54**) was prepared with methyl 6-*O*-benzyl-2,3-di-*O*-benzoyl-α-L-glucopyranoside (**53**, 92.6 mg, 0.188 mmol) using method B described for the preparation for methyl 6-*O*-benzyl-α-D-glucopyranoside (**45**). The crude product was purified through flash chromatography (DCM-MeOH, 0-10%) to yield the pure product (39.9 mg, 0.140 mmol, 75% yield). **m.p.** 50.0-56.0 °C (Lit.[419] m.p. 58-60 °C); **$[\alpha]^{22}_D$** -71.1 (*c*= 1.00, $CHCl_3$) [Lit.[419] ; $[\alpha]_D$ -83.1 (*c*= 0.81, $CHCl_3$)]; **^{1}HNMR** ($CDCl_3$, 400 MHz): δ 7.38-7.28 (m, 5H, Ar), 4.79 (d, *J*= 3.9 Hz, 1H, H-1), 4.64 (AB, *J*= 12.1 Hz, 1H, CH_2Ph), 4.57 (AB, *J*= 12.1 Hz, 1H, CH_2Ph), 3.77-3.69 (m, 4H, H-3, H-4 or 5, H-6 x2), 3.63-3.58 (m, 1H, H-2), 3.54 (apt td, *J*= 9.6, 3.9 Hz, 1H, H-4 or 5), 3.43 (s, 3H, OMe); **^{13}CNMR** ($CDCl_3$, 100 MHz): δ 138.1 (Ar), 128.5 (Ar), 127.79 (Ar), 127.77 (Ar), 99.6 (C-1), 74.5 (C-3,4 or 5), 73.7 (*C*H_2Ph), 72.1 (C-2), 70.9 (C-3,4 or 5), 70.6 (C-3,4 or 5), 69.7 (C-6), 55.4 (OMe).

Methyl 6-*O*-benzyl-α-L-glucopyranoside 2,3,4-tris(dibenzylphosphate) (**55**)

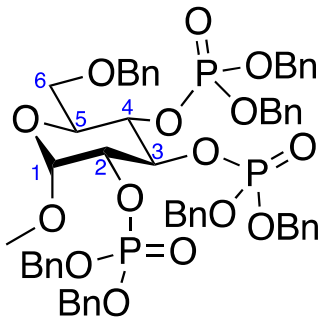

Methyl 6-*O*-benzyl-α-L-glucopyranoside 2,3,4-tris(dibenzylphosphate) (**55**) was prepared with methyl 6-*O*-benzyl-α-L-glucopyranoside (**54**, 33 mg, 0.116 mmol) in the same method as for methyl 6-*O*-benzyl-α-D-glucopyranoside 2,3,4-tris(dibenzylphosphate) (**48**). The crude product was purified through flash

chromatography (1. P.E.-EtOAc, 0-100%, 2. DCM-EtOAc, 0-100%) to yield the pure product as a colourless oil (63.8 mg, 0.060 mmol, 52% yield). **[α]$^{22}_{D}$** -34.7 (*c*= 0.68, $CHCl_3$); **^{1}HNMR** ($CDCl_3$, 400 MHz): δ 7.31-7.13 (m, 35H, Ar), 5.13 (d, *J*= 3.5 Hz, 1H, H-1), 5.08-4.92 (m, 13H, H-3, CH_2Ph x12), 4.57 (q, *J*= 9.5 Hz, 1H, H-4), 4.52 (AB, *J*= 11.9 Hz, 1H, C-6*H*$_2$Ph), 4.40 (AB, *J*= 11.9 Hz, 1H, C-6*H*$_2$Ph), 4.33-4.28 (m, 1H, H-2), 3.91-3.87 (m, 1H, H-5), 3.83-3.74 (m, 2H, H-6 x2), 3.32 (s, 3H, OMe); **^{31}PNMR** ($CDCl_3$, 162 MHz): δ -1.27, -2.22, -2.24; **^{13}CNMR** ($CDCl_3$, 100 MHz): δ 138.3 (Ar), 136.2-135.7 (m, Ar), 128.7-128.6 (m, Ar), 128.5-128.4 (m, Ar), 128.3-128.1 (m, Ar), 128.0 (Ar), 127.7 (Ar), 127.6 (Ar), 97.3 (C-1), 75.1 (m, C-2), 74.3 (m, C-4), 73.3 (*C*-6H_2Ph), 70.0 (d, J= 5.6 Hz, C-5), 69.8-69.5 (m, C-3, *C*H_2Ph x6), 68.1 (C-6), 55.6 (OMe); **HRMS (ESI)**: *m/z* calcd $[M+H]^+$ for $C_{56}H_{59}O_{15}P_3$: 1065.31396, found: 1065.31250.

Methyl 6-*O*-benzyl-α-L-glucopyranoside 2,3,4-trisphosphate triethylammonium salt (**41**)

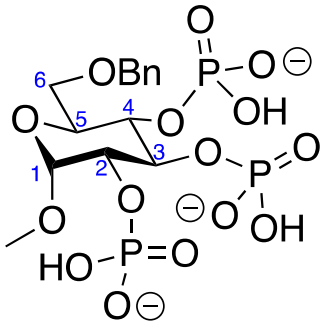

Methyl 6-*O*-benzyl-α-L-glucopyranoside 2,3,4-trisphosphate triethylammonium salt (**41**) was prepared with methyl 6-*O*-benzyl-α-L-glucopyranoside 2,3,4-tris(dibenzylphosphate) (**055**, 30 mg, 0.028 mmol) using the same method as that for the synthesis of methyl 6-*O*-benzyl-α-L-glucopyranoside 2,3,4-trisphosphate triethylammonium salt (**37**). The crude product was purified by ion-pair reverse-phase column chromatography and lyophilised to yield the pure product as a colourless glass (16.5 mg, calculated 3.0 TEA counterions per molecule of product, 0.020 mmol, 71% yield). **[α]$^{23}_{D}$** -29.9 (*c*= 1.02, MeOH); **^{1}HNMR** (d4-MeOH, 400 MHz): δ 7.38-7.22 (m, 5H, Ar), 4.93 (d, *J*= 3.6Hz, 1H, H-1), 4.61 (s, 2H, C*H*$_2$Ph x2), 4.56 (q, *J*= 9.3 Hz, 1H, H-3), 4.14-4.02 (m, 3H, H-2, H-4, H-6), 3.87 (brt, *J*= 8.7 Hz, 1H, H-5), 3.68 (dd, *J*= 11.1, 7.5 Hz, 1H, H-6), 3.40 (s, 3H, OMe), 3.19 (q, *J*= 7.4 Hz, approx. 18H, TEA C*H*$_2$CH$_3$), 1.30 (t, *J*= 7.4 Hz, approx. 27H, TEA CH$_2$C*H*$_3$); **^{31}PNMR** (d4-MeOH, 162 MHz): δ 1.87, 1.43, 0.05; **^{13}CNMR** (d4-MeOH, 100 MHz): δ 140.0 (Ar), 129.3 (Ar), 128.7 (Ar), 128.5 (Ar), 100.0 (C-1), 78.3 (m, C-3), 75.7 (m, C-2), 75.5 (m, C-4), 74.4 (C*H*$_2$Ph), 71.9 (m, C-5), 71.3 (C-6), 55.5 (OMe), 47.3 (TEA *C*H$_2$CH$_3$), 9.1 (TEA CH$_2$*C*H$_3$); **HRMS (ESI)**: *m/z* $[M-H]^-$ calcd for $C_{14}H_{23}O_{15}P_3$: 523.01770, found: 523.01800.

Methyl α-L-glucopyranoside 2,3,4-trisphosphate triethylammonium salt (**40**)

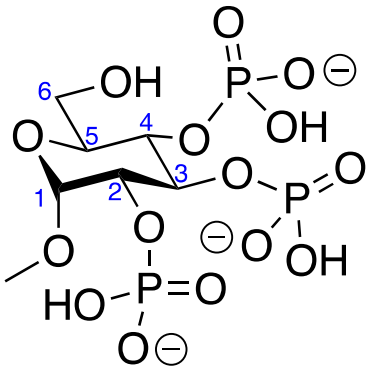

Methyl α-L-glucopyranoside 2,3,4-trisphosphate triethylammonium salt (**40**) was prepared with methyl 6-*O*-Benzyl α-L-glucopyranoside 2,3,4-tris(dibenzylphosphate) (**55**, 29.6 mg, 0.028 mmol) using the same method as for the synthesis of methyl α-D-glucopyranoside 2,3,4-trisphosphate triethylammonium salt (**38**). Upon NMR analysis of the product, no purification steps were deemed to be necessary, and the product converted to the triethylammonium salt with the addition of excess triethylamine. The product was concentrated *in vacuo* then lyophilised before being collected as a colourless glass (16 mg, calculated 3.0 TEA counterions per molecule of product, 0.022 mmol, 79% yield). **[α]$^{23}_{D}$** -42.9 (*c*= 0.98, MeOH); **^{1}HNMR** (d4-MeOH, 400 MHz): δ 4.92 (d, *J*= 3.8 Hz, H-1), 4.56 (q, *J*= 9.3 Hz, 1H, H-3), 4.16-4.09 (m, 2H, H-2, H-4), 3.93 (dd, *J*= 12.8, 4.0 Hz, 1H, H-6), 3.73 (dd, *J*= 12.9, 1.6 Hz, 1H, H-6), 3.61 (brdd, *J*= 10.0, 2.1 Hz, 1H, H-5), 3.38 (s, 3H, OMe), 3.20 (q, *J*= 6.6 Hz, approx. 18H, TEA C*H*$_2$CH$_3$), 1.31 (t, *J*= 7.0 Hz, approx. 27H, TEA CH$_2$C*H*$_3$); **^{31}PNMR** (d4-MeOH, 162 MHz): δ 2.38, 1.44, 0.72; **^{13}CNMR** (d4-MeOH, 100 MHz): δ 100.9 (C-1), 77.6 (C-3), 76.3 (C-2), 74.0 (C-4), 72.9 (C-5), 62.0 (C-6), 55.3 (OMe), 46.9 (TEA *C*H$_2$CH$_3$), 9.5 (TEA CH$_2$*C*H$_3$); **HRMS (ESI)**: *m/z* calcd [M-H]$^-$ for $C_{14}H_{23}O_{15}P_3$: 432.97075, found 432.97101.

Methyl α-L-glucopyranoside 2,3,4,6-tetrakis(dibenzylphosphate) (**50**)

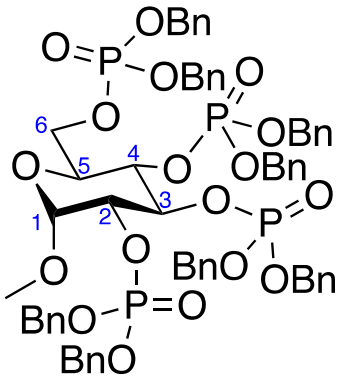

Methyl α-L-glucopyranoside 2,3,4,6-tetrakis(dibenzylphosphate) (**50**) was synthesised with methyl-α-L-glucopyranoside (**49**, 50 mg, 0.258 mmol) under the same conditions

as for the preparation of methyl-α-D-glucopyranoside 2,3,4,6-tetrakis(dibenzylphosphate) (**43**). The crude product was purified by flash chromatography (DCM-EtOAc, 0-100%), and the pure product was collected as a colourless oil (285.7 mg, 0.231 mmol, 90% yield). **[α]$^{23}_{D}$** -29.47 (*c*= 1.00, DCM); **^{1}HNMR** ($CDCl_3$, 400 MHz): δ 7.33-7.14 (m, 40H, Ar), 5.07 (d, *J*= 3.5 Hz, 1H, H-1), 5.05-4.93 (m, 17H, 16 x C*H*$_2$Ph, H-3), 4.47-4.42 (m, 1H, H-6), 4.40 (d, *J*= 9.3 Hz, 1H, H-4), 4.36-4.30 (m, 1H, H-6), 4.24-4.19 (m, 1H, H-2), 3.90-3.87 (m, 1H, H-5), 3.26 (s, 3H, OMe); **^{31}PNMR** ($CDCl_3$, 162 MHz): δ -1.00, -1.27, -1.90, -2.23; **^{13}CNMR** ($CDCl_3$, 100 MHz): δ 136.1-135.7 (m, Ar), 128.7-128.0 (m, Ar), 97.2 (C-1), 76.5 (C-3), 74.9 (C-2), 73.7 (C-4), 70.1-69.4 (m, *C*H_2Ph x 8), 68.8-68.7 (m, C-5), 66.0 (d, J= 5.3Hz, C-6), 55.8 (OMe); **HRMS (ESI)**: *m/z* calcd $[M+H]^+$ for $C_{63}H_{66}O_{18}P_4$: 1235.32724, found 1235.32348.

Methyl α-L-glucopyranoside 2,3,4,6-tetrakis phosphate triethylammonium salt (**39**)

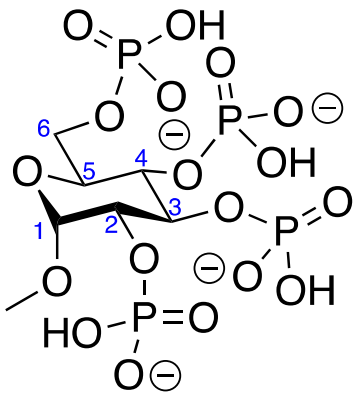

Methyl α-L-glucopyranoside 2,3,4,6-tetrakis phosphate triethylammonium salt (**39**) was synthesised with methyl-α-L-glucopyranoside 2,3,4,6-tetrakis(dibenzylphosphate) (**50**, 100 mg, 0.081 mmol) using the same method as the preparation for methyl α-D-glucopyranoside 2,3,4,6-tetrakis phosphate triethylammonium salt (**36**). Upon NMR analysis, no purification step was deemed necessary for the product, and it was converted to a triethylammonium salt, lyophilised and collected as a colourless glass (68.6 mg, calculated 3.9 TEA counterions per molecule of product, 0.076 mmol, 94% yield). **[α]$^{23}_{D}$** -33.3 (*c*= 1.53, MeOH); **^{1}HNMR** (d4-MeOH, 400 MHz): δ 4.89 (d, *J*= 3.7 Hz, 1H, H-1), 4.60 (q, *J*= 9.4 Hz, 1H, H-3), 4.29 (q, *J*= 9.6 Hz, 1H, H-4), 4.26-4.21 (m, 1H, H-6), 4.12-4.06 (m, 2H, H-2, H-6), 3.74 (brd, *J*= 9.6 Hz, 1H, H-5), 3.38 (s, 3H, OMe), 3.20 (q, *J*= 6.9 Hz, approx. 23H, TEA C*H*$_2$CH$_3$), 1.31 (t, *J*= 6.9 Hz, approx. 35H, TEA CH$_2$C*H*$_3$); **^{31}PNMR** (d4-MeOH, 162 MHz): δ 1.60, 1.26, 0.92, -0.30; **^{13}CNMR** (d4-MeOH, 100 MHz): δ 100.5 (C-1), 78.0 (C-3), 75.9 (C-2), 74.6 (C-4), 71.8 (C-5), 64.7 (C-6), 55.4 (OMe), 46.9 (TEA *C*H$_2$CH$_3$), 9.1 (TEA CH$_2$*C*H$_3$); **HRMS (ESI)**: m/z calcd $[M-H]^-$ for $C_7H_{18}O_{18}P_4$: 512.93708, found: 512.93713.

Synthesis of $InsP_3R$ carbohydrate polyphosphates

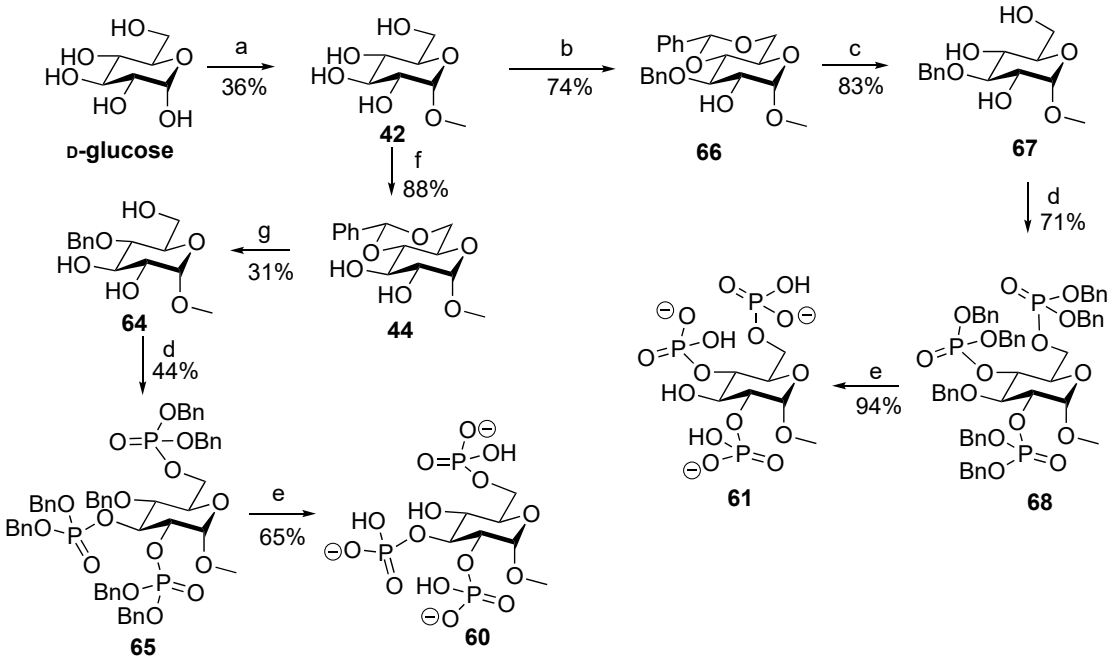

Scheme 8: Synthetic routes for the $InsP_3R$ ligands derived from D-glucose: methyl α-D-glucopyranoside 2,3,6-trisphosphate (**60**) and methyl α-D-glucopyranoside 2,4,6-trisphosphate (**61**).

Reagents and conditions: (a) MeOH, AcCl, reflux, 5d; (b) 1. TMSCl, py, 22h 2. DCM, benzaldehyde, $Fe(II)Cl_2 \bullet 6H_2O$, MeCN, triethylsilane, 0°C-rt, 1.5h; (c) MeOH, H_2O, 1M $HCl_{(aq)}$, Reflux, 3h; (d) 1. DCM, 5-phenyl-1*H*-tetrazole, $(OBn)_2PN(^iPr)_2$, 20h 2. *m*CPBA, -78°C-rt; (e) MeOH:H_2O (10:1 v/v), cat. $Pd(OH)_2/C$, H_2, 24h; (f) MeCN, benzaldehyde dimethyl acetal, cat. CSA, 24h; (g) BH_3-THF, $La(Tf)_3$, 7d.

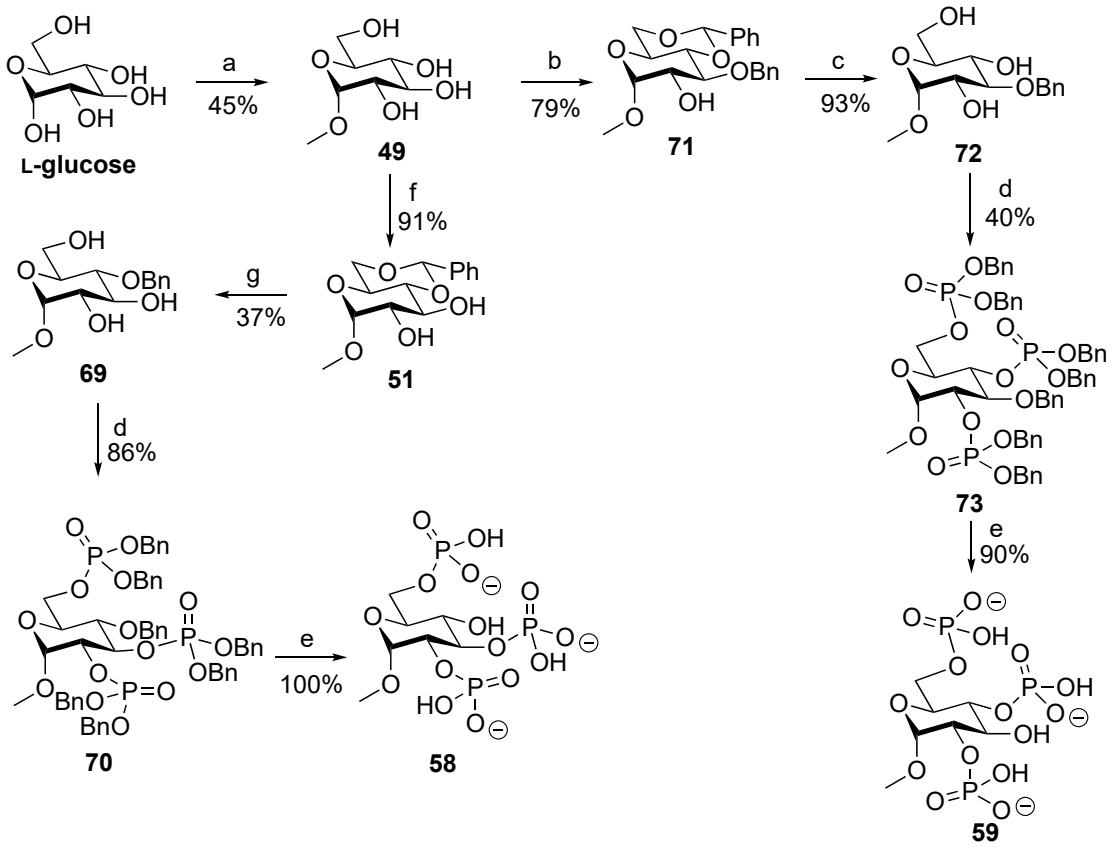

Scheme 9: Synthetic routes for the $InsP_3R$ ligands derived from L-glucose: methyl α-L-glucopyranoside 2,3,6-trisphosphate (**58**) and methyl α-L-glucopyranoside 2,4,6-trisphosphate (**59**)

Reagents and conditions: (a) MeOH, AcCl, reflux, 5d; (b) 1. TMSCl, py, 22h 2. DCM, benzaldehyde, $Fe(II)Cl_2{\cdot}6H_2O$, MeCN, triethylsilane, 0°C-rt, 1.5h; (c) MeOH, H_2O, 1M $HCl_{(aq)}$, Reflux, 3h; (d) 1. DCM, 5-phenyl-1*H*-tetrazole, $(OBn)_2PN(^iPr)_2$, 20h 2. *m*CPBA, -78°C-rt; (e) MeOH:H_2O (10:1 v/v), cat. $Pd(OH)_2/C$, H_2, 24h; (f) MeCN, benzaldehyde dimethyl acetal, cat. CSA, 24h; (g) BH_3-THF, $La(Tf)_3$, 7d.

Methyl 4,6-*O*-benzylidene-3-*O*-benzyl-α-D-glucopyranoside (**66**)

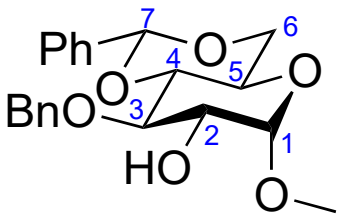

As described by Bourdreux *et al*.,[342] methyl α-D-glucopyranoside (**42**, 100 mg, 0.515 mmol) was dissolved in dry pyridine (1 mL) and put under argon. To this solution, trimethylsilyl chloride (0.33 mL, 2.57 mmol, 5 equiv) was added dropwise. The solution was allowed to stir for 22 h at RT. The reaction was then diluted with EtOAc and washed with water (2 x 30 mL). The organic phase was dried over $MgSO_4$ and concentrated *in vacuo* to yield the per-silylated glucopyranoside crude product. The

per-silylated product was not purified, but NMR spectroscopy was used to confirm that the reaction had proceeded to completion. The per-silylated product was dissolved and co-evaporated twice with toluene, before being dissolved in dry DCM (0.7 mL) and put under argon. To this solution, benzaldehyde (0.16 mL, 1.55 mmol, 3 equiv) was added and the reaction was cooled to 0°C. To this chilled solution, iron (III) chloride hexahydrate (3.6 mg, 0.013 mg, 0.026 equiv) dissolved in MeCN (0.12 mL) was added dropwise. Triethylsilane (0.09 mL, 0.568 mmol, 1.1 equiv) was then added dropwise, and the reaction was allowed to warm to RT and stir for 1 h 30 min. After this time, the solution was diluted with EtOAc (50 mL), washed with sat. $NaHCO_3$ solution (50 mL), and extracted from the aqueous phase twice more with EtOAc (2 x 30 mL). The combined organic phases were dried over $MgSO_4$ and concentrated *in vacuo* to yield the crude product. The crude product was purified with flash chromatography (P.E.-EtOAc, 0-100%) to be collected as a white solid (143 mg, 0.384 mmol, 74% yield). **m.p.** 178.4-181.0 °C (Lit.[422] m.p. 184 °C); **$[\alpha]^{22}_D$** 87.7 (*c*= 0.70, $CHCl_3$) [Lit.[422] $[\alpha]^{20}_D$ 77 (*c*= 0.91, $CHCl_3$)]; **^{1}HNMR** ($CDCl_3$, 400 MHz): δ 7.52-7.27 (m, 10H, Ar), 5.57 (s, 1H, H-7), 4.97 (d, *J*= 11.6 Hz, 1H, C*H*$_2$Ph), 4.82 (d, *J*= 3.8 Hz, 1H, H-1), 4.79 (d, *J*= 11.6 Hz, 1H, C*H*$_2$Ph), 4.30 (dd, *J*= 4.3, 9.8 Hz, 1H, H-6), 3.87-3.71 (m, 4H, H-2, H-3, H-5, H-6), 3.65 (t, 1H, *J*= 9.1 Hz, H-4), 3.45 (s, 3H, OMe), 2.29 (d, 1H, *J*= 7.4 Hz, OH); **^{13}CNMR** ($CDCl_3$, 100 MHz): δ 138.6 (Ar), 137.4 (Ar), 129.1 (Ar), 128.5 (Ar), 128.4 (Ar), 128.1 (Ar), 127.9 (Ar), 126.1 (Ar), 101.4 (H-7), 100.0 (C-1), 82.1 (C-4), 79.0 (C-2 or 3 or 5), 74.9 (*C*H$_2$Ph), 72.5 (C-2 or 3 or 5), 69.1 (C-6), 62.7 (C-2 or 3 or 5), 55.5 (OMe).

Methyl 3-*O*-benzyl-α-D-glucopyranoside (**67**)

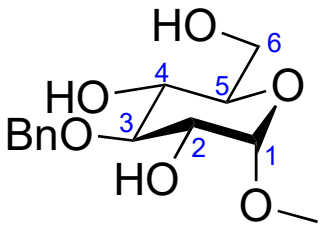

Methyl 4,6-*O*-benzylidene-3-*O*-benzyl-α-D-glucopyranoside (**66**, 120 mg, 0.322 mmol) was dissolved in MeOH (3 mL). To this solution, water (0.15 mL) and 1 M HCl $_{(aq)}$ (0.3 mL) were added. The reaction was heated to reflux for 3 h. After this time, the reaction was quenched with the addition of $NaHCO_{3\ (aq)}$ (25 mg in 5 mL water). The solution was concentrated *in vacuo* and the residue was dissolved and co-evaporated with toluene twice to yield the crude product. The product was purified with flash chromatography (petroleum ether/EtOAc, 0-100%) to yield the pure product as a white solid (75.7 mg, 0.266 mmol, 83% yield). **m.p.** 92.1- 93.9 °C (Lit.[423] m.p. ($CHCl_3$) 85-86 °C); **$[\alpha]^{23}_D$** 89.9 (*c*= 1.05, $CHCl_3$) [Lit.[423] $[\alpha]^{23}_D$ 95.1 (*c*=1.16, $CHCl_3$)]; **^{1}HNMR** ($CDCl_3$, 400 MHz): δ 7.39-7.27 (m, 5H, Ar), 4.99 (AB, *J*= 11.6, 1H, C*H*$_2$Ph), 4.74 (AB, *J*= 11.6 Hz, 1H, C*H*$_2$Ph), 4.73 (d, *J*= 3.7 Hz, 1H, H-1), 3.82-3.74 (m, 2H, H-6 x2), 3.67-3.52

(m, 4H, H-2, H-3, H-4, H-5), 3.42 (s, 3H, OMe), 2.74 (d, *J*= 2.5 Hz, 1H, OH), 2.32 (d, *J*= 8.7 Hz, 1H, OH), 2.27 (t, *J*= 6.4 Hz, 1H, OH); **^{13}CNMR** ($CDCl_3$, 100 MHz): δ 138.6 (Ar), 128.7 (Ar), 128.10 (Ar), 128.07 (Ar), 99.7 (C-1), 82.8 (C-3), 75.1 (*C*H_2Ph), 72.9 (C-2), 71.2 (C-5), 70.1 (C-4), 62.3 (C-6), 55.5 (OMe).

Methyl 3-*O*-benzyl-α-D-glucopyranoside 2,4,6-tris(dibenzylphosphate) (**68**)

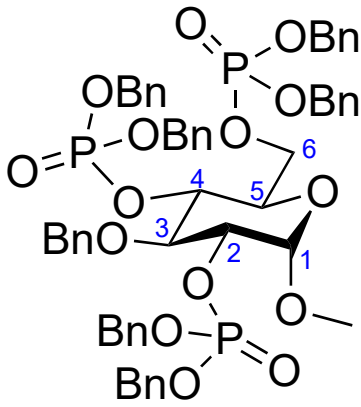

Methyl 3-*O*-benzyl-α-D-glucopyranoside (**67**, 51.9 mg, 0.183 mmol) was dissolved in dry DCM (2 mL) and the solution was put under argon. 5-Phenyl-1*H*-tetrazole (160 mg, 1.10 mmol, 6 equiv) was added to the solution, followed by dibenzyl phosphoramidite (0.30 mL, 0.82 mmol, 4.5 equiv). The reaction was allowed to stir at RT overnight. After confirmation of successful phosphitylation with ^{31}PNMR spectroscopy, the reaction flask was cooled to -78°C and *m*CPBA (270.7 mg, 70% purity, 1.10 mmol, 6 equiv) was added. The reaction was allowed to stir at RT for 10 min before the solution was diluted with EtOAc (50 mL), washed with 10% Na_2SO_3 solution (2 x 30 mL), dried over $MgSO_4$ and concentrated to yield the crude product. The product was purified with flash chromatography (P.E.-EtOAc, 0-100%) to yield the pure product as a colourless oil (138.1 mg, 0.130 mmol, 71% yield). **[α]$^{21}_D$** 41.4 (*c*= 0.61, $CHCl_3$); **^{1}HNMR** ($CDCl_3$, 400 MHz): δ 7.35-7.08 (m, 35H, Ar), 5.03 (s, 2H, C*H*$_2$Ph x2), 5.01 (s, 2H, C*H*$_2$Ph x2), 4.98 (d, *J*= 3.2 Hz, 1H, C*H*$_2$Ph), 4.97 (d, *J*= 3.2 Hz, 1H, C*H*$_2$Ph), 4.94-4.85 (m, 6H, H-1, C*H*$_2$Ph x5), 4.81-4.75 (m, 3H, C*H*$_2$Ph x3), 4.43-4.18 (m, 4H, H-2, H-3, H-6 x2), 3.98 (t, *J*= 9.3 Hz, 1H, H-4), 3.86 (dd, *J*= 10.0, 5.2 Hz, 1H, H-5), 3.28 (s, 3H, OMe); **^{31}PNMR** ($CDCl_3$, 162 MHz): δ -0.98, -1.73, -1.85; **^{13}CNMR** ($CDCl_3$, 100 MHz): δ 138.1 (Ar), 136.0 (Ar), 135.9 (Ar), 135.8-132.6 (m, Ar), 128.7-128.5 (m, Ar), 128.3 (Ar), 128.0 (m, Ar), 127.8 (Ar), 127.7 (Ar), 127.5 (Ar), 97.6 (C-1), 78.3 (m, C-4), 76.7 (m, C-2 or 3), 75.0 (C-2 or 3, *C*H_2Ph), 69.6 (m, *C*H_2Ph), 69.4 (m, CH_2Ph), 68.9 (m, C-5), 66.1 (m, C-6), 55.7 (OMe); **HRMS (ESI)**: *m/z* calcd $[M+H]^+$ for $C_{56}H_{59}O_{15}P_3$: 1065.31396, found: 1065.31336.

Methyl α-D-glucopyranoside 2,4,6-trisphosphate triethylammonium salt (**61**)

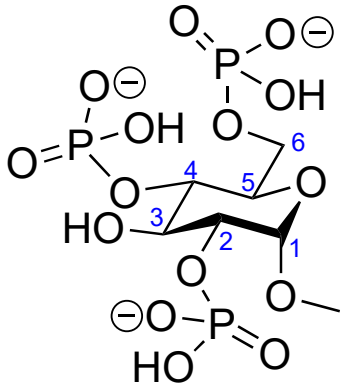

Methyl 3-*O*-benzyl-α-D-glucopyranoside 2,4,6-tris(dibenzylphosphate) (**68**, 132.4 mg, 0.124 mmol) was dissolved in MeOH (6.6 mL). Ultrapure water (0.66 mL) was added dropwise to the solution, ensuring that the precipitate formed upon addition was able to dissolve back into solution. 20% $Pd(OH)_2/C$ (≥50% wet, 66.2 mg) was added to the solution, and the reaction flask was flushed with hydrogen. The reaction was allowed to stir at RT for 24 h, after which the catalyst was filtered off and the collected filtrate was evaporated to yield the product as a free acid. Upon NMR analysis, no purification steps were deemed to be necessary. Excess triethylamine was added to sharpen the ^{31}PNMR signals and to convert the product from the free acid into the triethylammonium salt. The product was concentrated *in vacuo* before being lyophilised and collected as a colourless glass (86 mg, calculated 3.3 TEA counterions per molecule of product, 0.10 mmol, 94% yield). **$[\alpha]^{22}_D$** 39.3 (*c*= 0.43, MeOH); **^{1}H NMR** (d4-MeOH, 400 MHz): δ 4.91 (d, *J*= 2.8 Hz, 1H, H-1), 4.26-4.16 (m, 2H, H-3, H-6), 4.05-3.98 (m, 3H, H-2, H-4, H-6), 3.70 (brd, *J*= 9.8 Hz, 1H, H-5), 3.39 (s, 3H, OMe), 3.12 (q, *J*= 7.5 Hz, approx. 20H, TEA C*H*$_2$CH$_3$), 1.29 (t, *J*= 7.5 Hz, approx. 30H, TEA CH$_2$C*H*$_3$); ^{31}PNMR (d4-MeOH, 162 MHz): δ 1.99, 1.75, 1.32; **^{13}C NMR** (d4-MeOH, 100 MHz): δ 100.2 (C-1), 76.3 (d, 5.6 Hz, C-2 or 4), 74.6 (d, 3.4 Hz, C-2 or 4), 73.5 (d, 5.5 Hz, C-3), 71.1 (m, C-5), 63.9 (C-6), 55.6 (OMe), 47.0 (TEA *C*H$_2$CH$_3$), (TEA CH$_2$*C*H$_3$) 9.3; **HRMS (ESI)**: *m/z* calcd $[M-H]^-$ for $C_7H_{17}O_{15}P_3$: 432.97075, found: 432.97063.

Methyl 3-*O*-benzyl-4,6-*O*-benzylidene-α-L-glucopyranoside (**71**)

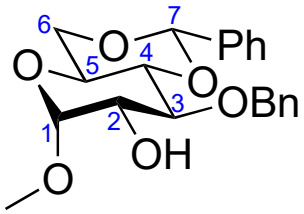

Methyl 3-*O*-benzyl-4,6-*O*-benzylidene-α-L-glucopyranoside (**71**) was synthesized with methyl α-L-glucopyranoside (**49**, 93 mg, 0.479 mmol) using the same method used to make methyl 3-*O*-benzyl-4,6-*O*-benzylidene-α-D-glucopyranoside (**66**). The crude product was purified with flash chromatography (P.E.-EtOAc, 0-100%) to yield the pure product as a white solid (140.7 mg, 0.378 mmol, 79% yield). **m.p.** 184.0-185.3 °C; **[α]$^{21}_{D}$** -87.5 (*c*= 1.00, $CHCl_3$); **^{1}HNMR** ($CDCl_3$, 400 MHz): δ 7.51-7.27 (m, 10H, Ar), 5.57 (s, 1H, H-7), 4.97 (d, *J*= 11.6 Hz, 1H, C*H*$_2$Ph), 4.82 (d, *J*= 3.9 Hz, 1H, H-1), 4.79 (d, *J*= 11.6 Hz, 1H, C*H*$_2$Ph), 4.30 (dd, *J*= 4.3, 9.8 Hz, 1H, H-6), 3.87-3.71 (m, 4H, H-2, H-3, H-5, H-6), 3.65 (t, *J*= 9.2 Hz, 1H, H-4), 3.45 (s, 3H, OMe), 2.29 (d, *J*= 7.2 Hz, 1H, OH); **^{13}CNMR** ($CDCl_3$, 100 MHz): δ 138. 6 (Ar), 137.5 (Ar), 129.1 (Ar), 128.6 (Ar), 128.4 (Ar), 128.2 (Ar), 127.9 (Ar), 126.2 (Ar), 101.4 (C-7), 100.0 (C-1), 82.1 (C-4), 79.0 (C-2 or 3 or 5), 75.0 (*C*H$_2$Ph), 72.6 (C-2 or 3 or 5), 69.2 (C-6), 62.7 (C-2 or 3 or 5), 55.6 (OMe); **HRMS (ESI)**: *m/z* calcd $[M+Na]^+$ for $C_{21}H_{24}O_6$: 395.14651, found: 395.14658.

Methyl 3-*O*-benzyl-α-L-glucopyranoside (**72**)

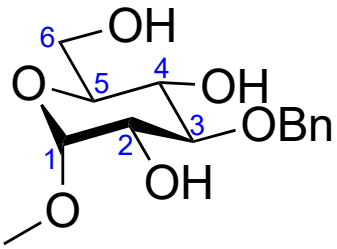

Methyl 3-*O*-benzyl-α-L-glucopyranoside (**72**) was made with methyl 3-*O*-benzyl-4,6-*O*-benzylidene-α-L-glucopyranoside (**71**, 135.7 mg, 0.364 mmol) using the same method as described for the synthesis of methyl 3-*O*-benzyl-α-D-glucopyranoside (**67)**. The crude product was purified with flash chromatography (P.E.-EtOAc, 0-100%) to yield the pure product as a white solid (96.3 mg, 0.339 mmol, 93% yield). **m.p.** 91.2- 93.8 °C; **[α]$^{22}_{D}$** -89.5 (*c*= 0.93, $CHCl_3$); **^{1}HNMR** ($CDCl_3$, 400 MHz): δ 7.39-7.29 (m, 5H, Ar), 5.03 (d, *J*= 11.5 Hz, 1H, C*H*$_2$Ph), 4.76 (d, *J*= 3.9 Hz, 1H, C*H*$_2$Ph), 4.73 (d, *J*= 11.5 Hz, 1H, H-1,), 3.88-3.75 (m, 2H, H-6 x2), 3.70-3.52 (m, 4H, H-2, H-3, H-4, H-5), 3.44 (s, 3H, OMe), 2.30 (d, *J*= 2.4 Hz, 1H, OH), 2.14 (d, *J*= 9.2 Hz, 1H, OH), 1.93 (dd, *J*= 5.7, 7.2 Hz, 1H, OH); **^{13}CNMR** ($CDCl_3$, 100 MHz): δ 138.6 (Ar), 128.8 (Ar), 128.1 (Ar), 99.7 (C-1), 82.8 (C-3),

75.1 (*C*H_2Ph), 72.9 (C-2), 71.1 (C-5), 70.2 (C-4), 62.5 (C-6), 55.5 (OMe); **HRMS (ESI)**: *m/z* calcd $[M+Na]^+$ for $C_{14}H_{20}O_6$: 307.11521, found: 307.11515.

Methyl 3-*O*-benzyl-α-L-glucopyranoside 2,4,6-tris(dibenzylphosphate) (**73**)

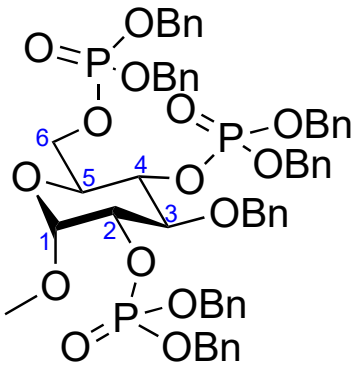

Methyl 3-*O*-benzyl-α-L-glucopyranoside 2,4,6-tris(dibenzylphosphate) (**73**) was synthesized with methyl 3-*O*-benzyl-α-L-glucopyranoside (**72**, 96.3 mg, 0.339 mmol) using the same method used for the synthesis of methyl 3-*O*-benzyl-α-D-glucopyranoside 2,4,6-tris(dibenzylphosphate) (**68**). The crude product was purified with flash chromatography (P.E.-EtOAc, 0-100%) to yield the pure product as a colourless oil (144.2 mg, 0.135 mmol, 40% yield). **$[\alpha]^{21}_D$** -38.8 (*c*= 1.01, $CHCl_3$); **^{1}HNMR** ($CDCl_3$, 400 MHz): δ 7.34-7.08 (m, 35H, Ar), 5.03 (s, 2H, C*H*$_2$Ph x2), 5.01 (s, 2H, C*H*$_2$Ph x2), 4.98 (d, *J*= 3.2 Hz, 1H, C*H*$_2$Ph), 4.96 (d, *J*= 3.2 Hz, 1H, C*H*$_2$Ph), 4.94-4.85 (m, 6H, H-1, C*H*$_2$Ph x5), 4.80-4.75 (m, 3H, C*H*$_2$Ph x3), 4.42-4.18 (m, 4H, H-2, H-3, H-6 x2), 3.98 (t, *J*= 9.4 Hz, 1H, H-4), 3.86 (dd, *J*= 10.0, 5.2 Hz, 1H, H-5), 3.28 (s, 3H, OMe); **^{31}PNMR** ($CDCl_3$, 162 MHz): δ -0.99, -1.74, -1.86; **^{13}CNMR** ($CDCl_3$, 100 MHz): δ 138.1 (Ar), 136.0 (Ar), 135.9 (Ar), 135.8-135.6 (m, Ar), 128.7-128.5 (m, Ar), 128.3 (Ar), 128.0 (m, Ar), 127.9 (Ar), 127.7 (Ar), 127.5 (Ar), 97.6 (C-1), 78.4-78.3 (m, C-4), 76.8-76.7 (m, C-2 or 3), 75.1 (C-2 or 3, *C*H_2Ph), 69.8-69.4 (m, *C*H_2Ph), 69.0-68.9 (m, C-5), 66.1 (d, J= 5.1 Hz, C-6), 55.7 (OMe); **HRMS (ESI)**: *m/z* calcd $[M+H]^+$ for $C_{56}H_{59}O_{15}P_3$: 1065.31396, found: 1065.31280.

Methyl α-L-glucopyranoside 2,4,6-trisphosphate triethylammonium salt (**59**)

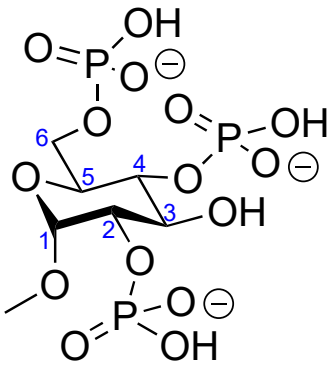

Methyl α-L-glucopyranoside 2,4,6-trisphosphate triethylammonium salt (**59**) was synthesized with methyl 3-*O*-benzyl-α-L-glucopyranoside 2,4,6-tris(dibenzylphosphate) (**73**, 141.9 mg, 0.133 mmol) using the same hydrogenation method as the preparation of methyl α-D-glucopyranoside 2,4,6-trisphosphate (**61**). Upon NMR analysos, no purification was deemed necessary, and the product was lyophilised and collected as a colourless glass (96.1 mg, calculated 3.1 TEA counterions per molecule of product, 0.120 mmol, 90% yield). **[α]$^{22}_{D}$** -46.5 (*c*= 0.88, MeOH); **^{1}HNMR** (d4-MeOH, 400 MHz): δ 4.90 (d, *J*= 3.0 Hz, 1H, H-1), 4.29-4.18 (m, 2H, H-3, H-6), 4.05-3.97 (m, 3H, H-2, H-4, H-6), 3.68 (d, *J*= 10.0 Hz, 1H, H-5), 3.38 (s, 3H, OMe), 3.14 (q, *J*= 7.3 Hz, approx. 18H, TEA C*H*$_2$CH$_3$), 1.30 (t, *J*= 7.3 Hz, approx. 28H, TEA CH$_2$C*H*$_3$); **^{31}PNMR** (d4-MeOH, 162 MHz): δ 1.90, 1.71, 1.28; **^{13}CNMR** (d4-MeOH, 100 MHz): δ 100.2 (d, *J*= 4.0 Hz, C-1), 76.3 (d, *J*= 5.1 Hz, C-2 or 4), 74.6 (d, *J*= 4.0 Hz, C-2 or 4), 73.5 (d, *J*= 4.9 Hz, C-3), 71.0-71.2 (m, C-5), 63.9 (d, *J*= 4.7 Hz, C-6), 55.6 (OMe), 46.9 (TEA *C*H$_2$CH$_3$), 9.4 (TEA CH$_2$*C*H$_3$); **HRMS (ESI)**: *m/z* calcd [M-H]$^-$ for $C_7H_{17}O_{15}P_3$: 432.97075, found: 432.97065.

Methyl 4-*O*-benzyl-α-D-glucopyranoside (**64**)

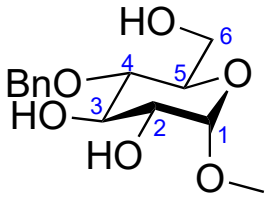

Method A: methyl 4,6-*O*-benzylidene-α-D-glucopyranoside (**44**, 100 mg, 0.354 mmol) was dissolved in dry DCM (5.3 mL) and put under argon. The solution was cooled to 0°C, and borane-THF (1 M, 1.8 mL, 1.77 mmol, 5 equiv) was added, followed by a solution of $AlCl_3$ (94.4, 0.708 mmol, 2 equiv) in dry diethyl ether (0.9 mL). The solution was allowed to gradually warm to RT and then stir for 24 h. After this time, the reaction was quenched with the addition of triethylamine (0.2 mL), followed by MeOH (0.9 mL). The reaction solution was concentrated *in vacuo* to form a solid residue. This residue

was dissolved in DCM (50 mL) and washed with 1 M $HCl_{(aq)}$, sat. $NaHCO_{3(aq)}$ and water. The combined aqueous washes were also extracted three times with EtOAc, and the organic layers were combined, dried over $MgSO_4$ and concentrated to yield the crude product. The product was purified through silica column chromatography using (P.E.-EtOAc, 0-100%) to yield the product. It should be noted that this product was not entirely pure, as a very small amount of methyl 6-*O*-benzyl-α-D-glucopyranoside (**45**) was generated as well. This regioisomer could not be separated from the desired product (although separation of the regioisomers post-phosphorylation was achievable).

Method B: In an adapted version of the Shie *et al.* protocol.,[338] methyl 4,6-*O*-benzylidene α-D-glucopyranoside (**44**, 100 mg, 0.355 mmol) was added to borane-THF (1M, 1.8 mL, 1.8 mmol, 5 equiv) and the reaction was put under argon. The solution was allowed to stir for 10 min before lanthanum triflate (31.2 mg, 0.053 mmol, 0.15 equiv) was added, and the reaction was allowed to stir at RT for a week. The reaction was then cooled to 0°C and quenched with triethylamine (0.5 mL, 1 equiv), followed by MeOH (0.7 mL). The reaction was concentrated *in vacuo* and co-evaporated with MeOH twice before the crude product was isolated as a white solid. The product was purified with flash chromatography (1. P.E.-EtOAc, 0-100% 2. DCM-EtOAc, 0-100%). As impurities were still present, an aqueous work-up was carried out. The product was dissolved in EtOAc and washed with 1 M $HCl_{(aq)}$, sat. $NaHCO_3$ and water. The aqueous washes were extracted with EtOAc again and the organic phases were combined, dried over $MgSO_4$ and concentrated to yield the pure product as a white solid (30.8 mg, 0.108 mmol, 31% yield).

Method C: In an adapted version of the Tanaka *et al*. protocol,[337] methyl 4,6-*O*-benzylidene α-D-glucopyranoside (**44**, 141.2 mg, 0.50 mmol) was suspended in toluene and cooled to 0°C. To this suspension, DIBAL-H in toluene (1.5 mL, 1M, 1.5 mmol, 3 equiv) was added dropwise, and the reaction was allowed to warm to RT and stir for 1 hour 30 min. After this time, the reaction was cooled to 0°C, and methanol (1 mL) was added to quench the reaction. 10% $KOH_{(aq)}$ (50 mL) was then added to the reaction, and the product was extracted with Et_2O (150 mL). The organic layer was separated, dried over $MgSO_4$ and concentrated to yield the crude product (which was not purified, but ^{1}HNMR indicated it was approximately 90% 4-*O*-benzyl regioisomer, **64**, with trace amounts of the 6-*O*-benzyl regioisomer, **45**).

m.p. 123.9−129.0 °C (Lit.[424] m.p. 126-127 °C); **$[\alpha]^{21}_D$** 116.2 (*c*=1.47, $CHCl_3$) [Lit.[424] $[\alpha]_D$ 154.1 (*c*= 1, $CHCl_3$)]; **^{1}HNMR** ($CDCl_3$, 400MHz): δ 7.36-7.28 (m, 5H, Ar), 4.86 (AB, *J*= 11.4 Hz, 1H, C*H*$_2$Ph), 4.75 (d, *J*= 3.9 Hz, 1H, H-1), 4.72 (AB, *J*= 11.4 Hz, 1H, C*H*$_2$Ph), 3.86 (t, *J*= 9.2 Hz, 1H, H-3), 3.83 (ABX, *J*= 11.6, 2.6 Hz, 1H, H-6), 3.75 (ABX, *J*= 11.9, 3.6 Hz, H-6), 3.63 (apt dt, *J*= 9.8, 3.3 Hz, 1H, H-5), 3.51 (brs, 1H, H-2), 3.45 (t, *J*= 9.4 Hz, 1H, H-4), 3.39 (s, 3H, OMe); **^{13}CNMR** ($CDCl_3$, 100 MHz): δ 138.3 (Ar), 128.7 (Ar), 128.2 (Ar), 128.1

(Ar), 99.2 (C-1), 77.2 (C-4), 75.1 (C-3), 74.8 (*C*H_2Ph), 72.8 (C-2), 70.9 (C-5), 62.0 (C-6), 55.5 (OMe).

Methyl 4-*O*-benzyl-α-D-glucopyranoside 2,3,6-tris(dibenzylphosphate) (**65**)

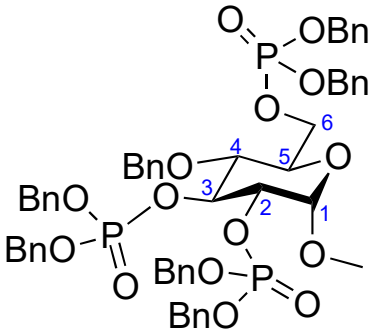

Methyl 4-*O*-benzyl-α-D-glucopyranoside (**64**, 50 mg, 0.176 mmol) was dissolved in dry DCM (2 mL), and the solution was put under argon. 5-Phenyl-1*H*-tetrazole (154 mg, 1.06 mmol, 6 equiv) was added to the solution followed by dibenzyl diisopropylphosphoramidite (0.27 mL, 0.792 mmol, 4.5 equiv). The reaction was allowed to stir at RT overnight. The following day, the reaction was cooled to -78°C, and *m*CPBA (70% pure, 261 mg, 1.06 mmol, 6 equiv) was added. The reaction was allowed to stir for 10 min at RT before it was diluted with EtOAc (50 mL) and washed twice with 10% Na_2SO_3 solution (2 x 30 mL). The organic layer was dried over $MgSO_4$ and concentrated *in vacuo* to yield the crude product. The product was purified with flash chromatography (1. P.E.-EtOAc, 0-100% and 2. DCM-EtOAc, 0-100%). The pure product was collected as a colourless oil (81.9 mg, 0.077 mmol, 44% yield). **[α]$^{22}_D$** 35.7 (*c*= 1.00, $CHCl_3$); **^{1}HNMR** ($CDCl_3$, 400 MHz): δ 7.33-7.09 (m, 35H, Ar), 5.05-4.82 (m, 16H, H-1, H-3, H-6, C*H*$_2$Ph), 4.47 (d, *J*= 10.7 Hz, 1H, C*H*$_2$Ph), 4.26 (ddd, *J*= 9.6, 6.2, 3.6 Hz, 1H, H-2), 4.19-4.16 (m, 1H, H-6), 3.76 (dq, *J*= 9.6, 2.7 Hz, 1H, H-5), 3.50 (t, *J*= 9.4 Hz, 1H, H-4), 3.25 (s, 3H, OMe); **^{31}PNMR** ($CDCl_3$, 162 MHz): δ -0.76, -1.32, -2.01; **^{13}CNMR** ($CDCl_3$, 100 MHz): δ 137.6 (Ar), 136.1-135.7 (m, Ar), 128.7-128.0 (m, Ar), 97.6 (C-1), 78.5-78.4 (m, C-3), 76.2 (C-4), 75.4-75.3 (m, C-2), 74.6 (*C*H_2Ph), 69.8 (d, *J*= 5.6 Hz, *C*H_2Ph), 69.6-69.4 (m, *C*H_2Ph), 69.1 (d, *J*= 8.1 Hz, C-5), 65.8 (d, *J*= 5.5 Hz, C-6), 55.5 (OMe); **HRMS (ESI)**: *m/z* calcd $[M+H]^+$ for $C_{56}H_{59}O_{15}P_3$: 1065.31396, found: 1065.31364.

Methyl α-D-glucopyranoside 2,3,6-trisphosphate triethylammonium salt (**60**)

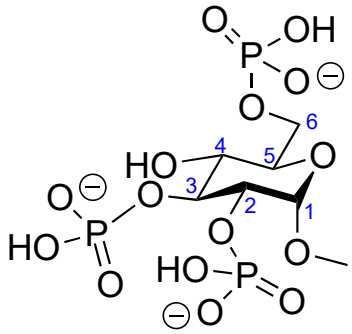

Methyl 4-*O*-benzyl-α-D-glucopyranoside 2,3,6-tris(dibenzylphosphate) (**65**, 55.5 mg, 0.052 mmol) was dissolved in MeOH (2.8 mL). To this solution, ultrapure water (0.28 mL) was added dropwise, ensuring that the white precipitate that formed returned to solution. 20% $Pd(OH)_2/C$ (≥50% wet, 27.8 mg) was added to the solution, and the flask was flushed with hydrogen. The reaction was left to stir under hydrogen at RT overnight. The palladium catalyst was filtered off with a PTFE filter, and the solution was concentrated *in vacuo* to yield the product as a free acid. Upon NMR analysis, no purification was deemed necessary. The free acid was converted to the triethylammonium salt through the addition of excess triethylamine, followed by concentration *in vacuo*. The product was lyophilised and collected as a colourless glass (24.8 mg, calculated 3.2 TEA counterions per molecule of product, 0.034 mmol, 65% yield). **$[\alpha]^{22}_D$** 38.2 (*c*= 1.00, MeOH); **^{1}H NMR** (d4-MeOH, 400 MHz): δ 4.91 (d, J= 3.6 Hz, 1H, H-1), 4.35 (q, *J*= 8.7 Hz, 1H, H-3), 4.17 (ddd, *J*= 11.0, 5.2, 2.0 Hz, 1H, H-6), 4.07-3.98 (m, 2H, H-2, H-6), 3.72-3.68 (m, 1H, H-5), 3.54 (dd, *J*= 9.8, 8.8 Hz, 1H, H-4), 3.39 (s, 3H, OMe), 3.11 (q, *J*= 7.3 Hz, approx. 19H, TEA CH_2CH_3), 1.28 (t, *J*= 7.3 Hz, approx. 29H, TEA CH_2CH_3); **^{31}PNMR** (d4-MeOH, 162 MHz): δ 2.21, 1.25, 0.94; **^{13}CNMR** (d4-MeOH, 100 MHz): δ 100.2 (C-1), 78.5 (t, *J*= 5.7 Hz, C-3), 75.3 (t, *J*= 4.9 Hz, C-2), 72.2 (d, *J*= 8.3 Hz, C-5), 71.7 (C-4), 65.6 (d, *J*= 5.2 Hz, C-6), 55.5 (OMe), 47.2 (TEA CH_2CH_3), 9.1 (TEA CH_2CH_3); **HRMS (ESI)**: *m/z* calcd $[M-H]^-$ for $C_7H_{17}O_{15}P_3$: 432.97075, found: 432.97076.

Methyl 4-*O*-benzyl-α-L-glucopyranoside (**69**)

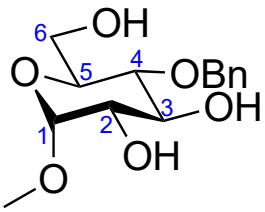

Methyl 4-*O*-benzyl-α-L-glucopyranoside (**69**) was made using method A, as described for the synthesise of methyl 4-*O*-benzyl-α-D-glucopyranoside (**64**). The desired product regioisomer generated using the method A reaction could not be entirely isolated from the small amounts of methyl 6-*O*-benzyl-α-L-glucopyranoside (**54**) also formed in the reaction. However, after the phosphorylation in the next step, it was possible to separate these regioisomers and remove the remaining traces of the unwanted regioisomer. Method A was much higher yielding and took less time than method B and so was used to generate the majority of the product (**69**), but method B was also carried out from methyl 4-*O*-benzyl-α-D-glucopyranoside (**64,** 71.5 mg, 0.253 mmol) to generate a small amount of pure product for characterisation (26 mg, 37% yield). **m.p.** 128.5- 132.0 (Lit.[425] m.p. 125-127 °C); **$[\alpha]^{25}_{D}$** -142.5 (c= 0.3, MeOH) [Lit.[425] $[\alpha]^{25}_{D}$ -144.2 (*c*= 1.2, MeOH)]; **^{1}HNMR** ($CDCl_3$, 400 MHz): δ 7.37-7.27 (m, 5H, Ar), 4.87 (AB, *J*= 11.5 Hz, 1H, CH_2Ph), 4.75 (d, *J*= 3.9 Hz, 1H, H-1), 4.72 (AB, *J*= 11.4 Hz, 1H, CH_2Ph), 3.86 (t, *J*= 9.2 Hz, 1H, H-3), 3.83 (ABX, *J*= 11.8, 2.6 Hz, 1H, H-6), 3.75 (ABX, *J*= 11.8, 3.8 Hz, H-6), 3.67-3.62 (m, 1H, H-5), 3.50 (dd, *J*= 3.9, 9.4 Hz,1H, H-2), 3.45 (t, *J*= 9.4 Hz, 1H, H-4), 3.40 (s, 3H, OMe); **^{13}CNMR** ($CDCl_3$, 100 MHz): δ 138.3 (Ar), 128.7 (Ar), 128.2 (Ar), 127.9 (Ar), 99.2 (C-1), 77.3 (C-4), 75.3 (C-3), 74.8 (*C*H_2Ph), 72.9 (C-2), 70.9 (C-5), 62.1 (C-6), 55.5 (OMe).

Methyl 4-*O*-benzyl-α-L-glucopyranoside 2,3,6-tris(dibenzylphosphate) (**70**)

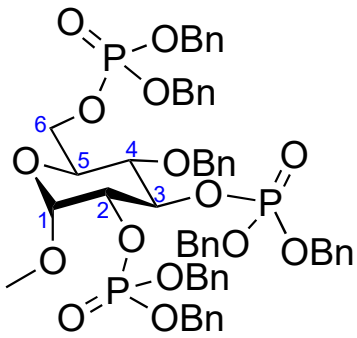

Methyl 4-*O*-benzyl α-L-glucopyranoside 2,3,6-tris(dibenzylphosphate) (**70**) was synthesised with methyl 4-*O*-benzyl-α-L-glucopyranoside (**69**, 65.5 mg, 0.230 mmol) using the same method as described to make methyl 4-*O*-benzyl-α-D-glucopyranoside 2,3,6-tris(dibenzylphosphate) (**65**). The crude product was purified with flash chromatography (petroleum ether/EtOAc, 0-100%) to yield the pure product as a

colourless oil (210.5 mg, 0.198 mmol, 86% yield). **[α]$^{21}_{D}$** -42.3 (*c*= 1.06, $CHCl_3$); **^{1}HNMR** ($CDCl_3$, 400 MHz): δ 7.33-7.09 (m, 35H, Ar), 5.05-4.81 (m, 16H, H-1, H-3, H-6, C*H*$_2$Ph), 4.46 (d, *J*= 10.7 Hz, 1H, C*H*$_2$Ph), 4.25 (ddd, *J*=13.3, 6.2, 3.6 Hz, 1H, H-2), 4.19-4.16 (m, 1H, H-6), 3.75 (dq, *J*= 10.0, 2.3 Hz, 1H, H-5), 3.50 (t, *J*= 9.5 Hz, 1H, H-4), 3.24 (s, 3H, OMe); **^{31}PNMR** ($CDCl_3$, 162 MHz): δ -0.76, -1.32, -2.01; **^{13}CNMR** ($CDCl_3$, 100 MHz): δ 137.6 (Ar), 136.1-135.7 (m, Ar), 128.7-127.8 (m, Ar), 97.6 (C-1), 78.4 (dd, J= 8.7, 6.5 Hz, C-3), 76.2 (C-4), 75.3 (dd, J= 4.7, 3.2 Hz, C-2), 74.6 (*C*H_2Ph), 69.8 (d, J= 5.6 Hz, *C*H_2Ph), 69.6-69.4 (m, *C*H_2Ph), 69.1 (d, J= 8.3 Hz, C-5), 65.8 (d, J= 5.6 Hz, C-6), 55.5 (OMe); **HRMS (ESI)**: *m/z* calcd $[M+H]^+$ for $C_{56}H_{59}O_{15}P_3$: 1065.31396, found: 1065.31297.

Methyl α-L-glucopyranoside 2,3,6-trisphosphate triethylammonium salt (**58**)

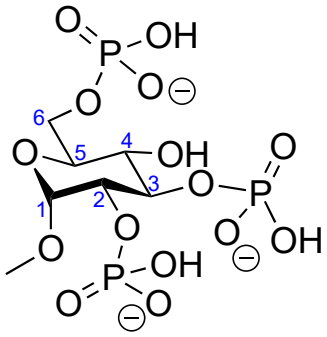

The methyl 4-*O*-benzyl-α-L-glucopyranoside 2,3,6-trisphosphate (**58**) was prepared with methyl 4-*O*-benzyl-α-L-glucopyranoside 2,3,6-tris(dibenzylphosphate) (**70**, 60 mg, 0.056 mmol) using the same method as for the preparation of methyl 4-*O*-benzyl-α-D-glucopyranoside 2,3,6-trisphosphate (**60**)**.** Upon NMR analysis of the product, no purification steps were deemed to be necessary. The product was then converted from a free acid to the triethylammonium salt with excess triethylamine, before it was lyophilised and collected as a colourless glass (44.5 mg, calculated 3.1 TEA counterions per molecule of product, 0.056 mmol, 100% yield). **[α]$^{21}_{D}$** -37.6 (*c*= 1.00, MeOH); **^{1}HNMR** ($CDCl_3$, 400 MHz): δ 4.92 (d, *J*= 3.6 Hz, 1H, H-1), 4.35 (q, *J*= 8.7 Hz, 1H, H-3), 4.17 (ddd, *J*= 11.1, 5.2, 2.0 Hz, 1H, H-6), 4.07-3.98 (m, 2H, H-2, H-6), 3.73-3.68 (m, 1H, H-5), 3.55 (dd, *J*= 9.8, 8.7 Hz, 1H, H-4), 3.39 (s, 3H, OMe), 3.09 (q, *J*= 7.3 Hz, approx. 19H, TEA C*H*$_2$CH$_3$), 1.27 (t, *J*= 7.3 Hz, approx. 28H, TEA CH$_2$C*H*$_3$); **^{31}PNMR** ($CDCl_3$, 162 MHz): δ 2.50, 1.53, 1.15; **^{13}CNMR** ($CDCl_3$, 100 MHz): δ 100.5 (C-1), 78.5 (C-3), 75.5 (C-2), 72.4 (d, *J*= 8.7 Hz, C-5), 72.0 (C-4), 65.7 (d, *J*= 4.9 Hz, C-6), 55.4 (OMe), 47.0 (TEA *C*H$_2$CH$_3$), 9.4 (TEA CH$_2$*C*H$_3$); **HRMS (ESI)**: *m/z* calcd $[M-H]^-$ for $C_7H_{17}O_{15}P_3$: 432.97075, found: 432.97067.

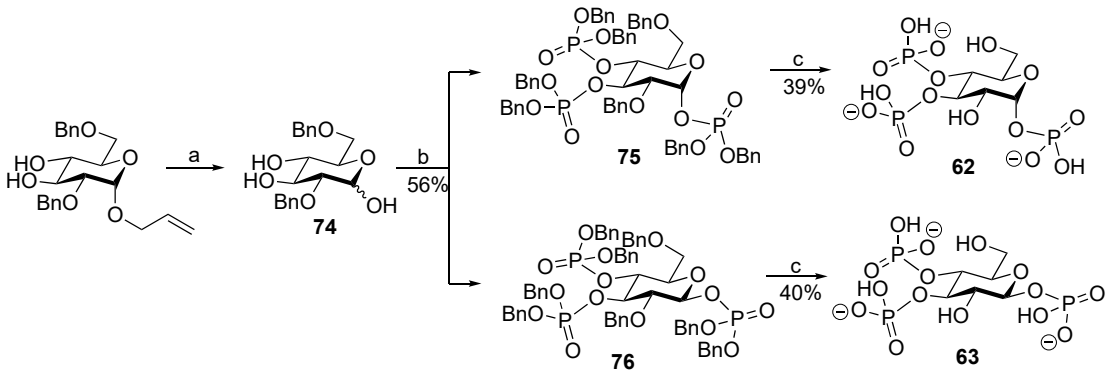

Scheme 10: Synthesis of the D-glucose based $InsP_3R$ ligands that have phosphates bound to the 1-position anomeric hydroxyl: α-D-glucosyl 1,3,4-trisphosphate (**62**) and β-D-glucosyl 1,3,4-trisphosphate (**63**).

Reagents and conditions: (a) MeOH, cat. $PdCl_2$, 6h; (b) 1. DCM, 5-phenyl-1*H*-tetrazole, $(OBn)_2PN(^iPr)_2$, 20h 2. *m*CPBA, -78°C -RT; (c) MeOH:H_2O (10:1 v/v), cat. $Pd(OH)_2/C$, H_2, $NaHCO_3$, 24h.

2,6-Di-*O*-benzyl-D-glucopyranose (**74**)

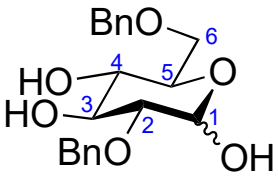

As described in Ogawa and Yamamoto,[353] allyl 2,6-di-*O*-benzyl-D-glucopyranoside (which can be synthesised as described in Rosenberg *et al.*,[282] 60mg, 0.133 mmol) was dissolved in dry MeOH (1.54 mL). To this solution, $PdCl_2$ (6.2 mg, 0.03 mmol, 0.25 equiv) was added and the reaction was allowed to stir at RT for 6 h, with a drying tube affixed to the flask. The reaction was then quenched with the addition of excess $NaHCO_3$, and allowed to stir for 5 minutes before being filtered through celite and concentrated to yield the crude product. (Lit.[357] m.p. 103-105 °C); [Lit.[357] mutarotation $[\alpha]_D$ 31-35 (*c*= 2.1, $CHCl_3$)]. The product of this reaction could not be successfully purified (although following phosphorylation, the products were successfully isolated).

2,6-Di-*O*-benzyl-α-D-glucopyranosyl 1,3,4-tris(dibenzylphosphate) (**75**) and 2,6-di-*O*-benzyl-β-D-glucopyranosyl 1,3,4-tris(dibenzylphosphate) (**76**)

2,6-Di-*O*-benzyl-D-glucopyranose (**74**, 154.7 mg, 0.429 mmol) was added to dry DCM (4.5 mL). To this suspension, 5-phenyl-1*H*-tetrazole (376 mg, 2.58 mmol, 6 equiv) was added, followed by dibenzyl phosphoramidite (0.67 mL, 1.93 mmol, 4.5 equiv). The reaction was allowed to stir under argon at RT overnight, after which it was cooled to

-78°C, and *m*CPBA (70% purity, 636 mg, 2.58 mmol, 6 equiv) was added. The reaction was then diluted with EtOAc (100 mL) and washed twice with 10% Na_2SO_3 solution (2 x 30 mL). The organic phase was dried over $MgSO_4$ and concentrated to yield the crude product. The product was purified using flash chromatography (P.E.-EtOAc, 0-100%). The stereoisomers of the product were partially isolated and collected as colourless oils (total: 276.6 mg, 0.242 mmol, 56% yield; α-anomer (**75**): 70.4 mg, 0.062 mmol, 14% yield; β-anomer (**76**): 92.4 mg, 0.081 mmol, 19% yield; remaining unseparated mix of anomers: 113.8 mg, 0.100 mmol, 23% yield).

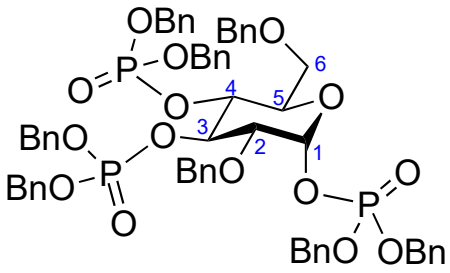

2,6-di-*O*-benzyl-α-D-glucopyranosyl 1,3,4-tris(dibenzylphosphate) (**75**): ***Rf*** (EtOAc) 0.63; **[α]$^{20}_D$** 35.7 (*c*= 0.71, chloroform); **^{1}HNMR** ($CDCl_3$, 400 MHz): δ 7.35-7.09 (m, 40H, Ar), 5.91 (dd, *J*= 3.3, 7.0 Hz, 1H, H-1α), 5.07-4.81 (m, 13H, H-3, C*H*$_2$Ph x12), 4.72-4.61 (m, 3H, H-4, C*H*$_2$Ph x2), 4.44 (d, *J*= 12.0 Hz, 1H, C*H*$_2$Ph), 4.31 (d, *J*= 12.0 Hz, 1H, C*H*$_2$Ph), 3.96 (dq, *J*= 10.0, 1.6 Hz, 1H, H-5), 3.70 (dd, *J*= 11.2, 3.9 Hz, 1H, H-6), 3.65 (dt, *J*= 9.7, 3.1 Hz, 1H, H-2), 3.54 (dd, *J*= 11.2, 1.8 Hz, 1H, H-6); **^{31}PNMR** ($CDCl_3$, 162 MHz): δ -1.66, -2.31, -2.50; **^{13}CNMR** ($CDCl_3$, 100 MHz): δ 138.0 (Ar), 137.0 (Ar), 136.2-135.6 (m, Ar), 128.6-127.6 (m, Ar), 94.8 (d, *J*= 5.6 Hz, C-1), 77.9-77.8 (m, C-3), 77.0 (m, C-2), 73.7-73.6 (m, C-4), 73.3 (*C*H$_2$Ph), 73.0 (*C*H$_2$Ph), 71.6 (C-5), 70.0-69.9 (m, *C*H$_2$Ph), 69.7-69.6 (m, *C*H$_2$Ph), 69.5-69.4 (m, *C*H$_2$Ph), 67.5 (C-6); **HRMS (ESI)**: *m/z* calcd $[M+Na]^+$ for $C_{62}H_{63}O_{15}P_3$: 1163.32720, found: 1163.32495.

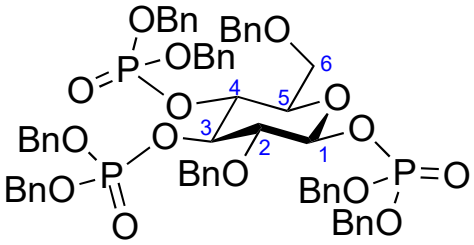

2,6-di-*O*-benzyl-β-D-glucopyranosyl 1,3,4-tris(dibenzylphosphate) (**76**)**:** ***Rf*** (EtOAc) 0.57; **[α]$^{21}_D$** 2.68 (*c*= 1.01, chloroform); **^{1}HNMR** ($CDCl_3$, 400 MHz): δ 7.31-7.03 (m, 40H, Ar), 5.31 (t, *J*= 7.2 Hz, 1H, H-1β), 5.04-4.87 (m, 11H, C*H*$_2$Ph x11), 4.81-4.60 (m, 5H, C-3, C-4, C*H*$_2$Ph x3), 4.42 (d, *J*= 12.0 Hz, 1H, C*H*$_2$Ph), 4.31 (d, *J*= 12.0 Hz, 1H, C*H*$_2$Ph), 3.77-3.55 (m , 4H, C-2, C-5, C-6 x2); **^{31}PNMR** ($CDCl_3$, 162 MHz): δ -1.90, -2.22, -2.59; **^{13}CNMR** ($CDCl_3$, 100 MHz): δ 138.0 (Ar), 137.7 (Ar), 136.1-135.4 (m, Ar), 128.6-127.6 (m, Ar), 98.6 (C-1), 80.1 (m, C-3 or 4), 79.7-79.6 (m, C-2 or 5), 74.5 (d, *J*= 3.5 Hz, C-3 or 4), 74.1 (*C*H$_2$Ph), 74.0-73.9 (m, C-2 or 5), 73.3 (*C*H$_2$Ph), 70.0 (d, *J*= 5.8 Hz, *C*H$_2$Ph), 69.8-69.7 (m,

*C*H$_2$Ph), 69.6-69.5 (m, *C*H$_2$Ph), 68.1 (C-6); **HRMS (ESI)**: *m/z* calcd [M+Na]$^+$ for $C_{62}H_{63}O_{15}P_3$: 1163.32720, found: 1163.32505.

β-D-Glucopyranosyl 1,3,4-trisphosphate triethylammonium salt (**63**)

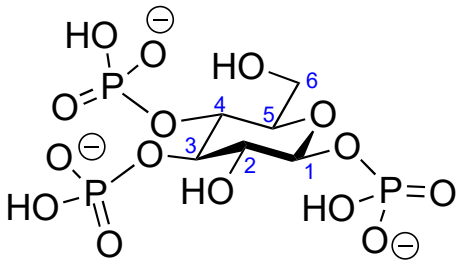

2,6-Di-*O*-benzyl-β-D-glucopyranosyl 1,3,4-tris(dibenzylphosphate) (**76**, 23.3 mg, 0.020 mmol) was dissolved in MeOH (1.5 mL). To this solution, ultrapure water (0.15 mL) was added dropwise, ensuring that the precipitate that formed upon addition returned to solution. $NaHCO_3$ (5.15 mg, 0.061 mmol, 3 equiv) was then added, followed by 20% $Pd(OH)_2$/C (≥50% wet, 11.7 mg). The reaction flask was flushed with hydrogen and left to stir at RT for 24 h. The catalyst was then filtered off, and the collected filtrate was evaporated *in vacuo* to yield the crude product as a sodium salt. The product was purified by ion-pair reverse-phase column chromatography and lyophilised to yield the triethylammonium salt of the product as a colourless glass (6.7 mg, calculated 3.2 TEA counterions per molecule of product, 0.008 mmol, 40% yield). **[α]$^{21}_D$** 3.76 (*c*=0.61, methanol); **^{1}HNMR** (d4-MeOH, 500 MHz): δ 4.98 (t, *J*= 7.6 Hz, 1H, H-1), 4.23 (q, *J*= 8.8 Hz, 1H, H-3), 4.08 (q, *J*= 9.8 Hz, 1H, H-4), 3.89 (dd, *J*= 12.7, 4.4 Hz, 1H, H-6), 3.84 (dd, *J*= 12.7, 2.1 Hz, 1H, H-6), 3.43-3.38 (m, 2H, H-2, H-5), 3.13 (q, *J*= 7.0 Hz, approx. 19H, TEA C*H*$_2$CH$_3$), 1.29 (t, *J*= 7.2 Hz, approx. 29H, TEA CH$_2$C*H*$_3$); **^{31}PNMR** (d4-MeOH, 162 MHz): δ 1.38, 1.06, -0.77; **^{13}C NMR** (d4-MeOH, 125 MHz): δ 99.3 (C-1), 81.4 (C-3), 77.9 (C-2 or 5), 76.2 (C-2 or 5), 73.8 (C-4), 62.4 (C-6), 47.2 (TEA *C*H$_2$CH$_3$), 9.3 (TEA CH$_2$*C*H$_3$); **HRMS (ESI)**: *m/z* calcd [M-H]$^-$ for $C_6H_{15}O_{15}P_3$: 418.9551, found: 418.95425.

α-D-Glucopyranosyl 1,3,4-trisphosphate triethylammonium salt (**62**)

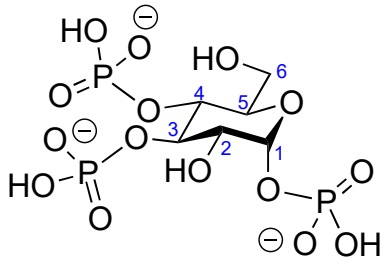

The α-D-glucopyranosyl 1,3,4-trisphosphate triethylammonium salt (**62**) was prepared with 2,6-di-*O*-benzyl-α-D-glucopyranosyl 1,3,4-tris(dibenzylphosphate) (**75**, 31.9 mg, 0.028 mmol) using the same hydrogenation method described for the synthesis of β-D-glucopyranosyl 1,3,4-trisphosphate triethylammonium salt (**63**). The crude sodium salt of the product was purified by ion-pair reverse-phase column chromatography, and lyophilised to yield the triethylammonium salt of the product as a colourless glass (8.0 mg, calculated 3.1 TEA counterions per molecule of product, 0.011 mmol, 39% yield). **[α]$^{20}_{D}$** 33.9 (*c*=0.97, methanol); **^{1}HNMR** (d4-MeOH, 400 MHz): δ 5.58 (dd, *J*= 7.0, 3.6 Hz, 1H, H-1), 4.45 (q, *J*= 9.0 Hz, 1H, H-3), 4.12 (q, *J*= 9.8 Hz, 1H, H-4), 3.98-3.91 (m, 2H, H-5, H-6), 3.76-3.72 (m, 1H, H-6), 3.61 (ddd, *J*= 9.5, 3.5, 2.4 Hz, 1H, H-2), 3.16 (q, *J*= 7.3 Hz, approx. 18H, TEA C*H*$_2$CH$_3$), 1.31 (t, *J*= 7.3 Hz, approx. 28H, TEA CH$_2$C*H*$_3$); **^{31}PNMR** (d4-MeOH, 162 MHz): δ 2.06, 2.06, -0.62; **^{13}CNMR** (d4-MeOH, 100 MHz): δ 96.3 (d, *J*= 5.4 Hz, C-1), 79.2-79.1 (m, C-3), 73.8-73.6 (m, C-2, C-4, C-5), 62.1 (C-6), 47.3 (TEA *C*H$_2$CH$_3$), 9.2 (TEA CH$_2$*C*H$_3$); **HRMS (ESI)**: *m/z* calcd [M-H]$^-$ for $C_6H_{15}O_{15}P_3$: 418.9551, found: 418.95422.

Synthesis of diphospho myo-inositol bisphosphate and diphospho myo-inositol phosphate [PP-InsP$_2$/PP-InsP] target compounds

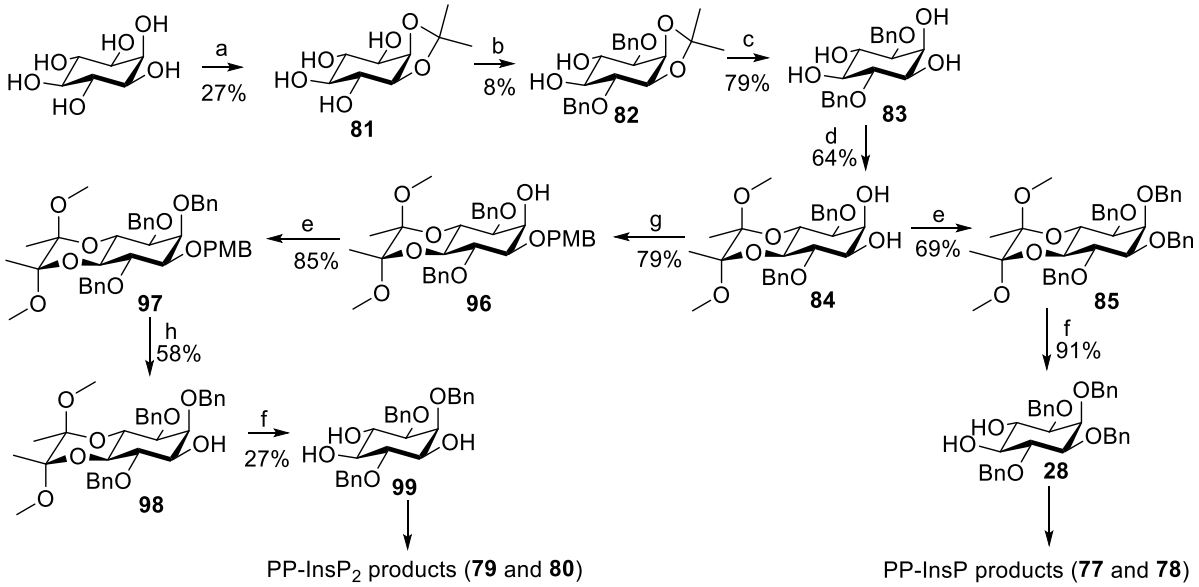

Scheme 12: Early synthetic steps in the routes to generate PP-InsP and PP-InsP$_2$ products: 5-PP-Ins(4)P (**77**), 4-PP-Ins(5)P (**78**), 5-PP-Ins(1,4)P$_2$ (**79**) and 4-PP-Ins(1,5)P$_2$ (**80**).

Reagents and conditions: (a) 2,2-isopropylidene, *p*TSA, DMSO, 110°C, 3h; (b) Bu$_2$SnO, BnBr, TBAB, MeCN, reflux, 24h; (c) 80% AcOH, 100°C, 4h; (d) trimethyl orthoformate, butanedione, CSA, MeOH, reflux, 24h; (e) BnBr, NaH, DMF, 0°C-RT, 3h; (f) TFA, H$_2$O, RT, 10 min; (g) 1. Bu$_2$SnO, MeOH, reflux, 24h, 2. PMBCl, CsF, DMF; (h) DDQ, DCM, H2O, RT, 90 min.

DL-1,2-Isopropylidene-*myo*-inositol (**81**)

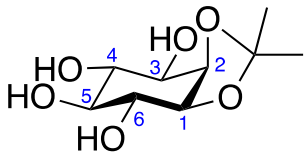

As described by Gigg *et al.*,[391] half of the *myo*-inositol (total amount: 5g, 0.0278 mol) was suspended in dry DMSO (50 mL), to which *para*-toluene sulfonic acid (75 mg, 0.436 mmol, 0.015 equiv) and 2,2-dimethoxypropane (50 mL, 0.408 mol, 14.7 equiv) were added. The reaction was heated to 110 °C and left to stir 1.5 h. After this time, the other half of the *myo*-inositol was added and the reaction was allowed to stir at 110 °C for a further 1.5 h. The reaction was then quenched with the addition of potassium carbonate (40 mg) and the DMSO was removed *in vacuo*. The resulting brown residue was then triturated in EtOH to yield a solid, which was recrystallized from boiling EtOH to yield the pure product as a white, crystalline solid (3.26 g, 0.0148 mol, 27% yield). **m.p**. 181.9-183.8 °C (lit.[393] mp 182-184°C); **^{1}HNMR** (D$_2$O, 400 Hz): 4.48 (t, *J*= 4.6 Hz, 1H, H-2), 4.06 (dd, *J*= 4.9, 7.8 Hz, 1H, H-3), 3.85 (dd, *J*= 4.2, 9.8 Hz, 1H, H-1), 3.65-3.56 (m, 2H, H-4 and H-6), 3.25 (t, *J*= 10.0 Hz, 1H, H-5), 1.53 (s, 3H, CH$_3$), 1.39

(s, 3H, CH_3); **^{13}CNMR** (D_2O, 100 Hz): 110.4 ($C(CH_3)_2$), 78.5 (C-3), 76.1 (C-2), 74.6 (C-4 or C-6), 72.6 (C-5), 72.2 (C-4 or C-6), 69.4 (C-1), 27.3 (CH_3), 25.1 (CH_3).

DL-3,6-Di-*O*-benzyl-1,2-isopropylidene-*myo*-inositol (**82**)

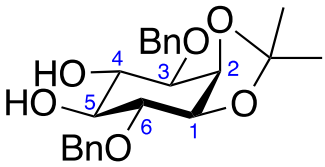

As described by Desai *et al*.,[393,394] the 1,2-isopropylidene *myo*-inositol (**81**, 4.3 g, 19.5 mmol) was dissolved in dry acetonitrile (100 mL). To this solution, dibutyltin oxide (12 g, 48.2 mmol, 2.5 equiv), tetrabutyl ammonium bromide (12.7 g, 39.4 mmol, 2 equiv) and benzyl bromide (6 mL, 50.5 mmol, 2.6 equiv) were added. The reaction was allowed to reflux for 24 h after which time the progress of the reaction was confirmed with TLC. The reaction was then allowed to cool to RT before triethylamine (2 mL) was added to destroy the excess benzyl bromide. The reaction mixture was concentrated *in vacuo* and the resultant residue was dissolved in diethyl ether and water (1:1, 100 mL). The product crashed out as a white solid and was purified through column chromatography (1. Et_2O, 2. Pet. ether-Et_2O, 0-100%) to yield a white solid (638 mg, 1.59 mmol, 8% yield). **m.p**. 156.7-161.6 °C (lit.[393] mp 161-163°C); **^{1}HNMR** ($CDCl_3$, 400 Hz): 7.42-7.27 (m, 10 Hz, Ar), 4.93 (d, J= 11.6 Hz, 1H, CH_2Ar), 4.80 (AB, *J*= 12.2 Hz, 1H, CH_2Ar), 4.77 (AB, *J*= 12.2 Hz, 1H, CH_2Ar), 4.68 (d, *J*= 11.6, 1H, CH_2Ar), 4.31 (dd, *J*= 4.2, 5.0 Hz, 1H, H-2), 4.09 (dd, *J*= 5.2, 6.9 Hz, 1H, H-1), 3.94 (dt, *J*= 1.7, 9.4 Hz, 1H, H-4), 3.56-3.52 (m, 2H, H-3 and H-6), 3.37 (dt, *J*= 1.9, 9.5 Hz, 1H, H-5), 2.71 (d, *J*= 1.9 Hz, 1H, OH), 2.69 (d, *J*= 2.0 Hz, 1H, OH), 1.50 (s, 3H, CH_3), 1.34 (s, 3H, CH_3); **^{13}CNMR** ($CDCl_3$, 100 Hz): 138.3 (Ar), 138.0 (Ar), 128.7 (Ar), 128.6 (Ar), 128.3 (Ar), 128.21 (Ar), 128.17 (Ar), 128.0 (Ar), 110.1 ($C(CH_3)_2$), 82.2 (C-3 or C-6), 79.4 (C-1), 77.2 (C-3 or C-6), 74.2 (C-2), 73.5 (CH_2Ar), 73.2 (C-5), 72.8 (CH_2Ar), 71.7 (C-4), 28.2 (CH_3), 26.1 (CH_3).

DL-3,6-Di-*O*-benzyl-*myo*-inositol (**83**)

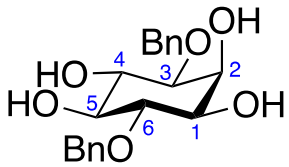

1,2-Isopropylidene 3,6-di-*O*-benzyl inositol (**82**, 2.9 g, 7.241 mmol) was dissolved in 80% aq acetic acid (50 mL). The reaction was allowed to stir at 100 °C for 4 hours. The reaction was then concentrated *in vacuo* and to yield the crude product. The crude product was recrystallized from ethanol to yield the pure product as a white,

crystalline solid (2.07 g, 5.74 mmol, 79% yield). **mp**: 203.6-204.7 °C (lit.[426] 204 °C); **^{1}HNMR** (dmso, 400 Hz): 7.21-7.43 (m, 10H, Ar), 4.73-4,82 (m, 5H, 2 x CH_2Ar and 3 x OH), 4.65 (dd, *J*= 2.2, 9.2 Hz, 1H, OH), 4.65 (AB, obscured, 1H, CH_2Ar), 4.57 (AB, *J*= 12.1 Hz, 1H, CH_2Ar), 3.96 (br d, *J*= 3.0 Hz, 1H, H-2), 3.60 (dt, *J*= 4.5, 9.0 Hz, 1H, H-4), 3.42 (t, *J*= 9.5 Hz, 1H, H-6), 3.27-3.32 (m, 1H, H-1), 3.13 (apt dt, *J*= 4.7, 9.0 Hz, 1H, H-5), 3.10 (dd, *J*= 2.3, 9.8 Hz, 1H, H-3); **^{31}CNMR** (dmso, 100 Hz): 139.9 (Ar), 139.3 (Ar), 128.0 (Ar), 127.9 (Ar), 127.52 (Ar), 127.48 (Ar), 127.1 (Ar), 126.9 (Ar), 81.8 (C-6), 79.8 (C-3), 75.0 (C-5), 73.6 (CH_2Ar), 72.3 (C-4), 71.4 (C-1), 70.7 (CH_2Ar), 69.7 (C-2).

DL-3,6-Di-*O*-benzyl-4,5-*O*-(2,3-dimethoxybutane-2,3-diyl)-*myo*-inositol (**84**)

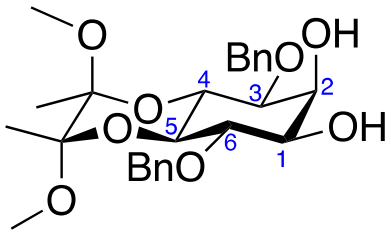

As described by Riley *et al.*,[397] 3,6-di-*O*-benzyl inositol (**83**, 4.70g, 13.04 mmol) was dissolved in dry methanol (100 mL). To this solution, trimethyl orthoformate (10 mL), butanedione (1.305 mL, 15.00 mmol, 1.15 equiv) and camphorsulfonic acid (250 mg, 1.075 mmol, 0.8 equiv) were added. This reaction was allowed to reflux for 24 hours, during which time the solution turned a dark red. The progress of the reaction was confirmed with TLC (Rf 0.5, EtOAc:DCM, 1:3). The solution was allowed to cool to RT, 0.5 mL triethylamine was added, and the solution was concentrated under reduced pressure to yield a red foam. This foam was purified by column chromatography (5-25% EtOAc in DCM) and recrystallized from ethanol to yield the pure product as a white solid (3.98 g, 8.40 mmol, 64% yield). **m.p.** 141.6-142.6 °C (lit.[397] 141-143°C); **^{1}HNMR** ($CDCl_3$, 400 Hz): 7.38-7.27 (m, 10H, Ar), 5.05 (AB, *J*= 11.2 Hz, 1H, C*H*$_2$Ph), 4.88 (AB, *J*= 11.9 Hz, 1H, C*H*$_2$Ph), 4.72 (AB, *J*= 11.0 Hz, 1H, C*H*$_2$Ph), 4.71 (AB, *J*= 12.2 Hz, 1H, C*H*$_2$Ph), 4.21 (t, *J*= 3.0 Hz, 1H, H-2), 4.16 (t, *J*= 10.0 Hz, 1H, H-4 or H-6), 3.84 (t, *J*= 9.5 Hz, 1H, H-4 or H-6), 3.65 (t, *J*= 9.9 Hz, 1H, H-5), 3.50 (dd, *J*= 9.9, 3.0 Hz, 1H, H-1), 3.46 (dd, *J*= 9.9, 2.6 Hz, 1H, H-3), 3.33 (s, 3H, OC*H*$_3$), 3.30 (s, 3H, OC*H*$_3$), 2.52 (brs, 1H, O*H*), 2.50 (brs, 1H, O*H*), 1.37 (s, 3H, CC*H*$_3$), 1.36 (s, 3H, CC*H*$_3$); **^{31}CNMR** ($CDCl_3$, 100 Hz): 138.9 (Ar), 128.7-127.8 (m, Ar), 99.5 (BDA), 78.5 (C-4 or C-6), 76.8 (C-1), 75.6 (*C*H_2Ph), 73.5 (*C*H_2Ph), 72.1 (C-3), 71.8 (C-5), 70.6 (C-2), 69.8 (C-4 or C-6), 48.1 x2 (O*C*H_3), 18.0 (C*C*H_3). **HRMS (ESI)**: *m/z* calcd $[M+Na]^+$ for $C_{26}H_{34}O_8$: 497.2170, found: 497.2145.

Synthesis of diphospho myo-inositol phosphate [PP-InsP] targets

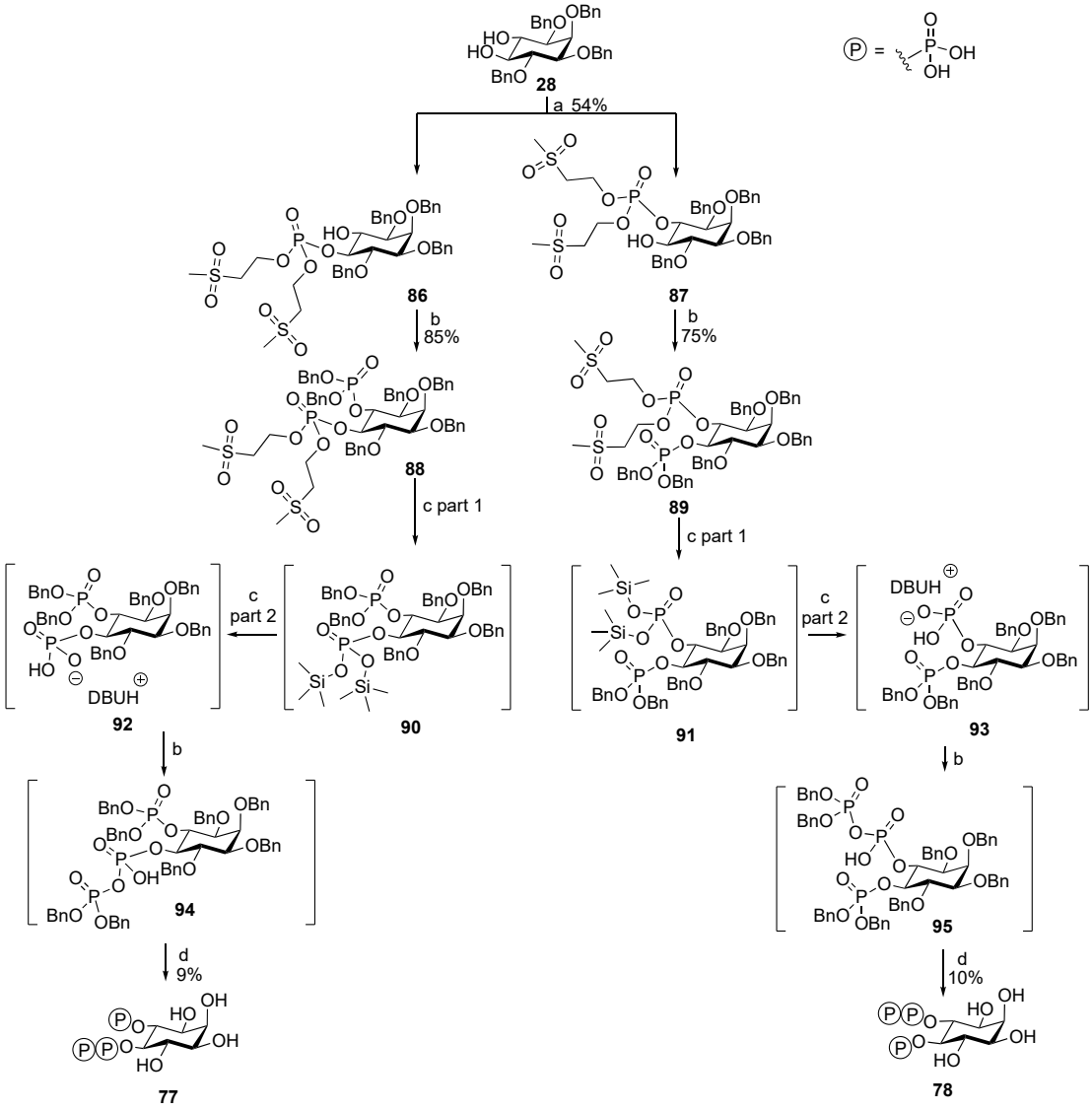

Scheme 13: Later steps in the synthetic route to form both target racemic regioisomers of PP-InsP:5-PP-Ins(4)P (**77**) and 4-PP-Ins(5)P (**78**).

Reagents and conditions: (a) 1. *N,N*-diisopropylamino-bis-[2-(methylsulfonyl)ethyloxy]phosphine (**1**), 5-phenyl-1*H*-tetrazole, DCM, RT, 3h, 2. *m*CPBA, -78°C -0°C, 10 min; (b) 1. dibenzyl diisopropylphosphoramidite, 5-phenyl-1*H*-tetrazole, DCM, RT, 3h, 2. *m*CPBA, -78°C -0°C, 10 min; (c) 1. BSTFA, $CDCl_3$ 2. MeOH, TFA; (d) H_2, $Pd(OH)_2/C$, $NaHCO_3$, H_2O, isopropanol. Non-isolated intermediates are shown in brackets.

DL-1,2,3,6-Tetra-*O*-benzyl-4,5-*O*-(2,3-dimethoxybutane-2,3-diyl)-*myo*-inositol (**85**)

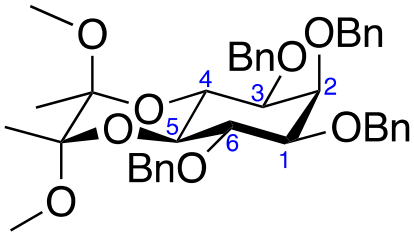

3,6-Di-*O*-benzyl-4,5-*O*-(2,3-dimethoxybutane-2,3-diyl)-*myo*-inositol (**84**, 500 mg, 1.05 mmol) was dissolved in dry DMF (20 mL). The solution was cooled to 0°C, and sodium hydride (81 mg, 3.37 mmol, 3.2 equiv) was added to the reaction followed by benzyl bromide (0.19 mL, 1.58 mmol, 1.5 equiv). The reaction was allowed to stir for 3h at RT, after which time brine (100 mL) was added to the flask and the product was extracted with EtOAc (150 mL). The organic phase was dried over $MgSO_4$ and concentrated under reduced pressure to yield the crude product. The product was purified with silica column chromatography (1. DCM-EtOAc, 0-100%, 2. Pet. ether-EtOAc, 0-100%) to yield the pure product as a colourless solid (476 mg, 0.727 mmol, 69% yield). **m.p**. 86.1-88.0°C; **^{1}HNMR** ($CDCl_3$, 400 Hz): 7.39-7.23 (m, 20H, Ar), 4.93-4.79 (m, 5H, CH_2Ar), 4.70-4.57 (m, 3H, CH_2Ar), 4.29 (t, *J*= 10.0 Hz, 1H, H-4 or H-6), 4.04 (t, *J*= 10 Hz, 1H, H-4 or H-6), 4.03 (t, *J*= 2.6 Hz, 1H, H-2), 3.64 (t, *J*= 9.9 Hz, 1H, H-5) 3.43 (dd, *J*= 2.5, 10.1 Hz, 1H, H-1 or H-3), 3.32 (dd, *J*= 2.5, 9.5 Hz, 1H, H-1 or H-3), 3.31 (s, 3H, OCH_3), 3.30 (s, 3H, OCH_3), 1.36 (s, 3H, CCH_3), 1.34 (s, 3H, CCH_3); **^{13}CNMR** ($CDCl_3$, 100 Hz): 139.34 (Ar), 139.30 (Ar), 139.2 (Ar), 138.7 (Ar), 128.43 (Ar), 128.37 (Ar), 128.3 (Ar), 128.2 (Ar), 128.1 (Ar), 128.0 (Ar), 127.7 (Ar), 127.64 (Ar), 127.55 (Ar), 127.4 (Ar), 127.3 (Ar), 127.2 (Ar), 99.52 (BDA), 99.46 (BDA), 81.1(C-1 or C-3), 79.0 (C-4 or C-6), 78.3 (C-1 or C-3), 76.7 (C-2), 75.8 (CH_2Ar), 74.7 (CH_2Ar), 73.4 (CH_2Ar), 73.2 (CH_2Ar), 72.0 (C-5), 70.0 (C-4 or C-6), 48.0 (OCH_3), 47.9 (OCH_3), 18.01 (CCH_3), 17.95 (CCH_3); **HRMS (ESI)**: *m/z* calcd $[M+Na]^+$ for $C_{40}H_{46}O_8$: 677.3085, found: 677.3081.

DL-1,2,3,6-Tetra-*O*-benzyl-*myo*-inositol (**28**)

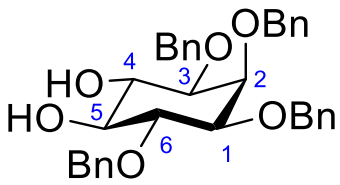

1,2,3,6-Tetra-*O*-benzyl-4,5-*O*-(2,3-dimethoxybutane-2,3-diyl)-*myo*-inositol (**85**, 400 mg, 0.611 mmol) was dissolved in a mixture of TFA (4.5 mL) and water (0.5 mL). The solution was allowed to stir for 10 minutes at RT, during which time the solution turned dark yellow. The reaction was then concentrated *in vacuo* to yield the crude

product, which was subsequently purified using silica column chromatography (DCM-EtOAc, 0-100%) to yield the pure product as a white solid (299.4 mg, 0.554 mmol, 91% yield). **m.p.** 85.1-86.4°C (lit.[400] value: 103-104°C); **^{1}HNMR** ($CDCl_3$, 400 Hz): 7.30-7.12 (m, 20H, Ar), 4.86 (d, *J*= 11.0 Hz, 1H, C*H*$_2$Ar), 4.78-4.68 (m, 3H, C*H*$_2$Ar), 4.57-4.42 (m, 4H, C*H*$_2$Ar), 3.95 (t, *J*= 9.5 Hz, 1H, H-4 or H-6), 3.95 (t, *J*= 2.4 Hz, 1H, H-2), 3.83 (t, *J*= 9.5 Hz, 1H, H-5), 3.34 (t, *J*= 9.2 Hz, 1H, H-4 or H-6), 3.27 (dd, *J*= 2.3, 9.7 Hz, 1H, H-1 or H-3), 3.08 (dd, *J*= 2.3, 9.7 Hz, 1H, H-1 or H-3), 2.65 (brs, 2H, 4-OH and 5-OH); **^{13}CNMR** ($CDCl_3$, 100 Hz): 138.93 (Ar), 138.91 (Ar), 138.3 (Ar), 138.0 (Ar), 128.6 (Ar), 128.5 (Ar), 128.3 (Ar), 128.1 (Ar), 128.0 (Ar), 127.9 (Ar), 127.83 (Ar), 127.77 (Ar), 127.74 (Ar), 127.69 (Ar), 127.5 (Ar), 81.1 (C-1 or C-3), 81.0 (C-5), 80.1 (C-1 or C-3), 75.5 (*C*H$_2$Ar), 74.9 (C-4 or C-6), 74.3 (*C*H$_2$Ar), 73.9 (C-2), 72.8 (*C*H$_2$Ar), 72.5 (C-4 or C-6), 72.4 (*C*H$_2$Ar); **HRMS (ESI)**: *m/z* calcd $[M+H]^+$ for $C_{34}H_{36}O_6$: 541.2585, found: 541.2583.

DL-1,2,3,6-Tetra-*O*-benzyl-*myo*-inositol-5-bis[2-(methanesulfonyl)ethyl]phosphate (**86**), DL-1,2,3,6-tetra-*O*-benzyl-*myo*-inositol-4-bis[2-(methanesulfonyl)ethyl]phosphate (**87**) and DL-1,2,3,6-tetra-*O*-benzyl-*myo*-inositol-4,5-bisbis[2-(methanesulfonyl)ethyl]phosphate (**29**)

DL-1,2,3,6-Tetra-*O*-benzyl-*myo*-inositol (**28**, 200 mg, 0.370 mmol) was dissolved in dry DCM (10 mL) and the solution was put under argon. 5-Phenyl-1*H*-tetrazole (81 mg, 0.555 mmol, 1.5 equiv) was added to the solution followed by MSE phosphoramidite (**1**, 168 mg, 0.444 mmol, 1.2 equiv). The reaction was allowed to stir at RT overnight. The following day, the reaction was cooled to -78°C and *m*CPBA (70% pure, 182 mg, 0.740 mmol, 2 equiv) was added. The reaction was allowed to stir for 10 min at RT before it was diluted with EtOAc (100 mL) and washed twice with 10% Na_2SO_3 solution (2 x 30 mL). The organic layer was dried over $MgSO_4$ and concentrated *in vacuo* to yield the crude product. The product was purified with flash chromatography (1. EtOAc-MeOH, 0-10%, 2. DCM-EtOAc, 0-100%, 3. Pet. ether-EtOAc, 0-100%) before being collected as a colourless oil that was a partially separated mixture of regioisomers (**87**: 7.5 mg, **86**: 14.1 mg, mixed **86** and **87**: 144.9 mg, overall 0.200 mmol, overall 54% yield). A larger-scale repeat of the reaction resulted in the generation of some of the bisphosphorylated product (mixed **86** and **87**: 571.1 mg, 33% yield; **29**: 825.8 mg, 31% yield).

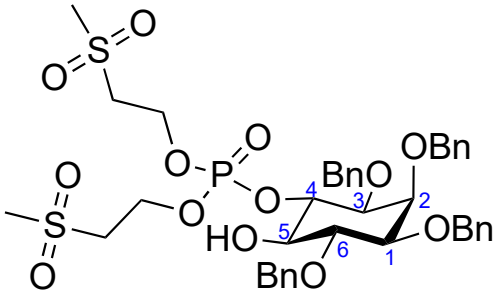

DL-1,2,3,6-Tetra-*O*-benzyl-*myo*-inositol-4-bis[2-(methanesulfonyl)ethyl]phosphate (**87**): **^{1}HNMR** ($CDCl_3$, 400 Hz): 7.38-7.28 (m, 20H, Ar), 4.96 (AB, *J*= 11.1 Hz, 1H, C*H*$_2$Ph), 4.90 (AB, *J*= 11.7, 1H, C*H*$_2$Ph), 4.81-4.56 (m, 6H, CH_2Ph), 4.50-4.28 (m, 5H, H-4, OCH_2), 4.10 (brs, 1H, H-2), 3.93 (t, *J*= 9.4 Hz, 1H, H-6), 3.58 (t, *J*= 9.2 Hz, 1H, H-5), 3.39 (dt, *J*= 2.6, 9.8 Hz, 2H, H-1, H-3), 3.23-3.18 (m, 3H, OH, CH_2S), 3.10-3.02 (m, 1H, CH_2S), 2.95-2.91 (m, 1H, CH_2S), 2.88 (s, 3H, SMe), 2.80 (s, 3H, SMe); **^{31}PNMR** ($CDCl_3$, 162 Hz): -2.56; **^{13}CNMR** ($CDCl_3$, 100 Hz): 138.5 (Ar), 138.0 (Ar), 128.8 (Ar), 128.7 (Ar), 128.5 (Ar), 128.4 (Ar), 128.3 (Ar), 128.00 (Ar), 127.95 (Ar), 127.8 (Ar), 80.9 (C-6), 80.6 (C-1 or C-3), 78.7 (C-1 or C-3), 75.9 (*C*H_2Ar), 74.7 (*C*H_2Ar), 73.9 (C-5), 73.3 (C-2), 73.1 (*C*H_2Ar), 72.2 (*C*H_2Ar), 61.9 (OCH_2), 61.7 (OCH_2), 55.0 (SCH_2), 54.8 (SCH_2), 42.83 (SMe), 42.76 (SMe); **HRMS (ESI)**: *m/z* calcd $[M+Na]^+$ for $C_{40}H_{49}O_{13}PS_2$: 855.2244, found: 355.2235.

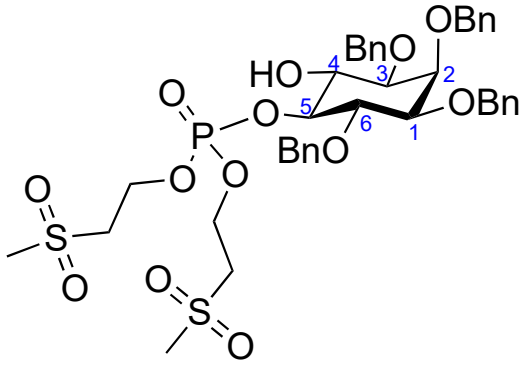

DL-1,2,3,6-Tetra-*O*-benzyl-*myo*-inositol-5-bis[2-(methanesulfonyl)ethyl]phosphate (**86**)**: ^{1}HNMR** ($CDCl_3$, 400 Hz): 7.40-7.25 (m, 2H, Ar), 5.09 (AB, *J*= 11.5 Hz, 1H, C*H*$_2$Ph), 4.85 (AB, *J*= 11.9 Hz, 1H, C*H*$_2$Ph), 4.78 (AB, *J*= 11.8 Hz, 1H, C*H*$_2$Ph), 4.66 (AB, *J*= 11.5 Hz, 1H, C*H*$_2$Ph), 4.62-4.50 (m, 6H, C*H*$_2$Ph, H-5, OC*H*$_2$), 4.36-4.02 (m, 6H, OC*H*$_2$, H-2, H-4, H-6), 3.41 (dd, *J*= 9.8, 2.2 Hz, 1H, H-1), 3.29 (t, *J*= 5.4 Hz, 2H, C*H*$_2$S), 3.18 (dd, *J*= 9.7, 2.2 Hz, 1H, H-3), 3.09 (brs, 1H, OH), 2.94 (s, 3H, SMe), 2.98-2.88 (m, 1H, C*H*$_2$S) 2.77 (s, 3H, SMe), 2.80-2.70 (m, 1H, C*H*$_2$S); **^{31}PNMR** ($CDCl_3$, 162 Hz): -2.20; **^{13}CNMR** ($CDCl_3$, 100 Hz): 138.7 (Ar), 138.6 (Ar), 137.7 (Ar), 137.6 (Ar), 128.7 (Ar), 128.6 (Ar), 128.5 (Ar), 128.3 (Ar), 128.1 (Ar), 128.0 (Ar), 127.9 (Ar), 127.7 (Ar), 127.1 (Ar), 82.2 (C-5), 80.5 (C-1), 79.5 (C-3), 79.1 (C-2 or C-4 or C-6), 74.7 (*C*H_2Ar), 74.5 (*C*H_2Ar), 73.2 (C-2 or C-4 or C-6), 72.9 (*C*H_2Ar), 72.7 (*C*H_2Ar), 71.4 (C-2 or C-4 or C-6), 61.9 (OC*H*$_2$), 61.5 (OC*H*$_2$), 55.1 (SC*H*$_2$), 54.5 (SC*H*$_2$), 42.9 (SMe), 42.7 (SMe); **HRMS (ESI)**: *m/z* calcd $[M+H]^+$ for $C_{40}H_{49}O_{13}PS_2$: 833.2425, found: 833.2414.

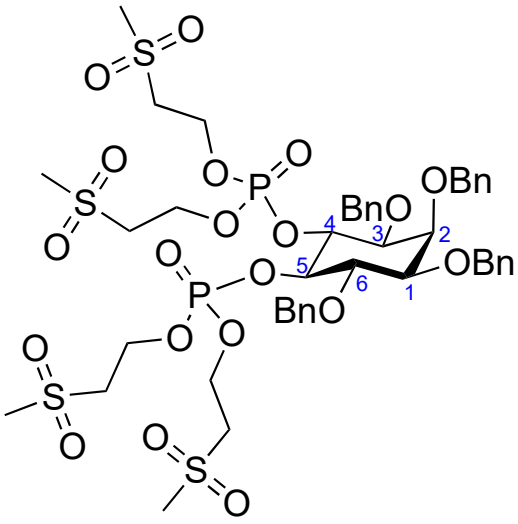

DL-1,2,3,6-tetra-*O*-benzyl-*myo*-inositol-4,5-bisbis[2-(methanesulfonyl)ethyl]phosphate (**29**)**:** **^{1}HNMR** ($CDCl_3$, 400 Hz): 7.37-7.21 (m, 20H, Ar), 5.08 (d, *J*= 11.3 Hz, 1H, C*H*$_2$Ar), 4.87 (d, *J*= 11.6 Hz, 1H, C*H*$_2$Ar), 4.83 (q, *J*= 9.4 Hz, 1H, H-4 or -6), 4.75 (d, *J*= 11.7 Hz, C*H*$_2$Ar), 4.74 (d, *J*= 11.3 Hz, C*H*$_2$Ar), 4.60-4.28 (m, 12H, H-5, C*H*$_2$Ar, MSE CH_2), 4.20-4.13 (m, 1H, MSE CH_2), 4.07 (t, *J*= 9.6 Hz, 1H, H-4 or -6), 4.04 (t, *J*= 2.2 Hz, 1H, H-2), 3.44-3.41 (m, 2H, H-1 and H-3), 3.40-3.24 (m, 4H, MSE CH_2), 3.10-2.97 (m, 2H, MSE CH_2), 2.94 (s, 3H, MSE C*H*$_3$), 2.92 (s, 3H, MSE C*H*$_3$), 2.89-2.87 (m, 1H, MSE CH_2), 2.85 (s, 3H, MSE C*H*$_3$), 2.80 (s, 3H, MSE C*H*$_3$), 2.78-2.73 (m, 1H, MSE CH_2); **^{31}PNMR** ($CDCl_3$, 162 Hz): -2.99, -3.46; **^{13}CNMR** ($CDCl_3$, 100 Hz): 138.2 (Ar), 137.4 (Ar), 128.9 (Ar), 128.7 (Ar), 128.6 (Ar), 128.5 (Ar), 128.2 (Ar), 128.08 (Ar), 128.06 (Ar), 128.0 (Ar), 127.8 (Ar), 127.0 (Ar), 80.5 (C-5), 80.1 (C-1 or -3), 79.1 (C-4 or -6), 78.7 (C-4 or -6), 77.9 (C-1 or -3), 74.8 (*C*H_2Ar), 74.63 (*C*H_2Ar), 74.56 (*C*H_2Ar), 73.0 (*C*H_2Ar), 72.8 (C-2), 61.8 (MSE *C*H_2), 61.4 (MSE *C*H_2), 54.54 (MSE *C*H_2), 54.46 (MSE *C*H_2), 42.7 (MSE *C*H_3), 42.6 (MSE *C*H_3), 42.52 (MSE *C*H_3), 42.45 (MSE *C*H_3); **HRMS (ESI)**: *m/z* calcd $[M+Na]^+$ for $C_{46}H_{62}O_{20}P_2S_4$: 1147.2085, found: 1147.2084.

DL-1,2,3,6-Tetra-*O*-benzyl-*myo*-inositol-4-dibenzylphosphate-5-bis[2-(methanesulfonyl)ethyl]phosphate (**88**)

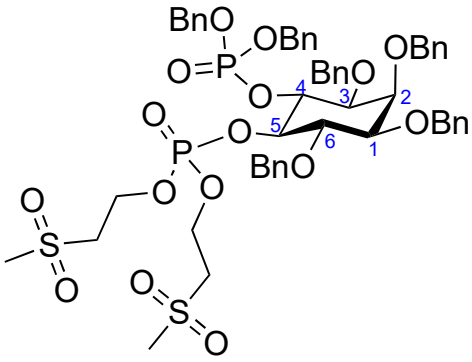

DL-1,2,3,6-Tetra-*O*-benzyl-*myo*-inositol-5-bis[2-(methanesulfonyl)ethyl]phosphate (**86**, 70 mg, 0.084 mmol) was first thoroughly dried on a vacuum line after dissolving it in dry acetonitrile and concentrating it under reduced pressure. The starting material (**86**) was then dissolved in dry DCM (10 mL), and to this solution, 5-phenyl-1*H*-tetrazole (98 mg, 0.672 mmol, 8 equiv) followed by dibenzyl phosphoramidite (0.17 mL, 0.504 mmol, 6 equiv) were added. The reaction was allowed to stir at RT under argon overnight. The solution was then cooled to -78°C, and *m*CPBA (70% pure, 124 mg, 0.504 mmol, 6 equiv) was added. The reaction was allowed to stir for 10 min at RT before it was diluted with EtOAc (100 mL) and washed with 10% Na_2SO_3 solution (60 mL). The organic layer was dried over $MgSO_4$ and concentrated to yield the crude product. The product was purified with flash chromatography (DCM-EtOAc, 0-100%) to yield the pure product as a colourless oil (77.7 mg, 0.071 mmol, 85% yield). **^{1}HNMR** ($CDCl_3$, 400 Hz): 7.38-7.18 (m, 30H, Ar), 5.10 (AB, *J*= 11.5 Hz, 1H, C*H*$_2$Ar), 5.05-5.00 (m, 2H, C*H*$_2$Ar), 4.97-4.90 (m, 3H, H-4 or H-5 and C*H*$_2$Ar), 4.82-4.77 (m, 2H, C*H*$_2$Ar), 4.70 (AB, *J*= 11.5 Hz, 1H, C*H*$_2$Ar), 4.57-4.41 (m, 6H, H-6 and MSE CH_2 and C*H*$_2$Ar), 4.33-4.21 (m, 2H, MSE CH_2), 4.10-4.05 (m, 2H, H-4 or H-5 and MSE CH_2), 3.94 (t, *J*= 2.2 Hz, 1H, H-2), 3.39 (t, *J*= 2.4Hz, 1H, H-1 or H-3), 3.37 (t, *J*= 2.4 Hz, 1H, H-1 or H-3), 3.10-2.98 (m, 2H, MSE CH_2), 2.83-2.77 (m, 1H, MSE CH_2), 2.74 (s, 3H, SMe), 2.67 (s, 3H, SMe), 2.66-2.62 (m, 1H, MSE CH_2); **^{31}PNMR** ($CDCl_3$, 162 Hz): -2.40 (benzyl-protected phosphate), -2.97 (MSE-protected phosphate); **^{13}CNMR** ($CDCl_3$, 100 Hz): 171.3 (Ar), 138.7 (Ar), 138.4 (Ar), 137.5 (Ar), 137.4 (Ar), 136.11 (Ar), 136.06 (Ar), 135.91 (Ar), 135.85 (Ar), 128.8 (Ar), 128.73 (Ar), 128.66 (Ar), 128.63 (Ar), 128.55 (Ar), 128.5 (Ar), 128.3 (Ar), 128.2 (Ar), 128.12 (Ar), 128.05 (Ar), 128.03 (Ar), 128.02 (Ar), 127.9 (Ar), 127.7 (Ar), 126.9 (Ar), 80.3 (C-6), 79.8 (C-1 or C-3), 78.7 (C-4 or C-5), 78.6 (C-4 or C-5), 78.1 (C-1 or C-3), 74.6 (*C*H$_2$Ar), 74.3 (*C*H$_2$Ar), 73.1 (C-2), 72.67 (*C*H$_2$Ar), 72.66 (*C*H$_2$Ar), 69.9 (d, *J*= 6.4 Hz, *C*H$_2$Ar), 69.6 (d, *J*= 5.0 Hz, *C*H$_2$Ar), 62.1 (d, *J*= 5.3 Hz, MSE CH_2), 61.4 (d, *J*= 4.6 Hz, MSE CH_2), 54.5 (d, *J*= 9.0 Hz, MSE CH_2), 54.2 (d, J= 8.0 Hz, MSE CH_2), 42.7 (SMe), 42.5 (SMe); **HRMS (ESI)**: *m/z* calcd $[M+H]^+$ for $C_{54}H_{62}O_{16}P_2S_2$: 1093.3027, found: 1093.3021.

DL-5-Diphospho-*myo*-inositol-4-phosphate triethylammonium salt (**77**)

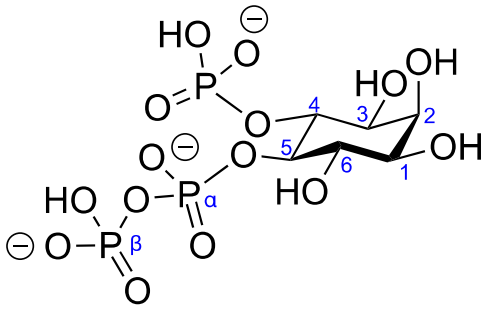

DL-1,2,3,6-Tetra-*O*-benzyl-*myo*-inositol-4-dibenzylphosphate-5-bis[2-(methanesulfonyl)-ethyl]phosphate (**88,** 77.7 mg, 71.1 µmol) was dissolved in $CDCl_3$ (1.5 mL) in an NMR tube, and to this solution DBU 49 µL, 0.284 mmol, 4 equiv) followed by BSTFA (0.38 mL, 1.42 mmol, 20 equiv) were added. ^{31}PNMR was used to ensure the silylation was complete with a diagnostic singlet at -17.8 ppm (**90**). Methanol (0.14 mL, 3.55 mmol, 50 equiv) was then added to the reaction and, after 7 min, TFA (46 µL, 0.604 mmol, 8.5 equiv) was added. ^{31}PNMR confirmed that desilylation was completed with the diagnostic signal shifting to around 0 ppm. The reaction was concentrated *in vacuo* and the residue (**92**) was thoroughly dried on a vacuum line.

This crude residue (**92**) was then dissolved in dry DCM (10 mL), and to this solution, 5-phenyl-1*H*-tetrazole (166 mg, 1.14 mmol, 16 equiv) and a portion of the dibenzyl phosphoramidite (0.15 mL; total: 0.23 mL, 0.654 mmol, 9.2 equiv) were added and the reaction was allowed to stir at RT for an hour. The remaining dibenzyl phosphoramidite (0.08 mL) was then added and the reaction was allowed to stir for another hour. The reaction was then cooled to -78 °C before *m*CPBA (280 mg, 70%, 1.14 mmol, 16 equiv) was added. The solution was allowed to warm to RT, before being concentrated *in vacuo* without heat. The residue generated at this point in the reaction (**94**) was immediately deprotected crude via hydrogenation to avoid possible product decomposition (the compound was also not studied or even thoroughly dried at this stage).

The protected pyrophosphate compound (**94**, assumed 71.1 µmol) was dissolved in a mixture of isopropanol (8 mL) and mQ (2 mL). To this solution, sodium bicarbonate (21 mg, 0.249 mmol, 3.5 equiv) and $Pd(OH)_2/C$ (20%, ≥50% wet, 135 mg) were added. The flask was evacuated and flushed with hydrogen three times, before being left to stir in an atmosphere of hydrogen. After 2 h, an additional 6 mL of mQ was added to the reaction, and the flask was evacuated and flushed with hydrogen three times again. The solution was allowed to stir at RT under hydrogen for three days. The crude product was purified on an RP-18 column (0-70% MeCN in 0.05 TEAB) to separate the partially deprotected product, which was subsequently hydrogenated again to fully remove the remaining benzyl groups. The product was purified with a Q Sepharose Fast Flow resin ion exchange column (0-1.5 M TEAB) and a final RP-18 column (0-10%

MeCN in 0.05 TEAB). The presence of product in the collected fractions was confirmed using a Briggs qualitative phosphate assay, and the product-containing fractions were concentrated *in vacuo* without heat. The excess TEAB buffer was decomposed through successive additions of methanol and *in vacuo* concentration. The final product was lyophilised and collected as an off-white glass (5.2 mg, calculated 3.8 TEA counterions per molecule of product, 6.50 µmol, 9% yield).

^{1}HNMR (D_2O, 400 Hz): 4.19 (dt, *J*= 9.3, 7.0 Hz, 1H, H-4), 4.02 (t, *J*= 2.8 Hz, 1H, H-2), 3.98 (q, J= 9.3 Hz, 1H, H-5), 3.86 (t, *J*= 9.6 Hz, 1H, H-6), dd (3.69, *J*= 9.6, 2.8 Hz, 1H, H-3), dd (3.57, *J*= 10.1, 2.9 Hz, 1H, H-1), 3.17 (q, *J*= Hz, approx. 23H, TEA C*H*$_2$), 1.26 (q, *J*= Hz, approx. 34H, TEA C*H*$_3$); **^{31}PNMR** (D_2O, 162 Hz): 4.28 (P-4), -6.30 (d, *J*= 23.9 Hz, pyrophosphate β-P), -11.25 (d, *J*= 23.7 Hz, pyrophosphate α-P); **^{13}CNMR** (D_2O, 100 Hz): 79.9 (C-5), 76.3 (C-4), 71.6 (C-3), 71.3 (C-2), 71.0 (C-6), 70.4 (C-1), 46.7 (TEA *C*H_2), 8.2 (TEA *C*H_3); **HRMS (ESI)**: *m/z* calcd $[M-H]^-$ for $C_6H_{19}O_{30}P_8$: 418.9551, found: 418.9552.

DL-1,2,3,6-Tetra-*O*-benzyl-*myo*-inositol-5-dibenzylphosphate-4-bis[2-(methanesulfonyl)ethyl]phosphate (**89**)

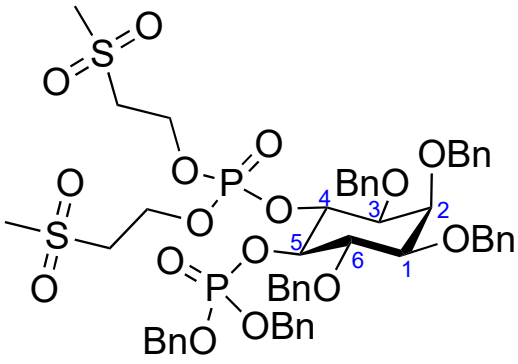

DL-1,2,3,6-Tetra-*O*-benzyl-*myo*-inositol-4-bis[2-(methanesulfonyl)ethyl]phosphate (**87**, 91.9 mg, 0.110 mmol) was first thoroughly dried on a vacuum line after dissolving it in dry acetonitrile and concentration under reduced pressure. The starting material (**87**) was then dissolved in dry DCM (10 mL), and to this solution, 5-phenyl-1*H*-tetrazole (129 mg, 0.883 mmol, 8 equiv), followed by dibenzyl phosphoramidite (0.23 mL, 0.662 mmol, 6 equiv) were added, and the solution was allowed to stir at RT under argon overnight. The solution was then cooled to -78°C, and *m*CPBA (70% pure, 163.2 mg, 0.662 mmol, 6 equiv) was added. The reaction was allowed to stir for 10 min at RT before it was diluted with EtOAc (100 mL) and washed with 10% Na_2SO_3 solution (60 mL). The organic layer was dried over $MgSO_4$ and concentrated to yield the crude product. The product was purified with flash chromatography (DCM-EtOAc, 0-100%) to yield the pure product as a colourless oil (90.4 mg, 0.083 mmol, 75% yield).**^{1}HNMR** ($CDCl_3$, 400 Hz): 7.38-7.07 (m, 30H, Ar), 5.07-4.76 (m, 8H, CH_2Ar and H-4 or H-6), 4.66-4.47 (m, 6H, CH_2Ar and H-5), 4.44-4.37 (m, 1H, MSE CH_2), 4.35-4.19 (m, 3H, MSE CH_2),

4.11 (t, *J*= 9.5 Hz, 1H, H-4 or H-6), 4.05 (t, *J*= 2.1 Hz, H-2), 3.42 (d, *J*= 9.9 Hz, 1H, H-1 or H-3), 3.41 (d, *J*= 9.9 Hz, 1H, H-1 or H-3), 2.99 (t, *J*= 5.3 Hz, 2H, MSE CH_2), 2.96-2.90 (m, 1H, MSE CH_2), 2.85-2.81 (m, 1H, MSE CH_2), 2.79 (s, 3H, MSE CH_3), 2.64 (s, 3H, MSE CH_3); **^{31}PNMR** ($CDCl_3$, 162 Hz): -2.07, -3.51; **^{13}CNMR** ($CDCl_3$, 100 Hz): 138.8 (Ar), 138.3 (Ar), 137.6 (Ar), 137.3 (Ar), 135.8 (Ar), 128.8 (Ar), 128.73 (Ar), 128.67 (Ar), 128.6 (Ar), 128.5 (Ar), 128.4 (Ar), 128.3 (Ar), 128.2 (Ar), 128.11 (Ar), 128.06 (Ar), 128.0 (Ar), 127.9 (Ar), 127.3 (Ar), 127.1 (Ar), 80.4 (C-1 or C-3), 79.9 (C-5), 79.3 (C-4 or C-6), 78.9 (C-4 or C-6), 78.1 (C-1 or C-3), 74.8 (*C*H_2Ar), 74.7 (*C*H_2Ar), 73.2 (*C*H_2Ar), 72.7 (C-2), 72.1 (*C*H_2Ar), 69.9 (*C*H_2Ar), 69.8 (*C*H_2Ar), 69.60 (*C*H_2Ar), 69.55 (*C*H_2Ar), 61.50 (MSE *C*H_2), 61.45 (MSE *C*H_2), 54.6 (MSE *C*H_2), 54.5 (MSE *C*H_2), 42.7 (MSE *C*H_3), 42.6 (MSE *C*H_3); **HRMS (ESI)**: *m/z* calcd $[M+H]^+$ for $C_{54}H_{62}O_{16}P_2S_2$: 1093.3027, found: 1093.3014.

DL-4-Diphospho-*myo*-inositol-5-phosphate triethylammonium salt (**78**)

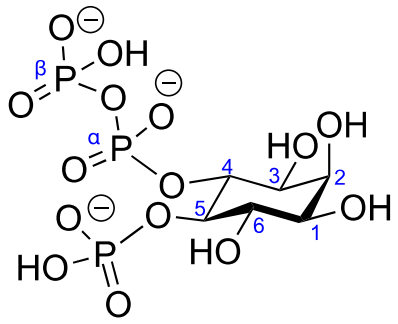

DL-1,2,3,6-Tetra-*O*-benzyl-*myo*-inositol-5-dibenzylphosphate-4-bis[2-(methanesulfonyl)-ethyl]phosphate (**89**, 90.4 mg, 82.7 µmol) was dissolved in $CDCl_3$ (1.5 mL) in an NMR tube, and to this solution DBU 49 µL, 0.331 mmol, 4 equiv) followed by BSTFA (0.44 mL, 1.65 mmol, 20 equiv) were added. ^{31}PNMR was used to ensure the silylation was complete with a diagnostic singlet at -17.8 ppm (**91**). Methanol (0.17 mL, 4.14 mmol, 50 equiv) was then added to the reaction and after 7 min, TFA (54 µL, 0.703 mmol, 8.5 equiv) was added. ^{31}PNMR spectroscopy confirmed that desilylation was completed with the diagnostic peak shifting to -0.1 ppm. The reaction was concentrated *in vacuo* and the residue (**93**) was thoroughly dried on a vacuum line.

This crude residue (**93**) was then dissolved in dry DCM (10 mL), and to this solution, 5-phenyl-1*H*-tetrazole (193 mg, 1.32 mmol, 16 equiv) and a portion of the dibenzyl phosphoramidite (0.17 mL; total: 0.25 mL, 0.730 mmol, 8.8 equiv) were added, and the reaction was allowed to stir at RT for an hour. The remaining dibenzyl phosphoramidite (0.08 mL) was then added, and the reaction was allowed to stir for another hour. The reaction was then cooled to -78 °C before *m*CPBA (326 mg, 70%, 1.32 mmol, 16 equiv) was added. The solution was allowed to warm to RT before being concentrated *in vacuo* without heat. The residue generated at this point in the reaction (**95**) was immediately deprotected crude via hydrogenation to avoid possible

product decomposition (the compound was also not studied or even thoroughly dried at this stage).

The protected pyrophosphate compound (**95**, assumed 82.7 µmol) was dissolved in a mixture of isopropanol (8 mL) and mQ (2 mL). To this solution, sodium bicarbonate (24 mg, 0.290 mmol, 3.5 equiv) and $Pd(OH)_2/C$ (20%, ≥50% wet, 150 mg) were added. The flask was evacuated and flushed with hydrogen three times before the mixture being left to stir in an atmosphere of hydrogen. After 2 h, an additional 6 mL of mQ was added to the reaction, and the flask was evacuated and flushed with hydrogen three times again. The solution was allowed to stir at RT under hydrogen for three days. The crude product was purified on an RP-18 column (0-10% MeCN in 0.05 TEAB), but the debenzylation was found to be incomplete (indicated by NMR spectroscopy results). The hydrogenation was repeated (as written, except omitting the sodium bicarbonate), and the product was still found to be incomplete. The product was purified using another reverse-phase column (0-70% MeCN in 0.05 TEAB), before being subjected to a third hydrogenation which proved to be successful. The product was then purified by an ion exchange column (0-1.5 M TEAB) and a final RP-18 column (0-10% MeCN in 0.05 TEAB). The presence of product in the collected column fractions was confirmed with a Briggs qualitative phosphate assay, and the product-containing fractions were concentrated *in vacuo* without heat. The excess TEAB buffer was decomposed through successive additions of methanol and *in vacuo* concentration. The final product was lyophilised and collected as an off-white glass (6.1 mg, calculated 3.5 TEA counterions per molecule of product, 7.92 µmol, 10% yield).

^{1}HNMR (D_2O, 400 Hz): 4.37 (q, *J*= 9.3 Hz, 1H, H-4), 4.08 (t, *J*= 2.7 Hz, 1H, H-2), 4.00 (q, *J*= 9.1 Hz, 1H, H-5), 3.82 (t, *J*= 9.6 Hz, 1H, H-6), 3.75 (dd, *J*= 9.8, 2.8 Hz, 1H, H-3), 3.62 (dd, *J*= 10.0, 2.9 Hz, 1H, H-1), 3.19 (q, *J*= 7.3 Hz, approx. 21H, TEA C*H*$_2$), 1.27 (t, *J*= 7.3 Hz, approx. 32H, TEA C*H*$_3$); **^{31}PNMR** (D_2O, 162 Hz): 4.15 (P-5), -6.13 (d, *J*= 23.6 Hz, pyrophosphate β-P), -10.86 (d, *J*= 23.6 Hz, pyrophosphate α-P); **^{13}CNMR** (D_2O, 100 Hz): 78.4-78.2 (C-4 and C-5), 72.0 (C-6), 71.5 (C-2), 70.9 (C-1), 70.2 (C-3), 46.7 (TEA *C*H_2), 8.2 (TEA *C*H_3); **HRMS (ESI)**: *m/z* calcd $[M-H]^-$ for $C_6H_{19}O_{30}P_8$: 418.9551, found: 418.9552.

Synthesis of diphospho myo-inositol bisphosphate [PP-InsP$_2$] targets

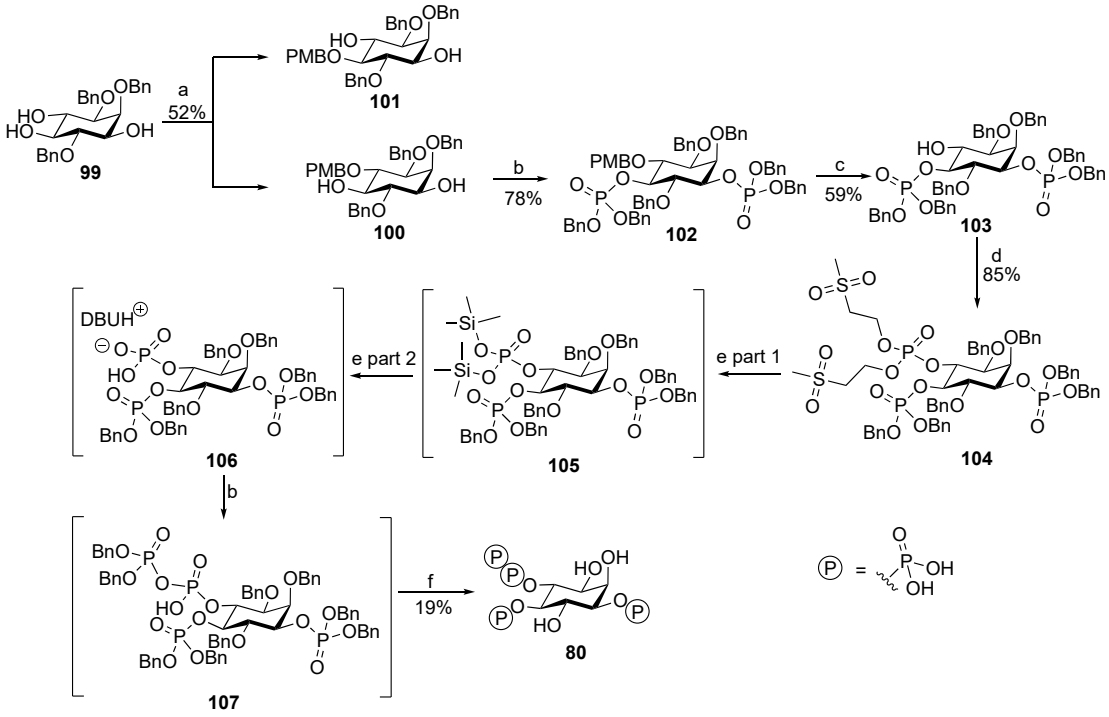

Scheme 14: Later steps in synthesis route to generate 4-PP-Ins(1,5)P$_2$.

Reagents and conditions a) 1. Bu_2SnO, MeCN, reflux, 24h, 2. PMBCl, TBAI, reflux, 24h; b) 1. dibenzyl diisopropylphosphoramidite, 5-phenyl-1*H*-tetrazole, DCM, RT, 3h, 2. *m*CPBA, -78°C -0°C, 10 min; c) DDQ, DCM, H2O, RT, 90 min; d) 1. *N,N*-diisopropylamino-bis-[2-(methylsulfonyl)ethyloxy]phosphine , 5-phenyl-1*H*-tetrazole, DCM, RT, 3h, 2. *m*CPBA, -78°C -0°C, 10 min; e) 1. BSTFA, $CDCl_3$ 2. MeOH, TFA; f) H_2, $Pd(OH)_2/C$, $NaHCO_3$, H_2O, isopropanol.

DL-3,6-Di-*O*-benzyl-4,5-*O*-(2,3-dimethoxybutane-2,3-diyl)-1-*O*-para-methoxybenzyl-*myo*-inositol (**96**)

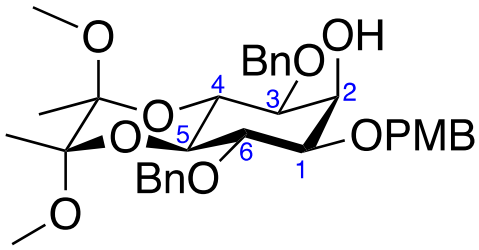

As described by Riley *et al.*[399], to a solution of 3,6-di-*O*-benzyl-4,5-*O*-(2,3-dimethoxybutane-2,3-diyl)-*myo*-inositol (**84**, 500 mg, 1.05 mmol) in MeOH (50 mL), dibutyltin oxide (315 mg, 1.26 mmol, 1.2 equiv) was added. This suspension was then refluxed overnight using a Soxhlet apparatus containing 3 Å molecular sieves to remove water. During the reflux, the solution turned yellow. The solution was then allowed to cool and concentrated *in vacuo*. The subsequent residue was dissolved in anhydrous DMF (10 mL) and to this solution caesium fluoride (352 mg, 2.32 mmol, 2.2

equiv) followed by 4-methoxybenzyl chloride (0.21 mL, 1.58 mmol, 1.5 equiv) were added, and the solution was allowed to stir at RT overnight. Progress of the reaction was confirmed with TLC (diethyl ether-PE, 2:1) indicating that the starting diol (Rf 0.11) was converted into a less polar product (Rf 0.44). The solution was then concentrated *in vacuo* to form a residue that was then dissolved in diethyl ether, washed with water (100 mL), filtered over Celite and concentrated *in vacuo* to yield the crude product. The product was purified with silica column chromatography (1. PE-EtOAc, 0-100%, 2. DCM-EtOAc, 0-100%) and recrystallised from diethyl ether-hexane as a white solid (495.4 mg, 0.833 mmol, 79% yield). **m.p.** 95.6-98.1 °C; **^{1}HNMR** ($CDCl_3$, 400 Hz): 7.40-7.23 (m, 12H, Ar), 6.86-6.83 (m, 2H, Ar), 4.94-4.59 (m, 6H, C*H*$_2$Ar), 4.19 (t, *J*= 10.1 Hz, 1H, H-4 or H-6), 4.16 (t, *J*= 2.8 Hz, 1H, H-2), 3.69 (t, *J*= 9.6 Hz, 1H, H-4 or H-6), 3.81 (s, 3H, ArOC*H*$_3$), 3.61 (t, *J*= 10.0 Hz, 1H, H-5), 3.42 (dd, *J*= 9.9, 2.9 Hz, 1H, H-1 or H-3), 3.33 (dd, *J*= 9.2, 2.8 Hz, 1H, H-1 or H-3), 3.32 (s, 3H, bda OC*H*$_3$), 3.29 (s, 3H, bda OC*H*$_3$), 2.50 (s, 1H, OH), 1.37 (s, 3H, bda CC*H*$_3$), 1.35 (s, 3H, bda CC*H*$_3$); **^{13}CNMR** ($CDCl_3$, 100 Hz): 159.4 (Ar), 139.2 (Ar), 138.6 (Ar), 133.3 (Ar), 129.6 (Ar), 128.7 (Ar), 128.43 (Ar), 128.36 (Ar), 128.1 (Ar), 127.73 (Ar), 127.70 (Ar), 127.6 (Ar), 114.1 (Ar), 113.9 (Ar), 99.5 (quaternary bda), 99.4 (quaternary bda), 79.7 (C-1 or C-3), 78.5 (C-4 or C-6), 76.8 (C-1 or C-3), 75.8 (*C*H$_2$Ar), 73.4 (*C*H$_2$Ar), 72.9 (*C*H$_2$Ar), 71.5 (C-5), 69.48 (C-4 or C-6), 69.45 (C-2), 65.1 (*C*H$_2$Ar), 55.4 (ArO*C*H$_3$), 48.1 (bda O*C*H$_3$), 48.0 (bda O*C*H$_3$), 17.9 (bda *C*CH$_3$); **HRMS (ESI)**: *m/z* calcd $[M+Na]^+$ for $C_{34}H_{42}O_9$: 617.2721, found: 617.2717.

DL-2,3,6-Tri-*O*-benzyl-4,5-*O*-(2,3-dimethoxybutane-2,3-diyl)-1-*O*-para-methoxybenzyl-*myo*-inositol (**97**)

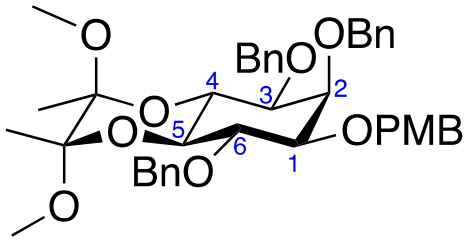

3,6-Di-*O*-benzyl-4,5-*O*-(2,3-dimethoxybutane-2,3-diyl)-1-*O*-para-methoxybenzyl-*myo*-inositol (**96**, 300 mg, 0.504 mmol) was dissolved in dry DMF (10 mL). To this solution, sodium hydride (27 mg, 1.01 mmol, 2 equiv) and benzyl bromide (0.19 mL, 0.807 mmol, 1.6 equiv) were added, and the solution was allowed to stir under argon at RT overnight. The reaction was then quenched through the addition of 1 mL water. The DMF reaction solution was diluted with DCM (150 mL) and washed with water (100 mL). The organic layer was dried over $MgSO_4$ and concentrated *in vacuo* to yield the crude product. The product was purified through silica column chromatography (P.E.- EtOAc, 0-50%) and collected as colourless oil (292.7 mg, 0.427 mmol, 85% yield). **^{1}HNMR** ($CDCl_3$, 400 Hz): 7.39-7.21 (m, 17H, Ar), 6.85-6.82 (m, 2H, Ar), 4.91-4.79 (m,

5H, C*H*$_2$Ar), 4.63 (m, 2H, C*H*$_2$Ar), 4.52 (AB, *J*= 11.3 Hz, 1H, C*H*$_2$Ar), 4.28 (t, *J*= 10.1 Hz, 1H, H-4 or H-6), 4.02 (t, *J*= 9.6 Hz, 1H, H-4 or H-6), 3.99 (t, *J*= 2.5 Hz, 1H, H-2), 3.80 (s, 3H, ArOC*H*$_3$), 3.63 (t, *J*= 9.8 Hz, 1H, H-5), 3.42 (dd, *J*= 10.1, 2.4 Hz, 1H, H-1 or H-3), 3.30 (dd, *J*= 9.1, 2.5 Hz, 1H, H-1 or H-3), 3.30 (s, 3H, bda OC*H*$_3$), 3.29 (s, 3H, bda OC*H*$_3$), 1.36 (s, 3H, bda CC*H*$_3$), 1.34 (s, 3H, bda CC*H*$_3$); **^{13}CNMR** ($CDCl_3$, 100 Hz): 199.3 (Ar), 139.4 (Ar), 139.32 (Ar), 139.26 (Ar), 130.8 (Ar), 129.3 (Ar), 128.4 (Ar), 128.3 (Ar), 128.1 (Ar), 128.0 (Ar), 127.5 (Ar), 127.4 (Ar), 127.3 (Ar), 127.2 (Ar), 113.8 (Ar), 99.52 (bda quaternary C), 99.45 (bda quaternary C), 80.8 (C-1 or C-3), 79.0 (C-4 or C-6), 78.2 (C-1 or C-3), 76.7 (C-2), 75.8 (*C*H$_2$Ar), 74.7 (*C*H$_2$Ar), 73.4 (*C*H$_2$Ar), 72.9 (*C*H$_2$Ar), 72.0 (C-5), 70.0 (C-4 or C-6), 55.4 (ArO*C*H$_3$), 48.0 (bda O*C*H$_3$), 47.9 (bda O*C*H$_3$), 18.00 (bda C*C*H$_3$), 17.95 (bda C*C*H$_3$); **HRMS (ESI)**: *m/z* calcd $[M+Na]^+$ for $C_{41}H_{48}O_9$: 707.3191, found: 707.3185.

DL-2,3,6-Tri-*O*-benzyl-4,5-*O*-(2,3-dimethoxybutane-2,3-diyl)-*myo*-inositol (**98**)

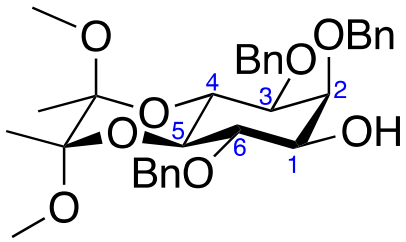

2,3,6-Tri-*O*-benzyl-4,5-*O*-(2,3-dimethoxybutane-2,3-diyl)-1-*O*-para-methoxybenzyl-*myo*-inositol (**97**, 280 mg, 0.409 mmol) was dissolved in a mixture of DCM-water (8 mL, 19-1). DDQ (167 mg, 0.735 mmol, 1.8 equiv) was then added to the flask, and the reaction was allowed to stir for 1h 30 min, during which time a pink precipitate formed. More DCM (100 mL) was then added and the precipitate was removed by filtration. The red reaction solution was washed with 10% sodium sulphite solution (100 mL) and then saturated sodium bicarbonate solution (100 mL). The organic layer was dried over $MgSO_4$ and concentrated to yield the crude product. The product was purified with silica column chromatography (DCM-EtOAc, 0-100%) to yield the pure product as a colourless oil (134.1 mg, 0.237 mmol, 58% yield). **^{1}HNMR** ($CDCl_3$, 400 Hz): 7.31-7.16 (m, 15H, Ar), 4.91 (AB, *J*= 11.2 Hz, 1H, C*H*$_2$Ar), 4.90 (AB, *J*= 11.4 Hz, 1H, C*H*$_2$Ar), 4.83 (AB, *J*= 12.0 Hz, 1H, C*H*$_2$Ar), 4.64 (AB, *J*= 11.3 Hz, 1H, C*H*$_2$Ar), 4.61 (AB, *J*= 11.4 Hz, 1H, C*H*$_2$Ar), 4.60 (AB, *J*= 12.0 Hz, 1H, C*H*$_2$Ar), 4.17 (t, *J*= 10.1 Hz, 1H, H-4), 3.95 (t, *J*= 2.7 Hz, 1H, H-2), 3.70 (t, *J*= 9.5 Hz, 1H, H-6), 3.57 (t, *J*= 9.7 Hz, 1H, H-5), 3.44 (dd, *J*= 10.2, 2.5 Hz, 1H, H-3), 3.41-3.36 (m, 1H, H-1), 3.24 (s, 3H, bda OC*H*$_3$), 3.22 (s, 3H, bda OC*H*$_3$), 2.28 (d, *J*= 2.28 Hz, OH), 1.29 (s, 3H, bda CC*H*$_3$), 1.27 (s, 3H, bda CC*H*$_3$); **^{13}CNMR** ($CDCl_3$, 100 Hz): 139.1 (Ar), 139.0 (Ar), 138.9 (Ar), 128.5 (Ar), 12.39 (Ar), 128.35 (Ar), 128.03 (Ar), 128.00 (Ar), 127.8 (Ar), 127.6 (Ar), 127.5 (Ar), 127.2 (Ar), 99.44 (bda quaternary C), 99.42 (bda quaternary C), 79.4 (C-6), 78.8 (C-2), 78.3 (C-3),

75.5 (*C*H_2Ar), 75.3 (*C*H_2Ar), 73.6 (*C*H_2Ar), 72.5 (C-1), 72.0 (C-5), 70.1 (C-4), 48.0 (bda O*C*H_3), 47.9 (bda O*C*H_3), 18.0 (bda C*C*H_3), 17.9 (bda C*C*H_3); **HRMS (ESI)**: *m/z* calcd $[M+Na]^+$ for $C_{33}H_{40}O_6$: 587.2615, found: 587.2610.

DL-2,3,6-Tri-*O*-benzyl-*myo*-inositol (**99**)

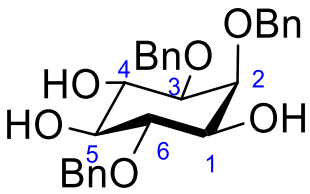

DL-2,3,6-Tri-*O*-benzyl-4,5-*O*-(2,3-dimethoxybutane-2,3-diyl)-*myo*-inositol (**98**, 130 mg, 0.230 mmol) was dissolved in a mixture of TFA (4.5 mL) and water (0.5 mL) and left to stir at RT for 10 min. After this time, the reaction was concentrated under reduced pressure, without heating, to yield the crude product. The product was purified via silica column chromatography (DCM-EtOAc, 0-100%) to yield the pure product as a colourless solid (28.2 mg, 0.063 mmol, 27% yield). **m.p.** 115.9-117.4°C (lit.[400] value: 121-123°C); **^{1}HNMR** ($CDCl_3$, 400 Hz): 7.40-7.26 (m, 15H, Ar), 4.94 (AB, *J*= 11.5 Hz, 1H, C*H*$_2$Ar), 4.89 (AB, *J*= 11.3 Hz, 1H, C*H*$_2$Ar), 4.83 (AB, *J*= 11.3 Hz, 1H, C*H*$_2$Ar), 4.72 (AB, *J*= 11.5 Hz, 1H, C*H*$_2$Ar), 4.68 (AB, *J*= 11.6 Hz, 1H, C*H*$_2$Ar), 4.59 (AB, *J*= 11.6 Hz, 1H, C*H*$_2$Ar), 4.07 (t, *J*= 2.5 Hz, 1H, H-2), 4.02 (t, *J*= 9.4 Hz, 1H, H-4 or H-6), 3.69 (t, *J*= 9.3 Hz, 1H, H-4 or H-6), 3.53 (dd, *J*= 2.7, 9.5 Hz, 1H, H-1 or H-3), 3.47 (t, *J*= 9.1 Hz, 1H, H-5), 3.28 (dd, *J*= 2.4, 9.7 Hz, 1H, H-1 or H-3), 2.67 (brs, 3H, OH); **^{13}CNMR** ($CDCl_3$, 100 Hz): 138.7 (Ar), 138.6 (Ar), 137.8 (Ar), 128.71 (Ar), 128.67 (Ar), 128.5 (Ar), 128.2 (Ar), 128.1 (Ar), 128.0 (Ar), 127.94 (Ar), 127.86 (Ar), 81.8 (C-4 or C-6), 80.3 (C-1 or C-3), 76.5 (C-2), 75.2 (*C*H_2Ar), 75.0 (C-5), 74.9 (*C*H_2Ar), 72.7 (*C*H_2Ar), 72.6 (overlapping C-1 or C-3 and C-4 or C-6).

Fe(dpm)$_3$ (dpm = 2,2,6,6-tetramethyl-3,5-heptanedionate) (**108**)

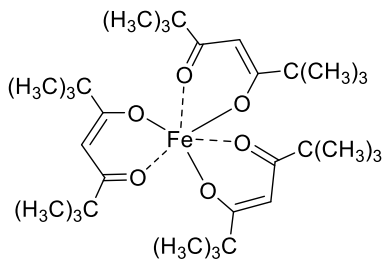

As described by Hammond *et al.*,[408] 2,2,6,6-Tetramethylheptan-3,5-dione (2.50 g, 13.54 mmol, 3 equiv) and sodium acetate (1.10 g, 1.34 mmol, 3 equiv) were added to a mixture of EtOH-H_2O (1:1, 50 mL). To this solution, $FeCl_3.6H_2O$ (1.22 g, 4.51 mmol)

was added, and the reaction mixture was allowed to stir at 60°C for 1 hour. The solution was then cooled to 0°C and the crude solid product was filtered off (washing the orange solid with water). The product was recrystallized from a 1:1 mixture of ethanol and water to be collected as an orange solid (2.30 g, 3.80 mmol, 84% yield). **m.p.** (EtOH:H_2O, 1:1): 166.2-166.7°C (Lit value:[427] 165°C)

DL-2,3,6-Tri-*O*-benzyl-4-*O*-*para*-methoxybenzyl-*myo*-inositol (**100**) and DL-2,3,6-tri-*O*-benzyl-5-*O*-PMB-*myo*-inositol (**101**)

Multiple methods for *para*-methoxybenzyl (PMB) protection were attempted to try to find the most suitable reaction conditions for synthesising, purifying and separating both the 4-position (**100**) and 5-position (**101**) product regioisomers.

Method A— dibutyltin oxide and tetrabutylammomium iodide (TBAI)

In a version of the protocol described by Wagner *et al*.,[407] DL-2,3,6-tri-*O*-benzyl -*myo*-inositol (**99**, 200 mg, 0.444 mmol) was dissolved in dry MeCN (50 mL). To this solution, dibutyltin oxide (147 mg, 0.592 mmol, 1.33 equiv) was added, and the reaction flask was fitted with a Soxhlet apparatus before the mixture was allowed to reflux for 24h. After 24h, tetrabutylammomium iodide (219 mg, 0.592 mmol, 1.33 equiv) and PMBCl (0.16 mL, 1.18 mmol, 2.67 equiv) were added, and the reaction mixture was allowed to reflux for another 24h. The reaction mixture was then allowed to cool, and the solvent was evaporated under reduced pressure to yield an orange residue. This residue was partitioned between water (150 mL) and diethyl ether (150 mL), and the organic layer was collected and allowed to stir with sat. aqueous $NaHCO_3$ (100 mL) for an hour. The organic layer was then separated again, filtered through Celite, dried over $MgSO_4$, and concentrated to yield the crude product. The crude product was purified by silica column chromatography (1. Pet ether- EtOAc, 0-100%, 2. DCM- EtOAc, 0-100%, 3. Pet ether- EtOAc, 0-100%,) to yield the partially separated product regioisomers (35.9 mg 4-PMB (**100**), 24.1 mg 5-PMB (**101**), 70 mg unseparated [approx. ratio of unseparated 1:1.4 in favour of 4-PMB (**100**)], 52% combined yield).

Method B—$Fe(dpm)_3$, Ag_2O and TBAB

In a version of the protocol described by Ren *et al*.,[404] DL-2,3,6-tri-*O*-benzyl-*myo*-inositol (**99**, 200 mg, 0.44 mmol) was dissolved in dry MeCN (10 mL). To this solution, $Fe(dpm)_3$ (32 mg, 0.05 mmol, 0.12 equiv), Ag_2O (70 mg, 0.266 mmol, 0.6 equiv), tetrabutylammionium bromide (TBAB, 16 mg, 0.050 mmol, 0.1 equiv), K_2CO_3 (76 mg,

0.550 mmol, 1.2 equiv) and PMBCl (0.1 mL, 0.74 mmol, 1.7 equiv) were added, and the reaction mixture was heated to 60°C for 12 h. The reaction mixture was then allowed to cool to RT before being diluted with DCM (100 mL). This organic solution was then washed with 5% $NaHCO_3$ (50 mL) and brine (50 mL), before being dried over $MgSO_4$ and concentrated *in vacuo* to yield the crude product. The crude product was purified by silica column chromatography (1. Pet ether- EtOAc, 0-100%, 2. DCM-EtOAc, 0-100%) to yield the partially-separated product (73.2 mg, approx. 30% yield).

Method C—dibutyltin oxide and caesium fluoride

In a version of the protocol described by Nagashima and Ohno,[403] DL-2,3,6-tri-*O*-benzyl-*myo*-inositol (500 mg, 1.11 mmol) was dissolved in dry MeOH (80 mL). To this solution, dibutyltin oxide (368 mg, 1.48 mmol, 1.33 equiv) was added, and the reaction flask was fitted with a Soxhlet apparatus before the mixture allowed to reflux for 24 h. After 24 h the reaction mixture was concentrated to a yellow foam *in vacuo.* The foam was redissolved in dry DMF (5 mL), and to this solution, caesium fluoride (225 mg, 1.47 mmol, 1.33 equiv) and PMBCl (0.4 mL, 2.96 mmol. 2.67 equiv) were added, and the reaction mixture was allowed to stir overnight at RT. The solution was then evaporated under reduced pressure to yield an orange residue. The residue was dissolved in diethyl ether (200 mL) and washed with water (100 mL) before the organic layer was separated, dried over $MgSO_4$, and concentrated *in vacuo* to yield the crude product. The crude product was purified by silica column chromatography (Pet ether-EtOAc, 0-100%) to yield the unseparated product regioisomers (70.1 mg).

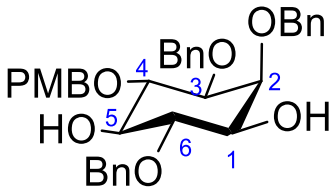

DL-2,3,6-Tri-*O*-benzyl-4-*O*-*para*-methoxybenzyl-*myo*-inositol (**100**): **^{1}HNMR** ($CDCl_3$, 400 Hz): 7.39-7.28 (m, 17H, Ar), 6.89-6.85 (m, 2H, Ar), 5.00 (d, *J*= 11.5 Hz, 1H, CH_2Ar), 4.91 (d, *J*= 11.0 Hz, 1H, CH_2Ar), 4.91 (d, *J*= 11.2 Hz, 1H, CH_2Ar), 4.80-4.68 (m, 5H, CH_2Ar), 4.06 (t, *J*= 2.5 Hz, 1H, H-2), 3.89 (t, *J*= 9.4 Hz, 1H, H-4), 3.80 (s, 3H, OCH_3), 3.69 (t, *J*= 9.3 Hz, 1H, H-6), 3.51 (t, *J*= 9.2 Hz, 1H, H-5), 3.52-3.47 (m, 1H, H-1), 3.44 (dd, *J*= 2.4, 9.7 Hz, 1H, H-3), 2.49 (brs, 1H, OH), 2.31 (brs, 1H, OH); **^{13}CNMR** ($CDCl_3$, 100 Hz): 159.5 (Ar), 138.9 (Ar), 138.8 (Ar), 138.3 (Ar), 131.0 (Ar), 129.9 (Ar), 128.7 (Ar), 128.6 (Ar), 128.5 (Ar), 128.2 (Ar), 127.92 (Ar), 127.89 (Ar), 127.8 (Ar), 127.7 (Ar), 114.1 (Ar), 81.8 (C-6), 81.09 (C-3), 81.05 (C-4), 77.3 (C-2), 75.3 (*C*H_2Ar), 75.14 (*C*H_2Ar), 75.07 (C-5), 74.9

(*C*H_2Ar), 72.9 (*C*H_2Ar), 72.4 (C-1), 55.4 (O*C*H_3); **HRMS (ESI)**: *m/z* calcd $[M+Na]^+$ for $C_{35}H_{38}O_7$: 593.2510, found: 593.2496;

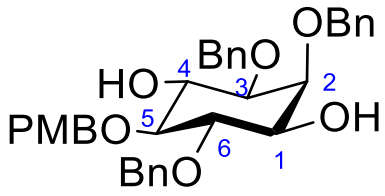

DL-2,3,6-Tri-*O*-benzyl-5-*O*-PMB-*myo*-inositol (**101**)**:** **^{1}HNMR** ($CDCl_3$, 400 Hz): 7.35-7.26 (m, 17H, Ar), 6.86-6.84 (m, 2H, Ar), 4.92 (d, *J*= 11.4 Hz, 1H, C*H*$_2$Ar) 4.90 (d, *J*= 11.1 Hz, 1H, C*H*$_2$Ar), 4.83-4.59 (m, 6H, C*H*$_2$Ar), 4.13 (t, *J*= 9.4 Hz, 1H, H-4), 4.06 (t, *J*= 2.5 Hz, 1H, H-2), 3.80-3.75 (m, 1H, H-6), 3.79 (s, 3H, OCH_3), 3.54-3.49 (m, 1H, H-1), 3.37 (t, *J*= 9.1 Hz, 1H, H-5), 3.29 (dd, J= 9.8, 2.4 Hz, 1H, H-3), 2.48 (s, 1H, OH-4), 2.25 (d, *J*= 6.2Hz, OH-1); **^{13}CNMR** ($CDCl_3$, 100 Hz): 128.8 (Ar), 128.71 (Ar), 128.64 (Ar), 128.5 (Ar), 128.2 (Ar), 128.1 (Ar), 127.9 (Ar), 127.8 (Ar), 114.0 (Ar), 83.1 (C-5), 82.7 (C-6), 80.6 (C-3), 77.4 (C-2), 75.6 (*C*H_2Ar), 75.1 (*C*H_2Ar), 74.8 (*C*H_2Ar), 73.4 (C-4), 72.8 (*C*H_2Ar), 72.7 (C-1), 55.4 (OCH_3); **HRMS (ESI)**: *m/z* calcd $[M+Na]^+$ for $C_{35}H_{38}O_7$: 593.2510, found: 593.2506.

DL-2,3,6-Tri-*O*-benzyl-4-*O*-*para*-methoxybenzyl-*myo*-inositol 1,5-bis(dibenzylphosphate) (**102**)

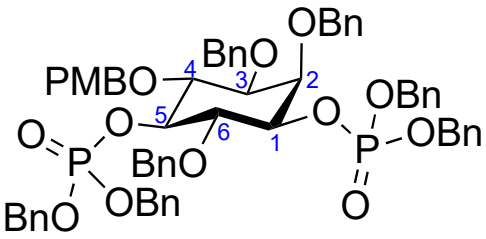

DL-2,3,6-Tri-*O*-benzyl-4-*O*-para-methoxybenzyl-*myo*-inositol (**100**, 70 mg, 0.123 mmol) was dissolved in dry DCM (10 mL). To this solution, 5-phenyl-1*H*-tetrazole (54 mg, 0.368 mmol, 3 equiv) was added, followed by dibenzyl diisopropylphosphoramidite (0.1 mL, 0.307 mmol, 2.5 equiv). The reaction mixture was allowed to stir under argon at RT overnight, after which it was cooled to -78°C and *m*CPBA (70% purity, 121 mg, 0.491 mmol, 4 equiv) was added. The reaction solution was then diluted with EtOAc (100 mL) and washed twice with 10% Na_2SO_3 solution (2 x 30 mL). The organic phase was dried over $MgSO_4$ and concentrated *in vacuo* to yield the crude product. The product was purified using flash chromatography (1. petroleum ether-EtOAc, 0-100%, 2. DCM-EtOAc, 0-100%) to yield the pure product as a colourless oil (104 mg, 78% yield). **^{1}HNMR** ($CDCl_3$, 400 Hz): 7.36-7.01 (m, 37H, Ar), 6.75-6.69 (m, 2H, Ar), 4.93-4.70

(m, 14H, C*H*$_2$Ar), 4.56-4.49 (m, 2H, C*H*$_2$Ar), 4.41 (q, *J*= 9.2 Hz, 1H, H-5), 4.33 (t, *J*= 2.3 Hz, 1H, H-2), 4.24-4.19 (m, 1H, H-1 or H-3), 4.07 (t, *J*= 9.6 Hz, 1H, H-4 or H-6), 4.03 (t, *J*= 9.6 Hz, 1H, H-4 or H-6), 3.74 (s, 3H, OC*H*$_3$), 3.38 (dd, *J*= 9.8, 2.2 Hz, 1H, H-1 or H-3); **^{31}PNMR** ($CDCl_3$, 162 Hz): -1.46, -1.82; **^{13}CNMR** ($CDCl_3$, 100 Hz): 159.0 (Ar), 130.8 (Ar), 129.5 (Ar), 128.7 (Ar), 128.6 (Ar), 128.5 (Ar), 128.43 (Ar), 128.37 (Ar), 128.2 (Ar), 127.9 (Ar), 127.81 (Ar), 127.77 (Ar), 127.7 (Ar), 127.6 (Ar), 127.4 (Ar), 113.6 (Ar), 80.7 (C-5), 80.1 (C-1 or C-3), 78.82 (C-4 or C-6), 78.78 (C-4 or C-6), 78.5 (C-1 or C-3), 76.1 (C-2), 69.62 (*C*H$_2$Ar), 69.56 (*C*H$_2$Ar), 69.5 (*C*H$_2$Ar), 69.4 (*C*H$_2$Ar), 69.34 (*C*H$_2$Ar), 69.28 (*C*H$_2$Ar), 69.25 (*C*H$_2$Ar), 55.4 (O*C*H$_3$); **HRMS (ESI)**: *m/z* calcd $[M+H]^+$ for $C_{63}H_{65}O_{13}P_2$: 1091.3895, found: 1091.3835.

DL-2,3,6-Tri-*O*-benzyl-*myo*-inositol 1,5-bis(dibenzylphosphate) (**103**)

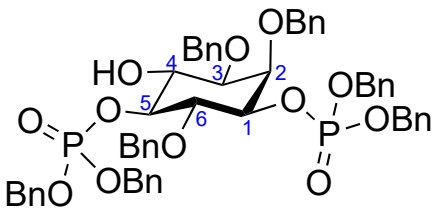

DL-2,3,6-Tri-*O*-benzyl-4-*O*-*para*-methoxybenzyl-*myo*-inositol 1,5-bis(dibenzylphosphate) (**102**, 50 mg, 0.0433 mmol) was dissolved in DCM-H_2O (7.6:0.4 mL). To this solution, DDQ (17.7 mg, 0.0780 mmol, 1.8 equiv) was added, and the reaction mixture was allowed to stir at RT for 90 min, during which time a peach precipitation formed. The reaction mixture was then diluted with more DCM (100 mL) and filtered to remove the solid precipitate. The organic DCM layer was washed with 10% aqueous Na_2SO_3 (100 mL) and sat. aqueous $NaHCO_3$ (100 mL), before being dried over $MgSO_4$ and concentrated *in vacuo* to yield the crude product. The product was then purified through column chromatography (DCM-EtOAc, 0-100%) to yield the pure product as a white solid (26.6 mg, 0.0257 mmol, 59% yield). **m.p.** 115-117 °C; **^{1}HNMR** ($CDCl_3$, 400 Hz): 7.35-7.12 (m, 35H, Ar), 5.04-4.83 (m, 9H, C*H*$_2$Ar), 4.75-4.69 (m, 3H, C*H*$_2$Ar), 4.63-4.56 (m, 2H, C*H*$_2$Ar), 4.29 (t, *J*= 2.3 Hz, 1H, H-2), 4.24-4.17 (m, 3H, H-1/3/4/5/6), 4.02 (t, *J*= 9.4 Hz, 1H, H-4/5/6), 3.86 (brs, 1H, OH), 3.24 (dd, *J*= 9.5, 2.3 Hz, 1H, H-1/3); **^{31}PNMR** ($CDCl_3$, 162 Hz): 0.09, -1.72; **^{13}CNMR** ($CDCl_3$, 100 Hz): 128.7-127.7 (m, Ar), 81.5 (C-1/3/4/5/6), 78.3 (C-4/5/6), 75.2(C-1/3/4/5/6), 74.2 (*C*H$_2$Ar), 72.2 (*C*H$_2$Ar), 72.1 (C-1/3/4/5/6), 69.8 (*C*H$_2$Ar), 69.2 (*C*H$_2$Ar), 64.2 (C-2), 42.1 (C-1/3); **HRMS (ESI)**: *m/z* calcd $[M+Na]^+$ for $C_{55}H_{54}O_{11}P_2$: 971.3320, found: 971.3310.

DL-2,3,6-Tri-*O*-benzyl-*myo*-inositol-1,5-bis(dibenzylphosphate)-4-bis[2-(methanesulfonyl)-ethyl]phosphate (**104**)

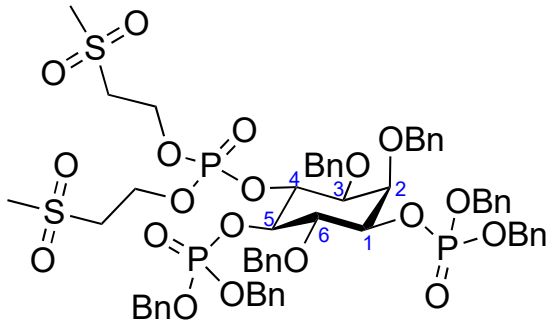

DL-2,3,6-Tri-*O*-benzyl-*myo*-inositol 1,5-bis(dibenzylphosphate) (**103**, 100 mg, 0.0966 mmol) was dissolved in dry DCM (8 mL). To this solution, 5-Phenyl-1*H*-tetrazole (57 mg, 0.386 mmol, 4 equiv) and *N,N*-diisopropylamino-bis-[2-(methylsulfonyl)ethyloxy]phosphine (109 mg, 0.290 mmol, 3 equiv) were added. The reaction was allowed to stir at RT under argon for 4h. After this time, the solution was cooled to -78°C and *m*CPBA (119 mg, 70% pure, 0.483 mmol, 5 equiv) was added. The reaction mixture was allowed to warm to RT (5 min), before being diluted with EtOAc (150 mL) and washed with 10% aqueous Na_2SO_3 (50 mL). The organic layer was then dried over $MgSO_4$ and concentrated *in vacuo* to yield the crude product. The product was purified with silica column chromatography (1. DCM-MeOH, 0-20%, 2. EtOAc) to yield the pure product as a colourless oil (103.3 mg, 0.0818 mmol, 85% yield). **^{1}HNMR** ($CDCl_3$, 400 Hz): 7.38-7.04 (m , 35 H, Ar), 5.03 (d, *J*= 11.4 Hz, 1H, C*H*$_2$Ar), 5.02 (d, *J*= 11.4 Hz, 1H, C*H*$_2$Ar), 4.94-4.74 (m, 11H, C*H*$_2$Ar, H-4 or H-6), 4.60 (t, *J*= 11.2 Hz, 1H, C*H*$_2$Ar), 4.53 (d, *J*= 11.2 Hz, 1H, C*H*$_2$Ar), 4.50 (q, *J*= 9.1 Hz, 1H, H- 5), 4.44-4.37 (m, 3H, H-2 and OCH_2 and C*H*$_2$Ar), 4.33-4.15 (m, 4H, H-1 or H-3 and OCH_2), 4.11 (t, *J*= 9.5 Hz, 1H, H-4 or H-6), 3.45 (dd, *J*= 2.71, 10.0 Hz, 2.2 Hz, 1H, H-1 or H-3), 2.98 (apt t, *J*= 5.6 Hz, 2H, C*H*$_2$S), 2.91-2.84 (m, 1H, C*H*$_2$S), 2.78-2.71 (m, 1H, C*H*$_2$S), 2.76 (s, 3H, SCH_3), 2.64 (s, 3H, SCH_3); **^{31}PNMR** ($CDCl_3$, 162 Hz): -1.67, -2.07, -3.47; **^{13}CNMR** ($CDCl_3$, 100 Hz): 138.2 (Ar), 138.0 (Ar), 137.1 (Ar), 135.6 (Ar), 135.5 (Ar), 128.82 (Ar), 128.80 (Ar), 128.76 (Ar), 128.73 (Ar), 128.68 (Ar), 128.5 (Ar), 128.33 (Ar), 128.28 (Ar), 128.2 (Ar), 128.0 (Ar), 127.9 (Ar), 127.7 (Ar), 127.1 (Ar), 79.2 (C-5), 78.8 (C-4 or C-6), 78.2 (C-1 or C-3), 77.7 (C-4 or C-6), 77.4 (C-1 or C-3), 75.6 (*C*H$_2$Ar), 74.9 (*C*H$_2$Ar), 74.6 (C-2), 72.0 (*C*H$_2$Ar), 69.9 (*C*H$_2$Ar), 69.83 (*C*H$_2$Ar), 69.76 (*C*H$_2$Ar), 69.6 (*C*H$_2$Ar), 62.2 (OCH_2), 61.5 (OCH_2), 54.5 (CH_2S), 54.4 (CH_2S), 42.6 (SCH_3), 42.5 (SCH_3); **HRMS (ESI)**: *m/z* calcd $[M+Na]^+$ for $C_{61}H_{70}O_{19}P_3S_2$: 1263.3160, found: 1263.3139.

DL-4-Diphospho-*myo*-inositol 1,5-bisphosphate triethylammonium salt (**80**)

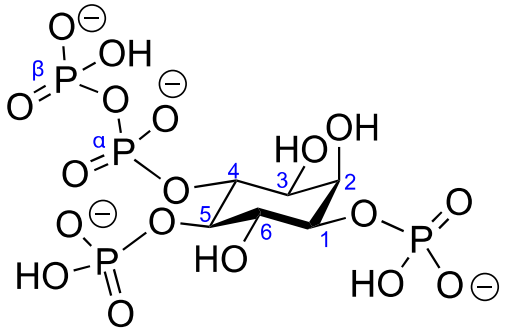

DL-2,3,6-Tri-*O*-benzyl-*myo*-inositol-1,5-bis(dibenzylphosphate)-4-bis[2-(methanesulfonyl)-ethyl]phosphate (**104**, 103.3 mg, 81.8 µmol) was dissolved in $CDCl_3$ (1 mL) in an NMR tube, and to this solution DBU 49 µL, 0.327 mmol, 4 equiv) followed by BSTFA (0.44 mL, 1.64 mmol, 20 equiv) were added. ^{31}PNMR spectroscopy was used to ensure the silylation was complete with a diagnostic singlet at -17.75 ppm (**105**). Methanol (0.17 mL, 4.09 mmol, 50 equiv) was then added to the reaction and, after 7 min, TFA (53 µL, 0.695 mmol, 8.5 equiv) was added. ^{31}PNMR spectroscopy initially indicated that desilylation was incomplete (with the presence of the diagnostic signal at -9.30 ppm), and a second portion of methanol (0.17 mL, 4.09 mmol, 50 equiv) was added and, after another 7 min, the solution was concentrated *in vacuo*. ^{31}PNMR spectroscopy then confirmed that desilylation was completed with the diagnostic signal shifting to around 0 ppm (**106**). The reaction mixture was concentrated *in vacuo* and the residue was thoroughly dried on a vacuum line.

This crude residue (**106**) was then dissolved in dry DCM (10 mL), and to this solution, 5-phenyl-1*H*-tetrazole (191 mg, 1.31 mmol, 16 equiv) and half of the dibenzyl phosphoramidite (total: 0.34 mL, 0.981 mmol, 12 equiv) were added and phosphitylation was allowed to take place for an hour. The second half of the dibenzyl phosphoramidite was then added, and the reaction was allowed to stir at RT for another hour. The reaction mixture was then cooled to -78 °C, before *m*CPBA (323 mg, 70%, 1.31 mmol, 16 equiv) was added. The solution was allowed to warm to RT before undergoing a very brief aqueous work-up, in which the reaction was diluted with more DCM (200 mL) before being washed with 10% aqueous sodium sulphite (15 mL). The organic layer was quickly separated, dried over $MgSO_4$, and concentrated *in vacuo* without heat. The protected pyrophosphate (**107**) was then purified using silica column chromatography (DCM-MeOH, 0-20%), before the final deprotection via hydrogenation was carried out. Due to suspected instability of the protected pyrophosphate groups at this stage, the compound (**107**) was not characterised and instead hydrogenated immediately.

The protected pyrophosphate compound (**107**, assumed 81.8 µmol) was dissolved in a mixture of isopropanol (8 mL) and mQ water (2 mL). To this solution, sodium

bicarbonate (24 mg, 0.286 mmol, 4.5 equiv) and $Pd(OH)_2/C$ (20%, ≥50% wet, 135 mg) were added. The flask was evacuated and flushed with hydrogen three times before the mixture being left to stir in an atmosphere of hydrogen. After 2 h, an additional 6 mL of mQ water was added to the reaction and the flask was evacuated and flushed with hydrogen three times again. The solution was allowed to stir at RT under hydrogen for 24h. The crude product was purified on an RP-18 column (0-70% MeCN in 0.05 M TEAB), followed by ion exchange chromatography (0-2.0 M TEAB) and a second RP-18 column (0-10% MeCN in 0.05 M TEAB). The presence of product in the collected fractions for each of the columns was confirmed with a Briggs qualitative phosphate assay, and the product-containing fractions were concentrated *in vacuo* without heat. The excess TEAB buffer was decomposed through successive additions of methanol and *in vacuo* concentration. The final product was lyophilised and collected as an off-white glass (13.4 mg, calculated 3.7 TEA counterions per molecule of product, 15.4 µmol, 19% yield). **^{1}HNMR** (D_2O, 400 Hz): 4.34 (q, *J*= 9.2 Hz, 1H, H-4), 4.23 (t, *J*= 2.5 Hz, 1H, H-2) 4.02-3.92 (m, 2H, H-5 and H-1), 3.85 (t, *J*= 9.4 Hz, 1H, H-6), 3.71 (dd, *J*= 9.7, 2.5 Hz, 1H, H-3), 3.12 (q, *J*= 7.2 Hz, approx. 22 H, TEA CH_2CH_3), 1.20 (t, *J*= 7.2 Hz, approx. 33H, TEA CH_2CH_3); **^{13}CNMR** (D_2O, 100 Hz): 78.3 (C-4), 77.9 (C-5), 75.2 (C-1), 71.2 (C-6), 70.5 (C-2), 69.9 (C-3), 46.6 (TEA CH_2), 8.2 (TEA CH_3); **^{31}PNMR** (D_2O, 162 Hz): 1.17, 0.18, -9.19 (d, *J*=20.6 Hz, pyrophosphate β-P), -10.20 (d, *J*=20.1 Hz, pyrophosphate α-P); **HRMS (ESI)**: *m/z* calcd $[M-H]^-$ for $C_6H_{16}O_{18}P_4$: 498.9214, found: 498.9207.

References

(1) Thomas, M. P.; Mills, S. J.; Potter, B. V. L. The “Other” Inositols and Their Phosphates: Synthesis, Biology, and Medicine (with Recent Advances in *Myo*-Inositol Chemistry). *Angew. Chemie Int. Ed.* **2016**, *55*, 1614–1650.

(2) Potter, B. V. L.; Lampe, D. Chemistry of Inositol Lipid Mediated Cellular Signaling. *Angew. Chemie Int. Ed. English* **1995**, *34*, 1933–1972.

(3) Wickner, R. B.; Edskes, H. K.; Bezsonov, E. E.; Son, M.; Ducatez, M. Prion Propagation and Inositol Polyphosphates. *Curr. Genet.* **2018**, *64* (3), 571–574.

(4) Conway, S. J.; Miller, G. J. Biology-Enabling Inositol Phosphates, Phosphatidylinositol Phosphates and Derivatives. *Nat. Prod. Rep.* **2007**, *24*, 687–707.

(5) Agranoff, B. W. Turtles All the Way: Reflections on *Myo*-Inositol. *J. Biol. Chem.* **2009**, *284* (32), 21121–21126.

(6) Yang, P.; Murthy, P. P. N.; Brown, R. E. Synergy of Intramolecular Hydrogen-Bonding Network in *Myo*-Inositol 2-Monophosphate: Theoretical Investigations into the Electronic Structure, Proton Transfer, and PKa. *J. Am. Chem. Soc.* **2005**, *127* (45), 15848–15861.

(7) Streb, H.; Irvine, R. F.; Berridge, M. J.; Schulz, I. Release of Ca^{2+} from a Nonmitochondrial Intracellular Store in Pancreatic Acinar Cells by Inositol-1,4,5-Trisphosphate. *Nature*. 1983, pp 67–69.

(8) Wilson, M. S. C.; Livermore, T. M.; Saiardi, A. Inositol Pyrophosphates: Between Signalling and Metabolism. *Biochem. J.* **2013**, *452*, 369–379.

(9) Shears, S. B. Intimate Connections: Inositol Pyrophosphates at the Interface of Metabolic Regulation and Cell Signaling. *J. Cell. Physiol.* **2018**, *233*, 1897–1912.

(10) Stephens, L. R.; Radenberg, T.; Thiel, U.; Vogel, G.; Khoo, K. H.; Dell, A.; Jackson, T. R.; Hawkins, P. T.; Mayr, G. W. The Detection, Purification, Structural Characterization, and Metabolism of Diphosphoinositol Pentakisphosphate(s) and Bisdiphosphoinositol Tetrakisphosphate(S). *J. Biol. Chem.* **1993**, *268* (6), 4009–4015.

(11) Hand, C. E.; Honek, J. F. Phosphate Transfer from Inositol Pyrophosphates $InsP_5PP$ and $InsP_4(PP)_2$: A Semi-Empirical Investigation. *Bioorganic Med. Chem. Lett.* **2007**, *17*, 183–188.

(12) Stockbridge, R. B.; Wolfenden, R. Enhancement of the Rate of Pyrophosphate Hydrolysis by Nonenzymatic Catalysts and by Inorganic Pyrophosphatase. *J. Biol. Chem.* **2011**, *286* (21), 18538–18546.

(13) Westheimer, F. H. Nature Chose Phosphates The Role of Phosphates The

Importance of Being Ionized. *Science* **1987**, *235* (1), 1173–1178.

(14) Borkovec, M.; Spiess, B. Microscopic Ionization Mechanism of Inositol Tetrakisphosphates. *Phys. Chem. Chem. Phys.* **2004**, 1144–1151.

(15) Desfougères, Y.; Wilson, M. S. C.; Laha, D.; Miller, G. J.; Saiardi, A. ITPK1 Mediates the Lipid-Independent Synthesis of Inositol Phosphates Controlled by Metabolism. *Proc. Natl. Acad. Sci. U. S. A.* **2019**, *116* (49), 24551–24561.

(16) Berridge, M. J. Inositol Trisphosphate and Diacylglycerol: Two Interacting Second Messengers. *Ann. Rev. Biochem.* **1987**, *56*, 159–193.

(17) Putney, Jr., J. W. The Role of Phosphoinositide Metabolism in Signal Transduction in Secretory Cells. *J. exp. Biol.* **1988**, *139*, 135–150.

(18) Irvine, R. F.; Schell, M. J. Back in the Water: The Return of the Inositol Phosphates. *Nat. Rev. Mol. Cell Biol.* **2001**, *2*, 327–338.

(19) Freed, C.; Adepoju, O.; Gillaspy, G. Can Inositol Pyrophosphates Inform Strategies for Developing Low Phytate Crops? *Plants* **2020**, *9* (115).

(20) Martin, K. L.; Smith, T. K. The Glycosylphosphatidylinositol (GPI) Biosynthetic Pathway of Bloodstream-Form *Trypanosoma Brucei* Is Dependent on the *de Novo* Synthesis of Inositol. *Mol. Microbiol.* **2006**, *61* (1), 89–105.

(21) Qiu, D.; Wilson, M. S.; Eisenbeis, V. B.; Harmel, R. K.; Riemer, E.; Haas, T. M.; Wittwer, C.; Jork, N.; Gu, C.; Shears, S. B.; Schaaf, G.; Kammerer, B.; Fiedler, D.; Saiardi, A.; Jessen, H. J. Analysis of Inositol Phosphate Metabolism by Capillary Electrophoresis Electrospray Ionization Mass Spectrometry. *Nat. Commun.* **2020**, *11* (1), 1–12.

(22) Gonzalez-Salgado, A.; Steinmann, M. E.; Greganova, E.; Rauch, M.; Mäser, P.; Sigel, E.; Bütikofer, P. *Myo*-Inositol Uptake Is Essential for Bulk Inositol Phospholipid but Not Glycosylphosphatidylinositol Synthesis in Trypanosoma Brucei. *J. Biol. Chem.* **2012**, *287* (16), 13313–13323.

(23) Majumder, A. L.; Johnson, M. D.; Henry, S. A. 1L-*Myo*-Inositol-1-Phosphate Synthase. *Biochim. Biophys. Acta - Lipids Lipid Metab.* **1997**, *1348* (1–2), 245–256.

(24) Stephens, L. R.; Irvine, R. F. Stepwise Phosphorylation of *Myo*-Inositol Leading to *Myo*-Inositol Hexakisphosphate in *Dictyostelium*. *Nature* **1990**, *346*, 580–583.

(25) Gregory J., M. *Inositol Phosphates*; *Laboratory Techniques in Biochemistry and Molecular Biology,* 2020.

(26) Shears, S. B. Metabolism of the Inositol Phosphates Produced upon Receptor Activation. *Biochem. J.* **1989**, *260* (2), 313–324.

(27) Oliver, K. G.; Putney, Jr., J. W.; Obie, J. F.; Shears, S. B. The Interconversion of

Inositol 1,3,4,5,6-Pentakisphosphate and Inositol Tetrakisphosphates in AR4-2J Cells. *J. Biol. Chem.* **1992**, *267* (30), 21528–21534.

(28) Mitchell, J.; Wang, X.; Zhang, G.; Gentzsch, M.; Nelson, D. J.; Shears, S. B. An Expanded Biological Repertoire for Ins(3,4,5,6)P_4 through Its Modulation of ClC-3 Function. *Curr. Biol.* **2008**, *18* (20), 1600–1605.

(29) Guse, A. H.; Emmrich, F. T-Cell Receptor-Mediated Metabolism of Inositol Polyphosphates in Jurkat T-Lymphocytes. *J. Biol. Chem.* **1991**, *266*, 24498–24502.

(30) Saiardi, A.; Caffrey, J. J.; Snyder, S. H.; Shears, S. B. The Inositol Hexakisphosphate Kinase Family. Catalytic Flexibility and Function in Yeast Vacuole Biogenesis. *J. Biol. Chem.* **2000**, *275* (32), 24686–24692.

(31) Shears, S. B. Inositol Pyrophosphates: Why so Many Phosphates? *Adv. Biol. Regul.* **2015**, *57*, 203–216.

(32) Thota, S. G.; Bhandari, R. The Emerging Roles of Inositol Pyrophosphates in Eukaryotic Cell Physiology. *J. Biosci.* **2015**, *40* (3), 593–605.

(33) Wundenberg, T.; Mayr, G. W. Synthesis and Biological Actions of Diphosphoinositol Phosphates (Inositol Pyrophosphates), Regulators of Cell Homeostasis. *Biol. Chem.* **2012**, *393* (9), 979–998.

(34) Hatch, A. J.; York, J. D. SnapShot : Inositol Phosphates. *Cell* **2010**, *143* (6), 1–3.

(35) Hermosura, M. C.; Takeuchi, H.; Fleig, A.; Riley, A. M.; Potter, B. V. L.; Hirata, M.; Penner, R. $InsP_4$ Facilitates Store-Operated Calcium Influx by Inhibition of $InsP_3$ 5-Phosphatase. *Cell* **2000**, *408*, 735–740.

(36) Tsubokawa, H.; Oguro, K.; Robinson, H. P. C.; Masuzawa, T.; Kawai, N. Intracellular Inositol 1,3,4,5-Tetrakisphosphate Enhances the Calcium Current in Hippocampal CA1 Neurones of the Gerbil after Ischaemia. *J. Physiol.* **1996**, *497* (1), 67–78.

(37) Ivarsson, M. E.; Durantie, E.; Huberli, C.; Huwiler, S.; Hegde, C.; Friedman, J.; Altamura, F.; Lu, J.; Verdu, E. F.; Bercik, P.; Logan, S. M.; Chen, W.; Leroux, J. C.; Castagner, B. Small-Molecule Allosteric Triggers of *Clostridium Difficile* Toxin B Auto-Proteolysis as a Therapeutic Strategy. *Cell Chem. Biol.* **2019**, *26* (1), 17-26.e13.

(38) Mayr, G. W.; Radenberg, T.; Thiel, U.; Vogel, G.; Stephens, L. R. Phosphoinositol Diphosphates: Non-Enzymic Formation *in Vitro* and Occurrence *in Vivo* in the Cellular Slime Mold Dictyostelium. *Carbohydr. Res.* **1992**, *234*, 247–262.

(39) Menniti, F. S.; Miller, R. N.; Putney, J. W.; Shears, S. B. Turnover of Inositol Polyphosphate Pyrophosphates in Pancreatoma Cells. *J. Biol. Chem.* **1993**, *268* (6), 3850–3856.

(40) Glennon, M. C.; Shears, S. B. Turnover of Inositol Pentakisphosphates, Inositol Hexakisphosphate and Diphosphoinositol Polyphosphates in Primary Cultured Hepatocytes. *Biochem. J.* **1993**, *293* (2), 583–590.

(41) Shah, A.; Ganguli, S.; Sen, J.; Bhandari, R. Inositol Pyrophosphates: Energetic, Omnipresent and Versatile Signalling Molecules. *J. Indian Inst. Sci.* **2017**, *97* (1), 23–40.

(42) Thomas, M. P.; Potter, B. V. L. The Enzymes of Human Diphosphoinositol Polyphosphate Metabolism. *FEBS J.* **2014**, *281*, 14–33.

(43) Saiardi, A.; Erdjument-Bromage, H.; Snowman, A. M.; Tempst, P.; Snyder, S. H. Synthesis of Diphosphoinositol Pentakisphosphate by a Newly Identified Family of Higher Inositol Polyphosphate Kinases. *Curr. Biol.* **1999**, *9* (22), 1323–1326.

(44) Choi, J. H.; Williams, J.; Cho, J.; Falck, J. R.; Shears, S. B. Purification, Sequencing, and Molecular Identification of a Mammalian PP-InsP_5 Kinase That Is Activated When Cells Are Exposed to Hyperosmotic Stress. *J. Biol. Chem.* **2007**, *282* (42), 30763–30775.

(45) Mulugu, S.; Bai, W.; Fridy, P. C.; Bastidas, R. J.; Otto, J. C.; Dollins, D. E.; Haystead, T. A.; Ribeiro, A. A.; York, J. D. A Conserved Family of Enzymes That Phosphorylate Inositol Hexakisphosphate. *Science.* **2007**, *316*, 106–109.

(46) Lin, H.; Fridy, P. C.; Ribeiro, A. A.; Choi, J. H.; Barma, D. K.; Vogel, G.; Falck, J. R.; Shears, S. B.; York, J. D.; Mayr, G. W. Structural Analysis and Detection of Biological Inositol Pyrophosphates Reveal That the Family of VIP/Diphosphoinositol Pentakisphosphate Kinases Are1/3-Kinases. *J. Biol. Chem.* **2009**, *284* (3), 1863–1872.

(47) Wang, H.; Falck, J. R.; Hall, T. M. T.; Shears, S. B. Structural Basis for an Inositol Pyrophosphate Kinase Surmounting Phosphate Crowding. *Nat. Chem. Biol.* **2012**, *8* (1), 111–116.

(48) Chakraborty, A. The Inositol Pyrophosphate Pathway in Health and Diseases. *Biol. Rev.* **2018**, *93* (2), 1203–1227.

(49) Weaver, J. D.; Wang, H.; Shears, S. B. The Kinetic Properties of a Human PPIP5K Reveal That Its Kinase Activities Are Protected against the Consequences of a Deteriorating Cellular Bioenergetic Environment. *Biosci. Rep.* **2013**, *33* (2), 229–242.

(50) Safrany, S. T.; Ingram, S. W.; Cartwright, J. L.; Falck, J. R.; McLennan, A. G.; Barnes, L. D.; Shears, S. B. The Diadenosine Hexaphosphate Hydrolases from *Schizosaccharomyces Pombe* and *Saccharomyces Cerevisiae* Are Homologues of the Human Diphosphoinositol Polyphosphate. Overlapping Substrate Specificities in a Mutt-Type Protein Phosphohydrolase. *J. Biol. Chem.* **1999**, *274* (31), 21735–21740.

(51) Safrany, S. T. A Novel Context for the `MutT' Module, a Guardian of Cell Integrity, in a Diphosphoinositol Polyphosphate Phosphohydrolase. *EMBO J.* **1998**, *17* (22), 6599–6607.

(52) Caffrey, J. J.; Safrany, S. T.; Yang, X.; Shears, S. B. Discovery of Molecular and Catalytic Diversity among Human Diphosphoinositol-Polyphosphate Phosphohydrolases. An Expanding NUDT Family. *J. Biol. Chem.* **2000**, *275* (17), 12730–12736.

(53) Kilari, R. S.; Weaver, J. D.; Shears, S. B.; Safrany, S. T. Understanding Inositol Pyrophosphate Metabolism and Function: Kinetic Characterization of the DIPPs. *FEBS Lett.* **2013**, *587*, 3464–3470.

(54) Lonetti, A.; Szijgyarto, Z.; Bosch, D.; Loss, O.; Azevedo, C.; Saiardi, A. Identification of an Evolutionarily Conserved Family of Inorganic Polyphosphate Endopolyphosphatases. *J. Biol. Chem.* **2011**, *286* (37), 31966–31974.

(55) Wu, M.; Chong, L. S.; Capolicchio, S.; Jessen, H. J.; Resnick, A. C.; Fiedler, D. Elucidating Diphosphoinositol Polyphosphate Function with Nonhydrolyzable Analogues. *Angew. Chemie - Int. Ed.* **2014**, *53*, 7192–7197.

(56) Saiardi, A.; Sciambi, C.; McCaffery, J. M.; Wendland, B.; Snyder, S. H. Inositol Pyrophosphates Regulate Endocytic Trafficking. *Proc. Natl. Acad. Sci. U. S. A.* **2002**, *99* (22), 14206–14211.

(57) Draškovič, P.; Saiardi, A.; Bhandari, R.; Burton, A.; Ilc, G.; Kovačevič, M.; Snyder, S. H.; Podobnik, M. Inositol Hexakisphosphate Kinase Products Contain Diphosphate and Triphosphate Groups. *Chem. Biol.* **2008**, *15* (3), 274–286.

(58) Phillippy, B. Q.; Bland, J. M. Gradient Ion Chromatography of Inositol Phosphates. *Anal. Biochem.* **1988**, *175*, 162–166.

(59) Whitfield, H.; Riley, A. M.; Diogenous, S.; Godage, H. Y.; Potter, B. V. L.; Brearley, C. A. Simple Synthesis of ^{32}P-Labelled Inositol Hexakisphosphates for Study of Phosphate Transformations. *Plant Soil* **2018**, *427* (1–2), 149–161.

(60) Blaabjerg, K.; Hansen-Møller, J.; Poulsen, H. D. High-Performance Ion Chromatography Method for Separation and Quantification of Inositol Phosphates in Diets and Digesta. *J. Chromatogr. B Anal. Technol. Biomed. Life Sci.* **2010**, *878* (3–4), 347–354.

(61) Lee, S.; Kim, M. G.; Ahn, H.; Kim, S. Inositol Pyrophosphates: Signaling Molecules with Pleiotropic Actions in Mammals. *Molecules* **2020**, *25* (9), 7–9.

(62) Worley, J.; Luo, X.; Capaldi, A. P. Inositol Pyrophosphates Regulate Cell Growth and the Environmental Stress Response by Activating the HDAC Rpd3L. *Cell Rep.* **2013**, *3* (5), 1476–1482.

(63) Pulloor, N. K.; Nair, S.; Kostic, A. D.; Bist, P.; Weaver, J. D.; Riley, A. M.; Tyagi, R.; Uchil, P. D.; York, J. D.; Snyder, S. H.; García-Sastre, A.; Potter, B. V. L.; Lin, R.; Shears, S. B.; Xavier, R. J.; Krishnan, M. N. Human Genome-Wide RNAi Screen Identifies an Essential Role for Inositol Pyrophosphates in Type-I Interferon Response. *PLoS Pathog.* **2014**, *10* (2).

(64) Choi, K.; Mollapour, E.; Choi, J. H.; Shears, S. B. Cellular Energetic Status Supervises the Synthesis of Bis-Diphosphoinositol Tetrakisphosphate Independently of AMP-Activated Protein Kinase. *Mol. Pharmacol.* **2008**, *74* (2), 527–536.

(65) Saiardi, A. How Inositol Pyrophosphates Control Cellular Phosphate Homeostasis? *Adv. Biol. Regul.* **2012**, *52* (2), 351–359.

(66) Dubois, E.; Scherens, B.; Vierendeels, F.; Ho, M. M. W.; Messenguy, F.; Shears, S. B. In Saccharomyces Cerevisiae, the Inositol Polyphosphate Kinase Activity of Kcs1p Is Required for Resistance to Salt Stress, Cell Wall Integrity, and Vacuolar Morphogenesis. *J. Biol. Chem.* **2002**, *277* (26), 23755–23763.

(67) Gokhale, N. A.; Zaremba, A.; Janoshazi, A. K.; Weaver, J. D.; Shears, S. B. PPIP5K1 Modulates Ligand Competition between Diphosphoinositol Polyphosphates and PtdIns(3,4,5)P_3 for Polyphosphoinositide-Binding Domains. *Biochem. J.* **2013**, *453* (3), 413–426.

(68) Chakraborty, A.; Koldobskiy, M. A.; Bello, N. T.; Maxwell, M.; Potter, J. J.; Juluri, K. R.; Maag, D.; Kim, S.; Huang, A. S.; Dailey, M. J.; Saleh, M.; Snowman, A. M.; Moran, T. H.; Mezey, E.; Snyder, S. H. Inositol Pyrophosphates Inhibit Akt Signaling, Thereby Regulating Insulin Sensitivity and Weight Gain. *Cell* **2010**, *143* (6), 897–910.

(69) Prasad, A.; Jia, Y.; Chakraborty, A.; Li, Y.; Jain, S. K.; Snyder, S. H.; Luo, H. R. Inositol Hexakisphosphate Kinase 1 (InsP6K1) Regulates Neutrophil Function in Innate Immunity by Inhibiting PtdIns(3,4,5)P_3 Signaling. *Nat. Immunol.* **2011**, *12* (8), 752–760.

(70) Luo, H. R.; Huang, Y. E.; Chen, J. C.; Saiardi, A.; Iijima, M.; Ye, K.; Huang, Y.; Nagata, E.; Devreotes, P.; Snyder, S. H. Inositol Pyrophosphates Mediate Chemotaxis in *Dictyostelium* via Pleckstrin Homology Domain-Ptdins(3,4,5)P_3 Interactions. *Cell* **2003**, *114* (5), 559–572.

(71) Lee, Y. S.; Huang, K.; Quiocho, F. A.; O'Shea, E. K. Molecular Basis of Cyclin-CDK-CKI Regulation by Reversible Binding of an Inositol Pyrophosphate. *Nat. Chem. Biol.* **2008**, *4* (1), 25–32.

(72) Rao, F.; Cha, J.; Xu, J.; Xu, R.; Vandiver, M. S.; Tyagi, R.; Tokhunts, R.; Koldobskiy, M. A.; Fu, C.; Barrow, R.; Wu, M.; Fiedler, D.; Barrow, J. C.; Snyder, S. H. Inositol Pyrophosphates Mediate the DNA-PK/ATM-P53 Cell Death Pathway by Regulating CK2 Phosphorylation of Tti1/Tel2 Feng. *Mol. Cell* **2014**,

54 (1), 119–132.

(73) Wild, R.; Gerasimaite, R.; Jung, J. Y.; Truffault, V.; Pavlovic, I.; Schmidt, A.; Saiardi, A.; Jessen, H. J.; Poirier, Y.; Hothorn, M.; Mayer, A. Control of Eukaryotic Phosphate Homeostasis by Inositol Polyphosphate Sensor Domains. *Science.* **2016**, *352* (6288), 986–990.

(74) Bhandari, R.; Saiardi, A.; Ahmadibeni, Y.; Snowman, A. M.; Adam, R. C.; Kristiansen, T. Z.; Molina, H.; Pandey, A.; Werner, J. K.; Juluri, K. R.; Ku, Y.; Prestwich, G. D.; Parang, K.; Snyder, S. H. Protein Pyrophosphorylation by Inositol Pyrophosphates Is a Posttranslational Event. *Proc. Natl. Acad. Sci. U. S. A.* **2007**, *104* (39), 15305–15310.

(75) Saiardi, A.; Bhandari, R.; Resnick, A. C.; Snowman, A. M.; Snyder, S. H. Phosphorylation of Proteins by Inositol Pyrophosphates. *Science.* **2004**, *306* (5704), 2101–2105.

(76) Yates, L. M.; Fiedler, D. Establishing the Stability and Reversibility of Protein Pyrophosphorylation with Synthetic Peptides. *ChemBioChem* **2015**, *16* (3), 415–423.

(77) Thota, S. G.; Unnikannan, C. P.; Thampatty, S. R.; Manorama, R.; Bhandari, R. Inositol Pyrophosphates Regulate RNA Polymerase I-Mediated RRNA Transcription in Saccharomyces Cerevisiae. *Biochem. J.* **2015**, *466*, 105–114.

(78) Azevedo, C.; Burton, A.; Ruiz-Mateos, E.; Marsh, M.; Saiardi, A. Inositol Pyrophosphate Mediated Pyrophosphorylation of AP3B1 Regulates HIV-1 Gag Release. *Proc. Natl. Acad. Sci. U. S. A.* **2009**, *106* (50), 21161–21166.

(79) Ruben, E. A. Florida State University Libraries Stereoelectronic Effects in Phosphates. **2007**.

(80) Gorenstein, D. G. Stereoelectronic Effects in Biomolecules. *Chem. Rev.* **1987**, *87* (5), 1047–1077.

(81) Freitas, M. P. The Anomeric Effect on the Basis of Natural Bond Orbital Analysis. *Org. Biomol. Chem.* **2013**, *11* (17), 2885–2890.

(82) Duss, M.; Capolicchio, S.; Linden, A.; Ahmed, N.; Jessen, H. J. Desymmetrization of *Myo*-Inositol Derivatives by Lanthanide Catalyzed Phosphitylation with C_2-Symmetric Phosphites. *Bioorganic Med. Chem.* **2015**, *23* (12), 2854–2861.

(83) Jones, S.; Selitsianos, D. A Simple and Effective Method for Phosphoryl Transfer Using $TiCl_4$ Catalysis. *Org. Lett.* **2002**, *4* (21), 3671–3673.

(84) Burgess, K.; Cook, D. Syntheses of Nucleoside Triphosphates. *Chem. Rev.* **2000**, *100* (6), 2047–2059.

(85) Nifantiev, E. E.; Grachev, M. K.; Burmistrov, S. Y. Amides of Trivalent

Phosphorus Acids as Phosphorylating Reagents for Proton-Donating Nucleophiles. *Chem. Rev.* **2000**, *100*, 3755–3799.

(86) Evans, D. A.; Gage, J. R.; Leighton, J. L. Asymmetric Synthesis of Calyculin A. 3. Assemblage of the Calyculin Skeleton and the Introduction of a New Phosphate Monoester Synthesis. *J. Org. Chem.* **1992**, *57* (7), 1964–1966.

(87) Brady, P. B.; Morris, E. M.; Fenton, O. S.; Sculimbrene, B. R. Efficient Catalyst Turnover in the Phosphitylation of Alcohols with Phosphoramidites. *Tetrahedron Lett.* **2009**, *50*, 975–978.

(88) Lampe, D. Synthesis of Novel Analogues of Myo-Inositol 1,4,5-Trisphosphate, University of Bath, 1993.

(89) Capolicchio, S.; Thakor, D. T.; Linden, A.; Jessen, H. J. Synthesis of Unsymmetric Diphospho-Inositol Polyphosphates. *Angew. Chemie - Int. Ed.* **2013**, *52* (27), 6912–6916.

(90) Li, W.; Schultz, C.; Llopis, J.; Tsien, R. Y. Membrane-Permeant Esters of Inositol Polyphosphates, Chemical Syntheses and Biological Applications. *Tetrahedron* **1997**, *53* (35), 12017–12040.

(91) Riley, A. M.; Unterlass, J. E.; Konieczny, V.; Taylor, C. W.; Helleday, T.; Potter, B. V. L. A Synthetic Diphosphoinositol Phosphate Analogue of Inositol Trisphosphate. *Medchemcomm* **2018**, *9* (7), 1105–1113.

(92) Van Der Heden Van Noort, G. J.; Van Der Horst, M. G.; Overkleeft, H. S.; Van Der Marel, G. A.; Filippov, D. V. Synthesis of Mono-ADP-Ribosylated Oligopeptides Using Ribosylated Amino Acid Building Blocks. *J. Am. Chem. Soc.* **2010**, *132* (14), 5236–5240.

(93) Jessen, H. J.; Schulz, T.; Balzarini, J.; Meier, C. Bioreversible Protection of Nucleoside Diphosphates. *Angew. Chemie - Int. Ed.* **2008**, *47*, 8719–8722.

(94) Nurminen, E. J.; Mattinen, J. K.; Lönnberg, H. Kinetics and Mechanism of Tetrazole-Catalyzed Phosphoramidite Alcoholysis. *J. Chem. Soc. Perkin Trans. 2* **1998**, No. 7, 1621–1628.

(95) Li, Y.; Manickam, G.; Ghoshal, A.; Subramaniam, P. More Efficient Palladium Catalyst for Hydrogenolysis of Benzyl Groups. *Synth. Commun.* **2006**, *36* (7), 925–928.

(96) Bianco, A.; Passacantilli, P.; Righi, G. Mild Hydrogenolysis Process by Catalytic Transfer Hydrogenation. *Tetrahedron Lett.* **1989**, *30* (11), 1405–1408.

(97) Capolicchio, S.; Wang, H.; Thakor, D. T.; Shears, S. B.; Jessen, H. J. Synthesis of Densely Phosphorylated Bis-1,5-Diphospho-*Myo*-Inositol Tetrakisphosphate and Its Enantiomer by Bidirectional P-Anhydride Formation. *Angew. Chemie - Int. Ed.* **2014**, *53* (36), 9508–9511.

(98) Marlow, A. L.; Kiessling, L. L. Improved Chemical Synthesis of UDP-Galactofuranose. *Org. Lett.* **2001**, *3* (16), 2517–2519.

(99) Wagner, G. K.; Pesnot, T.; Field, R. A. A Survey of Chemical Methods for Sugar-Nucleotide Synthesis. *Nat. Prod. Rep.* **2009**, *26* (9), 1172–1194.

(100) Xu, Z. A Review on the Chemical Synthesis of Pyrophosphate Bonds in Bioactive Nucleoside Diphosphate Analogs. *Bioorganic Med. Chem. Lett.* **2015**, *25* (18), 3777–3783.

(101) Zhang, H.; Thompson, J.; Prestwich, G. D. A Scalable Synthesis of the IP_7 Isomer , 5-PP-Ins(1,2,3,4,6)P_5. *Org. Lett.* **2009**, *11* (7), 1551–1554.

(102) Jessen, H. J.; Ahmed, N.; Hofer, A. Phosphate Esters and Anhydrides – Recent Strategies Targeting Nature's Favoured Modifications. *Org. Biomol. Chem.* **2014**, *12*, 3526–3530.

(103) Gold, H.; Van Delft, P.; Meeuwenoord, N.; Codée, J. D. C.; Filippov, D. V.; Eggink, G.; Overkleeft, H. S.; Van Der Marel, G. A. Synthesis of Sugar Nucleotides by Application of Phosphoramidites. *J. Org. Chem.* **2008**, *73* (23), 9458–9460.

(104) Falck, J. R.; Reddy, K. K.; Ye, J.; Saady, M.; Mioskowski, C.; Shears, S. B.; Tan, Z.; Safrany, S. T. Synthesis and Structure of Cellular Mediators: Inositol Polyphosphate Diphosphates. *J. Am. Chem. Soc.* **1995**, *117*, 12172–12175.

(105) Reddy, K. M.; Reddy, K. K.; Falck, J. R. Synthesis of 2- and 5-Diphospho-*Myo*-Inositol Pentakisphosphate (2- and 5-PP-InsP_5), Intracellular Mediators. *Tetrahedron Lett.* **1997**, *38* (28), 4951–4952.

(106) Wu, M.; Dul, B. E.; Trevisan, A. J.; Fiedler, D. Synthesis and Characterization of Non-Hydrolysable Diphosphoinositol Polyphosphate Second Messengers. *Chem. Sci.* **2013**, *4* (1), 405–410.

(107) Wang, H.; Godage, H. Y.; Riley, A. M.; Weaver, J. D.; Shears, S. B.; Potter, B. V. L. Synthetic Inositol Phosphate Analogs Reveal That PPIP5K2 Has a Surface-Mounted Substrate Capture Site That Is a Target for Drug Discovery. *Chem. Biol.* **2014**, *21*, 689–699.

(108) Guynn, R. W.; Veech, R. L. The Equilibrium Constants of the Adenosine Triphosphate Hydrolysis and the Adenosine Trisphosphate-Citrate Lyase Reactions. *J. Biol. Chem.* **1973**, *248* (20), 6966–6972.

(109) Banait, N. S.; Jencks, W. P. Elimination Reactions: Experimental Confirmation of the Predicted Elimination of (β-Cyanoethyl)Sulfonium Ions through a Concerted, E2 Mechanism. *J. Am. Chem. Soc.* **1990**, *112* (19), 6950–6958.

(110) Swarbrick, J. M.; Graeff, R.; Garnham, C.; Thomas, M. P.; Galione, A.; Potter, B. V. L. 'Click Cyclic ADP-Ribose': A Neutral Second Messenger Mimic. *Chem. Commun.* **2014**, *50* (19), 2458–2461.

(111) Flohr, A.; Aemissegger, A.; Hilvert, D. α-Functionalized Phosphonylphosphinates: Synthesis and Evaluation as Transcarbamoylase Inhibitors. *J. Med. Chem.* **1999**, *42* (14), 2633–2640.

(112) Watson, P. J.; Millard, C. J.; Riley, A. M.; Robertson, N. S.; Wright, L. C.; Godage, H. Y.; Cowley, S. M.; Jamieson, A. G.; Potter, B. V. L.; Schwabe, J. W. R. Insights into the Activation Mechanism of Class I HDAC Complexes by Inositol Phosphates. *Nat. Commun.* **2016**, *7* (11262), 1–13.

(113) Riley, A. M.; Wang, H.; Weaver, J. D.; Shears, S. B.; Potter, B. V. L. First Synthetic Analogues of Diphosphoinositol Polyphosphates: Interaction with PP-InsP_5 Kinase. *Chem. Commun.* **2012**, *48* (92), 11292.

(114) Riley, A. M.; Wang, H.; Shears, S. B.; Potter, B. V. L. Synthesis of an α-Phosphono-α,α-Difluoroacetamide Analogue of the Diphosphoinositol Pentakisphosphate 5-InsP_7. *Medchemcomm* **2019**, *10* (7), 1165–1172.

(115) Blackburn, G. M.; Kent, D. E.; Kolkmann, F. Three New β,γ-Methylene Analogues of Adenosine Triphosphate. *J. Chem. Soc. Chem. Commun.* **1981**, No. 22, 1188–1190.

(116) Engel, R. Phosphonates as Analogues of Natural Phosphates. *Chem. Rev.* **1977**, *77* (3), 349–367.

(117) Romanenko, V. D.; Kukhar, V. P. Fluorinated Phosphonates: Synthesis and Biomedical Application. *Chem. Rev.* **2006**, *106* (9), 3868–3935.

(118) Puschmann, R.; Harmel, R. K.; Fiedler, D. From the Bench Scalable Chemoenzymatic Synthesis of Inositol Pyrophosphates Scalable Chemoenzymatic Synthesis of Inositol Pyrophosphates. *Biochemistry* **2019**. h

(119) Swarbrick, J. M.; Riley, A. M.; Mills, S. J.; Potter, B. V. L. Designer Small Molecules to Target Calcium Signalling. *Biochem. Soc. Trans.* **2015**, *43* (3), 417–425.

(120) Adams, S. R.; Tsien, R. Y. Controlling Cell Chemistry with Caged Compounds. *Annu. Rev. Physiol.* **1993**, *55*, 755–784.

(121) Dinkel, C.; Moody, M.; Traynor-kaplan, A.; Schultz, C. Membrane-Permeant 3-OH-Phosphorylated Phosphoinositide Derivatives. *Angew. Chemie - Int. Ed.* **2001**, *40* (16), 3004–3008.

(122) Li, W.; Llopis, J.; Whitney, M.; Zlokarnik, G.; Tsien, R. Y. Cell-Permeant Caged InsP_3 Ester Shows That Ca^{2+} Spike Frequency Can Optimize Gene Expression. *Nature* **1998**, *392*, 936–941.

(123) Mentel, M.; Laketa, V.; Subramanian, D.; Gillandt, H.; Schultz, C. Photoactivatable and Cell-Membrane-Permeable Phosphatidylinositol 3,4,5-Trisphosphate. *Angew. Chemie - Int. Ed.* **2011**, *50*, 3811–3814.

(124) Jessen, H. J. The Hitchhiker's Guide to Organophosphate Chemistry. *Synlett* **2018**, *29*, 699–713.

(125) Li, X.; Gu, C.; Hostachy, S.; Sahu, S.; Wittwer, C.; Jessen, H. J.; Fiedler, D.; Wang, H.; Shears, S. B. Control of XPR1-Dependent Cellular Phosphate Efflux by $InsP_8$ Is an Exemplar for Functionally-Exclusive Inositol Pyrophosphate Signaling. *Proc. Natl. Acad. Sci. U. S. A.* **2020**, *117* (7), 3568–3574.

(126) Chin, A. C.; Gao, Z.; Riley, A. M.; Furkert, D.; Wittwer, C.; Dutta, A.; Rojas, T.; Semenza, E. R.; Felder, R. A.; Pluznick, J. L.; Jessen, J.; Fiedler, D.; Potter, B. V. L.; Snyder, S. H.; Fu, C. The Inositol Pyrophosphate 5-$InsP_7$ Drives Sodium-Potassium Pump Degradation by Relieving an Autoinhibitory Domain of PI3K P85a. **2020**, 1–14.

(127) Wilson, M. S.; Jessen, H. J.; Saiardi, A. The Inositol Hexakisphosphate Kinases IP6K1 and -2 Regulate Human Cellular Phosphate Homeostasis, Including XPR1-Mediated Phosphate Export. *J. Biol. Chem.* **2019**, *294* (30), 11597–11608.

(128) Shears, S. B. Diphosphoinositol Polyphosphates: Metabolic Messengers? *Mol. Pharmacol.* **2009**, *76* (2), 236–252.

(129) Burton, A.; Hu, X.; Saiardi, A. Are Inositol Pyrophosphates Signalling Molecules? *J. Cell. Physiol.* **2009**, *220* (1), 8–15.

(130) Luo, H. R.; Saiardi, A.; Yu, H.; Nagata, E.; Ye, K.; Snyder, S. H. Inositol Pyrophosphates Are Required for DNA Hyperrecombination in Protein Kinase C1 Mutant Yeast. *Biochemistry* **2002**, *41* (8), 2509–2515.

(131) Lee, T. S.; Lee, J. Y.; Kyung, J. W.; Yang, Y.; Park, S. J.; Lee, S.; Pavlovic, I.; Kong, B.; Jho, Y. S.; Jessen, H. J.; Kweon, D. H.; Shin, Y. K.; Kim, S. H.; Yoon, T. Y.; Kim, S. Inositol Pyrophosphates Inhibit Synaptotagmindependent Exocytosis. *Proc. Natl. Acad. Sci. U. S. A.* **2016**, *113* (29), 8314–8319.

(132) Nagata, E.; Saiardi, A.; Tsukamoto, H.; Okada, Y.; Itoh, Y.; Satoh, T.; Itoh, J.; Margolis, R. L.; Takizawa, S.; Sawa, A.; Takagi, S. Inositol Hexakisphosphate Kinases Induce Cell Death in Huntington Disease. *J. Biol. Chem.* **2011**, *286* (30), 26680–26686.

(133) Illies, C.; Gromada, J.; Fiume, R.; Leibiger, B.; Yu, J.; Juhl, K.; Yang, S.-N.; Barma, D. K.; Falck, J. R.; Saiardi, A.; Barker, C. J.; Berggren, P.-O. Requirement of Inositol Pyrophosphates for Full Exocytotic Capacity in Pancreatic beta-Cells. *Science.* **2007**, *318*, 1299–1302.

(134) Gerasimaite, R.; Pavlovic, I.; Capolicchio, S.; Hofer, A.; Schmidt, A.; Jessen, H. J.; Mayer, A. Inositol Pyrophosphate Specificity of the SPX-Dependent Polyphosphate Polymerase VTC. *ACS Chem. Biol.* **2017**, *12*, 648–653.

(135) Azevedo, C.; Saiardi, A. Eukaryotic Phosphate Homeostasis: The Inositol

Pyrophosphate Perspective. *Trends Biochem. Sci.* **2017**, *42* (3), 219–231.

(136) Potapenko, E.; Cordeiro, C. D.; Huang, G.; Storey, M.; Wittwer, C.; Dutta, A. K.; Jessen, H. J.; Starai, V. J.; Docampo, R. 5-Diphosphoinositol Pentakisphosphate (5-IP_7) Regulates Phosphate Release from Acidocalcisomes and Yeast Vacuoles. *J. Biol. Chem.* **2018**, *293* (49), 19101–19112.

(137) Desmarini, D.; Lev, S.; Furkert, D.; Crossett, B.; Saiardi, A.; Kaufman-francis, K.; Li, C.; Sorrell, T. C.; Wilkinson-White, L.; Matthews, J.; Fiedler, D.; Djordjevic, J. T. IP_7-SPX Domain Interaction Controls Fungal Virulence by Stabilizing Phosphate Signaling Machinery. *MBio* **2020**, *11* (5), 1–20.

(138) Thorsell, A. G.; Persson, C.; Gräslund, S.; Hammarström, M.; Busam, R. D.; Hallberg, B. M. Crystal Structure of Human Diphosphoinositol Phosphatase 1. *Proteins Struct. Funct. Bioinforma.* **2009**, *77* (1), 242–246.

(139) Eric Dollins, D.; Bai, W.; Fridy, P. C.; Otto, J. C.; Neubauer, J. L.; Gattis, S. G.; Mehta, K. P. M.; York, J. D. Vip1 Is a Kinase and Pyrophosphatase Switch That Regulates Inositol Diphosphate Signaling. *Proc. Natl. Acad. Sci. U. S. A.* **2020**, *117* (17), 9356–9364.

(140) Caffrey, J. J.; Shears, S. B. Genetic Rationale for Microheterogeneity of Human Diphosphoinositol Polyphosphate Phosphohydrolase Type 2. *Gene* **2001**, *269* (1–2), 53–60.

(141) Li, C.; Lev, S.; Saiardi, A.; Desmarini, D.; Sorrell, T. C.; Djordjevic, J. T. Identification of a Major IP_5 Kinase in *Cryptococcus Neoformans* Confirms That PP-IP_5/IP_7, Not IP_6, Is Essential for Virulence. *Sci. Rep.* **2016**, *6* (March), 1–13.

(142) York, S. J.; Armbruster, B. N.; Greenwell, P.; Petes, T. D.; York, J. D. Inositol Diphosphate Signaling Regulates Telomere Length. *J. Biol. Chem.* **2005**, *280* (6), 4264–4269.

(143) Saiardi, A.; Resnick, A. C.; Snowman, A. M.; Wendland, B.; Snyder, S. H. Inositol Pyrophosphates Regulate Cell Death and Telomere Length through Phosphoinositide 3-Kinase-Related Protein Kinases. *Proc. Natl. Acad. Sci. U. S. A.* **2005**, *102* (6), 1911–1914.

(144) Watanabe, Y.; Mitani, M.; Morita, T.; Ozaki, S. Highly Efficient Protection by the Tetraisopropyldisiloxane-1,3-Diyl Group in the Synthesis of *Myo*-Lnositol Phosphates and Inositol 1,3,4,6-Tetrakisphosphate. *J Chem Soc Chem Commun* **1989**, 482–483.

(145) Jessen, H. J.; Capolicchio, S.; Pavlovic, I.; Thakor, D. T. Diphosphoinositol Polyphosphates: Polar Stars in Cell Signaling. *Synlett* **2014**, *25*, 1494–1498.

(146) Riley, A. M.; Jenkins, D. J.; Potter, B. V. L. A Concise Synthesis of *Neo*-Inositol. *Carbohydr. Res.* **1998**, *314*, 277–281.

(147) Engelsma, S. B.; Meeuwenoord, N. J.; Overkleeft, H. S.; van der Marel, G. A.;

Filippov, D. V. Combined Phosphoramidite-Phosphodiester Reagents for the Synthesis of Methylene Bisphosphonates. *Angew. Chemie - Int. Ed.* **2017**, *56*, 2955–2959.

(148) Bradshaw, B.; Dinsmore, A.; Ajana, W.; Collison, D.; Garner, C. D.; Joule, J. A. Synthesis of the Organic Ligand of the Molybdenum Cofactor, in Protected Form. *J. Chem. Soc. Perkin Trans. 1* **2001**, 3239–3244.

(149) Brown, D. M. Aspects of Phosphate Ester Chemistry As Applied To the Phosphoinositides. *Ann. N. Y. Acad. Sci.* **1970**, *165* (2), 687–694.

(150) Laussmann, T.; Eujen, R.; Weisshuhn, C. M.; Thiel, U.; Vogel, G. Structures of Diphospho-*Myo*-Inositol Pentakisphosphate and Bisdiphospho-*Myo*-Inositol Tetrakisphosphate from *Dictyostelium* Resolved by NMR Analysis. *Biochem. J.* **1996**, *315*, 715–720.

(151) McLennan, A. G. The Nudix Hydrolase Superfamily. *Cell. Mol. Life Sci.* **2006**, *63* (2), 123–143.

(152) Fisher, D. I.; Safrany, S. T.; Strike, P.; McLennan, A. G.; Cartwright, J. L. Nudix Hydrolases That Degrade Dinucleoside and Diphosphoinositol Polyphosphates Also Have 5-Phosphoribosyl 1-Pyrophosphate (PRPP) Pyrophosphatase Activity That Generates the Glycolytic Activator Ribose 1,5-Bisphosphate. *J. Biol. Chem.* **2002**, *277* (49), 47313–47317.

(153) Yang, X.; Safrany, S. T.; Shears, S. B. Site-Directed Mutagenesis of Diphosphoinositol Polyphosphate Phosphohydrolase, a Dual Specificity NUDT Enzyme That Attacks Diadenosine Polyphosphates and Diphosphoinositol Polyphosphates. *J. Biol. Chem.* **1999**, *274* (50), 35434–35440.

(154) Zong, G.; Jork, N.; Hostachy, S.; Fiedler, D.; Jessen, H. J.; Shears, S. B.; Wang, H. New Structural Insights Reveal an Expanded Reaction Cycle for Inositol Pyrophosphate Hydrolysis by Human DIPP1. *FASEB J.* **2021**, *35* (2), 1–14.

(155) Hidaka, K.; Caffrey, J. J.; Hua, L.; Zhang, T.; Falck, J. R.; Nickel, G. C.; Carrel, L.; Barnes, L. D.; Shears, S. B. An Adjacent Pair of Human NUDT Genes on Chromosome X Are Preferentially Expressed in Testis and Encode Two New Isoforms of Diphosphoinositol Polyphosphate Phosphohydrolase. *J. Biol. Chem.* **2002**, *277* (36), 32730–32738.

(156) Márquez-Moñino, M. Á.; Ortega-García, R.; Shipton, M. L.; Franco-Echevarría, E.; Riley, A. M.; Sanz-aparicio, J.; Potter, B. V. L.; González, B. Multiple Substrate Recognition by Yeast Diadenosine and Diphosphoinositol Polyphosphate Phosphohydrolase through Phosphate Clamping. *Sci. Adv.* **2021**, *7*, 1–16.

(157) Parker, D. Luminescent Lanthanide Sensors for PH, pO_2 and Selected Anions. *Coord. Chem. Rev.* **2000**, *205* (1), 109–130.

(158) Thibon, A.; Pierre, V. C. Principles of Responsive Lanthanide-Based Luminescent Probes for Cellular Imaging. *Anal. Bioanal. Chem.* **2009**, *394* (1), 107–120.

(159) Mailhot, R.; Traviss-Pollard, T.; Pal, R.; Butler, S. J. Cationic Europium Complexes for Visualizing Fluctuations in Mitochondrial ATP Levels in Living Cells. *Chem. - A Eur. J.* **2018**, *24* (42), 10745–10755.

(160) Hewitt, S. H.; Ali, R.; Mailhot, R.; Antonen, C. R.; Dodson, C. A.; Butler, S. J. A Simple, Robust, Universal Assay for Real-Time Enzyme Monitoring by Signalling Changes in Nucleoside Phosphate Anion Concentration Using a Europium(III)-Based Anion Receptor. *Chem. Sci.* **2019**, *10* (20), 5373–5381.

(161) Pal, R.; Parker, D.; Costello, L. C. A Europium Luminescence Assay of Lactate and Citrate in Biological Fluids. *Org. Biomol. Chem.* **2009**, *7* (8), 1525–1528.

(162) Butler, S. J.; Delbianco, M.; Lamarque, L.; Mcmahon, B. K.; Neil, E. R.; Pal, R.; Parker, D.; Walton, J. W.; Zwier, J. M. EuroTracker® Dyes: Design, Synthesis, Structure and Photophysical Properties of Very Bright Europium Complexes and Their Use in Bioassays and Cellular Optical Imaging. *Dalt. Trans.* **2015**, *44* (11), 4791–4803.

(163) Vicentini, G.; Zinner, L. B.; Zukerman-Schpector, J.; Zinner, K. Luminescence and Structure of Europium Compounds. *Coord. Chem. Rev.* **2000**, *196* (1), 353–382.

(164) Heffern, M. C.; Matosziuk, L. M.; Meade, T. J. Lanthanide Probes for Bioresponsive Imaging. *Chem. Rev.* **2014**, *114* (8), 4496–4539.

(165) Bodman, S. E.; Butler, S. J. Advances in Anion Binding and Sensing Using Luminescent Lanthanide Complexes. *Chem. Sci.* **2021**, *12* (8), 2716–2734.

(166) Hewitt, S. H.; MacEy, G.; Mailhot, R.; Elsegood, M. R. J.; Duarte, F.; Kenwright, A. M.; Butler, S. J. Tuning the Anion Binding Properties of Lanthanide Receptors to Discriminate Nucleoside Phosphates in a Sensing Array. *Chem. Sci.* **2020**, *11* (14), 3619–3628.

(167) Døssing, A. Luminescence from Lanthanide(3+) Ions in Solution. *Eur. J. Inorg. Chem.* **2005**, No. 8, 1425–1434.

(168) Pesesse, X.; Choi, K.; Zhang, T.; Shears, S. B. Signaling by Higher Inositol Polyphosphates: Synthesis of Bisdiphosphoinositol Tetrakisphosphate ("$InsP_8$") Is Selectively Activated by Hyperosmotic Stress. *J. Biol. Chem.* **2004**, *279* (42), 43378–43381.

(169) Choi, K.; Mollapour, E.; Shears, S. B. Signal Transduction during Environmental Stress: $InsP_8$ Operates within Highly Restricted Contexts. *Cell. Signal.* **2005**, *17*, 1533–1541.

(170) Gu, C.; Nguyen, H. N.; Hofer, A.; Jessen, H. J.; Dai, X.; Wang, H.; Shears, S. B.

The Significance of the Bifunctional Kinase/Phosphatase Activities of Diphosphoinositol Pentakisphosphate Kinases (PPIP5Ks) for Coupling Inositol Pyrophosphate Cell Signaling to Cellular Phosphate Homeostasis. *J. Biol. Chem.* **2017**, *292* (11), 4544–4555.

(171) Khaled, M. L.; Bykhovskaya, Y.; Gu, C.; Liu, A.; Drewry, M. D.; Chen, Z.; Mysona, B. A.; Parker, E.; McNabb, R. P.; Yu, H.; Lu, X.; Wang, J.; Li, X.; Al-Muammar, A.; Rotter, J. I.; Porter, L. F.; Estes, A.; Watsky, M. A.; Smith, S. B.; Xu, H.; Abu-Amero, K. K.; Kuo, A.; Shears, S. B.; Rabinowitz, Y. S.; Liu, Y. PPIP5K2 and PCSK1 Are Candidate Genetic Contributors to Familial Keratoconus. *Sci. Rep.* **2019**, *9* (1), 1–16.

(172) Yousaf, R.; Gu, C.; Ahmed, Z. M.; Khan, S. N.; Friedman, T. B.; Riazuddin, S.; Shears, S. B.; Riazuddin, S. Mutations in Diphosphoinositol-Pentakisphosphate Kinase PPIP5K2 Are Associated with Hearing Loss In Human and Mouse. *PLoS Genet.* **2018**, 1–20.

(173) Bednarek, M. A.; Bodanszky, M. 9-Fluorenylmethyl Esters. *Int. J. Pept. Protein Res.* **1983**, *21*, 196–201.

(174) Riley, A. M.; Wang, H.; Shears, S. B.; Potter, B. V. L. Synthetic Tools for Studying the Chemical Biology of $InsP_8$. *Chem. Commun.* **2015**, *51*, 12605–12608.

(175) Swarbrick, J. M.; Cooper, S.; Bultynck, G.; Gaffney, P. R. J. Regioselective Deprotection of Orthobenzoates for the Synthesis of Inositol Phosphates. *Org. Biomol. Chem.* **2009**, *7* (8), 1709–1715.

(176) Riley, A. M.; Godage, H. Y.; Mahon, M. F.; Potter, B. V. L. Chiral Desymmetrisation of *Myo*-Inositol 1,3,5-Orthobenzoate Gives Rapid Access to Precursors for Second Messenger Analogues. *Tetrahedron Asymmetry* **2006**, *17* (2), 171–174.

(177) Hussain, J.; Chhabria, D.; Kirubakaran, S. Design, Synthesis and Biological Evaluation of New *Myo*-Inositol Derivatives as Potential RAS Inhibitors. *Bioorganic Med. Chem. Lett.* **2020**, *30* (16), 127290.

(178) Westerduin, P.; Willems, H. A. M.; van Boeckel, C. A. A. Total Synthesis of New 1,5-Bissubstituted *Myo*-Inositol Derivatives. Synthesis of D-*Myo*-Inositol 1,5-Bisphosphate, 3,5-Bisphosphophosphate and of Rac. 1,5-Bissulphated and 1,5-Bissulphamoylated Isosteric Analogues. *Tetrahedron Lett.* **1990**, *131* (47), 6915–6918.

(179) Pavlovic, I.; Thakor, D. T.; Bigler, L.; Wilson, M. S. C.; Laha, D.; Schaaf, G.; Saiardi, A.; Jessen, H. J. Prometabolites of 5-Diphospho-*Myo*-Inositol Pentakisphosphate. *Angew. Chemie - Int. Ed.* **2015**, *54*, 9622–9626.

(180) Laussmann, T.; Reddy, K. M.; Reddy, K. K.; Falck, J. R.; Vogel, G. Diphospho-Myo-Inositol Phosphates from *Dictyostelium* Identified as D-6-Diphospho-

Myo-Inositol Pentakisphosphate and D-5,6-Bisdiphospho-*Myo*-Inositol Tetrakisphosphate. *Biochem. J.* **1997**, *322*, 31–33.

(181) Laussmann, T.; Hansen, A.; Reddy, K. M.; Reddy, K. K.; Falck, J. R.; Vogel, G. Diphospho-*Myo*-Inositol Phosphates in *Dictyostelium* and *Polysphondylium*: Identification of a New Bisdiphospho-*Myo*-Inositol Tetrakisphosphate. *FEBS Lett.* **1998**, *426*, 145–150.

(182) Wang, H.; Falck, J. R.; Hall, T. M. T.; Shears, S. B. Structural Basis for an Inositol Pyrophosphate Kinase Surmounting Phosphate Crowding. *Nat. Chem. Biol.* **2011**, *8* (1), 111–116.

(183) Noble, N. J.; Potter, B. V. L. Desulphurisation of Vicinal Bisphosphorothioates: A Novel Synthetic Route to Substituted Cyclic Pyrophosphates. *J. Chem. Soc., Chem. Commun.* **1989**, 1194–1195.

(184) Noble, N. J.; Dubreuil, D.; Potter, B. V. L. Total Synthesis of *Myo*-Inositol-1-Phosphate-4,5-Pyrophosphate, a Novel Second Messenger Analogue, via *Myo*-Inositol-1-Phosphate-4,5-Bisphosphorothioate. *Bioorg. Med. Chem. Lett.* **1992**, *2* (5), 471–476.

(185) Felsenfeld, G.; Groudine, M. Controlling the Double Helix. *Nature* **2003**, *421*, 448–453.

(186) Joshi, P.; Greco, T. M.; Guise, A. J.; Luo, Y.; Yu, F.; Nesvizhskii, A. I.; Cristea, I. M. The Functional Interactome Landscape of the Human Histone Deacetylase Family. *Mol. Syst. Biol.* **2013**, *9* (672), 1–21.

(187) Seto, E.; Yoshida, M. Erasers of Histone Acetylation: The Histone Deacetylase Enzymes. *Cold Spring Harb. Perspect. Biol.* **2014**, *6* (4), 1–26.

(188) Marmorstein, R.; Zhou, M.-M. Writers and Readers of Histone Acetylation: Structure, Mechanism, and Inhibition. *Cold Spring Harb. Perspect. Biol.* **2014**, *6* (7), 1–26.

(189) Gui, C.-Y.; Ngo, L.; Xu, W. S.; Richon, V. M.; Marks, P. A. Histone Deacetylase (HDAC) Inhibitor Activation of P21WAF1 Involves Changes in Promoter-Associated Proteins, Including HDAC1. *Proc. Natl. Acad. Sci. U. S. A.* **2004**, *101* (5), 1241–1246.

(190) Witt, O.; Deubzer, H. E.; Milde, T.; Oehme, I. HDAC Family: What Are the Cancer Relevant Targets? *Cancer Lett.* **2009**, *277* (1), 8–21.

(191) Smith, K. T.; Workman, J. L. Histone Deacetylase Inhibitors: Anticancer Compounds. *Int. J. Biochem. Cell Biol.* **2009**, *41* (1), 21–25.

(192) Maolanon, A. R.; Madsen, A. S.; Olsen, C. A. Innovative Strategies for Selective Inhibition of Histone Deacetylases. *Cell Chem. Biol.* **2016**, *23*, 759–768.

(193) Ververis, K.; Hiong, A.; Karagiannis, T. C.; Licciardi, P. V. Histone Deacetylase

Inhibitors (HDACIS): Multitargeted Anticancer Agents. *Biol. Targets Ther.* **2013**, *7*, 47–60.

(194) Millard, C. J.; Watson, P. J.; Fairall, L.; Schwabe, J. W. R. Targeting Class I Histone Deacetylases in a "Complex" Environment. *Trends Pharmacol. Sci.* **2017**, *38* (4), 363–377.

(195) Guenther, M. G.; Yu, J.; Kao, G. D.; Yen, T. J.; Lazar, M. A. Assembly of the SMRT-Histone Deacetylase 3 Repression Complex Requires the TCP-1 Ring Complex. *Genes Dev.* **2002**, *16*, 3130–3135.

(196) Watson, P. J.; Fairall, L.; Santos, G. M.; Schwabe, J. W. R. Structure of HDAC3 Bound to Co-Repressor and Inositol Tetraphosphate. *Nature* **2012**, *481* (7381), 335–340.

(197) Itoh, T.; Fairall, L.; Muskett, F. W.; Milano, C. P.; Watson, P. J.; Arnaudo, N.; Saleh, A.; Millard, C. J.; El-Mezgueldi, M.; Martino, F.; Schwabe, J. W. R. Structural and Functional Characterization of a Cell Cycle Associated HDAC1/2 Complex Reveals the Structural Basis for Complex Assembly and Nucleosome Targeting. *Nucleic Acids Res.* **2015**, *43* (4), 2033–2044.

(198) Millard, C. J.; Watson, P. J.; Celardo, I.; Gordiyenko, Y.; Cowley, S. M.; Robinson, C. V.; Fairall, L.; Schwabe, J. W. R. Class I HDACs Share a Common Mechanism of Regulation by Inositol Phosphates. *Mol. Cell* **2013**, *51*, 57–67.

(199) Marcum, R. D.; Radhakrishnan, I. Inositol Phosphates and Core Subunits of the Sin3L/Rpd3L Histone Deacetylase (HDAC) Complex up-Regulate Deacetylase Activity. *J. Biol. Chem.* **2019**, *294* (38), 13928–13938.

(200) Li, C.-W.; Dong, H.-J.; Cui, C.-B. The Synthesis and Antitumor Activity of Twelve Galloyl Glucosides. *Molecules* **2015**, *20*, 2034–2060.

(201) Tseberlidis, G.; Zardi, P.; Caselli, A.; Cancogni, D.; Fusari, M.; Lay, L.; Gallo, E. Glycoporphyrin Catalysts for Efficient C-H Bond Aminations by Organic Azides. *Organometallics* **2015**, *34*, 3774–3781.

(202) Van Cleve, J. W. Improved Preparation of Methyl 4,6-*O*-Benzylidene-α-D-Glucopyranoside. *Carbohydr. Res.* **1971**, *17*, 461–464.

(203) Tatina, M.; Yousuf, S. K.; Mukherjee, D. 2,4,6-Trichloro-1,3,5-Triazine (TCT) Mediated One-Pot Sequential Functionalisation of Glycosides for the Generation of Orthogonally Protected Monosaccharide Building Blocks. *Org. Biomol. Chem.* **2012**, *10*, 5357–5360.

(204) Chambers, D. J.; Evans, G. R.; Fairbanks, A. J. A Facile Synthesis of 4,6-O-Benzylidene Glucal. *Tetrahedron Asymmetry* **2003**, *14*, 1767–1769.

(205) Spanevello, R. A.; Saavedra, D. D. Improved Preparation of Methyl 4,6-*O*-Benzylidene- α-D-Glucopyranoside. *Org. Prep. Proced. Int.* **1999**, *31* (4), 460–462.

(206) Ohlin, M.; Johnsson, R.; Ellervik, U. Regioselective Reductive Openings of 4,6-Benzylidene Acetals: Synthetic and Mechanistic Aspects. *Carbohydr. Res.* **2011**, *346*, 1358–1370.

(207) Johnsson, R.; Ohlin, M.; Ellervik, U. Reductive Openings of Benzylidene Acetals Revisited: A Mechanistic Scheme for Regio- and Stereoselectivity. *J. Org. Chem.* **2010**, *75*, 8003–8011.

(208) Rao, K. V.; Patil, P. R.; Atmakuri, S.; Kartha, K. P. R. Iodine-Sodium Cyanoborohydride-Mediated Reductive Ring Opening of 4,6-*O*-Benzylidene Acetals of Hexopyranosides. *Carbohydr. Res.* **2010**, *345*, 2709–2713.

(209) Johnsson, R.; Olsson, D.; Ellervik, U. Reductive Openings of Acetals: Explanation of Regioselectivity in Borane Reductions by Mechanistic Studies. *J. Org. Chem.* **2008**, *73*, 5226–5232.

(210) Ek, M.; Garegg, P. J.; Hultberg, H.; Oscarson, S. Reductive Ring Openings of Carbohydrate Benzylidene Acetals Using Borane-Trimethylamine and Aluminium Chloride. Regioselectivity and Solvent Dependance. *J. Carbohydr. Chem.* **1983**, *2* (3), 305–311.

(211) Zhang, Y.-J.; Dayoub, W.; Chen, G. R.; Lemaire, M. TMDS as a Dual-Purpose Reductant in the Regioselective Ring Cleavage of Hexopyranosyl Acetals to Ethers. *European J. Org. Chem.* **2012**, No. 10, 1960–1966.

(212) Jiang, L.; Chan, T.-H. Borane/Bu_2BOTf: A Mild Reagent for the Regioselective Reductive Ring Opening of Benzylidene Acetals in Carbohydrates. *Tetrahedron Lett.* **1998**, *39*, 355–358.

(213) Ansell, E. G.; Honeyman, J. Sugar Nitrates. Part I. Removal of Nitrate and Toluene-*p*-Sulphonyl Groups from Esters of Substituted Methyl-D-Glucosides. *J. Chem. Soc.* **1952**, 2778–2789.

(214) Smith, A. B. I.; Hale, K. J.; Vaccaro, H. A.; Rivero, R. A. Phyllanthoside-Phyllanthostatin Synthetic Studies. 9. Total Syntheses of (-)-Phyllanthostatin 1, (+)-Phyllanthostatin 2, and (+)-Phyllanthostatin 3. *J. Am. Chem. Soc.* **1991**, *113*, 2112–2122.

(215) Marchant, J. S.; Beecroft, M. D.; Riley, A. M.; Jenkins, D. J.; Marwood, R. D.; Taylor, C. W.; Potter, B. V. L. Disaccharide Polyphosphates Based upon Adenophostin A Activate Hepatic D-*Myo*-Inositol 1,4,5-Trisphosphate Receptors. *Biochemistry* **1997**, *36*, 12780–12790.

(216) Pradere, U.; Garnier-Amblard, E. C.; Coats, S. J.; Amblard, F.; Schinazi, R. F. Synthesis of Nucleoside Phosphate and Phosphonate Prodrugs. *Chem. Rev.* **2014**, *114* (18), 9154–9218.

(217) Chougrani, K.; Niel, G.; Boutevin, B.; David, G. Regioselective Ester Cleavage during the Preparation of Bisphosphonate Methacrylate Monomers. *Beilstein*

J. Org. Chem. **2011**, *7*, 364–368.

(218) Justyna, K.; Małolepsza, J.; Kusy, D.; Maniukiewicz, W.; Błażewska, K. M. The McKenna Reaction – Avoiding Side Reactions in Phosphonate Deprotection. *Beilstein J. Org. Chem.* **2020**, *16*, 1436–1446.

(219) Ponpipom, M. M. Synthesis of 3-*O*-Substituted D-Mannoses. *Carbohydr. Res.* **1977**, *59*, 311–317.

(220) Gillard, J. W.; Israel, M. Trimethylsilyl Bromide as a Mild, Stereoselective Anomeric Brominating Agent. *Tetrahedron Letters*. 1981, pp 513–516.

(221) Wegener, D.; Wirsching, F.; Riester, D.; Schwienhorst, A. A Fluorogenic Histone Deacetylase Assay Well Suited for High-Throughput Activity. *Chem. Biol.* **2003**, *10*, 61–68.

(222) Berridge, M. J.; Irvine, R. F. Inositol Trisphosphate, a Novel Second Messenger in Cellular Signal Transduction. *Nature* **1984**, *312*, 315–321.

(223) Berridge, M. J.; Lipp, P.; Bootman, M. D. The Versatility and Universality of Calcium Signalling. *Nat. Rev. Mol. Cell Biol.* **2000**, *1*, 11–21.

(224) Hanson, C. J.; Bootman, M. D.; Roderick, H. L. Cell Signalling: IP_3 Receptors Channel Calcium into Cell Death. *Curr. Biol.* **2004**, *14* (21), 933–935.

(225) Taylor, C. W.; Da Fonseca, P. C. A.; Morris, E. P. IP_3 Receptors: The Search for Structure. *Trends Biochem. Sci.* **2004**, *29* (4), 210–219.

(226) Wojcikiewicz, R. J. H. The Making and Breaking of Inositol 1,4,5-Trisphosphate Receptor Tetramers. *Messenger* **2019**, *6* (1), 45–49.

(227) Chandrasekhar, R.; Alzayady, K. J.; Yule, D. I. Using Concatenated Subunits to Investigate the Functional Consequences of Heterotetrameric Inositol 1,4,5-Trisphosphate Receptors. *Biochem. Soc. Trans.* **2015**, *43* (3), 364–370.

(228) Wojcikiewicz, R. J. H.; He, Y. Type I, II and III Inositol 1,4,5-Trisphosphate Receptor Co-Immunoprecipitation as Evidence for the Existence of Heterotetramric Receptor Complexes. *Biochem. Biophys. Res. Commun.* **1995**, *213* (1), 334–341.

(229) Sudhof, T. C.; Newton, C. L.; Archer, B. T.; Ushkaryov, Y. A.; Mignery, G. A. Structure of a Novel $InsP_3$ Receptor. *EMBO J.* **1991**, *10* (11), 3199–3206.

(230) Chan, J.; Yamazaki, H.; Ishiyama, N.; Seo, M. D.; Mal, T. K.; Michikawa, T.; Mikoshiba, K.; Ikura, M. Structural Studies of Inositol 1,4,5-Trisphosphate Receptor: Coupling Ligand Binding to Channel Gating. *J. Biol. Chem.* **2010**, *285* (46), 36092–36099.

(231) Monkawa, T.; Miyawaki, A.; Sugiyama, T.; Yoneshima, H.; Yamamoto-Hino, M.; Furuichi, T.; Saruta, T.; Hasegawa, M.; Mikoshiba, K. Heterotetrameric Complex Formation of Inositol 1,4,5-Trisphosphate Receptor Subunits. *Journal*

of Biological Chemistry. **1995**, 14700–14704.

(232) Nerou, E. P.; Riley, A. M.; Potter, B. V. L.; Taylor, C. W. Selective Recognition of Inositol Phosphates by Subtypes of the Inositol Trisphosphate Receptor. *Biochem. J.* **2001**, *355* (Pt 1), 59–69.

(233) Newton, C. L.; Mignery, G. A.; Südhof, T. C. Co-Expression in Vertebrate Tissues and Cell Lines of Multiple Inositol 1,4,5-Trisphosphate ($InsP_3$) Receptors with Distinct Affinities for $InsP_3$. *J. Biol. Chem.* **1994**, *269* (46), 28613–28619.

(234) Irvine, R. F.; Letcher, A. J.; Heslop, J. P.; Berridge, M. J. The Inositol Tris/Tetrakisphosphate Pathway--Demonstration of Ins(1,4,5)P_3 3-Kinase Activity in Animal Tissues. *Nature* **1986**, *320*, 631–634.

(235) Changya, L.; Gallacher, D. V.; Irvine, R. F.; Petersen, O. H. Inositol 1,3,4,5-Tetrakisphosphate and Inositol 1,4,5-Trisphosphate Act by Different Mechanisms When Controlling Ca^{2+} in Mouse Lacrimal Acinar Cells. *FEBS Lett.* **1989**, *251* (1,2), 43–48.

(236) Ehrlich, B. E.; Watras, J. Inositol 1,4,5-Trisphosphate Activates a Channel From Smooth Muscle Sarcoplasmic Reticulum. *Nature* **1988**, *336* (8), 583–586.

(237) Guse, A. H.; Roth, E.; Emmrich, F. D-*Myo*-Inositol 1,3,4,5-Tetrakisphosphate Releases Ca^{2+} from Crude Microsomes and Enriched Vesicular Plasma Membranes, but Not from Intracellular Stores of Permeabilized T-Lymphocytes and Monocytes. *Biochem. J.* **1992**, *288*, 489–495.

(238) Ely, J. A.; Hunyady, L.; Baukal, A. J.; Catt, K. J. Inositol 1,3,4,5-Tetrakisphosphate Stimulates Calcium Release from Bovine Adrenal Microsomes by a Mechanism Independent of the Inositol 1,4,5-Trisphosphate Receptor. *Biochem. J.* **1990**, *268*, 333–338.

(239) Gawler, D. J.; Potter, B. V. L.; Gigg, R.; Nahorski, S. R. Interactions between Inositol Tris- and Tetrakis-Phosphates. Effects on Intracellular Ca^{2+} Mobilization in SH-SY5Y Cells. *Biochem J* **1991**, *276*, 163–167.

(240) Luckhoff, A.; Clapham, D. E. Inositol 1,3,4,5-Tetrakisphosphate Activates an Endothelial Ca^{2+}-Permeable Channel. *Nature* **1992**, *355*, 356–358.

(241) Burford, N. T.; Nahorski, S. R.; Chung, S.-K.; Chang, Y.-T.; Wilcox, R. A. Binding and Activity of the Nine Possible Regioisomers of Myo-Inositol Tetrakisphosphate at the Inositol 1,4,5-Trisphosphate Receptor. *Cell Calcium* **1997**, *21* (4), 301–310.

(242) Polokoff, M. A.; Bencen, G. H.; Vacca, J. P.; DeSolms, S. J.; Young, S. D.; Huff, J. R. Metabolism of Synthetic Inositol Trisphosphate Analogs. *J. Biol. Chem.* **1988**, *263* (24), 11922–11927.

(243) Wilcox, R. A.; Challiss, R. A. J.; Baudin, G.; Vasella, A.; Pottert, B. V. L.;

Nahorski, S. R. Stereoselectivity of Ins(1,3,4,5)P_4 Recognition Sites: Implications for the Mechanism of the Ins(1,3,4,5)P_4-Induced Ca^{2+} Mobilization. *Biochem. J.* **1993**, *294*, 191–194.

(244) Wilcox, R. A.; Whitham, E. M.; Potter, B. V. L.; Nahorski, S. R. *Myo*-Inositol 1,3,4,5-Tetrakisphosphate Can Independently Mobilise Intracellular Calcium, via the Inositol 1,4,5-Trisphosphate Receptor: Studies with *Myo*-Inositol 1,4,5-Trisphosphate-3-Phosphorothioate and *Myo*-Inositol Hexakisphosphate. *FEBS* **1993**, *336* (2), 267–271.

(245) Wilcox, R. A.; Challiss, R. A. J.; Liu, C.; Potter, B. V. L.; Nahorski, S. R. Neuroblastoma Induces Calcium Mobilization Receptor in SH-SY5Y. *Mol. Pharmacol.* **1993**, *44*, 810–817.

(246) Miller, A. T.; Chamberlain, P. P.; Cooke, M. P. Beyond IP_3: Roles for Higher Order Inositol Phosphates in Immune Cell Signaling. *Cell Cycle* **2008**, *7* (4), 463–467.

(247) Bosanac, I.; Alattia, J.-R.; Mal, T. K.; Chan, J.; Talarico, S.; Tong, F. K.; Tong, K. I.; Yoshikawa, F.; Furuichi, T.; Iwai, M.; Michikawa, T.; Mikoshiba, K.; Ikura, M. Structure of the Inositol 1, 4, 5-Trisphosphate Receptor Binding Core in Complex with Its Ligand. *Nature* **2002**, *420* (December), 3–7.

(248) Yoshikawa, F.; Morita, M.; Monkawa, T.; Michikawa, T.; Furuichi, T.; Mikoshiba, K. Mutational Analysis of the Ligand Binding Site of the Inositol 1,4,5-Trisphosphate Receptor. *J. Biol. Chem.* **1996**, *271* (30), 18277–18284.

(249) Seo, M.-D.; Velamakanni, S.; Ishiyama, N.; Stathopulos, P. B.; Rossi, A. M.; Khan, S. A.; Dale, P.; Li, C.; Ames, J. B.; Ikura, M.; Taylor, C. W. Structural and Functional Conservation of Key Domains in $InsP_3$ and Ryanodine Receptors. *Nature* **2012**, *483*, 108–114.

(250) Rossi, A. M.; Riley, A. M.; Tovey, S. C.; Rahman, T.; Dellis, O.; Taylor, E. J. A.; Veresov, V. G.; Potter, B. V. L.; Taylor, C. W. Synthetic Partial Agonists Reveal Key Steps in IP_3 Receptor Activation. *Nat. Chem. Biol.* **2009**, *5* (9), 631–639.

(251) Bello, D.; Aslam, T.; Bultynck, G.; Slawin, A. M. Z.; Roderick, H. L.; Bootman, M. D.; Conway, S. J. Synthesis and Biological Action of Novel 4-Position-Modified Derivatives of D-*Myo*-Inositol 1,4,5-Trisphosphate. *J. Org. Chem.* **2007**, *72*, 5647–5659.

(252) Bootman, M. D.; Lipp, P. Calcium Signalling: Ringing Changes to the "Bell-Shaped Curve." *Curr. Biol.* **1999**, *9* (23), 876–878.

(253) Paknejad, N.; Hite, R. K. Structural Basis for the Regulation of Inositol Trisphosphate Receptors by Ca^{2+} and IP_3. *Nat. Struct. Mol. Biol.* **2018**, *25*, 660–668.

(254) Mak, D.-O. D.; McBride, S.; Foskett, J. K. Inositol 1,4,5-Tris-Phosphate

Activation of Inositol Tris-Phosphate Receptor Ca^{2+} Channel by Ligand Tuning of Ca^{2+} Inhibition. *Proc. Natl. Acad. Sci. USA* **1998**, *95*, 15821–15825.

(255) Franco-Echevarría, E.; Baños-Sanz, J. I.; Monterroso, B.; Round, A.; Sanz-Aparicio, J.; González, B. A New Calmodulin-Binding Motif for Inositol 1,4,5-Trisphosphate 3-Kinase Regulation. *Biochem. J.* **2014**, *463* (3), 319–328.

(256) Baker, M. R.; Fan, G.; Seryshev, A. B.; Agosto, M. A.; Baker, M. L.; Serysheva, I. I. Cryo-EM Structure of Type 1 IP_3R Channel in a Lipid Bilayer. *Commun. Biol.* **2021**, *4* (1).

(257) Iwai, M.; Michikawa, T.; Bosanac, I.; Ikura, M.; Mikoshiba, K. Molecular Basis of the Isoform-Specific Ligand-Binding Affinity of Inositol 1,4,5-Trisphosphate Receptors. *J. Biol. Chem.* **2007**, *282* (17), 12755–12764.

(258) Nahorski, S. R.; Potter, B. V. L. Molecular Recognition of Inositol Polyphosphates by Intracellular Recpetors and Metabolic Enzymes. *Trends Pharmacol. Sci.* **1989**, *10*, 139–144.

(259) Takahashi, M.; Tanzawa, K.; Takahashi, S. Adenophostins, Newly Discovered Metabolites of Penicillium Brevicompactum, Act as Potent Agonists of the Inositol 1,4,5-Trisphosphate Receptor. *J. Biol. Chem.* **1994**, *269* (1), 369–372.

(260) Takahashi, M.; Kagasaki, T.; Hosoya, T.; Takahashi, S. Adenophostins A and B: Potent Agonists of Inositol-1,4,5-Trisphosphate Receptor Produced by Penicillium Brevicompactum. *J. Antibiot. (Tokyo).* **1993**, *46* (11), 1643–1647.

(261) Sureshan, K. M.; Riley, A. M.; Thomas, M. P.; Tovey, S. C.; Taylor, C. W.; Potter, B. V. L. Contribution of Phosphates and Adenine to the Potency of Adenophostins at the IP_3 Receptor: Synthesis of All Possible Bisphosphates of Adenophostin A. *J. Med. Chem.* **2012**, *55* (4), 1706–1720.

(262) Dreef, C. E.; Schiebler, W.; van der Marel, G. A.; van Boom, J. H. Synthesis of 5-Phosphonate Analogues of Myo-Inositol 1,4,5-Trisphosphate: Possible Intracellular Calcium Antagonists. *Tetrahedron Lett.* **1991**, *32* (42), 6021–6024.

(263) Kozikowski, A. P.; Ognyanov, V. I.; Fauq, A. H.; Nahorski, S. R.; Wilcox, R. A. Synthesis of 1D-3-Deoxy-, 1D-2,3-Dideoxy-, and 1D-2,3,6-Trideoxy-*Myo*-Inositol 1,4,5-Trisphosphate from Quebrachitol, Their Binding Affinities, and Calcium Release Activity. *J. Am. Chem. Soc.* **1993**, *115*, 4429–4434.

(264) Terauchi, M.; Abe, H.; Tovey, S. C.; Dedos, S. G.; Taylor, C. W.; Paul, M.; Trusselle, M.; Potter, B. V. L.; Matsuda, A.; Shuto, S. A Systematic Study of C-Glucoside Trisphosphates as *Myo*-Inositol Trisphosphate Receptor Ligands. Synthesis of β-C-Glucoside Trisphosphates Based on the Conformational Restriction Strategy. *J. Med. Chem.* **2006**, *49*, 1900–1909.

(265) Safrany, S. T.; Wilcox, R. A.; Liu, C.; Potter, B. V. L.; Nahorski, S. R. 3-Position Modification of *Myo*-Inositol 1,4,5-Trisphosphate: Consequences for

Intracellular Ca^{2+} Mobilisation and Enzyme Recognition. *Eur. J. Pharmacol.* **1992**, *226*, 265–272.

(266) Wilcox, R. A.; Fauq, A. H.; Kozikowski, A. P.; Nahorski, S. R. Defining the Minimal Structural Requirements for Partial Agonism at the Type I *Myo*-Inositol 1,4,5-Triphosphate Receptor. *FEBS Lett.* **1997**, *402* (2–3), 241–245.

(267) Irvine, R. F.; Brown, K. D.; Berridge, M. J. Specificity of Inositol Trisphosphate-Induced Calcium Release from Permeabilized Swiss-Mouse 3T3 Cells. *Biochem J* **1984**, *221*, 269–272.

(268) Safrany, S. T.; Wojcikiewicz, R. J. H.; Strupish, J.; Nahorski, S. R.; Dubreuil, D.; Cleophux, J.; Gero, S. D.; Potter, B. V. L. Interaction of Synthetic D-6-Deoxy-*Myo*-Inositol 1,4,5-Trisphosphate with the Ca^{2+}- Releasing D-*Myo*-Inositol 1,4,5-Trisphosphate Receptor, and the Metabolic Enzymes 5-Phosphatase and 3-Kinase. *FEBS Lett.* **1991**, *278* (2), 252–256.

(269) Liu, C.; Potter, B. V. L. Synthesis of 3-Position-Modified Analogues of *Myo*-Inositol 1,4,5-Trisphosphate, Tools for Investigation of the Polyphosphoinositide Pathway of Cellular Signaling. *J. Org. Chem.* **1997**, *62*, 8335–8340.

(270) Riley, A. M.; Dozol, H.; Spiess, B.; Potter, B. V. L. 2-*O*-(2-Aminoethyl)-*Myo*-Inositol 1,4,5-Trisphosphate as a Novel Ligand for Conjugation: Physicochemical Properties and Synthesis of a New Ins(1,4,5)P_3 affinity Matrix. *Biochem. Biophys. Res. Commun.* **2004**, *318*, 444–452.

(271) Noble, N. J.; Cooke, A. M.; Potter, B. V. L. Synthesis of (+/-)-*Myo*-Inositol 1,4,5-Trisphosphate and the Novel Analogue (+/-)-*Myo*-Inositol 1,4-Bisphosphate 5-Phosphorothioate. *Carbohydr. Res.* **1992**, *234*, 177–187.

(272) Cooke, A. M.; Noble, N. J.; Payne, S.; Gigg, R.; Potter, B. V. L. Synthesis *Myo*-Inositol 1,4-Bisphosphate-5-Phosphorothioate. *J. Chem. Soc., Chem. Commun.* **1989**, 269–271.

(273) Keddie, N. S.; Ye, Y.; Aslam, T.; Luyten, T.; Bello, D.; Garnham, C.; Bultynck, G.; Galione, A.; Conway, S. J. Development of Inositol-Based Antagonists for the D-*Myo*-Inositol 1,4,5-Trisphosphate Receptor. *Chem. Commun.* **2011**, *47*, 242–244.

(274) Riley, A. M.; Guédat, P.; Schlewer, G.; Spiess, B.; Potter, B. V. L. A Conformationally Restricted Cyclic Phosphate Analogue of Inositol Trisphosphate: Synthesis and Physicochemical Properties. *J. Org. Chem.* **1998**, *63*, 295–305.

(275) Poirot, E.; Bourdon, H.; Chrétien, F.; Chapleur, Y.; Berthon, B.; Hilly, M.; Mauger, J.-P.; Guillon, G. Influence of the Absolute Configuration at C-4 in the Binding of D-*Myo* Inositol 1,4,5 Trisphosphate Analogues to IP_3 Receptor. *Bioorg. Med. Chem. Lett.* **1995**, *5* (6), 569–572.

(276) Wilcox, R. A.; Challiss, R. A. J.; Traynor, J. R.; Fauq, A. H.; Ognayanov, V. I.; Kozikowski, A. P.; Nahorski, S. R. Molecular Recognition at the *Myo*-Inositol 1,4,5-Trisphospahte Receptor. *J. Biol. Chem.* **1994**, *269* (43), 26815–26821.

(277) Mills, S. J.; Riley, A. M.; Murphy, C. T.; Bullock, A. J.; Westwick, J.; Potter, B. V. L. Myo-Inositol 1,4,6-Trisphosphorothioate and *Myo*-Inositol 1,3,4-Trisphosphorothioate: New Synthetic Ca^{2+}-Mobilising Partial Agonists at the Inositol 1,4,5-Trisphosphate Receptor. *Bioorg. Med. Chem. Lett.* **1995**, *5* (3), 203–208.

(278) Safrany, S. T.; Wilcox, R. A.; Liu, C.; Dubreuil, D.; Potter, B. V. L.; Nahorski, S. R. Identification of Partial Agonists with Low Intrinsic Activity at the Inositol-1,4,5-Trisphosphate Receptor. *Mol. Pharmacol.* **1993**, *43* (4), 499–503.

(279) Murphy, C. T.; Riley, A. M.; Mills, S. J.; Lindley, C. J.; Potter, B. V. L.; Westwick, J. *Myo* Inositol 1,4,6-Trisphorothioate and 1,3,6-Trisphosphorothioate: Partial Agonists with Very Low Intrinsic Activity at the Platelet *Myo*-Inositol 1,4,5-Trisphosphate Receptor. *Mol. Pharmacol.* **2000**, *57*, 595–601.

(280) Wilcox, R. A.; Safrany, S. T.; Lampe, D.; Mills, S. J.; Nahorski, S. R.; Potter, B. V. L. Modification at C2 of *Myo*-inositol 1,4,5-trisphosphate Produces Inositol Trisphosphates and Tetrakisphosphates with Potent Biological Activities. *Eur. J. Biochem.* **1994**, *223*, 115–124.

(281) Vibhute, A. M.; Pushpanandan, P.; Varghese, M.; Koniecnzy, V.; Taylor, C. W.; Sureshan, K. M. Synthesis of Dimeric Analogs of Adenophostin A That Potently Evoke Ca^{2+} Release through IP_3 Receptors. *RSC Adv.* **2016**, *6*, 86346–86351.

(282) De Kort, M.; Regenbogen, A. D.; Valentijn, A. R. P. M.; Challiss, R. A. J.; Iwata, Y.; Miyamoto, S.; Van Der Marel, G. A.; Van Boom, J. H. Spirophostins: Conformationally Restricted Analogues of Adenophostin A. *Chem. - A Eur. J.* **2000**, *6* (15), 2696–2704.

(283) Abe, H.; Shuto, S.; Matsuda, A. Synthesis of the C-Glycosidic Analogue of Adenophostin A and Its Uracil Congener as Potential IP_3 Receptor Ligands. Stereoselective Construction of the C-Glycosidic Structure by a Temporary Silicon-Tethered Radical Coupling Reaction. *J. Org. Chem.* **2000**, *65*, 4315–4325.

(284) Riley, A. M.; Unterlass, J.; Koniecnzy, V.; Taylor, C. W.; Helleday, T.; Potter, B. V. L. 1-PP-Ins(4,5)P_2: A Diphosphate Analogue of Ins(1,4,5)P_3. *Medchemcomm* **2018**, 9 (7), 1105-1113.

(285) Tegge, W.; Denis, G. V.; Ballou, C. E. Synthesis and Ca2+-Release Activity of D- and L-*Myo*-Inositol 2,4,5-Trisphosphate and D- and L-*Chiro*-Inositol 1,3,4-Trisphosphate. *Carbohydr. Res.* **1991**, *217*, 107–116.

(286) Rosenberg, H. J.; Riley, A. M.; Correa, V.; Taylor, C. W.; Potter, B. V. L. C-Glycoside Based Mimics of D-*Myo*-Inositol 1,4,5-Trisphosphate. *Carbohydr.*

Res. **2000**, *329*, 7–16.

(287) Rosenberg, H. J.; Riley, A. M.; Laude, A. J.; Taylor, C. W.; Potter, B. V. L. Synthesis and Ca^{2+}-Mobilizing Activity of Purine-Modified Mimics of Adenophostin A: A Model for the Adenophostin-Ins(1,4,5)P_3 Receptor Interaction. *J. Med. Chem.* **2003**, *46*, 4860–4871.

(288) De Kort, M.; Correa, V.; Valentijn, A. R. P. M.; Van der Marel, G. A.; Potter, B. V. L.; Taylor, C. W.; Van Boom, J. H. Synthesis of Potent Agonists of the D-*Myo*-Inositol 1,4,5-Trisphosphate Receptor Based on Clustered Disaccharide Polyphosphate Analogues of Adenophostin A. *J. Med. Chem.* **2000**, *43*, 3295–3303.

(289) De Kort, M.; Luijendijk, J.; van der Marel, G. A.; van Boom, J. H. Synthesis of Photoaffinity Derivatives of Adenophostin A. *European J. Org. Chem.* **2000**, 3085–3092.

(290) Correa, V.; Riley, A. M.; Shuto, S.; Horne, G.; Nerou, E. P.; Marwood, R. D.; Potter, B. V. L.; Taylor, C. W. Structural Determinants of Adenophostin A Activity at Inositol Trisphosphate Receptors. *Mol. Pharmacol.* **2001**, *59* (5), 1206–1215.

(291) Riley, A. M.; Correa, V.; Mahon, M. F.; Taylor, C. W.; Potter, B. V. L. Bicyclic Analogues of D-*Myo*-Inositol 1,4,5-Trisphosphate Related to Adenophostin a: Synthesis and Biological Activity. *J. Med. Chem.* **2001**, *44* (13), 2108–2117.

(292) Vibhute, A. M.; Konieczny, V.; Taylor, C. W.; Sureshan, K. M. Triazolophostins: A Library of Novel and Potent Agonists of IP_3 Receptors. *Org. Biomol. Chem.* **2015**, *13*, 6698–6710.

(293) Hirata, M.; Watanabe, Y.; Yoshida, M.; Koga, T.; Ozaki, S. Roles for Hydroxyl Groups of D-*Myo*-Inositol 1,4,5-Trisphosphate in the Recognition by Its Receptor and Metabolic Enzymes. *J. Biol. Chem.* **1993**, *268* (26), 19260–19266.

(294) Ballereau, S.; Guédat, P.; Poirier, S. N.; Guillemette, G.; Spiess, B.; Schlewer, G. Synthesis, Acid-Base Behavior, and Binding Properties of 6-Modified *Myo*-Inositol 1,4,5-Tris(Phosphate)s. *J. Med. Chem.* **1999**, *42* (23), 4824–4835.

(295) Guedat, P.; Poitras, M.; Spiess, B.; Guillemette, G.; Schlewer, G. Rapid Synthesis and Properties of (+)-6-Deoxy-6-Fluoro-*Myo*-Inositol-1,4,5-Tris(Phosphate) an Analogue of *Myo*-Inositol-1,4,5-Tris(Phosphate). *Bioorg. Med. Chem. Lett.* **1996**, *6* (10), 1175–1178.

(296) Liu, C.; Nahorski, S. R.; Potter, B. V. L. Synthesis from Quebrachitol of 1L-*Chiro*-Inositol 2,3,5-Trisphosphate, an Inhibitor of the Enzymes of 1D-*Myo*-Inositol 1,4,5-Trisphosphate Metabolism. *Carbohydr. Res.* **1992**, *234*, 107–115.

(297) Kozikowski, A. P.; Fauq, A. H.; Aksoy, I. A.; Seewald, M. J.; Powis, G. Synthesis of the First Optically Pure, Fluorinated Inositol 1,4,5-Trisphosphate of *Myo*-

Inositol. Stereochemistry and Its Effect on Calcium(2+) Release in Swiss 3T3 Cells. *J. Am. Chem. Soc.* **1990**, *112*, 7403–7404.

(298) Kozikowski, A. P.; Fauq, A. H.; Wilcox, R. A.; Nahorski, S. R. Chemical Synthesis and Biological Evaluation of 1D-1,2,4,5-$InsP_4$ and Its 3-Fluorinated Counterpart 1D-3-F-1,2,4,5-$InsP_4$ - Potent 1D-1,4,5-$InsP_3$-like Calcium Mobilizing Analogues. *Bioorg. Med. Chem. Lett.* **1995**, *5* (12), 1295–1300.

(299) Seewald, M. J.; Aksoy, I. A.; Powis, G.; Fauq, A. H.; Kozikowski, A. P. Synthesis of D-3-Deoxy-*Myo*-Inositol-1,4,5-Trisphosphate and Its Effects on Ca^{2+} Release in NIH 3T3 Cells. *J. Chem. Soc., Chem. Commun.* **1990**, No. 1638, 1638–1639.

(300) Howard, J. A. K.; Hoy, V. J.; O'Hagan, D.; Smith, G. T. How Good Is Fluorine as a Hydrogen Bond Acceptor? *Tetrahedron* **1996**, *52* (38), 12613–12622.

(301) Wilcox, R. A.; Primrose, W. U.; Nahorski, S. R.; Challiss, R. A. J. New Developments in the Molecular Pharmacology of the *Myo*-Inositol 1,4,5-Trisphosphate Receptor. *Trends Pharmacol. Sci.* **1998**, *19*, 467–475.

(302) Liu, C.; Potter, B. V. L. Synthesis of (±)-3-*O*-Alkylated Myo-Inositol 1,4,5-Trisphosphate Analogues as Potent Receptor Ligands and Enzyme Inhibitors. *Tetrahedron Lett.* **1994**, *35* (45), 8457–8460.

(303) Fauq, A. H.; Kozikowski, A. P.; Ognayanov, V. I.; Wilcox, R. A.; Nahorski, S. R. Probing of the D-1,4,5-IP_3/D-1,3,4,5-IP_4 Functional Interface. Synthesis and Pharmacology of Novel D-3-Modified Myo-Inositol Trisphosphate Analogues. *J. Chem. Soc., Chem. Commun.* **1994**, 1301–1302.

(304) Hirata, M.; Watanabe, Y.; Kanematsu, T.; Ozaki, S.; Koga, T. D-Myo-Inositol 1,4,5-Trisphosphate Analogues Substituted at the 3-Hydroxyl Group. *Biochim. Biophys. Acta* **1995**, *1244*, 404–410.

(305) Riley, A. M.; Murphy, C. T.; Lindley, C. J.; Westwick, J.; Potter, B. V. L. 6-Deoxy-6-Hydroxymethyl *Scyllo*-Inositol 1,2,4-Trisphosphate: A Potent Agonist at the Inositol 1,4,5-Trisphosphate Recpeptor. *Bioorg. Med. Chem. Lett.* **1996**, *6* (18), 2197–2200.

(306) Konieczny, V.; Stefanakis, J. G.; Sitsanidis, E. D.; Ioannidou, N.-A. T.; Papadopoulos, N. V.; Fylaktakidou, K. C.; Taylor, C. W.; Koumbis, A. E. Synthesis of Inositol Phosphate-Based Competitive Antagonists of Inositol 1,4,5-Trisphosphate Receptors. *Org. Biomol. Chem.* **2016**, *14*, 2504–2514.

(307) Hirata, M.; Watanabe, Y.; Ishimatsu, T.; Ikebe, T.; Kimura, Y.; Yamaguchi, K.; Ozaki, S.; Koga, T. Synthetic Inositol Trisphosphate Analogs and Their Effects on Phosphatase, Kinase, and the Release of Ca^{2+}. *J. Biol. Chem.* **1989**, *264* (34), 20303–20308.

(308) Hirata, M.; Yanaga, F.; Koga, T.; Ogasawara, T.; Watanabe, Y.; Ozaki, S. Stereospecific Recognition of Inositol 1,4,5-Trisphosphate Analogs by the

Phosphatase, Kinase, and Binding Proteins. *J. Biol. Chem.* **1990**, *265* (15), 8404–8407.

(309) Safrany, S. T.; Sawyer, D. A.; Wojcikiewicz, R. J. H.; Nahorski, S. R.; Potter, B. V. L. Ca^{2+}-Mobilising Properties of Synthetic Fluoro-Analogues of *Myo*-Inositol 1,4,5-Trisphosphate and Their Interaction with *Myo*-Inositol 1,4,5-Trisphosphate 3-Kinase and 5-Phosphatase. *FEBS Lett.* **1990**, *276* (1,2), 91–94.

(310) Ding, Z.; Rossi, A. M.; Riley, A. M.; Rahman, T.; Potter, B. V. L.; Taylor, C. W. Binding of Inositol 1,4,5-Trisphosphate (IP_3) and Adenophostin A to the N-Terminal Region of the IP_3 Receptor: Thermodynamic Analysis Using Fluorescence Polarization with a Novel IP_3 Receptor Ligand. *Mol. Pharmacol.* **2010**, *77* (6), 995–1004.

(311) Poitras, M.; Bernier, S.; Boulay, G.; Fournier, A.; Guillemette, G. Interaction of Benzene 1, 2,4-Trisphosphate with Inositol 1,4,5-Trisphosphate Receptor and Metabolizing Enzymes. *Eur. J. Pharmacol.* **1993**, *244*, 203–210.

(312) Mills, S. J.; Luyten, T.; Erneux, C.; Parys, J. B.; Potter, B. V. L. Multivalent Benzene Polyphosphate Derivatives Are Non-Ca^{2+}-Mobilizing Ins(1,4,5)P_3 Receptor Antagonists. *Messenger* **2012**, *2* (1), 167–181.

(313) Riley, A. M.; Jenkins, D. J.; Potter, B. V. L. Pentagon IP_3: Synthesis of a Ring-Contracted Mimic of a Second Messenger. *J. Am. Chem. Soc.* **1995**, *117* (11), 3300–3301.

(314) Takahashi, S.; Kinoshita, T.; Takahashi, M. Adenophostins A and B: Potent Agonists of Inositol-1,4,5-Trisphosphate Receptor Produced by *Penicillium Brevicompactum*. *J. Antibiot. (Tokyo).* **1994**, *47* (1), 95–100.

(315) Saleem, H.; Tovey, S. C.; Riley, A. M.; Potter, B. V. L.; Taylor, C. W. Stimulation of Inositol 1,4,5-Trisphosphate (IP_3) Receptor Subtypes by Adenophostin A and Its Analogues. *PLoS One* **2013**, *8* (2), e58027.

(316) Jenkins, D. J.; Potter, B. V. L. A Ca^{2+}-Mobilising Carbohydrate-Based Polyphosphate : Synthesis of 2-Hydroxyethyl α-D-Glucopyranoside 2',3,4-Trisphosphate. *Carbohydr. Res.* **1996**, *287*, 169–182.

(317) Shuto, S.; Tatani, K.; Ueno, Y.; Matsuda, A. Synthesis of Adenophostin Analogues Lacking the Adenine Moiety as Novel Potent IP_3 Receptor Ligands: Some Structural Requirements for the Significant Activity of Adenophostin A. *J. Org. Chem.* **1998**, *63*, 8815–8824.

(318) Van Straten, N. C. R.; van der Marel, G. A.; Van Boom, J. H. An Expeditious Route to the Synthesis of Adenophostin A. *Tetrahedron* **1997**, *53* (18), 6509–6522.

(319) De Kort, M.; Valentijn, A. R. P. M.; Van Der Marel, G. A.; Van Boom, J. H. Synthesis of Clustered Disaccharide Polyphosphate Analogues of

Adenophostin A. *Tetrahedron Lett.* **1997**, *38* (43), 7629–7632.

(320) Van Straten, N. C. R.; Kriek, N. M. A. J.; Cziria, Z. A. C.; Van der Marel, G. A.; Van Boom, J. H. Synthesis of 3',4'-Bisphosphate-Containing Analogs of Adenophostin A. *Tetrahedron* **1997**, *53* (18), 6539–6554.

(321) Dohle, W.; Su, X.; Mills, S. J.; Rossi, A. M.; Taylor, C. W.; Potter, B. V. L. A Synthetic Cyclitol-Nucleoside Conjugate Polyphosphate Is a Highly Potent Second Messenger Mimic. *Chem. Sci.* **2019**, 5382–5390.

(322) Sureshan, K. M.; Riley, A. M.; Rossi, A. M.; Tovey, S. C.; Dedos, S. G.; Taylor, C. W.; Potter, B. V. L. Activation of IP_3 Receptors by Synthetic Bisphosphate Ligands. *Chem. Commun.* **2009**, 1204–1206.

(323) Jenkins, D. J.; Marwood, R. D.; Potter, B. V. L. A Concise Route from D-Glucose and D-Ribose to a Potent Sugar Polyphosphate Second Messenger Mimic Related to Adeno- Phostin A Is Described; a Role for the Adenine Base of the Adenophostins Is Suggested. *Chem. Commun.* **1997**, 449–450.

(324) Wilcox, R. A.; Erneux, C.; Primrose, W. U.; Gigg, R.; Nahorski, S. R. 2-Hydroxyethyl-α-D-Glucopyranoside-2,3',4'-Trisphosphate, a Novel, Metabolically Resistant, Adenophostin A and *Myo*-Inositol-1,4,5-Trisphosphate Analogue, Potently Interacts with the *Myo*-Inositol-1,4,5-Trisphosphate Receptor. *Mol. Pharmacol.* **1995**, *47*, 1204–1211.

(325) Hotoda, H.; Murayama, K.; Miyamoto, S.; Iwata, Y.; Takahashi, M.; Kawase, Y.; Tanzawa, K.; Kaneko, M. Molecular Recognition of Adenophostin, a Very Potent Ca^{2+} Inducer, at the D-*Myo*-Inositol 1,4,5-Trisphosphate Receptor. *Biochemistry* **1999**, *38*, 9234–9241.

(326) Felemez, M.; Marwood, R. D.; Potter, B. V. L.; Spiess, B. Inframolecular Studies of the Protonation of Adenophostin A: Comparison with 1-D-*Myo*-Inositol 1,4,5-Trisphosphate. *Biochem. Biophys. Res. Commun.* **1999**, *266* (2), 334–340.

(327) Rossi, A. M.; Sureshan, K. M.; Riley, A. M.; Potter, B. V. L.; Taylor, C. W. Selective Determinants of Inositol 1,4,5-Trisphosphate and Adenophostin A Interactions with Type 1 Inositol 1,4,5-Trisphosphate Receptors. *Br. J. Pharmacol.* **2010**, *161*, 1070–1085.

(328) Sureshan, K. M.; Trusselle, M.; Tovey, S. C.; Taylor, C. W.; Potter, B. V. L. 2-Position Base-Modified Analogues of Adenophostin A as High-Affinity Agonists of the D-*Myo*-Inositol Trisphosphate Receptor: *In Vitro* Evaluation and Molecular Modeling. *J. Org. Chem.* **2008**, *73*, 1682–1692.

(329) Shuto, S.; Yahiro, Y.; Ichikawa, S.; Matsuda, A. Synthesis of 3,7-Anhydro-D-Glycero-D-Ido-Octitol 1,5,6-Trisphosphate as an IP_3 Receptor Ligand Using a Radical Cyclization Reaction with a Vinylsilyl Tether as the Key Step. Conformational Restriction Strategy Using Steric Repulsion between Adjacent Bulky Protecting groups on a Pyranose Ring. *J. Org. Chem.* **2000**, *65* (18),

5547–5557.

(330) Beecroft, M. D.; Marchant, J. S.; Riley, A. M.; Van Straten, N. C. R.; Van Der Marel, G. A.; Van Boom, J. H.; Potter, B. V. L.; Taylor, C. W. Acyclophostin: A Ribose-Modified Analog of Adenophostin A with High Affinity for Inositol 1,4,5-Trisphosphate Receptors and PH-Dependent Efficacy. *Mol. Pharmacol.* **1999**, *55* (1), 109–117.

(331) Murphy, C. T.; Riley, A. M.; Lindley, C. J.; Jenkins, D. J.; Westwick, J.; Potter, B. V. L. Structural Analogues of D-*Myo*-Inositol-1,4,5-Trisphosphate and Adenophostin A: Recognition by Cerebellar and Platelet. *Mol. Pharmacol.* **1997**, *52*, 741–748.

(332) Fan, G.; Baker, M. R.; Wang, Z.; Seryshev, A. B.; Ludtke, S. J.; Baker, M. L.; Serysheva, I. I. Cryo-EM Reveals Ligand Induced Allostery Underlying $InsP_3R$ Channel Gating. *Cell Res.* **2018**, *28*, 1158–1170.

(333) Gambardella, J.; Morelli, M. B.; Wang, X.; Castellanos, V.; Mone, P.; Santulli, G. The Discovery and Development of IP_3 Receptor Modulators: An Update. *Expert Opin. Drug Discov.* **2021**, 1–10.

(334) Saleem, H.; Tovey, S. C.; Molinski, T. F.; Taylor, C. W. Interactions of Antagonists with Subtypes of Inositol 1,4,5-Trisphosphate (IP_3) Receptor. *Br. J. Pharmacol.* **2014**, *171* (13), 3298–3312.

(335) Shipton, M. L.; Riley, A. M.; Rossi, A. M.; Brearley, C. A.; Taylor, C. W.; Potter, B. V. L. Both D- and L-Glucose Polyphosphates Mimic D-*Myo*-Inositol 1,4,5-Trisphosphate: New Synthetic Agonists and Partial Agonists at the $Ins(1,4,5)P_3$ Receptor. *J. Med. Chem.* **2020**, *63* (10), 5442–5457.

(336) Van Straten, N. C. R.; Van der Marel, G. A.; Van Boom, J. H. Synthesis of 2',3',4'-Trisphosphate-Containing Analogs of Adenophostin A. *Tetrahedron* **1997**, *53* (18), 6523–6538.

(337) Tanaka, N.; Ogawa, I.; Yoshigase, S.; Nokami, J. Regioselective Ring Opening of Benzylidene Acetal Protecting Group(s) of Hexopyranoside Derivatives by DIBAL-H. *Carbohydr. Res.* **2008**, *343*, 2675–2679.

(338) Shie, C.-R.; Tzeng, Z.-H.; Wang, C.-C.; Hung, S.-C. Metal Trifluoromethanesulfonate Catalyzed Regioselective Reductive Ring Opening of Benzylidene Acetals. *J. Chin. Chem. Soc.* **2009**, *56*, 510–523.

(339) Daragics, K.; Fügedi, P. Regio- and Chemoselective Reductive Cleavage of 4,6-*O*-Benzylidene-Type Acetals of Hexopyranosides Using BH_3·THF-TMSOTf. *Tetrahedron Lett.* **2009**, *50* (24), 2914–2916.

(340) Tani, S.; Sawadi, S.; Kojima, M.; Akai, S.; Sato, K. A Novel Method for Regioselective Ring-Opening Reduction of 4,6-*O*-Benzylidene Hexopyranoside Derivatives Using $CoCl_2$ and BH_3·THF. *Tetrahedron Lett.* **2007**, *48*, 3103–3104.

(341) Jensen, H. H.; Nordstrøm, L. U.; Bols, M. The Disarming Effect of the 4,6-Acetal Group on Glycoside Reactivity: Torsional or Electronic? *J. Am. Chem. Soc.* **2004**, *126*, 9205–9213.

(342) Bourdreux, Y.; Lemétais, A.; Urban, D.; Beau, J.-M. Iron(III) Chloride-Tandem Catalysis for a One-Pot Regioselective Protection of Glycopyranosides. *Chem. Commun.* **2011**, *47*, 2146–2148.

(343) Wang, C.-C.; Lee, J.-C.; Luo, S.-Y.; Fan, H.-F.; Pai, C.-L.; Yang, W.-C.; Lu, L.-D.; Hung, S.-C. Synthesis of Biologically Potent A1 →2-Linked Disaccharide Derivatives via Regioselective One-Pot Protection - Glycosylation. *Angew. Chemie - Int. Ed.* **2002**, *41* (13), 2360–2362.

(344) Dong, H.; Zhou, Y.; Pan, X.; Cui, F.; Liu, W.; Liu, J.; Ramström, O. Stereoelectronic Control in Regioselective Carbohydrate Protection. *J. Org. Chem.* **2012**, *77*, 1457–1467.

(345) Français, A.; Urban, D.; Beau, J.-M. Tandem Catalysis for a One-Pot Regioselective Protection of Carbohydrates: The Example of Glucose. *Angew. Chemie - Int. Ed.* **2007**, *46*, 8662–8665.

(346) Takahashi, H.; Mitsuzuka, H.; Nishiyama, K.; Ikegami, S. A Facile Synthesis of Neosaccharides: 2,6'-and 3,6'-Ether- Linked Sugars. *Synthesis (Stuttg).* **2006**, No. 9, 1415–1418.

(347) Ogawa, T.; Nakabayashi, S.; Kitajima, T. Synthesis of a Hexasaccharide Unit of a Complex Type of Glycan Chain of a Glycoprotein. *Carbohydr. Res.* **1983**, *114*, 225–236.

(348) Nakayama, K.; Uoto, K.; Higashi, K.; Soga, T.; Kusama, T. A Useful Method for Deprotection of the Protective Allyl Group at the Anomeric Oxygen of Carbohydrate Moieties Using Tetrakis(Tripehenylphosphine)Palladium. *Chem. Pharm. Bull* **1992**, *40* (7), 1718–1720.

(349) Boss, R.; Scheffold, R. Cleavage of Allyl Ether with Pd/C. *Angew. Chemie - Int. Ed.* **1976**, *15* (9), 558–559.

(350) Gigg, R.; Warren, C. D. A Synthesis of DL-2,3,4,5,6-Penta-*O*-Benzylmyoinositol. *Tetrahedron Lett.* **1966**, No. 22, 2415–2417.

(351) Gigg, J.; Gigg, R. The Allyl Ether as a Protecting Group in Carbohydrate Chemistry. *J. Chem. Soc.* **1966**, 82–86.

(352) Gigg, R.; Warren, C. D. Use of the Allyl Ether as a Protecting Group in a New Synthesis of L-Lyxose. **1965**, 2205–2210.

(353) Ogawa, T.; Yamamoto, H. Synthesis of a Model Linear Mannohexaose for the Backbone Structure of Fruit Body Polysaccharide of *Tremella Fuciformis* and *Dictyophora Indusiata* Fisch. *Agric. Biol. Chem.* **1985**, *49* (2), 475–482.

(354) Cunningham, J.; Gigg, R.; Warren, C. D. The Allyl Ether as a Protecting Group in Carbohydrate Chemistry. *Tetrahedron Lett.* **1964**, No. 19, 1191–1196.

(355) Bullock, A. L.; Cirino, V. O.; Rowland, S. P. Mono-*O*-(Methylsulfonylethyl)-D-Glucoses. *Can. J. Chem.* **1967**, *45*, 255–260.

(356) Eby, R.; Sondheimer, S. J.; Schuerch, C. Selective Acetolysis of Primary Benzyl Ethers. *Carbohydr. Res.* **1979**, *73*, 273–276.

(357) Desai, T.; Gigg, J.; Gigg, R. The Allyl Group for Protection in Carbohydrate Chemistry. *Aust. J. Chem.* **1996**, *49*, 305–309.

(358) Plante, O. J.; Andrade, R. B.; Seeberger, P. H. Synthesis and Use of Glycosyl Phosphates as Glycosyl Donors. *Org. Lett.* **1999**, *1* (2), 211–214.

(359) Garcia, B. A.; Gin, D. Y. Synthesis of Glycosyl-1-Phosphates via Dehydrative Glycosylation. *Org. Lett.* **2000**, *2* (14), 2135–2138.

(360) MacDonald, D. L. Separation of the Anomers of Glycosyl Phosphates. *Carbohydr. Res.* **1968**, *6*, 376–381.

(361) Fylaktakidou, K. C.; Duarte, C. D.; Koumbis, A. E.; Nicolau, C.; Lehn, J. M. Polyphosphates and Pyrophosphates of Hexopyranoses as Allosteric Effectors of Human Hemoglobin: Synthesis, Molecular Recognition, and Effect on Oxygen Release. *ChemMedChem* **2011**, *6*, 153–168.

(362) Sabesan, S.; Neira, S. Synthesis of Glycosyl Phosphates and Azides. *Carbohydr. Res.* **1992**, *223*, 169–185.

(363) Carrel, F. R.; Seeberger, P. H. Protecting Group Manipulations on Glycosyl Phosphate Triesters. *J. Carbohydr. Chem.* **2007**, *26*, 125–139.

(364) Jiang, J.; Biggins, J. B.; Thorson, J. S. A General Enzymatic Method for the Synthesis of Natural and " Unnatural " UDP- and TDP-Nucleotide Sugars. *J. Am. Chem. Soc.* **2000**, *122*, 6803–6804.

(365) Sabesan, S. Process for the Preparation of Glycosyl Phosphate Triesters. USA5,095,123, 1992.

(366) Cohn, M. Mechanisms of Cleavage of Glucose-1-Phosphate. *J. Biol. Chem.* **1949**, *180* (2), 771–781.

(367) Duarte, F.; Barrozo, A.; Åqvist, J.; Williams, N. H.; Kamerlin, S. C. L. The Competing Mechanisms of Phosphate Monoester Dianion Hydrolysis. *J. Am. Chem. Soc.* **2016**, *138* (33), 10664–10673.

(368) Mills, S. J.; Rossi, A. M.; Konieczny, V.; Taylor, C. W.; Potter, B. V. L. D-Chiro-Inositol Ribophostin: A Highly Potent Agonist at D-*Myo*-Inositol 1,4,5-Trisphosphate Receptors: Synthesis and Biological Activities. *J. Med. Chem.* **2020**, 3238–3251.

(369) Morgan, A. J.; Galione, A. Developmental Biology of the Sea Urchin and Other Marine Invertebrates. In *Developmental Biology of the Sea Urchin and Other Marine Invertebrates*; 2014; Vol. 1128, pp 161–173.

(370) Parys, J. B.; McPherson, S. M.; Mathews, L.; Campbell, K. P.; Longo, F. J. Presence of Inositol 1,4,5-Trisphosphate Receptor, Calreticulin, and Calsequestrin in Eggs of Sea Urchins and *Xenopus Laevis*. *Developmental Biology*. 1994, pp 466–476.

(371) Morgan, A. J.; Churchill, G. C.; Masgrau, R.; Ruas, M.; Davis, L. C.; Billington, R. A.; Patel, S.; Yamasaki, M.; Thomas, J. M.; Genazzani, A. A.; Galione, A. Methods in Cyclic ADP-Ribose and NAADP Research. *Calcium Signaling, Second Ed.* **2005**, 265–334.

(372) Denis, G. V.; Ballou, C. E. The Ca^{2+} Release Activities of D-*Myo*-Inositol 1,4,5-Trisphosphate Analogs Are Quantized. *Cell Calcium* **1991**, *12* (6), 395–401.

(373) Sun, Y.; Wilson, M. P.; Majerus, P. W. Inositol 1,3,4-Trisphosphate 5/6-Kinase Associates with the COP9 Signalosome by Binding to CSN1. *J. Biol. Chem.* **2002**, *277* (48), 45759–45764.

(374) Miller, G. J.; Wilson, M. P.; Majerus, P. W.; Hurley, J. H. Specificity Determinants in Inositol Polyphosphate Synthesis: Crystal Structure of Inositol 1,3,4-Trisphosphate 5/6-Kinase. *Mol. Cell* **2005**, *18* (2), 201–212.

(375) Wilson, M. P.; Sun, Y.; Cao, L.; Majerus, P. W. Inositol 1,3,4-Trisphosphate 5/6-Kinase Is a Protein Kinase That Phosphorylates the Transcription Factors c-Jun and ATF-2. *J. Biol. Chem.* **2001**, *276* (44), 40998–41004.

(376) Yang, X.; Shears, S. B. Multitasking in Signal Transduction by a Promiscuous Human Ins(3,4,5,6)P_4 1-Kinase/Ins(1,3,4)P_3 5/6-Kinase. *Biochem. J.* **2000**, *351* (3), 551–555.

(377) Field, J.; Wilson, M. P.; Mai, Z.; Majerus, P. W.; Samuelson, J. An *Entamoeba Histolytica* Inositol 1,3,4-Trisphosphate 5/6-Kinase Has a Novel 3-Kinase Activity. *Mol. Biochem. Parasitol.* **2000**, *108*, 119–123.

(378) Whitfield, H.; White, G.; Sprigg, C.; Riley, A. M.; Potter, B. V. L.; Hemmings, A. M.; Brearley, C. A. An ATP-Responsive Metabolic Cassette Comprised of Inositol Tris/Tetrakisphosphate Kinase 1 (ITPK1) and Inositol Pentakisphosphate 2-Kinase (IPK1) Buffers Diphosphosphoinositol Phosphate Levels. *Biochem. J.* **2020**, *477* (14), 2621–2638.

(379) Riemer, E.; Qiu, D.; Laha, D.; Harmel, R. K.; Gaugler, P.; Gaugler, V.; Frei, M.; Hajirezaei, M.; Laha, N. P.; Krusenbaum, L.; Schneider, R.; Saiardi, A.; Fiedler, D.; Jessen, H. J.; Schaaf, G.; Giehl, R. F. H. ITPK1 Is an $InsP_6$/ADP Phosphotransferase That Controls Phosphate Signaling in Arabidopsis. *Mol. Plant* **2021**.

(380) Laha, D.; Parvin, N.; Hofer, A.; Giehl, R. F. H.; Fernandez-Rebollo, N.; Von Wirén, N.; Saiardi, A.; Jessen, H. J.; Schaaf, G. Arabidopsis ITPK1 and ITPK2 Have an Evolutionarily Conserved Phytic Acid Kinase Activity. *ACS Chem. Biol.* **2019**, *14* (10), 2127–2133.

(381) Wilson, M. P.; Majerus, P. W. Characterization of a CDNA Encoding Arabidopsis Thaliana. *Biochem. Biophys. Res. Commun.* **1997**, *232* (3), 678–681.

(382) Martin, J. B.; Laussmann, T.; Bakker-Grunwald, T.; Vogel, G.; Klein, G. *Neo*-Inositol Polyphosphates in the Amoeba *Entamoeba Histolytica*. *J. Biol. Chem.* **2000**, *275* (14), 10134–10140.

(383) Ho, M. W. Y.; Yang, X.; Carew, M. A.; Zhang, T.; Hua, L.; Kwon, Y.; Chung, S.; Adelt, S.; Riley, A. M.; Potter, B. V. L.; Shears, S. B.; Carolina, N. By a Reversible Kinase/Phosphatase. *Current* **2002**, *12* (02), 477–482.

(384) Riley, A. M.; Deleu, S.; Qian, X.; Mitchell, J.; Chung, S. K.; Adelt, S.; Vogel, G.; Potter, B. V. L.; Shears, S. B. On the Contribution of Stereochemistry to Human ITPK1 Specificity: Ins(1,4,5,6)P_4 Is Not a Physiologic Substrate. *FEBS Lett.* **2006**, *580* (1), 324–330.

(385) Rosenberg, H. J.; Riley, A. M.; Marwood, R. D.; Correa, V.; Taylor, C. W.; Potter, B. V. L. Xylopyranoside-Based Agonists of D-*Myo*-Inositol 1,4,5-Trisphosphate Receptors: Synthesis and Effect of Stereochemistry on Biological Activity. *Carbohydr. Res.* **2001**, *332* (1), 53–66.

(386) Marwood, R. D.; Riley, A. M.; Correa, V.; Taylor, C. W.; Potter, B. V. L. Simplification of Adenophostin a Defines a Minimal Structure for Potent Glucopyranoside-Based Mimics of D-*Myo*-Inositol 1,4,5-Trisphosphate. *Bioorganic Med. Chem. Lett.* **1999**, *9* (3), 453–458.

(387) González, B.; Schell, M. J.; Letcher, A. J.; Veprintsev, D. B.; Irvine, R. F.; Williams, R. L. Structure of a Human Inositol 1,4,5-Trisphosphate 3-Kinase: Substrate Binding Reveals Why It Is Not a Phosphoinositide 3-Kinase. *Mol. Cell* **2004**, *15* (5), 689–701.

(388) Safrany, S. T.; Wojcikiewicz, R. J. H.; Strupish, J.; McBain, J.; Cooke, A. M.; Potter, B. V. L.; Nahorski, S. R. Synthetic Phosphorothioate-Containing Analogues of Inositol 1,4,5-Trisphosphate Mobilize Intracellular Ca^{2+} Stores and Interact Differentially with Inositol 1,4,5-Trisphosphate 5-Phosphatase and 3-Kinase. *Mol. Pharmacol.* **1991**, *39* (6), 754–761.

(389) Wickner, R. B.; Bezsonov, E. E.; Son, M.; Ducatez, M.; Dewilde, M.; Edskes, H. K. Anti-Prion Systems in Yeast and Inositol Polyphosphates. *Biochemistry* **2018**, *57* (8), 1285–1292.

(390) Wickner, R. B.; Kelly, A. C.; Bezsonov, E. E.; Edskes, H. K. [PSI+] Prion Propagation Is Controlled by Inositol Polyphosphates. *Proc. Natl. Acad. Sci.*

2017, 201714361.

(391) Gigg, R.; Warren, C. D. Derivatives of 2,3,4,5,6-Penta-*O*-Benzyl-*Myo*-Inositol. *J. Chem. Soc.* **1969**, 2367–2371.

(392) Angyal, S. J.; Macdonald, C. G. Angyal and Macdonald : Cyclitols. Part I . 324. Cyclitols. Part I . IsoPropylidene Derivatives of Inositols and Quercitols. The Structure of Pinitol and Quebrachitol. *J. Chem. Soc.* **1952**, No. 686, 686.

(393) Desai, T.; Gigg, J.; Gigg, R.; Martín-Zamora, E.; Schnetz, N. The Synthesis and Resolution of (±)-1,4-Di-*O*-Benzyl-2,3-*O*-Isopropylidene-*Myo*-Inositol. *Carbohydr. Res.* **1994**, *258* (C), 135–144.

(394) Gigg, J.; Gigg, R.; Martin-Zamora, E. The Alkylation of Dibutylstannylene Derivatives of 1,2-*O*-Isopropylidene-*Myo*-Inositol. *Tetrahedron Lett.* **1993**, *34* (17), 2827–2830.

(395) David, S.; Hanessian, S. Regioselective Manipulation of Hydroxyl Groups via Organotin Derivatives. *Tetrahedron* **1985**, *41* (4), 643–663.

(396) Grindley, T. B.; Thangarasa, R. The Structures and Reactions of Stannylene Acetals from Carbohydrate-Derived Trans-Diols. Part I. In the Absence of Added Nucleophiles. *Can. J. Chem.* **1990**, *68* (7), 1007–1019.

(397) Riley, A. M.; Potter, B. V. L. Bicyclic Analogues of Inositol 1,4,5-Trisphosphate Based upon Adenophostin A. *Tetrahedron Lett.* **1999**, *40*, 2213–2216.

(398) Montchamp, J. L.; Tian, F.; Hart, M. E.; Frost, J. W. Butane 2,3-Bisacetal Protection of Vicinal Diequatorial Diols. *J. Org. Chem.* **1996**, *61* (11), 3897–3899.

(399) Riley, A. M.; Potter, B. V. L. Poly(Ethylene Glycol)-Linked Dimers of D-*Myo*-Inositol 1,4,5- Trisphosphate. *Chem. Commun.* **2000**, No. 11, 983–984.

(400) Desai, T.; Gigg, J.; Gigg, R.; Payne, S. The Preparation, Resolution, and Phosphorylation of Some Benzyl Ethers of *Myo*-Inositol: Intermediates for the Synthesis of *Myo*-Inositol Phosphates of the Phosphatidylinositol Cycle. *Carbohydr. Res.* **1992**, *225* (2), 209–228.

(401) Desai, T.; Gigg, J.; Gigg, R.; Payne, S.; Penades, S. The Preparation of Intermediates for the Synthesis of 1D-*Myo*-Inositol 1,4,5-Trisphosphate, a Second Messenger for Signal Transduction in Cells. *Carbohydr. Res.* **1992**, *234* (C), 1–21.

(402) Xu, H.; Lu, Y.; Zhou, Y.; Ren, B.; Pei, Y.; Dong, H.; Pei, Z. Regioselective Benzylation of Diols and Polyols by Catalytic Amounts of an Organotin Reagent. *Adv. Synth. Catal.* **2014**, *356*, 1735–1740.

(403) Nagashima, N.; Ohno, M. Selective Monoalkylation of Acyclic Diols by Means of Dibutyltin Oxide and Fluoride Salts. *Chem. Pharm. Bull.* **1991**, *39* (8), 1972–

1982.

(404) Ren, B.; Yan, N.; Gan, L. Regioselective Alkylation of Carbohydrates and Diols: A Cheaper Iron Catalyst, New Applications and Mechanism. *RSC Adv.* **2017**, *7* (73), 46257–46262.

(405) Ren, B.; Lv, J.; Zhang, Y.; Tian, J.; Dong, H. Highly Efficient Selective Benzylation of Carbohydrates Catalyzed by Iron(III) with Silver Oxide and Bromide Anion as Co-Catalysts. *ChemCatChem* **2017**, *9*, 950–953.

(406) Dong, H.; Zhou, Y.; Pan, X.; Cui, F.; Liu, W.; Liu, J.; Ramström, O. Stereoelectronic Control in Regioselective Carbohydrate Protection. *J. Org. Chem.* **2012**, *77*, 1457–1467.

(407) Wagner, D.; Verheyden, J. P. H.; Moffatt, J. G. Preparation and Synthetic Utility of Some Organotin Derivatives of Nucleosides. *J. Org. Chem.* **1974**, *39* (1), 24–30.

(408) Hammond, G. S.; Nonhebel, D. C.; Wu, C.-H. Chelates of Beta-Diketones V. Preparation and Properties of Chelates Containing Sterically Hindered Ligands. *Inorg. Chem.* **1963**, *2* (1), 73–76.

(409) Laude, A. J.; Tovey, S. C.; Dedos, S. G.; Potter, B. V. L.; Lummis, S. C. R.; Taylor, C. W. Rapid Functional Assays of Recombinant IP_3 Receptors. *Cell Calcium* **2005**, *38*, 45–51.

(410) Tovey, S. C.; Sun, Y.; Taylor, C. W. Rapid Functional Assays of Intracellular Ca^{2+} Channels. *Nat. Protoc.* **2006**, *1* (1), 259–263.

(411) Jones, G.; Willett, P.; Glen, R. C.; Leach, A. R.; Taylor, R. Development and Validation of a Genetic Algorithm for Flexible Docking. *J. Mol. Biol.* **1997**, *267*, 727–748.

(412) Verdonk, M. L.; Berdini, V.; Hartshorn, M. J.; Mooij, W. T. M.; Murray, C. W.; Taylor, R. D.; Watson, P. Virtual Screening Using Protein-Ligand Docking: Avoiding Artificial Enrichment. *J. Chem. Inf. Comput. Sci.* **2004**, *44*, 793–806.

(413) Korb, O.; Stützle, T.; Exner, T. E. Empirical Scoring Functions for Advanced Protein-Ligand Docking with PLANTS. *J. Chem. Inf. Model.* **2009**, *49*, 84–96.

(414) Verdonk, M. L.; Chessari, G.; Cole, J. C.; Hartshorn, M. J.; Murray, C. W.; Nissink, J. W. M.; Taylor, R. D.; Taylor, R. Modeling Water Molecules in Protein-Ligand Docking Using GOLD. *J. Med. Chem.* **2005**, *48*, 6504–6515.

(415) Lampe, D.; Liu, C.; Potter, B. V. L. Synthesis of Selective Non-Ca^{2+} Mobilizing Inhibitors of D-*Myo*-Inositol 1,4,5-Trisphosphate 5-Phosphatase. *J. Med. Chem.* **1994**, *37* (7), 907–912.

(416) Godage, H. Y.; Riley, A. M.; Woodman, T. J.; Thomas, M. P.; Mahon, M. F.; Potter, B. V. L. Regioselective Opening of *Myo*-Inositol Orthoesters:

Mechanism and Synthetic Utility. *J. Org. Chem.* **2013**, *78* (6), 2275–2288.

(417) Szeleszczuk, Ł.; Gubica, T.; Zimniak, A.; Pisklak, D. M.; Dąbrowska, K.; Cyrański, M. K.; Kańska, M. The Potential for the Indirect Crystal Structure Verification of Methyl Glycosides Based on Acetates' Parent Structures: GIPAW and Solid-State NMR Approaches. *Chem. Phys. Lett.* **2017**, *686*, 7–11.

(418) Rocheleau, S.; Pottel, J.; Huskić, I.; Moitessier, N. Highly Regioselective Monoacylation of Unprotected Glucopyranoside Using Transient Directing-Protecting Groups. *European J. Org. Chem.* **2017**, *2017* (3), 646–656.

(419) Achmatowicz Jr., O.; Bielski, R. Stereoselective Total Synthesis of Methyl α-D- and α-L-Glucopyranosides. *Carbohydr. Res.* **1977**, *55*, 165–176.

(420) Daragics, K.; Szabó, P.; Fügedi, P. Some Observations on the Reductive Ring Opening of 4,6-*O*-Benzylidene Acetals of Hexopyranosides with the Borane Trimethylamine-Aluminium Chloride Reagent. *Carbohydr. Res.* **2011**, *346*, 1633–1637.

(421) Medgyes, A.; Farkas, E.; Lipták, A.; Pozsgay, V. Synthesis of the Monosaccharide Units of the *O*-Specific Polysaccharide of *Shigella Sonnei*. *Tetrahedron* **1997**, *53* (12), 4159–4178.

(422) Bauder, C. A Convenient Synthesis of Orthogonally Protected 2-Deoxystreptamine (2-DOS) as an Aminocyclitol Scaffold for the Development of Novel Aminoglycoside Antibiotic Derivatives against Bacterial Resistance. *Org. Biomol. Chem.* **2008**, *6*, 2952–2960.

(423) Liau, B. B.; Milgram, B. C.; Shair, M. D. Total Syntheses of HMP-Y1, Hibarimicinone, and HMP-P1. *J. Am. Chem. Soc.* **2012**, *134* (40), 16765–16772.

(424) Satomura, S.; Iwata, T.; Sakata, Y.; Omichi, K.; Ikenaka, T. Synthesis of *P*-Nitrophenyl 6-*O*-Benzyl-α-Maltopentaoside, a Substrate for α-Amylases. *Carbohydr. Res.* **1988**, *176*, 107–115.

(425) D'Alonzo, D.; Guaragna, A.; Napolitano, C.; Palumbo, G. Rapid Access to 1,6-Anhydro- L-Hexopyranose Derivatives via Domino Reaction : Synthesis of L-Allose and L-Glucose. *J. Org. Chem.* **2008**, *73*, 5636–5639.

(426) Tateishi, H.; Anraku, K.; Koga, R.; Okamoto, Y.; Fujita, M.; Otsuka, M. Design and Synthesis of Lipid-Coupled Inositol 1,2,3,4,5,6-Hexakisphosphate Derivatives Exhibiting High-Affinity Binding for the HIV-1 MA Domain. *Org. Biomol. Chem.* **2014**, *12* (27), 5006–5022.

(427) Ahmed, M. A. K.; Fjellvag, H.; Kjekshus, A.; Wragg, D. S. Structure and Polymorphism of $M(Thd)_3$ (M = Al, Cr, Mn, Fe, Co, Ga, and In). *Zeitschrift fur Anorg. und Allg. Chemie* **2013**, *639* (5), 770–778.

Spectra

Synthesis of 5-PP-InsP$_5$ (2) and 5-PP-InsP$_4$ (3)

2-*O*-Benzyl-1,6:3,4-bis-*O*-(2,3-dimethoxybutane-2,3-diyl)-*myo*-inositol (**5**)

^{1}HNMR, 400 MHz, $CDCl_3$

5

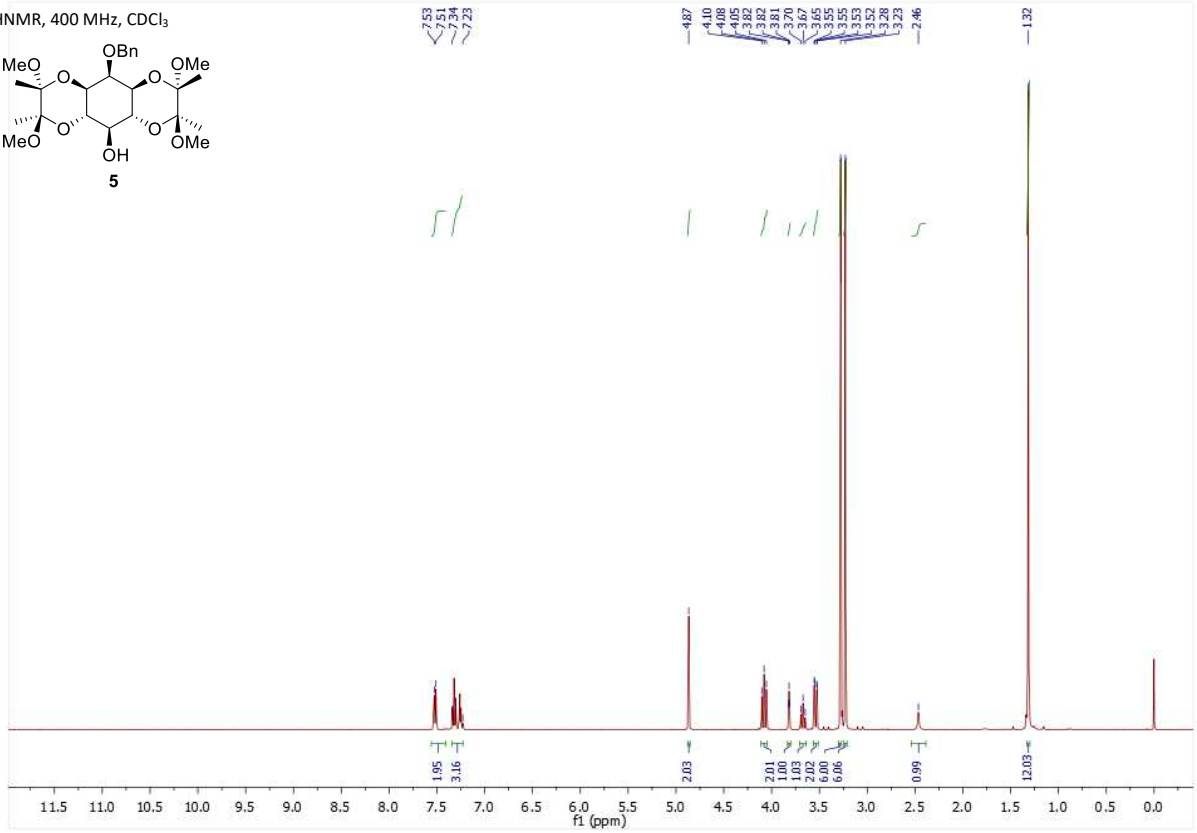

^{13}CNMR, 100 MHz, $CDCl_3$

5

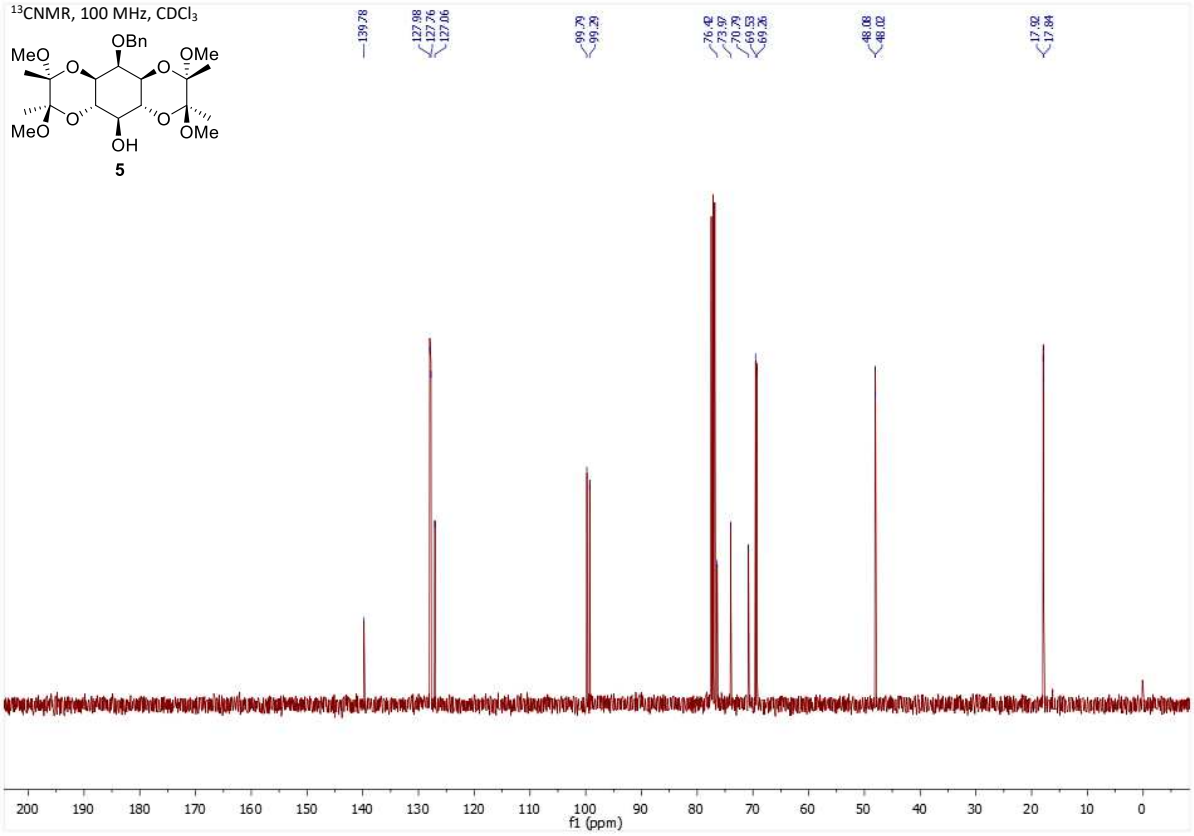

^{1}H-^{1}H COSY

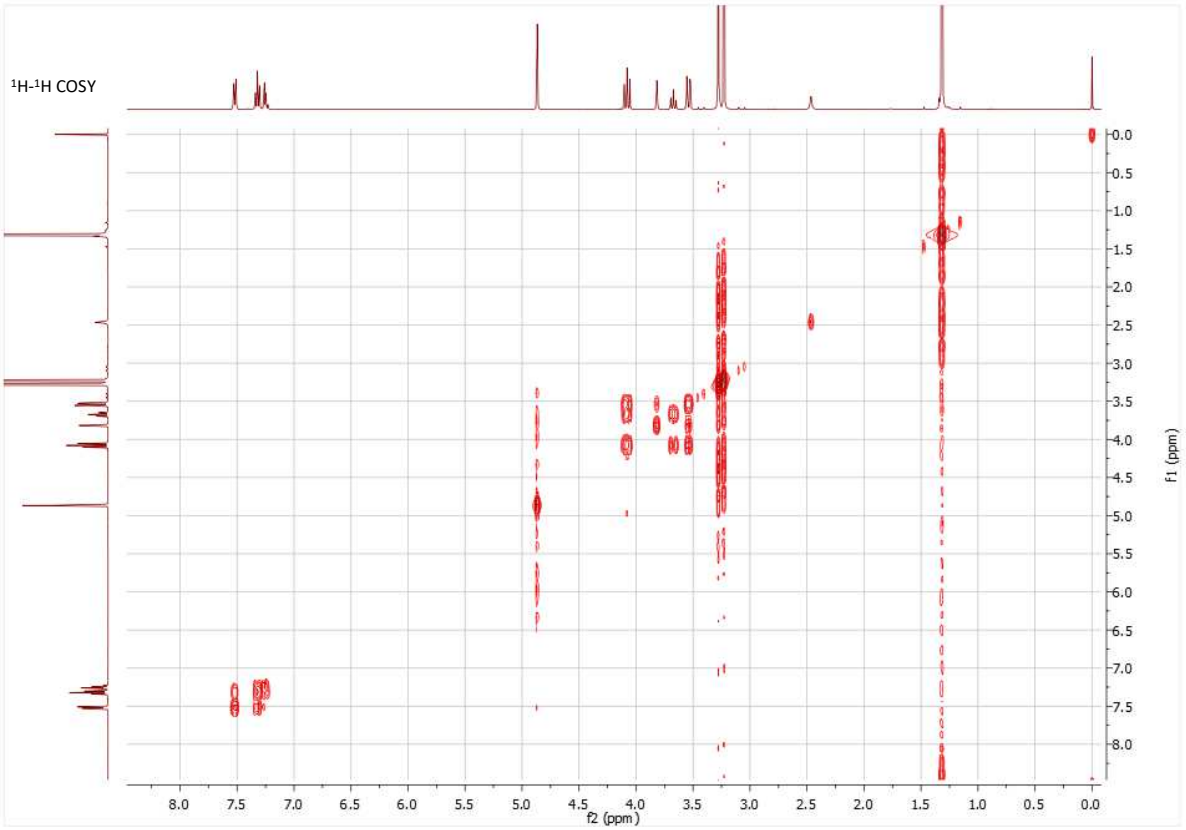

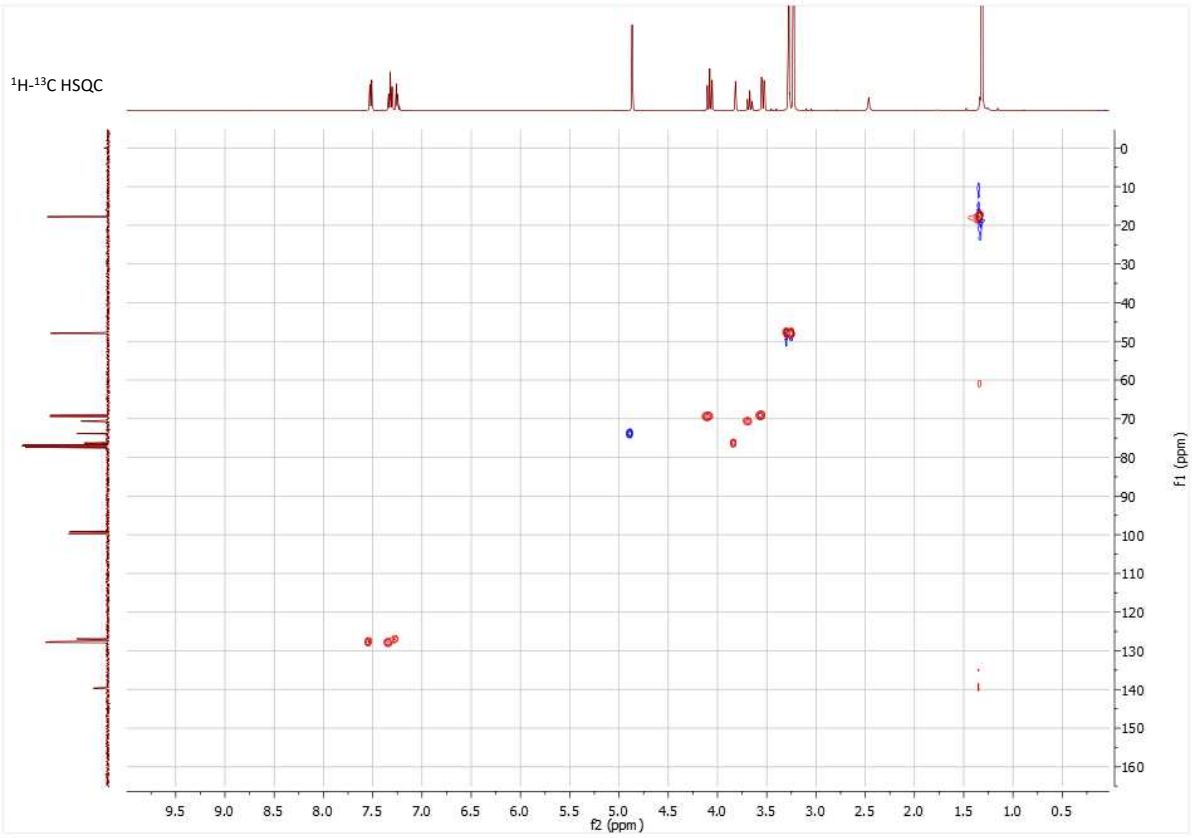

N,N-Diisopropylamino-bis-[2-(methylsulfonyl)ethyloxy]phosphine (**1**)

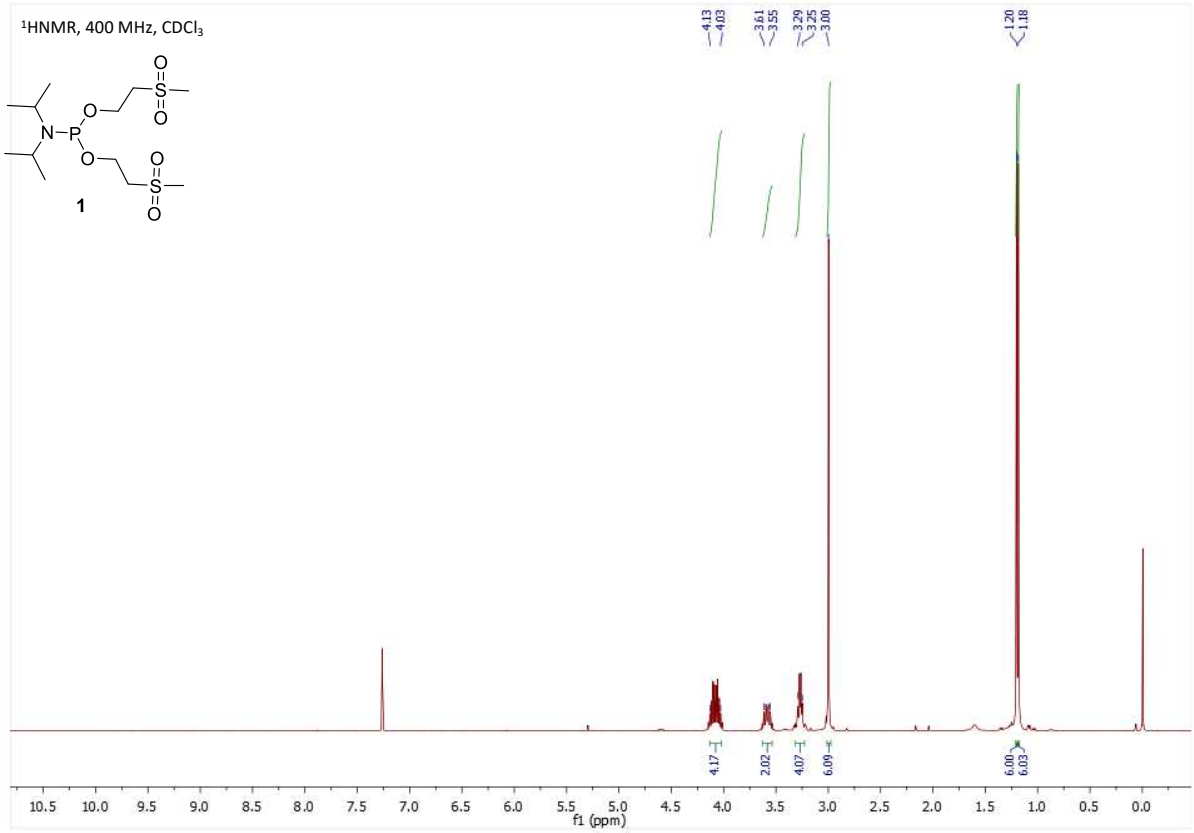

^{31}PNMR, 162 MHz, $CDCl_3$

1

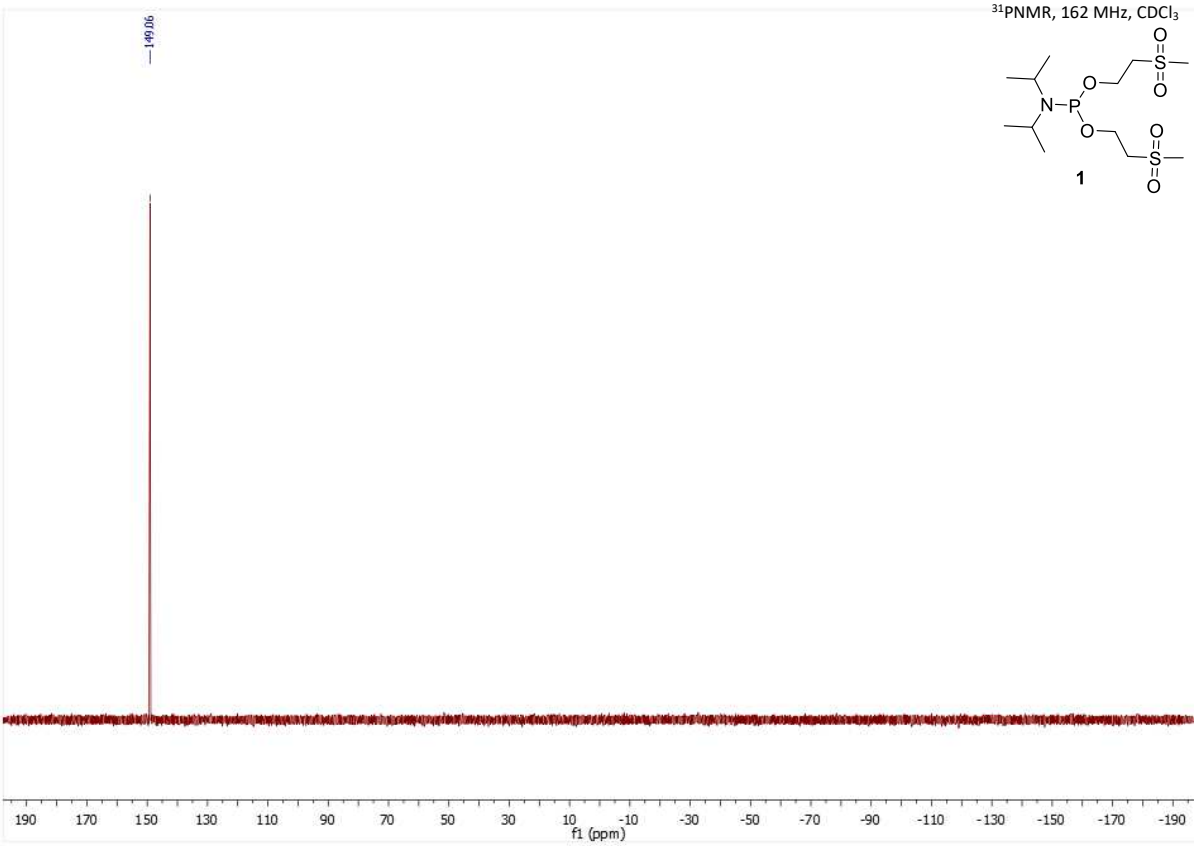

^{13}CNMR, 100 MHz, $CDCl_3$

1

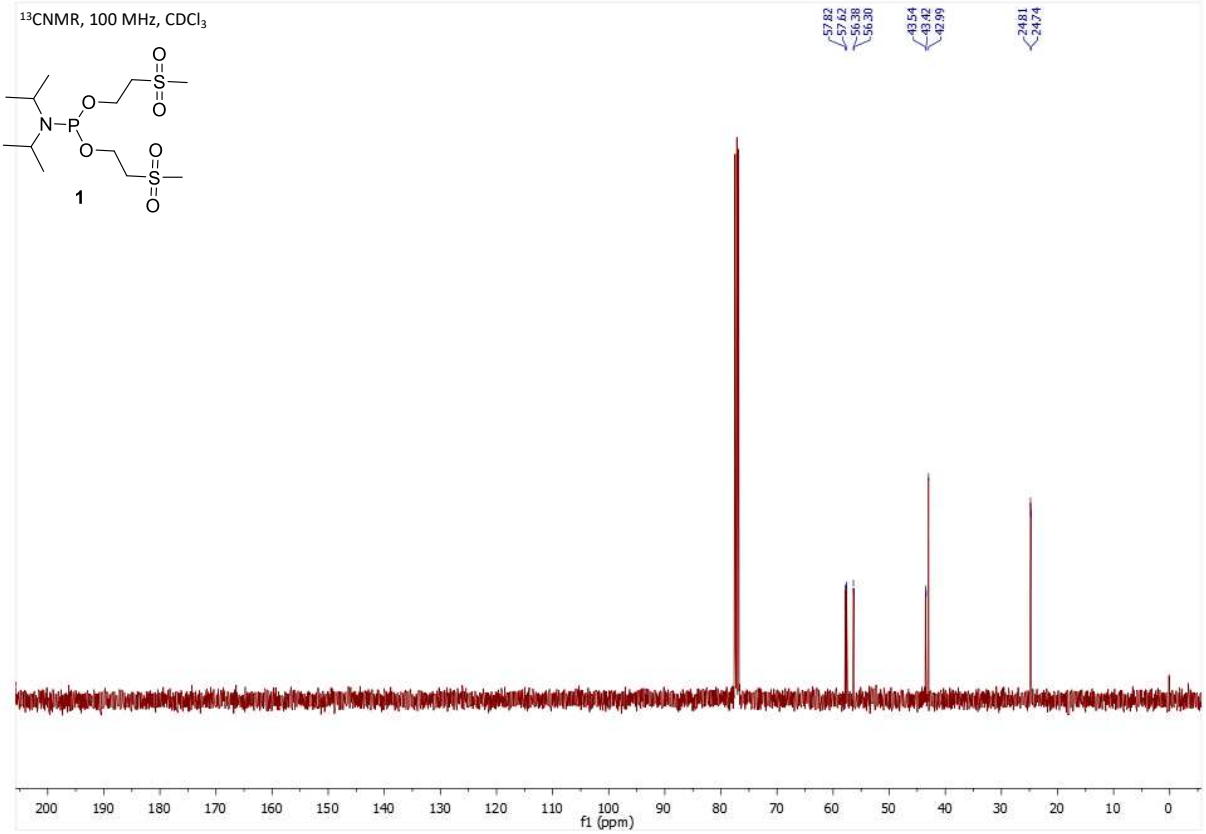

^{1}H-^{1}H COSY

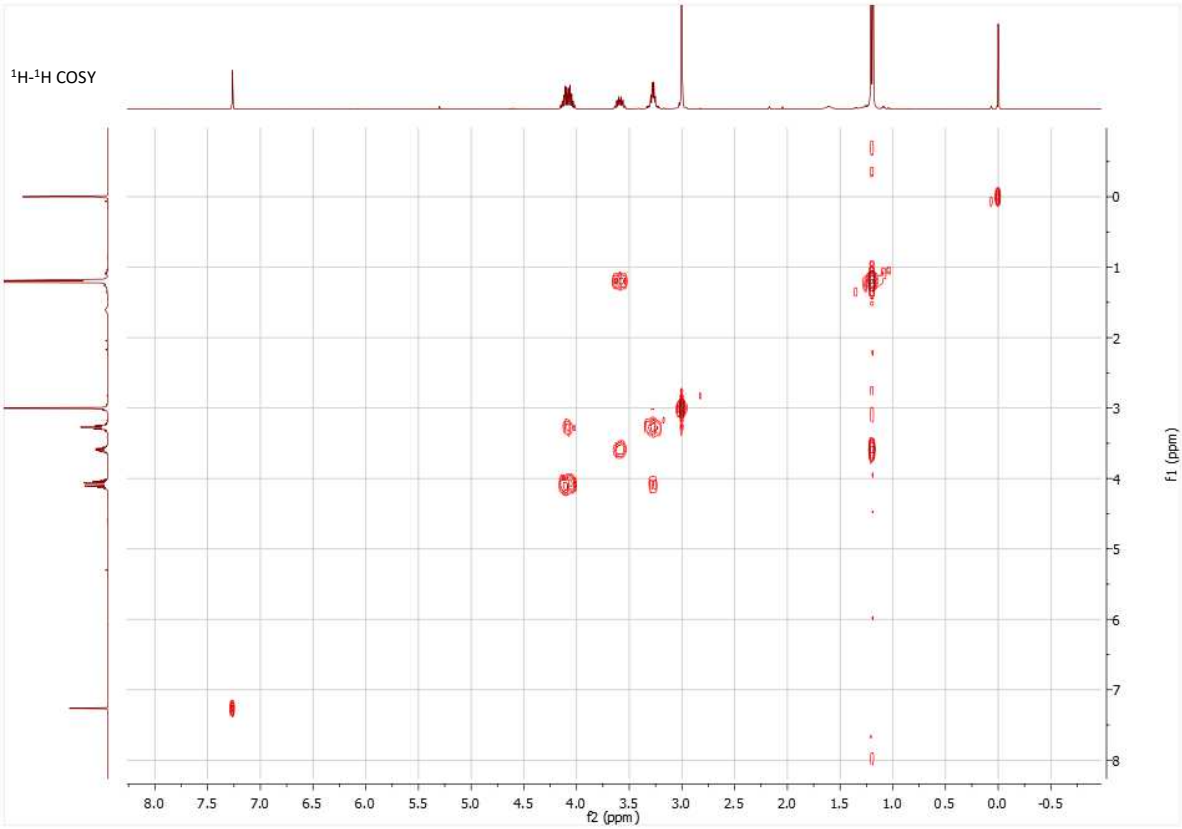

^{1}H-^{13}C HSQC

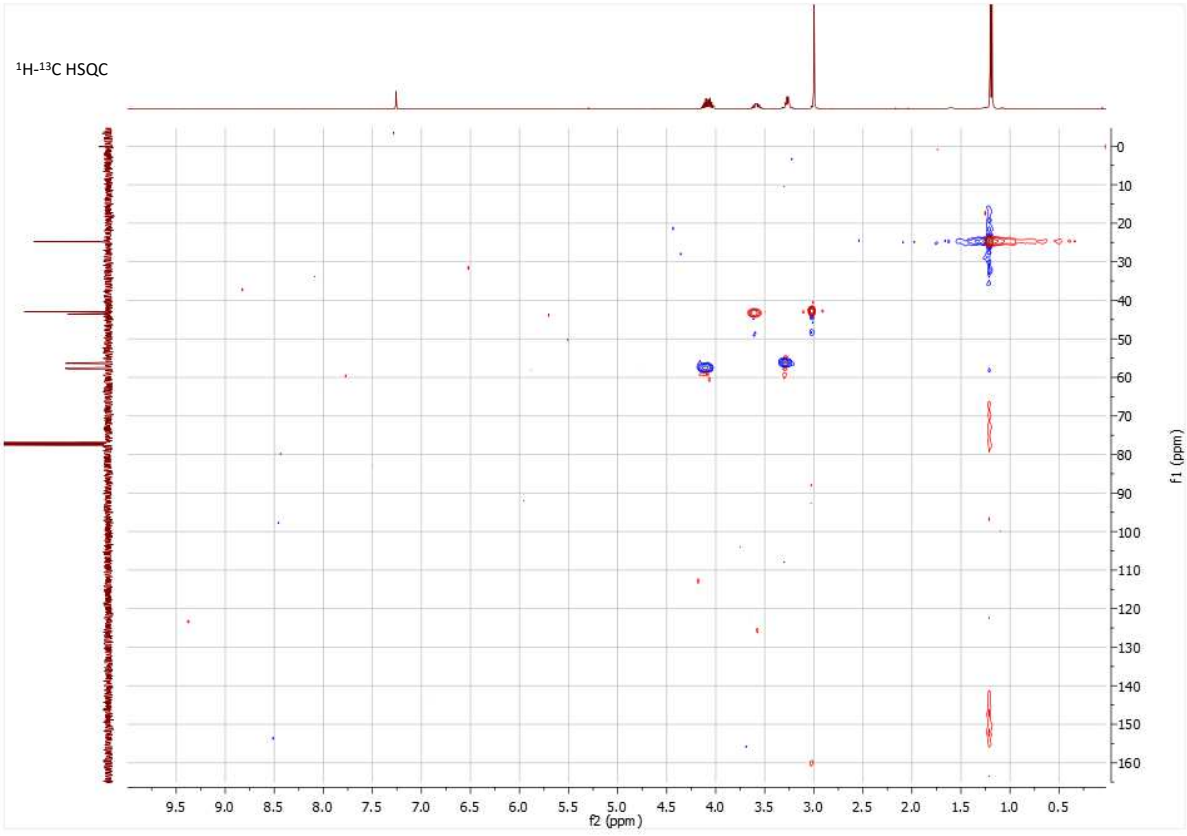

2-*O*-Benzyl-1,6:3,4-bis-*O*-(2,3-dimethoxybutane-2,3-diyl)-*myo*-inositol-5-bis[2-(methanesulfonyl)ethyl]phosphate (**6**)

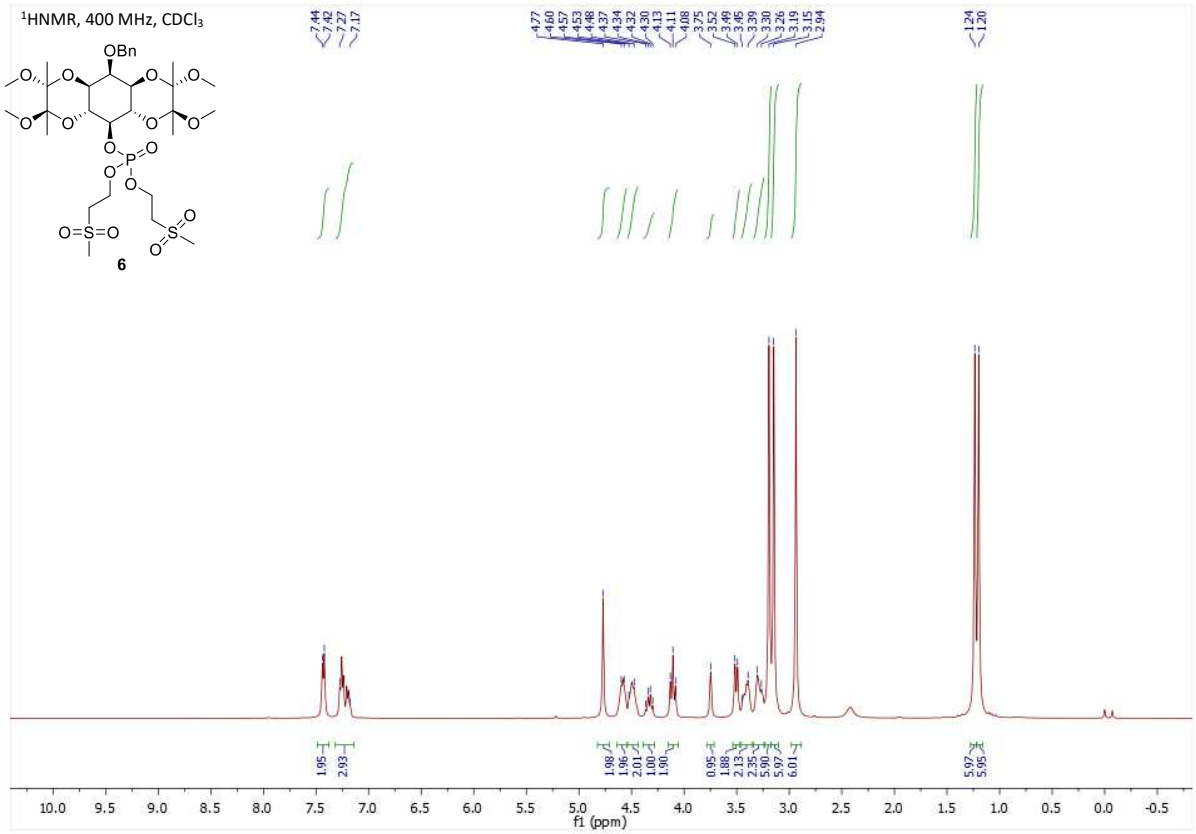

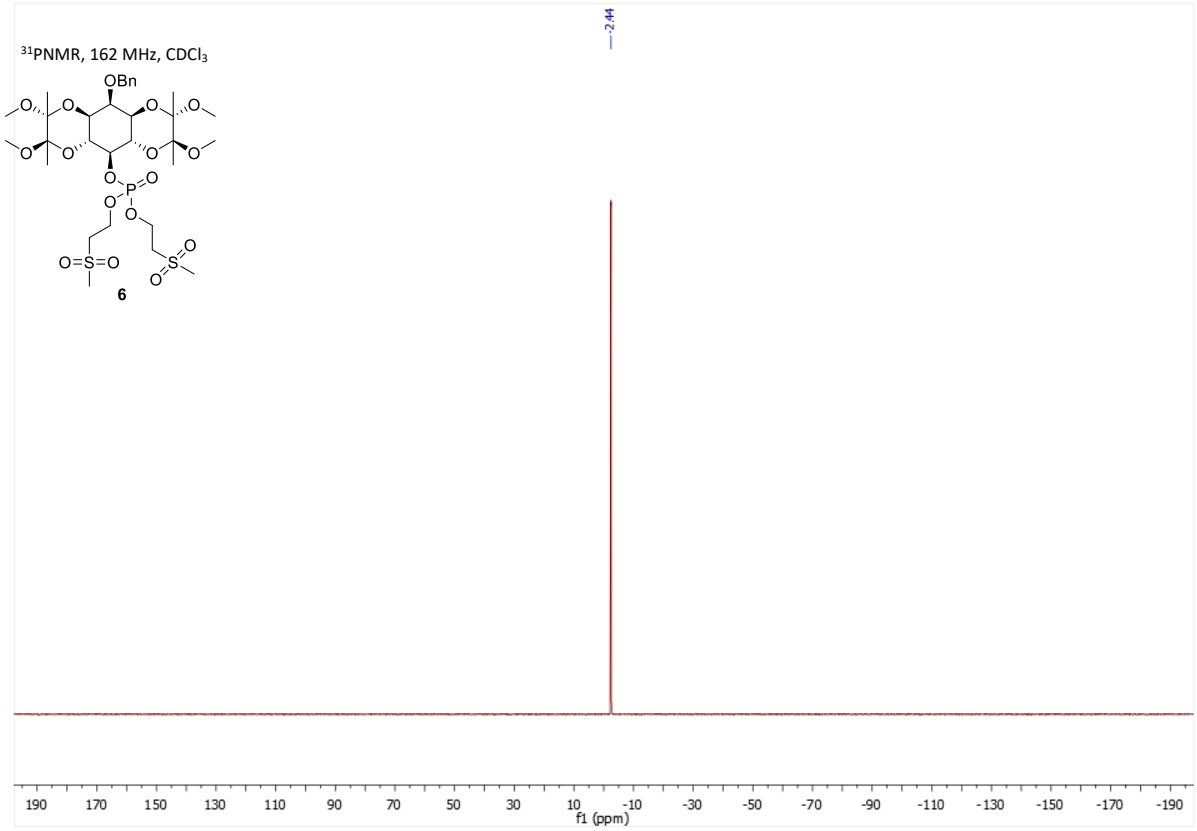

^{13}CNMR, 100 MHz, $CDCl_3$

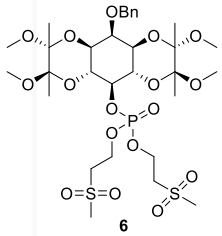

6

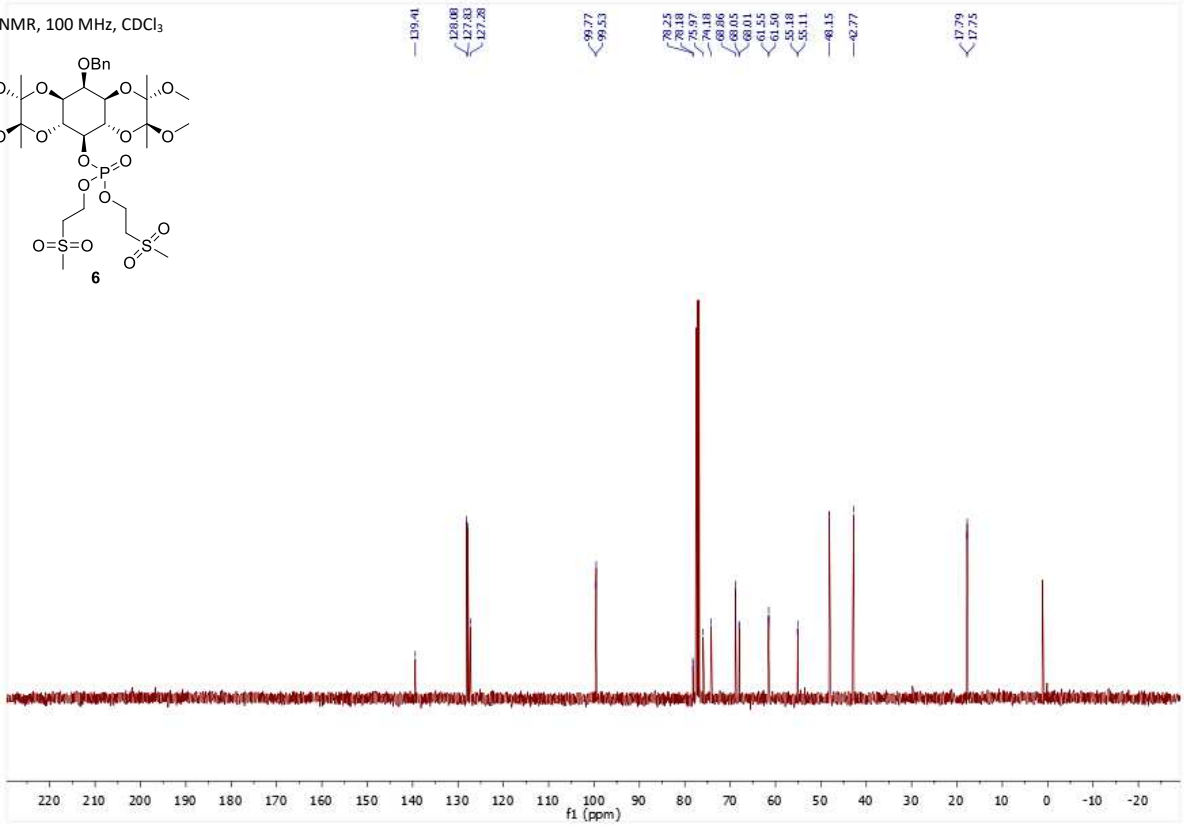

^{1}H-^{1}H COSY

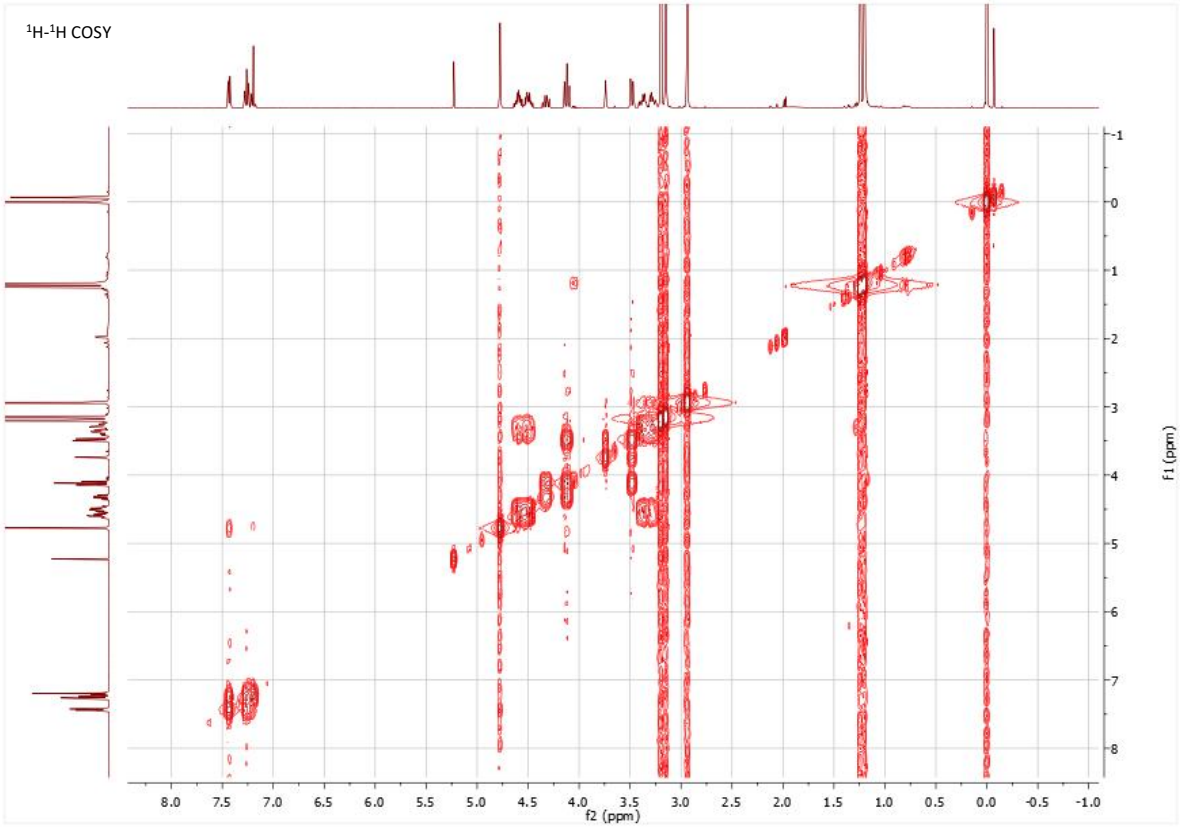

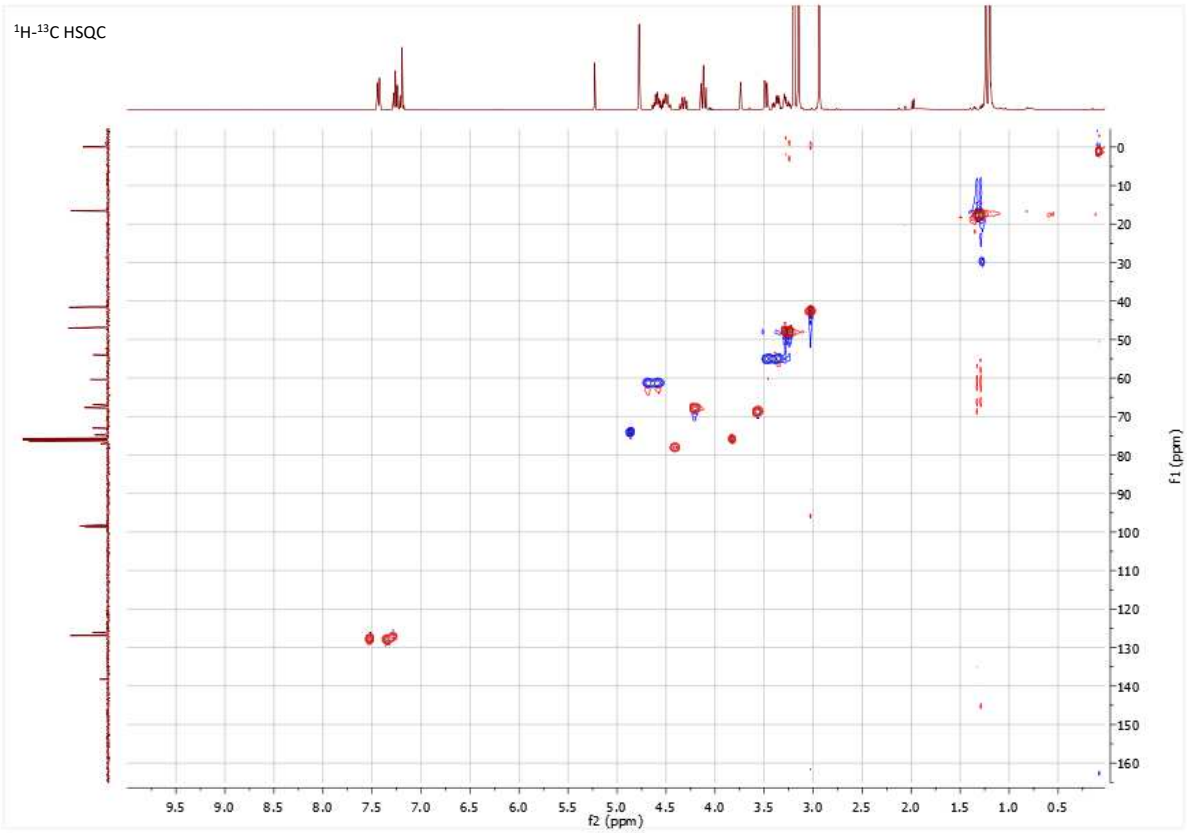

2-*O*-Benzyl-*myo*-inositol-5-bis[2-(methanesulfonyl)ethyl]phosphate (**7**)

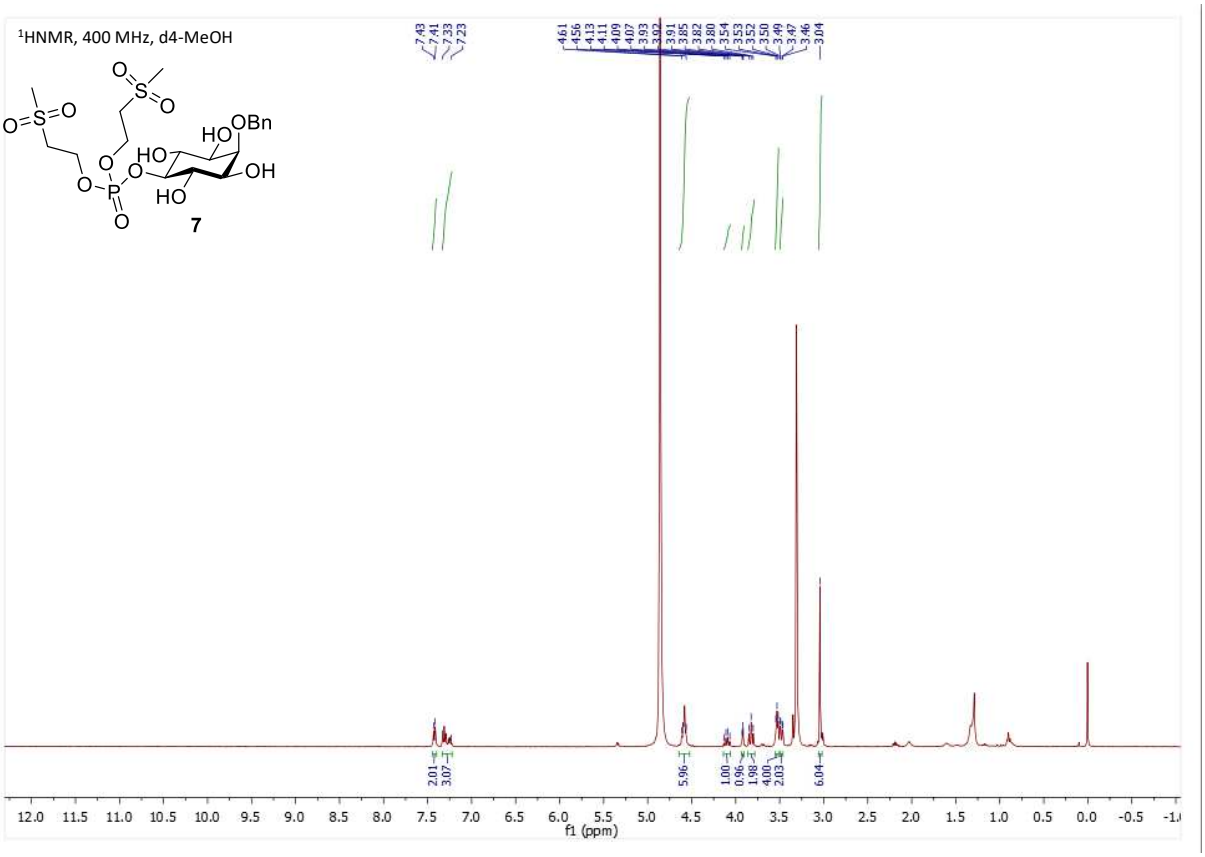

^{31}PNMR, 162 MHz, d6-DMSO

7

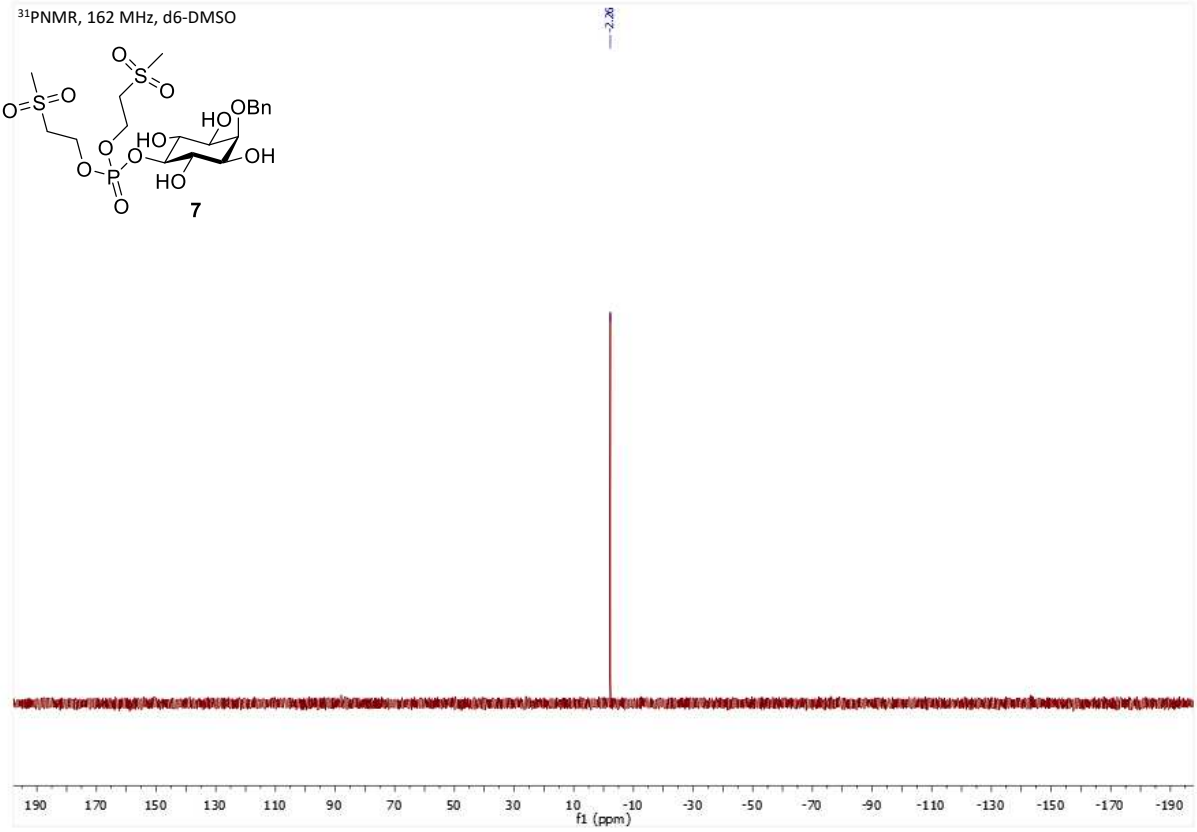

^{13}CNMR, 100 MHz, d6-DMSO

7

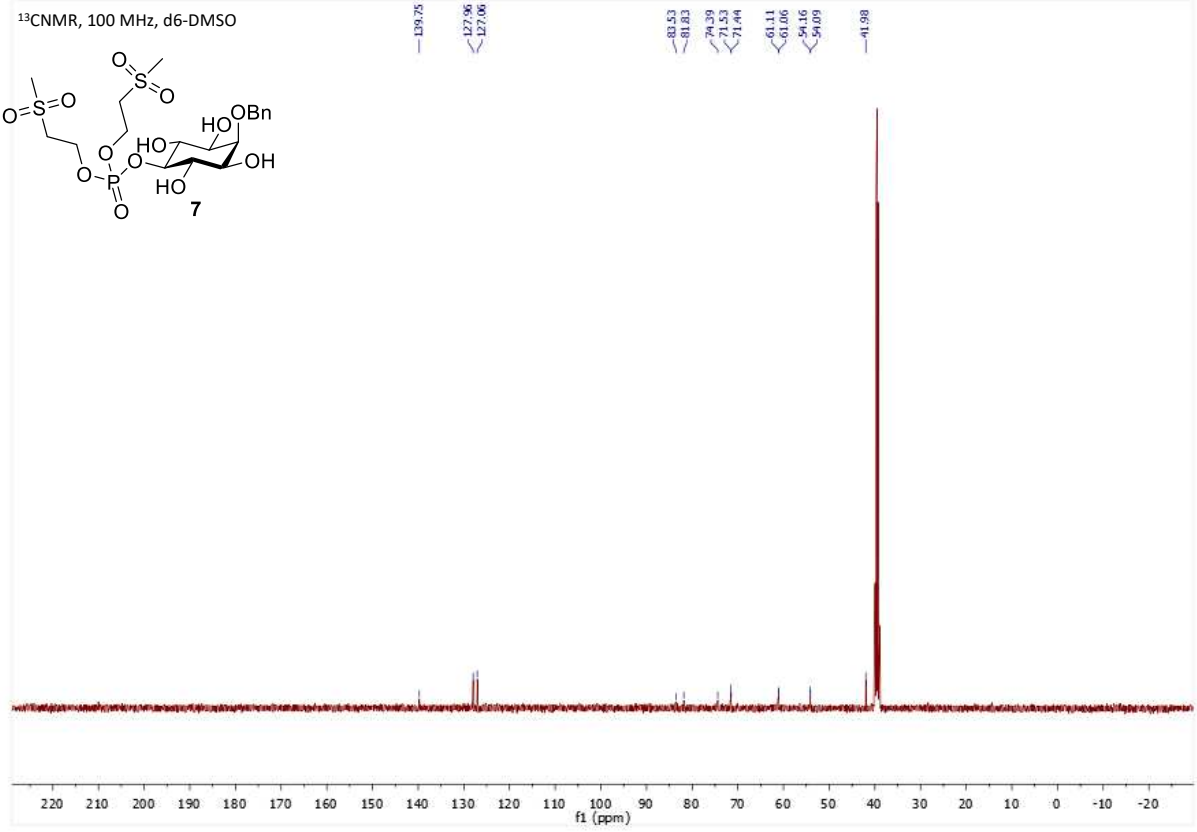

^{1}H-^{1}H COSY

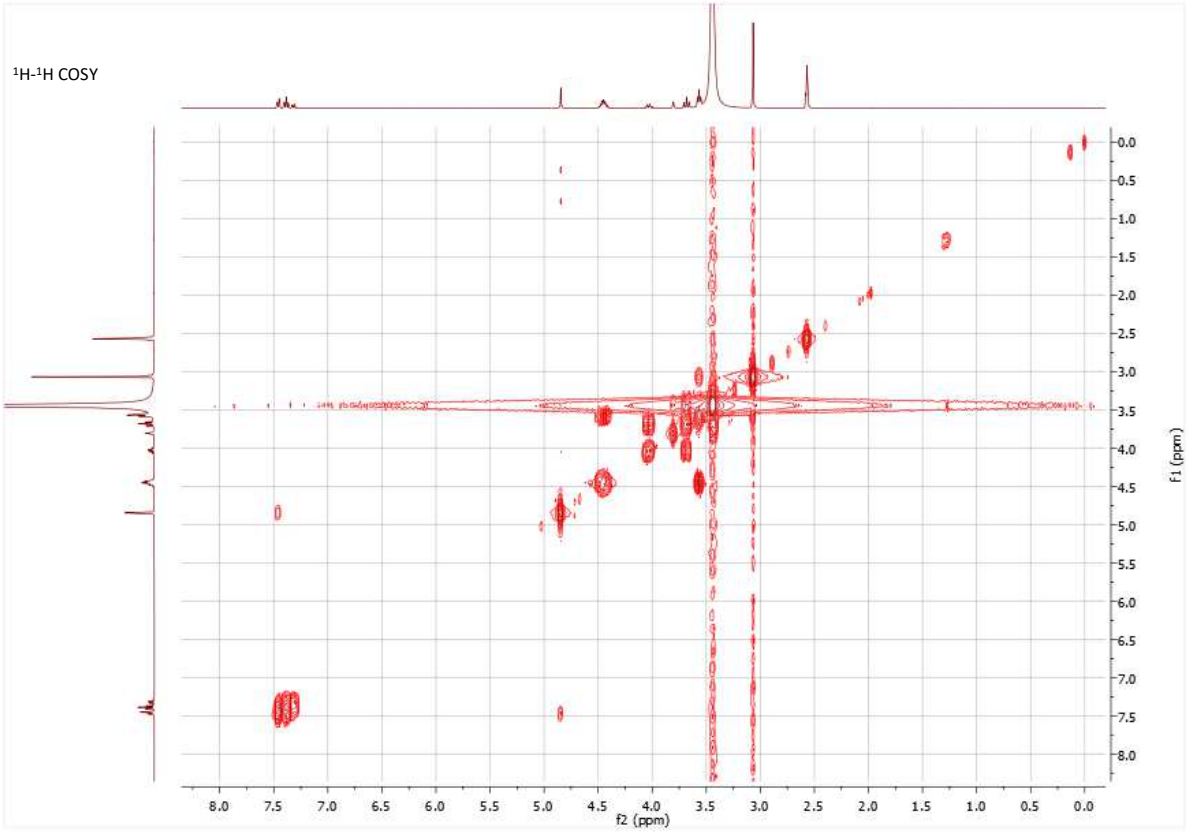

^{1}H-^{13}C HSQC

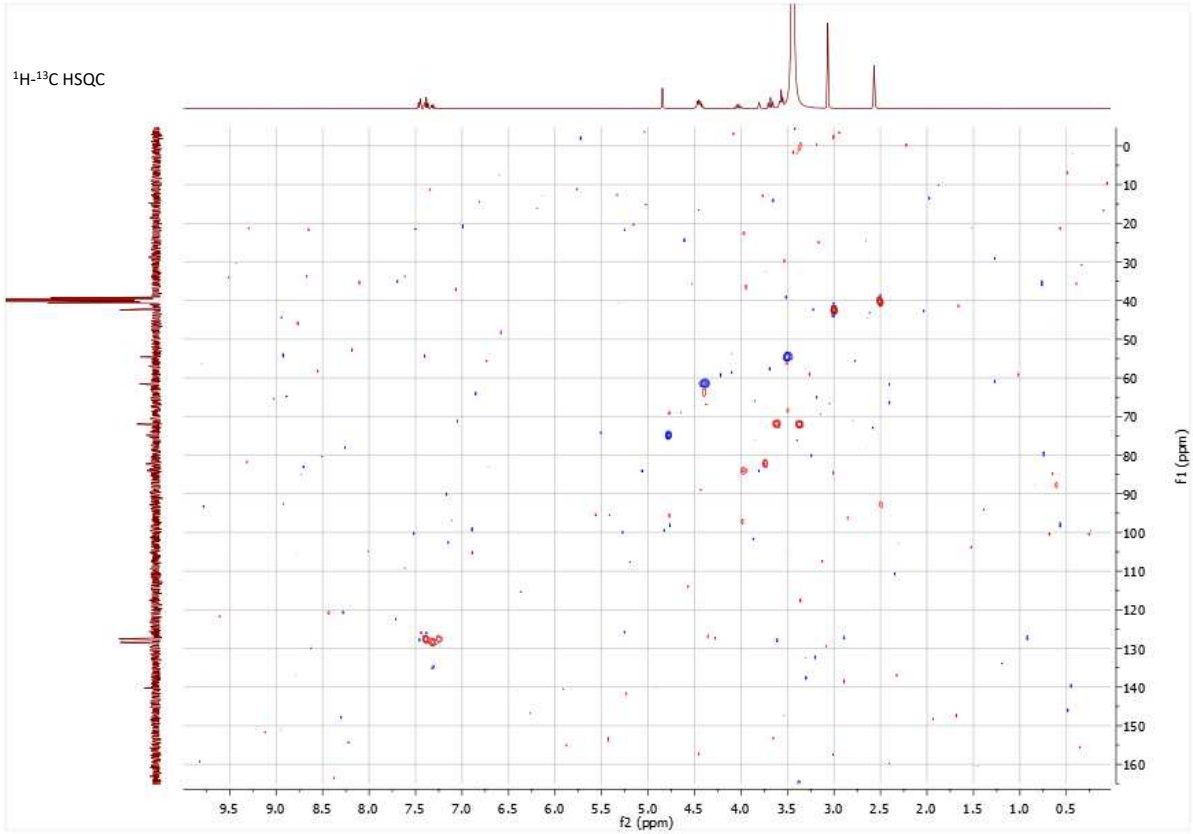

myo-Inositol-5-bis[2-(methanesulfonyl)ethyl]phosphate (**8**)

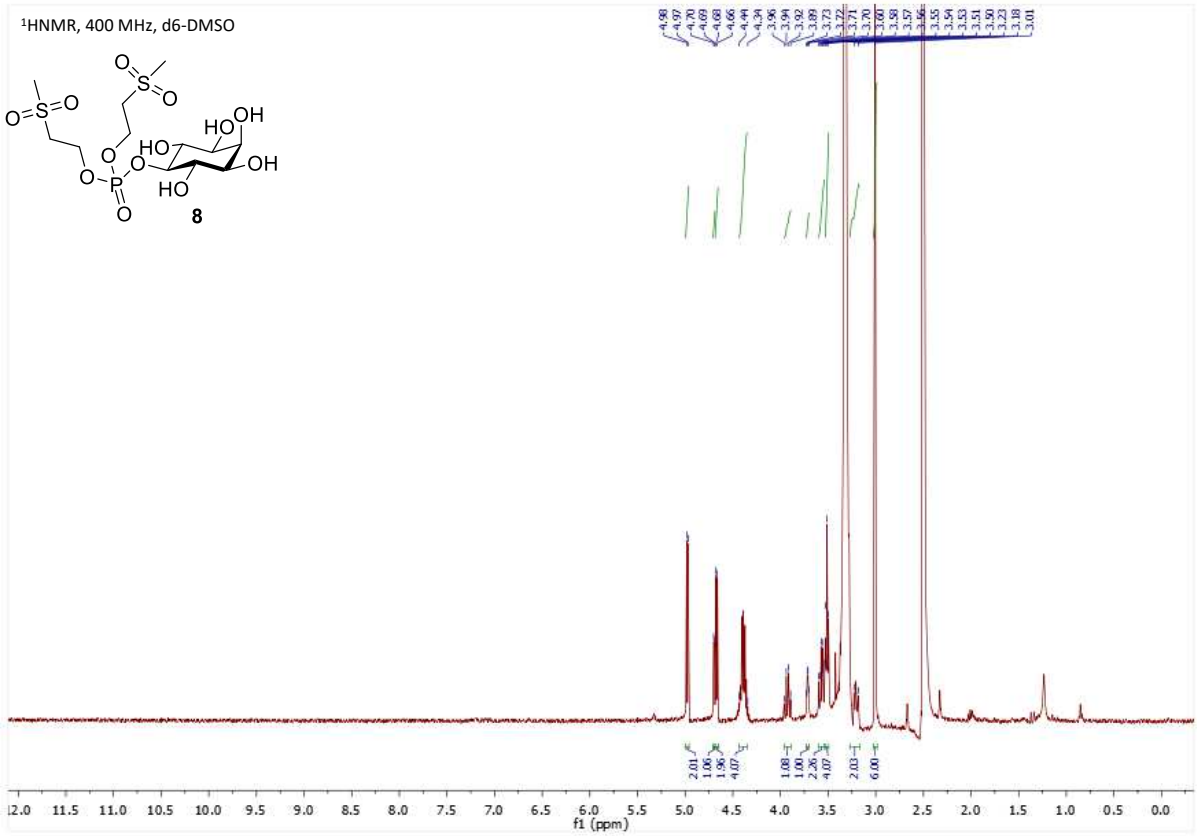

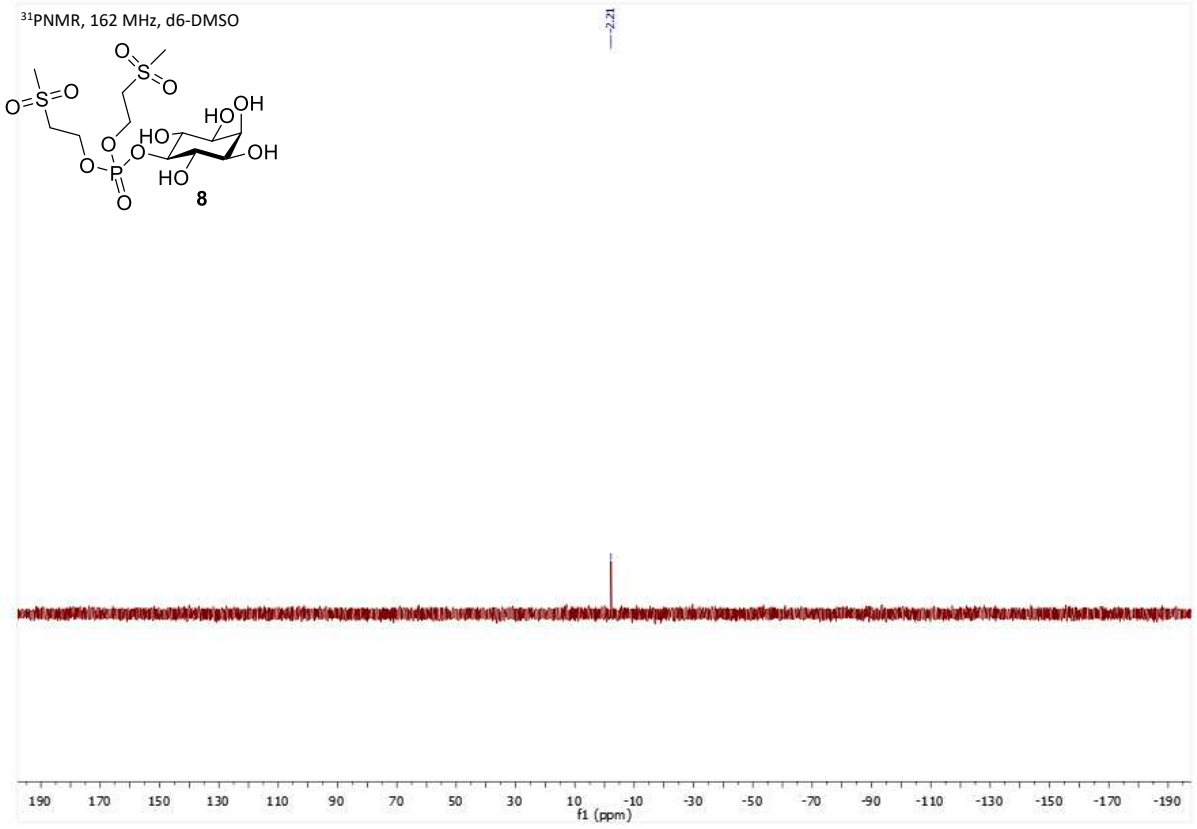

myo-Inositol-1,2,3,4,6-pentakis(dibenzyl)phosphate-5-bis[2-(methanesulfonyl)ethyl]-phosphate (**9**)

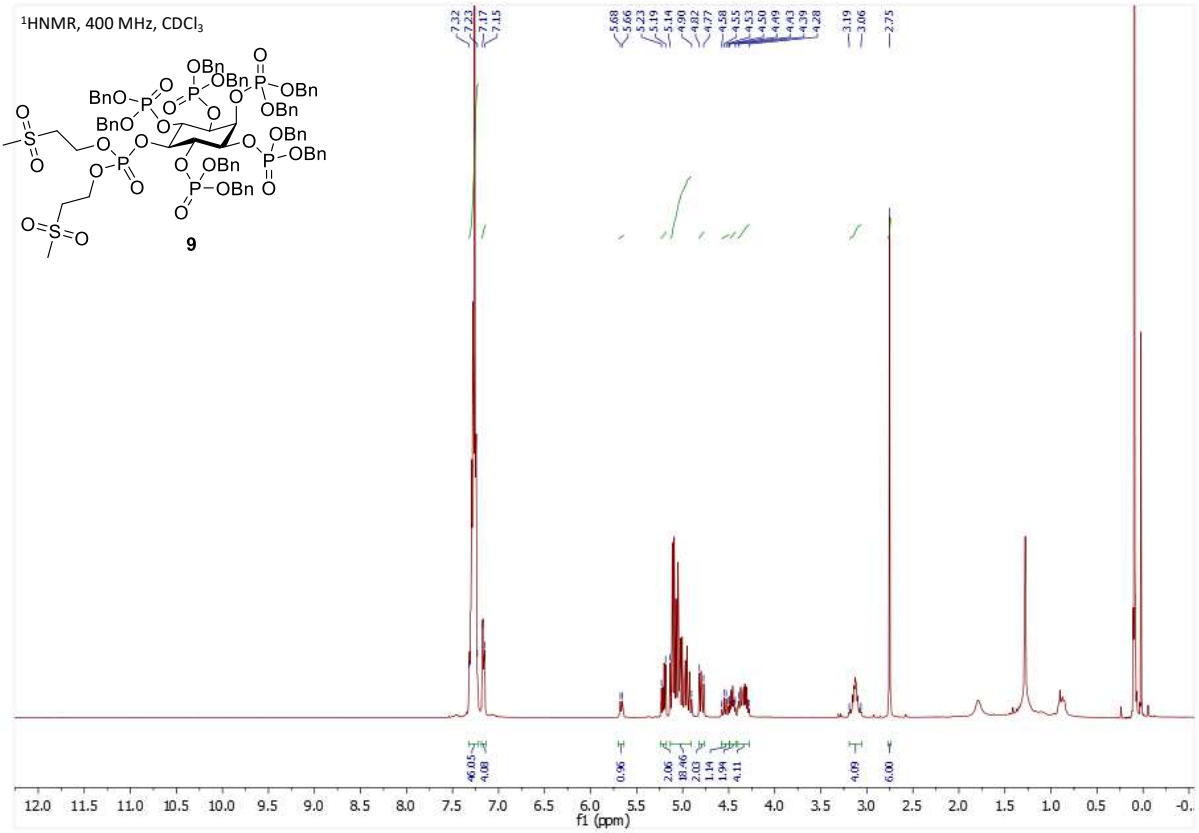

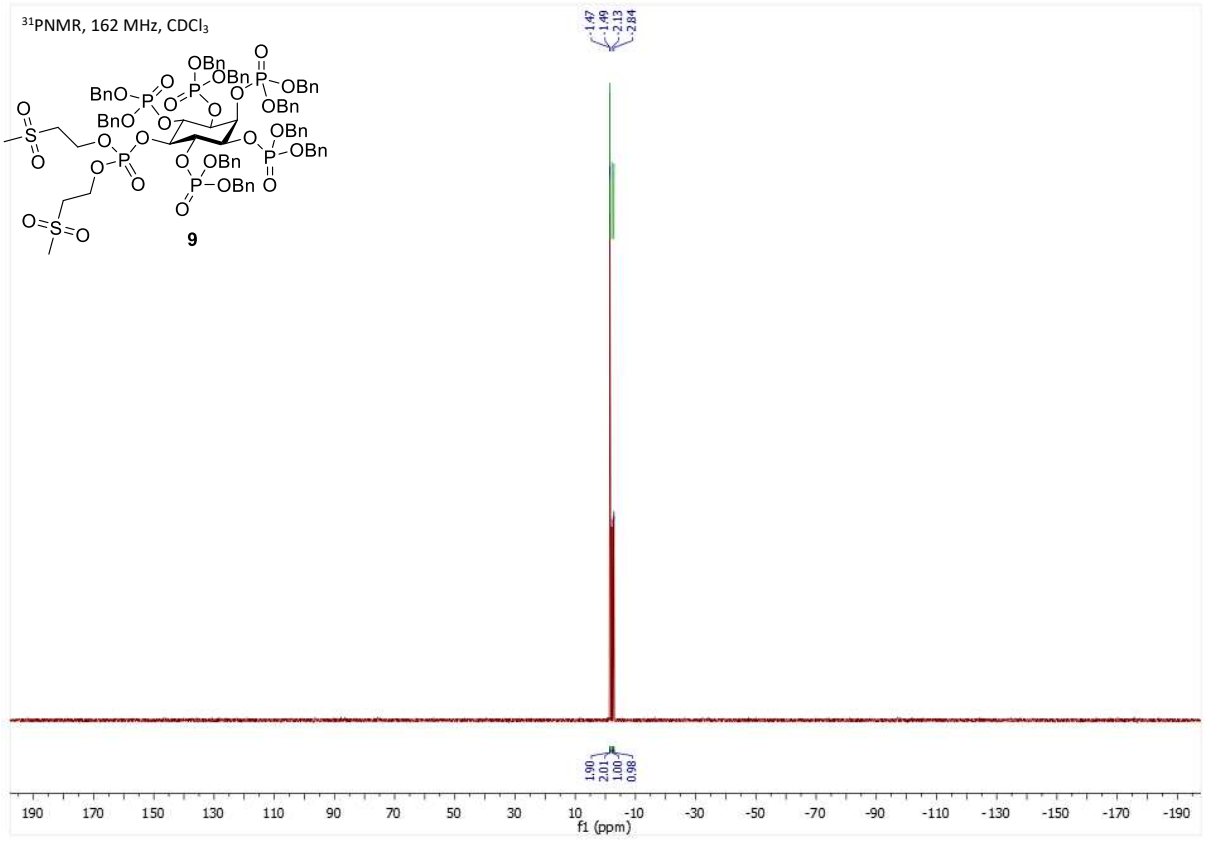

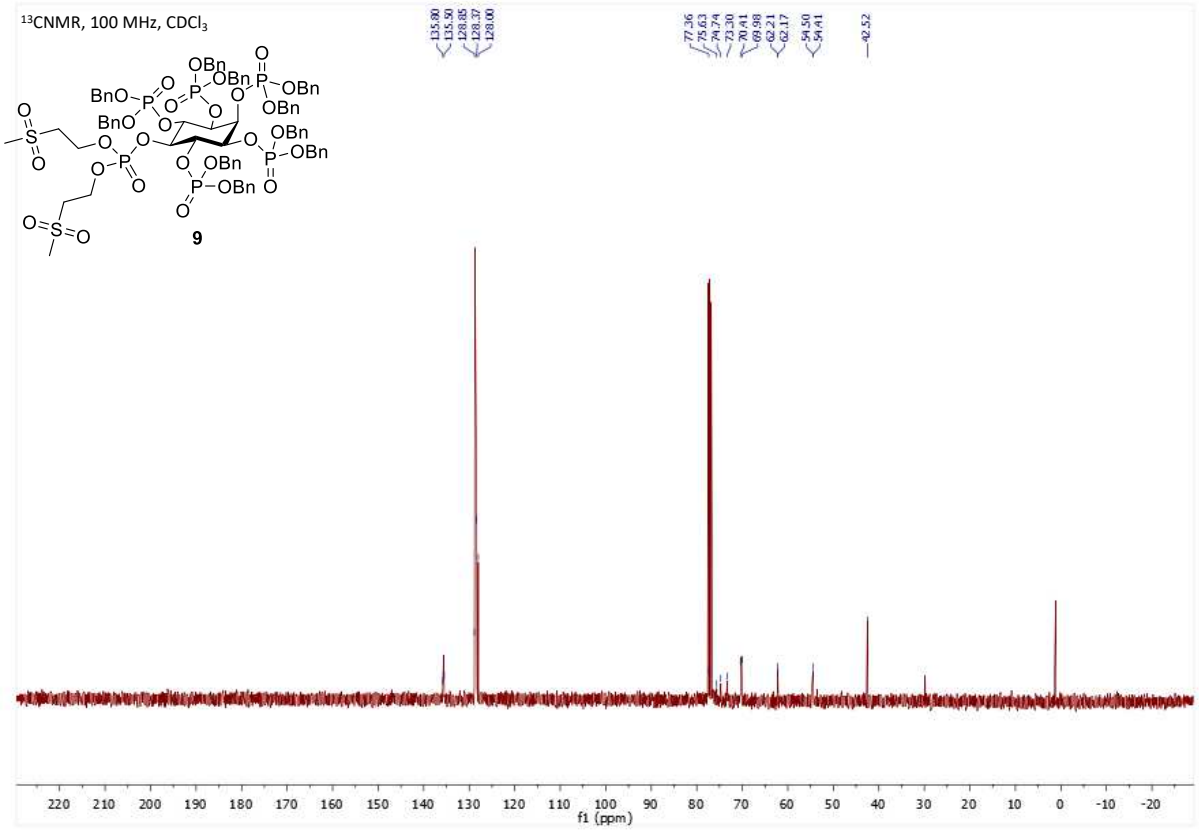
^{13}CNMR, 100 MHz, $CDCl_3$
9
135.90
135.50
128.85
128.37
128.00
77.36
75.63
74.74
73.30
70.41
69.98
62.21
62.17
54.50
54.41
42.52
f1 (ppm)

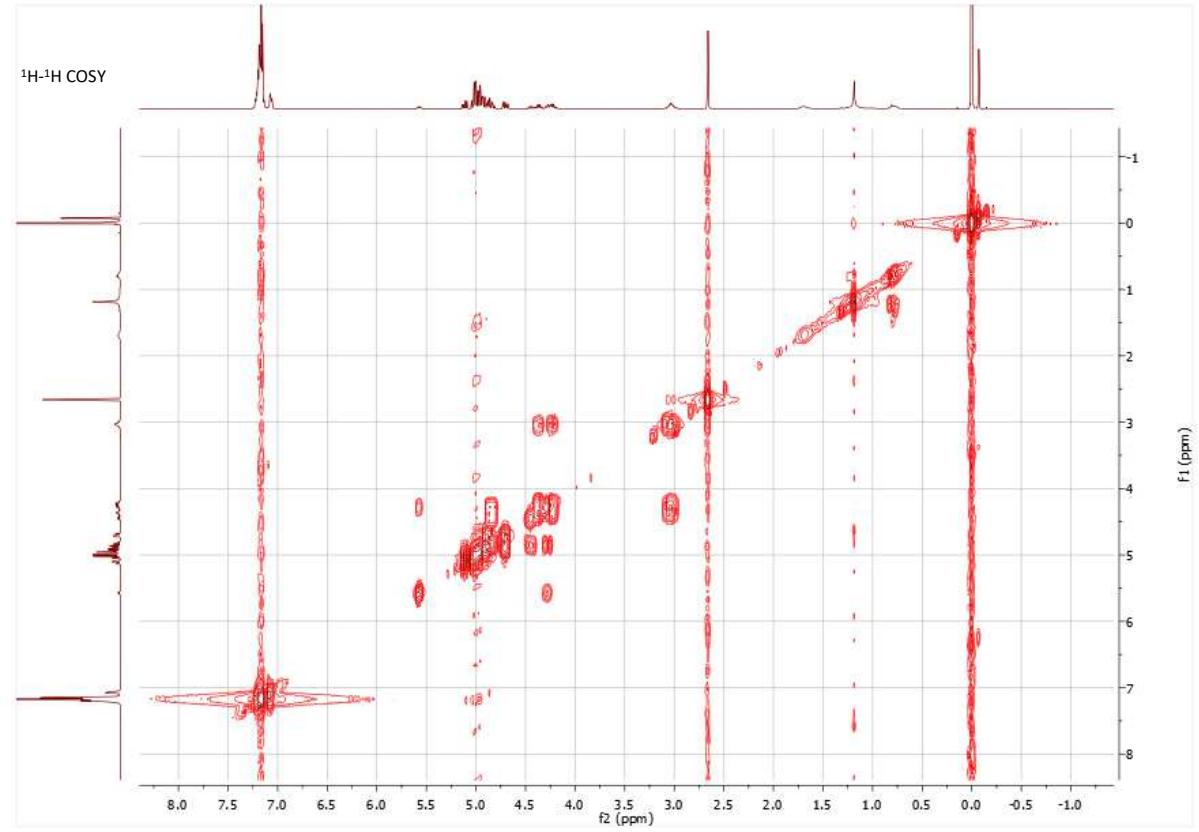
^{1}H-^{1}H COSY
f2 (ppm)
f1 (ppm)

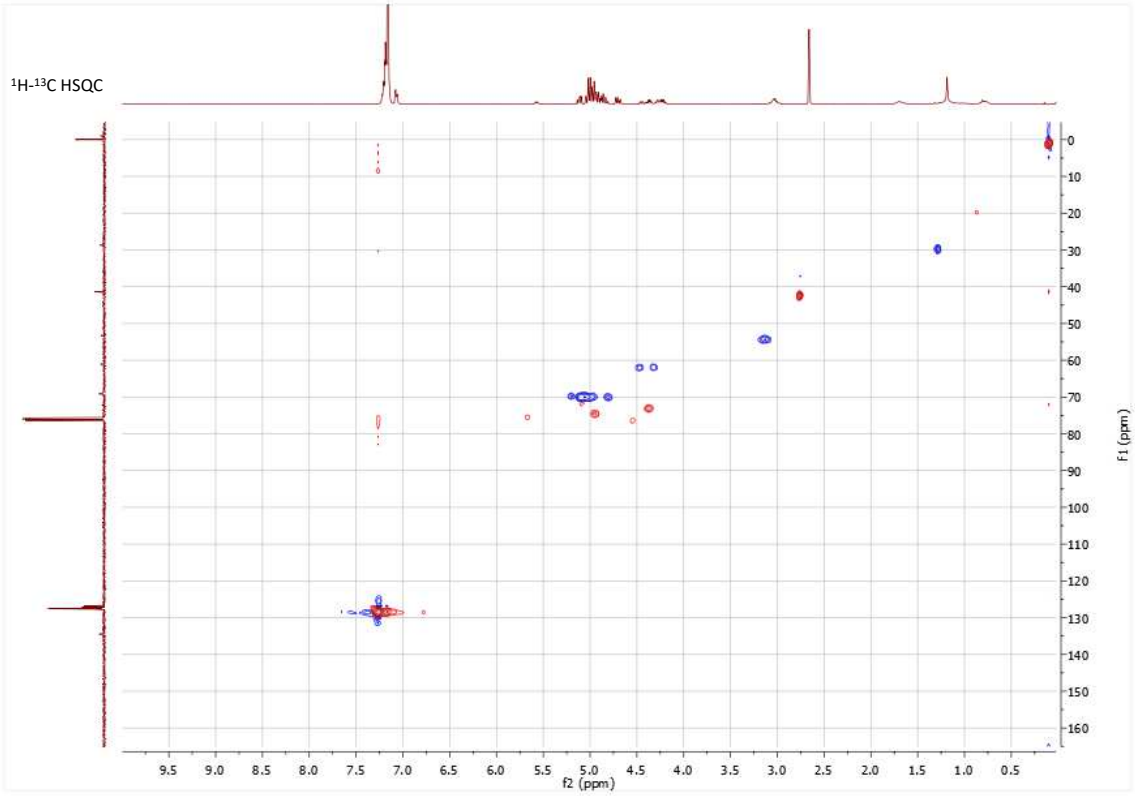

5-Diphospho-*myo*-inositol-1,2,3,4,6-pentakisphosphate triethylammonium salt (**2**)

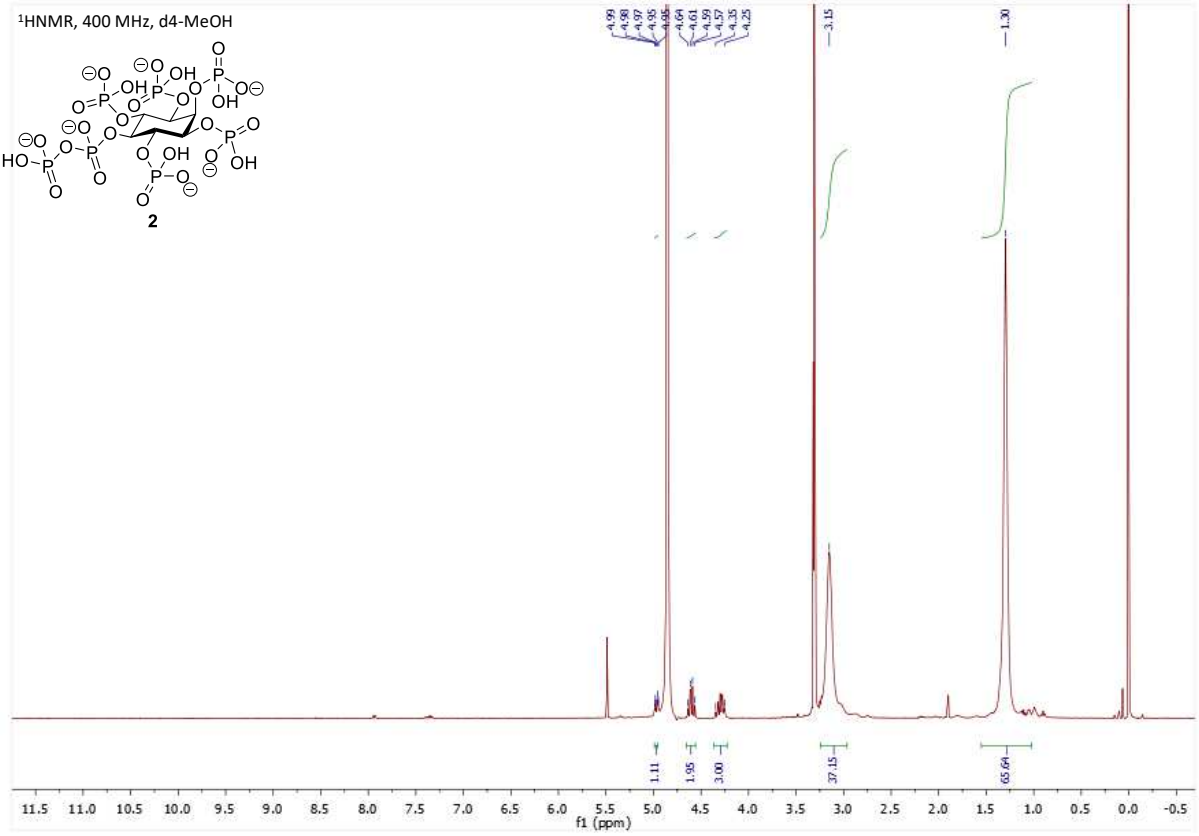

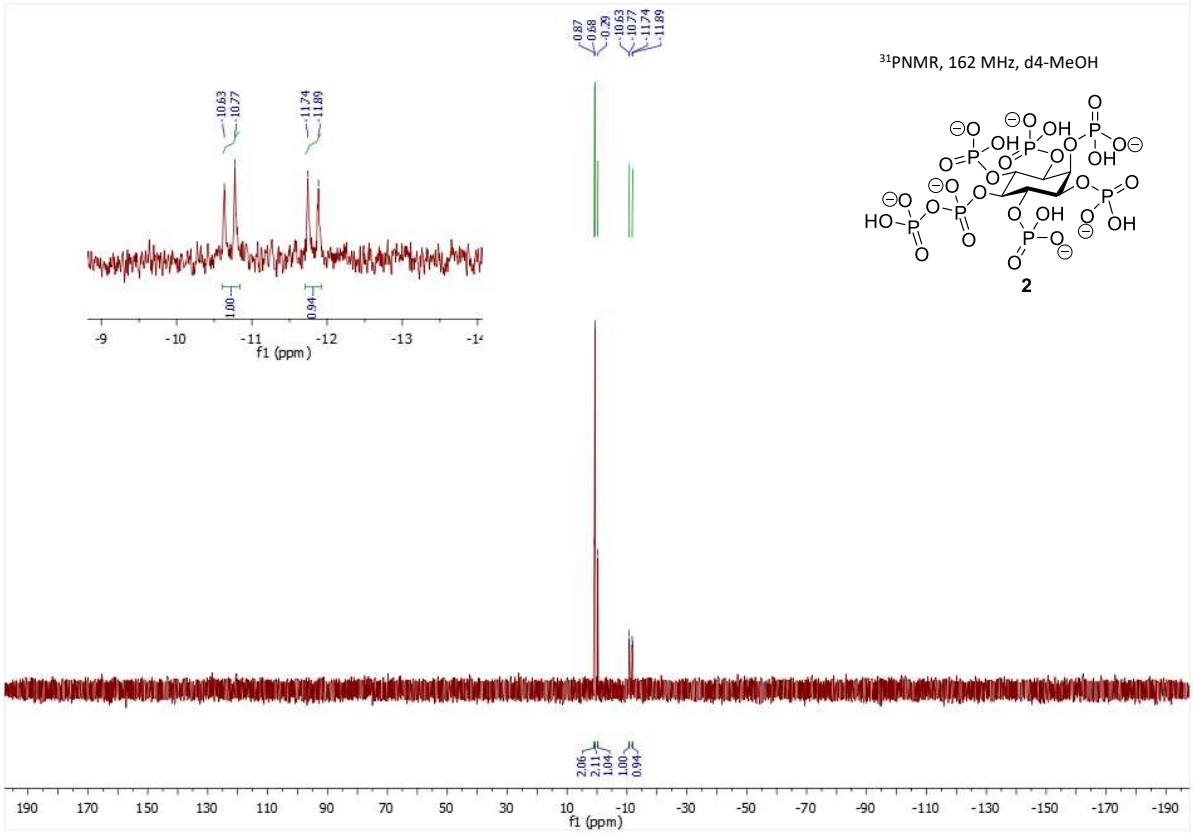
31PNMR, 162 MHz, d4-MeOH
2
f1 (ppm)

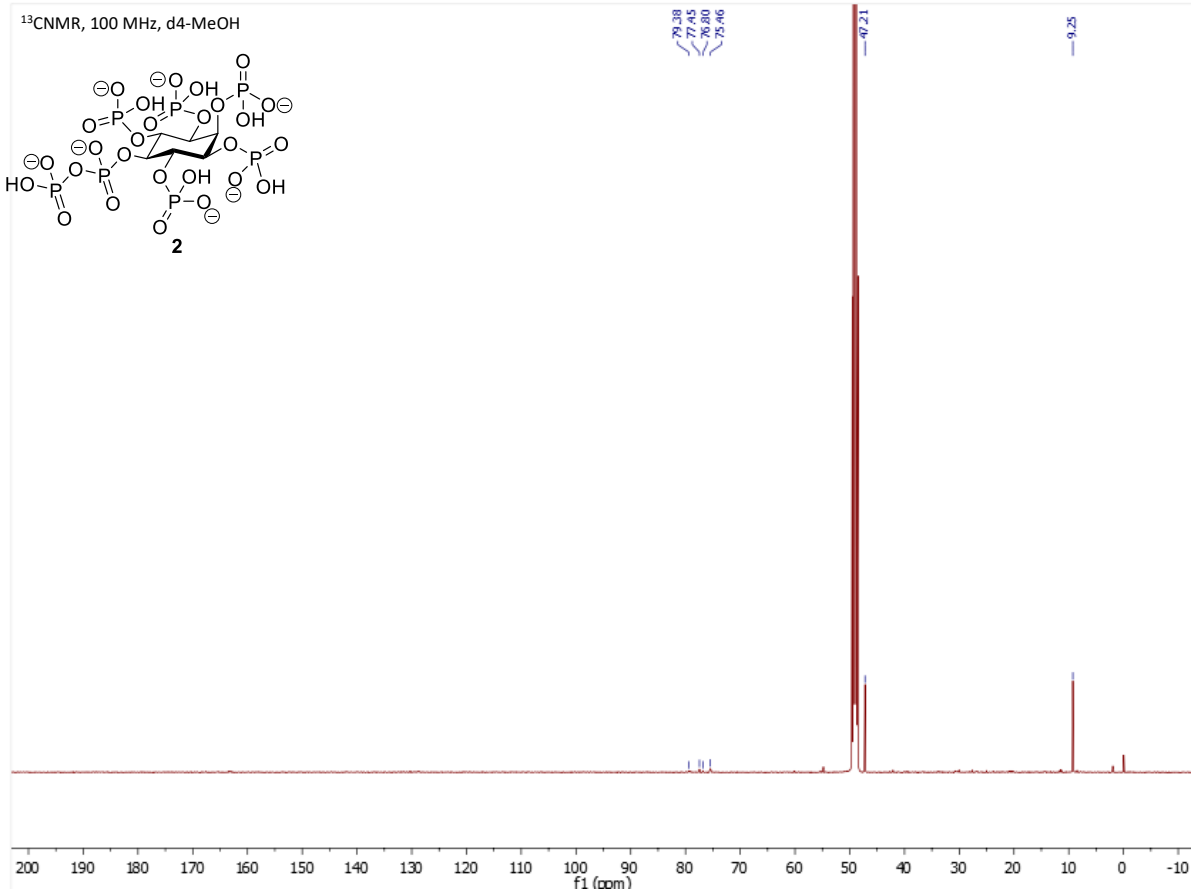
13CNMR, 100 MHz, d4-MeOH
2
f1 (ppm)

^{1}H-^{1}H COSY

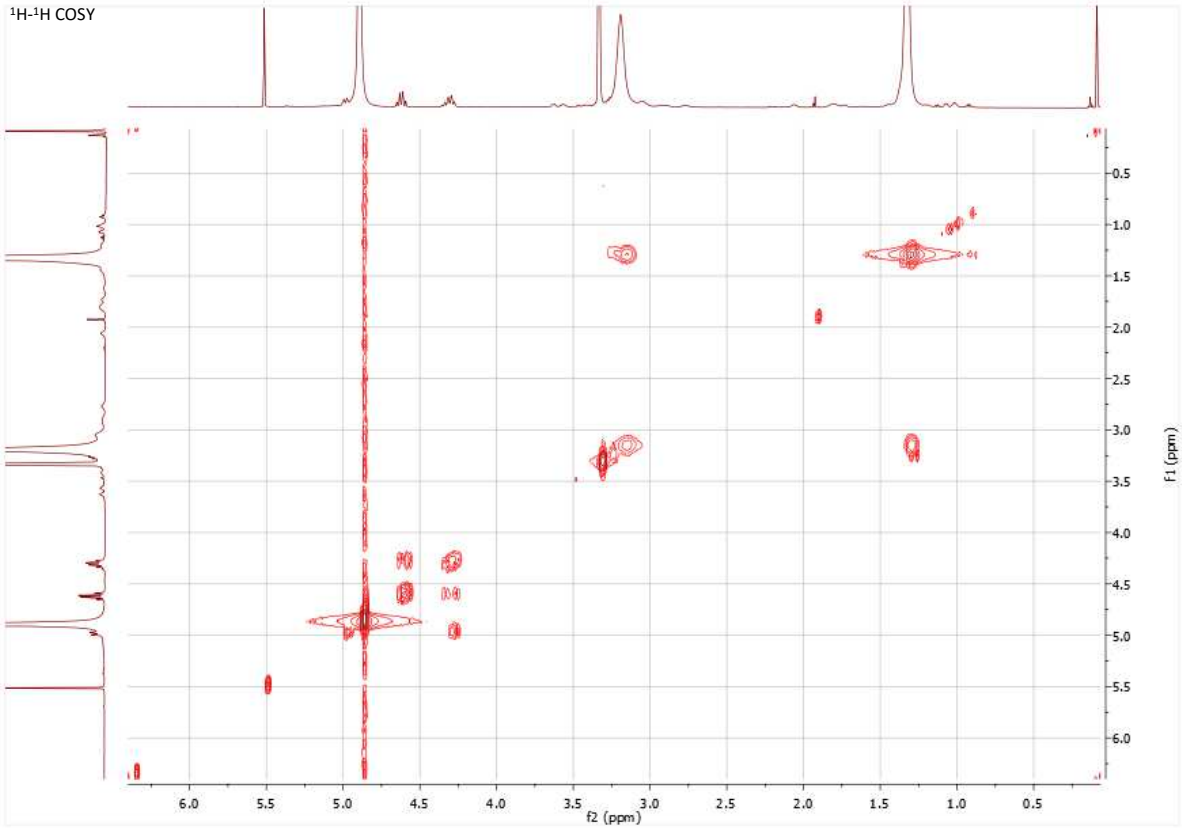

^{1}H-^{13}C HSQC

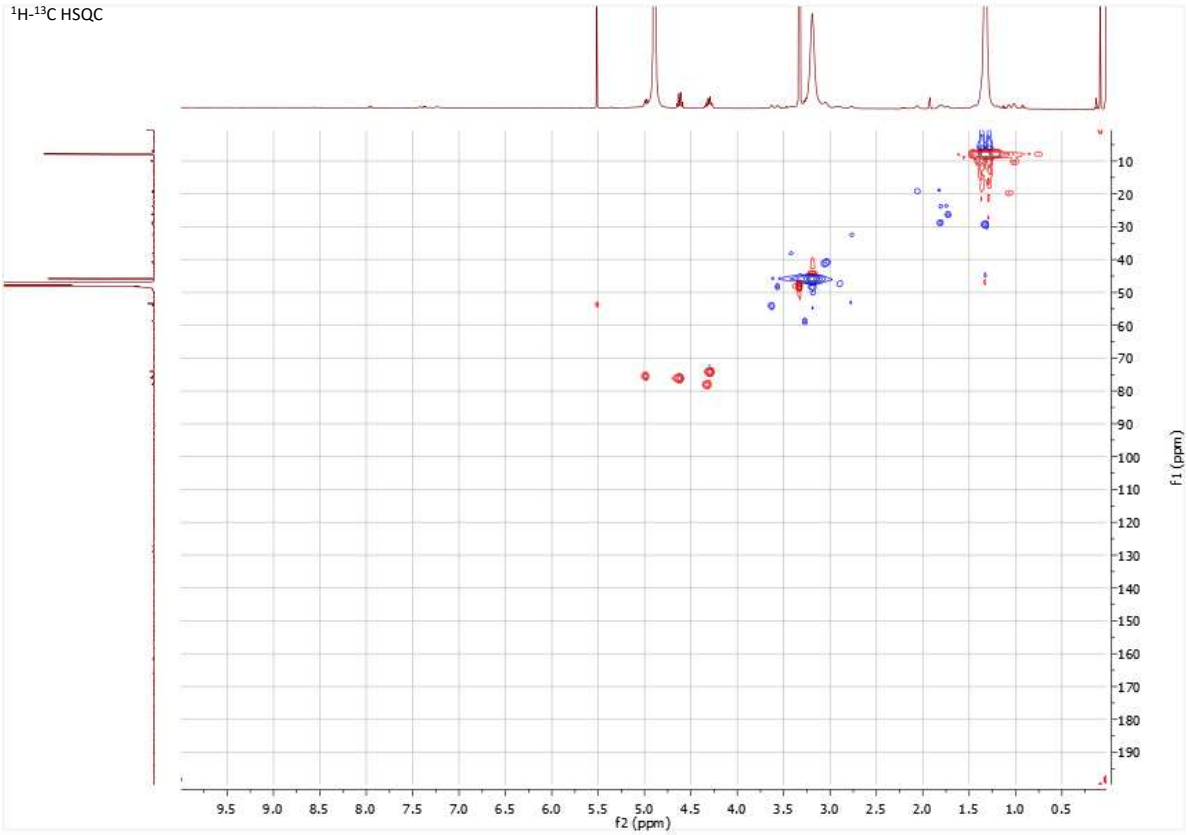

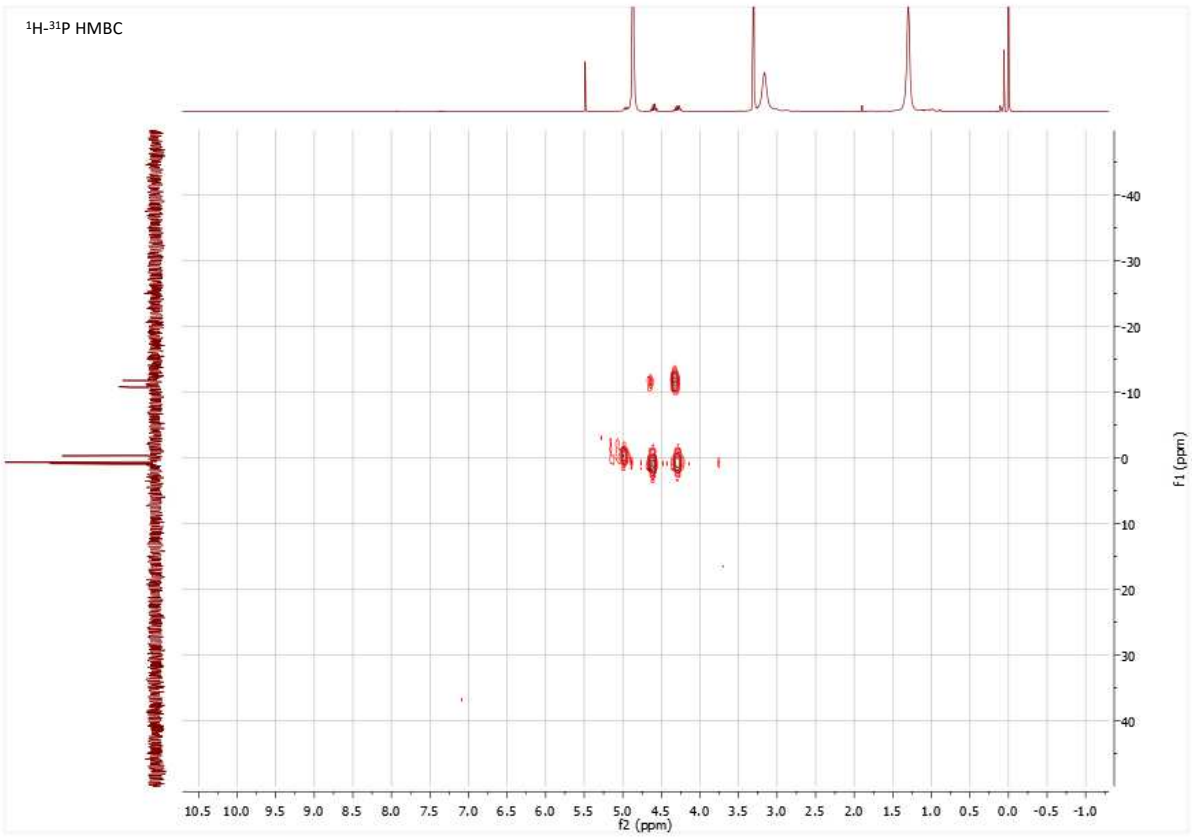

2-*O*-Benzyl-*myo*-inositol-1,3,4,6-tetrakis(dibenzyl)phosphate-5-bis[2-(methanesulfonyl)ethyl]-phosphate (**11**)

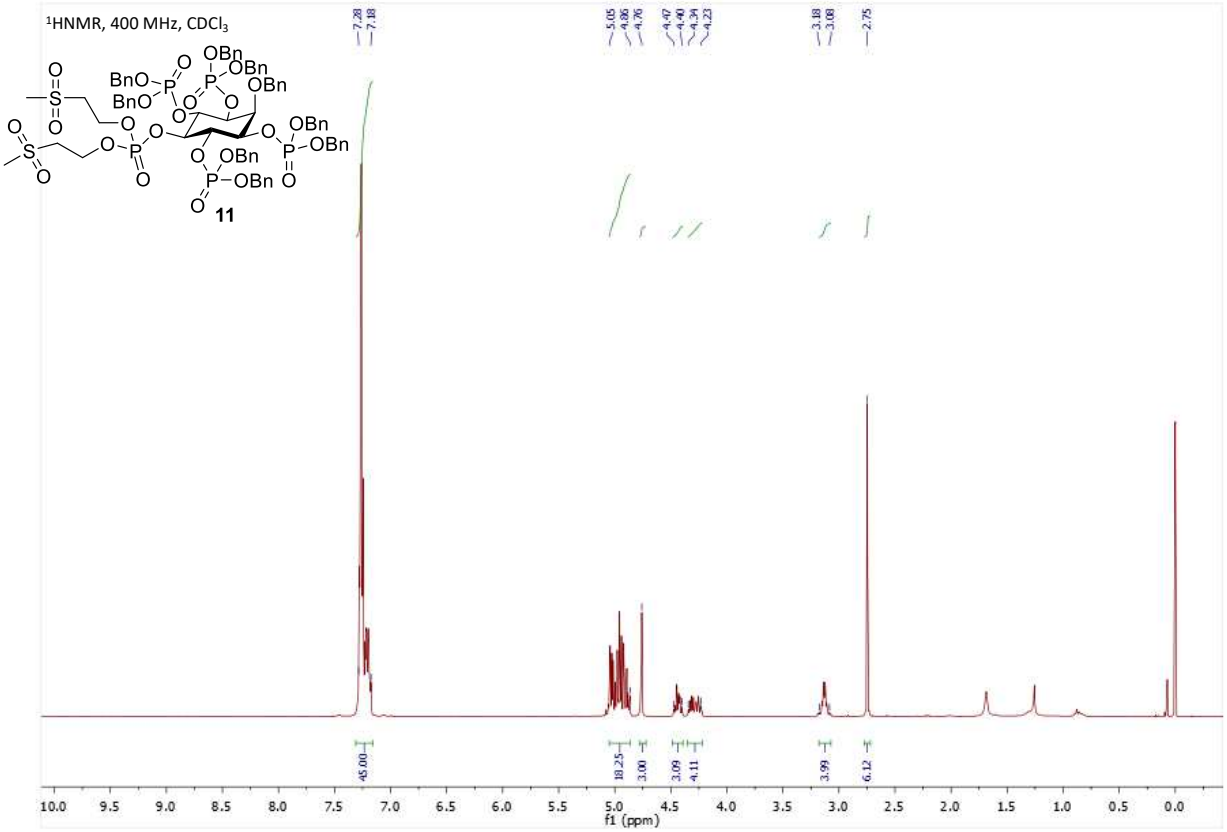

^{31}PNMR, 162 MHz, $CDCl_3$

11

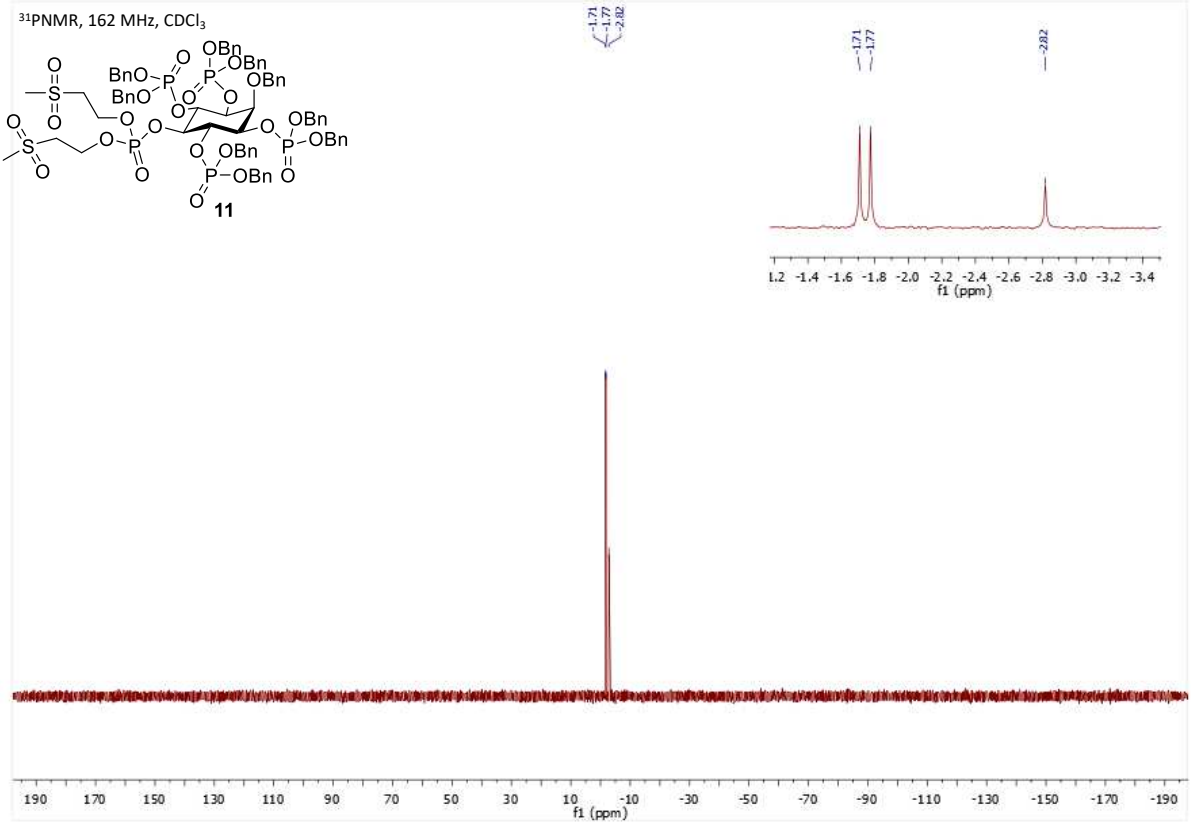

^{13}CNMR, 100 MHz, $CDCl_3$

11

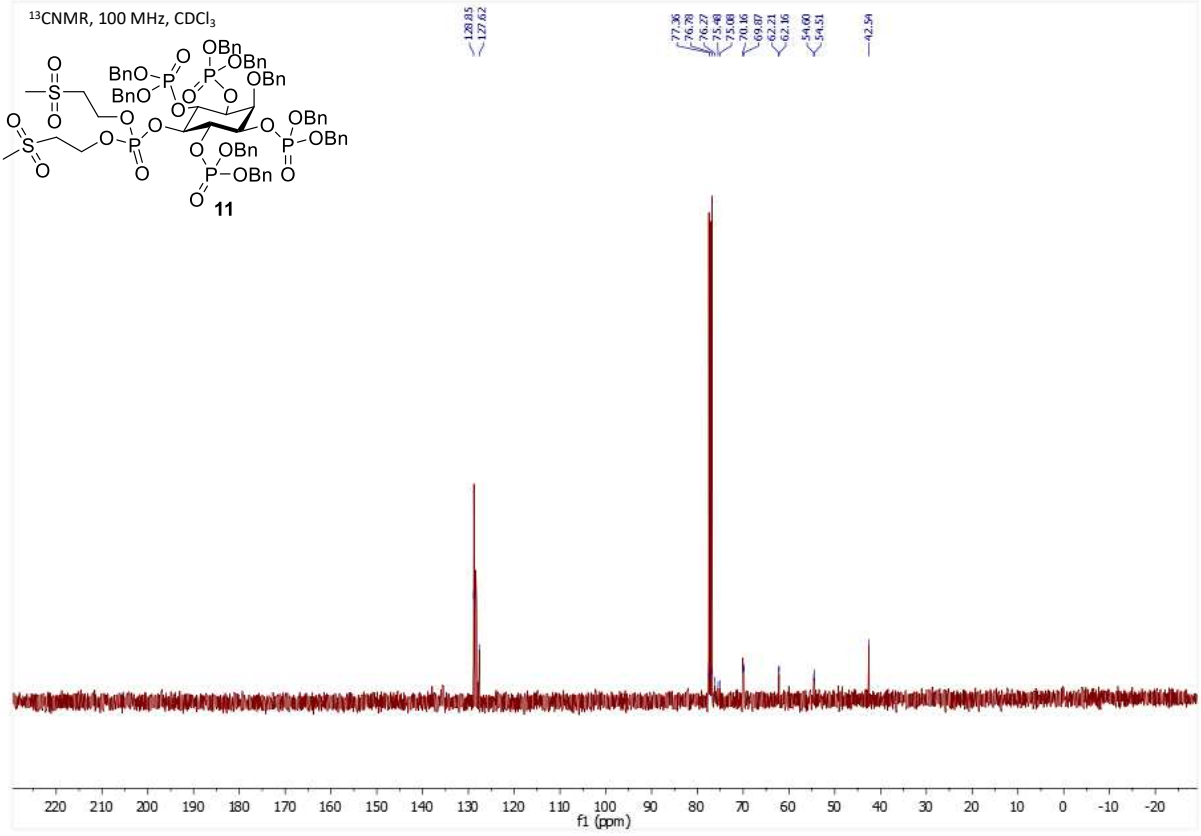

^{1}H-^{1}H COSY

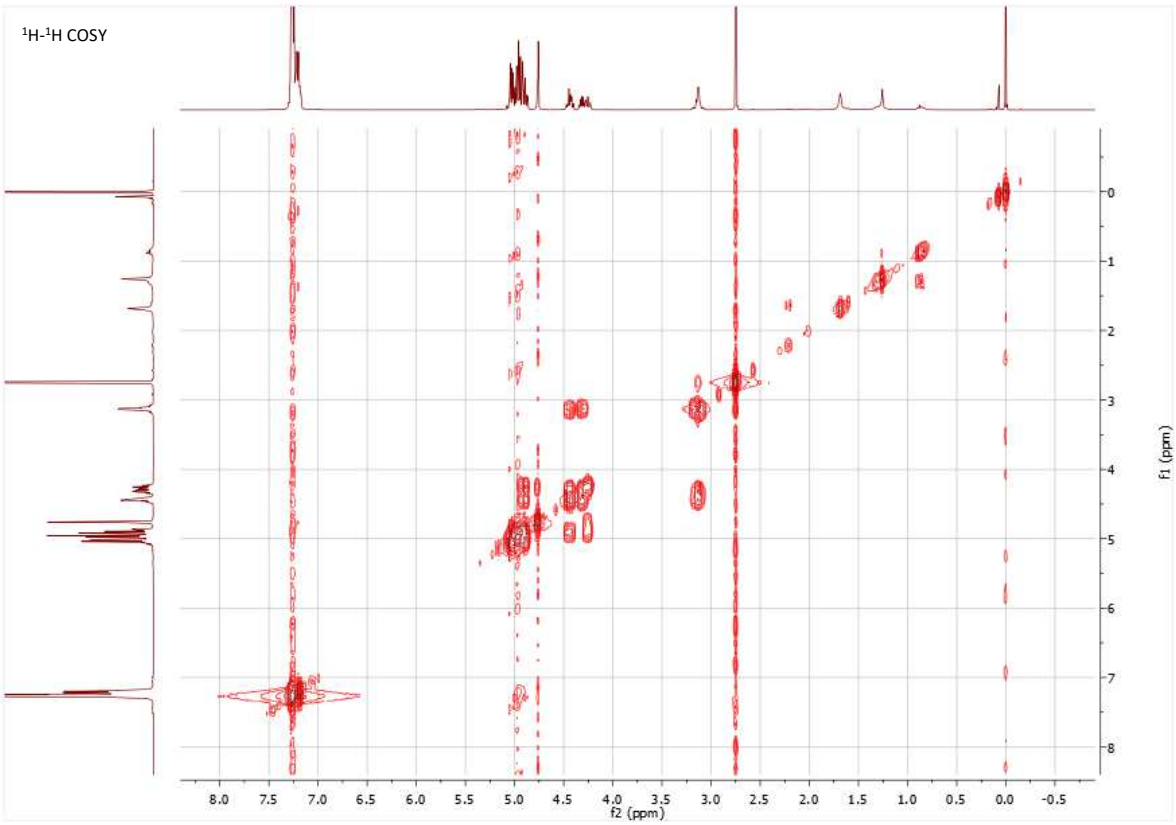

^{1}H-^{13}C HSQC

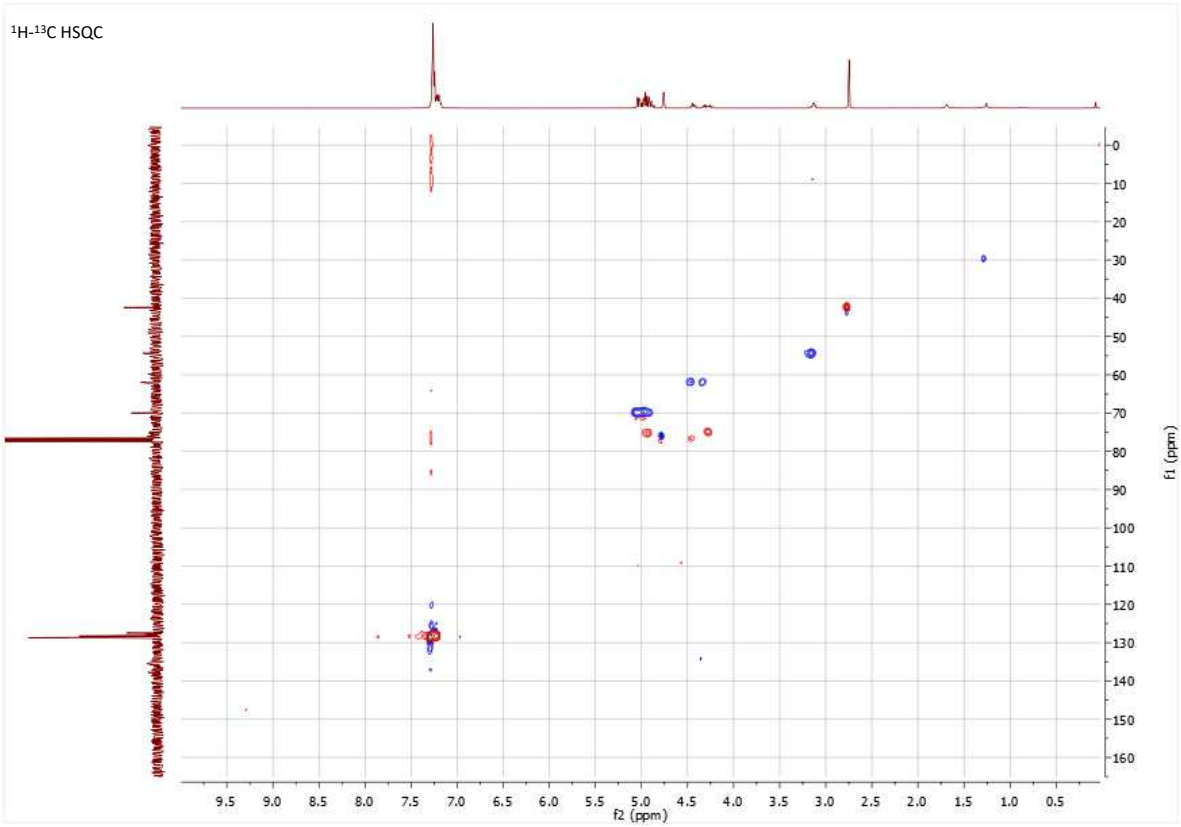

5-Diphospho-*myo*-inositol-1,3,4,6-tetrakisphosphate triethylammonium salt (**3**)

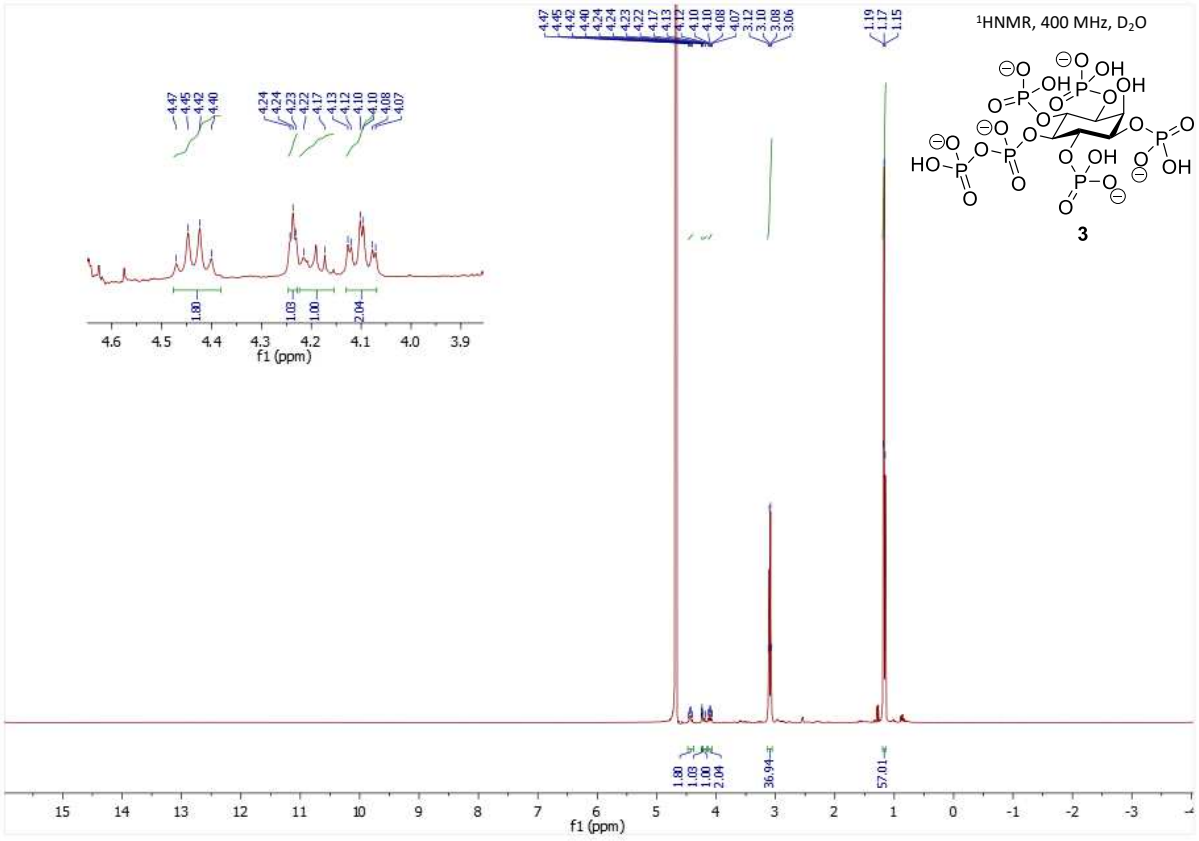

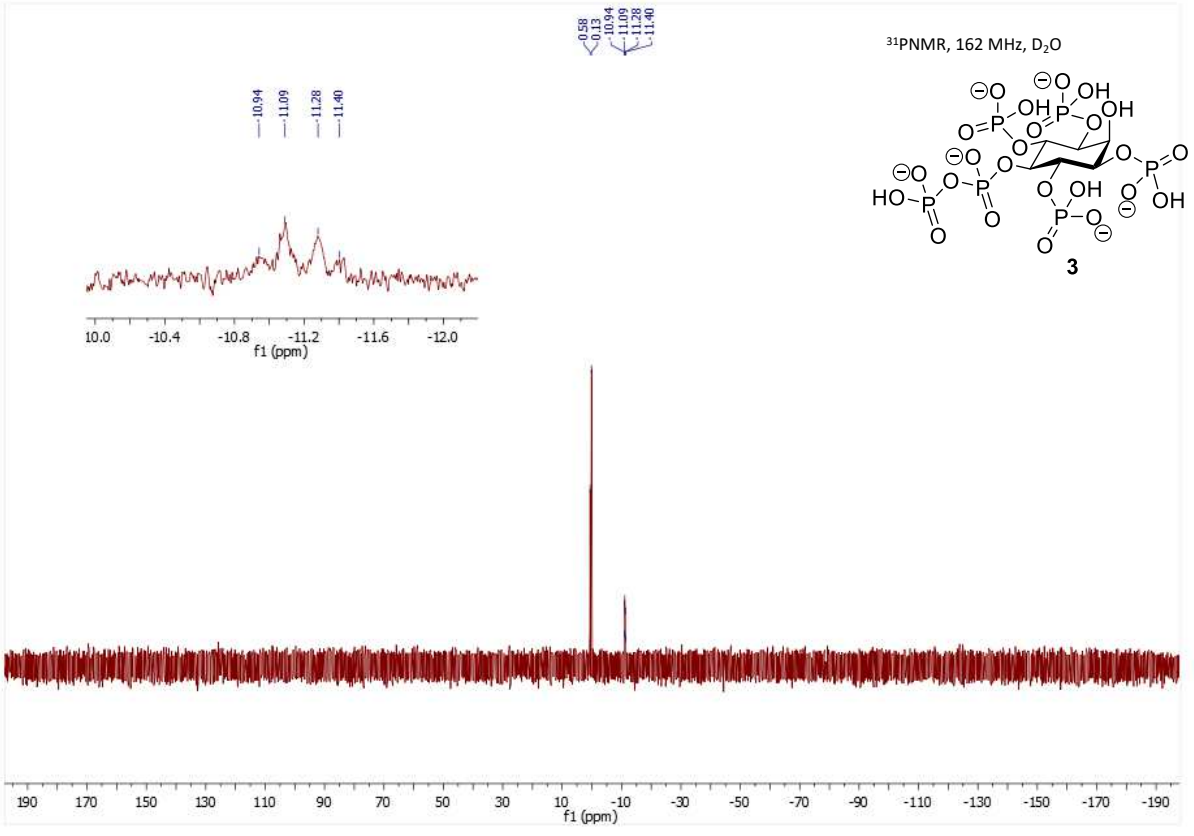

^{13}CNMR, 100 MHz, D_2O

3

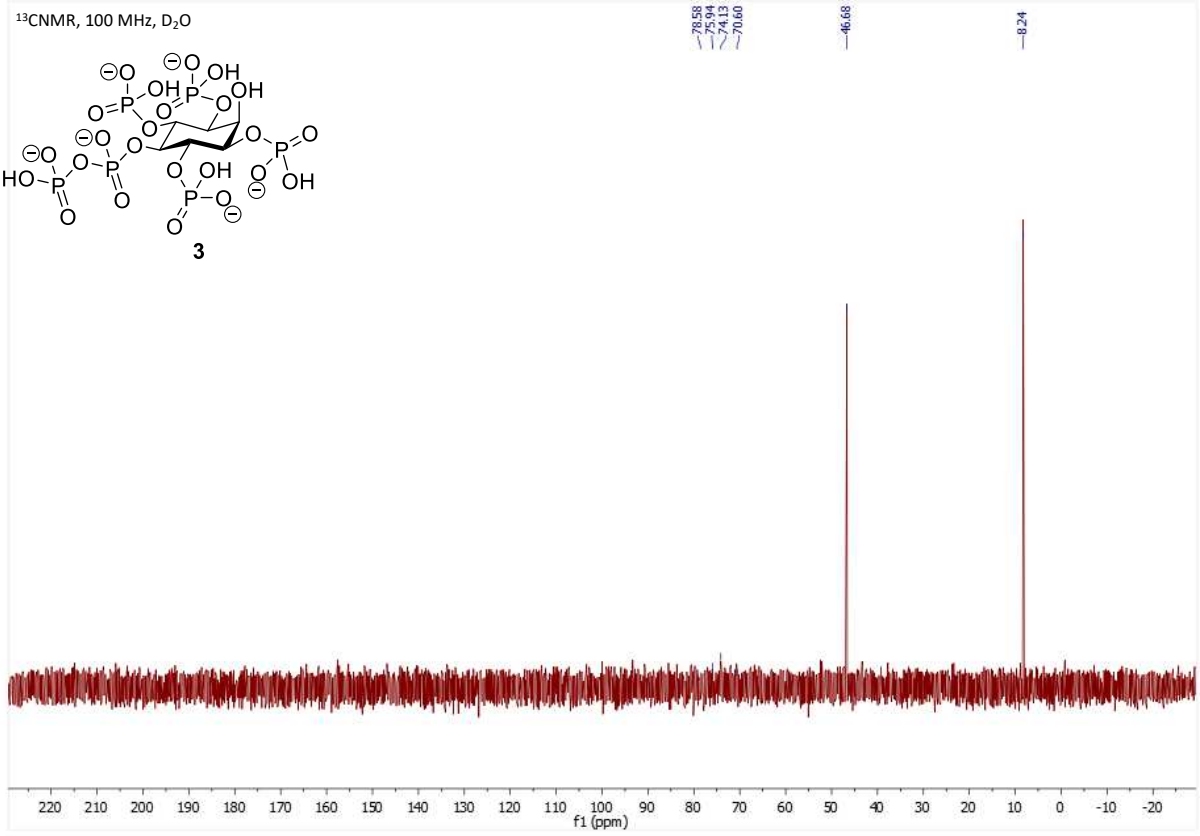

^{1}H-^{1}H COSY

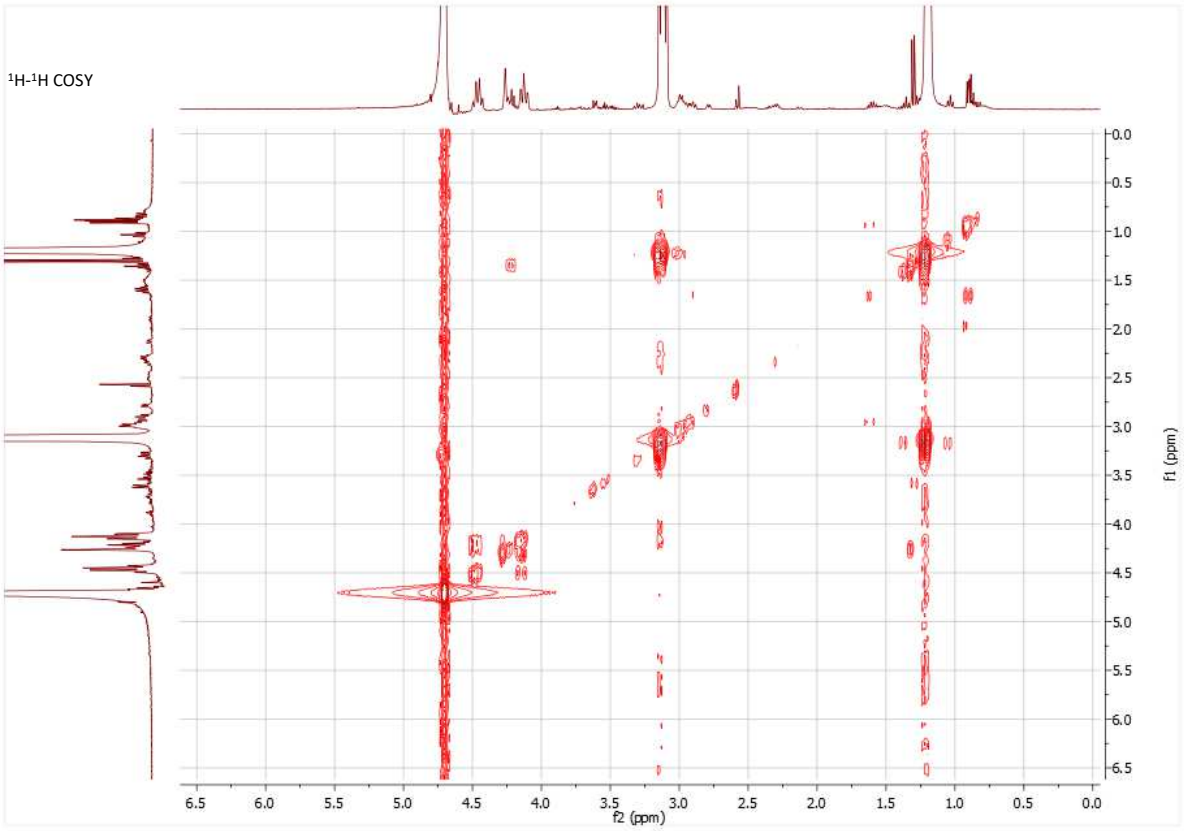

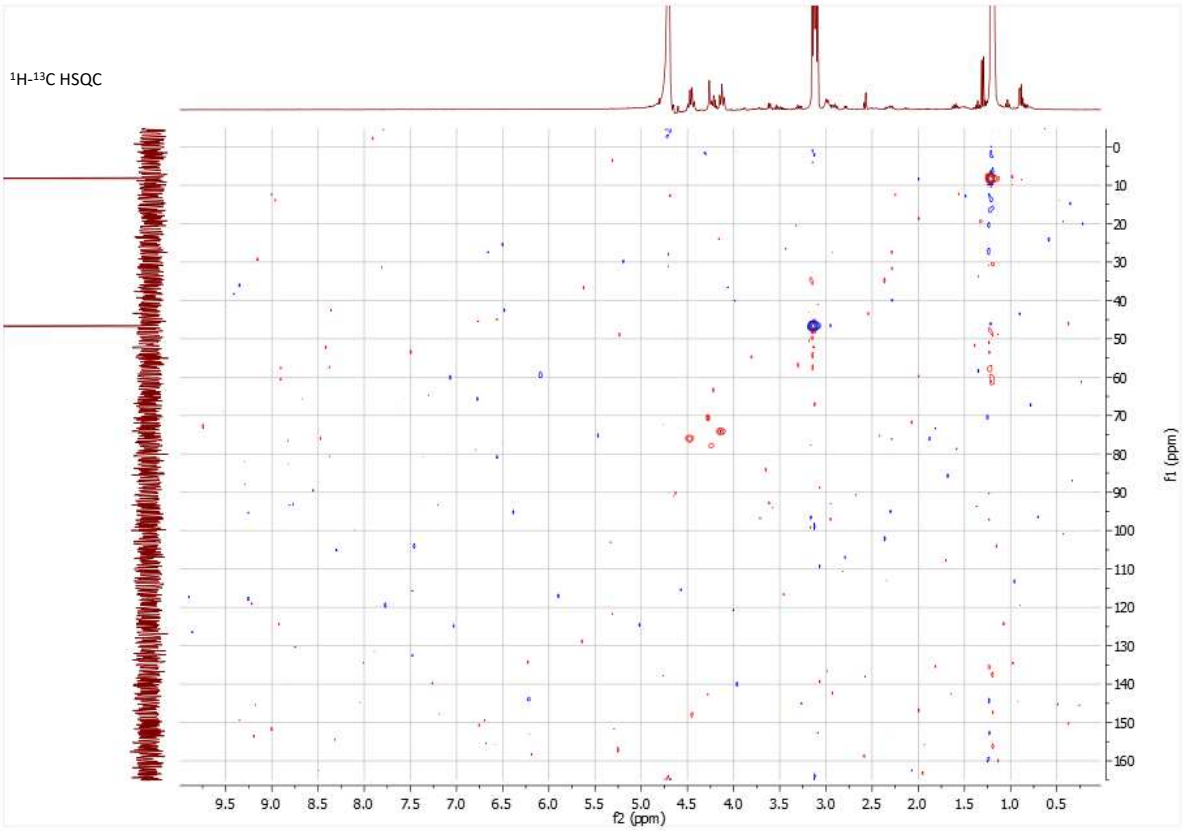

Synthesis of 1,5-bis(diphospho)-myo-inositol tetrakisphosphate [1,5-(PP)$_2$-InsP$_4$]

myo-Inositol orthobenzoate (**17**)

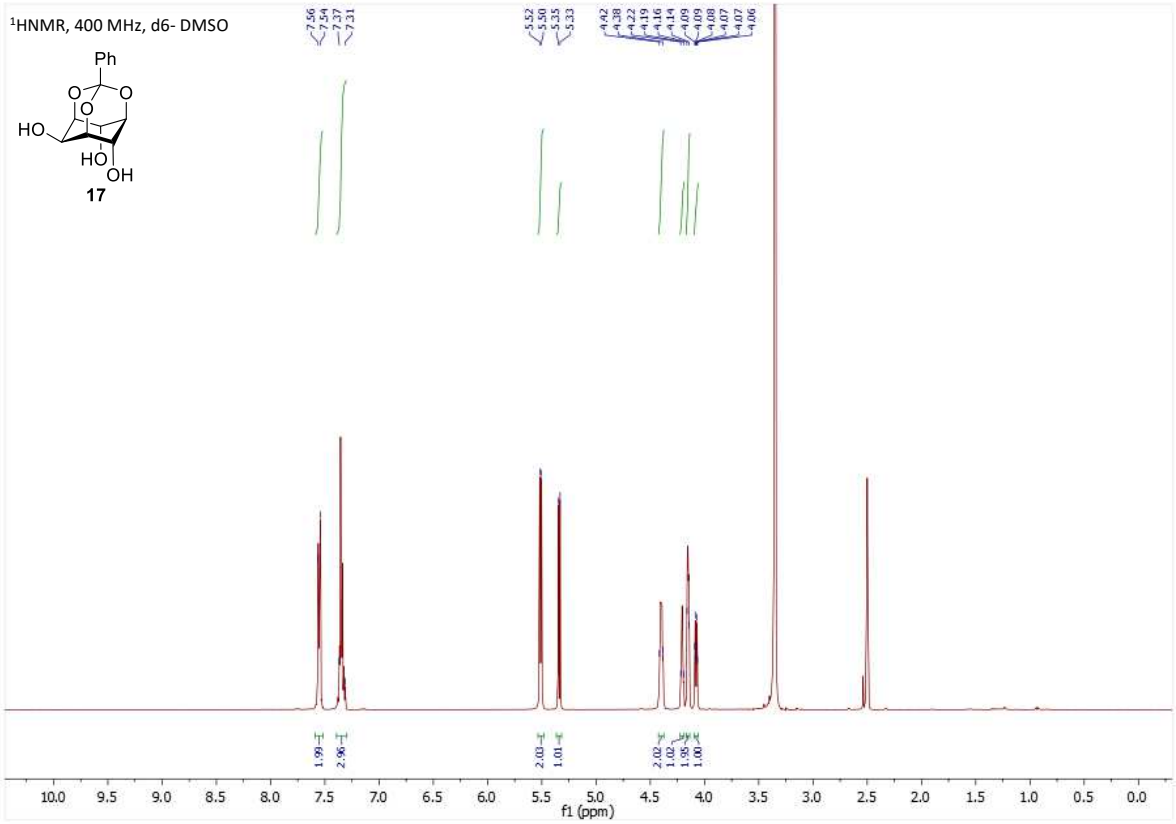

^{13}CNMR, 100 MHz, d6-DMSO

17

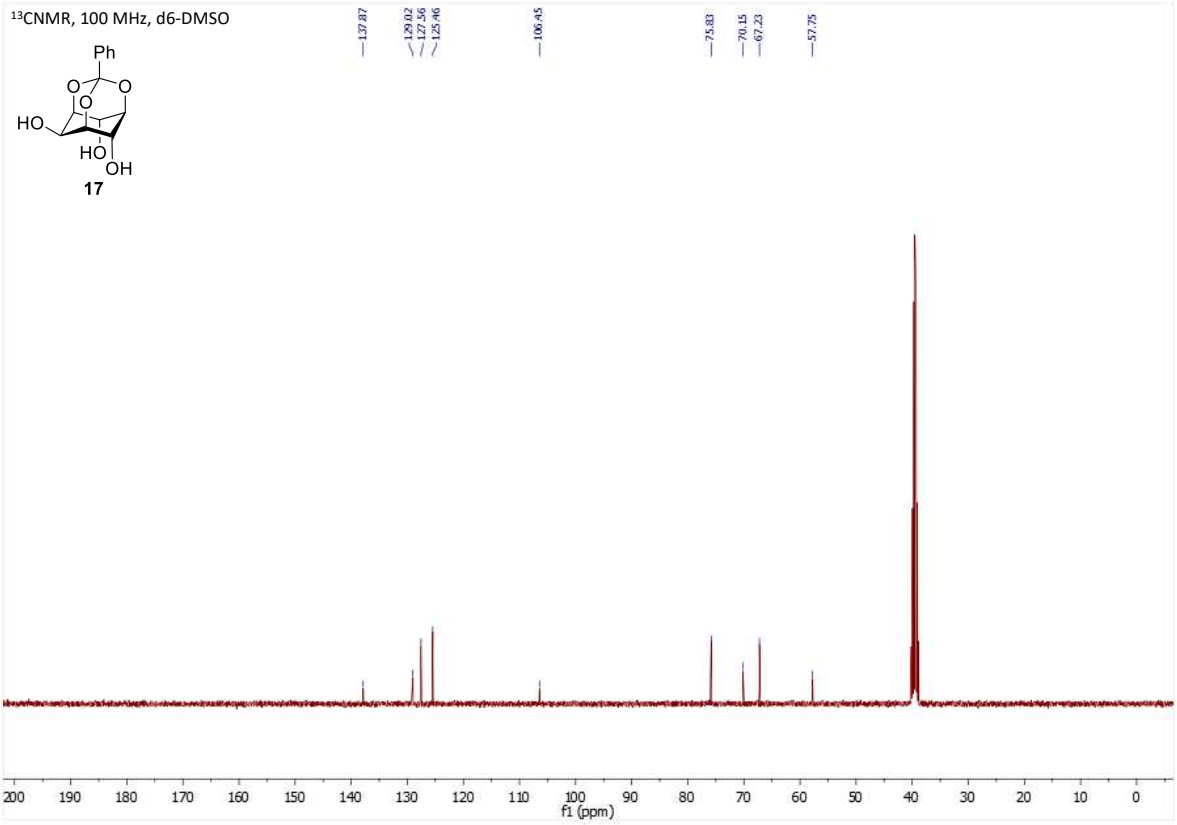

^{1}H-^{1}H COSY

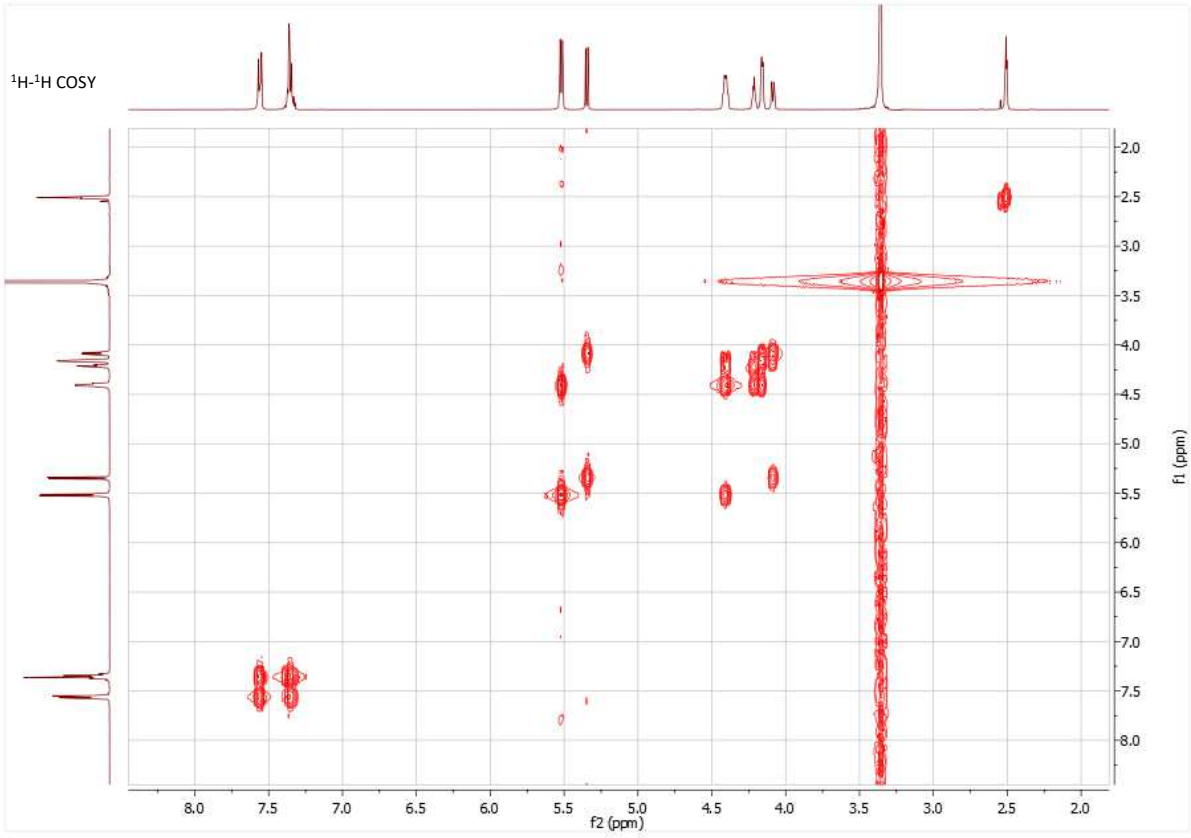

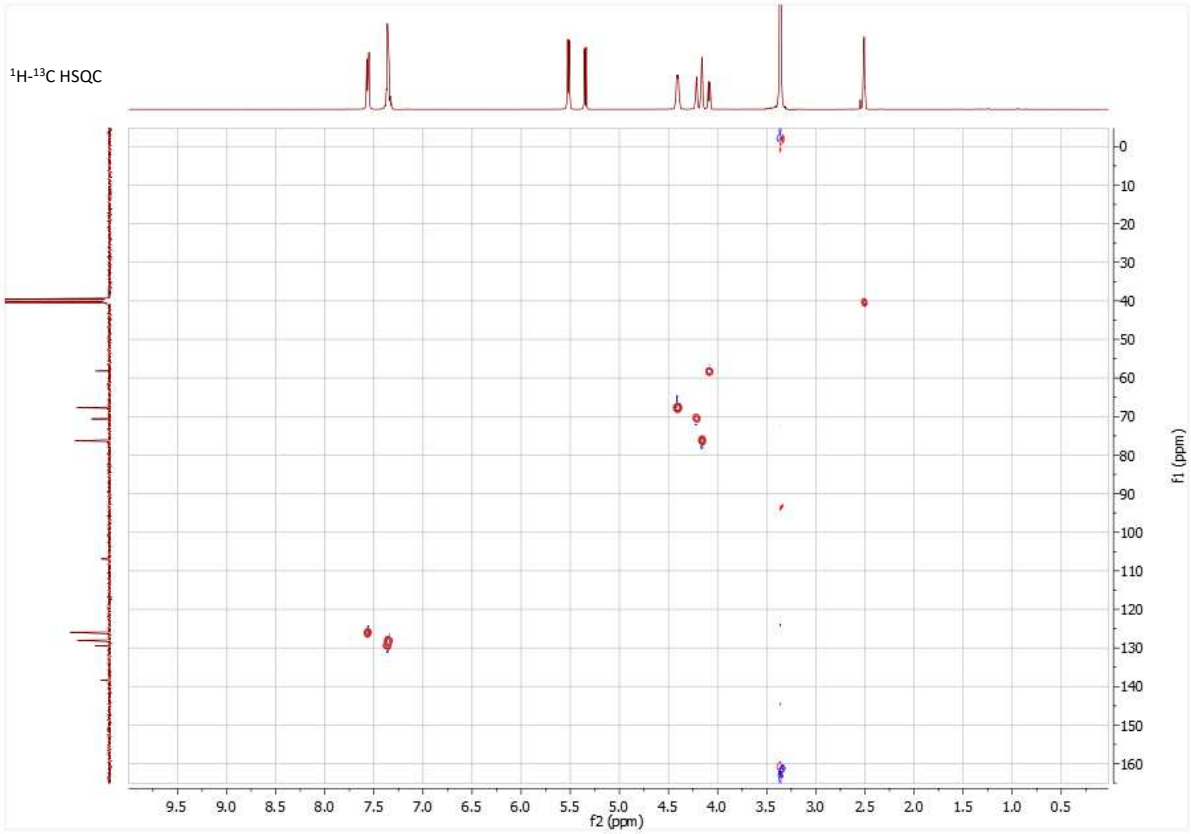

2,4,6-Tri-*O*-benzyl-*myo*-inositol orthobenzoate (**18**)

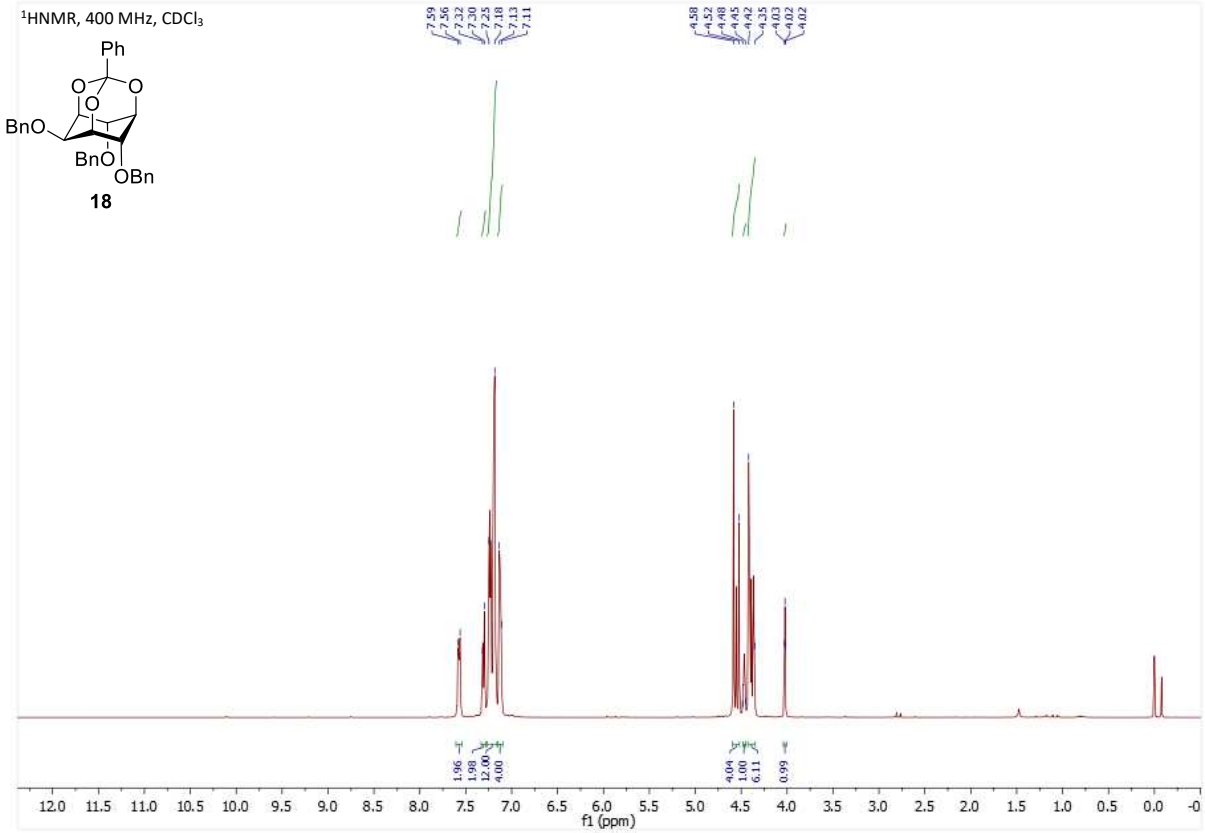

^{13}CNMR, 100 MHz, $CDCl_3$

18

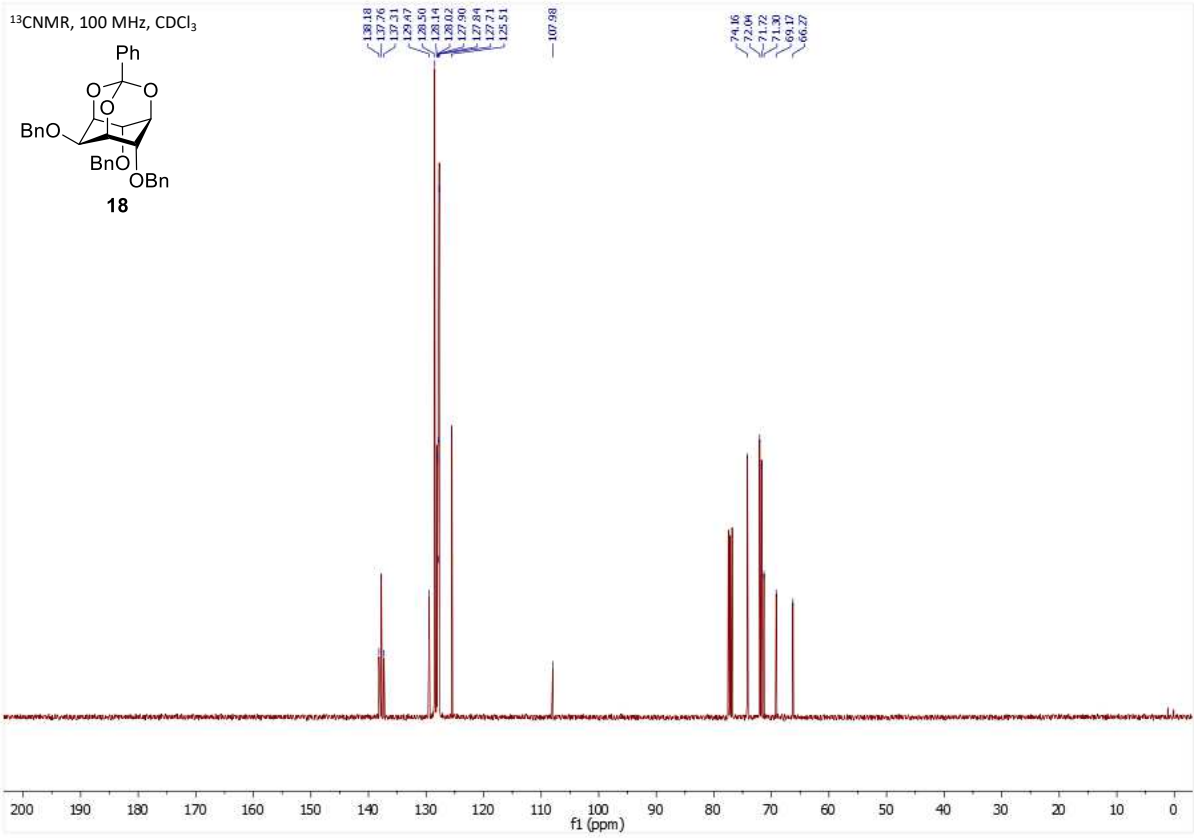

^{1}H-^{1}H COSY

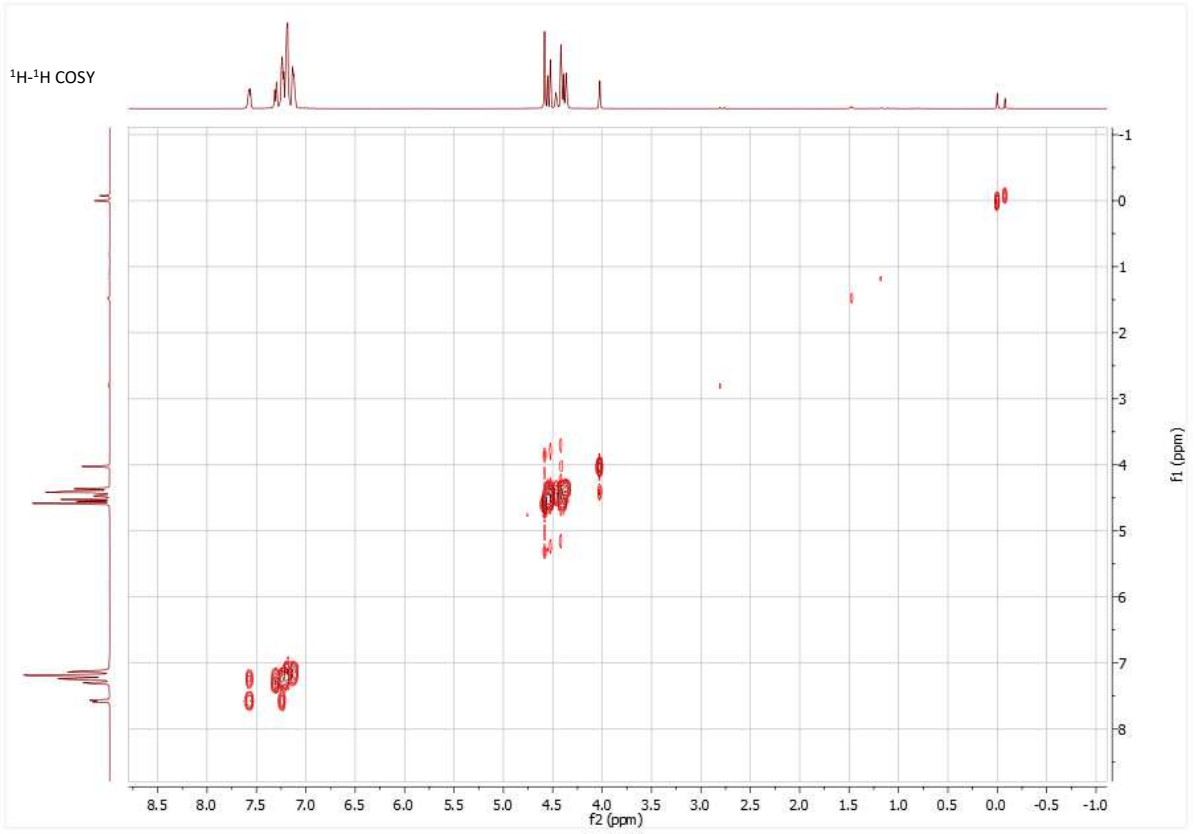

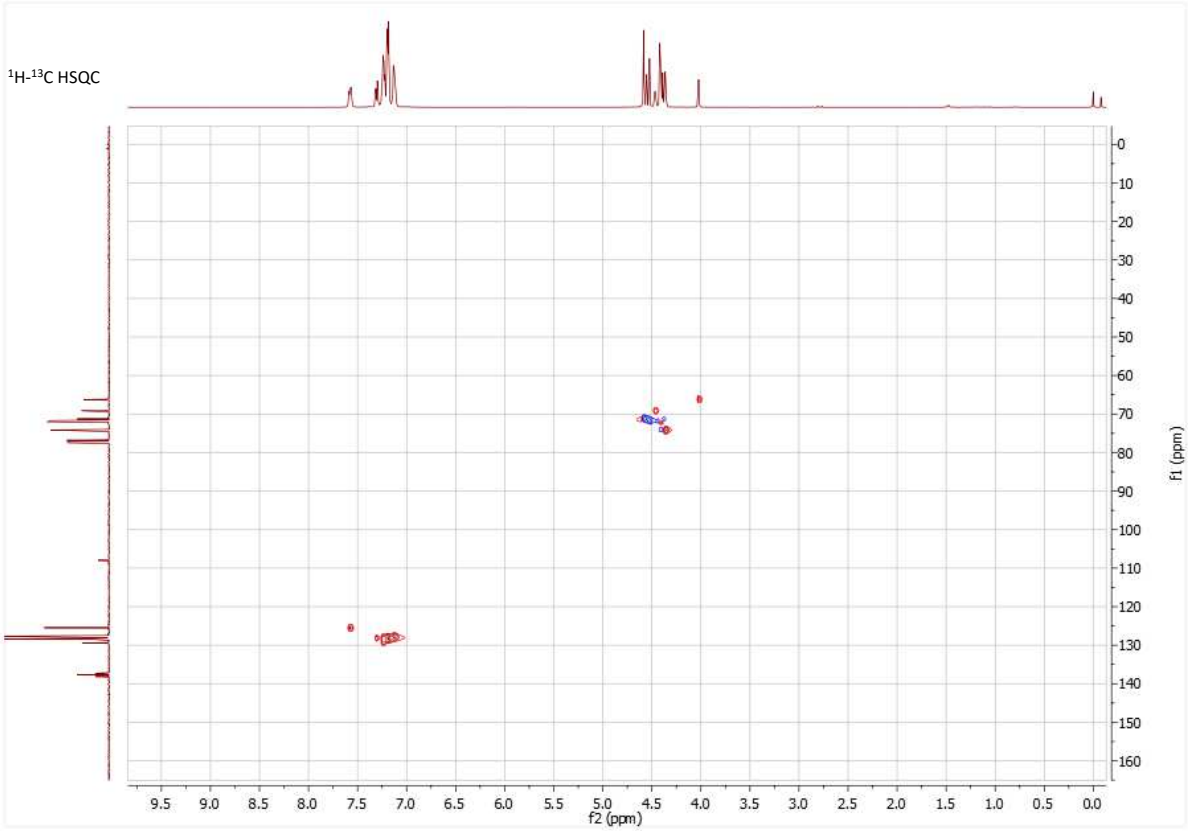

2,3,4,6-Tetra-*O*-benzyl-*myo*-inositol (**19**)

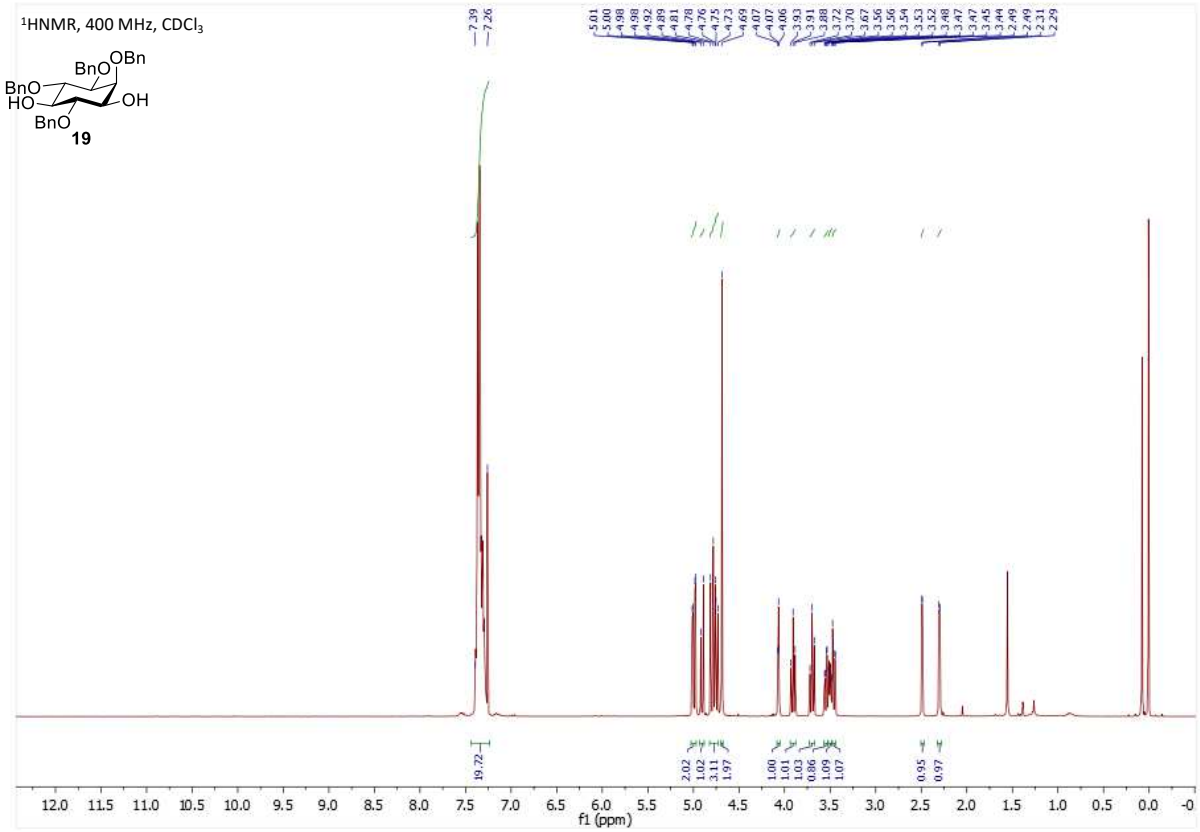

^{13}CNMR, 100 MHz, $CDCl_3$

19

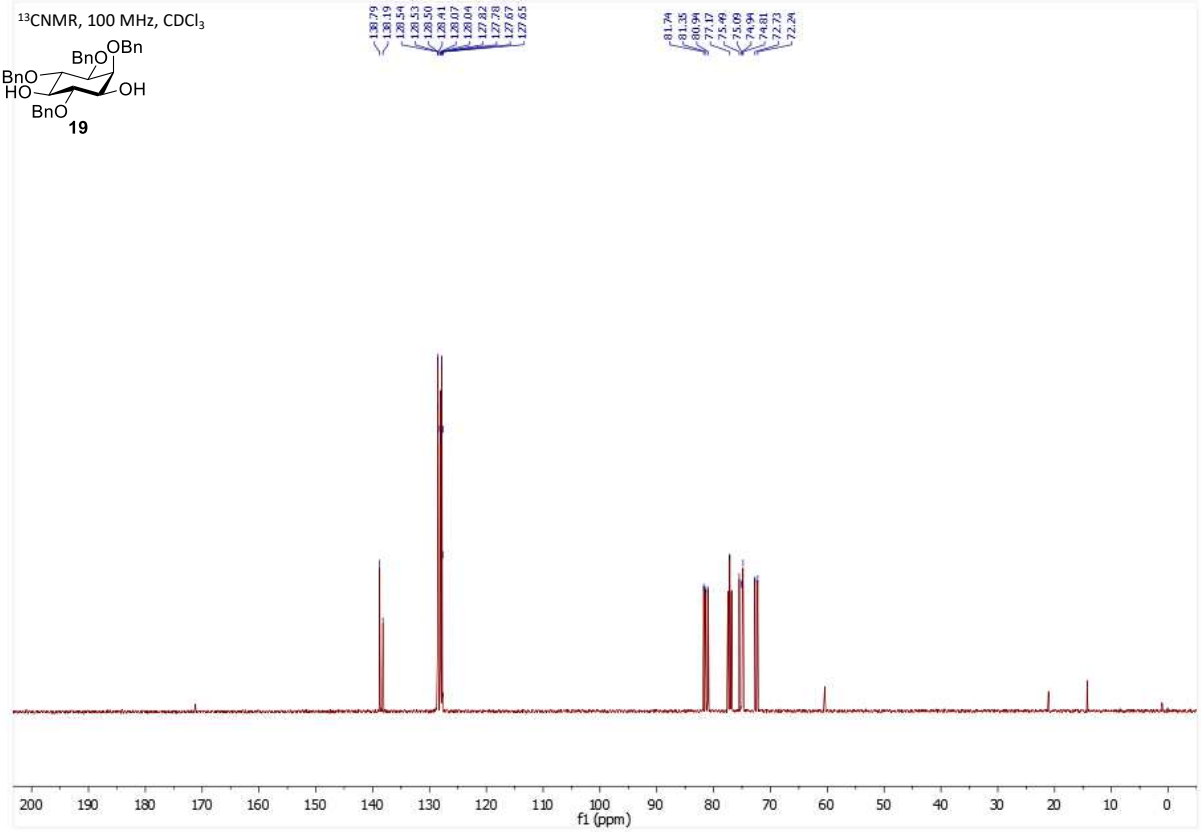

^{1}H-^{1}H COSY

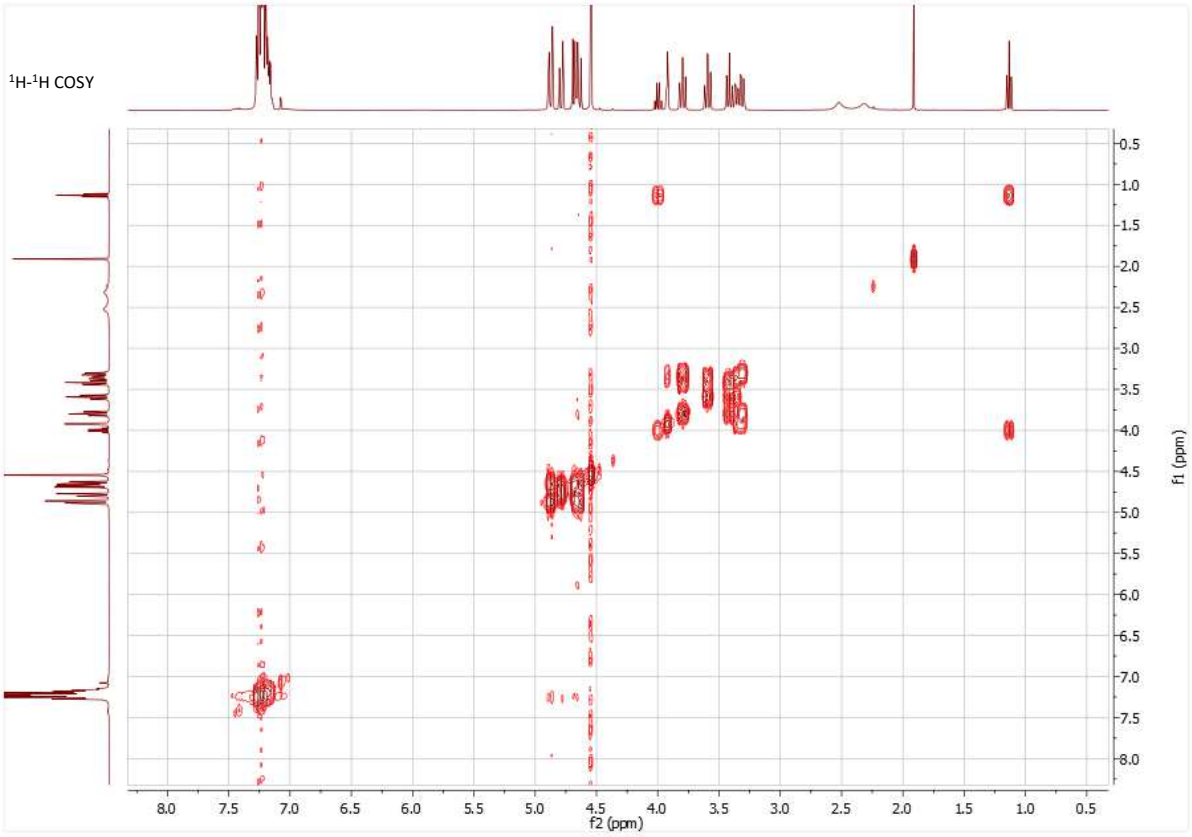

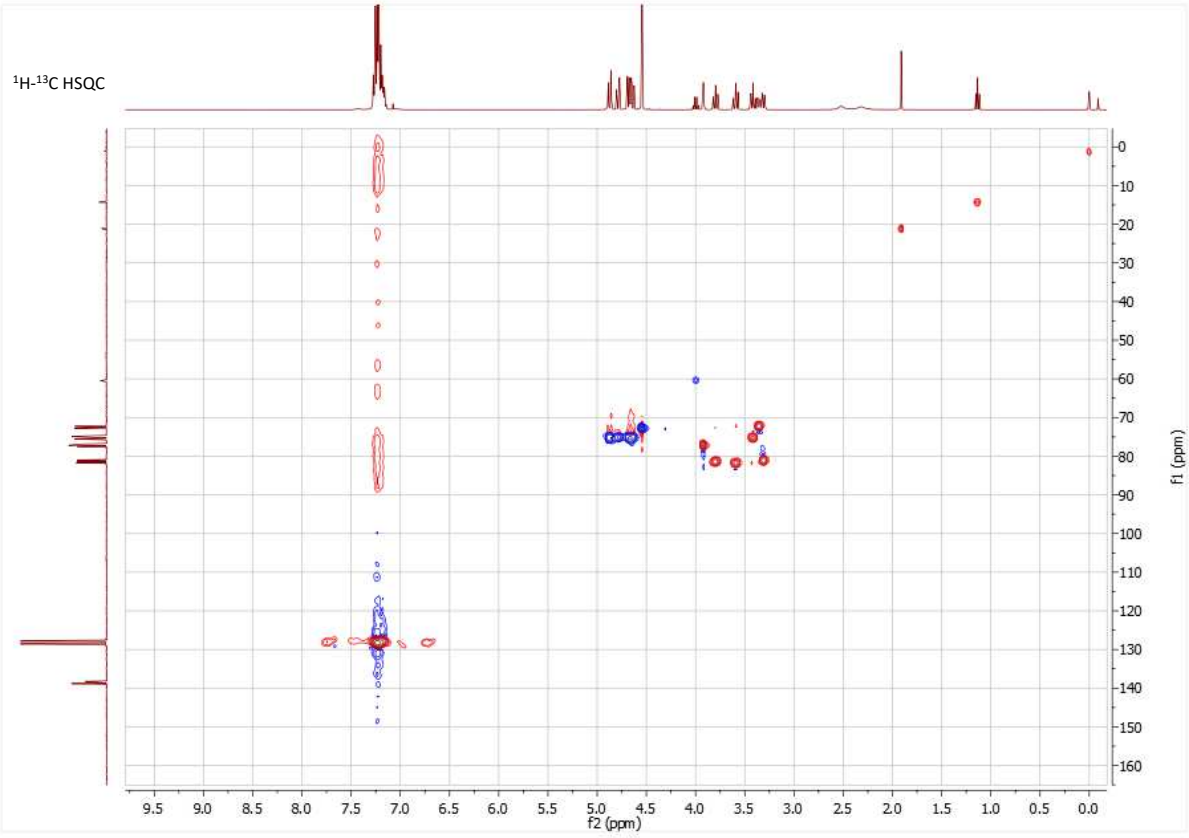

DL-2,3,4,6-Tetra-*O*-benzyl-*myo*-inositol-1,5-bis{bis[2-(methanesulfonyl)ethyl]phosphate} (**20**)

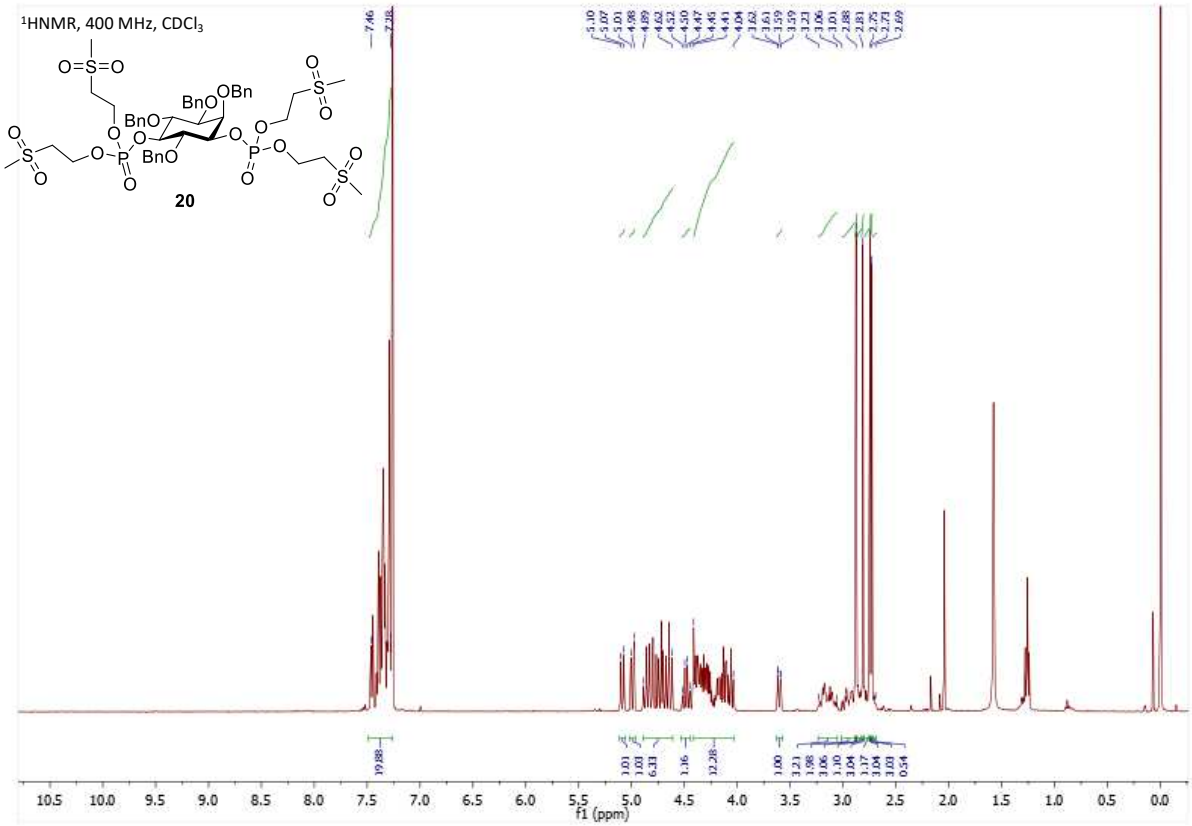

^{31}PNMR, 162 MHz, $CDCl_3$

20

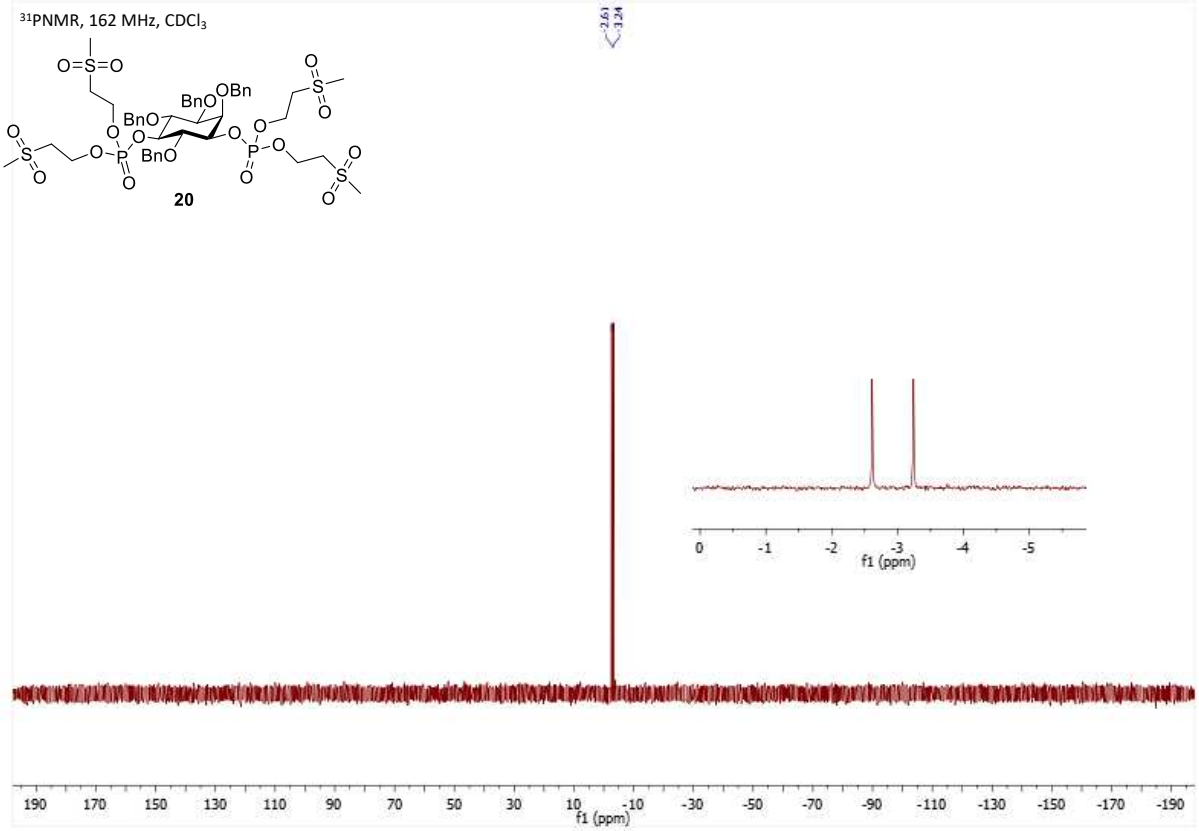

^{13}CNMR, 100 MHz, $CDCl_3$

20

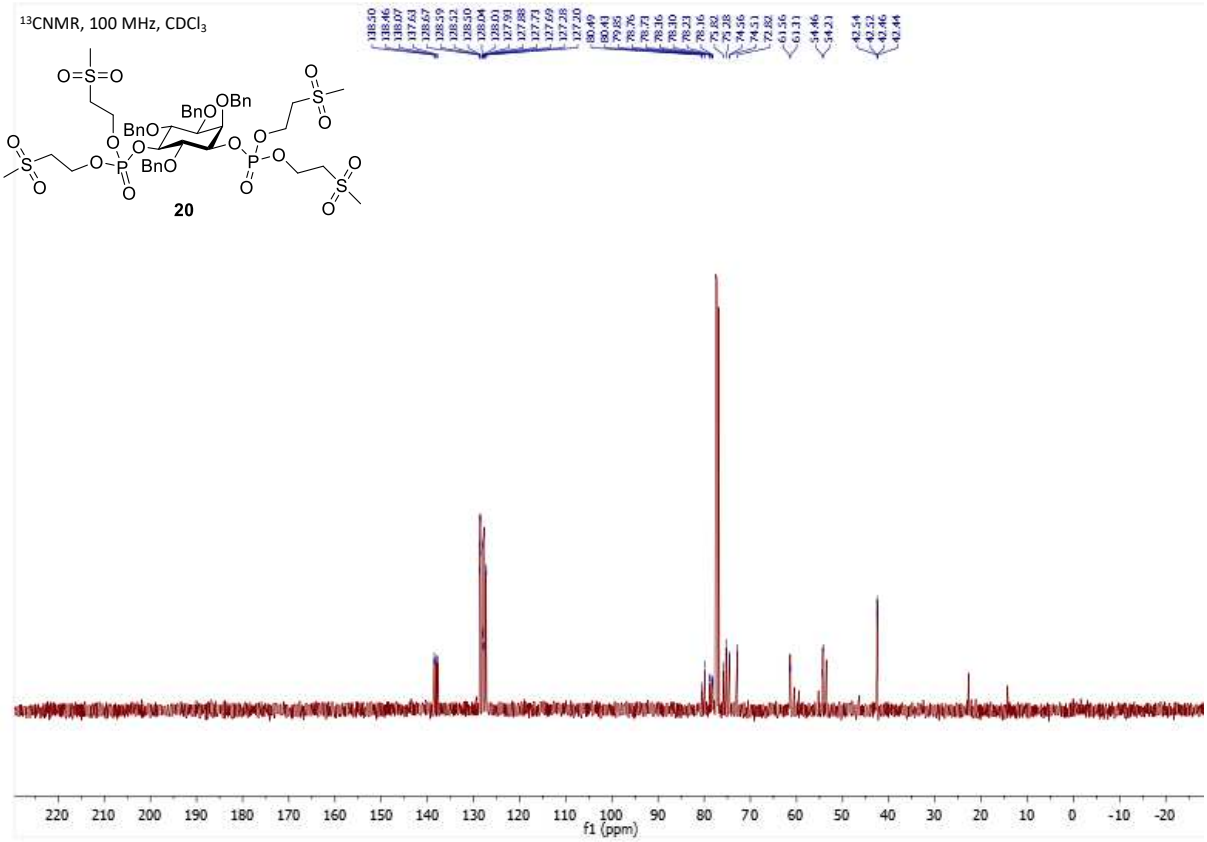

^{1}H-^{1}H COSY

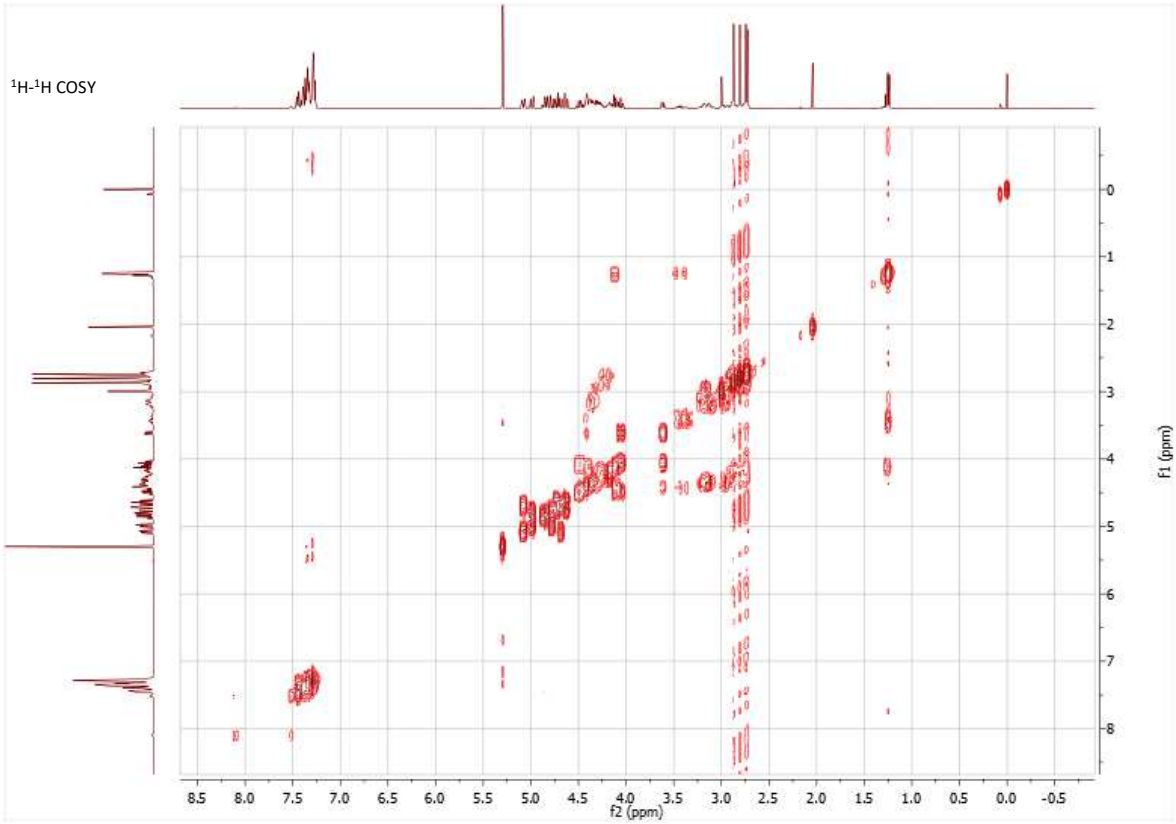

^{1}H-^{13}C HSQC

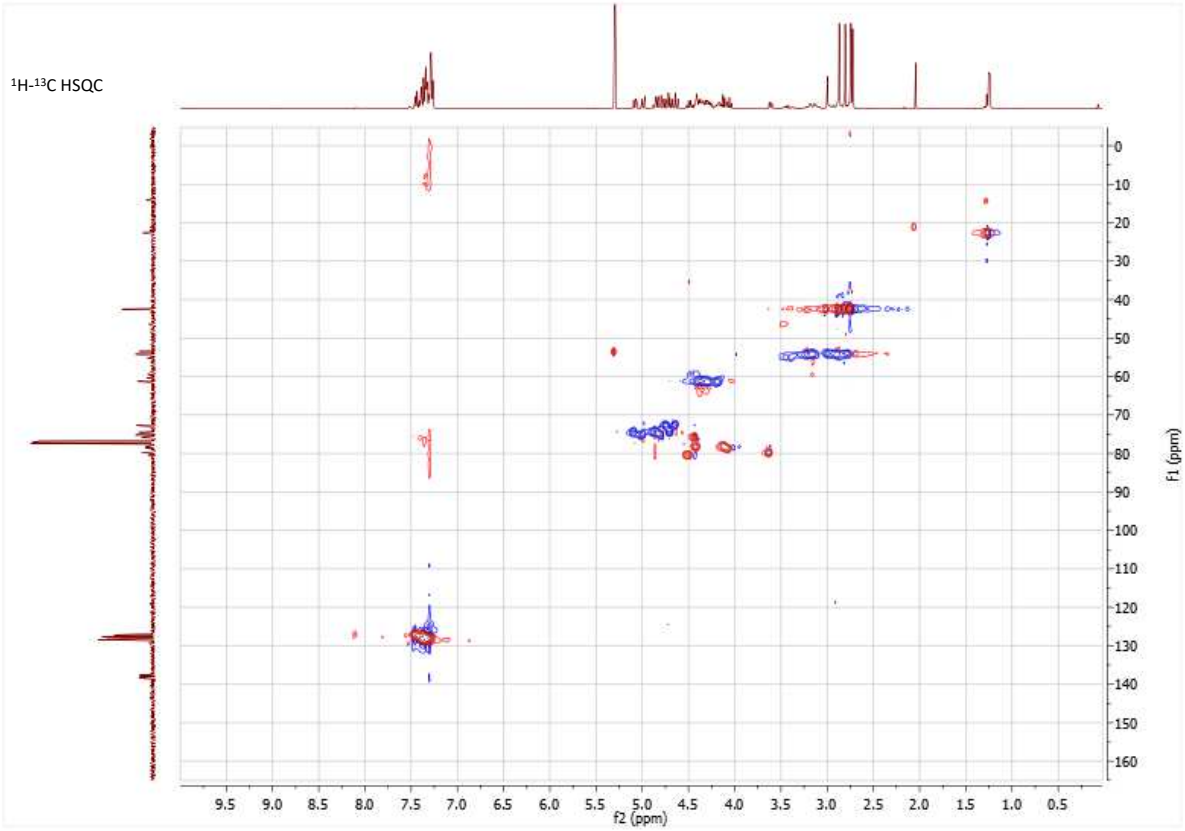

DL-*myo*-Inositol-1,5-bis{bis[2-(methanesulfonyl)ethyl]phosphate} (**21**)

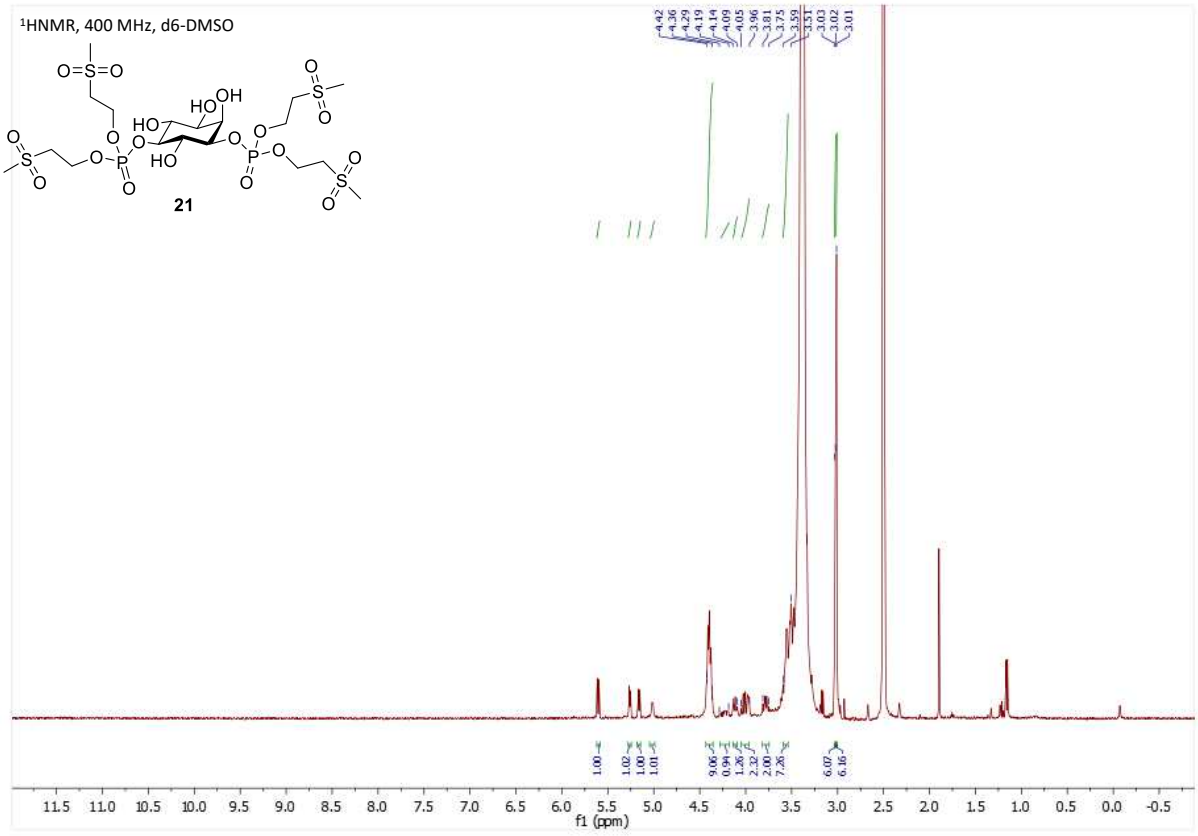

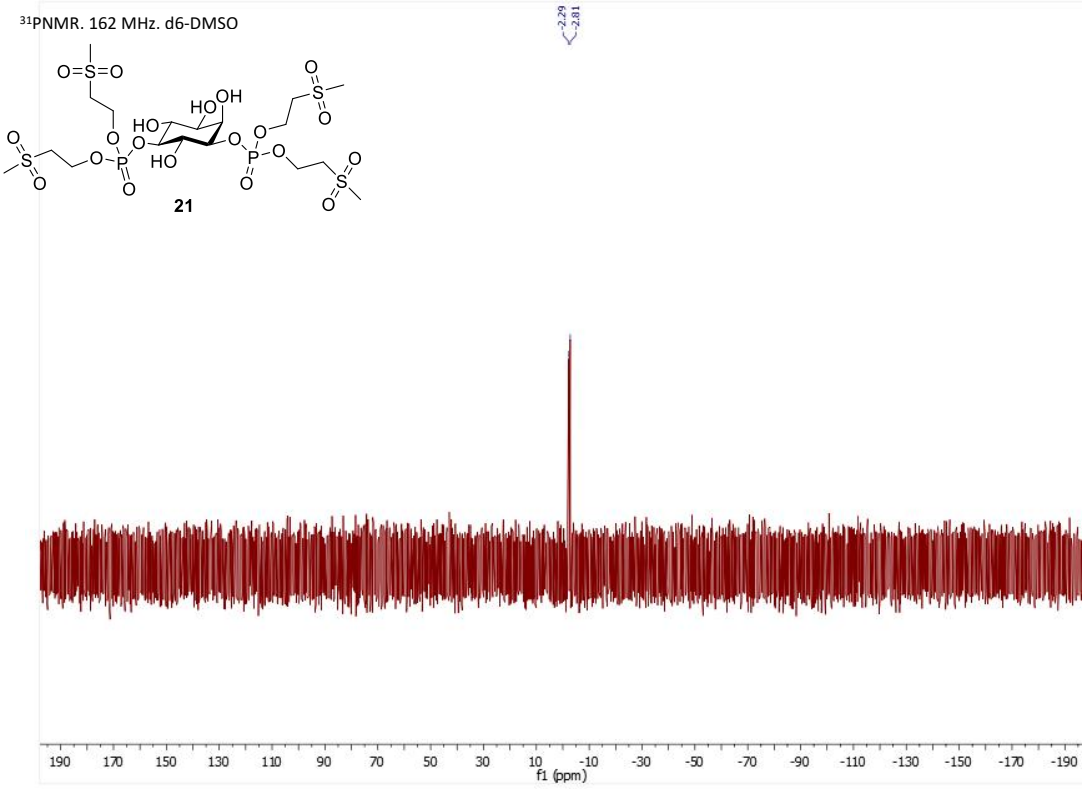

DL-*myo*-Inositol-1,5-bis{bis[2-(methanesulfonyl)ethyl]phosphate}-2,3,4,6-tetrakis(dibenzyl-phosphate) (**22**)

^{1}HNMR, 400 MHz, $CDCl_3$

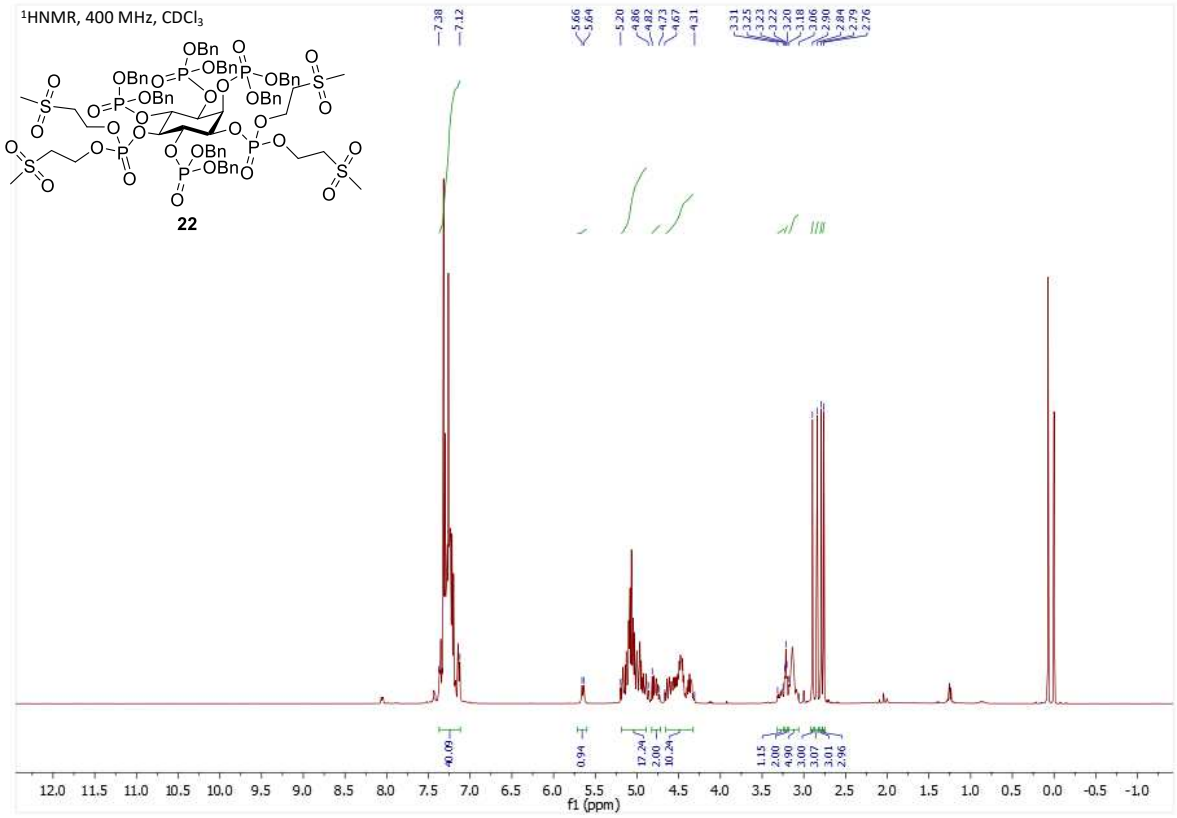

22

^{31}PNMR, 162 MHz, $CDCl_3$

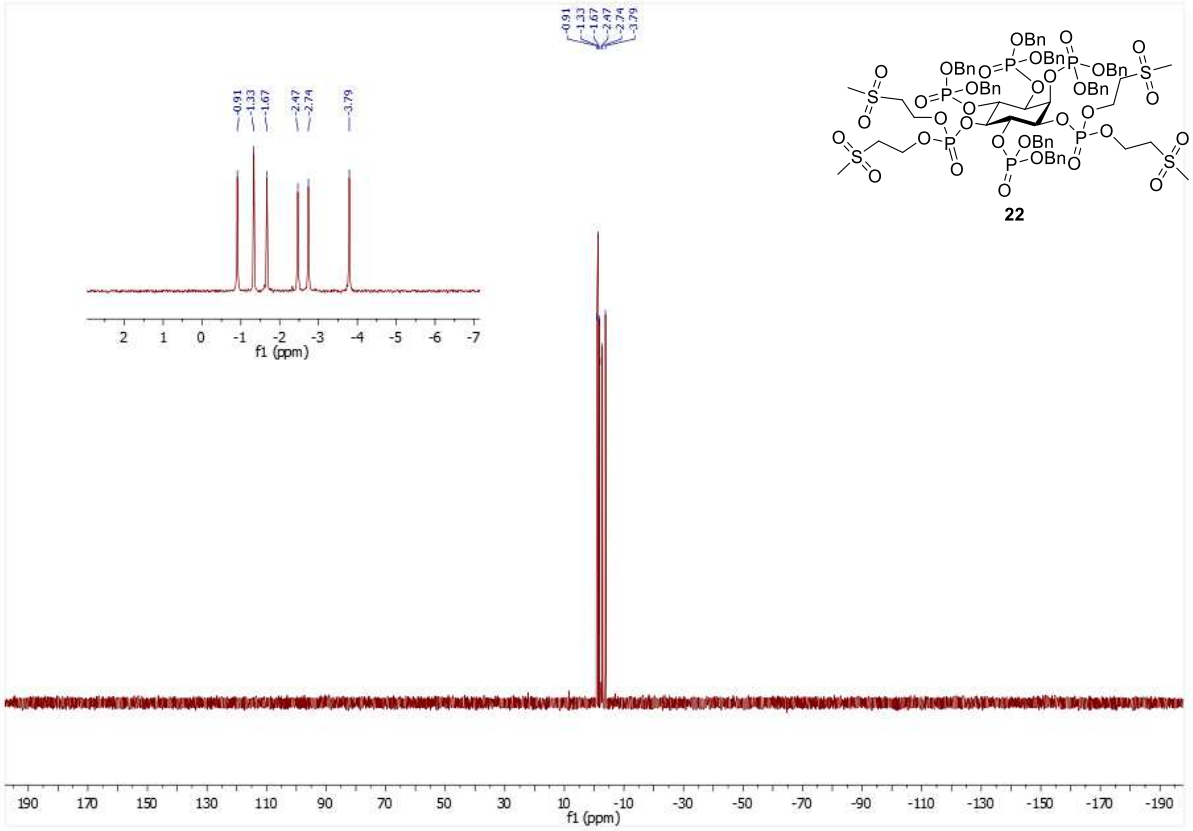
-0.91
-1.33
-1.67
-2.47
-2.74
-3.79
f1 (ppm)
22

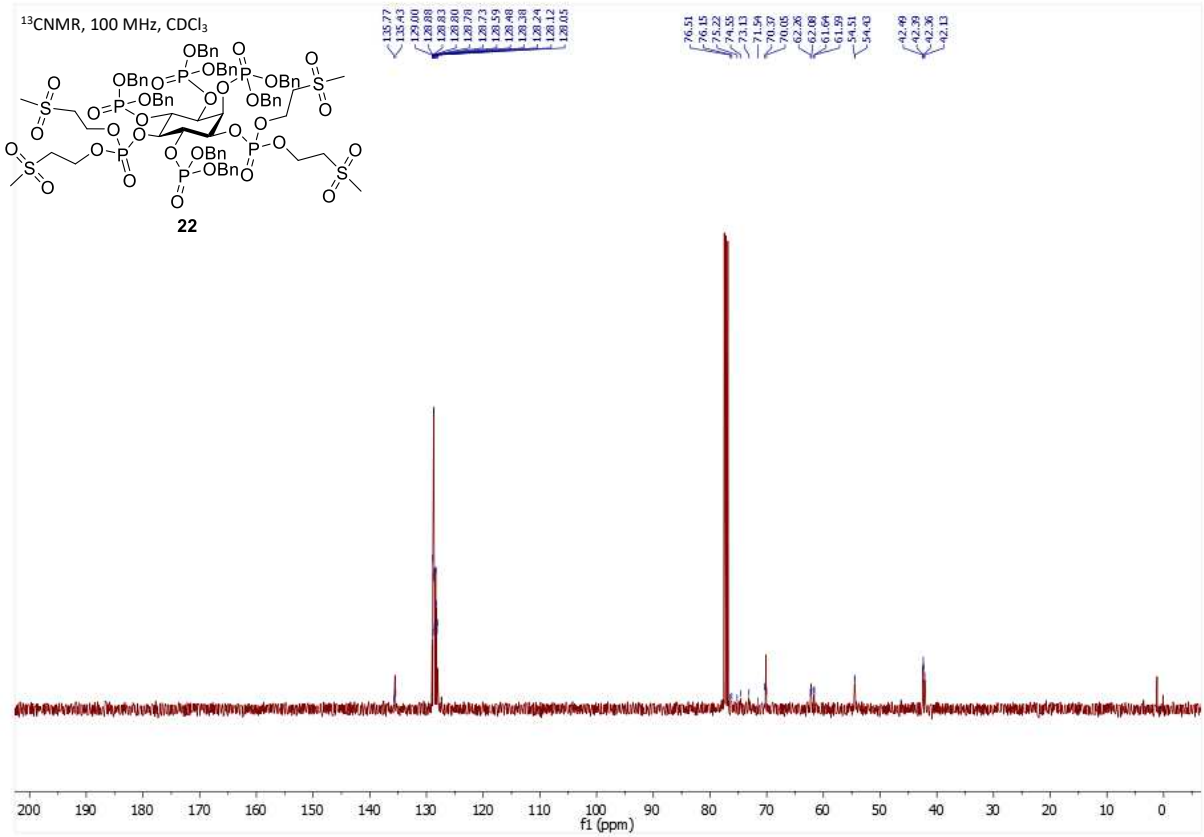
13CNMR, 100 MHz, CDCl3
22
f1 (ppm)

^{1}H-^{1}H COSY

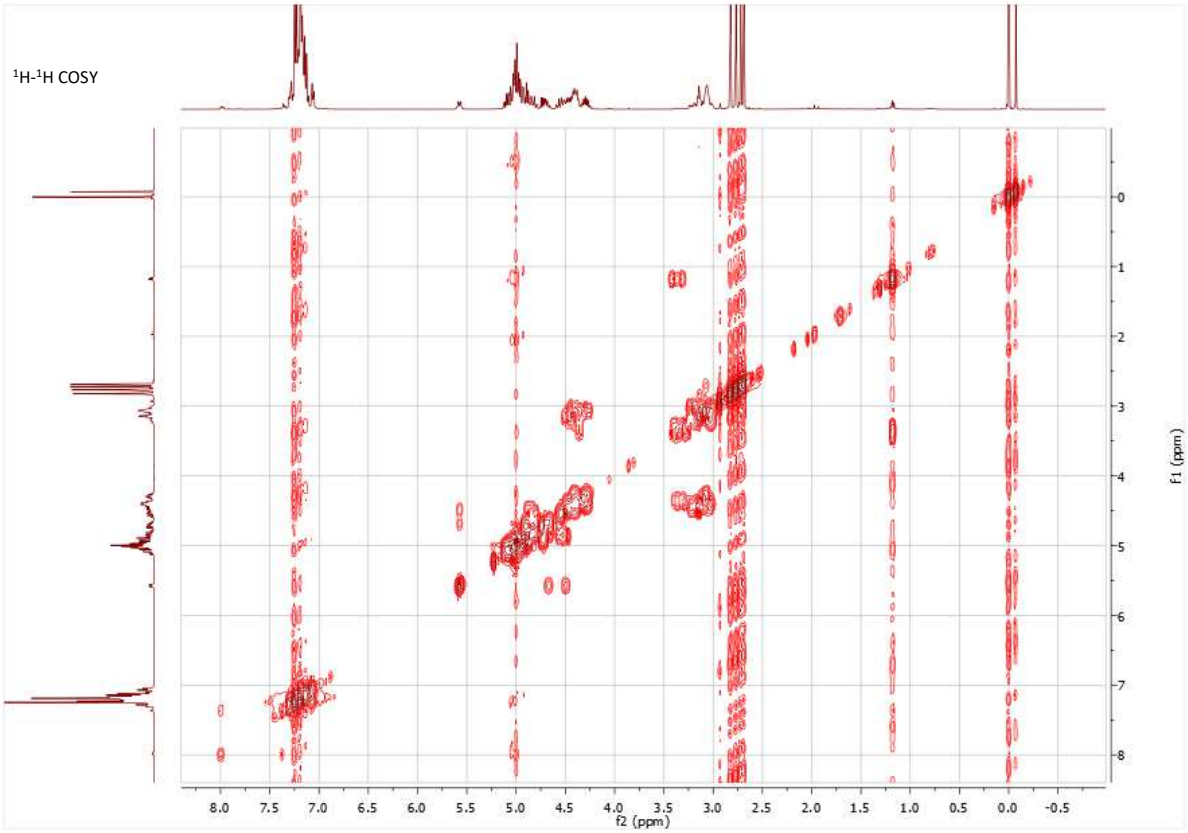

^{1}H-^{13}C HSQC

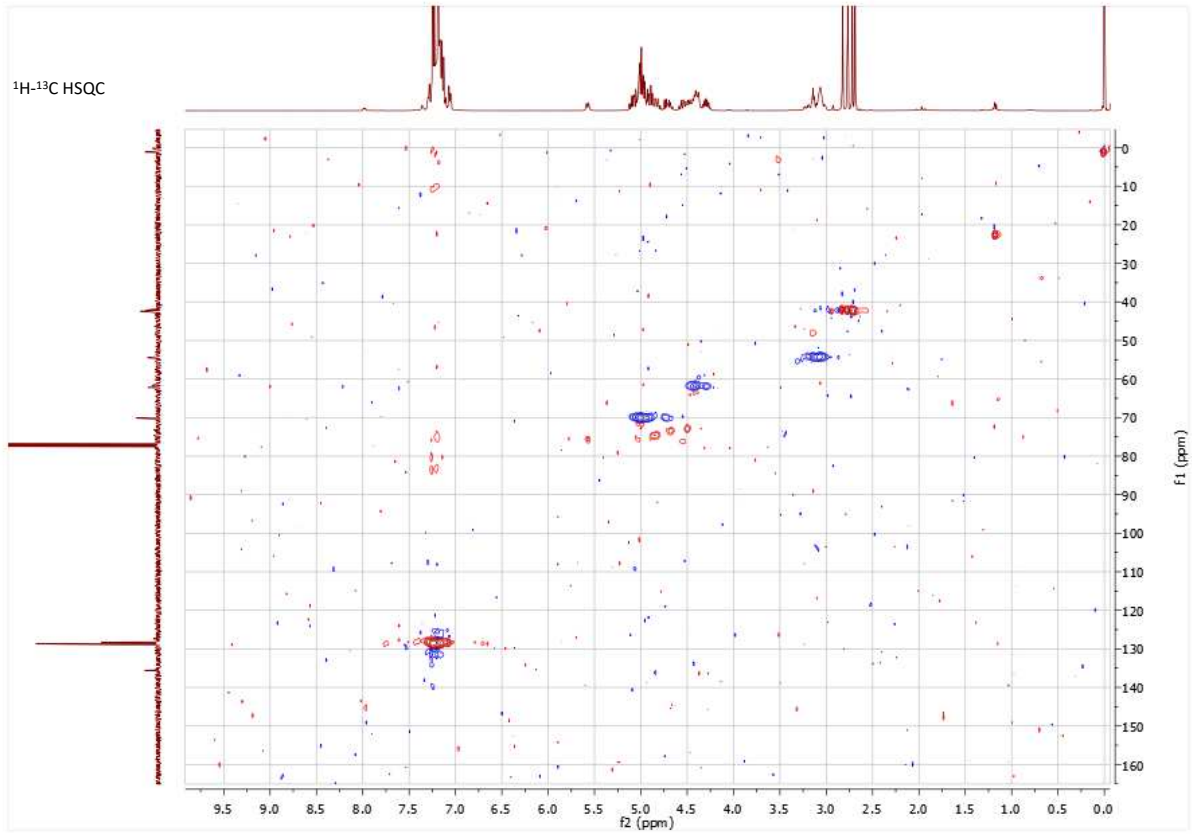

1,5-bis(diphospho)-*myo*-inositol-2,3,4,6-tetrakisphosphate triethylammonium salt (**16**)

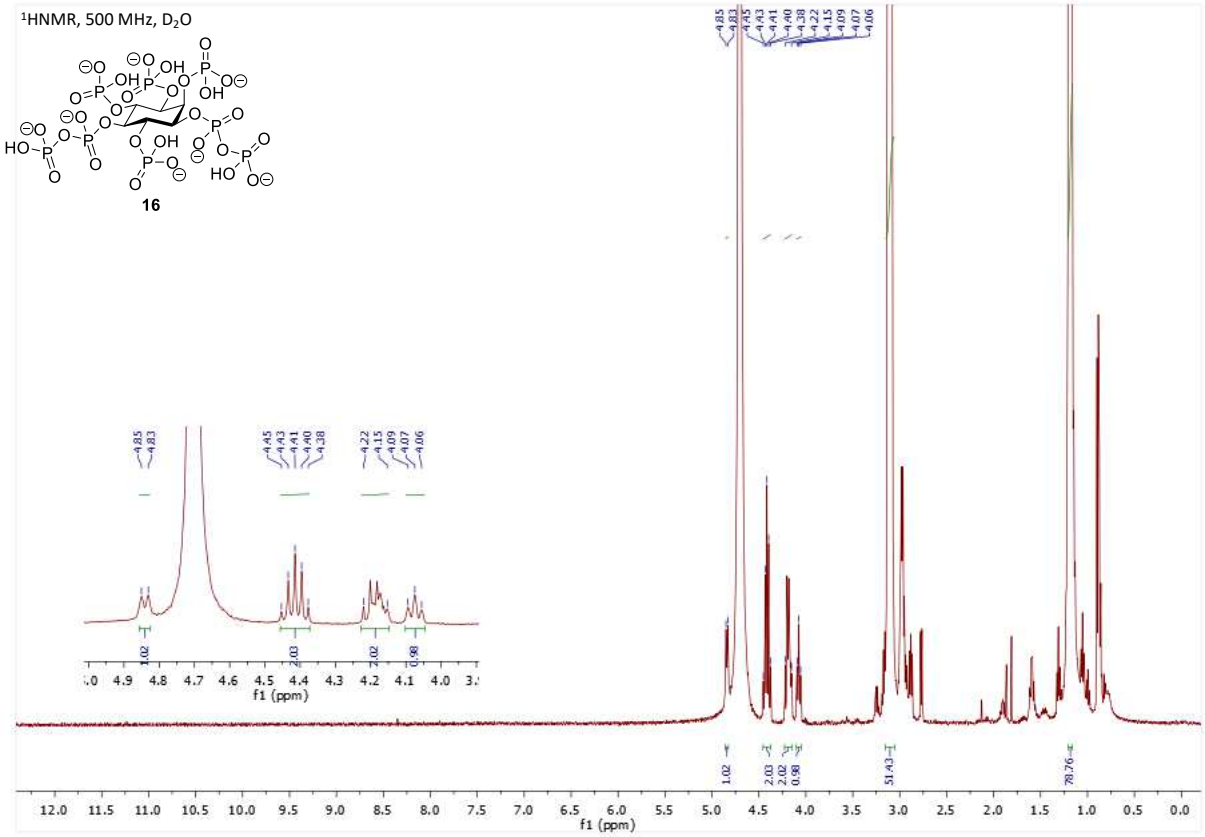

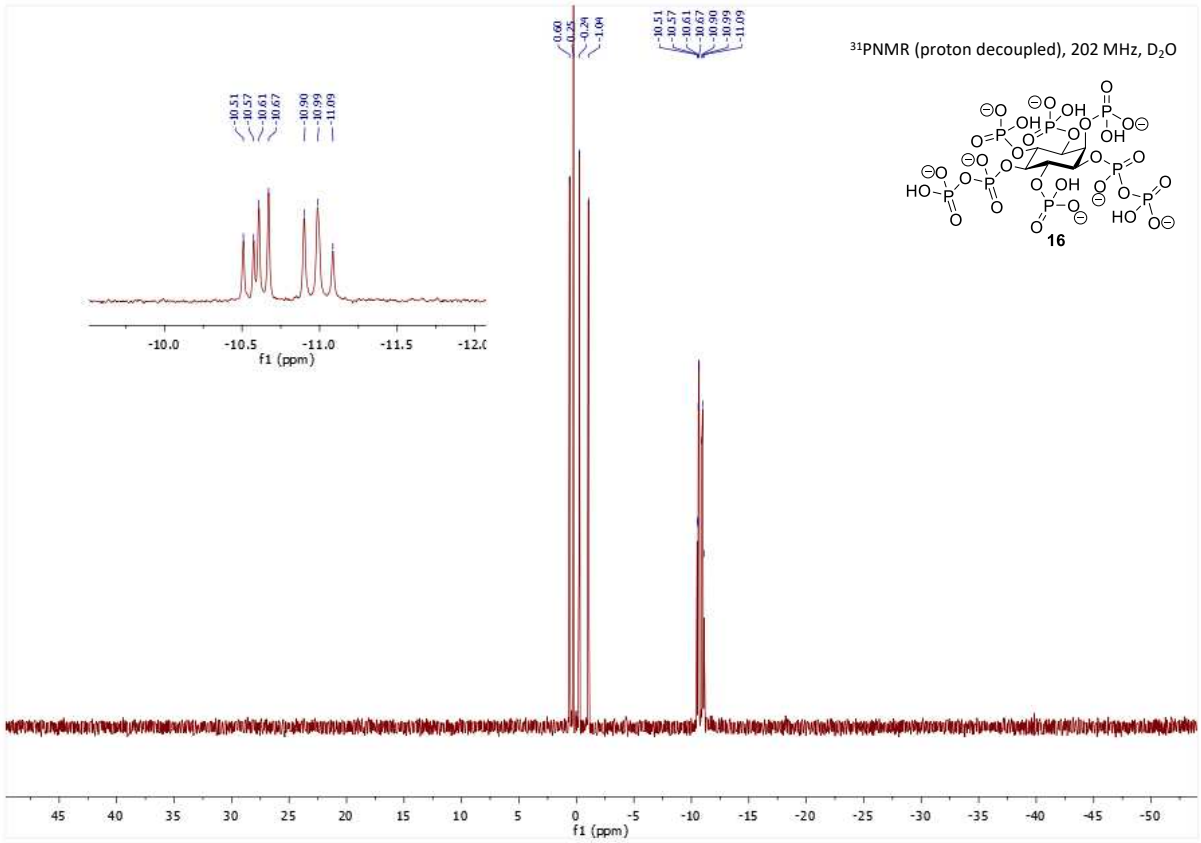

^{31}PNMR (proton coupled), 202 MHz, D_2O

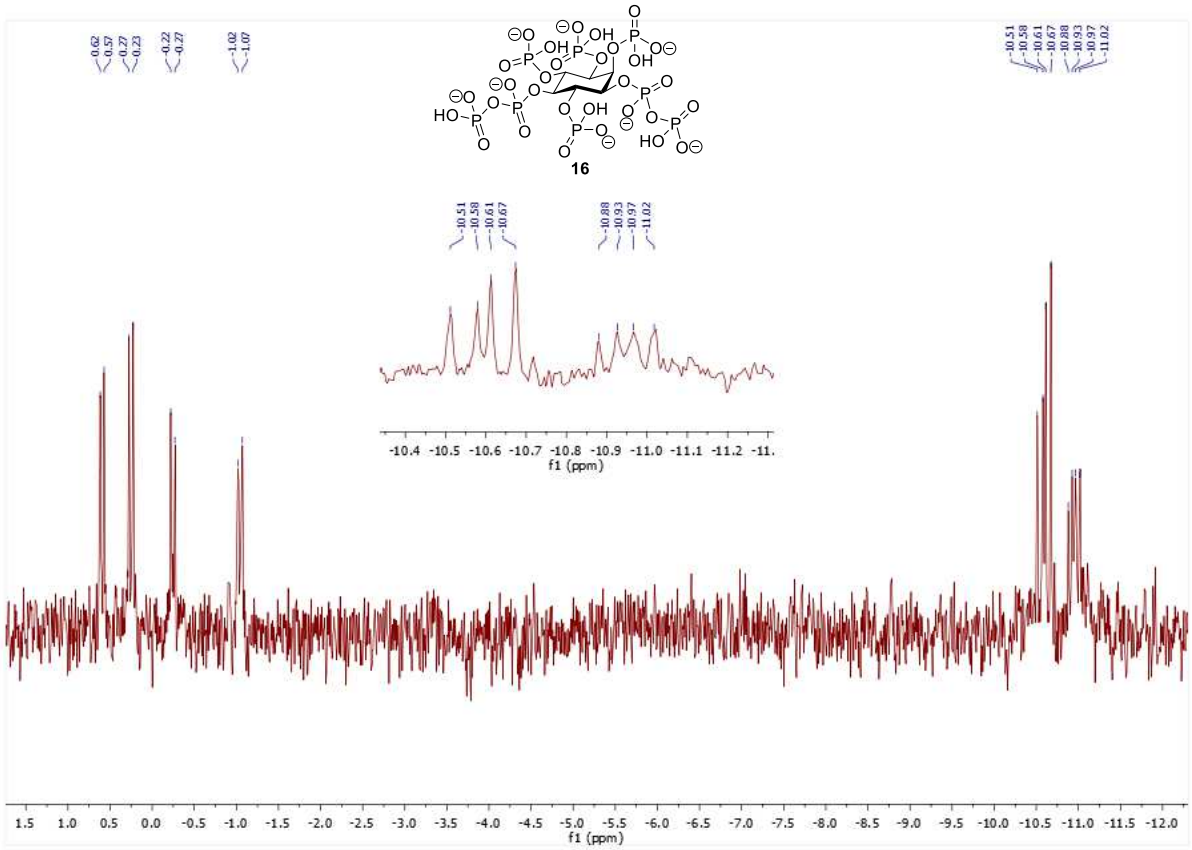

^{13}CNMR, 125 MHz, D_20

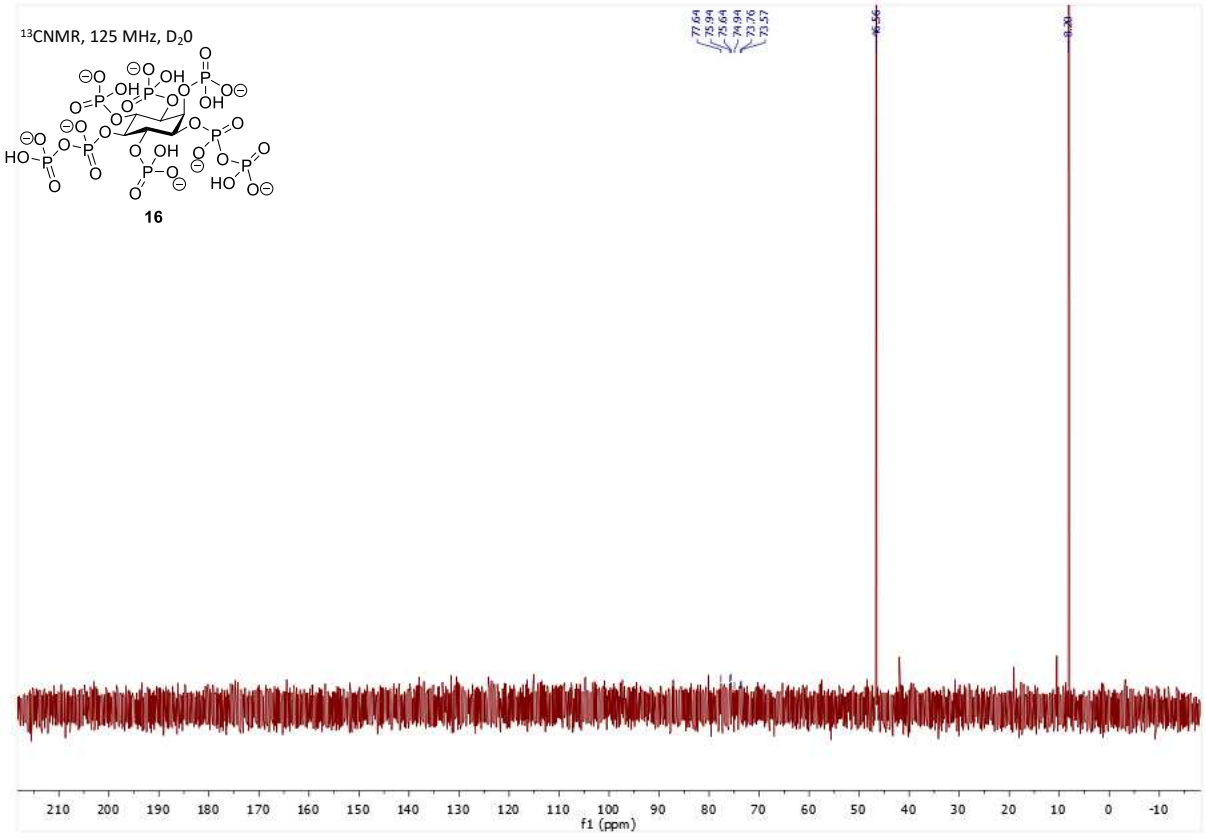

^{1}H-^{31}P HMBC

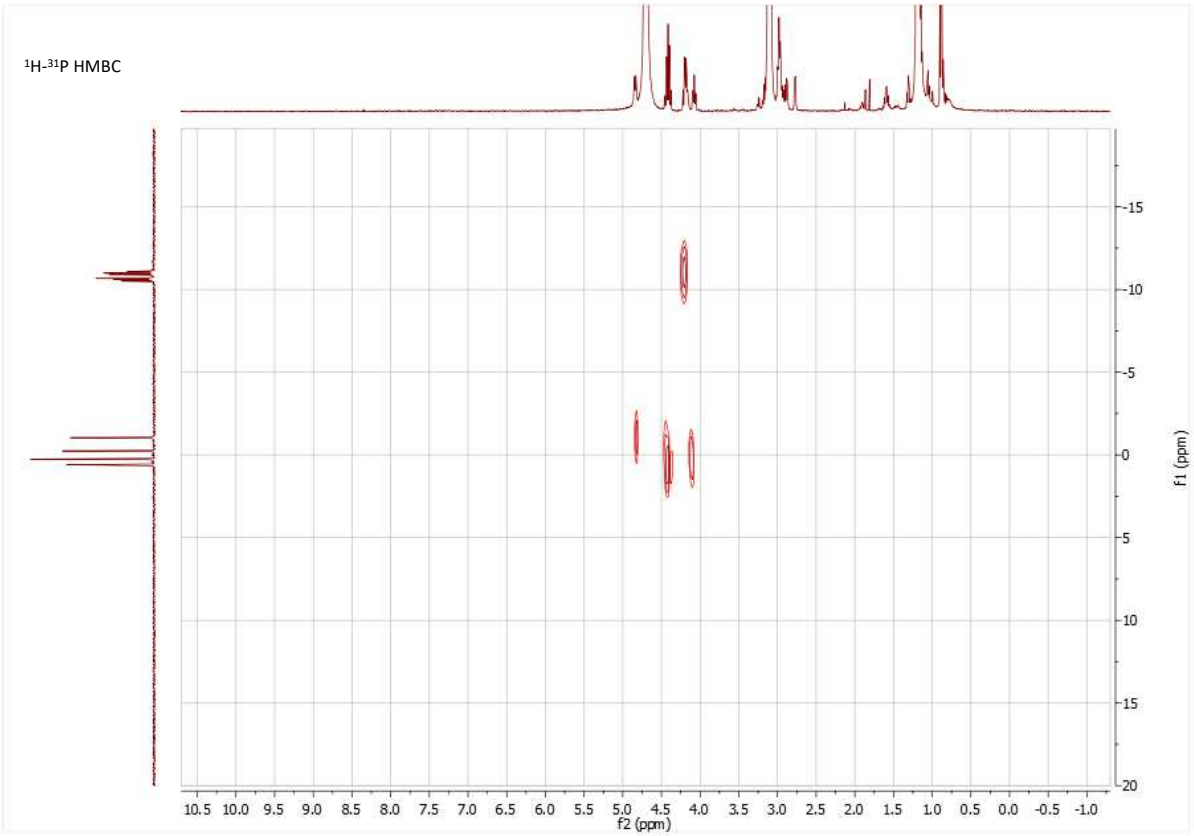

^{1}H-^{1}H COSY

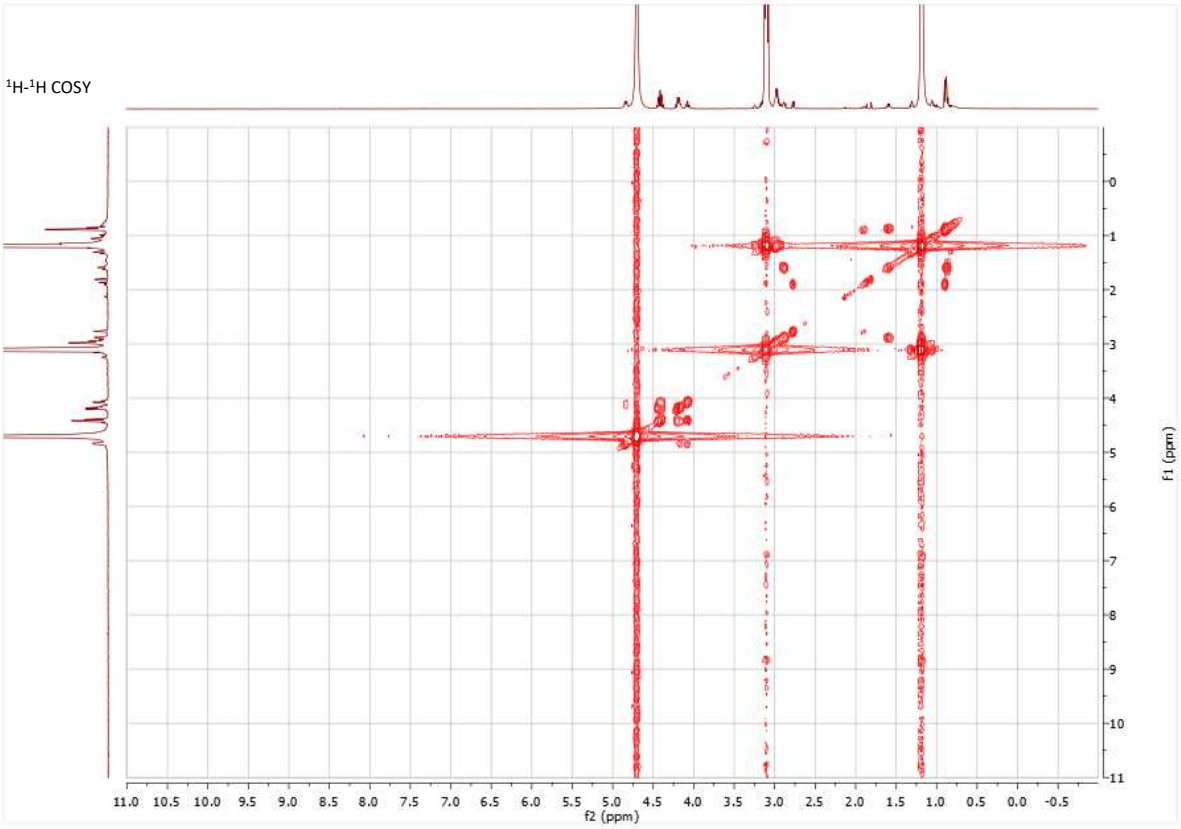

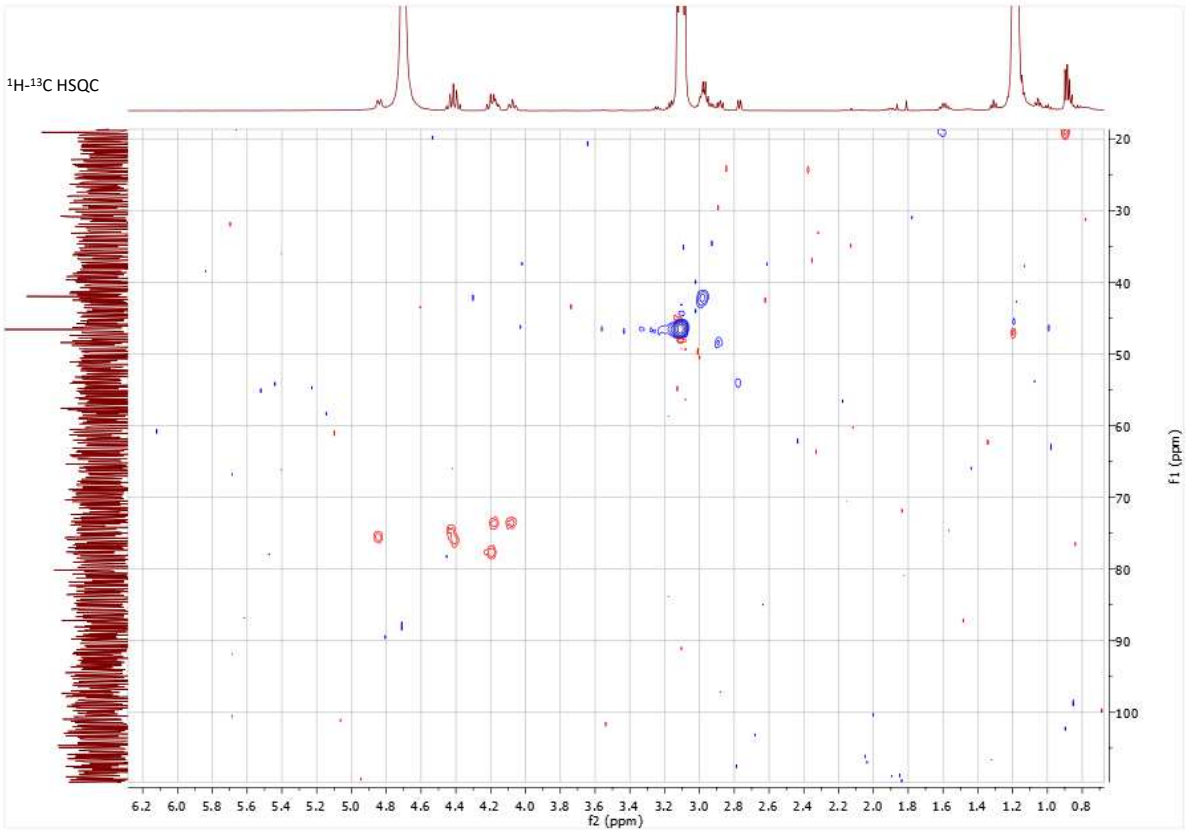
^{1}H-^{13}C HSQC
f2 (ppm)
F1 (ppm)

Synthesis of HDAC3-SMRT carbohydrate polyphosphates

Methyl α-D-glucopyranoside (**42**)

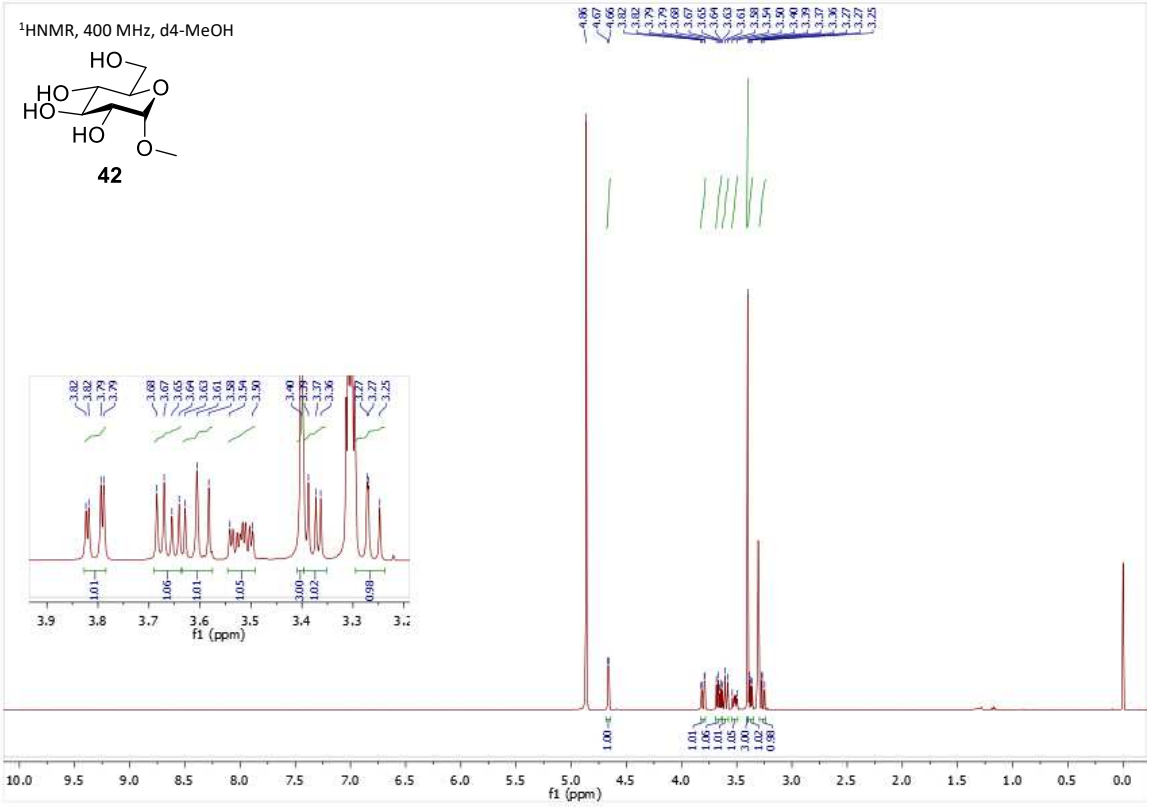

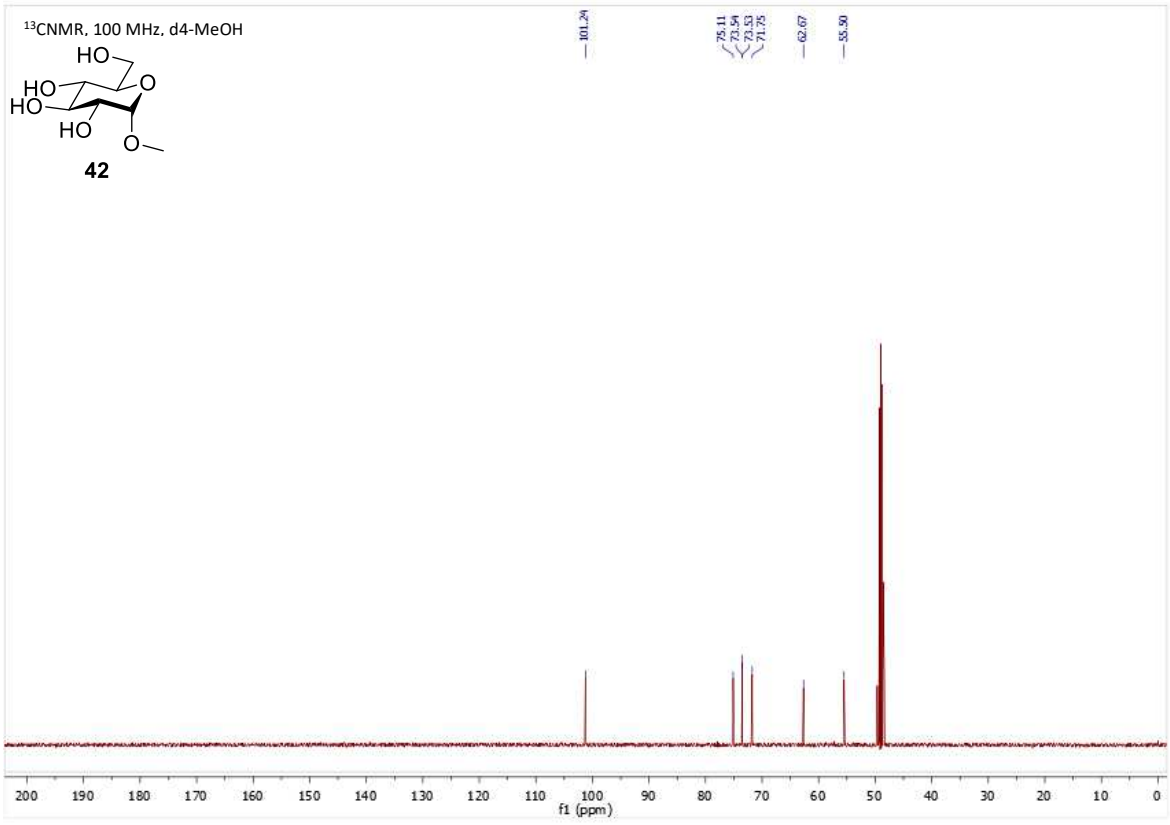

Methyl 4,6-*O*-benzylidene-α-D-glucopyranoside (**44**)

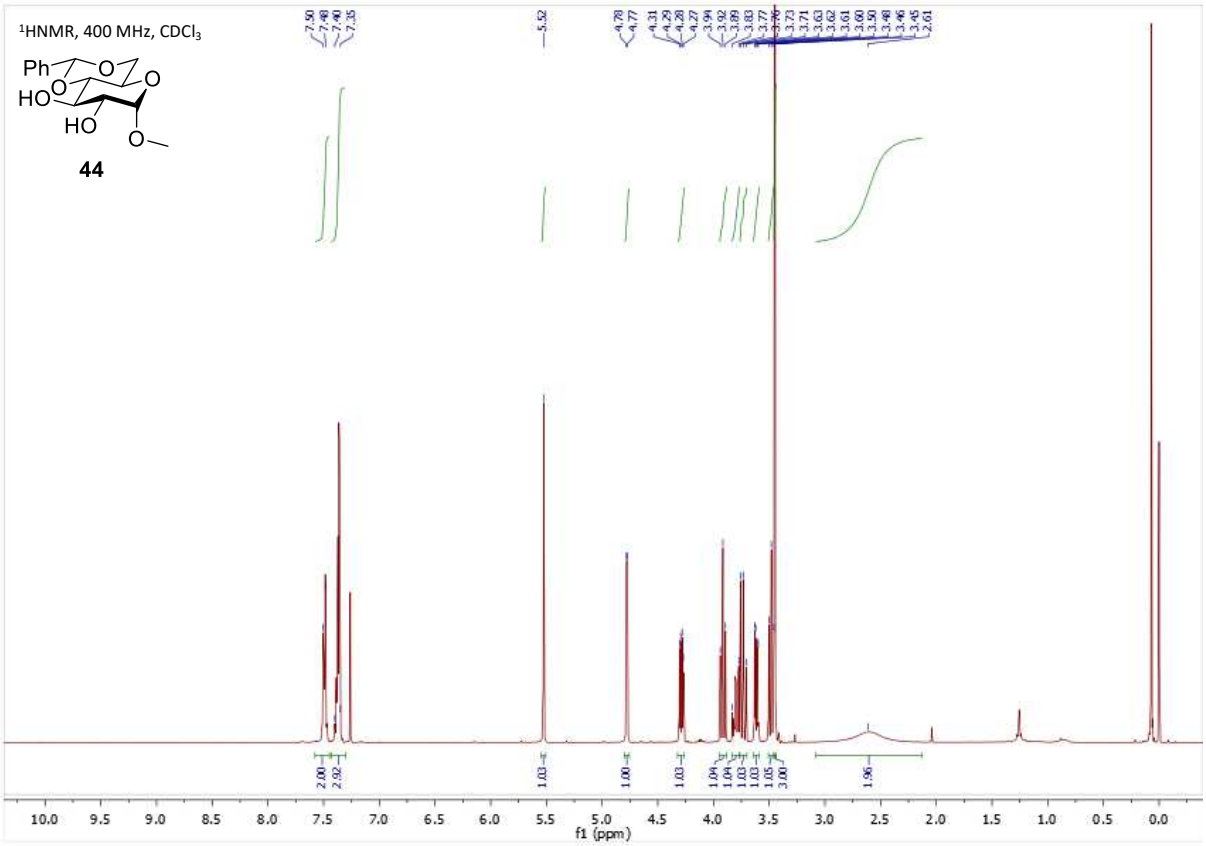

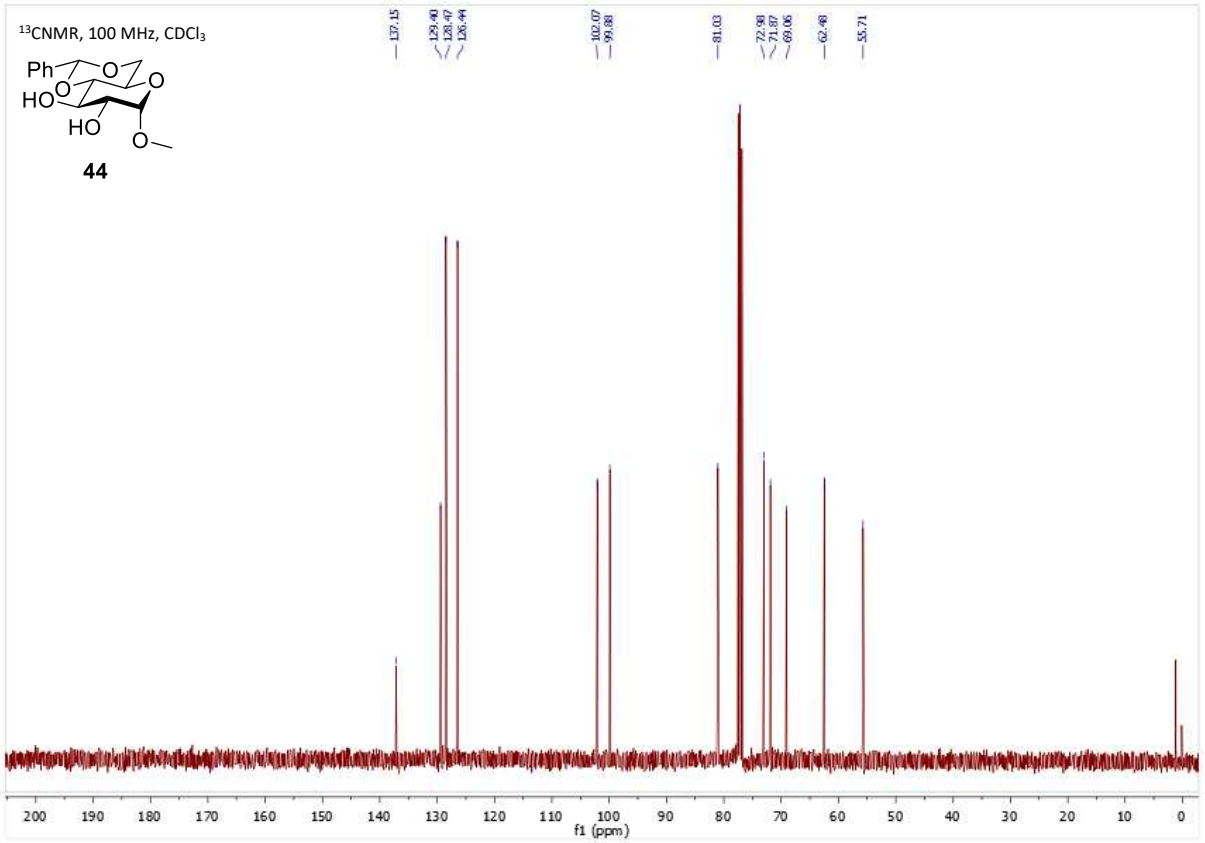

Methyl 6-*O*-benzyl α-D-glucopyranoside (**45**)

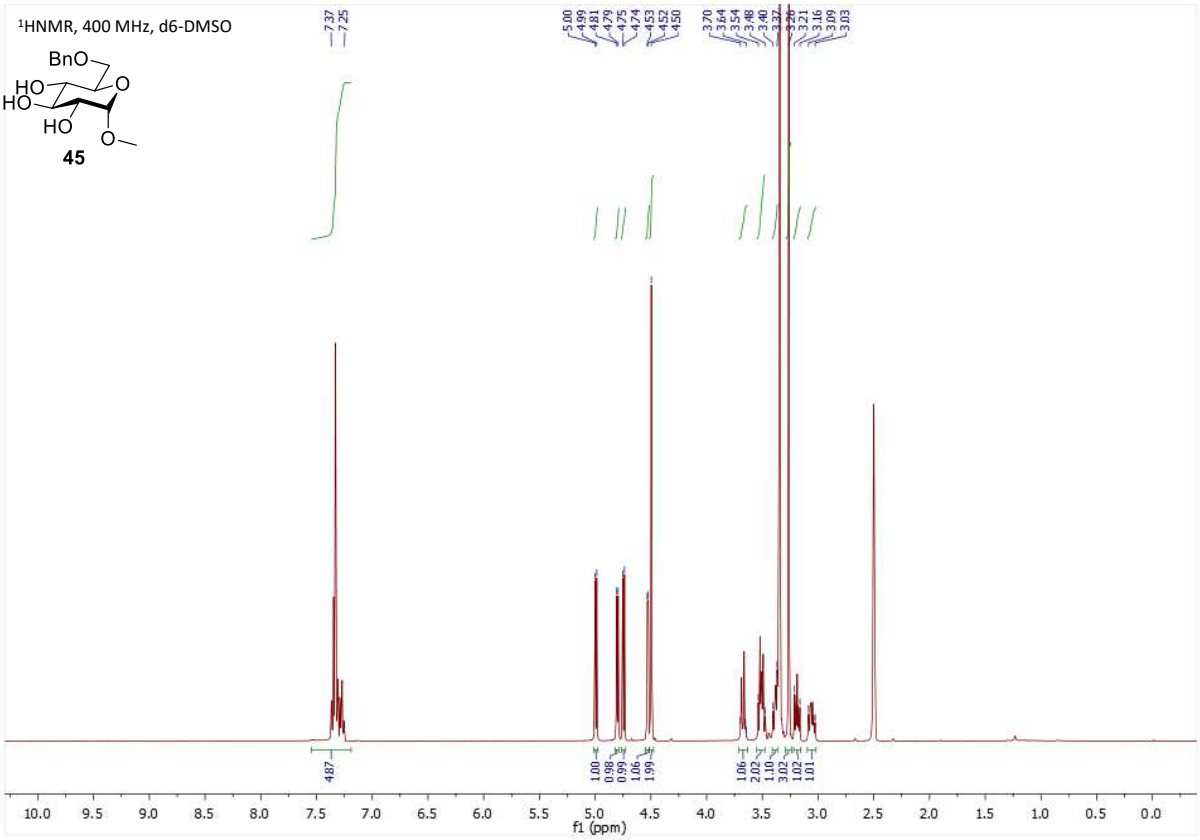

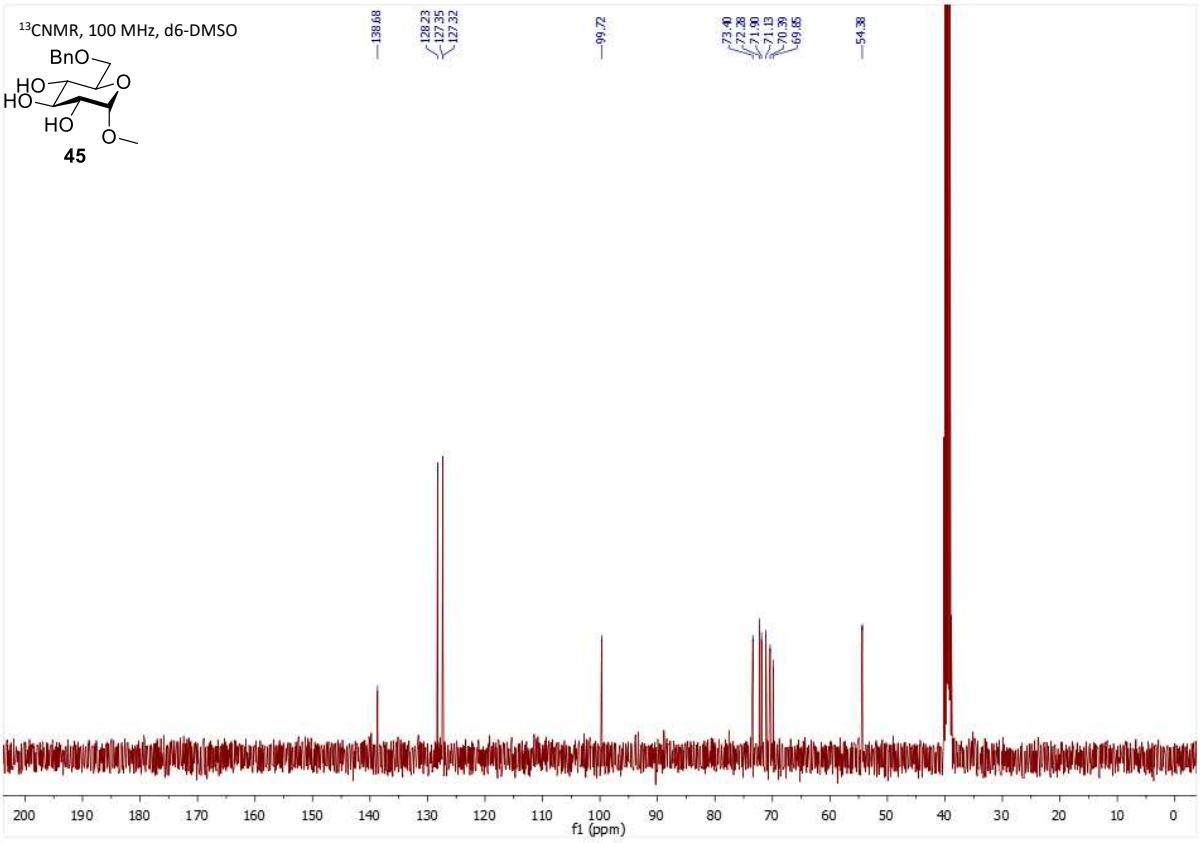

^{1}H-^{1}H COSY

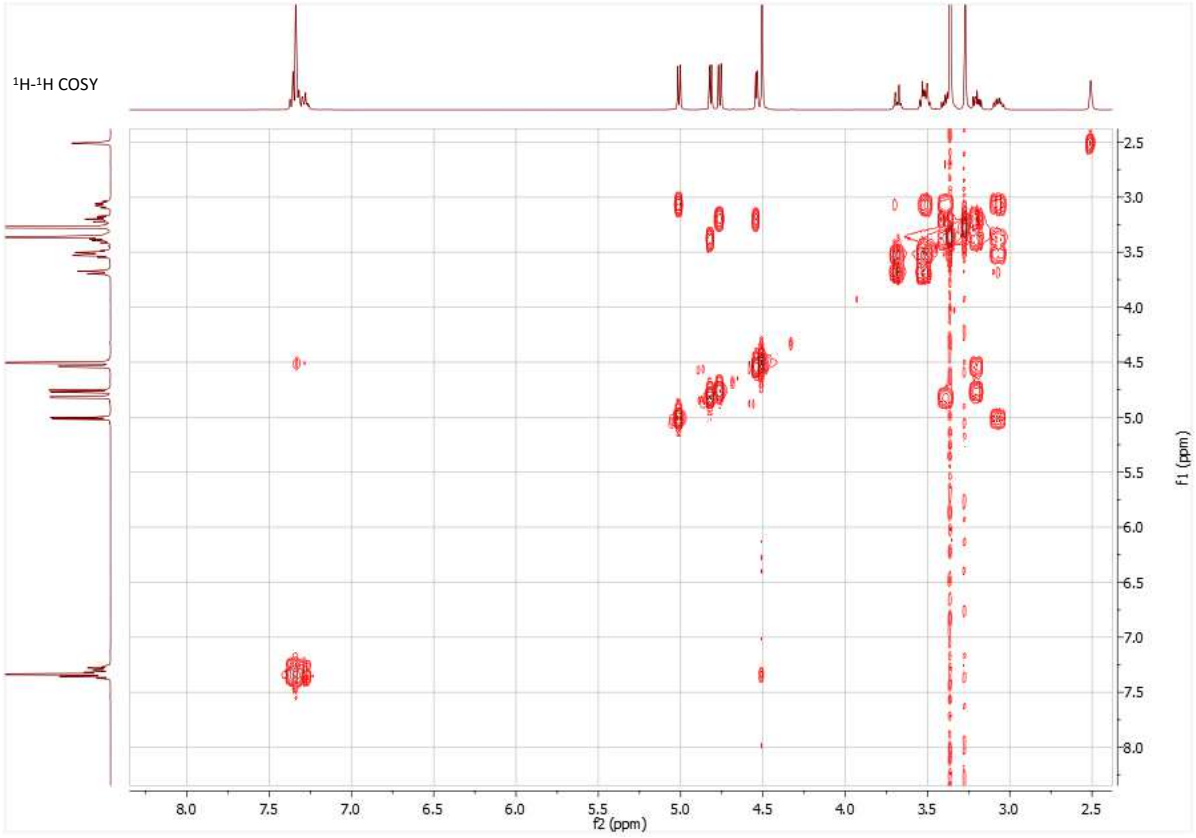

^{1}H-^{13}C HSQC

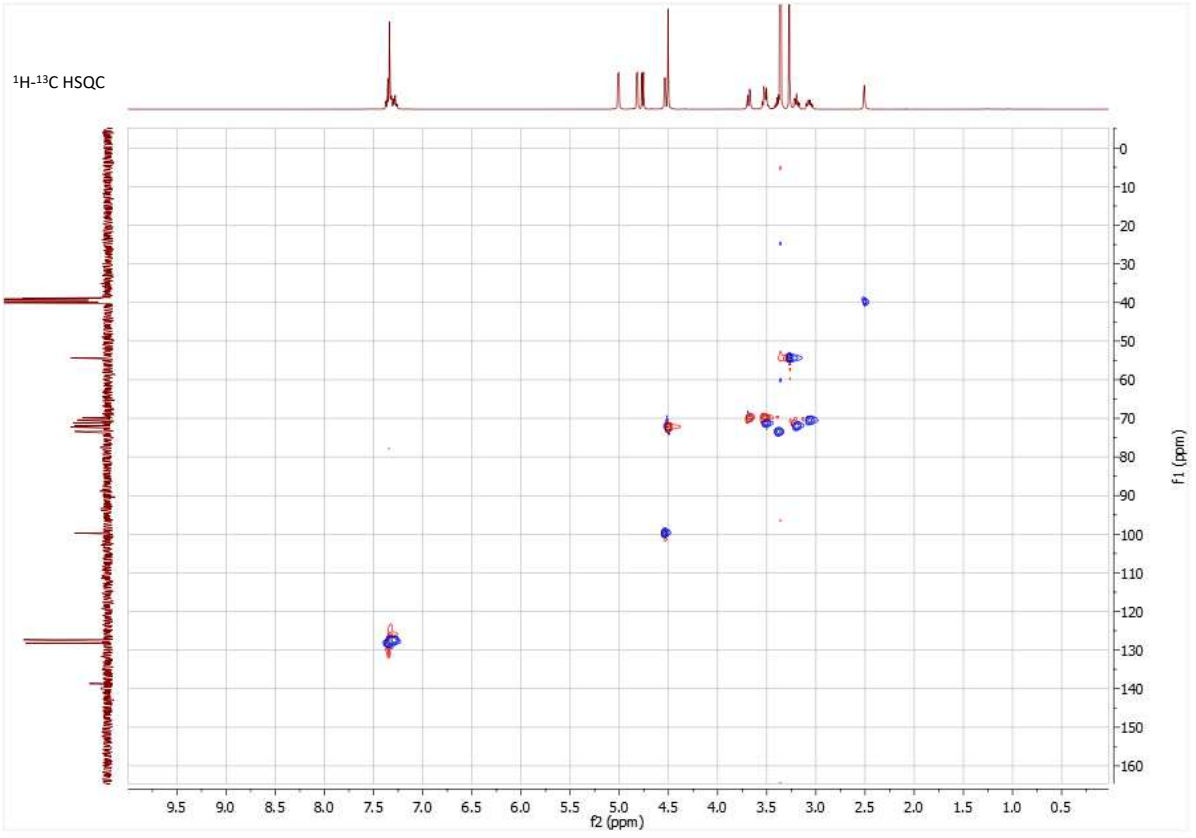

Methyl 2,3-di-*O*-benzoyl-4,6-*O*-benzylidene-α-D-glucopyranoside (**46**)

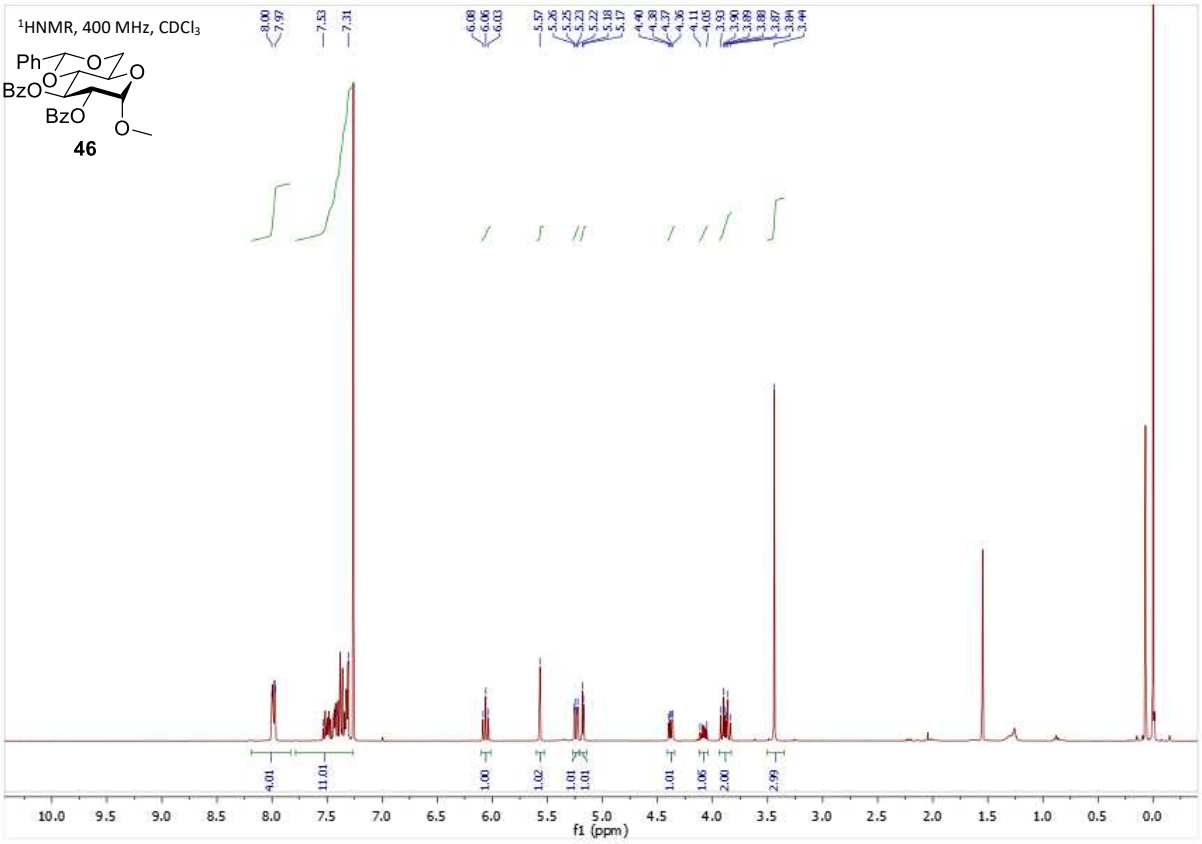

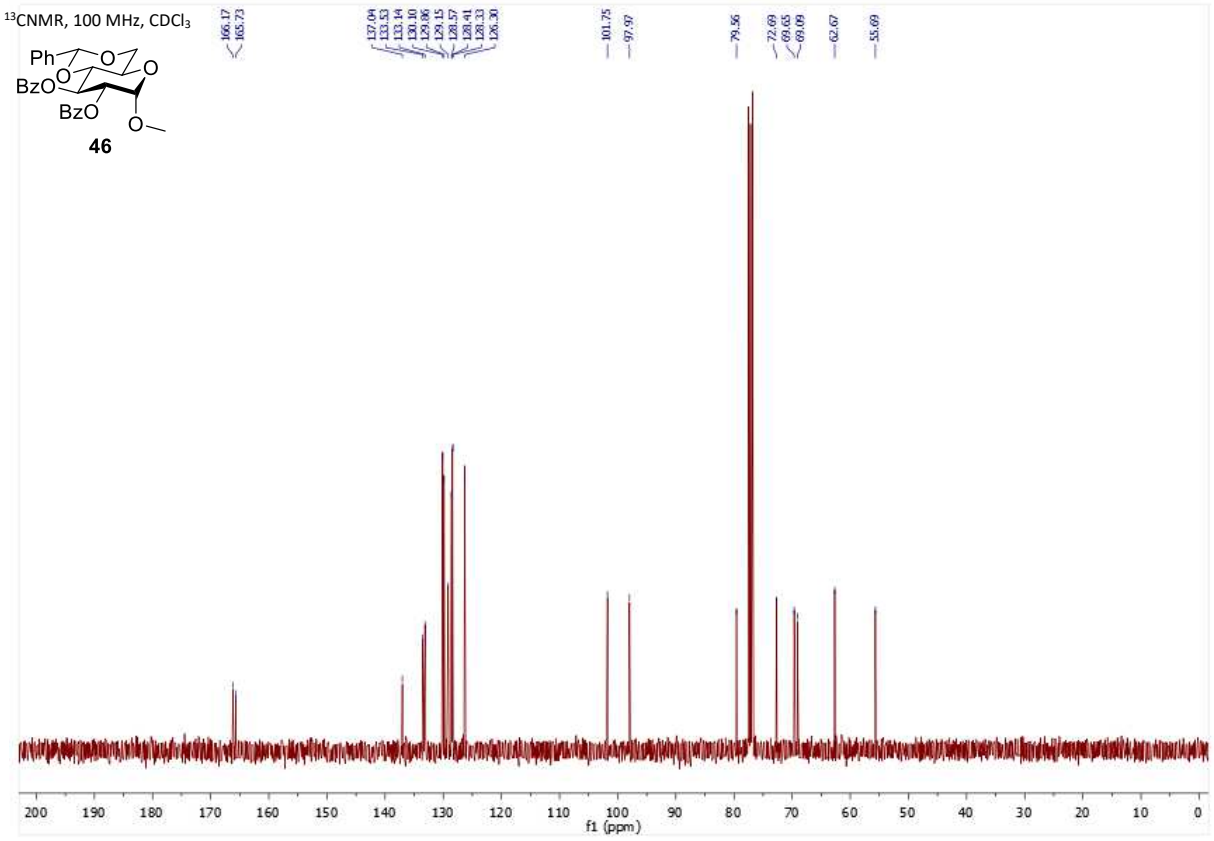

Methyl 2,3-di-*O*-benzoyl-6-*O*-benzyl-α-D-glucopyranoside (**47**)

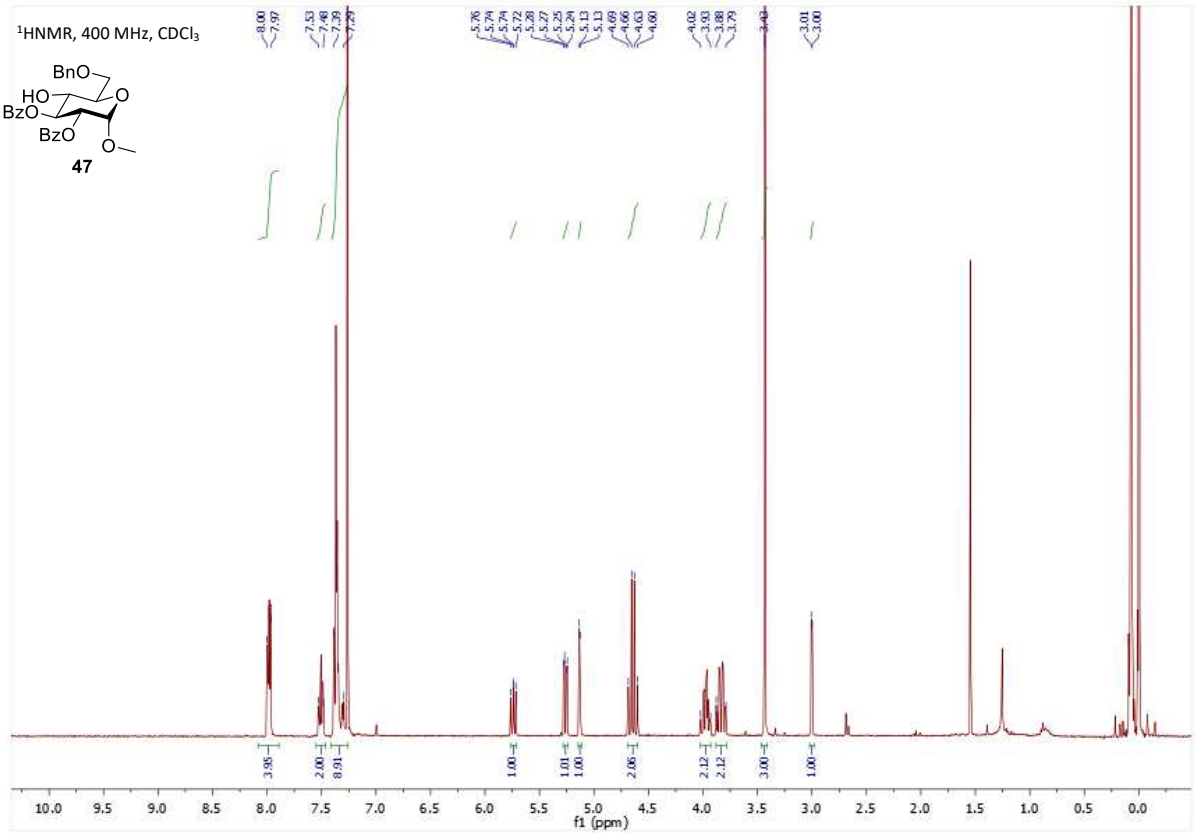

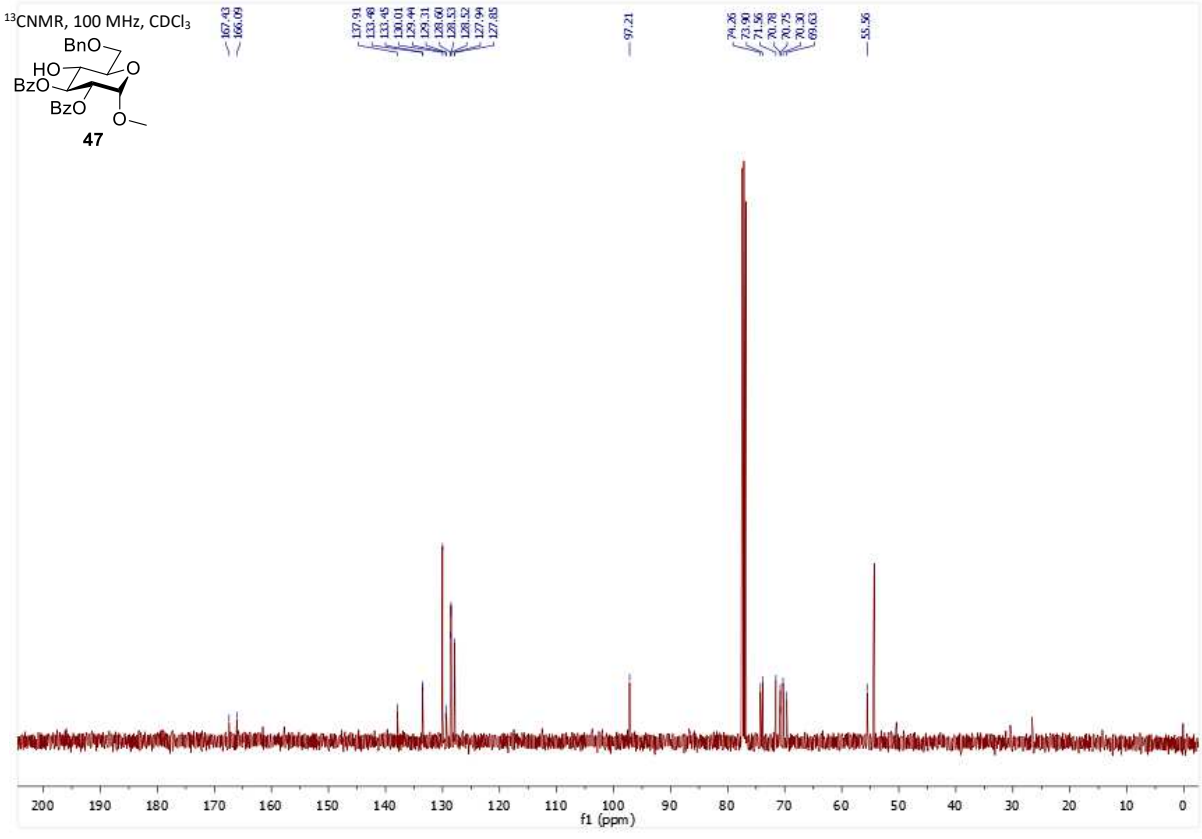

Methyl 6-*O*-benzyl-α-D-glucopyranoside 2,3,4-tris(dibenzylphosphate) (**48**)

^{1}HNMR, 400 MHz, $CDCl_3$

48

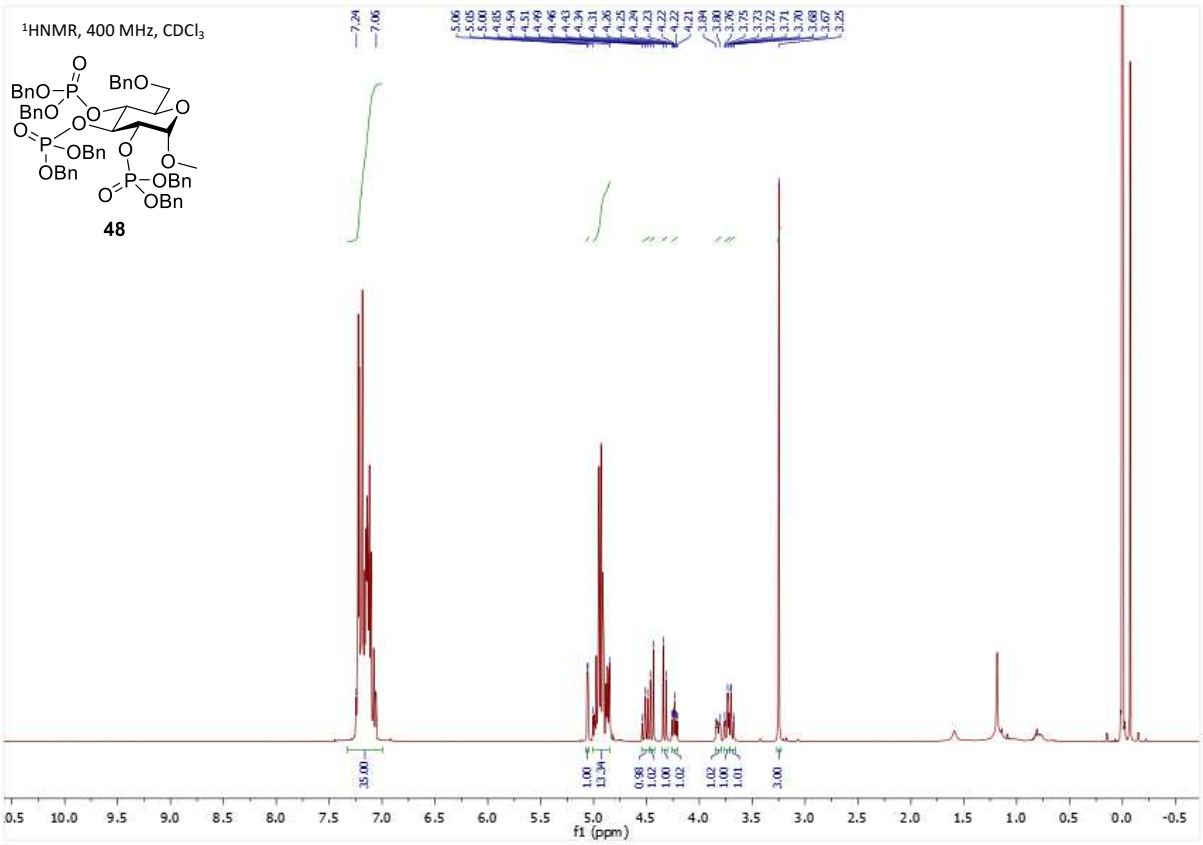

^{31}PNMR, 162 MHz, $CDCl_3$

48

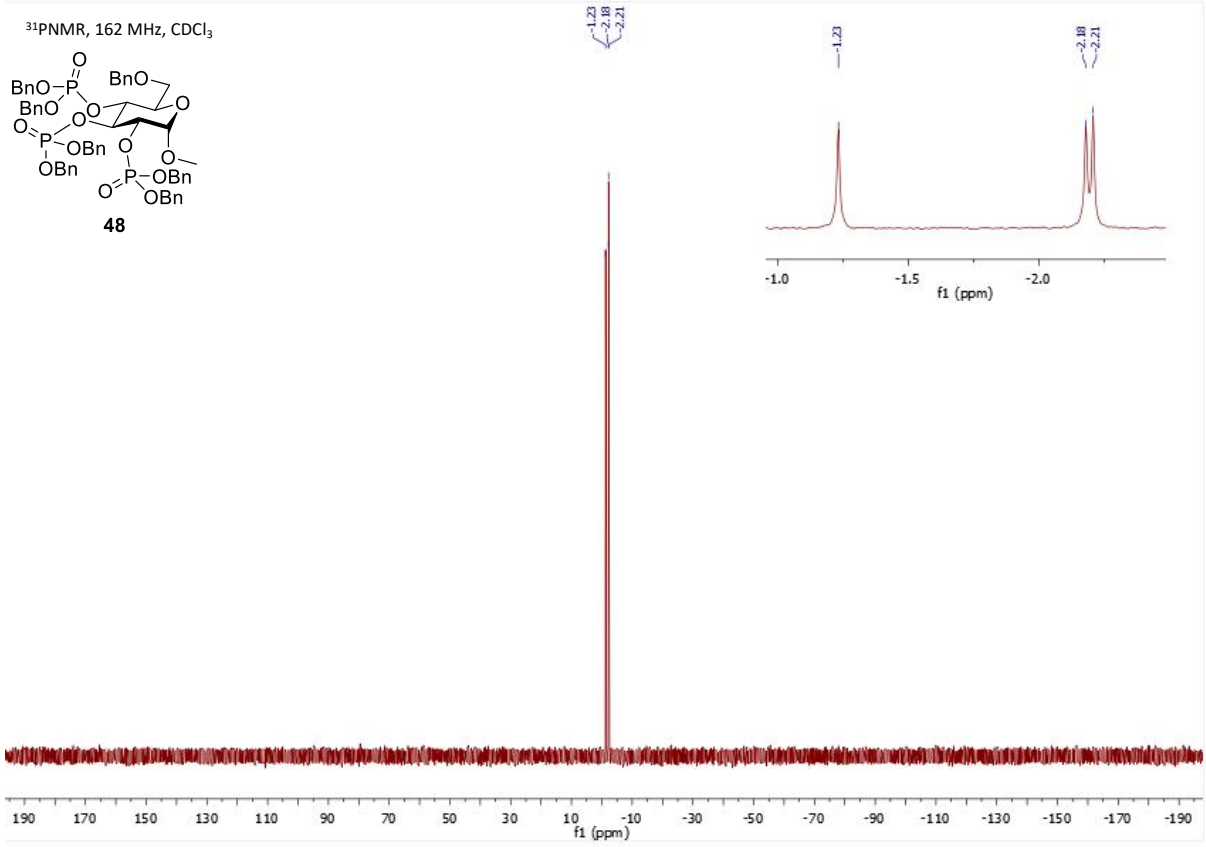

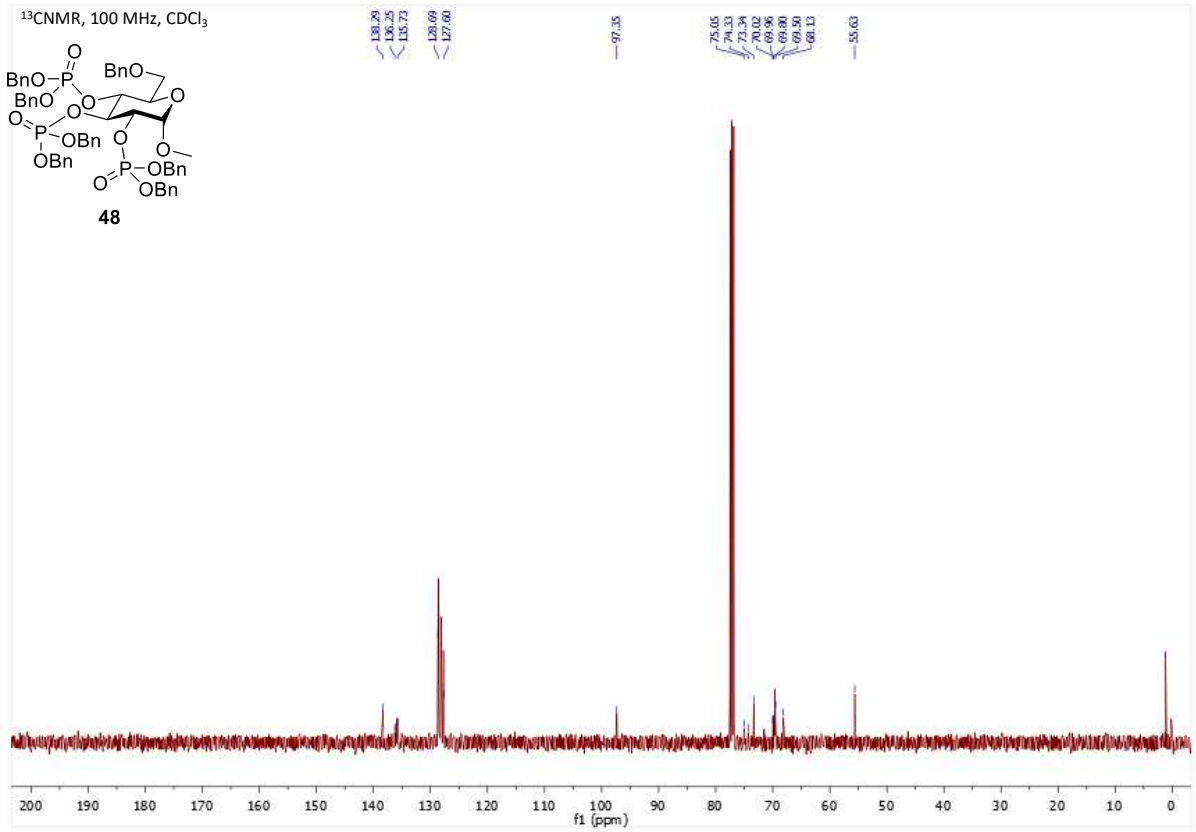

Methyl 6-*O*-benzyl-α-D-glucopyranoside 2,3,4-trisphosphate triethylammonium salt (**37**)

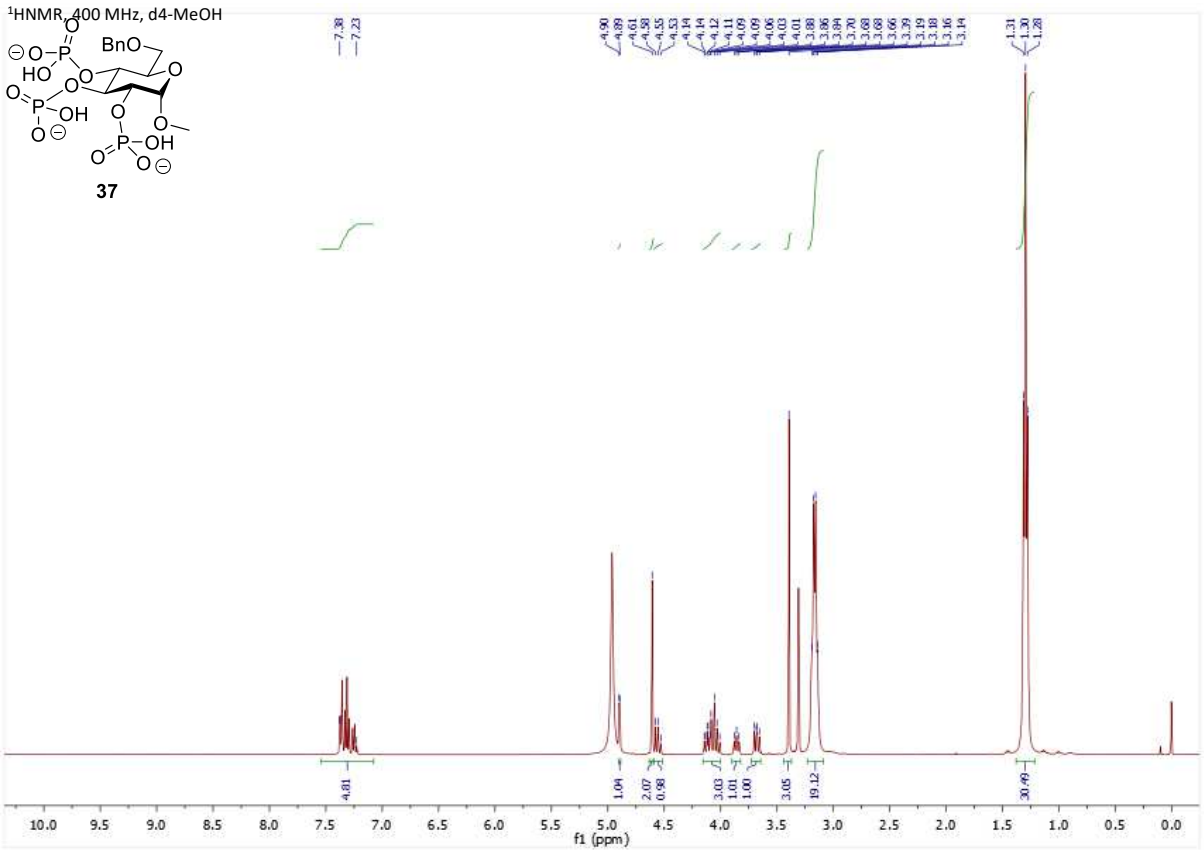

^{31}PNMR, 162 MHz, d4-MeOH

37

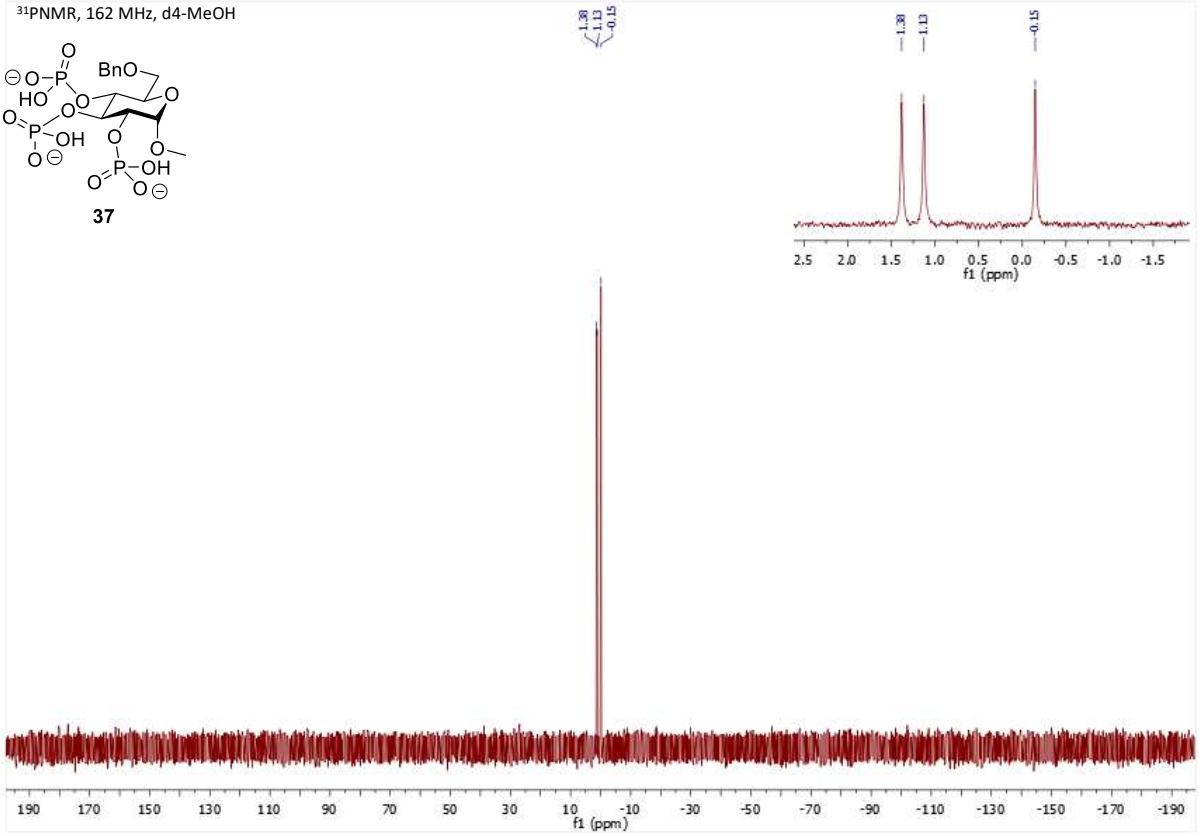

^{13}CNMR, 100 MHz, d4-MeOH

37

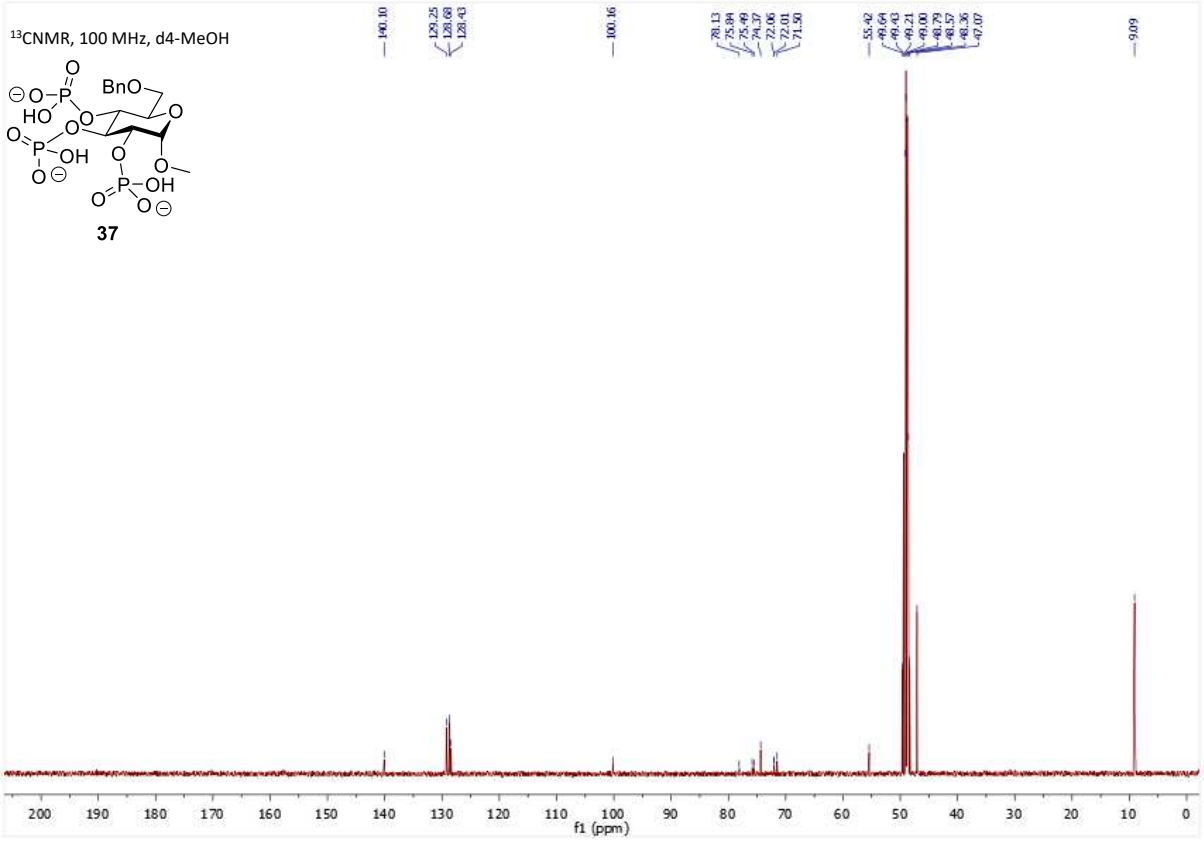

Methyl α-D-glucopyranoside 2,3,4-trisphosphate triethylammonium salt (**38**)

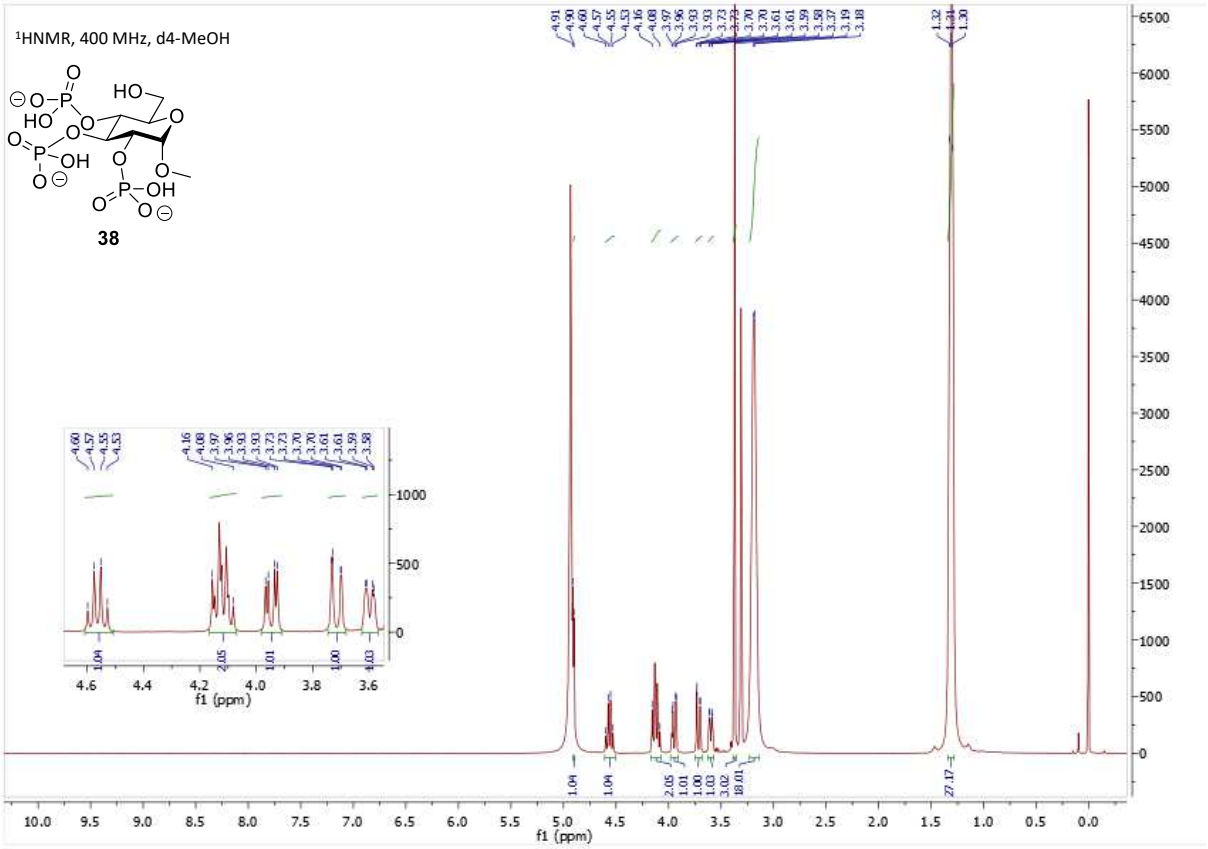

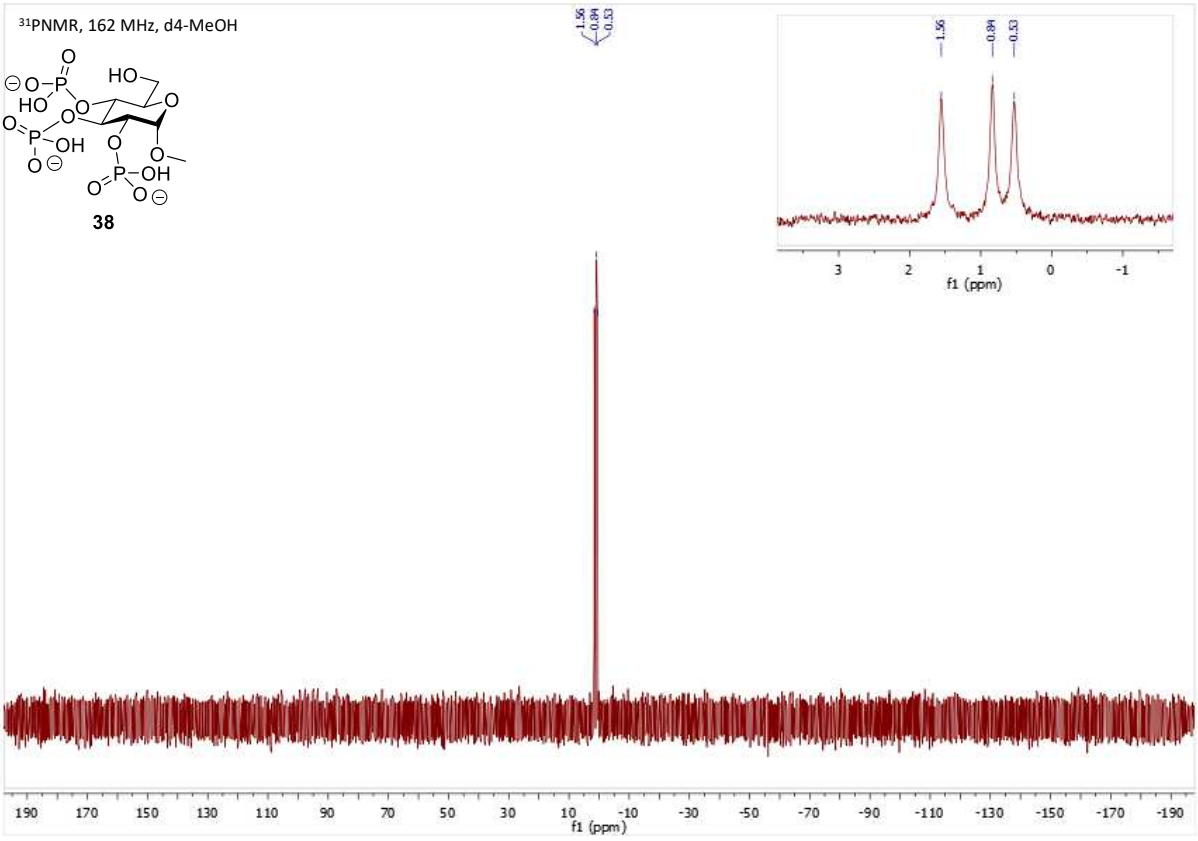

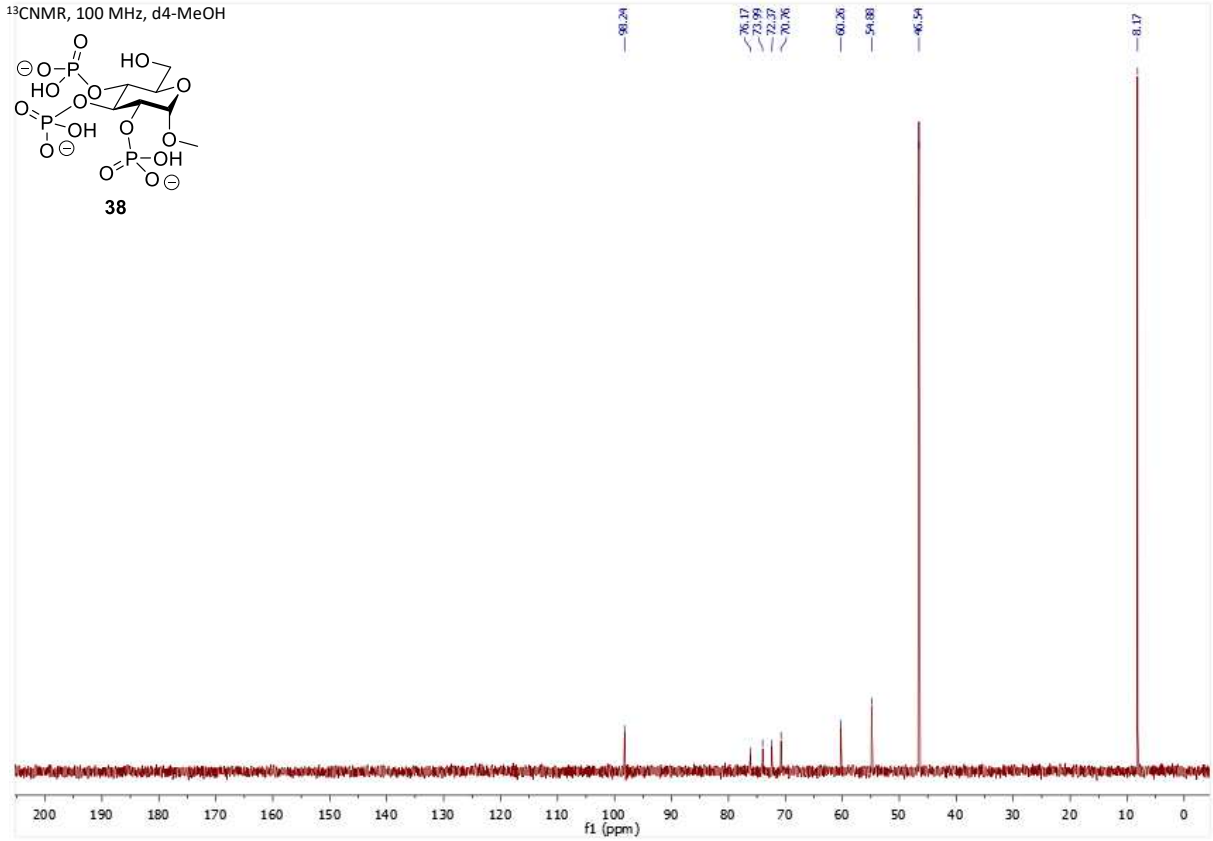

Methyl α-D-glucopyranoside 2,3,4,6-tetrakis(dibenzylphosphate) (**43**)

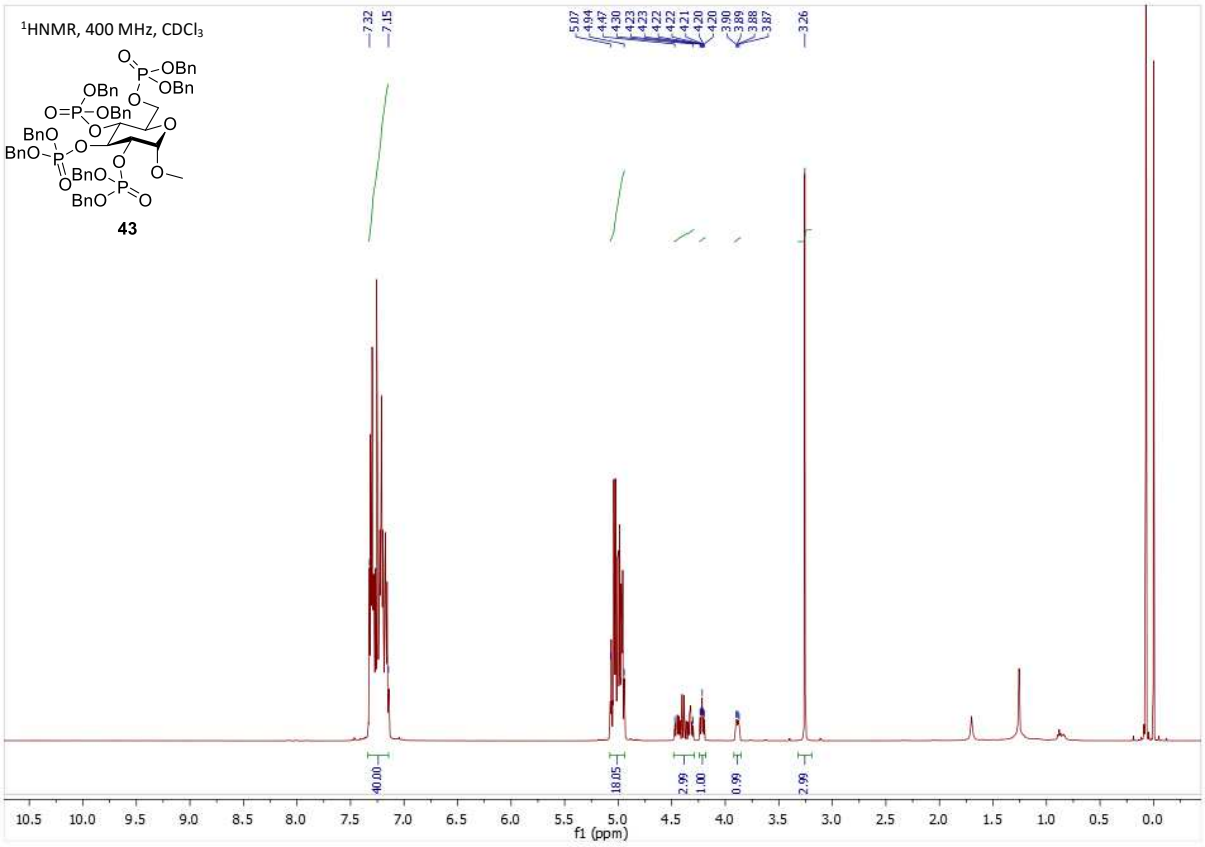

^{31}PNMR, 162 MHz, $CDCl_3$

43

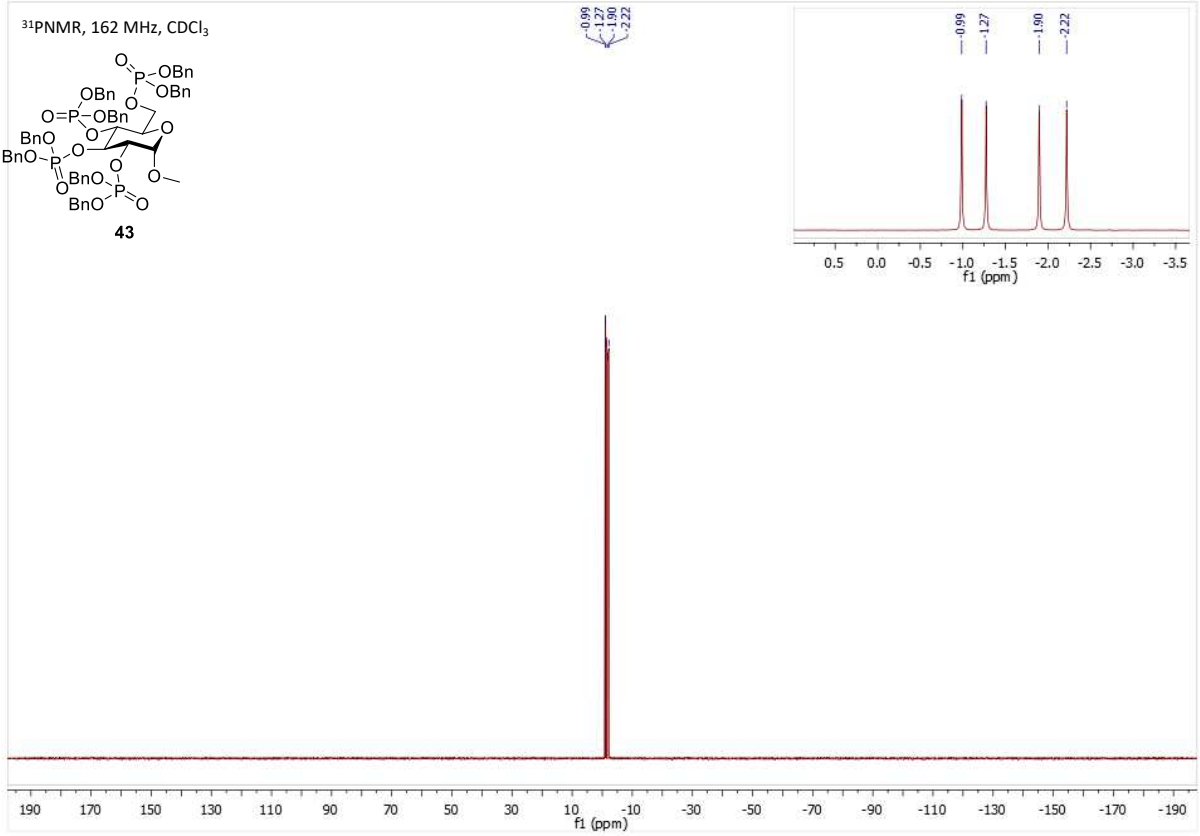

^{13}CNMR, 100 MHz, $CDCl_3$

43

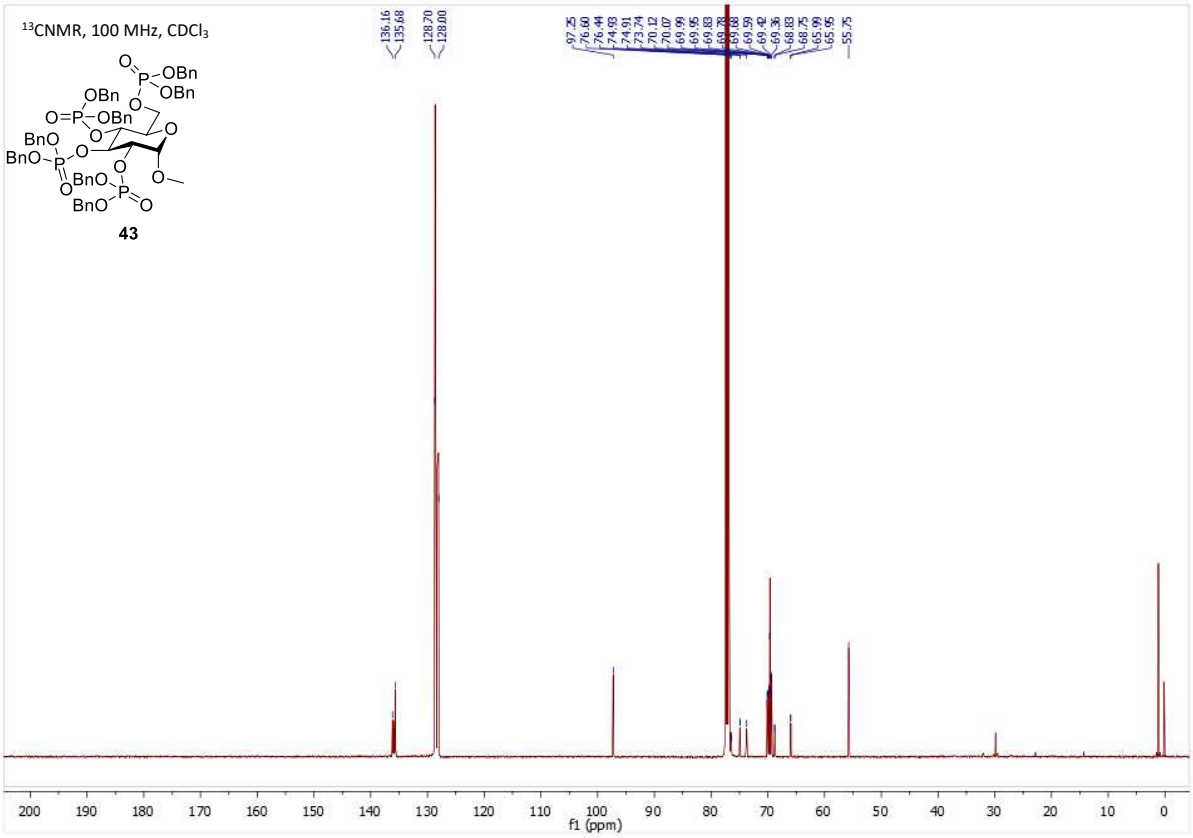

Methyl α-D-glucopyranoside 2,3,4,6-tetrakisphosphate triethylammonium salt (**36**)

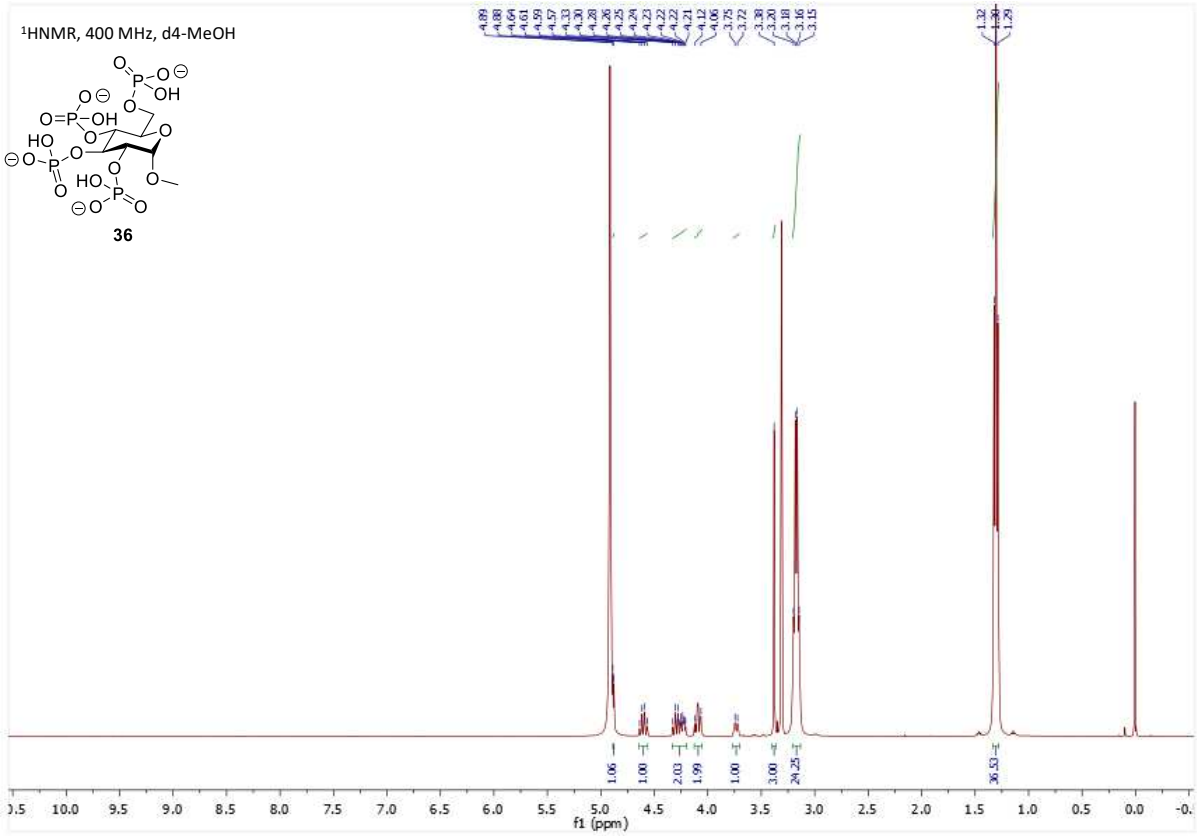

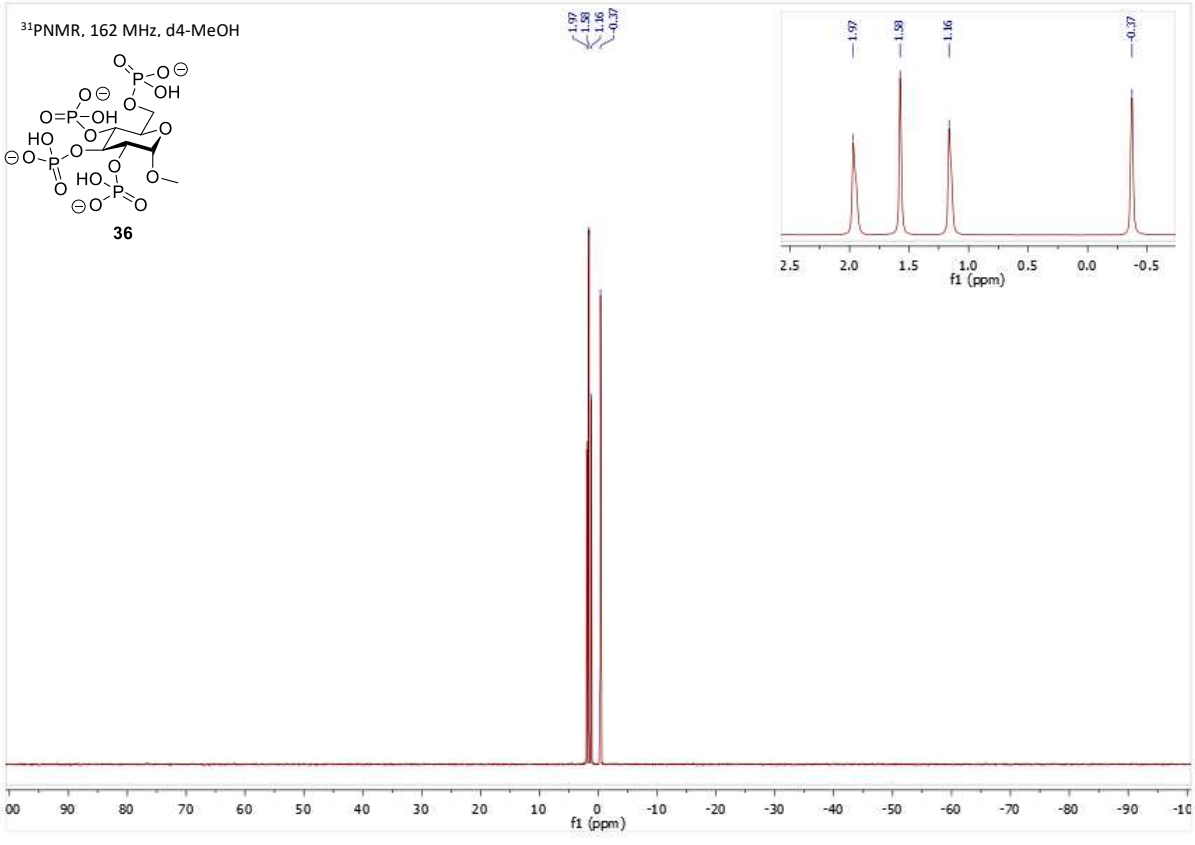

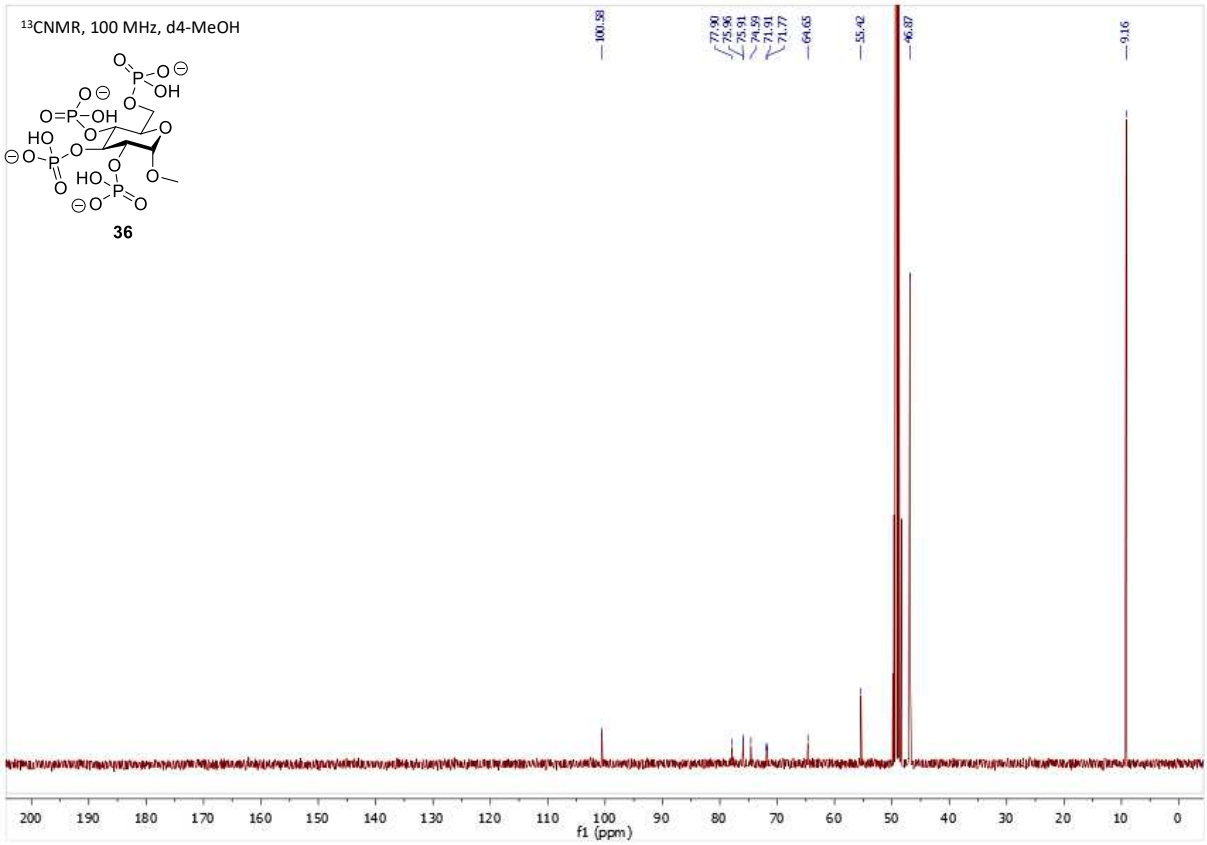

Methyl β-D-glucopyranoside 2,3,4,6-tetrakis(dibenzylphosphate) (**57**)

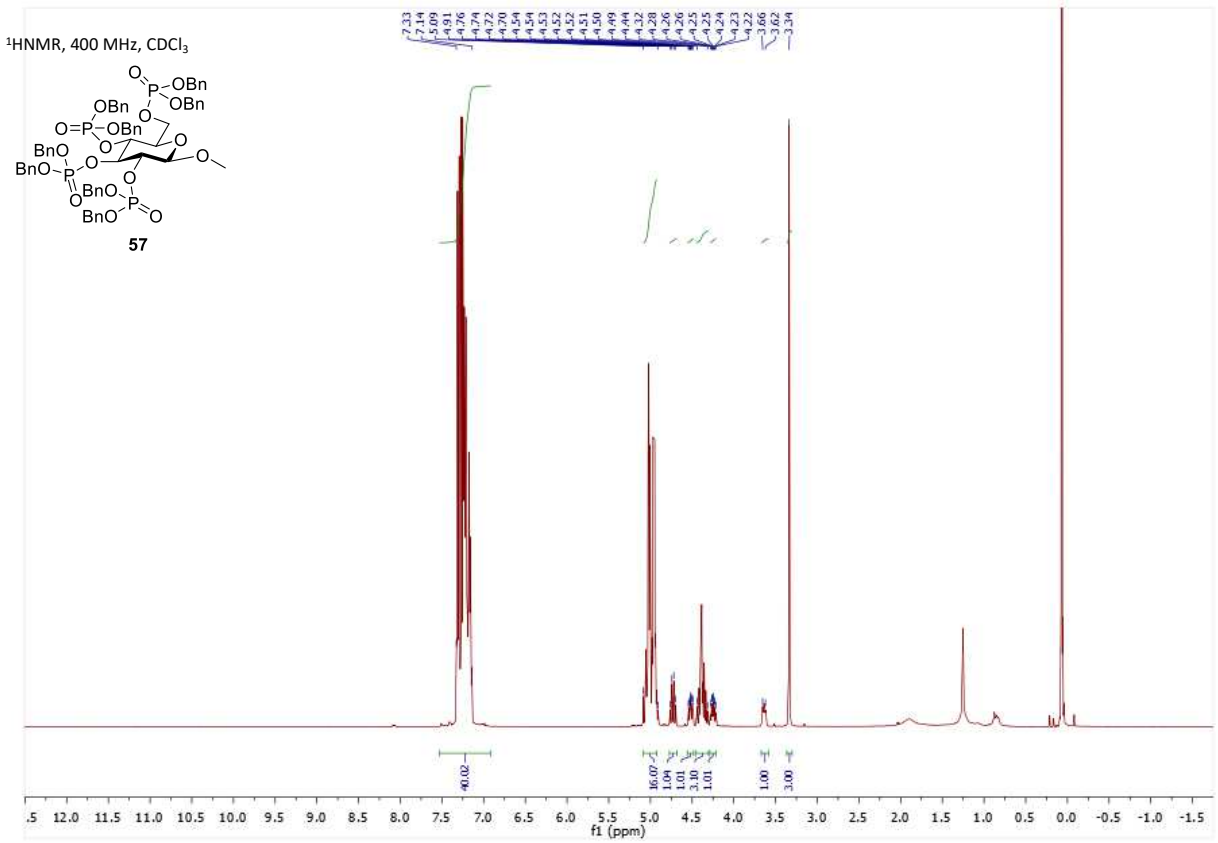

^{31}PNMR, 162 MHz, $CDCl_3$

57

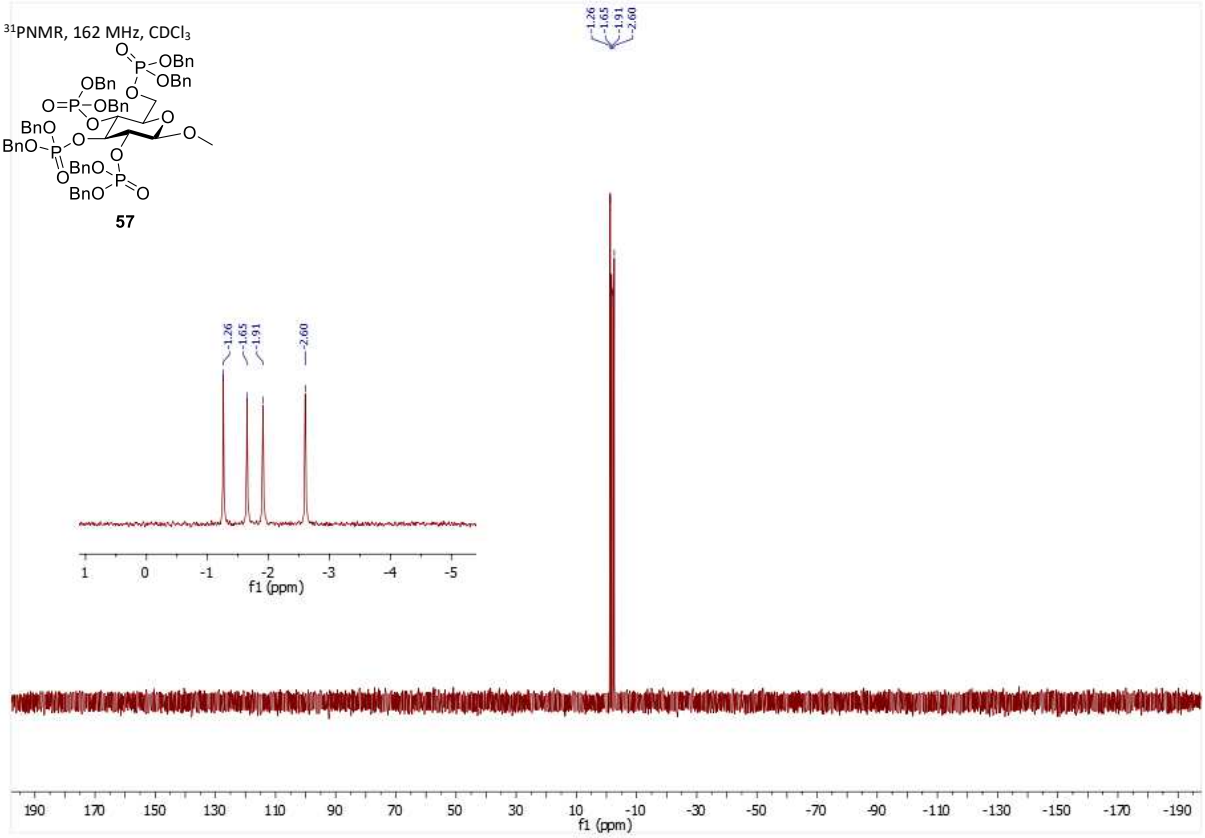

^{13}CNMR, 100 MHz, $CDCl_3$

57

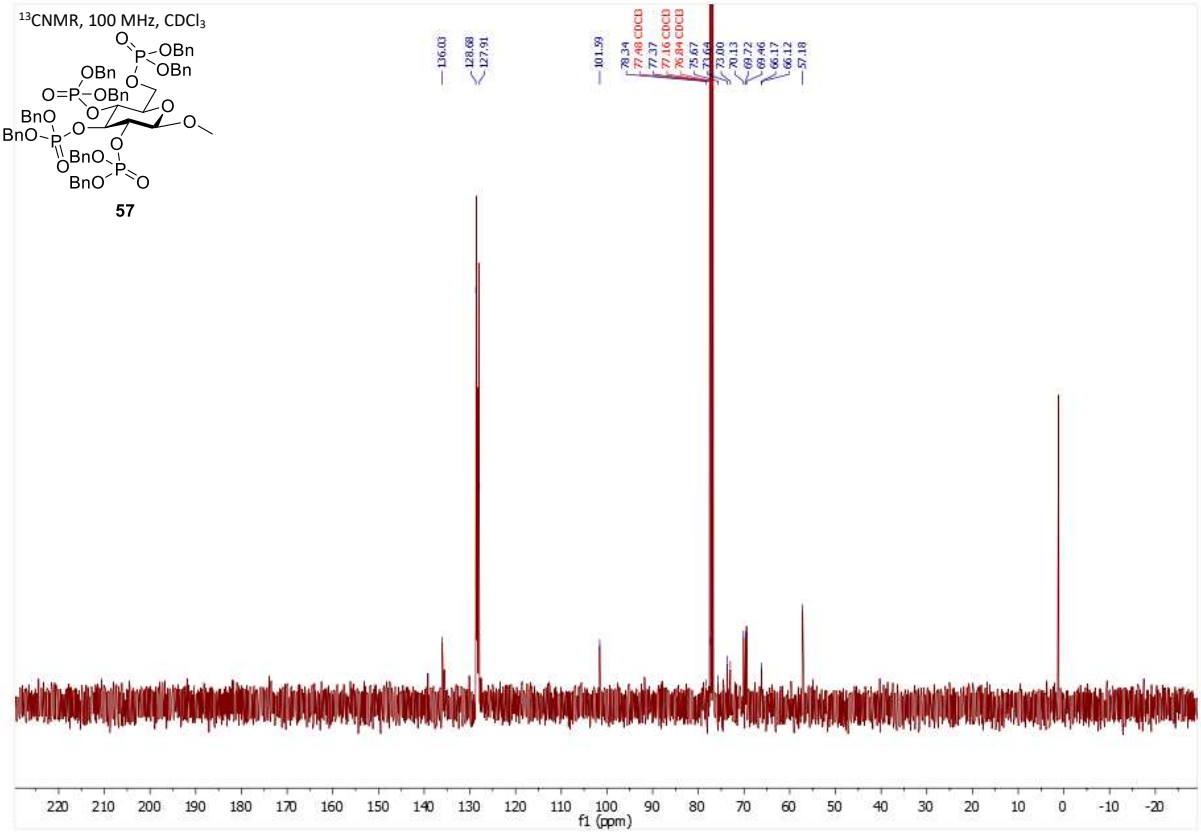

^{1}H-^{1}H COSY

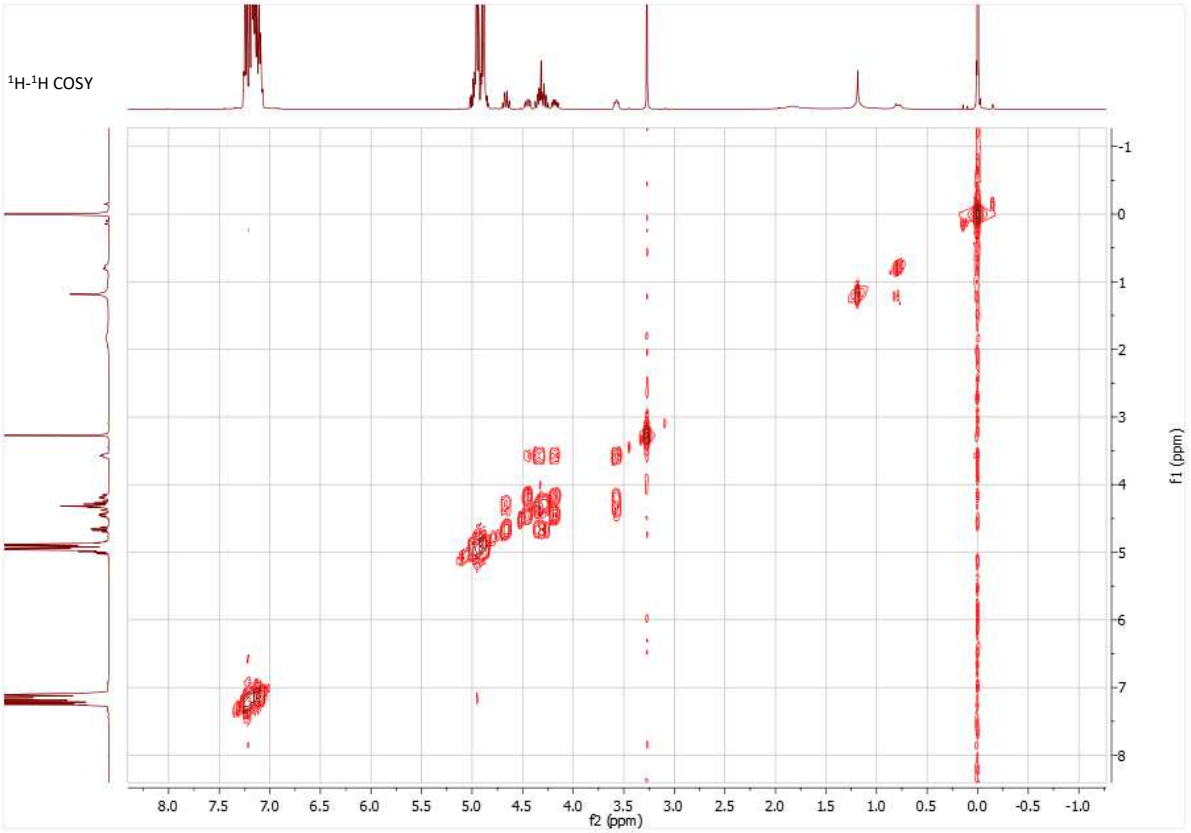

^{1}H-^{13}C HSQC

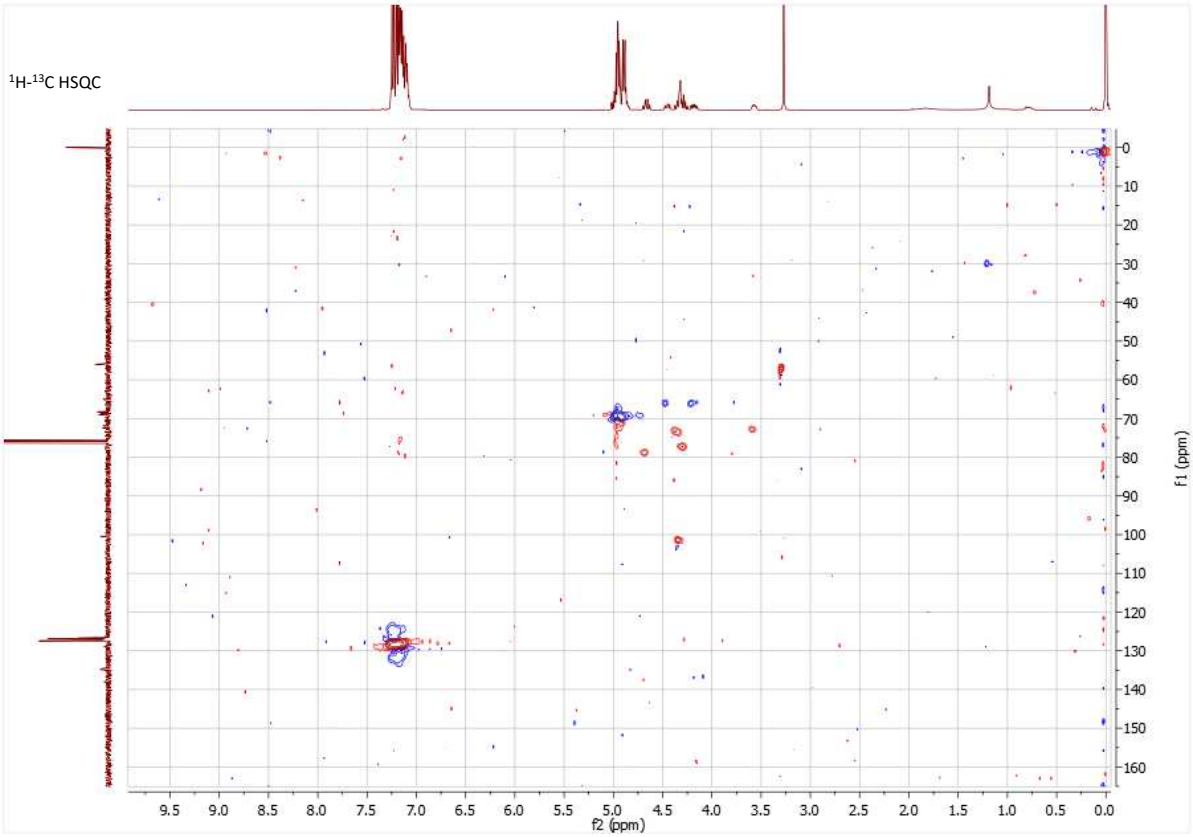

Methyl β-D-glucopyranoside 2,3,4,6-tetrakisphosphate triethylammonium salt (**56**)

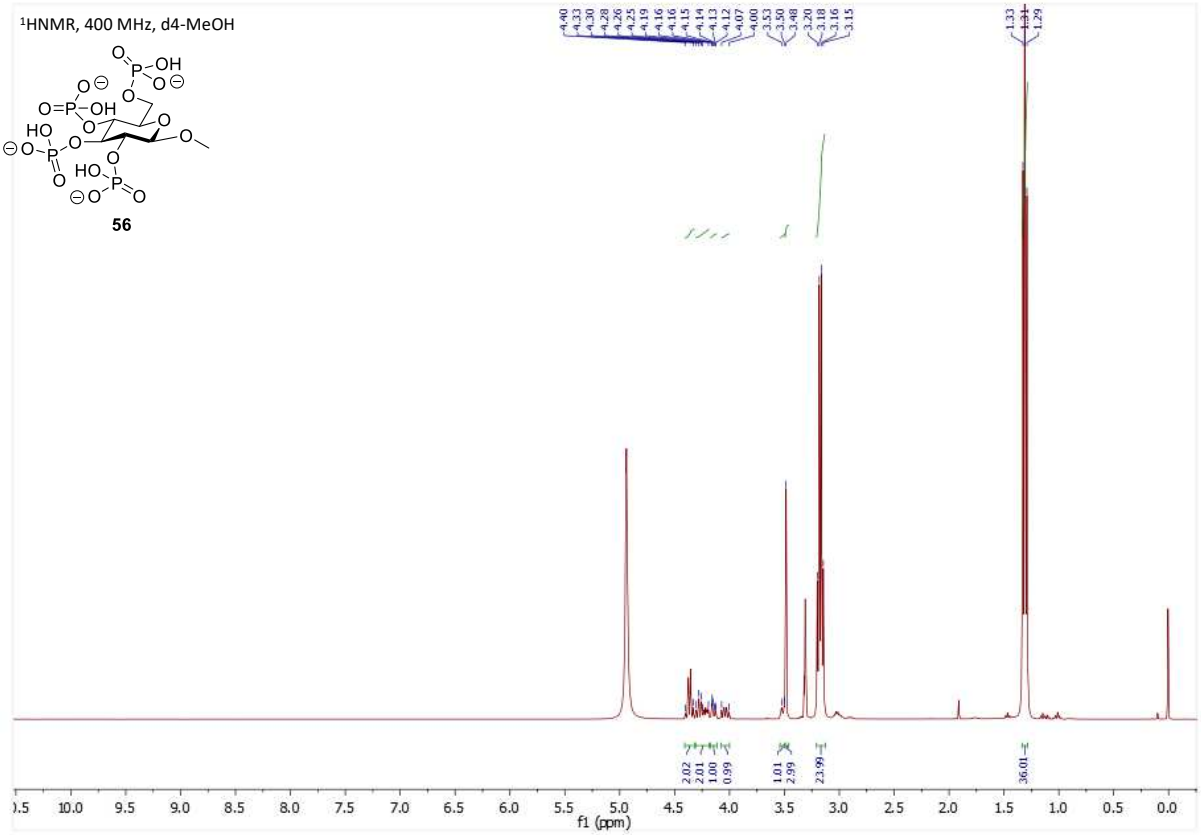

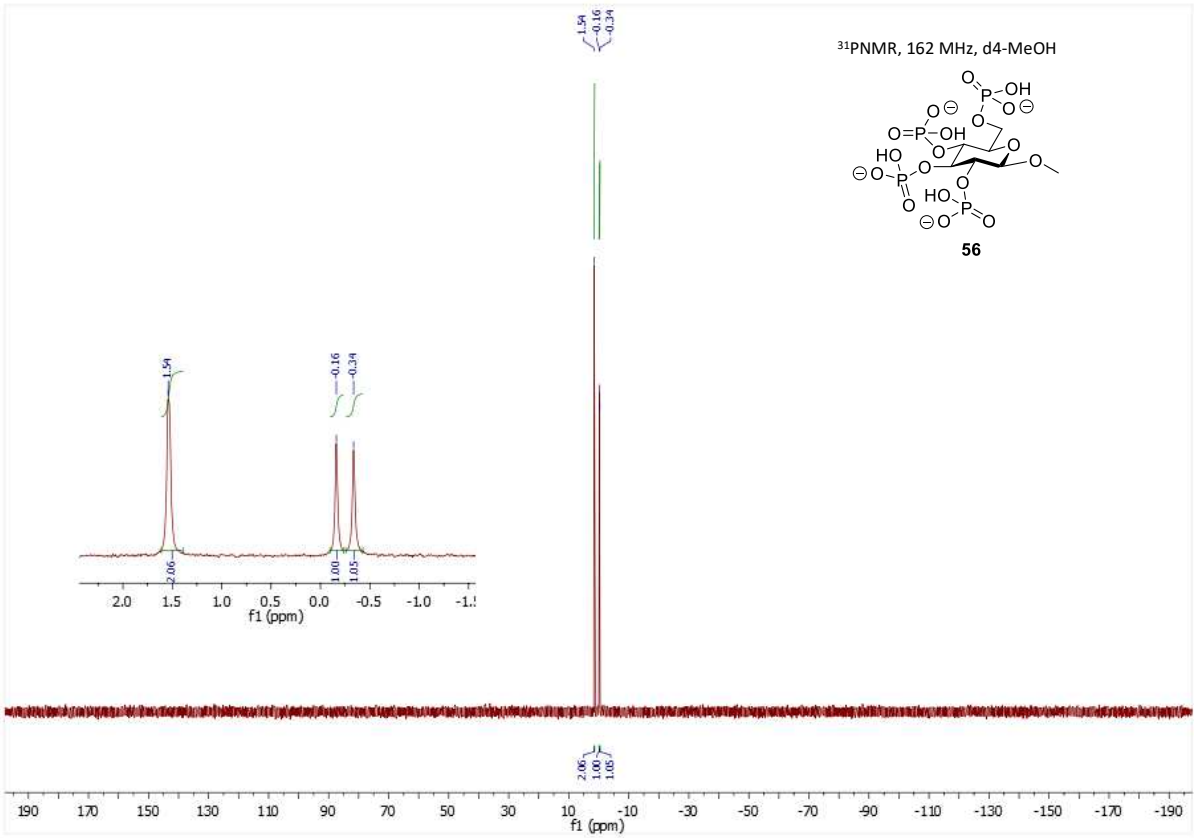

^{13}CNMR, 100 MHz, d4-MeOH

56

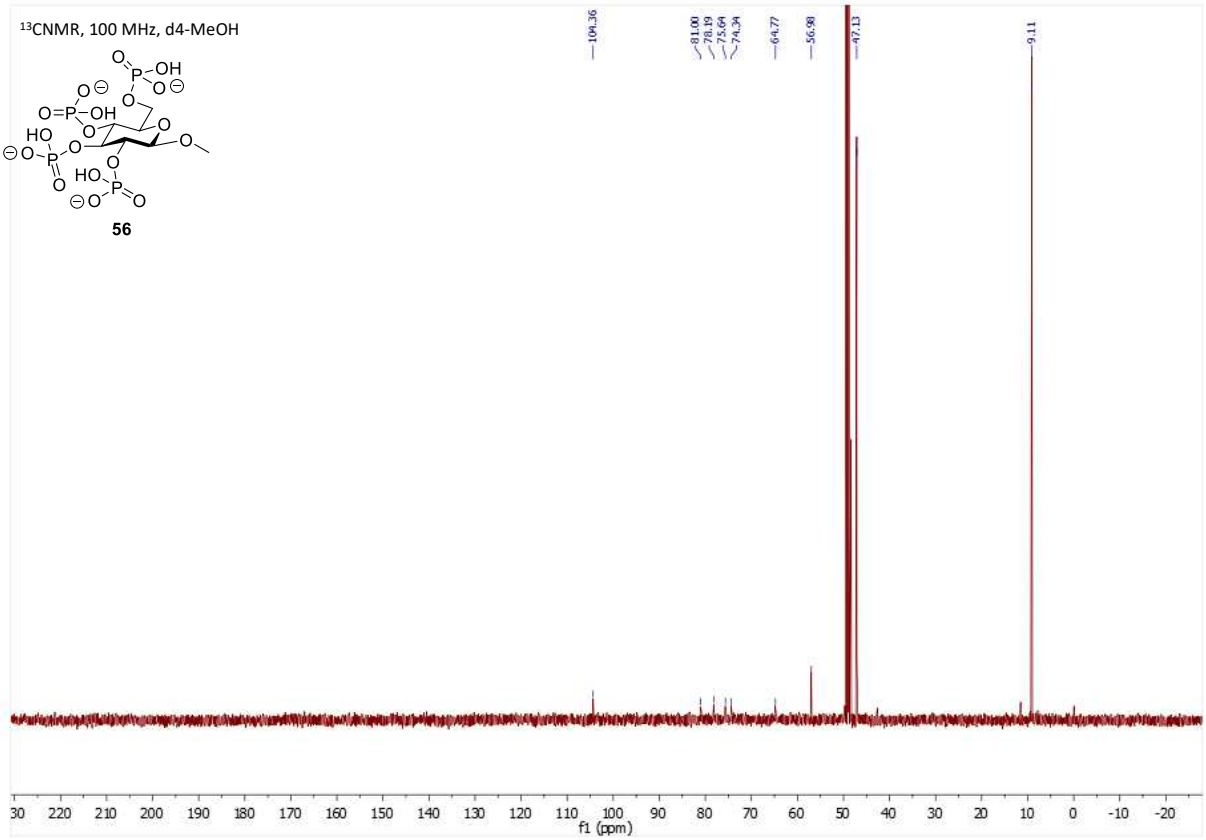

^{1}H-^{1}H COSY

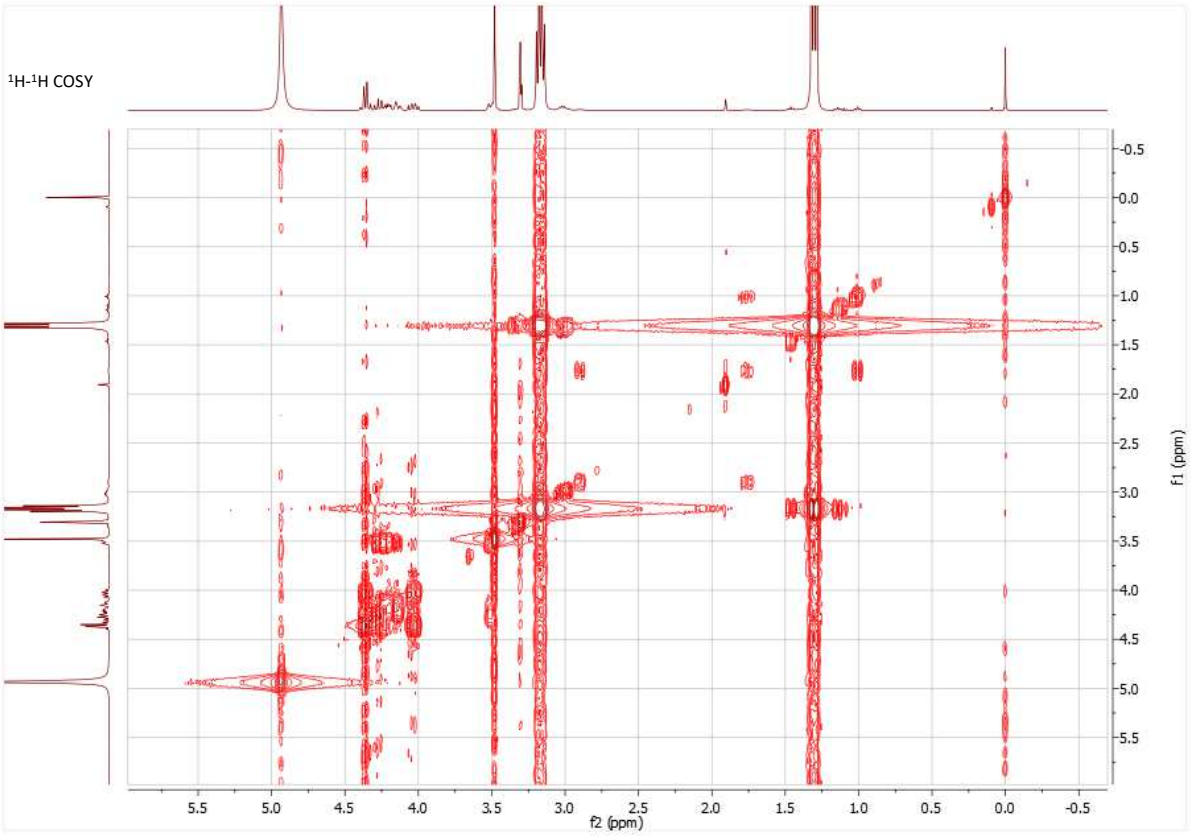

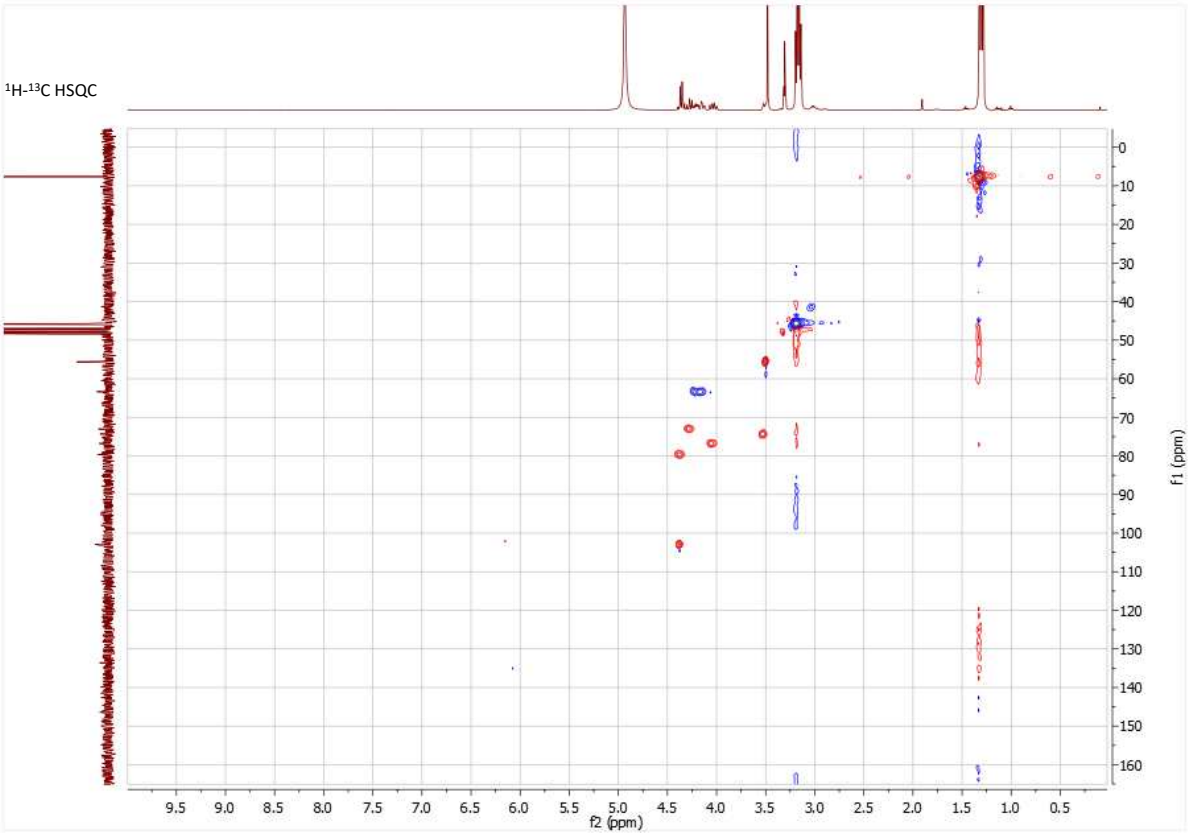

Methyl α-L-glucopyranoside (**49**)

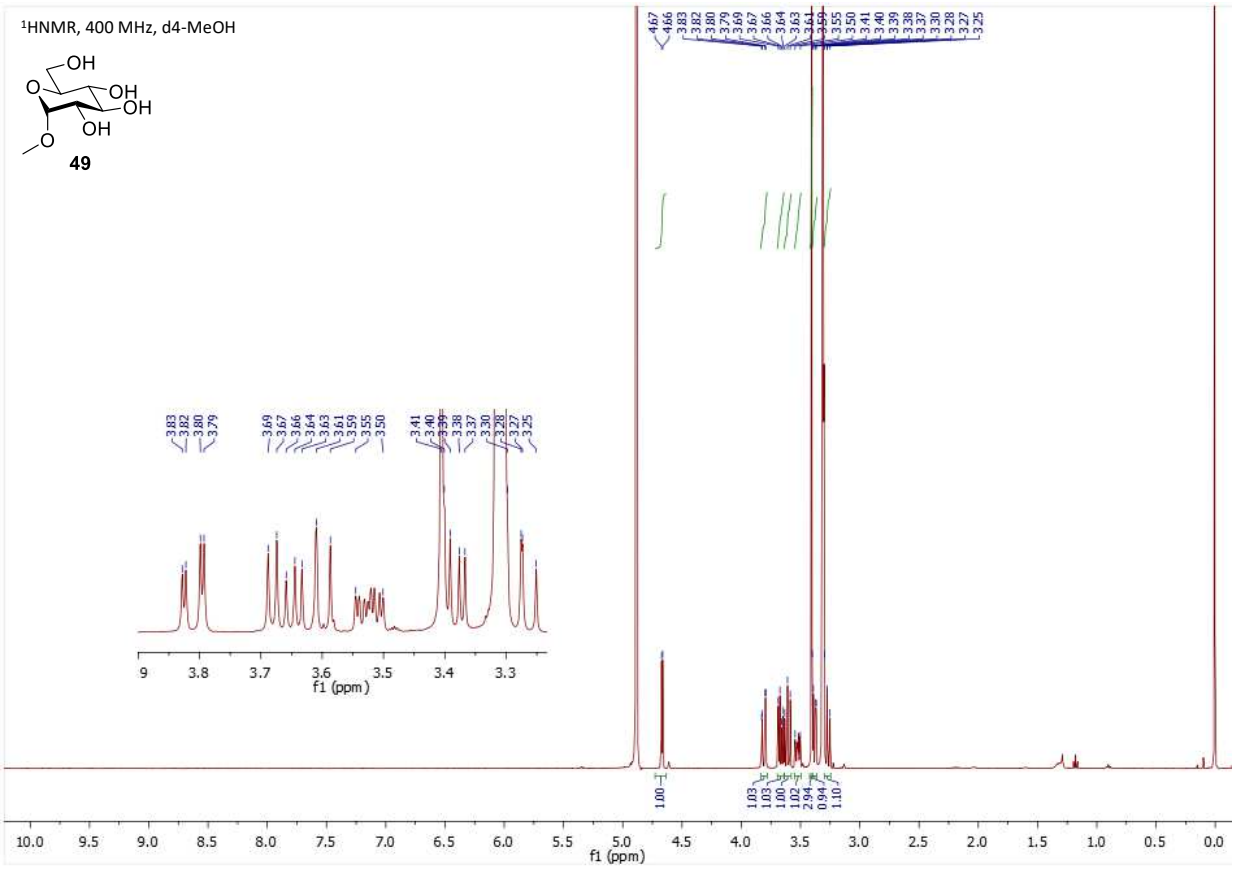

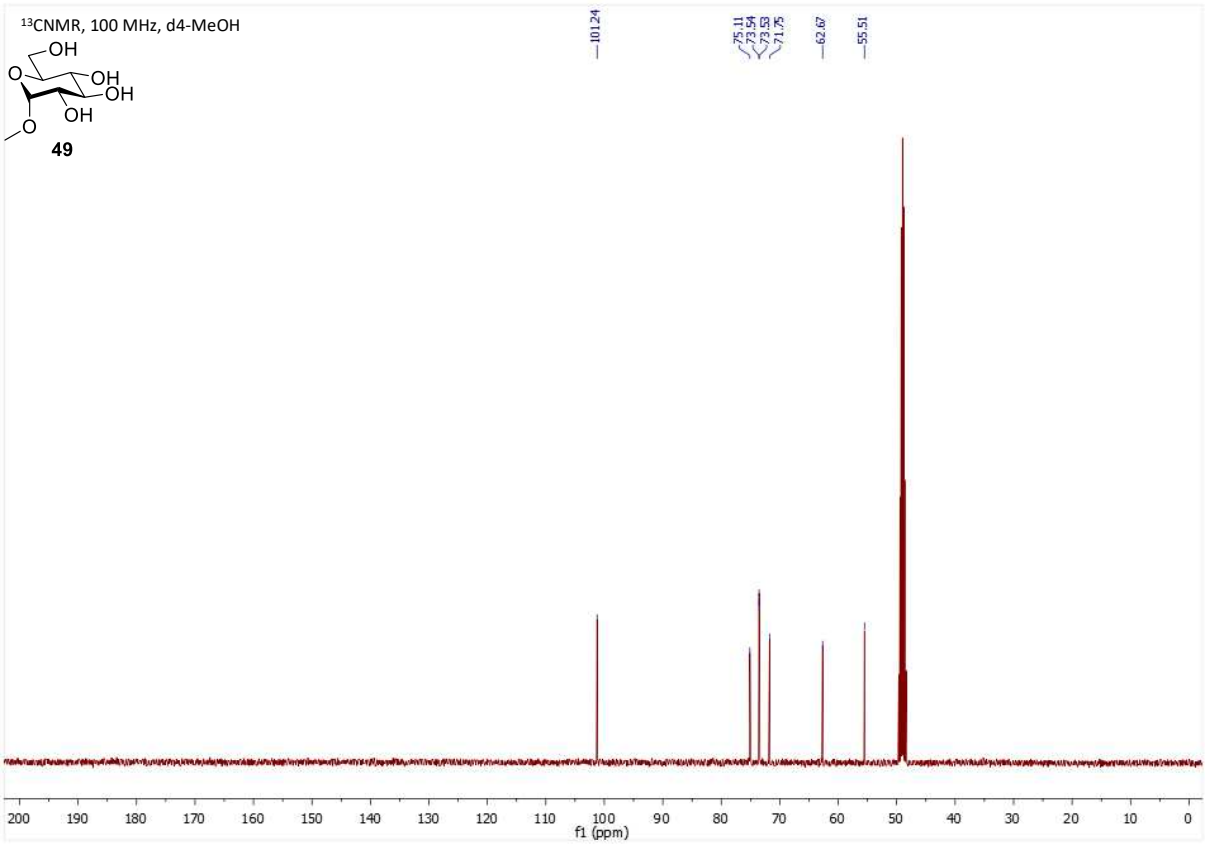

Methyl 4,6-*O*-benzylidene-α-L-glucopyranoside (**51**)

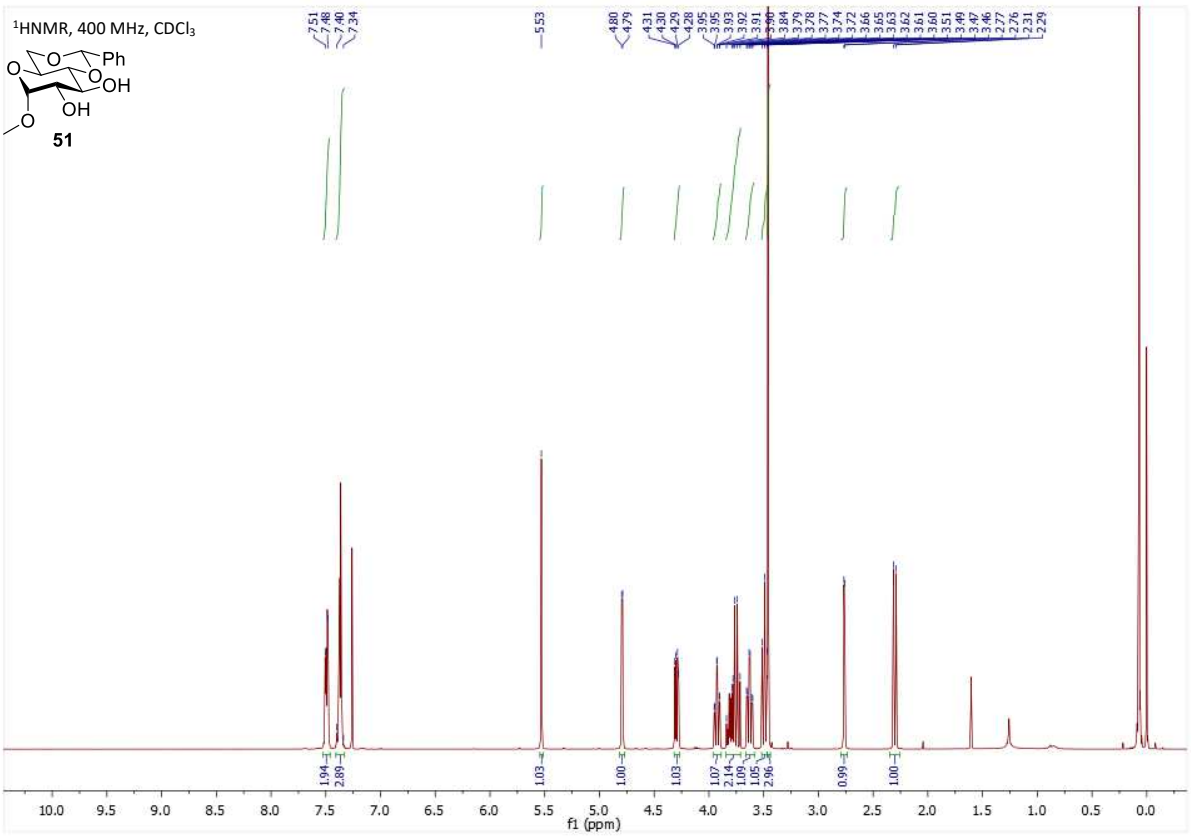

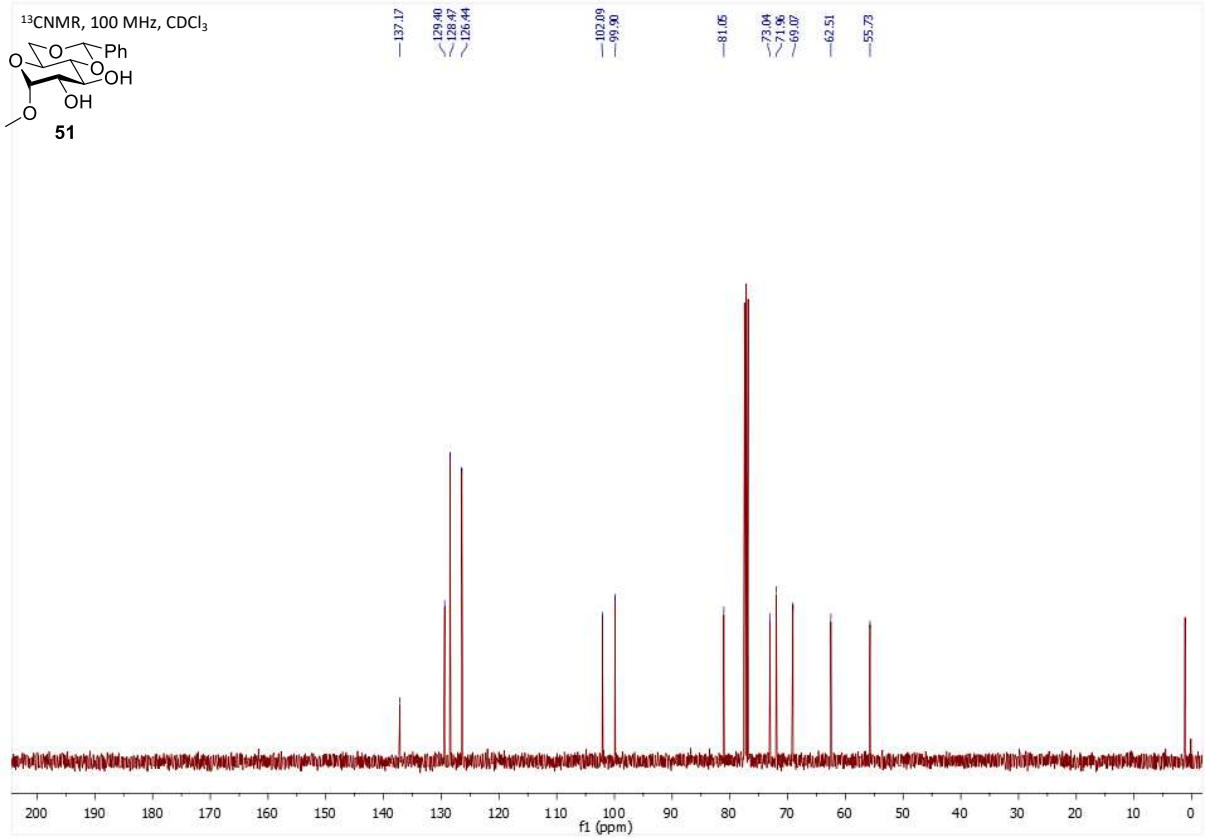

Methyl 2,3-di-*O*-benzoyl-4,6-*O*-benzylidene-α-L-glucopyranoside (**52**)

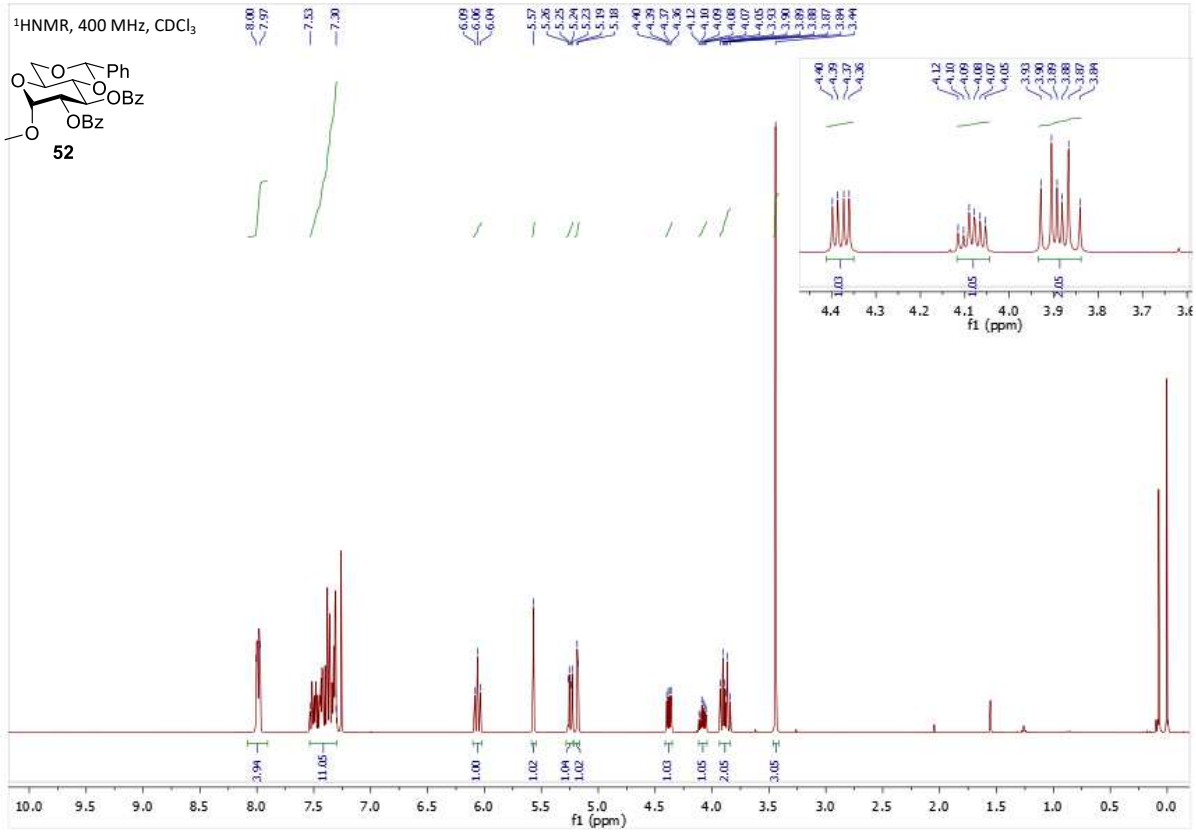

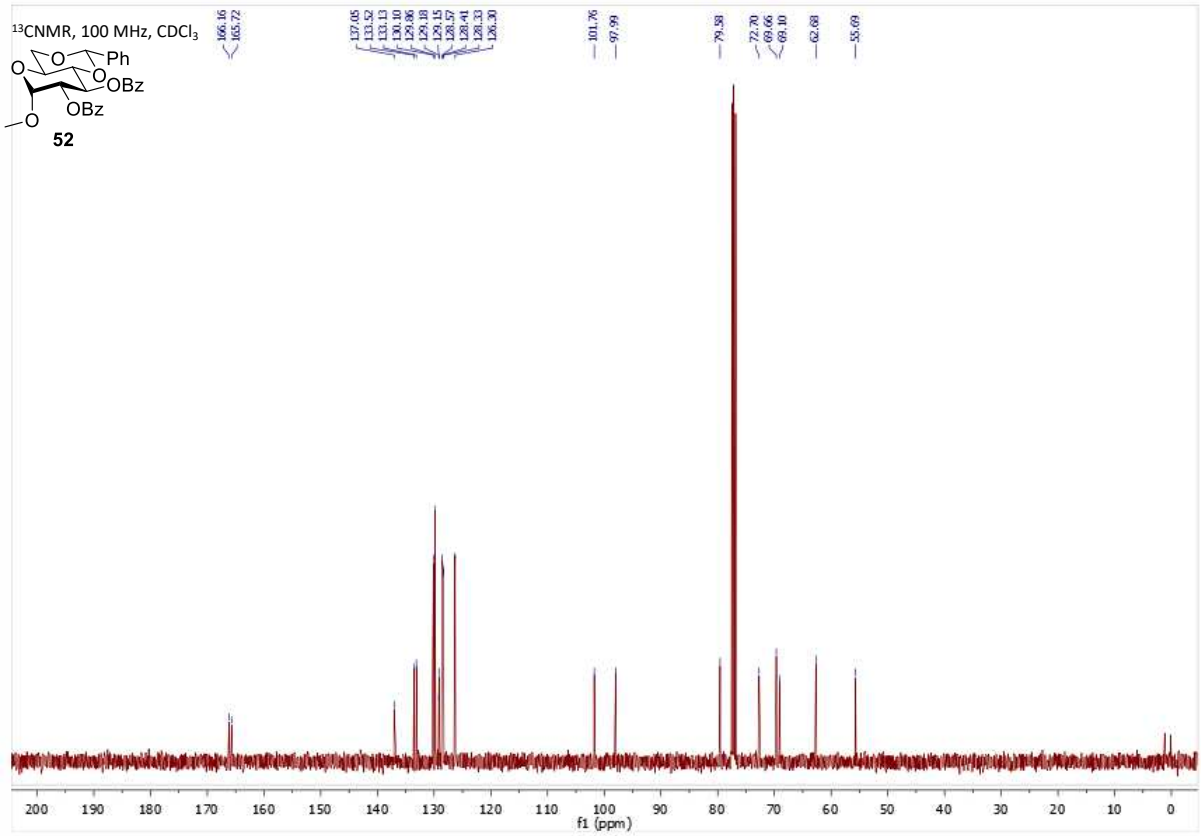

Methyl 2,3-di-*O*-benzoyl-6-*O*-benzyl-α-L-glucopyranoside (**53**)

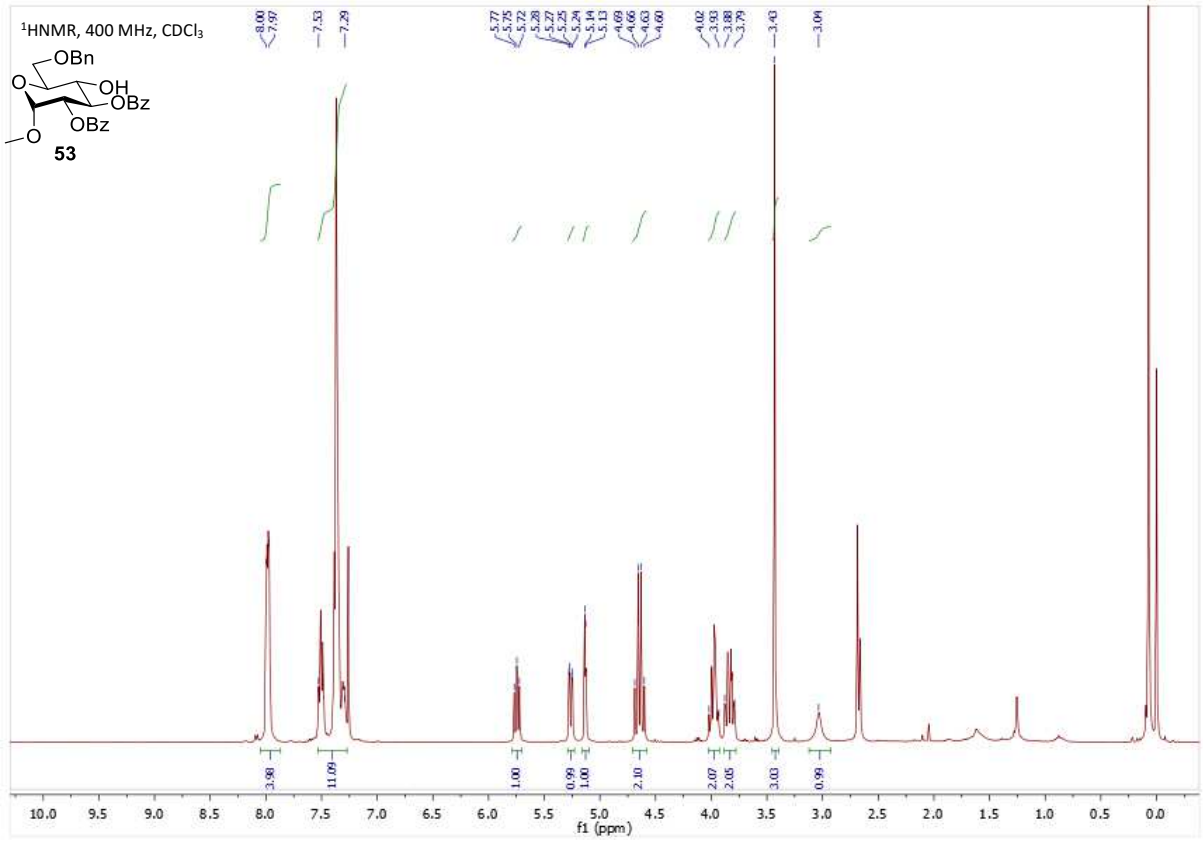

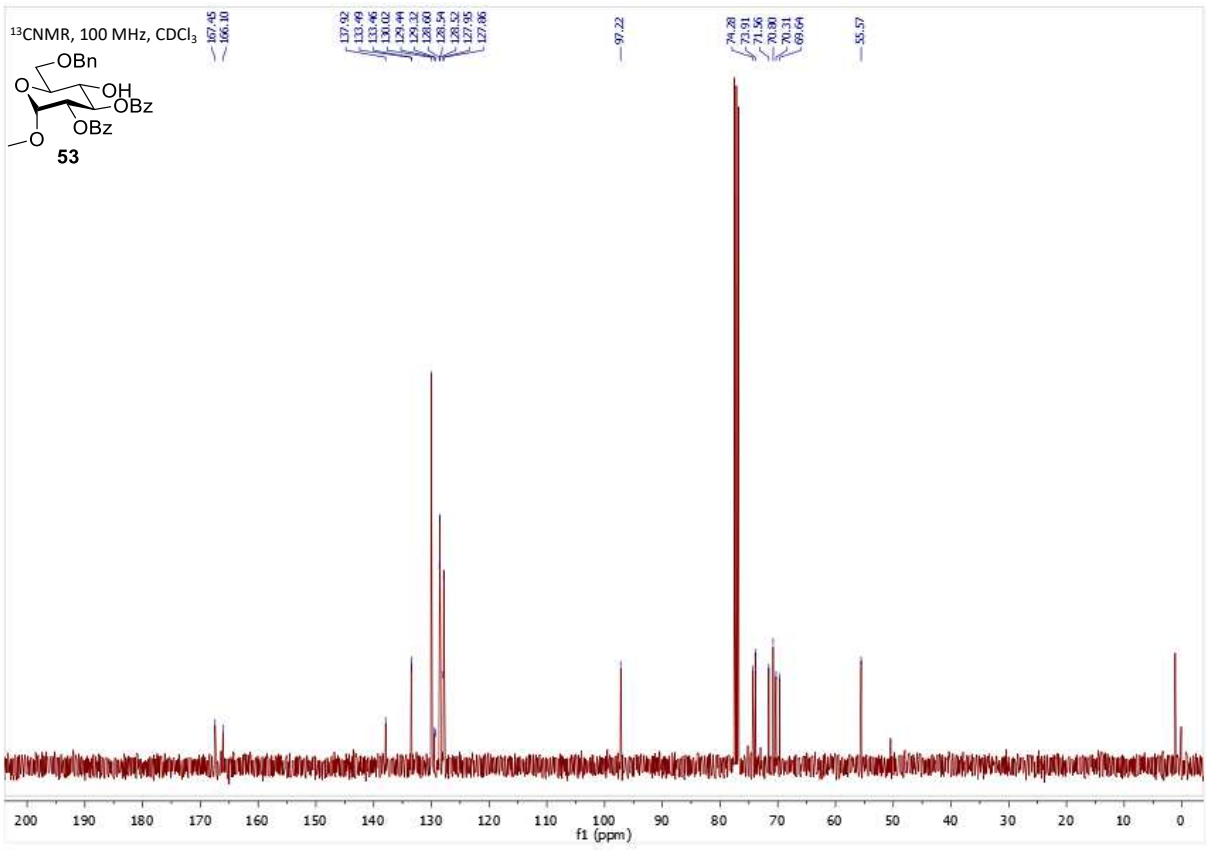

Methyl 6-*O*-benzyl-α-L-glucopyranoside (**54**)

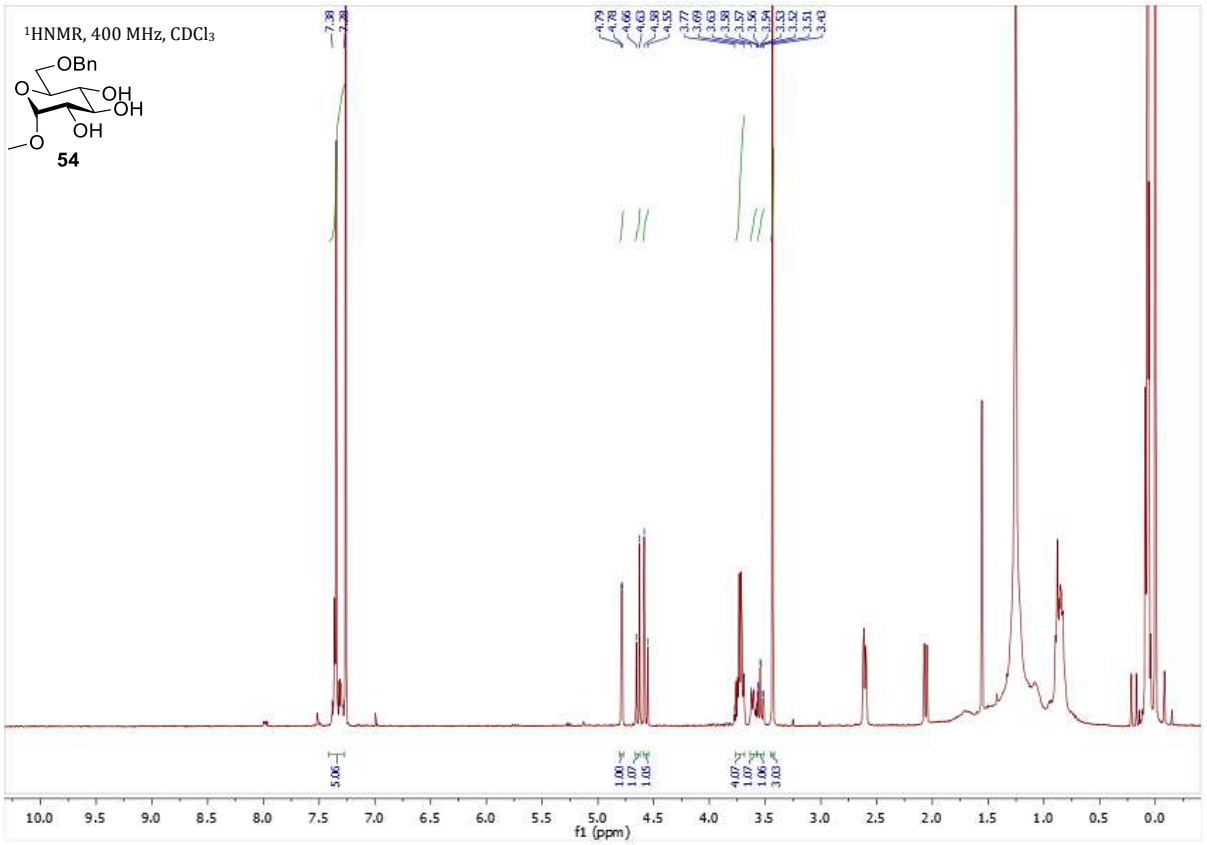

^{13}CNMR, 100 MHz, $CDCl_3$

54

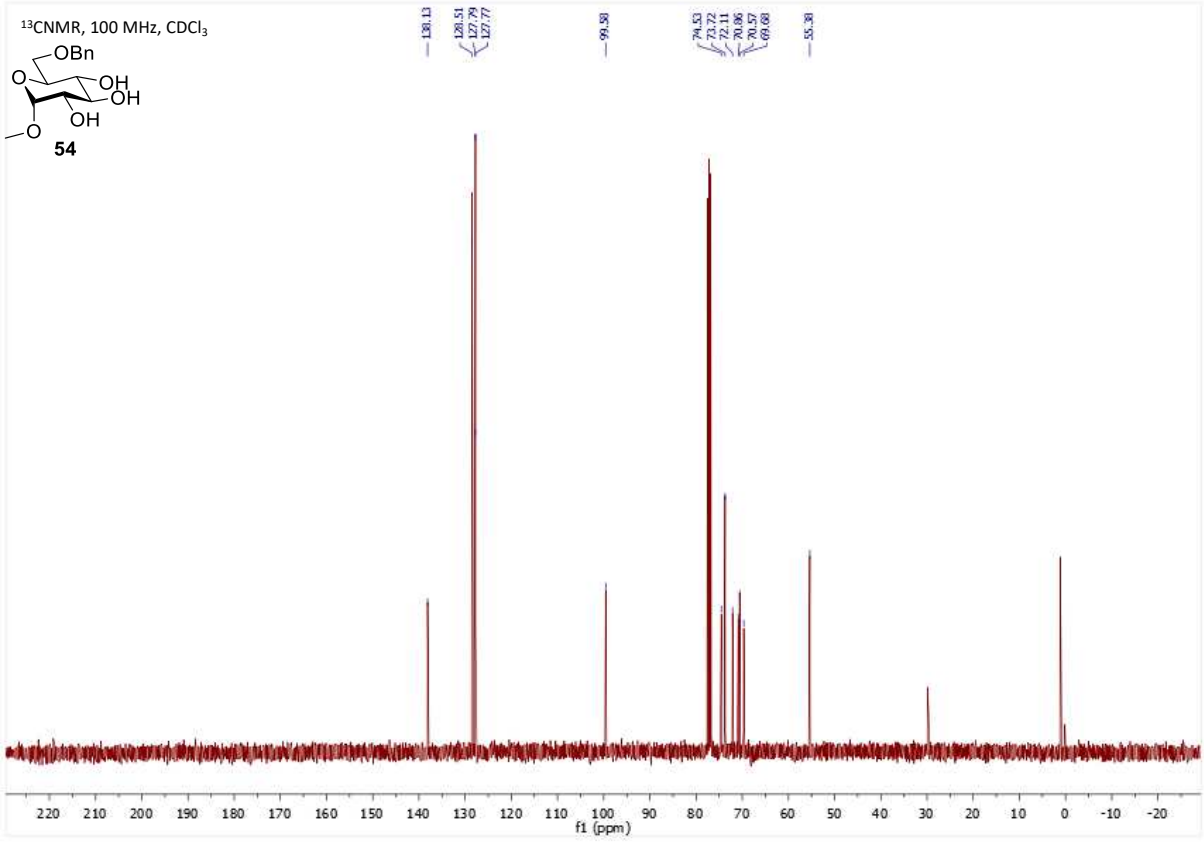

^{1}H-^{1}H COSY

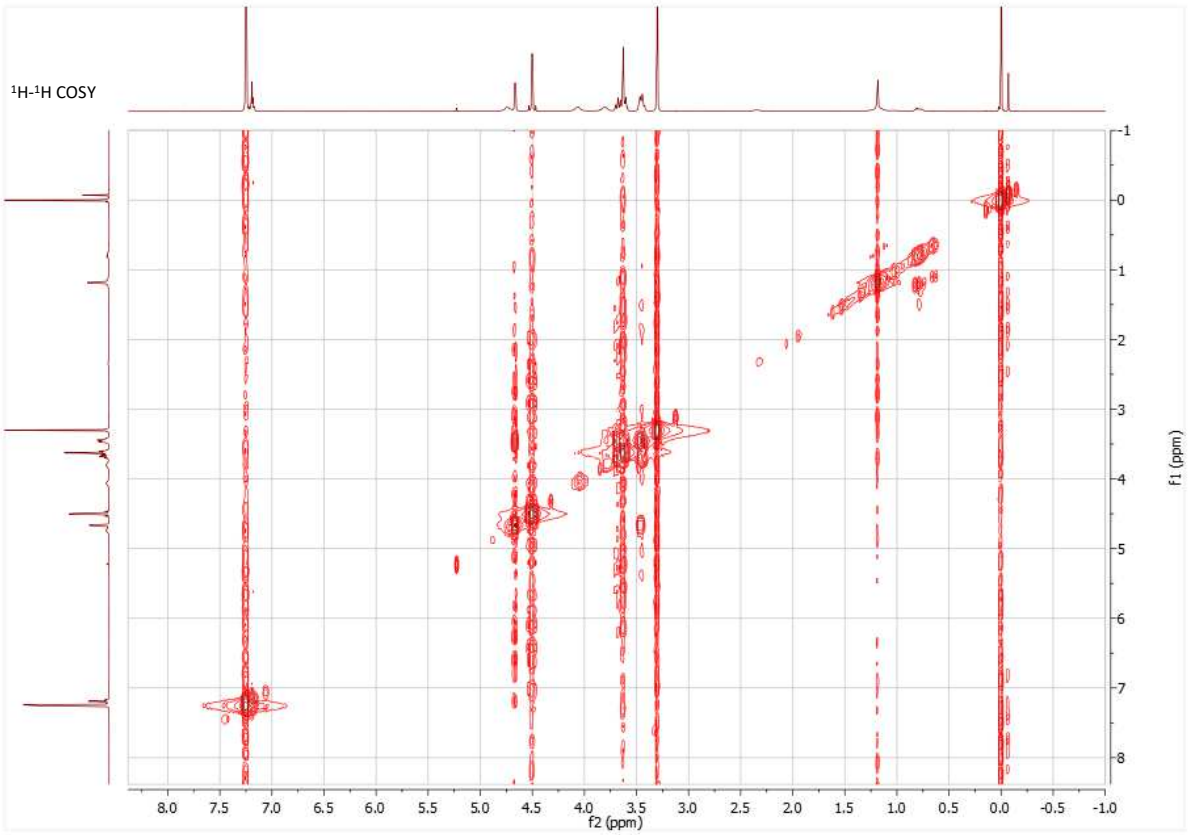

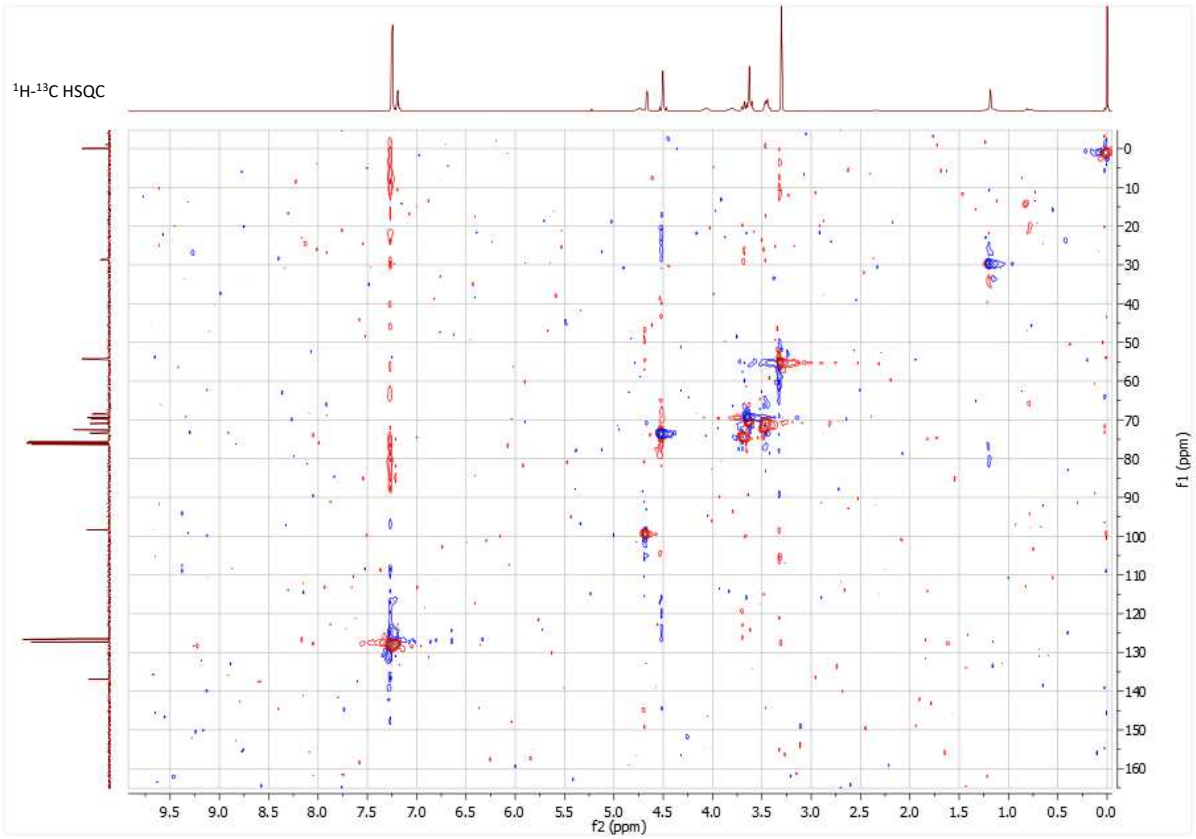

Methyl 6-*O*-benzyl-α-L-glucopyranoside 2,3,4-tris(dibenzylphosphate) (**55**)

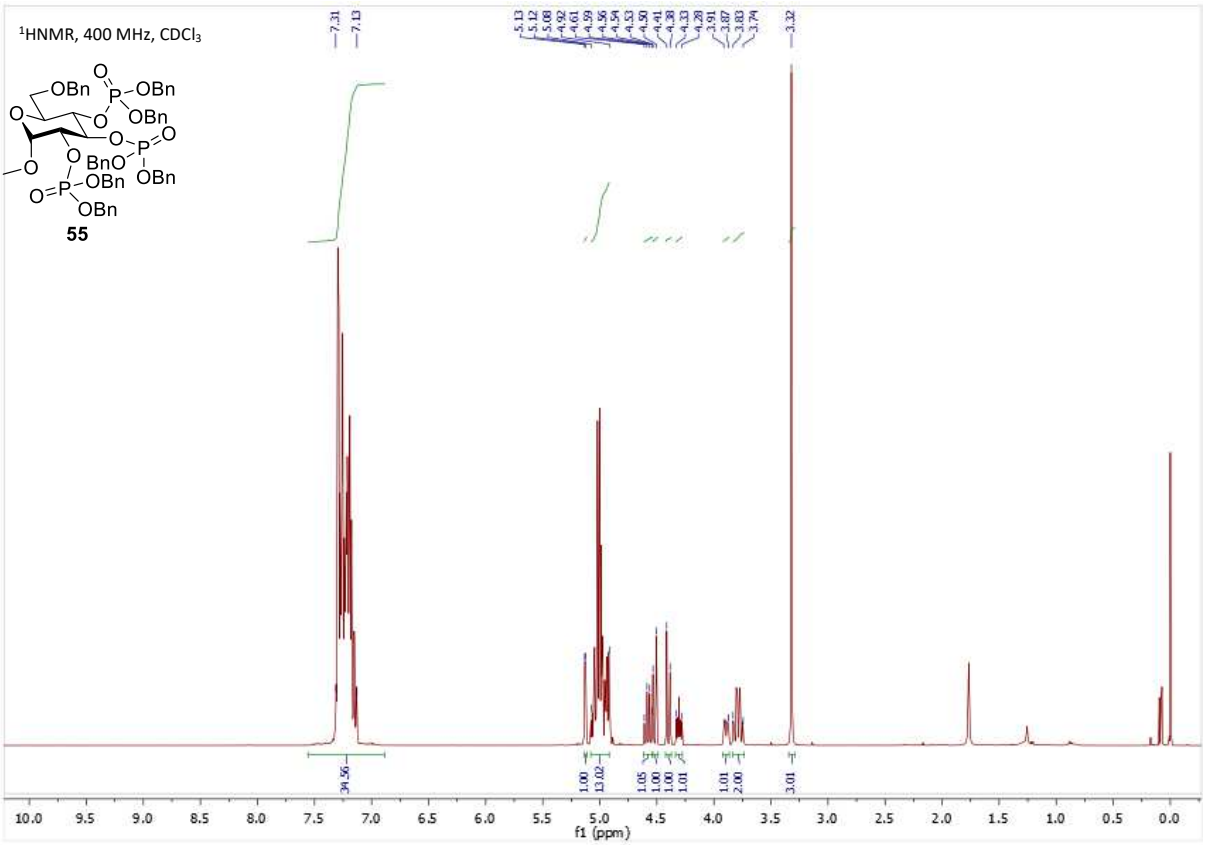

^{31}PNMR, 162 MHz, $CDCl_3$

55

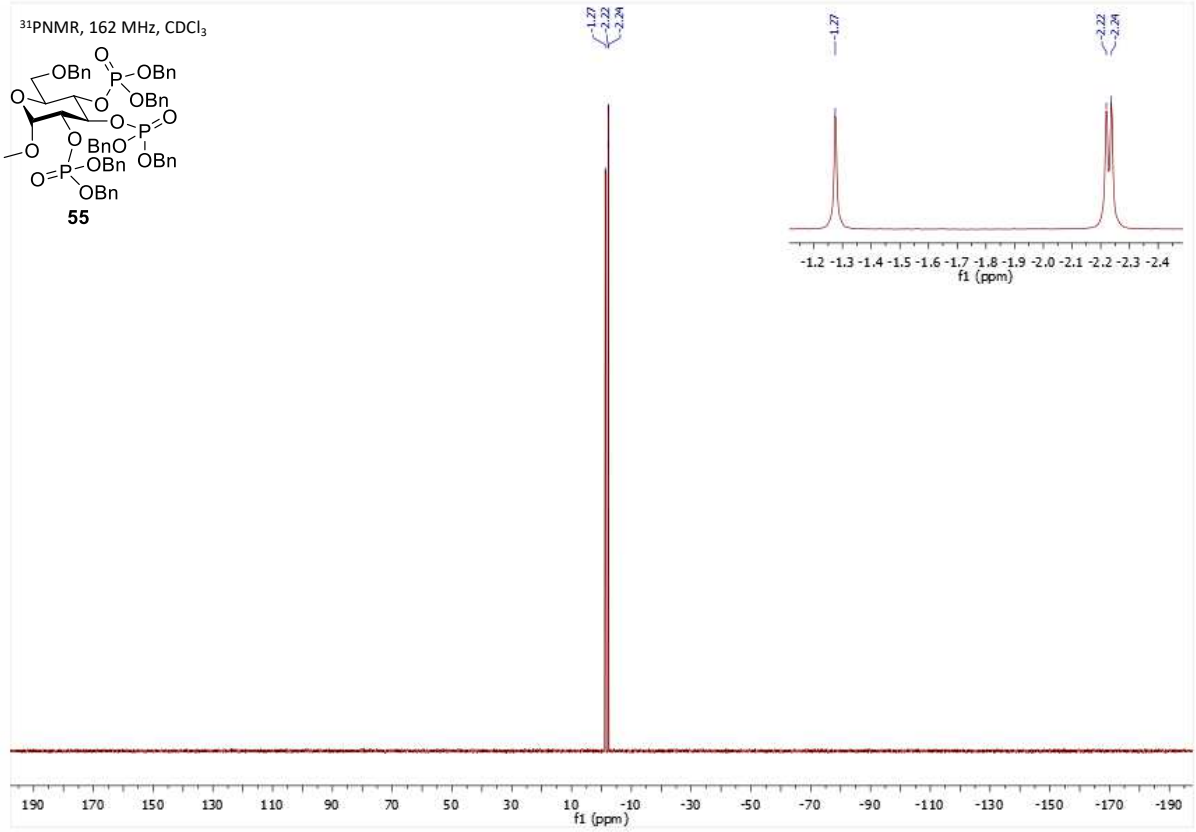

^{13}CNMR, 100 MHz, $CDCl_3$

55

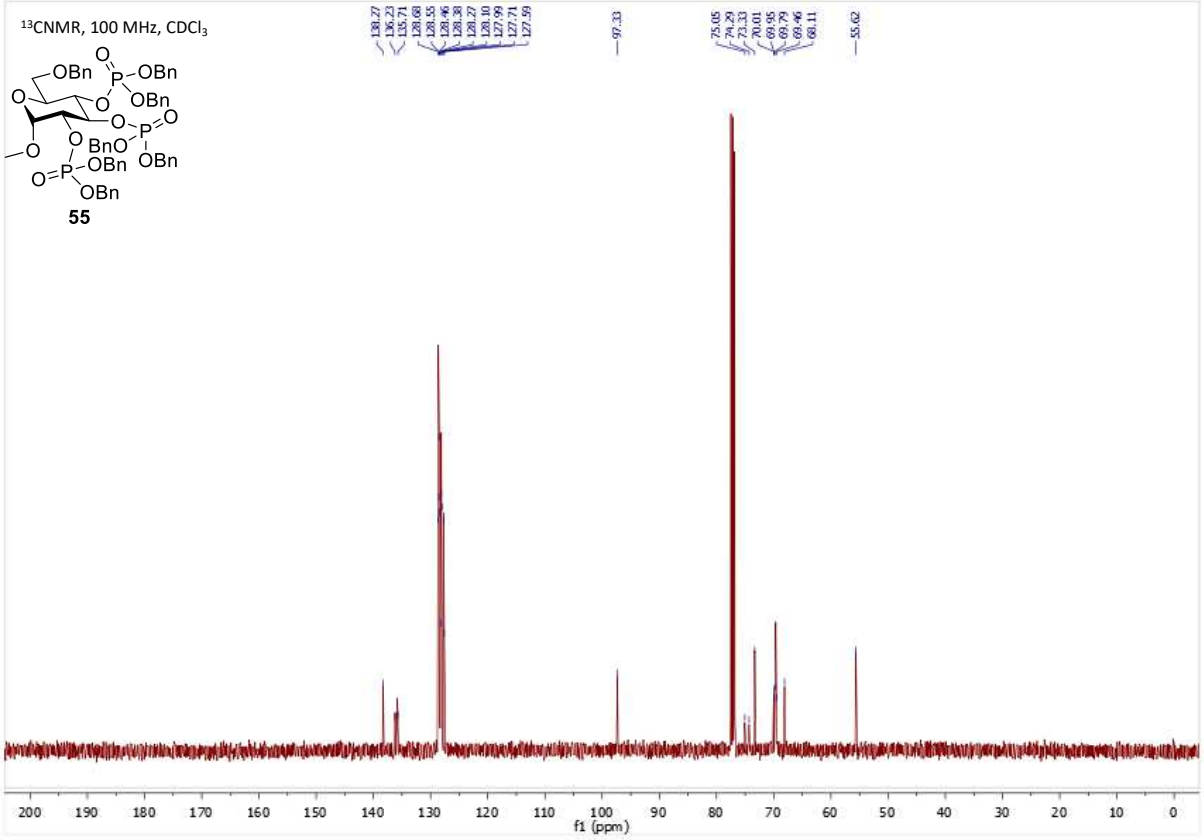

Methyl 6-*O*-benzyl-α-L-glucopyranoside 2,3,4-trisphosphate triethylammonium salt (**41**)

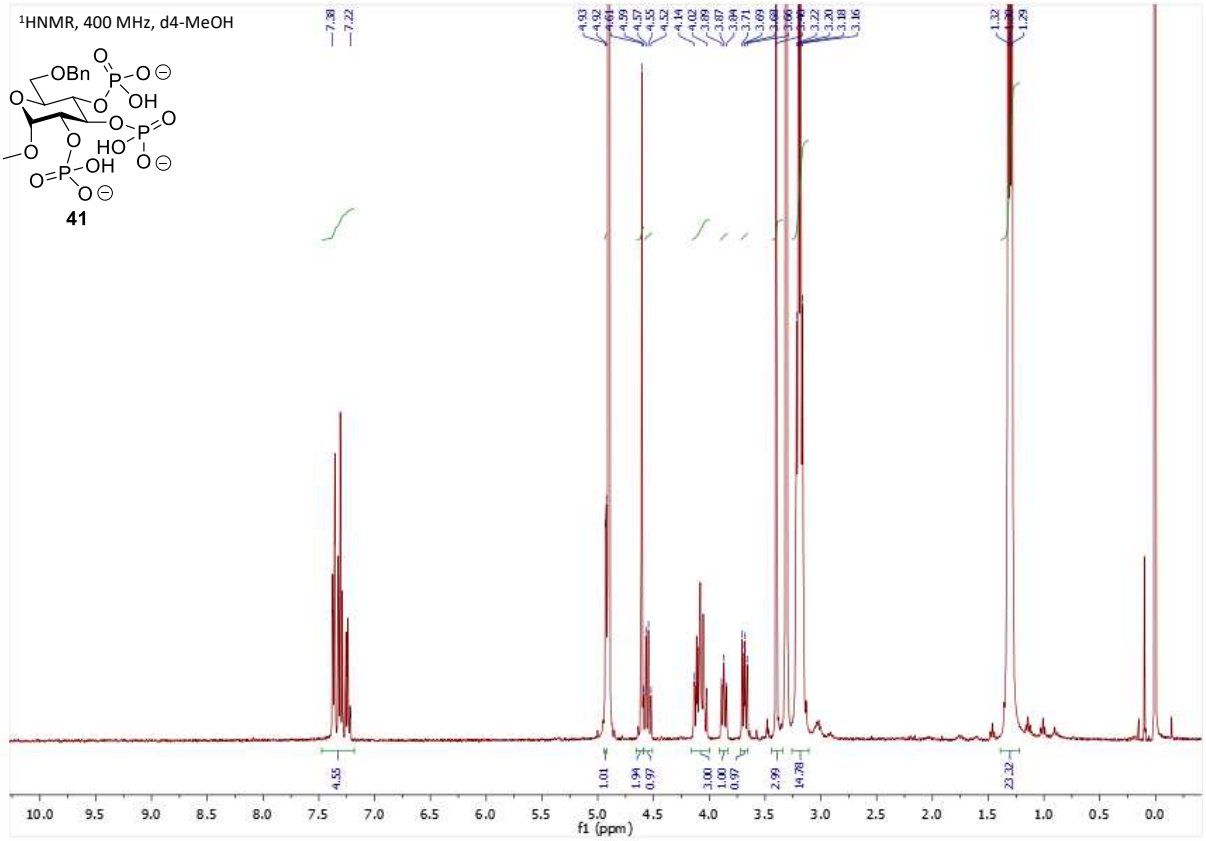

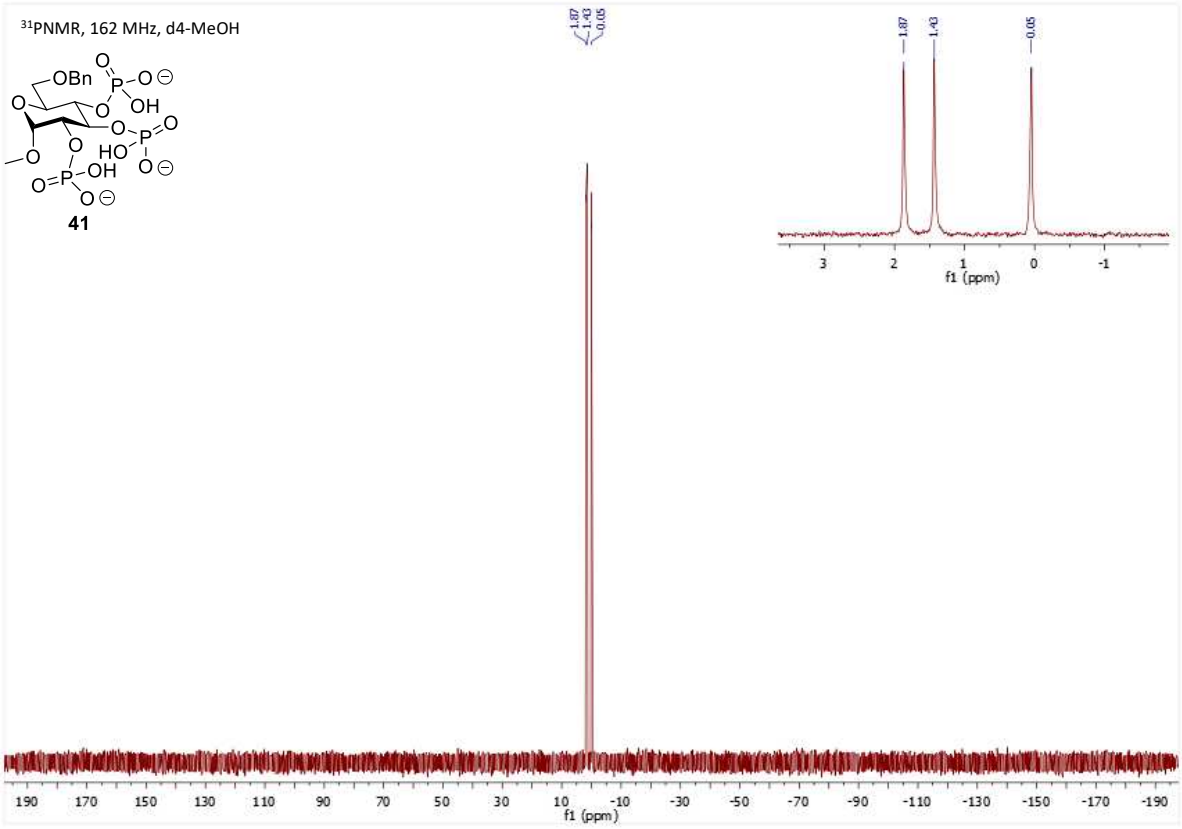

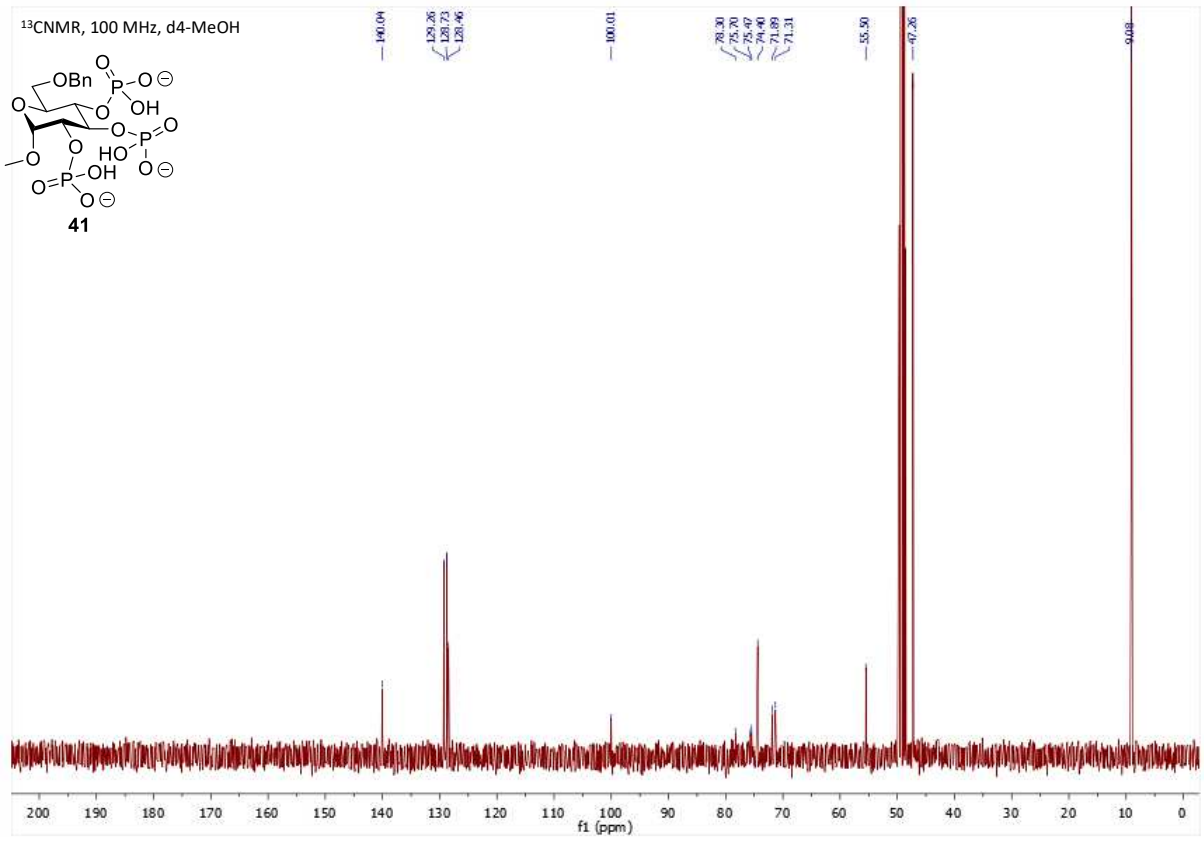

Methyl α-L-glucopyranoside 2,3,4-trisphosphate triethylammonium salt (**40**)

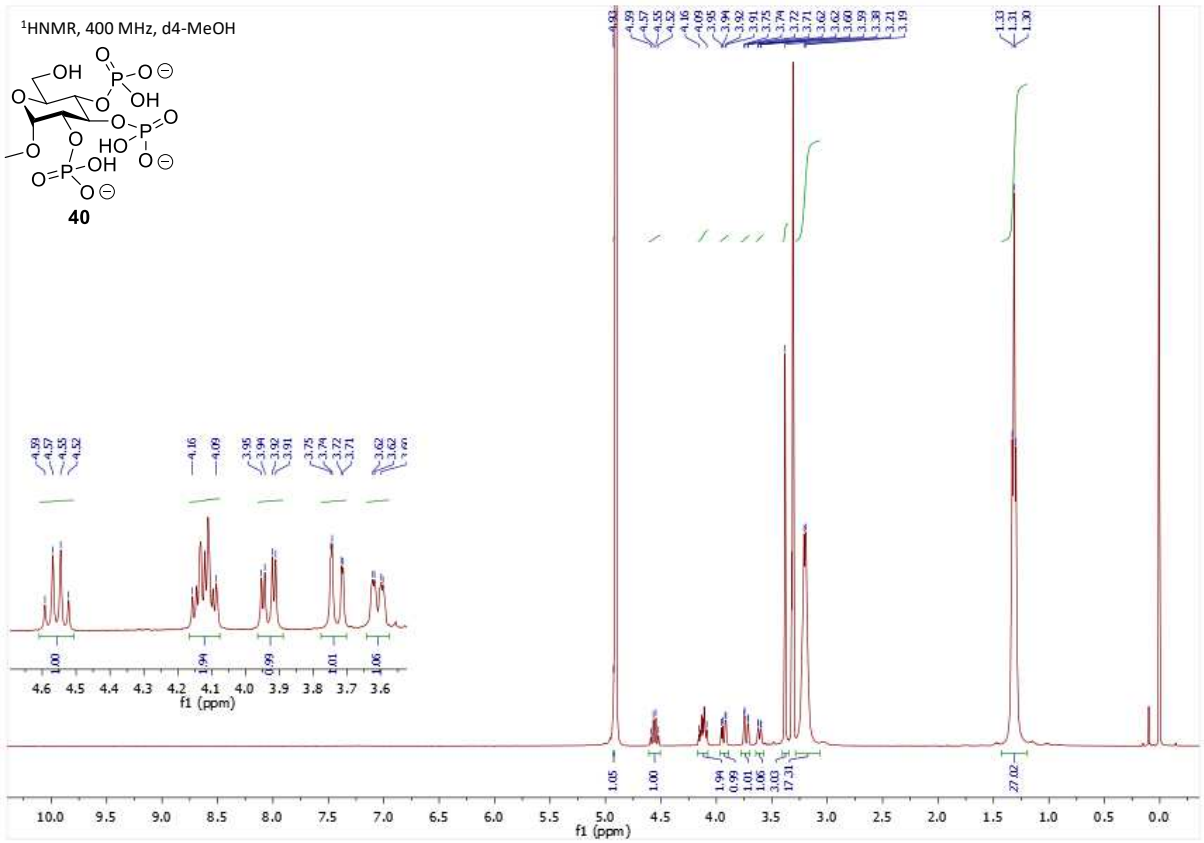

^{31}PNMR, 162 MHz, d4-MeOH

40

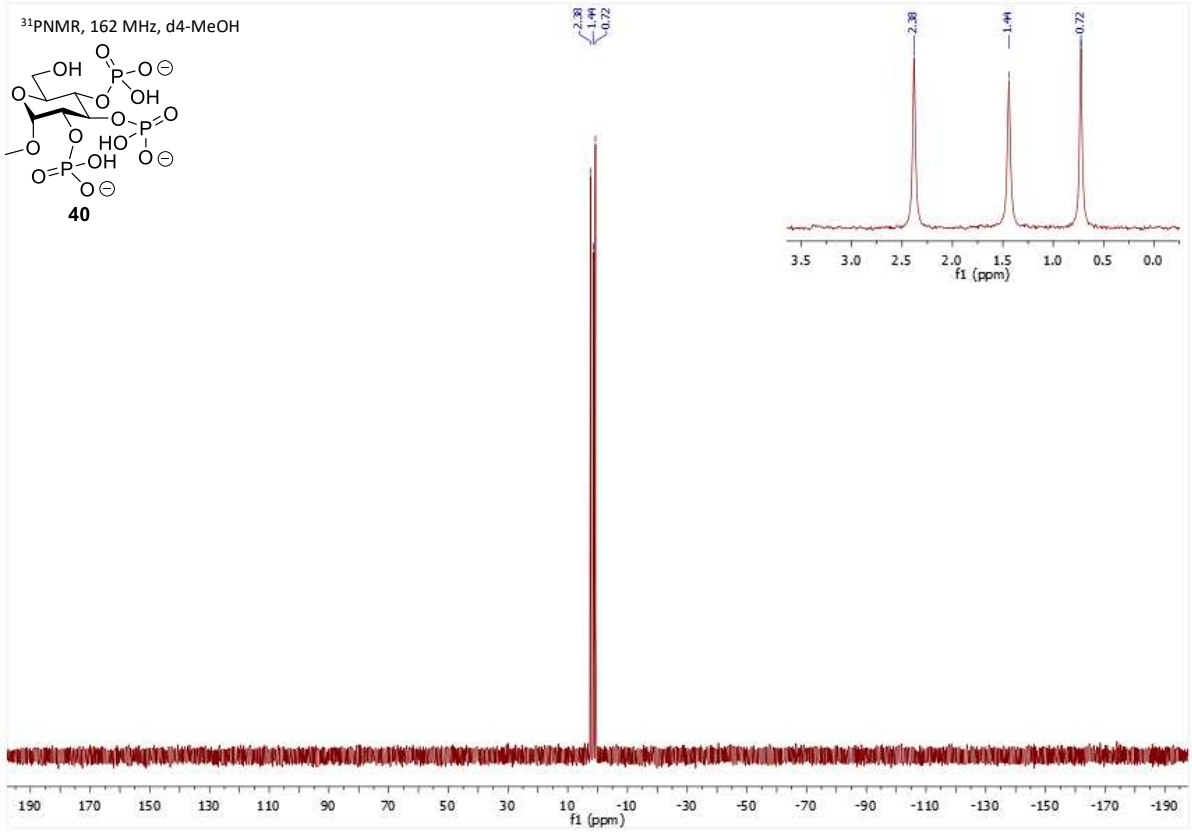

^{13}CNMR, 100 MHz, d4-MeOH

40

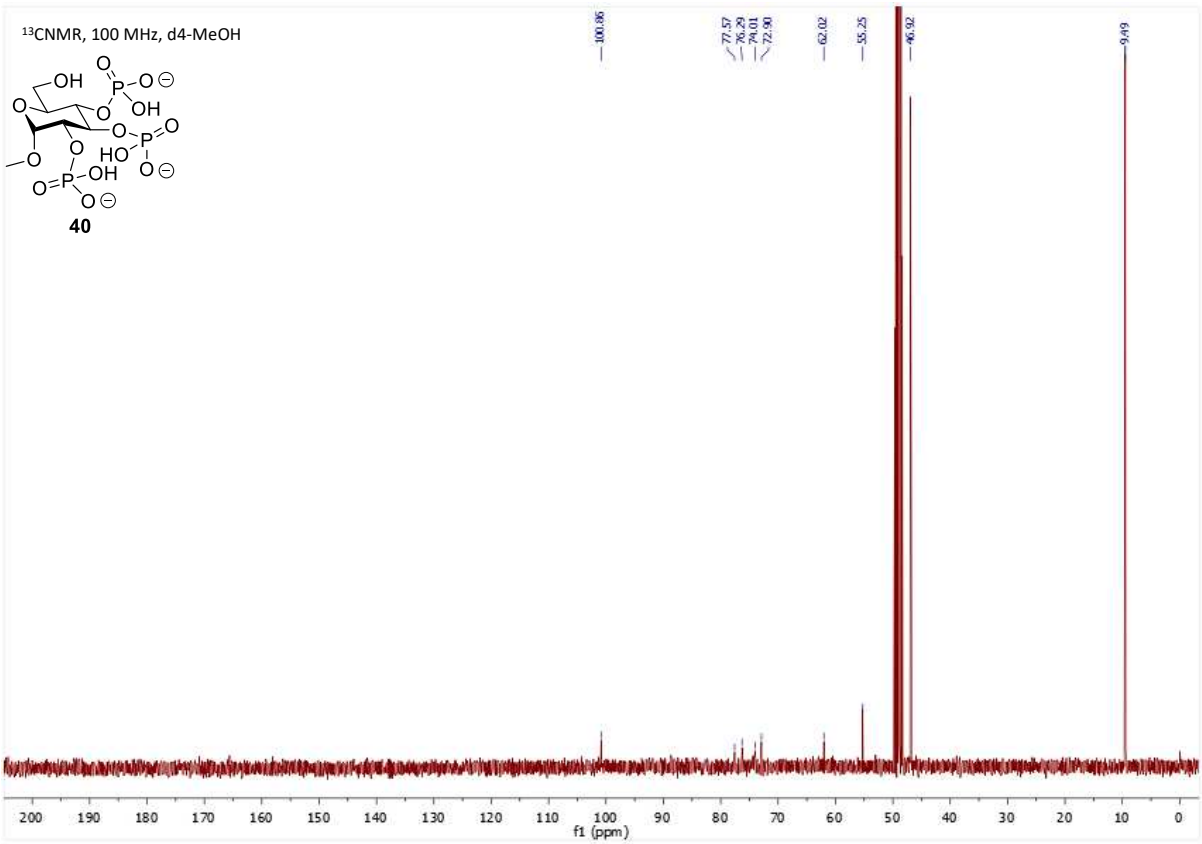

Methyl α-L-glucopyranoside 2,3,4,6-tetrakis(dibenzylphosphate) (**50**)

^{1}HNMR, 100 MHz, $CDCl_3$

50

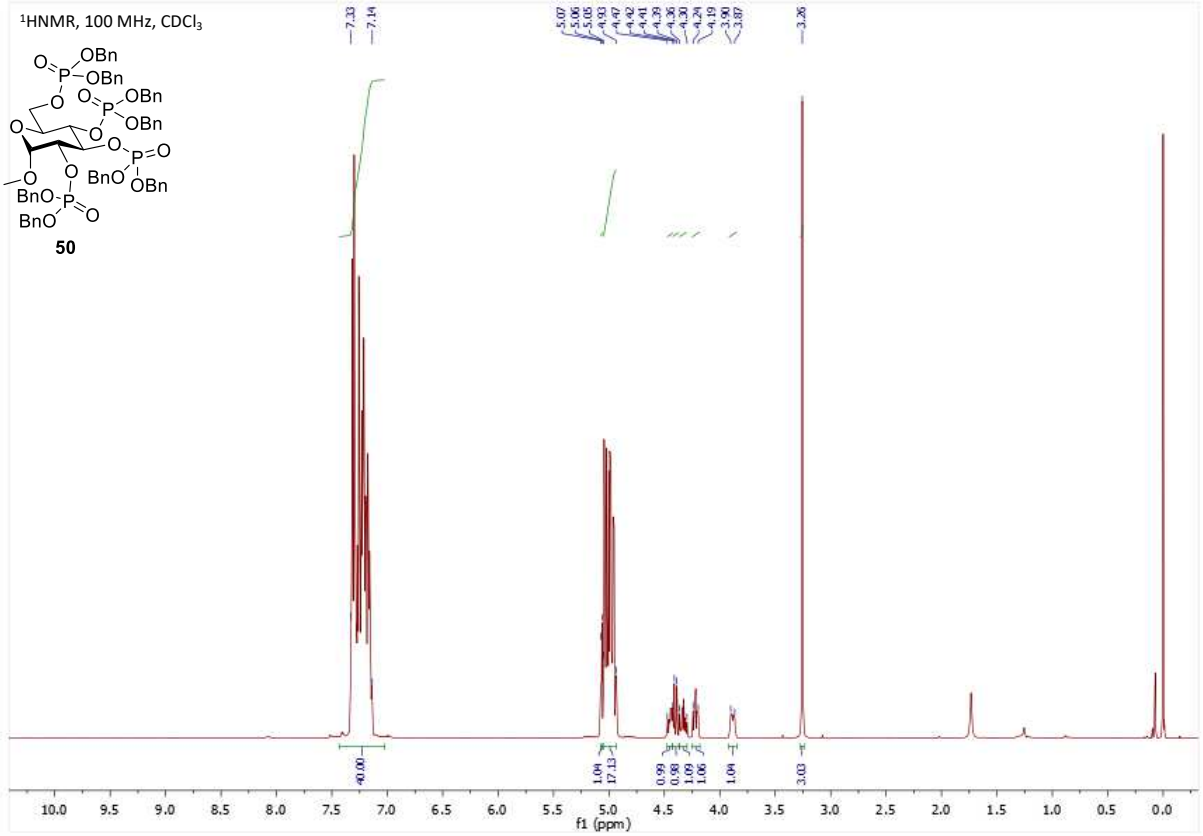

^{31}PNMR, 162 MHz, $CDCl_3$

50

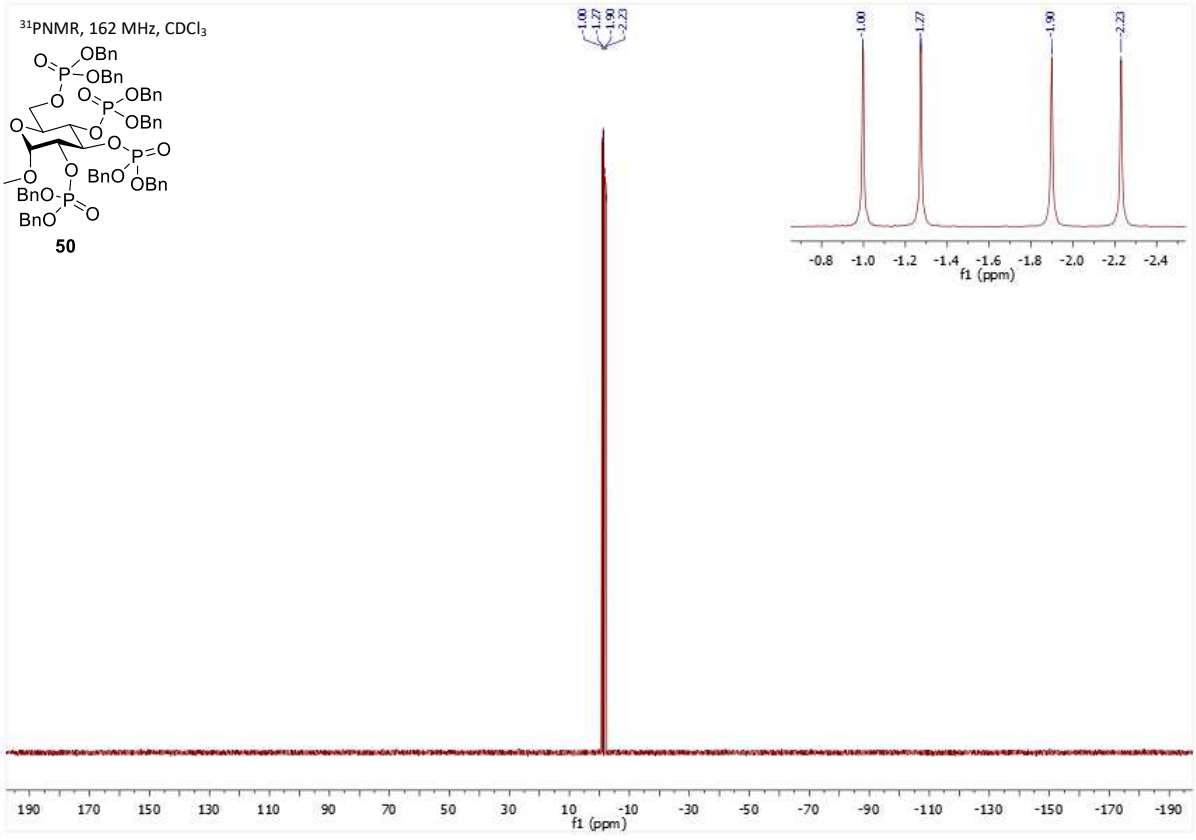

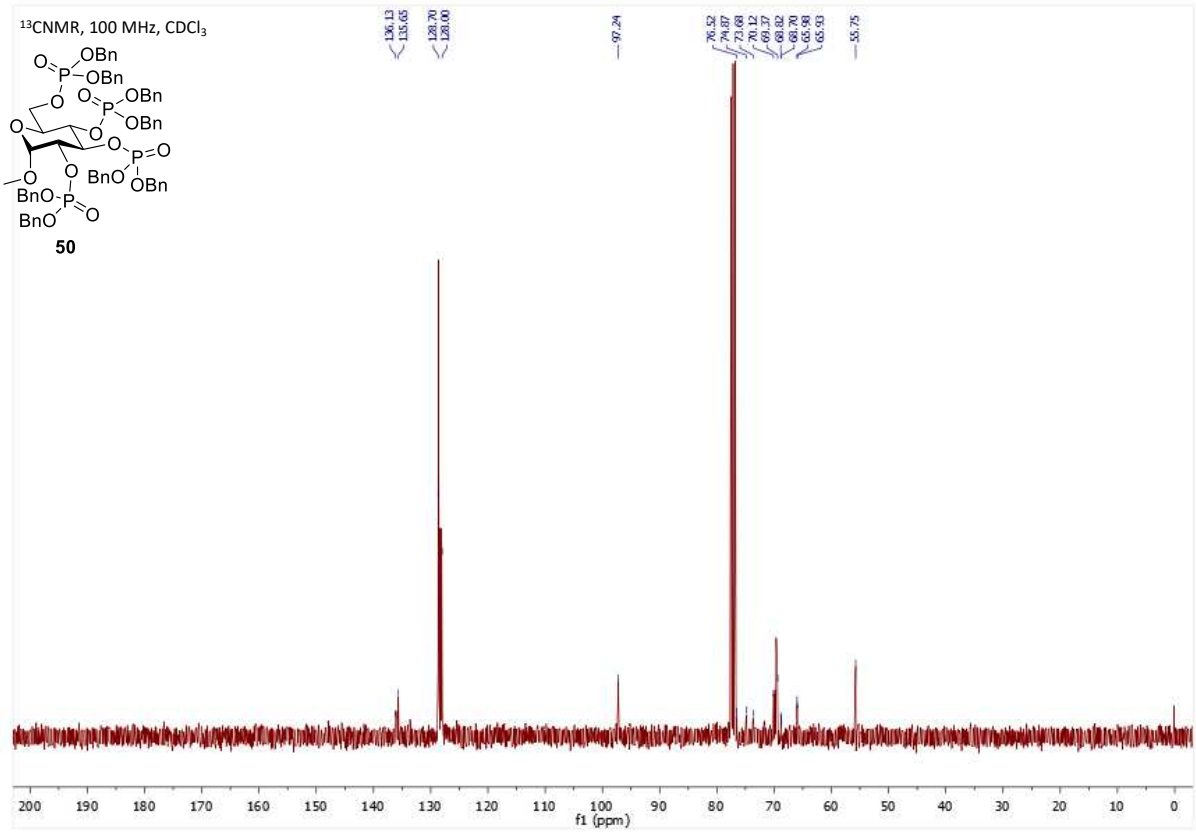

Methyl α-L-glucopyranoside 2,3,4,6-tetrakisphosphate triethylammonium salt (**39**)

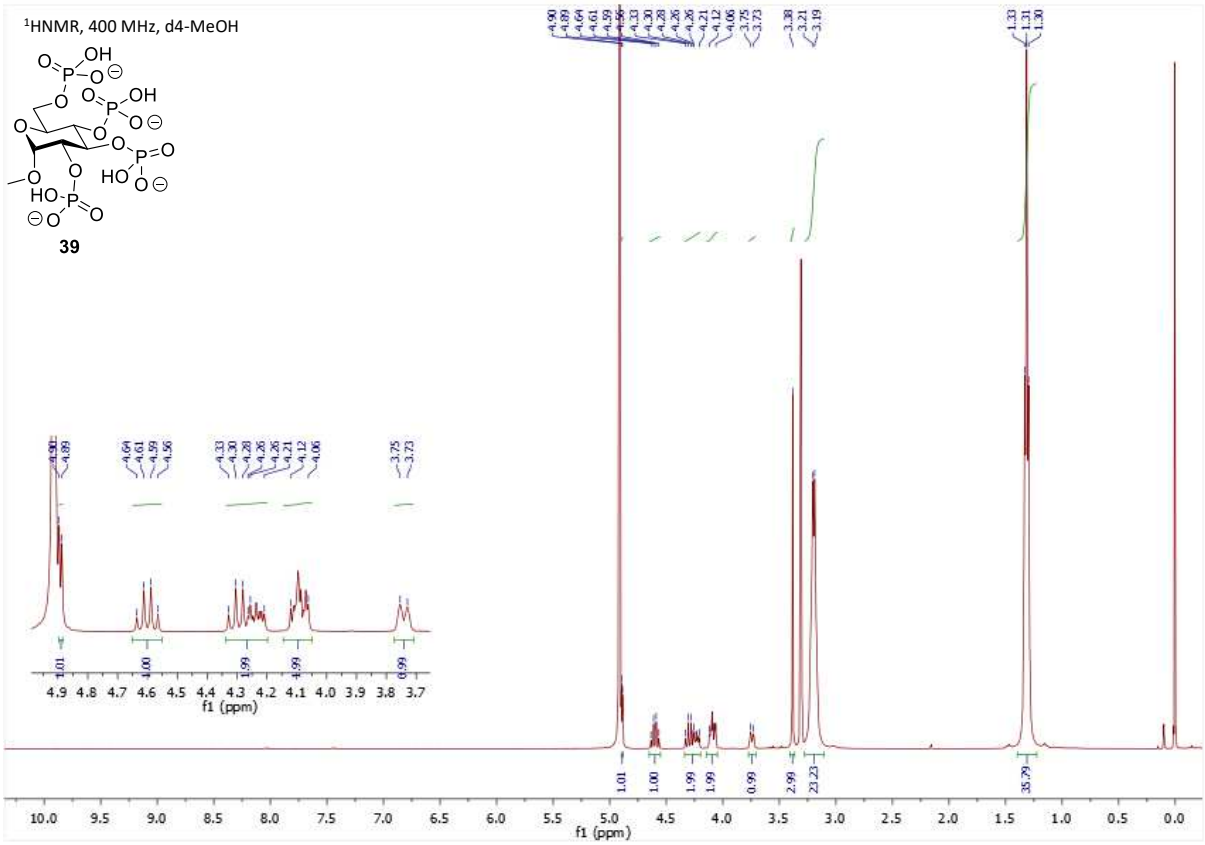

^{31}PNMR, 162 MHz, d4-MeOH

39

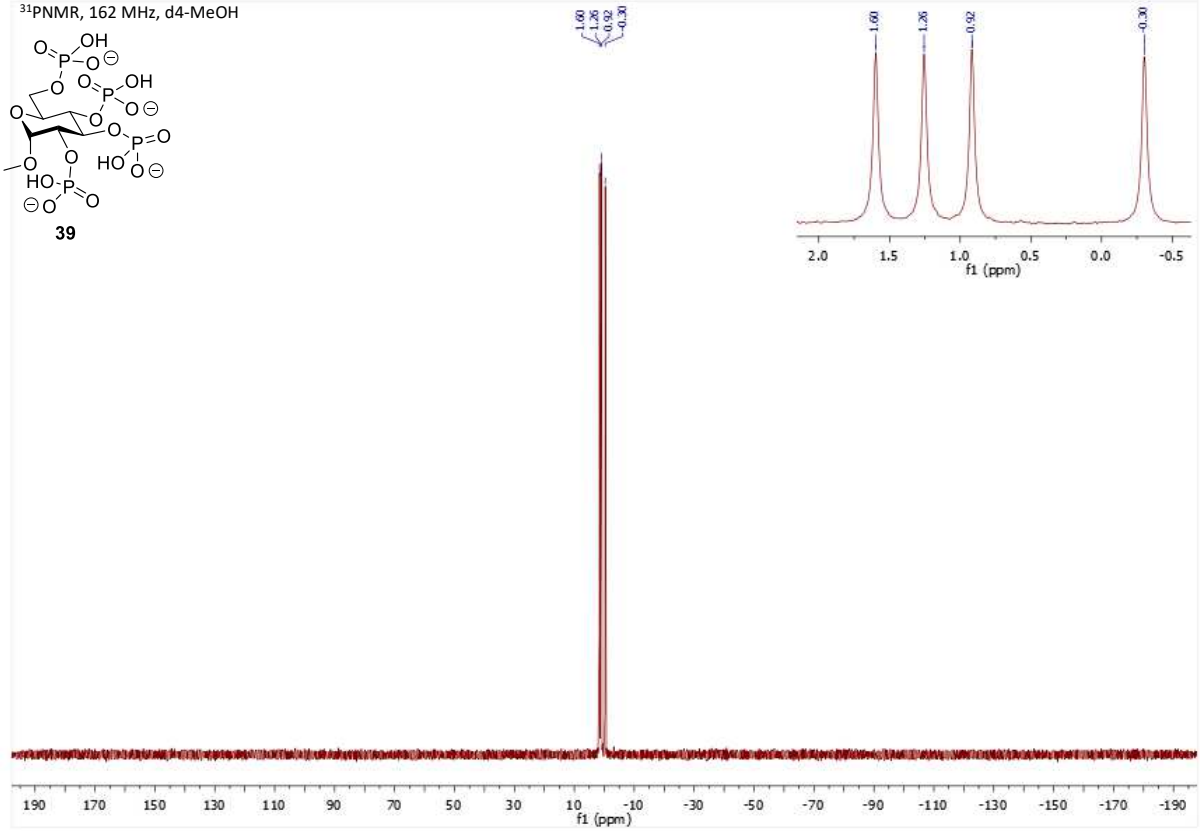

^{13}CNMR, 100 MHz, d4-MeOH

39

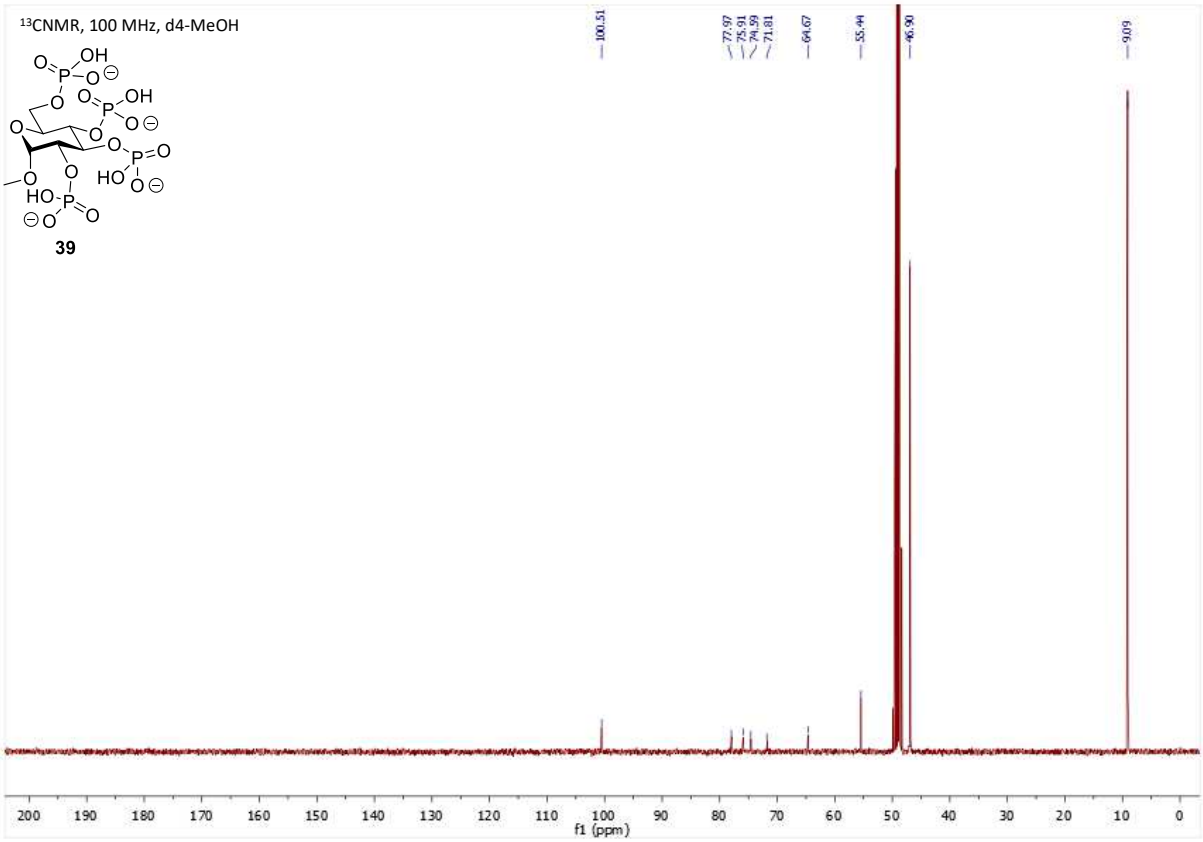

Synthesis of InsP$_3$R carbohydrate polyphosphates

Methyl 4,6-*O*-benzylidene-3-*O*-benzyl-α-D-glucopyranoside (**66**)

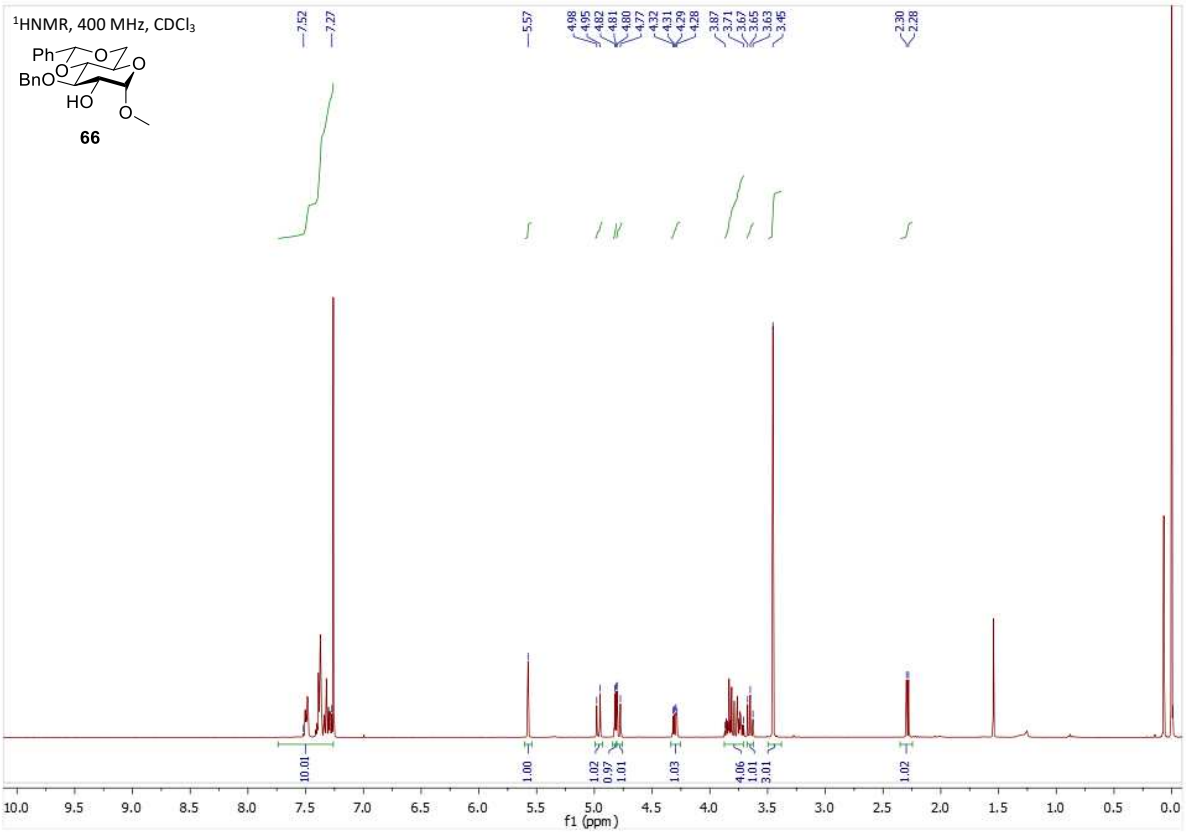

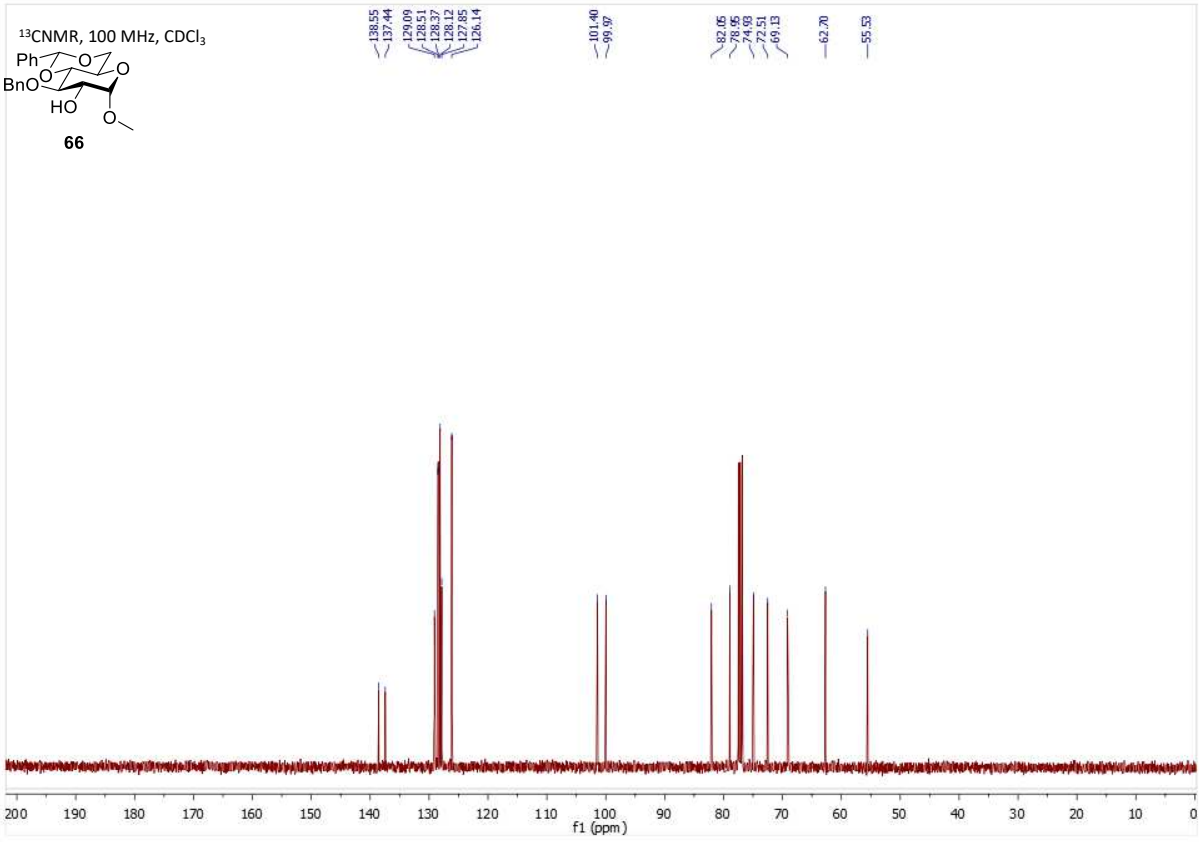

^{1}H-^{1}H COSY

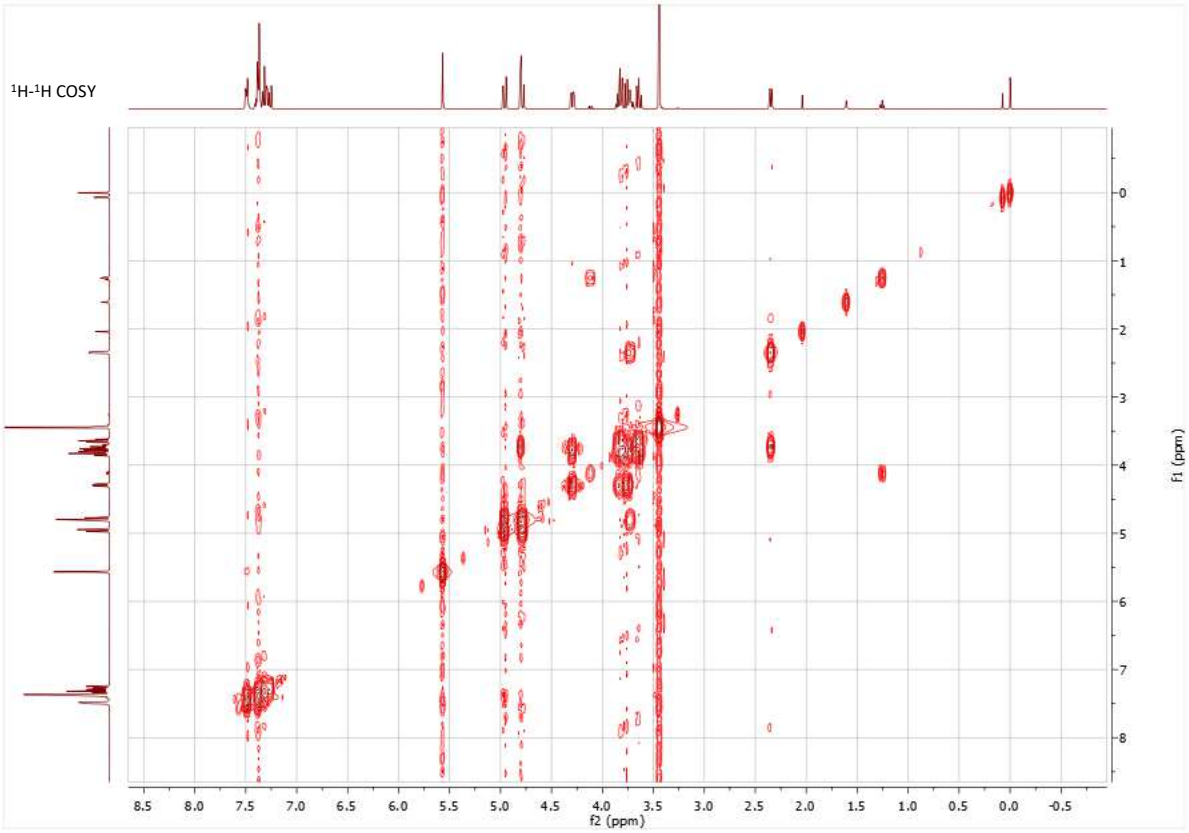

^{1}H-^{13}C HSQC

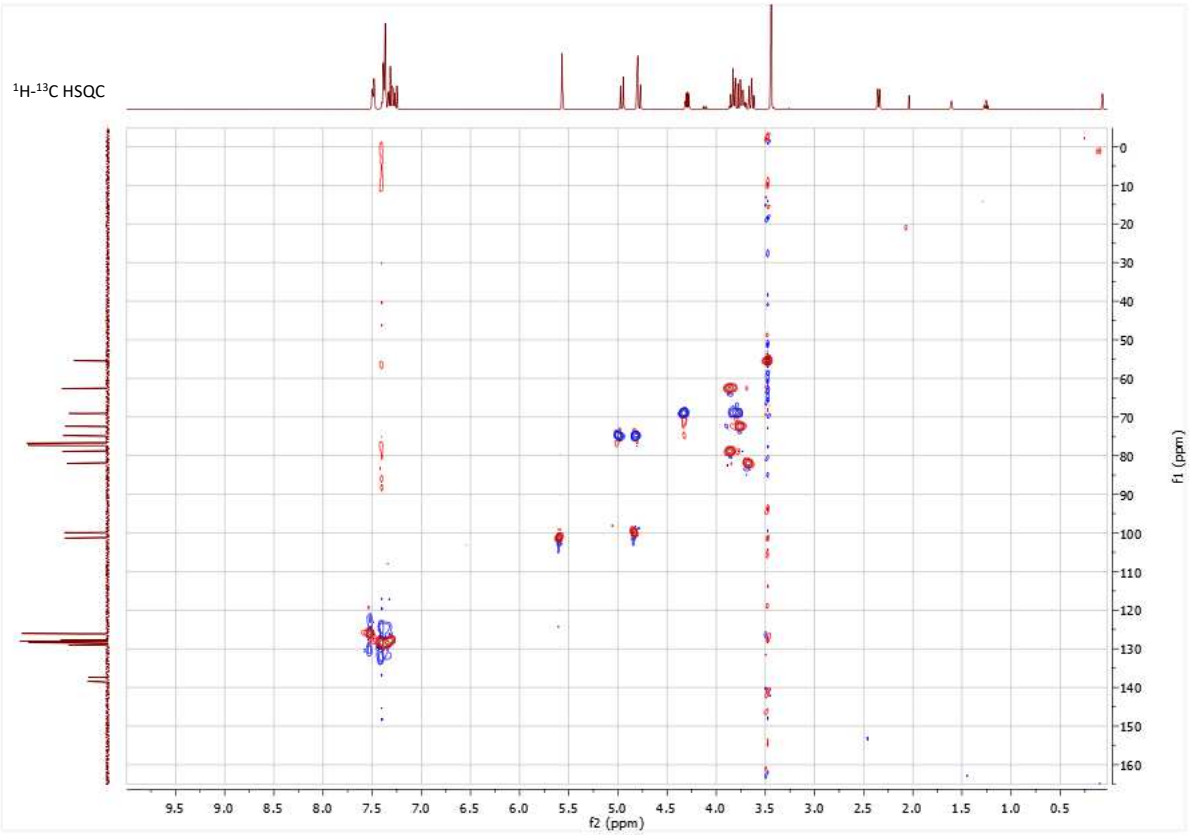

Methyl 3-*O*-benzyl-α-D-glucopyranoside (**67**)

^{1}HNMR, 400 MHz, $CDCl_3$

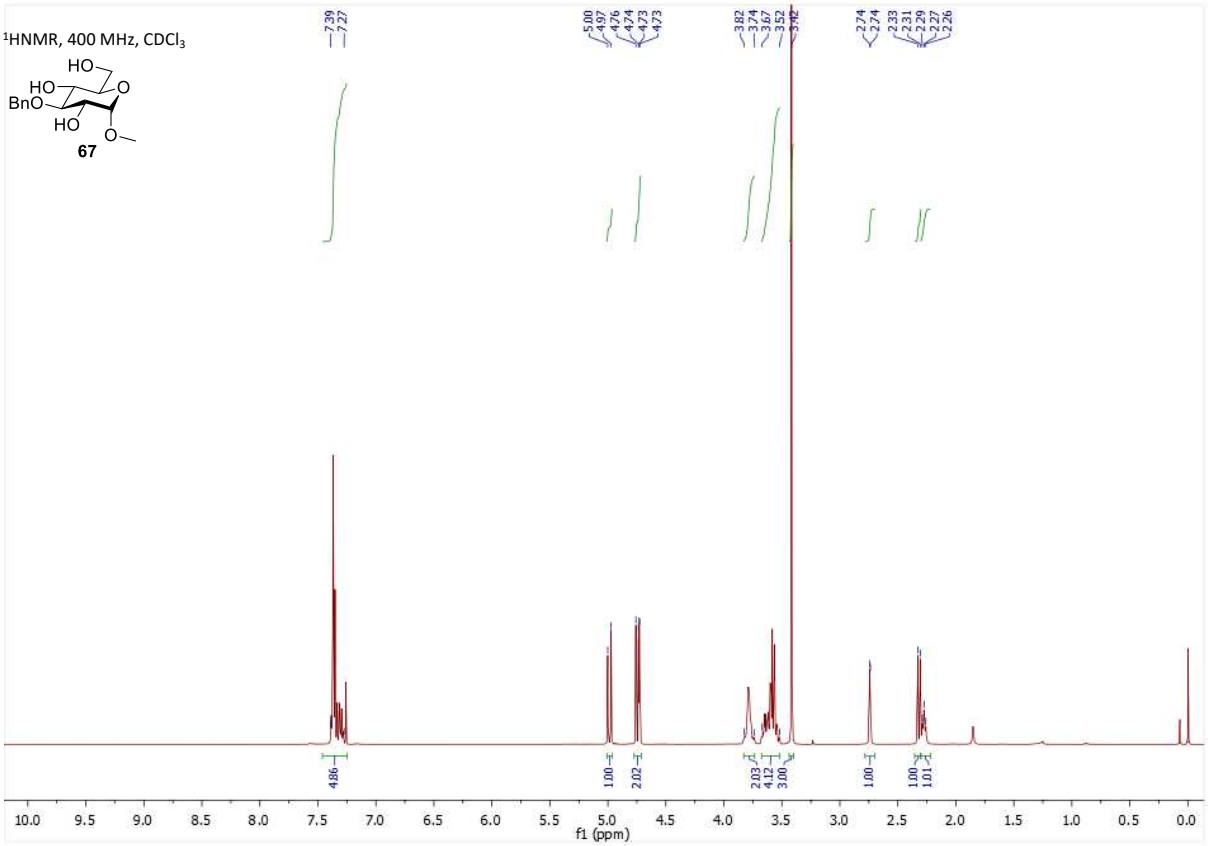

^{13}CNMR, 100 MHz, $CDCl_3$

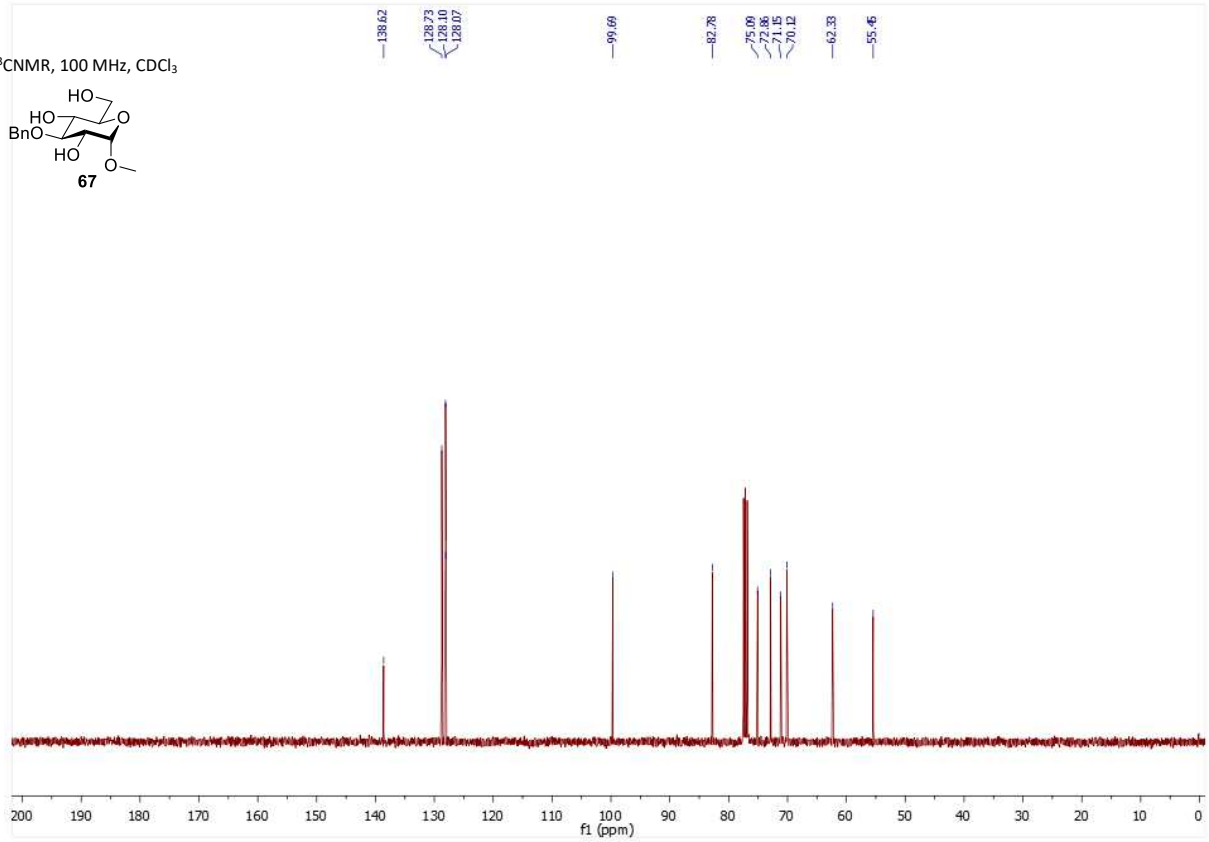

^{1}H-^{1}H COSY

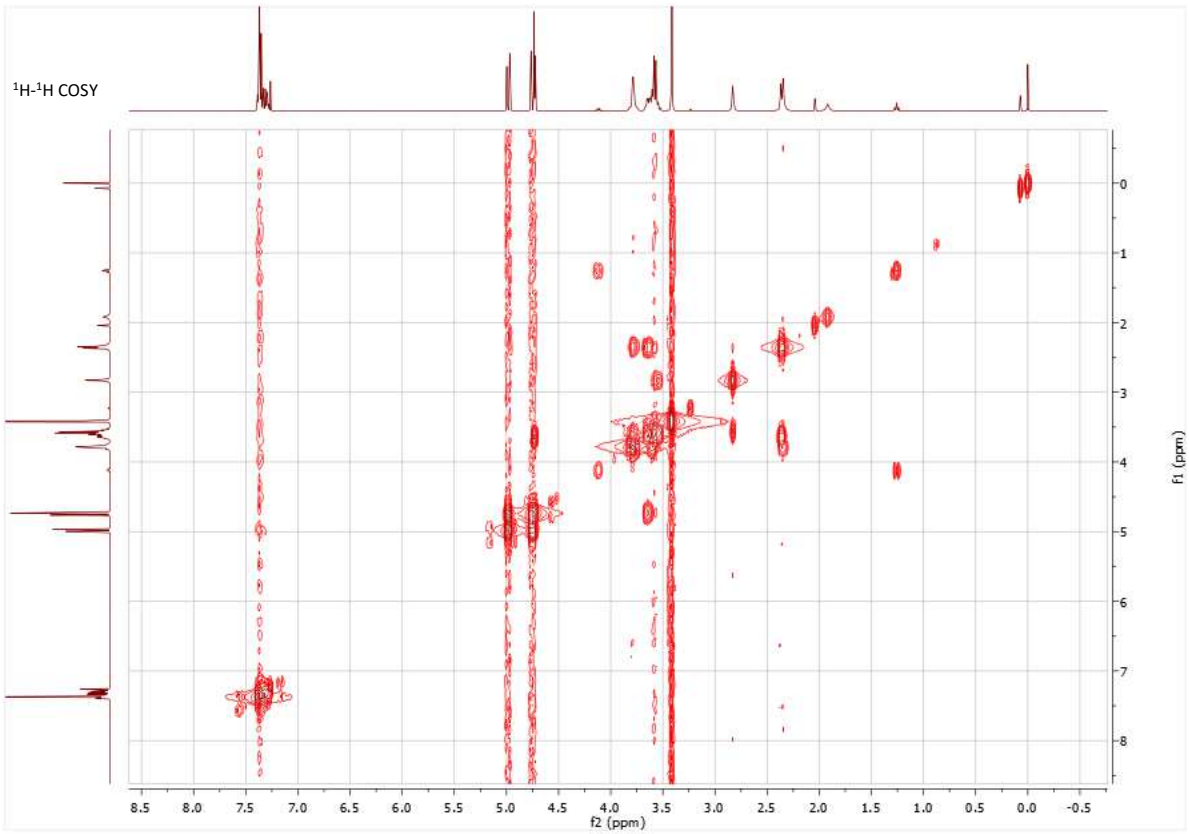

^{1}H-^{13}C HSQC

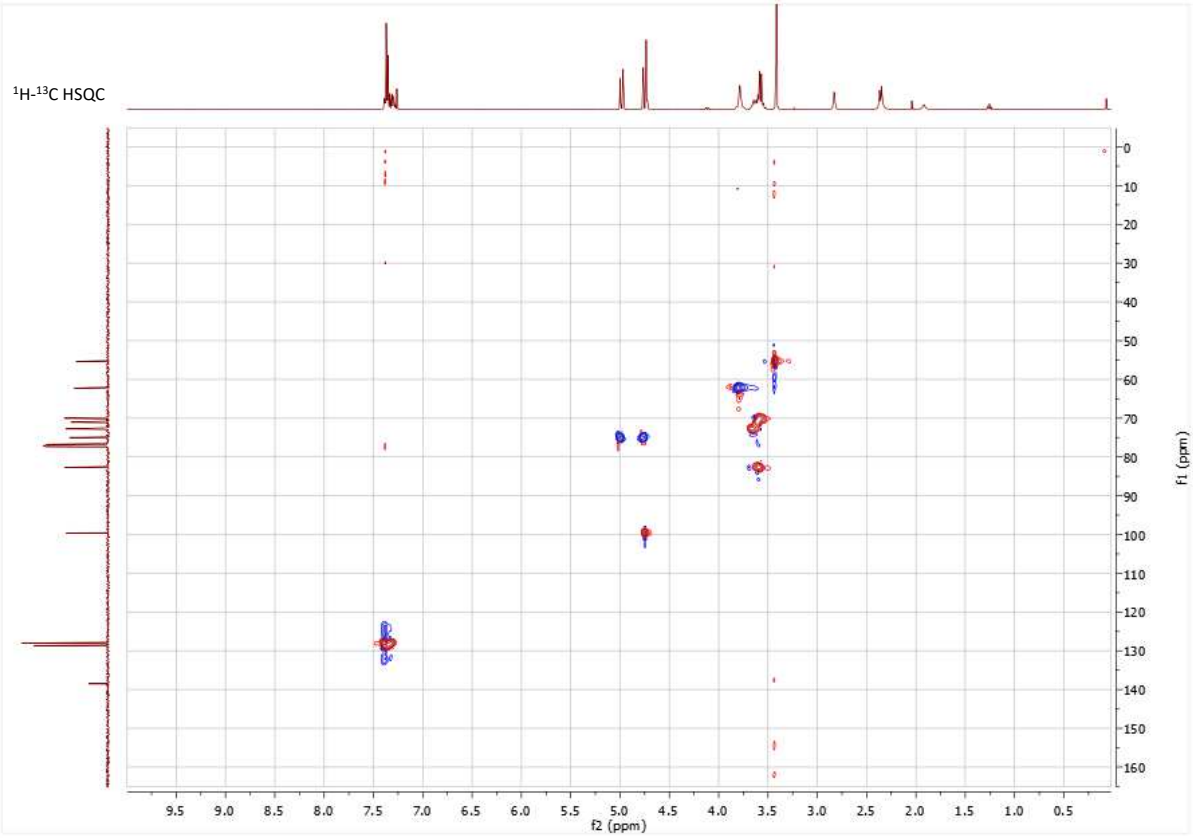

Methyl 3-*O*-benzyl-α-D-glucopyranoside 2,4,6-tris(dibenzylphosphate) (**68**)

^{1}HNMR, 400 MHz, $CDCl_3$

68

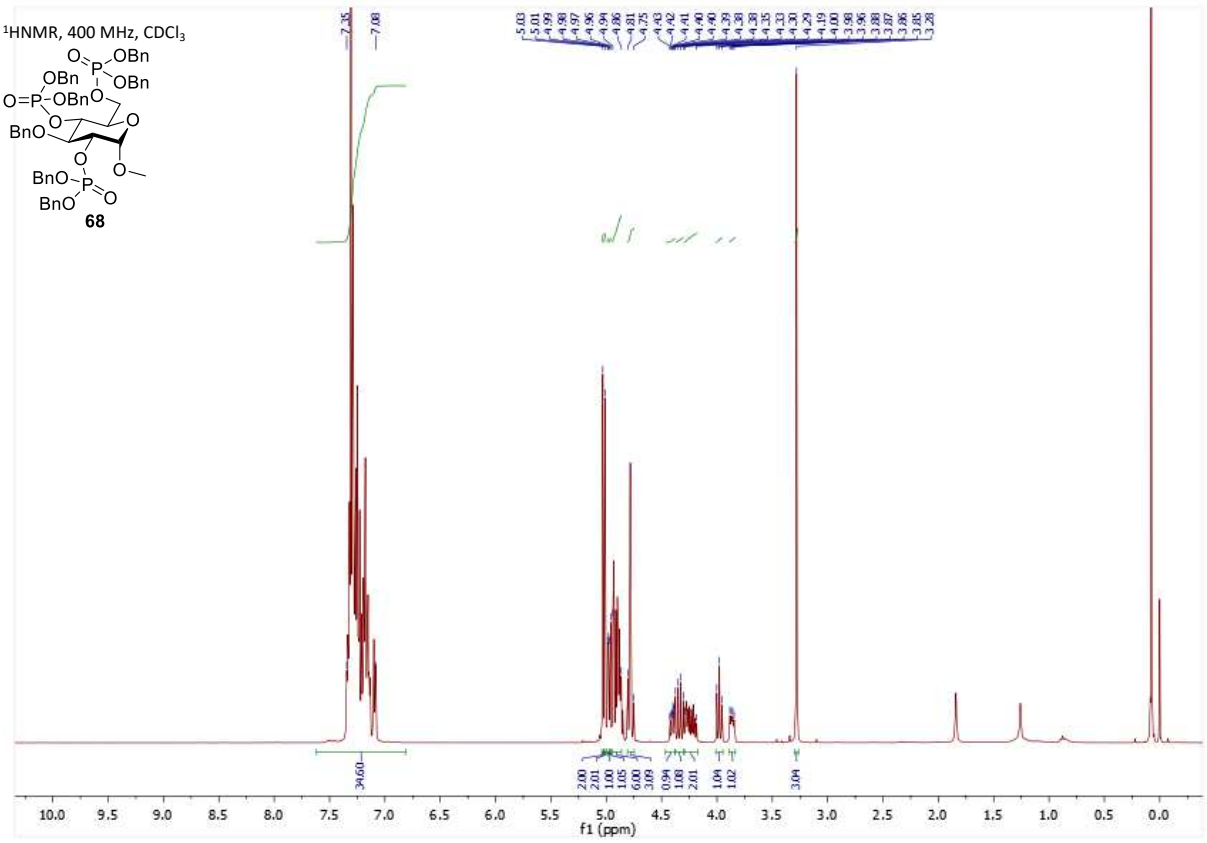

^{31}PNMR, 162 MHz, $CDCl_3$

68

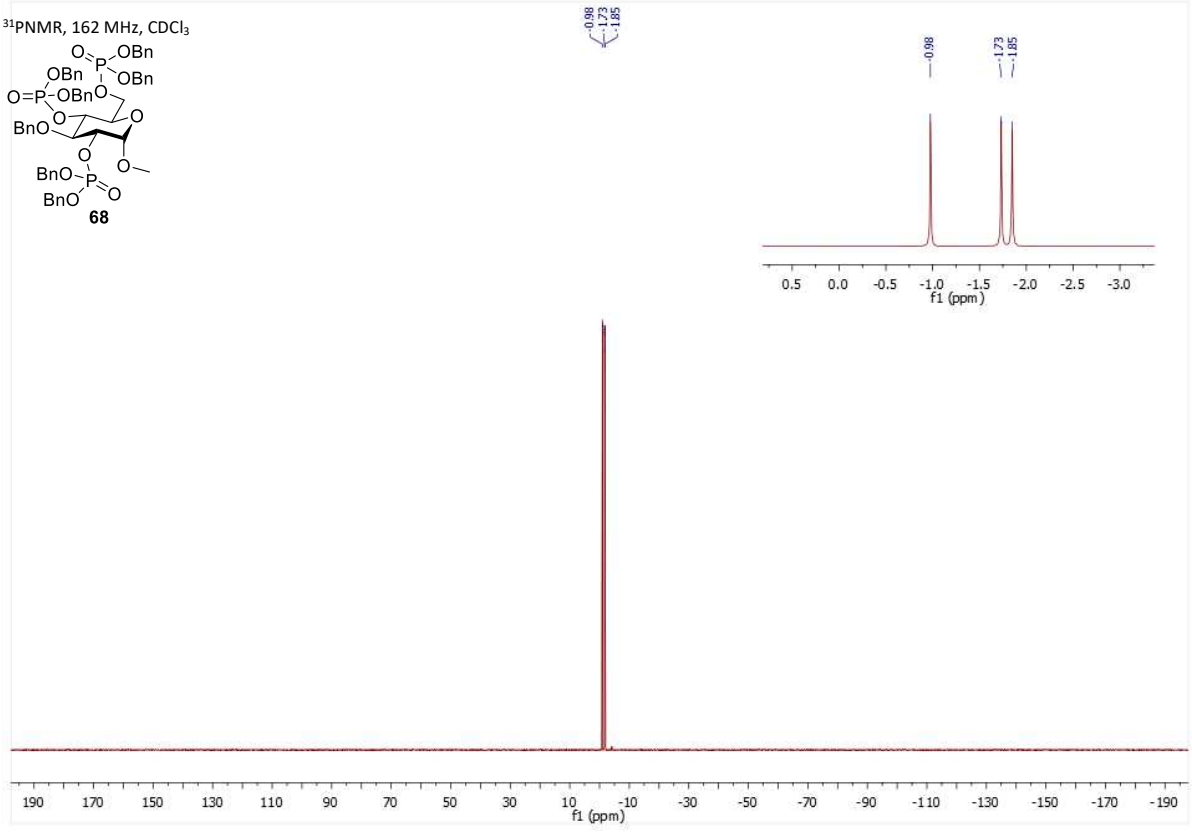

^{13}CNMR, 100 MHz, $CDCl_3$

68

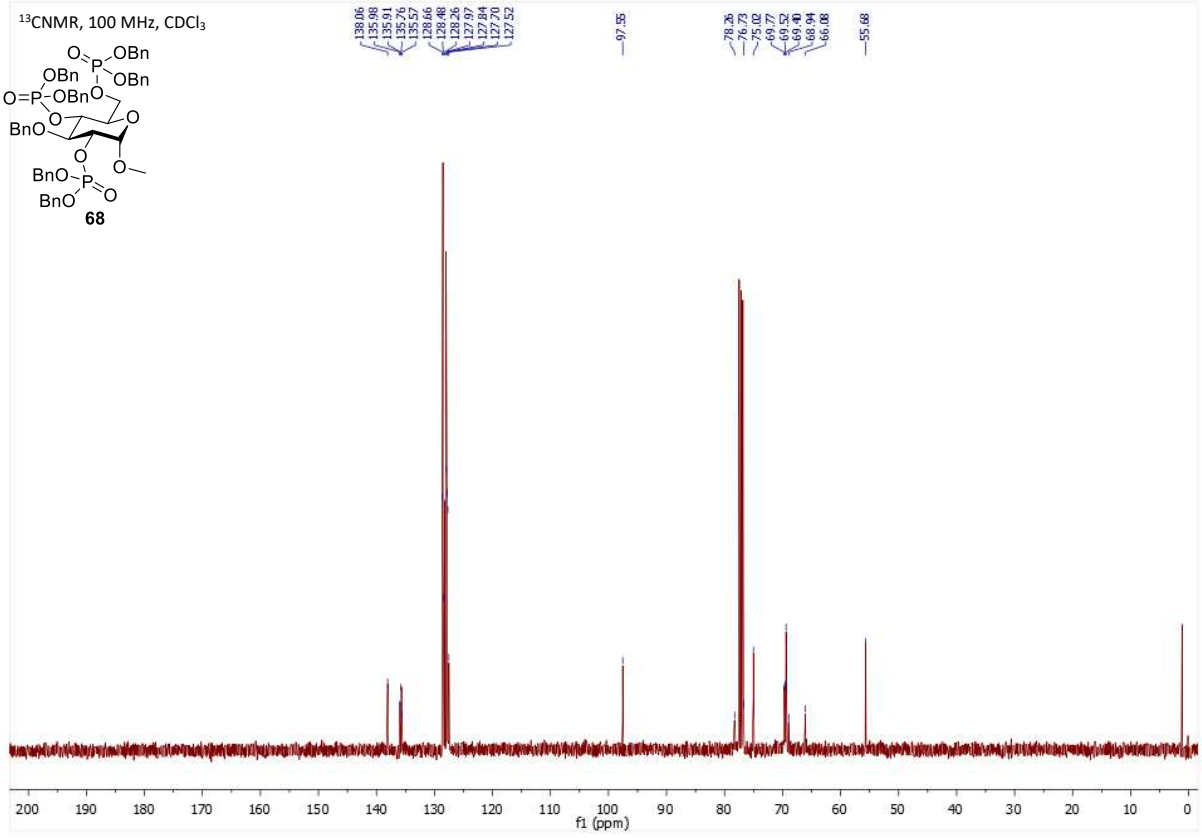

^{1}H-^{1}H COSY

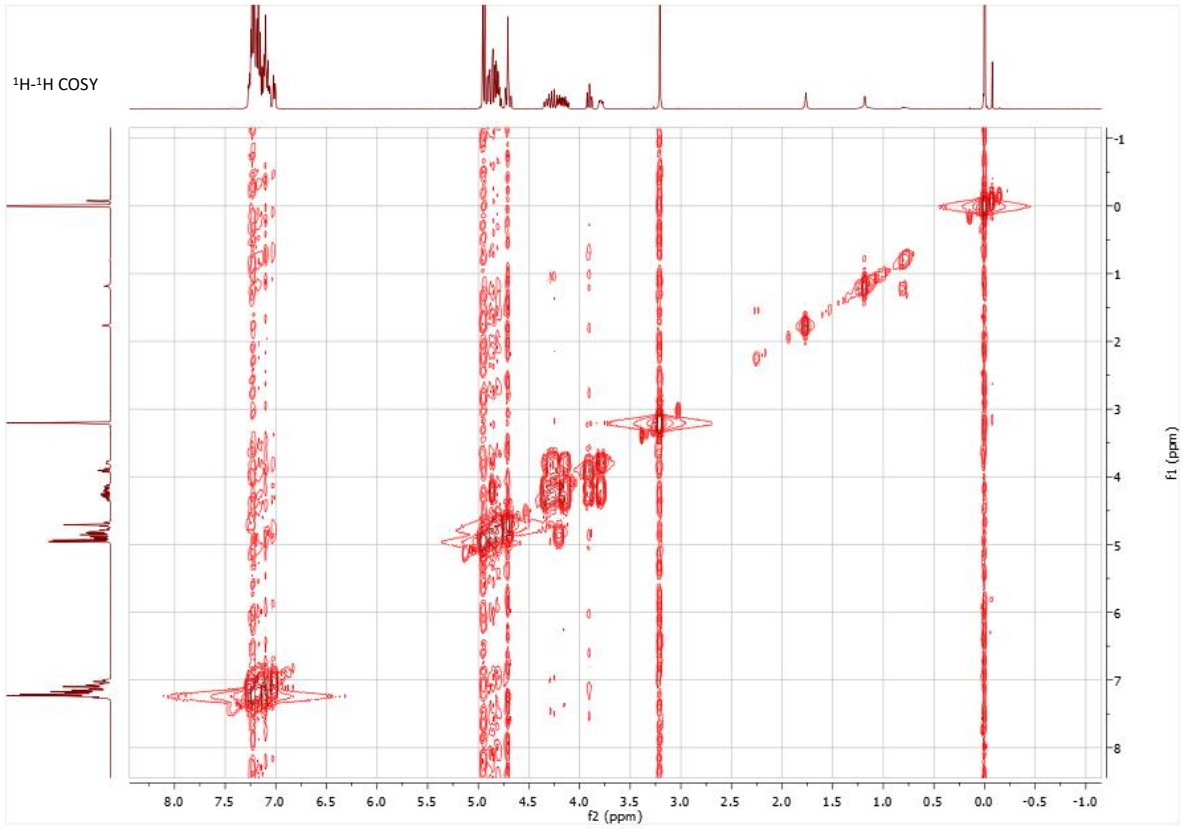

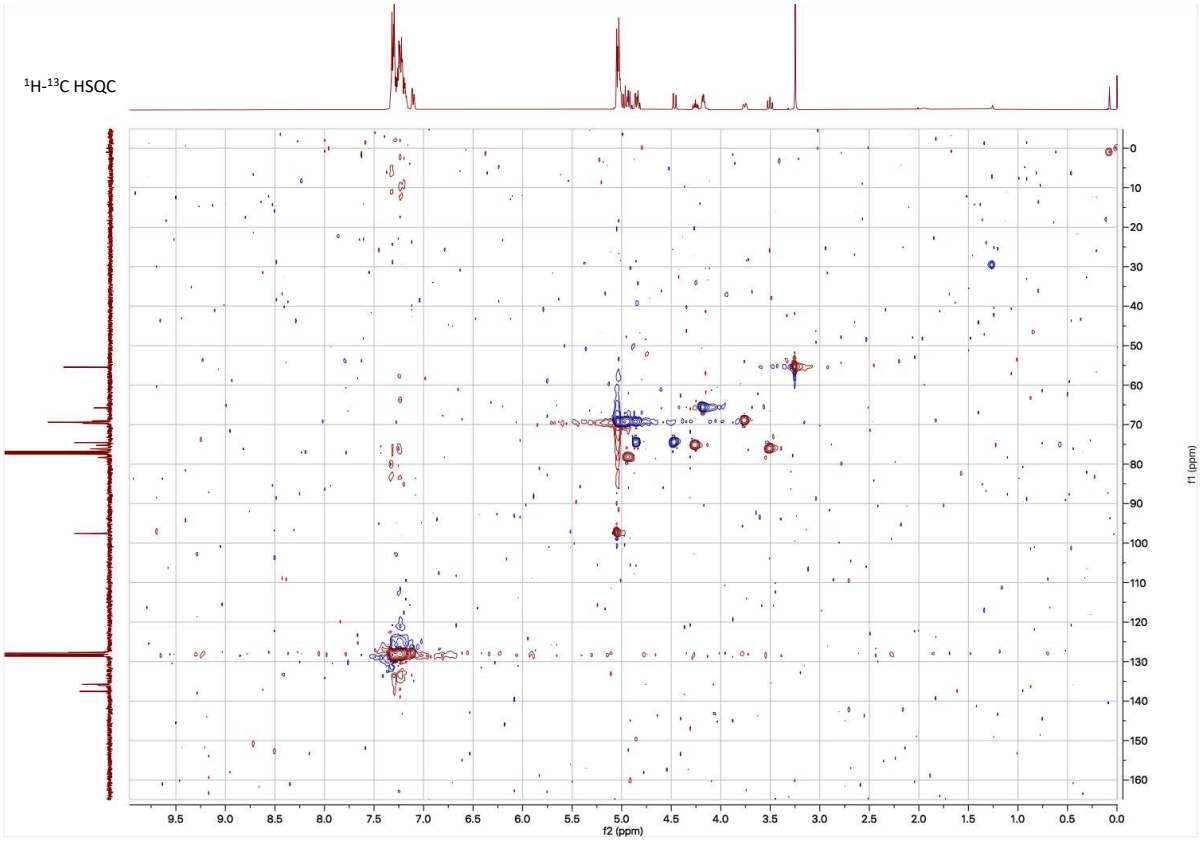

Methyl α-D-glucopyranoside 2,4,6-trisphosphate triethylammonium salt (**61**)

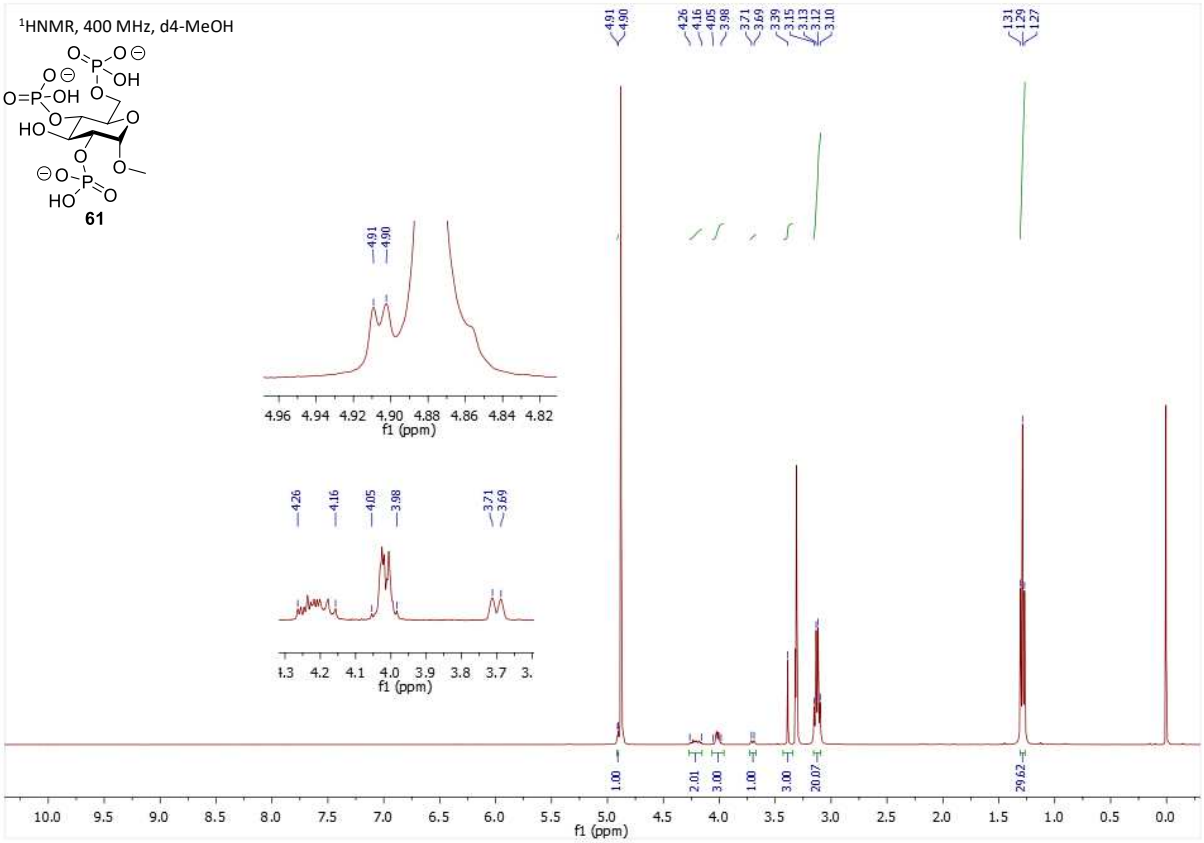

^{31}PNMR, 162 MHz, d4-MeOH

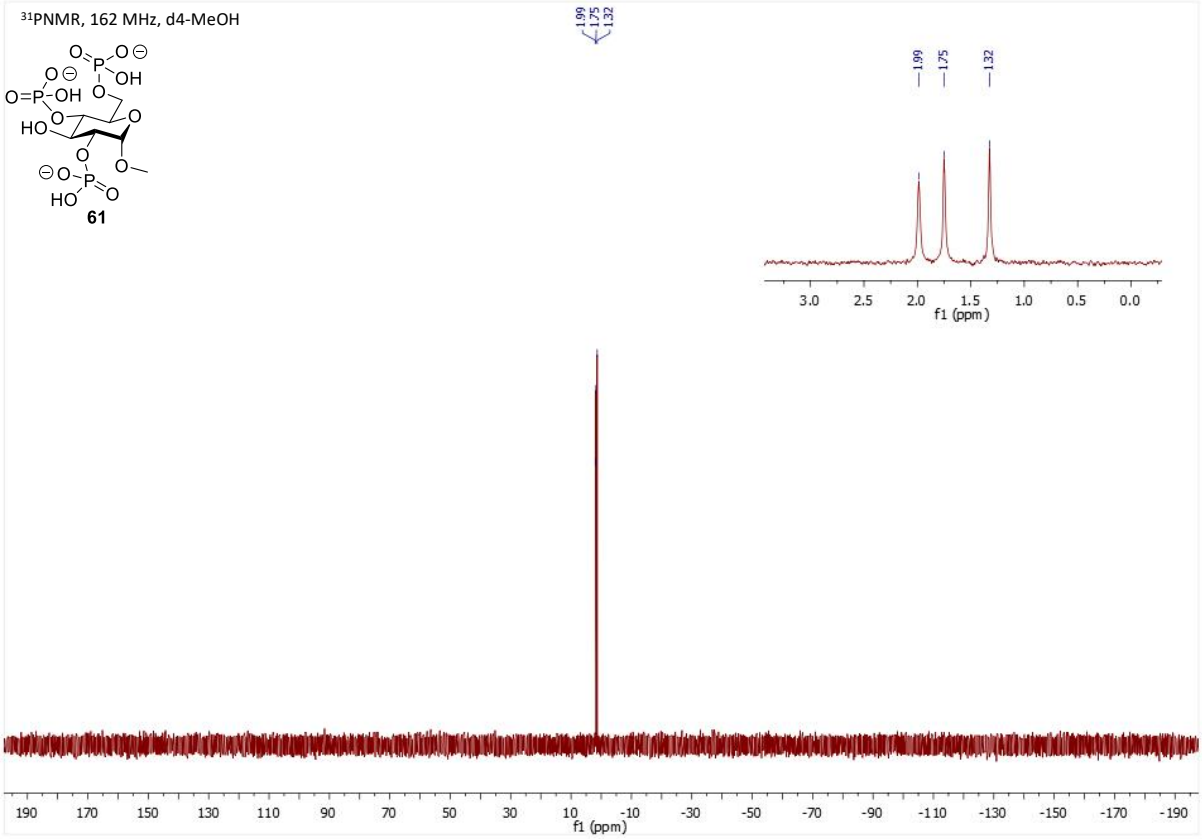

61

^{13}CNMR, 100 MHz, d4-MeOH

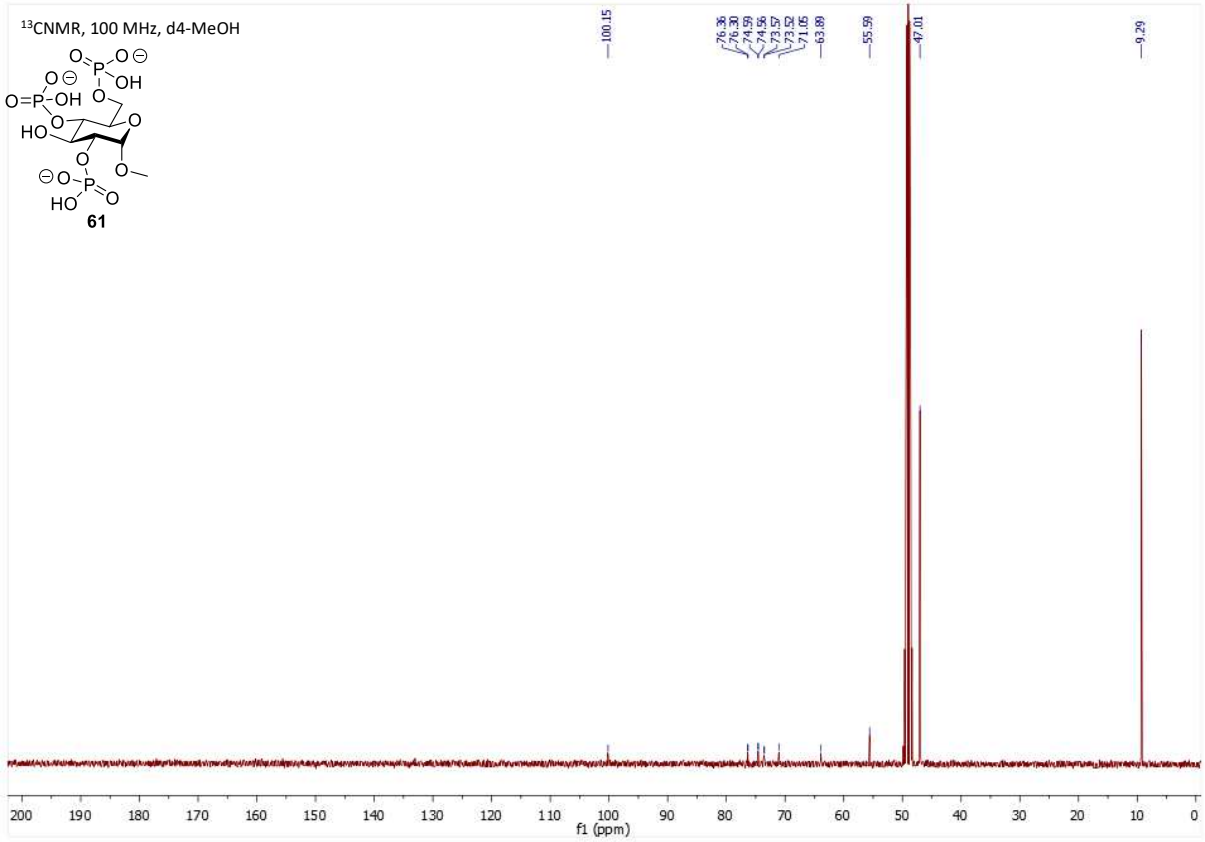

61

^{1}H-^{1}H COSY

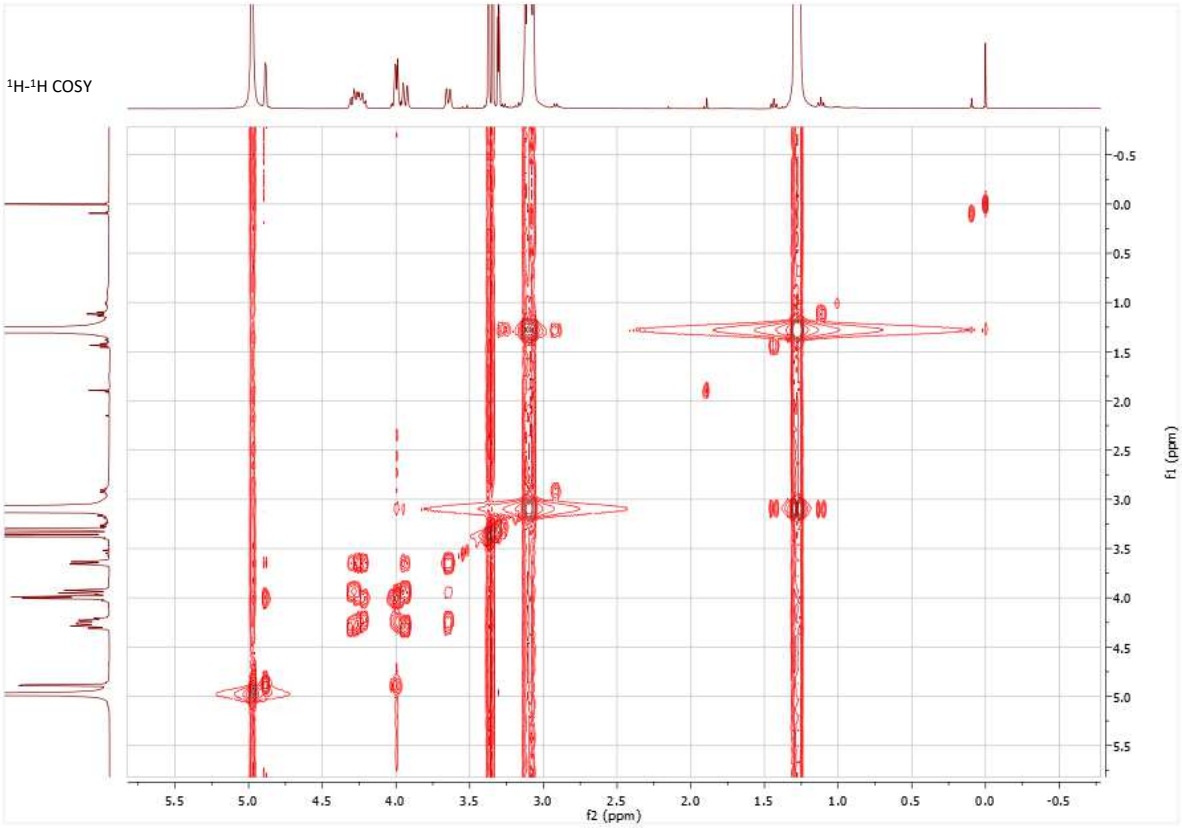

^{1}H-^{13}C HSQC

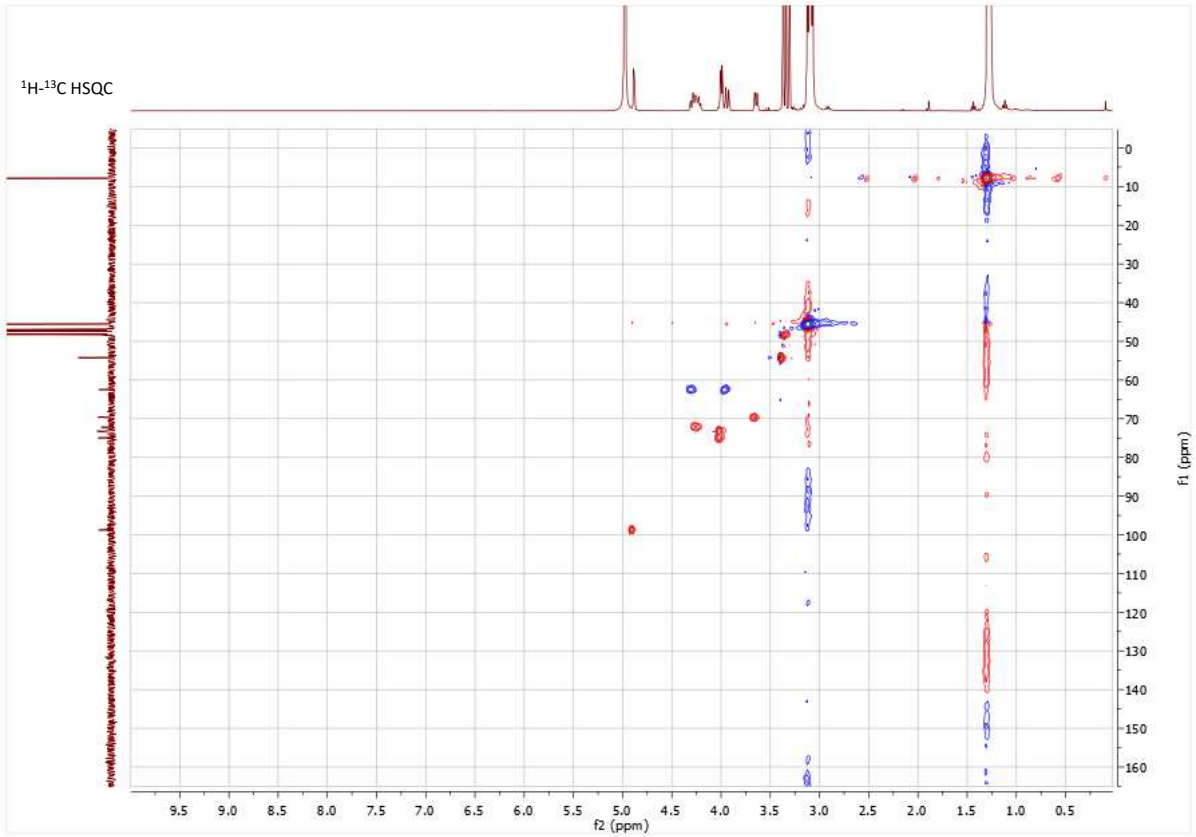

Methyl 3-*O*-benzyl-4,6-*O*-benzylidene-α-L-glucopyranoside (**71**)

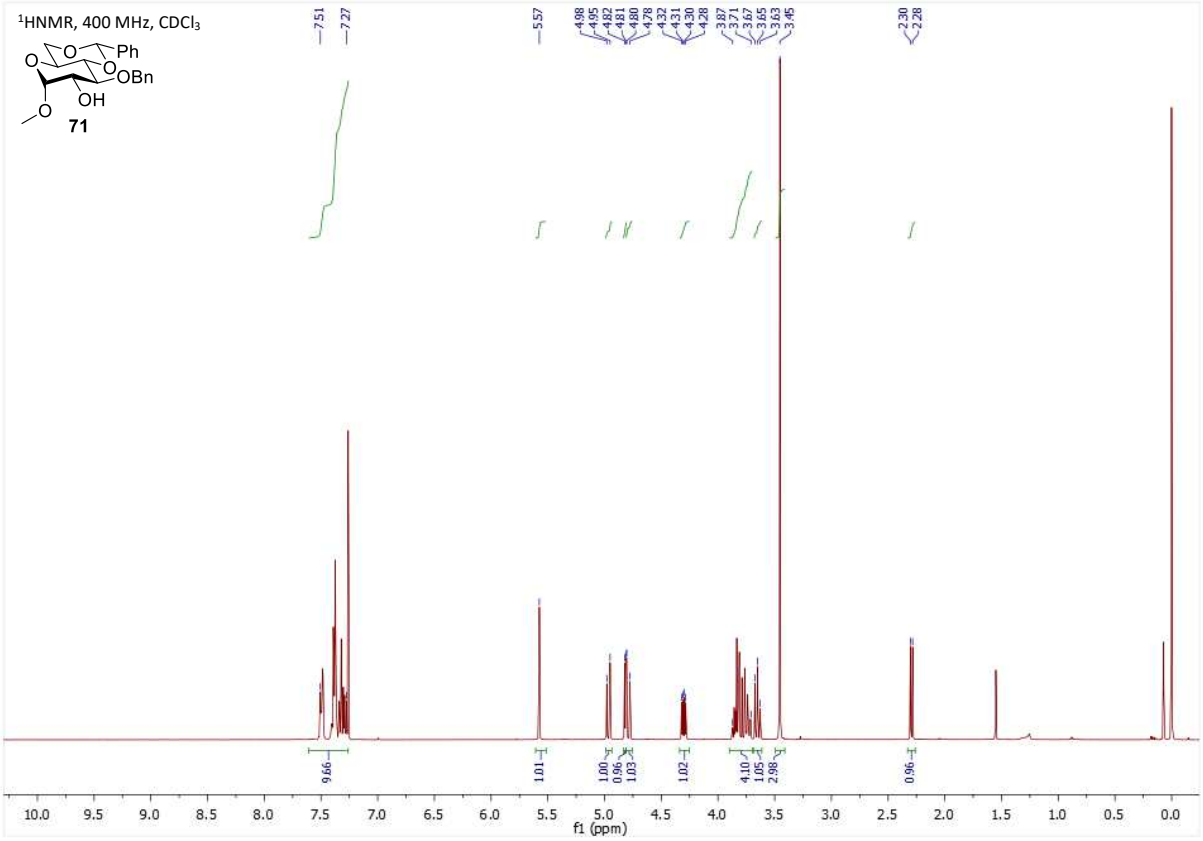

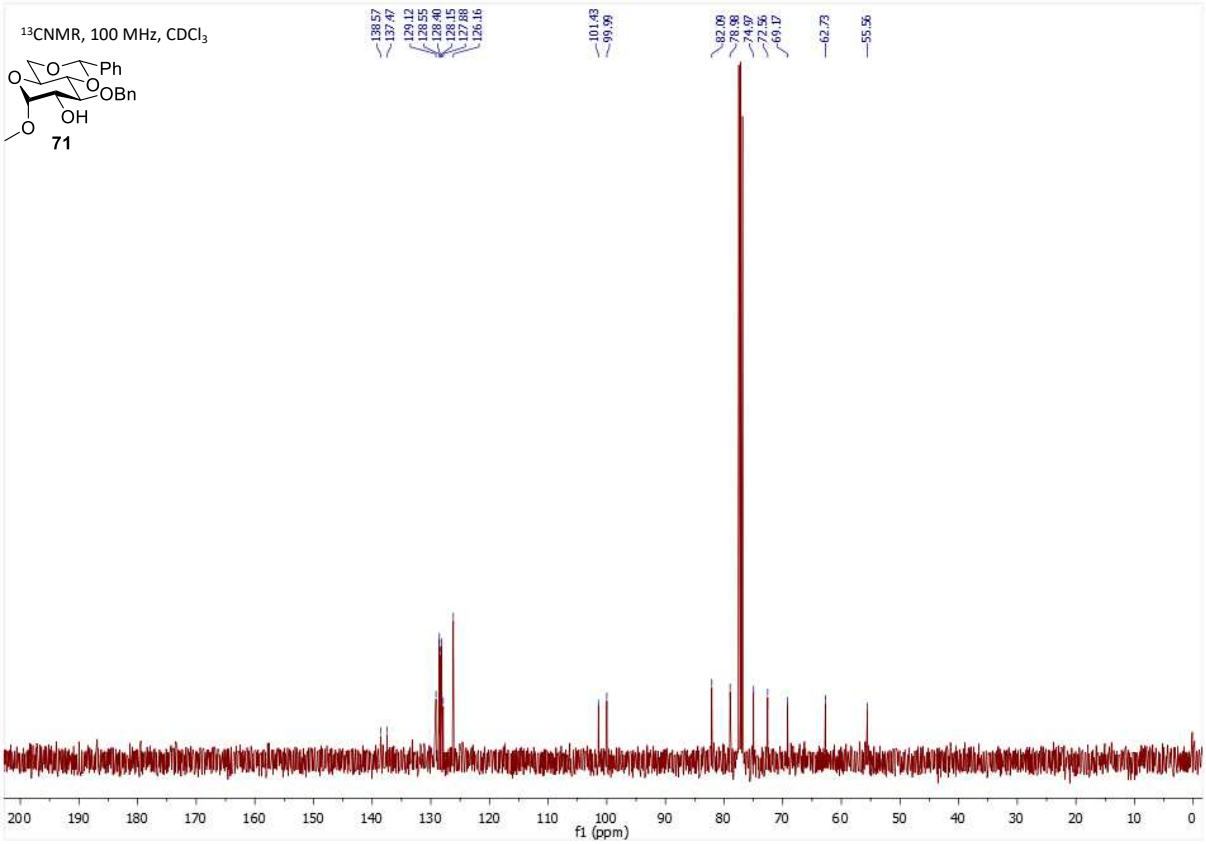

^{1}H-^{1}H COSY

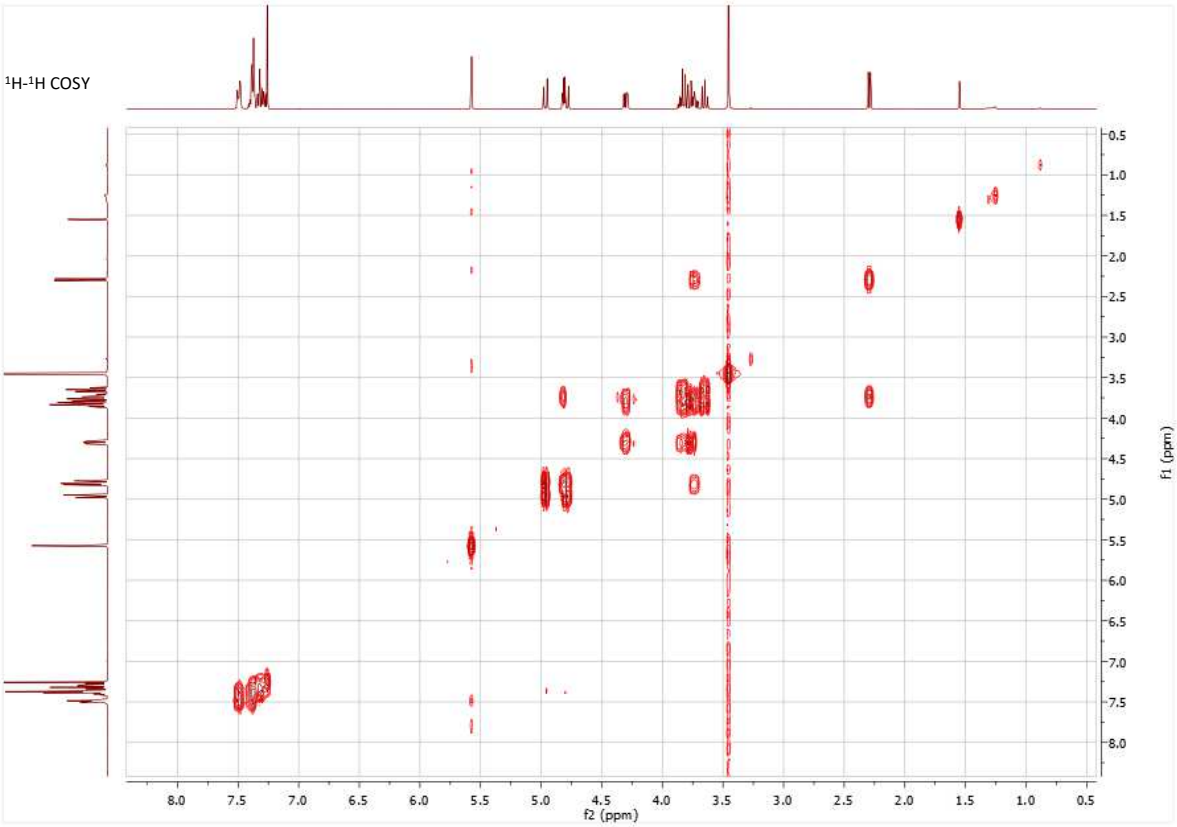

^{1}H-^{13}C HSQC

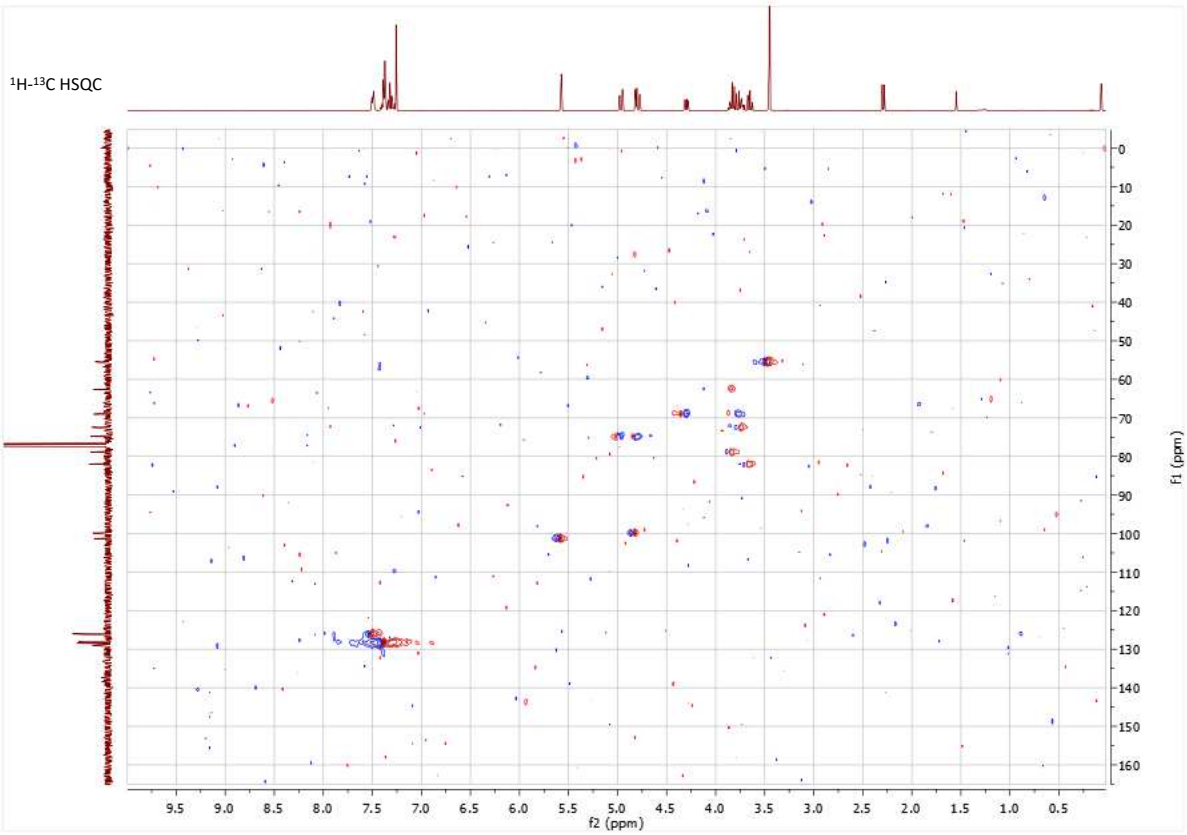

Methyl 3-*O*-benzyl-α-L-glucopyranoside (**72**)

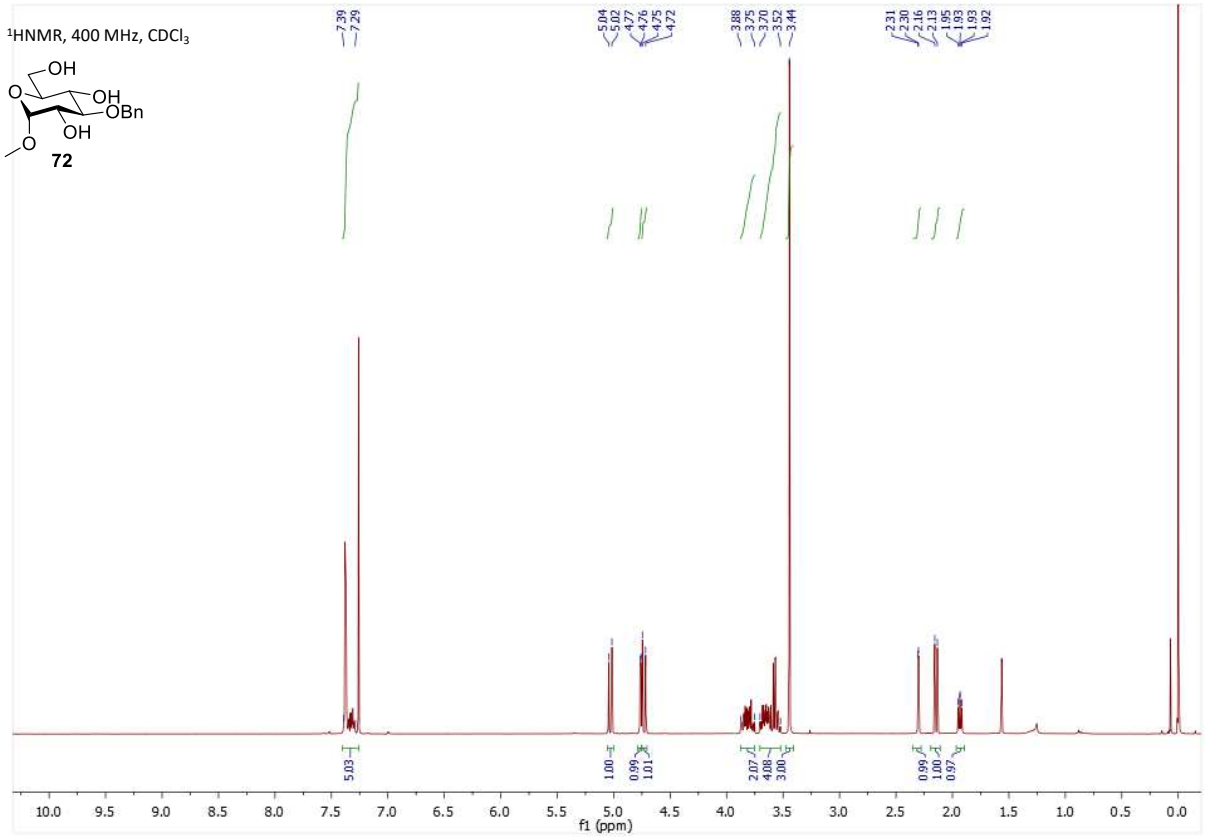

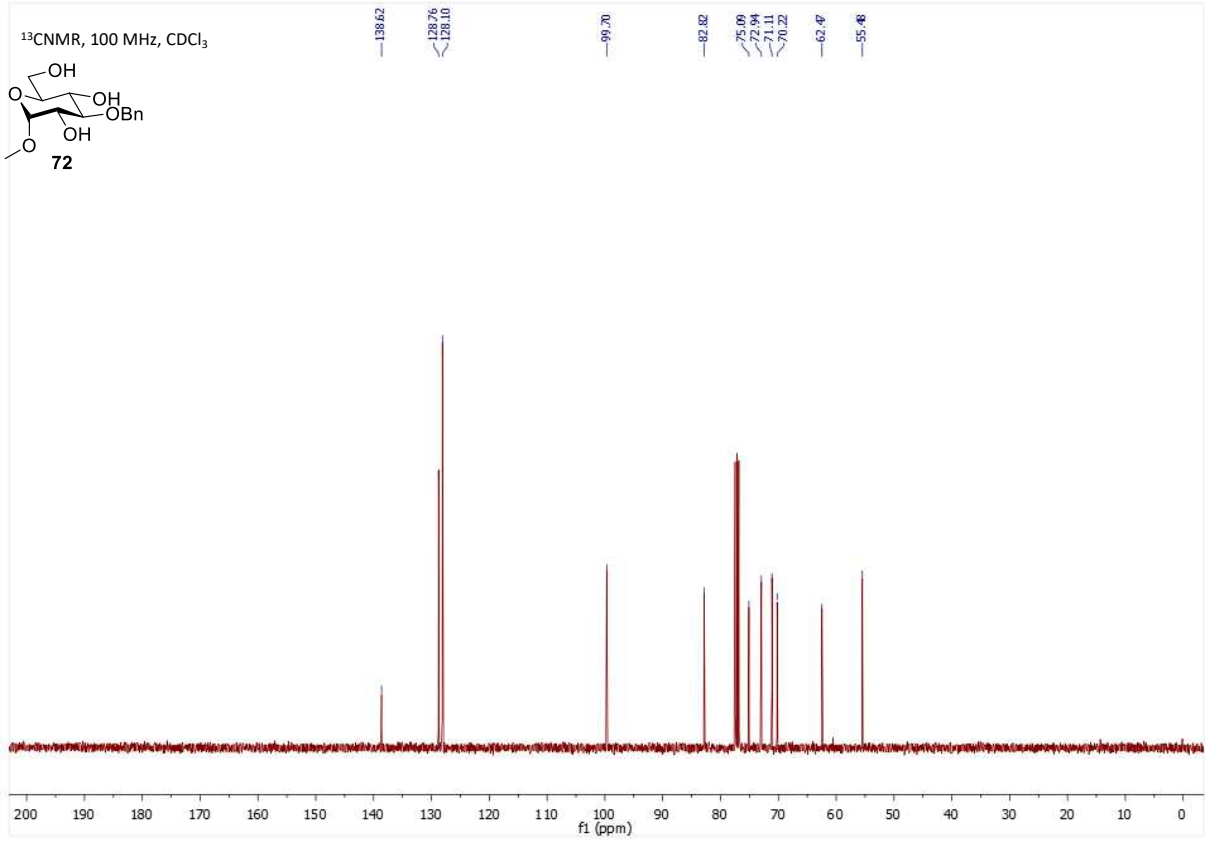

^{1}H-^{1}H COSY

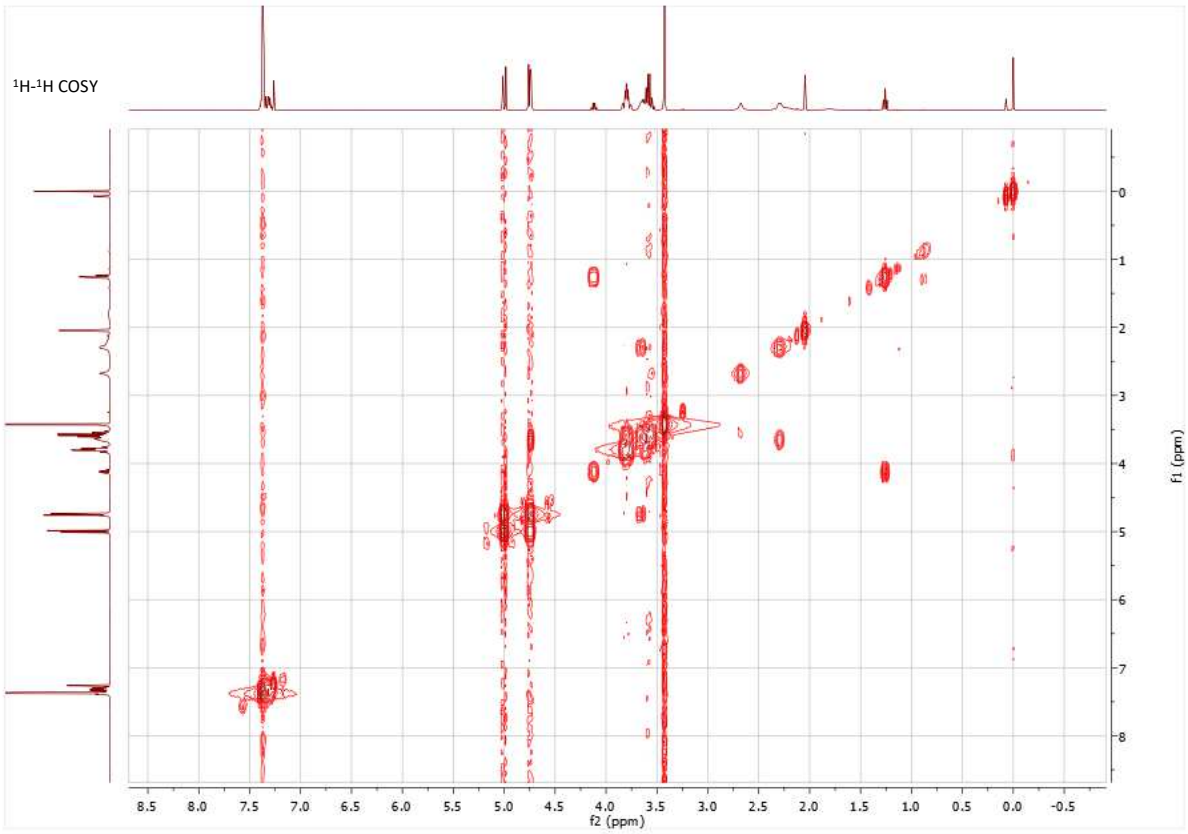

^{1}H-^{13}C HSQC

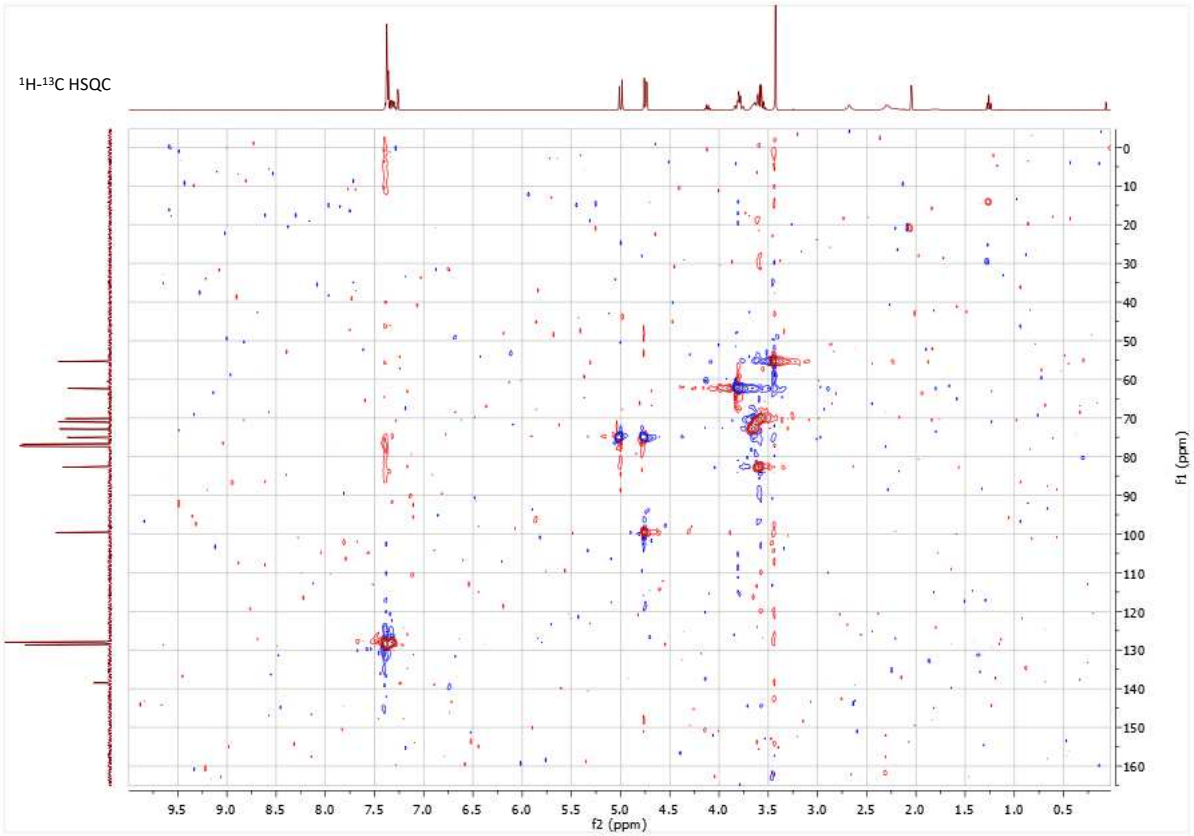

Methyl 3-*O*-benzyl-α-L-glucopyranoside 2,4,6-tris(dibenzylphosphate) (**73**)

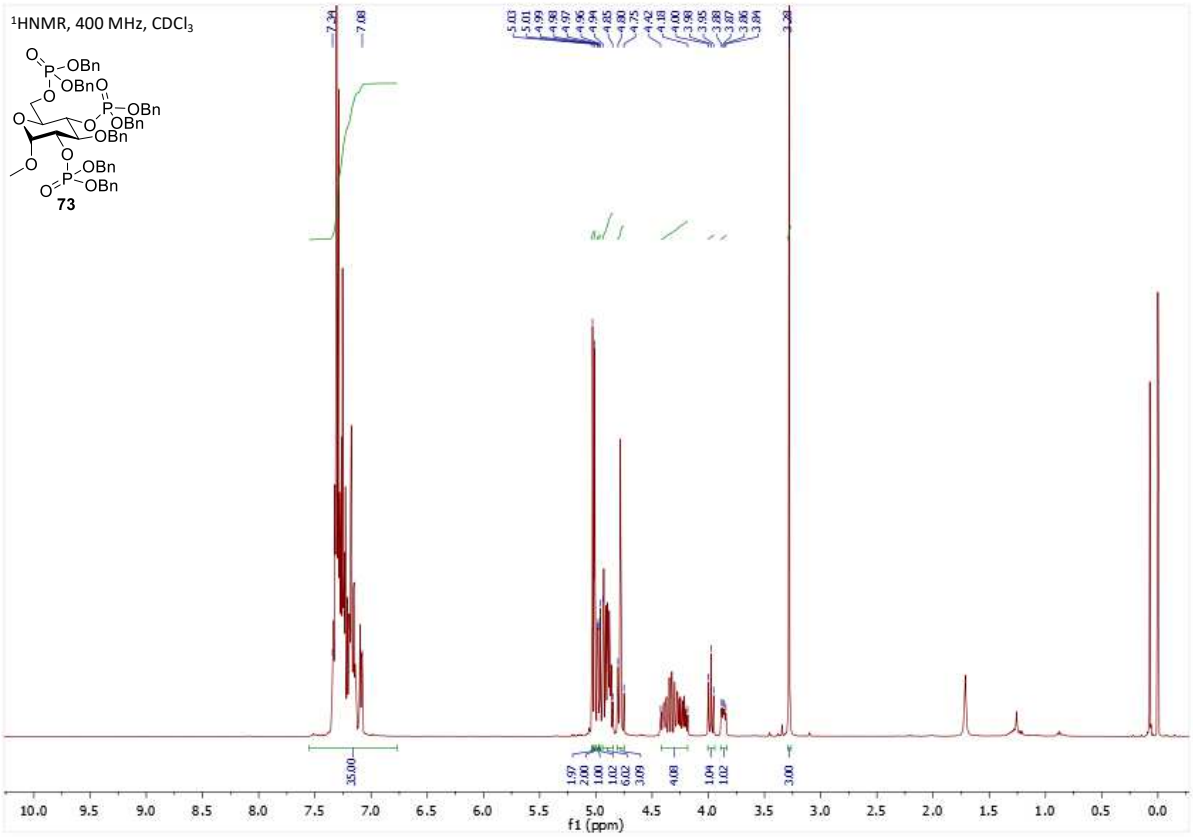

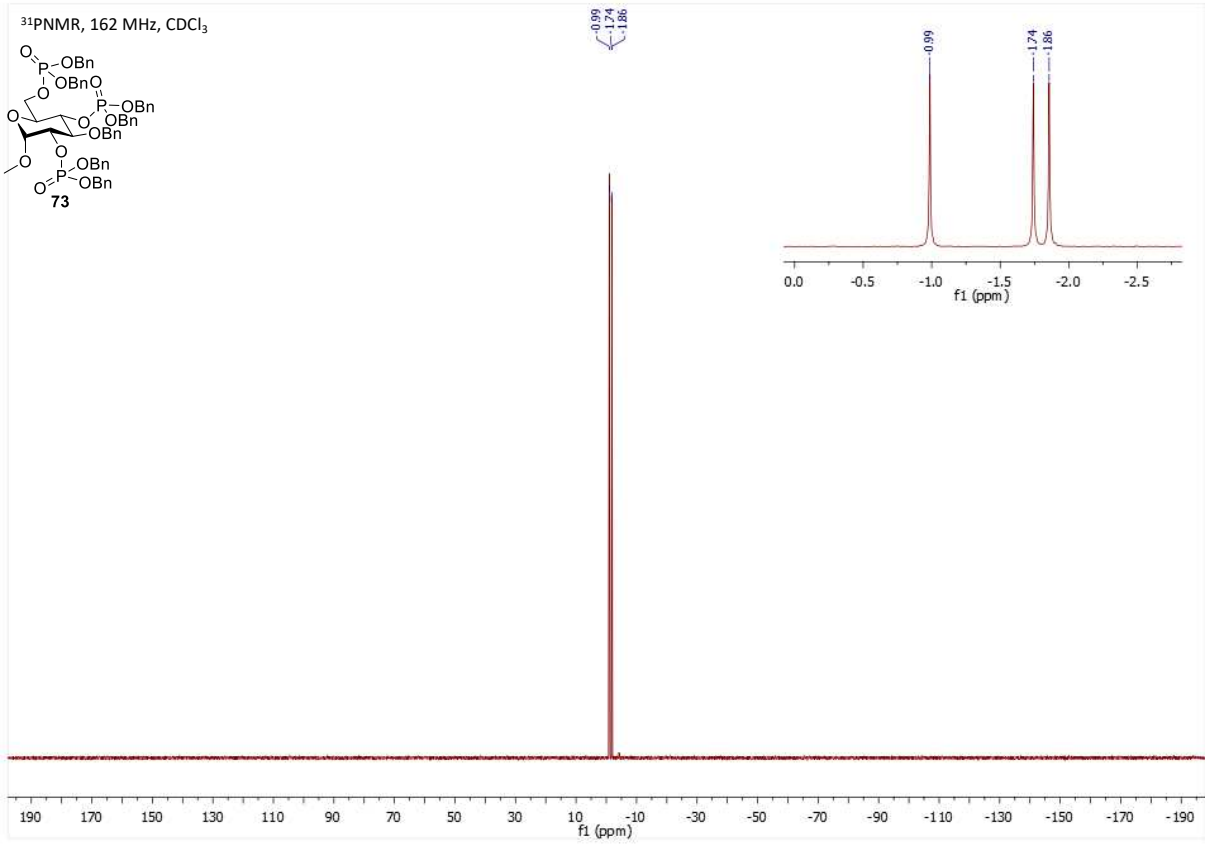

^{13}CNMR, 100 MHz, $CDCl_3$

73

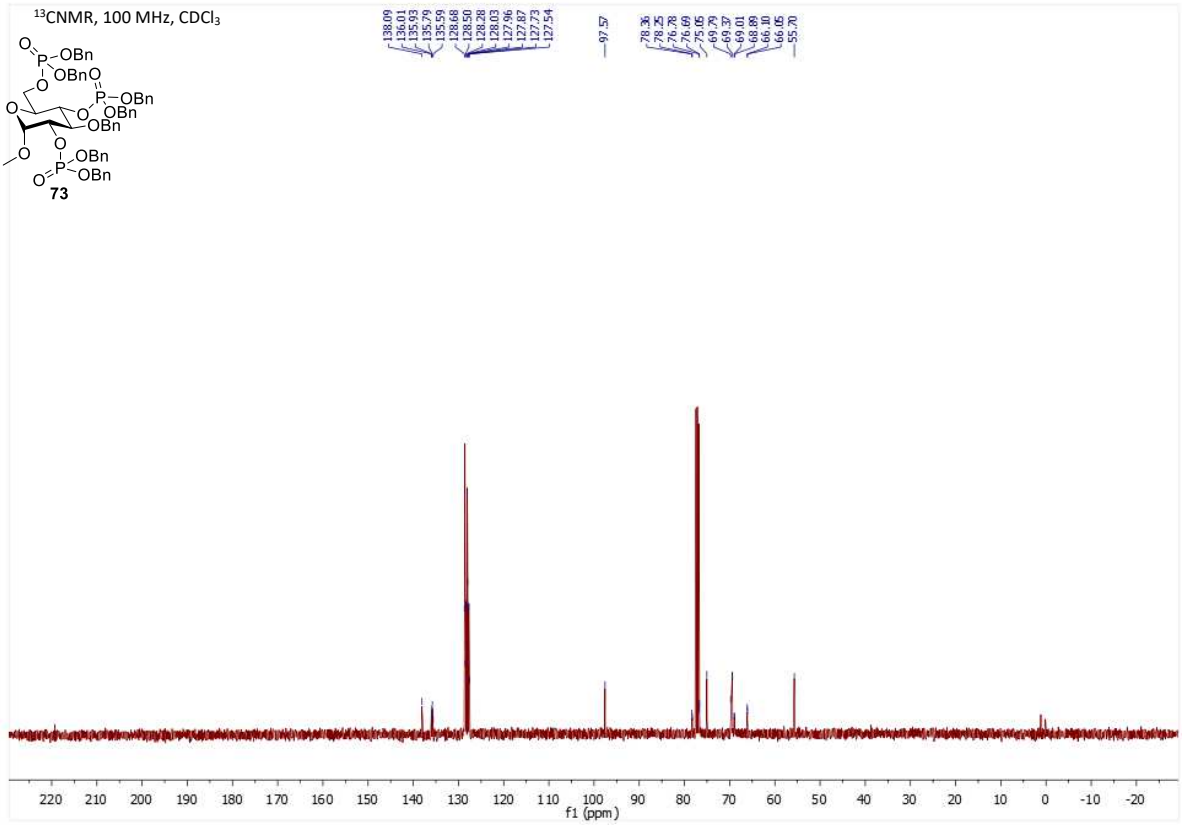

^{1}H-^{1}H COSY

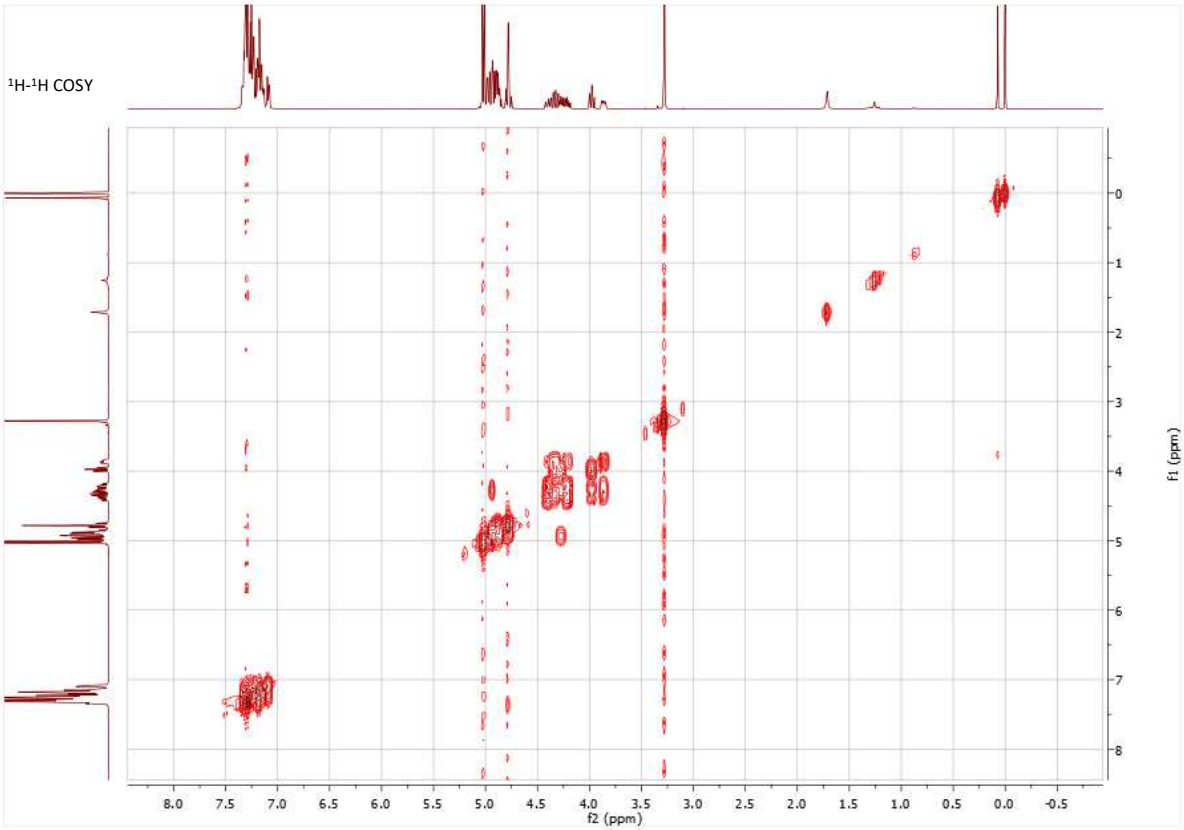

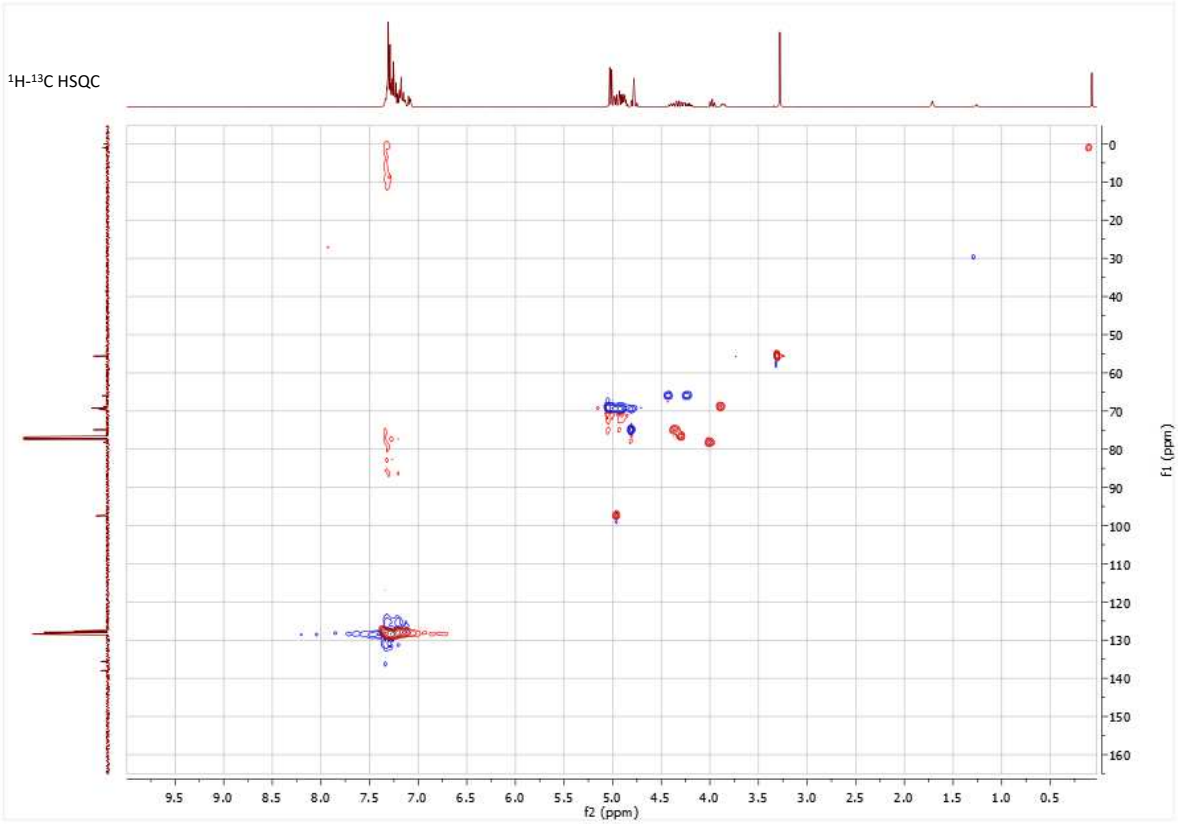

Methyl α-L-glucopyranoside 2,4,6-trisphosphate triethylammonium salt (**59**)

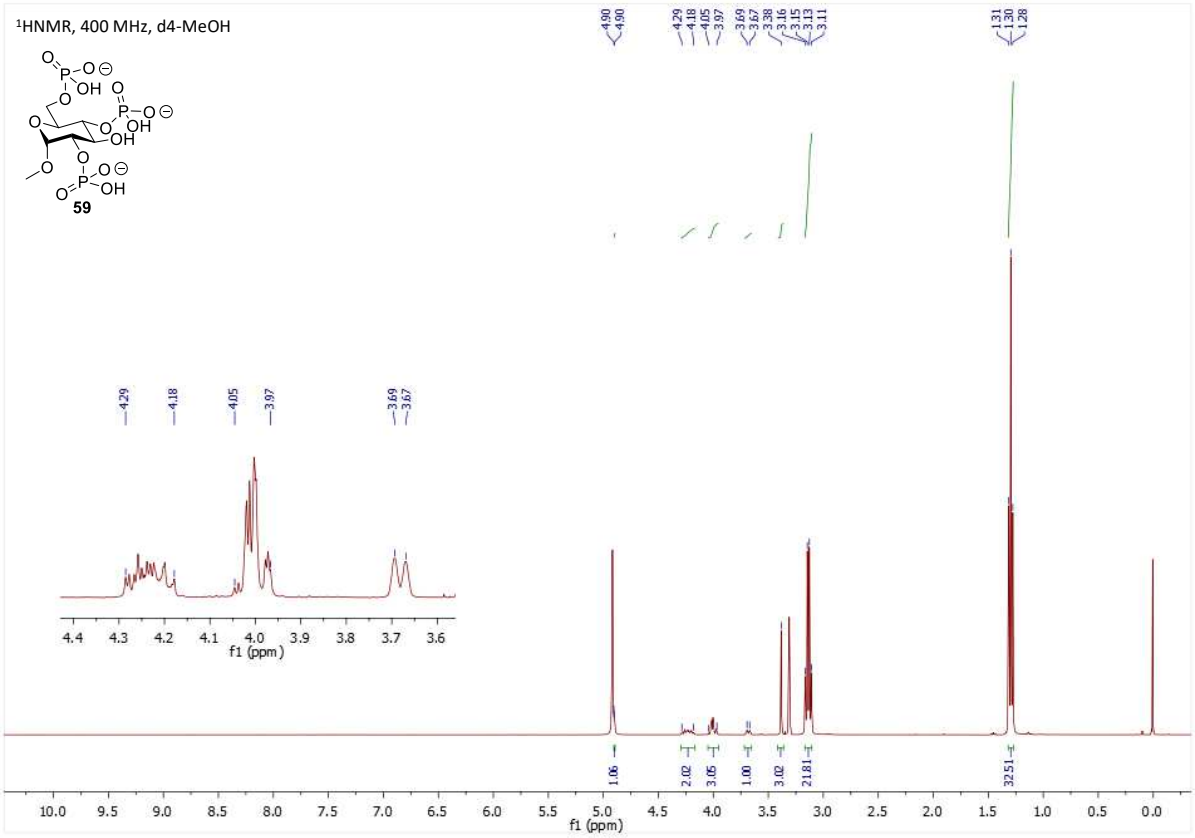

^{31}PNMR, 162 MHz, d4-MeOH

59

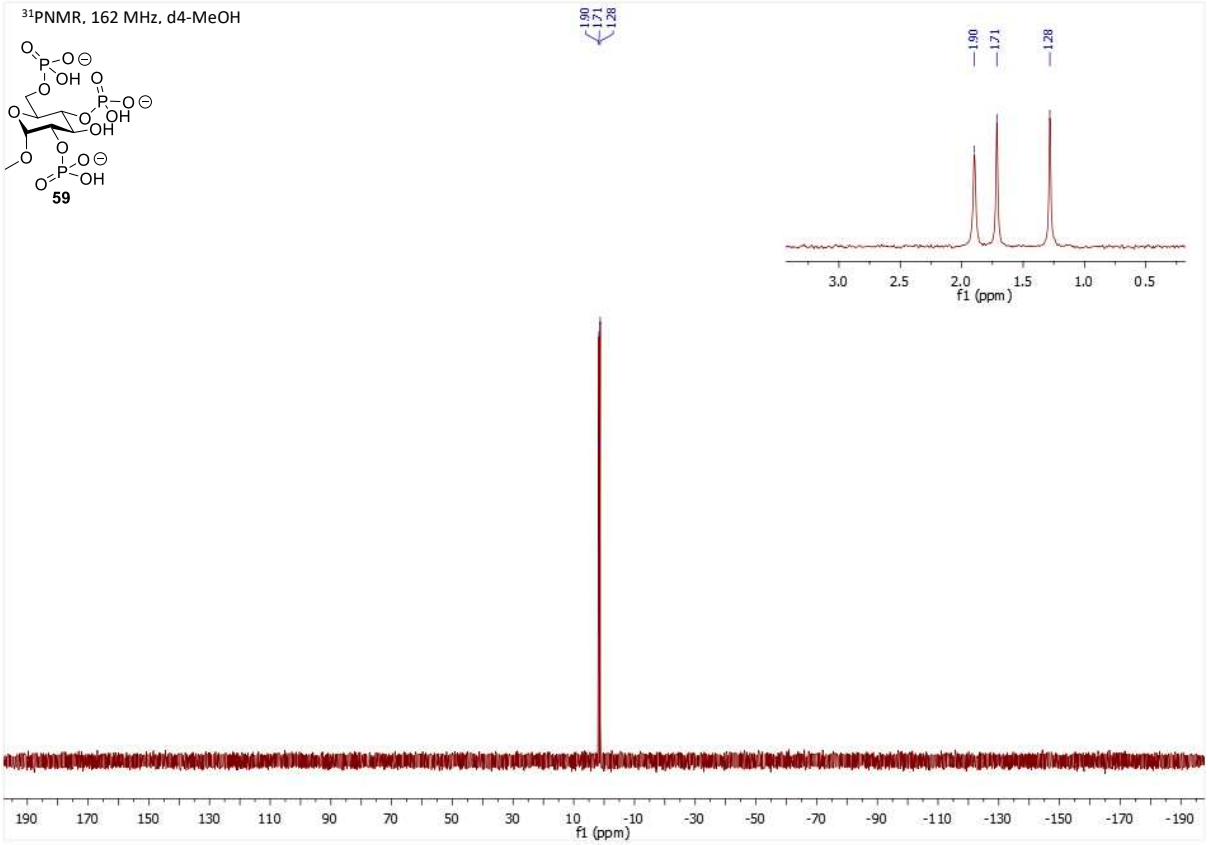

^{13}CNMR, 100 MHz, d4-MeOH

59

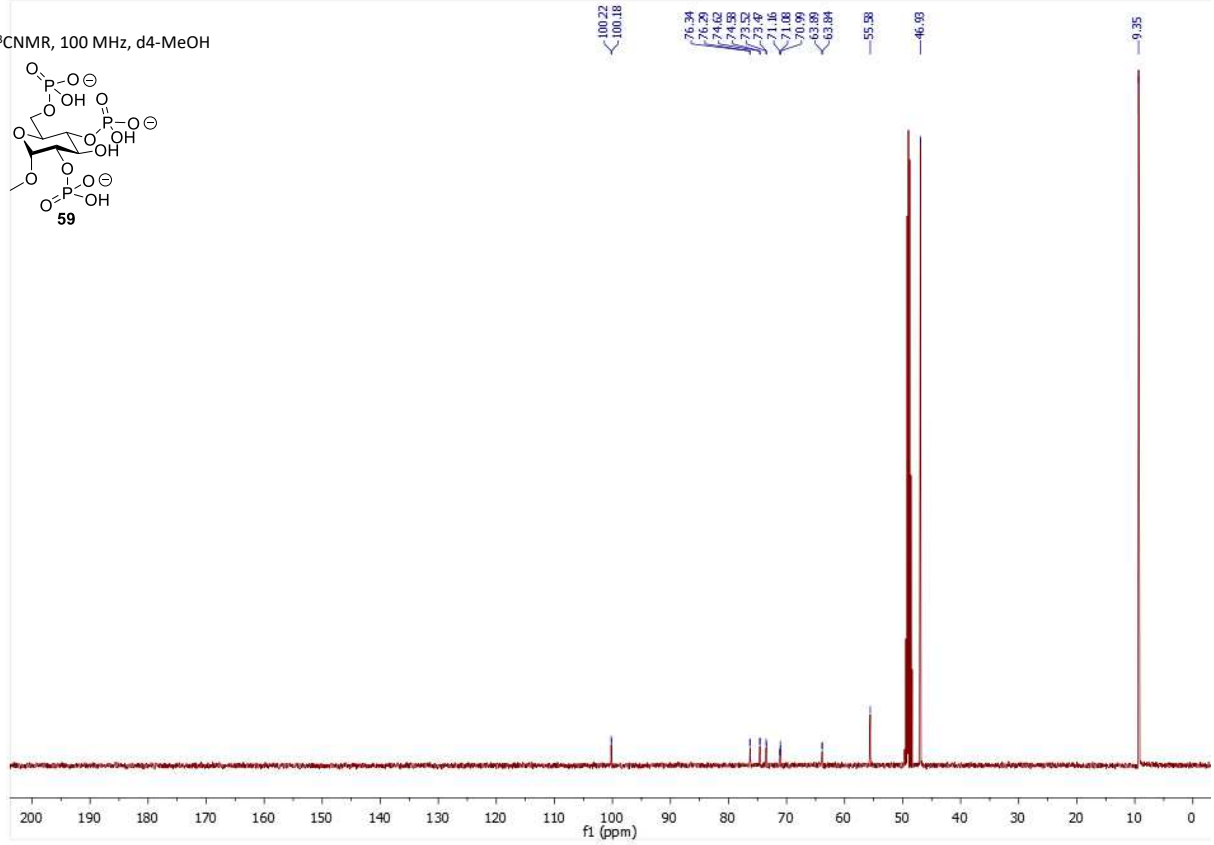

^{1}H-^{1}H COSY

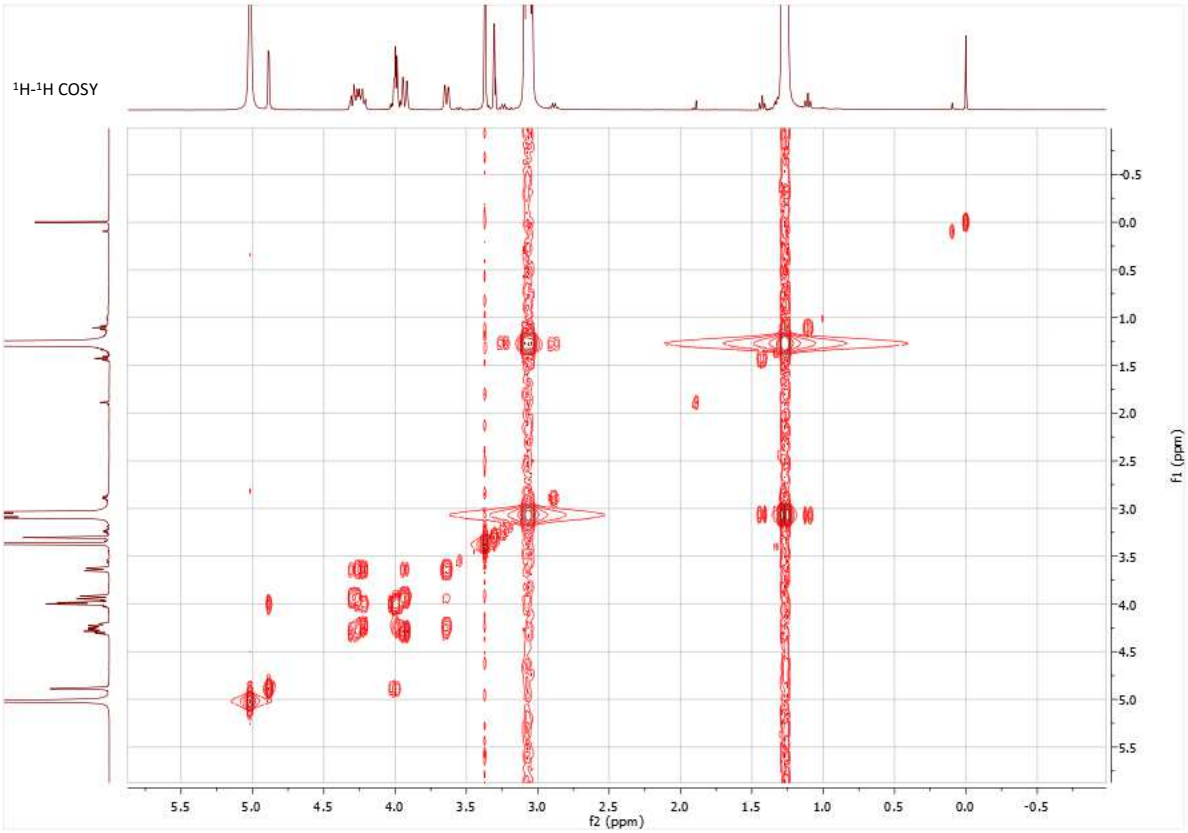

^{1}H-^{13}C HSQC

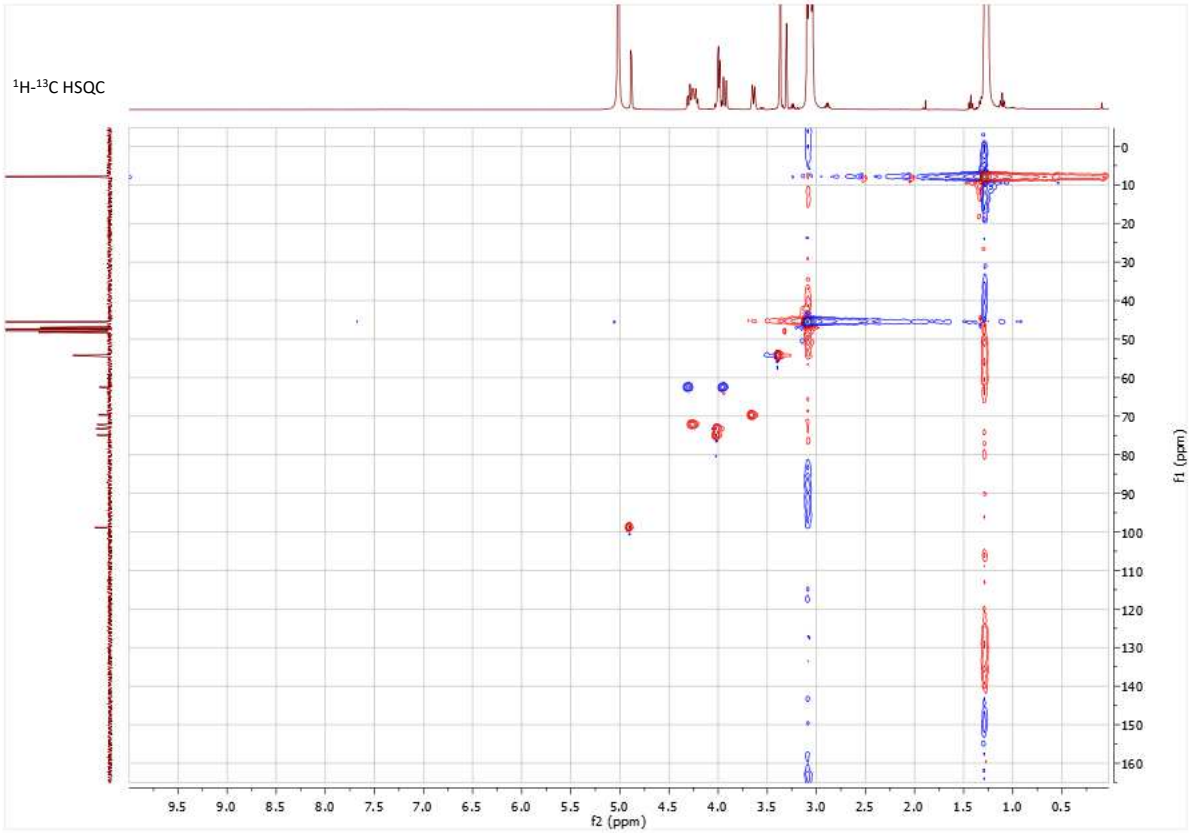

Methyl 4-*O*-benzyl-α-D-glucopyranoside (**64**)

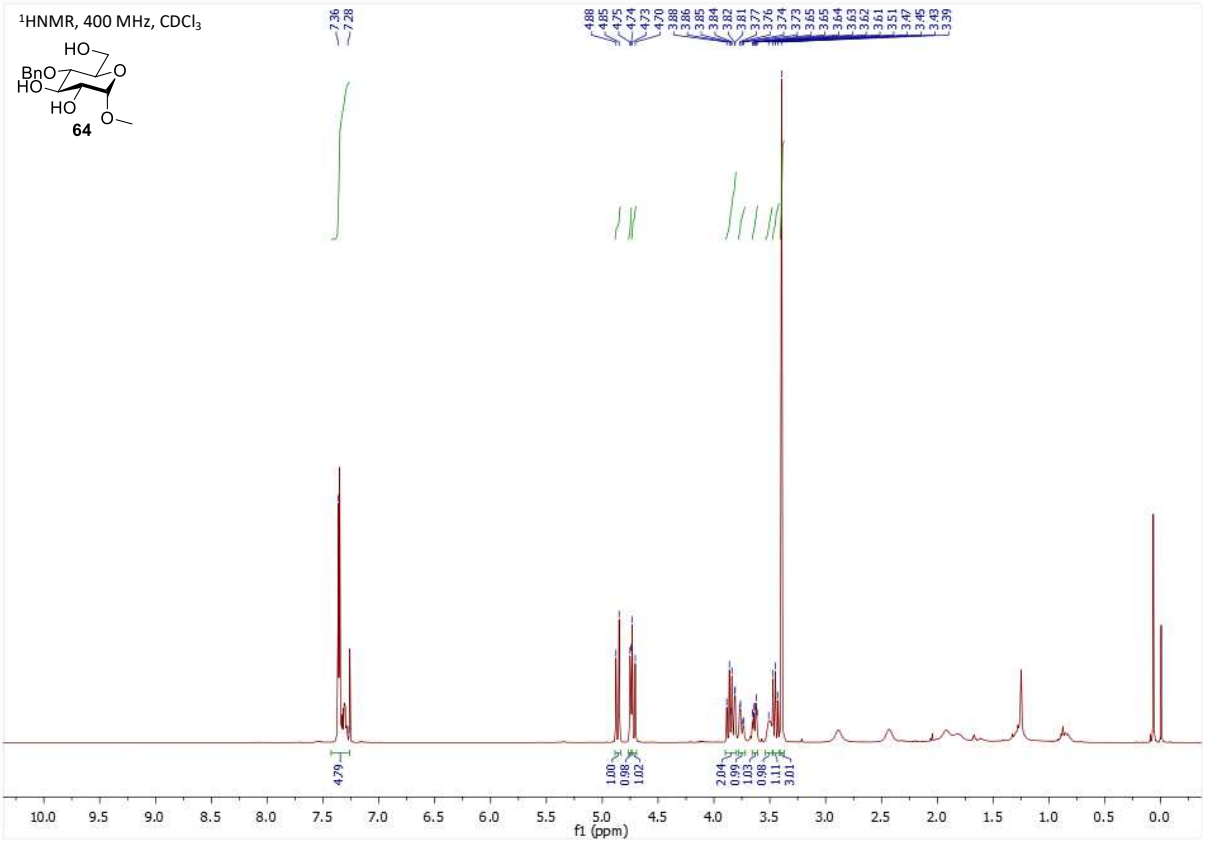

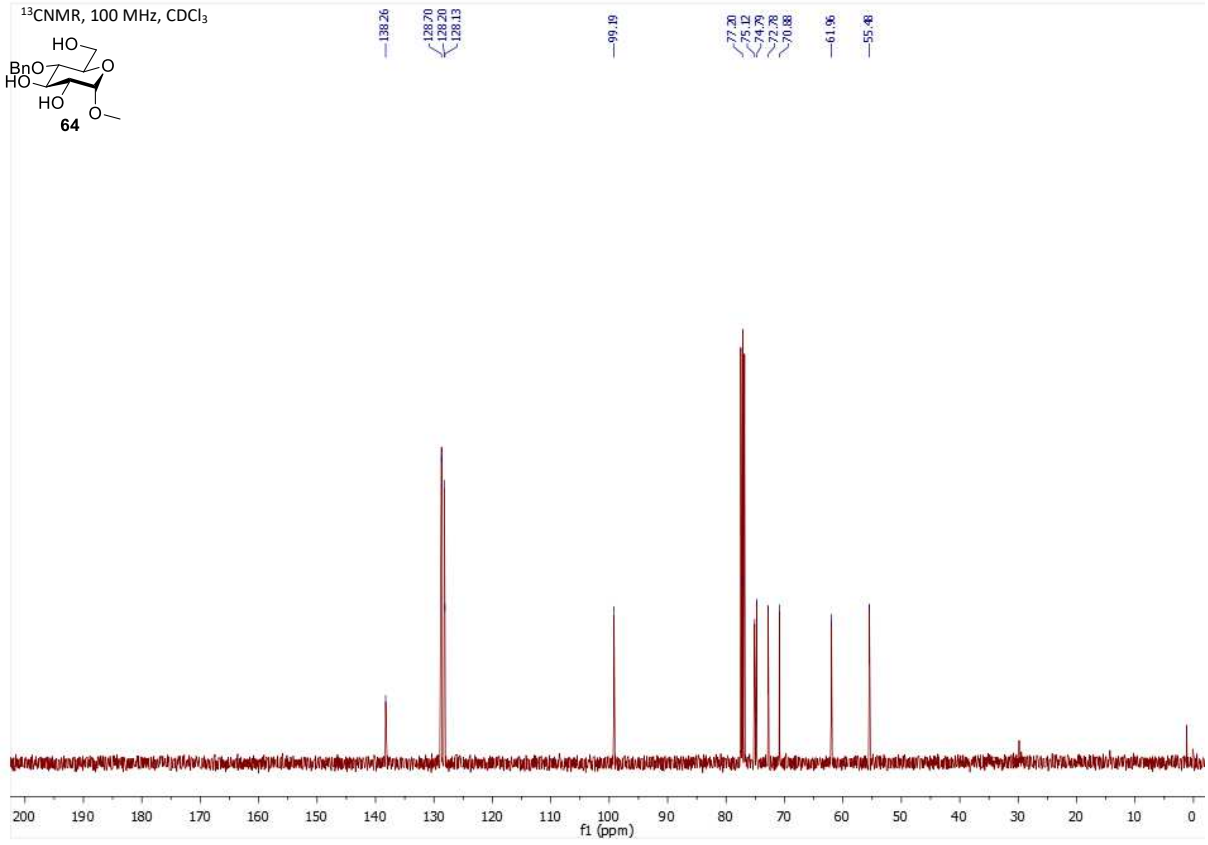

^{1}H-^{1}H COSY

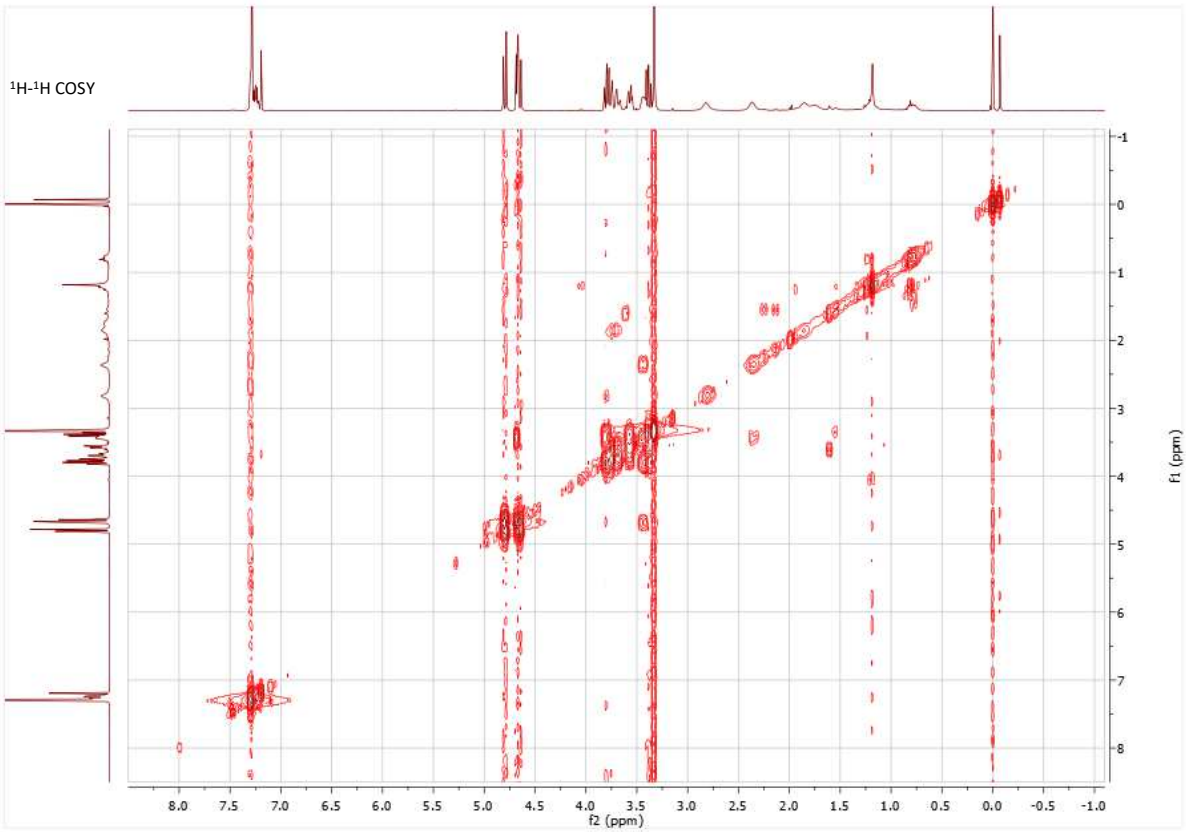

^{1}H-^{13}C HSQC

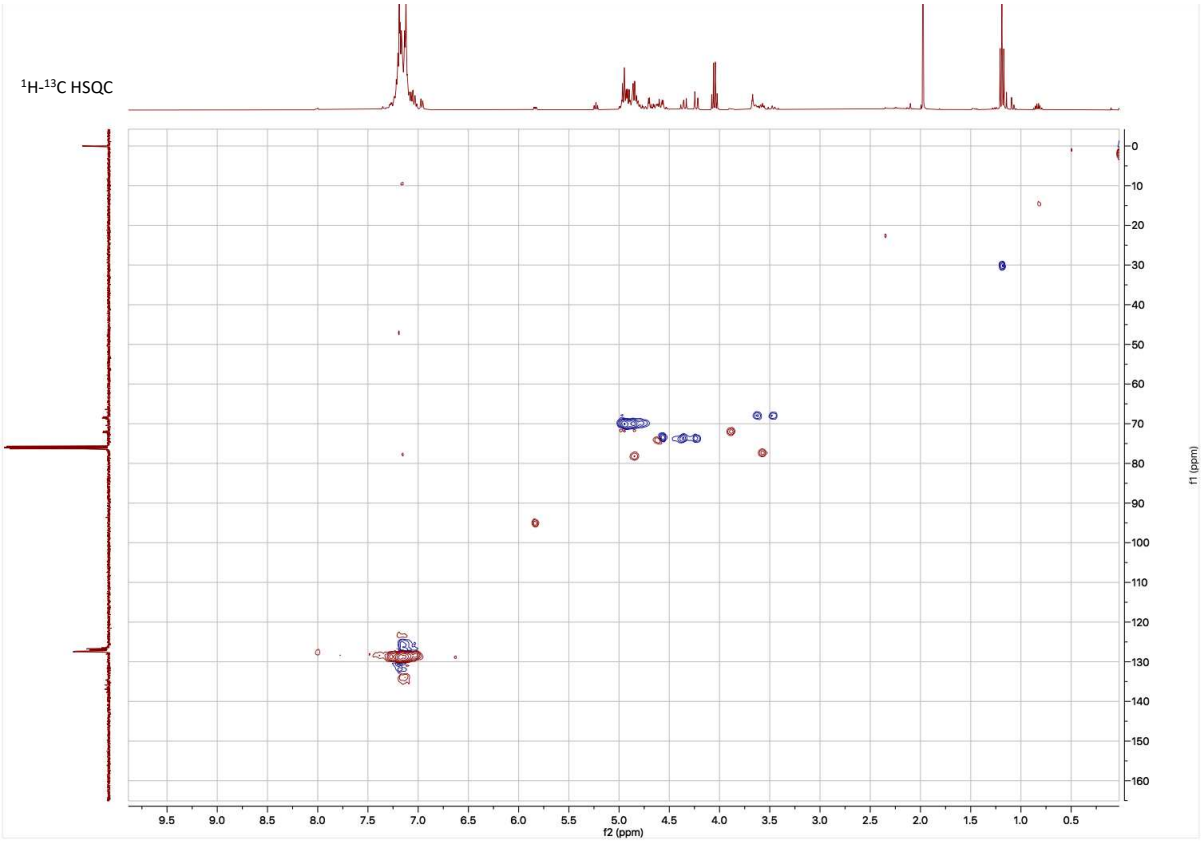

Methyl 4-*O*-benzyl-α-D-glucopyranoside 2,3,6-tris(dibenzyl phosphate) (**65**)

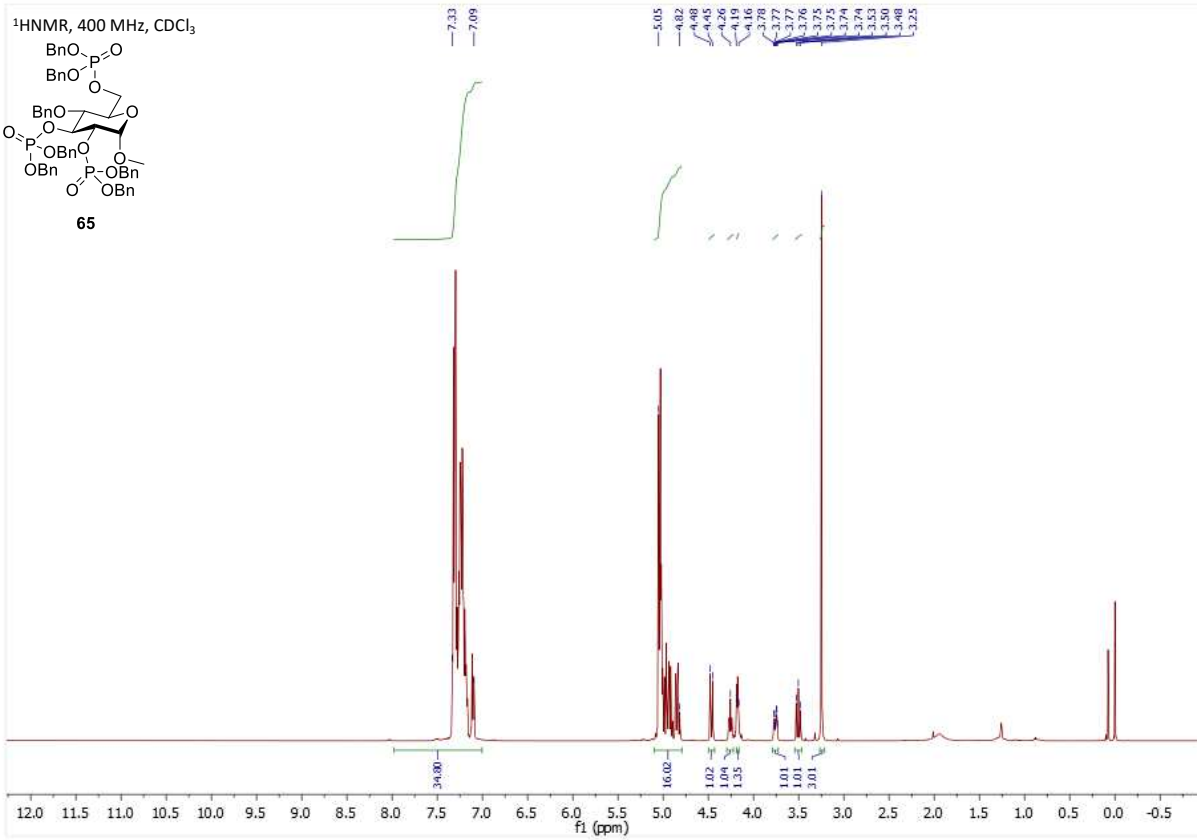

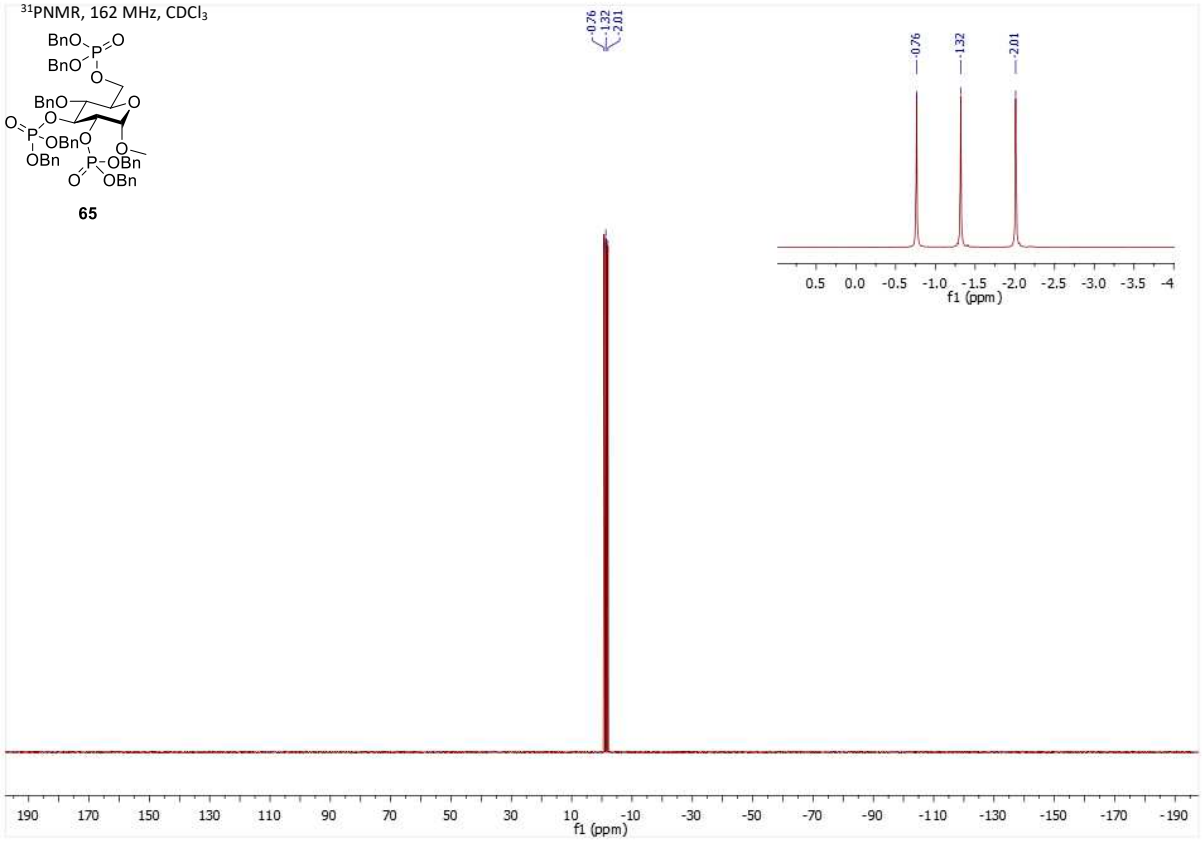

^{13}CNMR, 100 MHz, $CDCl_3$

65

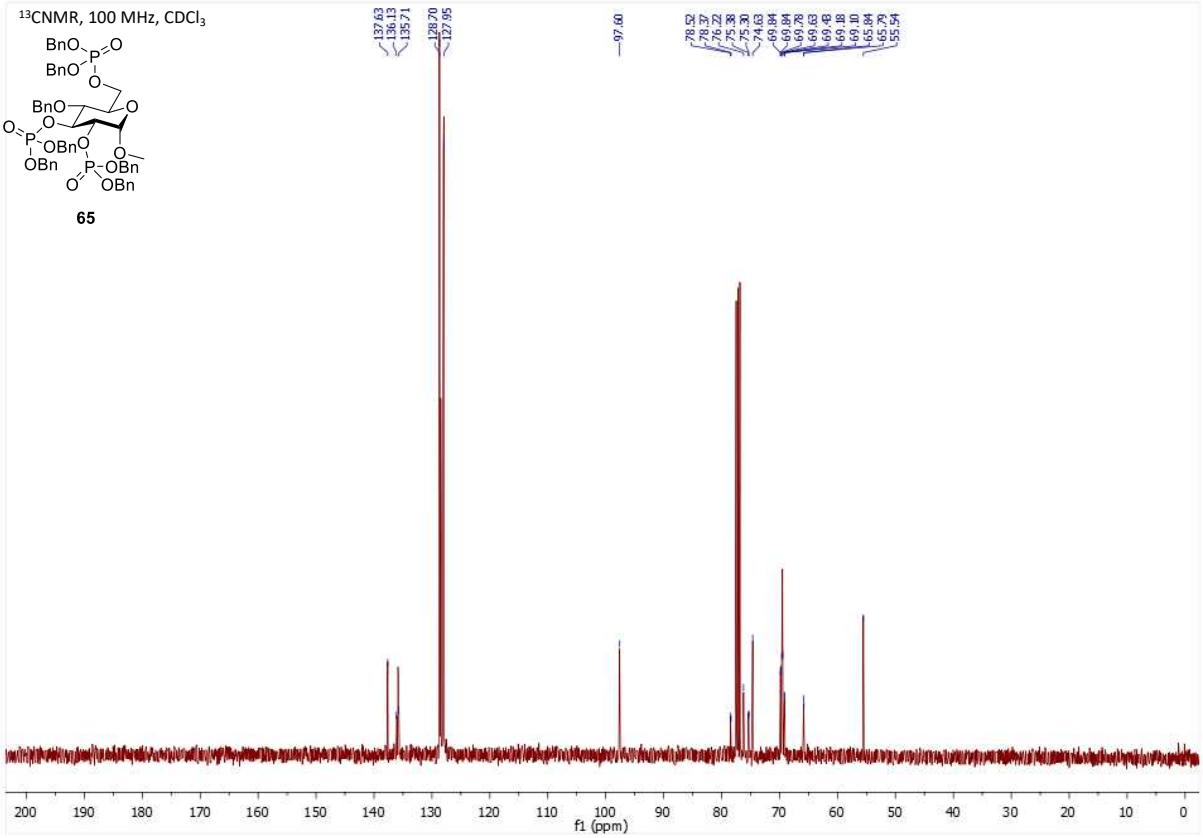

^{1}H-^{1}H COSY

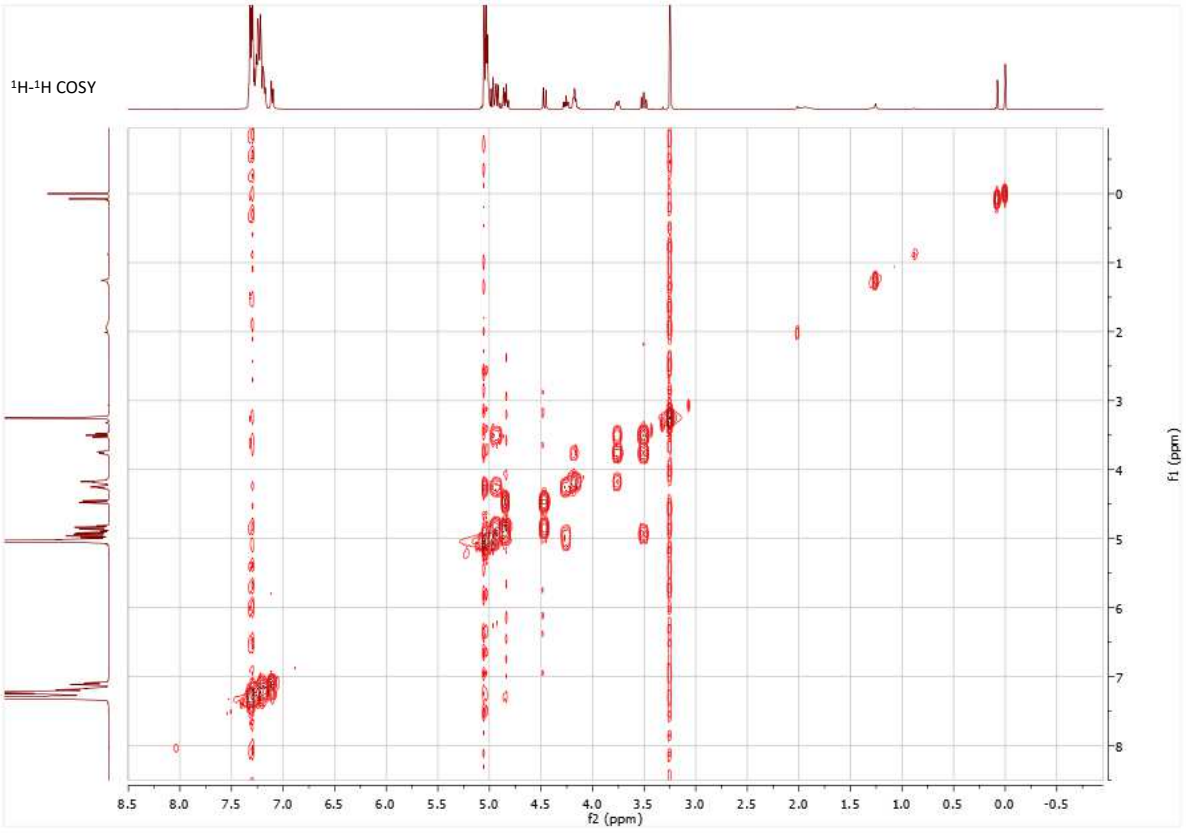

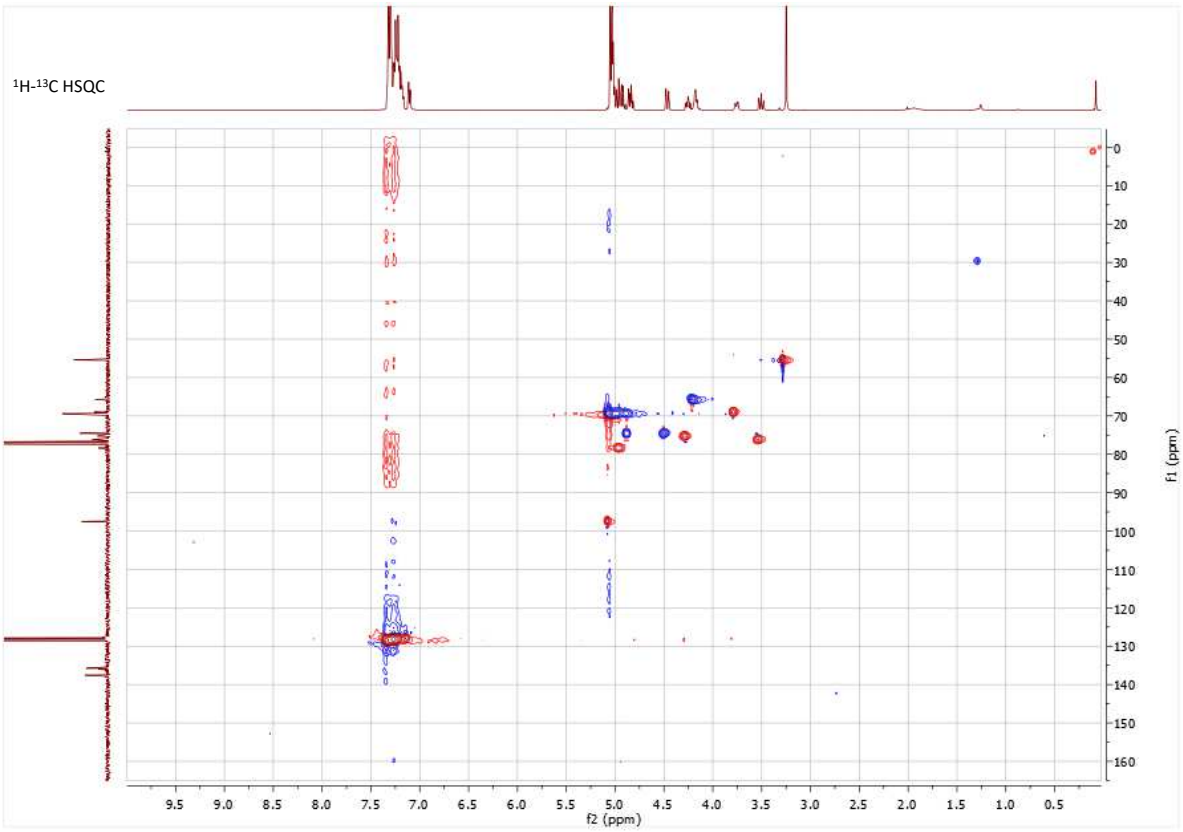

Methyl α-D-glucopyranoside 2,3,6-trisphosphate triethylammonium salt (**60**)

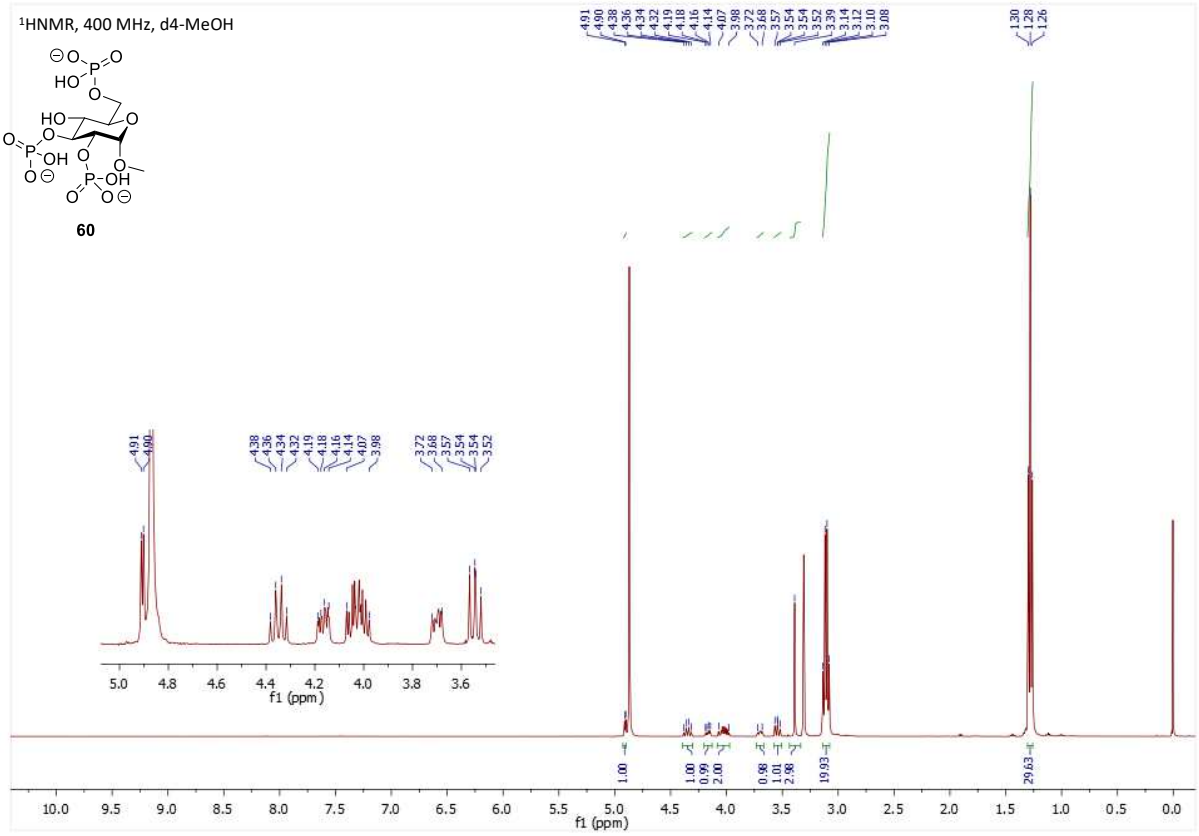

^{31}PNMR, 162 MHz, d4-MeOH

60

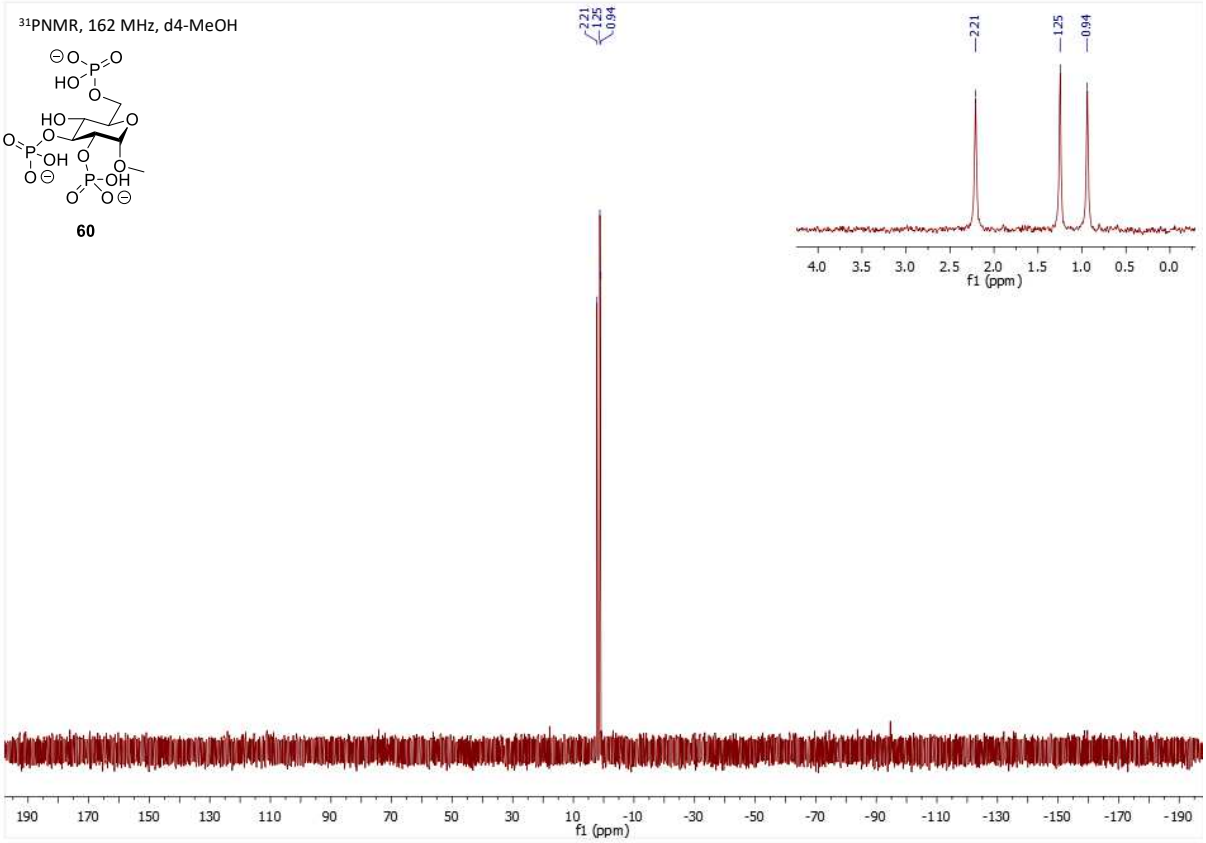

^{13}CNMR, 100 MHz, d4-MeOH

60

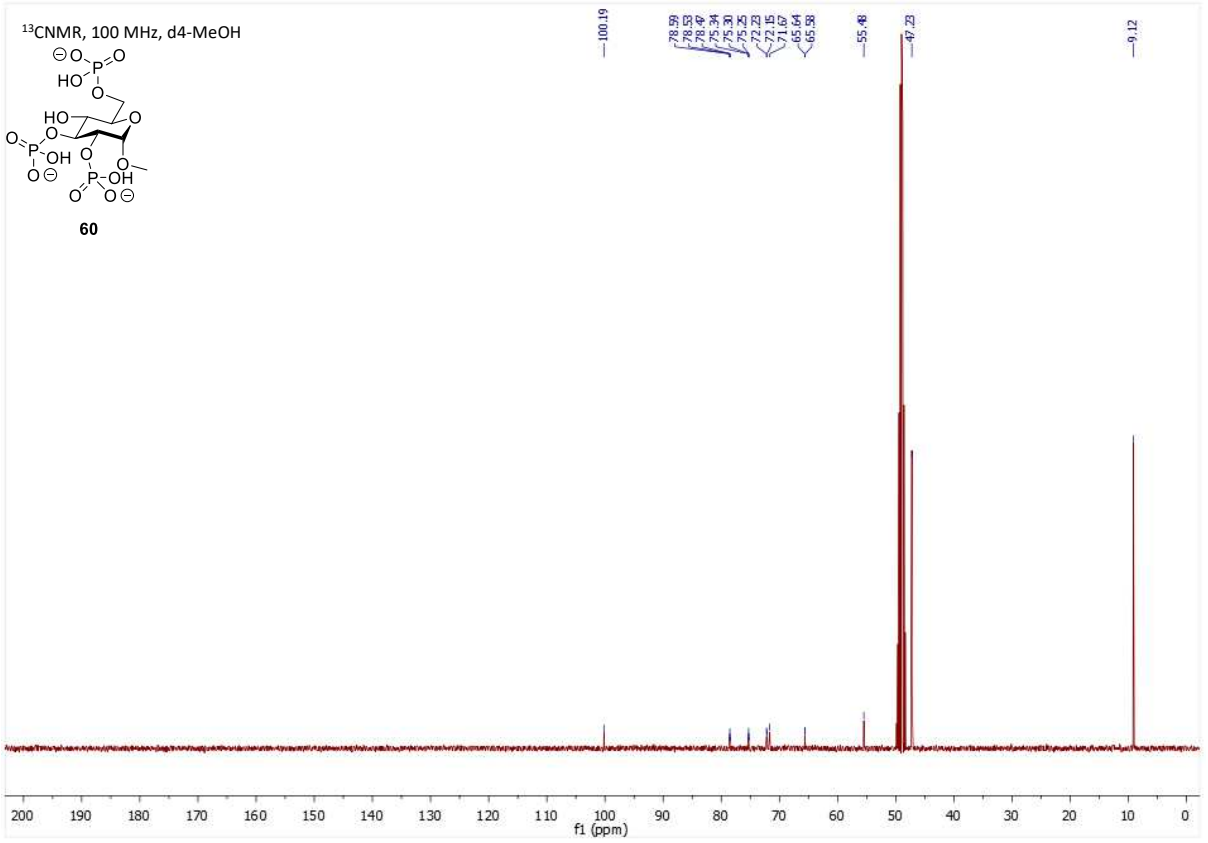

^{1}H-^{1}H COSY

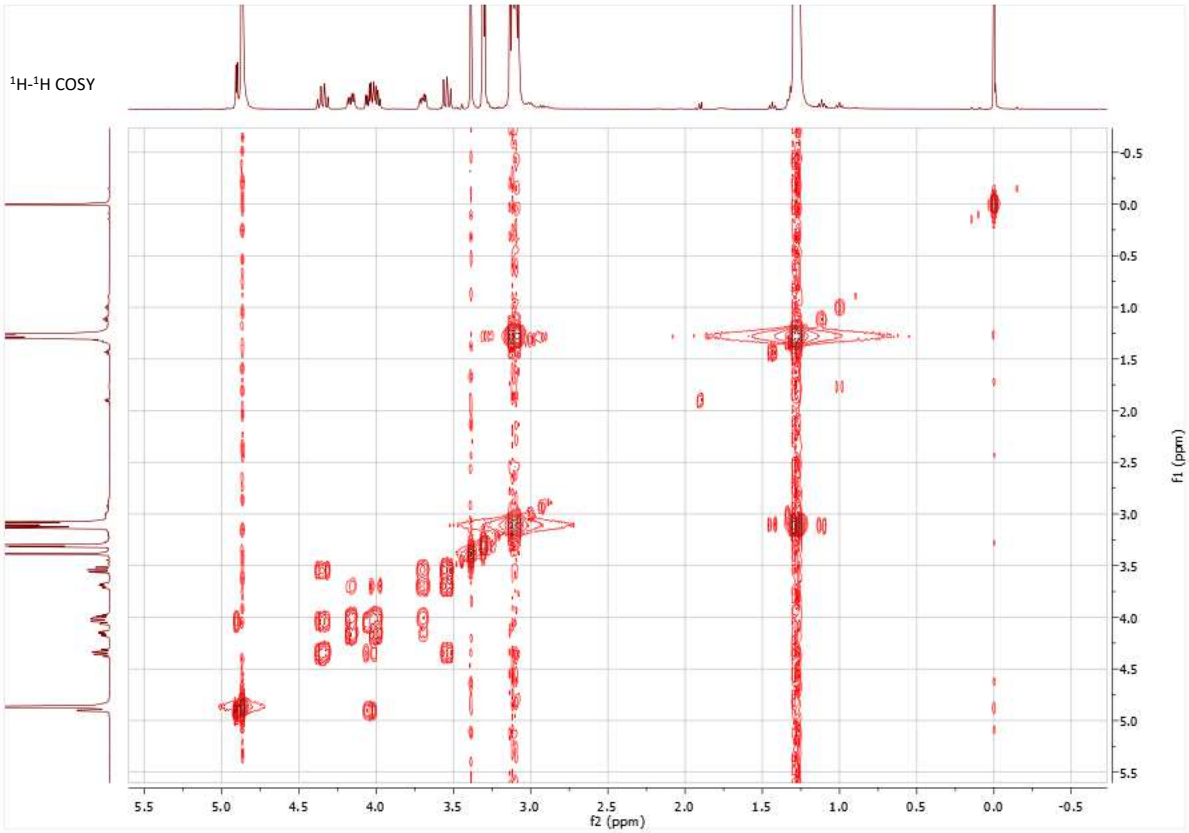

^{1}H-^{13}C HSQC

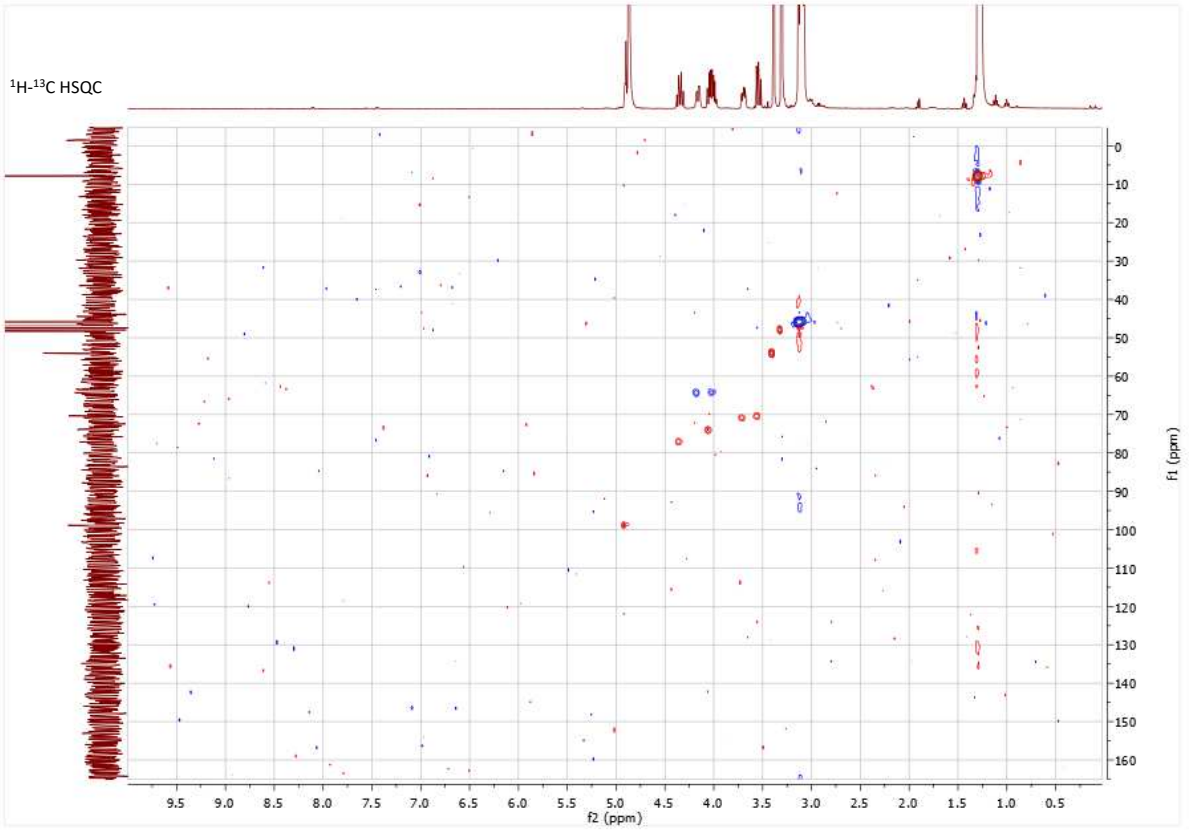

Methyl 4-*O*-benzyl-α-L-glucopyranoside (**69**)

^{1}HNMR, 400 MHz, $CDCl_3$

69

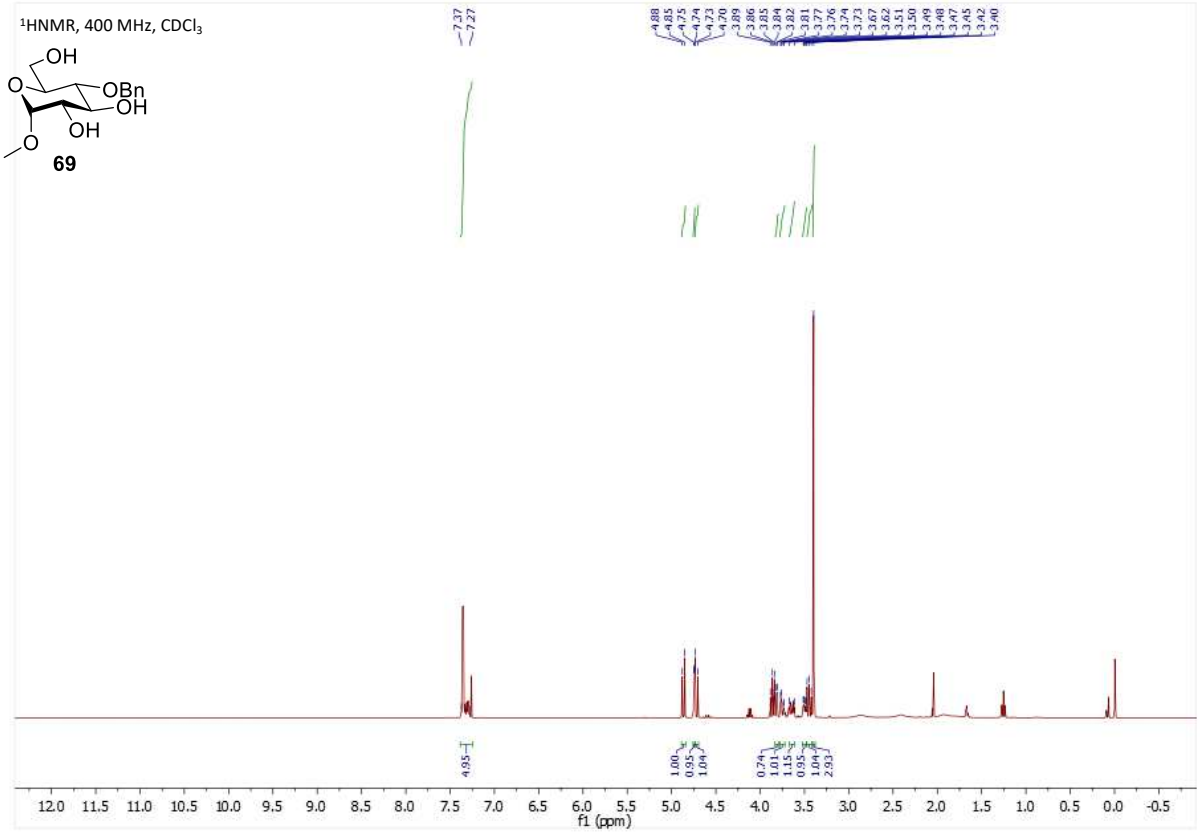

^{13}CNMR, 100 MHz, $CDCl_3$

69

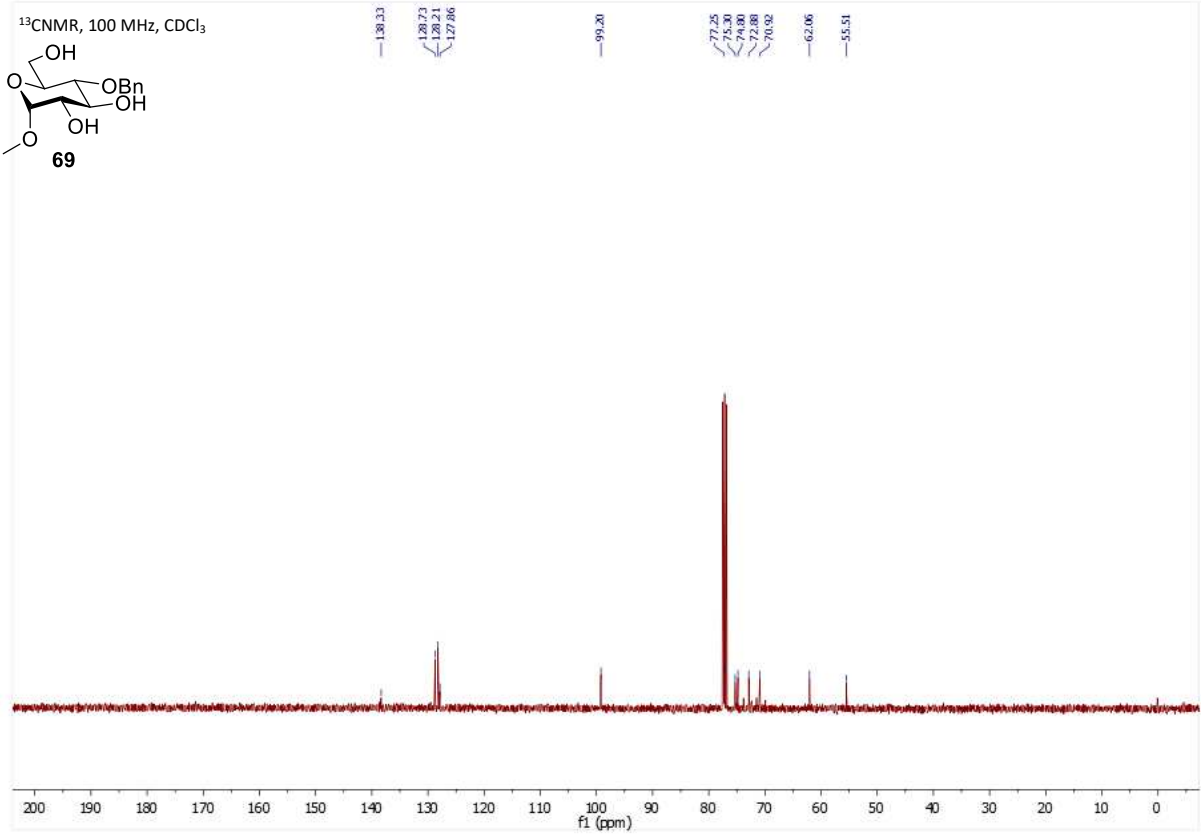

Methyl 4-*O*-benzyl-α-L-glucopyranoside 2,3,6-tris(dibenzylphosphate) (**70**)

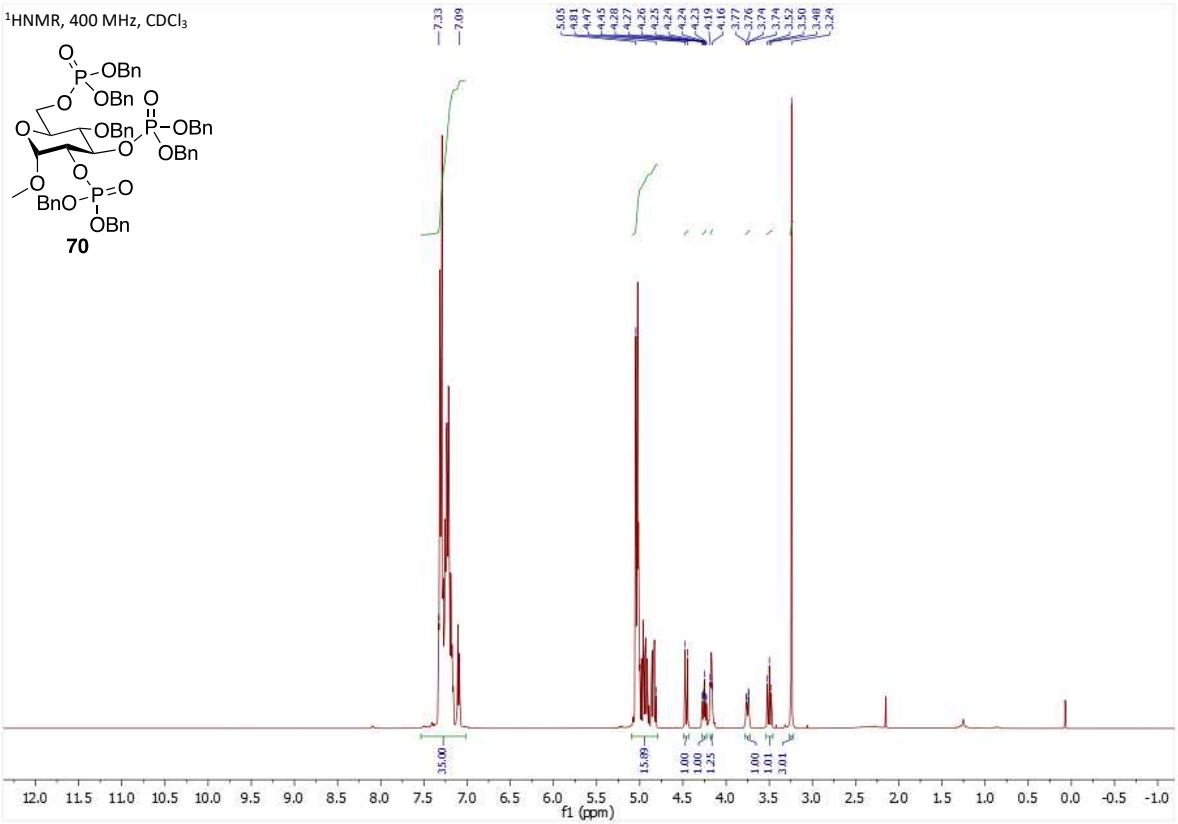

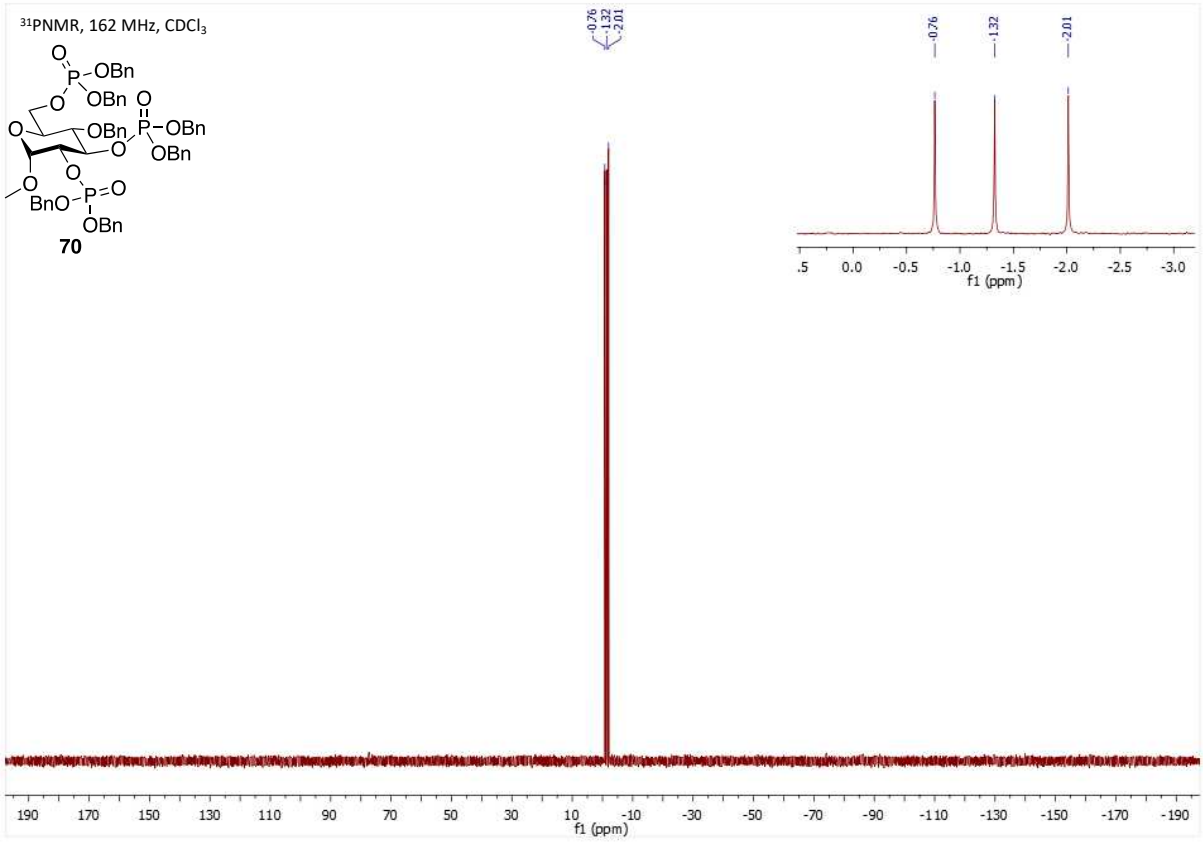

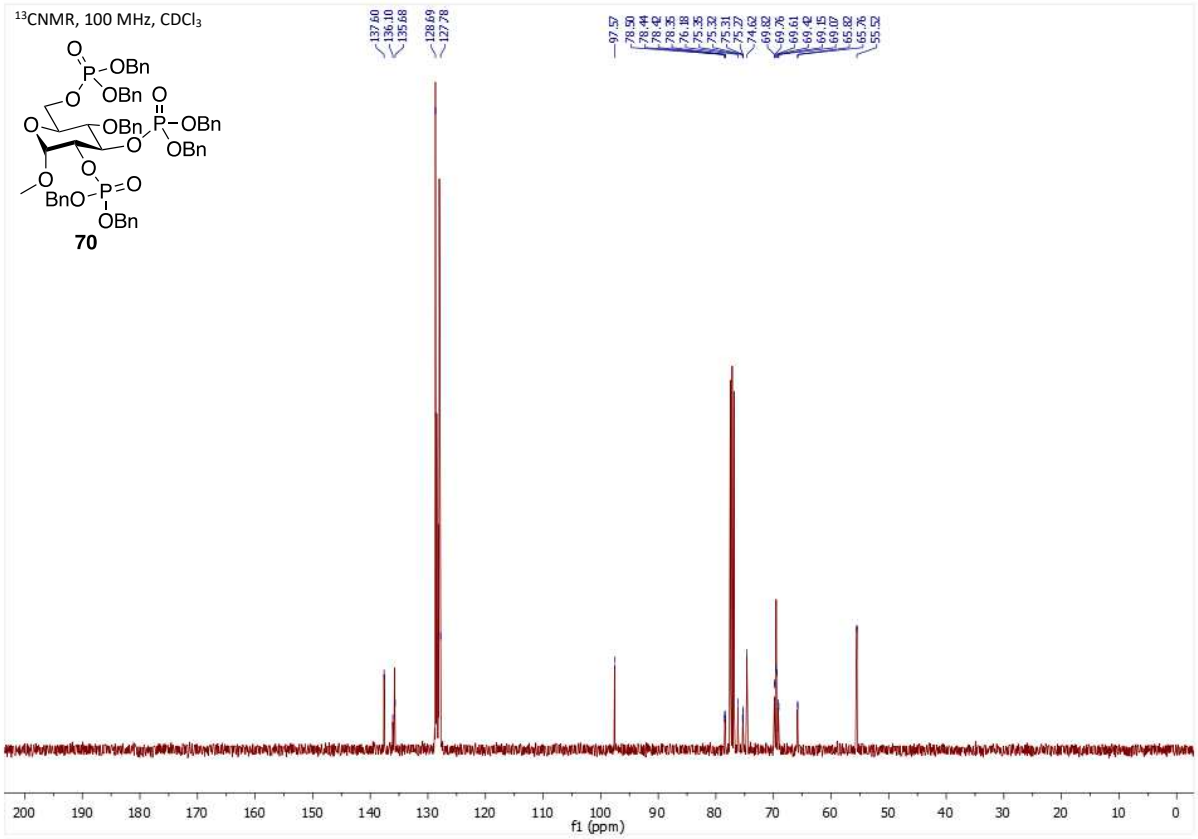

Methyl α-L-glucopyranoside 2,3,6-trisphosphate triethylammonium salt (**58**)

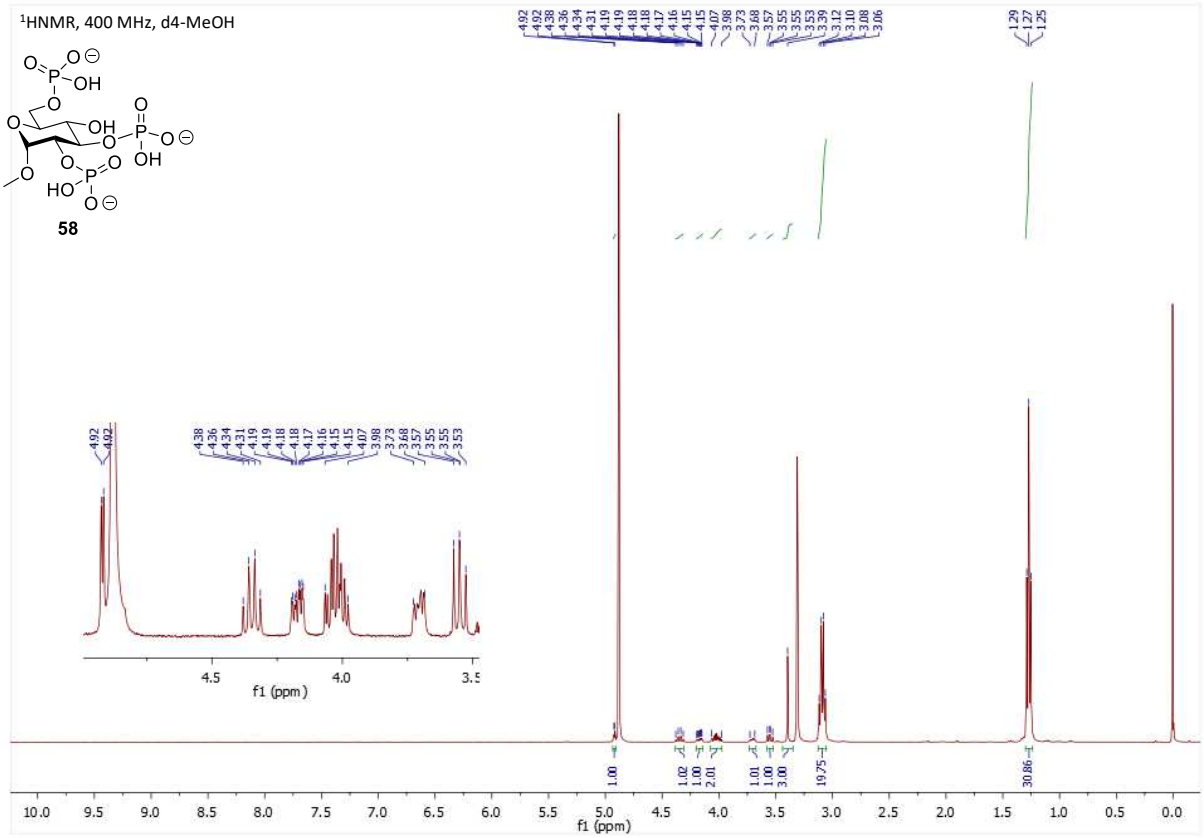

^{31}PNMR, 162 MHz, d4-MeOH

58

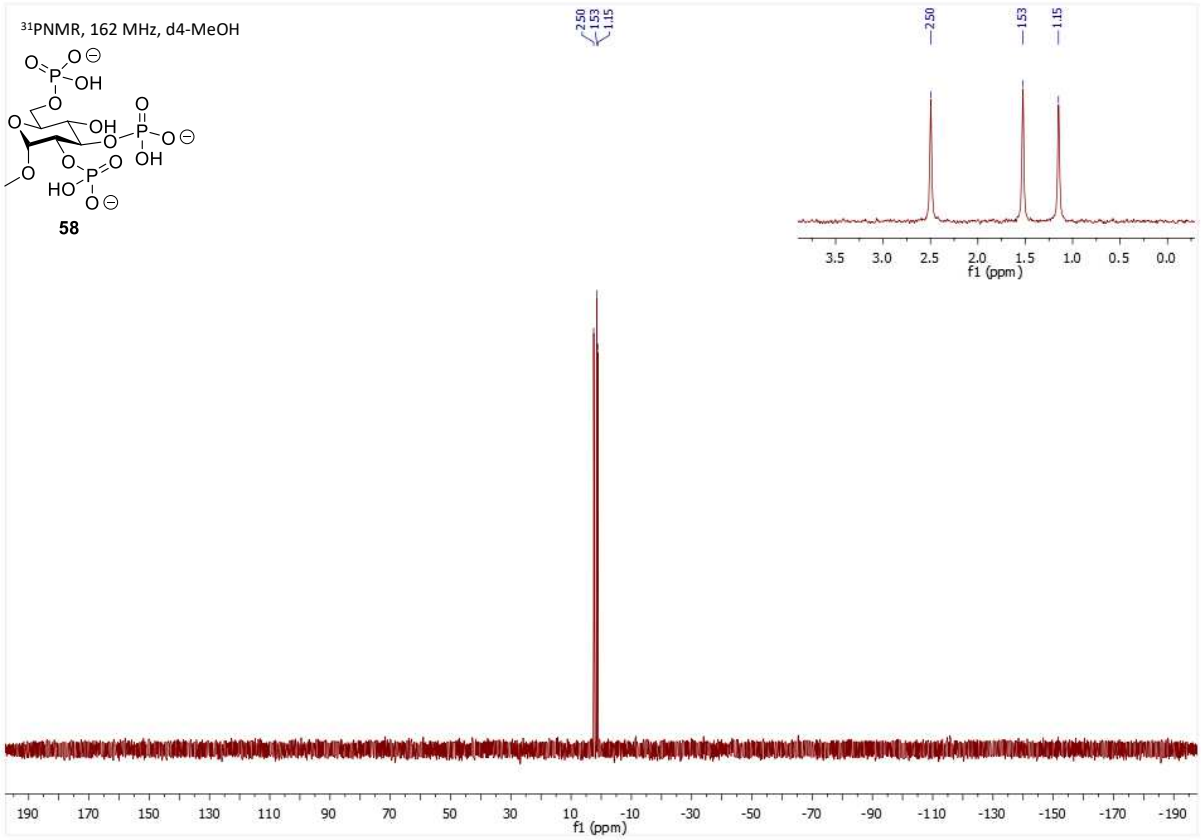

^{13}CNMR, 100 MHz, d4-MeOH

58

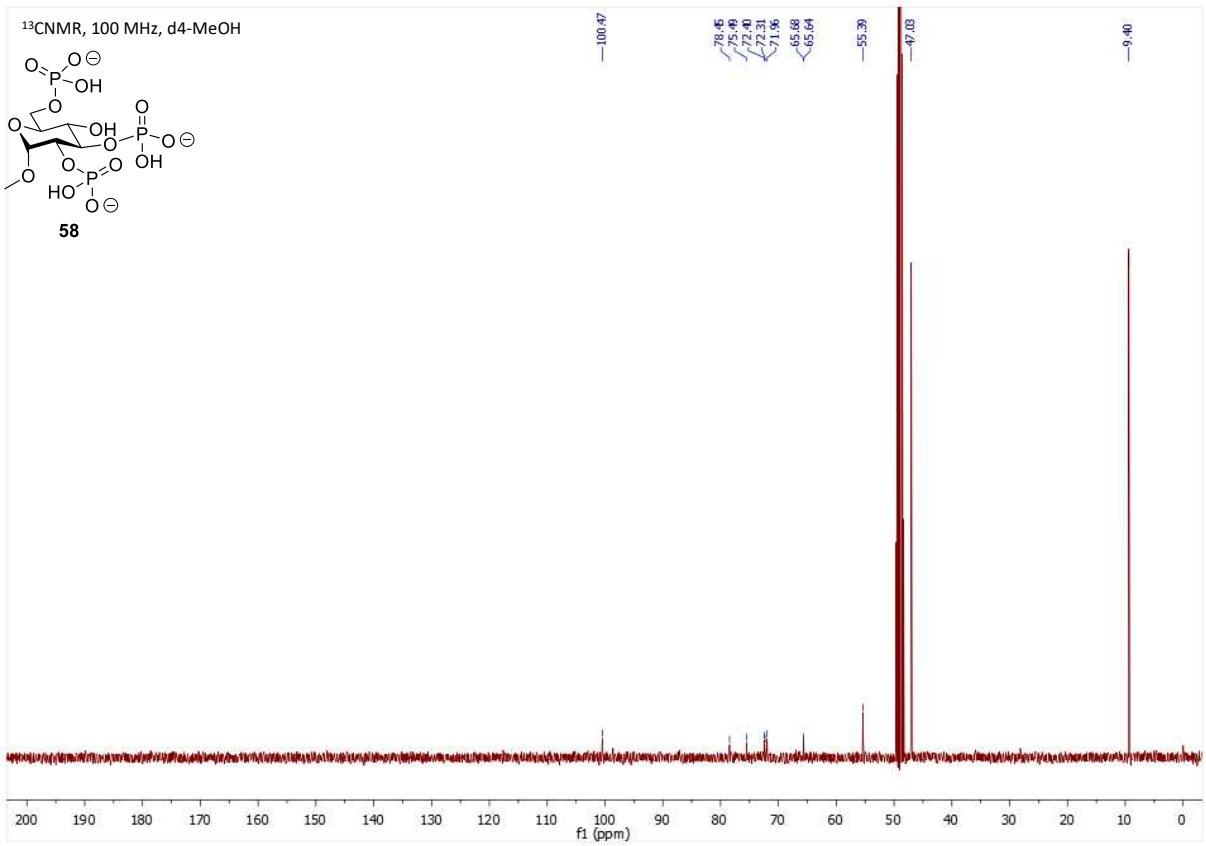

^{1}H-^{1}H COSY

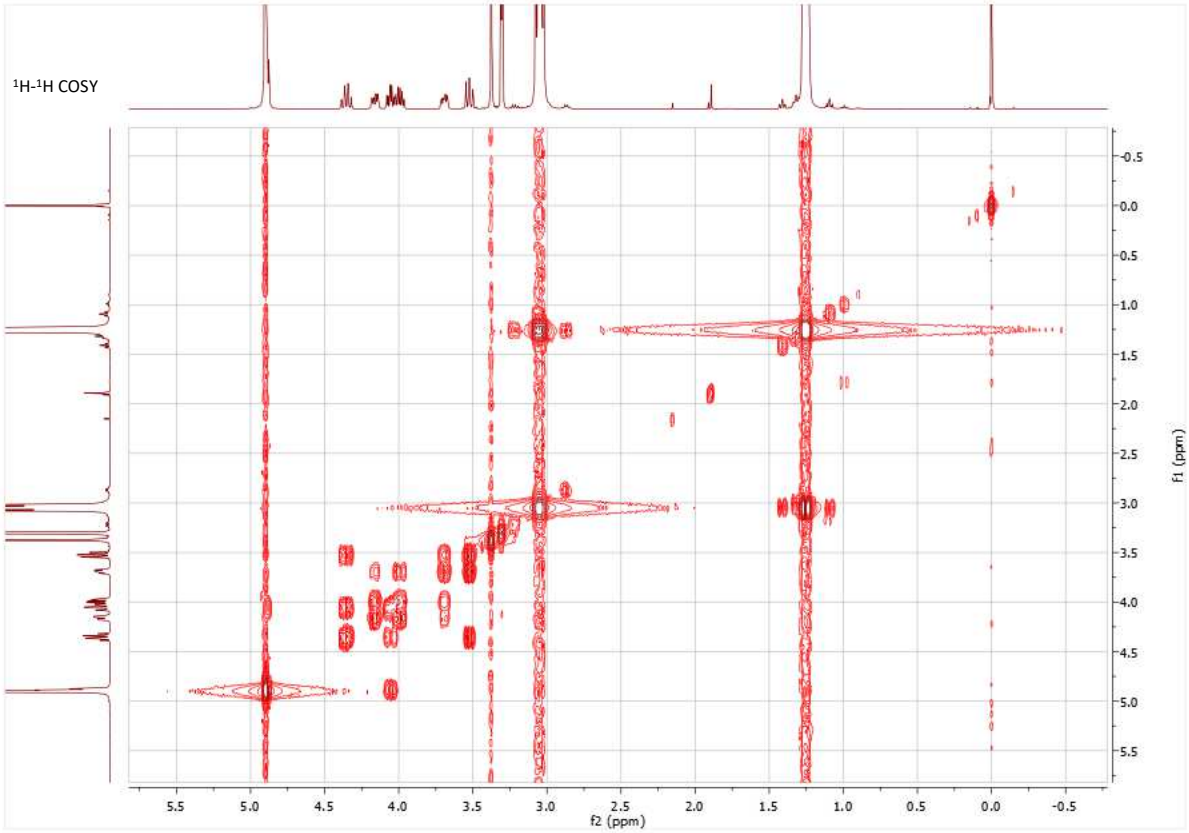

^{1}H-^{13}C HSQC

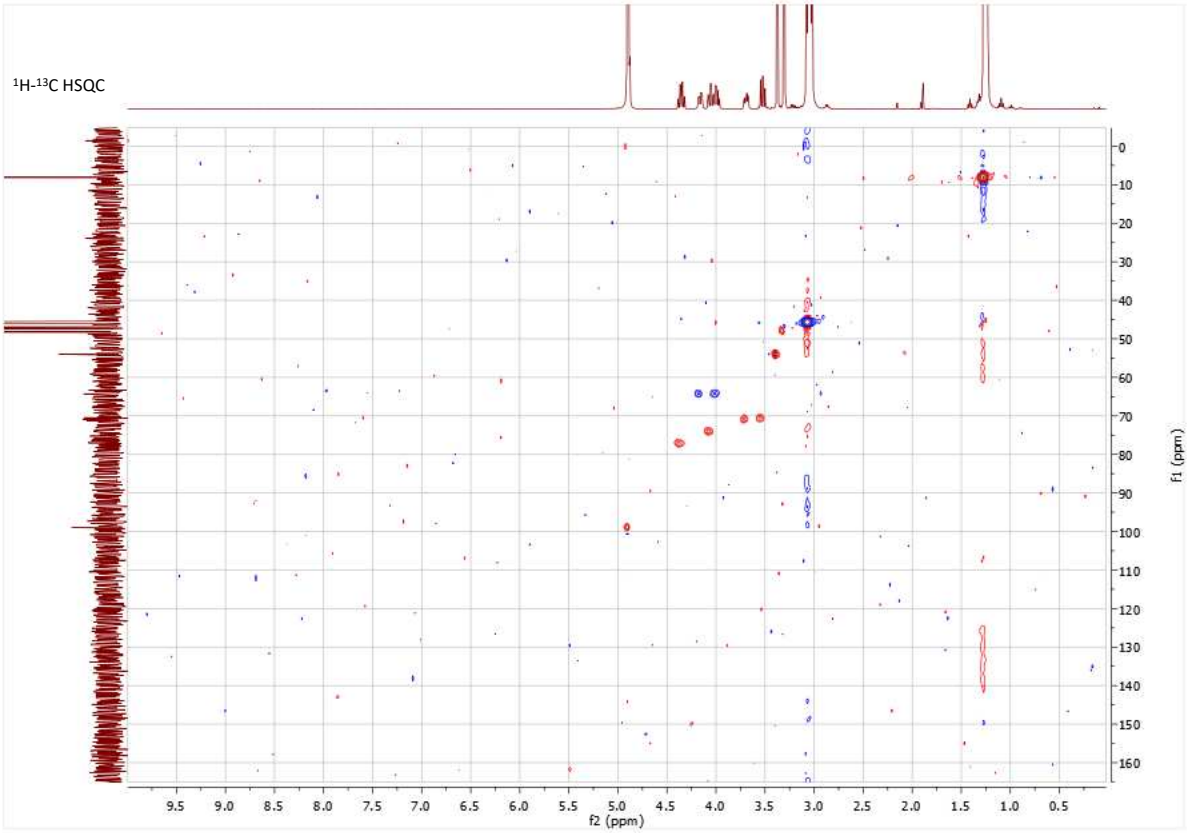

2,6-di-*O*-benzyl-α-D-glucopyranosyl 1,3,4-tris(dibenzylphosphate) (**75**)

^{1}HNMR, 400 MHz, $CDCl_3$

75

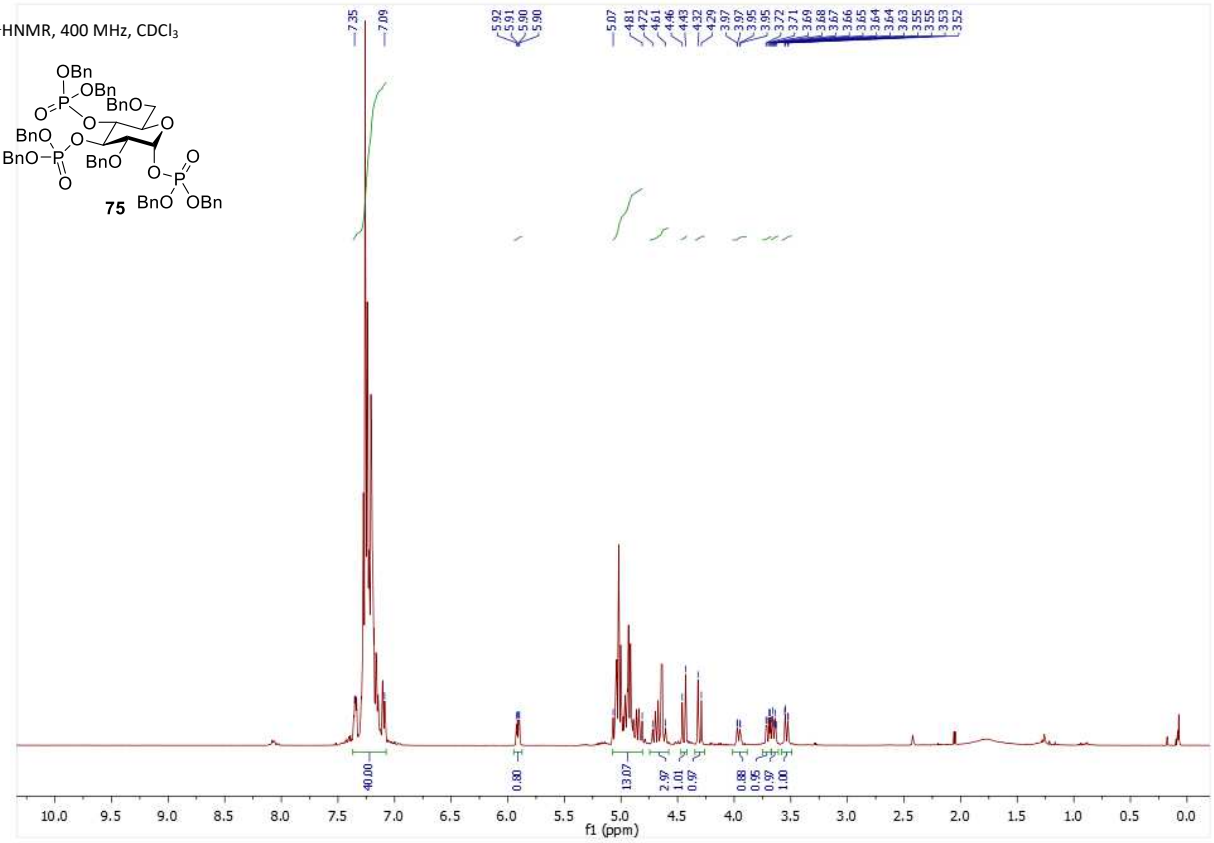

^{31}PNMR, 162 MHz, $CDCl_3$

75

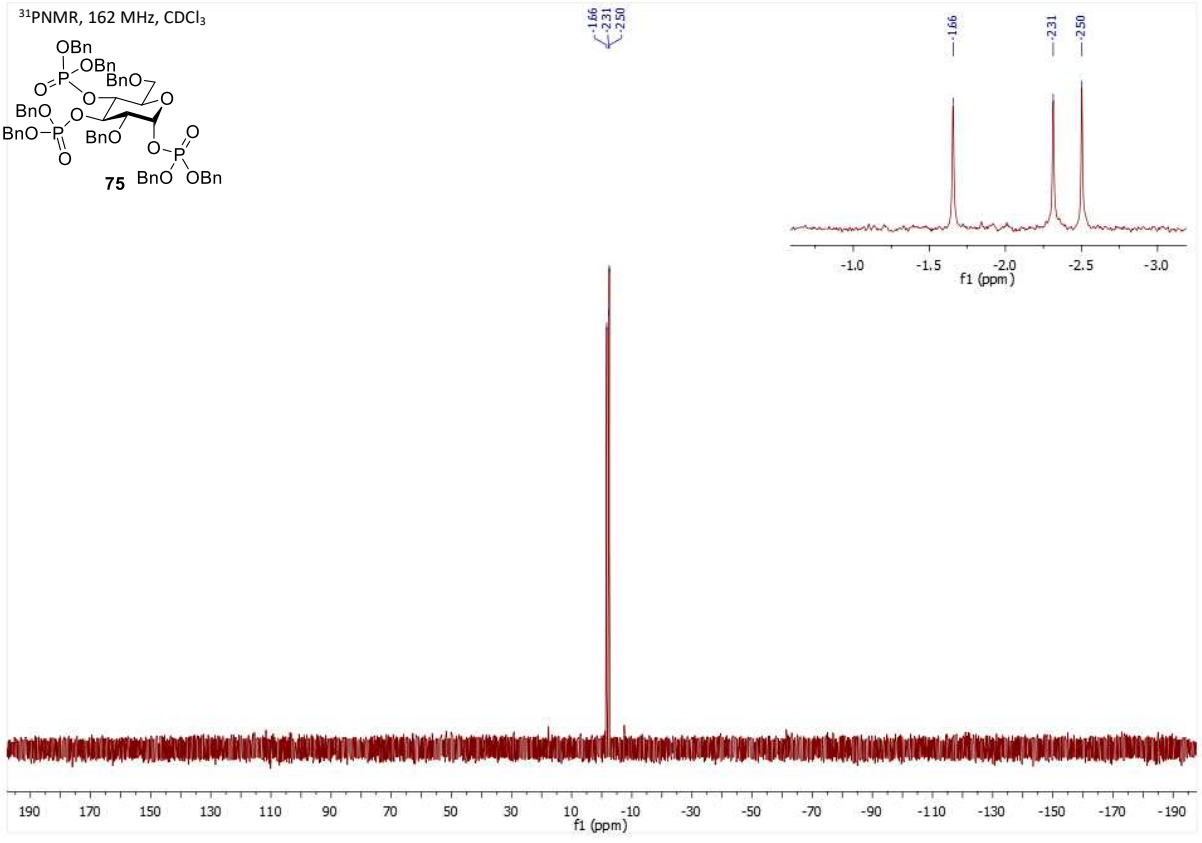

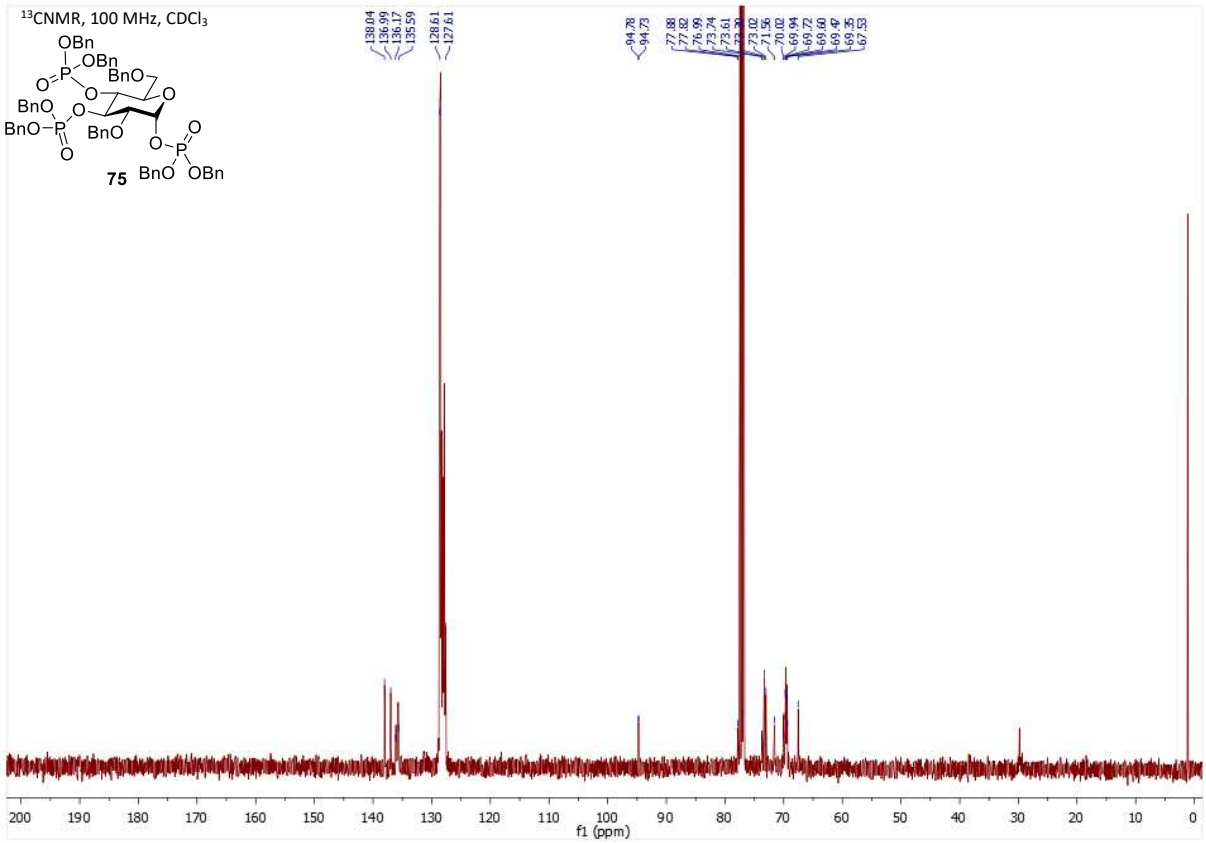
^{13}CNMR, 100 MHz, $CDCl_3$
75
138.04
136.99
136.17
135.59
128.61
127.61
94.78
94.73
77.88
77.82
76.99
73.74
73.61
73.30
73.02
71.96
70.02
69.94
69.72
69.60
69.47
69.35
67.53
f1 (ppm)

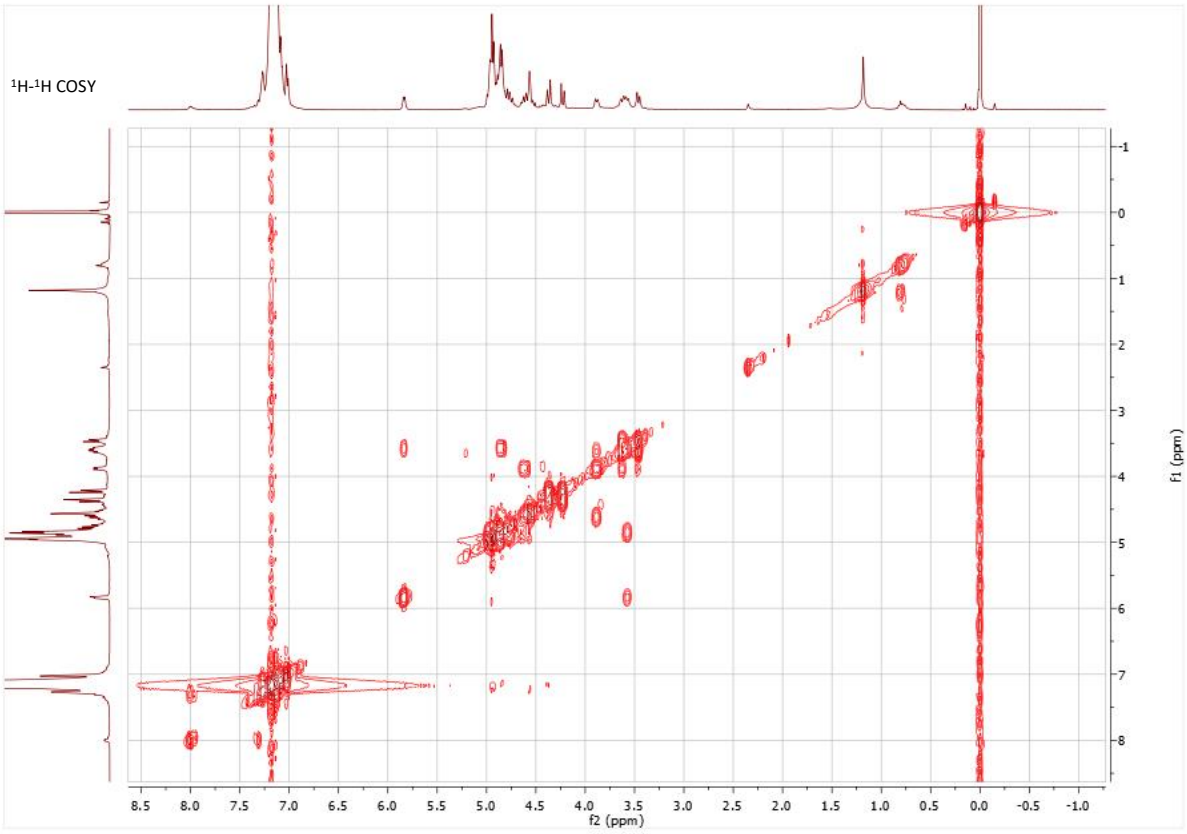
^{1}H-^{1}H COSY
f2 (ppm)
f1 (ppm)

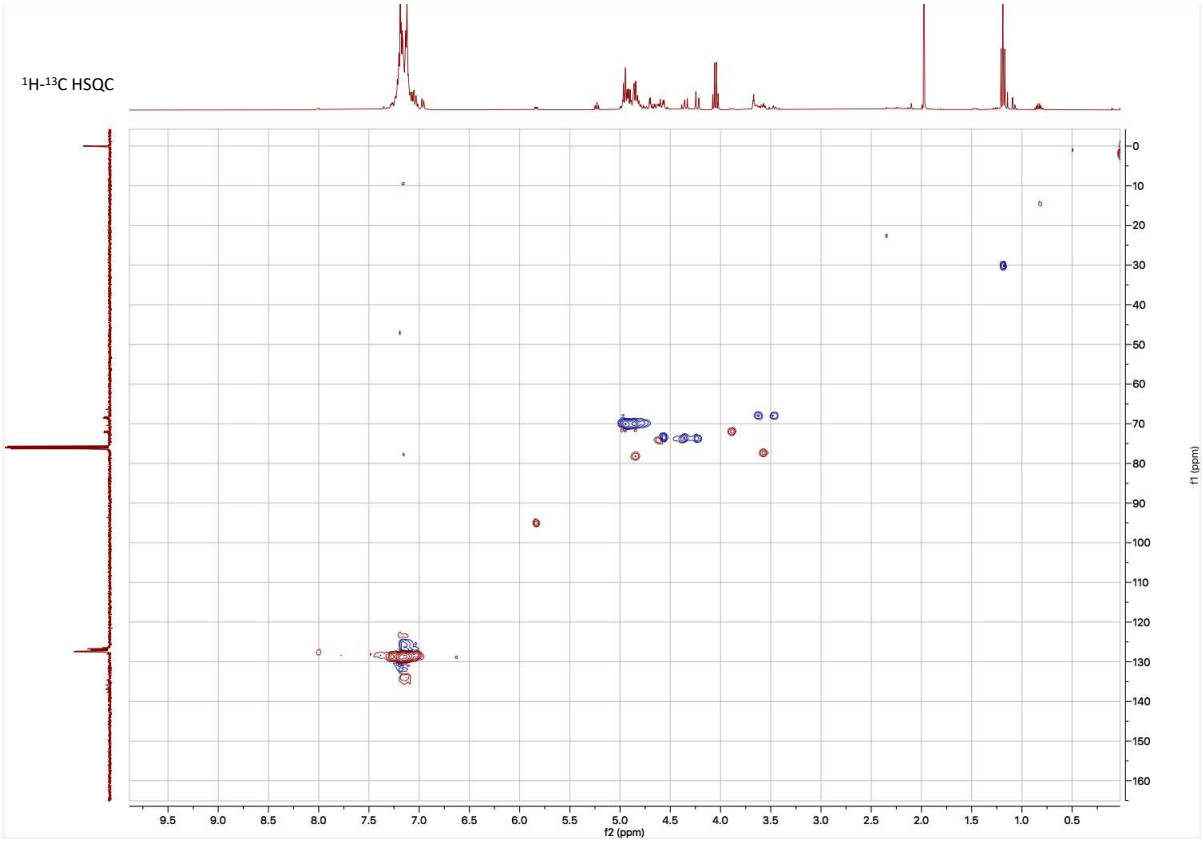

2,6-Di-*O*-benzyl-β-D-glucopyranosyl 1,3,4-tris(dibenzylphosphate) (**76**)

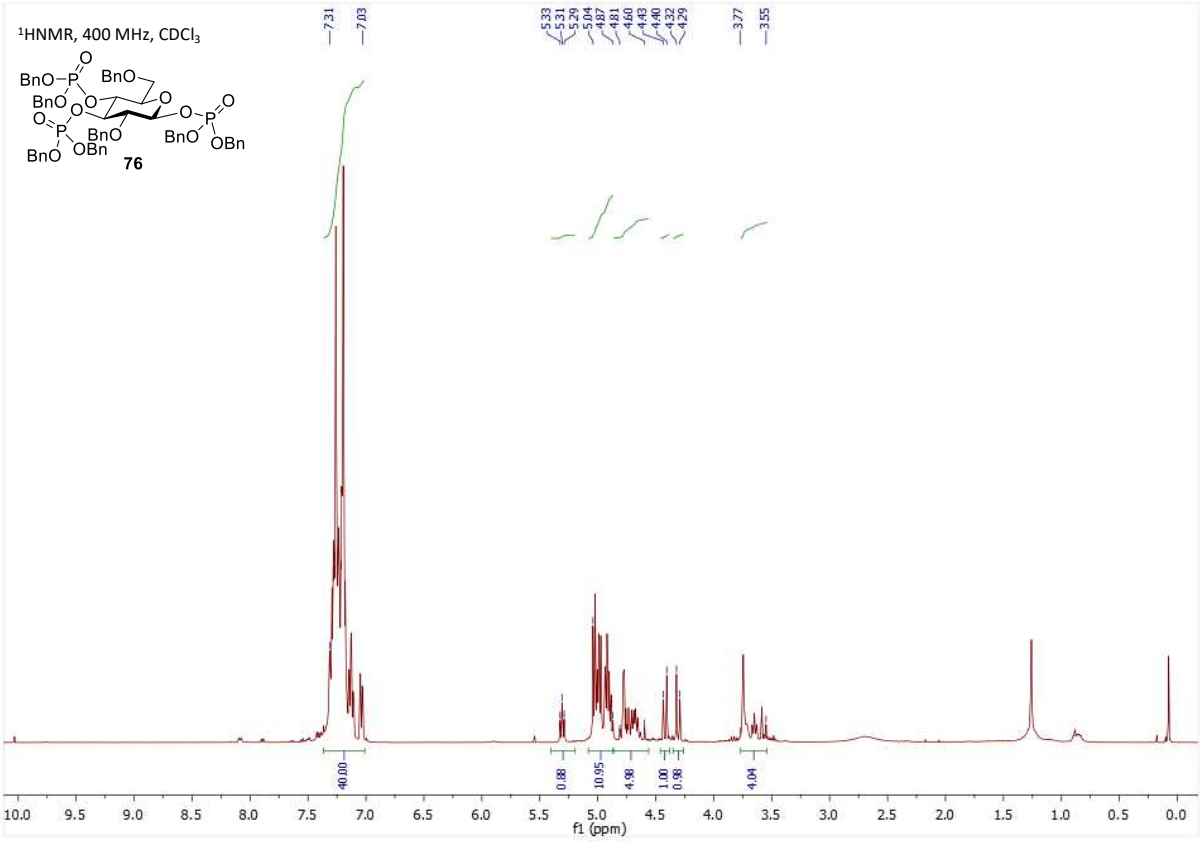

^{31}PNMR, 162 MHz, $CDCl_3$

76

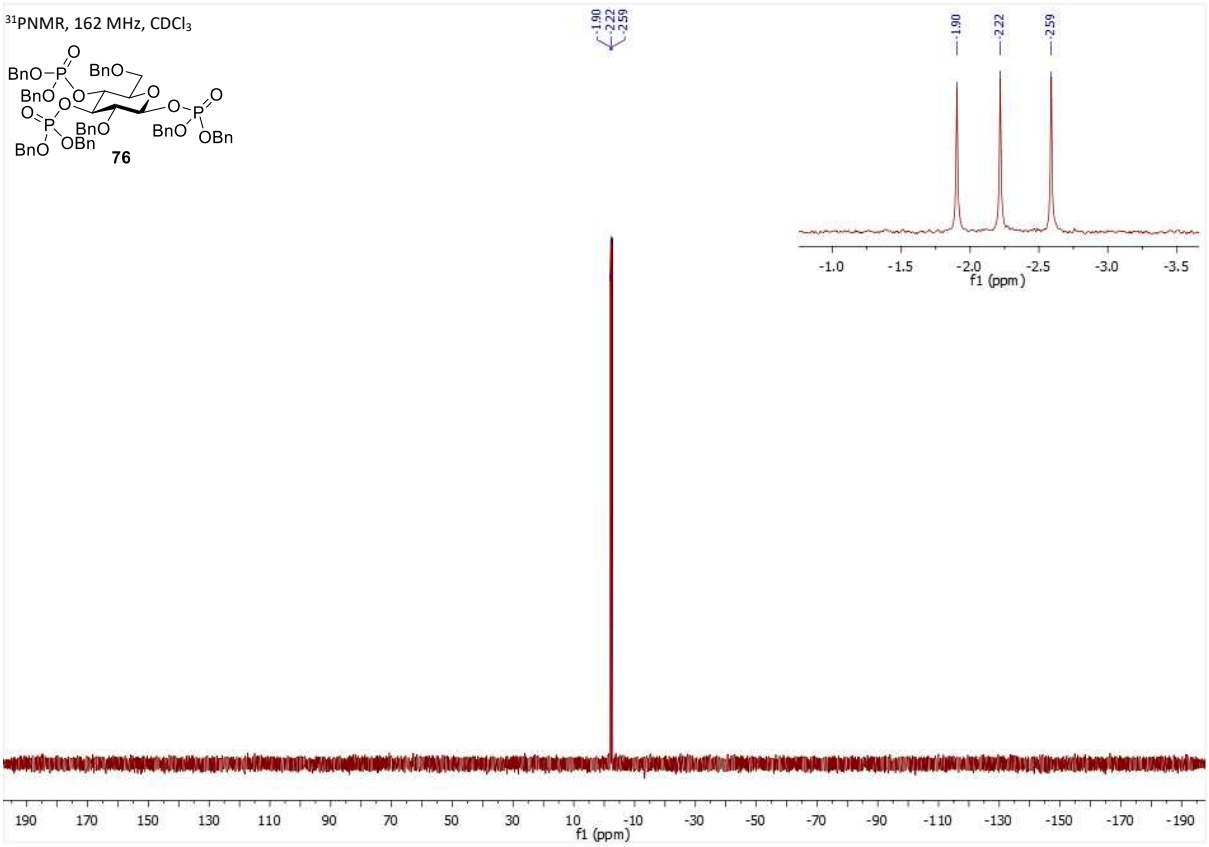

^{13}CNMR, 100 MHz, $CDCl_3$

76

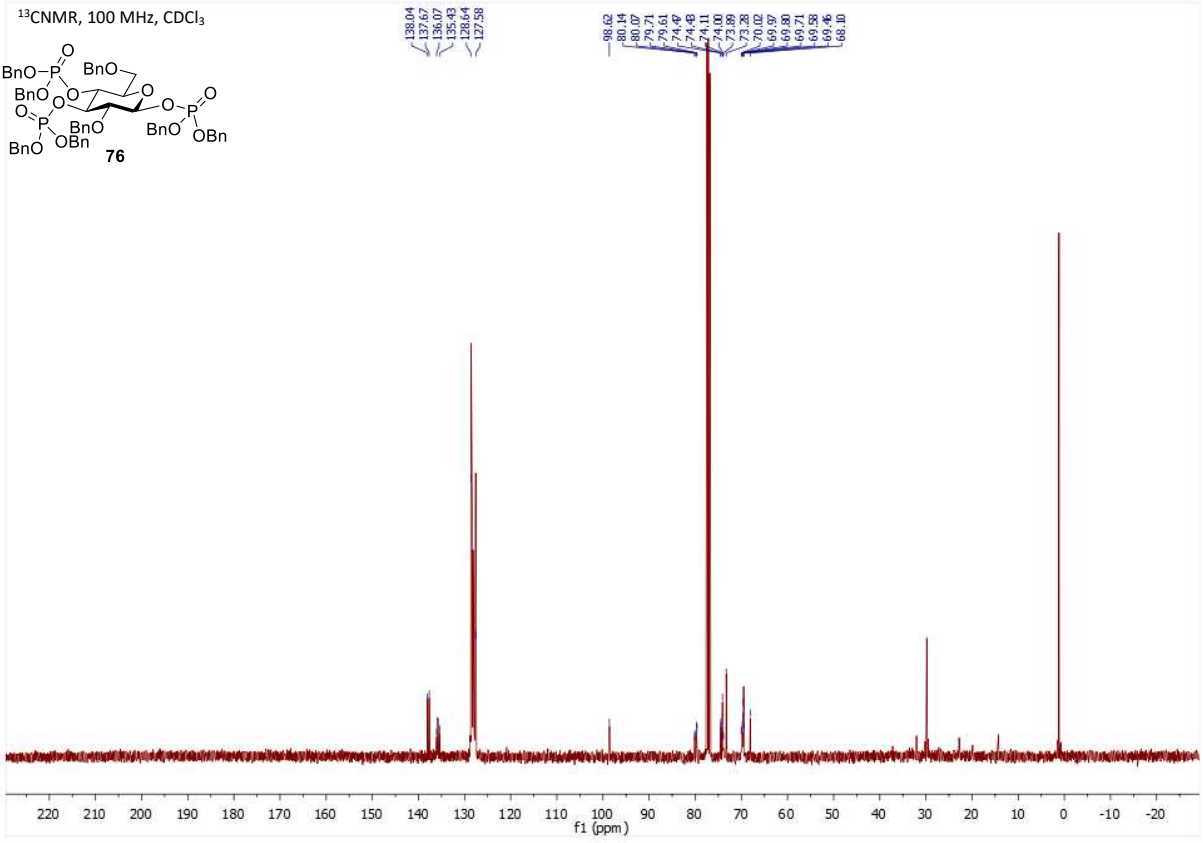

^{1}H-^{1}H COSY

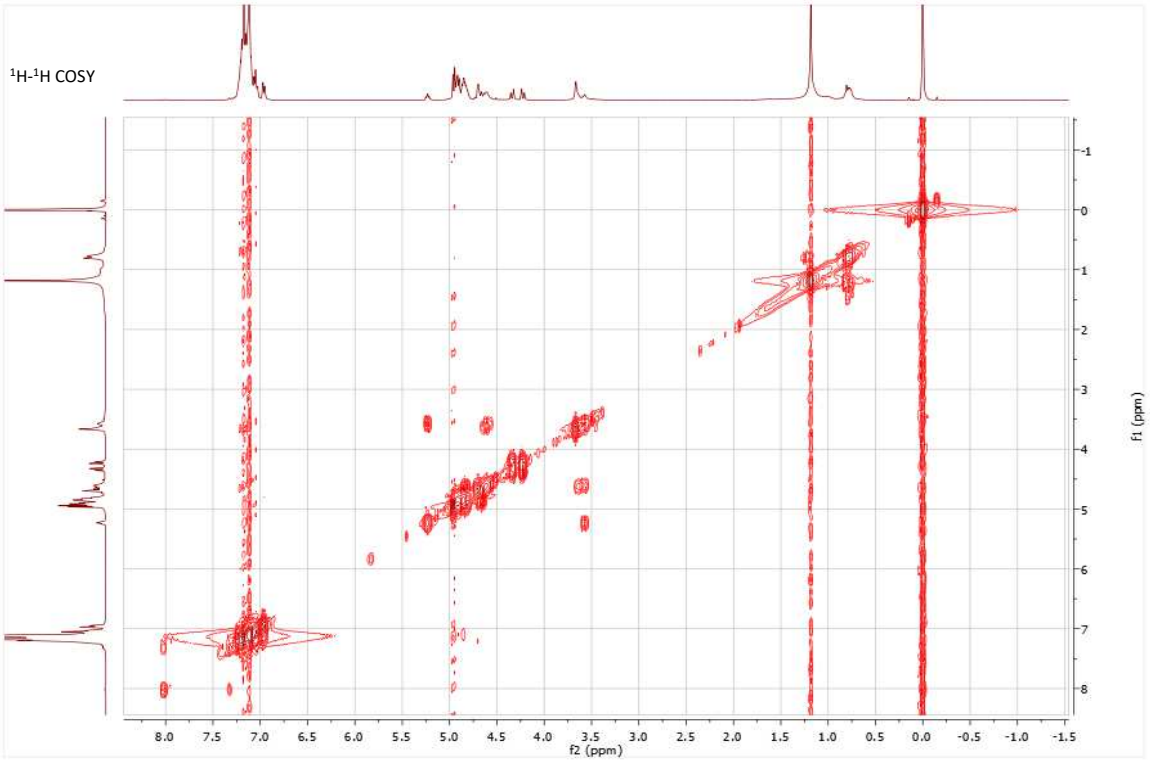

^{1}H-^{13}C HSQC

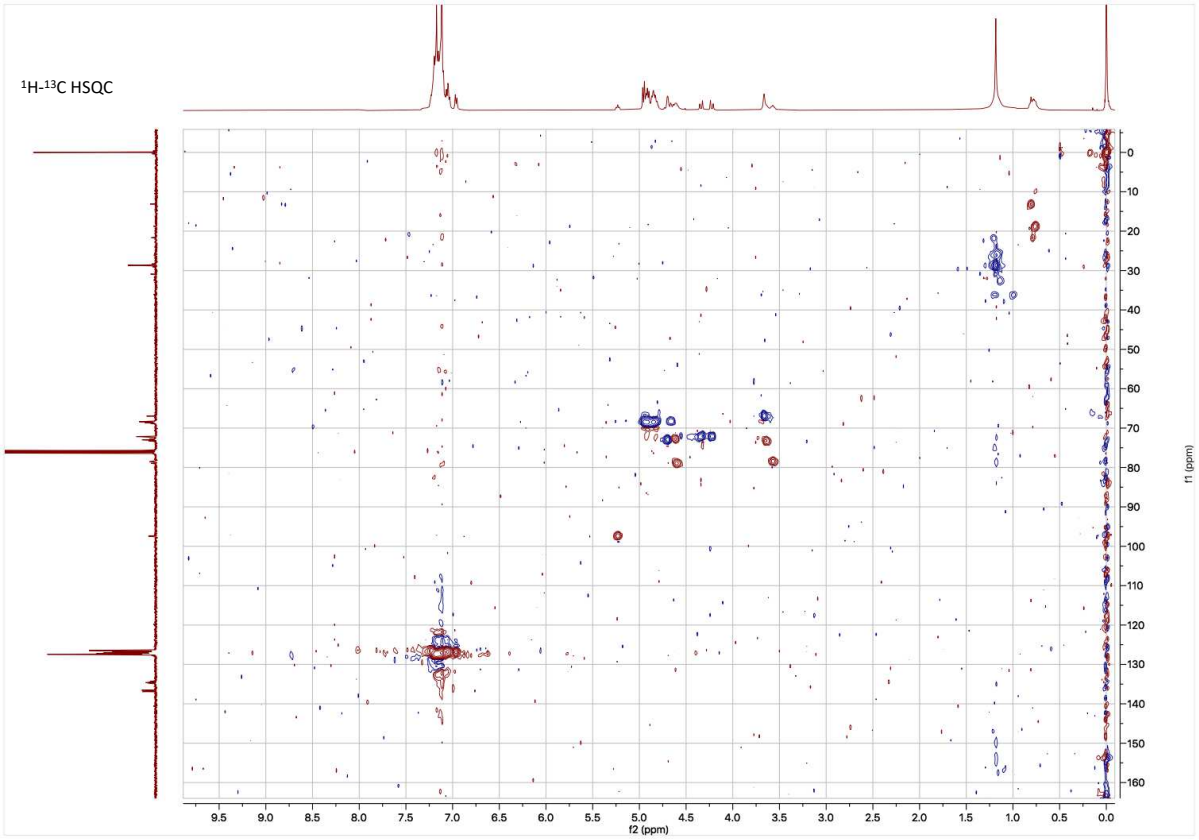

β-D-Glucopyranosyl 1,3,4-trisphosphate triethylammonium salt (**63**)

^{1}HNMR, 400 MHz, d4-MeOH

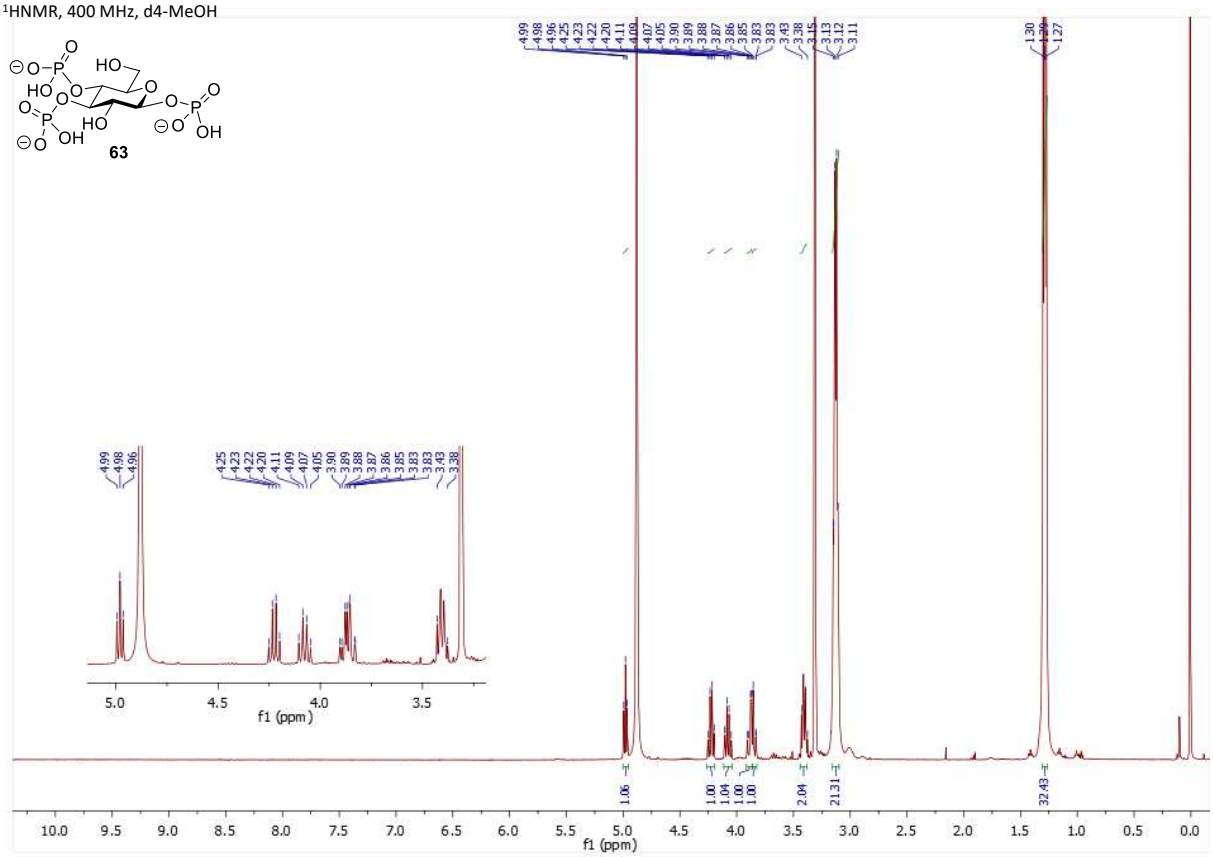

^{31}PNMR, 162 MHz, d4-MeOH

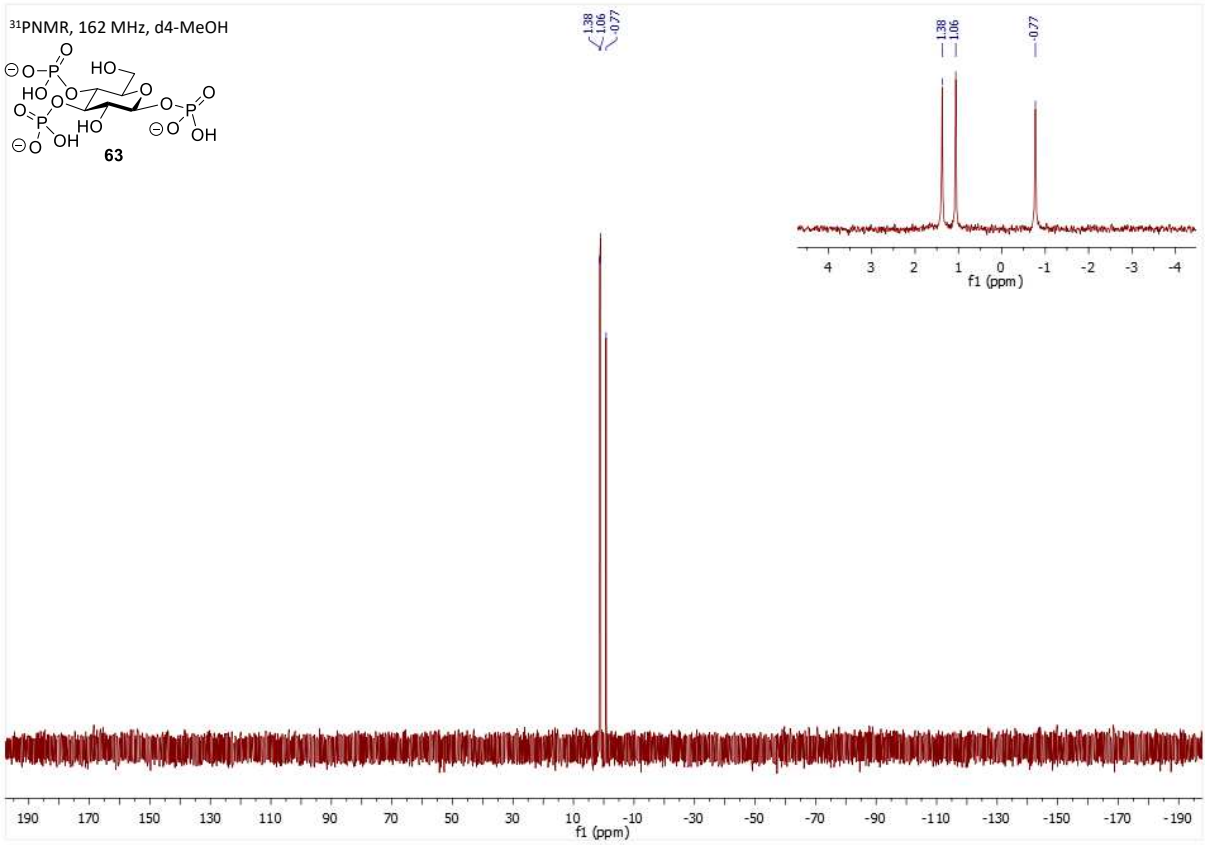

^{13}CNMR, 100 MHz, d4-MeOH

63

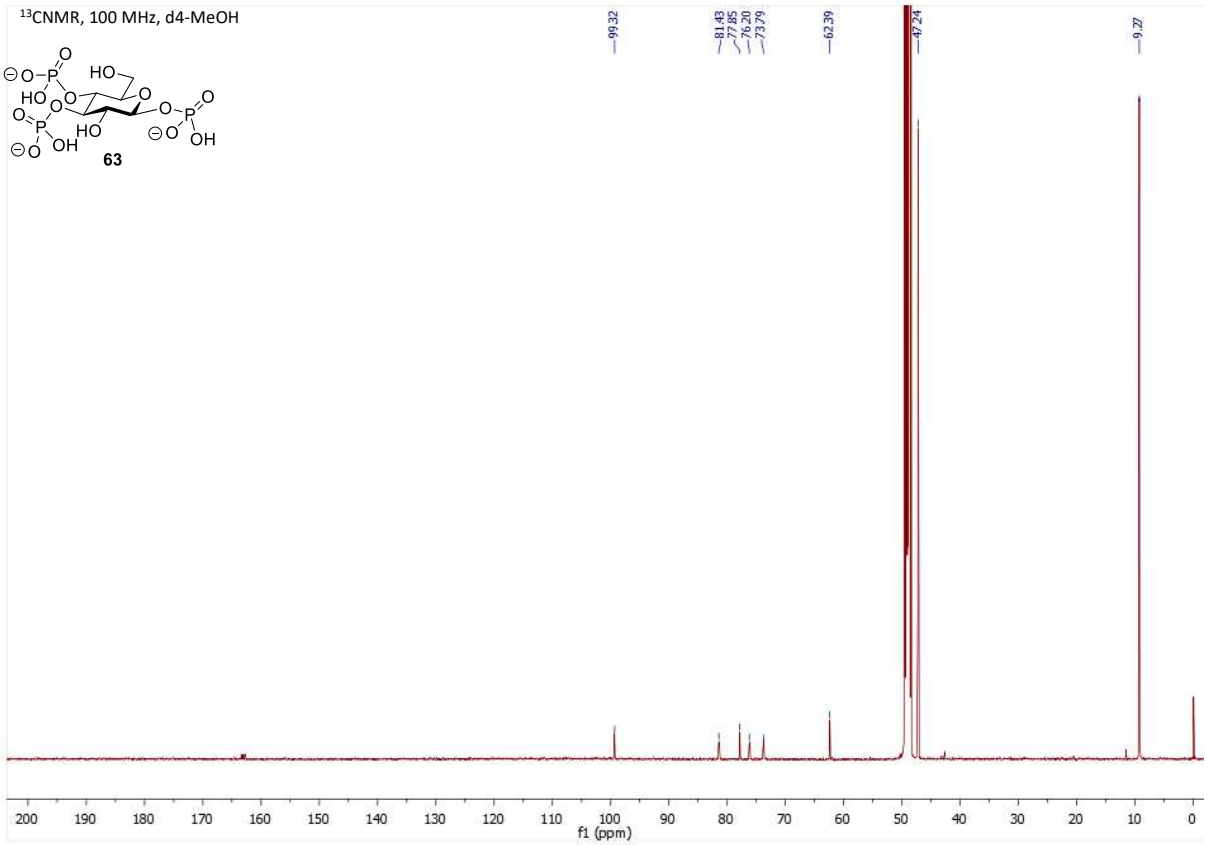

^{1}H-^{1}H COSY

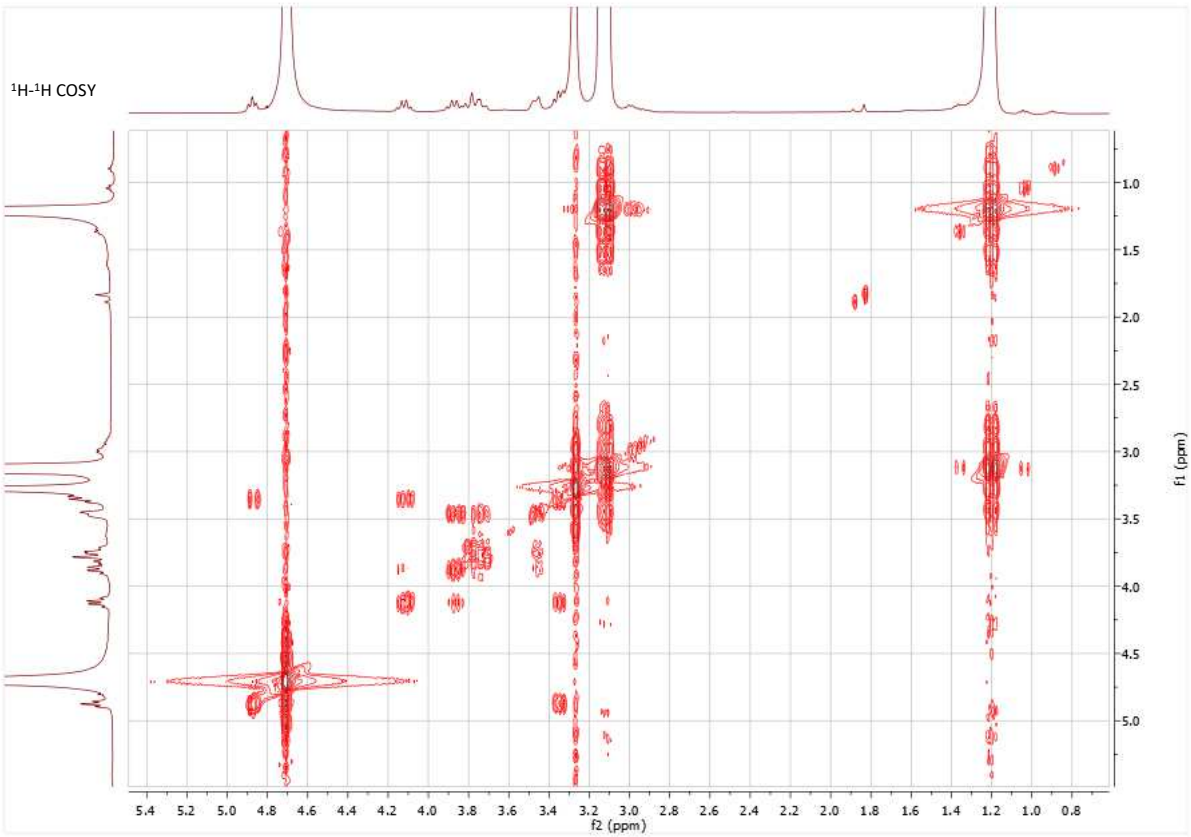

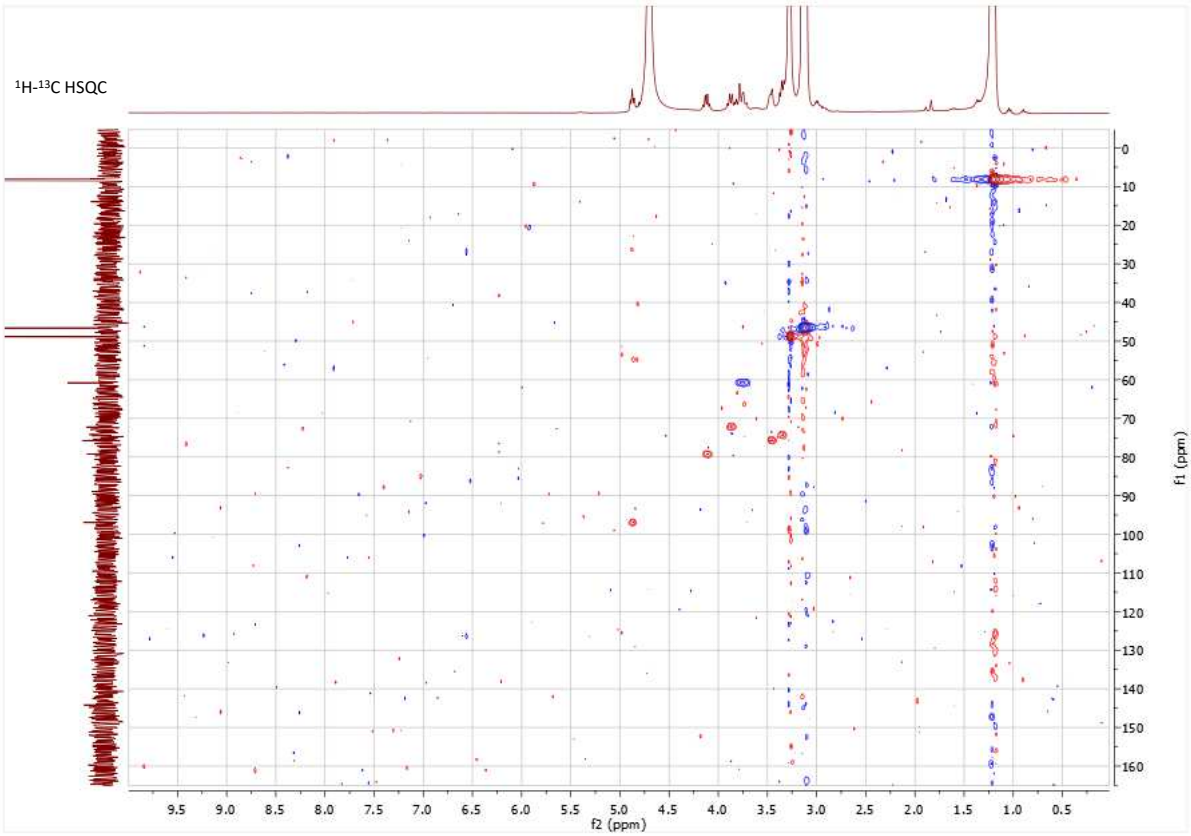

α-D-Glucopyranosyl 1,3,4-trisphosphate triethylammonium salt (**62**)

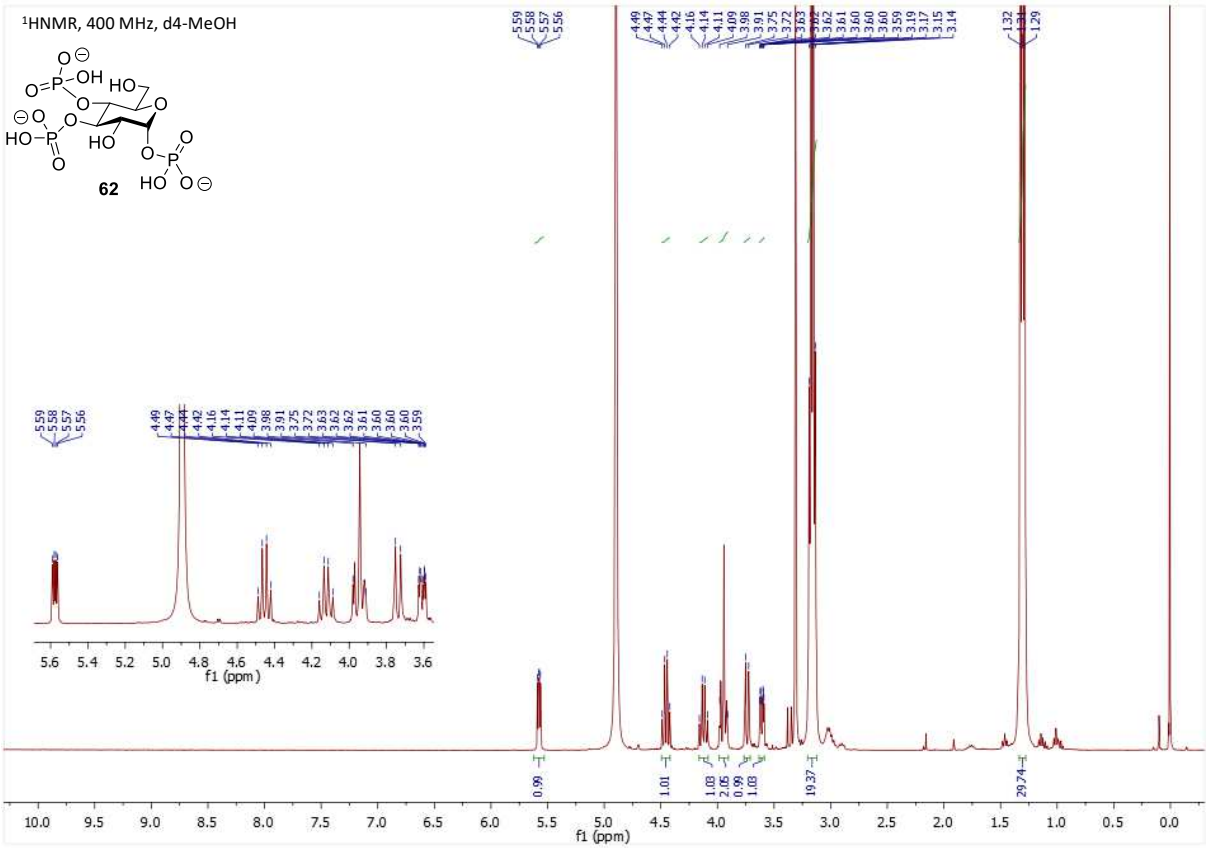

^{31}PNMR, 162 MHz, d4-MeOH

62

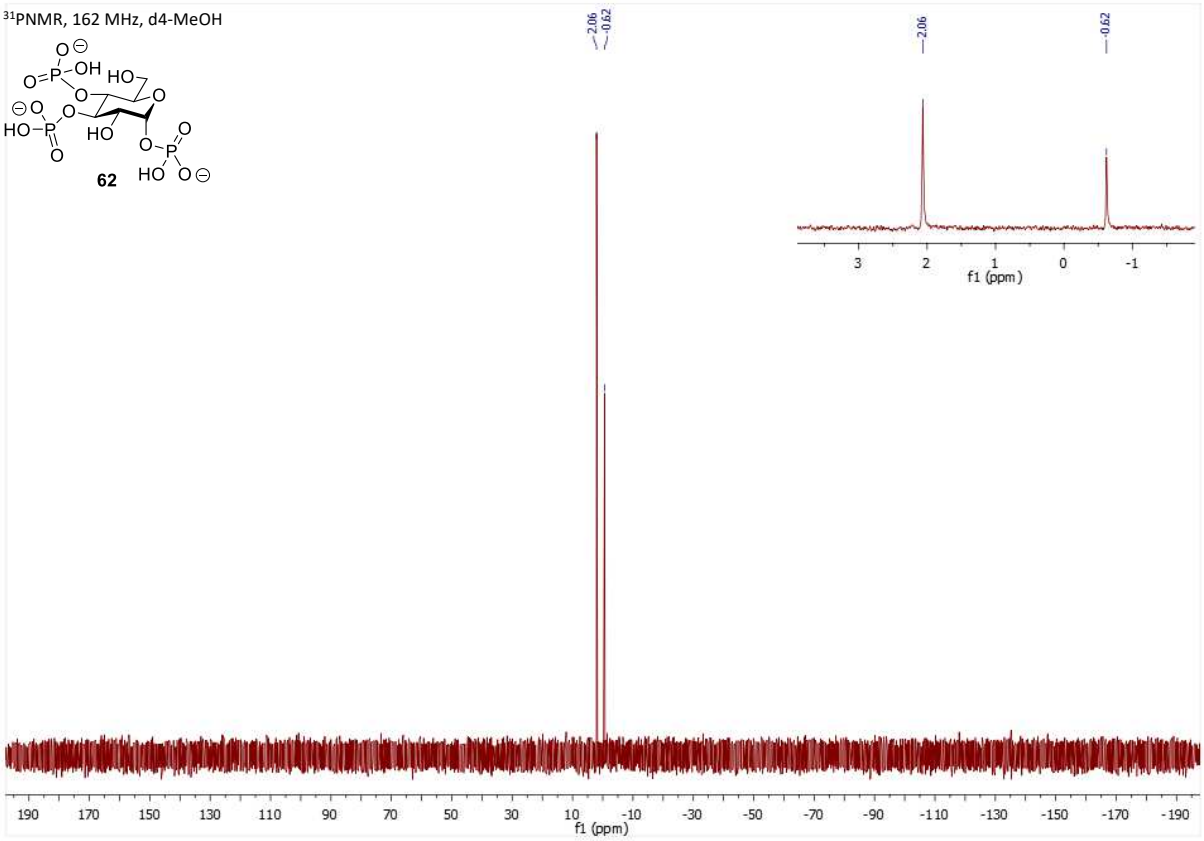

^{13}CNMR, 100 MHz, d4-MeOH

62

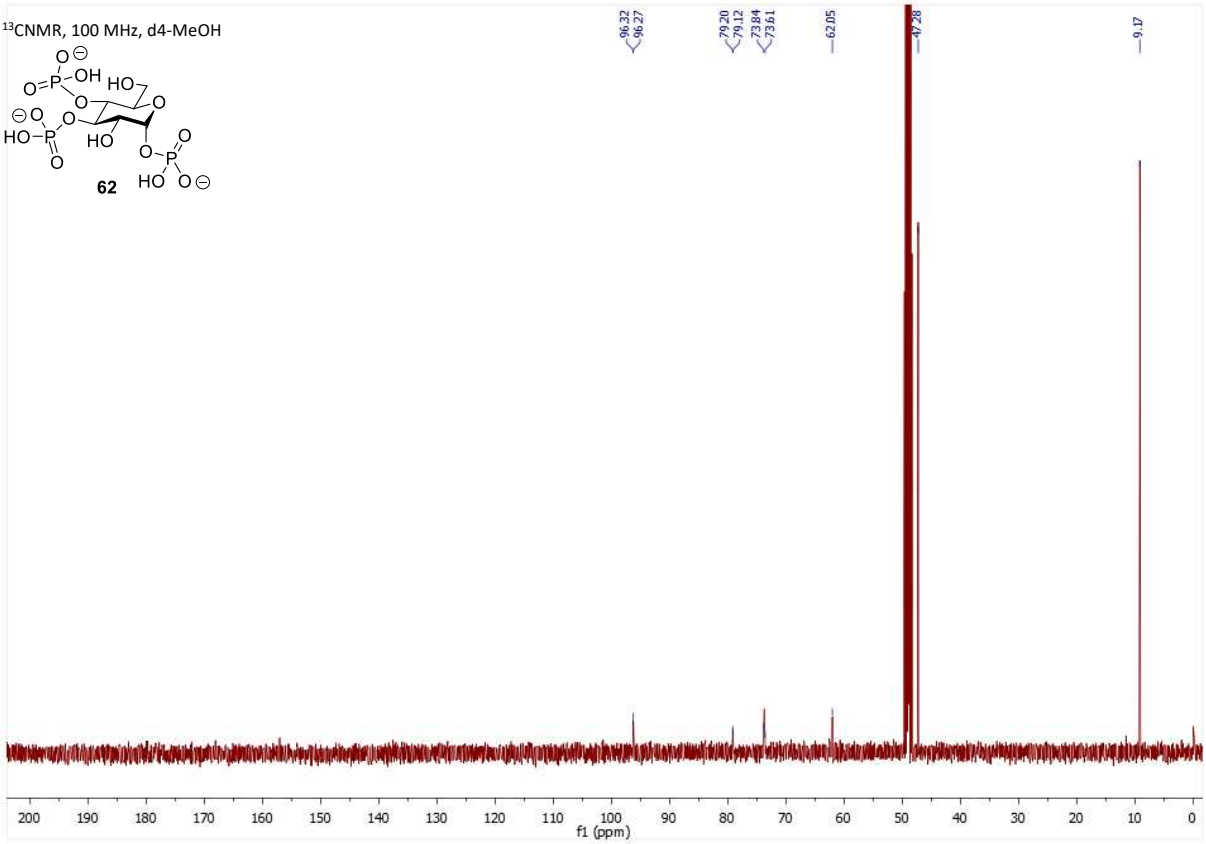

^{1}H-^{1}H COSY

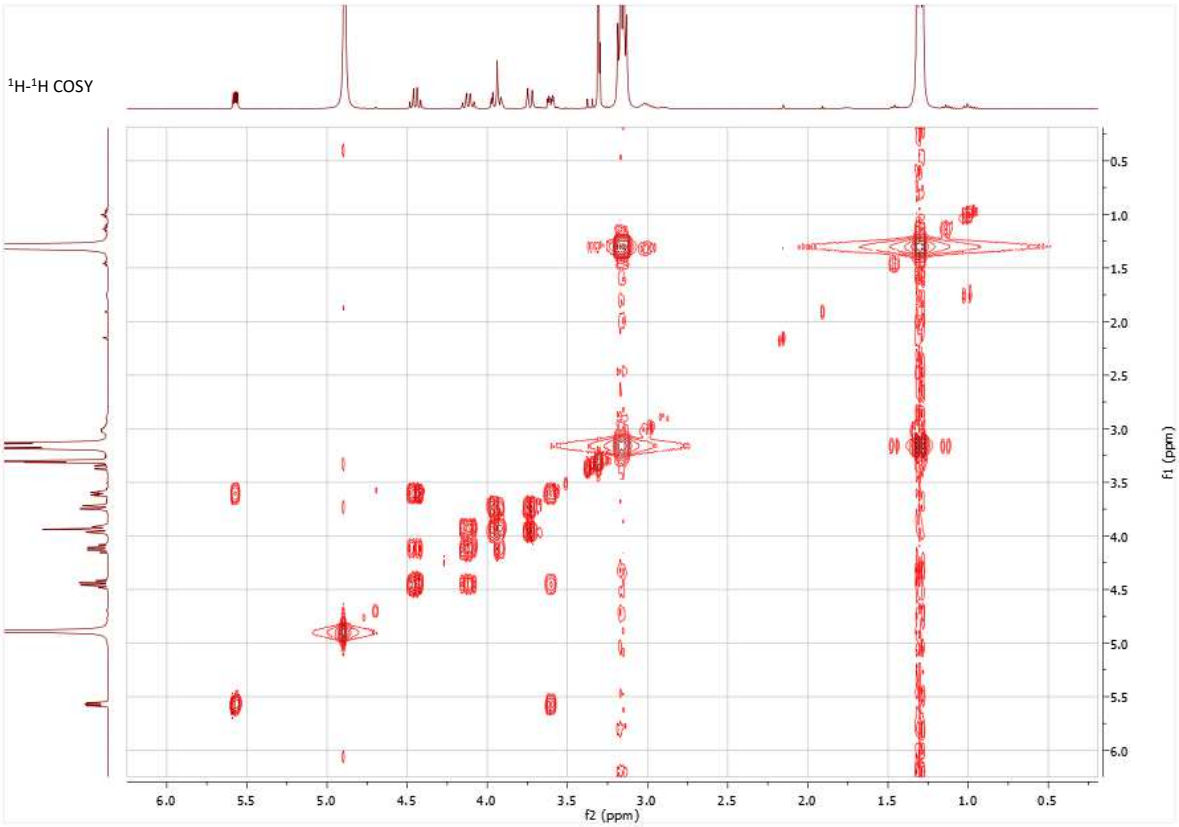

^{1}H-^{13}C HSQC

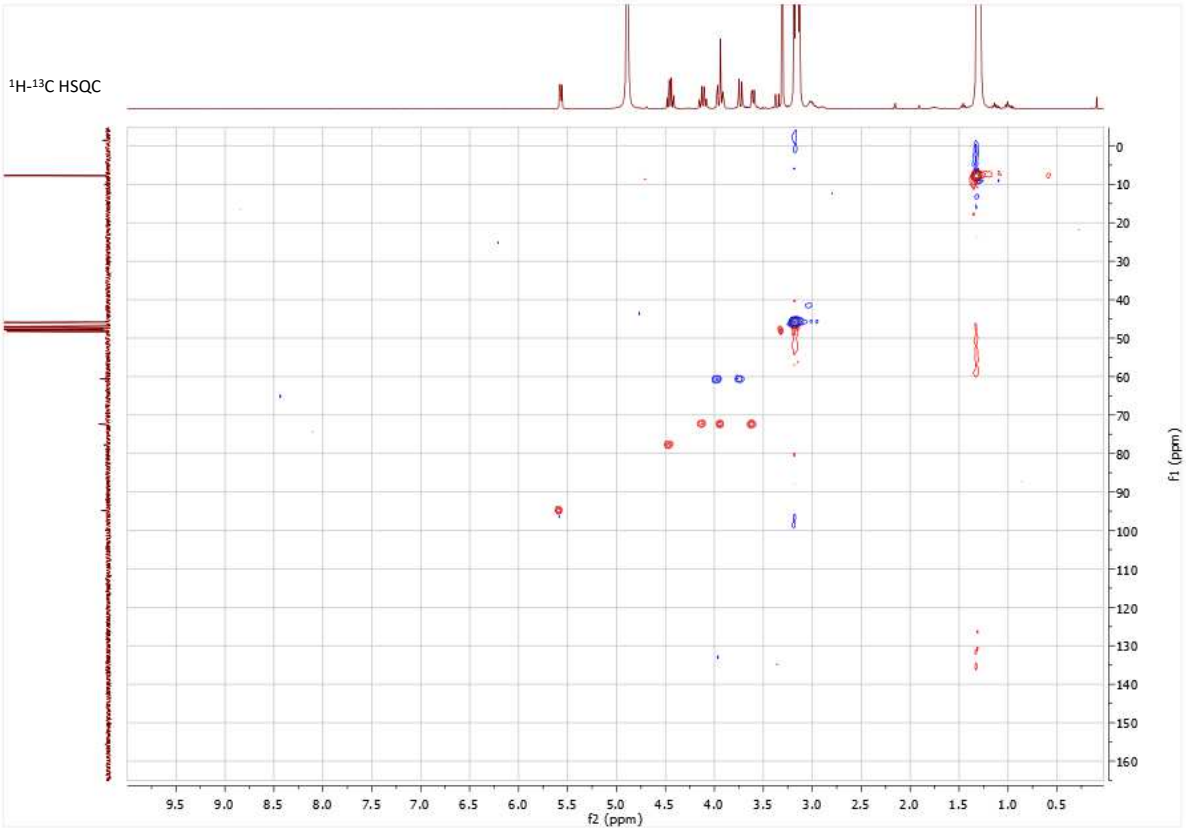

Synthesis of diphospho myo-inositol bisphosphate and diphospho myo-inositol phosphate [PP-InsP$_2$/PP-InsP] target compounds

DL-1,2-Isopropylidene-*myo*-inositol (**81**)

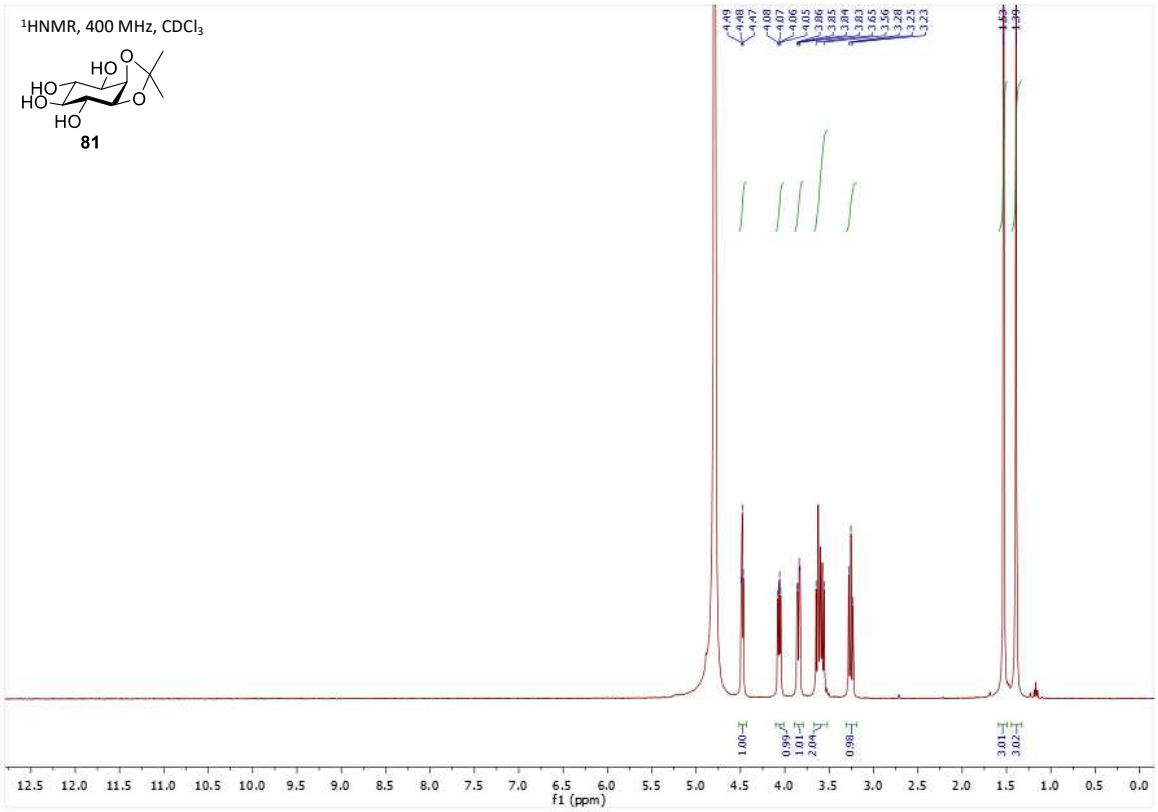

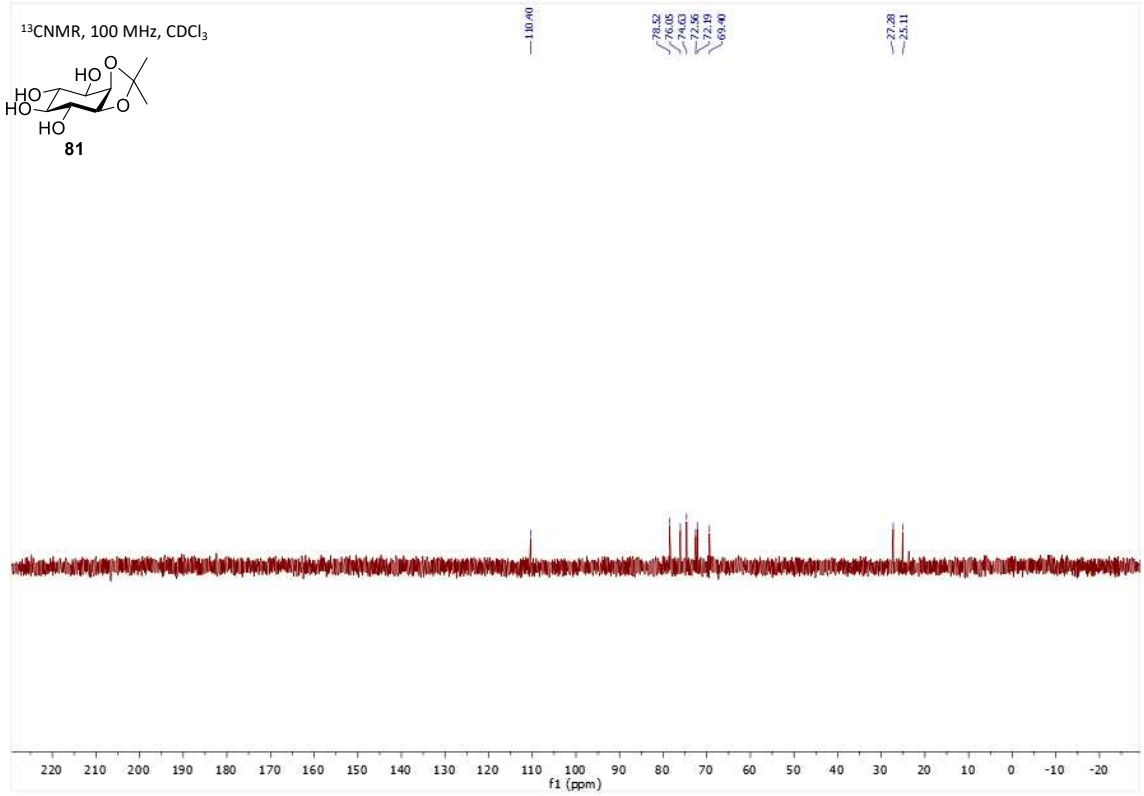

^{1}H-^{1}H COSY

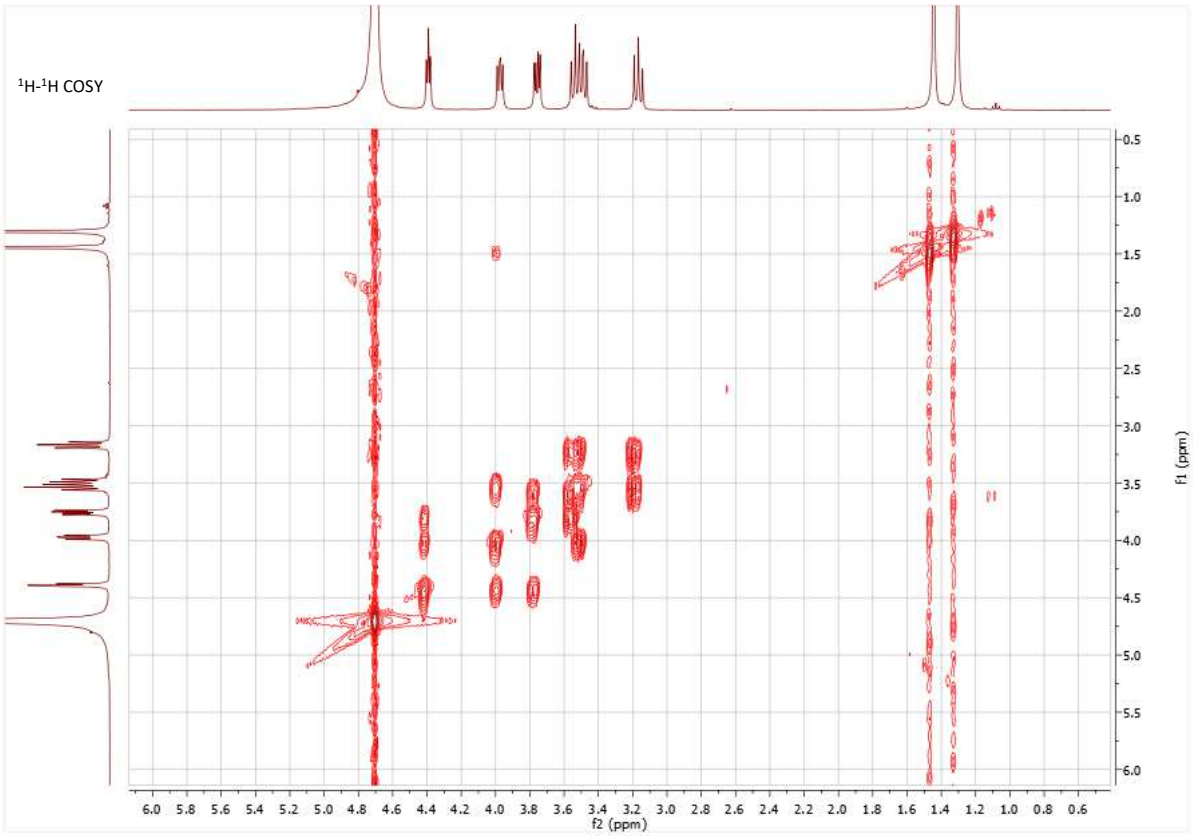

^{1}H-^{13}C HSQC

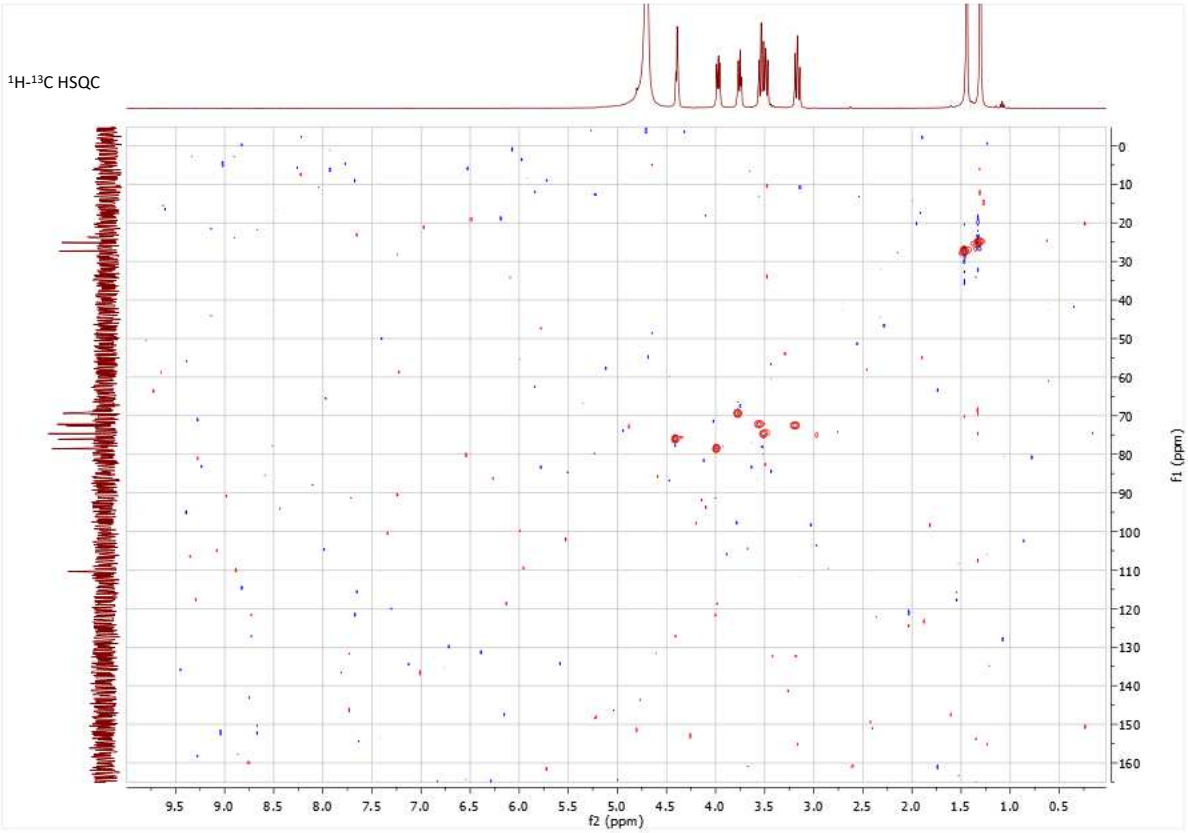

DL-3,6-Di-*O*-benzyl-1,2-isopropylidene-*myo*-inositol (**82**)

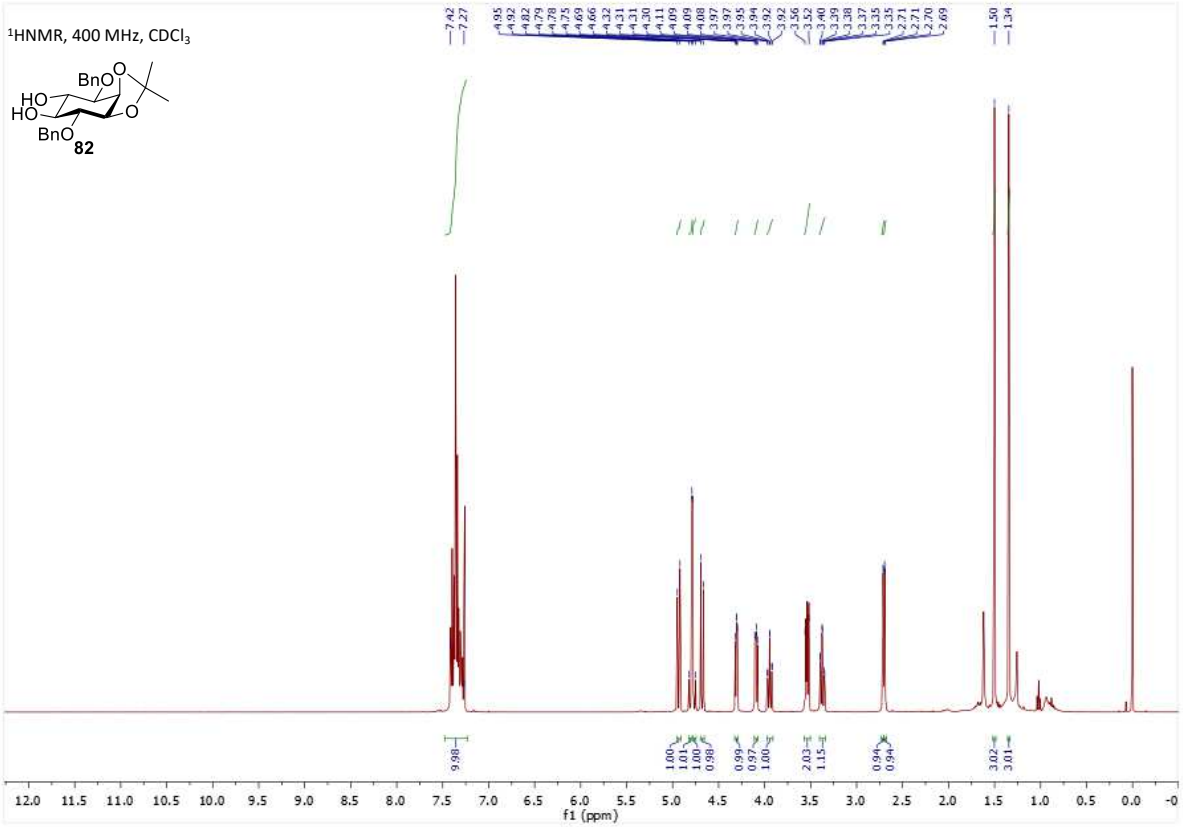

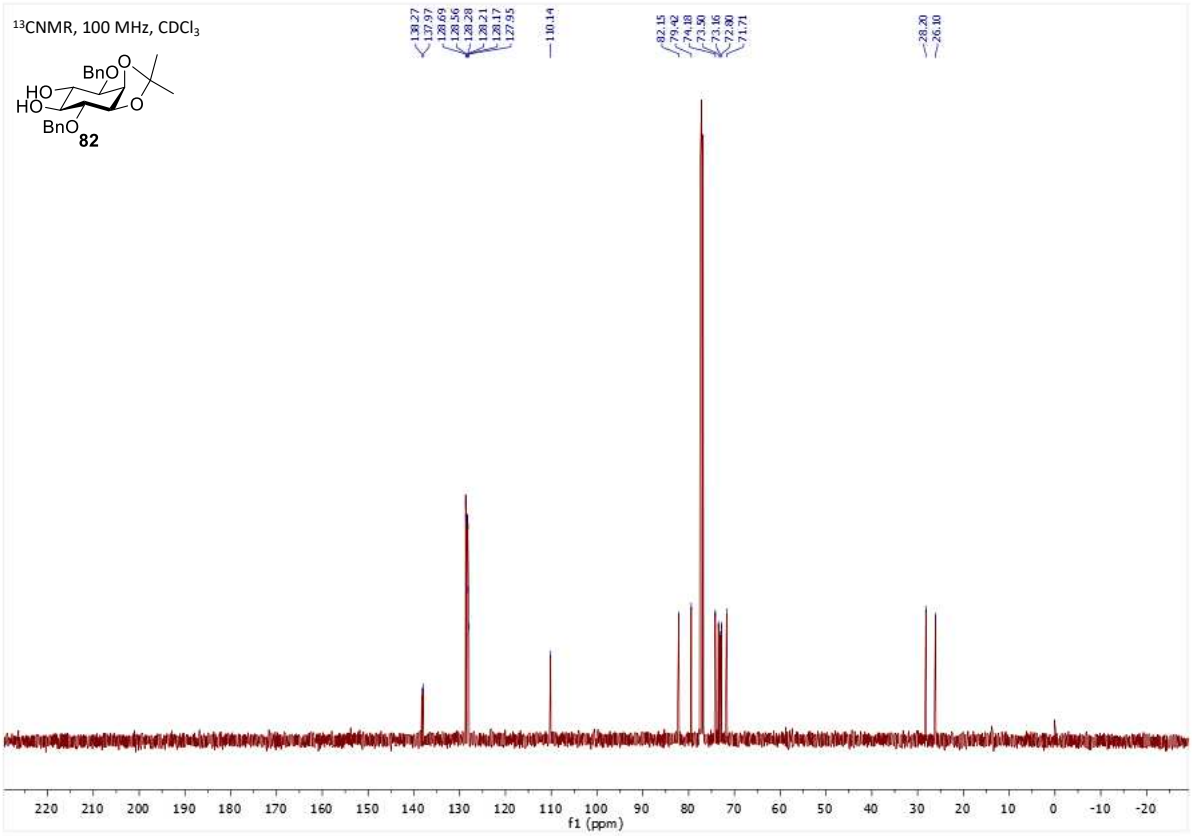

^{1}H-^{1}H COSY

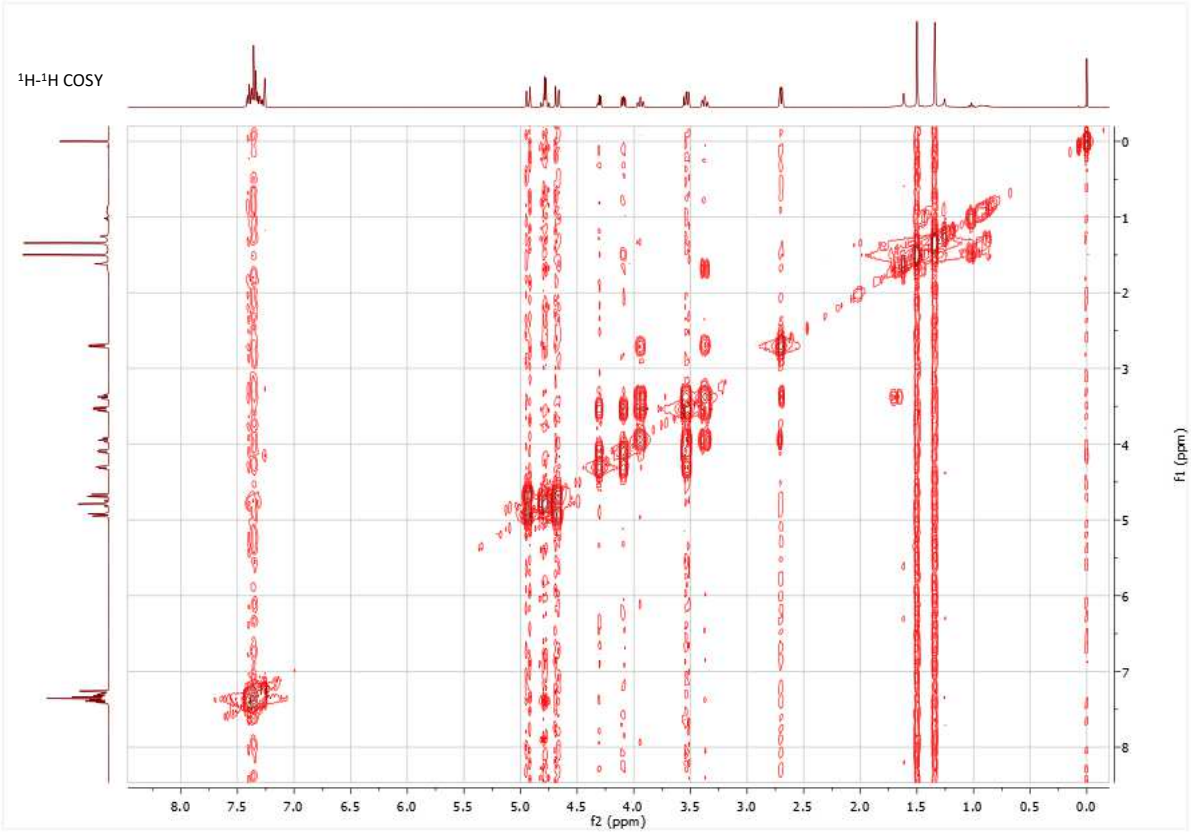

^{1}H-^{13}C HSQC

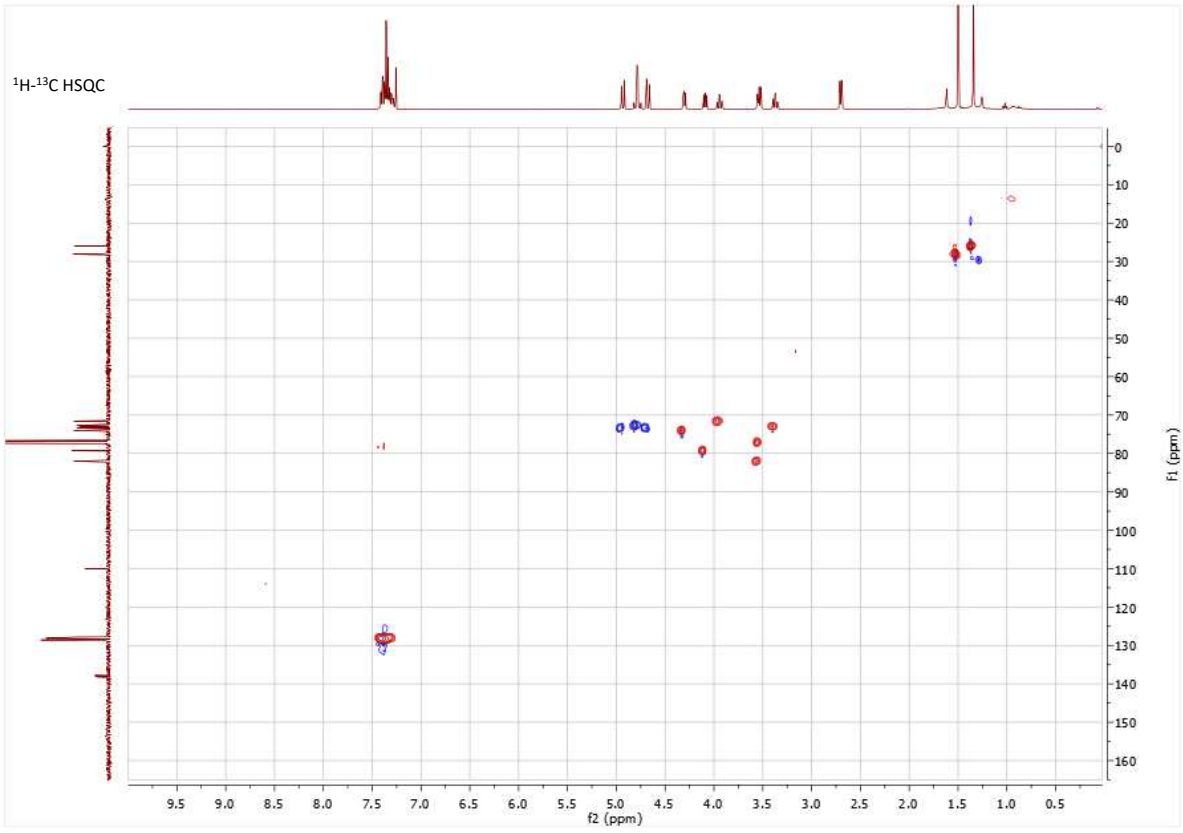

DL-3,6-Di-*O*-benzyl-*myo*-inositol (**83**)

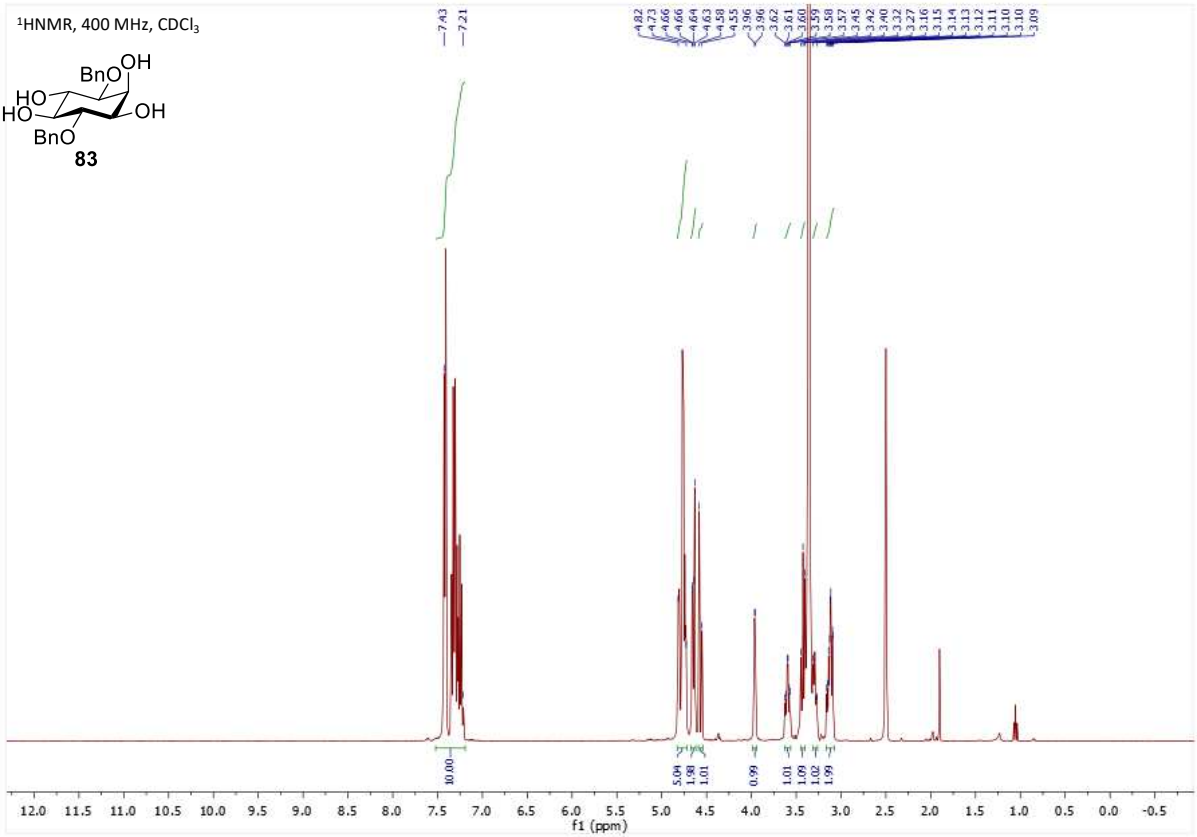

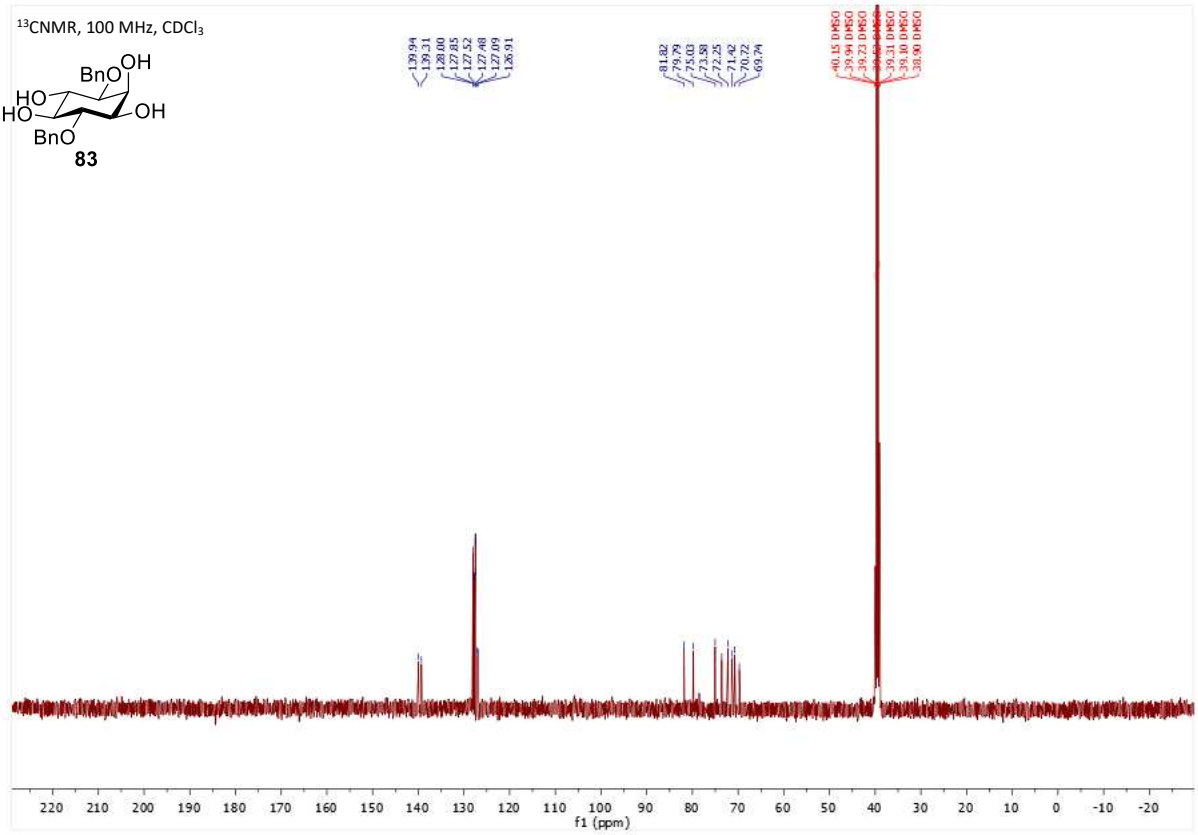

^{1}H-^{1}H COSY

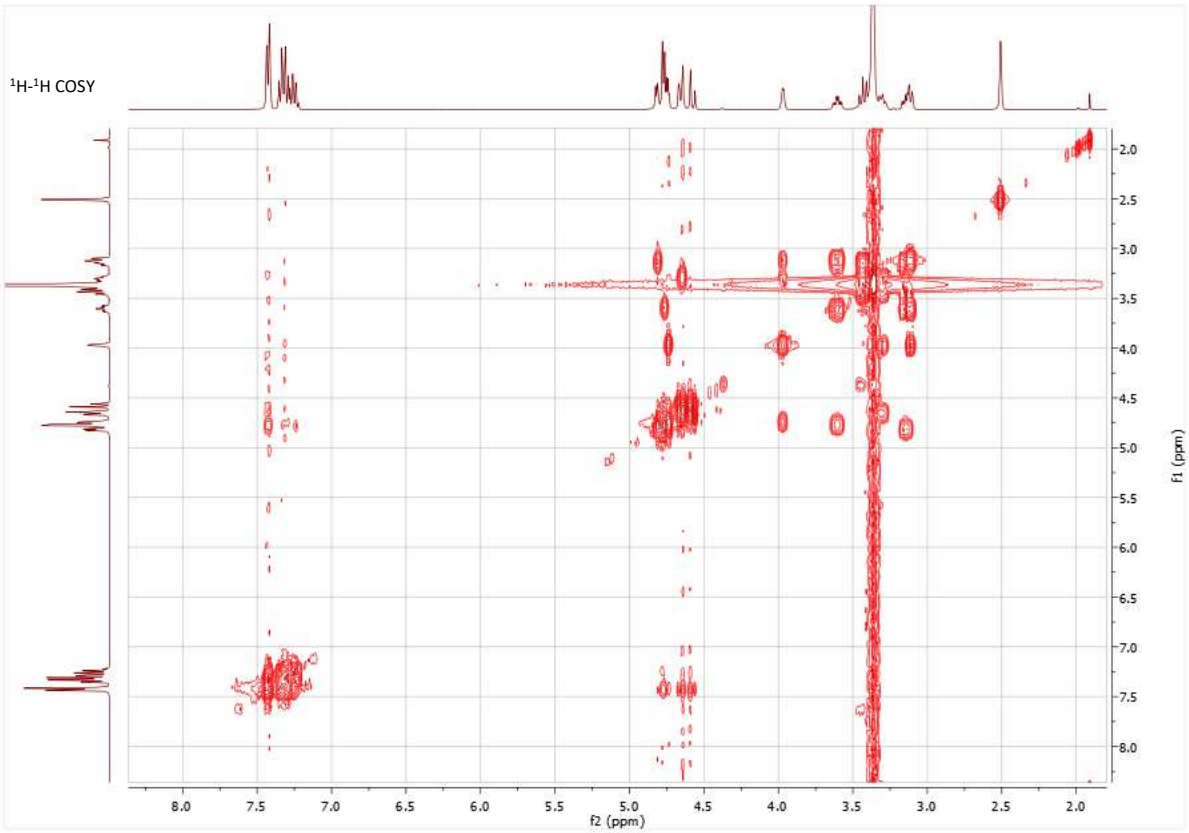

^{1}H-^{13}C HSQC

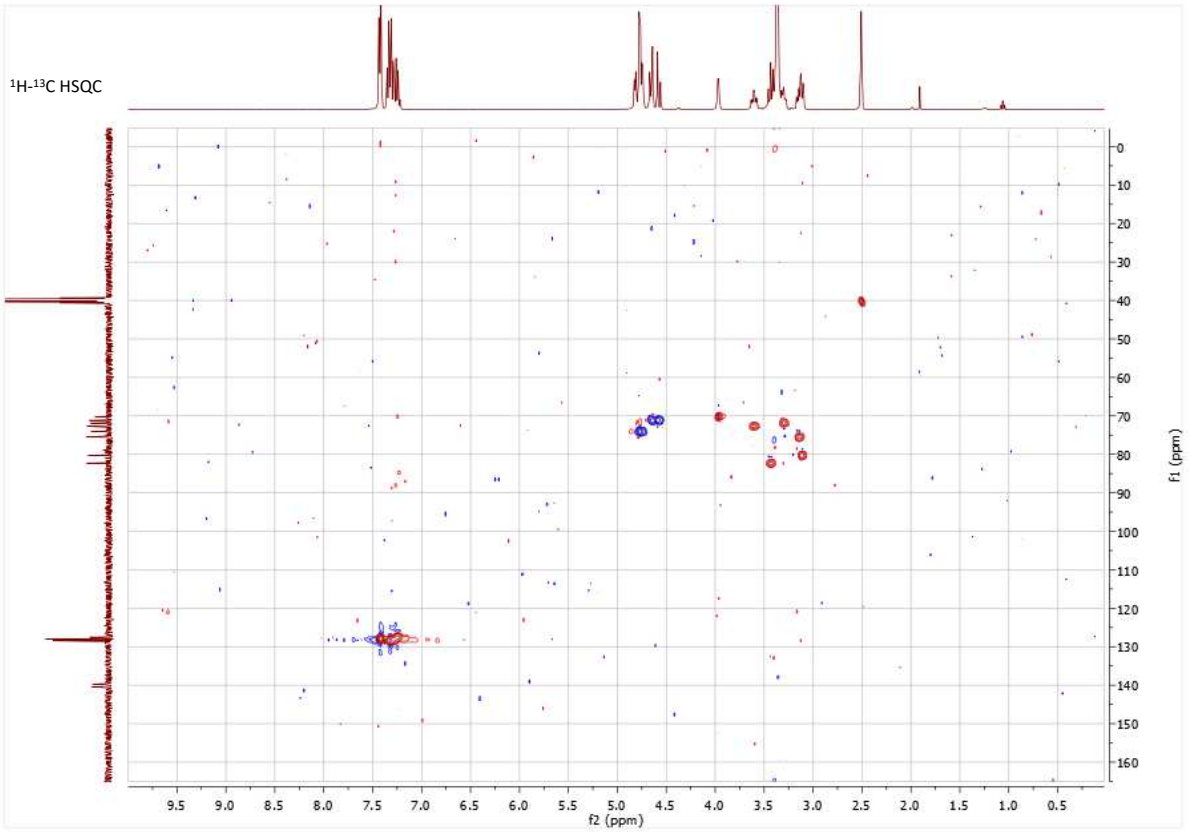

DL-3,6-Di-*O*-benzyl-4,5-*O*-(2,3-dimethoxybutane-2,3-diyl)-*myo*-inositol (**84**)

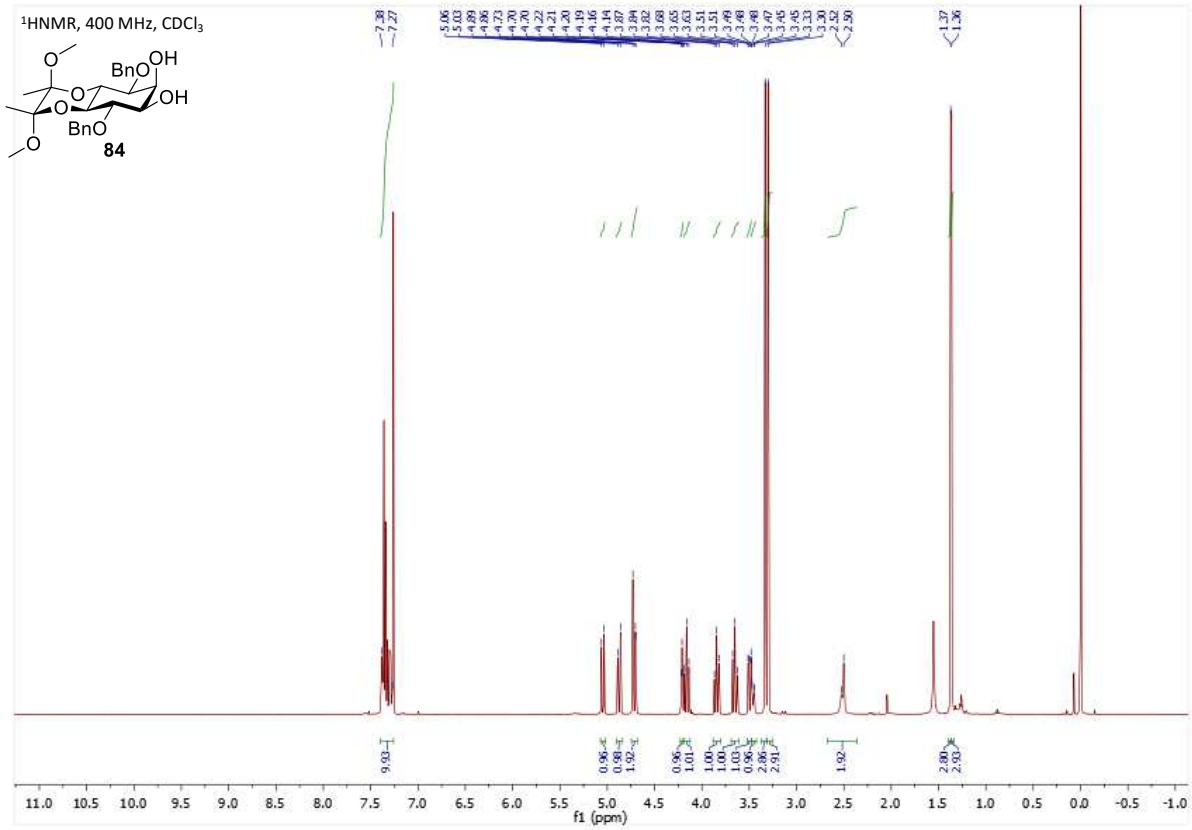

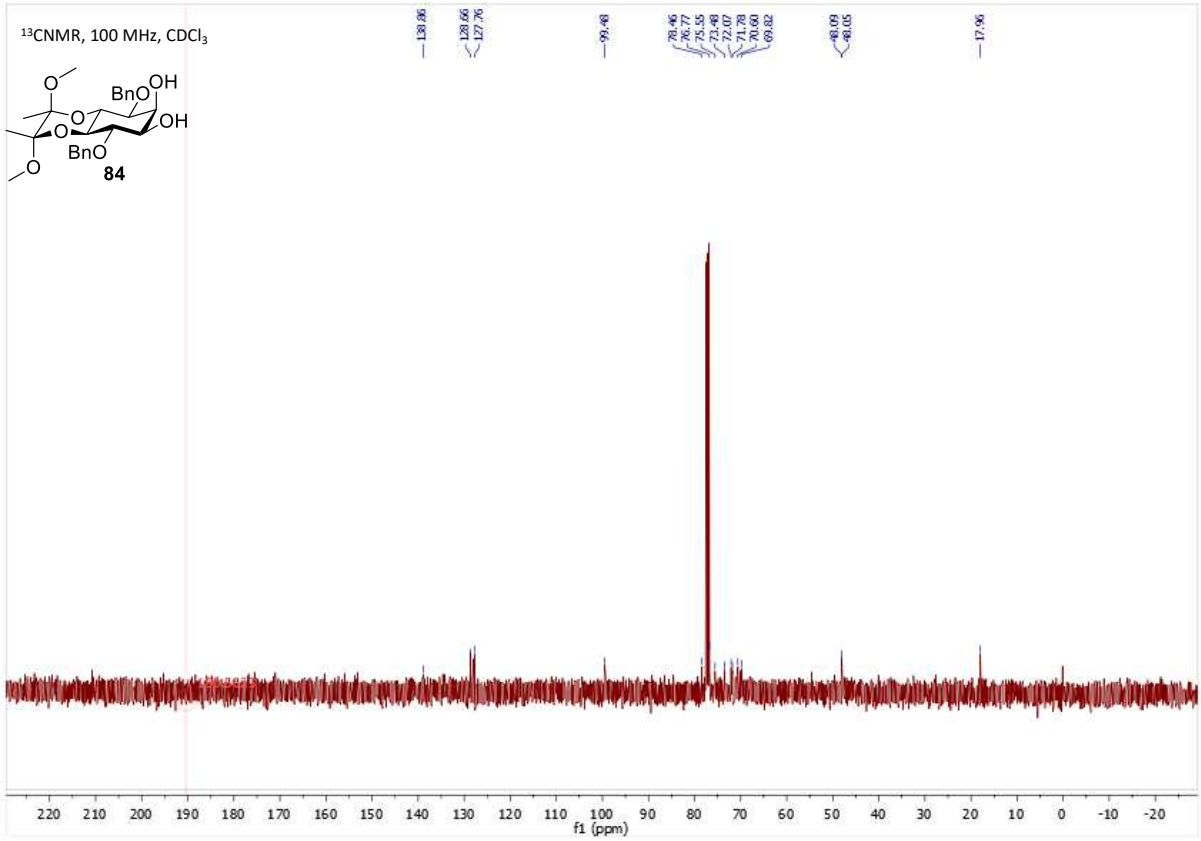

^{1}H-^{1}H COSY

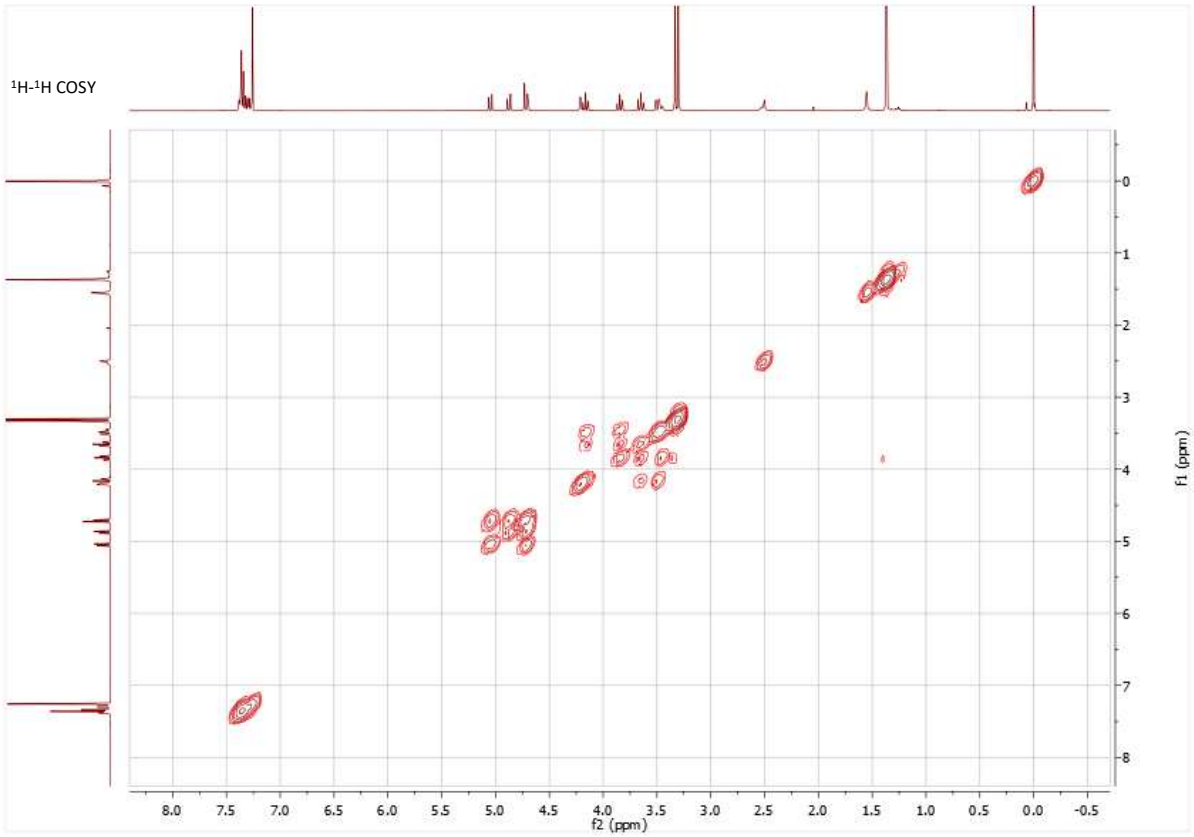

^{1}H-^{13}C HSQC

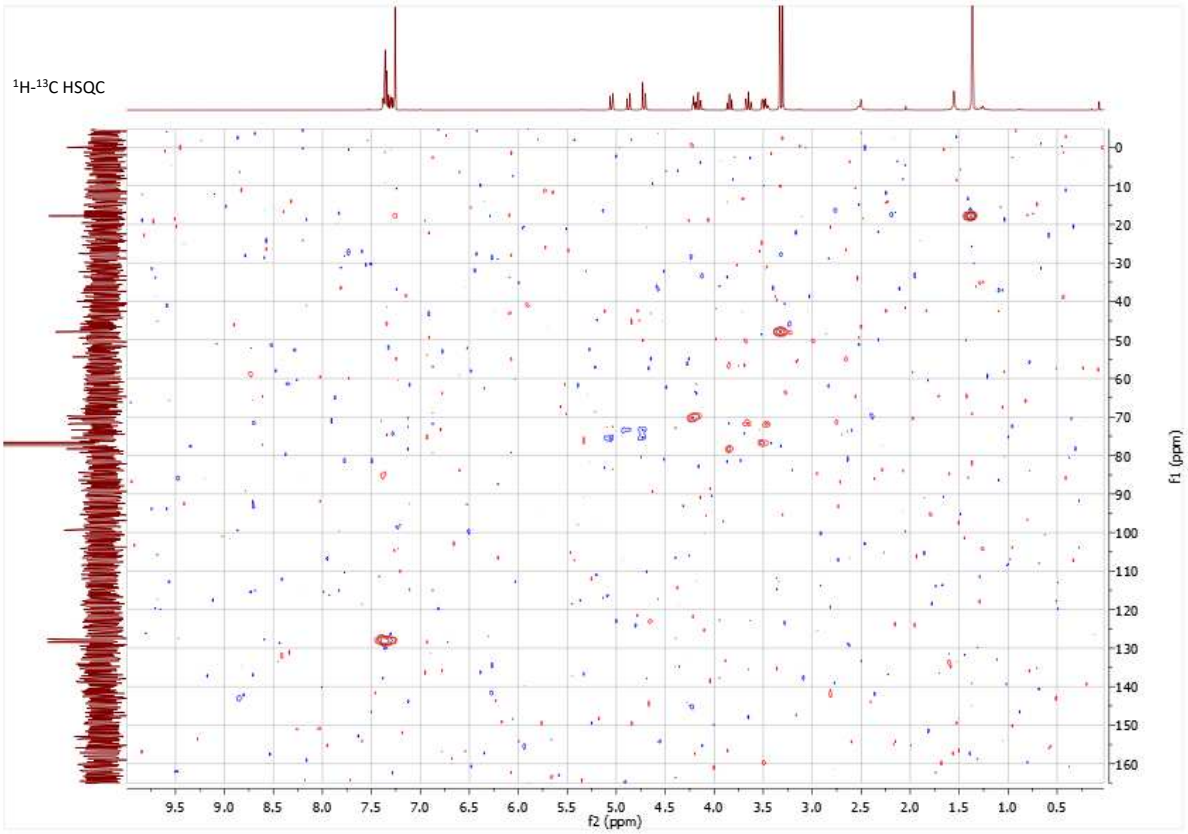

DL-1,2,3,6-Tetra-*O*-benzyl-4,5-*O*-(2,3-dimethoxybutane-2,3-diyl)-*myo*-inositol (**85**)

^{1}HNMR, 400 MHz, $CDCl_3$

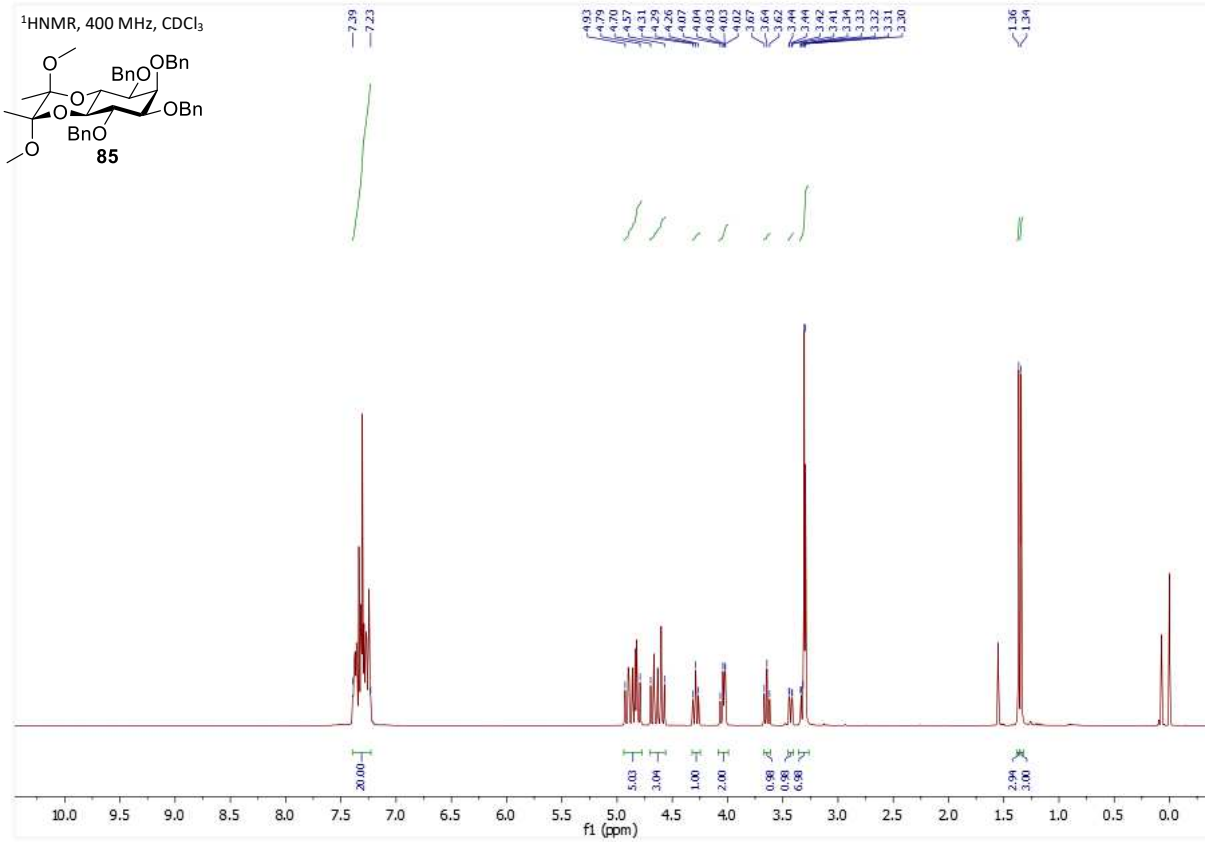

^{13}CNMR, 100 MHz, $CDCl_3$

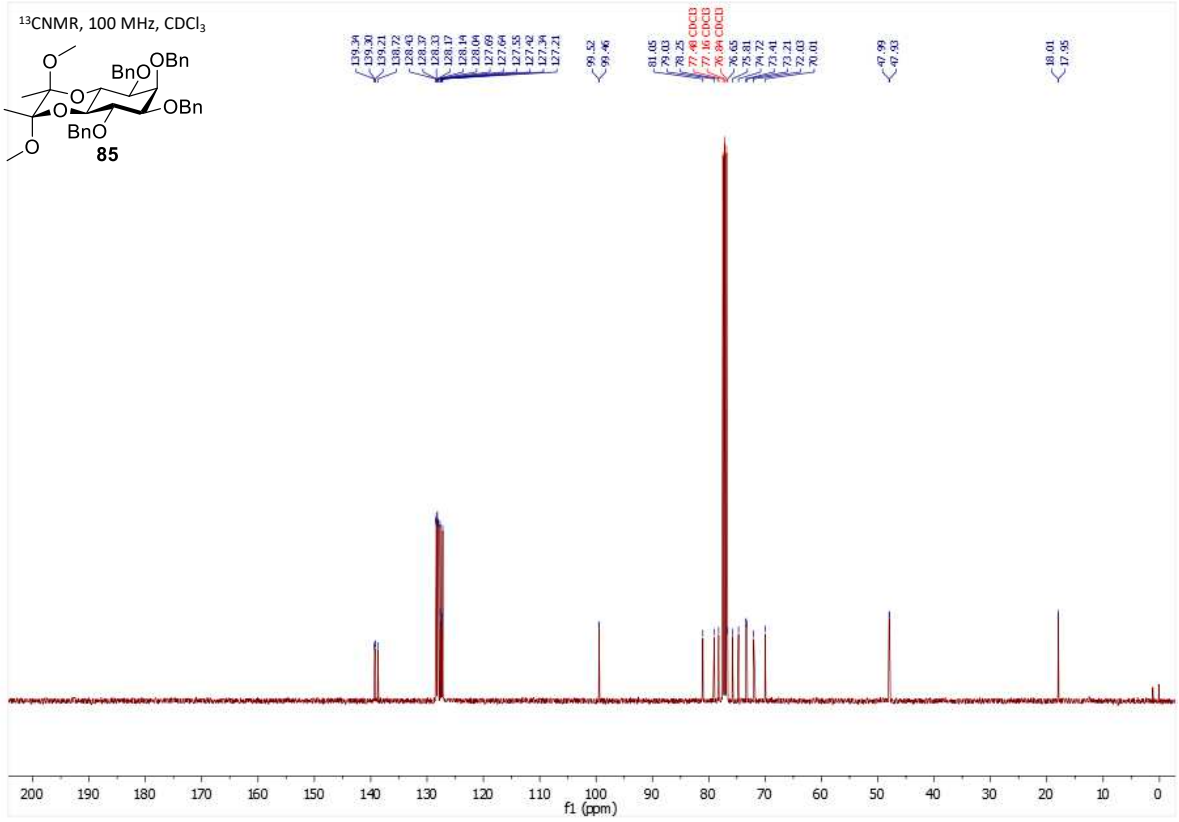

^{1}H-^{1}H COSY

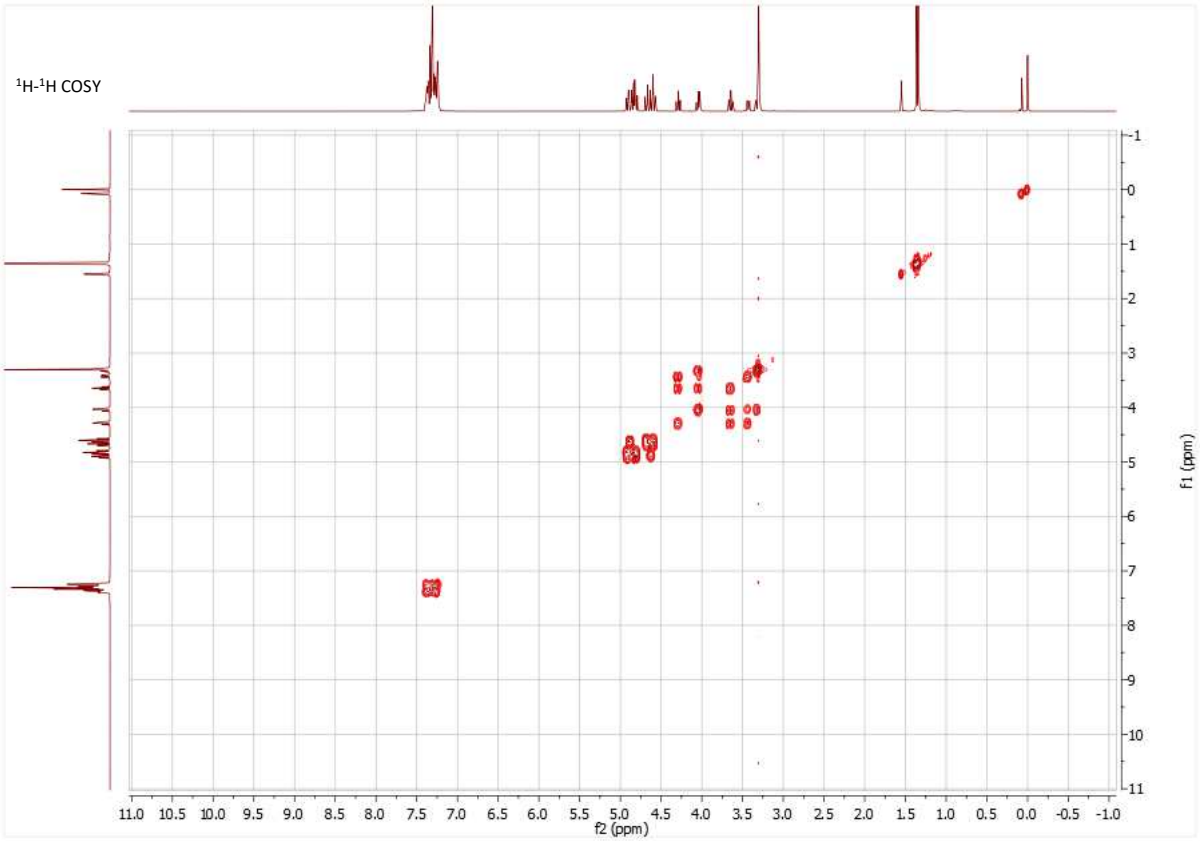

^{1}H-^{13}C HSQC

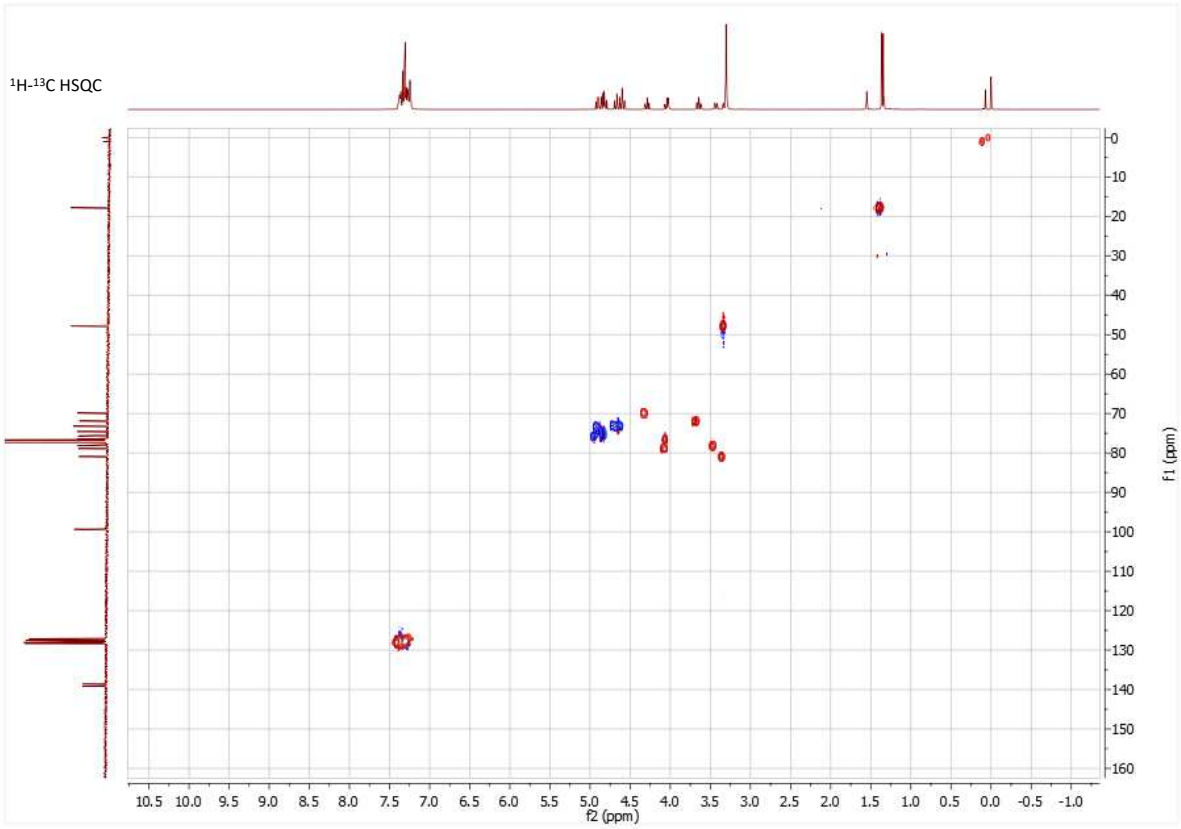

DL-1,2,3,6-Tetra-*O*-benzyl-*myo*-inositol (**28**)

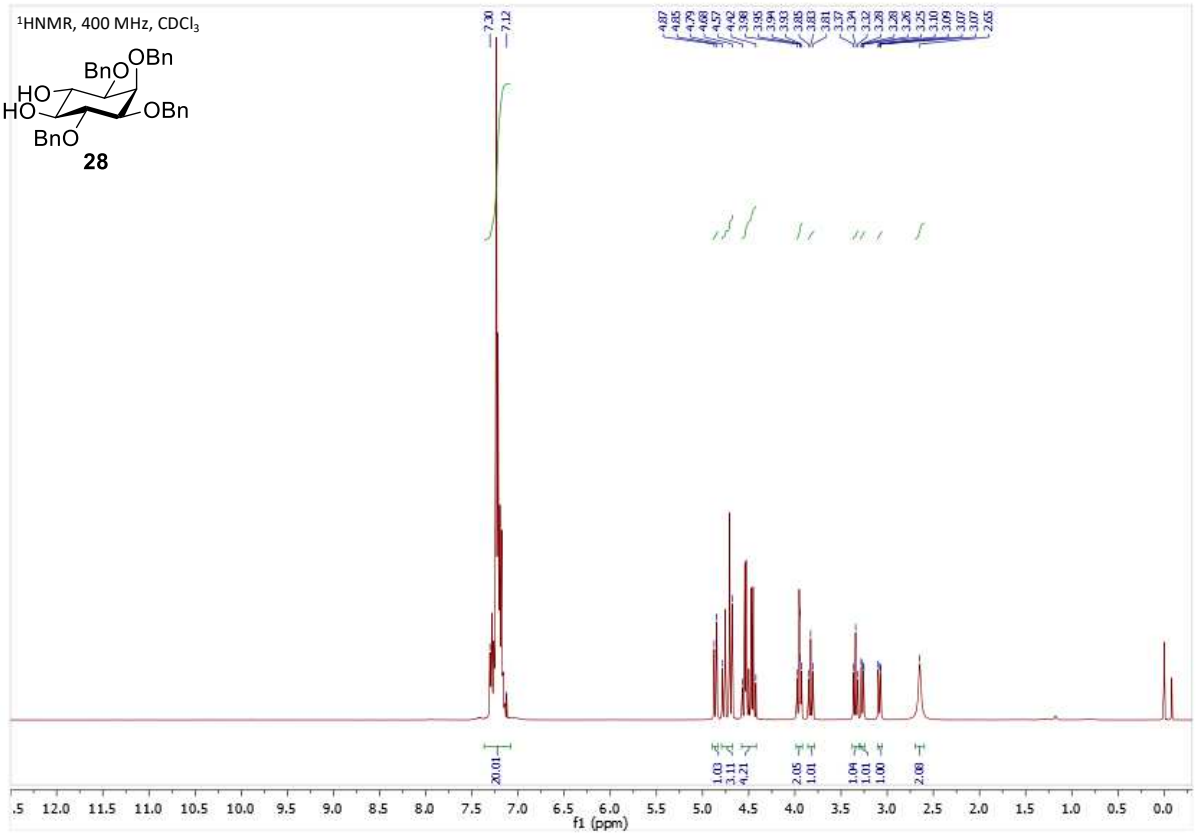

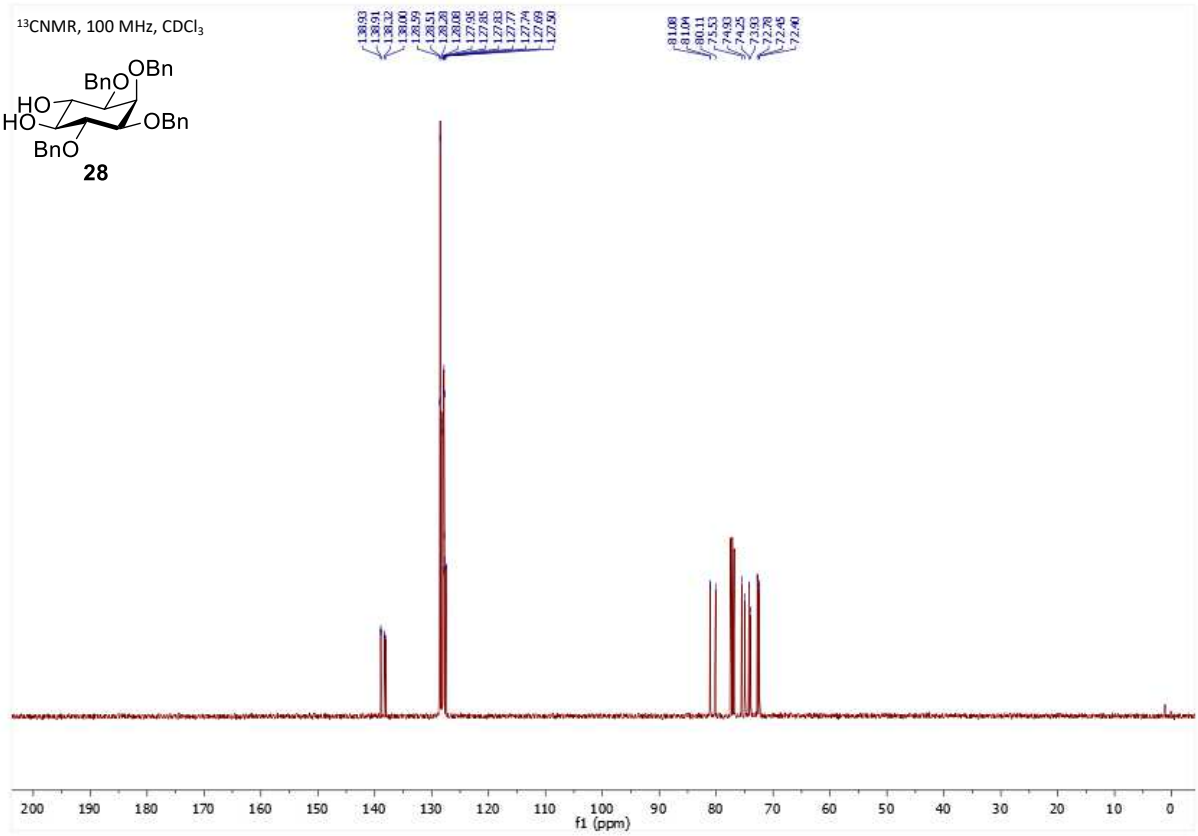

^{1}H-^{1}H COSY

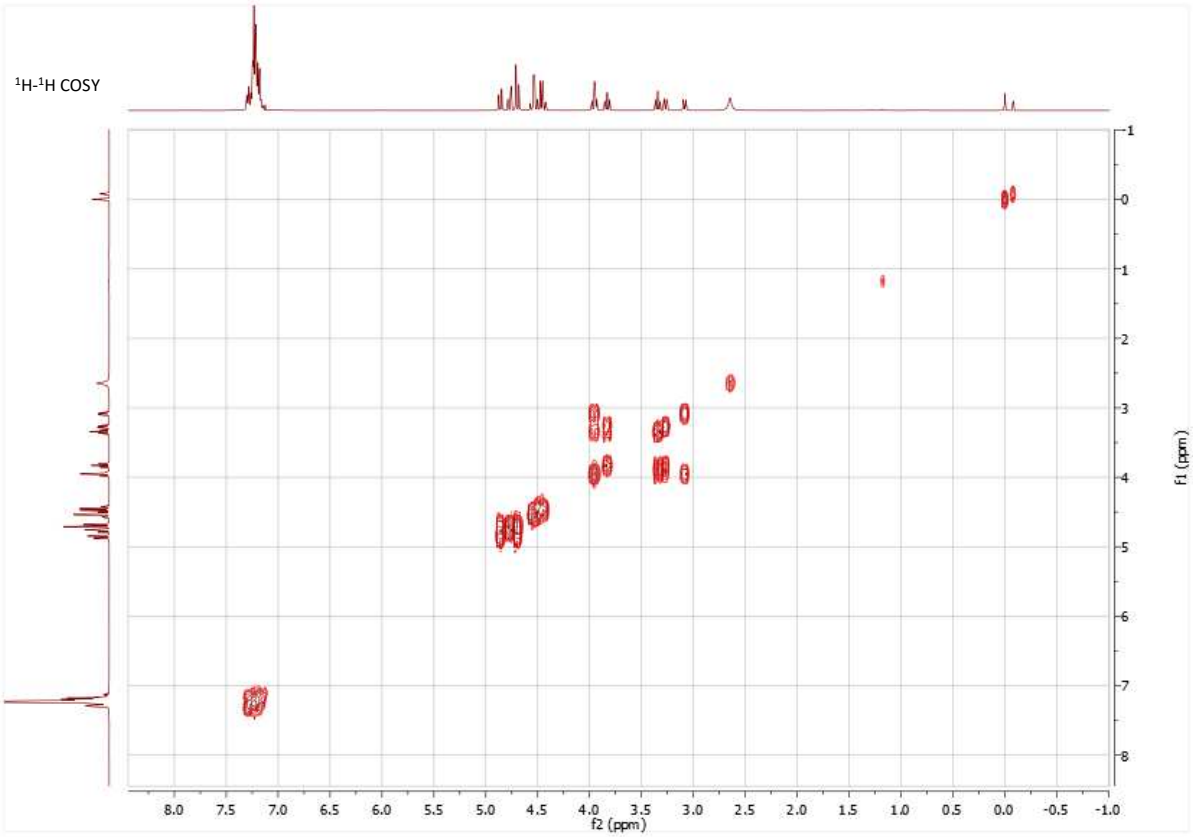

^{1}H-^{13}C HSQC

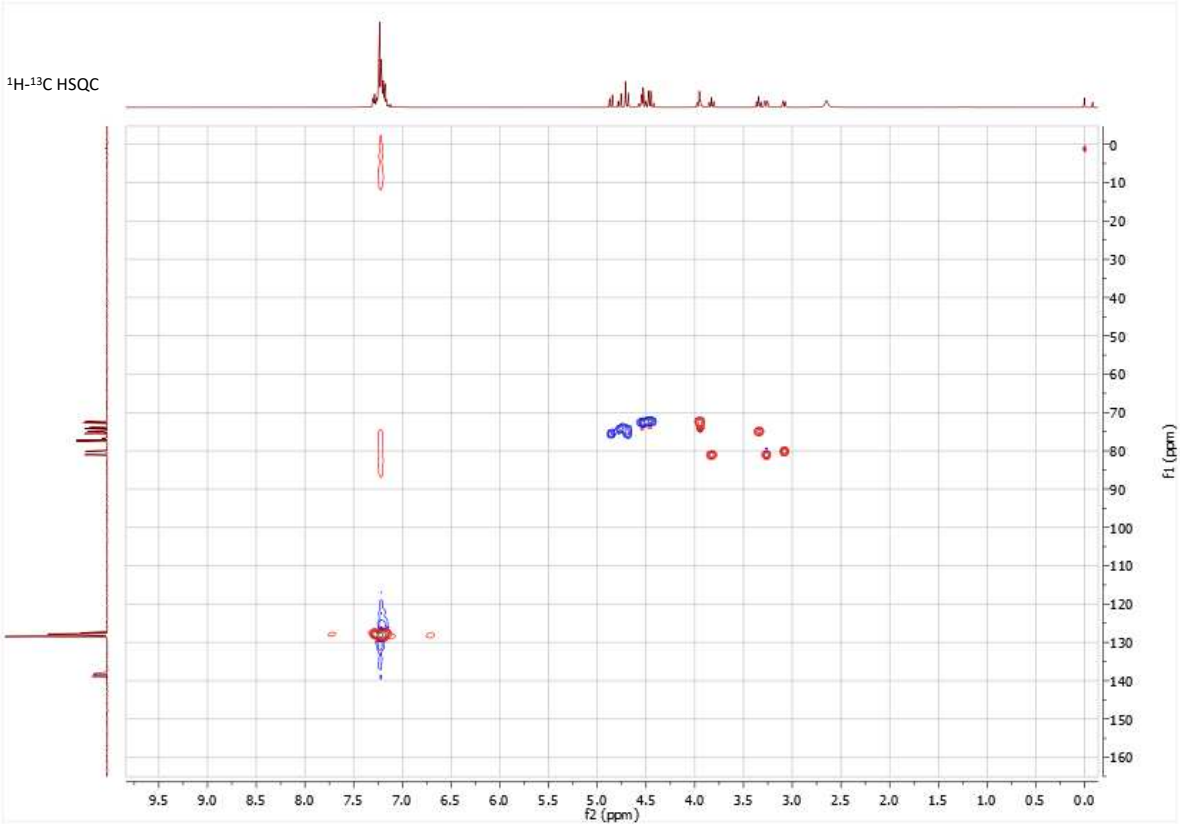

DL-1,2,3,6-Tetra-*O*-benzyl-*myo*-inositol-4-bis[2-(methanesulfonyl)ethyl]phosphate (**87**)

^{1}HNMR, 400 MHz, $CDCl_3$

87

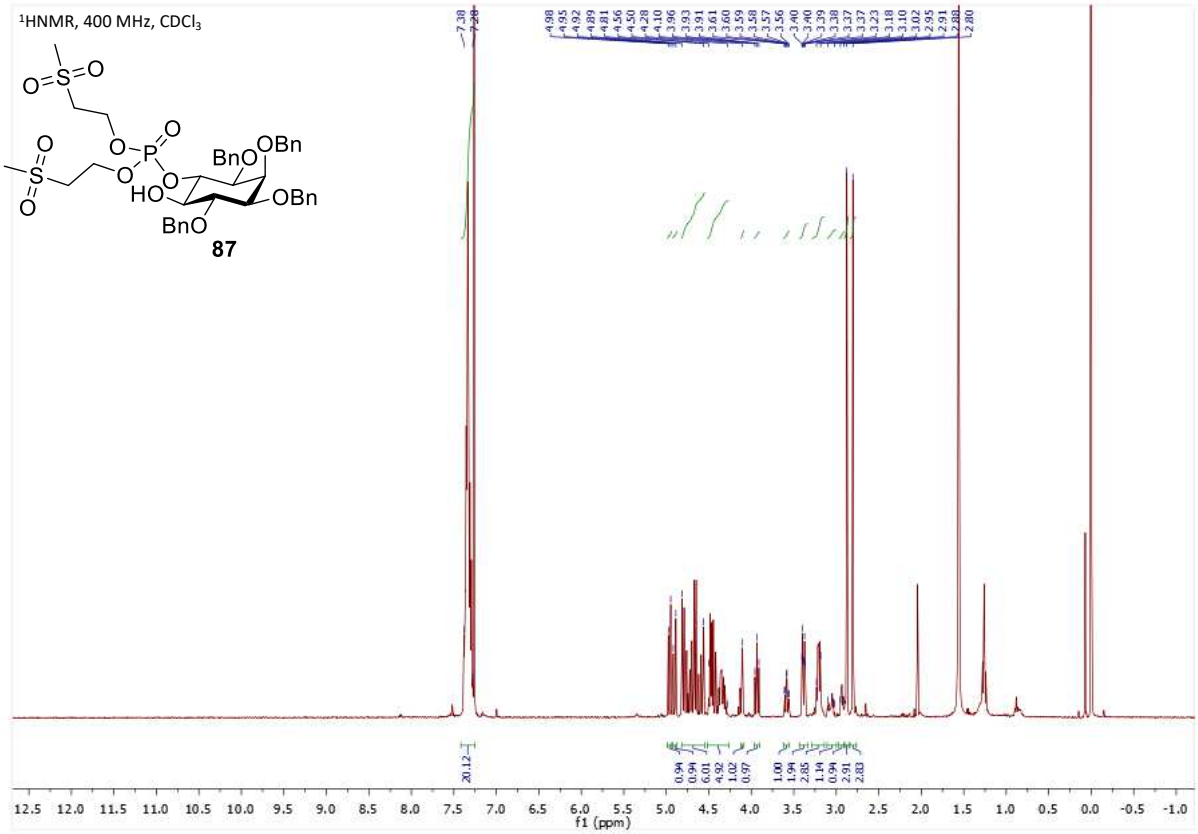

^{31}PNMR, 162 MHz, $CDCl_3$

87

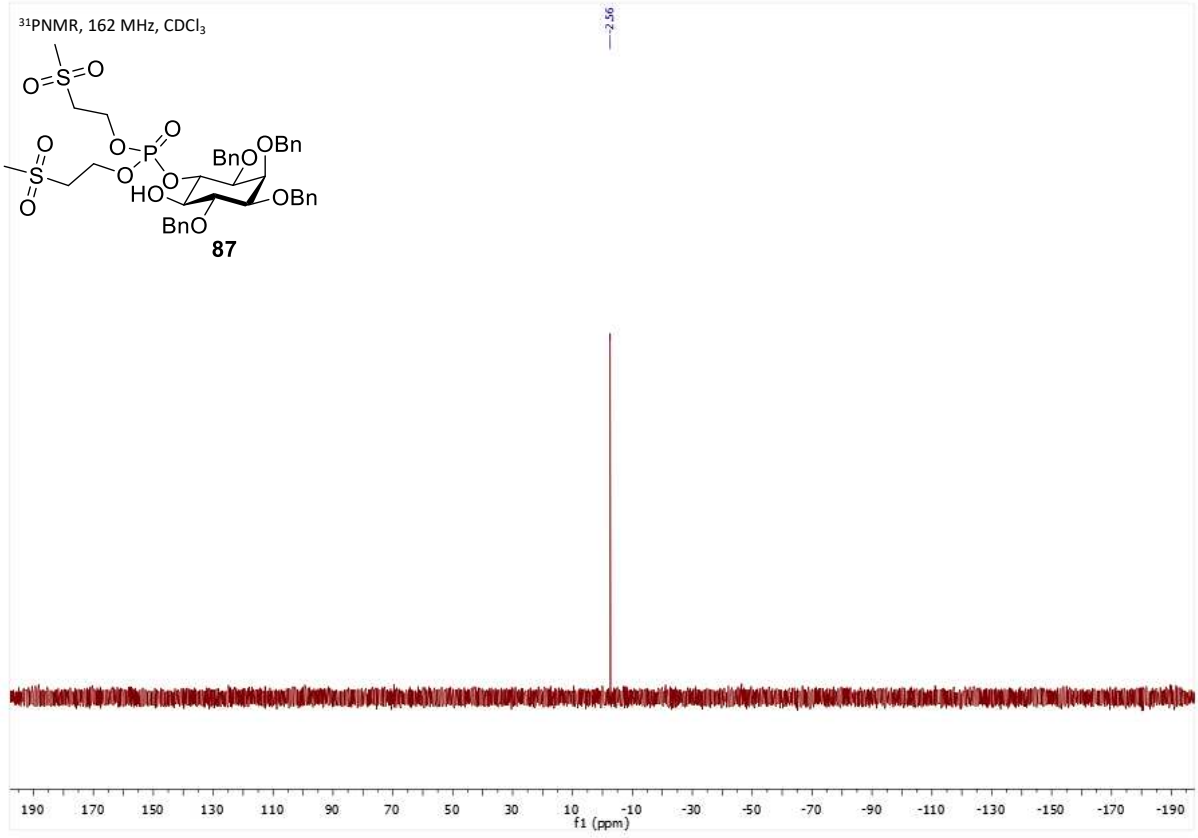

^{13}CNMR, 100 MHz, $CDCl_3$

87

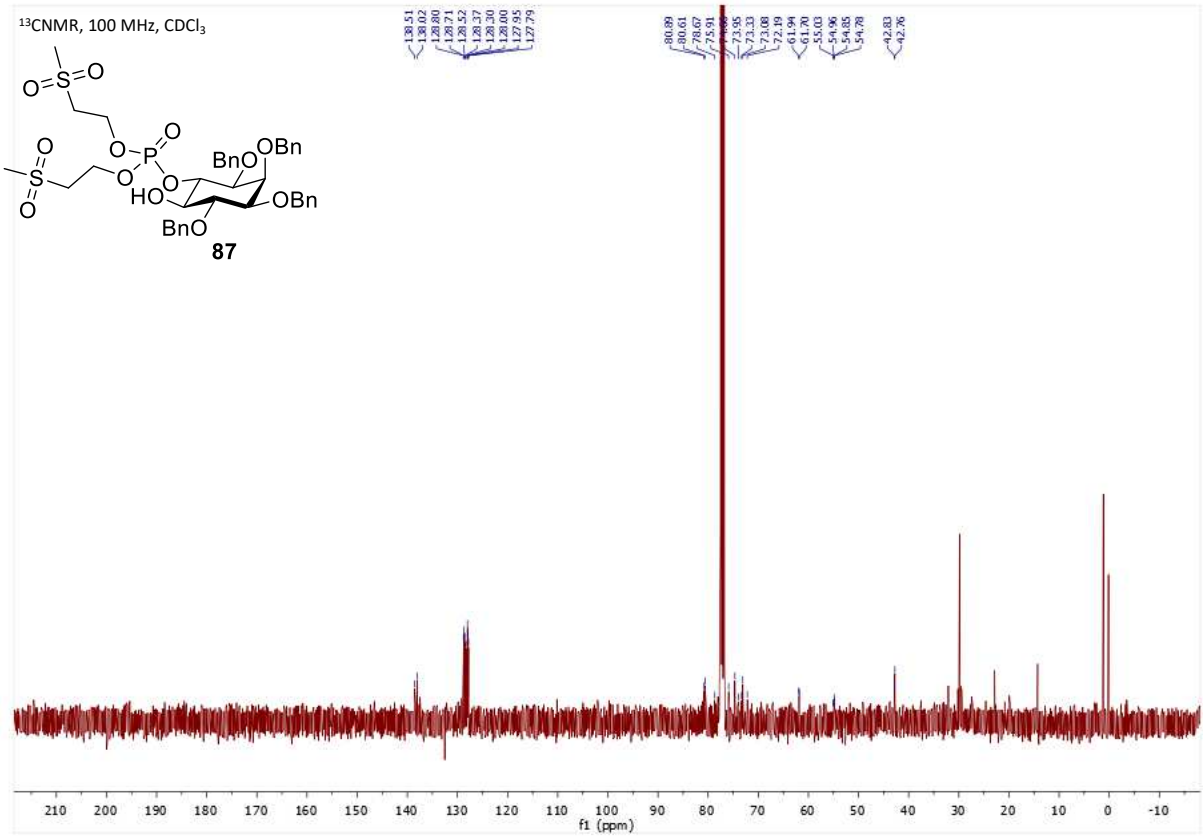

^{1}H-^{1}H COSY

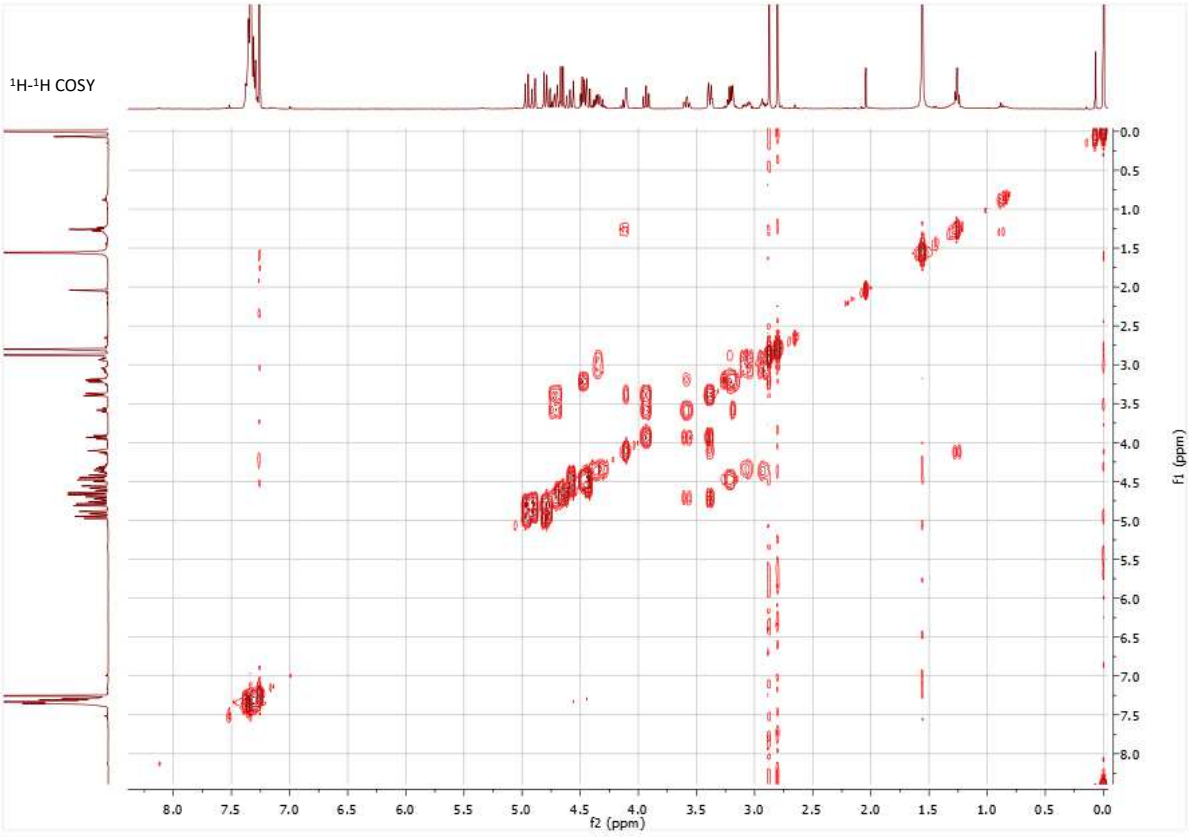

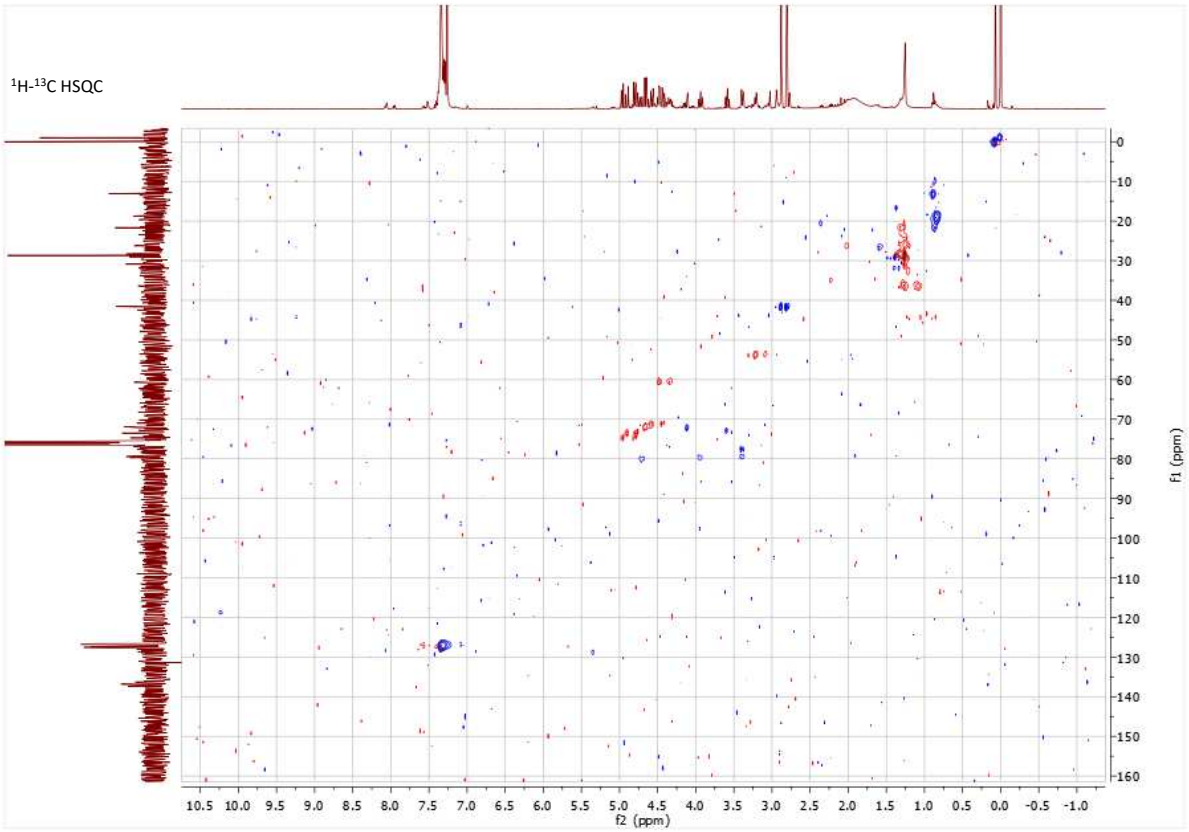

DL-1,2,3,6-Tetra-*O*-benzyl-*myo*-inositol-5-bis[2-(methanesulfonyl)ethyl]phosphate (**86**)

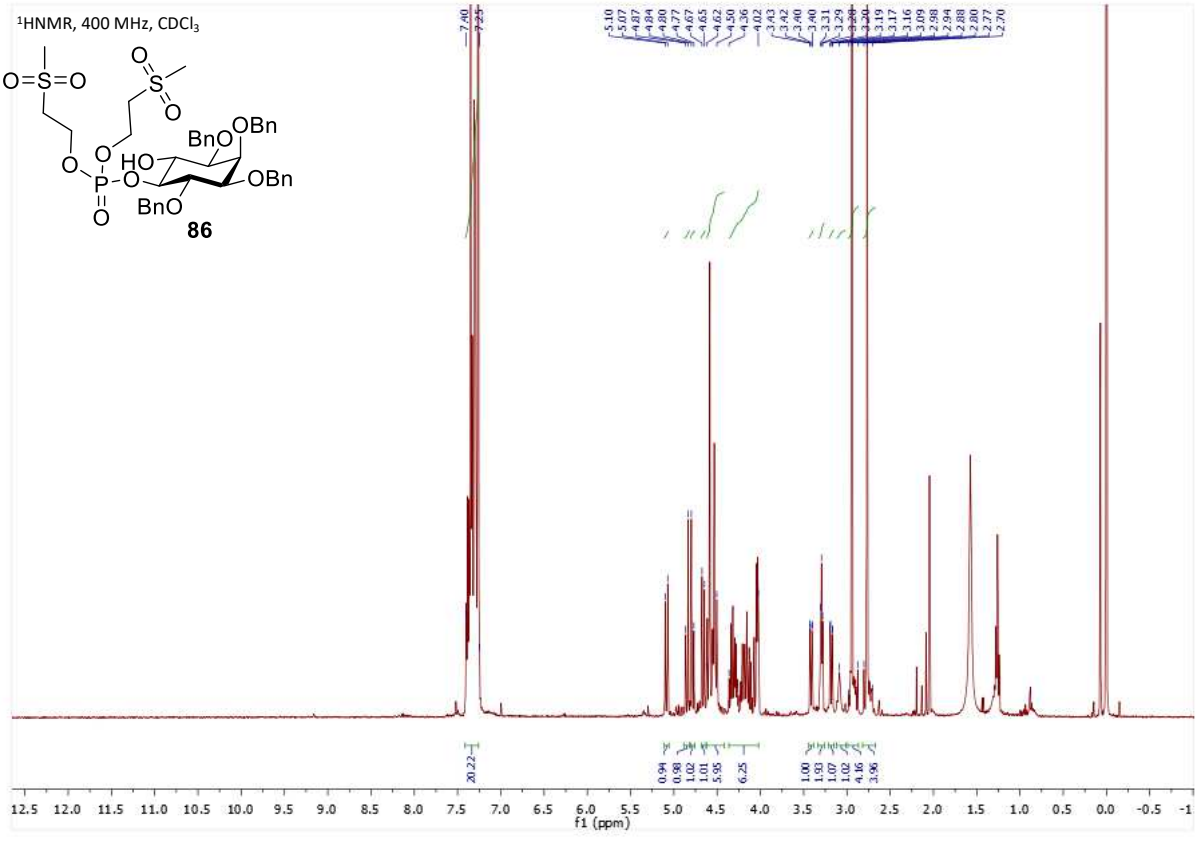

^{31}PNMR, 162 MHz, $CDCl_3$

86

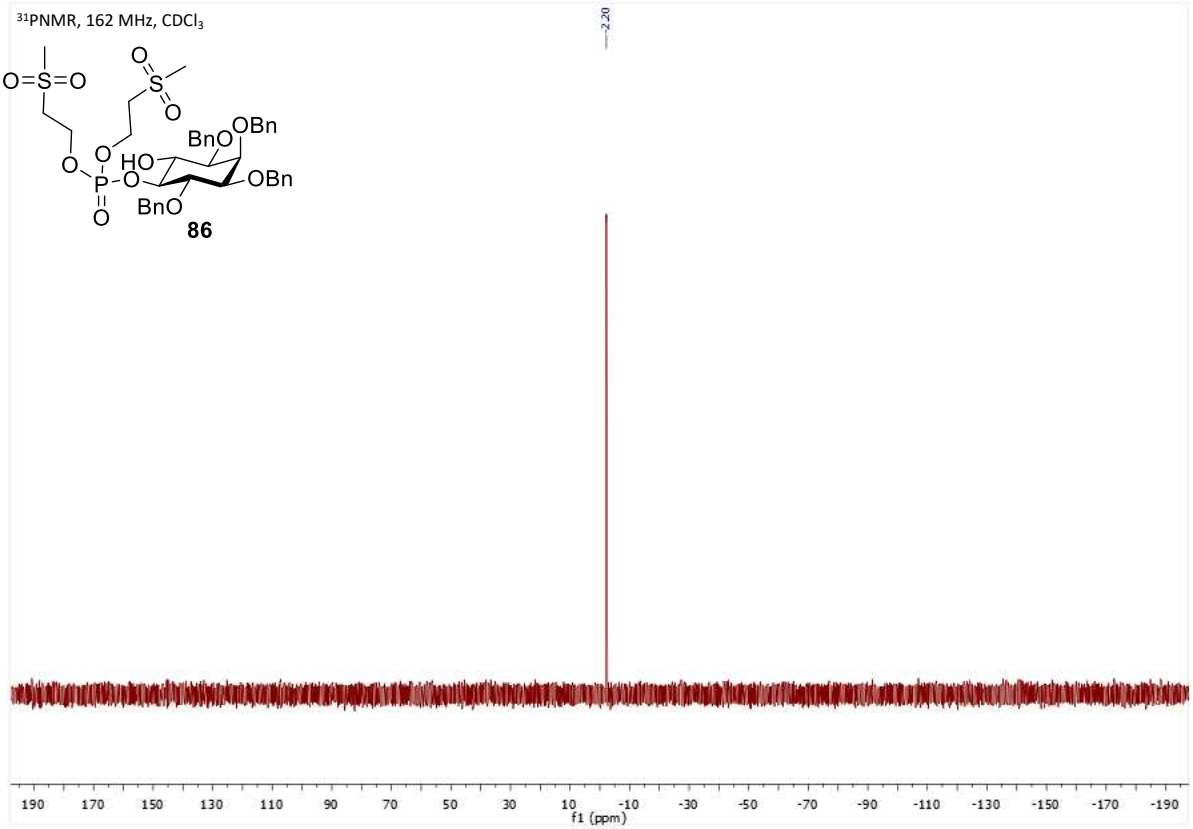

^{13}CNMR, 100 MHz, $CDCl_3$

86

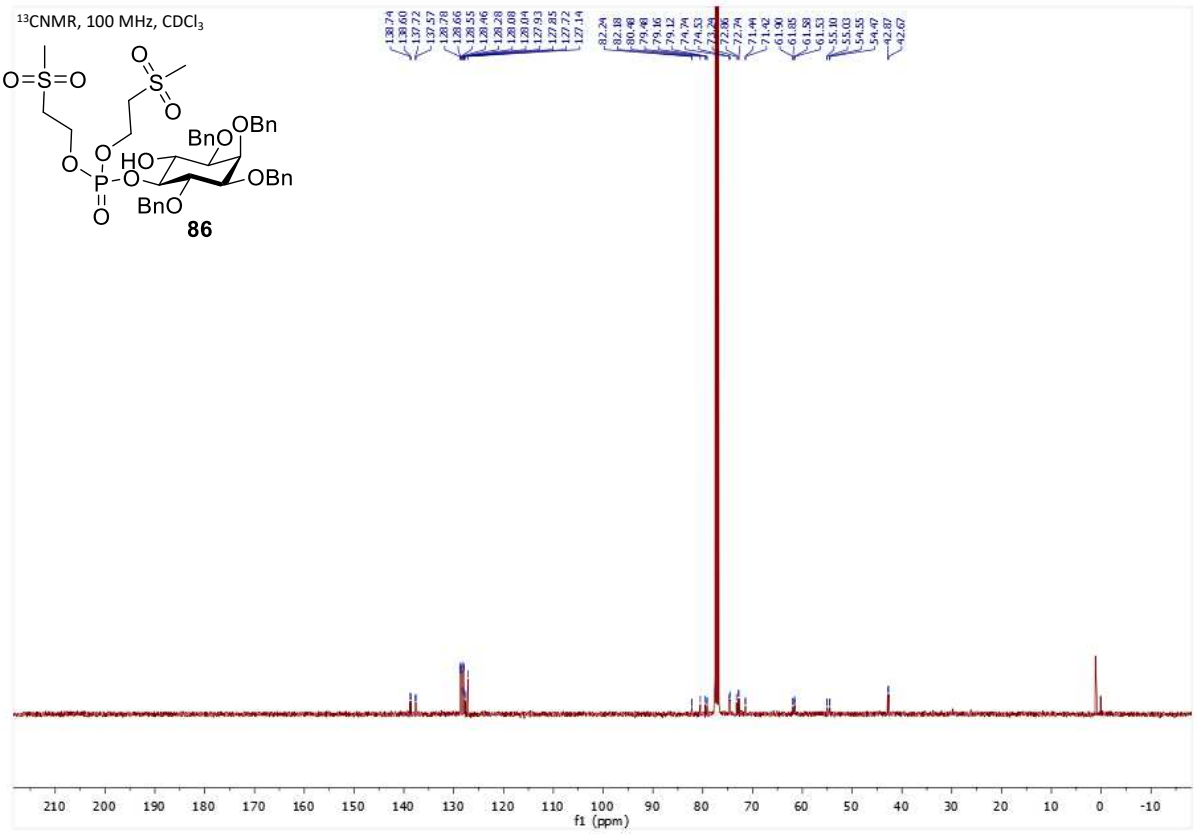

^{1}H-^{1}H COSY

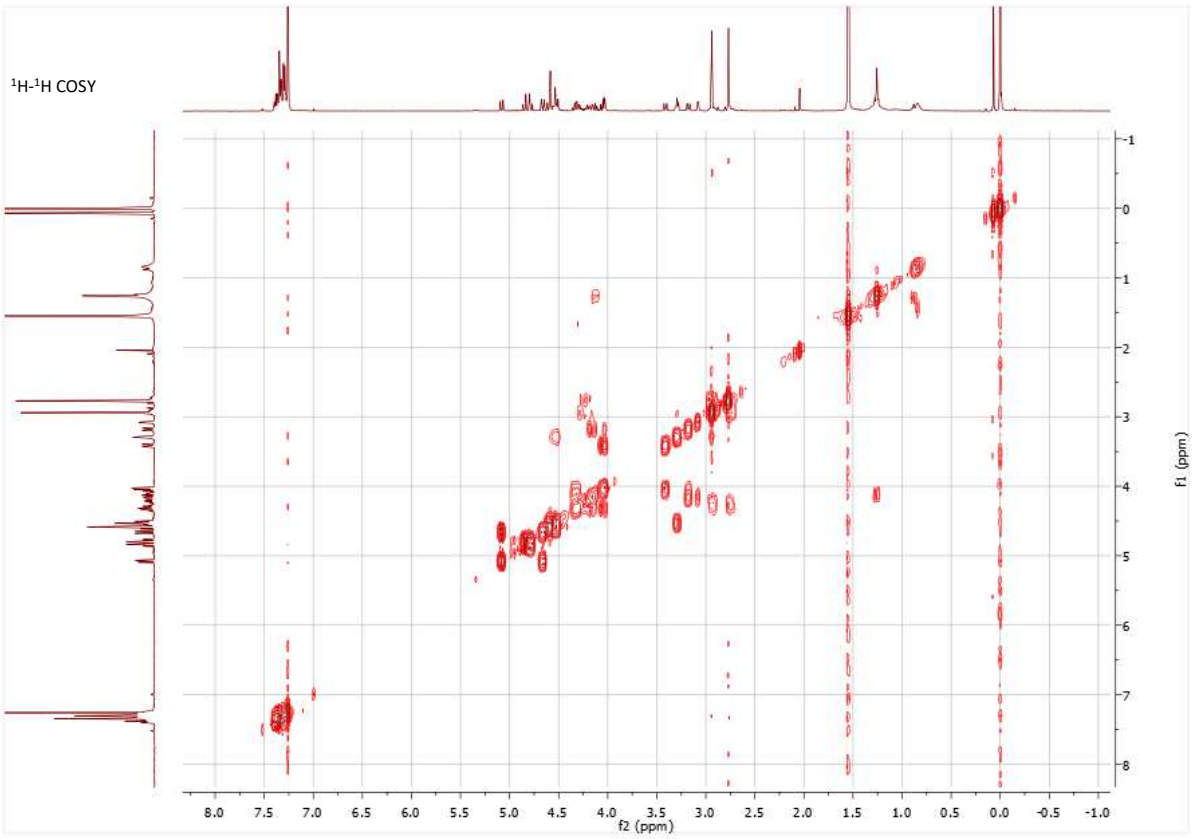

^{1}H-^{13}C HSQC

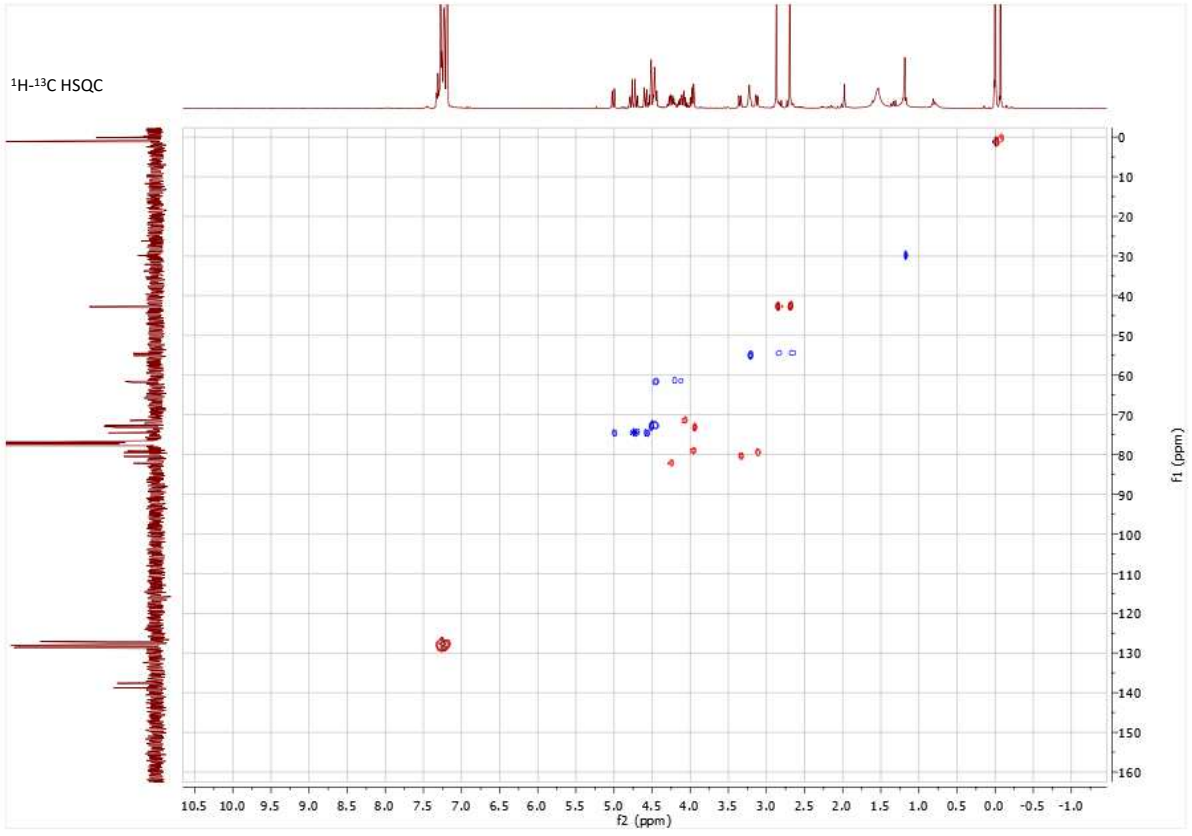

DL-1,2,3,6-Tetra-*O*-benzyl-*myo*-inositol-4,5-bisbis[2-(methanesulfonyl)ethyl]phosphate (**29**)

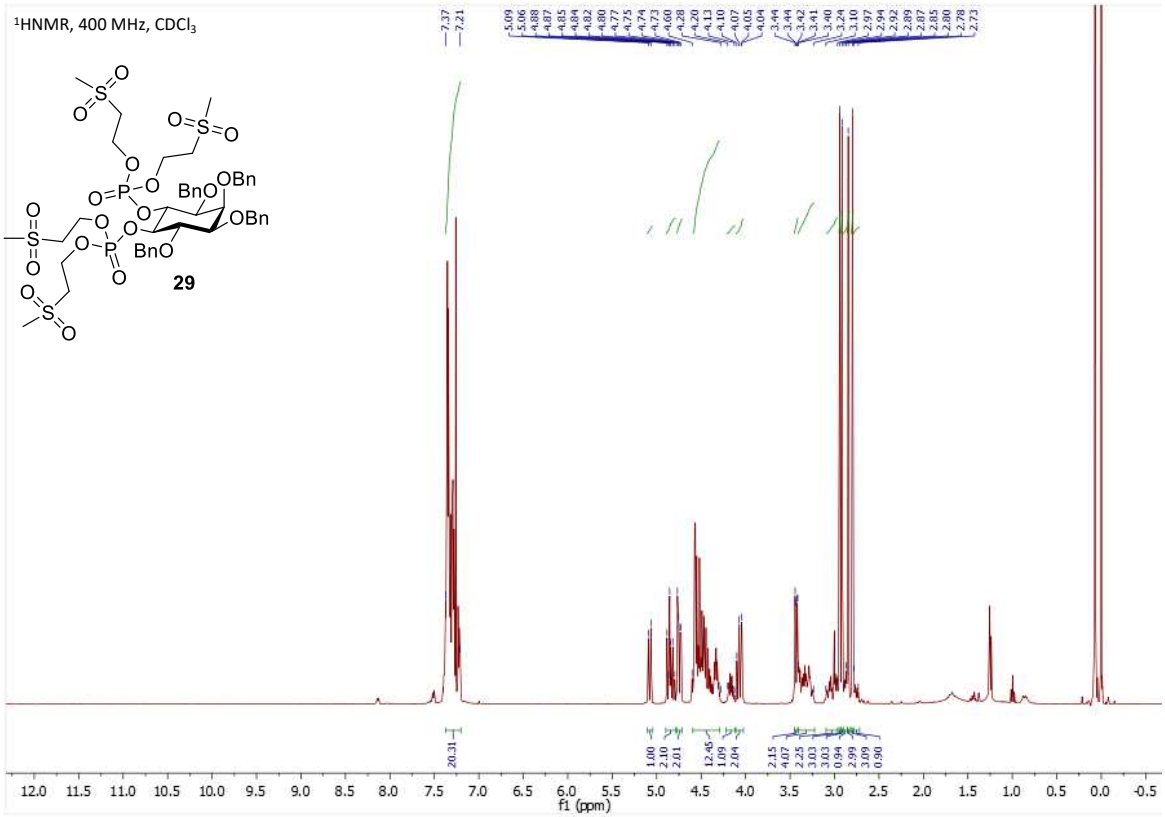

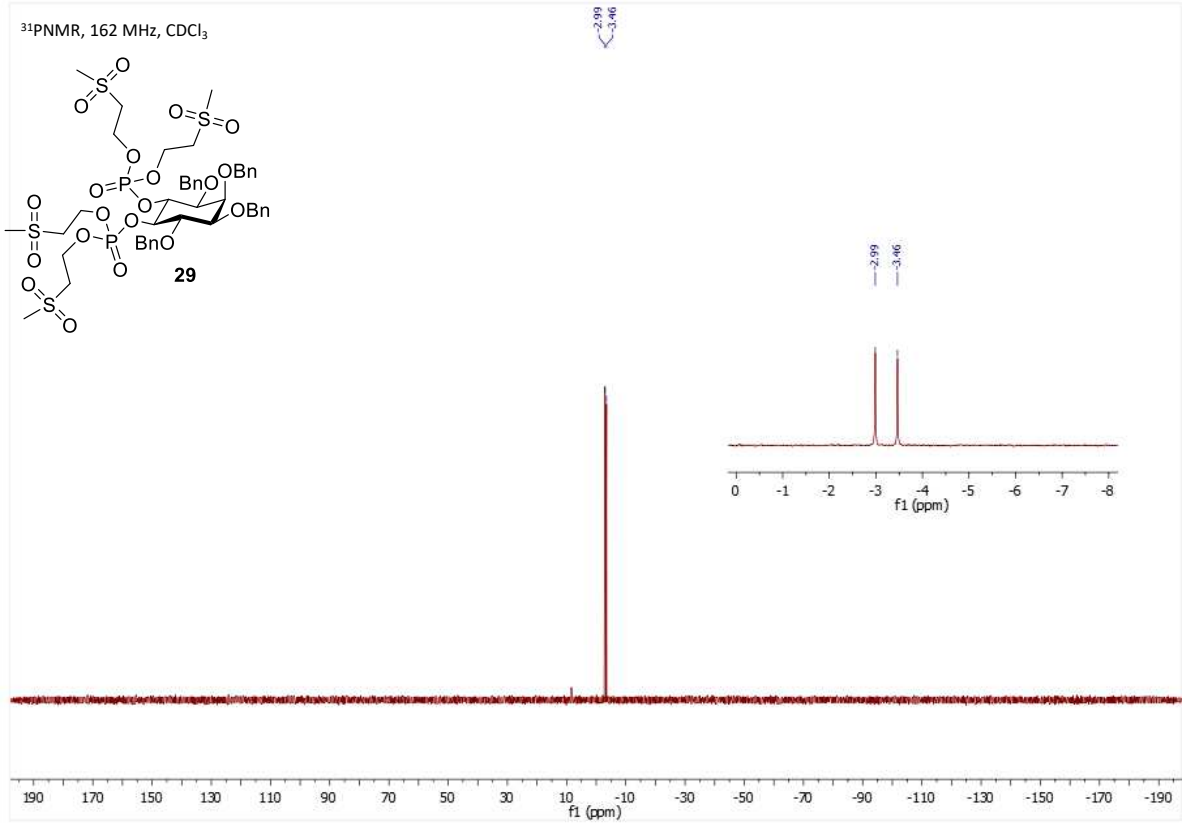

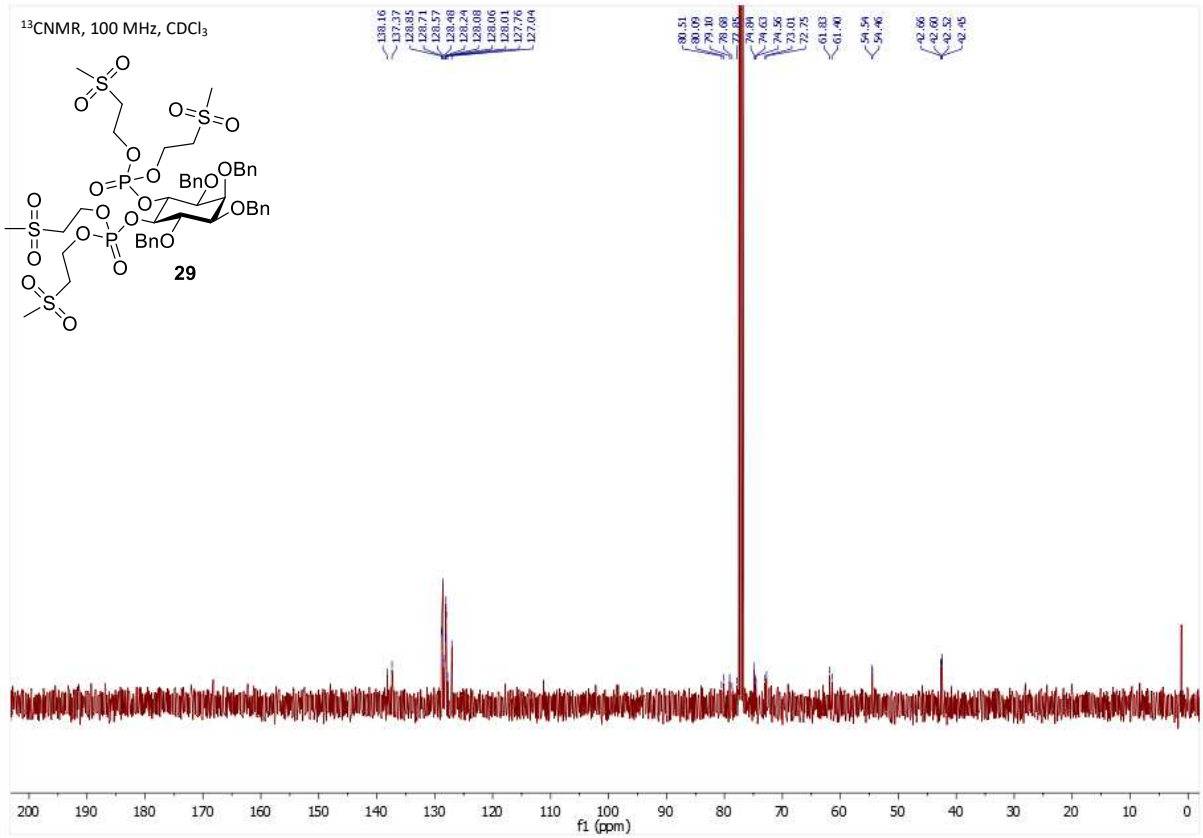
13CNMR, 100 MHz, CDCl3
29
f1 (ppm)

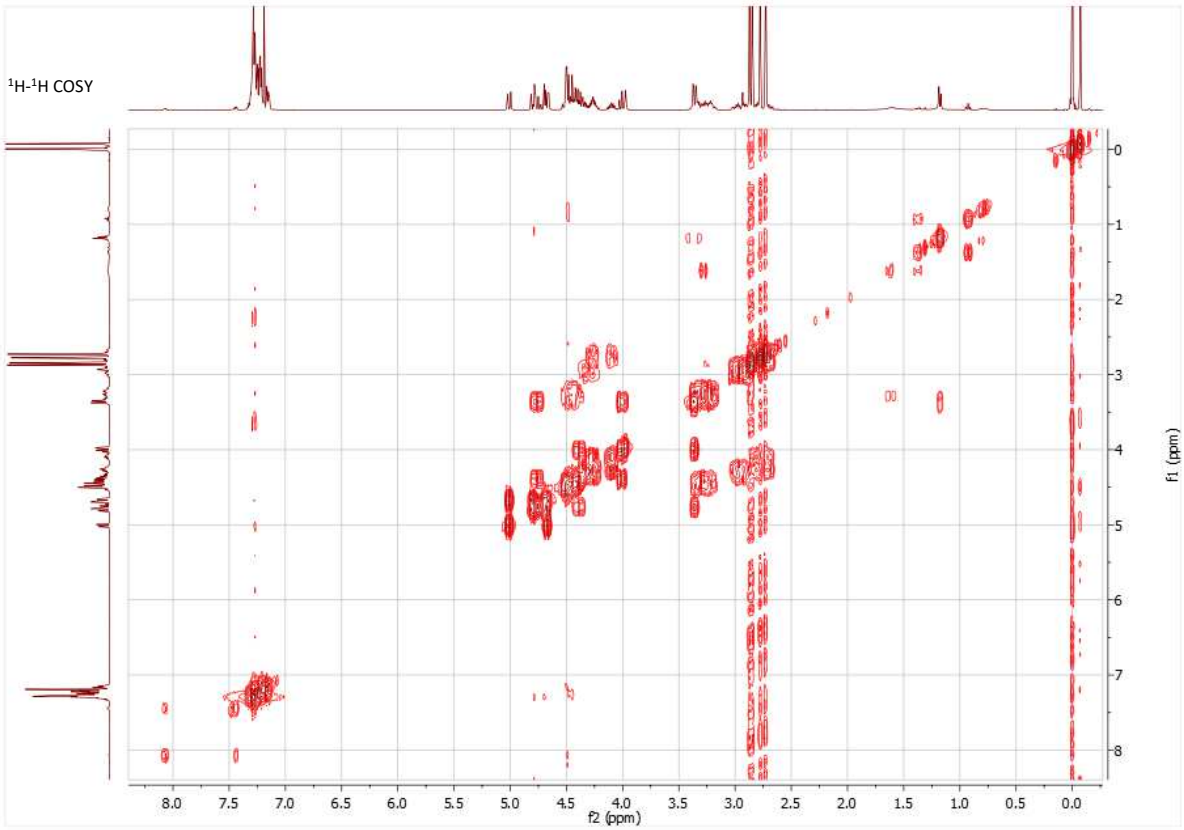
1H-1H COSY
f2 (ppm)
f1 (ppm)

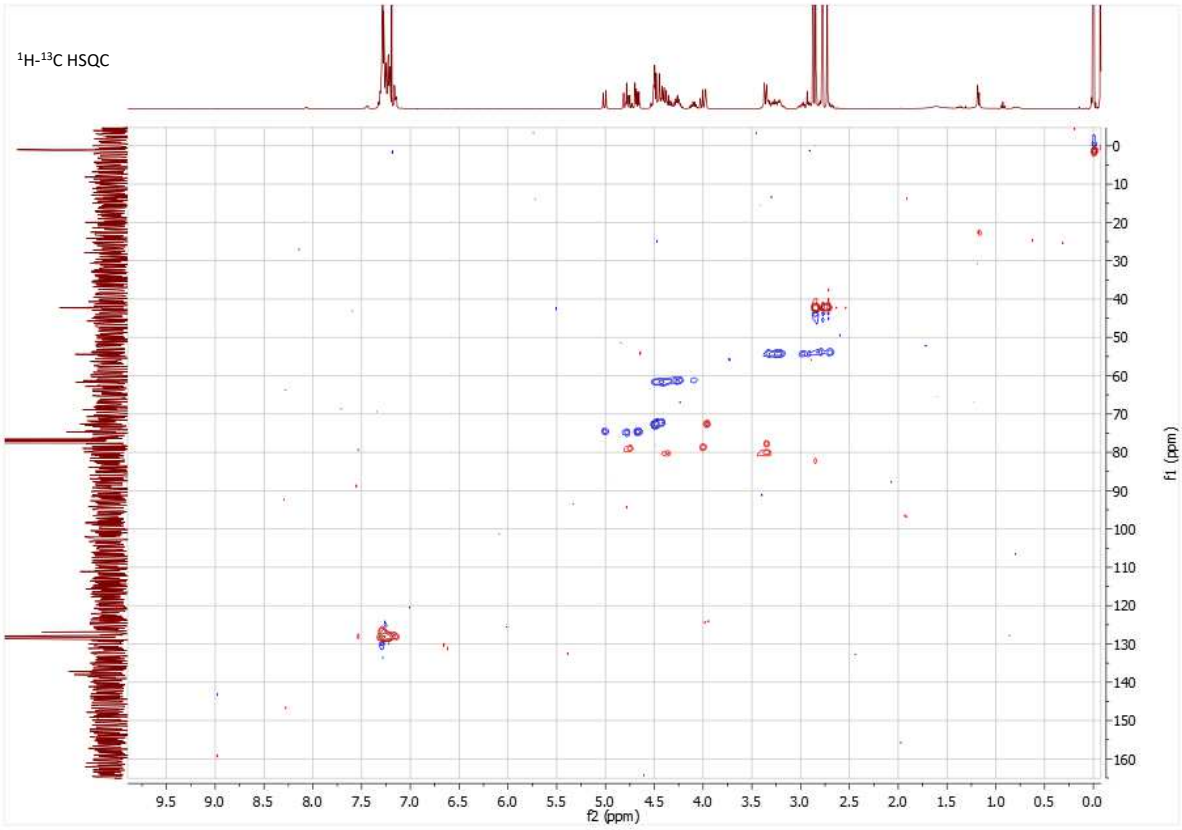

DL-1,2,3,6-Tetra-*O*-benzyl-*myo*-inositol-4-dibenzylphosphate-5-bis[2-(methanesulfonyl)ethyl]phosphate (**88**)

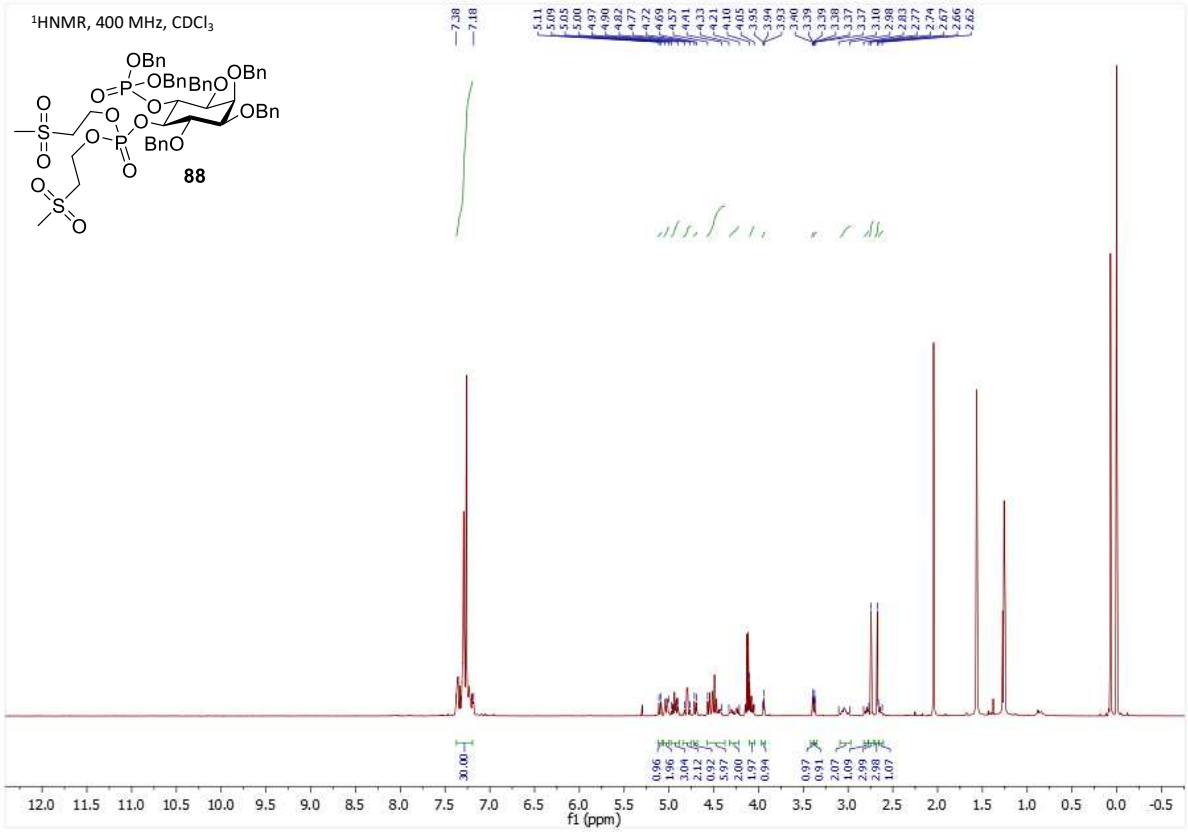

^{31}PNMR, 162 MHz, $CDCl_3$

88

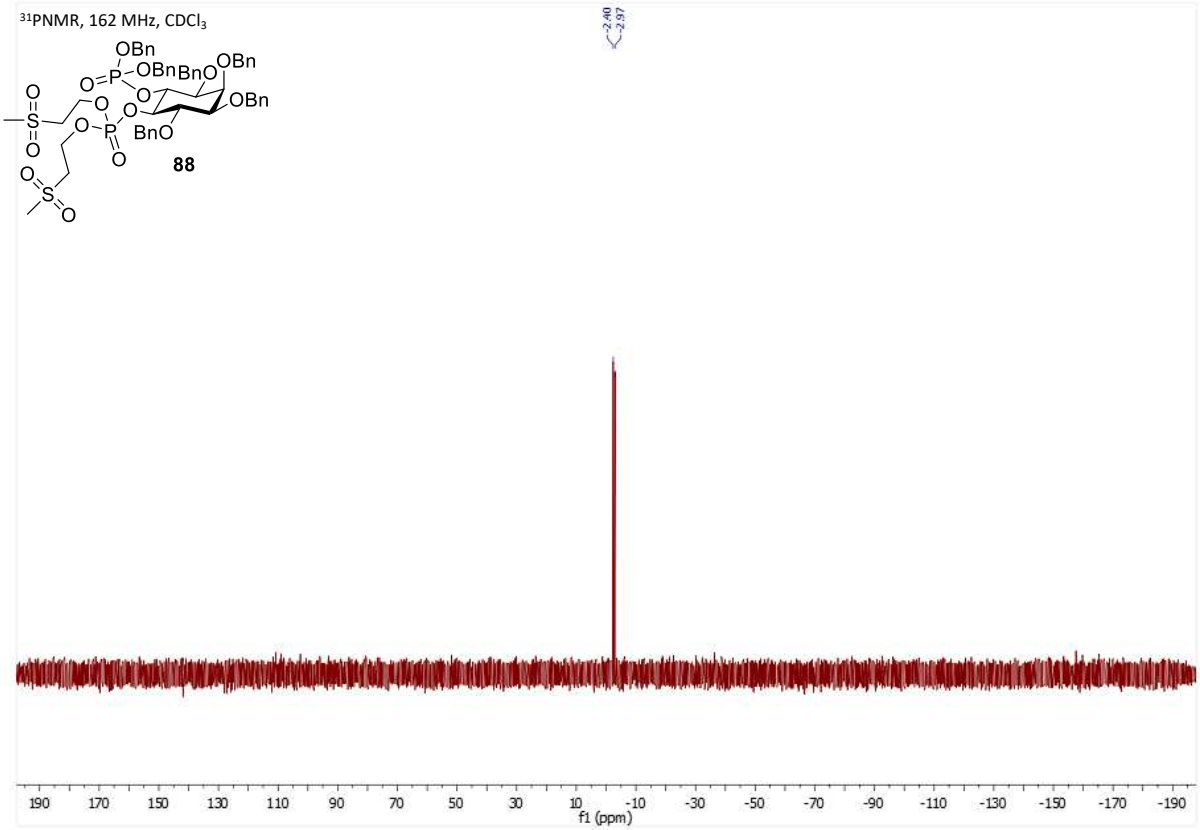

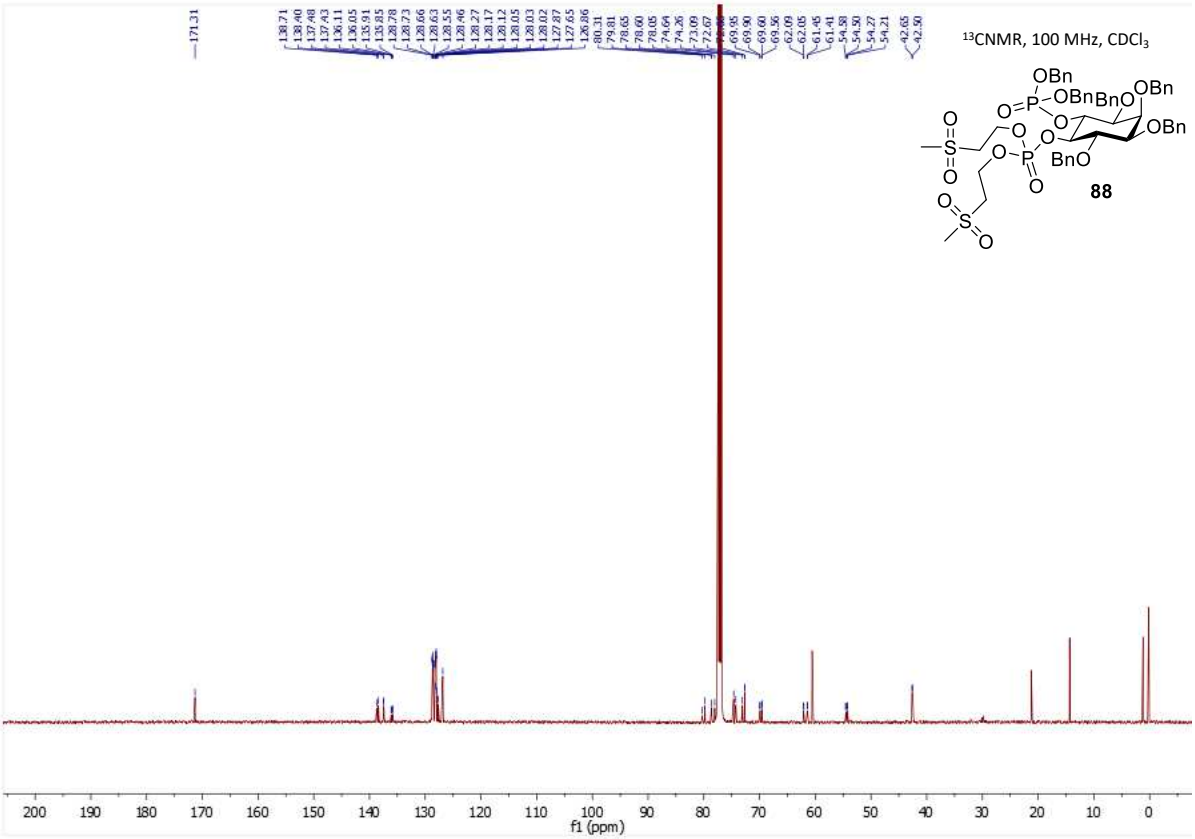

^{13}CNMR, 100 MHz, $CDCl_3$

88

^{1}H-^{1}H COSY

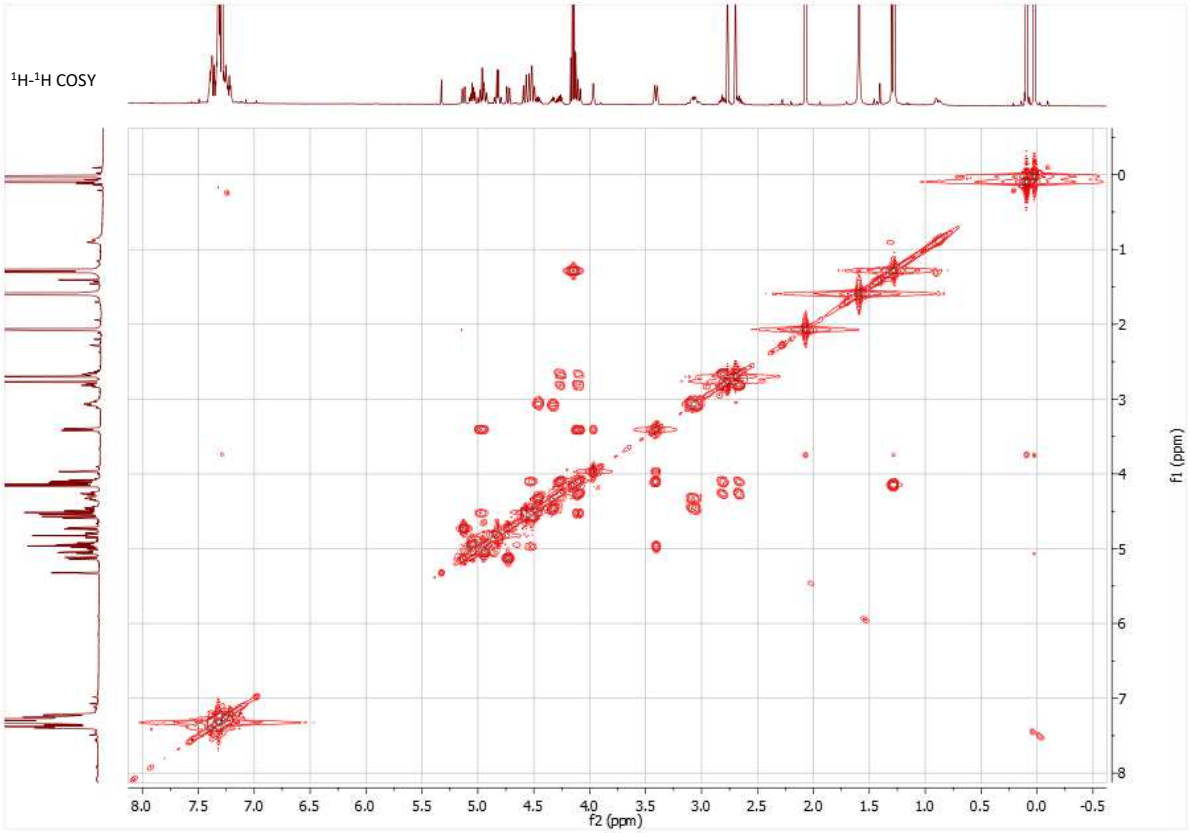

^{1}H-^{31}P HMBC

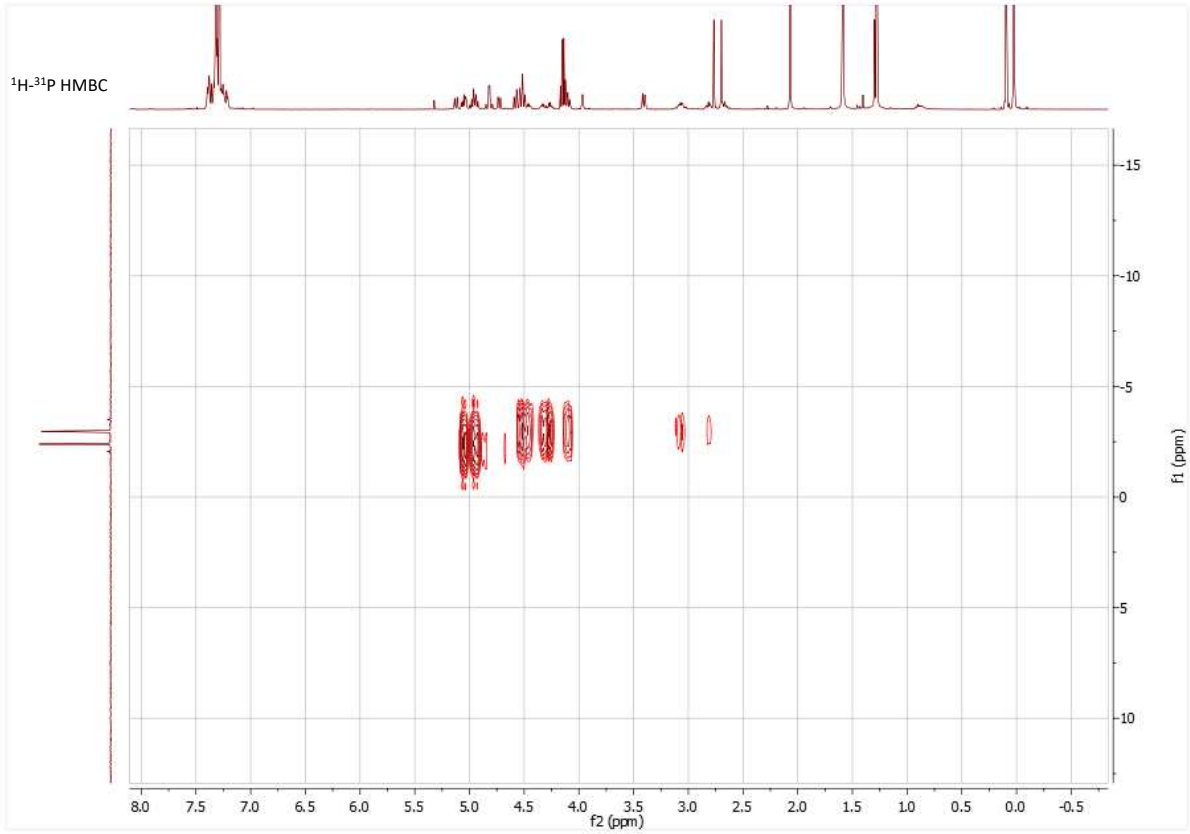

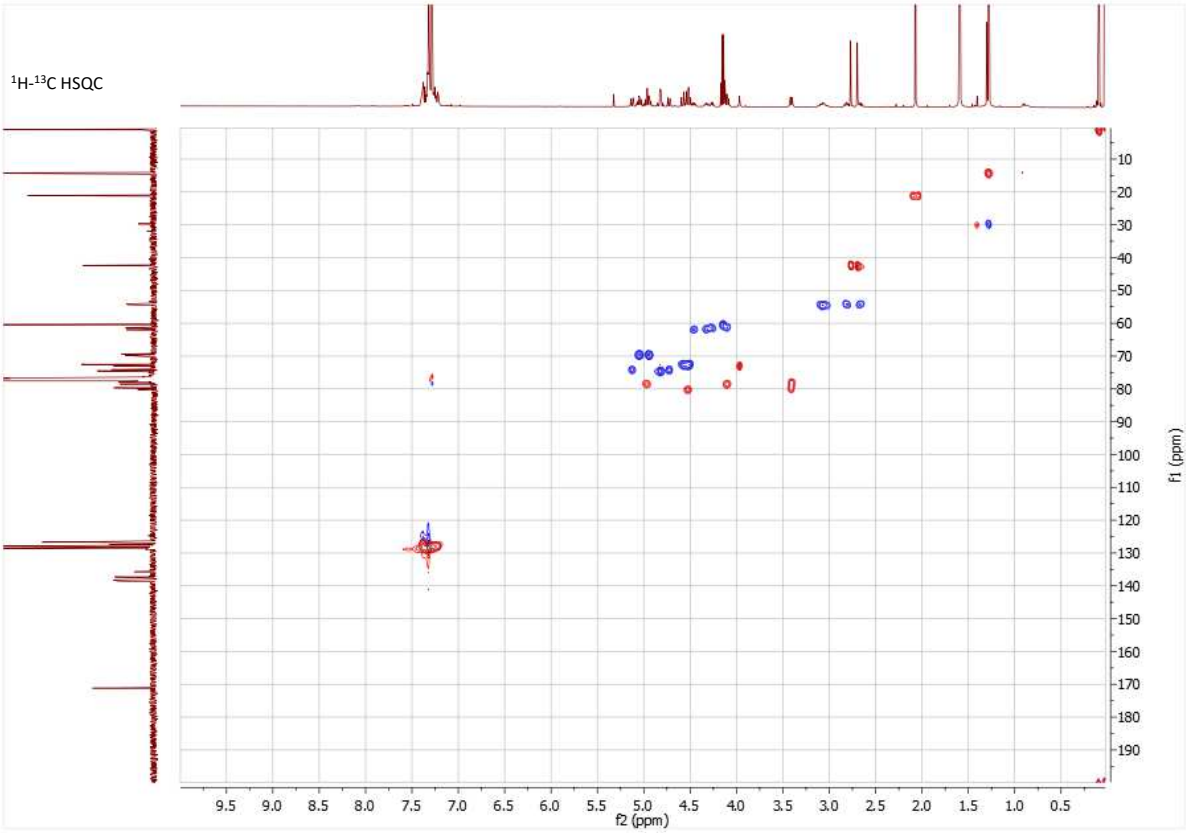

DL-5-Diphospho-*myo*-inositol-4-phosphate (**77**)

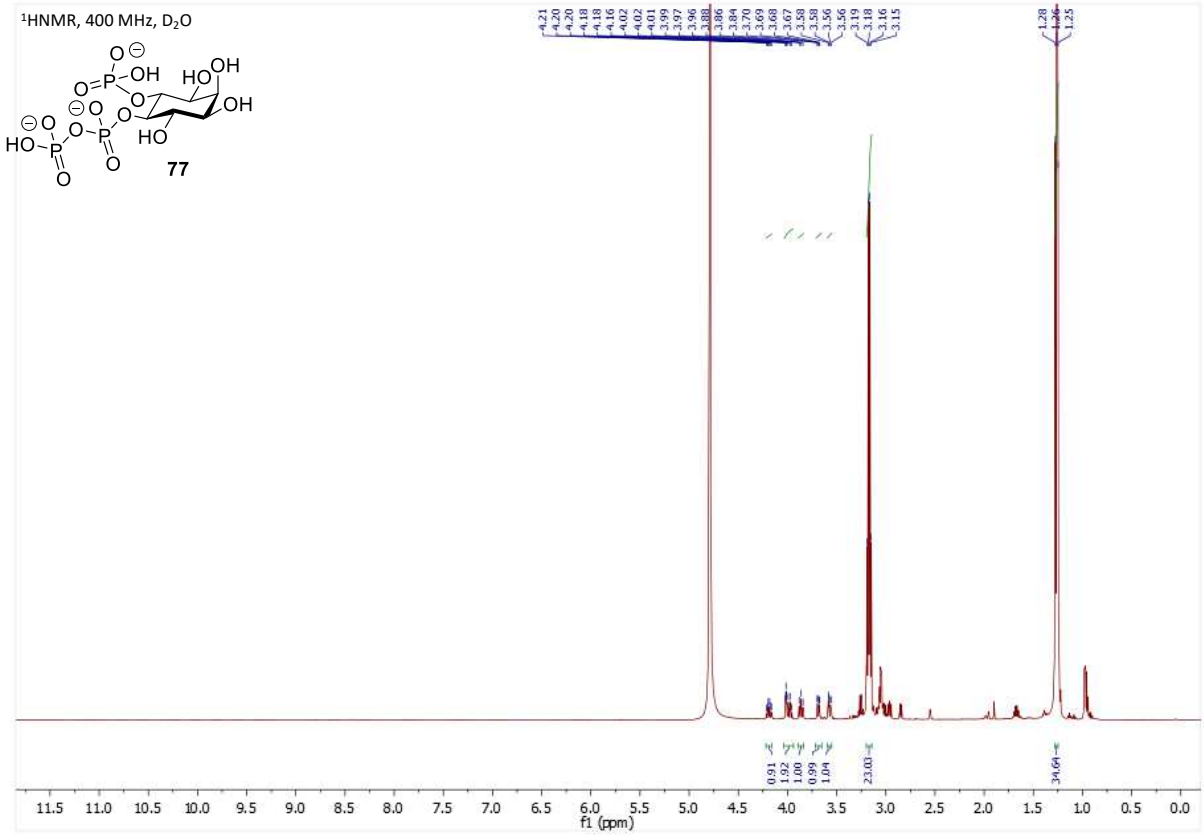

^{31}PNMR, 162 MHz, D_2O

77

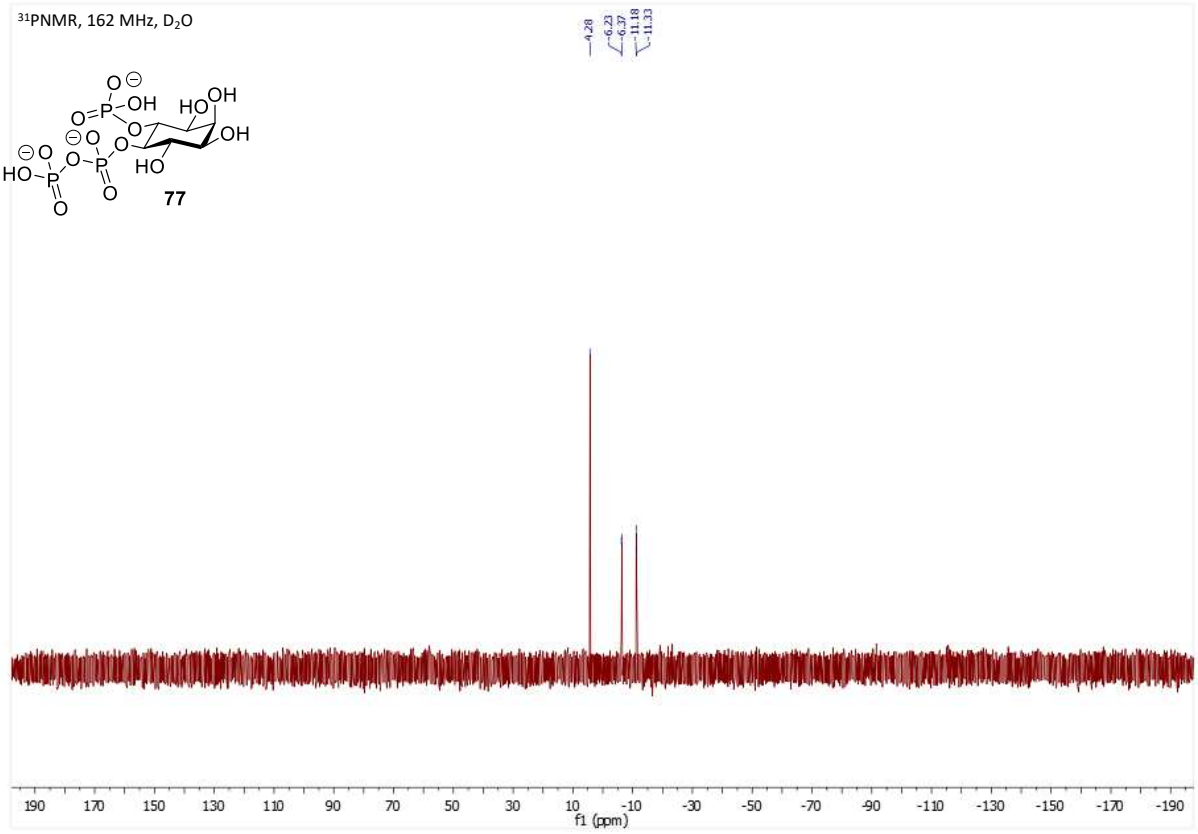

^{13}CNMR, 100 MHz, D_2O

77

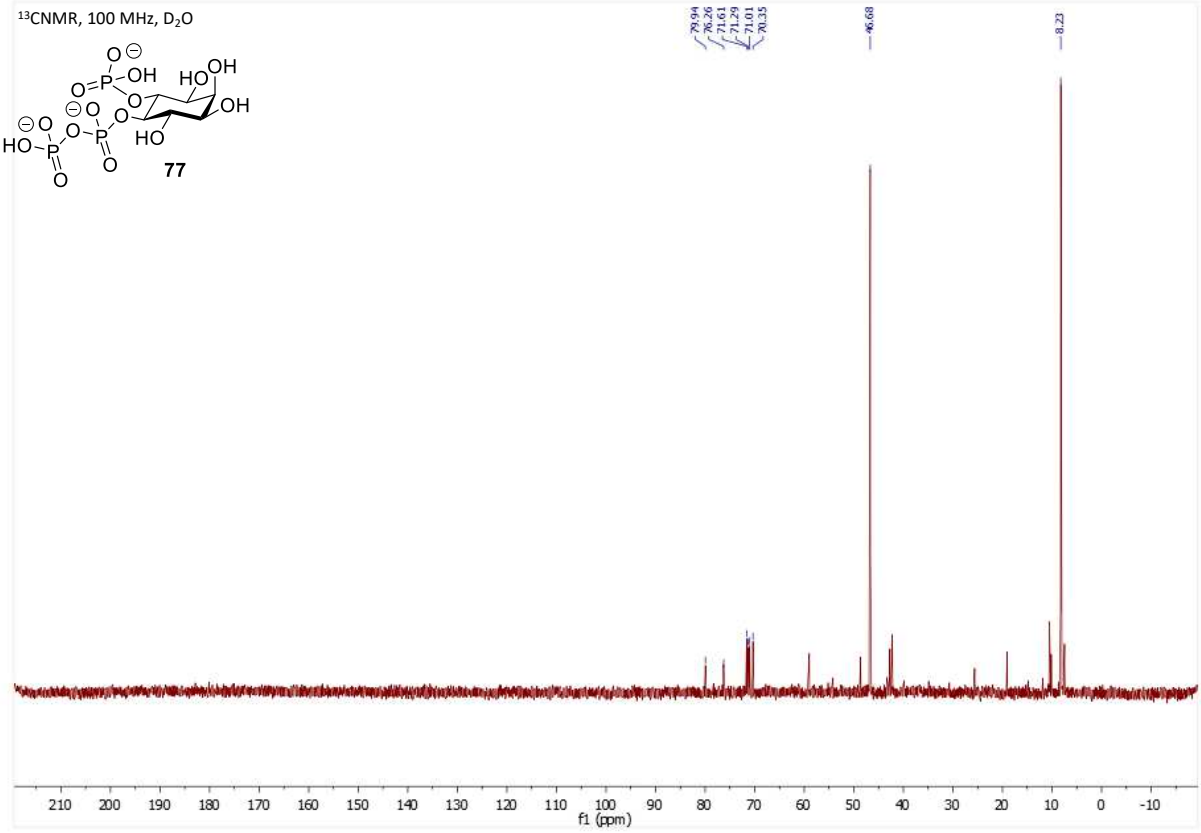

^{1}H-^{31}P HMBC

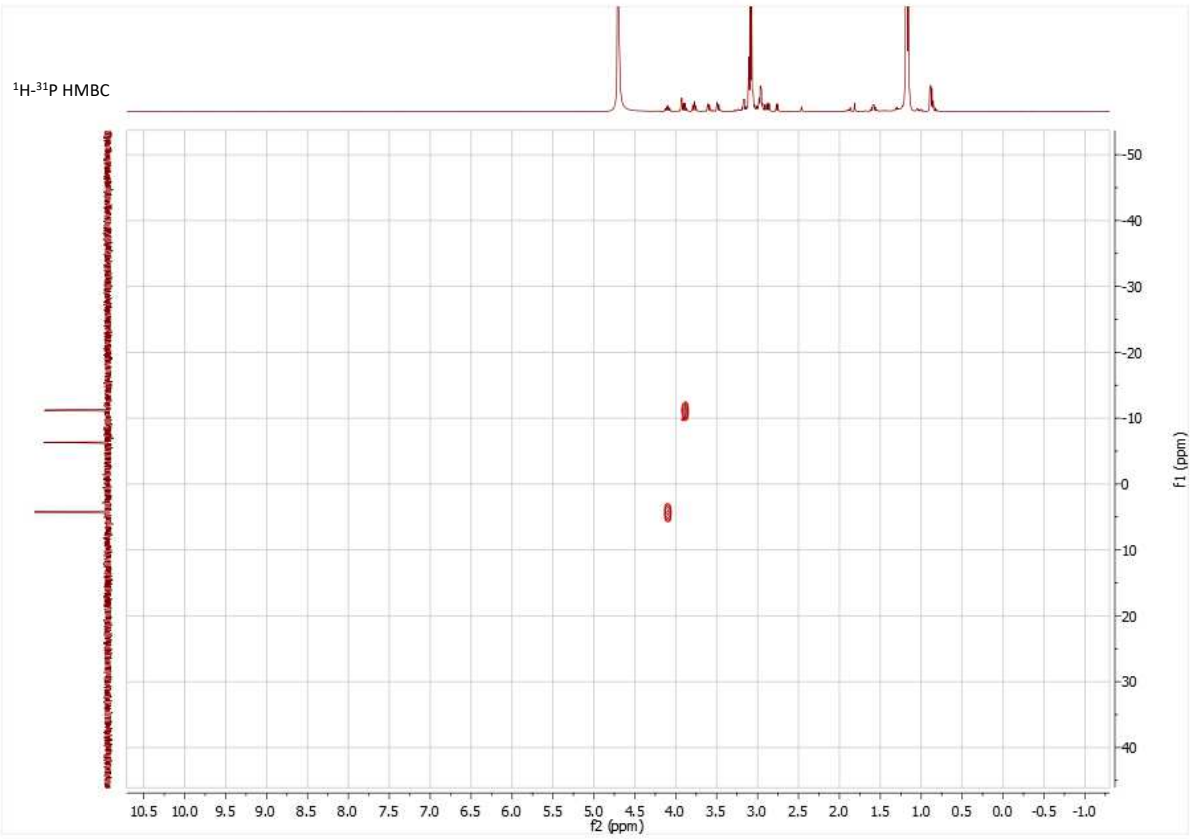

^{1}H-^{1}H COSY

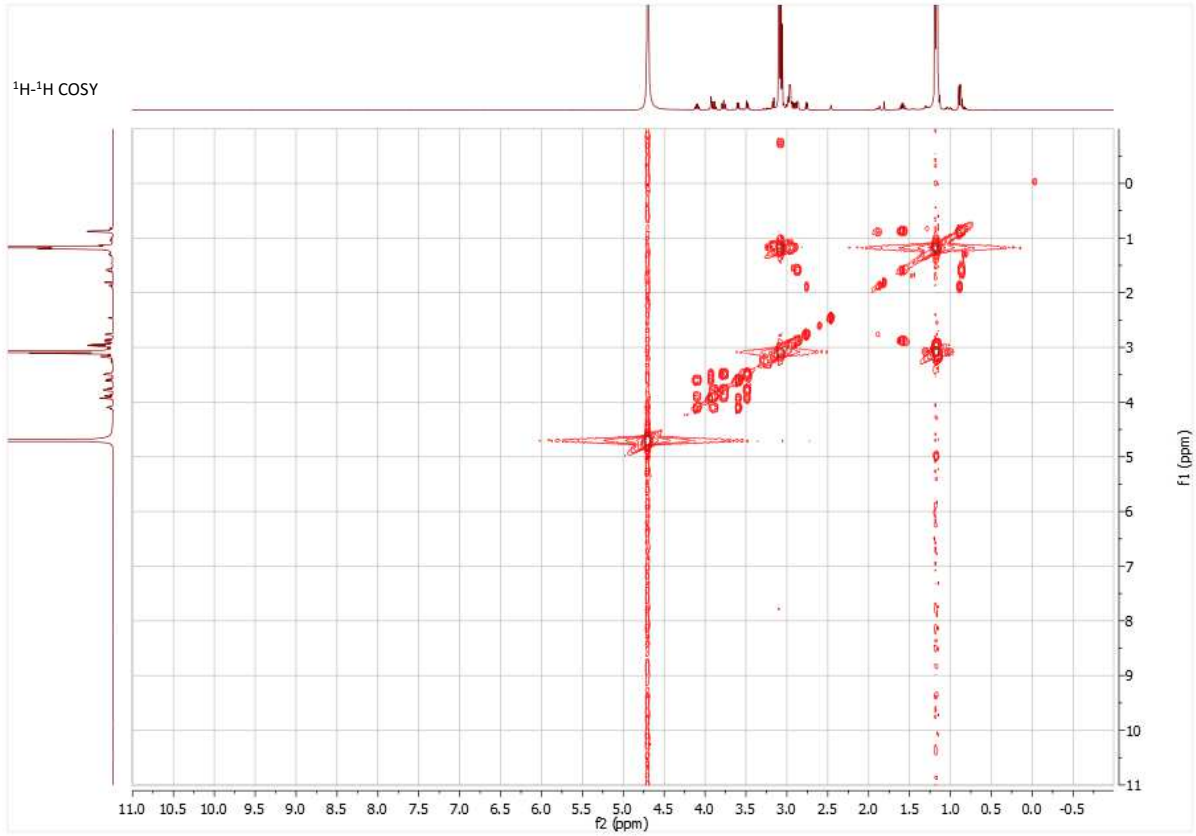

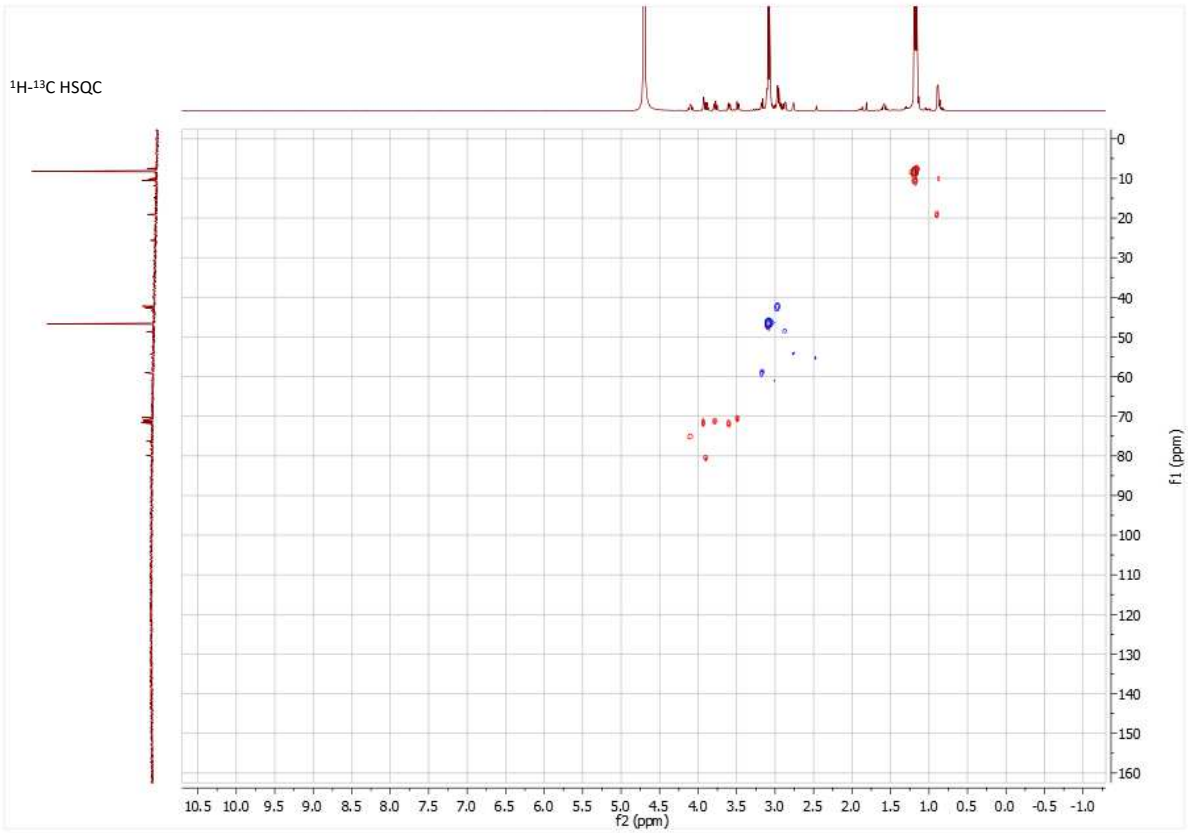

DL-1,2,3,6-Tetra-*O*-benzyl-*myo*-inositol-5-dibenzylphosphate-4-bis[2-(methanesulfonyl)ethyl]phosphate (**89**)

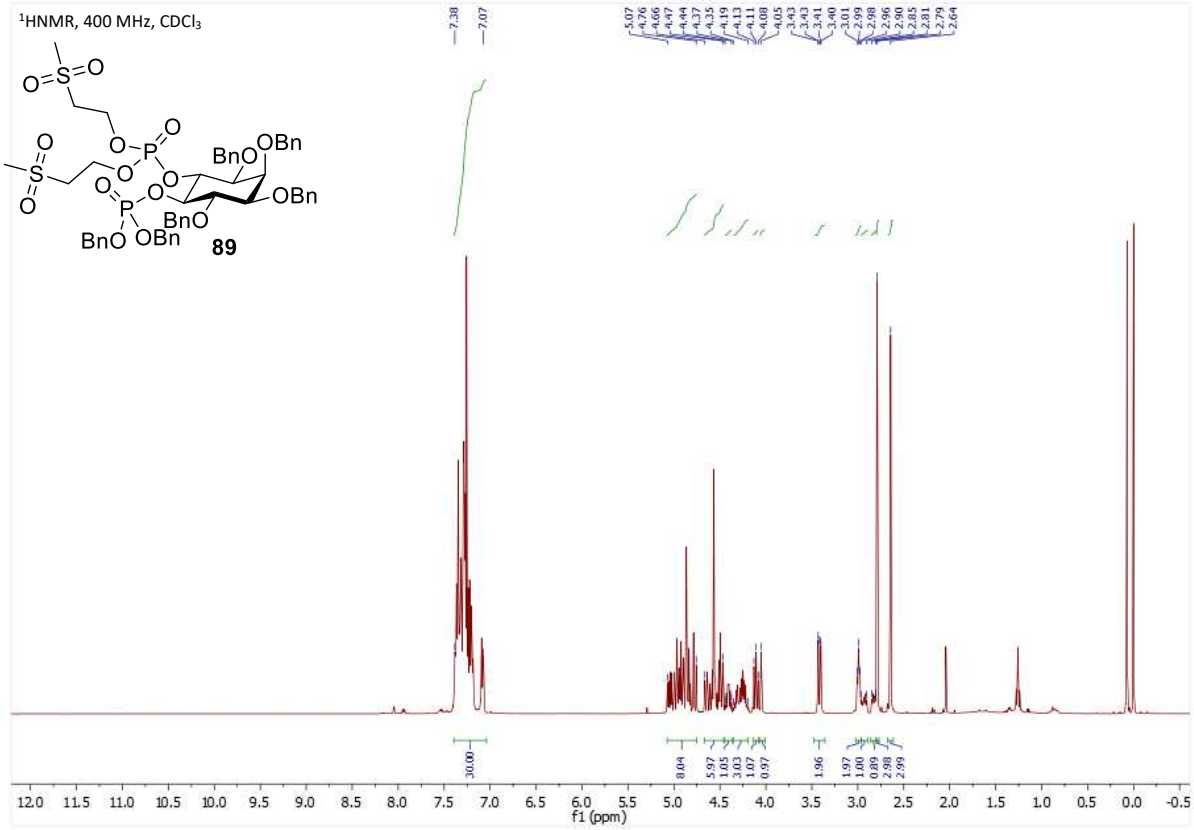

^{31}PNMR, 162 MHz, $CDCl_3$

89

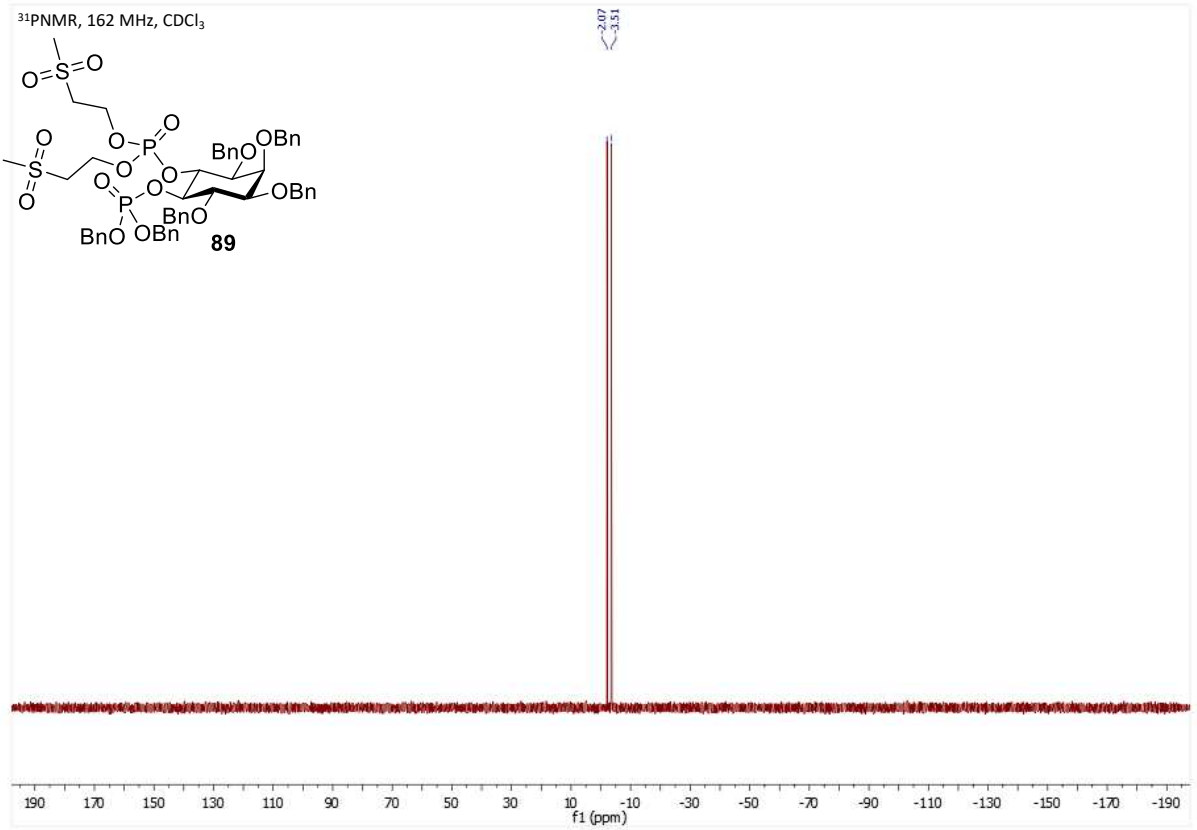

^{13}CNMR, 100 MHz, $CDCl_3$

89

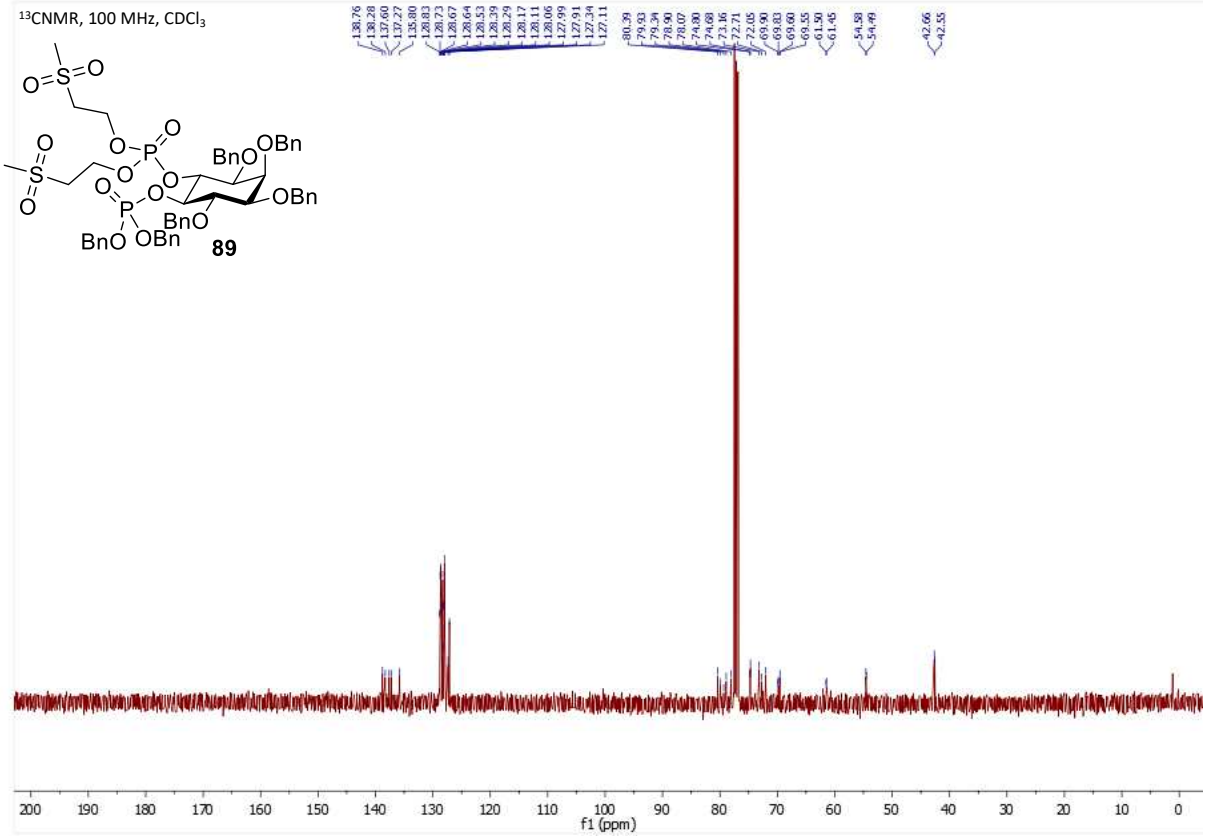

^{1}H-^{1}H COSY

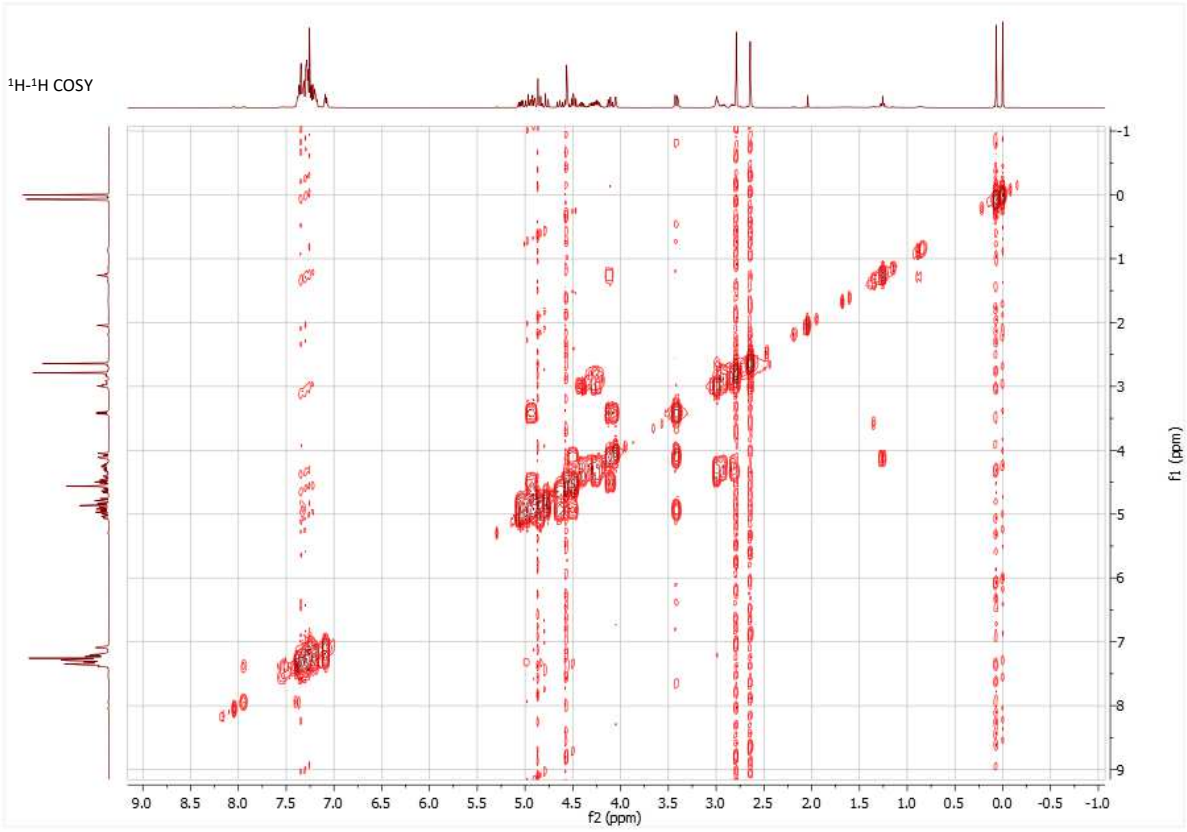

^{1}H-^{13}C HSQC

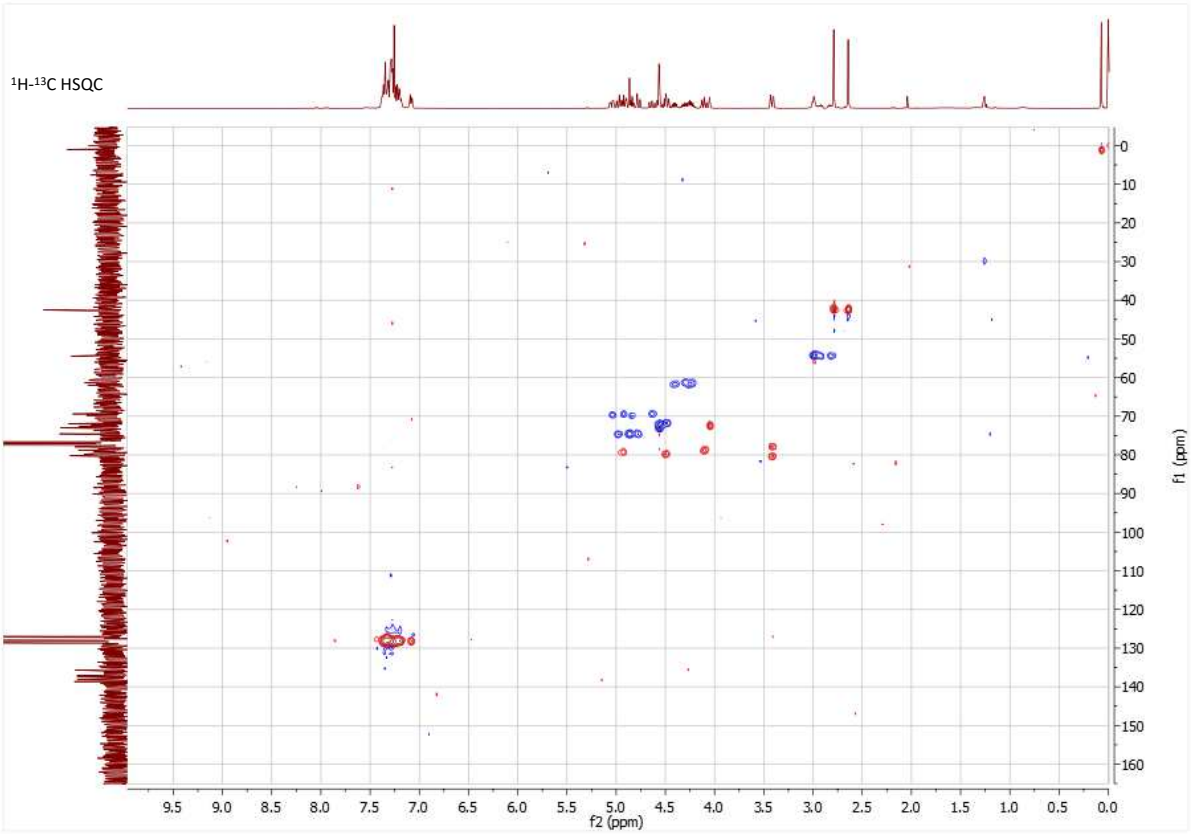

DL-4-Diphospho-*myo*-inositol-5-phosphate (**78**)

^{1}HNMR, 400 MHz, D_2O

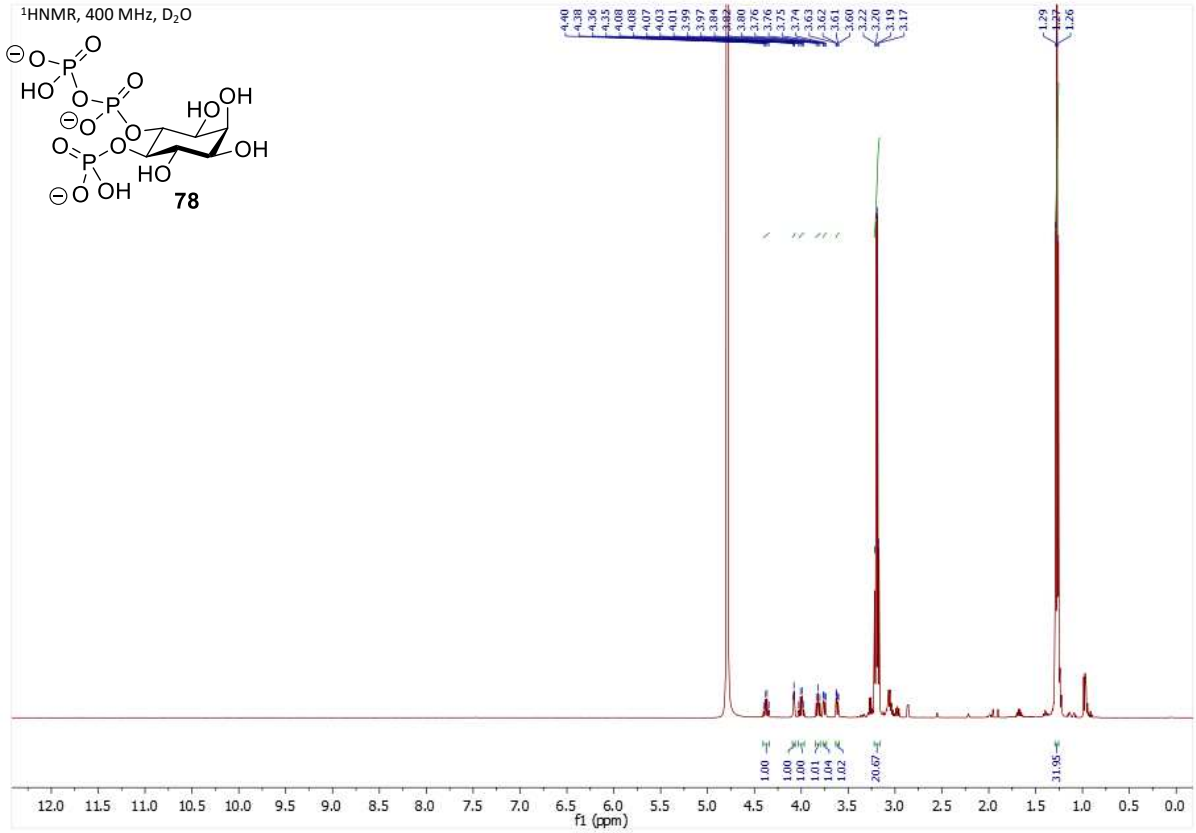

^{31}PNMR, 162 MHz, D_2O

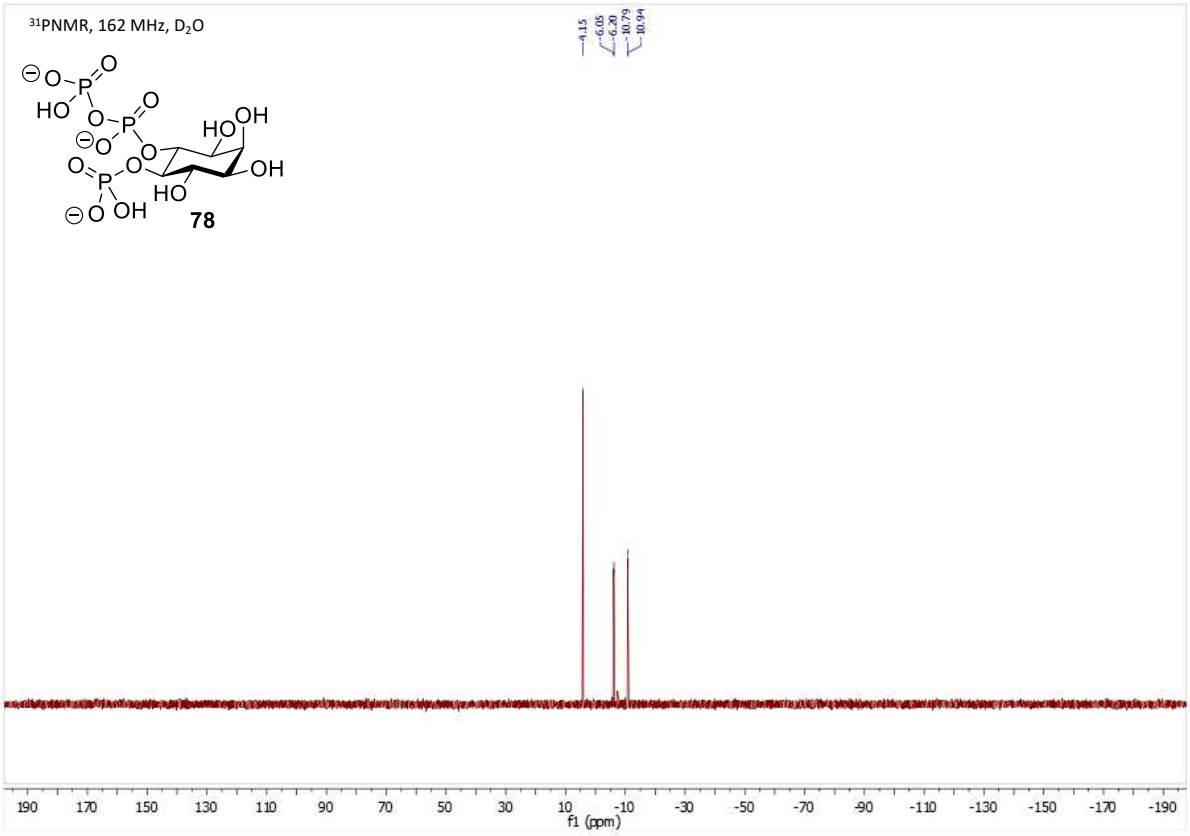

^{13}CNMR, 100 MHz, D_2O

78

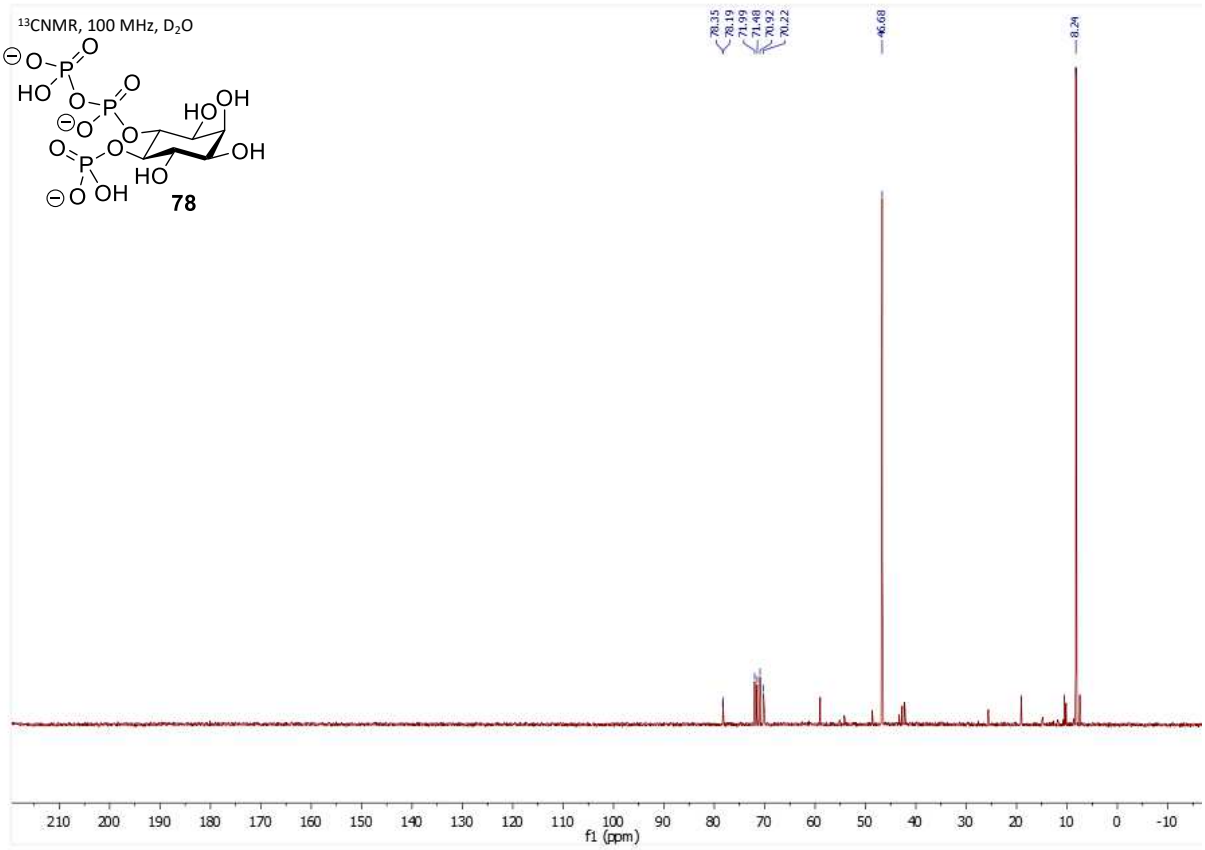

^{1}H-^{31}P HMBC

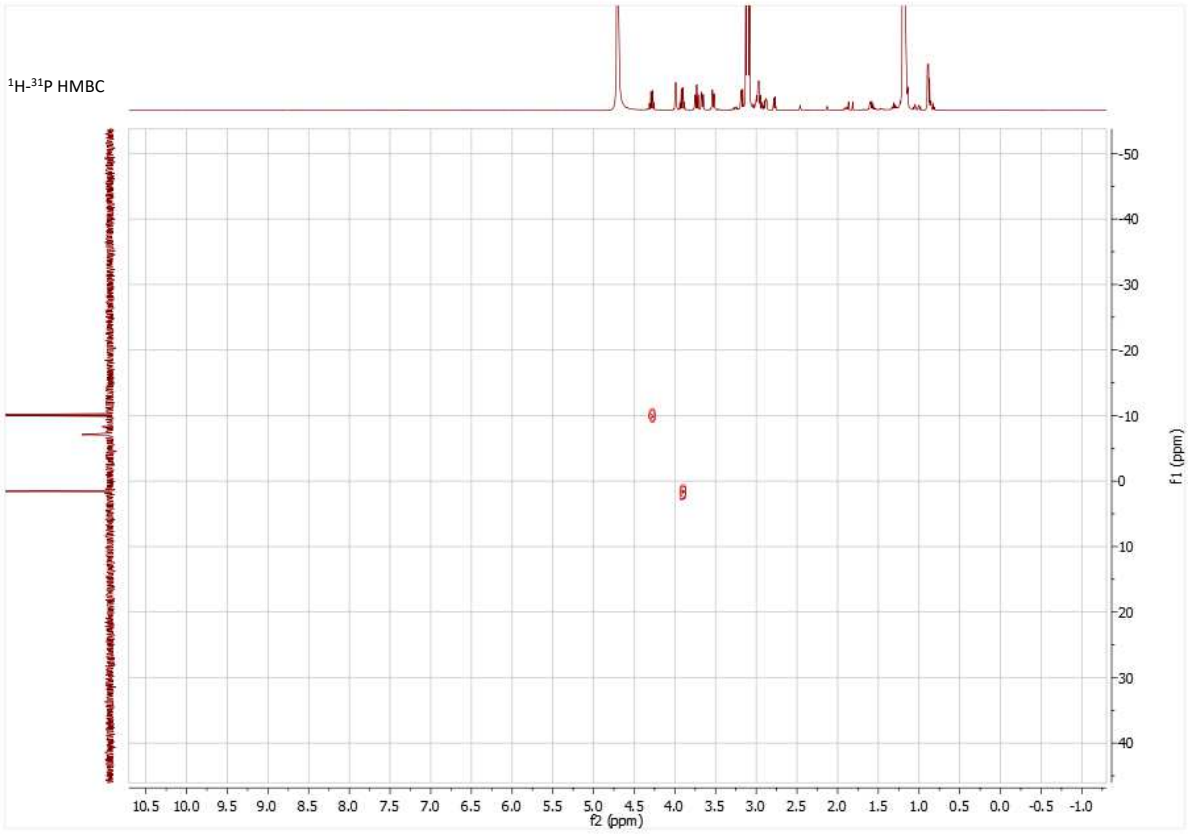

^{1}H-^{1}H COSY

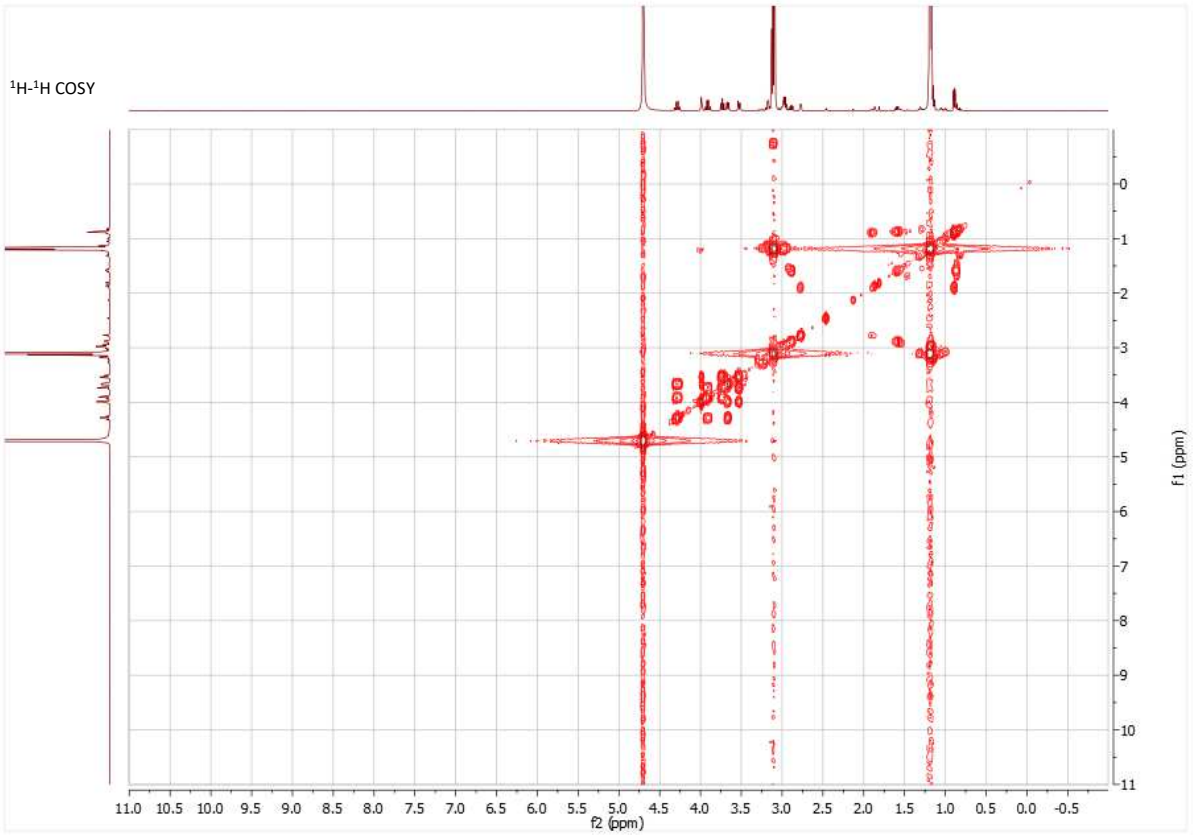

^{1}H-^{13}C HSQC

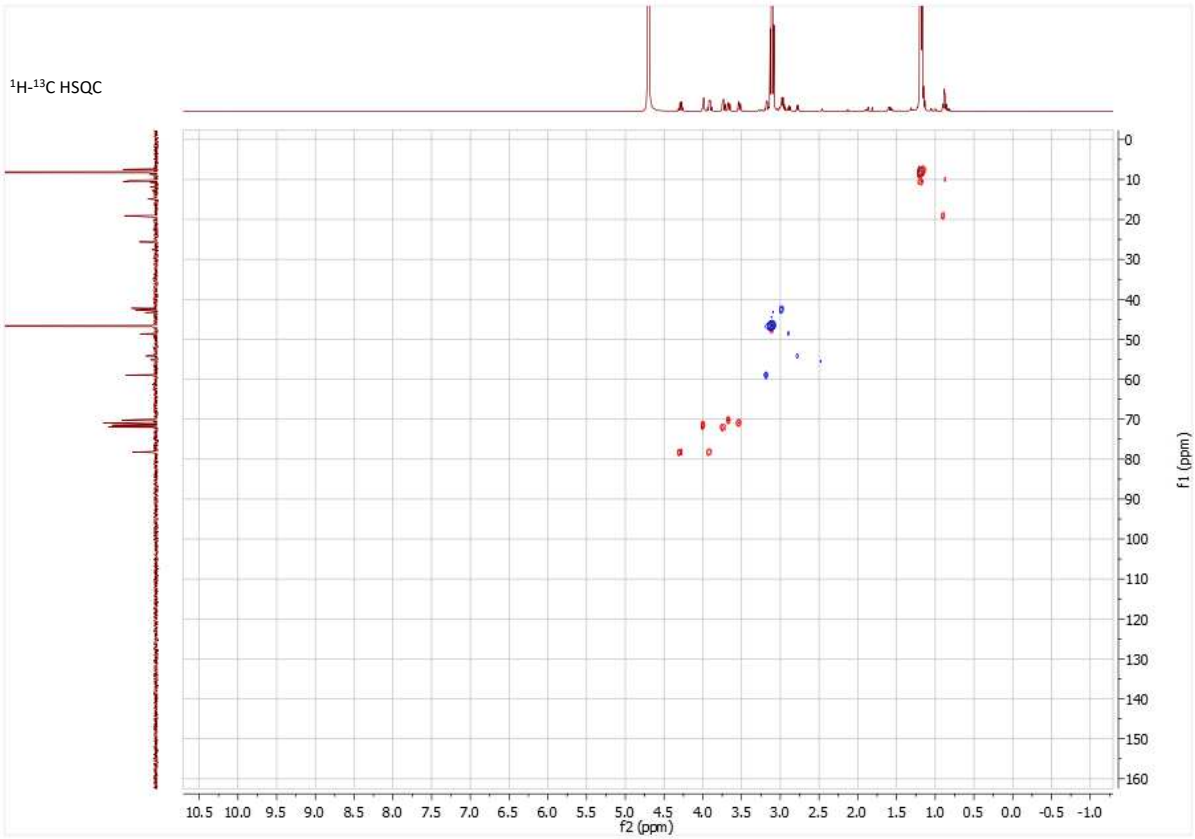

Synthesis of diphospho myo-inositol bisphosphate [PP-InsP$_2$] targets

DL-3,6-di-*O*-benzyl-4,5-*O*-(2,3-dimethoxybutane-2,3-diyl)-1-*O*-para-methoxybenzyl-*myo*-inositol (**96**)

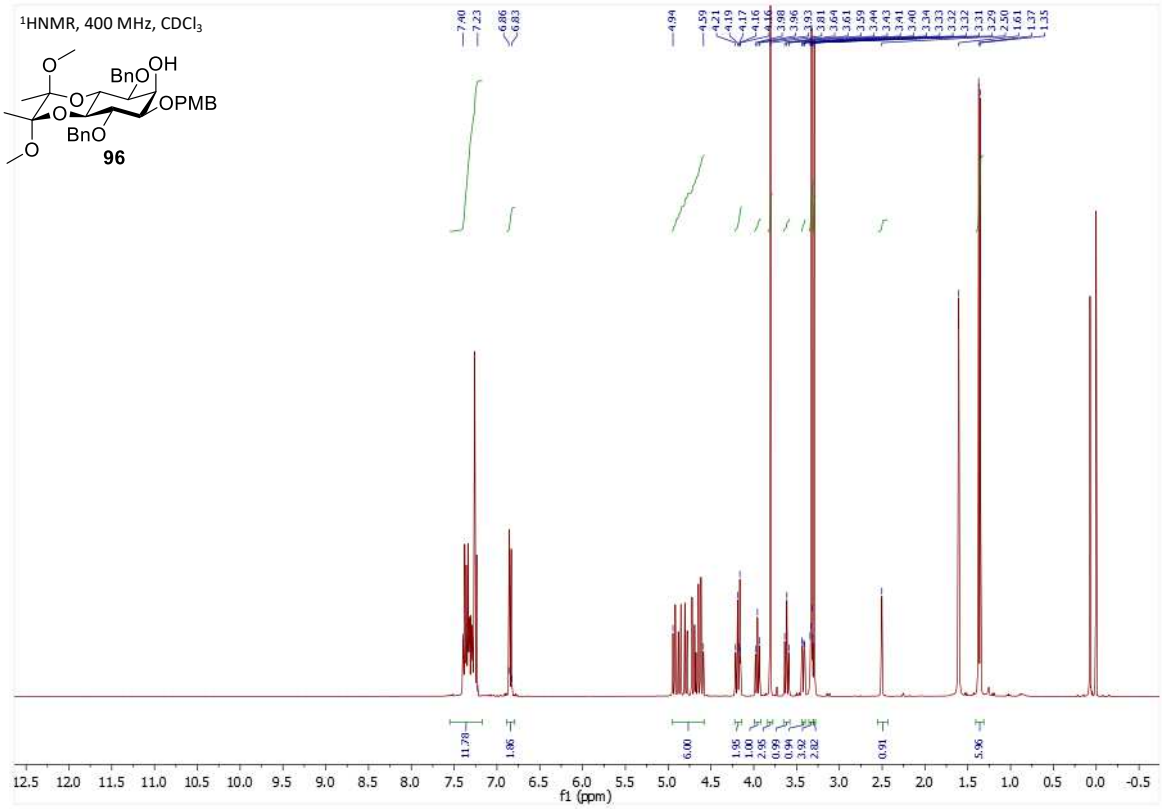

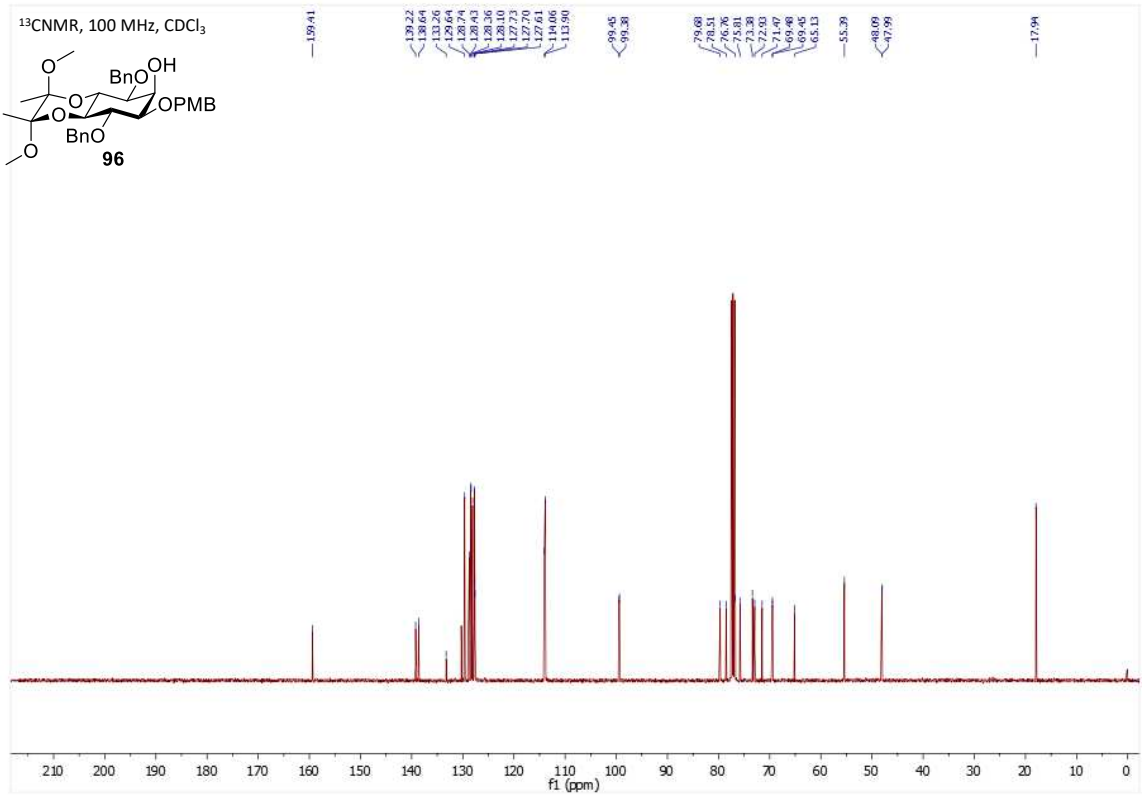

^{1}H-^{1}H COSY

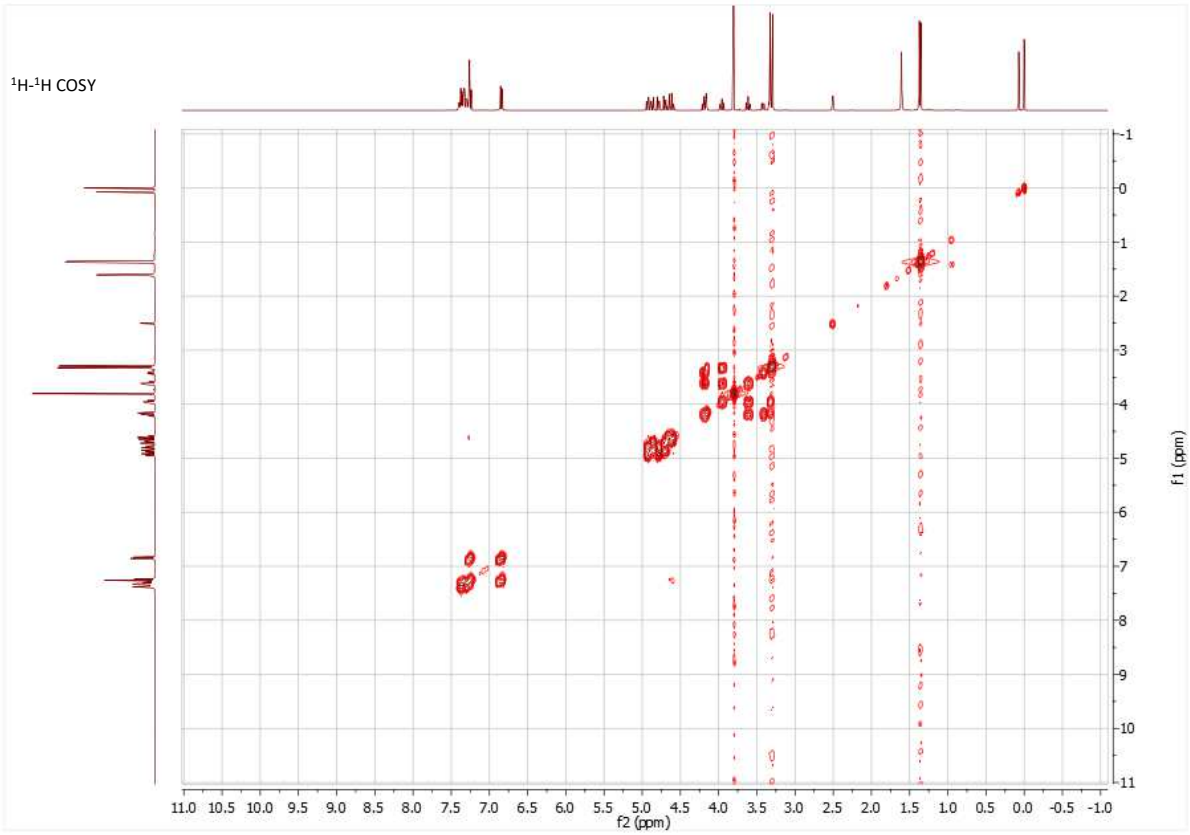

^{1}H-^{13}C HSQC

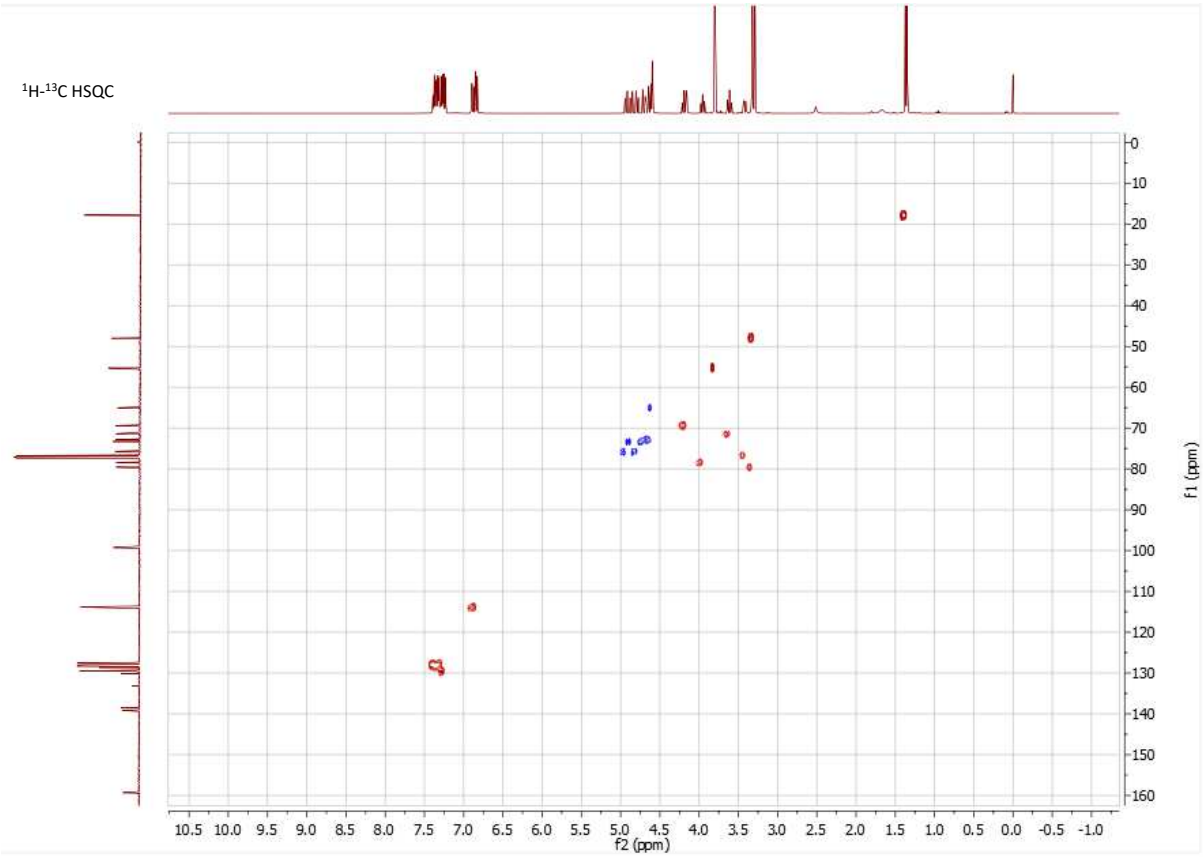

DL-2,3,6-Tri-*O*-benzyl-4,5-*O*-(2,3-dimethoxybutane-2,3-diyl)-1-*O*-para-methoxybenzyl-*myo*-inositol (**97**)

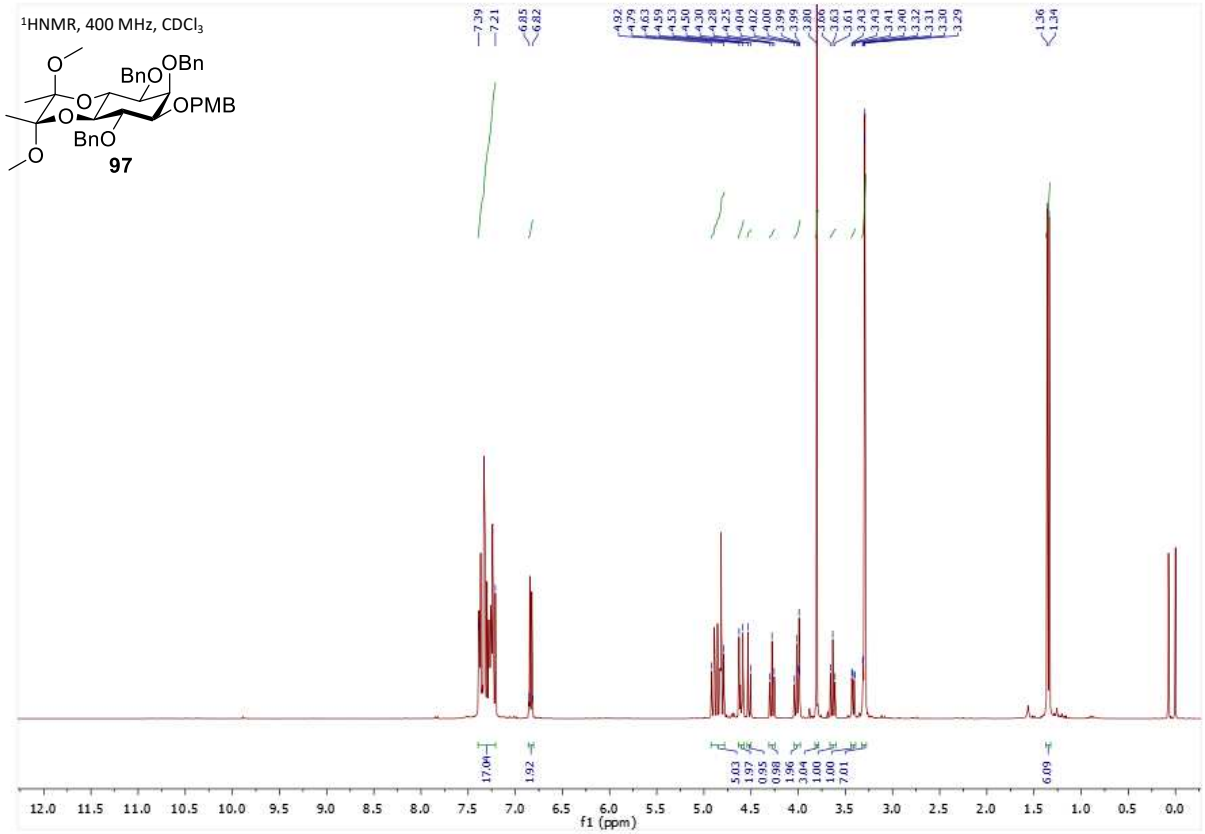

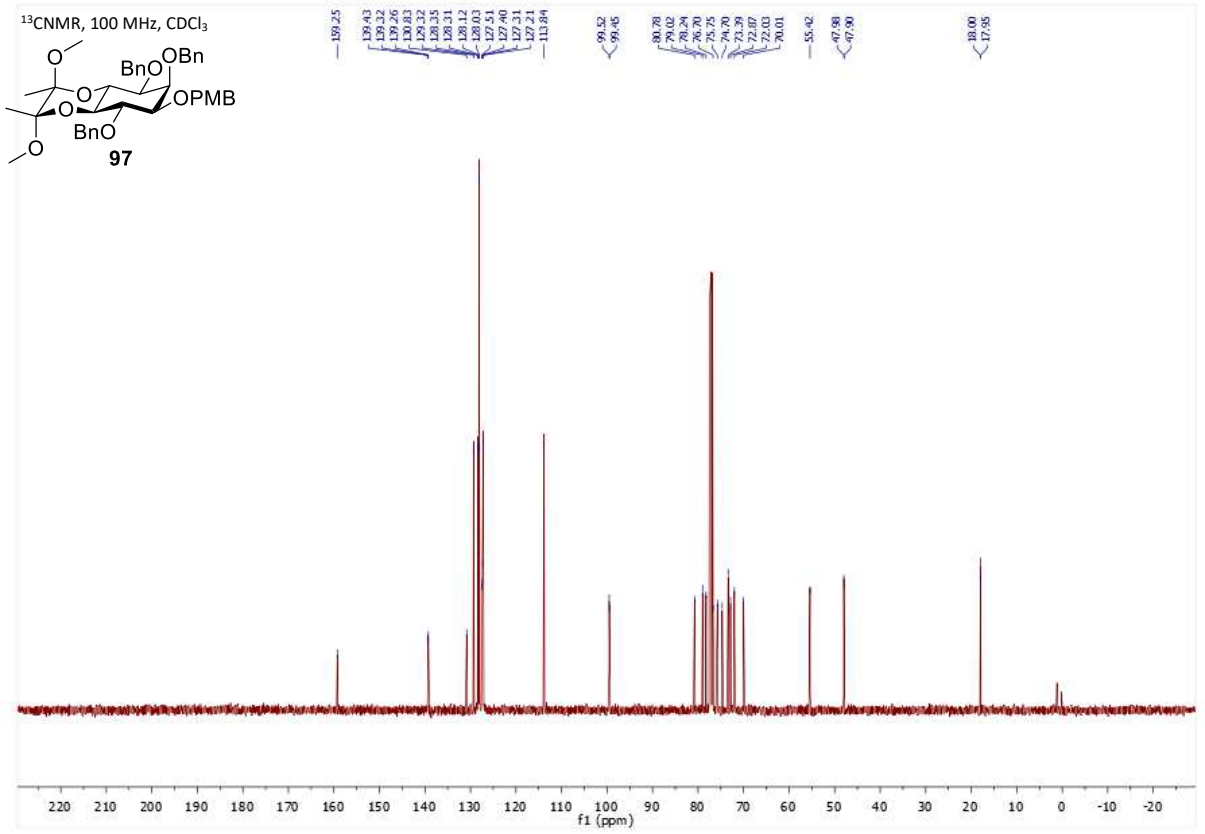

^{1}H-^{1}H COSY

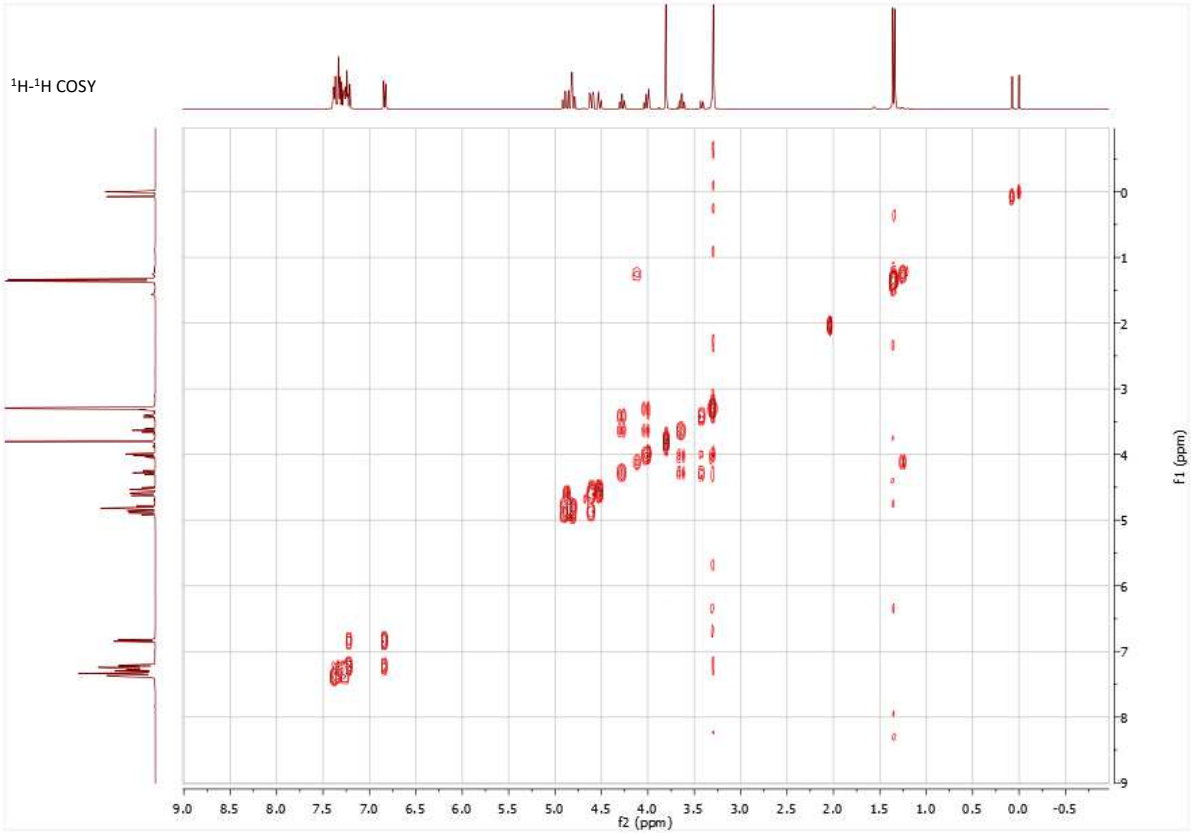

^{1}H-^{13}C HSQC

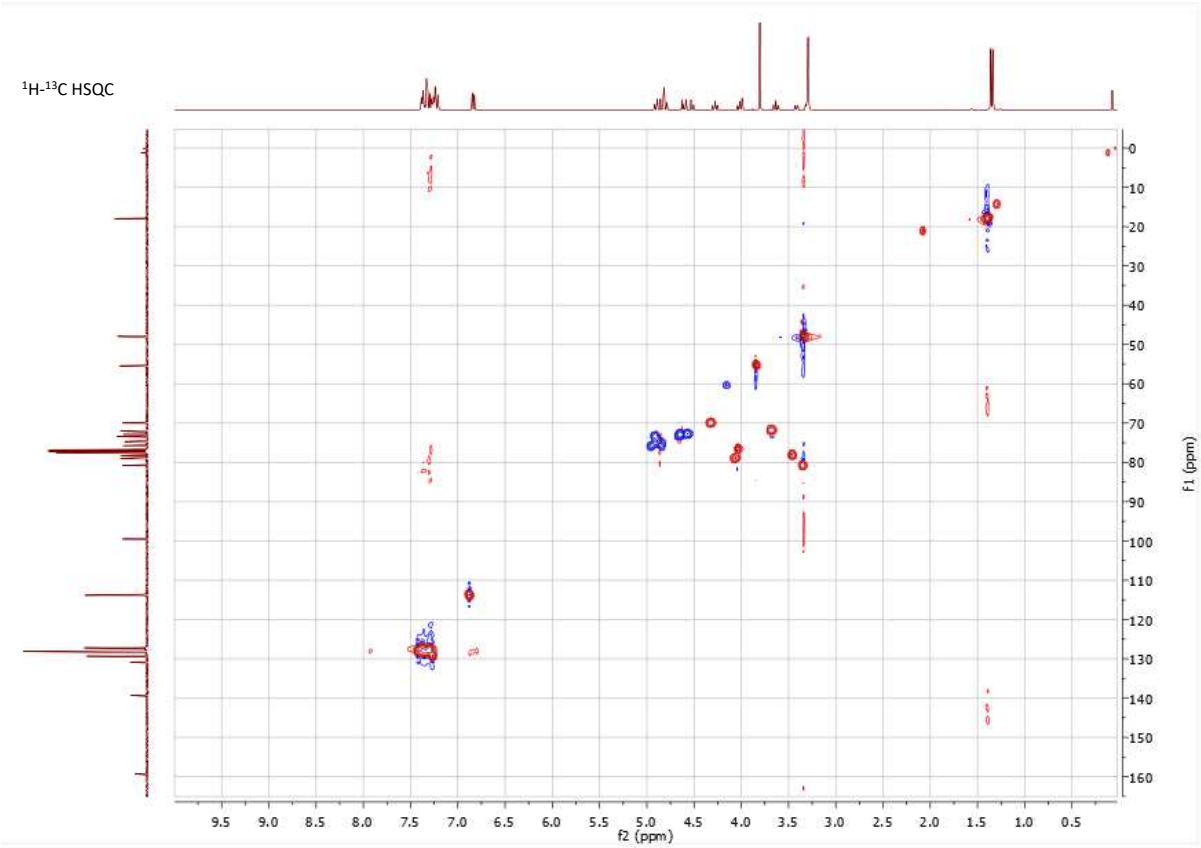

DL-2,3,6-Tri-*O*-benzyl-4,5-*O*-(2,3-dimethoxybutane-2,3-diyl)-*myo*-inositol (**98**)

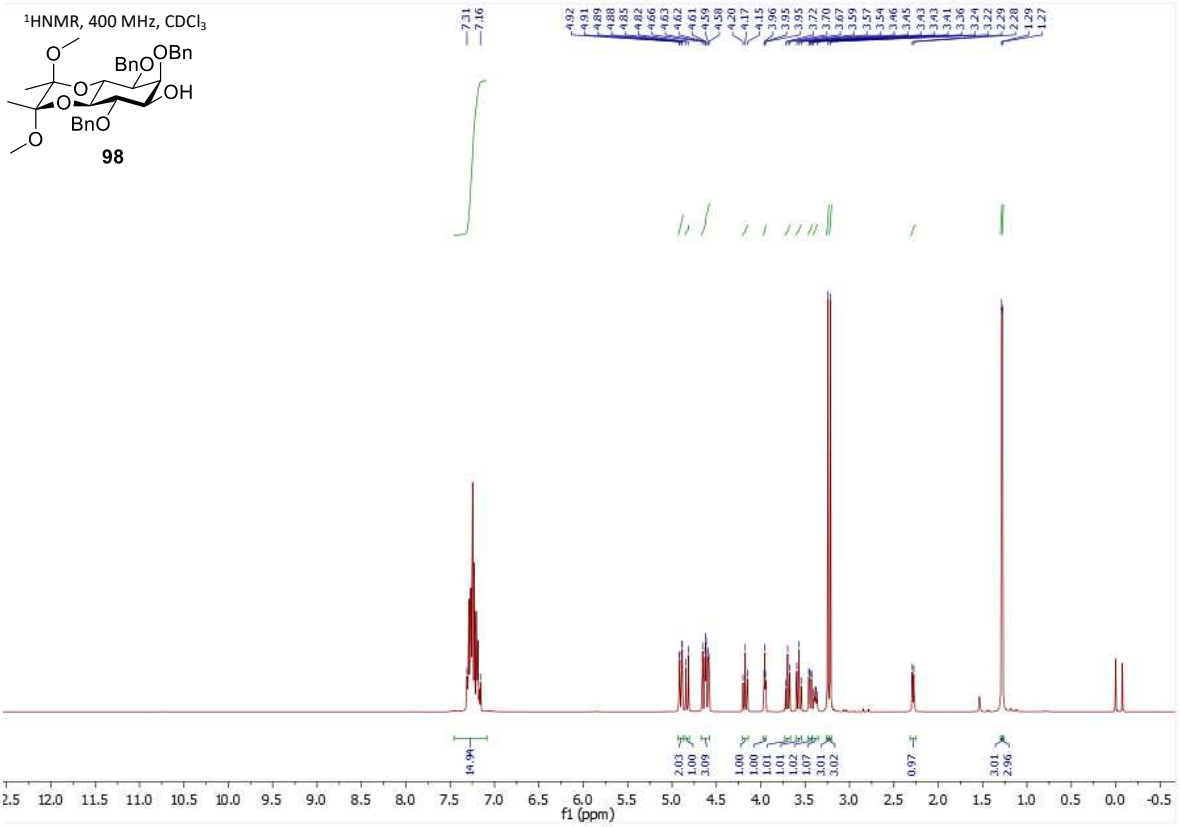

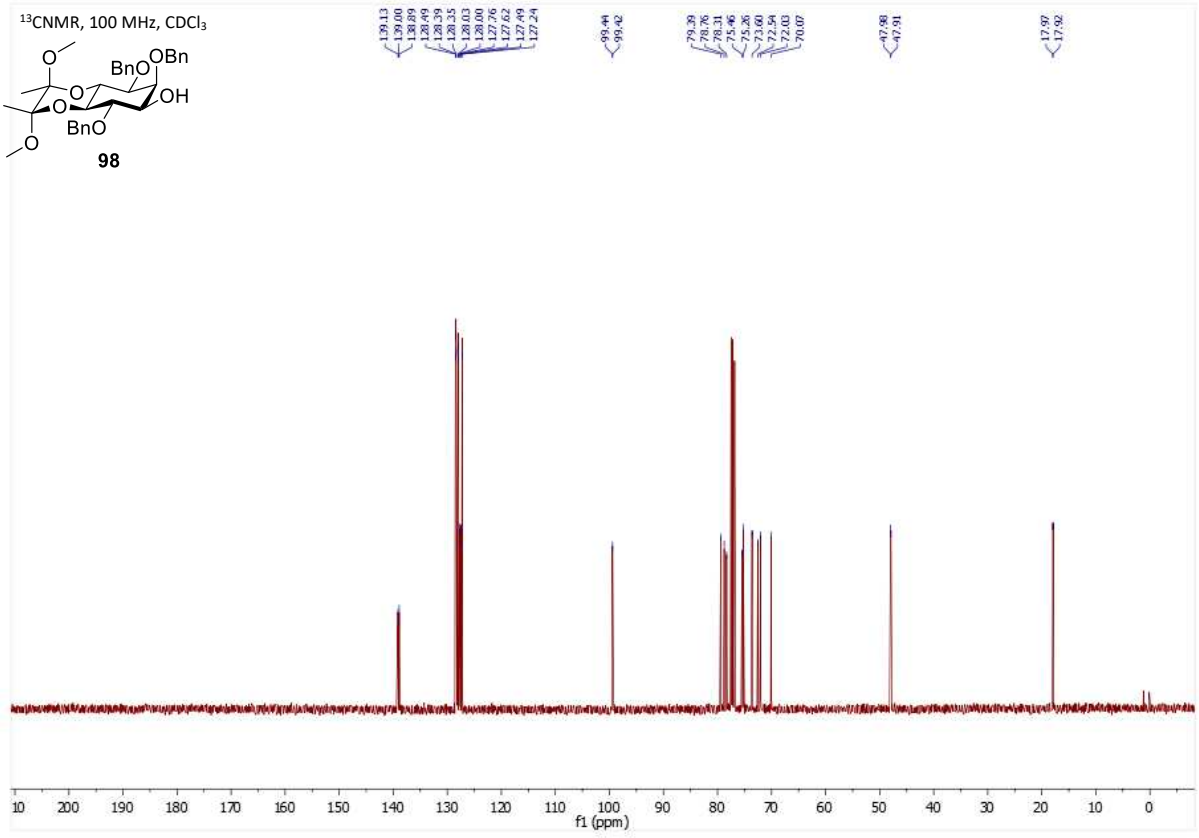

^{1}H-^{1}H COSY

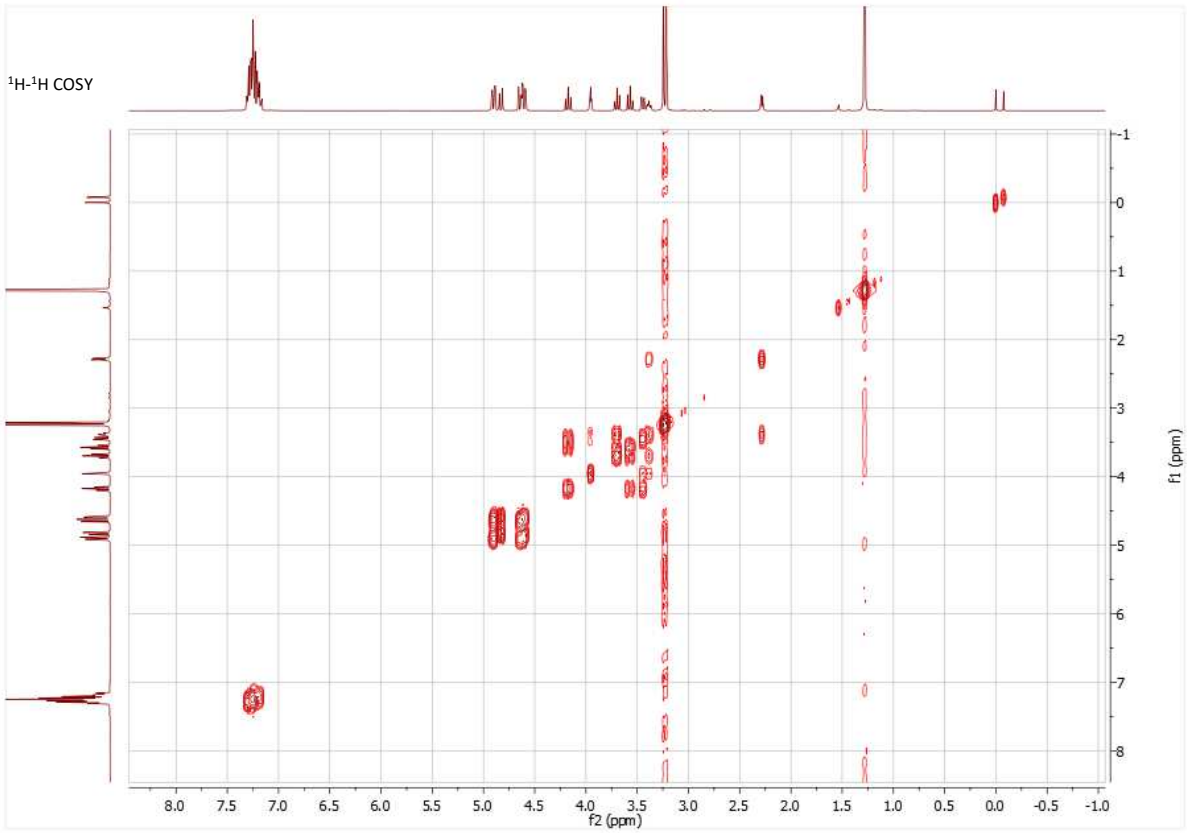

^{1}H-^{13}C HSQC

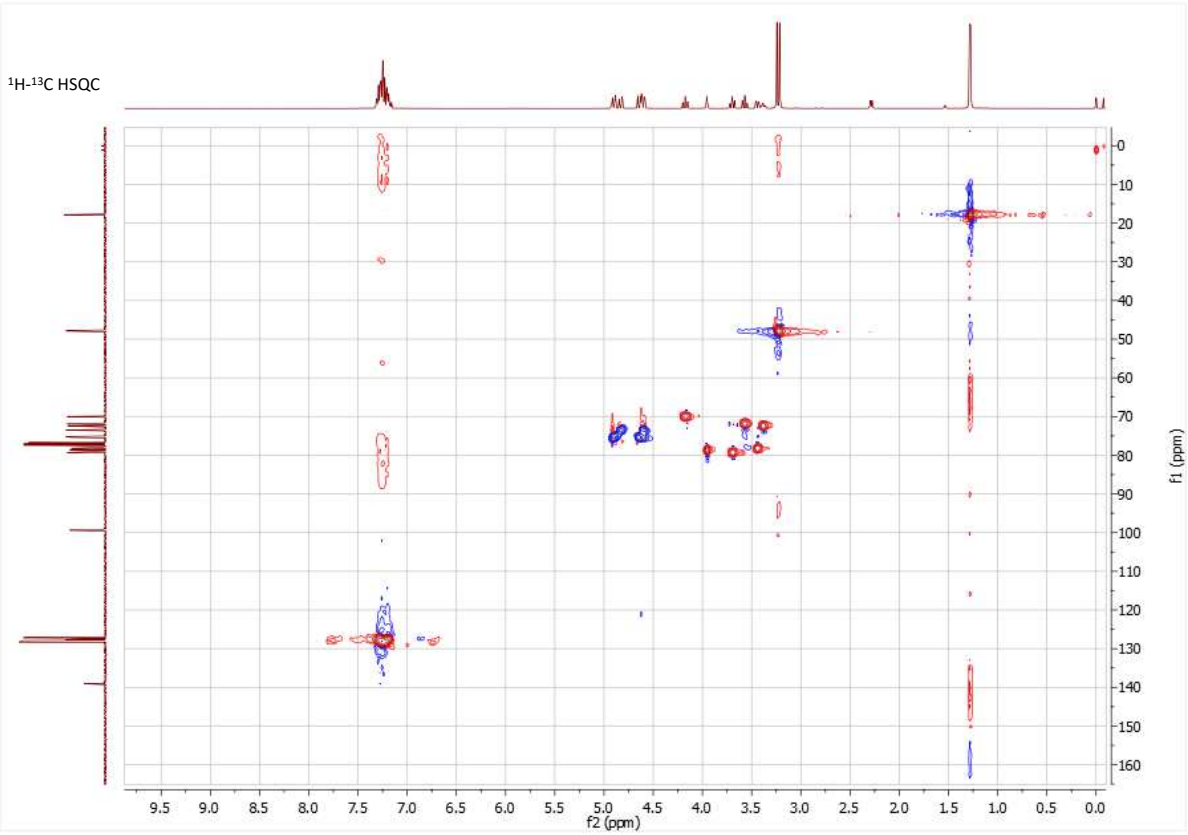

DL-2,3,6-Tri-*O*-benzyl-*myo*-inositol (**99**)

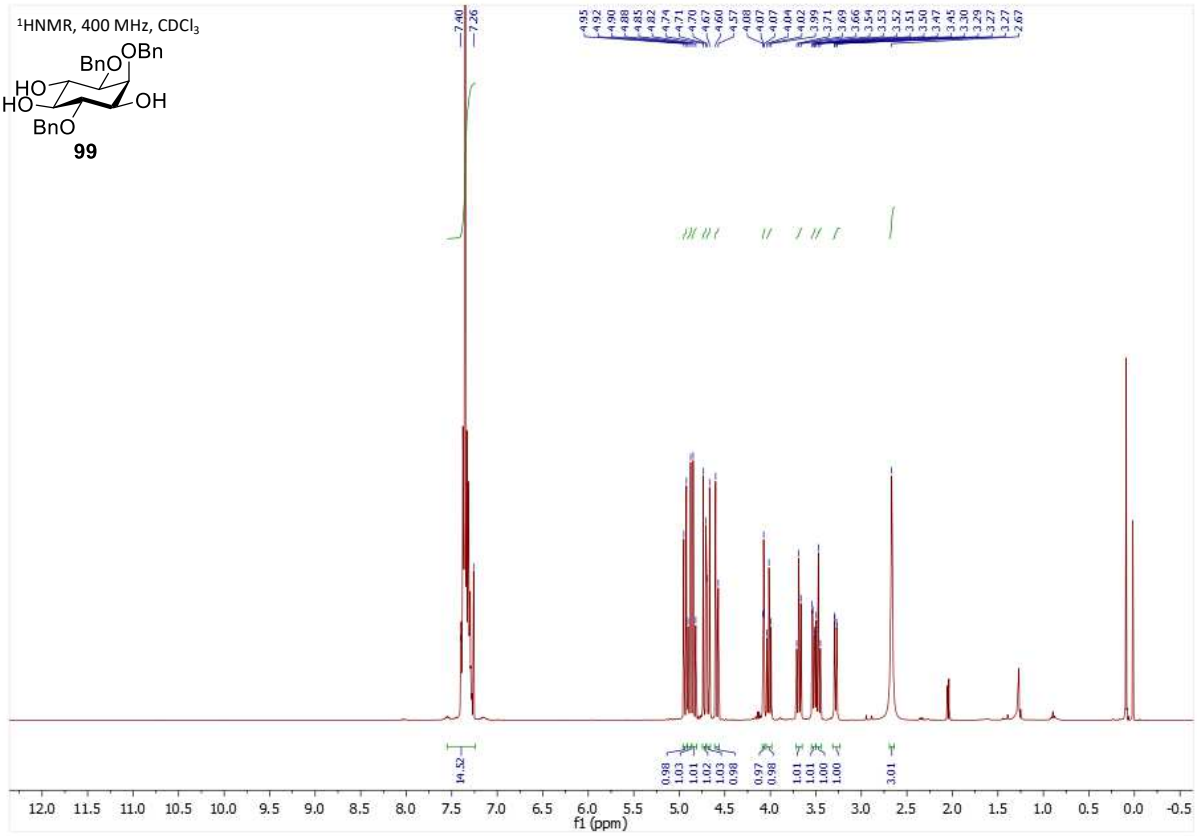

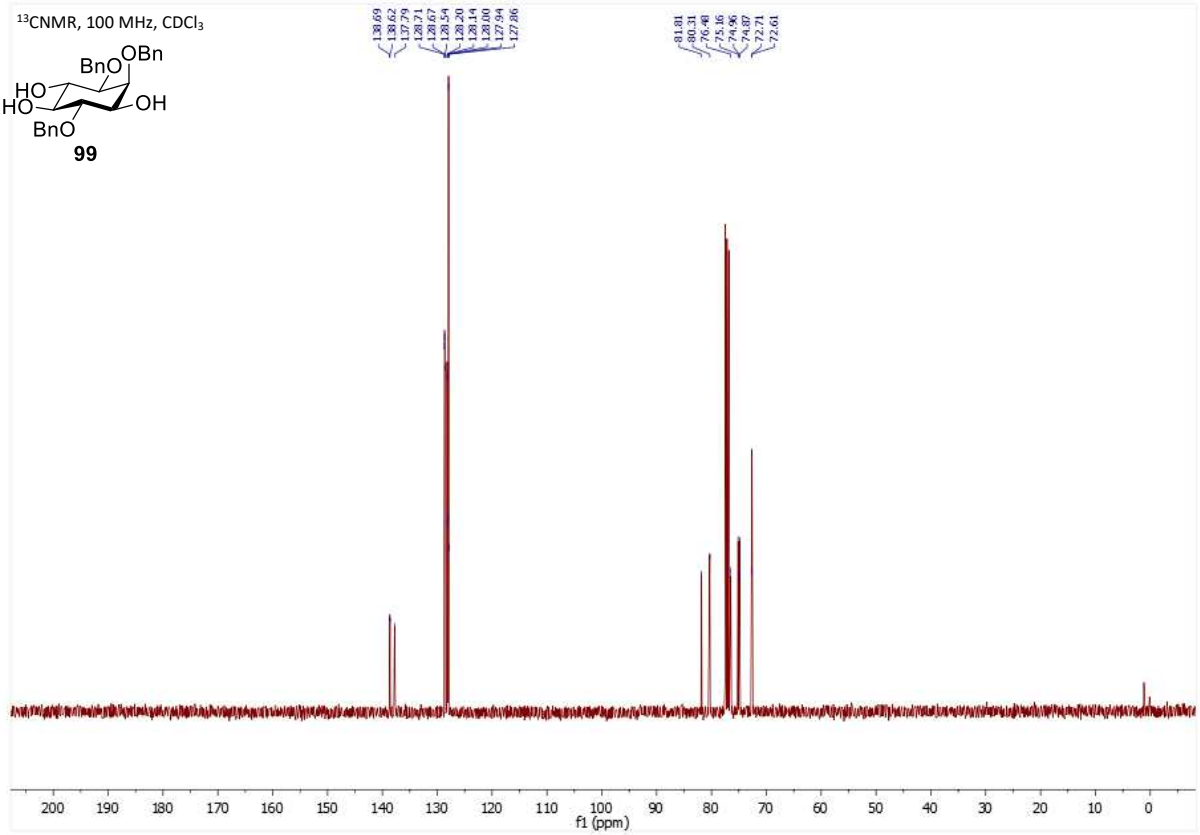

^{1}H-^{1}H COSY

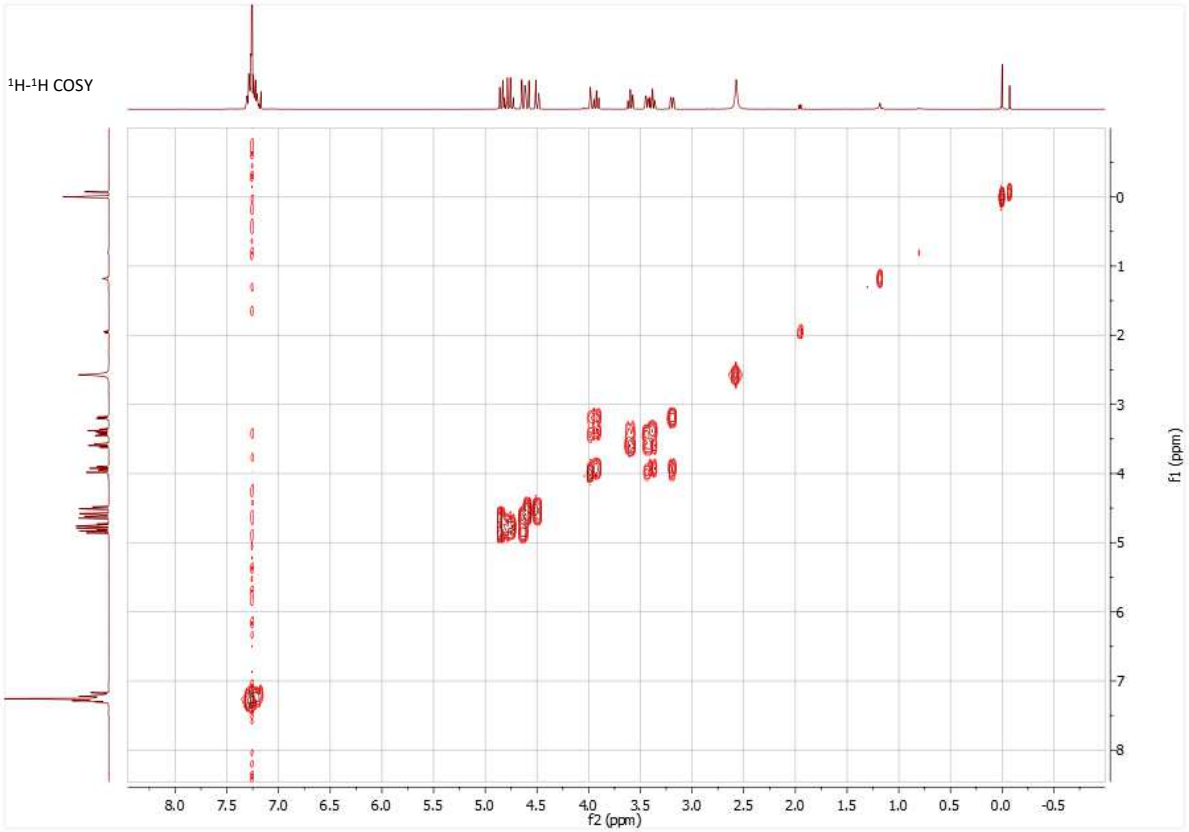

^{1}H-^{13}C HSQC

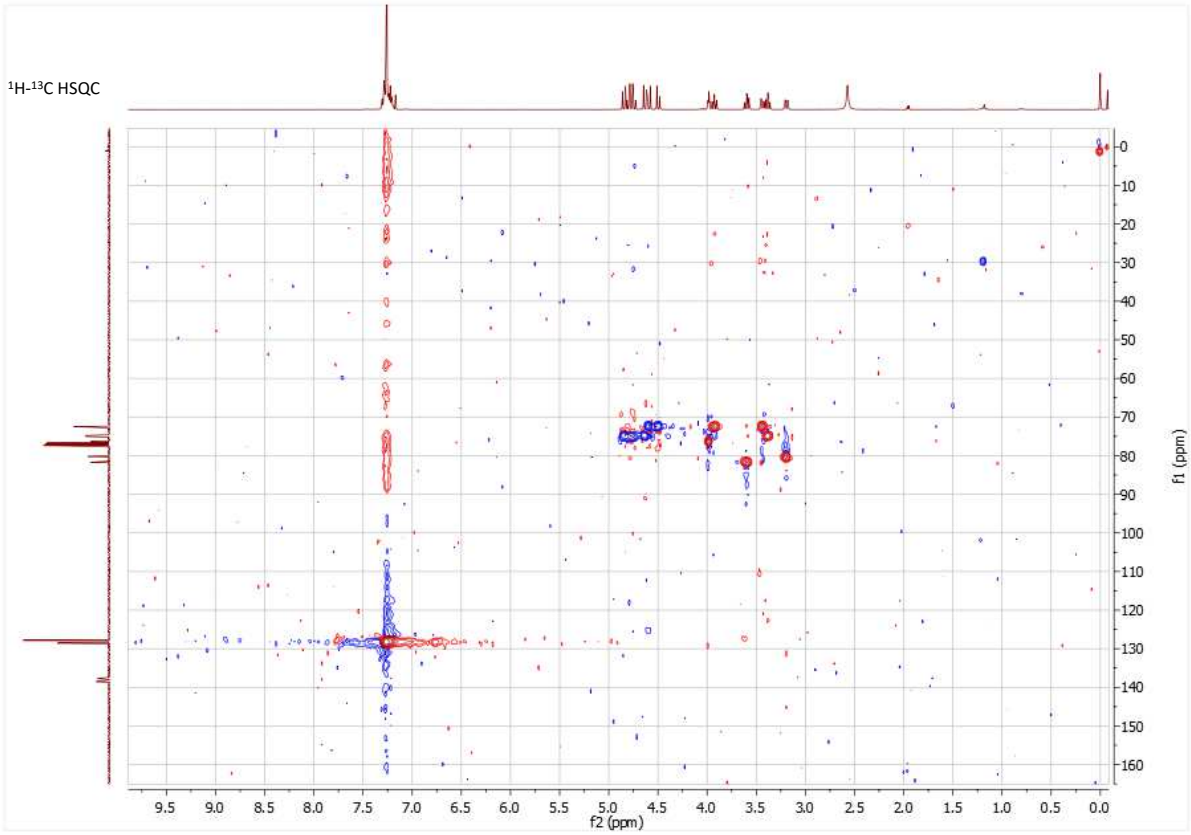

DL-2,3,6-Tri-*O*-benzyl-4-*O*- *para*-methoxybenzyl-*myo*-inositol (**100**)

^{1}HNMR, 400 MHz, $CDCl_3$

100

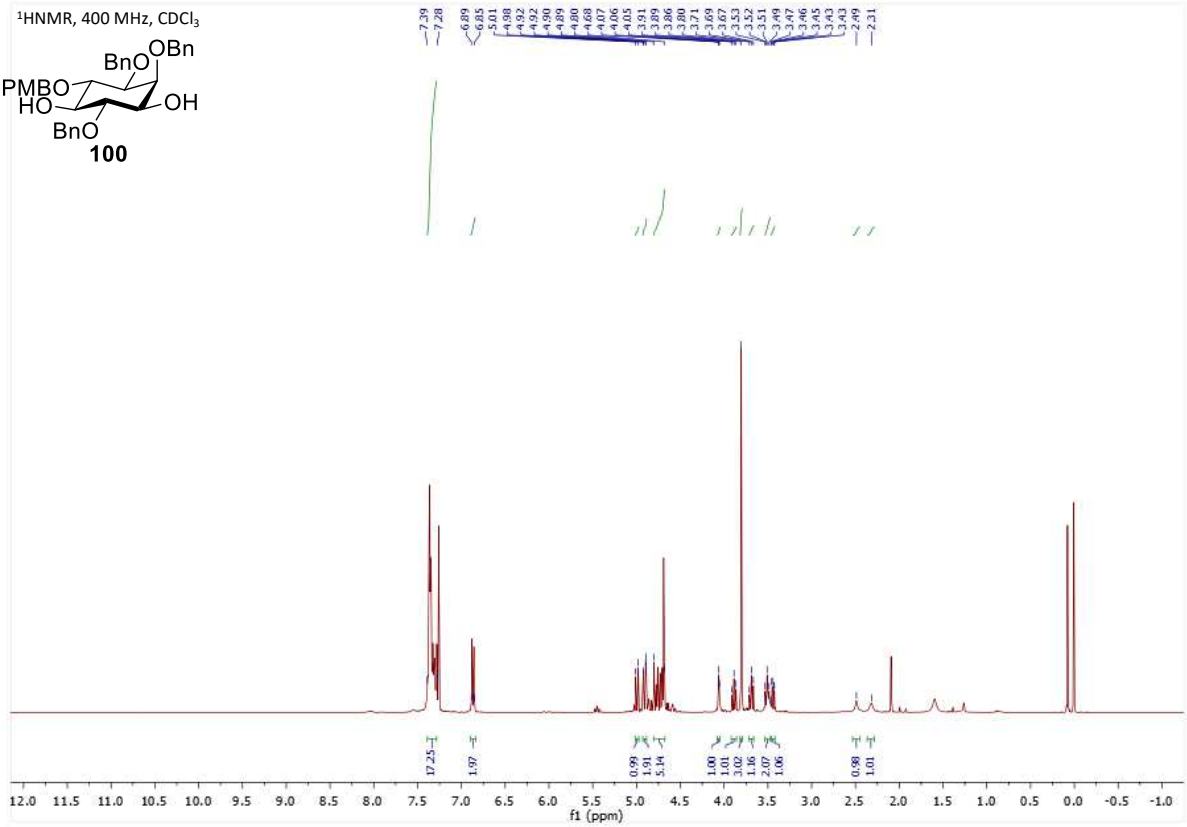

^{13}CNMR, 100 MHz, $CDCl_3$

100

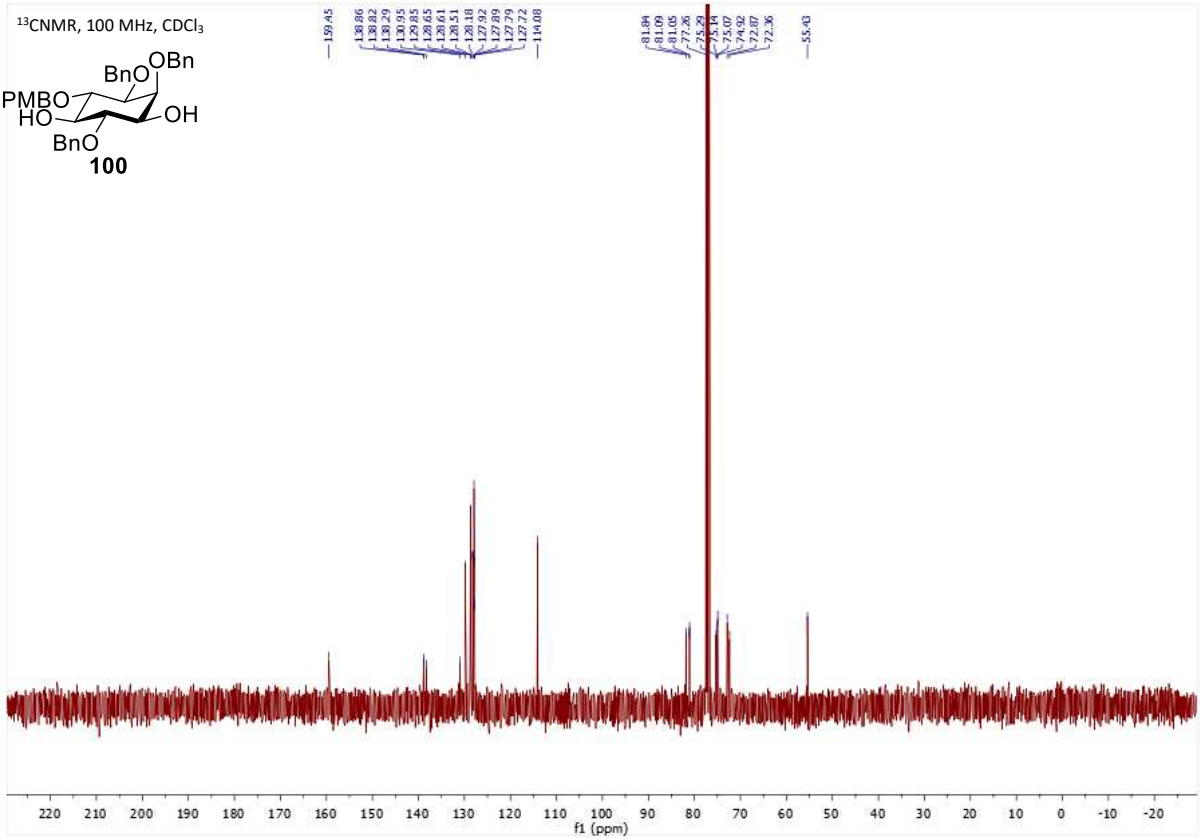

^{1}H-^{1}H COSY

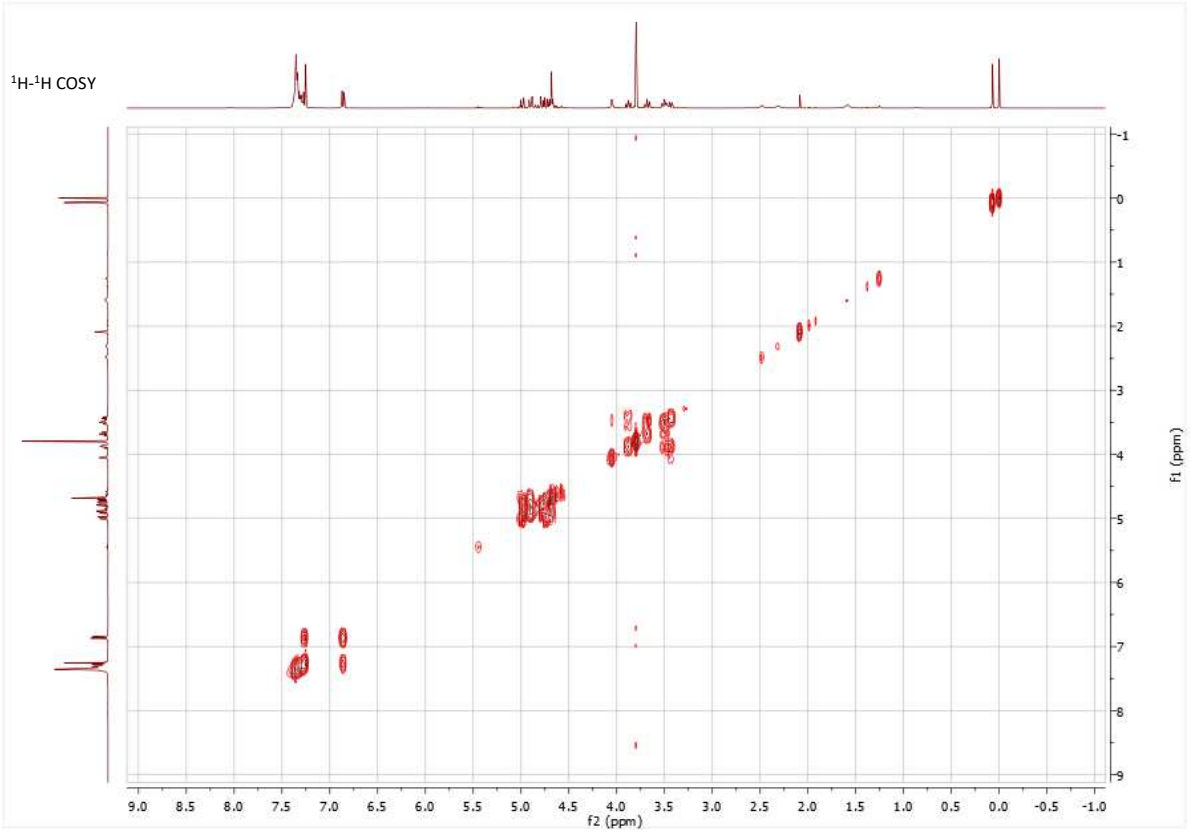

^{1}H-^{13}C HSQC

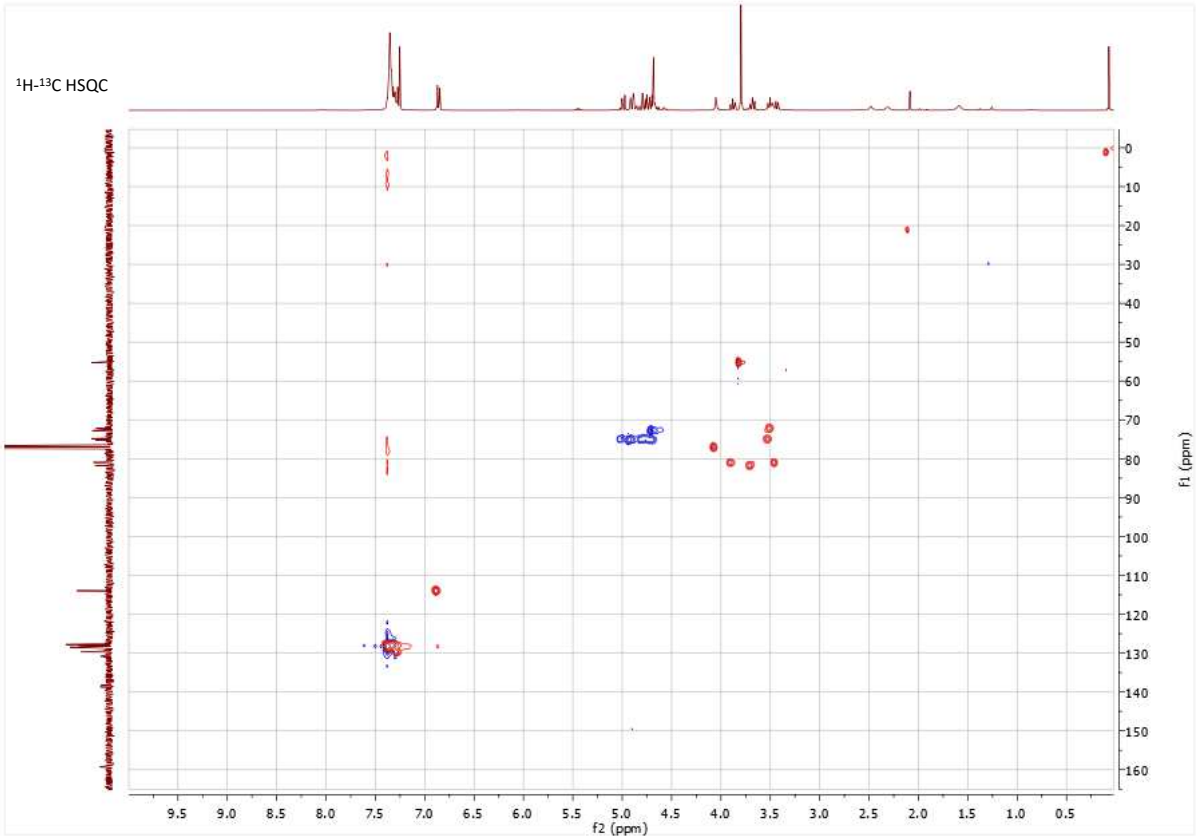

DL-2,3,6-Tri-*O*-benzyl-5-*O*-PMB-*myo*-inositol (**101**)

^{1}HNMR, 400 MHz, $CDCl_3$

101

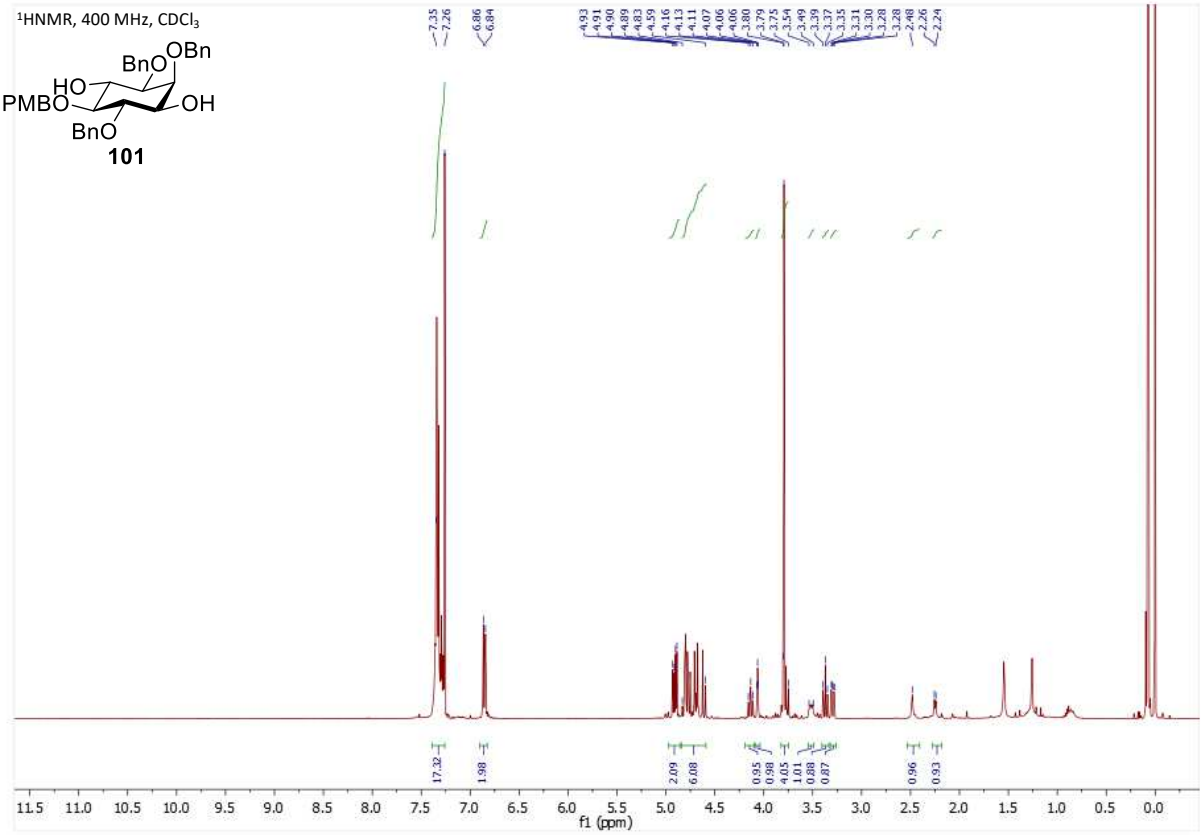

^{13}CNMR, 100 MHz, $CDCl_3$

101

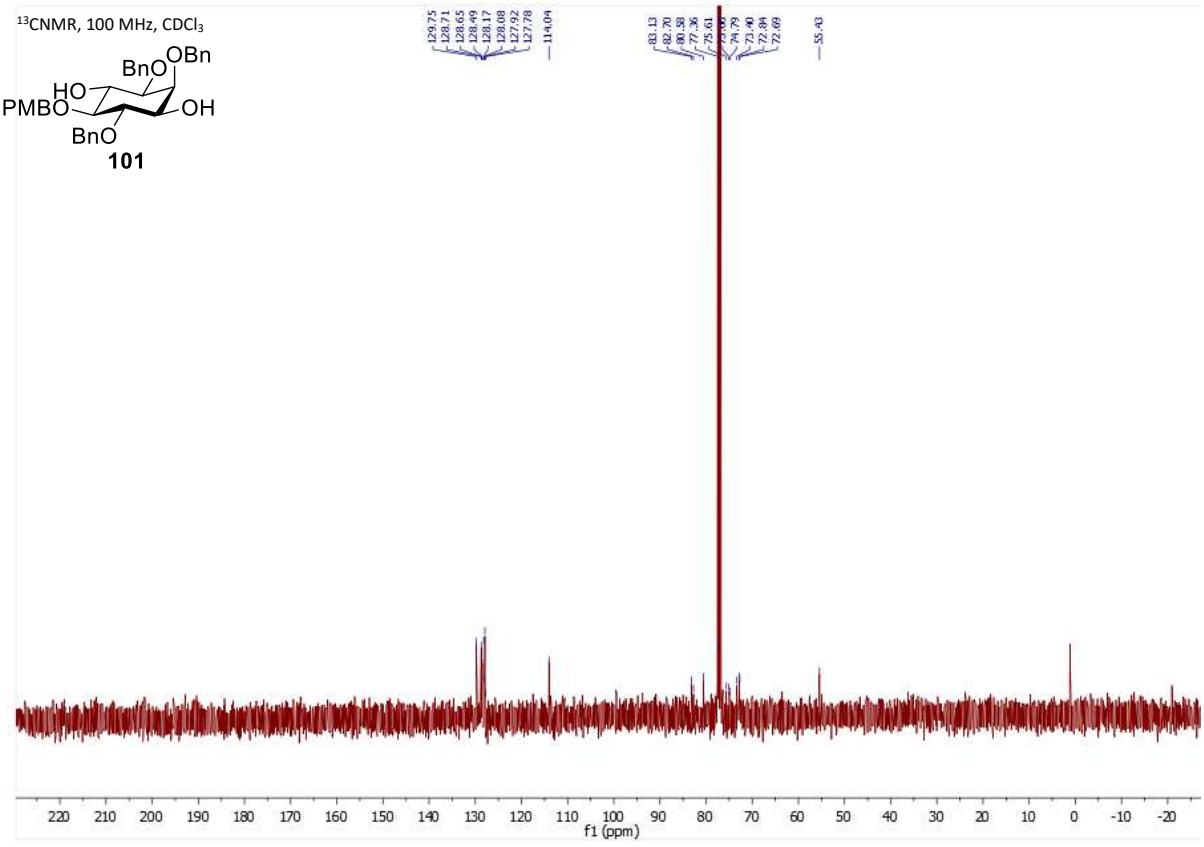

^{1}H-^{1}H COSY

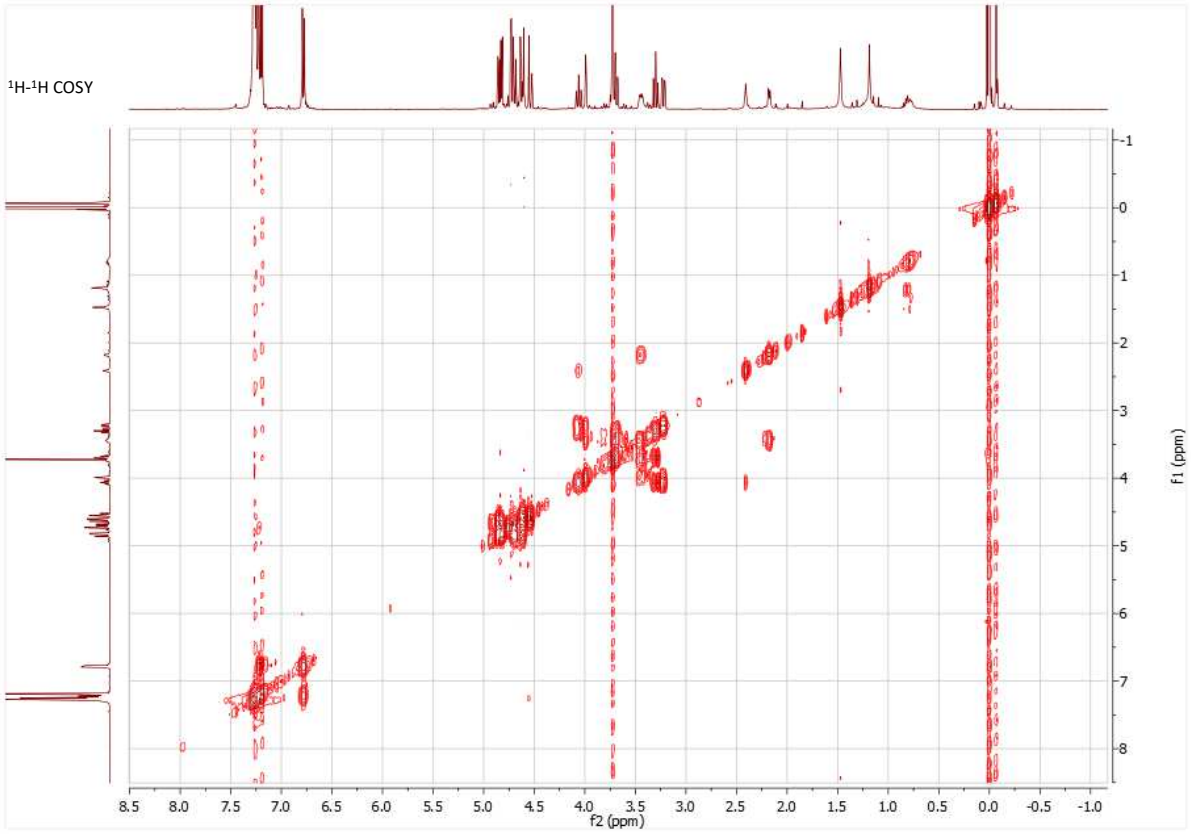

^{1}H-^{13}C HSQC

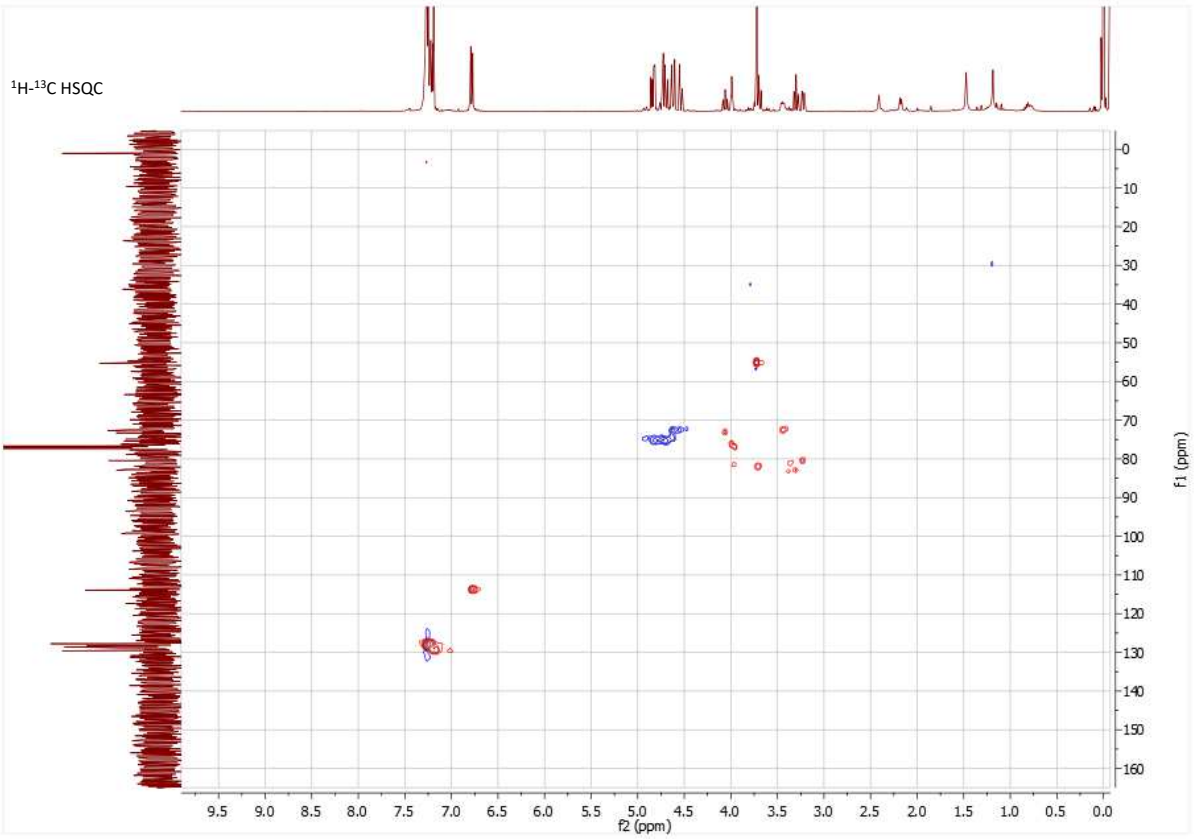

DL-2,3,6-Tri-*O*-benzyl-4-*O*-*para*-methoxybenzyl-*myo*-inositol 1,5-bis(dibenzylphosphate) (**102**)

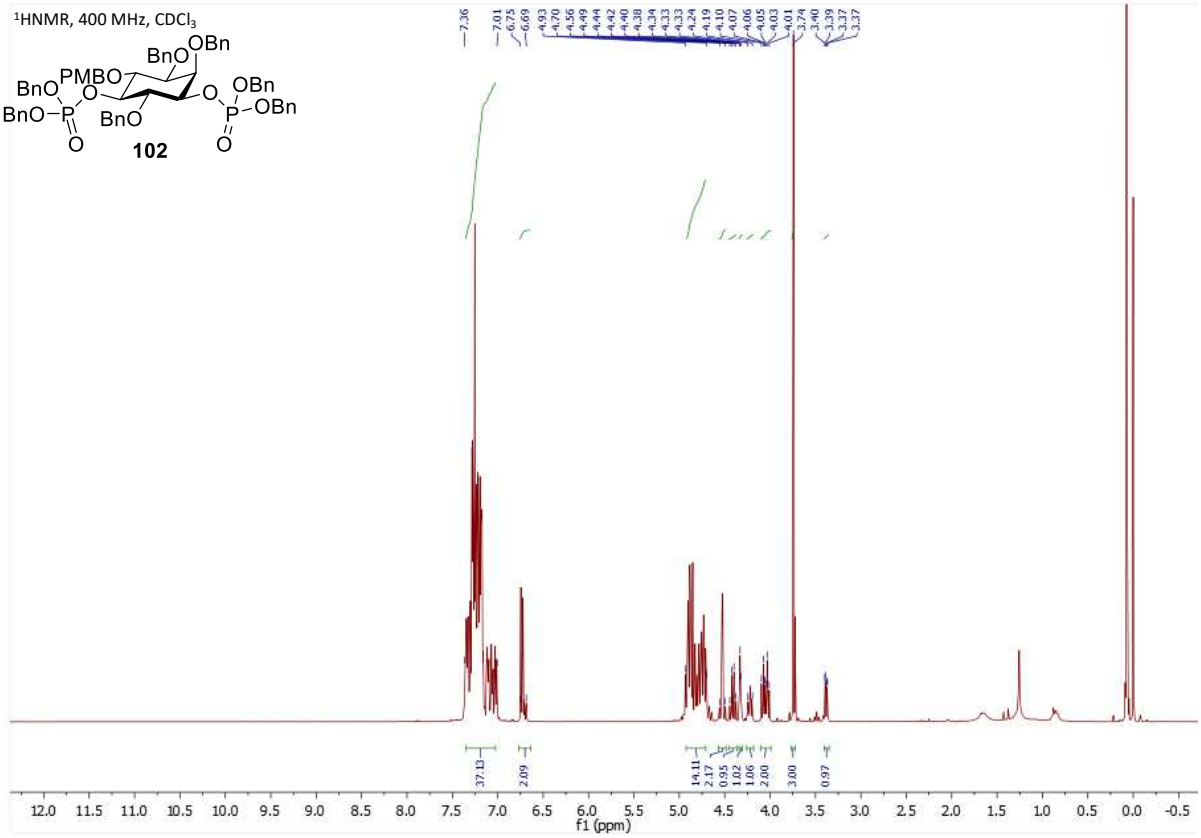

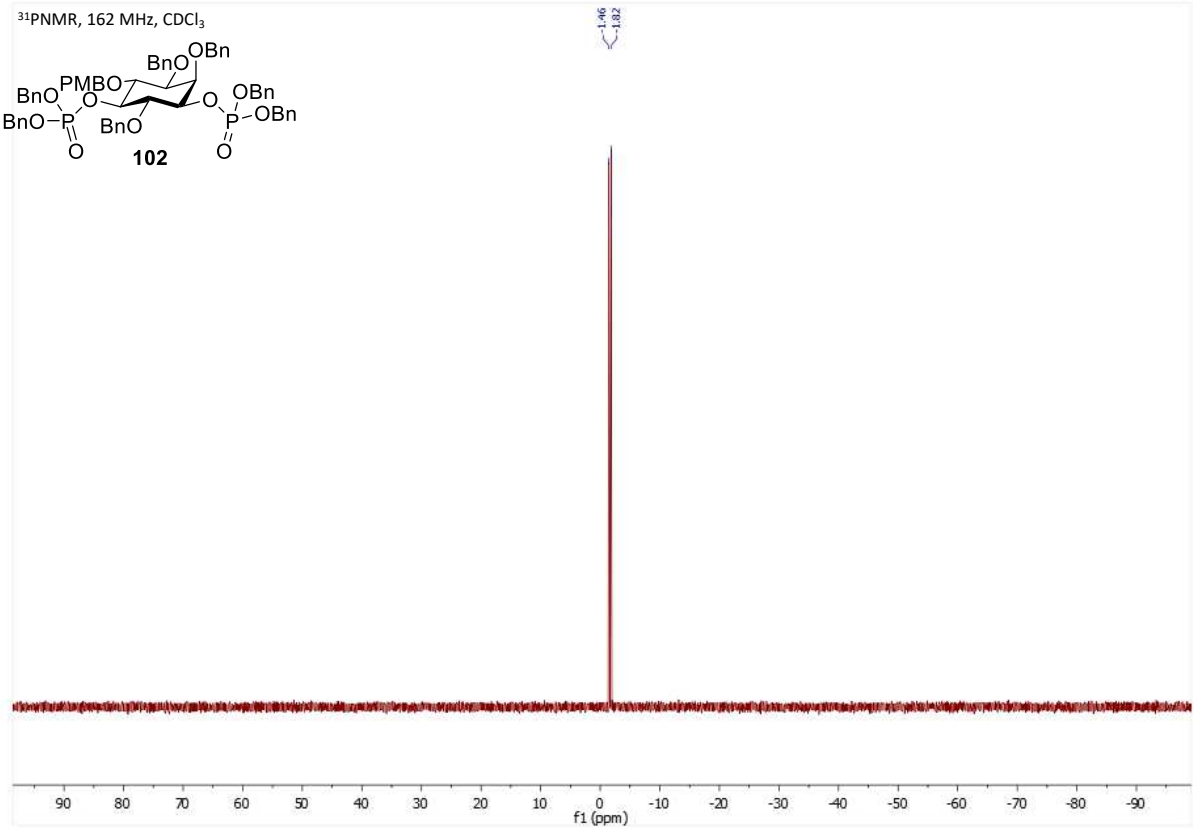

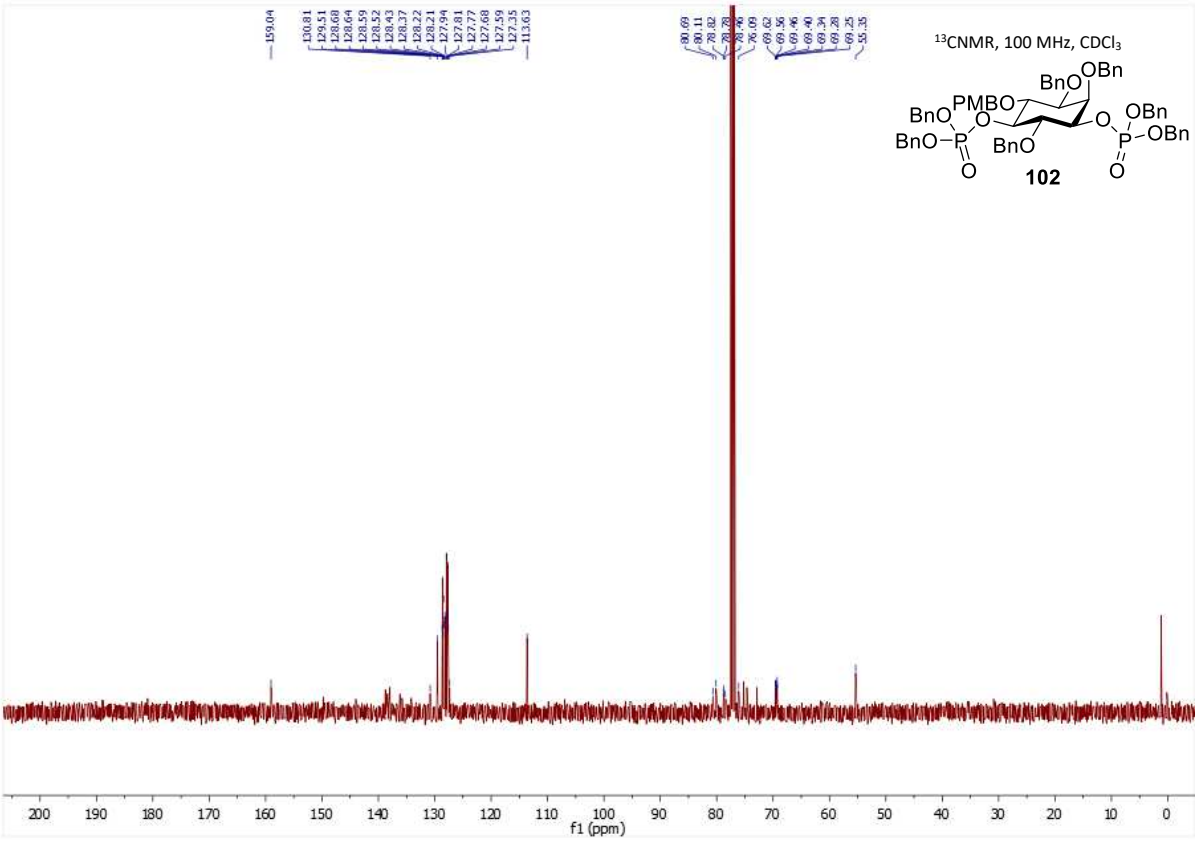
159.04
130.81
129.51
128.68
128.64
128.59
128.52
128.43
128.37
128.22
128.21
127.94
127.81
127.77
127.68
127.59
127.35
113.63
80.69
80.11
78.82
78.78
78.40
76.09
69.62
69.56
69.46
69.40
69.34
69.28
69.25
55.35
13CNMR, 100 MHz, CDCl3
BnO
OBn
PMBO
BnO
O
O
OBn
BnO
P
BnO
P
OBn
O
O
102
200 190 180 170 160 150 140 130 120 110 100 90 80 70 60 50 40 30 20 10 0
f1 (ppm)

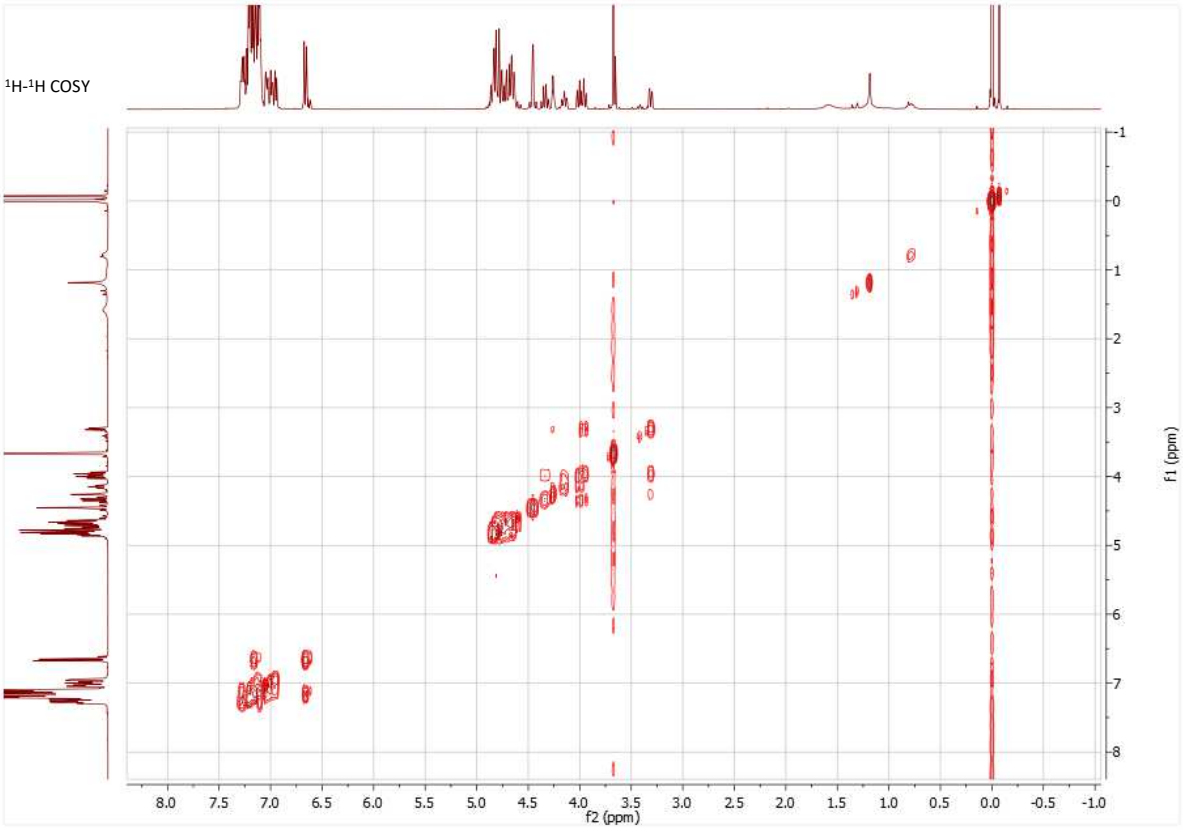
1H-1H COSY
8.0 7.5 7.0 6.5 6.0 5.5 5.0 4.5 4.0 3.5 3.0 2.5 2.0 1.5 1.0 0.5 0.0 -0.5 -1.0
f2 (ppm)
-1 0 1 2 3 4 5 6 7 8
f1 (ppm)

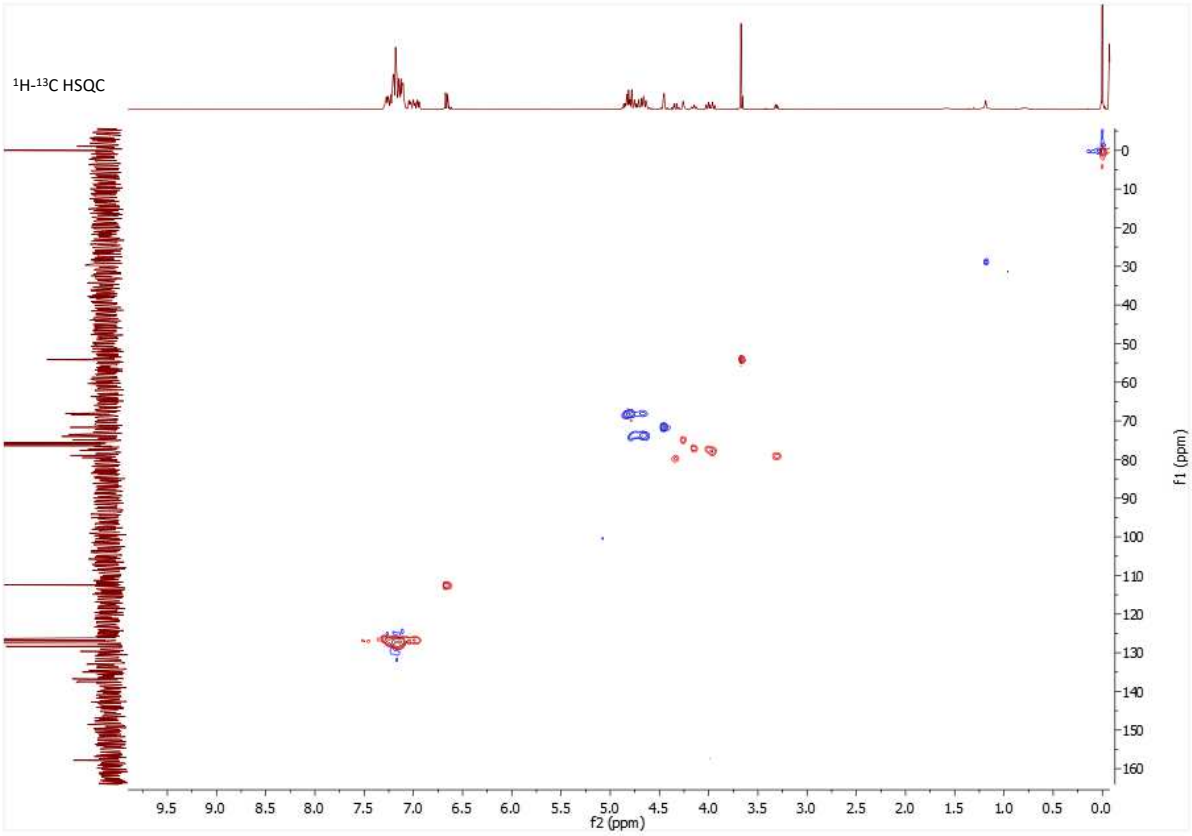

DL-2,3,6-Tri-*O*-benzyl-*myo*-inositol 1,5-bis(dibenzylphosphate) (**103**)

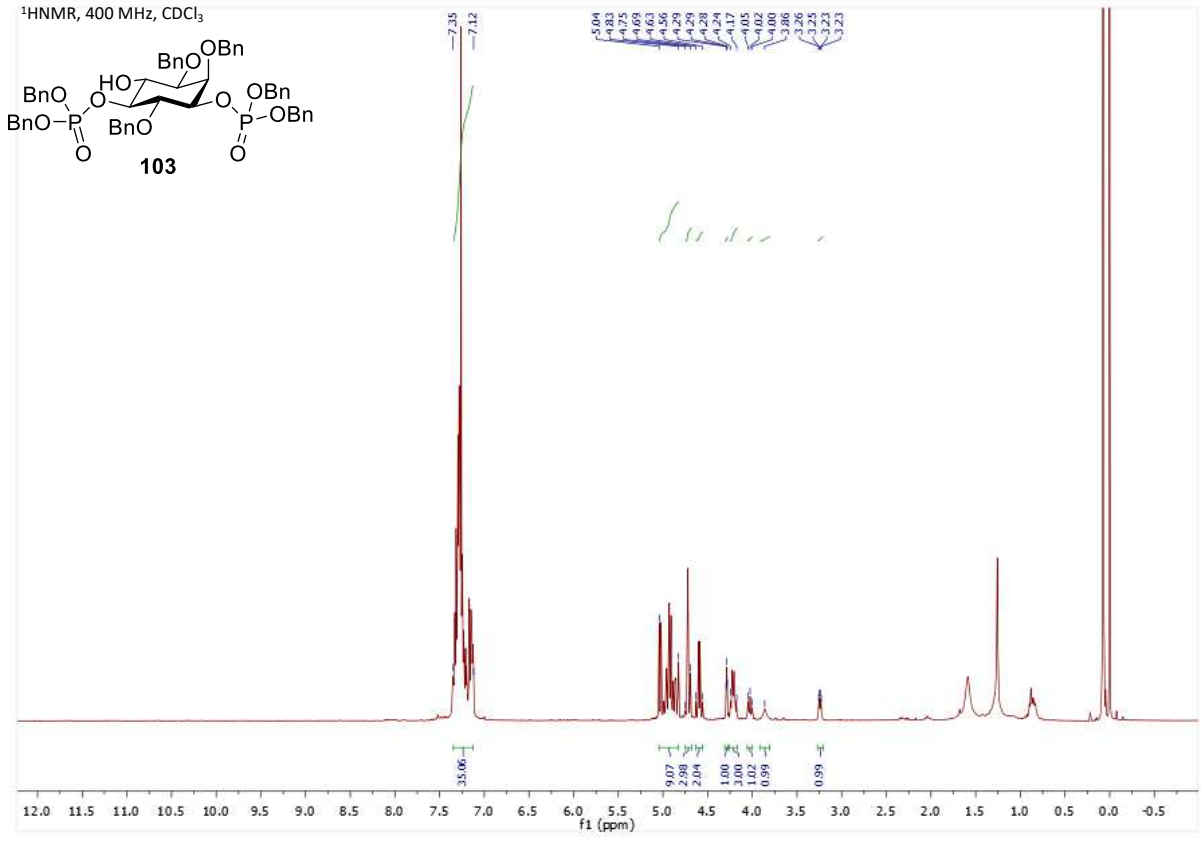

^{31}PNMR, 162 MHz, $CDCl_3$

103

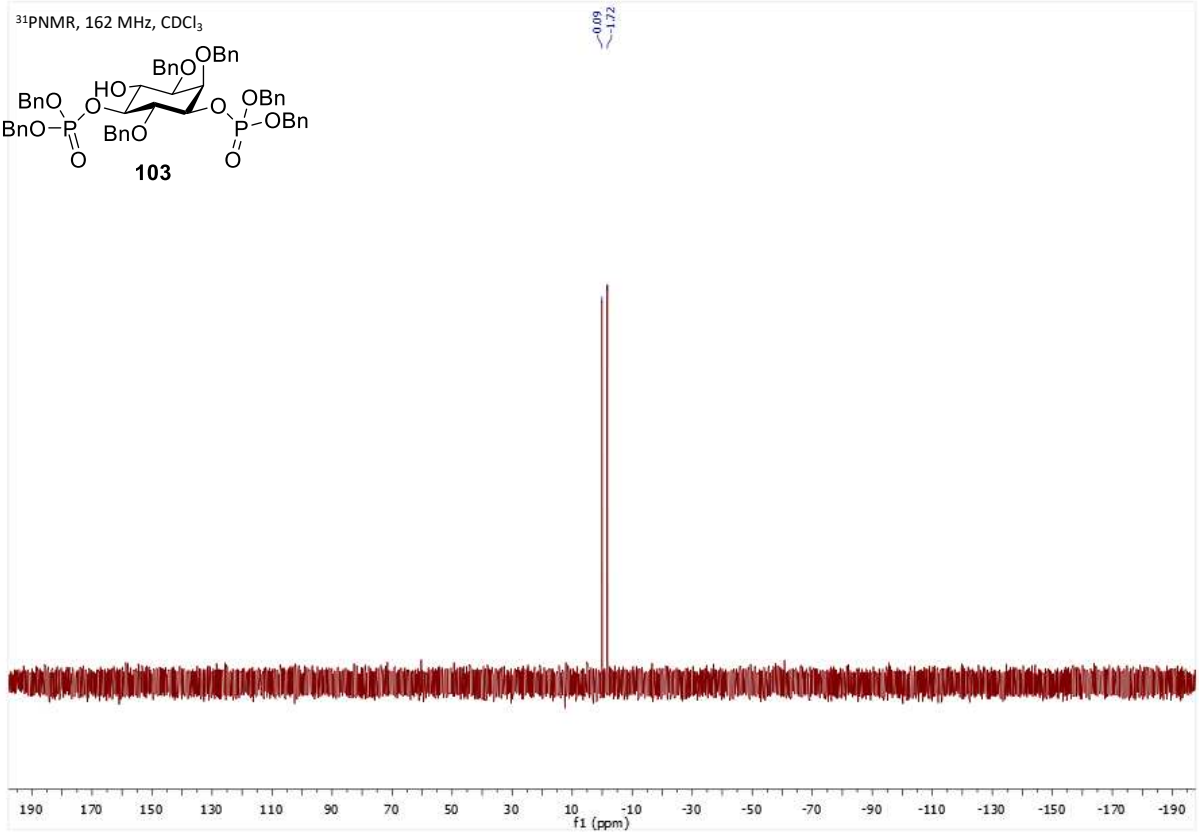

^{13}CNMR, 100 MHz, $CDCl_3$

103

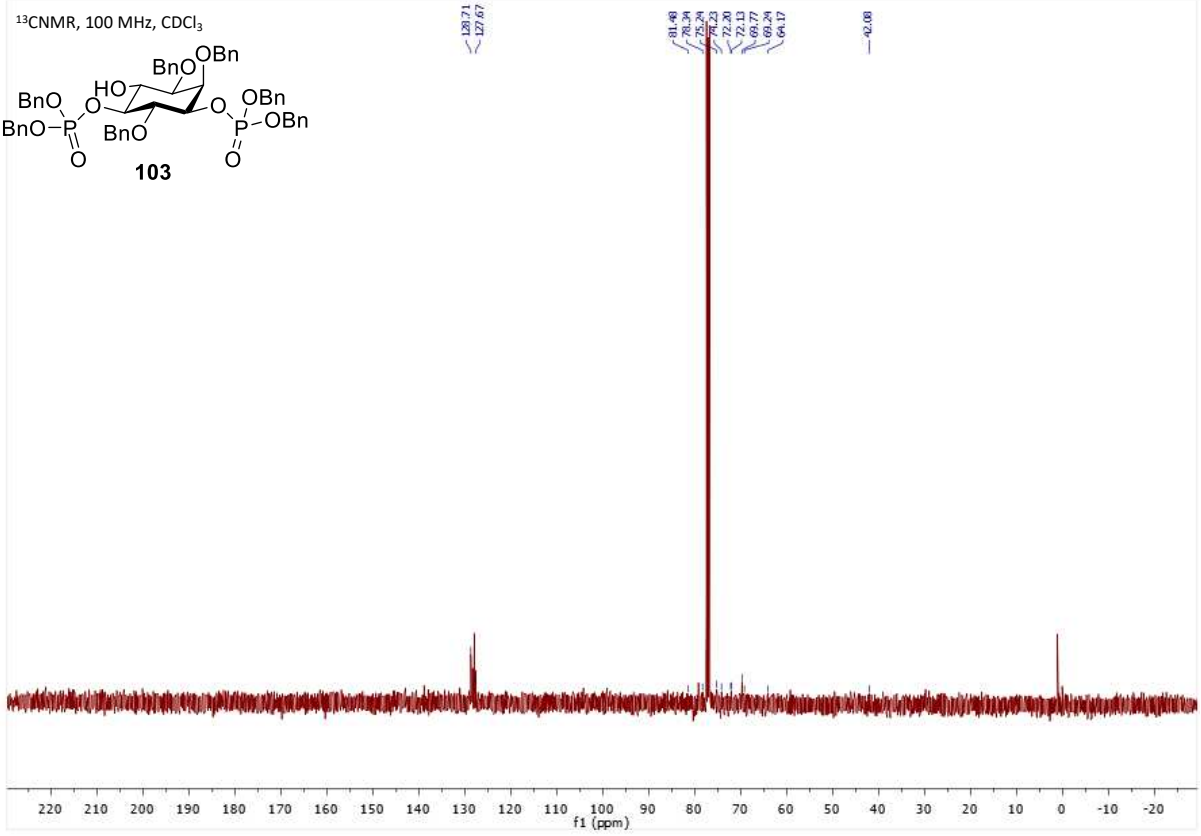

^{1}H-^{1}H COSY

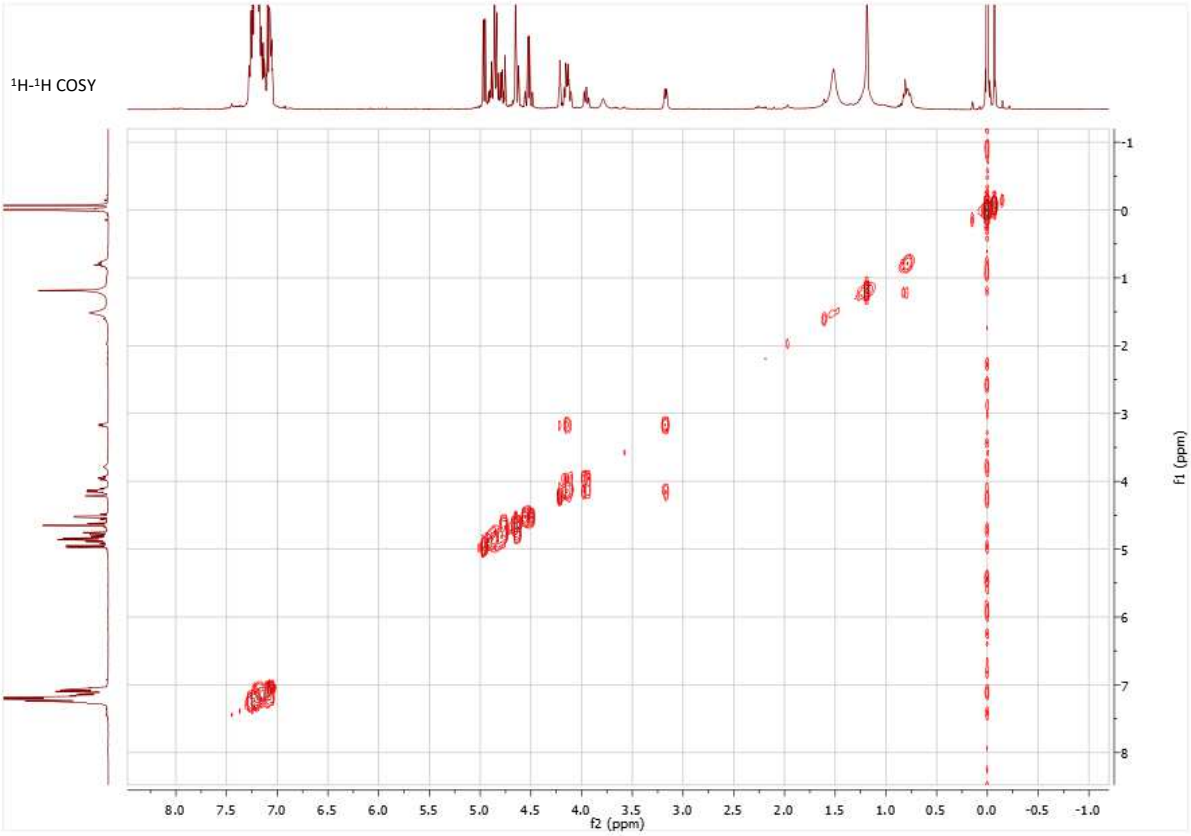

^{1}H-^{13}C HSQC

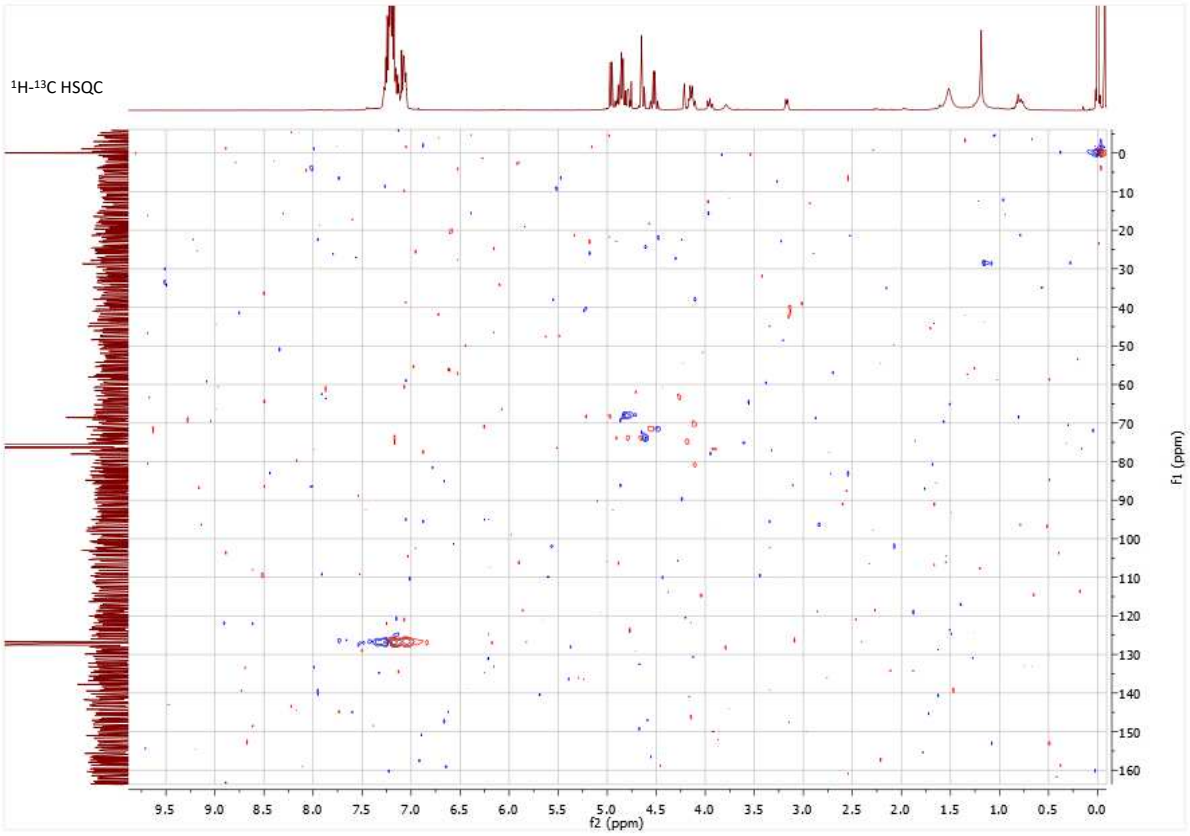

DL-2,3,6-Tri-*O*-benzyl-*myo*-inositol-1,5-bis(dibenzylphosphate)-4-bis[2-(methanesulfonyl)-ethyl]phosphate (**104**)

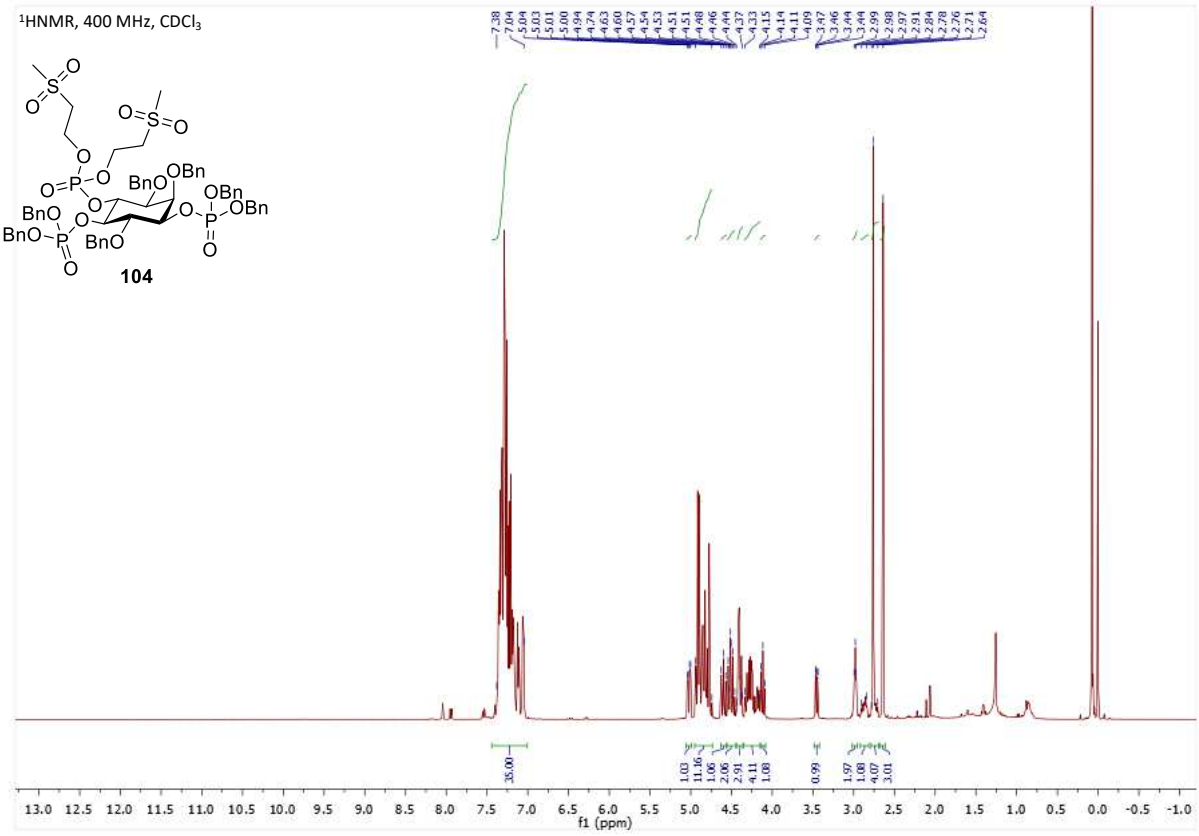

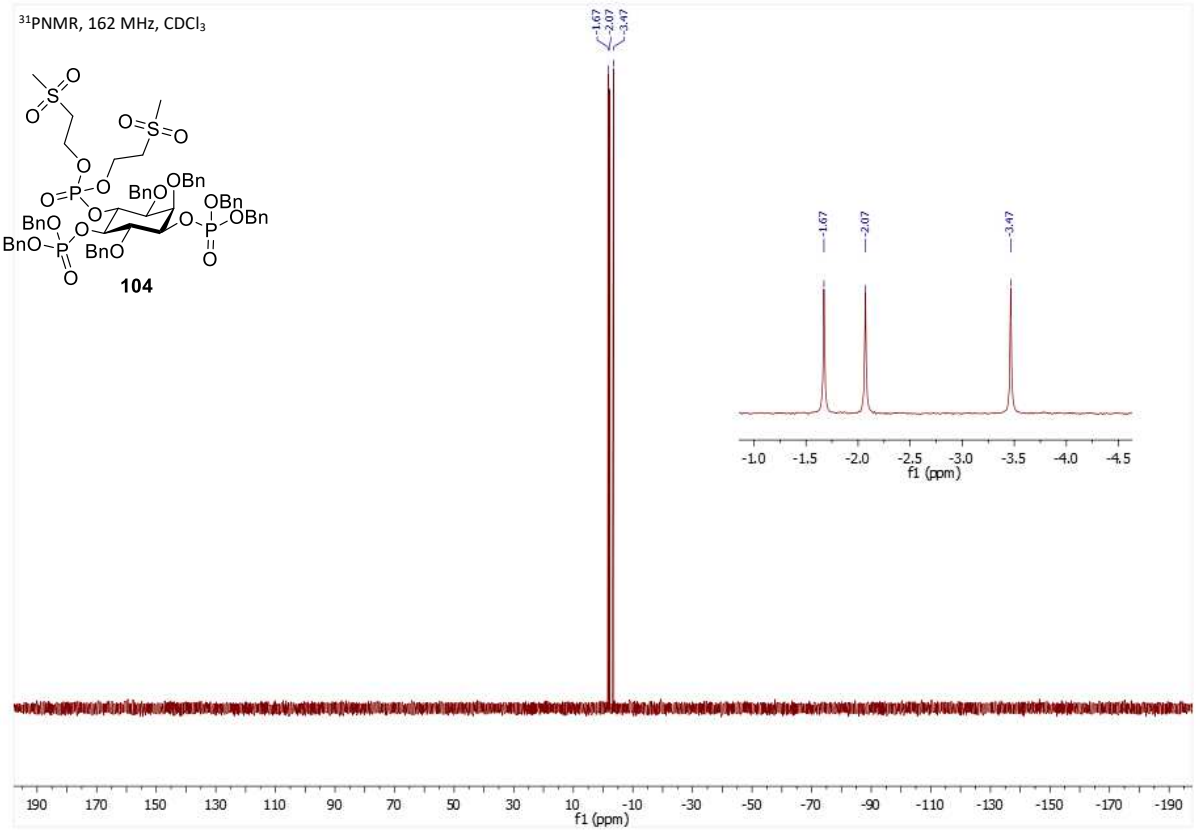

^{13}CNMR, 100 MHz, $CDCl_3$

104

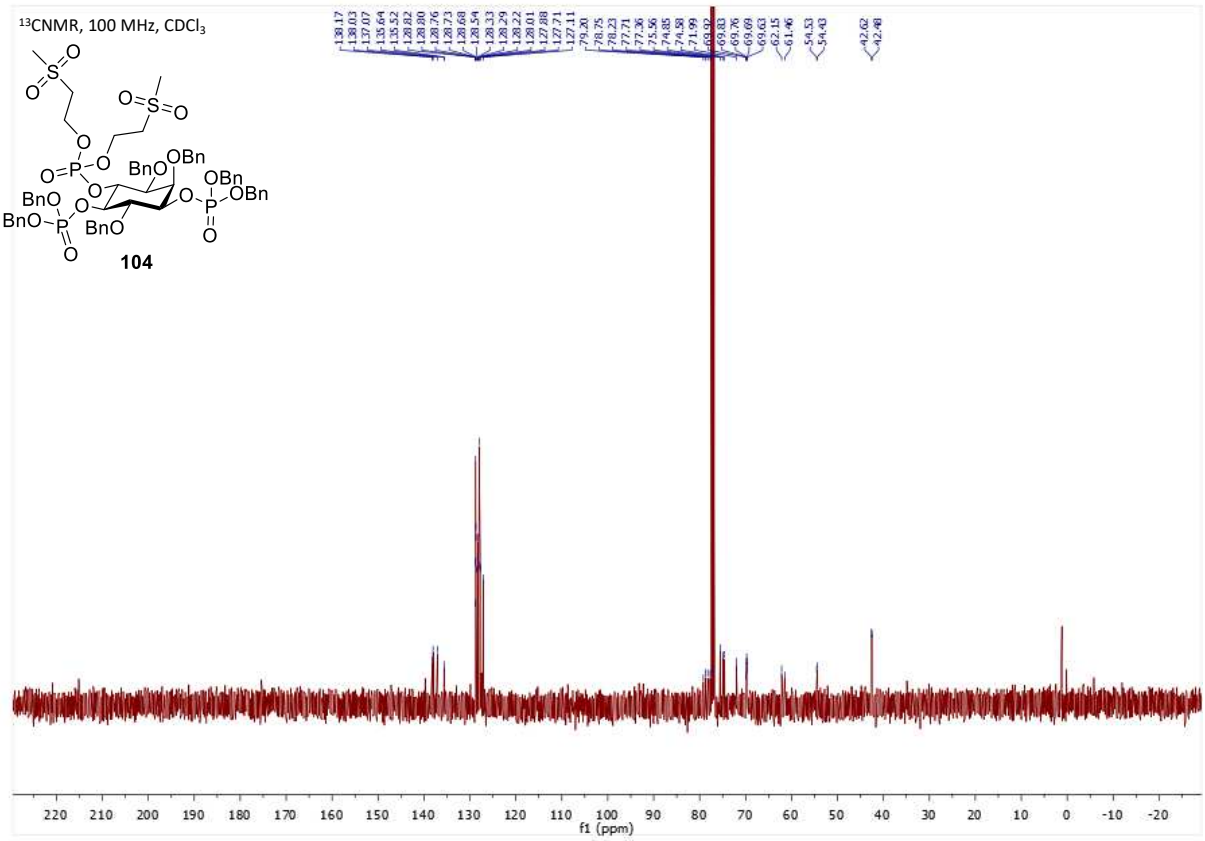

^{1}H-^{1}H COSY

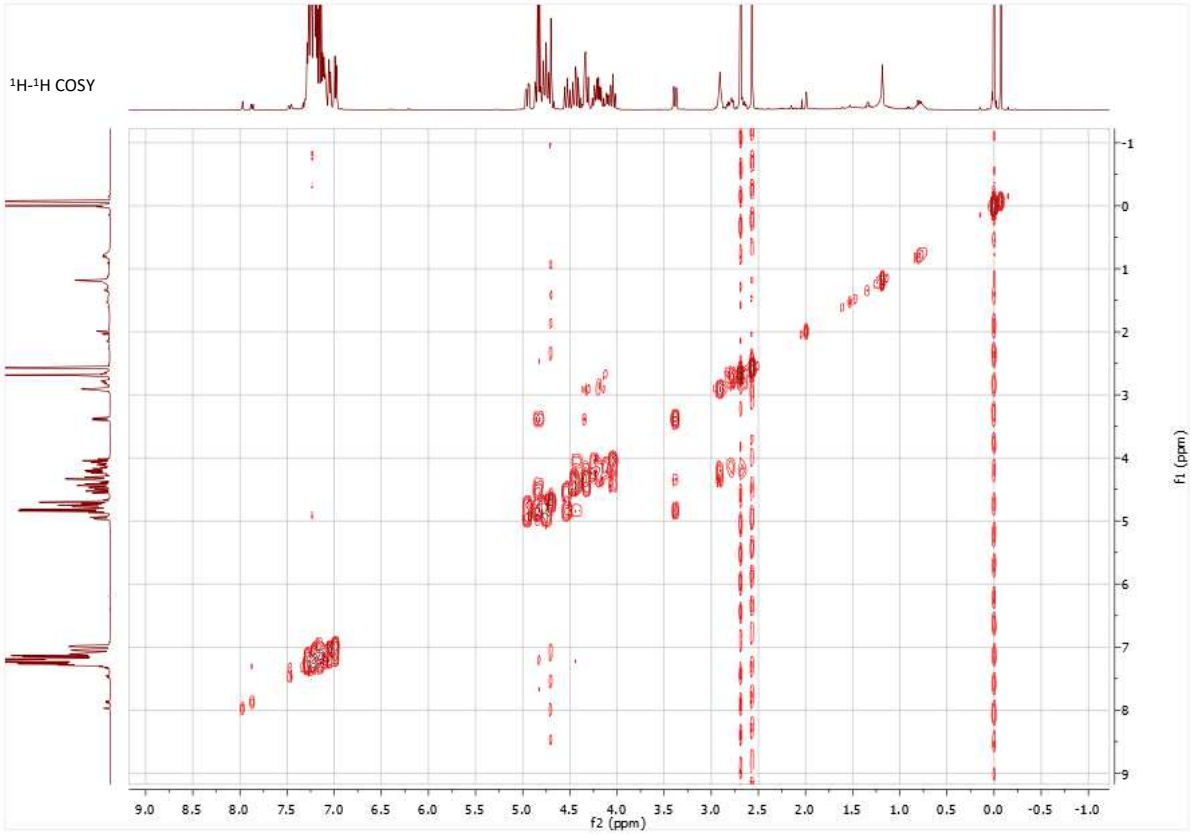

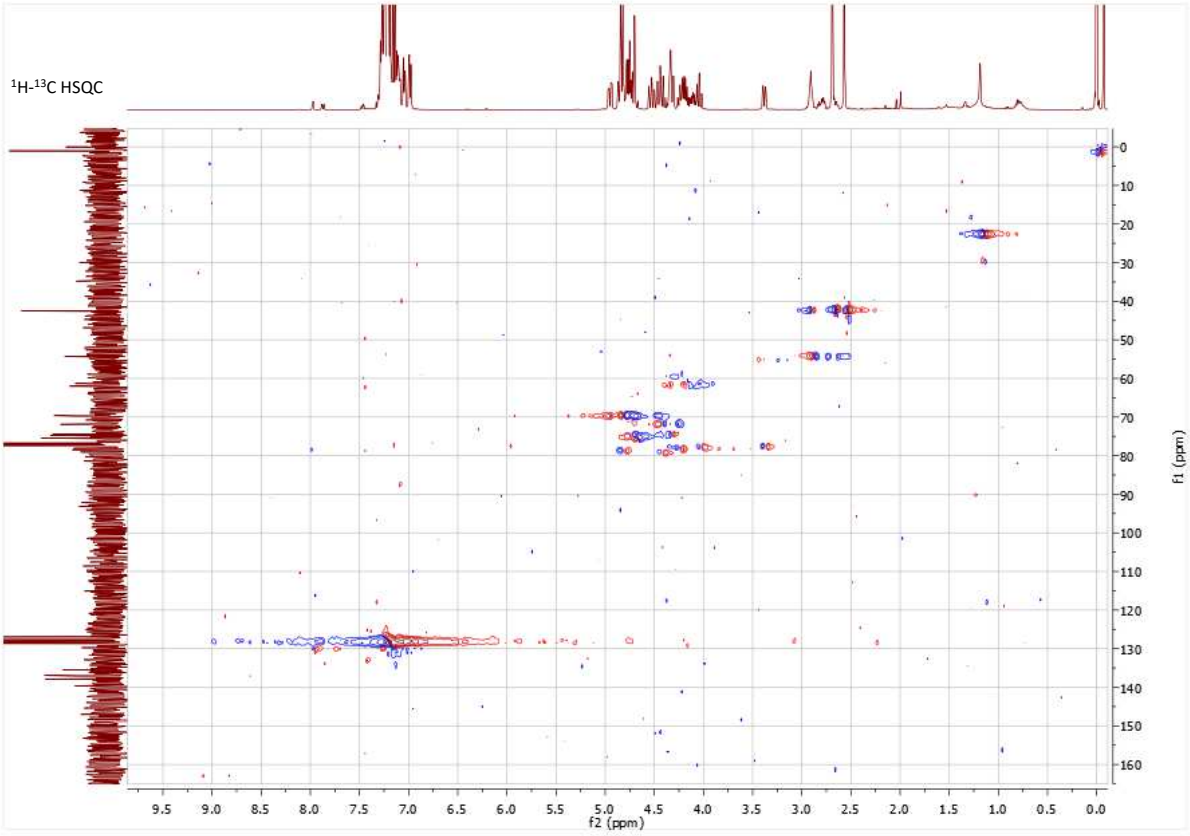

DL-4-Diphospho-*myo*-inositol 1,5-bisphosphate triethylammonium salt (**80**)

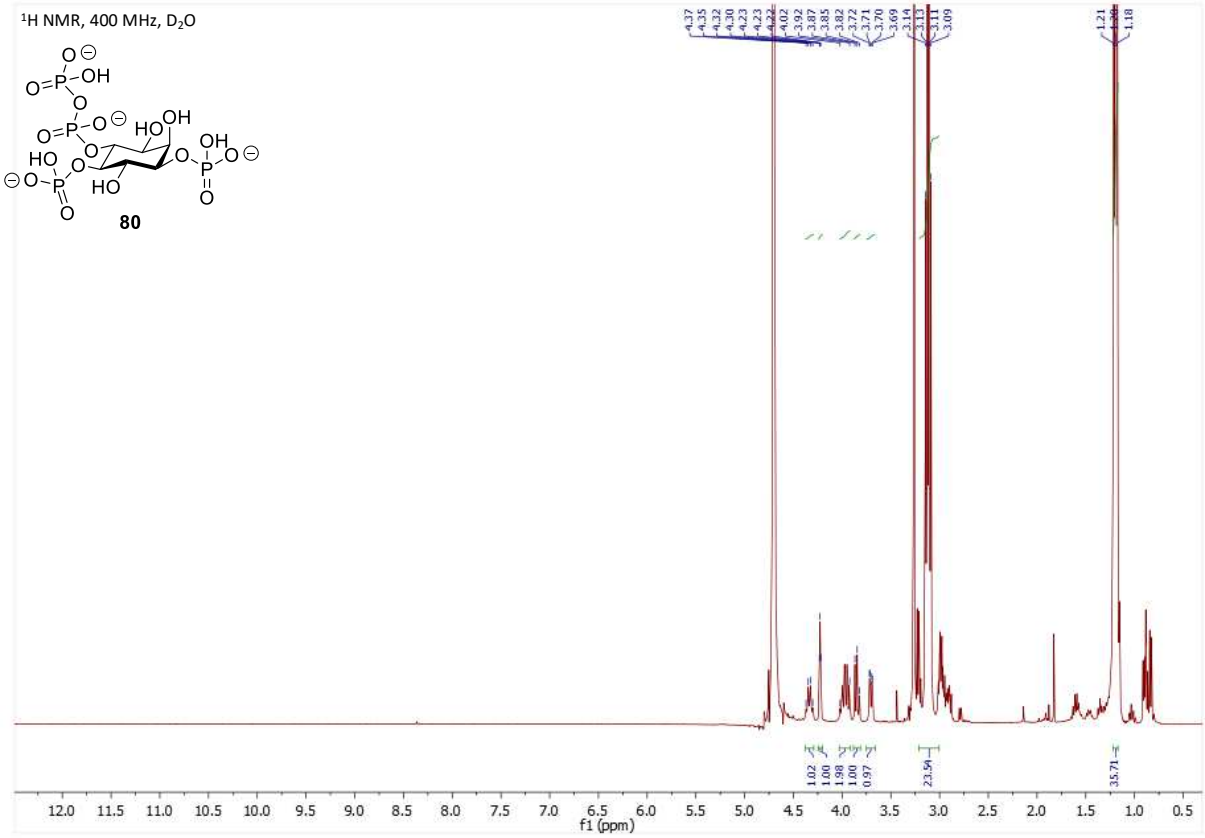

^{31}PNMR, 162 MHz, D_2O

80

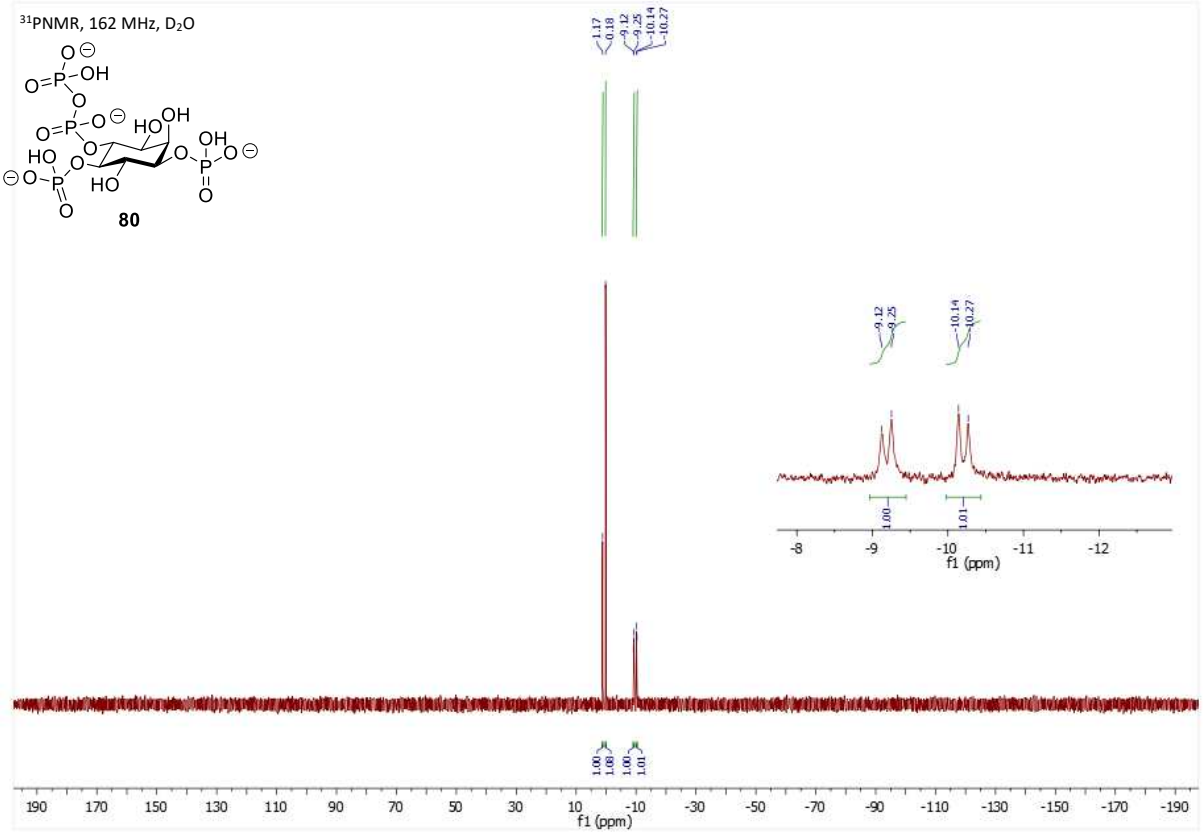

^{13}CNMR, 100 MHz, D_2O

80

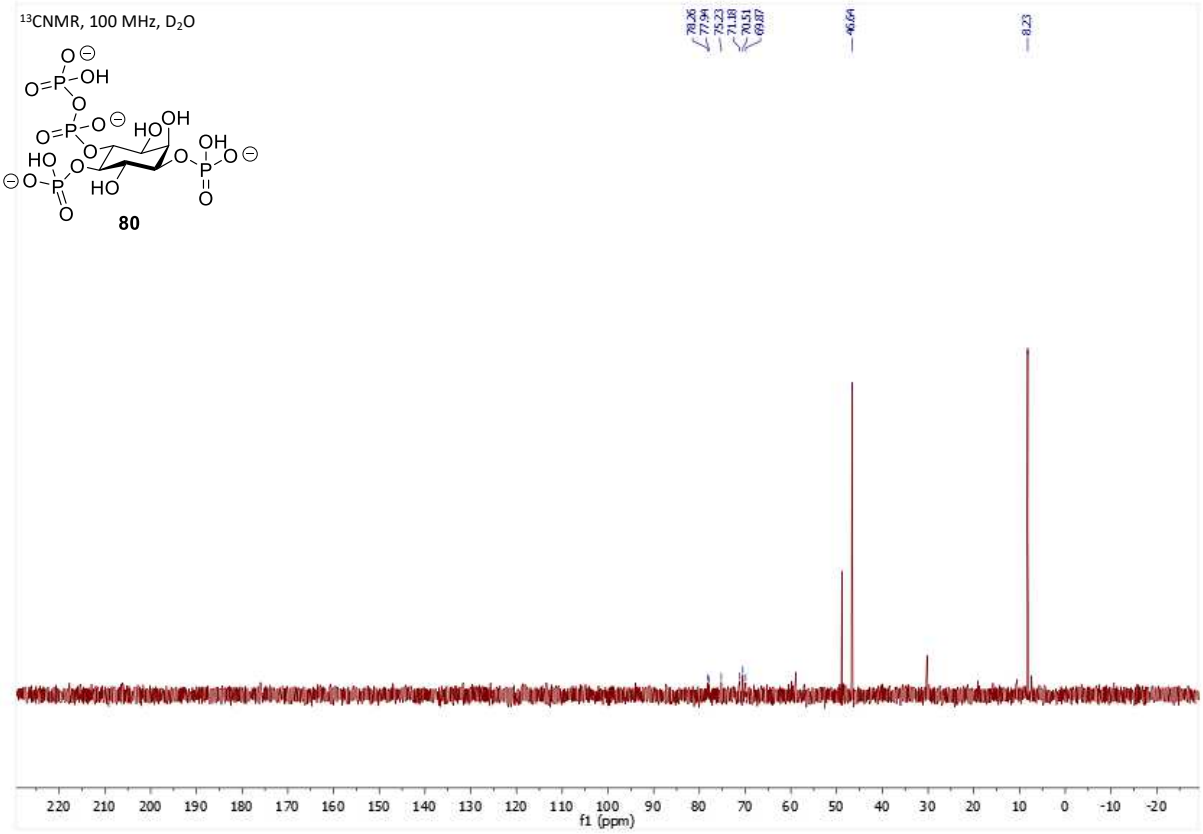

^{1}H-^{31}P HMBC

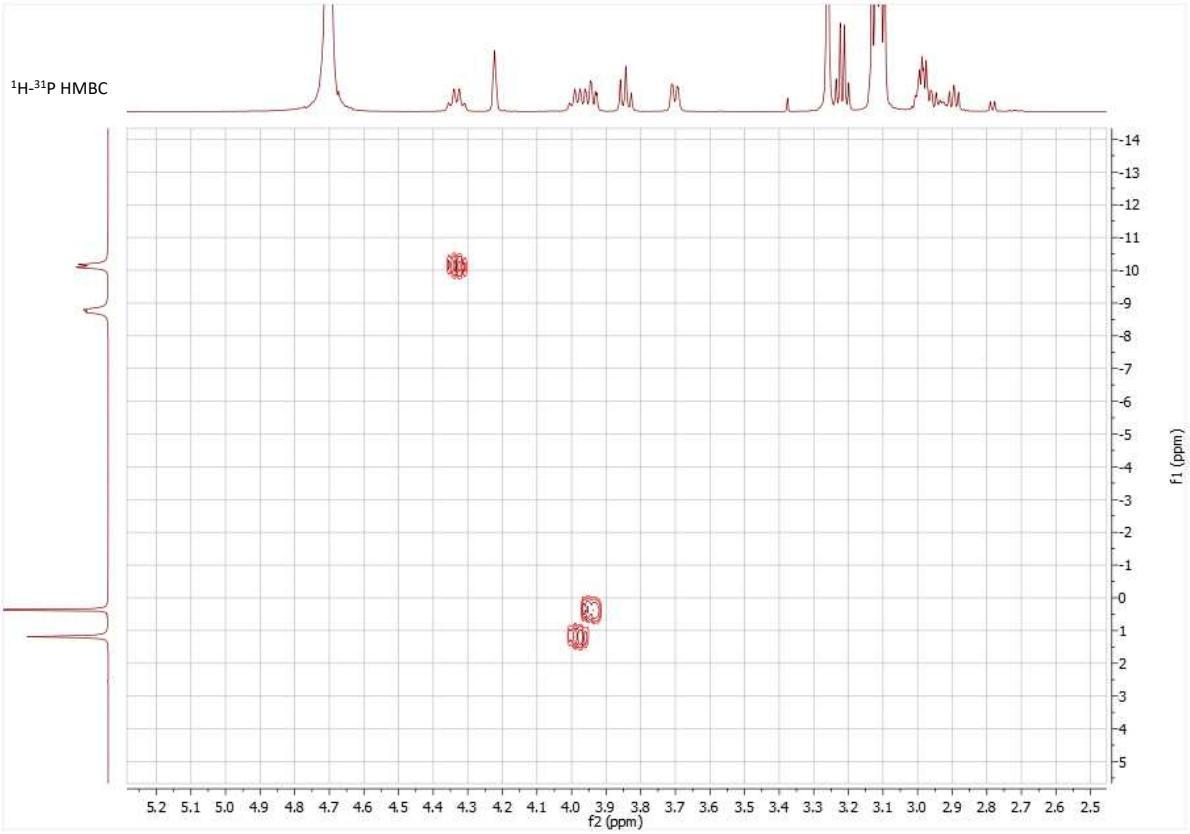

^{1}H-^{1}H COSY

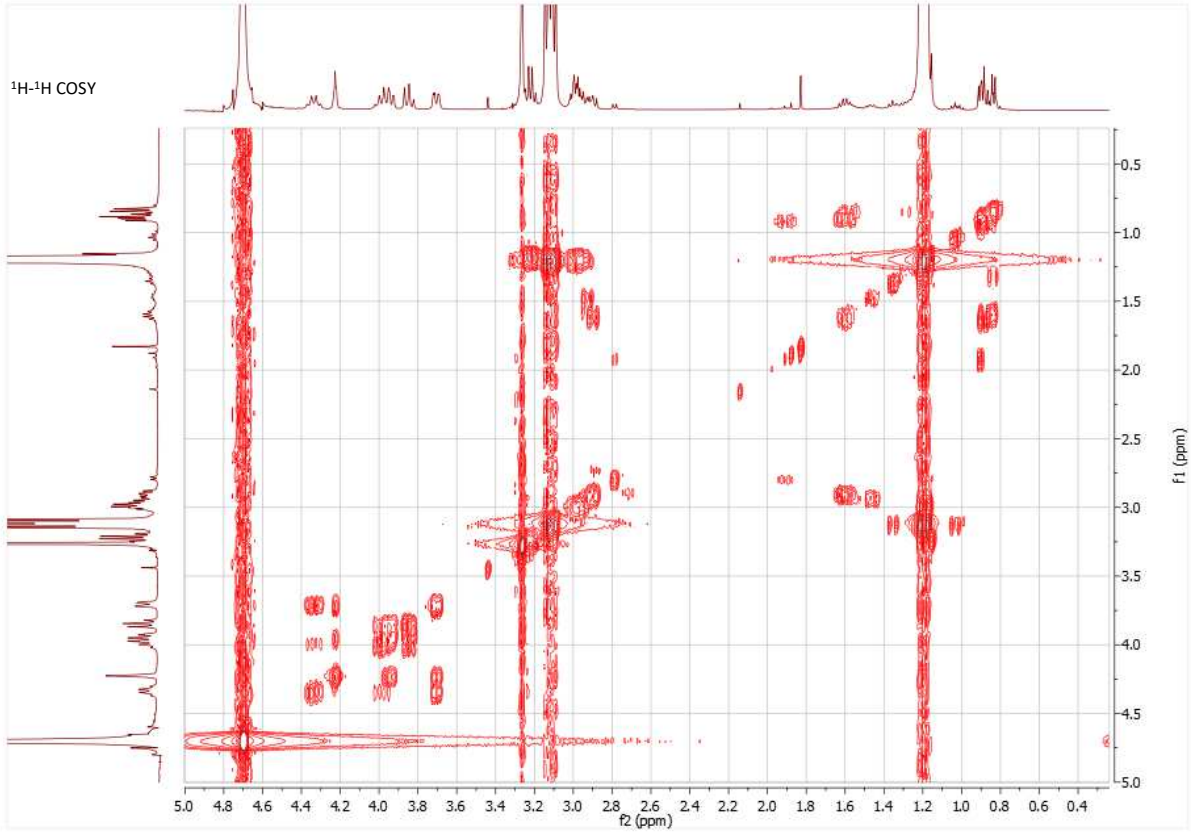

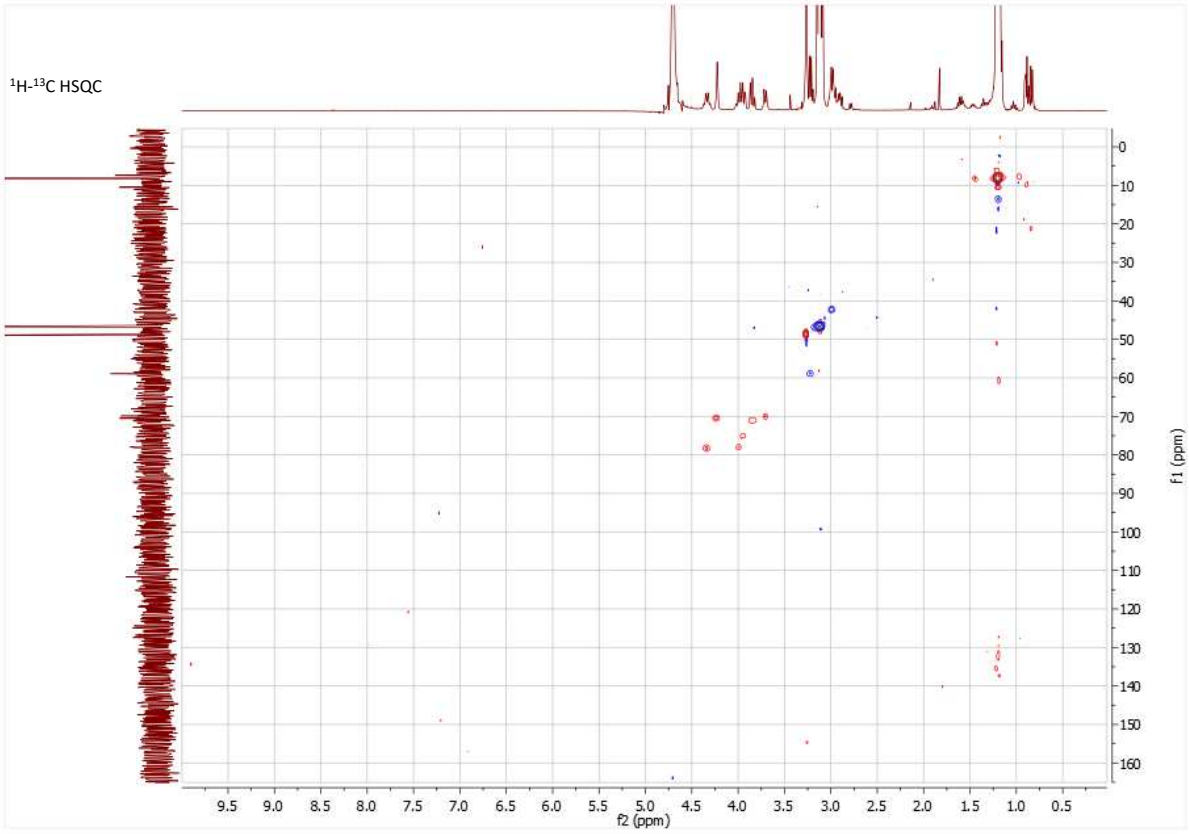
^{1}H-^{13}C HSQC
f2 (ppm)
f1 (ppm)